NASA/CP—2001-210427

Proceedings of the 4th Conference on Aerospace Materials, Processes, and Environmental Technology

D.E. Griffin, D. Cross Stanley, Editors
Marshall Space Flight Center, Marshall Space Flight Center, Alabama

Proceedings of a conference held in
Huntsville, Alabama, September 18–20, 2000

National Aeronautics and
Space Administration

Marshall Space Flight Center • MSFC, Alabama 35812

February 2001

NASA/CP—2001-210427

Proceedings of the 4th Conference on Aerospace Materials, Processes, and Environmental Technology

D.E. Griffin, D. Cross Stanley, Editors
Marshall Space Flight Center, Marshall Space Flight Center, Alabama

Proceedings of a conference held in
Huntsville, Alabama, September 18–20, 2000

February 2001

Available from:

NASA Center for AeroSpace Information
7121 Standard Drive
Hanover, MD 21076–1320
(301) 621–0390

National Technical Information Service
5285 Port Royal Road
Springfield, VA 22161
(703) 487–4650

The NASA STI Program Office...in Profile

Since its founding, NASA has been dedicated to the advancement of aeronautics and space science. The NASA Scientific and Technical Information (STI) Program Office plays a key part in helping NASA maintain this important role.

The NASA STI Program Office is operated by Langley Research Center, the lead center for NASA's scientific and technical information. The NASA STI Program Office provides access to the NASA STI Database, the largest collection of aeronautical and space science STI in the world. The Program Office is also NASA's institutional mechanism for disseminating the results of its research and development activities. These results are published by NASA in the NASA STI Report Series, which includes the following report types:

- TECHNICAL PUBLICATION. Reports of completed research or a major significant phase of research that present the results of NASA programs and include extensive data or theoretical analysis. Includes compilations of significant scientific and technical data and information deemed to be of continuing reference value. NASA's counterpart of peer-reviewed formal professional papers but has less stringent limitations on manuscript length and extent of graphic presentations.

- TECHNICAL MEMORANDUM. Scientific and technical findings that are preliminary or of specialized interest, e.g., quick release reports, working papers, and bibliographies that contain minimal annotation. Does not contain extensive analysis.

- CONTRACTOR REPORT. Scientific and technical findings by NASA-sponsored contractors and grantees.

- CONFERENCE PUBLICATION. Collected papers from scientific and technical conferences, symposia, seminars, or other meetings sponsored or cosponsored by NASA.

- SPECIAL PUBLICATION. Scientific, technical, or historical information from NASA programs, projects, and mission, often concerned with subjects having substantial public interest.

- TECHNICAL TRANSLATION. English-language translations of foreign scientific and technical material pertinent to NASA's mission.

Specialized services that complement the STI Program Office's diverse offerings include creating custom thesauri, building customized databases, organizing and publishing research results...even providing videos.

For more information about the NASA STI Program Office, see the following:

- Access the NASA STI Program Home Page at ***http://www.sti.nasa.gov***

- E-mail your question via the Internet to help@sti.nasa.gov

- Fax your question to the NASA Access Help Desk at (301) 621–0134

- Telephone the NASA Access Help Desk at (301) 621–0390

- Write to:
  NASA Access Help Desk
  NASA Center for AeroSpace Information
  7121 Standard Drive
  Hanover, MD 21076–1320
  (301)621–0390

4th Conference on Aerospace Materials, Processes and Environmental Technology
Sponsoring Agencies

National Aeronautics and Space Administration
George C. Marshall Space Flight Center
MSFC, AL 35812-9999

NASA Operational Environment Team
George C. Marshall Space Flight Center
MSFC, AL 35812-9999

NASA's Materials and Processes Working Group
Attn.: Dennis Griffin, Chairman
Mailstop: ED35
MSFC, AL 35812-9999

Office of Space Flight, NASA Headquarters
Washington, DC 20546-0001

Aerospace Institute of Aeronautics and Astronautics
1801 Alexander Bell Drive, Suite 500
Reston, VA 20191

National Center for Manufacturing Sciences
3025 Boardwalk Street
Ann Arbor, MI 48108-3266

ASM, International™
9639 Kinsman Road
Materials Park, OH 44073-0002

Aerospace Industries Association
1250 Eye Street, NW, 12th Floor
Washington, DC 20005

Environmental Protection Agency
86 T. W. Alexander Drive
Research Triangle Park, NC 27711

National Center for Advanced Manufacturing
Attn: John Vickers
Mailstop: ED35
MSFC, AL 35812

Sandia National Laboratories
Manufacturing Technology Center
P. O. Box 5800
Albuquerque, NM 87185

Society for Advancement of Materials and Processes Engineering
1161 Parkview Drive
Covina, CA 91724-3748

University of New Orleans
College of Engineering
New Orleans, LA 70148

Proceedings of 4th Conference on Aerospace Materials, Processes and Environmental Technology (AMPET)

Opening Session

Challenges for Aerospace Materials & Processes
Dr. Charles E. Browning

Advanced Space Flight and Environmental Concerns
Dr. Ann F. Whitaker

Session A1: Engineering Evaluation of Solvent Substitutes

Nonflammable, Nonaqueous, Low Atmospheric Impact, High Performance Cleaning Solvents
Patrick M. Dhooge, Suzanne M. Glass, and Jonathan S. Nimitz

Aerospace Applications for AK-225
Kenroh Kitamura, Masaaki Tsuzaki, and Stephen D. Stagliano

HFEs In The Aerospace Industry: A Logical Alternative To CFCs And Other Halogenated Cleaning Solvents
David A. Hesselroth

Elimination Of MEK And Lacquer Thinner In Department Of Defense Painting Operations
Joseph A. Lucas and Eric Lethe

Session A2: Advances In Materials Development

Lightweight Multi-Layer Structural Materials
H.H. Legner, W.T. Laughlin, V. Di Cristina, D. Marshall, and R. Singler

Asbestos Free Insulation Development For The Space Shuttle Solid Propellant Rocket Motor (RSRM)
Larry D. Allred and Norman F. Eddy

Aerogel Projects Ongoing In MSFC's Engineering Directorate
David Shular, Gweneth Smithers, and Joel Plawsky

Electroactive Polymers As Artificial Muscles – Reality And Challenges
Yoseph Bar-Cohen

Session A3: National Center For Advanced Manufacturing Workshop

National Center For Advanced Manufacturing Overview
John Vickers

Advanced Engineering Environments – Implications For Aerospace Manufacturing
Dale Thomas

State, Industry, And Education Partnerships Expanding Education To Meet Workforce Challenges
James E. Swindell, Donna C. Bass, and William R. Reynolds

Composite Manufacturing For Space Launch Vehicles
Donna Y. Knezevich

Session B1: Elimination Of Heavy Metals

Laser Cladding/Glazing As A Surface Coating Alternative
Rob Hull, Dave Firsich, Chuck Woods, and John Eric

Testing Of Environmentally Preferable Aluminum Pretreatments And Coating Systems For Use On Space Shuttle Solid Rocket Boosters (SRBs)
Catherine Clayton, Lee Zook, and Randy Raley

Trivalent Chromium/Organically-Modified Silicate Composite Coatings For Corrosion Protection Of Aluminum Alloys
Edward Knobbe, Elvira Stesikova, Tammy Metroke, and Olga Kachurina

HVOF Thermal Spray Coating As An Alternative To Hard Chrome Plating On Military Aircraft
Bruce D. Sartwell

The Use Of Ion Vapor Deposited (IVD) Aluminum For The Space Shuttle Solid Rocket Booster
Howard Novak, Bill Imre, and Randy Raley

Session B2: Advances In Materials Analysis And Testing Techniques I

High Temperature Material Performance Testing Using Continuous Wave Carbon Dioxide Lasers
Timothy Johnson

Thermographic Nondestructive Evaluation Of The Space Shuttle Main Engine Nozzle
James L. Walker, Samuel S. Russell, Matthew D. Lansing, and Paul Caraccioli

Verification Of Shearography NDE Methods On Space Shuttle, X-33, And Delta IV Launch Vehicles
John W. Newman

Thermographic Analysis Of Composite Cobonds On The X-33
James L. Walker, Matthew D. Lansing, and Samuel S. Russell

Session B3: Developments In Metals Processes I

Evaluation Of Forces On The Welding Probe Of The Automated Retractable Pin-Tool (RPT)
R. Jeffrey Ding

Friction Stir Weld Modeling At MSFC: Kinematics
Arthur C. Nunes, Jr.

Aluminum Lithium Alloy 2195 Fusion Welding Improvements With New Filler Wire
Carolyn Russell

Session B4: Non-Metals Processes I

Fabrication Of Composite Combustion Chamber/Nozzle For Fastrac Engine
T. Lawrence, R. Beshears, S. Burlingame, W. Peters, M. Prince, M. Suits, S. Tillery, L. Burns, M. Kovach, and K. Roberts

Large Composite Structures Processing Technologies For Reusable Launch Vehicles
R.G. Clinton, Jr., John H. Vickers, A. B. Hulcher, Norman J. Johnston, William M. McMahon, R. J. Cano, H. L. Belvin, Walter Franklin, Don Sidwell, Keith McIver, Tod Palm, and Robert Biggs

Composite, Cryogenic, Conformal, Common Bulkhead, Aerogel-Insulated Tank (CBAT) Materials And Processing Methodologies
Michael P. Kovach, J. Keith Roberts, William M. McMahon, and Jeffery L. Finckenor

Session C1: Developments In Coating Removal Processes

Coating Removal Technology Using Starch Based Abrasives, A Review Of Current Aerospace Applications Using The Envirostrip® Dry Stripping Process
Denis Monette and Cameron Drake

Removal Of Zirconia Thermal Barrier Coatings And MCrAlY Bond Coatings From Turbine Blades: A Comparison Of Methods Based On Chemical Stripping, Water Jet, And Salt Bath
A. Scrivani, U. Bardi, G. Ballerini, D. Bonacchi, M. Fantini, R. Groppetti, S. Ianelli, and G. Rizzi

Joint EPA/NASA/USAF Interagency Depainting Study
Marceia Clark-Ingram

Evaluation Of Various Depainting Processes On Mechanical Properties Of 2024-T3 Aluminum Substrate
Preston B. McGill

Session C2: Ceramic Matrix Composites

Concept For Determining The Life Of Ceramic Matrix Composites Using Nondestructive Characterization Techniques
Michael Effinger, Bill Ellingson, Todd Spohnholtz, and John Koenig

Low-Cost Ceramic Matrix Composites
Witold Kowbel, C. Bruce, K.T. Tsou, and J.C. Withers

Fabrication and Testing of Ceramic Matrix Composite Propulsion Components
Micheal Effinger, R. G. Clinton, Jr., Jay Dennis, Sandra Elam, Gary Genge, J. Doug Kiser, Andy Eckel, Martha Jaskowiak and Jerry Land

Rapid Fabrication Of Monolithic Ceramic Parts Reinforced With Fibrous Monoliths For Aerospace Applications
R. Vaidyanathan, J. Walish, J.L. Lombardi, M. Fox, M. Rigali, and M. Sutaria

Session C3: Rapid Prototyping

Solid Freeform Fabrication Of Continuous Fiber Reinforced Composites For Propulsion Applications
R. Vaidyanathan, J. Walish, M. Fox, M. Rigali, M. Sutaria, J.W. Gillespie, Jr., S. Yarlagadda, and M. Effinger

An Example Of Economic Value In Rapid Prototyping
John R. Reagan, Edward P. Braunscheidel, and Robert L. Hauer

High-Efficiency Monolithic Lightweight Aluminum Cast Structure
John Bowkett

Preliminary Component Integration Utilizing Rapid Prototyping Techniques
Ken Cooper and Pat Salvail

Session C4: Innovative Materials Applications

Multifunctional Carbon Foams For Aerospace Applications
Darren K. Rogers and Janusz Plucinski

Polymer Matrix Composite Materials Oxygen Compatibility
Tim Vaughn, Tom Owens, and Robert Jacobs

Low Density Monolithic Metal Honeycombs by Thermal Chemical Processing
Jim Lee, Joe Cochran, Dave McDowell, and Tom Sanders

TransHab Materials Selection
Michael Pedley

Session D1: Evaluating Pollution Prevention Methodologies

Identification Of High Performance, Low Environmental Impact Materials And Processes Using Systematic Substitution (Sys)
Patrick M. Dhooge and Jonathan S. Nimitz

Selection Criteria For Alternative Technologies, As A Method Of Hazardous Waste Minimization
Eric Lethe

Joint Group On Pollution Prevention, Partnering For Progress
Robert P. Hill and Michael McCall

Liquid Filtration For Component Reliability And Waste Minimization
Edward Kanegsberg and Barbara Kanegsberg

Chemical Aging Of Environmentally Friendly Cleaners
L.L. Biegert, K.B. Evans, B. D. Olsen, and B.L. Weber

Session D2: Advanced Materials For Extreme Environments

NAtional Materials Information System
Jeff Guthrie

Durability Characterization Of Advanced Polymeric Composites At Cryogenic Temperatures
Thomas S. Gates

Development Of Metal Matrix Composites For NASA's Advanced Propulsion Systems
Jonathan A. Lee and Sandy Elam

Inorganic-Organic Hybrid Polymers For High Temperature Aerospace Applications
Teddy M. Keller

Session D3: Manufacturing Technology Topics

Integrated High Payoff Rocket Propulsion Technologies Program Material Development Plan
R.G. Clinton, Jr., Brian Reed, Michael Stropki, Dan Cleyrat, Brian Stucke, and Shawn Phillips

X-33 LH_2 Tank Failure Investigation Findings
Mindy Niedermeyer

Assessment Of The State-Of-The-Art In The Design And Manufacturing Of Large Composite Structures
Charles E. Harris

Session D4: Evaluation Of Cleaning And Bonding Materials And Processes

A Mass Spectrometer-Based Tool For In-Process Analysis Of RSRM Components
Michael Meltzer, Carolyn Koester, and Neil Sagers

Effects And Detection Of Silicone And HD2 Grease Contaminants
Jerrell W. Blanks

Physical Evaluation Of Cleaning Performance – We Are Only Fooling Ourselves
Earl Pratz

Session E1: Alternatives For Chemical Replacements

Low Environmental Impact, High Performance Foam Blowing Agents Based On Iodofluorocarbons
Patrick M. Dhooge, Suzanne M. Glass, and Jonathan S. Nimitz

Update: HFC 245fa Blown Foam Development With External Tank Spray Foams
Simon Davis

High-Performance, Low Environmental Impact Refrigerants
Patrick M. Dhooge, Edward T. McCullough, Suzanne M. Glass, and Jonathan S. Nimitz

VOC Compliant Wax Removal Process
Alan Brown, David Grimmett, and Margarite Sylvia

Highly Effective, Low Toxicity, Low Environmental Impact Total Flooding Fire Suppressants
Patrick M. Dhooge, Suzanne M. Glass, and Jonathan S. Nimitz

Session E2: Advances In Materials Analysis And Testing Techniques II

Promoted Combustion Of Metals In A High-Pressure, Flowing Oxygen Environment
Miguel J. Maes and Joel M. Stoltzfus

Problem Solving Applications Of Chemical Fingerprinting
Michael O. Killpack, Dennis J. Fife, Chad R. Saunders, Charles R. Whitworth, and William H. McClennen

Resources Available For Hazards Analysis Of Aerospace Fluids
Stephen S. Woods, Walter F. Stewart, David L. Baker, and Harold D. Beeson

Chemical Fingerprinting Of Materials Developed Due To Environmental Issues
Doris A. Smith

Use Of GC/MS And Microtome Techniques To Evaluate ODC Cleaner Diffusion And Evaporation In Insulation And Phenolic Case Material
L.L. Biegert

Session E3: Non-Metals Processes II

Electron Beam-Cured Polymer Matrix Composites: Processing And Properties
George Wrenn, Barbara Frame, Brian Jensen, and Alan Nettles

Manufacture Of Porous Ceramic Materials By Combustion Synthesis
L. A. Whelan Robinson, H. C. Yi, and J.Y. Guigné

The Composites Affordability Initiative
John Mistretta

Advanced Ceramic Matrix Composites for Aerospace Applications
John Garnier, Bill Patterson, Bob Klacka and Paul Gray

Session E4: Developments In Metals Processes II

Aluminum Investment Cast Spacecraft And Aerospace Structures
John Bowkett

Vacuum Plasma Spray Of Cu-8Cr-4Nb Alloys For Advanced Liquid-Fuel Combustion Chambers
Frank Zimmerman, Sandra Elam, David Ellis, Heather Miller, Timothy McKechnie and Robert Hickman

Dynamic Oxidation Of A Plasma-Sprayed Cu-Cr Coating
K.T. Chiang

Manufacturing Challenges Implementing Material Changes For Super Lightweight Tank: A Welding Process Perspective
Chip Jones and Kirby G. Lawless

Cryogenic Tank Technology Program (CTTP)
Tim Vaughn

Session F1: Methods For Cleaning And Cleanliness Verification

Elimination of Carbon Tetrachloride for Quantitative Hydrocarbon Surface Analysis
Vonnie M. Douglas

Ellipsometric Verification And Evaluation Of Clean Surfaces
Wayne Thompson

Improved Detection Technique For Solvent Rinse Cleanliness Verification
Steven D. Hornung and Harold D. Beeson

Criteria For NVR Solvent Replacement
Kenneth Luey, Dianne J. Coleman, Joseph C. Uht, and Graham S. Arnold

Critical Surface Cleaning And Verification Alternatives
Donald M. Melton

Session F2: Advanced Metals Research

Effects Of Cryogenic Treatment On The Residual Stress And Mechanical Properties Of An Aerospace Aluminum Alloy
Po Chen, Robert Bond, Tina Malone, and Pablo Torres

Toughness Of Ultra High Strength AF1410 Type Steels
Luana E. Iorio and Warren M. Garrison, Jr.

Segregation Behavior Of Sulfur And Other Impurities Onto The Free Surfaces In ED-Ni Deposits
Binayak Panda and Gregory Jerman

Statistical Analysis Of Strength Data For An Aerospace Aluminum Alloy
Lynn Neergaard and Tina Malone

Electrostatic Levitation Processing Of Bulk Metallic Glass Forming Liquids
C. C. Hayes, J. Schroers, U. Geyer, and W. L. Johnson

Session F3: Emerging Technologies

Residual Stress Prediction In Machined Workpiece Surface
Troy Marusich and Paul Bayer

Easily Processable High Temperature And Flame Resistant Phthalonitrile Composites For Aerospace Applications
Teddy M. Keller and Harry N. Jones

Real Time Video Recording Of Extremely High Temperature Processes
Thad Hoffman

Vapor Grown Carbon Fiber/Phenolic Matrix Composites For Rocket Nozzles And Heat Shields
R. D. Patton, C. U. Pittman, Jr., L. Wang, J. R. Hill, and A. Day

Session F4: Environmental Monitoring Methods

Ambient Air Monitoring Of Respirable Particulate Matter (PM_{10}) And Total Suspended Particulate (TSP) From The RD180 Rocket Engine Tests At The NASA Marshall Space Flight Center
John Hughes and Kathy Lehr

Gas Emission Measurements From The RD 180 Rocket Engine Tests At The NASA Marshall Space Flight Center
H. Richard Ross

Overview of the City of Huntsville Air Pollution Control Program
Daniel Shea

Potential Effects on the Huntsville Area of Revised National Ambient Air Quality Standards for Ozone and Fine Particulate Matter
Daniel Shea

Posters

Development Of Lead-Free Energy For Space Shuttle Blast Container
Donald Balles, Thomas Ingram, Howard Novak, and Albert Schricker

Polymer Matrix Composites (PMCs) Cryopipe For Rocket Engine Lines And Ducts
David Bettinger

Nanotechnology Concepts At Marshall Space Flight Center – Engineering Directorate
Biliyar Bhat, Raj Kaul, Sandeep Shah, Gweneth Smithers, and Michael D. Watson

Microstructure, Mechanical Properties, Hot-Die Forming, And Joining Of 47XD Gamma TiAl Rolled Sheets
G. Das, S. Draper, J.D. Whittenberger, and P.A. Bartolotta

At Last, Something New! Cleaning Without Chemistry, And Reusing The Waste Water!
John Durkee

Polymer Matrix Composite (PMC) Analog Processes For Lightweight Aluminum Matrix Composite (AMC) Structures
Brian Gordon

Further Studies Of Materials Compatibility In High-Test Hydrogen Peroxide
Rudy Gostowski and Tom Owens

X-Traktor: A Rookie Robot, Simple, Yet Complex, Impeccably Designed, A Very Innovative Multidisciplinary Engineering Masterpiece
Arthur J. Henderson, Jr.

Laser Surface Modification of TiAl Intermetallics
Sherman McElroy and Ramana Reddy

Characterization Of Ceramic Matrix Composite Combustor Components: Pre And Post Exposure
G. Ojard, G. Linsey, J. Brennan, R. Naik, R. Cairo, R. Stephan, J. Hornick, and D. Brewer

Automated Acquisition And Analysis Of Digital Radiographic Images
Richard Poland, David Inmel, Boyd Howard, Randy Singer, and Bob Moore

Fabrication Of Low-Cost, High-Temperature Composites For Rocket Propulsion Systems
Mark J. Rigali, Manish Sutaria, Anthony C. Mulligan, and Ranji Vaidyanathan

Electro Spark Alloy Processing for Aerospace Components
Michael Riley

Detection, Identification, and Quantification of Surface Contamination
M. Martin Szczesniak, Michael Beecroft, and Phillip Mattison

Quadruple Lap Shear Processing Evaluation
Tony N. Thornton

5th Conference on

Aerospace Materials, Processes, and Environmental Technology (AMPET)

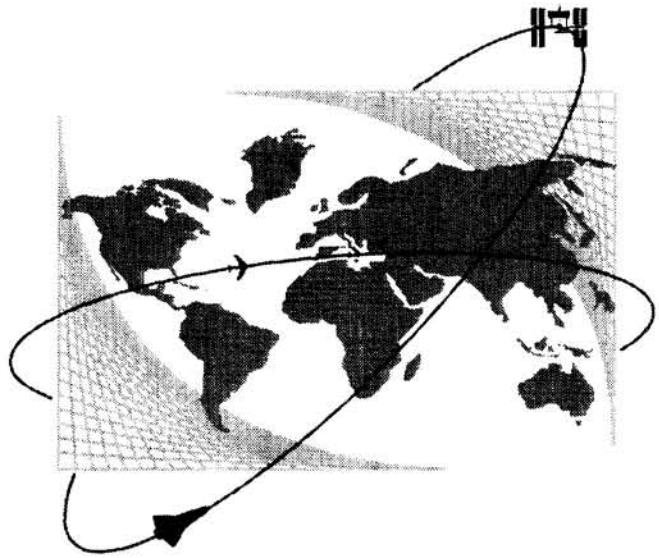

Week of September 16, 2002 (tentative)
Von Braun Center
Huntsville, Alabama

Objective: The purpose of this conference is to provide a forum for materials and processes engineers, manufacturing engineers, environmental engineers, scientists, and managers to describe, review, and critically assess the evolving advances in materials, manufacturing, replacement, and clean propulsion technologies from the standpoint of their significance, application, impact on aerospace systems, and utilization by the research and development community.

For additional information, contact Dawn Cross Stanley, Administrative Chair
Telephone: 256-544-1835
E-mail: dawn.cross@msfc.nasa.gov
Conference URL: http://ampet.msfc.nasa.gov/

Thomas, Dale	NASA/MARSHALL SPACE FLIGHT CENTER	VS10	MSFC, AL 35812			
Thompson, Wayne	UNIVERSITY OF ALABAMA IN HUNTSVILLE					
Thornton, Tony	THIOKOL PROPULSION	5983 Co. Rd. 92	Rogersville, AL 35652	(256) 544-6428	(256) 544-0732	tony.thornton@thiokol.com
Tinker, Michael	NASA/MARSHALL SPACE FLIGHT CENTER	ED21	MSFC, AL 35812			
Tira, James	HONEYWELL	2000 E. 95th St.	Kansas City, Mo 64141			
Tolliver, Nancy	THE BOEING COMPANY	799 James Record Road	Madison, AL 35758	(256) 961-0169		nancy.toilliver@hsc.boeing.com
Torres, Pablo	NASA/MARSHALL SPACE FLIGHT CENTER	ED33	MSFC, AL 35812			
Tygielski, Phillip	NASA/MARSHALL SPACE FLIGHT CENTER	ED62	MSFC, AL 35812			
Utreja, Laj	NAS, INC.	1500 Perimeter Pkwy	Huntsville, Al 35806	256 721 6695		lutreja@tecmasters.com
Vaidyanathan, Ranji	ADVANCED CERAMICS	3292 E. Hemisphere Loop	Tucson, AZ 85706	(520) 573-6300	(520) 573-2057	
Valentine, Pete	NASA/MARSHALL SPACE FLIGHT CENTER	ED34	MSFC, AL 35812			
Vandiver, Terry	US AVIATION & MISSILE COMMAND	3114 Shoreway Circle	Hampton Cove, AL 35763	256 876 1683	256 842 9800	
Vaughn, Tim	NASA/MARSHALL SPACE FLIGHT CENTER	ED35	MSFC, AL 35812			
Vickers, John	NASA/MARSHALL SPACE FLIGHT CENTER	ED34	MSFC, AL 35812			
Wagner, Carole	NASA/MARSHALL SPACE FLIGHT CENTER	ED35	MSFC, AL 35812			
Walker, James	NASA/MARSHALL SPACE FLIGHT CENTER	ED32	MSFC, AL 35812			
Walters, Patricia	WESTAR CORPORATION	28304 Capshaw Road	Harvest, AL 35749	(256) 313-4685	(256) 313-0274	pat.walters@redstone.army.mil
Waltz, Zachary	PRATT & WHITNEY LIQUID SPACE OPS	102 Wandering Trail	Jupiter, FL 33458	(561) 796-7678	(561) 796-6477	waltzz@pwfl.com
Ward, Carla	ITB, INC.	MS ITB HQ Rm 3481	Kennedy Space Center, Fl 32899	(321) 867-8477	(321) 867-8479	wardcn@kscgws00.ksc.nasa.gov
Washington, Janet	NASA/MARSHALL SPACE FLIGHT CENTER	ED37	MSFC, AL 35812			
Watring, Dale	NASA/MARSHALL SPACE FLIGHT CENTER	SD01	MSFC, AL 35812			
Watson, Gay	NASA/MARSHALL SPACE FLIGHT CENTER	2026 Princeton Blvd	Huntsville, AL 35801	(256) 544-0710		gay.watson@msfc.nasa.gov
Watson, Sherry	AMCOM	140 Fred Atkinson	Huntsville, AL 35806			sherry.watson@redstone.army.mil
Watts, Ed	NAS, INC.	1500 Perimeter Pkwy	Huntsville, Al 35806			ed.watts@msfc.nasa.gov
Wegrich, Richard	NASA/MARSHALL SPACE FLIGHT CENTER	ED35	MSFC, AL 35812			
Wenzel, Thomas	NAVAL SURFACE WARFARE CENTER	9500 MacArthur Blvd	West Bethesda, MD 20817	(703) 443-0802	(301) 227-4963	wenzelte@nswccd.navy.mil
Wertz, George	NASA/MARSHALL SPACE FLIGHT CENTER	ED31	MSFC, AL 35812			
Whelan Robinson, Lisa	GUIGNE INTERNATIONAL LIMITED	685 St. Thomas Line	Paradise, NF A1L1C1	(709) 895-3819	(709) 895-3999	dryan@guigne.com
Whitaker, Ann	NASA/MARSHALL SPACE FLIGHT CENTER	SD01	MSFC, AL 35812			
White, Jeffery	SVERDRUP TECHNOLOGY	620 Discovery Drive	Huntsville, AL 35806	(256) 971-9490	(256) 971-9475	jeff.white@hsv.sverdrup.com
White, Tyrus	NASA/MARSHALL SPACE FLIGHT CENTER	ED25	MSFC, AL 35812			
Whitfield, Steven	NASA/MARSHALL SPACE FLIGHT CENTER	ED36	MSFC, AL 35812			
Whitworth, Charles	THIOKOL PROPULSION	P.O. Box 707 MS LCO	Brigham city, UT 84302			
Wildes, Stephen	OMNI TECH INT'L LTD.	2715 Ashman Street	Midland, MI 48640	(517) 631-3377 x 235	(517) 631-0812	swildes@omnitechintl.com
Wilkerson, Chuck	NASA/MARSHALL SPACE FLIGHT CENTER	ED32	MSFC, AL 35812			
Wilkie, David	NAS, INC.	1500 Perimeter Pkwy	Huntsville, Al 35806	256		david.wilkie@msfc.nasa.gov
Wilson, Scott	QUALIS CORPORATION	604 Mt. Gap Dr.	Huntsville, AL 35803	(256) 658-9032		c /sw/@msn.com
Wise, Harry	NAS, INC.	213 Deanna Drive	Owens Cross Roads, AL 35763	(256) 544-3006	(256) 544-5478	harry.wise@msfc.nasa.gov
Wrenn, George	OAK RIDGE NATIONAL LAB	P.O. Box 2009, Bldg 9204-1	Oak Ridge, TN 37831	(865) 241-2521	(865) 574-8257	wreengejr@ornl.gov
Wright, Jerry	NASA/MARSHALL SPACE FLIGHT CENTER	ED37	MSFC, AL 35812			
Xenofos, George	NASA/MARSHALL SPACE FLIGHT CENTER	TD62	MSFC, AL 35812			
Yost, Vaughn	NASA/MARSHALL SPACE FLIGHT CENTER	Attn: MP 21	MSFC, AL 35812			
Zimmerman, Frank	NASA/MARSHALL SPACE FLIGHT CENTER	ED33	MSFC, AL 35812			

Russell, Carolyn	NASA/MARSHALL SPACE FLIGHT CENTER	ED33	MSFC, AL 35812			
Russell, Judy	LOCKHEED MARTIN SPACE SYSTEMS CO.	5512 Perrier St	New Orleans, LA 70115	(504) 257-4913	(504) 257-4440	judy.russel@maf.nasa.gov
Russell, Sam	NASA/MARSHALL SPACE FLIGHT CENTER	ED32	MSFC, AL 35812			
Sacks, Randy	NASA/MARSHALL SPACE FLIGHT CENTER	Attn: MP 71	MSFC, AL 35812			
Sadlowski, Dave	ICRC	8101 Resurrection Drive	Anchorage, Alaska 99504	907 560 5650	907 560 5651	dsadlowski@gci.net
Salvador, Costante	PRATT & WHITNEY	9743	, Fl 33410	561 796 3237	561 796 5866	salvador@pwfl.com
Sams, Madelyn	NASA/MARSHALL SPACE FLIGHT CENTER	ED36	MSFC, AL 35812			
Sartwell, Bruce	NAVAL RESEARCH LAB	4555 Overlook Avenue/Code 6170	Washington, DC 20375	(202) 767-0722	(202) 767-3321	sartwell@nrl.navy.mil
Sawyer, James	NASA/LANGLEY RESEARCH CENTER	430 Rockweel Road	Hampton, VA 23669	(757) 864-5432	(757) 864-7943	j.w.sawyer@larc.nasa.gov
Schantz, John	PUGET SOUND CLEAN AIR AGENCY	110 Union Street, Ste 500	Seattle, WA 98101	(206) 689-4027	(206) 343-7522	johnS@pscleanair.org
Schneider, Todd	NASA/MARSHALL SPACE FLIGHT CENTER	ED31	MSFC, AL 35812			
Schuster, John	3M COMPANY	3M Center, Bldg 223-6S-04	St. Paul, MN 55144-1000	(651) 736-6055	(651) 736-7542	jmschuster1@mmm.com
Schwinghammer, Bob	NAS, INC.	7314 Martha Drive	Huntsville, AL 35802	(256) 881-8705		
Scott, Joseph	AZ TECHNOLOGY, INC.	7047 Old Madison Pike, Ste 300	Huntsville, AL 35806	(256) 837-9877	(256) 837-1155	
Scroggins, Sharon	NASA/MARSHALL SPACE FLIGHT CENTER	AD10	MSFC, AL 35812			sharon.scroggins@msfc.nasa.gov
Semmel, Charles	NAS, INC.	1500 Perimeter Pkwy	Huntsville, Al 35806			charles.semmel@msfc.nasa.gov
Sempeles, John	LOCKHEED MARTIN AERONAUTICS	P.O. Box 748 Lockheed Blvd	Ft Worth, TX 76101	(817) 777-4018	(817) 763-4300	john.n.sempeles@lmco.com
Serrano, Odean	NASA/HQ					
Shah, Sandeep	NASA/MARSHALL SPACE FLIGHT CENTER	ED33	MSFC, AL 35812			
Sharpe, John	LOCKHEED MARTIN SPACE SYSTEMS CO.	P.O. Box 9008	MSFC, AL 35812	(256) 544-0441	(256) 544-5869	
Shea, Charlotte	NAS, INC.	Bldg 4612 Rm 1410	Huntsville, AL 35812	(256) 544-3029		charlotte.shea@msfc.nasa.gov
Shea, Danny	CITY OF HUNTSVILLE					
Shuart, Mark	NASA/LANGLEY RESEARCH CENTER	1 East Reid Street	Hampton, VA 23681	757 864 3492	7575 864 7792	m.j.shuart@larc.nasa.gov
Shular, David	NASA/MARSHALL SPACE FLIGHT CENTER	ED34	MSFC, AL 35812			
Singer, Jody	NASA/MARSHALL SPACE FLIGHT CENTER	Attn: MP 01	MSFC, AL 35812			
Singer, Randy	WESTINGHOUSE SRS	P.O. Box 616	, SC 29802	(805) 725-2407	(805) 725-1744	randy.singer@srs.gov
Sirchio, Scott	NAVAL SURFACE WARFARE CENTER	8375 Tamar Drive Apt #645	Columbia, MD 21045	(301) 227-5196	(301) 227-5359	sirchiosa@nswccd.navy.mil
Skarsgard, Erik	HONEYWELL	5444 Avenida del Sol	Las Cruces, NM 88011	505 524 5199	505 524 5083	eskarsga@wstf.nasa.gov
Smith, Andrew	NASA/MARSHALL SPACE FLIGHT CENTER	ED20	MSFC, AL 35812	(256) 544-4932		drew.smith@msfc.nasa.gov
Smith, Doris	LOCKHEED MARTIN SPACE SYSTEMS CO.	P.O. BOX 29304	New Orleans, LA 70189	(504) 257-0228	(504) 257-4438	doris.smith@maf.nasa.gov
Smith, Gregory	AJT & ASSOC., INC.	1211 Kathy Lane	Decatur, AL 35601	(256) 544-5729	(256) 544-5746	greg.smith@msfc.nasa.gov
Smith, Ryan	THE BOEING COMPANY	8550 Astronaut Blvd MS ZL96	Cape Canaveral, FL 32920	(321) 799-6923	(321) 799-6063	
Smithers, Gweneth	NASA/MARSHALL SPACE FLIGHT CENTER	ED34	MSFC, AL 35812			
Snyder, Jack	LOCKHEED MARTIN SPACE SYSTEMS CO.	P.O. Box 179 MS S9080	Denver, CO 80127	(303) 977-3322	(303) 977-3844	jack.snyder@lmco.com
Sparks, Scott	NASA/MARSHALL SPACE FLIGHT CENTER	ED34	MSFC, AL 35812			
Stack, Eric	LOCKHEED MARTIN SPACE SYSTEMS CO.	P.O. Box 29304	New Orleans, LA 70189	(504) 257-1428	(504) 257-4450	eric.stack@maf.nasa.gov
Staffer, Doug	WANG GOVERNMENT SERVICES					
Stanton, William	NASA/MARSHALL SPACE FLIGHT CENTER	ED33	MSFC, AL 35812			
Steel, Alexander	AMCOM	2528 Camp Creek	Huntsville, AL 35803			
Steeve, Brian	NASA/MARSHALL SPACE FLIGHT CENTER	ED22	MSFC, AL 35812			
Stevens, William	3M COMPANY	3M Center, Bldg 223-6S-04	St. Paul, MN 55144-1000	(936) 449-6359	(936) 449-6359	wmstevens@mmm.com
Stewart, Cynthia	NASA/MARSHALL SPACE FLIGHT CENTER	ED22	MSFC, AL 35812			
Stiene, Lucinda	AMCOM	Attn: AMSAM-RD-SE-PE	Redstone Arsenal, AL 35898	(256) 842-9259	(256) 313-6596	cindy.stiene@rdec.redstone.army.mil
Strong, Dexter	NASA/MARSHALL SPACE FLIGHT CENTER	ED32	MSFC, AL 35812			
Stroud, Richard	NASA/MARSHALL SPACE FLIGHT CENTER	TD62	MSFC, AL 35812			
Suits, Michael	NASA/MARSHALL SPACE FLIGHT CENTER	ED32	MSFC, AL 35812			
Sumner, Craig	UNITED SPACE ALLIANCE, INC.	555 Discovery Drive	Huntsville, AL 35806	(256) 971-3122	(256) 971-3212	
Swindell, James	CALHOUN COMMUNITY COLLEGE	P. O. Box 2216	Decatur, AL 35609			
Tackett, Wayne	THIOKOL PROPULSION	600 Boulevard South, Ste 112	Huntsville, AL 35802	(256) 880-0177	(256) 880-6988	tackeew@thiokol.com
Terek, Joanne	NASA/MARSHALL SPACE FLIGHT CENTER	ED36	MSFC, AL 35812			

Monette, Denis	ADM/OGILVIE	995 mill Street	Montreal,, H3C 1Y5 Canada	(514) 935-8717	(514) 935-8687	
Moore, Regina	NASA/MARSHALL SPACE FLIGHT CENTER	ED34	MSFC, AL 35812			
Moore, Robin	AZ TECHNOLOGY, INC.	7047 Old Madison Pike, Ste 300	Huntsville, AL 35806	(256) 837-1155	(256) 837-1155	
Munafo, Paul	NASA/MARSHALL SPACE FLIGHT CENTER	ED30	MSFC, AL 35812			
Murphy, Alan	NASA/MARSHALL SPACE FLIGHT CENTER	Attn: MP 71	MSFC, AL 35812			
Murray, Scott	NASA/KENNEDY SPACE CENTER	Mail Code YA-F1-M1	Kennedy Space Center, FL 32899	(321) 867-3400	(321) 867-7959	scott.murray-2@ksc.nasa.gov
Myers, Neil	NASA/MARSHALL SPACE FLIGHT CENTER	TD62	MSFC, AL 35812			
Neergaard, Lynn	IIT RESEARCH INSTITUTE	10001 Bayreuth Drive	Huntsville, AL 35803	(544)-5181	(256) 382-470	lynn.neergaard@msfc.nasa.gov
Newman, John	LASER TECHNOLOGY, INC.	1055 W. Germantown	Norristown, PA 19403	(610) 631-5043	(610) 631-0934	iti@laserNDT.com
Newton, Robert	NASA/MARSHALL SPACE FLIGHT CENTER	ED36	MSFC, AL 35812			
Nicolia, Vincent	EASTMAN KODAK COMPANY	800 Lee Road	Rochester, NY 14650-3116	(716) 588-7522	(716) 588-4939	vincent.nicolia@kodak.com
Niedermeyer, Melinda	NASA/MARSHALL SPACE FLIGHT CENTER	ED34	MSFC, AL 35812			
Norris, Jeff	LOCKHEED MARTIN	P.O. Box 9008	MSFC, AL 35812	(256) 544-1716	(256) 544-1660	jeffrey.norris@msfc.nasa.gov
Novak, Howard	UNITED SPACE ALLIANCE, INC.	M/S USK-864, 8550 Astronaut Blvd.	Cape Canaveral, FL 32920-4304	(407) 867-7052		novakh@usasrb.ksc.nasa.gov
Nunes, Jr., Arthur	NASA/MARSHALL SPACE FLIGHT CENTER	ED33	MSFC, AL 35812			
Obenhuber, Donald	MICRO CRAFT, INC.	ED36	MSFC, AL 35812	(256) 544-3761		donald.obenhuber@msfc.nasa.gov
Ortega, Rene	NASA/MARSHALL SPACE FLIGHT CENTER	ED22	MSFC, AL 35812			
Owen, Jim	NASA/MARSHALL SPACE FLIGHT CENTER	ED20	MSFC, AL 35812			
Panda, Binayak	IIT RESEARCH INSTITUTE	Bldg 4682	MSFC, AL 35812	(256) 544-6349	(256) 544-7473	binayak.panda@msfc.nasa.gov
Parham, James	MESA ASSOCIATES	9238 Madison Blvd, Bldg 2	Madison, A 35758	(256) 876-1074	(256) 842-1359	
Patton, R.D.	Mississippi State University	P. O. Box ME	Mississippi State, MS 39762			patton@me.msstate.edu
Paxton, James	PHYSITRON, INC.	3384 A Westmill Drive	Huntsville, AL 35805	(256) 534-4844	(256) 534-4896	paxton@physitron.com
Pearson, Steve	NASA/MARSHALL SPACE FLIGHT CENTER	ED03	MSFC, AL 35812			
Pedley, Michael	NASA/JOHNSON SPACE CENTER	NASA JSC/EM2	Houston, TX 77058	(281) 483-8913	(603) 971-8687	michael.d.pedley1@jsc.nasa.gov
Pelham, Larry	NASA/MARSHALL SPACE FLIGHT CENTER	ED34	MSFC, AL 35812			
Perkins, James	NASA/MARSHALL SPACE FLIGHT CENTER	ED36	MSFC, AL 35812			
Perkins, Leigh Ann	NASA/MARSHALL SPACE FLIGHT CENTER	ED22	MSFC, AL 35812			
Peters, Barrie	IIT RESEARCH INSTITUTE	215 Wynn Drive, Ste. 101	Huntsville, AL 35805	256 382 4790	256 382 4701	bpeters@iitri.org.
Piche, Joseph	EIKOS, INC.	2 Master Drive	Franklin, MA 02038	(508) 528-0300		jpiche@eikos.com
Pieterse, Herman	PIETERSE CONSULTING, INC.	6321 N. Calle Campeche	Tucson, AZ 85750	(520) 529-5547	(520) 529-5562	hpieterse@aol.com
Plaskon, Daniel	JPL/ACRO SERVICE CORP	P.O. Box 70345	Pasadena, CA 91117	(626) 795-4928	(626) 577-9504	daniel.plaskon@jpl.nasa.gov
Platt, Heidi	SHOT, INC.	7200 Hwy 150	Greenville, IN 47124	(812) 923-9591 x 202	(812) 923-9598	hplatt@shot.com
Pratz, Earl	LOCKHEED MARTIN SPACE SYSTEMS CO.	P.O. Box 29304	New Orleans, LA 70006	(504) 257-1261	(504) 257-4438	earl.h.pratz@maf.nasa.gov
Predmore, Roamer	NASA/GODDARD SPACE FLIGHT CENTER	Code 541	Goddard Space Flight Center, MD 20771	(301) 292-9319	(301) 286-5953	roamer.e.predmore@gsfc.nasa.gov
Price, Marlene	THE BOEING COMPANY	6633 Canoga Avenue	Canoga Park, CA 91309	818) 586-5122	(818) 586-9898	marlene.price@West.boeing.com
Prince, Mike	NASA/MARSHALL SPACE FLIGHT CENTER	ED34	MSFC, AL 35812			
Puskar, Michael	HAMILTON SUNDSTRAND	One Hamilton Road	windsor Locks, CT 06096			
Rathgeber, Kurt	HONEYWELL	2867 Morning Star Drive	Las Cruces, NM 88011	505 524 5603	505 524 5597	krathgeb@wstf.nasa.gov
Reddy, R.	THE UNIVERSITY OF ALABAMA	MTE, P.O. Box 870202	Tuscaloose, AL 35487	(205) 348-4246	(205) 348-2164	rreddy@coe.eng.us.edu
Reeves, Kevin	THE BOEING COMPANY	137 Foxridge Drive	Harvest, AL 35749	(256) 461-3547	(256) 461-3232	kevin.w.reeves@boeing.com
Reynolds, Michael	NASA/MARSHALL SPACE FLIGHT CENTER	AD10	MSFC, AL 35812			
Rice, Terrie	NASA/MARSHALL SPACE FLIGHT CENTER	ED35	MSFC, AL 35812			
Richardson, Erin	NASA/MARSHALL SPACE FLIGHT CENTER	ED36	MSFC, AL 35812			
Richardson, Stephen	NASA/MARSHALL SPACE FLIGHT CENTER	ED23	MSFC, AL 35812			
Rietz, Wolfgang	EASTMAN KODAK COMPANY	6335 North Avon Road	Honoye Falls, NY 14472	(716) 722-3868	(716) 588-4939	wolfgang.rietz@kodak.com
Riley, Michael	SURFACE TREATMENT TECHNOLOGIES, INC.	P.O. Box 907	Tullahoma, TN 37388	(931) 461-5900	(931) 461-2819	mriley@stt-inc.com
Robbins, John	MADYNE CORPORATION	600 Boulevard South, Ste 301	Huntsville, AL 35802	(256) 650-1466	(256) 880-5086	robbinsj@amdyne.com
Robinson, Paul	MADYNE CORPORATION	600 Boulevard South, Ste 301	Huntsville, AL 35802	(256) 313-1714	(256) 880-5086	james.robinson@redstone.army.mil
Rodriguez, Pete	NASA/MARSHALL SPACE FLIGHT CENTER	ED20	MSFC, AL 35812			
Rose, David	IIT RESEARCH INSTITUTE	201 Mill Street	Rome, NY 13440	315 339 7023	315 339 7107	drose@iitri.org.
Ross, Rick	STENNIS SPACE CENTER	Bldg 8110	Stennis Space Center, MS 39529	(228) 688-3260	(228) 688-3079	pshiffle@gbtech.net
Rowan, Greg	NAS, INC.	1500 Perimeter Parkway, Ste	Huntsville, AL 35806			

Kooney, Alexander	LOCKHEED MARTIN SPACE SYSTEMS CO.	218 Lake Tahoe	Slidell, LA 70461	504 257 0949	504 257 4461	alex.kooney@maf.nasa.gov
Kovach, Michael	THIOKOL PROPULSION	P.O. Box 9033, MS #61A	Huntsville, AL 35812	(256) 544-1478	(256) 544-0732	kovacmp@thiokol.com
Kowbel, Witold	MER CORPORATION	7960 S. Kolb Road	Tucson, AZ 85706			
Krienke, William	NASA/MARSHALL SPACE FLIGHT CENTER	TD62	MSFC, AL 35812			
Kumakawa, Akinaga	NATIONAL AEROSPACE LAB	Kimigaya	Kakuda, Miyagi 981-1525 Japan	011 81 224-68-3627	011 81 224-68-3939	kuma@kakuda-splab.go.jp
Lackey, Jeffrey	NASA/MARSHALL SPACE FLIGHT CENTER	TD62	MSFC, AL 35812			
Lambdin, Rob	NASA/MARSHALL SPACE FLIGHT CENTER	ED35	MSFC, AL 35812			
Landers, Tamara	NASA/MARSHALL SPACE FLIGHT CENTER	ED35	MSFC, AL 35812			
Lansing, Matt	NASA/MARSHALL SPACE FLIGHT CENTER	ED34	MSFC, AL 35812			
Lash, Rhonda	NASA/MARSHALL SPACE FLIGHT CENTER	ED31	MSFC, AL 35812			
Lawrence, Herbert	NASA/GLENN RESEARCH CENTER	6349 Ridge Plaza Drive	North Ridgeville, OH 44039	(216) 433-3364	(216) 433-3362	herbert.a.lawrence@grc.nasa.gov
Lawrence, Timothy	NASA/MARSHALL SPACE FLIGHT CENTER	ED34	MSFC, AL 35812			
LeBoeuf, Ralph	LOCKHEED MARTIN SPACE SYSTEMS CO.	P.O. Box 29304	New Orleans, LA 70189	(504) 257-1785	(504) 257-4438	leboerj@maf.nasa.gov
Ledbetter, Debbie	NASA/MARSHALL SPACE FLIGHT CENTER	ED38	MSFC, AL 35812	(256) 544-1088		deborah.ledbetter@msfc.nasa.gov
Ledbetter, Frank	NASA/MARSHALL SPACE FLIGHT CENTER	ED34	MSFC, AL 35812			
Lee, Jim	GEORGIA TECH	4059 Yellow Ginger Glen	Norcross, Ga 30092	404 894 7399		kj.lee@mse.gatech.edu
Lee, Jonathan	NASA/MARSHALL SPACE FLIGHT CENTER	ED33	MSFC, AL 35812			
Legner, H.H.	PHYSICAL SCIENCES, INC.	20 New England Business Center	Andover, MA 01810			
Lester, Carl	NASA/MARSHALL SPACE FLIGHT CENTER	ED34	MSFC, AL 35812			
Lester, William	NASA/HQ		Washington, DC			
Lethe, Eric	INLAND TECHNOLOGY INC.	401 East 27th Street	Tacoma, WA 98421	(253) 383-1177	(253) 593-8749	elethe@inlandtech.com
Liwag, Jose	QUALIS CORP.	102 Fairington Rd.	Huntsville, Al 35806	256-971-9574	256-971-9475	jose.liwag@hsv.sverdrup.com
Lucas, Joseph	INLAND TECHNOLOGY, INC.	401 East 27th stree	Tacoma, WA 98421	(253) 383-1177	(253) 593-8749	inland@inlandtech.com
Luey, Kenneth	THE AEROSPACE CORPORATION	4621 Maytime Lane	Culver City, CA 90230	(310) 336-5499	(4130 647-0479	kenluey@yahoo.com
Maes, Miguel	NASA/WSTF	PO Box 20	Las Cruces, NM 88004	505 524 5677	505 524 5260	mmaes@wstf.nasa.gov
Majchrowski, Thomas	UNIV OF CAL / S A I C	5335 Price Avenue	McClellan AFB, CA 95652	(916) 614-6209	(916) 6250	majchrowskit@saic.com
Malone, Tina	NASA/MARSHALL SPACE FLIGHT CENTER	ED33	MSFC, AL 35812			
Martin, Jolene	NASA/MARSHALL SPACE FLIGHT CENTER	Attn: MP 71	MSFC, AL 35812			
McCaleb, Rebecca	NASA/MARSHALL SPACE FLIGHT CENTER	AD10	MSFC, AL 35812			
McCarty, Dennis	PRATT & WHITNEY	4449 Fuchsia Circle North	Palm Beach Gardens, Fl 33410	561 796 4282	561 625 5652	mcrtydb@pwfl.com
McCool, Alex	NASA/MARSHALL SPACE FLIGHT CENTER	Attn: MP 01	MSFC, AL 35812			
McGaha, David	NASA/MARSHALL SPACE FLIGHT CENTER	ED37	MSFC, AL 35812			
McGill, Preston	NASA/MARSHALL SPACE FLIGHT CENTER	ED33	MSFC, AL 35812			
McHaffey, Jeanette	WR-ALC/TIEDM	420 2nd Street, Ste 100	Robins AFB, GA 31098-1640	(912) 926-4489	(912) 926-1743	jeanette.mchaffey@robins.af.mil
McKechnie, Timothy	PLASMA PROCESSES, INC.	4914 D. Moores Mill Road	Huntsville, AL 35811			
McMahon, Bill	NASA/MARSHALL SPACE FLIGHT CENTER	ED34	MSFC, AL 35812			
Medley, Jay	NASA/MARSHALL SPACE FLIGHT CENTER	ED38	MSFC, AL 35812			
Mellen, Dan	NASA/MARSHALL SPACE FLIGHT CENTER	ED22	MSFC, AL 35812			
Melton, Donald	LOCKHEED MARTIN MICHOUD OPERATIONS	2224 Cambridge	LaPlace, LA 40068	(504) 257-1782	(504) 257-4438	
Meltzer, Michael	LAWRENCE LIVERMORE NATIONAL LABORATORY					
Metroke, Tammy	OKLAHOMA STATE UNIVERSITY	Valerie Pogue/003 Life Science East Environmental Inst.	Stillwater , OK 74078			
Meyers, charles	NASA/MARSHALL SPACE FLIGHT CENTER	Ed22	MSFC, AL 35812			
Millimono, Fara	KIDS FACE	164 Fourah Bay Road	Freetown, Sierra Leone 00232			kidsfacesl@yahoo.com
Minor, Jody	NASA/MARSHALL SPACE FLIGHT CENTER	ED03, Bld 4487	MSFC, AL 35812	(256) 544-4041	(256) 544-8807	jody.minor@msfc.nasa.gov
Mistretta, John	WRIGHT PATTERSON AIR FORCE BASE					
Mitchell, Michael	NASA/MARSHALL SPACE FLIGHT CENTER	11117 HWY 231-431 N	Meridianville, AL 35759	(256) 544-2491		michael.mitchell@msfc.nasa.gov
Mize, Rondal	NASA/MARSHALL SPACE FLIGHT CENTER	QS01	MSFC, AL 35812	(256) 544-2485	(256) 544-2053	ron.c.mize@msfc.nasa.gov
Mohling, Robert	JOHNS HOPKINS UNIVERSITY	10630 Little Patuxent Parkway, Ste 202	Columbia, MD 21044-3204	(410) 992-7300	(410) 730-4969	bmohling@jhtechapps.com
Mojazza, Bob	TRITON SYSTEMS, INC.	200 Turnpike Road	Chelmsford, MA 01824			

Henderson, Arthur	NASA/MARSHALL SPACE FLIGHT CENTER	ED36	MSFC, AL 35812			
Henderson, Charles	NASA/MARSHALL SPACE FLIGHT CENTER	ED34	MSFC, AL 35812			
Henneberry, Mark	HENNEBERRY MARKETING	599 W. Jefferson	El Paso, IL 61738	(309) 527-2231	(309) 527-2230	henebery@elpaso.net
Hess, Rick	PUGET SOUND CLEAN AIR AGENCY	110 Union Street, Ste 500	Seattle, WA 98101	(206) 689-4027	(206) 343-7522	rickH@pscleanair.org
Hesselroth, David	3M COMPANY	Bld. 236-2B-01, 3M Center	St. Paul, MN 55144	651 736 6191	651 733 4335	dahesselroth@mmm.com
Hessler, Susan	IIT RESEARCH INSTITUTE	Bldg 4628	MSFC, AL 35812	(256) 544-8153		susan.hessler@msfc.nasa.gov
Hester, Jim	NASA/MARSHALL SPACE FLIGHT CENTER	ED37	MSFC, AL 35812			
Hill, Dewayne	NAS, INC.	1500 Perimeter Pkwy	Huntsville, Al 35806	256		dewayne.hill@msfc.nasa.gov
Hill, Robert	NASA/KENNEDY SPACE CENTER	Mail Code YA-E	Kennedy Space Center, FL 32899	321 867 8795	321 867 8479	robert.hill-3@kmail.ksc.nasa.gov
Hissam, Andy	NASA/MARSHALL SPACE FLIGHT CENTER	TD62	MSFC, AL 35812	(256) 544-8388		andy.hissam@msfc.nasa.gov
Hoffman, Thad	CONTROL VISION, INC.	P.O. Box 51505	Idaho Falls, ID 83405	(208) 523-5506	(208) 523-5520	vision@controlvisioninc.com
Hollingsworth, Joe	INTERNATIONAL TRADE BRIDGE, INC.	1701 Pell Street	Scottsboro, AL 35769	(256) 544-0591	(256) 544-9156	joe.hollingsworth@msfc.nasa.gov
Holmes, Steven	NASA/MARSHALL SPACE FLIGHT CENTER	Attn: MP 31	MSFC, AL 35812			
Holt, Carolyn	NAS, INC.	1500 Perimeter Parkway, Ste 215	Huntsville, AL 35806			
Hooper, Carlla	NASA/MARSHALL SPACE FLIGHT CENTER	ED30	MSFC, AL 35812			
Hopper, Stephanie	THE BOEING COMPANY	8550 Astronaut Blvd MS ZL96	Cape Canaveral, FL 32920	(321) 799-7206	(321) 799-6063	
Horiuchi, Gail	NASA/JOHNSON SPACE CENTER		Johnson Space Center, TX			
Hornung, Steve	HONEYWELL	PO Box 20	Las Cruces, NM 88004	505 524 5647	505 524 5597	shornung@wstf.nasa.gov
Housner, Jerrold	NASA/LANGLEY RESEARCH CENTER	MS 121	Hampton, VA 23621	(757) 864-3492	(757) 864-8543	j.m.housner@larc.nasa.gov
Howick, Bryan	THIOKOL PROPULSION	P.O. Box 707	Brigham City, UT 84302-0707	(435) 863-6481	(435) 863-4037	bryan.howick@thiokol.com
Hudson, Steve	NASA/MARSHALL SPACE FLIGHT CENTER	ED33	MSFC, AL 35812			
Huff, Timothy	NASA/MARSHALL SPACE FLIGHT CENTER	ED36	MSFC, AL 35812			
Hughes, John	STENNIS SPACE CENTER	Bldg 8110	Stennis Space Center, MS 39529	(228) 688-3260	(228) 688-3079	pshiffle@gbtech.net
Hulcher, Bruce	NASA/MARSHALL SPACE FLIGHT CENTER	ED34	MSFC, AL 35812			
Hundley, Nedra	NASA/MARSHALL SPACE FLIGHT CENTER	ED33	MSFC, AL 35812			
Iannucci, Vincenzo	Alenia Spazio S.P.A.	Via Saccomuro 23	Rome, Italy 00171	(011) 39-0604151-2260	(011) 39-06-4151-2433	v.iannucci@roma.alespazio.it
Jackson, James	NASA/GLENN RESEARCH CENTER	21000 Brookpark Road	Cleveland, OH 44135	(216) 433-6505	(216) 433-5270	james.b.jackson@grc.nasa.gov
Jacobs, Bob	NAS, INC.	1500 Perimeter Pkwy	Huntsville, Al 35806	256		bob.jacobs@msfc.nasa.gov
Jech, Ronald	US TECHNOLOGY COMPANY	220 Seventh St.	Canton, OH 44702	330 455 1181	330 455 1191	rjech@ustechnology.com
Jefferson, Pamela	NASA/MARSHALL SPACE FLIGHT CENTER	ED27	MSFC, AL 35812			
Jennings, Tommy	HYDRO-AIRE	3000 Winona Avenue	Burbanks, CA 91510			
Johnson, Sylvia	NASA	MS 231-1	Moffett Field, CA 94035	650 604-2636		
Johnson, Tim	ANTEON CORPORATION	5100 Springfield Pike Ste 509	Dayton, OH 35431-1264	(937) 252-3132	(937)252-0418	tjohnson@anteon.com
Jones, Clyde (Chip)	NASA/MARSHALL SPACE FLIGHT CENTER		MSFC, AL 35812			
Jones, Kenneth	UNITED SPACE ALLIANCE, INC.	555 Discovery Drive	Huntsville, AL 35806	(256) 971-3108	(256) 971-3212	
Jordan, Rebecca	LOCKHEED MARTIN SPACE SYSTEMS CO.	P.O. Box 29304	New Orleans, LA 70189	(504) 257-3436	(504) 257-4450	rebecca.jordan@maf.nasa.gov
Joseph, Brian	TOUCHSTONE RESEARCH LAB, LTD.	The Millenium Centre, R.D. 1, Box 100B	Triadelphia, WV 26059	304 547 5800	304 547 5764	bej@tril.com
Kanegsberg, Barbara	BFK SOLUTIONS	16924 Livorno Drive	Pacific Palisades, CA 90272			
Kanegsberg, Edward	BFK SOLUTIONS	16924 Livorno Drive	Pacific Palisades, CA 90272			
Kao, Wei	AEROSPACE CORPORATION	MS-242, P.O. Box 92957	Los Angeles, CA 90007			wei.h.kaor@aero.org
Kauffman, Billy	NASA/MARSHALL SPACE FLIGHT CENTER	ED03	MSFC, AL 35812			
Keele, Richard	THE BOEING COMPANY	325 N. Sweet Avenue	Fullerton, CA 92833	(714) 896-2101	(714) 896-1145	richard.p.keele@boeing.com
Keen, Jill	THIOKOL PROPULSION	P.O. Box 9033	Huntsville, AL 35812	(256) 544-2748	(256) 544-0732	keenjm@thiokol.com
Keller, Teddy	NAVAL RESEARCH LABORATORY	4555 Overlook AVenue	Washington, DC 20375-5320	(202) 767-3095	(202) 767-0594	keller1@ccf.nrl.navy.mil
Kennedy, Jim	NASA/MARSHALL SPACE FLIGHT CENTER	ED01	MSFC, AL 35812			
Key, Carlo "Frank"	NAS, INC.	101 Lynn Drive	Madison, AL 35758		(256) 544-5786	carlo.frank.key@msfc.nasa.gov
Killpak, Michael	THIOKOL PROPULSION	P.O. Box 707	Brigham City, UT 84032	(435) 863-3749	(435) 863-2271	killpmo@thiokol.com
Kilpatrick, Bill	NASA/MARSHALL SPACE FLIGHT CENTER	ED01	MSFC, AL 35812			
Kinchen, David	LOCKHEED MARTIN SPACE SYSTEMS CO.	13800 Old Gentilly Road	New Orleans, LA 70129	(504) 257-1454	(504) 257-4461	david.g.kinchen@maf.nasa.gov
Kitamura, Kenrah	ASAHI GLASS CO. LTD.	10 Gaiknigan	Ichihara Chiba, 270-8566 Japan	(81) 436-23-3151		kenro-kitamura@om.agc.co.jp
Knezevich, Donna	LOCKHEED MARTIN SPACE SYSTEMS CO.	D-4800	New Orleans, LA 70189			

Edwards, Dave	NASA/MARSHALL SPACE FLIGHT CENTER	ED31	MSFC, AL 35812			
Effinger, Mike	NASA/MARSHALL SPACE FLIGHT CENTER	ED34	MSFC, AL 35812			
Eichinger, Eric	THE BOEING COMPANY	5301 Bolsa Avenue	Huntington Beach, CA 92647	(714) 372-5197	(714) 896-3136	eric.c.eichinger@boeing.com
Engel, Carl	QUALIS CORPORATION	3225 Bob Wallace Avenue	Huntsville, AL 35805	533-9282	533-4442	carl.engel@qualis-corp.com
Ennis, Doug	US ARMY SPACE & MISSILE DEFENSE COMMAND	USASMDC Attn:SMDC-TC-BE	Huntsville, AL 35807-3801	256-955-2478	256-955-2497	martha.faircloth@smdc.army.mil
Eric, John	AF RESEARCH LAB	Attn: AFRL/MLPJ	Wright-Patterson AFB, OH 45433-7702	(937) 255-2334 x 3165	(937) 255-1128	john.eric@afrl.af.mil
Ezell, Kenneth	LOCKHEED MARTIN	P.O. Box 9008	MSFC, AL 35812	(256) 544-2746	(256) 544-1660	ezellkg@aol.com
Finchum, Andy	NASA/MARSHALL SPACE FLIGHT CENTER	ED31	MSFC, AL 35812			
Finckenor, Jeff	NASA/MARSHALL SPACE FLIGHT CENTER	ED23	MSFC, AL 35812			
Finckenor, Miria	NASA/MARSHALL SPACE FLIGHT CENTER	ED31	MSFC, AL 35812			
Fischer, Richard	NASA/MARSHALL SPACE FLIGHT CENTER	ED21	MSFC, AL 35812			
Forbes, David	THE BOEING COMPANY	P.O. Box 3707	Seattle, WA 98124	253 630-3091	(253) 351-1503	david.forbes@boeing.com
Foreman, Lawrence	NASA/MARSHALL SPACE FLIGHT CENTER	ED35	MSFC, AL 35812			
Frame, Barbara	OAK RIDGE NATIONAL LAB	P.O. Box 2009, BLDG 9204-1	Oak Ridge , TN 37831	(865) 576-1892	(865) 574-8257	framebj@ornl.gov
Frazier, Michael	NASA/MARSHALL SPACE FLIGHT CENTER	ED34	MSFC, AL 35812			
Gallus, Timothy	HONEYWELL	35 Leebarry Lane	Las Cruces, NM	505 524 5326		TGALLUS@WSTF.NASA.GOV
Garnier, John	HONEYWELL ADVANCED COMPOSITES	400 Bellevue Rd.	Newark, DE 19713	302 631 1323	302 631 1320	john.garnier@honeywell.com
Garriott, Owen	NATIONAL SPACE SCIENCE AND TECHNOLOGY CENTER		Huntsville, AL			
Garrison, Warren	CARNEGIE MELLON UNIVERSITY	Dept of Materials Sciences Carnegie Mellon University	Pittsburgh, PA 15213	9412) 268-3593	(412) 268-7596	wmg@andrew.cmu.edu
Gates, Thomas	NASA/LANGLEY RESEARCH CENTER	Mailstop: 188E	Hampton, VA 23681			
Gholston, Susan	NAS, INC.	Bldg 4612 Rm 1410	Huntsville, AL 35812	(256) 961-0350		susan.gholston@msfc.nasa.gov
Gibbs, Charles	WR-ALC/TIELC	420 2nd St. Ste 100	Robins AFB, GA 31098	(478) 926-4930	(478) 926-1276	charlie.gibbs@robins.af.mil
Gibbs, Wayne	NAS, INC.	1500 Perimeter Parkway, Ste 215	Huntsville, AL 35806			
Glass, Carolyn	NAS, INC.	Bldg 4612 Rm 1410	Huntsville, AL 35812	(256) 961-0355		carolyn.glass@msfc.nasa.gov
Glover, Steve	NASA/MARSHALL SPACE FLIGHT CENTER	Attn: MP 71	MSFC, AL 35812			
Golde, Rick	THIOKOL PROPULSION	P.O. Box 707	Brigham City, UT 84302	(435) 863-3423	(435) 863-8823	golderp@thiokol.com
Gooch, Glen	SVERDRUP TECHNOLOGY	620 Discovery Drive	Huntsville, Al 35806	256 971 9351	256 971 9403	glen.gooch@hsv.sverdrup.com
Gordon, Brian	TOUCHSTONE RESEARCH LABORATORY, LTD.	The Millennium Centre, R.D. 1, Box 100B	Triadelphia, WV 26059	(304) 547-5800	(304) 547-4069	blg@trl.com
Gordon, Gail	NASA/MARSHALL SPACE FLIGHT CENTER	ED34	MSFC, AL 35812			
Gostowki, Rudy	NASA/MARSHALL SPACE FLIGHT CENTER	ED36	MSFC, AL 35812			
Gowens, Gary	MESA ASSOCIATES, INC.	9238 Madison Blvd Bldg 2, Ste 116	Madison, AL 35758	(256) 772-7055		ggowens@hiwaay.net
Gray, Perry	NAS, INC.	1500 Perimeter Pkwy	Huntsville, Al 35806	256		perry.gray@msfc.nasa.gov
Greenwood, Terry	NASA/MARSHALL SPACE FLIGHT CENTER	Attn: MP 31	MSFC, AL 35812			
Gregg, Wayne	NASA/MARSHALL SPACE FLIGHT CENTER	ED22	MSFC, AL 35812			
Greszczuk, Longin	THE BOEING COMPANY	5301 Bolsa Avenue	Huntington Beach, CA 92647	(714) 896-3810		
Griffin, Dennis	NASA/MARSHALL SPACE FLIGHT CENTER	ED36	MSFC, AL 35812			
Grisham, Angela	MADYNE CORPORATION	600 Boulevard South, Ste 301	Huntsville, AL 35802	(256) 650-1466	(256) 880-5086	angela.grisham@redstone.army.mil
Gupte, Arun	SEMCOR	2901 Wall Triana Hwy	Huntsville, AL 35824			arun.gupte@redstone.army.mil
Guthrie, Jeffrey	IIT RESEARCH INSTITUTE	201 Mill Street	Rome, NY 13440	315 339 7058	315 339 7107	jguthrie@iitri.org.
Hampton, Tammy	NAS, INC.	1500 Perimeter Pkwy	Huntsville, Al 35806	256		atammy.hampton@msfc.nasa.gov
Harcrow, Aaron	MISSISSIPPI STATE UNIVERSITY	853 Blackjack Road	Starkville, MS 39759			harcrow@ae.msstate.edu
Harm, Eugene	UNITED SPACE ALLIANCE, INC.	8550 Astronaut Blvd.	Cape Canaveral, Fl 32920	321 867 9965	321 867 7162	harmg@vsasrb.ksc.nasa.gov
Harris, Charles	NASA/LANGLEY RESEARCH CENTER	MS 121	Hampton, VA 23681	(757) 868-0154	(757) 868-3447	c.e.harris@larc.nasa.gov
Harris, Sally	THE BOEING COMPANY/ROCKETDYNE	555 Discovery Drive	Huntsville, AL 35806	(256) 971-4508	(256) 971-4597	sally.l.harris@boeing.com
Harris, Yolanda	NASA/MARSHALL SPACE FLIGHT CENTER	Attn: MP 71	MSFC, AL 35812			
Hatchett, Nadra	NASA/MARSHALL SPACE FLIGHT CENTER	ED37	MSFC, AL 35812			
Hauer, Robert	NASA/GLENN RESEARCH CENTER	21000 Brookpard Road	Cleveland, OH 44135	(216) 433-5210	(216) 433-3362	robert.l.hauer@grc.nasa.gov
Hays, C.C.	CALIFORNIA INSTITUTE OF TECHNOLOGY					
Hedlund, Maurice	THE BOEING COMPANY	P.O. Box 3707	Seattle, WA 98124	(425) 234-5639	(425) 237-1465	maurice.c.hedlund@boeing.com
Heflin-Miller, Hilda	THE BOEING COMPANY	101 kestrel Court	Huntsville, AL 35824	(256) 461-5164	(256) 461-2323	hilda.a.heflin-miller@boeing.com

Carruth, Ralph	NASA/MARSHALL SPACE FLIGHT CENTER	ED31	MSFC, AL 35812			
Caruso, Sal	NASA/MARSHALL SPACE FLIGHT CENTER	ED30	MSFC, AL 35812			
Cash, Steve	NASA/MARSHALL SPACE FLIGHT CENTER	Attn: MP 51	MSFC, AL 35812			
Caverly, Jr., John	THE BOEING COMPA NY	P.O. Box 3707 MC 2T-48	Seattle, WA 98124	(253) 351-6118	(253) 931-5987	john.e.caverly@boeing.com
Chandler, John	THE BOEING COMPANY					
Chen, Po-Shou	IIT RESEARCH INSTITUTE	9421 O'Jay Drive	Huntsville, AL 35803	(256) 544-4171	(256) 544-7473	poshou.chen@msfc.nasa.gov
Chiang, Ken	THE BOEING COMPANY	6633 Canoga Avenue, MC GB19	Canoga Park, CA 91303	(818) 586-1211	(818) 586-0575	kunag-tsan.k.chiang@boeing.com
Chorba, John	3M COMPANY	3M Center, Bldg 223-6S-04	St. Paul, MN 55144-1000	(651) 736-7569	(651) 736-7542	jechorbal@mmm.com
Clark, Don	LOCKHEED MARTIN SPACE SYSTEMS CO.	1211 Chesser Drive	Huntsville, AL 35803	(256) 544-2999	(256) 544-9156	donald.clark@msfc.nasa.gov
Clark, Johnnie	NASA/MARSHALL SPACE FLIGHT CENTER	ED34	MSFC, AL 35812			
Clark, Linda	NASA/MARSHALL SPACE FLIGHT CENTER	ED32	MSFC, AL 35812			
Clark-Ingram, Marceia	NASA/MARSHALL SPACE FLIGHT CENTER	318 Greenstone Drive	Madison, Al 35758	256-544-6229	256-544-5478	marceia.a.clark.ingram@msfc.nasa.gov
Clayton, Catherine	UNITED SPACE ALLIANCE, INC.	8550 Astronaut Blvd.	Cape Canaveral, FL 32920	(321) 853-0523	(321) 853-4027	claytonc@usasrb.ksu.nasa.gov
Cleyrat, Daniel	AFRL/ML/ANTEON	2977 P. Street B 653 Ste 13	Wright Patterson AFB, OH 45433-7746	(937) 656- 6482		
Clifton, Stu	NASA/MARSHALL SPACE FLIGHT CENTER	ED03	MSFC, AL 35812			
Clinton, Jr., R.G.	NASA/MARSHALL SPACE FLIGHT CENTER	ED34	MSFC, AL 35812			
Coad, Dennis	THE BOEING COMPANY	499 Boeing Blvd	Huntsville, AL 35824-6204	(256) 461-2976	(256) 461-2988	dennis.l.choad@boeing.com
Coggins, Erin	NASA/MARSHALL SPACE FLIGHT CENTER	120 Mikelo Lane	Madison, AL 35758	(256) 544-0710		erin.coggins@msfc.nasa.gov
Colberg, Wendell	NASA/MARSHALL SPACE FLIGHT CENTER	ED30	MSFC, AL 35812			
Conte, Mamadouba	KIDS FACE	164 Fourah Bay Road	Freetown, Sierre Leone 00232		0023222-224439	
Cook, Beth	NASA/MARSHALL SPACE FLIGHT CENTER	ED30	MSFC, AL 35812			
Cooper, Carol	NAS, INC.	210 Nicki Lane	Arab, AL 35016	(256) 544-4794		carol.cooper@msfc.nasa.gov
Cooper, Ken	NASA/MARSHALL SPACE FLIGHT CENTER	ED34	MSFC, AL 35812			
cooper, Leighton	ALCOA	4079 State St.	Riverdale, IA 52722	(319) 459-3059		leighton.cooper@alcoa.com
Cooper, Steven	NAS, INC.	1500 Perimeter Parkway, Ste 215	Huntsville, AL 35806			
Cowan, Rusty	NASA/MARSHALL SPACE FLIGHT CENTER		MSFC, AL 35812			
Creel, Helen	NASA/MARSHALL SPACE FLIGHT CENTER	ED13	MSFC, AL 35812			
Cross, Dawn	NASA/MARSHALL SPACE FLIGHT CENTER	ED35	MSFC, AL 35812			
Crump, Chris	NASA/MARSHALL SPACE FLIGHT CENTER	ED30	MSFC, AL 35812			
Crutcher, Mickey	MAXIMUM TECHNOLOGY CORPORATION	P.O. Box 11817	Huntsville, AL 35814-1817	(256) 864-7630	)256) 864-0610	mickey@maxtc.com
Curtis, Gene	THIOKOL PROPULSION					
Darvin, Charles	U.S. EPA		Research Triangle, NC 27711			
Davis, Joe	NASA/MARSHALL SPACE FLIGHT CENTER	ED38	MSFC, AL 35812			
Davis, John	NASA/MARSHALL SPACE FLIGHT CENTER	ED35	MSFC, AL 35812			
Davis, Samuel	NASA/MARSHALL SPACE FLIGHT CENTER	ED36	MSFC, AL 35812			
Davis, Sheila	THE BOEING COMPANY	499 Boeing Blvd.	Huntsville, Al 358254	256 961 0160		sheila.s.davis@bboeing.com
Davis, Simon	LOCKHEED MARTIN SPACE SYSTEMS CO.	P.O. Box 9008	MSFC, AL 35812	(256) 544-6482		simon.davis@msfc.nasa.gov
Davis, Susan	DYNAMAC	DYN-5	Kennedy Space Center, FL 32899	(407) 867-8482	(407) 867-2502	susan.davis-1@ksc.nasa.gov
Deason, Doug	US ARMY SPACE & MISSILE DEFENSE COMMAND	P.O. Box 1500	Huntsville, AL 35807	(256) 955-1843	(256) 955-1432	doug.deason@smdc.army.mil
Deem, Victoria	UNITED SPACE ALLIANCE, INC.	8550 Astronaut Blvd	Cape Canaveral, FL 32920-5304	(321) 635-8329	(321) 861-5879	victoria.j.deem@usag.com
Denby, John	DYNCORP TECHNICAL SERVICES	P.O. Box 890949	Houston, TX 77289	(281) 244-9748	(281) 24-9713	
Dhooge, Patrick	ETEC	4500-B Hawkins St. NE	Albuquerque, NM 87109-4517	(505) 341-0893	(505) 345-4884	pdhooge@etec-nm.com
Dillard, Terry	THIOKOL PROPULSION	P.O. Box 9033	Huntsville, AL 35802	(256) 544-2287	(256) 544-0732	terry.dillard@thiokol.com
Ding, Jeffrey	NASA/MARSHALL SPACE FLIGHT CENTER	ED33	MSFC, AL 35812			
Dinges, Linda	NASA/MARSHALL SPACE FLIGHT CENTER	Attn: MP 71	MSFC, AL 35812			
Doktor, Gary	THE BOEING COMPANY	6633 Canoga Park Avenue	Canoga Park, CA 91309	(818) 586-5122	(818) 586-9898	gary.doktor@west.boeing.com
Dooley, Craig	LOCKHEED MARTIN SPACE SYSTEMS CO.	P.O. Box 29304 Dept 3614	New Orleans, LA 70129	(504) 257-0204	(504) 257-2869	craig.d.dooley@maf.nasa.gov
Douglas, Vonnie	THE BOEING COMPANY	6633 Canoga Avenue	Canoga Park, CA 91309-7922	818 586 1476	818 586 7219	
Drake, Cameron	ADM/OGLIVIE	302 Island Drive	Melbourne Beach, FL 32951	(321) 728-9100	(321) 728-0175	cdrake@mindspring.com
Durkee, John	CREATIVE ENTERPRISES	145 Oyster Creek Drive	Lake Jackson, TX 77566	(409) 612) 677-3170	(409) 292-0440	jdurkee@precisioncleaning.com
Eaker, David	TOXCO INCORPORATED	779 Oak Chase Blvd	Lenoir City, TN 37772	(865) 986-8890	(865) 986-8895	eakerd@bellsouth.net

Attendee	Business	Address	City, State	Phone Number	Fax Number	Email Address
Aggarwal, Pravin	NASA/MARSHALL SPACE FLIGHT CENTER	ED22	MSFC, AL 35812			
Albyn, Keith	NASA/JOHNSON SPACE CENTER		JSC, TX			
Allen, John	NASA/MARSHALL SPACE FLIGHT CENTER	ED38	MSFC, AL 35812			
Allred, Larry	THIOKOL PROPULSION	PO Box 707	Brigham City, UT 84302	435 863 6692	435 863 6282	allred@thiokol.com
Anderson, Brian	HONEYWELL	35 Leebarry Lane	Las Cruces, NM	505 524 5504	505 524 5597	banderson@wstf.nasa.gov
Andrasik, John	ZIN TECHNOLOGIES	3000 Aerospace Parkway	Brook Park, OH 44142	(216) 977-0353	(216) 977-0350	john.andrasik@zin-tech.com
Apel, Silke	THE BOEING COMPANY	5301 Bolsa Venue	Huntington Beach , CA 92647	(714) 372-5190	(714) 896-3136	silke.m.apel@boeing.com
Askins, Bruce	NASA/MARSHALL SPACE FLIGHT CENTER	ED38	MSFC, AL 35812			
Asphahani, Aziz	ASM INTERNATIONAL					
Bah, Alpha	KIDS FACE	164 Fourah Bay Road	Freetown, Sierre Leone 00232		0023222-224439	
Baillif, Faye	LOCKHEED MARTIN SPACE SYSTEMS CO.	37311 Rhonda Street	Pearl River, LA 70452	(504) 257-2794	(504) 257--4461	faye.baillif@maf.nasa.gov
Baker, Kathy	NAS, INC.	1500 Perimeter Pkwy	Huntsville, Al 35806			kathy.baker@msfc.nasa.gov
Bar-Cohen, Yoseph	JOINT PROPULSION LAB	4800 Oak Grove Drive (82-105)	Pasadena, Ca 91109-8099	(818) 354-2610	(818) 393-2879	yosi@jpl.nasa.gov
Barnett, Terry	SOUTHERN RESEARCH INSTITUTE	757 Tom Martin Drive	Birmingham, AL 35211	(205) 581-2378	(205) 581-2414	BARNETT@SRI.ORG
Baska, David	THE BOEING COMPANY	P.O. Box 21233	Kennedy Space Center, FL 32815	(321) 867-4287	(321) 867-2947	david.f.baska@boeing.com
Bass, Donna	ALABAMA INDUSTRIAL DEVELOPMENT TRAINING	P.O. Box 1763	Decatur, AL 35609			dbass@aidt.edu
Bayer, Paul	THIRD WAVE SYSTEMS, INC.	7301 Ohms Lane	Minneapolis, MN 55379			
Bayon, Maria	NASA/HQ	Code JE	Washington, DC 20354			
Beeson, Harold	NASA/WSTF	PO Box 20	Las Cruces, NM 88004	505 524 5542	505 524 5260	hbeeson@wstf.nasa.gov
Beishline, Rex	THE BOEING COMPANY	30608 Meadow Run Place	Menifee, CA 92584	(714) 896-1494		rex.a.beishline@boeing.com
Berry, David	SVERDRUP TECHNOLOGY	620 Discovery Drive	Huntsville, AL 35806	(256) 971-9484	(256) 971-9475	david.berry@hsv.sverdrup.com
Bettinger, David	THE TECHNOLOGY PARTNERSHIP	8030 Coventry	Grosse Pt, MI 48138			
Bevill, Mat	NASA/MARSHALL SPACE FLIGHT CENTER	Attn: MP 51	MSFC, AL 35812			
Bhat, Billiyar	NASA/MARSHALL SPACE FLIGHT CENTER	ED33	MSFC, AL 35812			
Biegert, Lydia	THIOKOL PROPULSION	PO Box 707	Brigham City, UT 84302	435 863 3958	435 863 2271	lydia.biegert@1
Bili, Tenina	NASA/MARSHALL SPACE FLIGHT CENTER	ED36	MSFC, AL 35812			
Bjorkman, Gerry	LOCKHEED MARTIN SPACE SYSTEMS CO.	108 Jenni Leigh Drive	Huntsville, AL 35806	(256) 961-4438	(256) 544-1660	gerry.bjorkman@msfc.nasa.gov
Black, Denise	UNITED SPACE ALLIANCE, INC.	Environmental Safety & Health DepartmnetComplex B, MC USK-142	Kennedy Space Center, FL	(321) 861-3881	(321) 867-8169	DENISE.L.BLACK@USAGO.KSC.NASA.GOV
Blanks, Jerrell	THIOKOL PROPULSION	P.O. Box 9033	Huntsville, AL 35812	(256) 544-7899	(256) 544-0732	blankjw@thiokol.com
Bolstad, Donald	LOCKHEED MARTIN SPACE SYSTEMS CO.	13800 Old Gentilly Road	New Orleans, LA 70129	(504) 257-4651	(504) 257-4461	donald.a.boldstad@maf.nasa.gov
Bonacchi, Daniele	TURBOCOATING	Via Volta, 3	Rubbiano, Italy	0039-525-406211	0039-525-406212	andreascrivani@turbocoating.it
Bond, Robert	IIT RESEARCH INSTITUTE	4028 Lucerne Dr.	Huntsville, AL 35802	(256) 544-8277	(256) 544-7473	robert.bond@msfc.nasa.gov
Bowkett, John	NU-CAST, INC.	29 Grenier Field Road	Londonderry, NH 03053	(603) 432-1600	(603) 432-0724	nci@grolen.com
Boyce, William	THE BOEING COMPANY	232 Goldenrod Lane	Madison, Al 35758	256 461 2372		william-e-boyce@boeing.com
Bradic, Jelena	COM DEV	155 Sheldon Drive	Cambridge, ON N1R7h0	(519) 622-2300		
Breitengross, Rick	NAVAL AIR WEAPONS STATION-CHINA LAKE	Code 826100D	China Lake, CA 93555-6100	(760) 375-3151	(760) 939-1619	breitengroRA@navair.navy.mil
Brobst, Keith	3M COMPANY	3M Center, Bldg 223-6S-04	St. Paul, MN 55144-1000	(800) 603-0377	(651) 736-7542	kebrobst@mmm.com
Brown, Alan	THE BOEING COMPANY	6633 Canoga Avenue	Canoga Park, CA 91309	(818) 586-6636	(818) 586-7219	alan.r.brown@boeing.com
Brown, Jerry	LOCKHEED MARTIN		Ft Worth, TX			
Browning, Charles	AF MATERIALS & MFG DIRECTORATE	AFRL/ML 2977 P Street Bldg 653	Wright Patterson AFB, OH 45433	(937) 255-4726	(937) 656-4068	charles.browning@wpafb.af.mil
Bryden, Philip	UNITED SPACE ALLIANCE	8550 Astronaut Blvd, USK-821	Cape Canaveral, FL 32920	(321) 853-5267	(321) 853-4027	brydenpd@usarb.ksc.nasa.gov
Bryson, Craig	NASA/MARSHALL SPACE FLIGHT CENTER	ED32	MSFC, AL 35812			
Burlingame, Steve	NASA/MARSHALL SPACE FLIGHT CENTER	ED34	MSFC, AL 35812			
Burnum, James	NASA/MARSHALL SPACE FLIGHT CENTER	Attn: MP 51	MSFC, AL 35812			
Byess, Dean	NAS, INC.	1500 Perimeter Pkwy	Huntsville, Al 35806	256 544 6283		dean.byess@msfc.nasa.gov
Campbell, David	THIOKOL PROPULSION	P.O. Box 1617 MS LFO	Brigham City , UT 84302	(435) 863-3463	(435) 863-2770	
Carey, Philip	EASTMAN KODAK COMPANY	800 Lee Road	Rochester, NY 14650-3119	716 588 8303	716 588 4939	philip.carey@kodak.com
Carpenter, Ronn	THIOKOL PROPULSION	P.O. Box 9033	Huntsville, AL 35812	(256) 544-0820	(256) 544-0857	brougjp@thiokol.com
Carr, Steven	U.S. ARMY AVIATION & MISSILE COMMAND	Attn: AMSAM-RD-PS-CM	Redstone Arsenal, AL 35898	(2560 876-7472	(256) 842-1359	steve.carr@redstone.army.mil

SEPTEMBER 20, 2000 *(CONTINUED)*

10:30 am – 12:30 pm — SESSION E *(continued)*

Session E1 (continued)

- High Performance, Low Environmental Impact Refrigerants
  Patrick Dhooge, Edward T. McCullough, Suzanne M. Glass, Jonathan S. Nimitz (Environmental Technology & Education Center)
- Volatile Organic Compound Compliant Wax Removal Process
  Alan Brown, David Grimmett, Margarite Sylvia (The Boeing Company – Rocketdyne)
- Highly Effective, Low Toxicity, Low Environmental Impact Total Flooding Fire Suppressants
  Patrick Dhooge, Suzanne M. Glass, Jonathan S. Nimitz (Environmental Technology & Education Center)

Session E2 (continued)

- Resources Available for Hazards Analysis of Aerospace Fluids
  Kurt Rathgeber (Honeywell); Stephen S. Woods (Allied Signal Technical Services Corporation); Walter F. Stewart (L&M Technologies, Inc.); David L. Baker, Harold Beeson (White Sands Test Facility)
- Chemical Fingerprinting of Materials Developed due to Environmental Issues
  Doris Smith, Mary Capezza, Emile Evans, Laurie Rando (Lockheed Martin Space Systems)
- Use of GC/MS and Microtome Techniques to Evaluate ODC Free Cleaner Diffusion and Evaporation in Insulation and Phenolic Case Material
  L.L. Biegert (Thiokol Propulsion Group)

Session E3 (continued)

- The Composites Affordability Initiative
  John Mistretta (Wright Patterson Air Force Base)
- Advanced Ceramic Matrix Composites for Aerospace Applications
  John Garnier, Bill Patterson, Bob Klacka, Paul Gray, Stan Hemstad (Honeywell Advanced Composites)

Session E4 (continued)

- Manufacturing Challenges Implementing Material Changes for Super Lightweight Tank: A Welding Process Perspective
  Chip Jones, Kirby G. Lawless (Marshall Space Flight Center)
- Cryotank Technology Program (CTTP)
  Tim Vaughn (Marshall Space Flight Center)

12:30 – 2:00 pm — *Lunch --- Poster Session People's Choice Award --- Exhibits*

1:30 pm **Demonstration**

Hybrid Propulsion (Exhibit Area)
Terry Abel (Marshall Space Flight Center)

2:00 – 4:00 pm — SESSION F

Session F1 (Orchestra)

Methods for Cleaning and Cleanliness Verification

Chair: Jerrell Blanks, Thiokol Propulsion Group

- Elimination of Carbon Tetrachloride for Quantitative Hydrocarbon Analysis
  Vonnie Douglas (The Boeing Company - Rocketdyne)
- Ellipsometric Verification and Evaluation of Clean Surfaces
  Wayne Thompson (University of Alabama in Huntsville)
- Improved Detection Technique for Solvent Rinse Cleanliness Verification
  Steven D. Hornung (Honeywell); Harold Beeson (White Sands Test Facility)
- Criteria for NVR Solvent Replacement
  Kenneth Luey, Dianne J. Coleman, Joseph C. Uht, Graham S. Arnold (The Aerospace Corporation)
- Critical Surface Cleaning and Verification Alternatives
  Donald M. Melton (Lockheed Martin Michoud Operations)

Session F2 (Salon 1A)

Advanced Metals Research

Chair: Eric Eichinger, Boeing

- The Effects of Cryogenic Treatment on the Mechanical Properties of an Al-Li Alloy 2195
  Po Chen, Robert Bond (IIT Research Institute); Tina Malone, Pablo Torres (Marshall Space Flight Center)
- Toughness of Ultra Strength AF 1410 Type Steels
  Warren M. Garrison, Jr., Luana Iorio (Carnegie Mellon University)
- Segregation Behavior of Sulfur and Other Impurities onto the Free Surfaces in ED-Ni Deposits
  Binayak Panda (IIT Research Institute); Gregory Jerman (Marshall Space Flight Center)
- Statistical Analysis of Al-Li 2195 Strength and Toughness Data
  Lynn Neerguard (IIT Research Institute); Tina Malone (Marshall Space Flight Center)
- Electrostatic Levitation Processing of Bulk Metallic Glass Forming Liquids
  C.C. Hays, J. Schroers, U. Geyer, W.L. Johnson (California Institute of Technology)

Session F3 (Salon 1B)

Emerging Technologies

Chair: R.D. Patton, Mississippi State University

- Residual Stress Prediction in Machined Workpiece Surfaces
  Paul Bayer, Troy Marusich (Third Wave Systems, Inc.)
- Easily Processable High Temperature and Flame Resistant Phthalonitrole Composites for Aerospace Applications
  Teddy M. Keller, Harry N. Jones (Naval Research Laboratory)
- Real Time Video Recording of Extremely High Temperature Processes
  Thad Hoffman (Control Vision, Inc.)
- Vapor Grown Carbon Fiber/ Phenolic Matrix Composites for Rocket Nozzles and Heat Shields
  R.D. Patton, C.U. Pittman, Jr., L. Wang (Mississippi State University); J.R. Hill (Charleston Air Force Base); A. Day (Thiokol)

Session F4 (Salon 2)

Environmental Monitoring Methods

Chair: Greg Smith, AJT & Associates, Inc.

- Ambient Air Monitoring of Respirable Particulate Matter (PM10) and Total Suspended Particulate (TSP) During the RD-180 Rocket Engine Tests at the NASA Marshall Space Flight Center
  John Hughes, Kathy Lehr (GB Tech)
- Gas Emission Measurements from the RD-180 Rocket Engine Tests at the NASA Marshall Space Flight Center
  H. Richard Ross (GB Tech)

4:00 pm — *End of Conference*

SEPTEMBER 20, 2000

7:00 am – 4:00 pm — *Poster Session Follow-On Discussions (Break-Out Room)*

8:00 – 10:00 am — SESSION D

Session D1 (Salon 1A)

Evaluating Pollution Prevention Methodologies

Chair: Odean Serrano, NASA Headquarters

- Identification of High Performance, Low Environmental Impact Materials and Processes Using Systematic Substitution (SyS)
  Patrick M. Dhooge, Jonathan S. Nimitz (Environmental Technology & Education Center)
- Selection Criteria for Alternate Technologies as a Method of Hazardous Waste Minimization
  Eric Lethe (Inland Technology, Incorporated)
- Joint Group on Pollution Prevention, Partnering for Progress
  Robert Hill (Kennedy Space Center); Michael McCall (Concurrent Technologies Corporation)
- Liquid Filtration for Component Reliability and Waste Minimization
  Edward Kanegsberg, Barbara Kanegsberg (BFK Solutions)
- Chemical Aging of Environmentally Friendly Cleaners
  L.L. Biegert, K.B. Evans, B.D. Olsen, B.L. Weber (Cordant Technologies: Thiokol Propulsion)

Session D2 (Salon 1B)

Advanced Materials for Extreme Environments

Chair: Teddy M. Keller, Naval Research Laboratory

- National Materials Information System
  Jeffrey Guthrie (AMPTIAC)
- Durability Characterization of Advanced Polymeric Composites at Cryogenic Temperatures
  Thomas S. Gates (Langley Research Center)
- Development of Metal Matrix Composites for NASA's Advanced Propulsion Systems
  Jonathan A. Lee, Sandy Elam (Marshall Space Flight Center)
- Inorganic-Organic Hybrid Polymers for High Temperature Aerospace Applications
  Teddy M. Keller (Naval Research Laboratory)

Session D3 (Orchestra)

Manufacturing Technology Topics

Chair: Charles Harris, Langley Research Center

- Integrated High-Payoff Rocket Propulsion Technologies Program Materials Development Plan
  R. G. Clinton (Marshall Space Flight Center); Brian Reed (Glenn Research Center); Michael Stropki, Dan Cleyrat, Brian Stucke, Shawn Phillips (Air Force Research Laboratory)
- Findings from the X-33 Hydrogen Tank Failure Investigation
  Mindy Niedermeyer (Marshall Space Flight Center)
- Assessment of the State of the Art in the Design and Manufacturing of Large Composite Structures
  Charles E. Harris (Langley Research Center)

Session D4 (Salon 2)

Evaluation of Cleaning and Bonding Materials and Processes

Chair: Jill Keen, Thiokol Propulsion Group

- A Mass Spectrometer-Based Tool for In-Process Analysis of RSRM Components
  Michael Meltzer, Carolyn Koester (Lawrence Livermore National Laboratory); Neil Sagers (Thiokol Propulsion)
- Effects and Detection of Silicone and HD2 Grease Contaminants
  Jerrell Blanks (Thiokol Propulsion Group)
- Physical Evaluation of Cleaning Performance – We Are Only Fooling Ourselves
  Earl Pratz (Lockheed Martin Space Systems)

10:00 – 10:30 am — ***Break --- Exhibits***

10:15 am — Demonstration

Pneumatic Impact (Exhibit Area)
Kurt Rathgeber (Honeywell)

10:30 am – 12:30 pm — SESSION E

Session E1 (Salon 1A)

Alternatives for Chemical Replacement

Chair: Alan Brown, The Boeing Company - Rocketdyne

- Low Environmental Impact, High-Performance Foam Blowing Agents Based on Iodofluorocarbons
  Patrick Dhooge, Suzanne M. Glass, Jonathan S. Nimitz (Environmental Techology & Education Center)
- Update: HFC 245fa Blown Foam Development with External Tank Spray Foams
  Simon Davis (Lockheed Martin Space Systems)

(continued on next page)

Session E2 (Salon 1B)

Advances in Materials Analysis and Testing Techniques II

Chair: Frank Key, Native American Services, Inc.

- Promoted Combustion of Metals in a High-Pressure, Flowing Oxygen Environment
  Miguel J. Maes (Allied Signal Technical Services Corporation); Joel M. Stoltzfus, (White Sands Test Facility)
- Problem Solving Applications of Chemical Fingerprinting
  Michael O. Killpack, Dennis J. Fife, Chad R. Saunders, Charles R. Whitworth, William H. McClennen (Thiokol Propulsion Group)

(continued on next page)

Session E3 (Salon 2)

Non-Metals Processes II

Chair: R.G. Clinton, Marshall Space Flight Center

- Electron Beam-Cured Polymer Matrix Composites: Processing and Properties
  George Wrenn, Barbara Frame (Oak Ridge National Laboratory); Brian Jensen (Langley Research Center); Alan Nettles (Marshall Space Flight Center)
- Manufacture of Porous Ceramic Materials by Combustion Synthesis
  L.A. Whelan Robinson, H.C. Yi, J.Y. Guigné (Guigné International Ltd.)

(continued on next page)

Session E4 (Orchestra)

Developments in Metals Processes II

Chair: Carolyn Russell, Marshall Space Flight Center

- Aluminum Investment Cast Spacecraft and Aerospace Structures
  John Bowkett (Nu-Cast, Inc.)
- Vacuum Plasma Spray of CuCrNb Alloy for Low-Cost, Long-Life Combustion Chambers
  Frank Zimmerman (Marshall Space Flight Center)
- Dynamic Oxidation of a Plasma Sprayed Cu-Cr Coating
  K.T. Chiang (The Boeing Company)

(continued on next page)

6:00 – 7:00 pm

POSTER SESSION — North Hall Gallery

Development of Lead-Free Energy Absorber for Space Shuttle Blast Container
Donald Balles, Thomas Ingram, Howard Novak, Albert Schricker (United Space Alliance)

Polymer Matrix Composites (PMCs) Cryopipe for Rocket Engine Lines and Ducts
David Bettinger (The Technology Partnership)

Nanotechnology Concepts at Marshall Space Flight Center – Engineering Directorate
Biliyar Bhat, Raj Kaul, Sandeep Shah, Gweneth Smithers, Michael D. Watson (Marshall Space Flight Center)

Microstructure, Mechanical Properties, Hot-Die Forming, and Joining of 47XD Gamma TiAl Rolled Sheets
G. Das (Pratt & Whitney); S. Draper, J.D. Whittenberger, P.A. Bartolotta (Glenn Research Center)

At Last, Something New! Cleaning without Chemistry, and Reusing the Waste Water!
John Durkee (Creative EnterpriZes)

Polymer Matrix Composite (PMC) Analog Processes for Lightweight Aluminum Matrix Composite (AMC) Structures
Brian Gordon (Touchstone Research Laboratory)

Further Studies of Materials Compatibility in High Test Hydrogen Peroxide
Rudy Gostowski (Austin Peay State University); Tom Owens (Marshall Space Flight Center)

X-Traktor: A Rookie Robot, Simple, Yet Complex, Impeccably Designed, A Very Innovative Multidisciplinary Engineering Masterpiece
Arthur J. Henderson, Jr. (Marshall Space Flight Center)

Laser Surface Modification of TiAl Intermetallics
Sherman McElroy, R.G. Reddy (The University of Alabama, Tuscaloosa)

Characterization of Ceramic Matrix Composite Combustor Components: Pre and Post Exposure
G. Ojard, G. Linsey, J. Brennan (United Technologies Research Center); R. Naik, R. Cairo, R. Stephan, J. Hornick (Pratt & Whitney); D. Brewer (Glenn Research Center)

Automated Acquisition and Analysis of Digital Radiographic Images
Richard Poland, David Inmel, Boyd Howard, Randy Singer, Bob Moore (Westinghouse Savannah River Company)

Fabrication of Low-Cost, High-Temperature Composites for Rocket Propulsion Systems
Mark J. Rigali, Manish Sutaria, Anthony C. Mulligan, Ranji Vaidyanathan (Advanced Ceramics Research, Inc.)

Electro Spark Alloy Processing for Aerospace Components
Michael Riley (Surface Treatment Technologies, Inc.)

Detection, Identification, and Quantification of Surface Contamination
M. Martin Szczesniak, Michael Beecroft, Phillip Mattison (Surface Optics Corporation)

Quadruple Lap Shear Processing Evaluation
Tony N. Thornton (Thiokol Propulsion, SEHO Operations)

PEOPLE'S CHOICE AWARD

Poster Session visitors will choose one poster presentation to receive the People's Choice Award.

- Posters will be judged on relevance, creativity, and speaker's presentation.
- Each Poster Session visitor who attends at least 4 presentations may vote for 3 presentations.
- Poster Session visitors who cast their ballots for the People's Choice Award will be entered in drawings for conference door prizes. Drawings will be immediately after the Poster Session (7 pm).
- The presentation receiving the most votes will win the People's Choice Award.
- Presentations that receive the second and third most votes will win runner-up prizes.
- The People's Choice Award and runner-up recognitions will be presented at the Wednesday luncheon.

POSTER SESSION FORMAT

- Presentations will be 5 minutes, followed by 5-minute question-and-answer periods.
- Presentations will be repeated throughout the Poster Session length.
- Detailed discussions can be scheduled with the presenter from 7 am - 4 pm Wednesday in the Break-Out Room.

INSTRUCTIONS FOR POSTER SESSION PRESENTERS

- Poster assembly in the North Hall Gallery must be completed by 9:30 am on Tuesday. You may set up your poster as early as Monday afternoon.
- Posters may be removed between 2 pm and 6 pm Wednesday.
- You must be available at your poster site during the Poster Session.
- The Break-Out Room is reserved from 7 am - 4 pm Wednesday for one-on-one or round-table discussions about your poster topic. Reserve space at the conference registration table.

SEPTEMBER 19, 2000 *(CONTINUED)*

1:30 – 3:30 pm — *SESSION B (continued)*

Session B1 (continued)

- HVOF Thermal Spray Coating as an Alternative to Hard Chrome Plating on Military Aircraft
  Bruce D. Sartwell (Naval Research Laboratory)
- The Use of Ion Vapor Deposited Aluminum (IVD) for the Space Shuttle Solid Rocket Booster
  Howard Novak, Bill Imre, Randy Raley (United Space Alliance)

3:30 – 4:00 pm — *Break --- Exhibits*

3:45 pm **Demonstration**

Robot Expo (Exhibit Area)
X-Traktor (MSFC/Lee High School, Huntsville, Alabama);
Patriot 4 (DaimlerChrysler/Bob Jones High School, Athens, Alabama);
Oscar (PRO-BOTS, Atlanta, Georgia)

4:00 – 5:30 pm — *SESSION C*

Session C1 (Salon 2)

Developments in Coating Removal Processes

Chair: Marceia Clark-Ingram
Marshall Space Flight Center

- Coating Removal Technology Using Starch-Based Abrasives: A Review of Current Aerospace Applications Using the EnviroStrip® Dry Stripping Process
  Denis Monette, Cameron Drake (ADM/EnviroStrip Division)
- Removal of Zirconia Thermal Barrier Coatings and MCrAlY Bond Coatings from Turbine Blades: A Comparison of Methods Based on Chemical Stripping, Water Jet, and Salt Bath
  A. Scrivani, U. Bardi, G. Ballerini, D. Bonacchi (University of Firenze); M. Fantini (Galvanica Parmense); R. Groppetti, S. Ianelli (University of Parma); G. Rizzi (Turbocoating S.p.A.)
- Joint EPA/NASA/USAF Interagency Depainting Study
  Marceia Clark-Ingram (Marshall Space Flight Center)
- Evaluation of Various Depainting Processes on Mechanical Properties of 2024-T3 Aluminum Substrate
  Preston McGill (Marshall Space Flight Center)

Session C2 (Orchestra)

Ceramic Matrix Composites

Chair: Mike Effinger
Marshall Space Flight Center

- Concept for Determining the Life of Ceramic Matrix Composites Using Nondestructive Characterization Techniques
  Michael Effinger (Marshall Space Flight Center); Bill Ellingson, Todd Spohnholtz (Argonne National Laboratory); John Koenig (Southern Research Institute)
- Low Cost Ceramic Matrix Composites
  Witold Kowbel, C. Bruce, K.T. Tsou, J.C. Withers (MER Corporation)
- Fabrication and Testing of Ceramic Matrix Composite Propulsion Components
  Michael Effinger, R.G. Clinton, Jr., Jay Dennis, Sandra Elam, Gary Genge (Marshall Space Flight Center); J. Doug Kiser, Andy Eckel, Martha Jaskowiak, Jerry Lang (Glenn Research Center)
- Rapid Fabrication of Monolithic Ceramic Parts Reinforced with Fibrous Monoliths for Aerospace Applications
  Ranji Vaidyanathan, J. Walish, J.L. Lombardi, D. Dent, M. Rigali, M. Sutaria (Advanced Ceramics Research, Inc.)

Session C3 (Salon 1B)

Rapid Prototyping

Chair: Ken Cooper
Marshall Space Flight Center

- Solid Freeform Fabrication of Continuous Fiber Reinforced Composites for Propulsion Applications
  Ranji Vaidyanathan, J. Walish, M. Fox, M. Rigali, M. Sutaria (Advanced Ceramics Research, Inc.); J.W. Gillespie, Jr., S.Yarlagadda (University of Delaware); M. Effinger (Marshall Space Flight Center)
- An Example of Economic Value in Rapid Prototyping
  Robert L. Hauer, John R. Reagan, Edward P. Braunscheidel, Herbert A. Lawrence, Jr. (Glenn Research Center)
- High-Efficiency Monolithic Lightweight Aluminum Cast Structure
  John Bowkett (Nu-Cast, Inc.)
- Preliminary Component Integration Utilizing Rapid Prototyping
  Ken Cooper (Marshall Space Flight Center); Pat Salvail (IIT Research Institute)

Session C4 (Salon 1A)

Innovative Materials Applications

Chair: Michael Pedley
Johnson Space Center

- Multifunctional Carbon Foams for Aerospace Applications
  Brian Joseph, Darren Rogers, Janusz Plucinski (Touchstone Research Laboratory)
- LOX Compatibility of Composite Materials
  Tim Vaughn (Marshall Space Flight Center)
- Low Density Monolithic Metal Honeycombs by Thermal Chemical Processing
  Jim Lee, Joe Cochran, Dave McDowell, Tom Sanders (Georgia Institute of Technology)
- Transhab Materials Selection
  Michael Pedley (Johnson Space Center)

5:30 – 6:30 pm — *EXHIBITORS' RECEPTION --- EXHIBIT AREA*

Relax and enjoy *hors d'oeuvres* and other refreshments with our conference exhibitors and your colleagues.

http://ampet.msfc.nasa.gov

SEPTEMBER 19, 2000 *(CONTINUED)*

Note: Each speaker is allotted 20 minutes of presentation time and 5 minutes for questions and answers.

10:00 am – 12:00 n — *SESSION A*

Session A1 (Orchestra)

Engineering Evaluation of Solvent Substitutes

Chair: Ralph LeBeouf
Lockheed Martin Space Systems

- Nonflammable, Nonaqueous, Low Atmospheric Impact, High Performance Cleaning Solvents
  Patrick M. Dhooge, Jonathan S. Nimitz, Suzanne M. Glass, (Environmental Technology & Education Center)
- Aerospace Applications for AK-225
  Kenroh Kitamura, Masaaki Tsuzaki, and Stephen D. Stagliano (Asahi Glass)
- HFEs in the Aerospace Industry: A Logical Alternative to CFCs and Other Halogenated Cleaning Solvents
  David A. Hesselroth (3M Company)
- Elimination of MEK and Lacquer Thinner in Department of Defense Painting Operations
  Joseph A. Lucas, Eric Lethe (Inland Technology Incorporated)

Session A2 (Salon 1B)

Advances in Materials Development

Chair: John Chandler
The Boeing Company

- Lightweight Multi-Layer Structural Materials
  H. H. Legner, W. T. Laughlin (Physical Sciences, Inc.); V. Di Cristina, D. Marshal (ThermoPhysical Sciences); R. Singler (Textron Systems)
- Asbestos Free Insulation Development for the Space Shuttle Solid Propellant Rocket Motor (RSRM)
  Larry D. Allred (Thiokol Propulsion Group)
- Aerogel Projects Ongoing in MSFC's Engineering Directorate
  David Shular, Gweneth Smithers (Marshall Space Flight Center); Joel Plawsky (Rensselaer Polytechnic Institute)
- Electroactive Polymers as Artificial Muscles - Reality and Challenges
  Yoseph Bar-Cohen (NDEAA Technologies)

Session A3 (Salon 1A)

National Center for Advanced Manufacturing Workshop

Chair: John Vickers
Marshall Space Flight Center

- Overview of the National Center for Advanced Manufacturing (NCAM)
  John Vickers (Marshall Space Flight Center)
- Advanced Engineering Environments - Implications for Aerospace Manufacturing
  Dale Thomas (Marshall Space Flight Center)
- Education, Industry and Government Partnerships Expanding Education and Meeting Workforce Challenges
  James E. Swindell, Richard Carpenter (Calhoun Community College); Donna C. Bass (Alabama Industrial Development Training); William R. Reynolds (Boeing, Delta IV Operations)
- Composite Manufacturing for Space Launch Vehicles
  Donna Y. Knezevich (Lockheed Martin Space Systems)

12:00 n – 1:30 pm

Lunch --- Exhibits

1:15 pm **Demonstration**

Rapid Prototyping (Exhibit Area)
Ken Cooper (Marshall Space Flight Center)

1:30 – 3:30 pm — *SESSION B*

Session B1 (Salon 1A)

Elimination of Heavy Metals

Chair: Howard Novak
United Space Alliance

- Laser Cladding/Glazing as a Surface Coating Alternative
  Rob Hull (Anteon Corporation); Dave Firish (Inorganic Specialists); Chuck Woods (Global Manufacturing Solutions); John Eric (AFRL/MLPJ)
- Testing of Environmentally Preferable Aluminum Pretreatments and Coating Systems for Use on Space Shuttle Solid Rocket Boosters (SRBs)
  Catherine Clayton, Lee Zook, Randy Raley (United Space Alliance)
- Trivalent Chromium/Organically-Modified Silicate Composite Coatings for Corrosion Protection of Aluminum Alloys
  Tammy Metroke, Edward Knobbe, Elvira Stesikova, Olga Kachurina (Oklahoma State University)

(continued on next page)

Session B2 (Salon 1B)

Advances in Materials Analysis and Testing Techniques I

Chair: Sam Russell
Marshall Space Flight Center

- High Temperature Material Performance Testing Using Continuous Wave Carbon Dioxide Lasers
  Timothy Johnson (Anteon Corporation)
- Thermographic Nondestructive Evaluation of the Space Shuttle Main Engine Nozzle
  James L. Walker, Samuel S. Russell, Matthew D. Lansing, Paul Caraccioli (Marshall Space Flight Center)
- Validation of Shearography NDE Methods on Space Shuttle, X-33, and Delta IV Launch Vehicles
  John Newman (Laser Technology, Inc.)
- Thermographic Analysis of Composite Cobonds on the X-33
  James L. Walker, Samuel S. Russell, Matthew D. Lansing (Marshall Space Flight Center)

Session B3 (Orchestra)

Developments in Metals Processes I

Chair: Don Bolstad
Lockheed Martin Space Systems

- Evaluation of Forces on the Welding Probe of the Automated Retractable Pin-Tool (RPT)
  R. Jeffery Ding (Marshall Space Flight Center)
- Friction Stir Weld Modeling at MSFC: Kinematics
  Arthur C. Nunes, Jr. (Marshall Space Flight Center)
- Aluminum Lithium Alloy 2195 Fusion Welding Improvements with New Filler Wire
  Gerry Bjorkman (Lockheed Martin Space Systems); Carolyn Russell (Marshall Space Flight Center)

Session B4 (Salon 2)

Non-Metals Processes I

Chair: Terry Dillard
Thiokol Propulsion Group

- Fabrication of Composite Combustion Chamber/Nozzle for Fastrac Engine
  Timothy Lawrence, R. Beshears, S. Burlingame, W. Peters, M. Prince, M. Suits, S. Tillery (Marshall Space Flight Center); L. Burns, M. Kovach, K. Roberts (Thiokol Propulsion Group)
- Large Composite Structures Processing Technologies For Reusable Launch Vehicles
  R.G. Clinton, Jr., John H. Vickers, William M. McMahon, et. al., (Marshall Space Flight Center); Norman J. Johnston (Langley Research Center)
- Composite, Cryogenic, Conformal, Common Bulkhead, Aerogel-Insulated Tank (CBAT) Materials and Processing Methodologies
  Michael P. Kovach, J. Keith Roberts (Thiokol Propulsion Group); William M. McMahon, Jeffery L. Finckenor (Marshall Space Flight Center)

Fourth Conference on Aerospace Materials, Processes, and Environmental Technology

September 18, 2000

AMPET Conference Venues

1. Von Braun Center (Conference Venue)
2. Huntsville Museum of Art (Welcoming Reception)
3. Hilton Huntsville (Lodging and Tour Start)

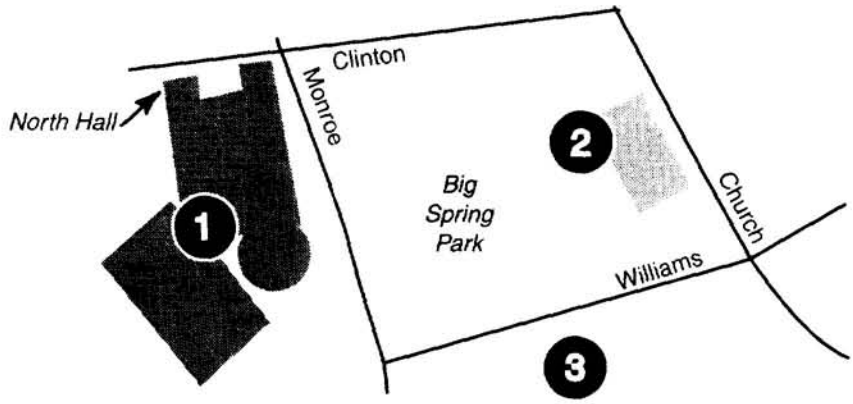

1:00 – 5:00 pm — *PRE-CONFERENCE TOURS*

1:00 pm — Buses depart from the Hilton Huntsville

US Citizens Tour
Boeing Delta IV Plant
MSFC Productivity Enhancement Complex
MSFC International Space Station Manufacturing Facility

International Guests Tour
US Space and Rocket Center (IMAX theater, guided tour, bus tour of MSFC)

5:00 pm — Buses return to the Hilton Huntsville

6:00 – 7:30 pm — *WELCOMING RECEPTION · HUNTSVILLE MUSEUM OF ART*

Enjoy an evening of art and southern hospitality at the AMPET Welcoming Reception in the elegant Great Hall of the Huntsville Museum of Art, overlooking Big Spring Park. This nationally accredited museum is the premier visual arts center in North Alabama and Southern Tennessee. In its seven spacious galleries, visitors enjoy a wide array of exhibitions, prestigious traveling exhibitions, works by nationally and regionally acclaimed contemporary artists, and shows featuring some of the 2,300 works in the Museum's permanent collection.

September 19, 2000

8:00 am — *OPENING SESSION*

Conference Welcome	*Dr. Ann F. Whitaker* Deputy Director, Science Directorate NASA/MSFC
Keynote Addresses	
Advanced Space Flight and Environmental Concerns	*Dr. Ann F. Whitaker* Deputy Director, Science Directorate NASA/MSFC
Science and Technology – Then and Now	*Dr. Owen K. Garriott* NASA Astronaut, Retired Interim Director, National Space Science and Technology Center
Materials Advancements in Aerospace	*Dr. Charles E. Browning* Director, Materials and Manufacturing Directorate Air Force Materiel Command Wright-Patterson Air Force Base

9:15 - 10:00 am — *Break — Exhibit Area*

9:30 am — Poster area (North Hall Gallery) opens for viewing.

http://ampet.msfc.nasa.gov

VBC North Hall Floor Plan

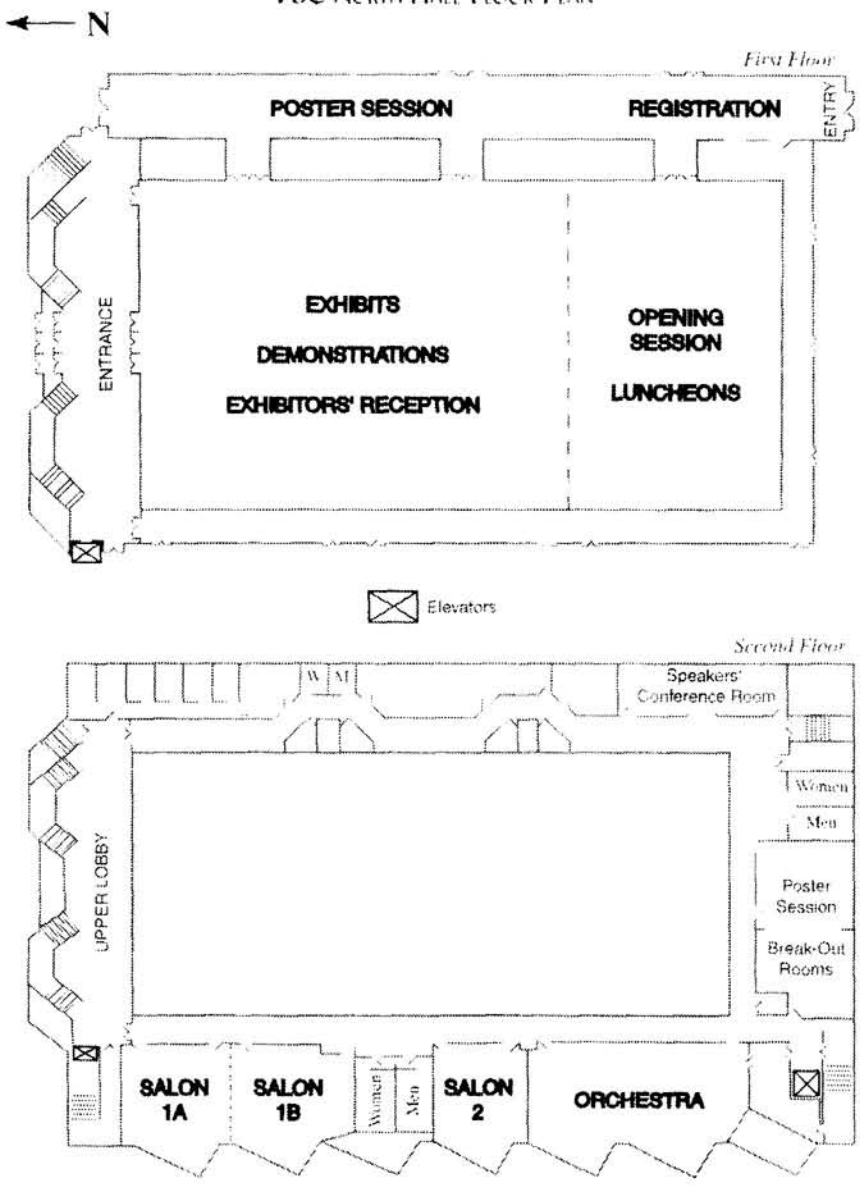

NP-2000-09-170-MSFC

PROGRAM

Fourth Conference on

Aerospace Materials, Processes, and Environmental Technology

September 18-20, 2000
Von Braun Center
Huntsville, AL

www.ampet.msfc.nasa.gov

Challenges for Aerospace Materials & Processes

19 Sep 00

Dr Charles E. Browning
Director, Materials & Manufacturing
AFRL/ML
Air Force Research Laboratory

OUTLINE

- A Material Life Cycle
- Aerospace Material Life Cycle
- Trends Impacting the Aerospace M&P Life Cycle
- Key Aerospace M&P Challenges
- Revolutionary Opportunity Areas
- Summary

A MATERIAL LIFE CYCLE

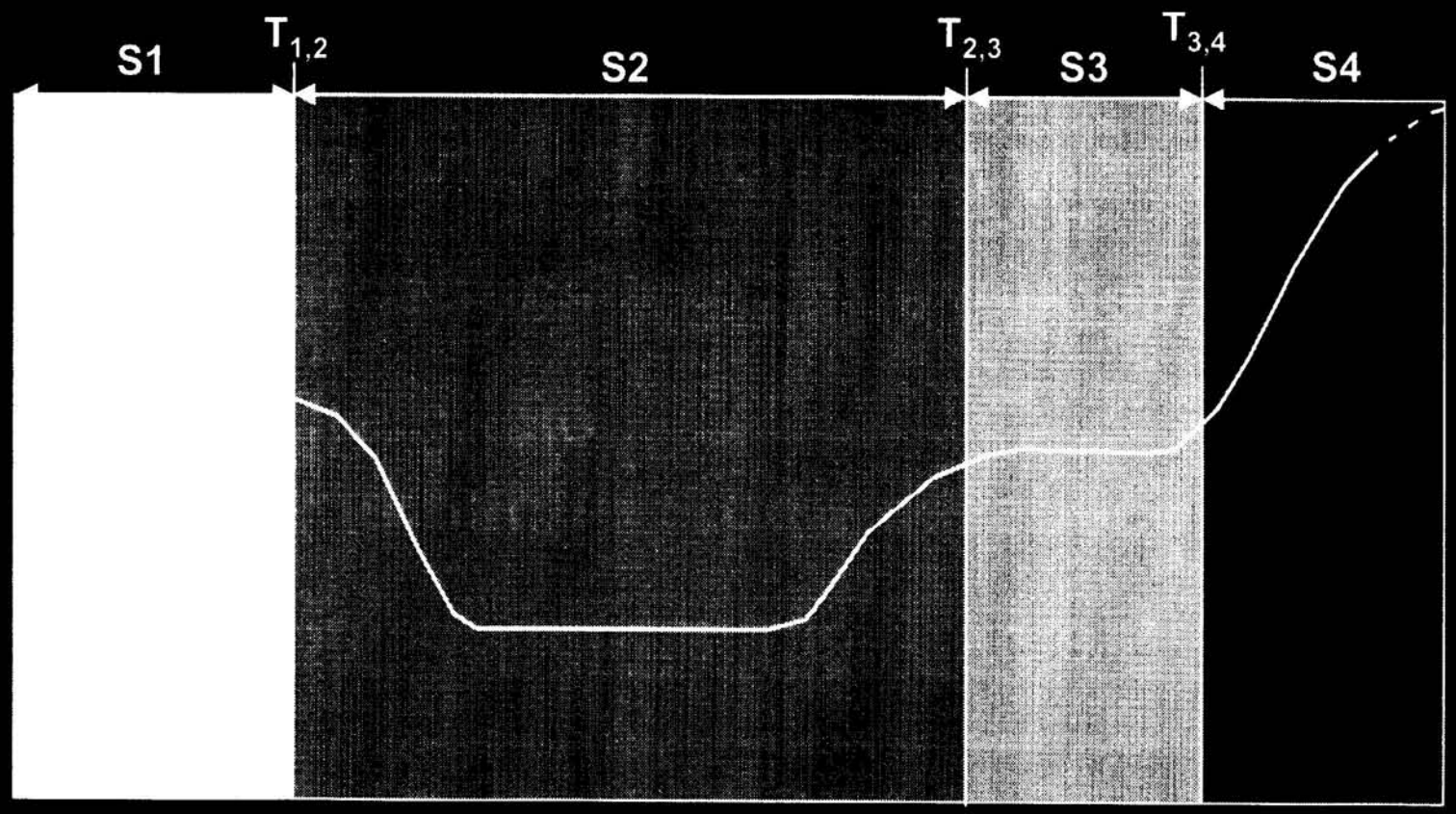

Stages
1 = Revolutionary
2 = [illegible]
3 = Specialty Material

acrp'00372-3

STAGE 1: REVOLUTIONARY

CHARACTERISTICS

- Significant New Capability Not Attainable with Today's Materials
- Potential for Dramatic Improvements in Key Parameters
- Traditionally Performance Driven
- Major Risk Taking
- Government Funding May Be Very Important
- Applications Window May Be Distant
- Tech Push
- Focus is on Materials; Processes May Be Dramatically Different
- Small Quantities
- High Materials Costs
- No to Little Data
- Length of Stage Variable

STAGE 2: EMERGING

CHARACTERISTICS

- Evolutionary Materials and Processes
- "M" and "p" giving way to "M" and "P"
- Process Development Activities Underway
- Scale-up Activities
- Intermediate Level Quantities Being Produced
- Cost Reducing Initiatives
- Moderate-High Risk
- Key Data Generation
- Tech Push; Some Tech Pull
- High Costs
- Preliminary Applications List Emerging
- Government Funding May Be Critical
- No Significant Application Quantities
- Potential Applications Influencing Development Activities
- Sufficient Interest to Keep Alive

STAGE 3: SPECIALTY MATERIAL

CHARACTERISTICS

- Significant Quantities Being Used
- Databases Continue to Be Populated
- Stable Materials/Stable Processes
- Production Environment
- Affordable Value
- Tech Pull
- Low Risk
- Vendor Data Sheets
- Little M, Some P (Affordability)
- Multiple Markets Emerging
- Repair Methods in Place
- No HazMat Issues

STAGE 4: COMMODITY MATERIAL

CHARACTERISTICS

- Very Large Quantities Being Produced
- Stable Material/Stable Process
- Major Databases
- Routine Usage in Many Commercial Sectors
- No M&P
- Affordable
- Readily Accessible to the Public

A MATERIAL LIFE CYCLE

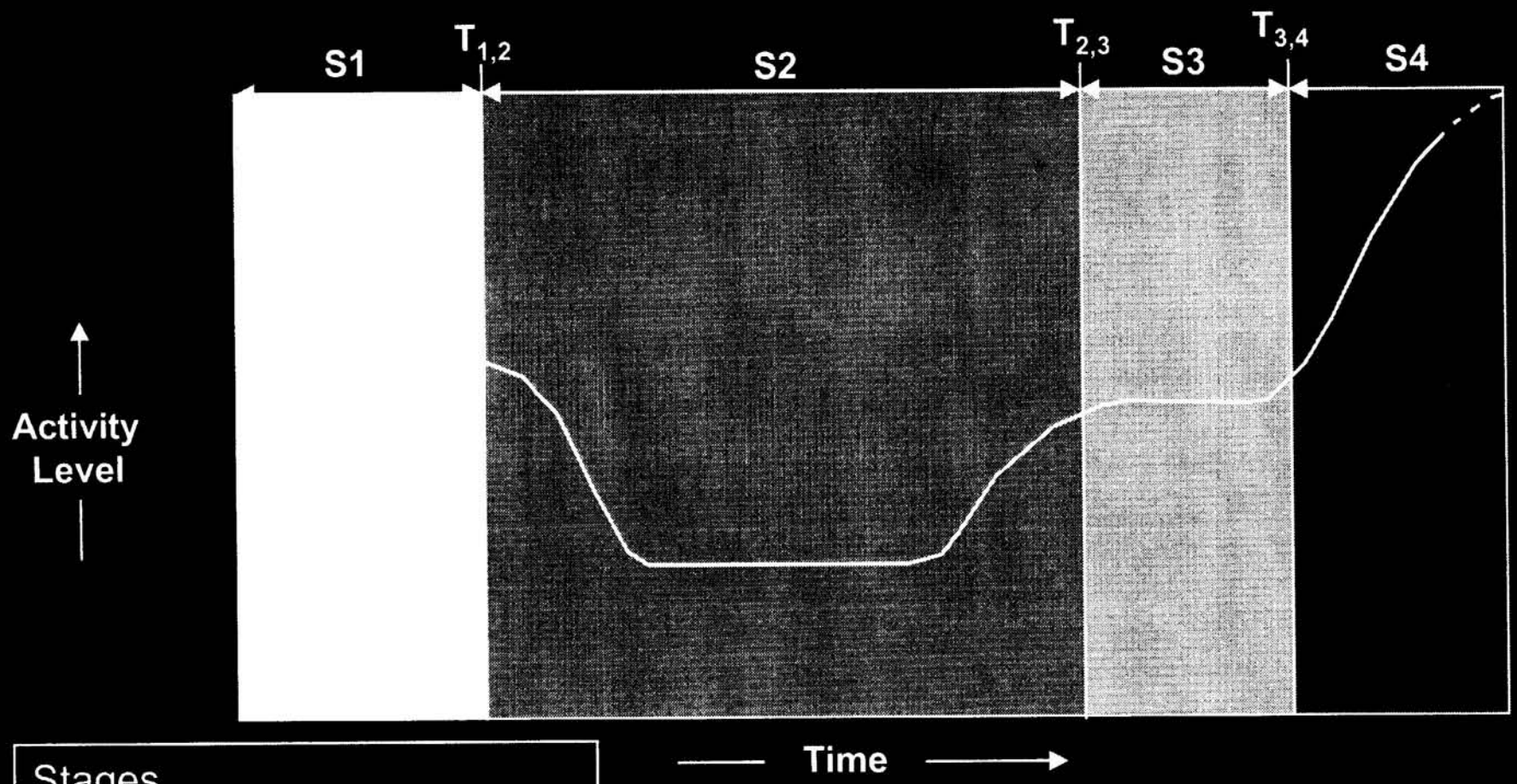

Stages
- 1 = Revolutionary
- 2 = Emerging
- 3 = Specialty Material

ac/rp/00372-8

TRANSITION FROM STAGE 1 TO STAGE 2

REQUIREMENTS

- Some Level of Properties Demonstrated
- Processable at Coupon Level
- Laboratory Scale-up Demonstrated
- Potential Applications Assessed
- No HazMat Issues
- Affordability Potential
- Sufficient Government/Industry Interest
- Positive Risk Assessment

TRANSITION FROM STAGE 2 TO STAGE 3

REQUIREMENTS

- Plant Level Scale-up Demonstrated
- Engineering Database
- Properties Continue to Look Good
- Processing of Structures Developed
- Affordability Moving in Right Direction
- Stable Materials/Stable Processes
- No "Surprises"
- Good Value
- Customer Demand

TRANSITION FROM STAGE 3 TO STAGE 4

REQUIREMENTS

- Plant Level Production Demonstrated
- Major Databases Developed
- Affordability Demonstrated
- Stable Materials/Stable Processes
- Strong Customer Demand
- "Routine"
- Large Markets Pull

AEROSPACE MATERIAL LIFE CYCLE

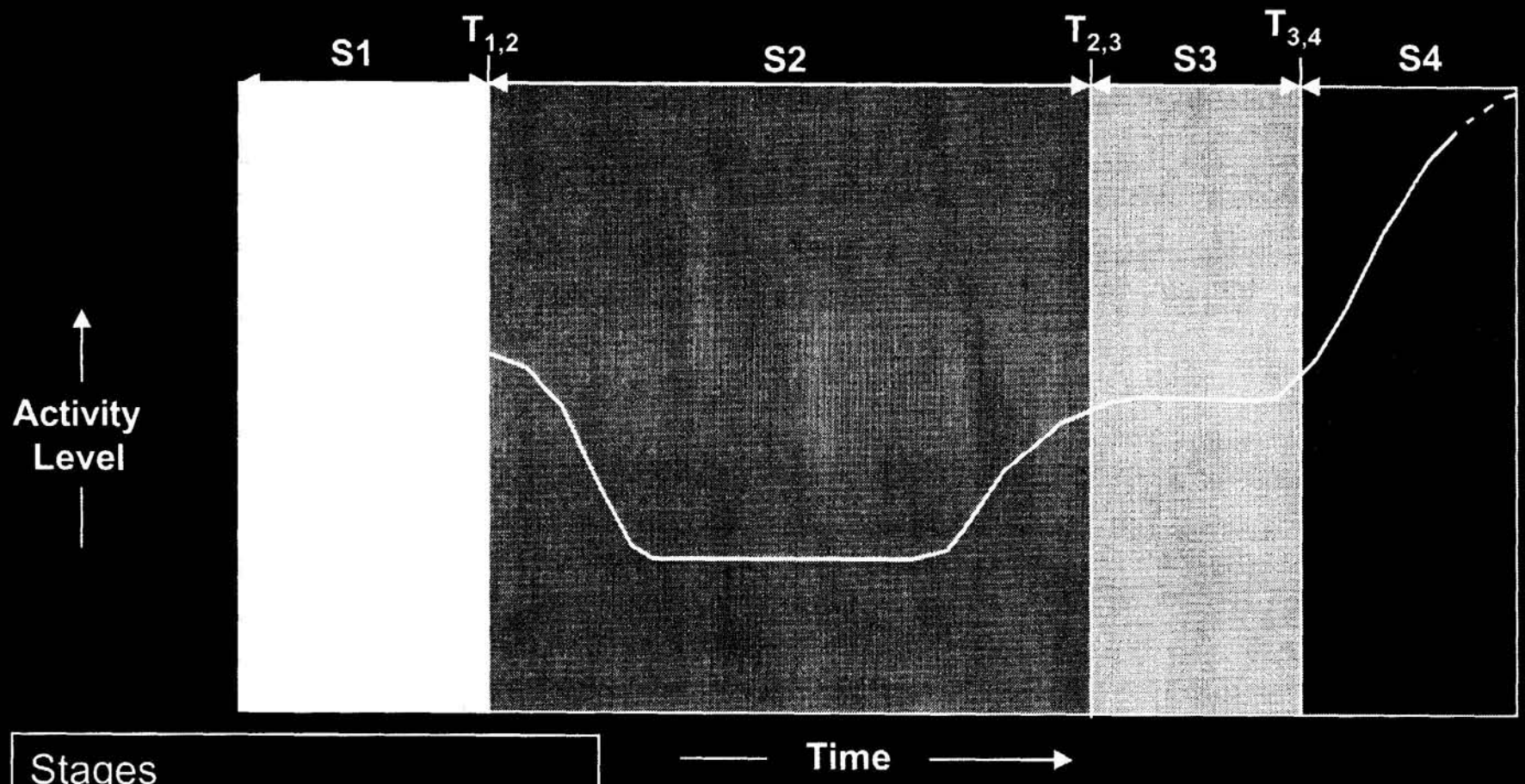

Stages
- 1 = Revolutionary
- 2 = Emerging
- 3 = Specialty Material

ac/rp/00372-12

AEROSPACE M&P CHARACTERISTICS

- Traditionally Performance Driven
- Characterized by Innovation
- Limited Markets (Niche Materials)
- Time Interval to Large Markets Can be Large (Relatively Long Life Cycles)
- Major Risk Taking
- Batch Processing
- "Craft" Processing
- Breakthrough Processing
- Data "Rules"
- May Not Make It Beyond Stage 3

AEROSPACE M&P EXAMPLES

- Advanced Composites
  - B
  - C
  - S-glass
  - B/Ep
  - Gr/Ep
  - C/C
  - MMCs
  - DRA
  - CMCs
- Mechanics of Composite Materials
- Electronic Materials
  - GaAs
  - SiC
- Advanced Metals & Processing
  - Ti
  - Al-Li
  - Superalloys
  - Superplastic Forming
  - TiAl
- Nonstructural Materials
  - Coatings
  - Sealants
  - Deposition Processes

ADVANCED COMPOSITES LIFE CYCLE

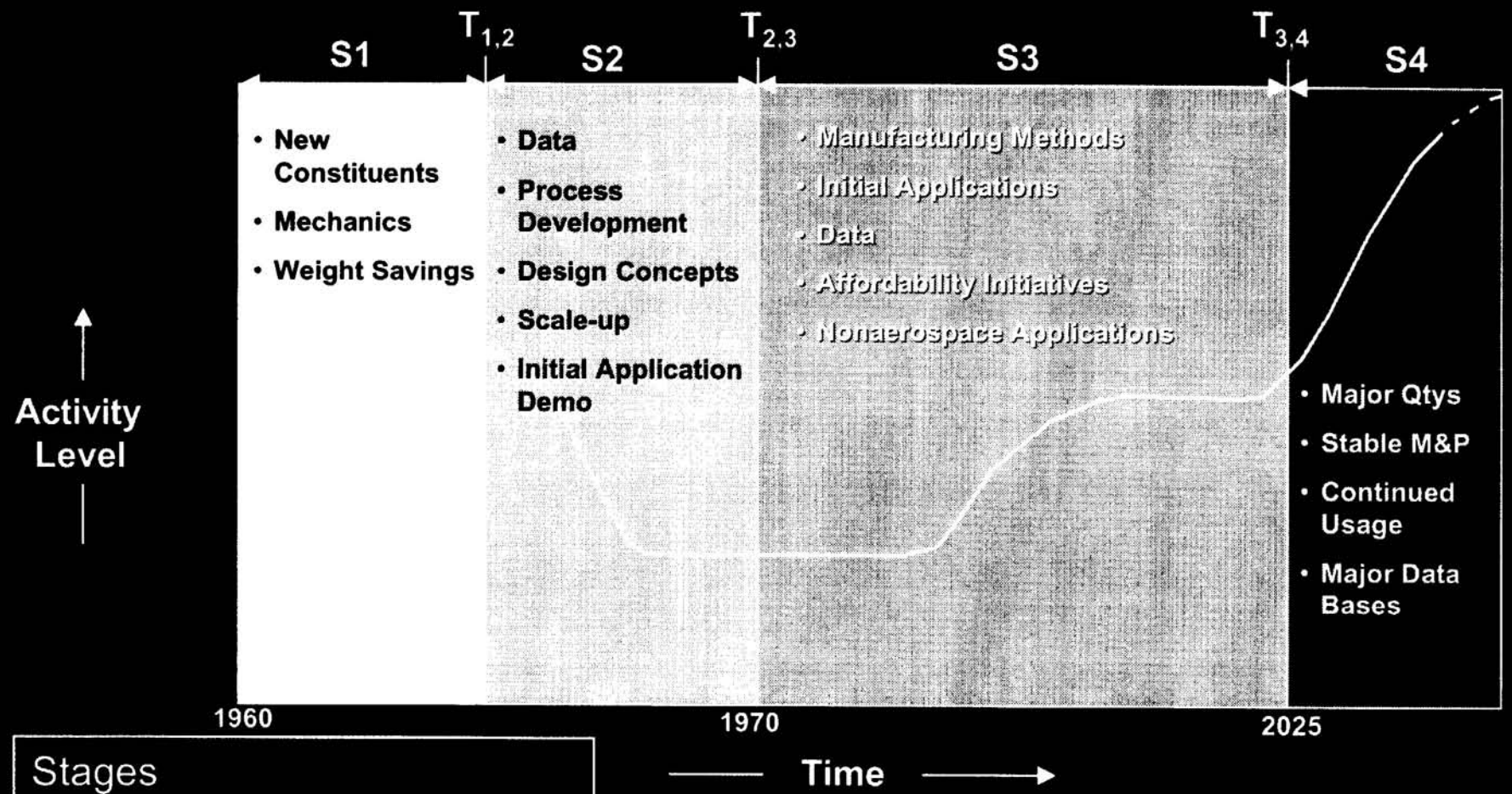

Stages
1 = Revolutionary
2 = Evolutionary
3 = Specialty Material

ac/rp/00372-15

STAGES OF CURRENT AEROSPACE M&P

- Stage 1
  - Compliant Substrates
  - MEMs M&P
  - Biologically-derived M&P
  - Computationally-derived M&P
  - Nano-tailored Materials

- Stage 2
  - Carbon-Carbon
  - SiC
  - TMC's
  - PLD
  - CMC's

- Stage 3
  - GaAs
  - Graphite Composites
  - DRA
  - Carbon-Carbon

- Stage 4
  - Aluminum Alloys
  - Glass Fiber Composites
  - Silicon
  - Urethane Coatings
  - GaAs

TRENDS IMPACTING THE AEROSPACE M&P LIFE CYCLE

- Military-Unique Industrial Base Will Continue to Decrease
- Military-Unique Requirements Will Continue to be Very Demanding and Push Envelope
- Reliance on Commercial Industrial Base Will Continue to Increase
- Commercial Requirements Not Likely to Push Envelope
- Commercial Sector Continues to be Near Term Oriented
- Computational Capabilities Will Grow Exponentially
- Emphasis on Reducing Cycle Times Will Be Strong
- Importance of Strategic Partnerships Will Continue to Grow
- Emphasis on Transitioning (Even Accelerating) M&P Already in the Life Cycle
- Emphasis on Affordability as Key to Transition will Continue
- Potential Loss of Key Talent to other Technical Areas will Continue

AEROSPACE MATERIAL LIFE CYCLE MAJOR CONCERN

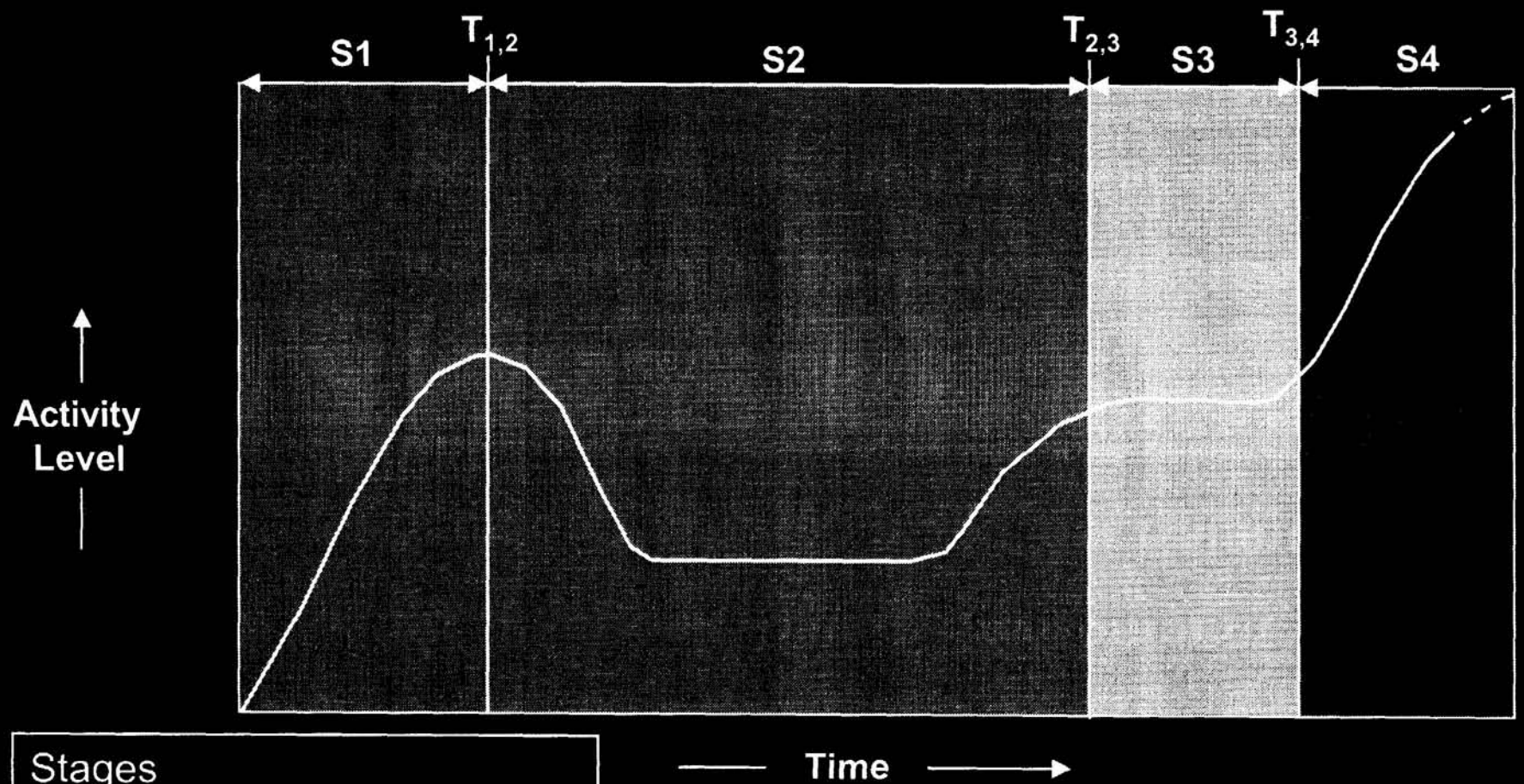

Stages
- 1 = Revolutionary
- 2 = Emerging
- 3 = Specialty Material

ac/rp/00372-18

KEY AEROSPACE MATERIALS & PROCESSES CHALLENGES

- Keeping the "Left Side" of the Cycle Strong
- "Risk Taking" in a Risk Averse Environment
- Keeping Focus on Performance - Cost Balance (Affordability)
- Decoupling Cost and Quantity
- Orchestrating "Win-Win" Strategic Partnerships
- Reducing R&D Cycle Times Without Sacrificing Quality
- Attracting Top Talent

AEROSPACE REVOLUTIONARY OPPORTUNITY AREAS (Circa 1965-85)

- Rare Earth Magnets
- Graphite/Epoxy Composites
- Carbon-Carbon Composites
- Gallium Arsenide Substrates
- Ti/Ni Aluminides
- Refractory Alloys
- Integral Fuel Tank Sealants

THE POTENTIAL OF ADVANCED COMPOSITE MATERIALS

High Performance Fibers
Reinforcing
High Performance Plastics

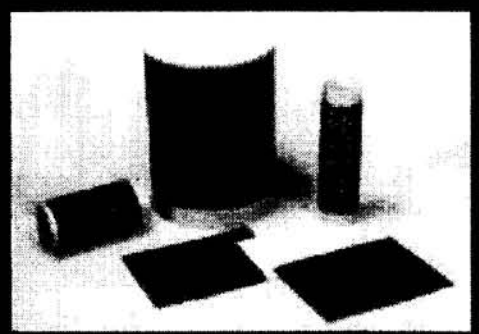

High Strength-to-Weight
High Stiffness-to-Weight
Tailorable Conductivity
Fatigue Resistance
Corrosion Resistance
Dimensional Control
Formable to complex shapes

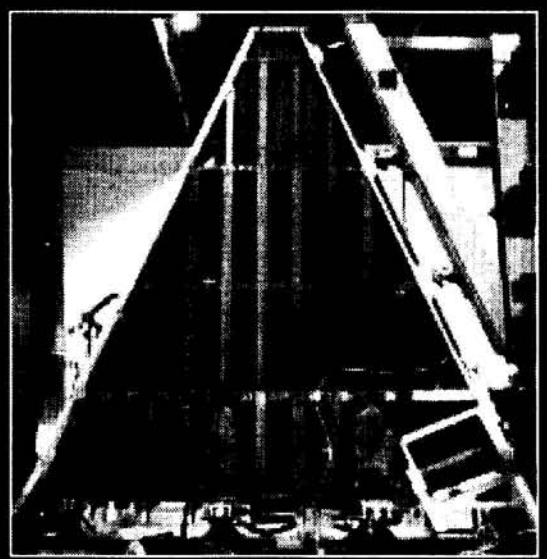

Higher Structural Efficiency
Lower Weight
Integrated Structures
Innovative Design Concepts
Environmental Durability

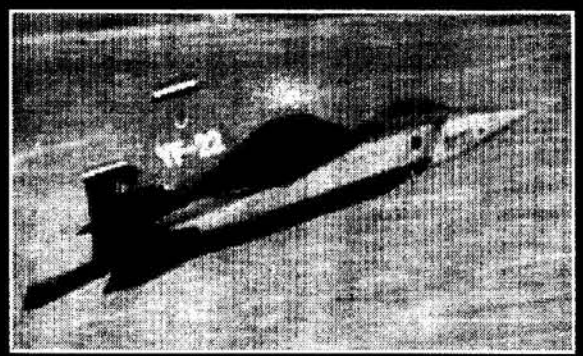

Increased Range
Increased Payload
Increased Manueverability
Lower Life Cycle Cost
Increased Survivability

REVOLUTIONARY OPPORTUNITY AREAS

- Multi-functional Materials
- Self-inspection Capabilities
- Nanostructured Materials
- Bioengineering
- Computationally-derived Structures
- Virtual Prototyping of M&P
- Virtual Databases
- Accelerated Insertion of Materials
- Combinatorial Materials Science
- Lean Research

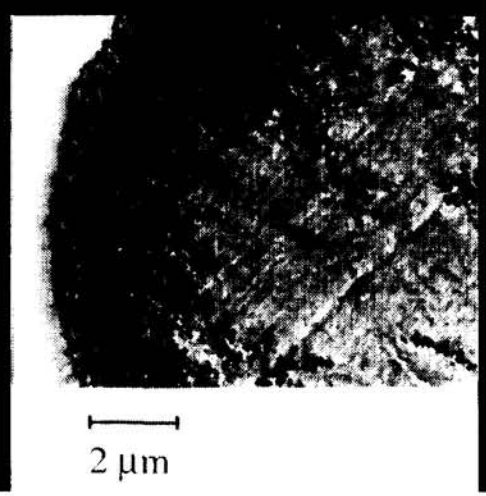

	Modulus (GPa)	Strength (MPa)	Strain (%)	Conductivity (S/cm)
Polymer Fiber	95.2	900	1.98	**10^{-12}-10^{-14}**
Nanostructured Fiber	51.8	1050	3.29	**2.5×10^{4}**
Metal Fiber (Ag)	76	55	60	**6.3×10^{5}**

50% lighter and 200x stronger than current signal lines

REVOLUTIONARY OPPORTUNITY

High Performance, Nanostructured Conducting Fibers

IMPACT

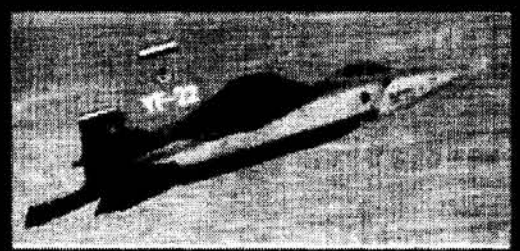

- Light Weight Signal Fibers
- Embedded Sensors
- Self Diagnostic Structural Component
- EM Shielding

Nanostructured Materials

Aerospace

Human Factors

Space

- Interactive Textiles
- Flexible Signal Routing
- Smart Fabrics

- Light Weight Signal Fibers
- Ultra High Performance Space Tethers
- Anti-Charging Panels
- Self Diagnostic Structural Components
- EM Shielding

ac/rp/00372-24

SUMMARY

- The Life Cycle of a Material Can Be Charted in Terms of Stages and Transitions
- Understanding This Life Cycle can be used to Manage M&P Strategies and Investments
- Key Trends Will Impact This Cycle
- Greatest Challenges in Revolutionary and Emerging Stages
- New Partnerships, Tools and M&P Processes Will Be Key to Meeting the Challenges

ML TECHNOLOGY PROGRAM
(CIRCA 1985)

Near-Term

- Retirement-for-Cause
- Stealth Materials
- Superplastic Forming
- Aluminum-Lithium
- 3-D Carbon-Carbon
- Mid-wave IR Sensor Mtls
- Thermal Control Coatings
- Thermoplastic Composites
- Composites Processing

- F-16
- DSP
- Space Bus Structure
- Pen Aids
- Space Antennas
- F117

Mid-Term

- Computed Tomography
- Gen II Stealth Materials
- Single-Line Laser Eye Prot
- PAO Dielectric Coolant
- HgCdTe
- SiC Ceramics
- Oxidation Resistant Alloys
- Composite Repair of Metals
- Composite Filament Winding
- Kapton Wire Insulation

- ALCs
- F-15
- C-141
- Sensors
- Titan/Delta
- F117
- B-2
- F-16
- A-10
- GTEs
- ATF

Far-Term

- Automated Ultrasonic NDI
- Mult-Line Laser Protection
- Hi Temp Super Conductivity
- Hi Temp Ceramics
- Ti/Ni Aluminides
- Large Integrated Structures
- Affordability Initiatives
- Gallium Arsenide Substrates
- Nonflam Hydraulic Fluids

- C-141
- F-22
- ALCs
- Turbine Engines
- IHPTET
- F119
- Sat Bus Str

ac/rp/00372-26

ML TECHNOLOGY PROGRAM
(CIRCA 1965)

Near-Term

- Aluminum
- Fiberglass
- Failure Analysis Methods
- Silicon Micro-circuits
- Ceramic Armor
- Ablative Materials
- Rain Erosion Coatings

- XB-70
- F-4
- Radomes
- ICBMs
- X-15
- Helicopters
- Turbine Engines
- RVs

Mid-Term

- 6-4 Titanium
- Boron/Epoxy Composites
- Aluminum Alloys
- Ferromagnetics
- Superalloys
- High Strength Steels
- Carbon-Carbon
- Composite RV Structures

- F-15
- Landing Gears
- RV Nosetips
- RV Heatshields
- A-4
- F-4

Far-Term

- NDI Methodolgies
- Early Stealth Materials
- Rare Earth Magnets
- Refractory Alloys
- Carbon-Carbon Processing
- Graphite/Epoxy Composites
- Integral Fuel Tank Sealants
- Mechanics of Materials

- F111
- F-16
- F-15
- Turbine Engines
- ICBMs
- T-39
- CH-47

ac/rp/00372-27

ML TECHNOLOGY PROGRAM
CURRENT EMPHASIS

Near-Term

- Multi-Line Laser Protection
- Composites Affordability
- Portable NDE
- CMC Brakes
- Long Wave IR Sensor Mtls
- Longer Life Coatings
- HCF Laser Shock Peening
- IR Coatings
- Aging Aircraft Inspn/Repair

- AFSOCOM
- JSF
- F-22
- ALCs
- DSP
- LACIRCM
- C-17
- Sensors
- SBIRS

Mid-Term

- CAI (Phase III)
- Agile Laser Protection (I)
- Durable Coatings
- Laser-Based Ultrasonic NDE
- SiC/GaN Hi Temp Device Mtl
- Metals Affordability Initiative
- LO Maintainability
- Aging Aircraft Inspn/Repair
- Engine Rotor Life Extension

- JSF
- ABL
- JDAM
- F119
- IHPRPT
- C-135
- UCAV
- F120
- HSI
- F-22
- IHPTET

Far-Term

- Bioengineered Materials
- Nano-Tailoring
- Computational Mtls Science
- Polymer Membranes
- Advd Thermal Protection
- Paint-for-Life
- Vehicle Health Monitoring
- Agile LEP (II)
- MEMs M&P

- SBR
- SBIRS
- UAVs
- Microsats
- SOV
- MSP
- ALCs
- Large Deployables
- JSF

ac/rp/00372-28

ADVANCED COMPOSITES CHANGING EMPHASIS

2020

2010

2000

1990

1980

1970

- WEIGHT

- WEIGHT
- DAMAGE TOLERANCE

- WEIGHT
- DAMAGE TOLERANCE
- LOW OBSERVABLE

- WEIGHT
- DAMAGE TOLERANCE
- LOW OBSERVABLE
- ***AFFORDABILITY***

ac/rp/00372-29

STAGE 1: REVOLUTIONARY

21st Century Characteristics

- Reduced Levels Initially
- Growth Later
- All Materials Classes
- Government Funding Vital
- Affordability-Driven From Start
- Emphasis on Lean Processes/Methodologies
- New Transition Strategies
- New Tools

SCALE OF MATERIALS AND PROCESSES REVOLUTION

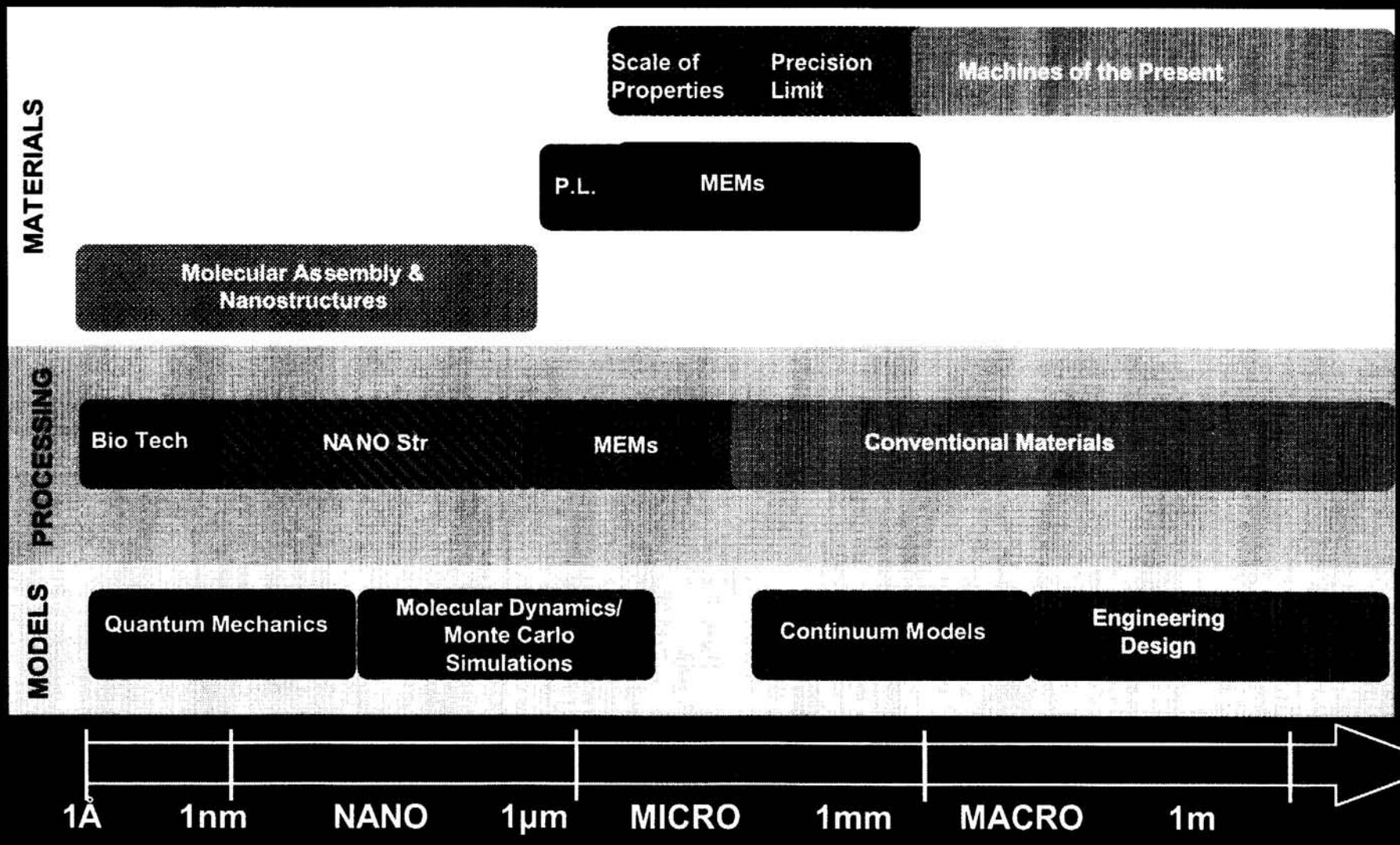

ac/rp/00372-31

STAGE 2: EMERGING

21st Century Characteristics

- Government Funding Vital
- Commercial Interest Vital
- Reduced Cycle Times
- New Strategies Will be Employed
- New Tools Will Be Employed
- Affordability a Key Driver
- Less Risk Taking

Advanced Space Flight and Environmental Concerns

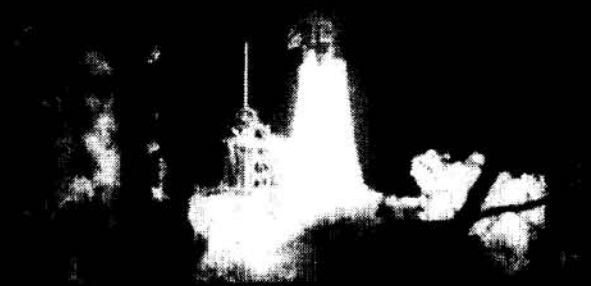

Dr. Ann Whitaker
NASA/MSFC
Deputy Director, Science Directorate

Environmental Challenges for Aerospace Industry

- Clean Air Act Amendments of 1990 (CAAA) presented new challenges for Aerospace Industry
  - Regulation of Ozone Depleting Chemicals (ODCs), Hazardous Air Pollutants, Volatile Organic Compounds (VOCs)
  - Acceleration of U.S. production ban of ODCs from 1/2000 to 1/1996
- Overwhelming environmental impact on traditional methodologies for manufacturing aerospace systems and vehicles

NASA Accepted the Challenge

- NASA Administrator, Mr. Daniel Goldin, established the NASA Operational Environment Team (NOET) in September 1992
  - Emphasis on development, test, production, and use of NASA's aerospace flight hardware
- NOET executed numerous technical forums
  - NASA Programs, Industry, Academia and Federal Agencies exchanged "lessons learned" on environmentally - driven materials replacement technology
- NOET continues to proactively serve as a champion of the "operational environment"

Examples of previous replacement activities

MARSHALL SPACE FLIGHT CENTER

Space Shuttle Environmental Replacement Technology

Examples of Previous Activities

Activity	NASA	Contractor				
Targeted Chemicals		Boeing-MDA	Lockheed Martin	Rocketdyne	Thiokol	UTC
Asbestos	IC				IC	
Aliphatic Glycidyl Ether (AGE)	T*					T*
Cadmium Compounds		PL		BR		
Carbon Tetrachloride				LA*		
Chlorofluorocarbons	LL, NVR	R*, DG	BA*, FC*	BA*, NVR	DG*, FC*	BA*, FC*
Chromium Lead Compounds			PR	A*, P*	S	A, P, S
Cyanides						AD
Dichloromethane (Methylene Chloride)	PS, T*		CA*, PS*			IC
Halons		F/S*				
Hydrazine						PR
Methylene Chloride						
Methylene Dianiline	AD					AD
Methyl Ethyl Ketone (MEK)			CA*			FC*, P
Perchloroethylene	T*			DW*	CA	IC, P
Toluene						FC, P
Trichloroethane (Methyl Chloroform, TCA)	DG*			DG*, NVR*	DG*, P*	FC*, P*
Trichloroethylene			DG, NVR	F		
Xylenes						P, AD
Alternate Propulsion	H		H	H	H	H
Cleaner Propellants	SRCS				SRCS	SRCS

* Completed Tasks

Legend

A	Anodizing
AD	Adhesives
BA	Blowing Agent
BR	Brazing Alloys
CA	Cleaning Agent
DG	Degreasing
DW	Dewaxing
F	Flushing
FC	Fine Cleaning
FS	Fuel Source
F/S	Fire Suppressant
IC	Insulating Compositions
LA	Late Analysis
LL	Long-Life Bearings
NVR	Nonvolatile Residue Analysis
PC	Precision Cleaning
P	Paints
PL	Plating
PR	Primers
PS	Paint Stripping
R	Refrigerant
S	Sealants
T	TPS
H	Hybrids
SRCS	Solid Rocket Combustion Simulator

NASA Assessed the Impact

- NASA's ODC usage in 1992 was 3 million pounds
  - Primarily Chlorofluorocarbons (CFCs) and Trichloroethane (TCA) for manufacture of programmatic hardware
- NASA's ODC usage decreased 87% by 1996
  - ODC usage in 1996 was 4[illegible]00 pounds
- Decrease accomplished [illegible] implementation of environmentally- [illegible]rials and processes
- NASA currently u[illegible]an 7[illegible] pounds/year fo[illegible]re of [illegible] hardware and [illegible]
  - Critical require[illegible]he Space Shuttle Transportation System

NASA's Teaming Successes

- Environmental challenges provided impetus for NASA to team with other Federal Agencies
  - Environmental Protection Agency (EPA)
  - Department of Defense (DoD)
- Interagency teaming resulted in collaborative working relationships that benefited the aerospace community
  - Cost Savings, Data Sharing and Technology Transfer
  - Rulemaking Process: Technically sound, Economically feasible and Environmentally friendly
- Teaming within NASA Centers and NASA programs resulted in resource savings and increasingly robust, advanced aerospace systems

Resulting Efforts and Studies

- NASA/EPA/DoD Interagency Depainting Study
- Non-ODC Surface Cleaning of Advanced Aerospace Systems
- Non-ODC Instrumentation for Cleanliness Verification
- 2nd Generation Blowing Agent for Thermal Protection System on External Tank
- Wire Arc Sprayed Aluminum Coatings
- Hot Oil Dewaxing
- Ultrasonic Cleaning
- Aerospace Manufacturing and Rework: National Emission Standards for Hazardous Air Pollutants (NESHAP)

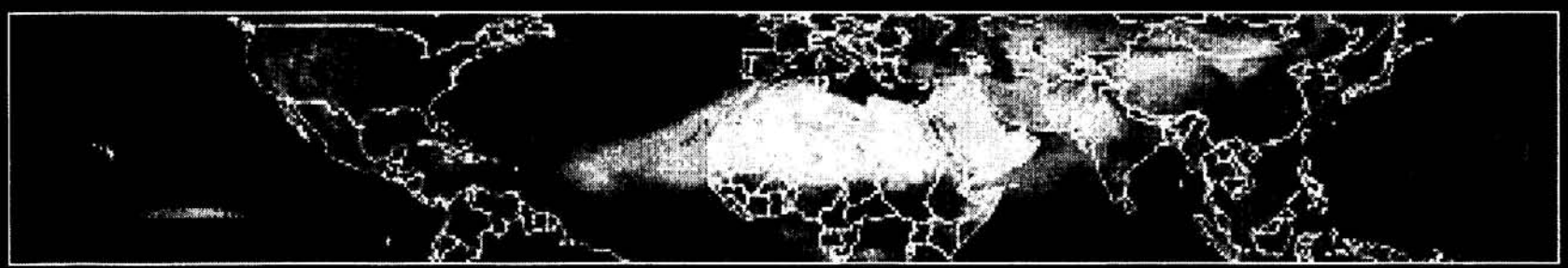

Manifestation of Environmental Challenges

- Manifestation of environmental challenges
  - Materials, Processes & Manufacturing
- Materials subtleties have surfaced in some environmentally - driven materials replacement technology
  - Decreased strength of materials
  - Post-flight anomalies
  - Consideration of synergistic effects of materials replacement
  - Performance of materials

Current Challenges

- Environmental challenges of new millennium for the manufacture of advanced aerospace flight systems
  - Development of 3rd Generation Blowing Agent
  - Elimination of TCA Rubber Activation & Cleaning
  - Reduction of Chromium in Primers & Conversion Coatings
  - Search for Better Cleaning Verification Solvents
  - Development of Low VOC Coatings

Future Environmental Concerns

- **Approximately 35 out of 150 NESHAPs potentially impact the materials, processes and manufacture of advanced aerospace flight systems**
  - Rocket Engine Test Firing
  - Paint Stripping Operations
  - Miscellaneous Organic Chemical Production & Process Usages
- **Increasing environmentally - driven materials obsolescence as suppliers comply with regulations**
  - Materials unavailability for advanced aerospace systems
  - Different performance characteristics of reformulated materials
  - Unexpected formulation change of material

Conclusions

- **Aerospace industry has conquered numerous environmental challenges during the last decade**
- **Aerospace industry of today has evolved due in part to the environmental challenges**
  - stronger
  - more robust
  - pushing limits of technology – materials and manufacturing
  - performing "cutting edge" engineering

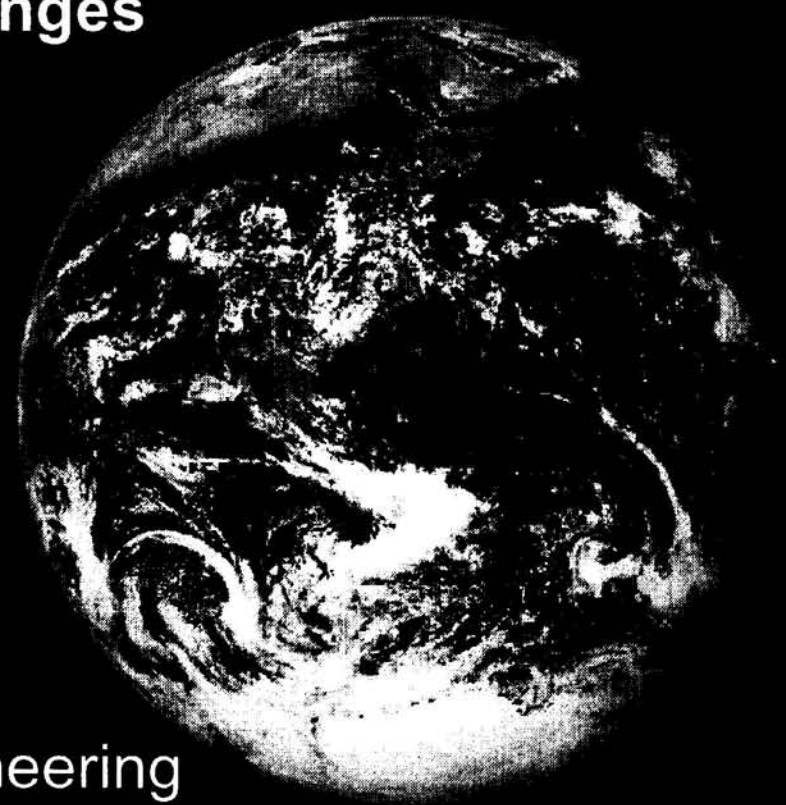

- **Aerospace Industry is viable and successful because of your commitment and contributions**

IN/23

Nonflammable, Nonaqueous, Low Atmospheric Impact, High Performance Cleaning Solvents

Patrick M. Dhooge, Suzanne M. Glass, and Jonathan S. Nimitz
Environmental Technology and Education Center (ETEC)
4500-B Hawkins St. NE
Albuquerque, NM 87109-4517
Phone: (505) 345-2707
http://www.etec-nm.com
pdhooge@etec-nm.com jnimitz@etec-nm.com

INTRODUCTION

For many years, chlorofluorocarbon (CFC) and chlorocarbon solvents have played an important part in aerospace operations. These solvents found extensive use as cleaning and analysis [EPA] solvents in precision and critical cleaning. However, CFCs and chlorocarbon solvents have deleterious effects on the ozone layer, are relatively strong greenhouse gases, and some are suspect or known carcinogens. Because of their ozone-depletion potential (ODP), the Montreal Protocol and its amendments, as well as other environmental regulations, have resulted in the phaseout of CFC-113 and 1,1,1-trichloroethane (TCA). Although alternatives have been recommended, they do not perform as well as the original solvents. In addition, some analyses, such as the infrared analysis of extracted hydrocarbons, cannot be performed with the substitute solvents that contain C-H bonds.

CFC-113 solvent has been used for many critical aerospace applications. CFC-113, also known as Freon® TF, has been used extensively in NASA's cleaning facilities for precision and critical cleaning, in particular the final rinsing in Class 100 areas, with gas chromatography analysis of rinse residue. While some cleaning can be accomplished by other processes, there are certain critical applications where CFC-113 or a similar solvent is highly cost-effective and ensures safety. Oxygen system components are one example where a solvent compatible with oxygen and capable of removing fluorocarbon grease is needed. Electronic components and precision mechanical components can also be damaged by aggressive cleaning solvents.

A number of alternative cleaning processes and solvents have been promoted in the last few years.

Supercritical carbon dioxide can provide excellent cleaning, but has the drawbacks that the high-pressure systems used are expensive and limited in size. The cleanliness obtained with supercritical CO_2 depends strongly on the pressure and temperature of the system, so these parameters must be closely controlled. In addition, the rapid temperature and pressure changes may damage structures and affect components.

Many conventional solvents (e.g., hydrocarbons) are effective cleaners but are flammable, not compatible with oxygen, and require special precautions.

Ethyl lactate has been developed as an effective, zero ODP, low GWP, biodegradable, low toxicity, solvent that can be made from renewable resources. However, its boiling point and

other physical properties are not suitable for cleaning many components and assemblies, as it evaporates too slowly and can become entrapped in small spaces. In addition, it is not compatible with oxygen.

Isopropyl alcohol (IPA) can be used in some cleaning, but engineering and safety measures are needed to minimize flammability risk. As a result, systems designed for IPA are expensive (on the order of $100,000). In addition, large volumes of IPA are often needed as final rinse and dry, generating large volumes of solvent waste.

Hydrofluorocarbons (HFCs) are nonflammable, have zero ODP and low toxicity, but they also have poor solvency and moderately high GWP. Some blends containing HFCs are under investigation.

Hydrofluoroethers (HFEs) have recently been introduced by 3M as cleaning solvents. HFEs possess the attractive properties of some solvency for oils and greases, low toxicity, reasonable cost, no ozone depletion, and modest global warming. However, their performance for many applications has had to be augmented by addition of better solvents such as dichloroethylene, which puts them back in the chlorinated solvent category.

One alternative solvent that is being investigated heavily and used in some applications is 1-bromopropane (EnSolv® and similar products). This solvent has good cleaning ability, relatively fast evaporation, is not flammable, and can be used in some precision cleaning applications. However, it is not compatible with oxygen, and there have been some reports of toxicity from exposure to 1-bromopropane. Haloalkanes also tend to be carcinogens.

Volatile methyl siloxane (VMS) solvents have been developed by Dow Corning. These compounds show promise as nonflammable (but combustible) cleaning solvents with good environmental properties. However, they are not compatible with oxygen and have relatively high boiling points and low volatilities, thus requiring longer drying times.

Plasma cleaning is being developed as a solvent-less process, but it requires sophisticated equipment and is not suitable for all materials.

Iodofluorocarbon (IFC) Solvents

Iodofluorocarbons (IFCs) were identified by Jon Nimitz and Lance Lankford as potentially attractive nonflammable, nonaqueous solvents for replacement of CFC and chlorocarbon solvents. The 3-carbon to 6-carbon IFCs containing one iodine atom have low boiling points, high volatilities, low viscosities, and low surface tension, which make them attractive candidates as alternative solvents. In addition, they have essentially zero ODP (<0.0025), extremely low global warming potential (GWP), acceptable toxicity, and good thermal stability. They are chemically similar enough to chlorofluorocarbon and chlorocarbon solvents that they also promised to have good soil removal abilities.

Although IFC solvents appeared to have much promise, there were a number of issues. There were little or no toxicity, stability, biodegradability, and compatibility data available on the compounds. For oxygen system cleaning, compatibility with liquid oxygen needed to be

determined. Atmospheric lifetime had to be calculated to obtain a good estimate of ODP and GWP. Cleaning abilities compared to CFC-113 and other solvents had to be established, as well as ability to purify and reuse the IFC solvent. Perhaps most importantly, since the IFCs are not bulk commercial products, a low cost synthetic route had to be identified.

From 1995 to 1999, in projects sponsored by the Air Force Research Laboratory and NASA, ETEC developed two new solvents, Ikon® Solvent P and Ikon® Solvent M, based on iodofluorocarbons (IFCs). The Air Force's interest in new solvents was for replacement of CFC-113 in mission-critical aircraft maintenance operations. NASA's interest in the solvents resulted from difficulties replacing CFC-113 in oxygen system cleaning.

RESULTS AND DISCUSSION

Cleaning Ability and Recovery for Reuse

A preliminary series of cleaning tests were performed with the three-carbon, four-carbon, and six-carbon IFCs. Testing was performed based on a procedure developed at Sandia National Laboratories. One by three inch tared coupons of substrate material were intentionally soiled with one of six representative soils: the three perfluorinated greases Braycote® 601 EF, Krytox® 240, and Tribolube® 16; Amoco Rykon® Grease No. 2EP (a hydrocarbon grease); Dow-Corning DC-55M (a silicone grease); and Royco 782 Superclean Hydraulic Fluid MIL-H-83282 (a fire-resistant hydraulic fluid containing phosphate esters). Soiling levels were from 1.0 to 5.0 g/ft^2. Each coupon was weighed to measure the amount of soil, then cleaned, air dried, and reweighed to determine soil removal effectiveness. Figure 1 shows some of the results from this testing. Perfluoro-n-butyl iodide ($CF_3CF_2CF_2CF_2I$, 1-C_4F_9I, Ikon® Solvent P), specified hereafter in this paper as PFBI, was identified as the most attractive cleaning solvent from this group, and as can be seen it removes perfluorinated greases significantly faster than CFC-113.

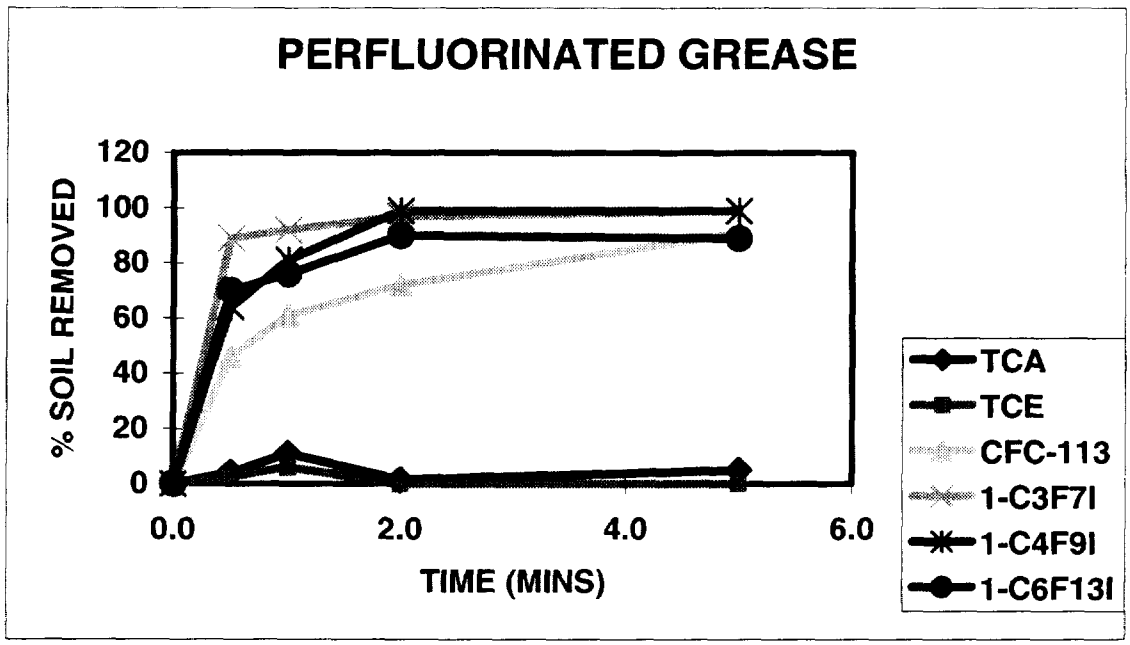

Figure 1. Removal of Perfluorinated Grease by Selected Solvents

Continued cleaning tests examined the ability of the IFC solvents and CFC-113 to remove a soil when the solvent was already saturated with that soil. Braycote® 601, Rykon® Grease No. 2, and Dow-Corning DC-55M were chosen as representative soils. The results of these tests were even more encouraging than the tests with clean solvents. As shown in Figure 2, Ikon Solvent P (PFBI) consistently removed the three soils from 316 stainless steel significantly faster than CFC-113, indicating superior cleaning ability over extended use applications.

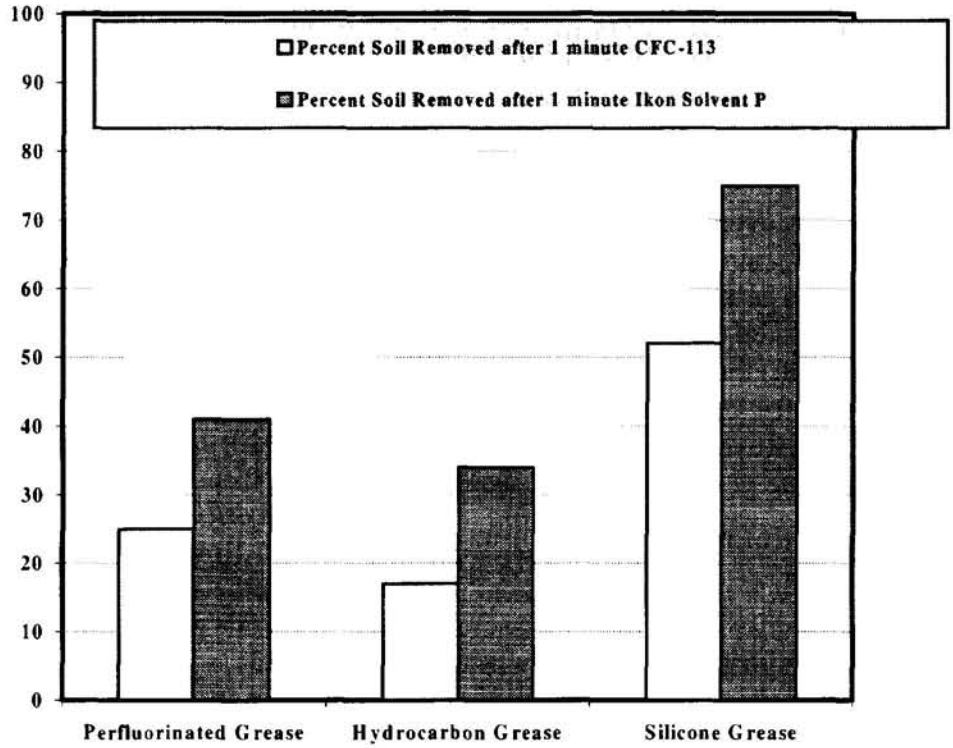

Figure 2. Soil Removal Ability of Soil-Saturated CFC-113 and Soil-Saturated PFBI

Upon determination of our best replacement solvent candidate, it was considered worthwhile to explore testing ability to recover the solvent to reduce its cost of use and the amount of waste solvent generated. This study was performed at the Air Force Research Laboratory/MLBT. They found that used or "dirty" PFBI could easily be distilled to a purity equal to that of new or unused solvent. At least 85-90% of the solvent was recoverable. AFRL/MLBT concluded that PFBI could be recovered easily and economically, greatly reducing the cost of using the solvent and the amount of waste solvent generated.

Compatibility and Stability

Compatibility tests consisted immersing selected materials in PFBI for 10 days at room temperature.

Of nineteen polymers and elastomers tested in this manner for compatibility, only Aflas, silicone rubber, and urethane were found to be incompatible. Compatible polymers included polyacrylic, cyanate ester, graphite/epoxy composite, nylon, phenolic, polyimide, poly (vinyl

chloride) and Teflon. Compatible elastomers included Buna-N, neoprene, EPDM, fluorosilicone, and Viton.

Compatibility tests were conducted with aluminum alloys 2024, 5052, 6061, and 7075T6; stainless steels 303 and 416; titanium; mild steel; cast iron; magnesium; copper; brass; bronze; acid-core solder; plumbing solder; and rosin core solder. PFBI was completely compatible with all metals tested except mild steel. Mild steel showed significant oxidation (rust), which was likely due to air and moisture that were not rigorously excluded, because there is no reaction between iron and PFBI alone that could have formed iron oxide. At the temperatures expected in cleaning operations, PFBI is also compatible with other common solvents, water, and adsorbents.

One indication of the relatively high stability of PFBI is its compatibility with liquid oxygen. This is a harsh test for any solvent, and almost all solvents will react with oxygen under these test conditions. In this test, a sample of the solvent is frozen in a pool of liquid oxygen and struck with a striker to attempt to initiate reaction. CFC-113 passes this test at 72 ft-lbs striking force. Only two out of seventeen samples of PFBI reacted at 72 ft-lbs, and none out of 20 samples at 65 ft-lbs. Thus, PFBI appears to be only slightly more reactive toward oxidation than CFC-113.

The autogenous ignition temperature of PFBI in 100% oxygen at 13.8 Mpa (2000 psia) was measured as 171 - 175°C. This test also reveals excellent stability for PFBI. In fact, PFBI is a known combustion suppressant.

Suppliers package, ship, and store PFBI without any special precautions. During our cleaning tests, PFBI was re-purified by distillation and reused many times without evidence of significant decomposition. PFBI often comes from the supplier with a slight pink color from free iodine in solution, and left out in the sun or under fluorescent lights for an extended period of time it will always develop a pink color from free iodine. The free iodine is a photolysis product from exposure of the solvent to UV light. The amount of iodine produced under these conditions is very small, at most several parts per million, and can easily be removed from the solvent with activated carbon.

Atmospheric Lifetime, ODP, and GWP

The estimated low atmospheric impact of the IFCs is a result of their susceptibility to short wavelength ultraviolet light. The carbon-iodine bond in these compounds is weak enough that UV wavelength photons in sunlight can break it. Breaking the C-I bond begins a decomposition chain that proceeds completely to CO_2, HF, and HI, as the fluorinated free radical from the C-I bond breakage reacts with water to form fluorinated alcohols that are highly unstable and quickly decompose.

Other than their susceptibility to photolysis, normal IFCs containing one iodine atom are stable because the fluorine atoms withdraw electron density from the iodine atom and make it much less reactive. The fluorines also block back-side attack on the iodinated carbon atom.

The atmospheric lifetimes, ODPs, and GWPs of the three-carbon, four-carbon, and six-carbon IFCs were determined by Dr. Don Wuebbles at the Department of Atmospheric Sciences

at the University of Illinois (Urbana-Champaign). Dr. Wuebbles is one of the world's foremost researchers on ODP and GWP. He concluded that the atmospheric lifetimes for these compounds are approximately 2 days. This is extremely short compared to most fluorinated chemicals, which have lifetimes ranging from years to centuries. He concludes that the ODPs of FICs are less than or equal to 0.0025, "much less than is of concern within the U.S. and international guidelines." The GWPs are also extremely small, less than 6 relative to CO_2 for the 20 year time horizon and less than 2 for the 100 and 500 year time horizons. Dr. Wuebbles concluded that "these results imply essentially a negligible effect on future climate from use of 1-C_3F_7I, 1-C_4F_9I, and1-$C_6F_{13}I$."

Toxicity and Biodegradability

Toxicity studies on PFBI were conducted by Huntingdon Life Sciences (HLS).

PFBI was found non-mutagenic in the Ames test and non-clastogenic in the human lymphocyte chromosome aberration test.

Twenty-eight day rat subchronic inhalation (6 hrs per day) exposure tests were performed. Results showed somewhat elevated thyroid hormone levels at 100 ppm exposure; elevated thyroid hormone, triglyceride, and iodide levels in the 1,000 and 10,000 ppm test groups; and some physical effects in the males (low weight and enlarged livers) at 10,000 ppm exposure. A medical expert in thyroid chemistry who has reviewed inhalation test data for the related compound CF_3I has noted that rats are much more sensitive to iodine levels than humans, and concluded that humans should suffer no effects at the recommended average 8-hour exposure level (AEL) of 150 ppmv for CF_3I (Capen). It cannot be stated positively that the same reasoning can be applied to the IFC solvents, but it seems likely.

Cardiac sensitization inhalation tests were performed on PFBI. Many gaseous or volatile hydrocarbons and halocarbons sensitize animal hearts to adrenalin through the inhalation pathway. The possibility of death from heart fibrillation after exposure to a halocarbon was first realized in the 1960s. A standard test was developed at that time to measure the relative cardiac sensitization of compounds. The test uses Beagle dogs that are injected with enough ephinephrine (adrenalin) to be barely under the amount that would cause that dogs' heart to go into fibrillation (this dosage is determined for each individual dog in the test group). After injection, the dogs are exposed to concentrations of the test compound in air. The minimum amount of the compound found to induce heart irregularities is the LOAEL, or Lowest Observable Affect Exposure Limit. The NOAEL, or No Observable Affect Exposure Limit, is the maximum concentration the dog can be exposed to with no affect. This test is quite rigorous, since the dogs are already just below the point of fibrillation due to the very high ephinephrine level, and the test was not originally intended to established exposure limits. It has been estimated that the ephinephrine levels used in this test may be 100 times or more higher than would be seen in even a very frightened test subject (Vinegar). The cardiac sensitization test's relevance is being questioned, but it remains the standard at this time. PFBI had a No Observable Adverse Effects Limit (NOAEL) of 0.4% (4,000 ppm), and a Low Observable Adverse Effects Limit (LOAEL) of 0.6% (6,000 ppm) in this test. PFBI's NOAEL is significantly higher than that of TCA (i.e., it is significantly less cardiac sensitizing than TCA), and only slightly lower than that of trichloroethylene (TCE). Figure 3 shows the comparison graphically.

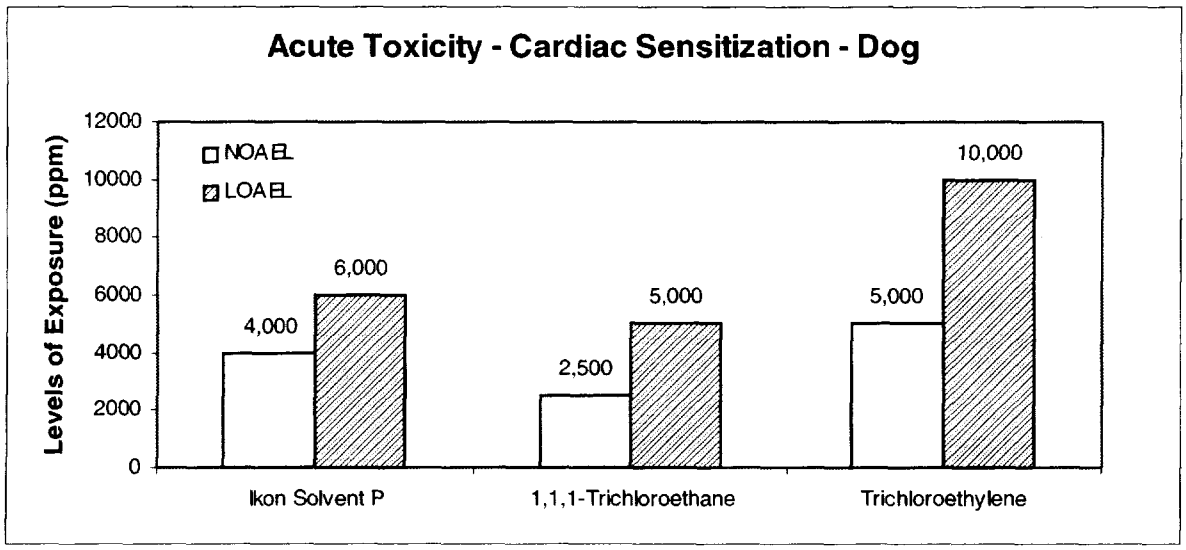

Figure 3. Comparison of Cardiac Sensitization NOAELS and LOAELS for Solvents

The aquatic toxicity of PFBI is considerably greater than for common chlorinated solvents. The 96 hour Fathead minnow LC_{50} was 2.3 ppm by weight for PFBI, compared to 40 ppm by weight for TCE and 53 ppm by weight for TCA.

Biodegradability testing was conducted by HLS in accordance with EEC Methods for Determination of Ecotoxicity Annex to Directive 92/69/EEC (O.J. No. L383A, 29.12.92) Part C, Method 4-E "Determination of Ready Biodegradability Closed Bottle Test" and the OECD Guideline for Testing of Chemicals No. 301D "Ready Biodegradability: Closed Bottle Test." Over 28 days, a mean PFBI concentration of 59 mg/L showed maximum oxygen depletion in the test vessels equivalent to 9% biodegradation, relative to the theoretical oxygen demand. Therefore, PFBI cannot be termed readily biodegradable as the 'pass level' of 60% was not attained. However, PFBI was not found to be inhibitory to activated sewage sludge bacteria under the conditions of this test.

Regulatory Status

PFBI is not a RCRA listed substance, but spent solvents are typically RCRA listed. The value of PFBI and its recoverability make it highly unlikely that spent liquid PFBI would be disposed of as hazardous waste.

For regulatory purposes, a chemical is classified as a volatile organic compound (VOC) if, when released into the air in the presence of sunlight and other common urban air contaminants, its breakdown results in production of higher ozone levels than an equivalent amount of ethane released (the standard). VOC testing on PFBI was conducted by the Environmental Science and Engineering Department at the University of North Carolina at Chapel Hill under the direction of Dr. Harvey Jeffries. The test is conducted on a summer day with high solar irradiance. Shortly before dawn a synthetic mixture simulating urban smog is injected into both of two large, clear plastic chambers, followed by samples of ethane into one chamber and the test substance into the other. The temperature, solar irradiance, and levels of ozone and nitrogen oxides are monitored until after sunset (about 13-hours total for the test). PFBI created more ozone than the ethane, and so would probably not be VOC-exempt, although there is an exclusion for point sources below a certain level of emissions per year.

The U.S. Environmental Protection Agency (EPA)'s Significant New Alternatives Policy (SNAP) program approves replacements for ozone-depleting substances. An application for Ikon® Solvent P has been submitted to EPA.

Occupational Exposure Assessment

Waldemar S. Nelson and Company, Inc. (Nelson) performed an occupational exposure assessment on PFBI. PFBI was compared to trichloroethylene, 1,1,1-trichloroethane, 1,1,2-trichloroethane, and CFC-113 using existing data to assess its relative occupational exposure. Nelson concluded that worker exposure to PFBI needed to be limited to 73 ppmv or less at present to freely substitute PFBI for other solvent chemicals without a potential increased health risk. This assumed the worst case (i.e., maximum continuous exposure level at the TLV) for the solvent, and it was Nelson's opinion that this assumption exaggerated anticipated exposure levels in a modern cleaning facility. Nelson stated, "It is unlikely that the exposure levels at a modern degreasing facility would approach the TLV for the solvent in use. If the real exposure level was far below the TLV, it would be far easier to achieve a level of comfort with the anticipated exposure to IKON-P." Nelson concluded that site-specific exposure information would be needed to evaluate this properly. Personnel protection equipment Nelson recommended for PFBI was similar to that for 1,1,1-trichloroethane and trichloroethylene.

Synthesis, Price, and Availability of the IFC Solvent

One of the greatest barriers to widespread use of IFC-based solvents is their current high cost. At present they are still essentially research chemicals, although PFBI's price continues to decrease and is now at about $60/lb versus over $200/lb several years ago. Successful introduction will require manufacturing PFBI at a sufficiently low cost that its selling price will be competitive with other alternative solvents.

The current method used for manufacturing PFBI is not disclosed in the literature, but we know from published patents and personal communications that PFBI is now made from tetrafluoroethylene. Tetrafluoroethylene ($CF_2=CF_2$) is a relatively inexpensive monomer used in manufacturing Teflon (a polymer of tetrafluoroethylene). Appropriate reactions of tetrafluoroethylene yield pentaiodoethane and higher even-carbon homologs, as shown in Reactions [1] and [2].

$$CF_2=CF_2 + IF_5 \rightarrow CF_3CF_2I \qquad [1]$$

$$CF_3CF_2I + CF_2=CF_2 \rightarrow 1\text{-}C_4F_9I + 1\text{-}C_6F_{13}I + \text{higher homologs} \qquad [2]$$

ETEC personnel identified and evaluated a number of alternative synthetic routes, including the Hunsdiecker reaction (iodination with decarboxylation of a fluorinated carboxylic acid), and alternative gas-phase reactions of several types. It was found that a modification of the gas-phase synthesis of PFBI from tetrafluoroethylene was by far the least expensive synthetic method. The yield reported in the literature is about 90% PFBI. ETEC's chemical engineering personnel prepared a conceptual design for a facility based on this process, producing 5 million pounds of PFBI per year. Equipment costs, materials costs, and operating costs were estimated from the design. Iodine is the principal cost driver in the synthesis. At the present bulk iodine cost of about $22/kg, the estimated cost of PFBI production is $18/kg. Assuming a markup of 25% by the manufacturer, 30% by the distributor, and a royalty of about $2/kg, this gives a retail selling price for PFBI of about $31/kg. This price is competitive with other fluorinated solvents

such as HFE-7100, and PFBI is a much more effective cleaning solvent than HFE-7100. Assuming bulk iodine price drops back to near its historic level, say $11/kg, PFBI could be produced for an estimated $15/kg. Under the same assumptions as above, the retail price of PFBI would be about $26/kg, significantly less than HFE-7100.

The available data indicate that iodine supply for producing PFBI and other IFCs as replacements for CFCs, HCFCs, and halons will not be a problem. Present world production of iodine is approximately 15 million kilograms per year. Currently, iodine prices are near a modern all time high due to China's decision several years ago to iodize their table salt. This decision caught iodine producers by surprise and raised iodine prices. New iodine production facilities are being built. Iodine price should return closer to its historic level of about $11/kg. Proven worldwide reserves of iodine recoverable at less than $15/kg are about 6.4 billion kilograms (Bureau of Mines). In addition, the oceans contain an estimated 34.5 billion kilograms of iodine, part of which can be recovered directly during extraction of chlorine, bromine, or magnesium from seawater, or indirectly by collecting and processing kelp. Seaweeds of the Laminaria family accumulate up to 0.45% iodine on a dry weight basis; before 1959 seaweed represented a major source of iodine. At least one company in China is now producing iodine extracted from seaweed at a quoted price of $23.50/kg. The price of iodine recovered from seaweed should decrease as production volume increases. Cultivation and harvesting of seaweed for iodine and food products such as alginates can create an alternative source of income for coastal peoples, reducing economic pressure to over-fish and providing marine habitat.

CONCLUSIONS

If PFBI is produced in quantity at a reasonable cost, it should be an effective substitute for CFC-113 and chlorinated solvents in a variety of critical cleaning and analytical applications.

ACKNOWLEDGEMENTS

The funding for this work was provided by the U.S. Air Force Research Laboratory/MLBT and NASA Kennedy Space Center. We would like to thank Dr. Edward Snyder of Wright Laboratories and Dr. Jamie Palou of NASA KSC for their valuable technical support during the efforts. We would also like to acknowledge the contribution of Ms. Kirby Olson, who performed many of the cleaning tests.

REFERENCES

Bureau of Mines, Mineral Commodity Summaries 1993, U.S. Department of the Interior, Washington, DC, 1993, pp. 86-87.

Capen, C. C., Letter report to S. Skaggs, Pacific Scientific, Re: Report "90_Day Nose-Only Inhalation Toxicology Study of Trifluoroiodomethane (CF_3I) to Male and Female Fischer 344 Rats," of study conducted by Mantech Environmental Technology, Inc., February 12, 1996.

EPA, Method 413.1 in Methods for Chemical Analysis of Water and Wastes (EPA-600/4-79-020) and also Method 5520B in Standard Methods for The Examination of Water and Wastewater, 18th Edition.

IN/5

Aerospace Applications for AK-225

Kenroh Kitamura, Masaaki Tsuzaki and Stephen Stagliano*

Technology and Process Development Center
Performance Chemicals General Division
Asahi Glass Co., Ltd.
10, Goikaigan, Ichihara-shi, Chiba 290-8566, JAPAN
Phone: +81-436-23-3151, Fax: +81-436-23-3164

* AGA Chemicals, Inc.
2201 Water Ridge Parkway, Suite 400, Charlotte, NC 28217
Phone: 704-357-3631, Fax: 704-357-6308

1. Introduction

HCFC-225 products are environmentally sensible alternatives in a variety of applications to CFC-113, perfluorocarbons (PFCs) and other hydrochlorofluorocarbons with high ODP values such as HCFC-141b. Many azeotrope-like mixtures and blends of AK-225 (a mixture of two isomers, HCFC-225ca ($CF_3CF_2CHCl_2$) and HCFC-225cb ($CClF_2CF_2CHClF$)) and AK-225G (HCFC-225cb) have been commercialized by Asahi Glass[1,2]. These HCFC-225 products are very similar to CFC-113 and its mixtures in physical properties, material compatibilities, and cleaning performance and are widely used in precision cleaning, electronics cleaning and a carrier solvent of fluorinated lubricants and silicones.

HCFC-225 products are thermally stable and non-flammable. They have substantially lower global warming potential (GWP) than PFCs and hydrofluorocarbons and an extremely low ozone depletion potential (ODP). AK-225 and most of HCFC-225 products are recoverable by distillation with no decomposition.

An azeotrope-like mixture of AK-225, ethanol and stabilizers (called AK-225AES) is suitable for many defluxing applications. The mixture of AK-225, ethanol, hydrocarbon and stabilizers (AK-225T) that provides increased solvency was developed to solve a white residue problem which occasionally forms on printed circuit boards cleaned with AK-225AES[3].

A blend of AK-225 and a surfactant (AK-225DH) for displacement drying after aqueous

cleaning and other processes using water was also developed. A few plastics such as acrylic resin and stressed polycarbonate may crack with AK-225. AK-225FPL, a mixture of AK-225 and a fluorinated solvent, was specifically developed for these plastic cleaning applications.

In this paper, fundamental properties and material compatibility of HCFC-225 products and their applications for aerospace related industries such as bearings, precision parts and PCBs will be discussed. Typical cleaning procedures of HCFC-225 products, the toxicological data and the status of regulations will be also described.

2. Fundamental Properties of HCFC-225 Products

Physical properties of HCFC-225 products are shown in Table 1 and 2. The boiling point, surface tension, KB value and latent heat of vaporization are critical properties for cleaning agents. To clean parts without raising their temperature to the point where the temperature sensitive materials are affected is of utmost importance. A boiling point in the range from 40 to 60 °C is suitable. A low surface tension enables a cleaning agent to penetrate into narrow gaps. KB value shows the solvency of a solvent. KB value around 30-40 shows a selective solvency to remove soils such as oil, grease and dirt without damage to materials. Smaller latent heat of vaporization results in less energy consumption for vaporization of a solvent and easier drying. HCFC-225 products have similar properties to those of CFC-113.

Table 3 shows the effect of AK-225 and CFC-113 on 20 kinds of plastics under typical cleaning conditions (at the boiling point for five minutes). The compatibilities of AK-225 are similar to those of CFC-113 except for acrylic resin. There are some cases where AK-225 shows cracking in parts made of polycarbonate that is caused by the residual stress from an injection molding process. Although some kinds of ABS resins are affected by AK-225, most ABS resins are compatible as shown in Table 3. AK-225FPL was developed to solve this issue. It is compatible with acrylic resin, stressed polycarbonate and ABS resin. Concerning AK-225G, the compatibilities are almost identical to those of AK-225.

The effects of AK-225 and CFC-113 on elastomers under boiling point exposure conditions for three days are shown in Table 4. The effects of AK-225 are slightly stronger than those of CFC-113. Gaskets and/or seals used in cleaning equipment should be made of polytetrafluoroethylene, EPDM or chloroprene. Mechanical pump seals in solvent recirculation pumps should be polytetrafluoroethylene. Sealless pumps are ideal.

AK-225 products are compatible with common metals.

Material compatibility can be affected by variations in material manufacturing and it is advisable to recheck critical components under use conditions before a final commitment is made to AK-225 products.

3. Applications of HCFC-225 Products in Precision Cleaning

AK-225 and AK-225G are mainly used in precision cleaning applications. Its cleaning performance is very similar to that of CFC-113. Cleaning procedures consist of immersing a work load into a warm solvent, rinsing or spraying with a cool solvent and drying in a solvent vapor. Figures 1 and 2 show the procedure in typical cleaning equipment.

AK-225 and AK-225G are applied for degreasing and dust removing of precision parts such as coils, relays, connectors, bearings, rocket engines and so on. These parts usually must avoid contact with water and they cannot be easily dried with aqueous, semi-aqueous and hydrocarbon cleaning systems because of their minute and complicated shapes.

Parts for medical equipment which are made of plastics are cleaned well with AK-225, AK-225G or AK-225FPL. The cleaning of the parts is difficult with other solvents due to the compatibility of plastics and requirement of high cleanliness.

Miniature bearings are precision parts requiring size accuracy and high reliability. In the manufacturing process, various processing oils are used for cutting and polishing. After assembling the bearings, the oils should be cleaned completely and an anti-rust agent would be administered simultaneously. AK-225 is used for cleaning and coating of anti-rust agents. The bearings are immersed in AK-225 to completely remove oils. During this process ultrasonic oscillation is sometimes used. They are then immersed in AK-225 and a few percent anti-rust agent solution to coat the surface.

AK-225 is also used to remove a fluorinated grease on bearings for maintenance cleaning. Other cleaning agents including HCFC-141b cannot dissolve the grease.

AK-225 and AK-225G are nonflammable and stable solvents and are compatible with liquid oxygen. It is used to manufacture rocket parts and manned spacecraft. In the steel manufacturing industry, AK-225 is used for maintenance of tubing, containers, valves, gauges and so on.

Systems using liquid oxygen should be cleaned completely. If a small amount of organic contamination remains on the surface, the liquid oxygen can easily ignite because of the strong oxidizing properties of oxygen that supports combustion.

Parts made of ceramic such as IC packages and parts made of sintered metal have very porous surfaces. It is difficult to clean them with an aqueous cleaning process due to the high surface tension of the rinse water. AK-225 has been adopted to remove soils on the their surface because of its very low surface tension, low viscosity, low latent heat of vaporization and high relative evaporation rate.

4. Applications of HCFC-225 Products in Electronics Cleaning

High reliability and durability are required for printed circuit boards (PCBs) installed in automobiles and other high technology equipment including aerospace equipment. Therefore, many are usually coated by resins. The manufacturing process of the PCBs consists of soldering electronic devices, cleaning and coating. It is necessary to clean them in a short time because of the huge number of PCBs for automobiles that are produced.

There are many manufacturers using AK-225AES for defluxing these PCBs. Most of them use fluxes and solder pastes developed for AK-225AES to shorten cleaning time and improve cleaning efficiency.

The cleaning procedure of AK-225AES is the same as that of AK-225 previously described. Usually, tact time for AK-225AES is shorter than that for AK-225. These customers do not clean all PCBs that had cleaned with CFC-113 several years ago. They evaluate the necessity of each cleaning application and use AK-225AES only in applications where it is essential. They also use AK-225AES with recovery and/or distillation equipment to reduce the consumption and solvent emission.

AK-225AES is also used for the defluxing of flexible circuits for printers, hard disk dives and so on. It is difficult to deflux them with aqueous and semi-aqueous cleaners, because flexible circuits are made of polyimide that is not compatible with alkaline and easily absorbs water.

Some fluxes and solder pastes for CFC-113 cause white residue on PCBs when the boards are cleaned with AK-225AES. AK-225T has developed to solve the problem. AK-225T can be used for removing most fluxes and solder pastes on PCBs.

5. Other Applications of HCFC-225 Products

AK-225 is used for refrigeration cycle cleaning where CFC-11 was used. It has also been adopted to verify cleanliness after cleaning in this application as well as others.

AK-225 is used as carrier solvents for silicones which is coated on needles of syringes and of fluorinated lubricants which is coated on hard disks. It is also used as a solvent in chemical reactions.

Aqueous or semi-aqueous cleaning is widely used to remove soils from parts. There are many cases that the drying of parts is difficult or may be the rate-determining step. Ak-225DH is a displacement drying system that can resolve this issue. AK225DH is used in a specially designed vapor degreaser with three or more sumps as shown in Figure 3. The procedure is as follows: wet parts are immersed in the dewatering sump containing boiling AK-225DH. Water adhering to the surface of the parts is separated by the surfactant in AK-225DH. The water rises to the surface of AK-225DH due to the density difference between them. It is necessary to rinse the treated parts with boiling AK-225 to remove the surfactant on the surface. At the end of the rinse, hold parts in the vapor zone of AK-225 to dry them and minimize solvent loss. Upon removal, parts are dry and spot free. AK-225DH is also used to dewater and dry wet parts after metal plating in the manufacturing of pin grid arrays and ball grid arrays.

6. Toxicological Studies

Many kinds of toxicological testing of HCFC-225 were carried out under the consortium of global fluorocarbon manufacturers called the Programme for Alternative Fluorocarbon Toxicity Testing (PAFT). Tests were conducted on HCFC-225ca and HCFC-225cb isomers and as a 45/55 weight percent mixture.

Data from acute toxicity studies indicate that HCFC-225ca and HCFC-225cb have very low acute toxicity. Neither isomer causes eye irritation nor dermal toxicity in standardized tests; skin application of both isomers at high dose (2,000mg/kg body weight) produces no adverse effects. Therefore, the dermal LD50s are greater than 2,000mg/kg body weight. Oral administration of either isomer at high doses (5,000mg/kg body weight) does not cause any mortality and the oral LD50s are greater than 5,000mg/kg body weight. Both isomers also have very low acute inhalation toxicity as measured by the concentration that cause 50% mortality in experimental

animals, the LC50. The 4-hour exposure LC50s for both isomers are approximately 37,000ppm in rats. Cardiac sensitization response in dogs is observed at approximately 15,000ppm for the mixture of HCFC-225ca/225cb (45/55% by weight) and 20,000ppm for HCFC-225cb. By comparison, a cardiac sensitization response is observed with CFC-113 at approximately 5,000ppm.

In 28-day inhalation studies with rat, the activity and responsiveness of the animals was reduced at 5,000ppm or greater for each isomer. Toxicity was otherwise confined to the liver; liver enlargement and induction of peroxisomes was seen following treatment with either of the isomers. HCFC-225ca was more potent than HCFC-225cb in eliciting these liver effects. In 90-day study of HCFC-225ca/225cb mixture (45/55% by weight) with rat, toxic effects were observed in liver; liver enlargement and induction of peroxisomes. In 28-day study with marmoset, exposure to HCFC-225ca at 1,000ppm caused effects on the liver, such as slight fat deposition associated with changes in serum biochemical parameters. In the same study, exposure to HCFC-225cb at 5,000ppm caused somnolence during exposure and an increase of cytochrome P-450, indicative of an adoptive response to HCFC-225cb. However, no liver enlargement was seen and virtually no peroxisome induction was observed in either isomer.

Animal testing with HCFC-225ca/225cb mixture (45/55% by weight) indicates that the compounds are not teratogenic. The compounds do not produce genetic damage in bacterial cell cultures (Ames Assay), CHL, and *in vivo* unscheduled DNA syntheses assay. The evidence from these studies implies that neither isomer is genotoxic.

Based on the test results, the AELs (Acceptable Exposure Limits) of AK-225 and AK-225G have been set as 50ppm 8-hrs TWA and 250ppm 8-hrs TWA, respectively.

7. Status of Regulation of HCFC-225

HCFC-225 is regulated under the Montreal Protocol. The production will be phased out in 2020 in most of developed countries. In the U.S. and the E.U., it will be phased out in 2015.

Final rule of Significant New Alternative Policy (SNAP) program based on Section 612 of the Clean Air Act Amendments of 1990 was published on June 13, 1995. HCFC-225 is listed as an acceptable substitute for electronics cleaning and precision cleaning applications. Concerning aerosol applications, HCFC-225 is also an acceptable substitute under SNAP program as described in the April 28, 1999 Federal Register.

HCFC-225 is exempted from VOC regulations by the U.S. EPA as written in the Federal Register published October 8, 1996.

8. Conclusion

CFC-113 was banned at the end of 1995 in non-Article 5 countries based on the Montreal Protocol. Solvent applications of HCFC-141b were banned at the end of 1996 in the U. S. based on the SNAP program. The applications have been frozen in 2000 and will be phased out by 2010 in Japan based on the guideline of MITI. HCFC-225 is an HCFC and considered as a transitional alternative which will be phased out by 2020 based on the Montreal Protocol and will be banned in 2015 in the U.S. and the E.U. However, as described in the report of the fifteenth meeting of the open-ended working group of the parties to the Montreal Protocol[4)], certain HCFC-225 applications and uses have been cited as critical. In view of the lack of appropriate alternatives with good technical or environmental performance, exemptions for AK-225 may be granted.

Such applications would include cleaning parts that require high reliability, and for newly developed applications that essentially require the performance of HCFC-225.

References

1. K. Kitamura et al.: Proceedings of the 1994 International CFC & Halon Alternatives Conference, p. 585, October 1994, Washington, D.C.
2. K. Kitamura et al.: ibid., p. 779, October 1995, Washington, D.C.
3. K. Kitamura et al.: Proceedings of the 1996 International Conference on Ozone Protection Technologies, p. 669, October 1996, Washington, D.C.
4. UNEP: Report of the fifteenth meeting of the open-ended working group of the parties to the Montreal Protocol (INEP/Ozl.Pro./WG.1/15/5, 12 June 1997).

Table 1. Physical Properties of AK-225, AK-225G and CFC-113

	AK-225	AK-225G	CFC-113
Molecular Weight	202.94	202.94	187.38
Boiling Point (°C)	54.0	56.1	47.6
Freezing Point (°C)	-131	-116	-35
Density (g/cm^3 25 °C)	1.55	1.56	1.57
Viscosity (cP, 25 °C)	0.59	0.60	0.65
Surface Tension (dyne/cm, 25 °C)	16.2	16.9	17.3
Vapor Pressure (kg/cm^2, 25 °C0	283	265	335
Latent Heat of Vaporization (cal/g, b.p.)	34.6	35.0	36.1
Specific Heat (cal/g°C, 25 °C)	0.24	0.26	0.23
Solubility of Water (wt%, 25 °C)	0.031	0.027	0.011
Solubility in Water (wt%, 25 °C)	0.033	0.016	0.017
Flash Point (°C)	None	None	None
KB Value	31	30	31
Solubility Parameter	6.9	6.9	7.5
Ozone Depletion Potential (CFC-11 = 1.0)	0.03	0.033	0.80
Global Warming Potential (CO_2=1.0, 100yr)	370	530	5000

Table 2. Physical Properties of AK-225AES, AK-225T and CFC-113AES

	AK-225AES	AK-225T	CFC-113AES*1
Boiling Point (°C)	52	54	46.5
Freezing Point (°C)	-138	-139	-41.8
Density (g/cm^2, 25 °C)	1.49	1.34	1.50
Viscosity (cP, 25 °C)	0.61	0.61	0.66
Surface Tension (dyne/cm, 25 °C)	16.8	17.6	18.5*2
Vapor Pressure (mmHg, 25 °C)	291	265	360
Latent Heat of Vaporization (cal/g, b.p.)	40.6	47.2	42.9
Relative Evaporation Rate (Ether=100)	81	72	120
Solubility of Water (wt%, 25 °C)	0.33	0.33	0.25
Solubility in Water (wt%, 25 °C)	0.053	0.062	---
Flash Point (°C)	None	None	None
KB Value	41	63	39
Ozone Depletion Potential (CFC-11=1.0)	0.03	0.03	0.8
Global Warming Potential (CO_2=1.0, 100yr)	350	310	4800

*1 CFC-113AES is an azeotrope of CFC-113 and ethanol. *2 measured at 20 °C

Table 3. Effect of AK-225 on Unstressed Plastics for 5 minutes at Boiling Point

	AK-225			CFC-113		
	Weight Change (%)	Linear Swell (%)	Extractables (%)	Weight Change (%)	Linear Swell (%)	Extractables (%)
Polyvinyl chloride	<0.1	<0.1	<0.1	<0.1	<0.1	<0.1
Polyvinyl chloride	0.9	<0.1	0.9	<0.1	<0.1	<0.1
Polyethylene (HP)	0.1	<0.1	<0.1	0.1	<0.1	<0.1
Polyethylene (LP)	0.3	0.4	<0.1	0.1	<0.1	<0.1
Polypropylene	0.1	<0.1	<0.1	0.1	<0.1	<0.1
Polystyrene	0.4	<0.1	0.1	<0.1	<0.1	<0.1
Polymethyl	crack	crack	crack	<0.1	<0.1	<0.1
Polycarbonate	<0.1	<0.1	<0.1	<0.1	<0.1	<0.1
Polyacetal	<0.1	<0.1	<0.1	<0.1	<0.1	<0.1
Polyphenylene oxide	<0.1	<0.1	<0.1	<0.1	<0.1	<0.1
Phenolic	<0.1	<0.1	<0.1	<0.1	<0.1	<0.1
ABS	<0.1	<0.1	<0.1	<0.1	<0.1	<0.1
Nylon 6	<0.1	<0.1	<0.1	<0.1	<0.1	<0.1
Nylon 66	<0.1	<0.1	<0.1	<0.1	<0.1	<0.1
Polyester (FR)	<0.1	<0.1	<0.1	<0.1	<0.1	<0.1
PTFE	<0.1	<0.1	<0.1	<0.1	<0.1	<0.1
PCTRE	<0.1	<0.1	<0.1	<0.1	<0.1	<0.1
Epoxy (FR)	<0.1	<0.1	<0.1	<0.1	<0.1	<0.1
Polyphenylene sulfide	<0.1	<0.1	<0.1	<0.1	<0.1	<0.1
Polybutylene	<0.1	<0.1	<0.1	<0.1	<0.1	<0.1

Table 4. Effect of AK-225 on Elastomers for 3 days at Boiling Point

	AK-225			CFC-113		
	Wt Change (%)	Linear Swell (%)	Extractables (%)	Wt Change (%)	Linear Swell (%)	Extractables (%)
Polysulfide rubber FA (T)	67.1	14.1	6.2	<0.1	0.7	<0.1
Natural rubber (NR)	23.5	6.1	2.9	3.5	0.3	2.1
Urethane rubber (U)	105.4	21.4	0.2	1.1	0.3	<0.1
Isobutylene isoprene	9.2	-0.2	14.4	4.7	0.3	3.3
Polychloroprene (CR)	21.6	3.8	7.3	1.1	<0.1	0.8
Fluoroelastomer E (FKM)	106.3	18.8	2.0	0.4	<0.1	<0.1
Chlorosulfonated polyethylene (CSM)	1.1	-3.1	17.4	0.9	<0.1	0.8
Silicone rubber (Q)	199.8	41.5	2.2	19.3	4.8	0.3
Nitryl Rubber (NBR)	102.5	21.7	11.4	0.8	<0.1	0.5
Ethylene propylene diene terpolymer (EPDM)	9.5	-0.1	14.4	4.7	0.3	3.6

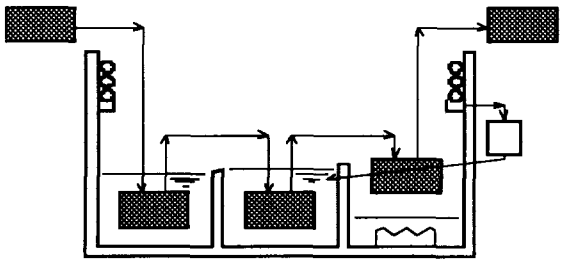

Fig. 1 Schematic Diagram of three-sump type cleaning equipment

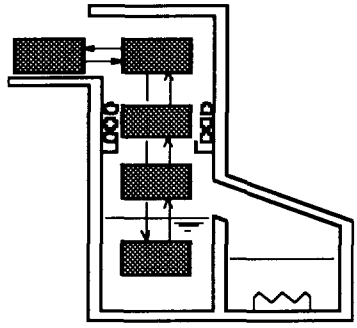

Fig. 2 Schematic Diagram of vertical two-sump type cleaning equipment

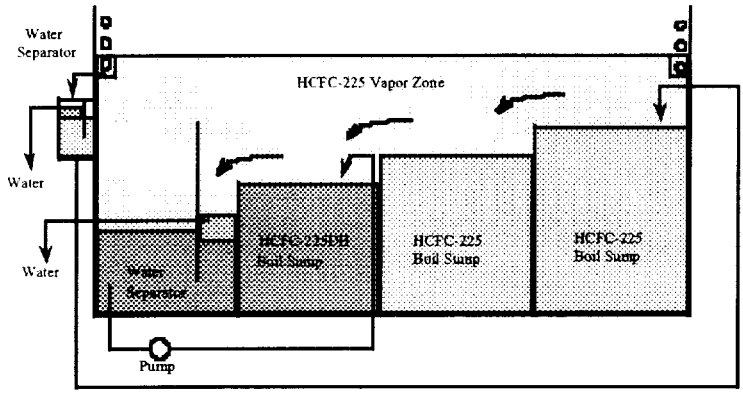

Fig. 3 Dewatering and Drying System for HCFC-225DH

CP/32/IN/23

HFEs in the Aerospace Industry: A Logical Alternative to CFCs and other Halogenated Cleaning Solvents.

David A. Hesselroth
3M Performance Materials

Introduction

The past several years have seen an effort to find suitable replacements for ozone-depleting substances (ODSs) such as CFC-113, HCFC-141b and 1,1,1 trichlorethane (TCA), as well as chlorinated solvents such as trichlorethylene, (TCE), and methylene chloride (CH_2Cl_2). Replacement solvents must meet more stringent environmental and toxicological requirements, and maintain the performance and compatibility characteristics of the products they are replacing. Segregated hydrofluoroethers (HFEs) are ethers with fluorocarbon on one side of the oxygen atom and hydrocarbon on the other. Non-segregated HFEs may have both hydrogen and fluorine on one or both sides of the oxygen. Tests have shown that the segregated HFEs have superior environmental properties. HFEs are non-ozone depleting, have a relatively low global warming potential (GWP) and most are exempt as volatile organic compounds (VOC) legislation. The commercially available HFEs have excellent toxicological properties. The HFEs and many of their azeotropes and co-solvents have excellent compatibility characteristics enabling them to be used with sensitive materials such as polycarbonate or acrylic. The use of HFEs neat, as azeotropic bends, or co-solvents enables them to clean a wide range of soils including light oils, silicones, waxes and heavy greases. HFEs have been used as direct replacement cleaning solvents in many applications.

As with CFC-113, HFEs can be used in a variety of non-cleaning applications. Heat transfer and electrical properties make them a suitable replacement in chillers, direct and indirect cooling, as well as dielectric constant temperature baths. HFEs and some of their azeotropes are used as carrier solvents for deposition of fluorochemical and silicone greases and coatings. HFEs with lubricious additives have proven to be an excellent near dry lubricant for drilling and machining aluminum, replacing CFC-113 with a similar additive. With performance and compatibility properties similar to CFC-113, HFEs can be a safe alternative with little or no modification to the existing systems.

Environmental

Background

The past decade has brought many changes in the way solvents are perceived for cleaning and other applications. The Montreal Protocol [1] forced the evaluation, reduction and elimination of ODSs. The elimination of CFC-113 and TCA production and phase out dates for HCFC-141b in 2001/2003, HCFC-225 in 2015, have established cut-off dates for conversion to solvents with better environmental properties. The Kyoto Protocol [2] established a classification system for GWPs. Although an actual phase out date has not been set, the GWP of a solvent should be considered. The protocol calls for voluntary reduction of green house gas emissions to be 5% below 1990 levels in 2008-2012. The

uses of VOCs have been restricted in many regions to help control the release of chemicals that contribute to the formation of photochemical smog. Most restrictions cover an entire site making it difficult to monitor emissions. These factors as well as the worker environment, are things that must be considered when evaluating alternatives.

The decomposition of chlorine or bromine containing molecules in the atmosphere contributes to stratospheric ozone depletion. Ozone or O_3 protects the earth from strong UV rays generated by the sun. Ozone absorbs the harmful UV rays. In this region the UV energy from the sun is at the proper level to decompose the solvent molecules releasing a chlorine or bromine free radical atom. The free radical enters a catalyic cycle that converts O_3 to O_2.

Global warming is being addressed for materials that have the potential to alter the earth's natural climatic balance. Water, CO_2 and other naturally occurring materials absorb some of the infrared (IR) radiation from the sun's rays to keep the earth at a relatively constant temperature. Greenhouse gasses upset this balance by adding additional IR absorbing materials or materials that absorb in IR regions that are naturally transparent. In either case the radiant heat from the earth's surface that typically passes through the atmosphere is absorbed by the greenhouse gases and not permitted to leave the earth's atmosphere. The term "greenhouse" is used to enable one to visualize the glass in a greenhouse as the gasses that accumulate in the atmosphere. When the sun's rays pass through the glass, the objects inside are warmed. The heat from the objects radiates inside the greenhouse warming the air. Objects outside the greenhouse are reflecting the same amount of heat, but without the glass, the reflected heat is permitted to disperse in the atmosphere. Reducing potential global warming materials emitted to the atmosphere will help maintain the earth's natural balance.

The GWP of a material is determined by two factors. One is the length of time that a material remains in the atmosphere. The other is the amount of IR radiation the material absorbs and/or the region of the IR spectrum in which it absorbs. The generally accepted scale sets CO_2 at a GWP of 1 on a 100-year horizon. A GWP is calculated based on the global warming contribution of a material compared to the equivalent contribution of and equal amount of CO_2 over a 100 year period of time. Both atmospheric lifetime and the level of IR absorption are used to calculate the GWP of a material.

Where greenhouse gases are typically found throughout the atmosphere, ODSs affect the ozone layer in the stratosphere about 50 km above the earth's surface. VOCs can cause problems in the lower atmosphere with contribution to the formation of ground level smog. Organic compounds, such as gasoline, hydrocarbon paint thinners, and many solvents, decompose in the lower atmosphere. Through a series of reactions the decomposition products change the O_2, to O_3 or ozone. At ground level, ozone reacts with the organic compounds to form that brown layer seen around large cities on bad smog days. The restriction of VOC emission is designed to reduce the overall concentration of materials that contribute to ground level smog.

Segregated HFEs have a balance of properties that is favorable in all three areas. As they are exempt as VOCs and do not contribute to smog formation, they can be used unrestricted in areas such as California's south coast and bay areas. They do not contribute to ozone depletion. The segregated HFEs global warming potentials are up to 10 times lower than their HCFC and HFC counterparts. Table 1 shows the properties of selected HFEs. Table 2 shows properties of solvents scheduled for phase out and other proposed replacement solvents.

Table 1: Environmental Properties

Environmental properties of commercially available segregated HFEs and selected commercial azeotropes

	HFE-7100 $C_4F_9OCH_3$	HFE-71DE[1]	HFE-71DA[2]	HFE-71IPA[3]	HFE-7200 $C_4F_9OC_2H_5$	L-13791 C3F7OCH3
Ozone Depletion Potential[4]	0	0	0	0	0	0
Global Warming Potential[5]	320	160	152	304	55	520
Volatile Organic Compound	Exempt	50% Exempt	52.7% Exempt	95% Exempt	Exempt	Pending
SNAP Approved	Yes	Yes	Yes	Yes	Yes	Pending

1) An azeotropic blend of 50% HFE-7100 and 50% trans-dichloroethylene 2) An azeotropic blend of 52.7% HFE-7100, 2.7% ethyl alcohol and 44.6% trans-dichloroethylene 3) An azeotropic blend of 95% HFE-7100 and 5% isopropyl alcohol. 4) CFC-11=1.0 5) CO_2 = 1, Source: WMO Global Ozone Research & Monitoring Project, Report No. 44, 1998

Table 2: Environmental Properties

Environmental properties of selected CFCs, HCFCs and chlorinated solvents

	CFC-113 CCl_2FCClF_2	HCFC-141b $C_2H_3Cl_2F$	HCFC-225 ca/cb $C_3HCl_2F_5$	TCE	TCA	CH_2Cl_2
Ozone Depletion Potential[1]	0.8	0.1	0.03	0	0.01	0
Global Warming Potential[2]	6000	700	180/620	-		-
Volatile Organic Compound	Exempt	Exempt	Exempt	Yes	Exempt	Exempt
SNAP Approved	No	No	Yes	No	No	No

1) CFC-11=1.0 2) CO_2 = 1, Source: WMO Global Ozone Research & Monitoring Project, Report No. 44, 1998

Segregation of the hydrocarbon and fluorocarbon portion of the ethers gives the HFEs favorable global warming properties. [3] Table 3 compares the GWP of hydrofluorocarbons (HFCs) and their HFE homologues. Table 4 shows the atmospheric lifetimes of segregated HFEs.

Table 3
Atmospheric Lifetimes and GWPs of Isomerically Similar HFEs and HFCs

Compound	Halocarbon Number	Atm. Lifetime (yrs) [3]	GWP [3] (100 Yr ITH)
CH_3CF_3	HFC-143a	53.5	5,400
CH_3OCF_3	HFE-143a	5.7	970
CF_2HCF_3	HFC-125	32.6	3800
CF_2HOCF_3	HFE-125	165	15,300
CF_3CFHCF_3	HFC-227ea	36.5	3,800
$CF_3CFHOCF_3$	HFE-227ea	11	1,500
$CF_3CH_2CF_3$	HFC-236fa	226	9,400
$CF_3CH_2OCF_3$	HFE-236fa	3.7	470
$CF_3CH_2CHF_2$	HFC-245fa	7.4	820
$CF_3CH_2OCHF_2$	HFE-245fa	4.4	570
$CF_3CF_2OCH_3$	HFE-245cb2	1.2	160
$C_4F_9OCH_3$	HFE-449s1 (HFE-7100)	4.1	320
$C_4F_9OC_2H_5$	HFE-569sf2 (HFE-7200)	0.8	55

Table 4
Atmospheric Lifetimes of Segregated HFEs

Compound	Atm. Lifetime (yrs)
n-$C_4F_9OCH_3$ (bp = 60°C)	4.7
i-$C_4F_9OCH_3$ (bp = 60°C)	3.7
n-$C_4F_9OC_2H_5$ (bp = 76°C)	0.9
i-$C_4F_9OC_2H_5$ (bp = 76°C)	0.7
n-$C_3F_7OCH_3$ (bp = 34°C)	4.9
$R_f^1OCH_3$ (bp ≈ 100°C)	2.7
$R_f^2OCH_3$ (bp ≈ 100°C)	3.8
$R_f^3OC_2H_5$ (bp ≈ 110°C)	1.0
$R_f^4OCH_3$ (bp ≈ 120°C)	5.0
$R_f^5OC_2H_5$ (bp ≈ 130°C)	2.5
$R_f^6OCH_3$ (bp ≈ 150°C)	4.2

Solvent Safety

Worker safety is an important consideration when evaluating a new material. While most any chemical can be handled safely, the margin of safety is important for comparing

different cleaning processes. Exposure limits including 8 hr. Time Weighted Average (TWA), No Effect Level (NOEL), ceiling exposure guidelines plus others should be known prior to evaluating candidates.

Product toxicity reveals significant differences in the margin of safety inherent to each solvent. Toxicological properties of common cleaning solvents are listed in Table 5. A compound's short term or acute toxicity, reflected in the 4-hour LC_{50}, needs to be considered in the event that a worker is exposed to high concentrations over a short period of time, as could be the case in the occurrence of a spill or equipment failure. The lower a compound's LC50, the higher its short-term toxicity, resulting in a smaller margin of safety.

A compound's exposure guideline (EG), typically an 8-hour time-weighted average, is an indication of a materials chronic or long-term toxicity. This number represents the time-weighted average concentration for a conventional 8-hour workday and a 40-hour workweek to which it is believed that nearly all workers may be repeatedly exposed, day after day, without adverse affect. A high exposure guideline will permit a greater margin of safety. Compounds with low exposure guidelines may require more extensive solvent containment or the use of some type of breathing apparatus to ensure the workers maintain an exposure level below recommended levels.

Table 5: Toxicological Properties

	CFC-113	HCFC-141b	HFE-7100	*trans*-1,2-dichloro ethylene	TCE	TCA	MeCl
Acute Lethal Concentration 4-Hr., ppm	55,000	62,000	>100,000	22,000[1]	8450	16,000	14,400
Ocular Irritant	No	No	No	Yes	Yes	Yes	Yes
Dermal Irritant	No	No	No	Yes	Yes	Yes	Yes
Exposure Guideline 8-hr. TWA, ppm	1000	500	750	200	50	350	25
STEL, 15 minute maximum exposure	None	None	None	None	100[2]	450[2]	125[2]

1) 6-hour exposure
2) ACGHI, 6th Edition of the "Documentation of the Threshold Limit Values and Biological Exposure Indices"

HFE Qualifications

When qualifying new solvents, the environmental and safety properties are only the beginning. Materials compatibility and performance also are critical. Selected HFEs, both commercial and experimental have been tested and meet the requirements for use in certain military and aerospace applications. The selective solvency enables the HFEs to fit in a variety of applications. The neat HFEs pass the most stringent oxygen compatibility tests, qualifying them for the NASA procurement specification SES-0073. HFEs and the 50% 1,2 trans dichloroethyene azeotrope blend has passed the primary testing for typical aerospace compatibility, required for various specifications such as the

Boeing, BAC D6-17487, Aerospace Materials, AMS 1526B and the AMCOM specification ADS-61-PRS, rev. P.
Table 6 contains the typical testing that is required for aerospace applications. HFE-7100, HFE-7200 conform to all the test requirements. HFE-71DE conforms to all test requirements except for acrylic stress crazing, ASTM 484. Table 7 contains additional testing typically required for oxygen compatibility.

Table 6, Compatibility Testing: HFE-7100, HFE-7200 and HFE-71DE

— Effect on Painted Surfaces	(ASTM F502)
— Residue Test	(ASTM F485)
— Sandwich Corrosion Test	(ASTM F1110)
— Acrylic Stress Crazing Test	(ASTM F484)
— Cadmium Removal Test	(ASTM F483)
— Low-Embrit. Cadmium Plate	(ASTM F519, 1C)
— Flash Point	(ASTM D56)
— Immersion Corrosion Test	(ASTM F483)
— Stress Corrosion	(ASTM D945)
— Stress Corrosion (modified*)	(ASTM D945)

— *Testing performed by Scientific Materials International.*

— * 3M performed ASTM D945 (modified). It was developed to accommodate solvents that are near residue free. In lieu of the short solvent exposure and high temperature exposure, the samples were held in the boiling solvents for five days, 8 hrs per day.

Table 7 : Oxygen Compatibility Testing

-Mechanical Impact	(NASA test)
-Autogenous Ignition Temp.	(ASTM G72 - 82)

-*Testing performed by, NASA, Johnson Space Center White Sands Test Facility.*
HFE-7100 and HFE-7200 met test criteria.

Solutions for aerospace cleaning challenges
Cleanliness is of vital importance for parts and equipment used in military and aerospace applications. However, when evaluating cleaning products, compatibility is as important as cleaning ability. This is not surprising, given the risks associated with poor compatibility in these applications. Qualification of new materials is an onerous and expensive process. Because of this, CFC-113 is still used in many applications. Replacement solvents must provide adequate cleaning performance and exhibit excellent materials compatibility. Extensive compatibility testing is performed before adopting a new cleaning process.

Another strong driver for selecting new cleaning processes is the environmental profile. Since qualification of new cleaning processes is neither cheap nor easy, users give the environmental profile of a replacement product more weight than other industries, in an effort to avoid future re-qualifications resulting from evolving environmental policy or new regulations. In addition, qualified product must be used throughout the world. Therefore, it is desirable that global regulatory bodies accept a new cleaning compound or process.

Cleaning gyroscopes and altimeters

Challenge: Find replacement for CFC-113 for use in a vapor degreaser that removed various hydrocarbon and silicone oils, as well as particulate. The cleaner had to perform quickly enough that it didn't affect the sensitive materials on the assemblies. The solvent of choice was to have zero ODP, low GWP, and provide users with a safety margin similar to that of CFC-113.

Solution: In cleaning altimeters and gyroscopes, the US Army and Airforce chose to qualify HFE-71DE, an azeotrope of HFE-7100 and *trans*-1, 2-dichloroethylene. An independent laboratory performed candidate screening and much of the qualification testing. The decision to employ HFE-71DE was based not only on the excellent cleaning results achieved, but also on comparative environmental and safety properties.

Oxygen gauge cleaning

Challenge: Find replacement for CFC-113 to remove light oils and particulate from oxygen gauges. The solution must be oxygen compatible and leave no residue. The process is listed in Mil Std. 1330 D.

Solution: For oxygen lines and storage tanks, an aqueous cleaning process (NOX) is used. However, the tight clearances on gauges require a solvent-based cleaner in order to avoid problematic residues.

For most oxygen gauge cleaning applications, HFE-7100 was found to be a suitable solution. However, where more aggressive cleaning is needed, a two-solvent process is being evaluated. The process will use HFE-71DE cold cleaning, followed by an HFE-7100 rinse. The HFE-71DE will easily remove the soils found in oxygen equipment. Rinsing with HFE-7100 ensures a clean and particulate-free part. The system uses products with the same base solvent (HFE-7100) to ensure good mixing, resulting in an efficient rinse.

The above same-solvent philosophy factored into the decision by the Royal Australian Air Force to approve an HFE-71DE clean/HFE-7100 rinse process for cleaning oxygen lines.

Cleaning transmissions, hydraulics, and various mechanical parts

Challenge: Replace chlorinated solvents for a variety of cleaning applications with a more environmentally acceptable and less toxic product. The process must be easy to operate and cannot introduce a corrosion risk.

Solution: Given the wide range of soils and substrates cleaned, process flexibility was important. The user decided on a co-solvent process, utilizing Petroferm's, solvating agent, SA-70 and HFE-7100. Aqueous cleaning was eliminated due to the risk of subsequent corrosion. The co-solvent process uses a high-boiling hydrocarbon solvent as a solvating agent to remove the soils. The solvating agent is miscible with HFE-7100 (the rinse solvent), allowing the user to vary operating temperature and ensuring a complete rinse. The solvating agent has extremely good solvency (Kauri Butanol value >150), yet is not aggressive toward sensitive parts. This, too, improves the flexibility of the process, allowing one machine to be used for a variety of cleaning applications.

Cleaning aircraft bearings.
Challenge: Removing soils that vary from light oils to very heavy greases from aircraft bearings.

Solution: A co-solvent process is under evaluation to replace a multi-step hydrocarbon solvent cleaning process. The improved flexibility of the co-solvent process has shown excellent cleaning results and will eliminate VOC emissions. The only emission from this process is the loss of the rinsing agent, HFE-7100. This allows for unrestricted use of the process to anywhere in the US.

Cleaning silicone mold-release from polycarbonate medical device parts
Challenge: Replace CFC-113 in a process used to remove silicone mold release from highly stressed, injection molded polycarbonate medical devices. The process must be of high enough solvency to remove the silicone, yet be compatible with the sensitive substrate.

Solution: Several potential solutions were evaluated. The first evaluation centered on using neat vapor cleaning with either HFE-7100 or HFE-7200. Cleaning with the HFE-7200 was found to be adequate, but the higher temperature resulted in increased stress cracking compared to the CFC-113 control. Stress cracking was not as prevalent with HFE-7100, but cleaning was not adequate.

An azeotrope of HFE-7100 and isopropyl alcohol, HFE-71IPA was evaluated and found to have good cleaning with compatibility similar to the control. It was noted that the slight decrease in boiling point, from 61°C to 56°C, significantly reduced the stress cracking.

A second solution proved to have the best performance. A co-solvent process used a blend of 90% HFE-7100 and 10% Isopar M as the solvating agent and HFE-7100 as the rinse aid. This solution resulted in excellent cleaning results and virtually no stress cracking, noticeably less than what was seen with CFC-113. However, the process

required close monitoring of the boil sump composition in order to maintain temperatures below 57°C. Ultimately, the manufacturer chose to implement HFE-71IPA cleaning, as it was an easier process.

Cleaning of polyurethane catheters

Challenge: To remove light oils and particulate from a polyurethane catheter. The manufacturer traditionally used a chlorinated solvent for cleaning applications but found them to be too aggressive on the sensitive catheters. In addition to compatibility, a second concern was that the parts had to be cleaned on the production floor in close proximity to production personnel and it would be difficult to control exposure of the cleaning solvent below 25ppm.

Solution: Given that application involved only light cleaning and that compatibility was the chief concern, HFE-7100 and HFE-71IPA were evaluated. Both proved to be effective cleaners for this application. Compatibility studies showed a negligible amount of extraction from the tubing on exposure to HFE-7100. Testing with HFE-71IPA showed a very low level of extraction (0.1%); even at this low level, a change in appearance and feel was observed. Due to this difference, neat cleaning with HFE-7100 was implemented.

Flux removal after high temperature soldering

Challenge: Replace methylene chloride in the removal of flux residue from a ceramic circuit board that had undergone solder reflow at 260°C. The manufacturer required no residual contamination visible on inspection under a 20X microscope and UV light. The evaluation was made more difficult as the parts were cleaned not immediately following the solder process but about one-week later.

Solution: Several boards were submitted for evaluation with different cleaning products and processes. A defluxing azeotrope was tested but did not adequately remove the residue--traces were visible on inspection. Co-solvent cleaning using SA-70 and HFE-7100 formulated to boil at 80°C in the boil sump and rinsing with HFE-7100. Ultrasonic agitation was used in both the boil and the rinse sump. The process, involving a six-minute dwell in the boil sump and a two-minute rinse, provided excellent cleaning results.

Drilling aluminum during assembly operations

Challenge: Find a replacement for Freon TB-1 and Boelube used to lubricate drilling operations during assembly of aircraft subassemblies and major components. Boelube has replaced Freon TB-1 in most operations, but requires significant effort to remove drilling residues from surfaces that will later be sealed or painted. In most cases, this cleaning is done by hand with solvents and wipes adding to labor costs and slowing production.

Solution: HFE-7100 based drilling fluids, MW-2400 and MW-2410 can be used much as Freon TB-1 was used in the past with good drilling performance, but does not leave oily, sticky drilling residues. Both MW fluids are formulated to lubricate aluminum drilling

when applied as a low volume jet or spray directed at the tooling. Both the HFE-7100 and the additives are fully volatile which leaves a clean and dry work surface, a dry work area (not slippery), and minimizes cleanup to removal of dry chips.

Conclusion

The conversion from ODSs or other chlorinated solvents, to more environmentally acceptable substitutes for cleaning applications continues. While many applications were a relatively easy conversion, there remain a number of more challenging applications for which a replacement is not easily found. Developing solutions for these difficult cleaning challenges requires a problem-solving mindset. Manufacturers need not sacrifice safety and environmental properties in exchange for performance. Effective and acceptable replacements can be found when suppliers and end-users work together to tailor an innovative solution to a specific application.

[1] Montreal Protocol on Substances that Deplete the Ozone Layer and its attendant amendments, United Nations Environment Programme, 1987.

[2] Kyoto Protocol to the United Nations Framework Convention on Climate Change, United Nations Environment Programme, 1997.

[3] Owens, J.G., Segregated Hydrofluoroethers: Low GWP Alternatives to HFCs and PFCs, Proceedings of the Joint IPCC/TEAP Expert Meeting on Options for the Limitation of Emissions of HFCs and PFCs, Energieonderzoek Centrum Nederland, Petten, The Netherlands, 1999.

Lightweight Multi-layer Structural Materials

H.H. LEGNER and W.T. Laughlin

Physical Sciences, Inc.
20 New England Business Center
Andover, MA 01810 USA
Phone: 978-689-0003 or 978-983-2234
Fax: 978-689-3232
E-mail: legner@psicorp.com

V. Di Cristina
ThermoPhysical Sciences

D. Marshall and R. Singler
Textron Systems

A new lightweight composite material with combined structural and thermal protection capability has been developed for both air vehicle and spacecraft application. The basic concept consists of the integration of a high-density outer layer with a low-density foam core, using stitching loops to integrate the material three-dimensionally. The layers are chemically bonded and mechanically linked. The generalization of this technique to integrated structural materials with two high-density face plates sandwiching the low-density inner layer provides an entirely new approach to fabricating cost-effective aero-shell and spacecraft structural materials. These materials have been evaluated structurally, as well as thermally in arc-jet and laser tests. Thermal insulation performance exceeds that of standard heat protection materials. Measured compressive and bending strengths have shown substantial residual load-carrying capabilities. In addition, damage tolerance and crush strength properties have been demonstrated to be superior to comparable honeycomb structures.

ELIMINATION OF MEK AND LACQUER THINNER IN DEPARTMENT OF DEFENSE PAINTING OPERATIONS

Authored by: Mr. Joseph Lucas and Mr. Eric Lethe
Inland Technology Incorporated
401 East 27th Street
Tacoma, WA 98421
(253) 383-1177
inland@inlandtech.com

Painting operations at aerospace and Department of Defense facilities create large and problematic waste streams as well as major emissions of hazardous air pollutants and VOC's. Some of these emissions are a result of the composition of the paints used, and as a result, create a waste stream that can only be addressed by a reformulation of the specific paints and coatings. However, the greatest percentage of waste and emissions generated by painting operations is a result of the use of MEK and lacquer thinner in clean up and surface preparation activities. Usage of these hazardous materials account for an excess of 50% of the overall waste generated by a painting facility. The successful elimination of MEK and lacquer thinner for these painting activities would clearly assist these facilities in meeting the requirements of the Aerospace NESHAPS and Executive Order # 12856, and would facilitate a considerable reduction in the overall generation of hazardous waste.

This presentation is an exemplary representation of successful replacement projects that have taken place at civilian manufacturers, aerospace, and Department of Defense installations. It will detail the substitution process from a chemical development standpoint, and will discuss the equipment validation procedures, work practice changes, and training required to make the substitution process successful. In each case study, the end result was a replacement process and chemistry that was more environmentally responsible and less regulated than the original process. In addition, each substitution project resulted in demonstrable cost savings.

Case Study # 1

US Army, Aberdeen Proving Ground had a strong incentive to reduce the hazardous waste generation caused by the use of paint thinner as a cleaning solvent at the Auto Body Shop. Ms. Amy Borman and Mr. Keith Katz determined the necessity for a substitution project, following an environmental audit which the safety and environmental officers conducted. The pre-existing conditions were; paint gun cleaning that consumed 70 or more gallons of lacquer thinner each month, and evaporative loss and contamination from usage, creating the need for frequent disposal of dirty lacquer thinner and replenishment with fresh material. This frequent disposal of lacquer thinner makes the cleaning process a major source of emissions and hazardous waste. The challenge for the research team was to provide a cleaning solution that would eliminate these problems. It was first necessary to develop a technology that would make the alternative material cost effective to use. The new cleaning solution ideally would contain no hazardous air pollutants, be non-flammable, and have minimal worker exposure risks associated with its use. The new material, therefore, would present considerable differences in behavior, even while accomplishing the cleaning task it was designed to do. Additionally, training procedures and work practice modifications required development in order to accommodate the differing characteristics between the new cleaner and the old style thinner. The research team took these criteria into the laboratory for experimentation.

The Solution-From a Chemical Standpoint

Inland Technology developed and patented "a low toxicity solvent composition" known as EP-921™. This solvent alternative was developed to mimic the Hansen's Solubility Parameters of MEK almost perfectly. It contains less than 1% VOC, has no ozone depleting or EPA 17 chemicals in the formula, and has a flashpoint of 156° F, EP-921™ eliminating the fire risks associated with lacquer thinner or MEK. This new cleaner proved effective in the removal of all uncured and semi-cured paints used by the Army, including the chemical resistant CARC coating. In December of 1998 EP-921™ was awarded a toxicity clearance from the US Army Center for Health Promotion and Preventative Medicine

The Solution - From an Equipment Standpoint

In order to maximize the cost effectiveness of the new cleaning compound, new equipment was engineered for the cleaning process. The Edge Tek™ Filtration System filters the EP-921™ on line as the cleaning station is being used. The system filters down to .1 micron nominal, and removes a major portion of the paint solids. This allows the EP-921™ to be re-used for a measure of months. Typically, the only wastes being disposed of are the filter elements, and a small amount of settled paint solids. The volume of hazardous waste disposed is reduced by greater than 85%.

The Solution -Work Practices, Training and Putting It All Together

Since there is no evaporative loss associated with EP-921™, most of the training and work practices necessary for the implementation of EP-921™ into a paint shop involve conservation techniques. It is also critically important to develop techniques for the removal of unevaporated EP-921™ from the surfaces of the painting equipment. Conservation techniques involve cascading the extremely dirty EP-921™ into a gross-cleaning operation, capture of the rinsate material, separation of the paint solids from the EP-921™, and filtration of that material in order to extend the usable life of the cleaner. The EP-921™ is unique in that its chemistry is able to attract the paint from the surfaces of the application equipment (paint lines, spray guns, pressure pots and cups) and form micelles of the free-floating paint. However, the paint has no opportunity to bond with or emulsify within the EP-921™. The greater specific gravity of the paint allows the paint to settle out, or to be easily filtered out, of the EP-921™. This lack of emulsification also prevents the EP-921™ from losing effectiveness, since the cleaner is not becoming saturated with paint. This exemplifies the nature of EP-921™ as a use-specific product which cannot be used as a surface preparation or thinner for paint or coating.

Final removal of EP-921™ from painting equipment involves the wiping of the surfaces with a dry rag inside the cup or pot and outside of the cup and gun head. Either rinse the inside of the cup with Teksol EP®, or, refill the cup or pot with fresh paint, and shoot it through the gun head into the waste paint container. The painter is now ready to begin the next painting job. It is of the utmost importance that the painter do a "pattern check" spray, (this takes 5 seconds or less spraying) to make sure all the EP-921™ is out of the gun head.

The Results

In May of 1996, two paint gun cleaning stations were filled with an initial charge of 5 gallons of EP-921™ and were put into service. A review of the performance was conducted 47 months later. It is notable that these same gun cleaning stations are still in use today. The records show that the total purchases for the stations during that 47-month period, consist of 95 gallons of EP-921™ and 15 cases of 12 Edge Tek™ Filter Elements, however, not all of these had been consumed after the 47 months. Emissions of hazardous air pollutants, VOC's, and EPA 17 chemicals have been cut to nearly zero. In a cost comparison with lacquer thinner, 47 months usage would have been 3,290 gallons at a cost of approximately $ 2.00 per gallon for a total of $ 6,580.00. The disposal volume for that same period would have been approximately 1,645 gallons, at a cost of $ 5.00 per gallon totaling $ 8,225.00 The costs of the traditional method of painting equipment cleaning had a total cost of $ 14,805. By comparison, the use of EP-921™ and the Edge Tek™ Filter System was: Acquisition of 95 gallons of EP-921™ at a cost of $ 28.95 per gallon, totaling $ 2,702.75, and the Edge Tek™ Filters, at a cost of $ 13.33 per filter element, totaling $ 2,079.48. The disposal cost for the 156 filter elements was $ 360.00. These filter elements were contained in one 55 gallon drum. The total cost for the 47 months usage of the EP-921™ was $ 5,142.23. This represents a cost savings of nearly 300%! This cost savings is strictly a monetary assessment, while volume of airborne emissions was reduced from 11,515 pounds of hazardous air pollutants from the cleaning process to zero pounds.

Case Study #2

Another example of the opportunity for minimization of airborne emissions from the painting equipment cleaning operations took place at Eglin Air Force Base. The point of contact was Mr. Al Holley, Painting Supervisor for the small parts painting shop. The mission at hand was to replace MEK in use as a clean-up solvent for the painting equipment. The replacement cleaner would have to be non-VOC, non-HAP, contain no ozone depleting chemicals, and contain none of the EPA 17 chemicals. The alternative clean-up solvent would need to be

effective in the removal of uncured epoxy primers and polyurethane topcoat paints, as well as have a compatibility with the gaskets and seals present in the painting equipment.

The previous conditions that were encountered at the small parts painting shop were: five full time painters who worked a day shift and a swing shift using high solids epoxy primers, and polyurethane top coats. The yearly consumption for the cleaning of the paint guns was approximately 5,200 gallons of MEK. The blend of waste paint and MEK accounted for 27,400 pounds of hazardous waste generated by this small shop per year. Additionally, the air emissions assessment for this shop showed more than 14,000 pounds of hazardous air pollutants and VOC emitted per year. Incoming MEK purchases totaled $ 6,000.00 per year, however, add to that the hazardous waste disposal cost of $ 12,450.00 per year.

The combined Eglin AFB, Inland Technology Task Force gathered data in order to develop and implement the ideal solution both for the air emission and solid waste issues. From interviews with the painters, it was learned that the current cleaning tanks were inefficient at cleaning all of the small openings and valves in the paint guns that were in use. After the paint guns were flushed in the tanks, the painters needed to disassemble the guns and hand detail all of the parts with a small bucket of MEK and a brush. The ideal piece of equipment would allow for both flushing of the gun heads, as well as detail work. This would be done preferably in the same piece of equipment, and with a non-hazardous cleaner. The performance criteria are the same as the previous case study, with a special emphasis on cleaning of high solids paints. If the paint is not completely removed from the equipment, the gun head will clog or spray in an erratic pattern. The high solids paints are also very prone to "clabbering" or congealing in the presence of water or incompatible solvent cleaners. The congealing of the paint in the gun head will cause such severe clogging, that the gun will need to be detailed with a stripper compound. This takes a long time, and the strippers are often destructive to the seals inside the gun head. The environmental criteria was driven by the need to reduce the generation of hazardous waste, with an emphasis on worker health and safety. Determination was made (using off-line trials) that the EP-921™ would remove the uncured and semi-cured paints used at Eglin AFB. The next order was to comply with the request for a piece of equipment which would allow for the flushing of the gun head assemblies, cleaning of the cup interiors, and cleaning of the cup and gun exteriors. Such a machine would need an air-operated pump, and would utilize the Edge Tek™ Filter System to minimize the disposal of the used EP-921™. The cleaning unit would need to be of a stainless steel construction in order to assure a long usable life for the unit. Based upon the requests of the environmental officers and the painting crew, the IT-45SSER™ was conceived.

Unit specifications for the IT-45SSER™ Paint Gun Washer

Measurements: 37" x 31" x 74" high, constructed of 14-gauge schedule 304 stainless steel, utilizes an air-operated diaphragm pump, and is equipped with the Edge Tek™ Filter System including a 25-micron resin prefilter.

The training procedures for implementing the EP-921™ and the IT-45SSER™ were overseen by the environmental officers, as well as the Paint Quality Assurance Team. Initially the new unit was placed along side the old style cleaning tanks. This provided a "security blanket" for the painters while they were becoming accustomed to using the non-evaporating EP-921™. After several days, in which the painters discovered that the EP-921™ was even more effective in the cleaning of the orifices of the gun heads, the old tanks were removed. The most radical change the painters experienced was the ability to clean the guns and cups in an open tank, without breathing the unpleasant fumes of the MEK. The other change was the need to follow the cleaning with a dry rag wipe to the exterior surfaces of the gun head and cup, as well as the interior of the cup. The EP-921™, which remained in the "barrel" of the gun head, was completely flushed away by the initial pattern-check spray of the next charge of paint. All of the various types of paint and primer that were cleaned in the old style washer were successfully tested in the IT-45SSER™ exhibiting no degradation of the gun seals, and no clogging of the spray ports in the gun heads.

After an assessment period of 14 months, the IT-45SSER™ at Eglin AFB showed these results: The shop now uses no MEK, and as a consequence, the paint shop emits zero Hazardous Air Pollutants or VOC's from the cleaning process. Additionally, the shop generates only 30 gallons (or 240 pounds) per year of hazardous waste from the cleaning of the painting equipment. Perhaps the most startling outcome is that the initial charge of 25 gallons of EP-921™ has lasted over one year. This is a comparable chemical purchase cost of $ 723.75 instead of $ 6,000.00. In addition, a volume reduction of hazardous waste of more than 27,000 pounds! The IT-45SSER™ Paint

Gun Washer and EP-921™ have now been given National Stock Numbers, and are currently in use in all branches of the Department of Defense.

In conclusion, these case studies are examples of successful process substitution projects. It should be noted that no one chemical, or piece of equipment, should be supposed to solve all environmental concerns. The greatest efforts were those involving the training and modifying of the SOP's (Standard Operating Procedures) for cleaning of the painting equipment and handling of the resultant wastes. It is a testimony to those training efforts, more than simply purchase of a new product, which resulted in the dramatic reduction of hazardous wastes from these sites.

Asbestos Free Insulation Development for the Space Shuttle Solid Propellant Rocket Motor (RSRM)

Larry D. Allred and Norman F. Eddy

Thiokol Propulsion

P.O. Box 707
Brigham City, Utah

(435) 863-6692
allreld@thiokol.com

(435) 863-2440
eddynf@thiokol.com

Copyright 2000 Thiokol Propulsion,
A Division of Cordant Technologies Inc.
All rights reserved

Asbestos Free Insulation Development for the Space Shuttle Solid Propellant Rocket Motor (RSRM)

ABSTRACT

Asbestos has been used for many years as an ablation inhibitor in insulating materials. It has been a constituent of the AS/NBR insulation used to protect the steel case of the RSRM (Reusable Solid Rocket Motor) since its inception. This paper discusses the development of a potential replacement RSRM insulation design, several of the numerous design issues that were worked and processing problems that were resolved. The earlier design demonstration on FSM-5 (Flight Support Motor) of the selected 7% and 11% Kevlar® filled EPDM (KF/EPDM) candidate materials was expanded. Full-scale process simulation articles were built and FSM-8 was manufactured using multiple Asbestos Free (AF) components and materials.

Two major problems had to be overcome in developing the AF design. First, bondline corrosion, which occurred in the double-cured region of the aft dome, had to be eliminated. Second, KF/EPDM creates high levels of electrostatic energy (ESE), which does not readily dissipate from the insulation surface. An uncontrolled electrostatic discharge (ESD) of this surface energy during many phases of production could create serious safety hazards. Numerous processing changes were implemented and a conductive paint was developed to prevent exposed external insulation surfaces from generating ESE/ESD.

Additionally, special internal instrumentation was incorporated into FSM-8 to record real-time internal motor environment data. These data included inhibitor insulation erosion rates and internal thermal environments. The FSM-8 static test was successfully conducted in February 2000 and much valuable data were obtained to characterize the AF insulation design.

INTRODUCTION

The primary insulation used on the current space shuttle RSRM is an asbestos and silicon dioxide filled acrylonitrile butadiene rubber (AS/NBR). Asbestos is also used in some RSRM adhesives, liner and castable inhibitor. Asbestos is a commercial term for a group of naturally occurring fibrous crystals made of hydrated silicates. Some forms of asbestos are considered a serious health hazard. Since the current regulatory policy in the United States does not differentiate between types of asbestos, the use of all asbestos could be restricted with little warning, which could affect production of the RSRM. Elimination of asbestos containing materials is also motivated by liability issues during the handling and processing of asbestos containing materials and the recurring costs associated with OSHA regulation compliance and indemnification. (4)

A development program was initiated in 1986 and numerous Asbestos Free (AF) insulation candidates were evaluated using seventy-pound charge (SPC) motors and Modified NASA (MNASA) motors. Kevlar® filled ethylene propylene diene monomer (KF/EPDM) insulation had previously been selected for use in several solid rocket motors (SICBM, CASTOR 4B, CASTOR 120). Several modifications of this KF/EPDM formulation were made to meet structural and ablation requirements and a 7% KF/EPDM was selected as the primary insulation for the AF RSRM.

This paper discusses the AF insulation design and some results of a full-scale static test using AF materials in the major components of the motor. The resolution of two major problems that had to be overcome in developing the AF design is also discussed. First, bondline corrosion, which occurred in the double-cured region of the aft dome, had to be eliminated. Second, KF/EPDM creates a high level of electrostatic energy (ESE), which does not readily dissipate from the insulation surface. An uncontrolled electrostatic discharge (ESD) of this surface energy during many phases of production could create serious safety hazards. Numerous processing changes were implemented and a conductive paint was developed to prevent exposed external insulation surfaces from generating ESE/ESD.

OVERVIEW

The thermal-ablative insulation development effort began by evaluating several families of base polymers (polyisoprene, styrene-butadiene, silicone, EPDM, NBR, etc.), fiber fillers (Kevlar®, Kynol®, polybenzimidazole, etc.), flame retardant and curative packages. The insulations were developed to provide erosion performance. The best formulations for erosion resistance were a family of Kevlar® fiber filled materials. An initial 11% KF/EPDM

Copyright 2000 Thiokol Propulsion,
A Division of Cordant Technologies Inc.
All rights reserved

formulation had been developed with a resin curative system and had been used in several space launch and strategic SRMs. The AF program developed a sulfur cured 7% KF/EPDM as the primary insulation. A sulfur-based cure was selected over a resin-based cure system for similarity of shrink characteristics with AS/NBR, higher strain capability and lower stiffness while sacrificing some ablation capability and perhaps across-ply fracture toughness. A backup 11% KF/EPDM was formulated to be similar to the 7% KF/EPDM that could be used in the aft dome in case of unexpectedly severe 7% KF/EPDM ablation with motor scale-up. Results of detailed structural characterization of the 7% KF/EPDM design showed the 7% KF/EPDM to have marginal across-ply and perpendicular to fiber stress and interlaminar fracture toughness capabilities. The marginal interlaminar capabilities result from the base polymers, Kevlar®, fire retardant and antioxidant fillers used to meet other process and design requirements. A silica filled NBR (SF/NBR) was selected for use in high structural load regions such as the propellant stress relief flap terminus. (1)

The original AF design goal was to have a single material replacement for the RSRM. The design would directly substitute an equal thickness of 7% KF/EPDM in place of AS/NBR and an increased thickness of 7% KF/EPDM in place of carbon fiber filled EPDM (CF/EPDM) in the aft dome. During the development process, the AF insulation was tested in progressively larger sub-scale motors. The KF/EPDM was first tested in seventy-pound propellant charge (SPC) motors. The SPC motor consists of an end burning propellant grain and attached blast tube. KF/EPDM rubbers and the RSRM baselines of CF/EPDM rubber and AS/NBR were then tested in modified National Aeronautic and Space Administration (MNASA) motors. The MNASA motor has a 1/5 scale RSRM aft segment blast tube and a 10,000-pound, center perforated propellant charge. The MNASA motor surpasses the SPC motor in reliability of results, but it has greater costs and cycle time. Thermal-ablative capability of 7% KF/EPDM in sub-scale motors was equivalent to AS/NBR. The thermal-ablative capability of 11% KF/EPDM was equivalent to CF/EPDM and its erosion rate was up to 40% lower than AS/NBR. (1)

The 7% KF/EPDM and 11% KF/EPDM were tested in the aft dome and partial aft segment regions of the full-scale static motor designated FSM-5. The 11% KF/EPDM performed as expected and equivalent to CF/EPDM in all but the two aft-most ablation stations designated 9.3 and 10.7-inch stations (measured axially from the nozzle boss). The within-motor variation was less than or equivalent to CF/EPDM. The CF/EPDM also shows increased ablation in these aft-most stations on static test motors, but is much less severe. The 7% KF/EPDM performed slightly worse than expected, in general. The surprising result was that 7% KF/EPDM performed better than the 11% KF/EPDM at the 9.3-inch station. This condition was likely due to the asymmetrical erosion caused by nozzle vectoring. The results of the FSM-5 full-scale static test showed that the baseline CF/EPDM was vastly superior to both KF/EPDM materials in the aft dome environment. CF/EPDM is used in RSRM aft domes because of its high thermal-ablative resistance. CF/EPDM remained the aft dome insulation for severs exposure regions in the AF design. (1)

RESULTS AND DISCUSSION

Asbestos Free Insulation Design Configuration

The AF insulation design that resulted following FSM-5 uses four insulation materials to satisfy competing structural and thermal-ablative requirements. A 7% KF/EPDM was selected as the overall best replacement insulation for igniter components, nozzle flex boot and the internal acreage regions of each segment. A comparison of the RSRM versus the AF RSRM is shown in Figure 1. The aft dome design uses 11% KF/EPDM as a substrate to CF/EPDM in a sandwich construction similar to the current RSRM. The CF/EPDM was implemented as a result of the severe erosion experienced on FSM-5 in the aft dome region. The 11% KF/EPDM was developed for highly ablative environments with low structural loads. The detailed aft dome design is shown in Figure 2. The 11% KF/EPDM substrate provides greater erosion margin than the AS/NBR with minimal impact on production and cost.

The AF design uses 7% KF/EPDM in the case cylinder regions of each segment, in the igniter components and in the nozzle flex boot. The cured KF/EPDM is an orthotropic material. As such, it was shown to have marginal across-ply and perpendicular to fiber stress and interlaminar fracture toughness capabilities. Because of the lower tensile capability of the KF/EPDM in the across-ply and perpendicular to ply orientations, structural safety factors could not be met in several high stress regions. In these regions, SF/NBR was used to satisfy the structural requirements. SF/NBR provides much higher structural capabilities with minimal impact on production. The areas in the segments, the igniter and the adapter where SF/NBR was used are low thermal exposure environments. Therefore, the lower thermal capability of the SF/NBR provided adequate protection for these areas of the motor.

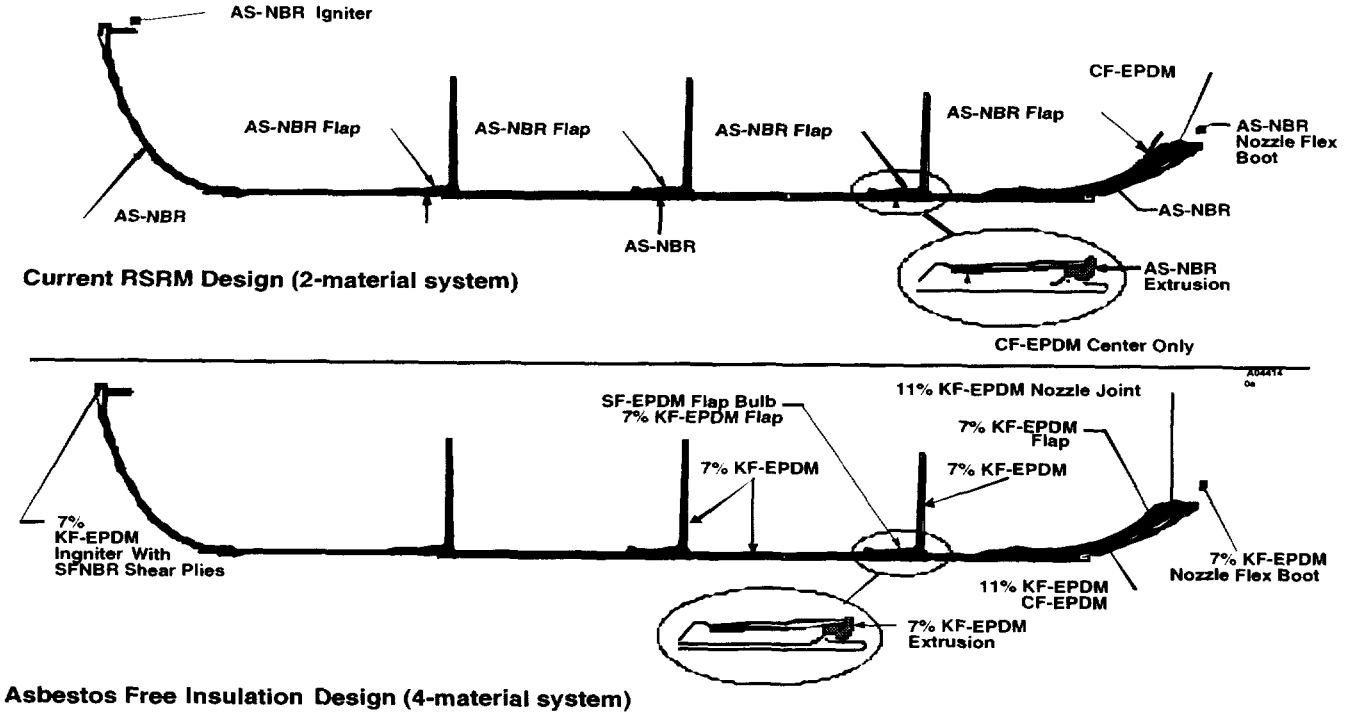

Figure 1 – Comparison of RSRM and AF Insulation Designs

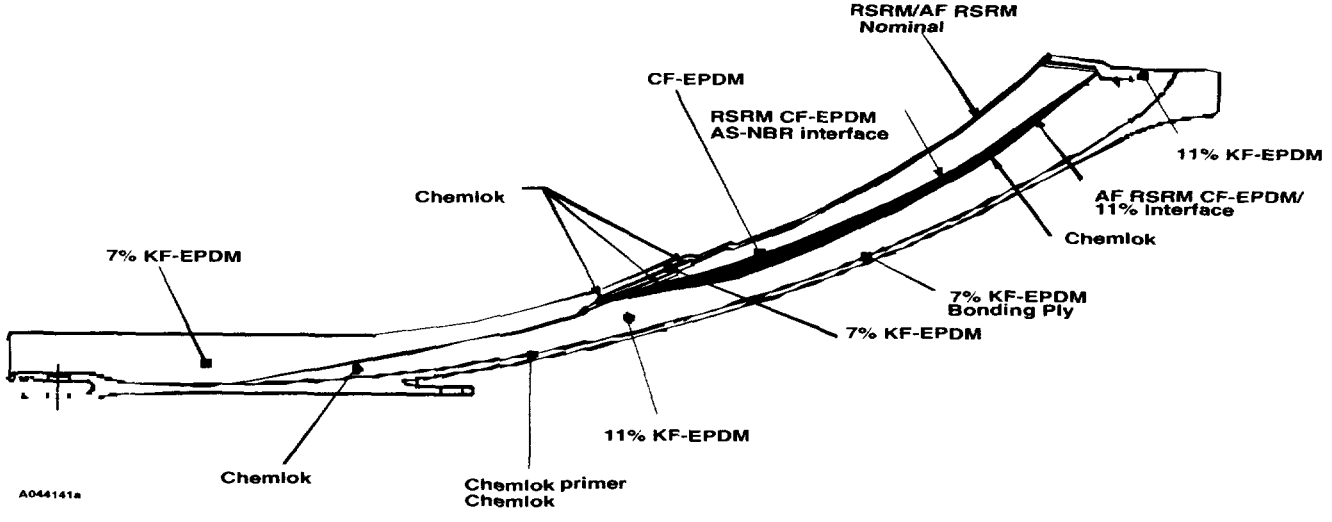

Figure 2 – AF Aft Dome Insulation Design

FSM-8 Design Demonstration

The intention of the AF insulation development program was to mature the design to the point that a demonstration of all major design features and components would be completed. Favorable results from a full-scale static test would confirm the validity of the design. However, full qualification of the design would require additional static tests and other qualification efforts. Thus, FSM-8 was selected as the demonstration test bed for the AF design. To cover the major design features, AF insulation, materials and processes were implemented on key portions of the static test motor in support of the AF replacement program. These areas are listed below and shown in Figure 3.

Internal insulation – igniter chamber (ID, OD and seal disks), adapter, initiator (helmet and seal disk) forward segment igniter boot region, aft/center segment, aft segment and nozzle flex boot
Joints – igniter inner (to adapter) and outer (to forward dome) joints, aft field joint
Liner – igniter chamber, initiator, aft/center segment and aft segment
Castable inhibitor – forward segment and aft/center segment
Forward-facing molded inhibitor – aft/center segment and aft segment
Adhesive – initiator, igniter chamber, initiator to adapter joint, seal disk bonds and insulation repairs

Erosion data from MNASA motors indicated that the performance of the AF insulation would be similar to the RSRM insulation. However, since the only actual performance data from a full-scale motor was in the aft dome region of FSM-5, the insulation thickness was increased in untested regions to meet a 2.0 thermal safety factor. Minimal impact was expected due to the increased insulation thickness for either ballistic or thermal performance.

As mentioned, the initiator to adapter joint was completed with AF adhesive. The igniter inner joint, mating the igniter adapter to the igniter chamber, was made of AF insulation. In order to have an AF igniter outer joint, the insulation at the forward dome mating surface was made of 7% KF/EPDM. The aft and aft/center segments, made of AF insulation, were mated to form an AF aft field joint. Because the center field joint would have mated dissimilar materials and served no demonstration function, the mating surface of the aft/center segment was changed to match the AS/NBR of the forward/center segment. A conflict of demonstration objectives existed on the FSM-8 nozzle-to-case joint. Because this joint had previously been successfully demonstrated on FSM-5, the mating surface material at the nozzle-to-case joint was changed to AS/NBR.

The igniter chamber and initiator were lined with AF liner, as were the entire aft/center and aft segments. The AF liner was similar to the RSRM liner except the asbestos fibers were replaced with Snow-Tex clay (silica) and a different thixotropic agent was used.

The AF castable inhibitor was applied to the FSM-8 forward segment to demonstrate the full-face inhibitor and to the aft/center segment, which is a short face inhibitor. The AF castable inhibitor was a material similar to the AF liner except for the amount of thixotrope used.

The RSRM forward-facing inhibitor thickness was maintained even though this was a first time demonstration on a full-scale motor. To compensate for the unproven inhibitor performance, the acreage insulation was increased to protect against inhibitor failure at motor ignition. This affected the insulation thickness in the acreage areas immediately aft of the inhibitors on the aft segment and on the aft/center segment.

AF adhesive was part of the AF baseline processes and was also used for insulation repairs. The adhesive was the same epoxy adhesive used on the RSRM with the asbestos fibers being replaced with Kevlar® fibers. The fiber loading required in the epoxy was less with the Kevlar® fibers because of their higher strength. The AF adhesive was used to secondarily bond several insulated components where the insulation had already been cured. The insulation bondlines that use the asbestos filled adhesive on the RSRM were completed using the AF adhesive on FSM-8. In addition, the igniter nozzle was a press-cured phenolic ring that was bonded to the steel case with the AF adhesive.

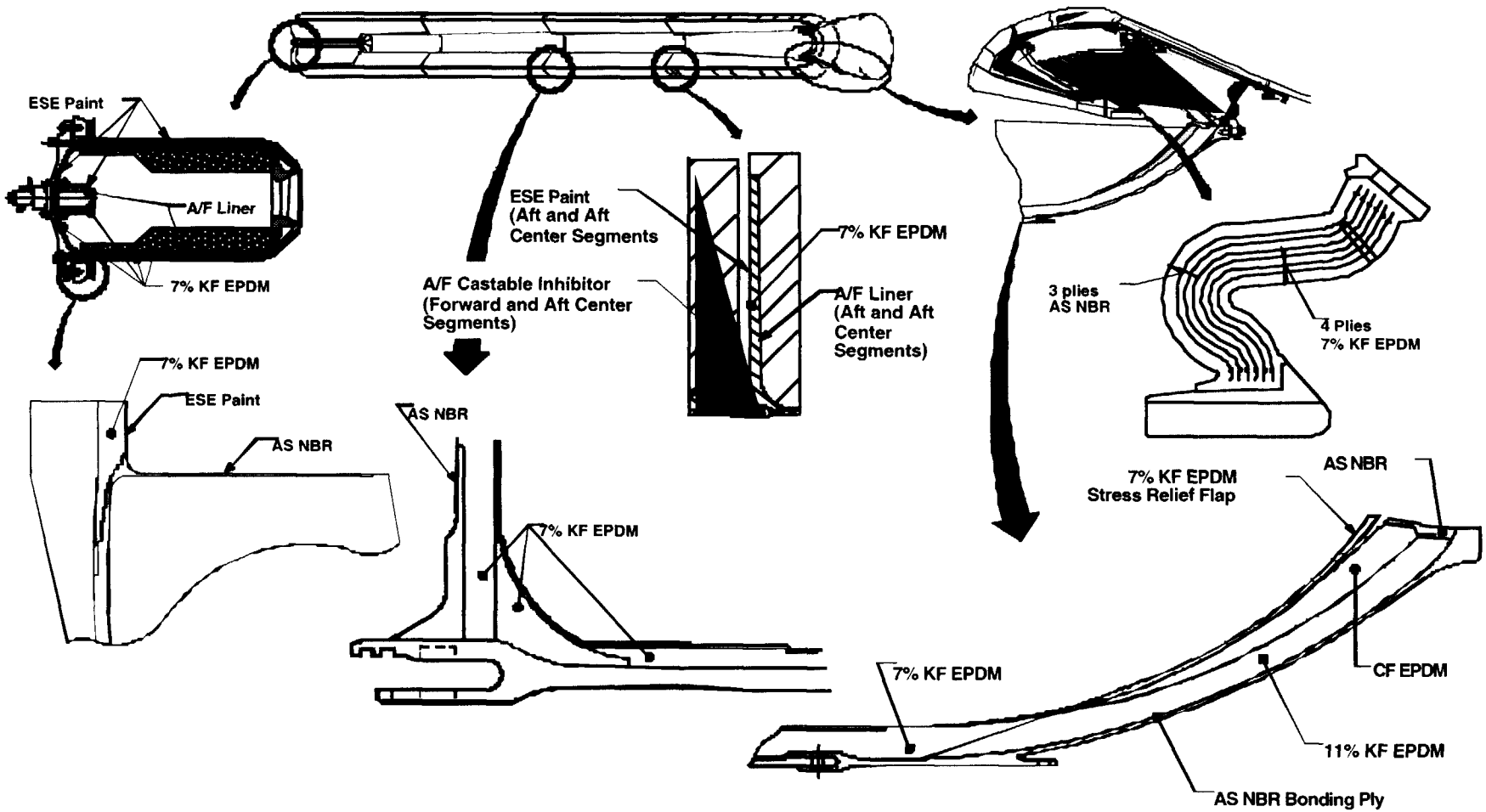

Figure 3 – FSM-8 Asbestos Free Insulation Configuration

Bondline Corrosion Corrective Action

Originally the AF insulation design had selected a Chemlok® 205 and Chemlok® 236X as the adhesive/primer system for the case to KF/EPDM insulation bondline. During subsequent process variability testing, indications of corrosion were found at the test specimen bondline. The corrosion on the specimens was generally accompanied by reductions in bondline strength, some of which were significant. Extensive testing was completed using design of experiment techniques to determine the cause of the bondline induced failures. The results indicated there were 6 factors that have some influence on the bondline corrosion formation. These factors were cure temperature, cure time, Chemlok® 205 age, Chemlok® 236X age, Chemlok® 205 thickness and Chemlok® 236X thickness.

An additional test effort was conducted to determine corrective actions that would eliminate the corrosion from the bondline. Three potential corrective actions were investigated. The corrective actions were to modify the cure cycle, to replace the Chemlok® 236X or to modify the Chemlok® 236X by adding a Dow Epoxy Resin 331 (DER331) additive to the Chemlok®. It was concluded from this testing, that using the Chemlok® 236X with the modified cure cycle was an acceptable solution to the corrosion problem. Significant corrosion reductions were observed at all processing variable conditions and no corrosion was seen with the nominal process conditions. It was also found that the replacement Chemlok® was clearly better than Chemlok® 236X or Chemlok® 236X/DER331 adhesives for corrosion inhibition and strength. This was particularly evident for the more corrosive environment using 2 year-old Chemlok® 205 primer under extended cure times and at the high side of the allowable cure temperature range.

The decision was made to replace Chemlok® 236X at the case to KF/EPDM insulation bondline because the replacement provided equal or better corrosion resistance and strength when using new Chemlok® 205. The more robust Chemlok® adhesive system provided by the replacement also allows greater process and material variations without creating bondline corrosion. This was the baseline planned for demonstration on FSM-8.

Prior to the actual build of the FSM-8 insulated components, process simulation articles were fabricated to evaluate the design and practice the manufacturing processes used in this design. The process simulation articles were built in a normal production environment using AF production procedures and materials. Part of the normal procedures was to construct witness panels that follow the full-scale hardware and were intended to represent, as close as possible, the material and bondlines that exist on the hardware. When the witness panels that represent the aft dome insulation configuration were tested, a shift in the bondline failure mode was noted. These witness panels typically fail cohesively within the insulation itself, indicating that the bondline is somewhat stronger than the material. However, the peel specimens indicated reduced peel strengths from what had been measured in the past and some failures were at the bondline rather than cohesive failures within the insulation.

An investigation of this bondline failure mode shift was initiated since this was the first time this observation had been seen on the program. Further laboratory investigation of this failure mode shift revealed that the Chemlok® system contains ingredients that may react with moisture in a slow exothermic reaction that occurs above 220 °F. During the extended cure times above 220 °F that the aft dome insulation bondline experiences, the reaction can occur and weaken the Chemlok® to KF/EPDM bond. KF/EPDM is cold stored prior to installation, which can result in moisture condensation on the rubber surface. This moisture can be trapped at the insulation to case interface and may not be absorbed into the rubber because of the hydrophobic nature of EPDMs. The RSRM does not experience this problem. The bond strength reduction and failure mode shift were duplicated in lab testing. The major contributors were determined to be full-scale double cure cycles, older Chemlok® 205 primer and higher moisture content in the bondline. The shift does not occur for shorter cure cycles, but only occurs with the extended cure times associated with the double cured aft dome. The final conclusion was that a combination of conditions in the aft dome must be present for the failure mode shift to occur, but their occurrence was a possibility on a full-scale motor in the aft dome region.

For FSM-8, a temporary solution to the problem was to install a thin ply of AS/NBR against the case and then vulcanize KF/EPDM to this ply. All of the bondlines that were created for this revised configuration had previously been tested and therefore represented an acceptable solution. This configuration had also previously been built on an earlier process simulation article. Other alternative solutions had not been fully developed at that time and any further development effort would have delayed the static test firing.

ESE/ESD Issue and Resolution

The AS/NBR used on the RSRM is a naturally dissipative insulation, which resists static charge generation. Any charge that is created dissipates throughout the insulation to the case and to a ground source. KF/EPDM is a very non-conductive and highly static producing insulation. This creates two major potential hazards during processing. The first hazard is from flammable vapor/air mixture ignition and the second is propellant ignition through a discharge from the insulation surface due to triboelectric charge build-up that cannot migrate to ground. The general approach to eliminating these potential hazards was to engineer the hazards out of the AF design and production processes rather than prove that the high voltage electrical charge generated during motor processing would not have sufficient energy to ignite vapors or propellant.

Process materials and operations were reviewed where improvements or changes could be made to reduce or eliminate the ESE/ESD potential. Slowing down contact-electrification type operations controlled many ESE generation processes. Use of ionizers, dissipative floor mats, conductive shoes and eliminating dry wipes were implemented. Vapor levels present in operations involving flammable solvents were monitored to ensure concentration levels were below acceptable limits. Wet abrading was required on all insulation surface repairs. Operators were retrained in dealing with ESE hazards. Inert process simulation articles were used to test changes made to the processes and to monitor levels of ESE generation. These implemented changes were sufficient to create safe operating environments in all areas and were demonstrated by monitoring hardware and personnel.

Other changes were made to the engineering design. For example, abrasion and cleaning of the RSRM field joints and igniter joints mating surfaces was done on loaded segments. Testing determined that abrasion of these joints could be completed on the insulated components prior to loading with propellant without creating a hazard and without impacting the bondline strength. Prior to lining, the RSRM cured internal insulated segment is hand cleaned with a flammable solvent, which has the potential to create a flammable vapor/air mixture inside the segment. It was noted that operators do routinely contact the KF/EPDM and could generate ESE in localized areas. To eliminate this potential hazard, another cleaning solvent, which is non-static producing and non-flammable, was tested for cured insulation and demonstrated on FSM-8.

The largest ESE/ESD concern existed for the exposed external surfaces of KF/EPDM. These surfaces are susceptible to contact-electrification both during planned processing as well as from incidental contact. The first approach to this issue was to select or develop a static dissipative paint that would mimic the bulk dissipative properties of AS/NBR. Even though conductive paints are used in several industries, an acceptable dissipative paint could not be found. Therefore, it was determined to modify the Hypalon® paint used to cover the RSRM forward-facing inhibitors and make it dissipative by using doped semiconductor additives from the paint industry. Several Electro-Conductive powders were selected to achieve the targeted surface resistivity. Several of the additives were able to initially match the desired surface resistivity, but the surface resistivity of each paint formulation varied after exposure to humidity, temperature and deformations. The data suggested that each of these type exposures changed the spatial relationship of the conductive powder, which affected the number of connecting paths within the paint. Since segment exposure to these conditions could not be controlled, the final resistivity would vary depending on the initial resistivity and the degree of exposure to these environments.

The solution of this issue was to make the ESE paint more conductive by increasing the concentration of Electro-Conductive powders in the Hypalon paint. A conductive paint complicated the processing by requiring that it be grounded at all times, but it allowed paint exposure to a much wider range of processing environments. The conductive paint was developed, tested on process simulation articles and then all live operations were monitored during the entire FSM-8 production process to assure safe operations.

The ESE/ESD hazards were successfully managed for FSM-8, although most operations were much more complicated and required more monitoring than was desired. An effort has been undertaken to modify the KF/EPDM itself and make it dissipative like AS/NBR. Several lab mixes of rubber have matched the AS/NBR ESE properties. However, any modification would be best if the thermal-ablative and structural material properties are not reduced. Combinations of conductive additives and polymer replacements have been tested. Full-scale production batches are planned and will be tested for acceptable material properties.

FSM-8 Test Results

FSM-8 was successfully static tested on February 17, 2000. The post-test evaluations indicated the components fabricated with AF insulation, liner or adhesives, performed as expected. Post-test inspections of the segments indicated no abnormal erosion or other abnormal conditions.

AF Igniter Components

The AF insulation in all igniter components performed as expected and all minimum thermal safety factors were acceptable. Generally, the igniter AF insulation performance was equal to that of the baseline AS/NBR insulation. No abnormal conditions were found. The Material Decomposition Depths (MDDs) for the FSM-8 igniter chamber and adapter were calculated from pre-fire and post-test insulation thicknesses. Data evaluations show that median MDDs for the FSM-8 igniter were slightly less than those for the FSM database for all but two stations. The increased MDDs at these two stations were only slightly higher. The adapter insulation performed as expected. The igniter chamber outer insulation appeared nominal. The 7% KF/EPDM had a thick char cap remaining. The underlying KF/EPDM was intact and uniform with small bubbles in the heat affected layer. No anomalous conditions were noted. The AF initiator helmet performed nominally. The entire helmet was intact and remained bonded to the initiator chamber. Heat effects and char of the KF/EPDM helmet were typical of static tested motors.

AF Internal Insulation

The performance of the AF insulation in the FSM-8 segments was as expected and no abnormal conditions were observed. The aft dome region of the motor experiences the most severe erosion environment. AF insulation had previously been tested in the aft dome of FSM-5 and some areas of severe pocket erosion resulted. The revised AF design on the FSM-8 aft dome region, with CF/EPDM used on the flame front, indicated no abnormal erosion. In the aft dome region where KF/EPDM was exposed, the MDDs were equal to or slightly better than the static test database. Aft of station 215, which is near the middle of the segment, to the stiffener factory joint, the MDDs were slightly higher than the database. Forward of station 215, in the low exposure locations of the segment, the MDDs were higher than the database. This may be due to different performance characteristics such as how the char layer was established or may have been affected by the AF liner that was also used on this segment. If the liner erosion were more severe for the AF liner, then the resulting MDDs would show this impact most dramatically in the low exposure areas.

Erosion performance of the AF 7% KF/EPDM in the aft segment acreage areas was near the predicted performance. Plots of performance, as shown by comparing median MDDs for FSM-8 aft segment versus the FSM static test database, are included in Figure 4. Similar observations can be made for the center/aft segment. Figure 5 indicates the 7% KF/EPDM has lower MDDs in the higher exposure region at the aft end of the segment. From station 40 going forward in the segment to station 275, these stations represent low exposure areas, which again indicate higher MDDs for FSM-8 than the database. The stations forward of 275 had liner remaining post-test and indicated no insulation erosion. All minimum safety factors for the AF case acreage insulation were acceptable.

AF Nozzle Hybrid Flex Boot

Some concern existed regarding the first-time use of 7% KF/EPDM in the nozzle flex boot. Although char tenacity tests had been conducted, it was still unknown how the AF insulation would perform with the standard nozzle vectoring duty cycle during a static test. The first 4 plies of the FSM-8 flex boot were 7% KF/EPDM and the remaining 3 plies were AS/NBR. Post-test inspections of the flex boot revealed it was in good condition. Of the original 7 plies of insulation, the number of remaining plies was nominal and was well within the static test experience. All performance thermal safety factor requirements were met.

AF Joints

The aft field joint was fabricated of AF insulation. The joint appeared to have remained sealed during motor operation with no leak paths observed. The post-test inspection of the pressure sensitive adhesive applied to

the joint mating surfaces indicated that typical bondline contact had been made. The exposed joint surfaces showed typical erosion. The igniter inner and outer joints also performed as designed and exhibited no leak paths.

AF Liner and Castable Inhibitor

The AF liner that remained was heavily heat-affected, but intact, and appeared to function well with no indication of unacceptable performance. Inspection of the acreage insulation gave no indication of liner or castable inhibitor failures that would result in increased erosion or might be indicated by pressure blips during motor operation.

AF Forward-facing Inhibitors

The AF forward-facing inhibitor heights were normal for a static test and indicated no abnormal areas of missing material. The remaining forward-facing inhibitors were measured on the aft and center/aft segments. Both of these inhibitors were made from 7% KF/EPDM and performed similar to the baseline AS/NBR insulation. The median remaining AF inhibitor heights were only slightly different than the median remaining static test inhibitor heights.

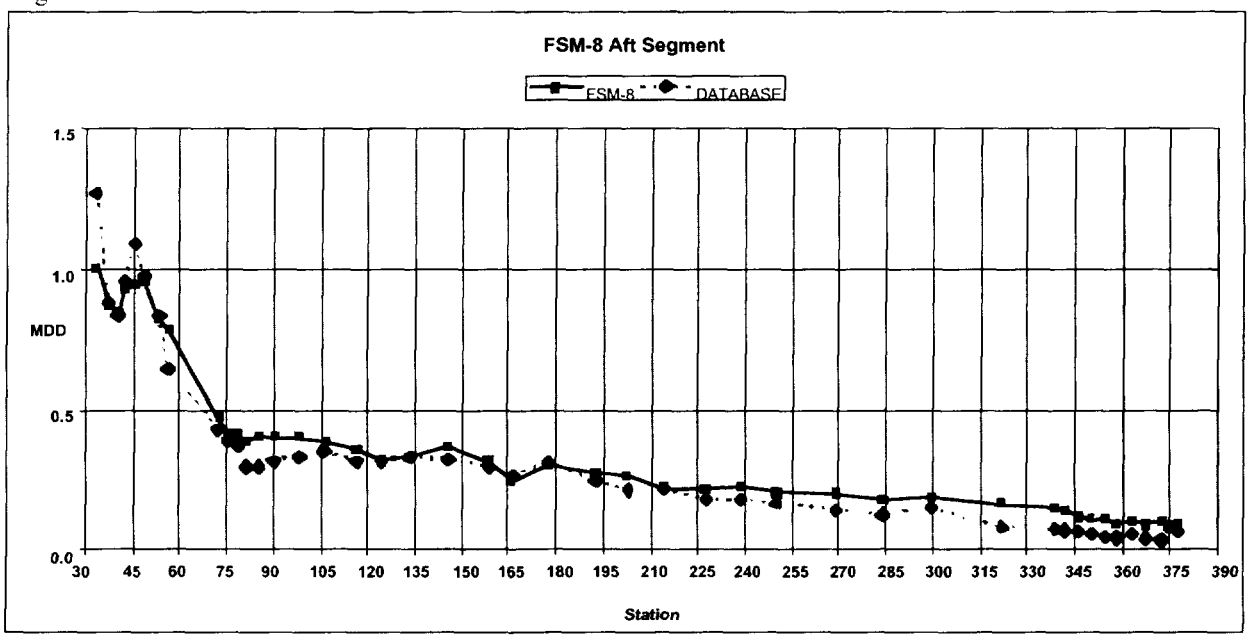

Figure 4 – Aft Segment Comparison of FSM-8 to Database

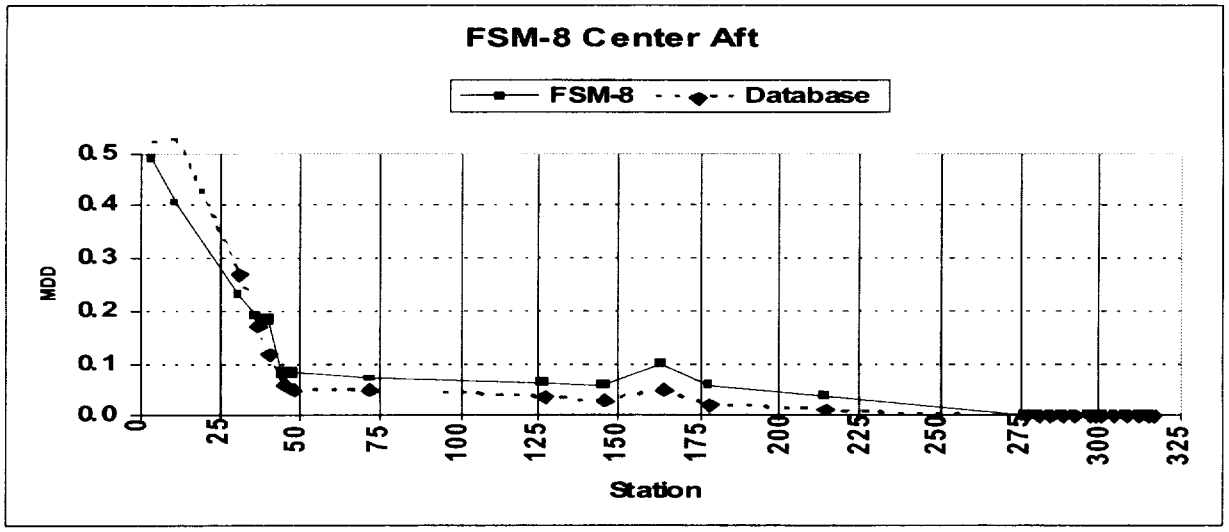

Figure 5 – Center/Aft Segment Comparison of FSM-8 to Database

Real-time Instrumentation Data

The RSRM forward-facing inhibitors restrict propellant surface burning on the forward face of the aft and center segments by insulating the propellant grain from the hot combustion gases, even though the inhibitors themselves are thermally ablating in the severe thermal environment. In the past, attempts have been made to predict the thermal performance of these inhibitors. However, since there is only a stub remaining for the aft joint and center joint inhibitors, it has been impossible to confirm the accuracy of these analyses. The FSM-8 aft and aft/center segment inhibitors were made of AF 7% KF/EPDM. These inhibitors were instrumented to obtain measured real-time inhibitor char line recession data for model calibration purposes and for a direct measurement of inhibitor safety factors. The instrumentation consisted of thermocouples and eroding potentiometers. The eroding potentiometer consisted of two small (3 mils diameter) twisted resistive wires that were polyimide insulated. (2) The wires were placed in the inhibitor during insulation lay-up parallel to the direction of erosion. During motor operation, the inhibitor eroded away, exposing the tip of the instrument to the heat of the internal motor environment, causing it to recede also. As the wires were heated, the polyimide insulation broke down at or near the tip and made an electrical junction. The electrical resistance of the wire pair decreased as its length receded and was measured as a function of time. Because the breakdown of the polyimide occurred near the pyrolysis/char interface of the decomposing insulation, the eroding potentiometer measured the continuous real-time char line recession of the inhibitors.

FSM-8 demonstrated the performance of the 7% KF/EPDM inhibitors in the motor environment. Real-time inhibitor eroding potentiometer and thermocouple data were successfully collected during motor operation for the first time on FSM-8. The comparison of the thermocouple data with the eroding potentiometer data gave good agreement, which indicated that the potentiometers worked well. The data showed the 7% KF/EPDM inhibitors performed well and there were no abnormally high char rates. The measured data verified that the thermal safety factors were greater than the 1.5 requirement for an assumed minimum inhibitor thickness. (3)

Conclusion

An Asbestos Free insulation design was successfully demonstrated on a full-scale Flight Support Motor. Major components were manufactured and shown to function well and as expected. Insulation thermal performance safety factors were calculated based on pre-test and post-test measurements and were found to meet all requirements. Several design issues were worked and acceptable solutions demonstrated. Some additional development work was started to make the design less complicated from a production standpoint. Further demonstration of the final design will be required prior to implementing an asbestos free insulation onto flight motors.

REFERENCES

1) Fitch, V. and Eddy, N., Space Shuttle Solid Rocket Motors, Asbestos Filled Insulation Replacement, AIAA 97-2992 Publication, July 1997.
2) McWhorter, B. B., Johnson, M. A, Bryner, B. B. and Ewing, M. E., An Instrument for Real-time Measurements of Solid Rocket Motor Insulation Erosion, AIAA 99-2136 Publication, June 1999.
3) McWhorter, B. B., Analysis of FSM-8 Inhibitor Instrumentation Data, TWR-77162, Thiokol Propulsion Publication, June 2000.
4) Mossman, B. T., Bignon, J., Corn, M., Seaton, A. and Gee, J. B. L., *Asbestos: Scientific Developments and Implications. for Public Policy*, Science, Vol. 247, pp. 294-301, January 1990.

Aerogel Projects Ongoing in MSFC's Engineering Directorate

David A. Shular
MSFC/NASA
Mailstop: ED25
Huntsville, AL 35812
(256) 544-8734 (ph)
(256) 544-0800 (f)
email: David.A.Shular@msfc.nasa.gov

Gweneth A. Smithers
MSFC/NASA
Mailstop: ED34
(256) 544-0282 (ph)
(256) 544-7255
email: Gweneth.Smithers@msfc.nasa.gov

Joel L. Plawsky
Rensselaer Polytechnic Institute
Troy, NY 12180-3590

Introduction

When we speak of an aerogel material, we are referring more to process and structure than to a specific substance. Aerogel, considered the lightest solid material, has been made from silica for seventy years. Resorcinol-formaldehyde, organic aerogels have been developed more recently. However, aerogel can be made from almost any type of substance, even lead. Because an aerogel is mostly air (about 99 %), the solid substance used will affect the weight very little.

The term "aerogel" connotes the sol-gel process used to manufacture the material. The aerogel begins as a liquid "sol," becomes a solid "alcogel," and is then dried to become an "aerogel." The final product has a unique structure, useful for exploitation. It is an "open pore" system with nano-sized particles and pores, has very high surface area, and is highly interconnected. Besides low weight, aerogels have ultimate (lowest) values in other properties: thermal conductivity, refractive index, sound speed, and dielectric constant. Aerogels were first prepared in 1931 by Steven Kistler, who used a supercritical drying step to replace the liquid in a gel with air, preserving the structure (1). Kistler's procedure involved a water-to-alcohol exchange step; in the 1970's, this step was eliminated when a French investigator introduced the use of tetramethylorthosilicate. Still, alcohol drying involved dangerously high temperatures and pressures. In the 1980's, the Microstructured Materials Group at Berkeley Laboratory found that the alcohol in the gel could be replaced with liquid carbon dioxide before supercritical drying, which greatly improved safety (2). The most recent major contribution has been that of Deshpande, Smith and Brinker in New Mexico, who are working to eliminate the supercritical drying step (3). When aerogels were first being developed, they were evaporatively dried. However, the wet gel, when dried, underwent severe shrinkage and cracking; this product was termed "xerogel." When the autoclave drying step was introduced, the final product was without

cracks and showed only minimal shrinkage; this product was termed "aerogel." In the 1990's, Deshpande, Smith and Brinker developed an evaporative drying procedure in which the wet gel is chemically "capped" so that the material, which undergoes shrinkage, springs back to its original size when evaporatively dried. This new type of xerogel, while uncracked and almost the same size as the wet gel, differs from the autoclave-dried product in that it is less porous (approximately 70%, as compared to 99% for aerogels).

The unique structure of an aerogel has suggested many diverse applications. In addition to the focus on superinsulation, aerogel has been considered or used in the following applications: catalyst support, micrometeroid capture, subatomic particle detection, impaction safety, desalination, toxicity sensing, acoustic and electrical insulation, and optical coatings (4, 5). Nanocomposite work is an active area in aerogel research. Aerogels are nanomaterials because of their nano-sized pores and particles. When aerogels are used in composite manufacture, the aerogel is the substrate, to which another phase (nano or larger) is added. The second phase can be added during the sol-gel processing (before drying), through the vapor phase (after drying), or the aerogel backbone can be chemically modified through reactive gas treatment.

The problem with aerogels is their low tensile strength and lack of elasticity. Therefore, the challenge is to find ways to make them stronger or ways to circumvent the strength issue. Organic aerogels have slightly higher strength than base silica aerogels, while the carbonized version has 3-5 times the break strength of the base aerogel.

A standard silica aerogel has a thermal conductivity of about 17 mW/M-°K (0.00980075 BTU-ft/hr-ft^2-F). This is an order of magnitude lower than the cryogenic foams that NASA currently uses today. A carbonized silica has about 13 mW/M-°K (0.0075 BTU-ft/hr-ft^2-F). These values are at atmospheric pressure. At pressures of around 50 torr, these values drop (and flatten out) to 8 and 4 mW/M-°K (0.0046 and 0.0023 BTU-ft/hr-ft^2-F) respectively.

The passage of thermal energy occurs in three modes, solid conductivity, gaseous conductivity, and radiative transmission. Solid conduction is limited due to the fact that the aerogels possess such a small amount of solid material. These solids consist of very small particles linked together in a three-dimensional network with many "dead-ends." This makes any thermal conduction extremely ineffective. Gaseous conduction is limited by the fact that the gas must follow a tortuous path, and with pore sizes less than the mean free path of air, the gaseous molecules are more likely to impact the pore surface before they collide with another gas molecule. The third method of transport, radiative transmission, is the primary mode of heat transfer in aerogels. Basic silica aerogels are reasonably transparent in the infrared region, especially between 3-5 microns. At low temperatures the radiative component is not a significant problem. At higher temperatures, carbon can be added as an effective absorber of infrared radiation.

There is work going on at NASA's Ames Research Center, and other places, to address radiative heat transfer. One method involves infusion or encapsulation of the aerogel into another material. Ames has developed an aerogel infused AETB (Alumina Enhanced Thermal Barrier)

tile, like what is currently flown on Shuttle, in hope of producing a single material that performs both cryo and aero-heating insulation duties in a single material.

In the Engineering Directorate at MSFC, our approach to the research and development of aerogel materials recognizes our relative inexperience in this technology area. We have chosen to partner with other NASA Centers, universities and industry to make the most of our mutual efforts in aerogel research.

Composite, Cryogenic, Conformal, Common Bulkhead, Aerogel-insulated Tank

Through award of a NASA Research Announcement (NRA), a Composite, Cryogenic, Conformal, Common Bulkhead, Aerogel-insulated Tank (CBAT) is being developed at MSFC. The CBAT team includes engineers from the Structures, Mechanics & Thermal Department (S.M & T) and the Materials, Processes & Manufacturing Department (MPM). Thiokol and Sverdrup also provide engineering support. This work is funded as a next generation RLV project. The intended propellants are liquid oxygen (LOX) and high-grade kerosene (RP); however, liquid nitrogen and water will be used to test this subscale tank. The tank will contain enough propellant to fire the Fastrac engine for 15 seconds. Tank pressure and compressive loads will also be based on the Fastrac engine. Aerogel insulation is being used at two locations: in the common bulkhead area (between the LOX and RP tanks) and around the skirt that surrounds the two tanks.

We explored a number of aerogel possibilities for the common bulkhead area. At the current time, Nanogel ™ (an evaporatively dried, silica-based xerogel which has been powdered and compressed, with additives, into a near monolith) is our baseline component. For testing, we obtained 8-inch diameter, _ inch thick disk samples of Nanogel ™ from Nanopore, Inc. in Albuquerque. The ASTM procedure for thermal conductivity testing requires samples of this size and shape. Because of the loads which will be experienced by the xerogel when the tank is pressurized, we asked Nanopore to compact this material at 75 psi, instead of 15 psi which is standard practice. Nanopore normally seals the material under a slight vacuum with a metallized, plastic laminate wrapper. We requested three types of samples: vacuum-sealed with air; sealed without vacuum; and krypton filled, sealed without vacuum. We also obtained one sample (vacuum-sealed with air) which was compacted with the standard 15 psi. The 75 psi samples were tested for thermal conductivity and compression strength. The 15 psi sample was tested for compression strength only. The results of these tests are shown in Tables 1 through 3 and Figures 1 through 4. Since the vacuum-sealed sample should insulate better than the Krypton-filled sample, we believe the vacuum-sealed sample may have lost vacuum. Attempts to perform thermal conductivity testing at cryogenic temperatures were not successful. The Holometrix Micromet Model GHP-200 employed was designed for higher temperatures. We are currently making plans to perform cryogenic testing of these samples at another facility. Thermal conductivity testing was performed by Scott Taylor of ASRI; he used ASTM Method C-177, Standard Test Method for Steady-State Heat Flux Measurements and Thermal Transmission Properties by Means of the Guarded-Hot-Plate Apparatus. Compressive fatigue testing was performed by Andrew Hodge, MPM Department.

In cooperation with Dr. Susan White at NASA's Ames Research Center, we are also pursuing an alternative type of aerogel for the common bulkhead area. Nomex™ honeycomb was cut into 8-inch disks here at MSFC, and subsequently shipped to Ames. In Dr. White's laboratory, an organic aerogel, formulated for compatibility with the honeycomb material will be used to fill the honeycombs, which will then be supercritically dried in an autoclave. These samples will be shipped back to MSFC for testing.

Around the skirt, we plan to install an aerogel blanket system. Because of his experience with aerogel blankets, we asked Mr. James Fesmire of Kennedy Space Center to assist us in this effort. The insulation system will include a Teflon-coated fiberglass cloth (beta cloth) on the cold side, an aerogel composite blanket (from Aspen Systems in Boston), and Silverlux™ film on the warm side. We are currently devising a mechanism by which CBAT team members at MSFC and Cryogenic Testbed personnel at KSC can exchange services in a way that is beneficial to both Centers.

Xerogel Optical Toxicity Sensor

Because of his expertise in aerogel materials, Dr. Joel Plawsky, a professor at Rensselaer Polytechnic Institute, was invited to spend the summers of 1999 and 2000 as a Faculty Fellow in the MPM Department at MSFC. Our awareness of the environmental and safety issues associated with the standard autoclave procedure used in production of aerogel and our study of recent advances in elimination of the autoclaved, supercritical drying step, led us to pursue, with Dr. Plawsky, aerogel production which employed evaporative drying rather than autolcave drying. This work, performed in 1999, laid the foundation for work performed in 2000 to develop an optical toxicity sensor.

Our goal during the summer of 1999 was to determine if the evaporative drying step used for thin-film aerogels in Dr. Plawsky's lab at RPI could be adapted to produce thicker, monolithic aerogels. Tetraethoxysilane (TEOS), ethanol, water, and hydrochloric acid were mixed and heated for 90 minutes. Acid catalysis promoted hydrolysis of the TEOS and initial polymerization. The precursor sol was then mixed with a solution of ammonium hydroxide. At room temperature, base catalysis promoted branching and crosslinking of the sol leading to gel formation in about 40 minutes. The wet gel was aged in a two-step process, performed at room temperature. In the first step, the gel was placed in a solution of ammonium hydroxide and ethanol, where it remained on a shaker table for 24 hours. The gel was then rinsed in ethanol and immersed in a solution of TEOS and ethanol. The gel was then aged from 24 to 72 hours at room temperature. Following this step, the gel was thoroughly rinsed in ethanol. Afterwards, the gel was immersed in hexamethyldisiloxane (HMDSO), and the capping agent was slowly added to yield a 10 mole% solution of trimethylchlorosilane in HMDSO. Gels were allowed to sit in the capping solution for 24 –48 hours on the shaker table. Subsequently they were flipped and immersed in a new solution to ensure complete treatment. After capping, the gels were washed in HMDSO again before drying began. Initial experiments drying the gels at room temperature failed. Eventually, the procedure was modified and resulted in successfully dried gels. The gel was placed in a closed petri dish (2" in diameter) which was drilled with a 1/16" hole at the top. The gels were placed on x-shaped teflon supports to elevate them from the bottom surface of the dish and remove any capillary suction there. This allowed the gels to

expand and contract freely during drying. The petri dishes were set on a hot plate, on top of a crucible insulator, and covered with a 600 ml fritted glass filter. The filter controlled the evaporation rate and kept the draft from the hood away from the specimen. Depending on the sample, drying took from 3 to 24 hours. Samples produced were 1/8" thick.

Aerogels exhibit high surface area, stability, and transparency. They can easily transport gases and can be filled with other phases. These properties make aerogels well-suited for use in optical sensors. When Dr. Plawsky returned to MSFC in the summer of 2000, we began work on a toxicity sensor which might have application in a closed-system situation like Space Station, where toxic chemicals must be monitored at a highly sensitive level. Figure 5 illustrates the plan for this sensor. Our plan for the summer was to continue development of various types of aerogel using the manufacturing procedure developed during the previous summer. These aerogels would be candidates for the layer that covers the waveguide. The waveguide element of this device is being developed at RPI by Dr. Plawsky and his graduate students. The aerogel or xerogel material forms the cladding of an integrated optical waveguide. The core material can be made of anything that has a higher refractive index than the xerogel and that the xerogel will adhere to. The xerogel component acts as the sensing element of the device since it can contain organic functionality that will interact with materials in the atmosphere. These are absorbed into the xerogel, changing its optical properties. The changes are read by the waveguide either as a change in the propagation characteristics of the waveguide or as a change in the intensity of the light as it passes through the waveguide. The sensitivity of the device comes from the great surface area of the xerogel and the large optical interaction length of the waveguide. At this writing, we are completing manufacture of these types of xerogels at MSFC. Two are hybrid silica-titania and silica-zirconia gels. These materials can be used as oxidation substrates for destruction of volatile organic compounds (6) in spacecraft. The high surface area of xerogels makes them well-suited for making compact chemical reactor systems (7). We are also making organic/inorganic hybrid xerogels with amino, mercapto, cyano, and saturated hydrocarbon functionality. Amino functional groups can be used to absorb and sense acid vapors, mercapto groups are useful for incorporating metals into the gels and using the metals as sensing elements, cyano groups are reactive functional groups to acidic and basic groups and the hydrocarbon groups are meant for absorption of nonpolar organic constituents. In addition, the amino and cyano groups can also be used to immobilize enzymes or antibodies into the gels for biological operations (8). In all cases the interaction of the compound of interest with the functional groups in the xerogel changes the optical properties of the xerogel and provides for the sensing function when the xerogel is used as a cladding for the optical waveguide.

Thermally Integrated Structures

Thermally Integrated Structures (ThIS) are a long-term goal at MSFC. NASA needs a reusable launch vehicle (RLV), single-stage-to-orbit, which utilizes liquid oxygen/liquid hydrogen chemical propulsion. To attain this goal, vehicle mass fraction must be high, 0.9 or greater. Vacuum specific impulse must be maximized, but realistically will be limited to ~ 460 seconds. The vehicle should look and operate as an aircraft. Vehicle volume must be reasonable to enable handling and operability.

A major difference between aircraft and RLV's is the "use temperature" of major structures. RLV aerodynamic surfaces can be exposed to environments resulting in surface temperatures up to 1800°F (leading edges, up to 3000°F). These hot surfaces must be non-catalytic. Cryogenic tankage will be exposed to –420°F, and must be compatible with liquid and gaseous oxygen and hydrogen. Heat leakage through the structure must be small. No cryopumping within the structure can be tolerated; the structure must be impermeable. The system must be durable, easily weatherproofed, lightweight, manufacturable and maintainable. It must have low operational costs. Material systems must be manufacturable in large sections. Joining and attachment techniques must be easily implemented.

Like aircraft, our current design approach includes use of lightweight materials of construction. Unlike aircraft, we add a Thermal Protection System (TPS) and cryogenic insulators to enable use temperatures for these structures. These additions add weight and cost, while reducing operability. These systems also add complexity in the area of attachments and add requirements such as allowable bond-line temperatures, complicating the design problem.

Estimates of RLV GLOW have indicated that this design approach, with these materials of construction and LOX/LH2 propulsion, does not meet SSTO feasibility requirements (mass fraction at an operable vehicle volume). Graphite-epoxy dry structures and integral cryotankage were thought to offer weight efficiency sufficient to enable SSTO, but if current RLV estimates derived from X-33 experience do not enable SSTO, then alternate approaches must be considered. One promising technology for RLV is advanced and integrated fundamental materials of construction for airframe and cryotank structures. We want to investigate feasibility of development of lightweight Thermally Integrated Structures with a large range of operating temperatures, and low heat transfer through the thickness of the material system.

The weight of such a material system must be significantly less than standard designs (which use lightweight materials with lightweight cryogenic insulators and TPS materials. For an investigation like this, we are considering a titanium honeycomb (use temperature ~ 1200F) filled with a high temperature aerogel. Very low heat transfer from face to face would be the goal of such as system, with all materials capable of withstanding both cryogenic to aero entry use temperature, as well as temperature gradients across the structure. Life should be at least 100 thermal/structural cycles. Manufacturability in very large sections is a key to operability. A severe limitation in the areas of cost and operability for current TPS material systems is the need to attach thousands of piece parts to very large structures.

The Thermodynamics and Heat Transfer Group in the Structures, Mechanics &Thermal Department (SMT) at MSFC have prepared a computational model which employs a titanium honeycomb core utilizing solid fill carbon aerogel. The facesheets are aluminum on the inside surface and titanium on the outer surface. The core dimensions consist of 3/8" diameter centers with a wall thickness of 0.005". The baseline design is for a 1" thick panel with counterbores of 2" diameter and 3/8" deep. The counterbores are oriented such that there is a slight overlap in order to provide a design in which there is no direct conduction path through the thickness of the panel. In the actual panel to be constructed, the counterbores will probably be square such that the edges can be aligned in order to ensure that there are no gaps created by the overlying circles which might allow for a more direct conduction path. Several densities of carbon aerogel have

been considered in an attempt to learn which density may be the best choice. According to the literature from the national labs, radiation is the primary mechanism of energy transport at elevated temperatures for generic aerogels; the solid conductivity is small in comparison. However, since this design is a closed system with direct contact among all materials (and the added carbon is an infrared absorber) conduction has been the primary focus. Property data is still being collected. The SMT and the MPM Departments are writing proposals and actively seeking funding for Thermally Integrated Structures projects.

Table 1. Apparent Thermal Conductivity of Nanogel™ TI-6000, 800 mbar abs. No Vacuum

Sample Position	*Thickness (mm)*	*Diameter (mm)*	*Mass (g)*	*Density (kg/m³)*
Top	13.20	203.20	96.20	224.73
Bottom	13.80	203.20	94.10	210.27

Mean Temperature, Degrees C (Deg F)	*Apparent Thermal Conductivity, W/mK*
4.2 (39.6)	0.016466
4.2 (39.6)	0.016826
9.4 (49.0)	0.017191
9.4 (48.9)	0.017326
18.4 (65.1)	0.018205
18.4 (65.2)	0.018246
35.1 (95.1)	0.019066
35.0 (95.0)	0.018990
56.4 (133.5)	0.020265
60.2 (140.3)	0.020675

Table 2. Apparent Thermal Conductivity of Nanogel™ TI-6000, 1 mbar abs. Vacuum

Sample Position	*Thickness (mm)*	*Diameter (mm)*	*Mass (g)*	*Density (kg/m³)*
Top	12.50	203.20	97.80	241.26
Bottom	12.40	203.20	94.50	235.00

Mean Temperature, Degrees C (Deg F)	*Apparent Thermal Conductivity, W/mK*
-5 (23)	0.011513
2.2 (36)	0.011339
13.8 (57)	0.012672
18.3 (65)	0.012885
32.8 (91)	0.013585
47.7 (118)	0.012485

Table 3. Apparent Thermal Conductivity of Nanogel™ TI-6000, 800 mbar abs. Krypton

Sample Position	*Thickness (mm)*	*Diameter (mm)*	*Mass (g)*	*Density (kg/m³)*
Top	12.80	203.20	96.90	233.44
Bottom	13.70	203.20	99.40	223.73

Mean Temperature, Degrees C (Deg F)	*Apparent Thermal Conductivity, W/mK*
1.1 (34)	0.010216
6.1 (43)	0.010266
21.7 (71)	0.011066
32.8 (91)	0.012039

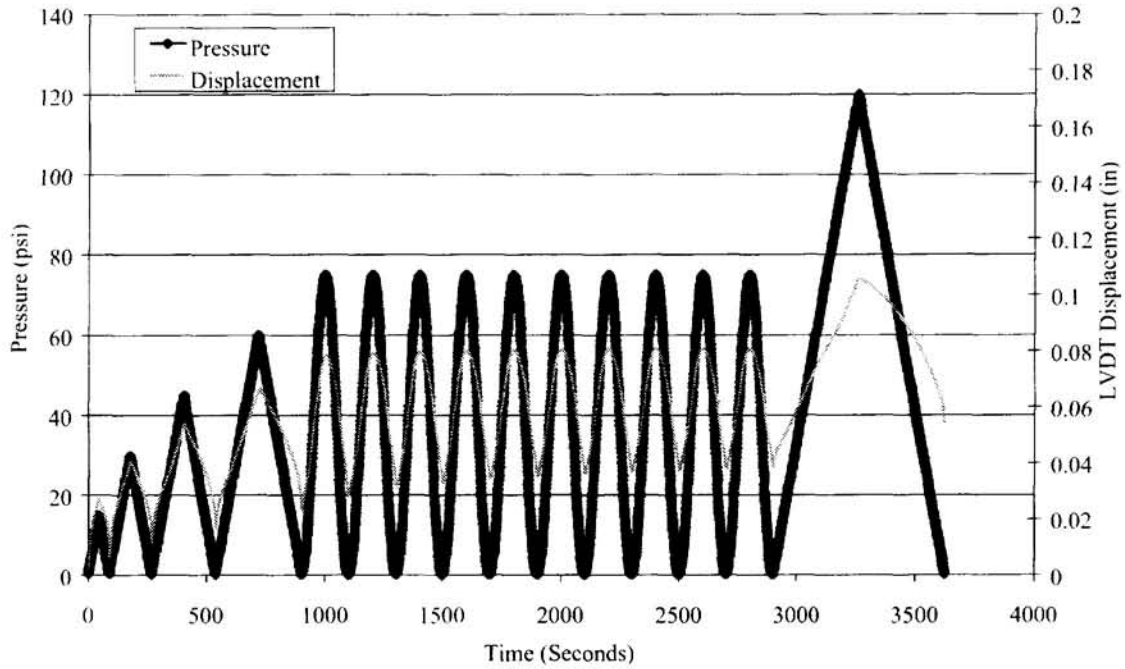

Figure 1. Compressive Fatigue Test of Xerogel Disk (75 psi, No Vacuum)

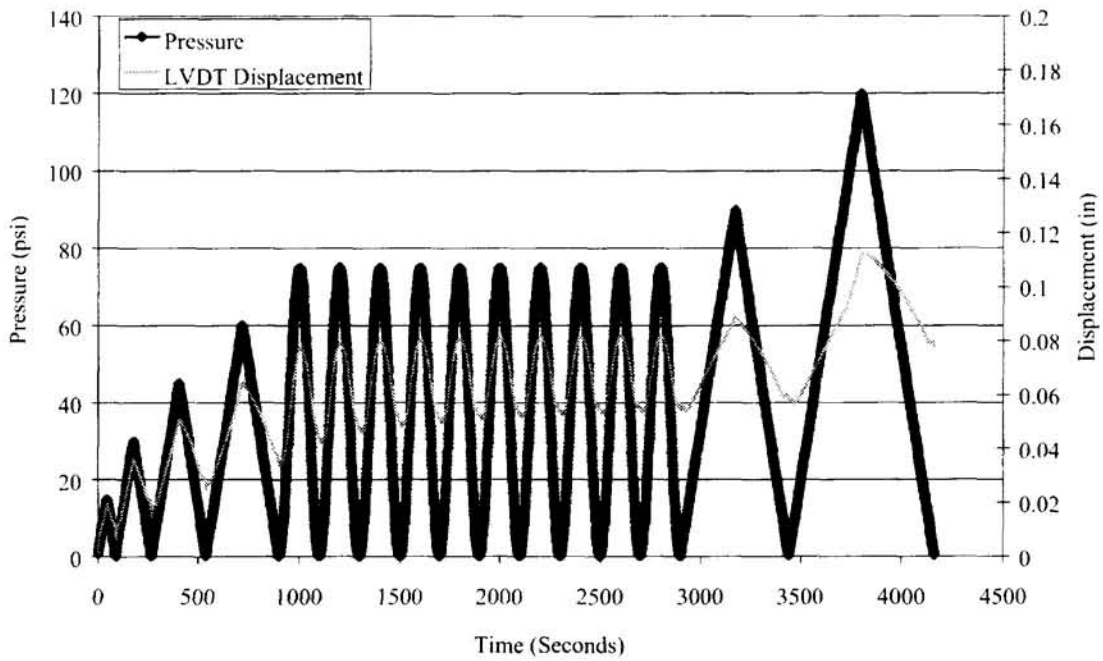

Figure 2. Compressive Fatigue Test of Xerogel Disk (75 psi, Vacuum)

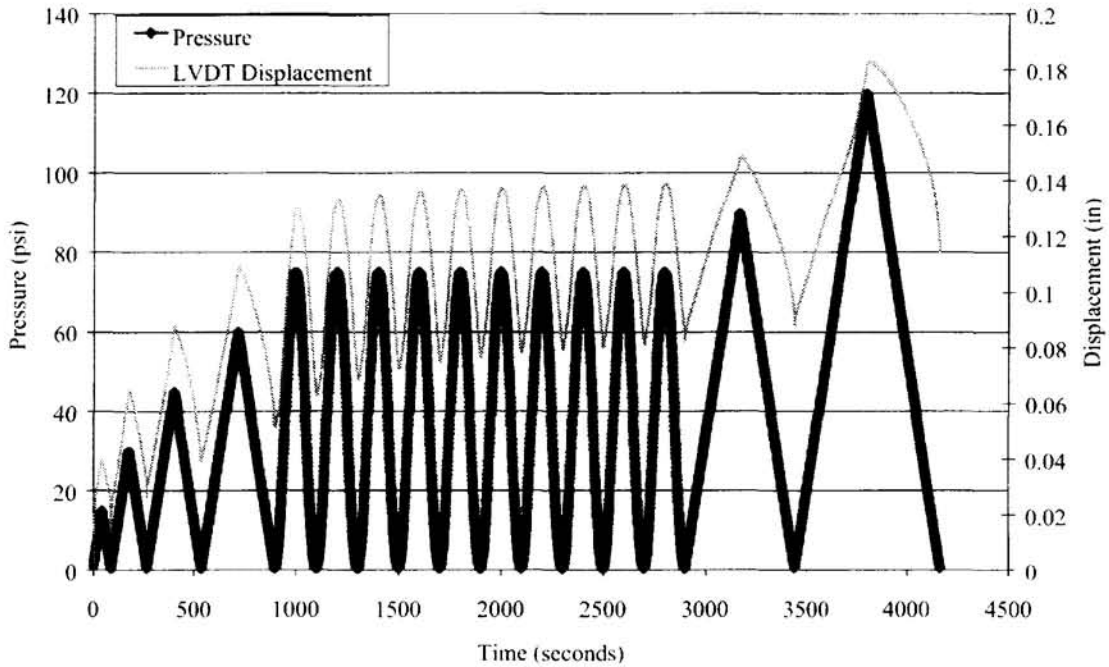

Figure 3. Compresive Fatigue Test of Xerogel Disk (75 psi, Krypton Filled)

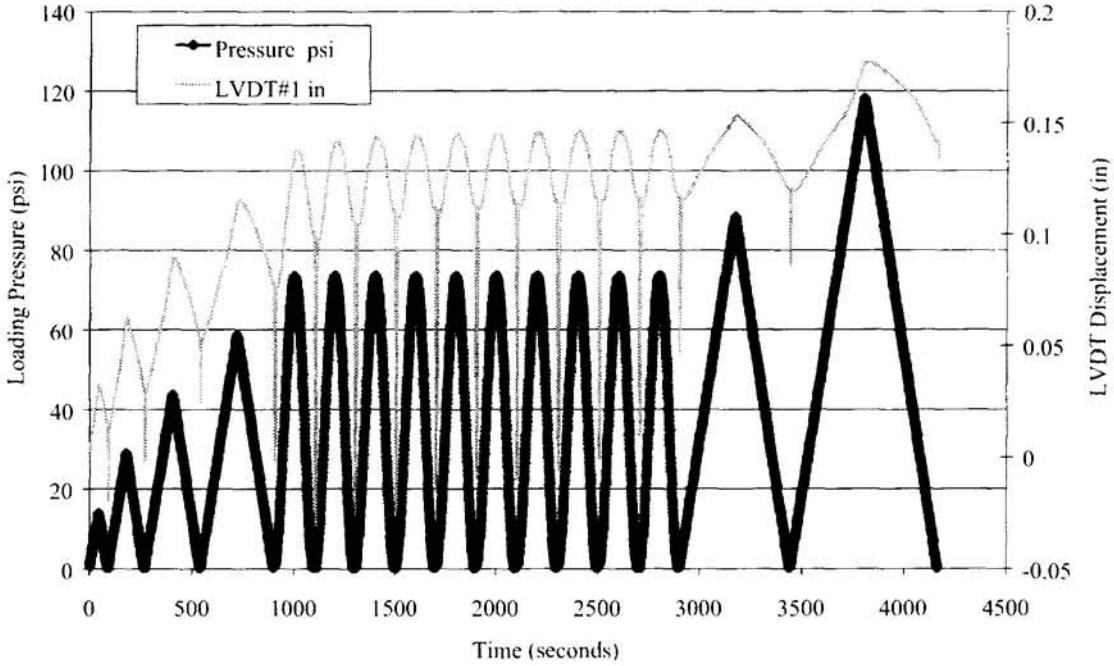

Figure 4. Compressive Fatigue Test of Xerogel Disk (15 psi, Vacuum)

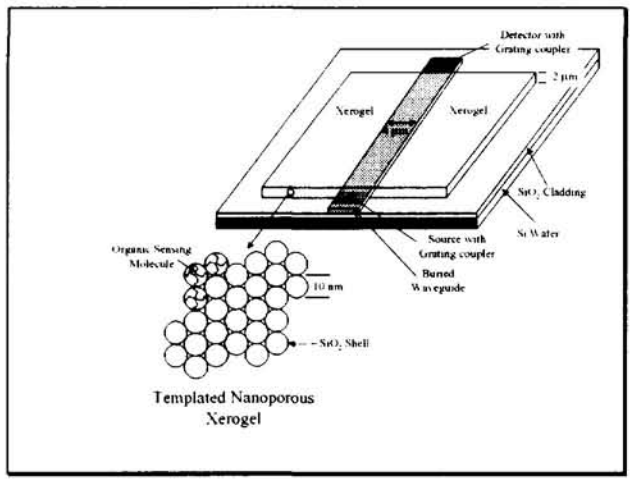

Figure 5. Xerogel Sensor Concept

References

1. S. S. Kistler, J. Phys. Chem., 34, 52 (1932).

2. Berkeley National Laboratory web site.

3. R. Deshpande, D.M. Smith and C.J. Brinker, US patent application (1992).

4. L. W. Hrubesh, Aerogel Applications, J. NonCryst. Solids, 225, 335, (1998).

5. Pacific-Sierra Research web site.

6. L.M. Hair, Coronado, P.R. and Reynolds, J.G. Mixed-metal Oxide Aerogels for Oxidation of Volatile Organic Compounds, J. NonCryst. Solids, 270, 115, (2000).

7. A. Sayari, Catalysis by Crystalline Mesoporous Molecular Sieves, Chemistry of Materials, 8, 1840, (1996).

8. M.A. Doody, Baker, G.A., Pandley, S., and Bright, F.V., Affinity and Mobility of Polyclonal Anti-Dansyl Antibodies Sequestered within Sol-Gel Derived Biogels, Chemistry of Materials, 12, 1142, (2000).

ELECTROACTIVE POLYMERS AS ARTIFICIAL MUSCLES – *REALITY AND CHALLENGES*

Yoseph Bar-Cohen, JPL/Caltech, Pasadena, CA
818-354-2610, yosi@jpl.nasa.gov

http://ndeaa.jpl.nasa.gov

Rover technology at JPL

Yoseph Bar-Cohen, 818-354-2610, yosi@jpl.nasa.gov

Polymer Actuators

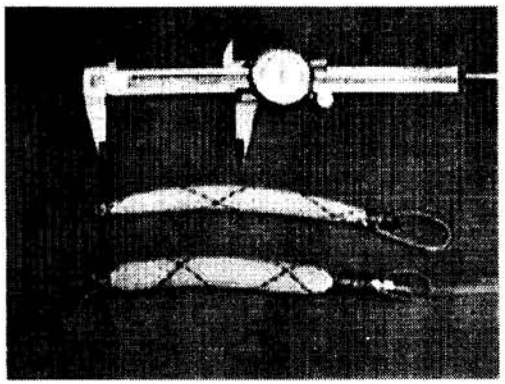

McKibben Artificial Muscles
Air Pressure activation (Hannaford, B.U. Washington)

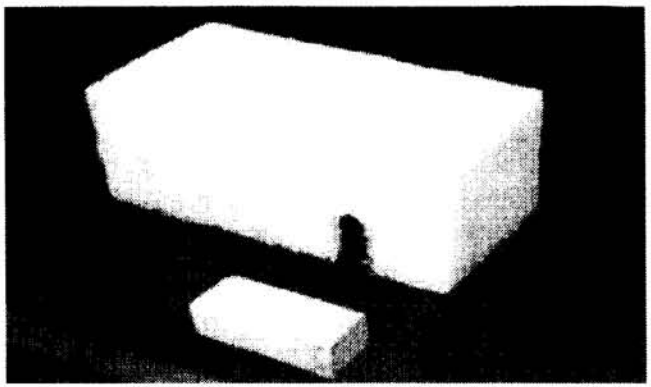

Shape Memory Polymers
Heat/pressure activation (W. Sokolowski, JPL)

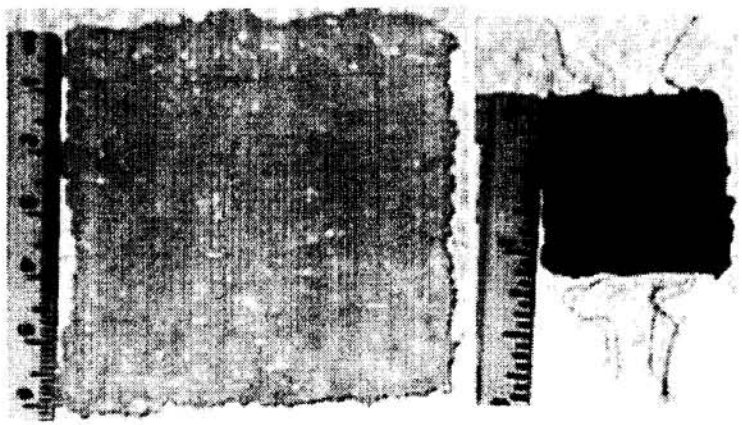

Ionic Gel Polymers
Chemical transduction (P. Calvert, UA)

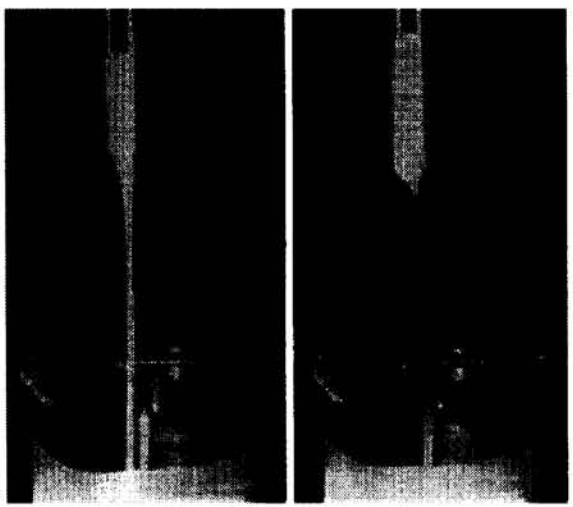

ElectroRheological Fluids
Electrical stimulation (Bayer Silicons Rheobay)

Y. Bar-Cohen, JPL, yosi@jpl.nasa.gov

Inflatable structures

Inflatable antennas & telescopes (A. Chmielewski, JPL)

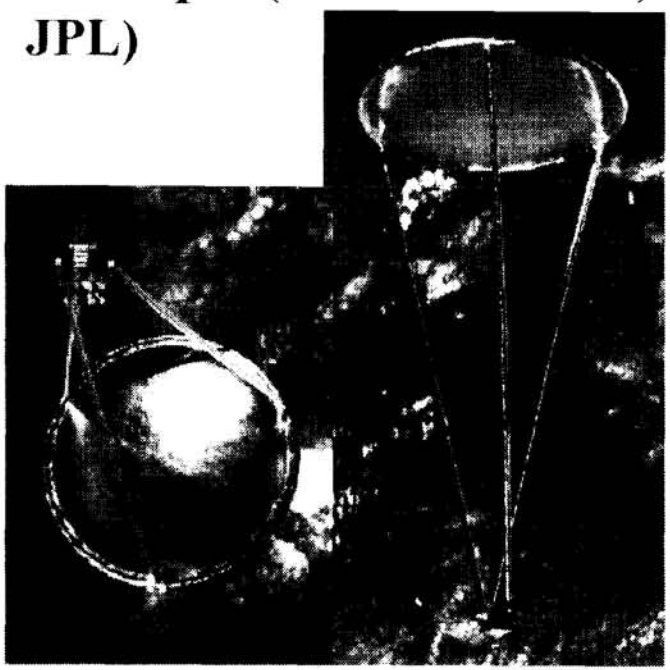

Inflatable vehicles (Jack Jones, JPL)

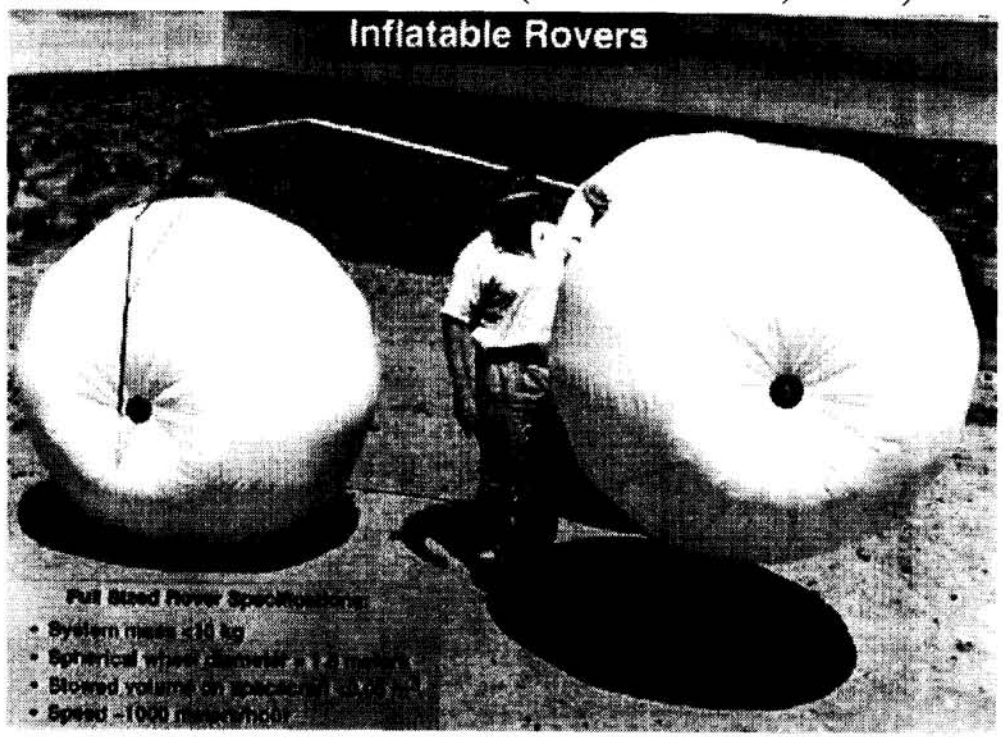

Yoseph Bar-Cohen, 818-354-2610, yosi@jpl.nasa.gov

Y. Bar-Cohen, JPL, yosi@jpl.nasa.gov

BACKGROUND AND MOTIVATION

- NASA is using actuation devices for many space applications.
- There is an increasing need for miniature, inexpensive, light and low power actuators.
- Existing transducing type actuators such as piezoceramics are inducing limited displacement levels.
- Electroactive polymers (EAP) ability to induce large displacements offer an enabling technology for unique mechanisms.
- EAP are activated by an electrical field and they can be used to emulate biological muscles.

EAP substituting mechanisms in robots and changing paradigms

- Conventional robots are driven by mechanisms that consist of motors, gears, bearings, etc.
- Electroactive polymers (EAP) offer alternative low mass, low power consuming, inexpensive actuators
- EAP are resilient, fracture tolerant, noiseless actuators.
- These materials allow emulation of biological muscles to produce insect-like robots and other mechanisms.
- Thus, robotic devices can be made that consist of materials only, serving as the structure and the actuators.

COMPARISON BETWEEN EAP AND WIDELY USED TRANSDUCING ACTUATORS

Property	EAP	EAC	SMA
Actuation strain	>10%	0.1 - 0.3 %	<8% short fatigue life
Force (MPa)	0.1 – 3	30-40	about 700
Reaction speed	μsec to sec	μsec to sec	sec to min
Density	1- 2.5 g/cc	6-8 g/cc	5 - 6 g/cc
Drive voltage	2-7V/ 10-100V/μm	50 - 800 V	NA
Consumed Power*	m-watts	watts	watts
Fracture toughness	resilient, elastic	fragile	elastic

* Note: Power values are compared for documented devices driven by such actuators.

Y. Bar-Cohen, JPL, yosi@jpl.nasa.gov

COMPARISON BETWEEN EAP AND WIDELY USED TRANSDUCING ACTUATORS

Property	Electro-static silicone elastomer [Kornbluh]	Polymer Electrostrictor [Zhang]	SMA	Single Crystal Electrostrictor [Shrout]	Single Crystal Magnetostrictor [Clark]
Actuation strain	32 %	4 %	8 %	1.7 %	2 %
Blocking Force/Area *	0.2 MPa	0.8 MPa	700 MPa	65 MPa	100 MPa
Reaction speed	μsec	μsec	sec to min	μsec	μsec
Density	1.5 g/cc	3 g/cc	6 g/cc	7.5 g/cc	9.2 g/cc
Drive field	144 V/μm	150 V/μm	--	12 V/μm	2500 Oe
Fracture toughness	large	large	large	low	large

*Note: Values were calculated assuming the elastic properties were independent of applied field and are therefore approximate.

Y. Bar-Cohen, JPL, yosi@jpl.nasa.gov

Bending and Longitudinal EAP Actuators

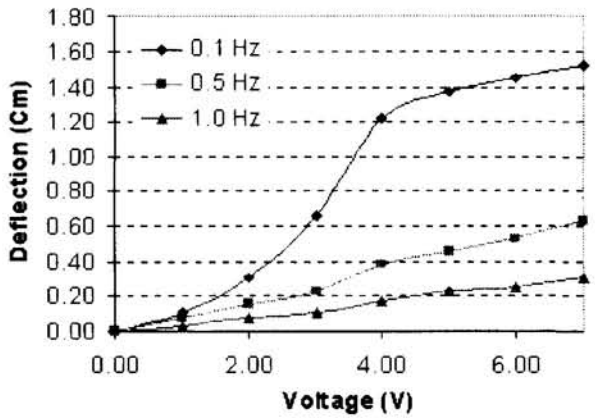

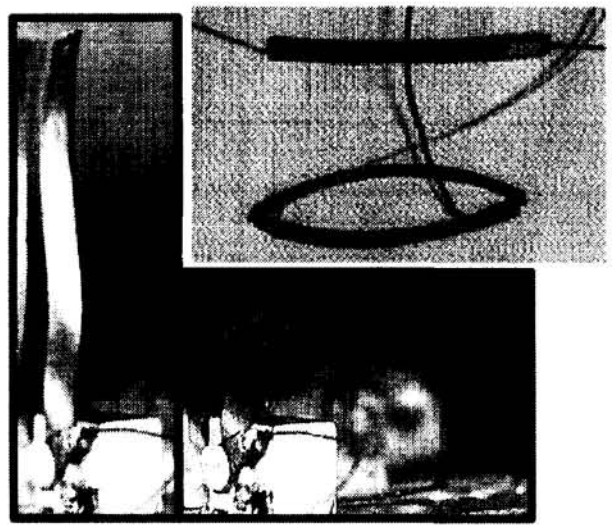

Ion-exchange Polymer membrane Metallic Composite (IPMC) can bend by over 90° under ~3-4V and ~30-50-mW.

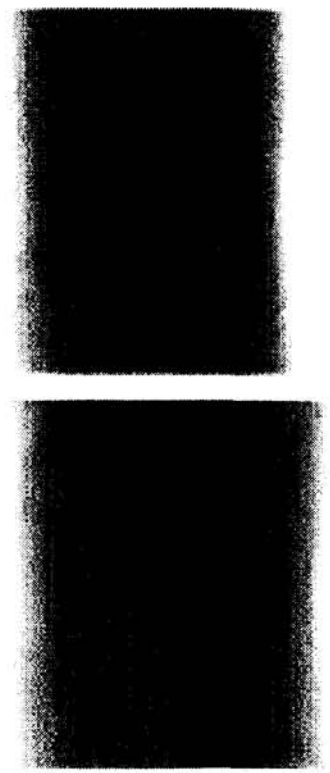

31-mm wide, 50-μm thick Electrostatically stricted polymer (ESSP) film extending over 12%

Y. Bar-Cohen, JPL, yosi@jpl.nasa.gov

ISSUES ASSOCITED IPMC AS BENDING EAP ACTUAORS

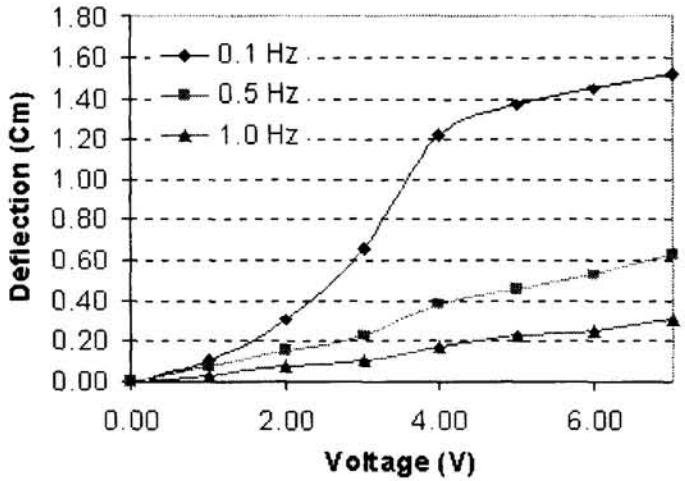

Reference

Activated

- Conductive ionic species is responsible for the actuation and it necessitates maintaining moist film.
- The Nafion base IPMC material behaves similar to Teflon and is difficult to bond or to coat.
- Coating IPMC deforms the film and blisters appeared after activation.
- The electrical response of the material is complex and need to be addressed to allow effective control of the electroactivation.

IPMC AS EAP BENDING ACTUATOR

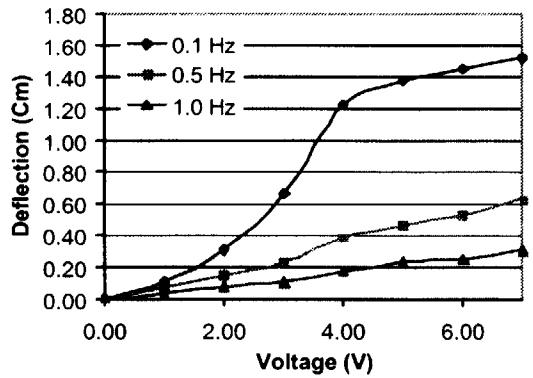

Charging capability

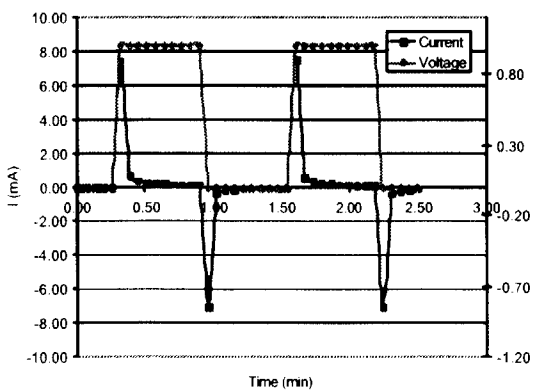

Higher resistance at Low Temp

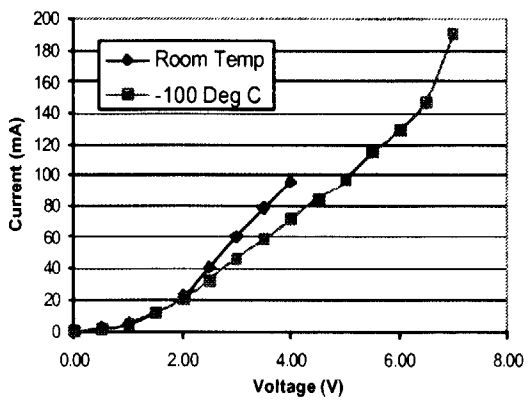

Response at Cryovac

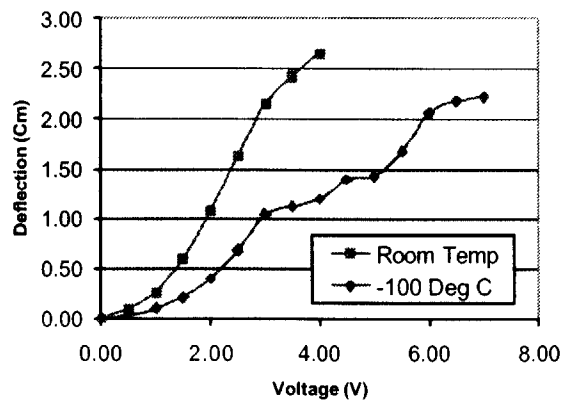

Y. Bar-Cohen, JPL, yosi@jpl.nasa.gov

Nanorover in action

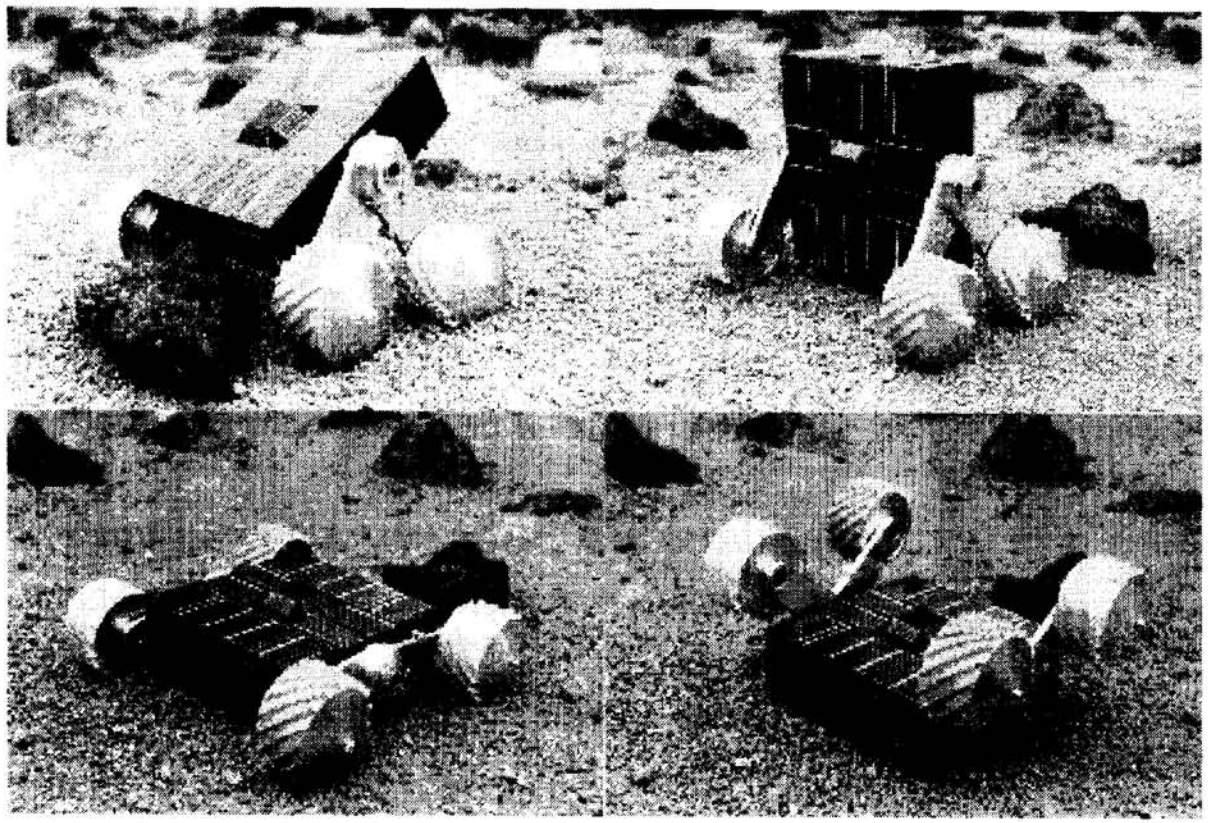

Nanorover - miniature rover to be launched in 2002
as part of the MUSES-CN mission to an asteroid.

Y. Bar-Cohen, JPL, yosi@jpl.nasa.gov

MUSES-CN Mission, the Nanorover and the EAP dust-wiper

- The MUSES-CN mission is planed for launch to an Asteroid in 2002.
- A probe will be dropped on the asteroid and blast-off dust.
- The imaging capability of the Nanorover will be affected by the dust.
- Pair of EAP wipers was basedlined to remove the dust.

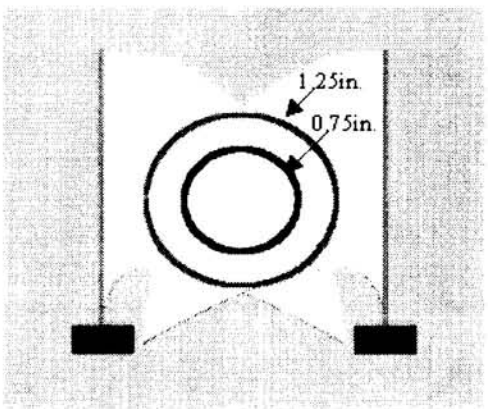

Simulated window and 2 side dust wipers

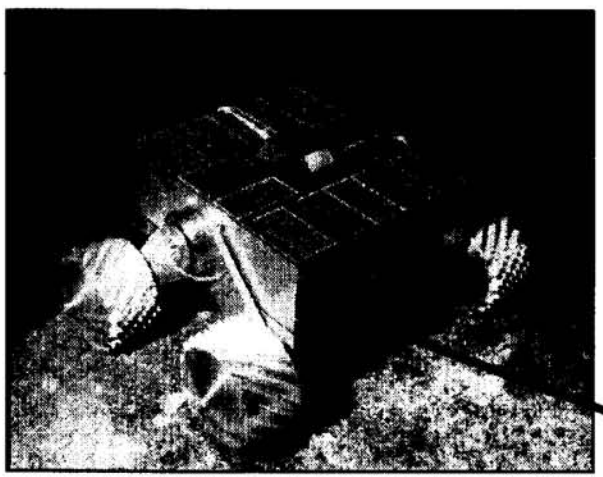

Imaging window

Y. Bar-Cohen, JPL, yosi@jpl.nasa.gov

MUSES-CN Nanorover EAP Dust Wiper

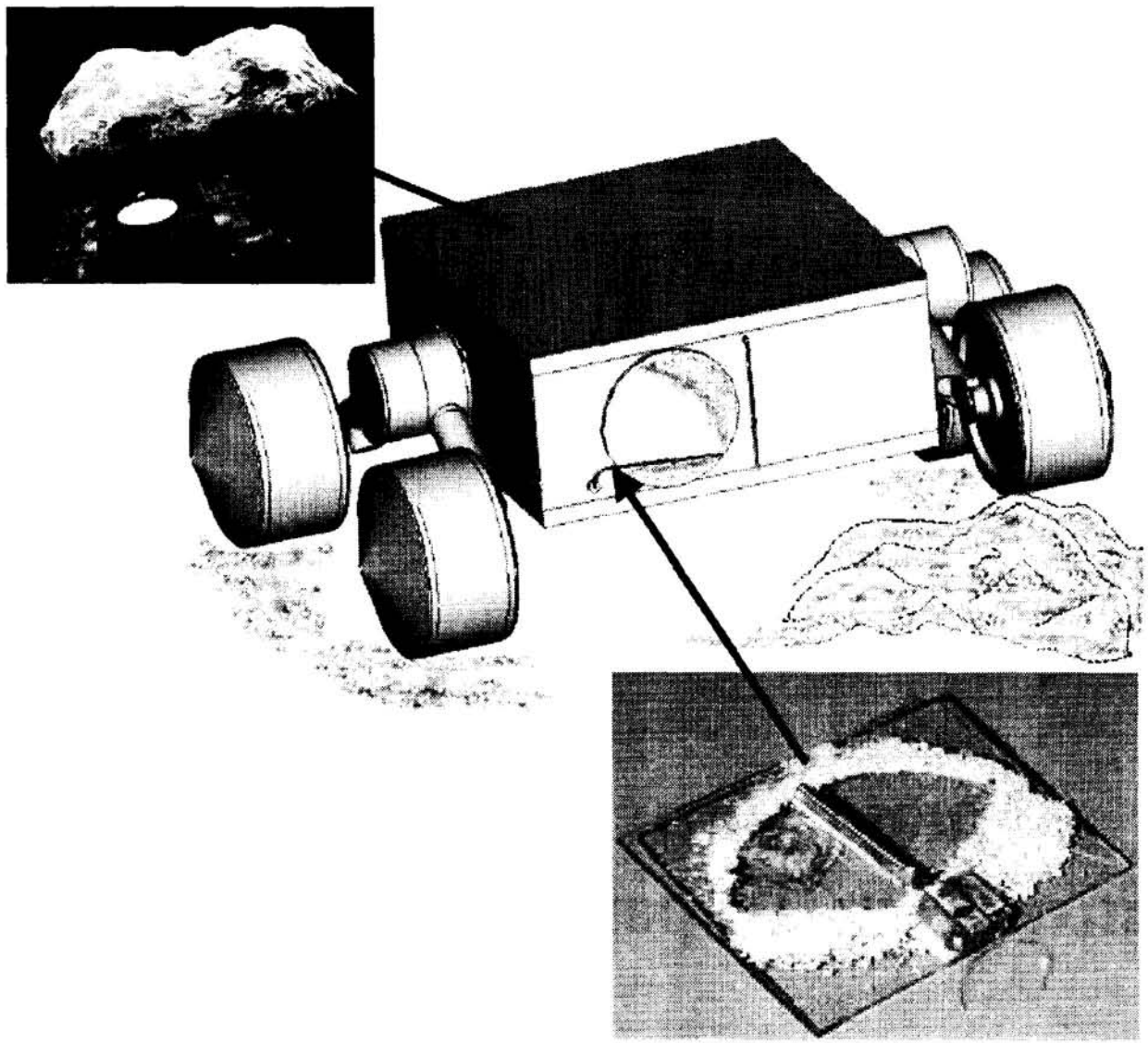

Y. Bar-Cohen, JPL, yosi@jpl.nasa.gov

Dust wiper activated by EAP using wiper blade attachment

Actuated by 1-3 volts

Biased with 1-2KV for dust repulsion

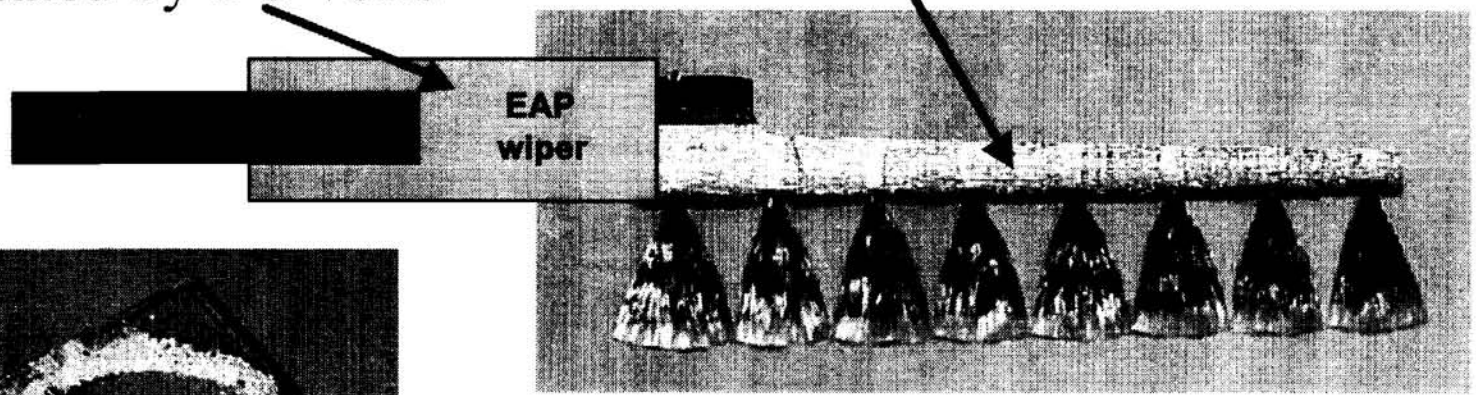

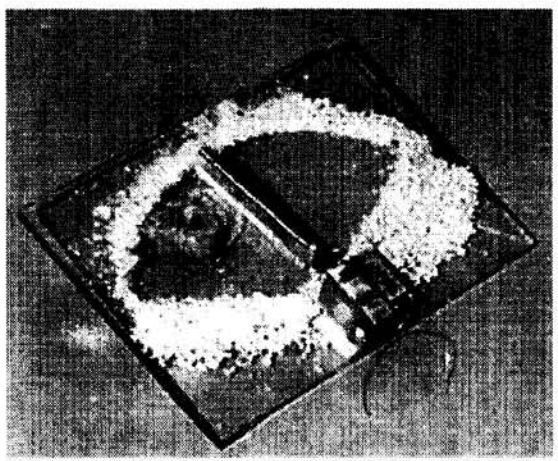

Graphite/Epoxy wiper blade* with fiberglass brush coated with gold

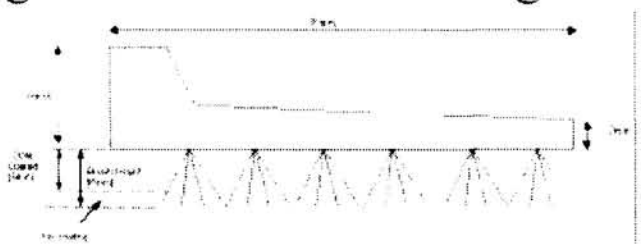

* Made by Energy Science Laboratories, Inc., San Diego, California

Y. Bar-Cohen, JPL, yosi@jpl.nasa.gov

Electroactive Polymers (EAP) Actuators Technology Transfer to MUSES-CN

EAP surface wiper for dust removal

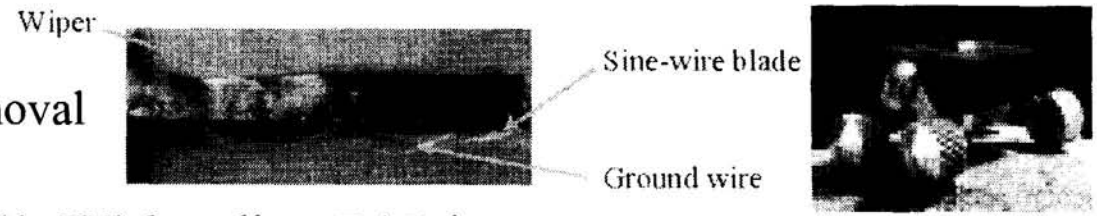

- Driven by low voltage (1-5V) bending-EAP is offering resilient, low-mass, miser, large displacement actuators.
- Bending EAP was shown to operate effectively down to -100°C.
- The technology rapidly emerged from basic research to the level that it address the critical issue of dust removal.
- EAP dust wiper was baselined for the optical/IR window of the MUSES-CN mission's NanoRover.
- Limitations of the EAP actuator are still challenges to the flight application of this technology.

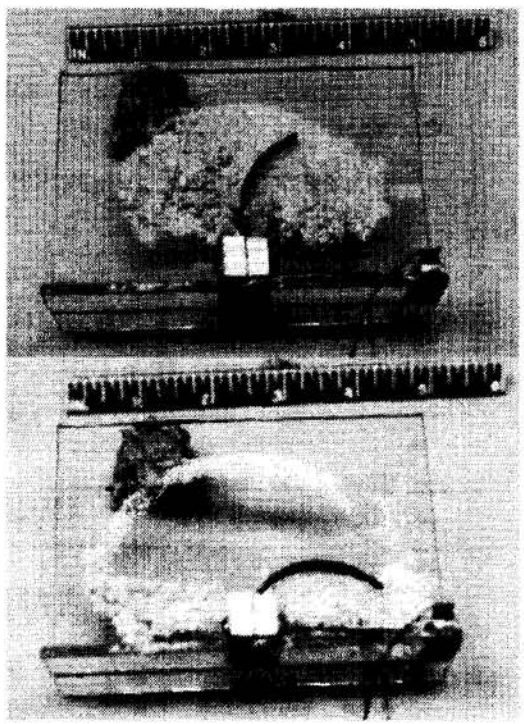

Y. Bar-Cohen, JPL, yosi@jpl.nasa.gov

Challenges and solutions to the application of IPMC as bending actuators

Challenge	Solution
Fluorinate base - difficult to bond	Pre-etching (LaRC)
Sensitive to dehydration (~5-min)	Etching and coating (NASA-LaRC)
Electroding points cause leakage	Effective compact electroding method was developed
Off-axis bending actuation	Use of load (e.g., wiper) to constrain the free end
Most bending occurs near the poles	Improve the metal layer uniformity
Electrolysis occurs at >1.23-V in Na+/Pt	• Minimize voltage • Use IPMC with gold electrodes and cations based on - Li^+ - Perfluorocarboxylate with tetra-n-butylammonium (ONRI)
• Survive -155°C to +125°C • Operate at -125°C to + 60°C	IPMC was demonstrated to operate at -140°C
Need to remove a spectrum of dust sizes in the range of >3μm	• Use effective wiper-blade design (ESLI, San Diego, CA) • Apply high bias voltage to repel the dust
Reverse bending under DC voltage	Limit application to dynamic/controlled operations
Developed coating is permeable	• Alternative polymeric coating • Metallic Self-Assembled Monolayer overcoat
No established quality assurance	• Use short beam/film • Efforts are underway to tackle the critical issues
Residual deformation	Still a challenge

Y. Bar-Cohen, JPL, yosi@jpl.nasa.gov

LONGITUDINAL EAP ACTUATOR

Under electro-activation, an EAP film with electrodes on both surfaces expands laterally.

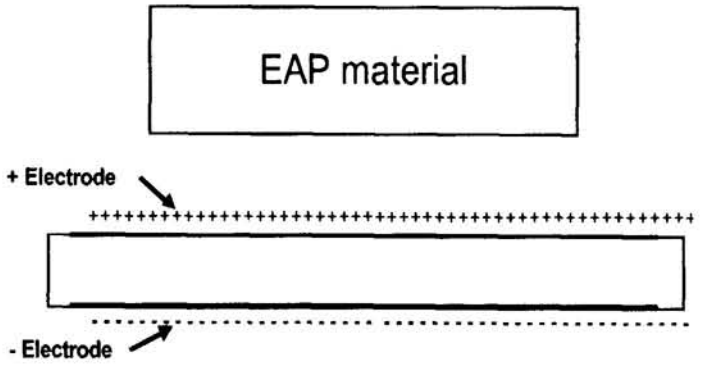

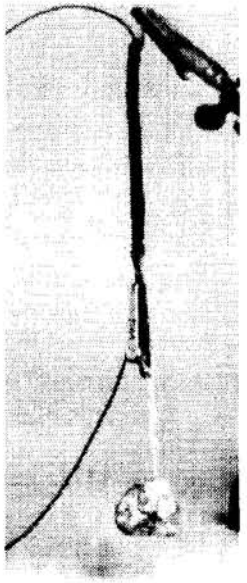

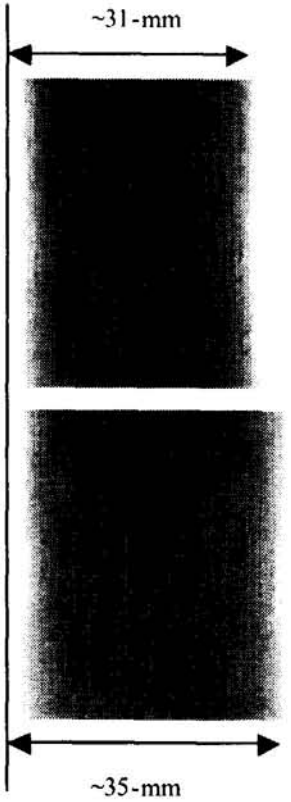

EAP film subjected to 25 V/μm induced over12% extension

Y. Bar-Cohen, JPL, yosi@jpl.nasa.gov

EAP ROBOTIC ARM FOR SAMPLE HANDLING AND MANIPULATION

Simulation

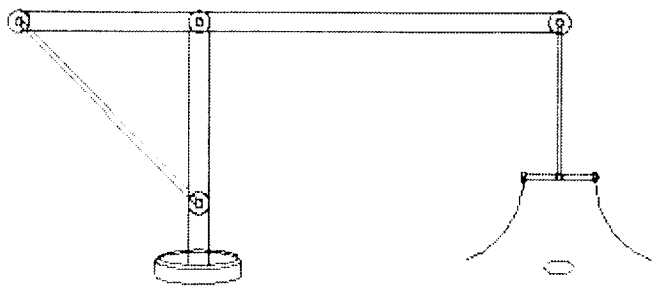

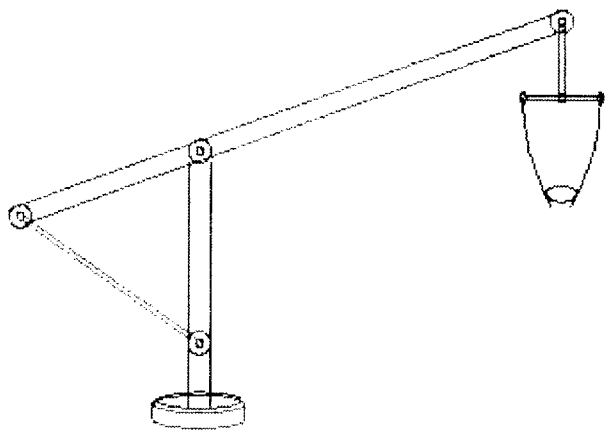

Y. Bar-Cohen, JPL, yosi@jpl.nasa.gov

Robotic arm

A computer controlled arm with longitudinal EAP actuator serving as the lifter and bending EAP fingers as the gripper

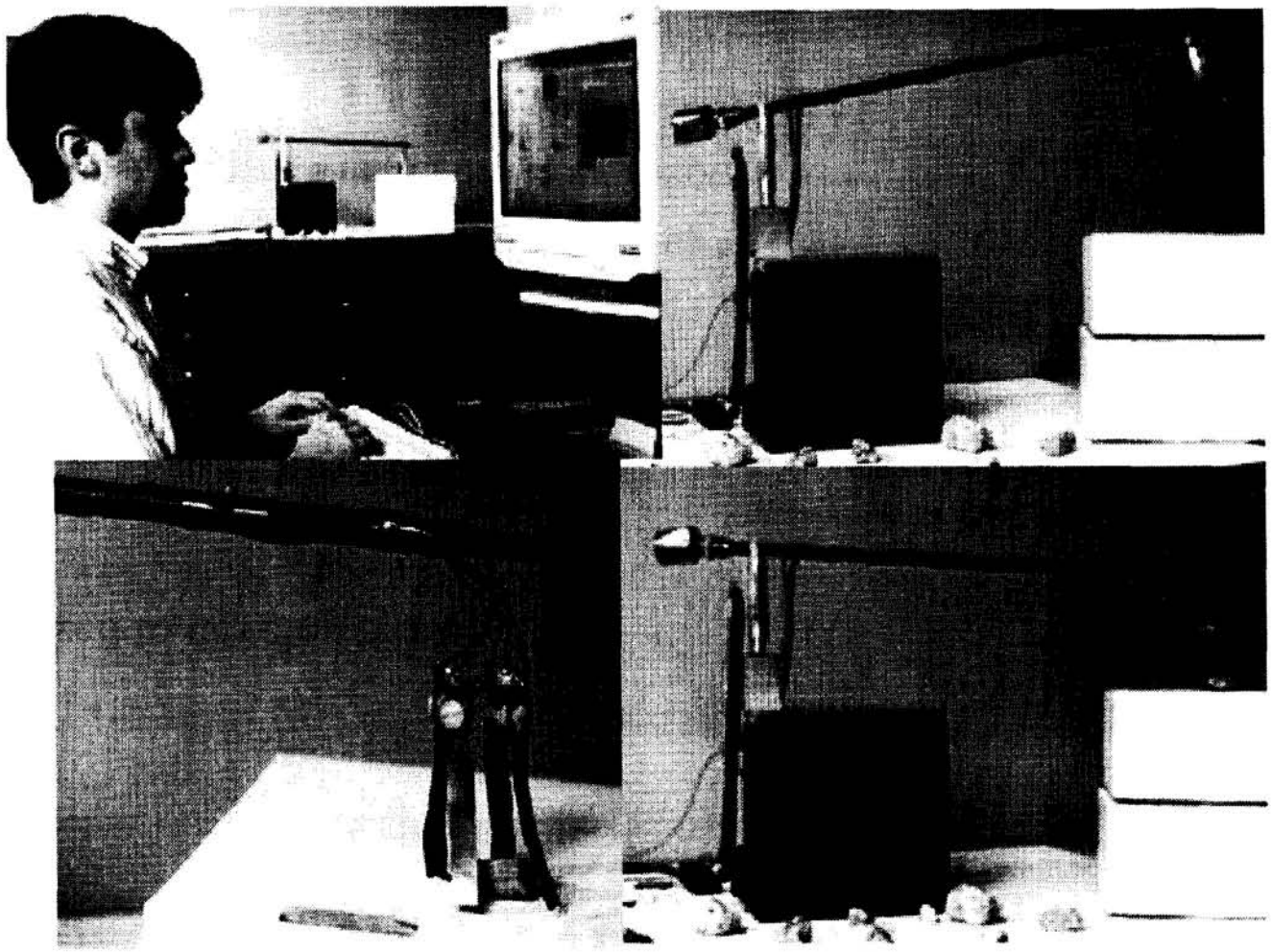

Electroactive Polymer (EAP) Actuators

Applications

Dust wiper

A bending EAP is used to develop a dust wiper

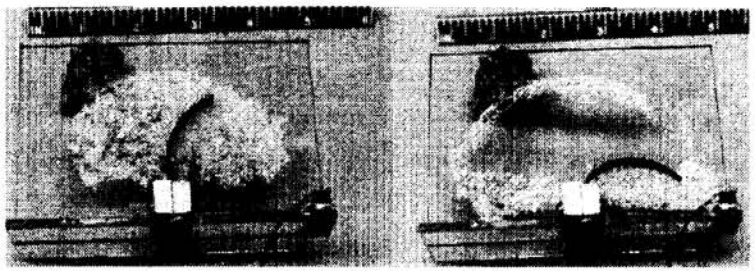

Miniature robotic arm

A stretching EAP is used to lower a robotic arm, while bending EAP fingers operate as a gripper. The technology is being developed to enable miniature sample handling robotics.

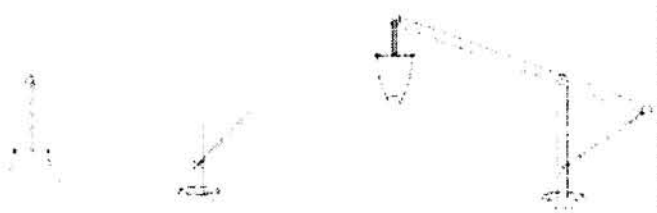

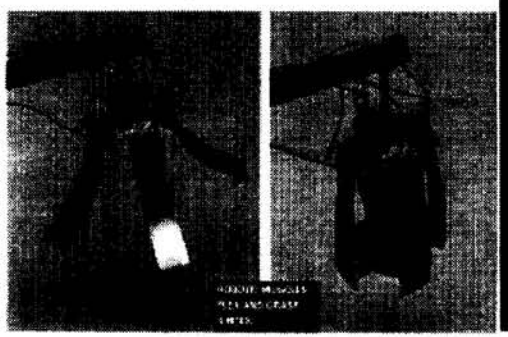

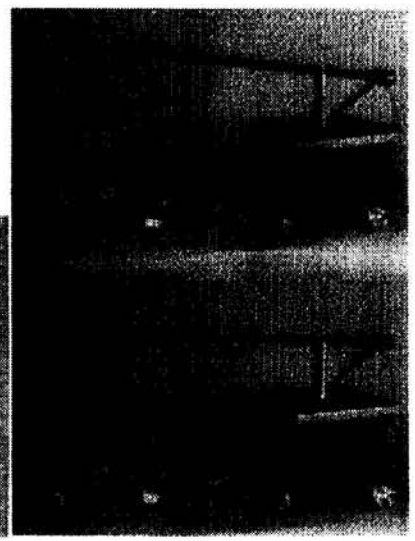

Y. Bar-Cohen, JPL, yosi@jpl.nasa.gov

ELEMENTS OF AN EAP ACTUATED ROBOTS

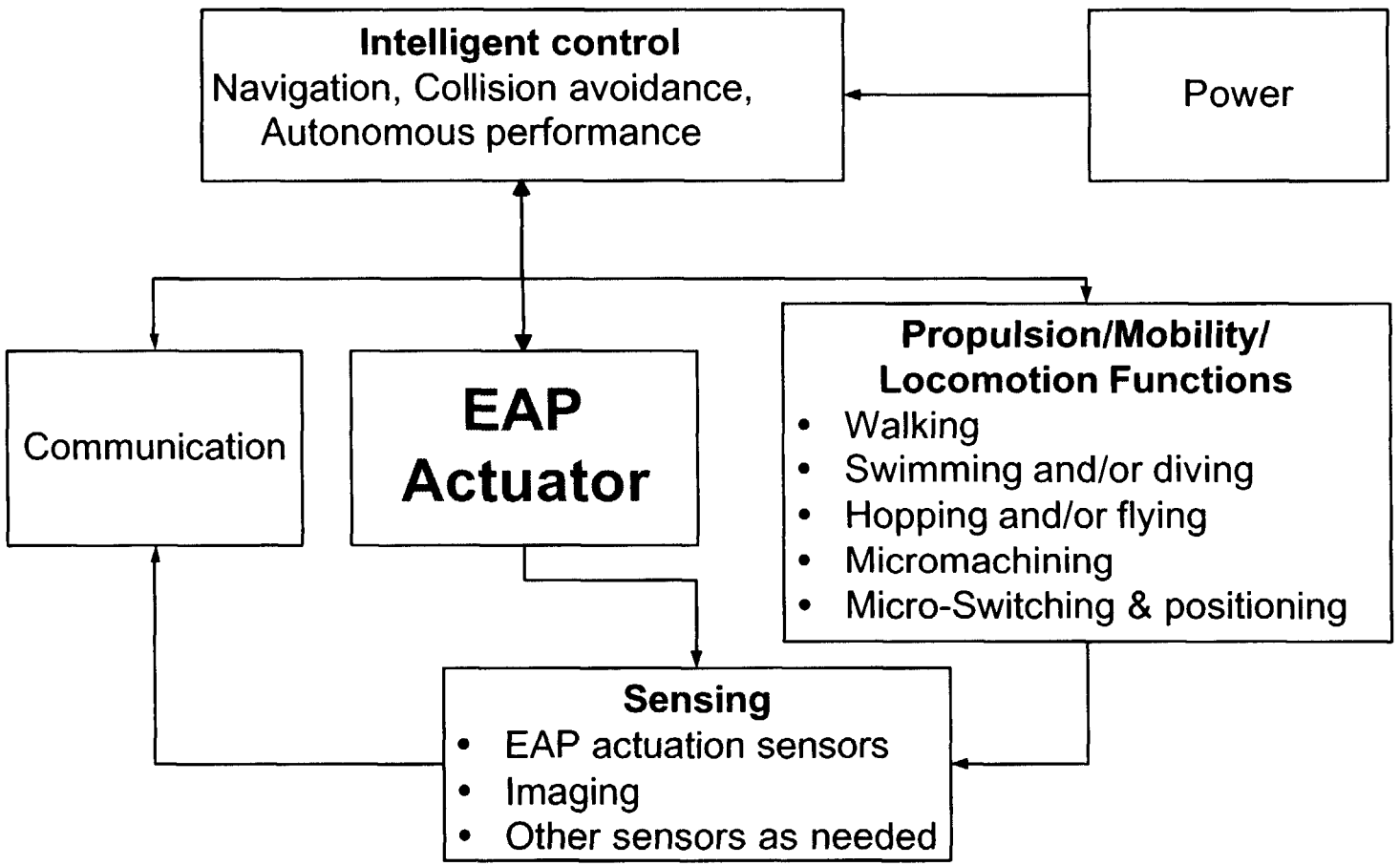

Y. Bar-Cohen, JPL, yosi@jpl.nasa.gov

EAP infrastructure

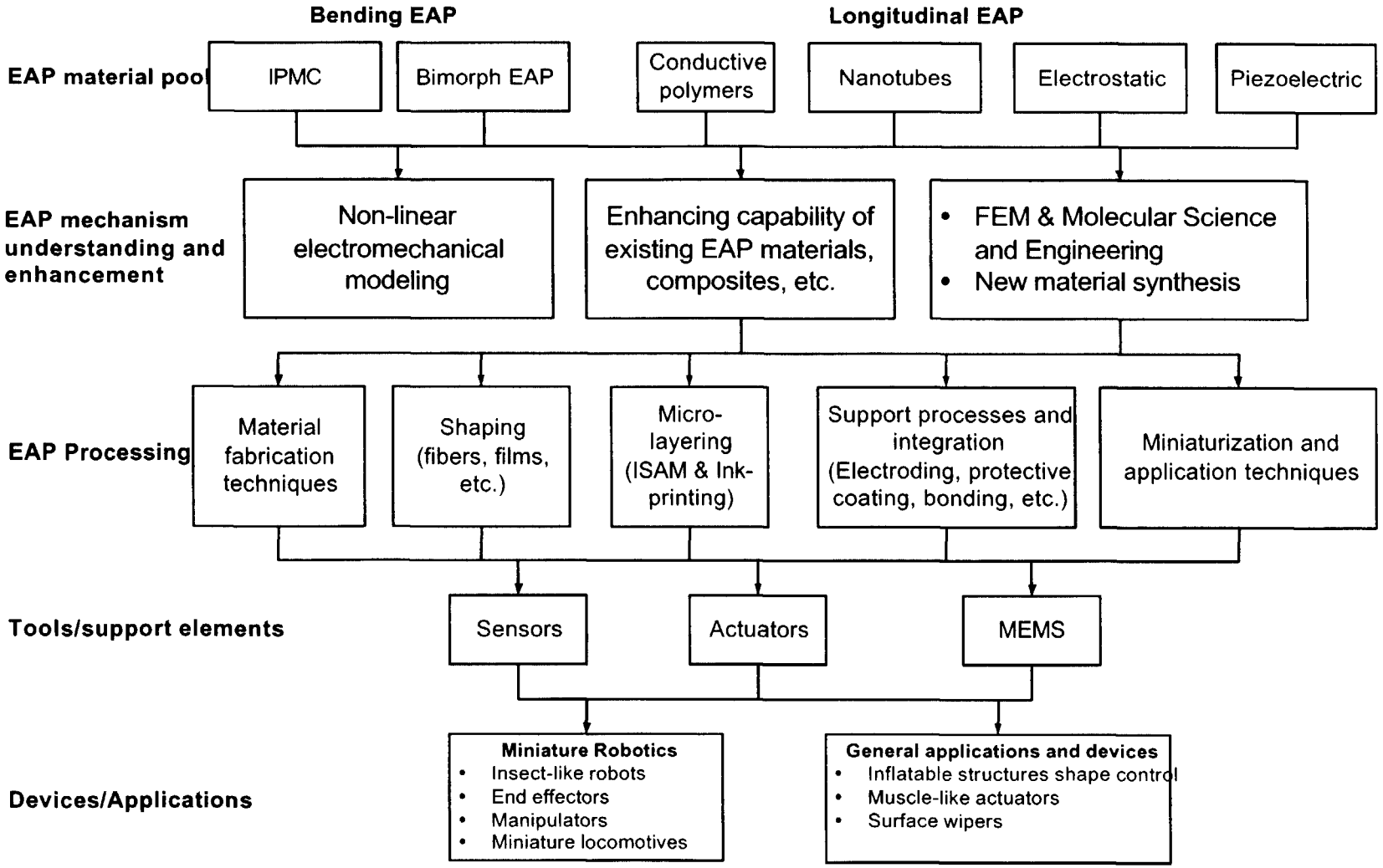

Y. Bar-Cohen, JPL, yosi@jpl.nasa.gov

Wet (Ionic) Electroactive Polymers

Actuator type	Principle	Advantages	Disadvantages	Reported types
Ionic Conductive Polymers (ICP)	Materials containing solvated ions that cause swelling in response to an applied voltage.	Use low voltage	Need surface protection to operate in dry environment	Polypyrrole, Polyethylenedioxythiophene, Poly(p-phenylene vinylene)s, Polyaniline, and Polythiophenes.
Ionic gels	Generally, activated by a chemical reaction (changing from acid ⇄ base increasing density and swelling, respectively.	• Potentially capable of matching the force and energy density of biological muscles	Operates very slowly and would require very thin layers and new type of electrodes to become practical	
Ion-Exchange Polymer Metal Composites (IPMC)	Bending is stimulated in IPMC, where the base polymer provides channels for mobility of positive ions in a fixed network of negative ions on interconnected clusters	• Activated by low voltage • Provides significant bending	• Operates at low frequency. • Sensitive to dehydration and developed coating is ineffective. • Subject to permanent deformation under DC • Subject to hydrolysis above 1.03V	Base polymer: • Nafion® (perfluorosulfonate made by DuPont) • Flemion® (perfluorocaboxylate, made by Asahi Glass, Japan). Cations: tetra-n-butylammonium, Li+, and Na+ Metal: Pt and Gold
Carbon Nanotubes	Using nanometer size tubes ionically activated. Showed induced stains of < 1% along the length and ~300% laterally.	• Potentially provide superior work/cycle & mechanical stresses. • Carbon offers high thermal stability towards >1000 °C.	Expensive. Difficulty to produce in large quantities.	Carbon

Y. Bar-Cohen, JPL, yosi@jpl.nasa.gov

Dry Electroactive Polymers

Actuator type	Principle	Advantages	Disadvantages	Reportec types
Ferroelectric Polymers	PVDF is involved with large dielectric loss. Recent introduction of electron radiation in P(VDF-TrFE) copolymer introduced defects into the crystalline structure dramatically lowering the dielectric losses.	• Demonstrates electrostrictive behavior • The relatively high elastic modulus offers high mechanical energy density • Induces relatively large strain (~5%) [being considered for sonar transducers]. • This permits AC switching with a lot less generated heat.	Requires high voltage (~150 MV/m)	Electron radiated P(VDF-TrF
Electro-Statically Stricted Polymer (ESSP) Actuators	Polymers with low elastic stiffness and high dielectric constant can be used to induce large actuation strain by subjecting them to an electrostatic field where Coulomb forces between electrodes to squeeze and thus stretch the material	• Large displacements reaching levels of 200% • Rapid response	• Requires large voltage. • Obtaining large displacements compromises the actuation force	• Silicone • Polyuretha

Y. Bar-Cohen, JPL, yosi@jpl.nasa.gov

Current EAP
Advantages and disadvantages

EAP type	Advantages	Disadvantages
Dry	• Can operate in room conditions for a long time • Can respond at very high frequencies • Provide large actuation forces	• Requires high voltages • Compromise between strain and stress is needed
Wet (Ionic)	• Provides mostly bending actuation (longitudinal mechanisms can be articulated) • Large bending displacements • Sustain hydrolysis at >1.23-V • Requires low voltage	• Does not hold strain under DC voltage • Operates at low frequencies (several Hertz) • Bending EAP presents a vary low actuation force

Y. Bar-Cohen, JPL, yosi@jpl.nasa.gov

BIOLOGICALLY INSPIRED ROBOTICS

MULTI-TASKING IN-SITU MISSIONS USING SCALABLE AUTONOMOUS ROBOTS FOR COLONIZED PLANETARY EXPLORATION

Multiple locomotion capabilities

Flying, walking, swimming & diving

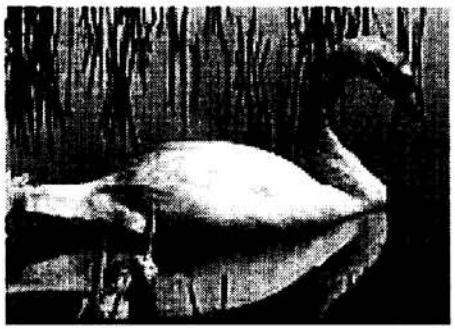

Hopping, flying, crawling & digging

Coordinated robotics

Models for EAP Actuated Flexible Robots

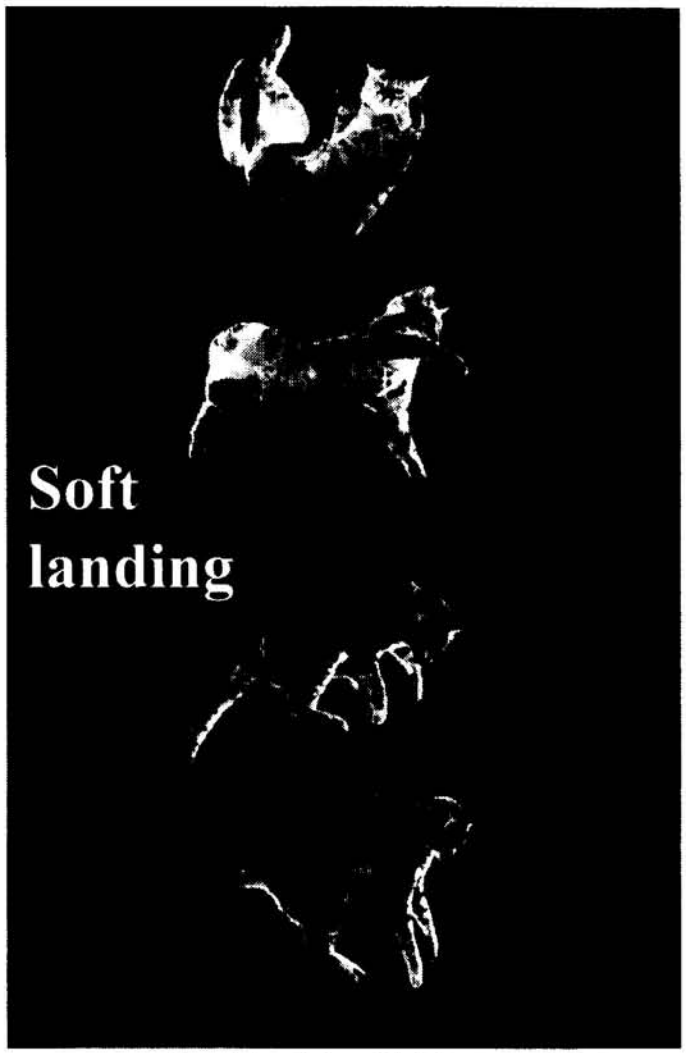

Yoseph Bar-Cohen, 818-354-2610, yosi@jpl.nasa.gov

INSECTS AS WORKHORSES AND ROBOTS

- Insects were used by various researchers (e.g., University of Tokyo, Japan) as locomotives to carry backpack of wireless electronics.
- EAP offer the potential of making insect-like robot to replace the "real thing".

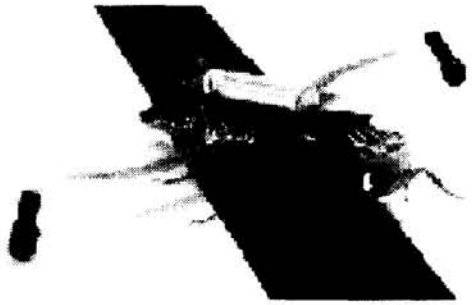

Cricket

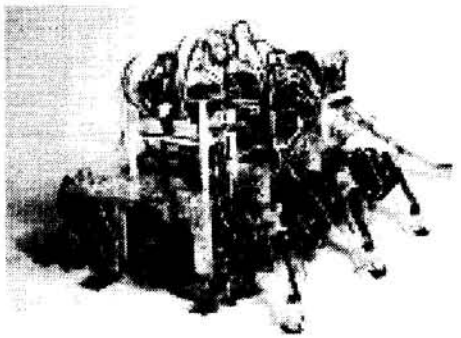

Spider

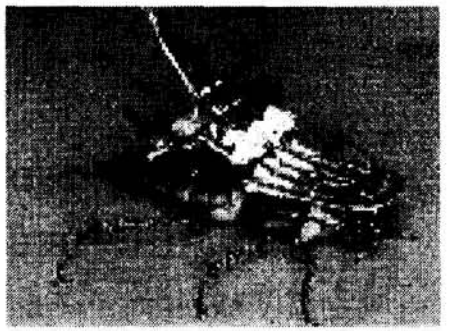

Cockroach

Reference: http://www.leopard.t.u-tokyo.ac.jp/

Insect walking process*

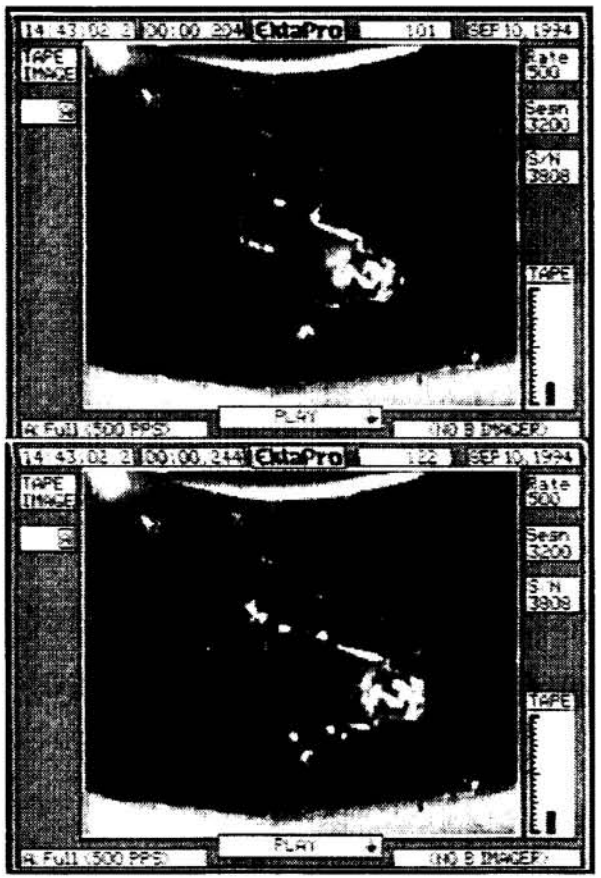

Photoelastic force platform is used at Berkeley to study insect walking mechanism.

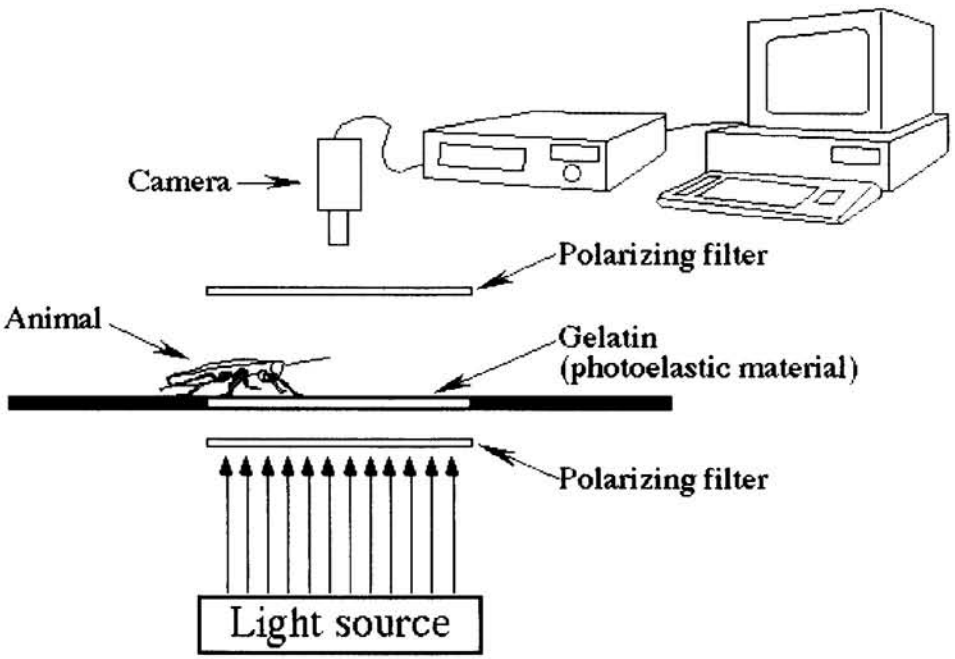

* Robert Full, Berkeley U.
Ref: http://rjf2.biol.berkeley.edu/Full_Lab/FL_Publications/PB_Posters/94ASZ_Turning/94ASZ_Turning.html

Key challenge to EAP

EAP materials induce low actuation force

New EAP materials and processes

New materials:
Ionic gel EAP

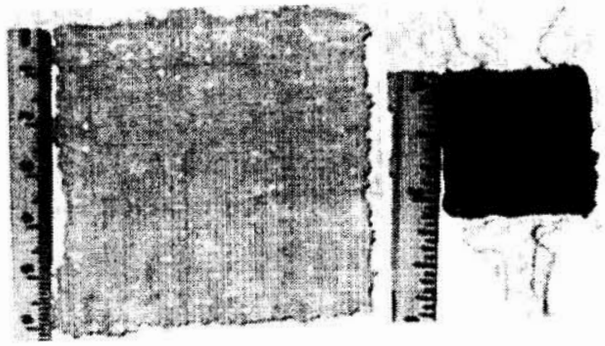

New material
design tools:
Computational
chemistry

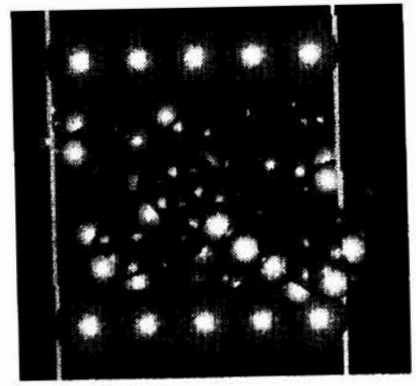

2000+ Layers Formed with Excellent Uniformity

Ionic Self-Assembled mono-layering

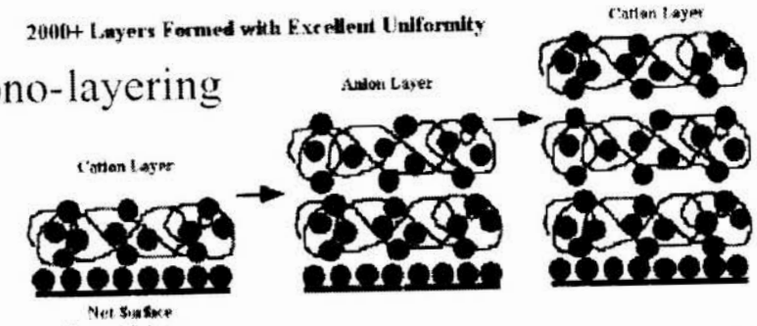

Micro-fabrication techniques:

Ink-printing

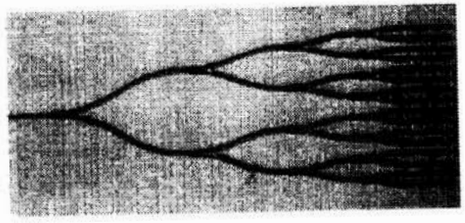

100-µm Waveguide

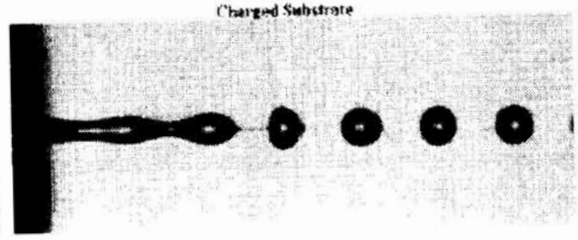

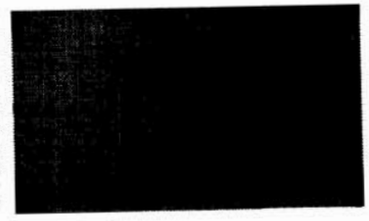

50-µm drops jet

Y. Bar-Cohen, JPL, yosi@jpl.nasa.gov

International technical forums for interaction and collaboration

- SPIE Smart Structures and Materials Symposium - EAP Actuators and Devices Conference - held at Newport Beach, CA, on March 1-2, 1999

- MRS Conference - Symposium FF: Electroactive Polymers - held in Boston, MA, on Nov. 29 to Dec. 3, 1999

- The first WW-EAP Newsletter issue was published electronically in June, 1999
  http//ndeaa.jpl.nasa.gov/nasa-nde/lommas/eap/WW-EAP-Newsletter.html

- On Nov. 19, 1999 - An electronic communication platform (newsgroup) was formed eap-request@artemis.arc.nasa.gov "subscribe eap"

- In March 1999 - An EAP Actuators Worldwide webhub was formed with links to EAP R&D sites, general information and databases.
  http://ndeaa.jpl.nasa.gov/nasa-nde/lommas/eap/EAP-web.htm

WW-EAP Homepages

Links for the Webhub: http://ndeaa.jpl.nasa.gov/nasa-nde/lommas/eap/EAP-web.htm

- Biological Muscles: Dr. Richard L. Lieber article
  http://eis.jpl.nasa.gov/ndeaa/ndeaa-pub/SPIE-lieber-muscle-99.pdf

- EAP Recipes: EAP preparation processes
  http://ndeaa.jpl.nasa.gov/nasa-nde/lommas/eap/EAP-recipe.htm

- EAP in Action: Short videos showing various EAP materials and mechanisms being activated
  http://ndeaa.jpl.nasa.gov/nasa-nde/lommas/EAP-video/EAP-videos.html

- EAP Database: A table of EAP was provided with a disclaimer
  http://ndeaa.jpl.nasa.gov/nasa-nde/lommas/eap/actuators-comp.pdf

- EAP References: A collection of references on EAP
  http://ndeaa.jpl.nasa.gov/nasa-nde/lommas/eap/EAP-references.htm

SPIE Conference - EAPAD

To accelerate the development of EAP actuators an SPIE International Conference and a committee were initiated to serve as a forum for collaboration among the developers and users of the technology.

Call for Papers and Announcement

Electro-active Polymer Actuators and Devices (EAPAD) (ss04)

Part of SPIE's 6th Annual International Symposium on Smart Structures and Materials
1–5 March 1999 • Newport Beach Marriott Hotel and Tennis Club • Newport Beach, California USA

Conference Chair: Yoseph Bar-Cohen, Jet Propulsion Lab.

Cochair: Mohsen Shahinpoor, Univ. of New Mexico

Program Committee: Carol Becker, Space and Naval Warfare Systems Ctr., San Diego; Paul D. Calvert, Univ. of Arizona; Richard O. Claus, Virginia Polytechnic Institute and State Univ.; Danilo De Rossi, Univ. degli Studi di Pisa (Italy); Michael Goldfarb, Vanderbilt Univ.; Chang Liu, Univ. of Illinois/Urbana-Champaign; Ajit K. Mal, Univ. of California/Los Angeles; Edward McCullough, Boeing North America; Jon S. McElvain, UNIAX Corp.; Yoshihito Osada, Hokkaido Univ. (Japan); Toribio F. Otero, Univ. del País Vasco (Spain); Francis Pettus, DARPA; Jaycelyn O. Simpson, NASA Langley Research Ctr.; Minoru Taya, Univ. of Washington; David B. Wallace, MicroFab Technologies, Inc.

For many years, electro-active ceramic and shape memory alloys have been the primary source of actuation materials for smart structures and drive mechanisms. Numerous applications have been reported including robotics, active damping, vibration isolation, manipulation, articulation, and many other functions. Electro-active polymers (EAP) received relatively little attention due to small number of available materials as well as their limited observed actuation capability.

In recent years, new and effective EAP materials have emerged that are changing the view of these materials capability and potential. Their key attraction is their ability to emulate biological muscles and their ability to induce strong levels of displacement strain. Recent studies of their operation at low temperatures and vacuum have been very promising, making them potential actuators for space mechanisms. Unique robotic components and MEMS devices have been reported, where EAP provided the actuation or mechanism of mobility. Insect-like mechanisms are becoming a possible reality and new enabling technologies are now feasible. This conference is seeking to turn the spotlight on these materials and their applications as well as to increase the recognition of EAP as viable option for smart structures.

Papers are solicited on but not limited to the following topics:

- electro-active polymers (EAP) materials and their characteristics
- muscles, actuators and sensors based on conducting (electronic and ionic) polymers
- MEMS and robotic applications of electro-active polymer actuators
- control, biomechanics and neuromuscular techniques, and applications of EAPs
- medical applications of artificial muscles, biotelemetry, cochlear implants,
- intelligent and adaptive processing of biological sensory information and implantable devices
- support electro-active polymer technology, including organic batteries
- modeling, analysis and simulation of EAP
- mechano-chemo-electrical devices as a reverse property of the artificial muscles (electro-chemo-mechanical devices)
- biomechanics and bio-mimetic application including walking, crawling, swimming and flying micro-devices
- miniature robo-creatures including flies, insects, worms, etc.

Abstracts and papers submitted MUST show an explicit connection to smart structures and materials in both the abstract and the main text in order to be considered. This connection can be either direct (the technique would be used directly in a smart structure) or indirect (the technique can be used to help create something that would be used directly in a smart structure).

Abstract Due Date: 3 August 1998
Manuscript Due Date: 1February 1999

SPIE—The International Society for Optical Engineering

SPIE is an international technical society dedicated to advancing engineering, scientific, and commercial applications of optical, photonic, imaging, electronic, and optomechanical technologies. Its members are engineers, scientists, and users interested in the development and application of these technologies. SPIE provides the means for communicating new developments and information to the engineering, scientific, and user communities through its publications, symposia, education programs, and other educational information services.

Y. Bar-Cohen, JPL, yosi@jpl.nasa.gov

INTERNATIONAL SPACE STATION - MISSE EXPERIMENT

- The International Space Station (ISS) is offering unprecedented opportunities for long-term experiments in space.
- One of the first of such experiments is the Materials International Space Station Experiment (MISSE) sponsored by the AFRL/ML and the NASA SEE Program [Cooperative effort between the Air Force, NASA and industry].
- Material specimens will be placed in 4 separate Passive Experiment Carriers (PECs) previously used to contain the MIR Environmental Effects Payload experiments on MIR from March 1996 to September 1997.
- The MISSE PECs will be installed external to the ISS in late 2000 to early 2001, subject to approval by the NASA ISS program and flown for periods of 1 to 3 years.
- The experiment time frame will correspond to solar maximum conditions, providing as severe a test environment in low earth orbit as possible.
- EAP was offered an opportunity to fly on the autonomous experiment and a small area was allocated.

PI: Suzanne L. B. Woll, Ph.D. Non-metallic Materials Technology Boeing Phantom Works, (425) 965-0672 Renton

SUMMARY

- Electroactive Polymers are emerging as effective displacement actuators.
- These materials offer the closest resemblance of biological muscle potentially enabling unique capabilities changing the paradigm about robots construction.
- Under a NASA task, several EAP driven mechanisms were developed including dust wiper, gripper and robotic arm
- EAP are inducing a low actuation force limiting the applications that can use their current capability
- In recognition of this limitation a series of international forums were established including SPIE conference, Webhub, Newsletter, and Newsgroup.
- A challenge was posed to the EAP community to have an arm wrestling between robot that is equipped with EAP actuators and human.

The grand challenge for EAP as
ARTIFICIAL MUSCLES

Y. Bar-Cohen, JPL, yosi@jpl.nasa.gov

National Center for Advanced Manufacturing

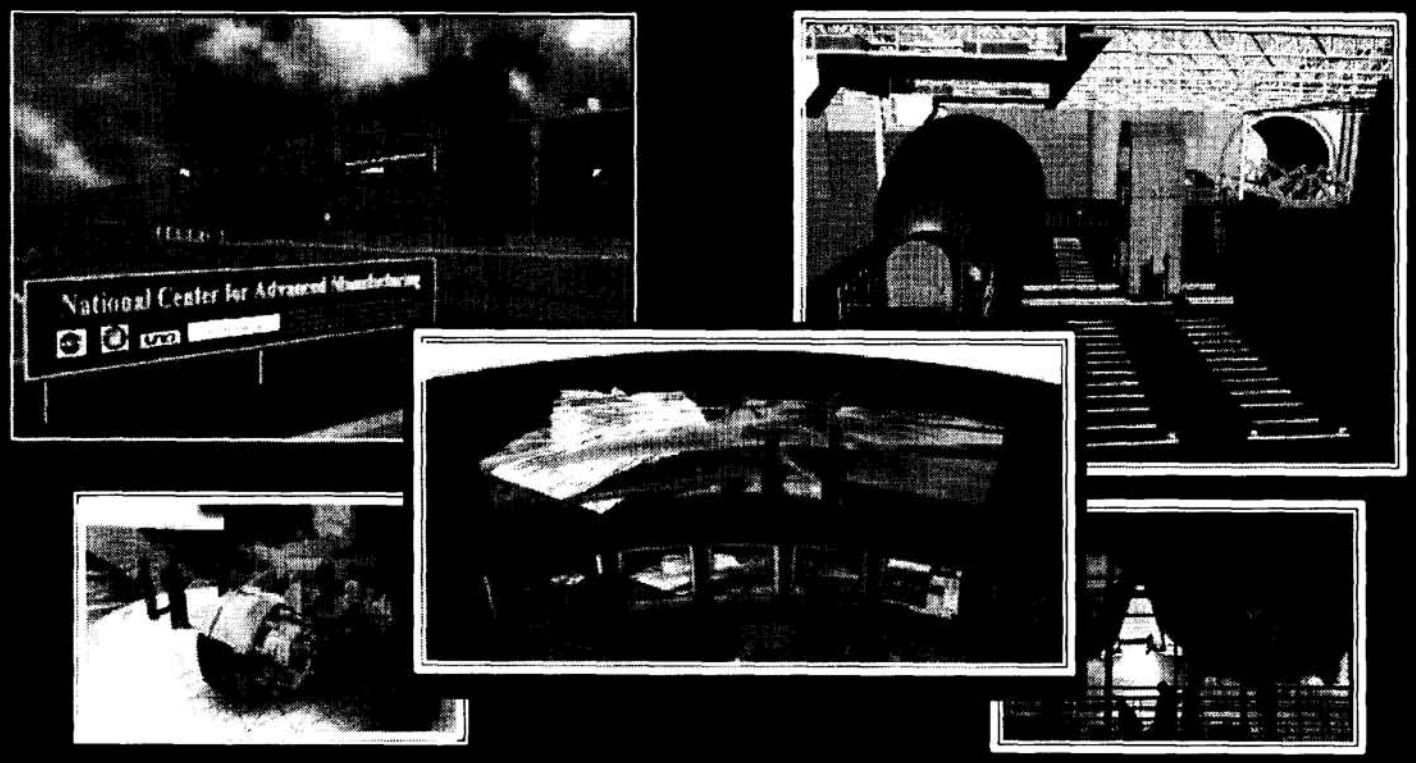

Fourth Conference on Aerospace Materials, Processes, and Environmental Technology

September 19, 2000

C/159/1M/31

Background

- Early '98 MSFC teamed with LMMSS to address large composite issues for VentureStar®
- The National Composite Center (NCC) concept was developed as strategy
- Presented the NCC concept to Dan Goldin and Senator Breaux, LA
  - Expand focus beyond VentureStar®, MAF, and composites (hence NCAM)
  - Structure as a virtual partnership involving - Industry, Government, and Education
  - MSFC to lead reporting to NASA HQ Chief Technologist, Sam Venneri

Background

George C. Marshall Space Flight Center

Primary-Assigned Missions
Space Transportation Systems Development
Microgravity
Space Optics Manufacturing Technology

Agency-Assigned Center of Excellence
Space Propulsion

Programmatic Assignments
Reusable Launch Vehicle Technology
Advanced Space Transportation Technology
Space Shuttle Elements
Microgravity Research and Space Product Development Programs
Space Product and Development Program
Chandra X-Ray Observatory
Space Station Support and Utilization
Scientific Payloads and Research
Global Hydrology and Climate Center

Agency Support Activities
Communication Architecture and Providing Agencywide Area Network (WAN)
NASA Automated Data Processing Consolidation Center
NASA Digital Television Transition
Earned-Value Management (EVM)
NASA Preferred Technical Standards
Space Environment and Effects
IFMP Training Activity
NASA Operational Environment Team (NOET)
NASA Acquisition Internet Service (NAIS)
NASA Integrated Services Network (NISN)
Defense Contract Administrative Service Financial Management Support
National Center for Advanced Manufacturing (NCAM)
NASA Engineering Excellence Initiative

Background

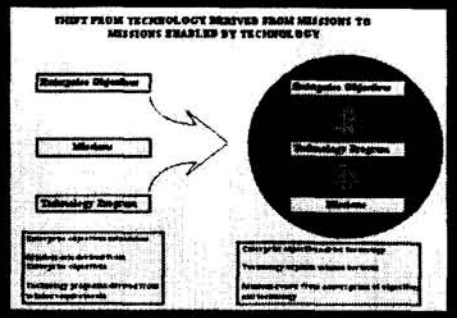

NASA Technology Plan

"Aerospace Manufacturing Technology Core Competency"

- Identify the long-term strategic technologies that are likely to be critical to the future missions of the Agency
- Determine those technologies where viable in-house "core competencies" will be essential to make that technology available to NASA in the future

Background

ED Strategic Plan

"Advanced Manufacturing Technology Thrust Area"

- ED seeks to focus its people and skill investments for a portion of its portfolio
- Technology thrust areas are intended to be crosscutting, high impact, and high value investments for ED customers

Mission

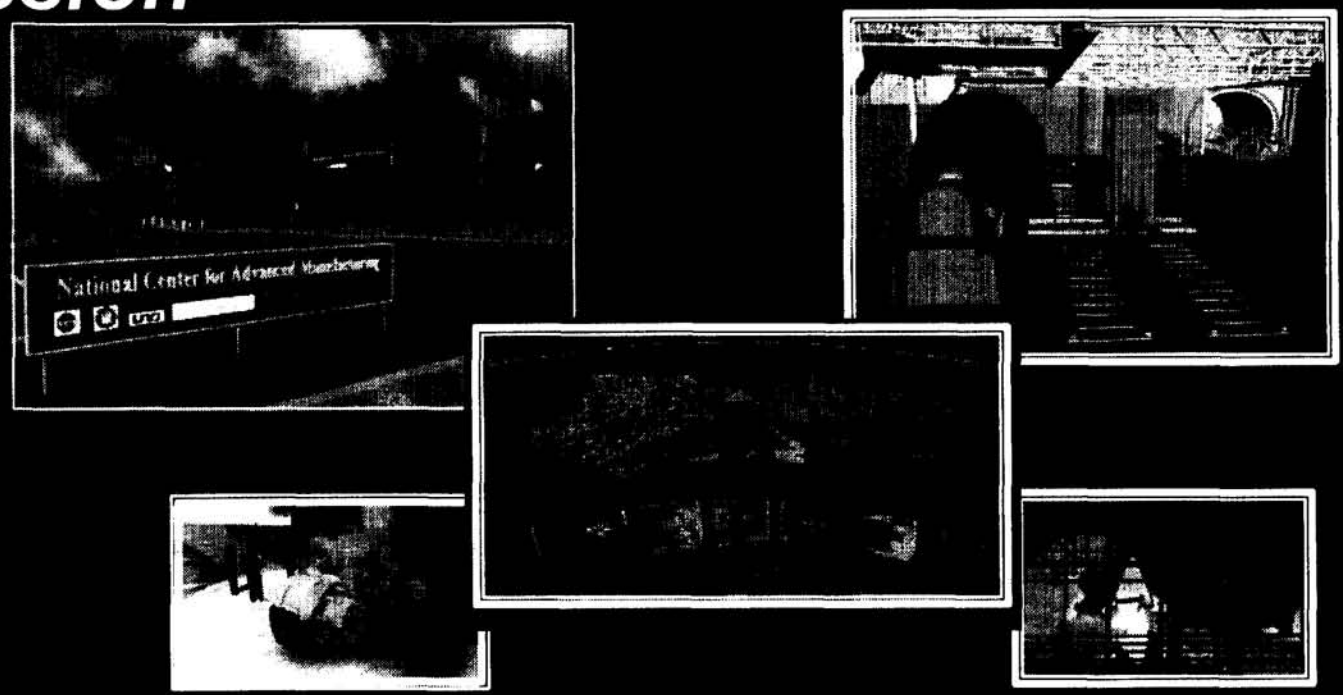

NASA's National Center for Advanced Manufacturing

- Assure World Class Manufacturing Capabilities Enabling Space Transportation Systems
- Effect Cultural Change in Manufacturing to Intelligent Environment
- Create Federal, State, University and Industry Mfg. Partnerships
- Enhance Educational Development for Manufacturing
- Strengthen U.S. Competitiveness in Aerospace/Commercial Markets

Technology Development Approach

World Class Manufacturing Capability

Technology Demonstration Opportunities

Advanced Manufacturing Technology Development

NCAM Capability Enhancements

Intelligent Processes and Equipment

Partnerships / Educational Development
Universities / NASA / Industry

Core Capabilities

Emerging Technologies

Technology Development Approach

- Strengthen overall long term investment in manufacturing technology
- Determine what technologies are critical to NASA and Industry missions
  - Understand technology readiness and gaps
  - Evaluate current/new technology for missions
  - Long term strategy, different from Project support
- Integrate manufacturing with counterpart discipline areas (systems, materials, design, operations, test, etc) "systems wise approach"
- Provide discipline leadership and authority
  - Develop a strategy to assure the technology base and national infrastructure availability

Partner and leverage

Space Transportation Significance

NCAM Supports Space Transportation

- Revolutionize space transportation by delivering advanced manufacturing research and technology development
  - Safe, affordable and reliable space transportation systems for the Nation and for NASA
  - Builds the technology base needed for next generation launch vehicles
- Affect a vigorous robust aerospace industry
- Provides environment to foster innovation and collaboration
  - Industry, Education and Government

Space Transportation Significance

Generations of Reusable Launch Vehicles

Today: Space Shuttle
1st Generation RLV
- Orbital Scientific Platform
- Satellite Retrieval and Repair
- Satellite Deployment

2010: 2nd Generation RLV
- Space Transportation
- Rendezvous, Docking, Crew Transfer
- Other on-orbit operations
- ISS Orbital Scientific Platform
- 10x Cheaper
- 100x Safer

2025: 3rd Generation RLV
- New Markets Enabled
- Multiple Platforms / Destinations
- 100x Cheaper
- 10,000x Safer

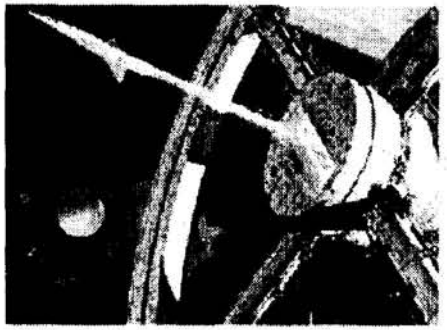

2040: 4th Generation RLV
- Routine Passenger Space Travel
- 1,000x Cheaper
- 20,000x Safer

Partnering

Strategic Partnerships and Alliances are Essential

- Common Set of Objectives and Goals
  - Maintain synergy, builds trust
  - Understand convergence issues government/industry
  - Eliminates redundant effort
- Increases competitively funded research
- Leverage assets and experience
- Cultural change to sharing of information

NCAM MAF Project

"A person of words and not of deeds is like a garden full of weeds"

- NASA
- State of Louisiana
- Academia – UNO
- U.S. Industry - LMMSS

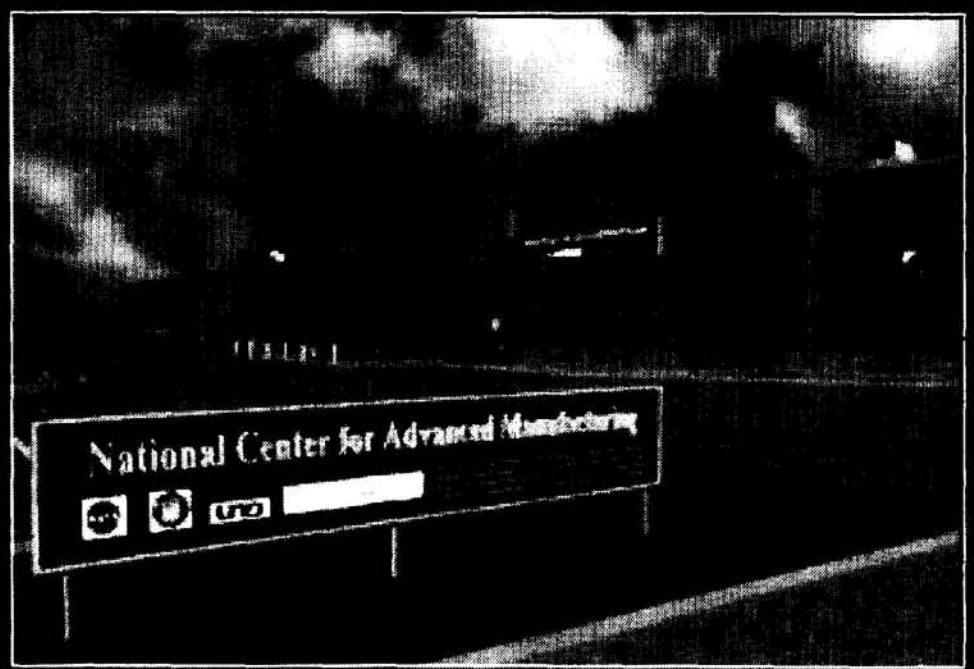

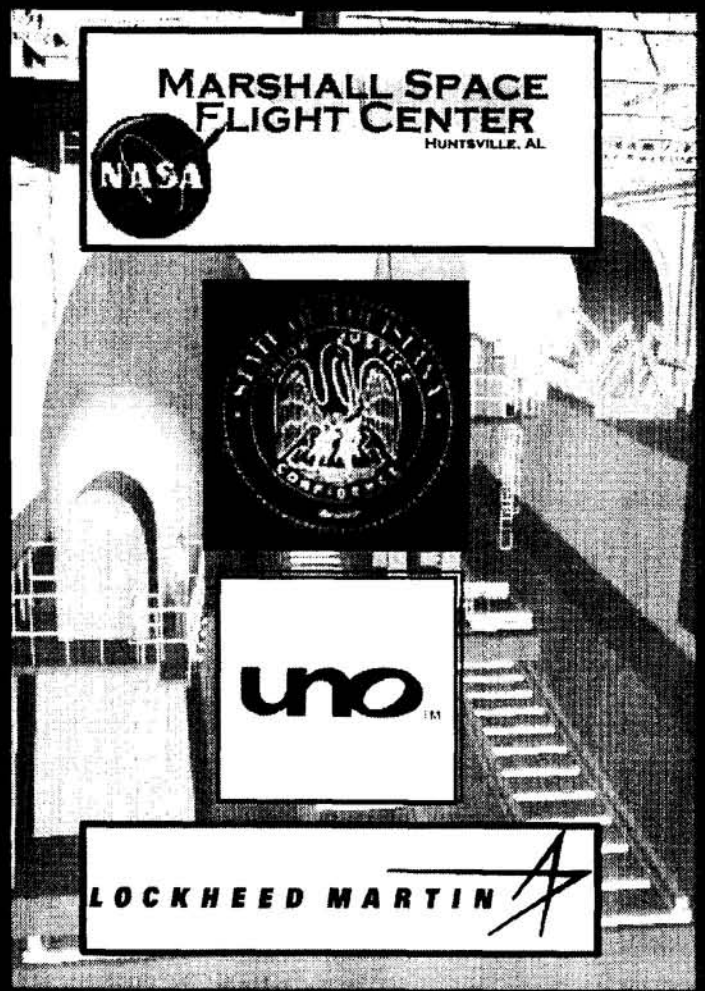

National Center for Advanced Manufacturing

NASA & Calhoun Community College

- NASA
- State of Alabama
- Calhoun Community College
- Boeing

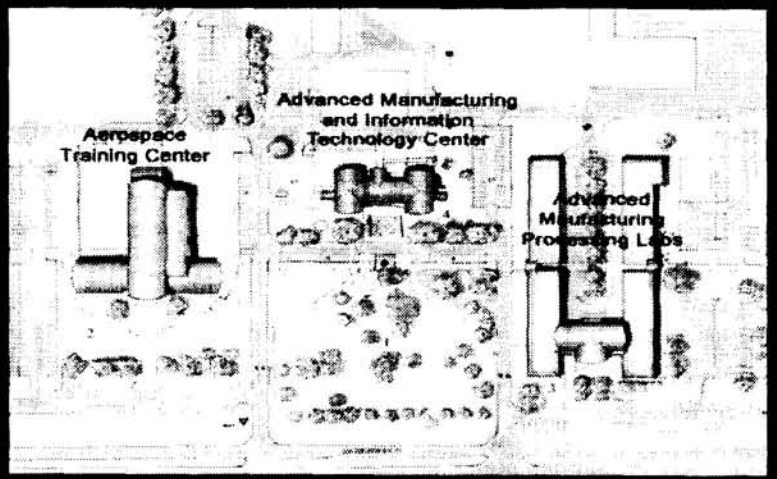

Calhoun

Aerospace and Advanced Technology Park

Productivity Enhancement Complex

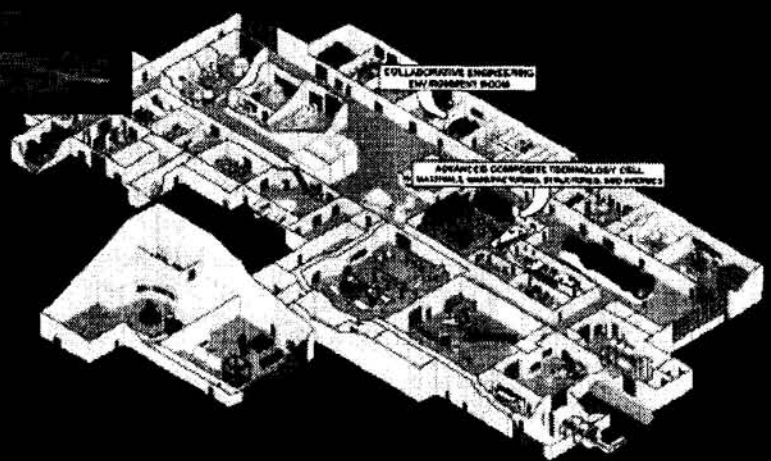

Boeing Delta IV Plant

Educational Development

- Develop advanced technical workforce for NASA and industry
- Focus research toward NASA and industry needs
- Increase number of high-value jobs

Why is NASA involved in education?

Education is critical to the development of revolutionary technology--the new set of "tools for our future."

Education is critical to the future of NASA. We depend on it for our highly skilled and knowledgeable workforce.

Education is critical to the vitality of the nation. Every American must have a fundamental understanding of science, and technology in order to fully participate in society.

Intelligent Synthesis Environment

"If the last century was the industrial revolution then this century will be the information revolution"

- Cultural changes required
- Leverage Information technology
- Collaboration through virtual centers
- Advances the state-of-practice of product development
- Broader than just manufacturing
  - Leverage other ISE areas
- NCAM serves as a user testbed for MSFC ISE initiatives
- A long term strategy (ISE is a journey not destination)
- "Poor Man" ISE approach being pursued

Summary

- The NCAM is a strategy, organization, & partnership
  "not a place or facility"
- Focused on long-term technology development
- The NCAM initially will be a regional partnership however the intent is National in scope
- Need benchmarking - concept to finished product not trial and error
- Significant progress has been made to date
  - Setting the vision for the future

Advanced Engineering Environments –
Implications for Aerospace Manufacturing

by

Dale Thomas, Ph.D., P.E.
NASA Marshall Space Flight Center
Mail Stop VS10
Huntsville, Alabama 35812

Telephone: 256-544-1180
Email: dale.Thomas@msfc.nasa.gov

INTRODUCTION

There are significant challenges facing today's aerospace industry. Global competition, more complex products, geographically-distributed design teams, demands for lower cost, higher reliability and safer vehicles, and the need to incorporate the latest technologies quicker, all face the developer of aerospace systems. New information technologies offer promising opportunities to develop advanced engineering environments (AEEs) to meet these challenges. Significant advances in the state-of-the-art of aerospace engineering practice are envisioned in the areas of engineering design and analytical tools, cost and risk tools, collaborative engineering, and high-fidelity simulations early in the development cycle. These advances will enable modeling and simulation of manufacturing methods, which will in turn allow manufacturing considerations to be included much earlier in the system development cycle. Significant cost savings, increased quality, and decreased manufacturing cycle time are expected to result.

This paper will give an overview of the NASA's Intelligent Synthesis Environment, the agency initiative to develop an AEE, with a focus on the anticipated benefits in aerospace manufacturing.

BACKGROUND

The development of aerospace systems has historically been a costly and time-consuming endeavor, particularly so for the systems developed for NASA missions. To illustrate, consider that the Apollo Saturn V launch vehicle required 8 years to develop (through first launch) at a cost of ~$5B, while the Space Shuttle required 11 years to develop at a cost of ~$11B; the unmanned Ariane V launch vehicle required 10 years and ~$7B to develop (all costs reflect actual year dollars). It should also be noted that the Ariane V may be considered to be an evolutionary development of the Ariane IV, otherwise the time and cost to develop would have been greater. A space transportation system typically includes a launch vehicle, a spacecraft, a ground launch processing infrastructure, and a mission operations infrastructure. Each of these component systems represents a significant development effort in its own right; developed in conjunction, the complexity of the development only increases.

In planning for the next generation of aerospace systems, NASA has chosen to focus on the life cycle cost of the system. In the case of a space transportation system, this would include a launch vehicle as well as its associated system components. The costs include the amortized cost to develop, the fabrication costs of the launch vehicle, and the development and operations costs of the associated/support systems. The operations costs are not negligible, even when compared to the significant development costs given in the foregoing paragraph. Consider that ~140,000 direct labor hours are required to process the Space Shuttle between flights, excluding propulsion elements and any servicing required on the launch pad. Hence, clearly all elements of the life cycle must be considered in development of any future space transportation system.

CURRENT SYSTEM DEVELOPMENT ENVIRONMENT

NASA aerospace systems are typified by small production lot size, complex architecture, and relatively little design heritage. Attempts to utilize legacy parts in a new design often result in spectacular failures, as evidenced by the failure of the inaugural launch of the Ariane V. (Gleick) In this instance, an Ariane IV subassembly and associated software used within the Ariane V Guidance, Navigation, and Control subsystem functioned per Ariane IV specification, but in a mode inconsistent with the Ariane V design. This subtle functional characteristic was not detected in the Ariane V qualification testing. As is commonly the case in complex systems including software, system testing can catch only the anticipated failure modes.

These development challenges are exacerbated by the nature of the development team. The development team typically consists of a systems integrator and many component vendors; the development team itself is usually dispersed across a large geographical area, often across international boundaries. Furthermore, the development team is rarely located proximate to the customer. When the complexity of the system development is considered, the communications problem becomes evident. Since the quality of any system engineering task depends on technical communication, the difficulty of system engineering grows as a function of geographical dispersion. Also, as the quantity of embedded software in today's systems grows, the system engineering challenge grows. Indeed, the Ariane V failure discussed in the foregoing paragraph has been attributed to poor system engineering. (Gerard, 1997) Likewise, failures in recent NASA missions have cited poor system engineering as a root cause. (McDonald, Spear, Stephenson, Young)

While advances in information technology have led to significant advances in engineering tools and infrastructure, engineering processes have remained largely unchanged since the days of drafting tables. The current engineering life cycle of a space transportation system is illustrated in Figure 1; this life cycle may be considered typical of the aerospace system life cycle. This traditional process is largely sequential in nature, usually requires long development times, and does not easily integrate customers and suppliers into the design process. Furthermore, following traditional design practices, approximately 90% of the total cost of an aerospace vehicle is built into the design in the first 10% of the development cycle. Unfortunately, the total cumulative knowledge of the design is still very low at this point, about 15-20% of the knowledge available at the end of the development cycle.

Efforts to accelerate the development cycle within NASA, commonly referred to as "Faster, Better, and Cheaper," have met with limited success. While in many cases the development cycle time and cost have indeed decreased, the mission success rate has likewise decreased. (Dickey) Given that the overall engineering process remains fundamentally unchanged, complex systems remain exceptionally expensive and time consuming to develop, as the quantum improvements in efficiency and quality that are characteristic of information technology applications in general have proven elusive.

ADVANCED ENGINEERING ENVIRONMENTS

Let the engineering environment be defined as the processes, tools, and infrastructure used by people to engineer systems. Here the engineering process describes the structured methods and procedures by which a complex system evolves through the conceptual definition, design, manufacture, integration and testing, and delivery for operations. The tools consist of hardware devices and software codes used by engineers to perform the various component tasks comprising the engineering process. The infrastructure is commonly described as the "physical plant" including office space, thermal vacuum chambers, etc. but has come to include the data networks and other elements of a computational and communications infrastructure.

AEEs are defined as particular implementations of computational and communications systems that create integrated virtual and/or distributed environments which link researchers, technologists, designers, analysts, manufacturers, suppliers, customers and managers involved in mission-oriented, leading-edge engineering teams comprised of industry, government, and academia. (NRC)

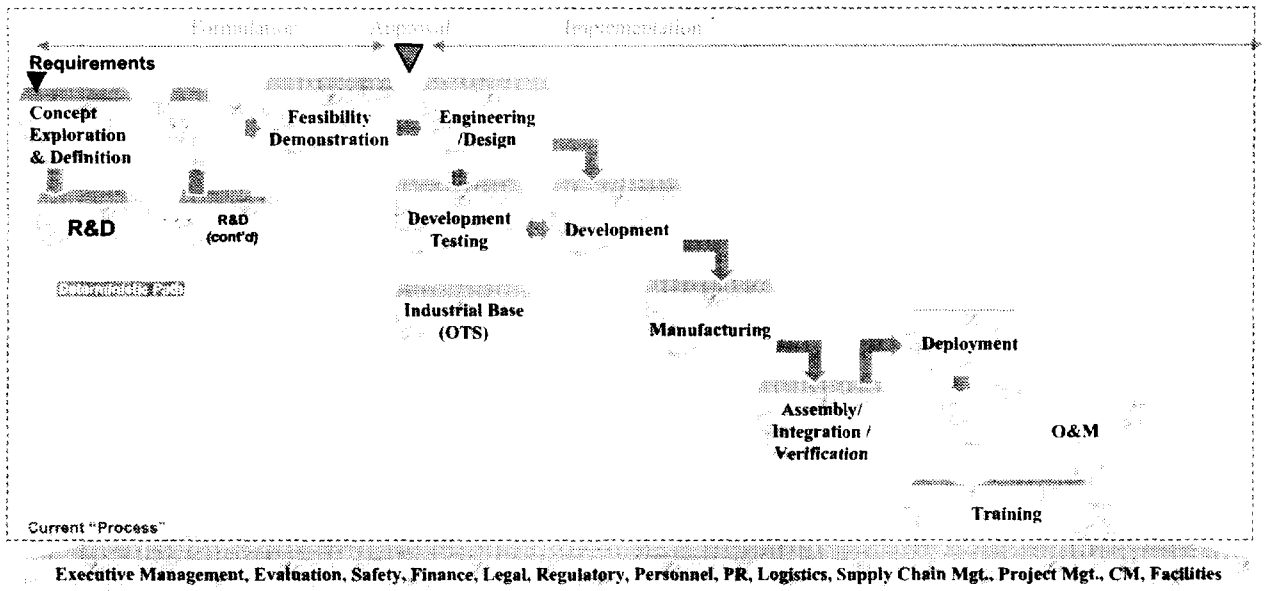

Figure 1. Current Life Cycle

THE INTELLIGENT SYNTHESIS ENVIRONMENT (ISE) CONCEPT

To meet NASA's unique needs the future product and mission development environment must accommodate different groups of people, such as engineers, designers, scientists and technology developers. These groups must be able to work together collaboratively, and must also be able to integrate both customers' and suppliers' requirements into the process (Goldin, Goldin, Noor). These diverse teams will collaborate in utilizing new computational resources in innovative and meaningful ways. Teams will not be in one location, so the design environment must support collaboration of geographically distributed teams. Computational tools that are utilized within this environment must be easy and intuitive to use, and make use of a balanced mix of multi-sensory technologies. The design environment must allow scientists to interact with simulated vehicles and missions so as to study science payload, mission performance and interaction of science requirements with vehicle and mission engineering. Ultimately, this environment should be usable by engineers, scientists, operators, program sponsors, and stakeholders.

Therefore, the vision of this new design and mission synthesis environment is:

To effect a cultural change that integrates into practice widely distributed science, technology and engineering teams to rapidly create innovative, affordable products. This is accomplished by using a combination of technologies to build/assemble an integrated Intelligent Synthesis Environment (ISE) for creative engineering and science.

ISE: A NEW NASA INITIATIVE

In order for NASA to meet its unique mission needs in space science, human exploration, earth science and aeronautics, NASA proposes a new Initiative to develop an Intelligent Synthesis Environment (ISE). ISE will utilize computational intelligence to synthesize existing, newly developing and future relevant technologies to provide the future product and mission development environment. In the ISE, synthesis takes place in three ways:

- Collaborative synthesis of scientists, engineers, technology developers, operational personnel and training personnel all working in geographically, as well as temporally, distributed locations;

- Synthesis of cutting-edge technologies and diverse, life cycle design tools seamlessly integrated together both horizontally and vertically at all levels of fidelity;

- Synthesis of humans, computers, intelligent hardware (e.g., robotics) and the synthetic (virtual reality) simulated designs and design languages.

The intelligent nature of ISE is derived from its concentrated use of non-traditional, intelligent computational systems such as intelligent product objects, intelligent agents and intelligent computational methods. The computational intelligence, which will be built into the design environment, will guide the utilization of the vast resources of knowledge and predictive capability to which the environment will have access.

Very importantly, the ISE program will make meaningful use of related developments sponsored by other government agencies and industry. This will be accomplished through the use of R&D ISE laboratories in which technologies from government, industry and universities will be synthesized, assessed, validated and demonstrated. To this end, NASA will form partnerships and coalitions with other government agencies, the software vendor industry, aerospace and non-aerospace industries and universities. In addition, ISE Large-Scale testbeds will be created to apply new ISE products to engineering projects and science missions of importance to NASA. These testbeds will be distributed geographically and will be reconfigurable to meet new requirements as these are identified. They will provide a showcase for demonstrating how state-of-the-art computational and communication facilities and tools can be synthesized with engineering, science, manufacturing, operations and training teams to dramatically improve productivity, enhance creativity and foster innovation at all levels of product and mission development.

THE ISE IN PRACTICE

The ISE Initiative will develop, validate, assess and demonstrate, through ISE LargeScale Applications, a revolutionary product and mission development environment which synthesizes existing, newly developing and future relevant technologies to provide the future environment for collaborative science, engineering, designing, manufacturing, certifying, operating and training. Such an environment will revolutionize design so that the conceptual, preliminary and detailed design phases merge, therefore dramatically shrinking the design cycle. Products and missions will be rapidly configured and assessed for scientific payoff or product performance leading to innovative and creative design solutions. Production, operations and training issues will be addressed early, and costs and risks accurately predicted and dramatically reduced. Redesign and manufacturing rework costs will be virtually eliminated. Certification testing requirements and costs will be dramatically reduced. In total, ISE will result in significant increases in productivity, affordability and performance.

The ISE is a comprehensive, completely integrated environment. It provides a holistic view of the product development process. It addresses the entire mission and life cycle of the aerospace system. It makes effective use of intelligent agents to increase the creativity bandwidth of the science and engineering teams. CEC's will be assembled/built to demonstrate the ISE concept, and to help in identifying technology developments needed for realizing its full potential in large-scale science and engineering applications. The

testbeds will be re-configurable, and will rapidly accommodate new synthesis paradigms as new technologies develop.

SPACE TRANSPORTATION SYSTEM DEVELOPMENT IN AN AEE

To illustrate the ISE concept of an AEE, consider the development of the NASA Spaceliner 100. (Lyles) The process of developing and deploying this vehicle is in its earliest stages such that the AEE can be illustrated throughout the full life cycle. Following are the primary goals for the vehicle:

- Increase Crew Safety
  - 1/1,000,000 probability of crew loss
  - Increase over current crew safety by a factor of over 10,000
- Increase Vehicle Reliability
  - 1/1,000,000 probability of vehicle loss
  - Increase over current reliability by a factor of over 10,000
- Lower launch vehicle costs
  - $100 per pound to LEO
  - Decrease current costs by a factor of 100.

The following paragraphs very briefly discuss the derivation of AEE functional requirements based on these Spaceliner 100 goals.

Orders of magnitude of vehicle endurance improvement are required. Specifically, the vehicle must turn out to be about 10,000 times more reliable/safe than the baseline vehicle – the Space Shuttle. This will require a combination of dramatic improvements involving principally materials and structural design – focused on increasing the overall fatigue life of the vehicle system, subsystems, and components. This focus will affect the conceptual through detailed design phases, as well as the manufacturing/ production phases. Thus, in order to support this focus, the AEE must facilitate design, materials selection, and loading simulation, and the AEE must facilitate the application of performance and fatigue life prediction tools at the vehicle system, subsystem, and component levels. This must include a probabilistic design approach that will provide multiple design alternatives, which will foster the understanding and reduction of risk, sensitivity and uncertainty. The AEE must enable and facilitate the prediction of performance and fatigue life at a level of accuracy far improved over such predictive capabilities as were available at the time of the Shuttle design. (Note, for example, that the Shuttle design plan predicted that the main engines would have to be removed and refurbished only after 20+ flights. As it turned out, they must be removed and refurbished after every flight – and at great cost.) In addition, the AEE must facilitate integration of comprehensive safety considerations and the "ilities" into the overall process and in all supporting subprocesses, as well.

The Spaceliner 100 goals require two orders of magnitude reduction in vehicle life cycle costs, with specific emphasis on the operations phase of the life cycle. Vehicle *development* cost is highly dependent on the overall length of time taken to complete the development. (The standing army of developers generally stays on the payroll throughout this length of time.) Thus, the AEE must provide methods and capabilities to accelerate the overall development process. A proposed, future, AEE-enabled engineering life cycle process is illustrated in Figure 2. This process utilizes state-of-the-art information technology to significantly reduce the vehicle development cycle time while simultaneously increasing the quality and thoroughness of the system engineering process as measured by increased system safety and reliability. The derived requirements for this AEE are further described in three paragraphs that follow. Subsequently, the AEE architecture will be described.

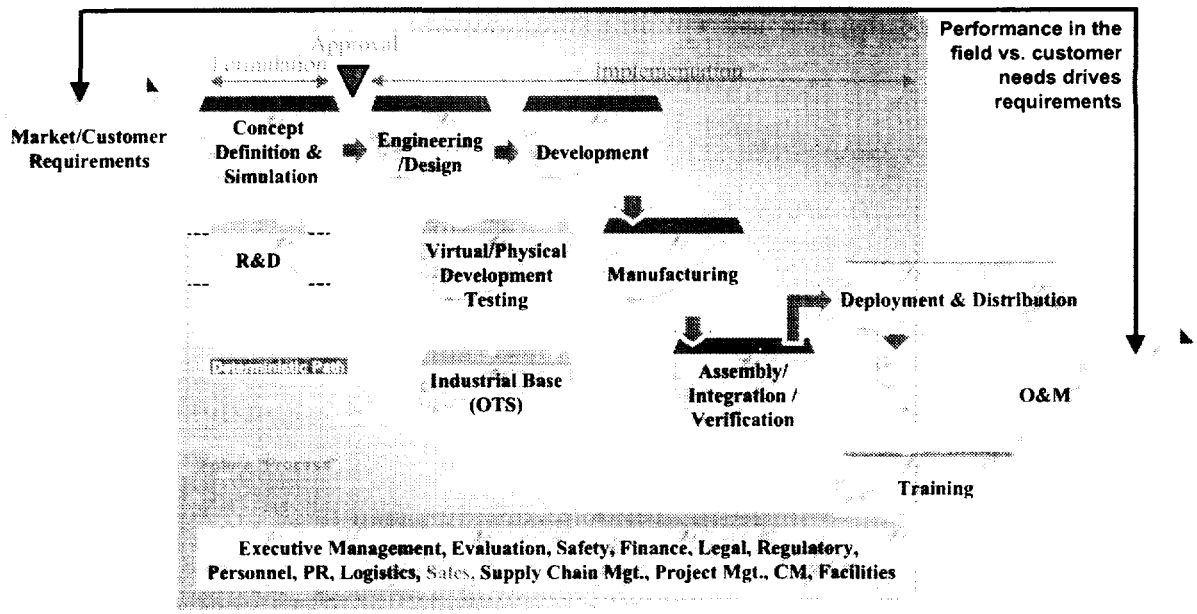

Figure 2. Future Life Cycle

Vehicle *development* (and ultimately operations) costs are principally driven by the decisions made in the conceptual and preliminary design phases. These decisions are based on lessons learned and particularly on the results of iterative rules-based design analyses. Vehicle performance and endurance capabilities are predicted based on anticipated loading/duty cycle/etc. These decisions include trades relative to utilization of actual and planned technology capabilities, such as materials performance characteristics. The speed at which these decisions can be made is dependent on the speed at which the computationally intensive iterations can occur in converging to a satisfactory design plan. Thus, in order to shorten the design phase while improving the quality of the outcome, the AEE must facilitate: rapid access to lessons learned and corporate knowledge, seamless integration of design/analysis tools, rapid completion of design and analysis steps/iterations, rapid insertion of alternative/ improved analysis tools, and intelligent selection of needed/compatible tools and techniques. These AEE-provided capabilities will require (and enable) a substantial accompanying process change from that of today since information derived in one process step/iteration will be immediately and seamlessly available as inputs for other process steps/iterations. This process change will enable the capability for essentially real-time/parallel processing among the engineering and analytical disciplines. To fully enable and implement this parallelism, the AEE implementation must facilitate integration of the people which support the engineering and analytical subprocesses. They must be trained to work in an environment that does not include the long periods of time – waiting for computations to complete, waiting for a colleague or supplier to finish a step, etc. – as is characteristic of current design environments.

The conceptual AEE architecture employs a building block approach to achieving the required AEE end-product capabilities. As shown in Figure 3 the blocks are analogous to the International Organization for Standardization (ISO) Open Systems Interconnect Model. Infrastructure blocks support tool and application blocks, and the aggregate of the blocks will be assembled within the architecture for a transportation vehicle – nominally the Spaceliner 100. It is noted that this architecture is readily applicable for the requirements of the other space transportation systems. The architecture provides these highlights:

- On-line/rapid connectivity and collaboration within MSFC and between MSFC and its supporting contractor, academic, and supplier communities. This enables the parallel processing required for shortening design cycles and/or enabling larger numbers of analysis iterations.
- On-line/rapid connectivity and collaboration between MSFC and the NASA Centers of Excellence. This enables MSFC organizations to expand the rapid/parallel processing capability to include Programs and Projects at the other Centers. This *external* connectivity and

collaboration is planned to be facilitated by the NASA Intelligent Synthesis Environment (ISE) Program. The AEE requirements in this regard will be developed to ensure MSFC's *internal* processes, tools, and infrastructure evolve to be compatible with the ISE.

- Tools integration and process automation environment. This enables the engineers and analysts to utilize the best tools available for each discipline in a plug-and-play environment. It also enables definition of multi-discipline analyses and optimization processes for automated solution convergence/ closure.

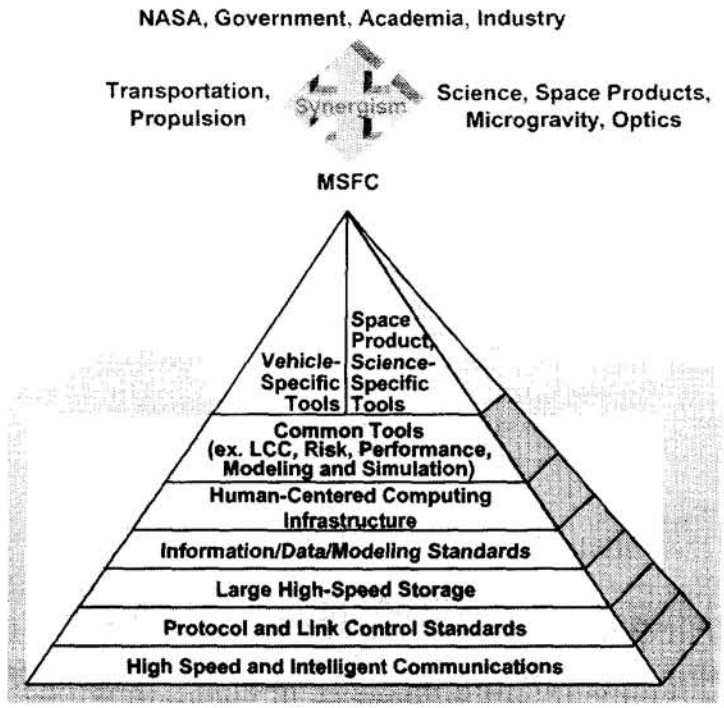

Figure 3. AEE Architecture

IMPLICATIONS FOR AEROSPACE MANUFACTURING

The Next-Generation Manufacturing Project (NGM) was initiated in 1995 to develop a framework for action that manufacturers can use to chart a course for success in an increasingly complex and competitive global environment. The NGM Project identified three high-leverage technology-related imperatives within an overall set of ten generic enabling practices and technologies deemed critical for NGM success:

- Next-Generation Manufacturing Processes and Equipment,
- Pervasive Modeling & Simulation,
- Adaptive, Responsive Information Systems.

Of these three imperatives, the second – Pervasive Modeling & Simulation, is most directly aligned with the goals and objectives of the Intelligent Synthesis Environment.

> "In the NGM Enterprise, modeling and simulation (M&S) will reflect a new way of doing business rather than a supporting technology. It will make virtual production a reality. All production decisions will be made on the basis of modeling and simulation methods, rather than on build-and-test methods. M&S tools will move from being the domain of the technologist, to being a tool for all involved in the product realization, production, and business processes. M&S will eliminate the need for developing hardware prototypes and allow for lot sizes of one. This will dramatically decrease time-

to-market for new products and services. It will provide products and services optimized for the customer and other stakeholders. It will require significantly fewer resources in the development process than build-and-test methods" (NGM)

Clearly, the inclusion of manufacturing M&S within the overall aerospace system development process will enable the consideration of manufacturing tradeoffs including the plant, the equipment, and the production processes at a much earlier point in the system design process than is typical today. Furthermore, this earlier inclusion of manufacturing considerations will include a higher degree of fidelity, enabling manufacturing plans to more appropriately influence the system design.

REMARKS

Today, the developer of an aerospace system is faced with more complex products, geographically-distributed design teams, demands for lower cost, higher reliability and safer vehicles, and the need to incorporate the latest technologies quicker. Within NASA, multiple technology development and demonstration projects are underway toward the objectives of safe, reliable, and affordable access to space. AEEs incorporating new information technologies offer promising opportunities to meet these challenges. The preceding discussion has identified significant advances in the state-of-the-art of aerospace engineering practice that are envisioned in the areas of engineering design and analytical tools, cost and risk tools, collaborative engineering, and high-fidelity simulations early in the development cycle for NASA aerospace systems. Furthermore, the implications of these advances within the specific context of aerospace manufacturing were discussed – namely, the routine usage of advanced manufacturing modeling and simulation methods, enabling manufacturing considerations to influence the system design much earlier in the development cycle than is common today.

REFERENCES

Dickey, B. "Midcourse Correction." Government Executive, September 2000.

Gerard, L. L. "Analysis of the Ariane V Flight 501 Failure – A System Engineering Perspective." Proceedings of the IEEE Conference and Workshop on Engineering of Computer-Based Systems, March 24-27, 1997, Monterey, California, pp. 339-46.

Gleick, J. M. "A Bug and a Crash." The New York Times Magazine, 1 December 1996.

Goldin, D. S., S. L. Venneri, and A. K. Noor. "Beyond Incremental Change", Computer, Vol. 31, No. 10, Oct. 1998, pp. 31-39.

Goldin, D.S., S. L. Venneri, A. K. Noor. "A New Frontier in Engineering", Mechanical Engineering Magazine, Vol. 120, No. 2, Feb. 1998, pp. 62-69.

Lyles, G. M. "Spaceliner 100 – Developing the Technologies to Enable 3rd Generation Launch Vehicles," Proceedings of the 1999 Space Transportation Day Conference, October 27, 1999, Huntsville, Alabama.

McDonald, H. (Chair) "Space Shuttle Independent Assessment Team – Report to Associate Administrator Office of Space Flight," March 7, 2000.

NGM (Next-Generation Manufacturing Project). 1997. Next-Generation Manufacturing Report, Volume 1, p. 48. Bethlehem, Pennsylvania: Agility Forum

Noor, A.K., S. L. Venneri,, J. M. Housner, and J. C. Peterson. "A Virtual Environment for Intelligent Design", Aerospace America, Vol. 35, No. 4, April 1997, pp. 28-35.

NRC (National Research Council). 1999. Advanced Engineering Environments: Achieving the Vision. Washington, D.C. National Academy Press.

Spear, T. (FBC Task Master). "NASA Faster, Better, Cheaper Task Final Report," March 2000.

Stephenson, A. G. (Chair). "Report on Project Management in NASA by the Mars Climate Orbiter Mishap Investigation Board," March 13, 2000.

Young, T. (Chair). "The Mars Program Independent Assessment Team Report." March 14, 2000.

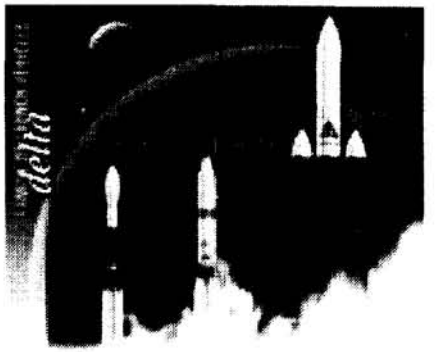

AMPET CONFERENCE

Huntsville, Alabama
September, 2000

State, Industry and Education Partnerships Expanding Education to Meet Workforce Challenges

James E. Swindell
Assistant Dean of Technology Programs
Calhoun Community College

William R. Reynolds
Delta Training Manager
The Boeing Company

Donna C. Bass
Project Coordinator for Boeing Decatur
Alabama Industrial Development Training

Presentation Overview

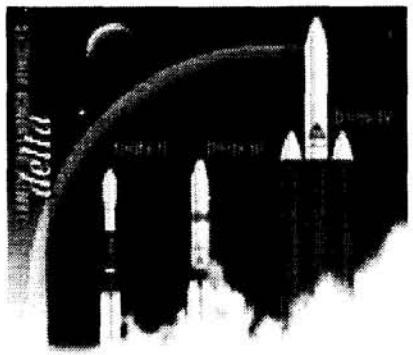

- America's Emerging Workforce
- Partnerships for Change
- Boeing Decatur – Meeting the Challenge with a New Approach
- AIDT – Tailored Training for Industry Startup
- Calhoun's Aerospace Technology and Beyond

Job Skill Level Changes
1950-2000

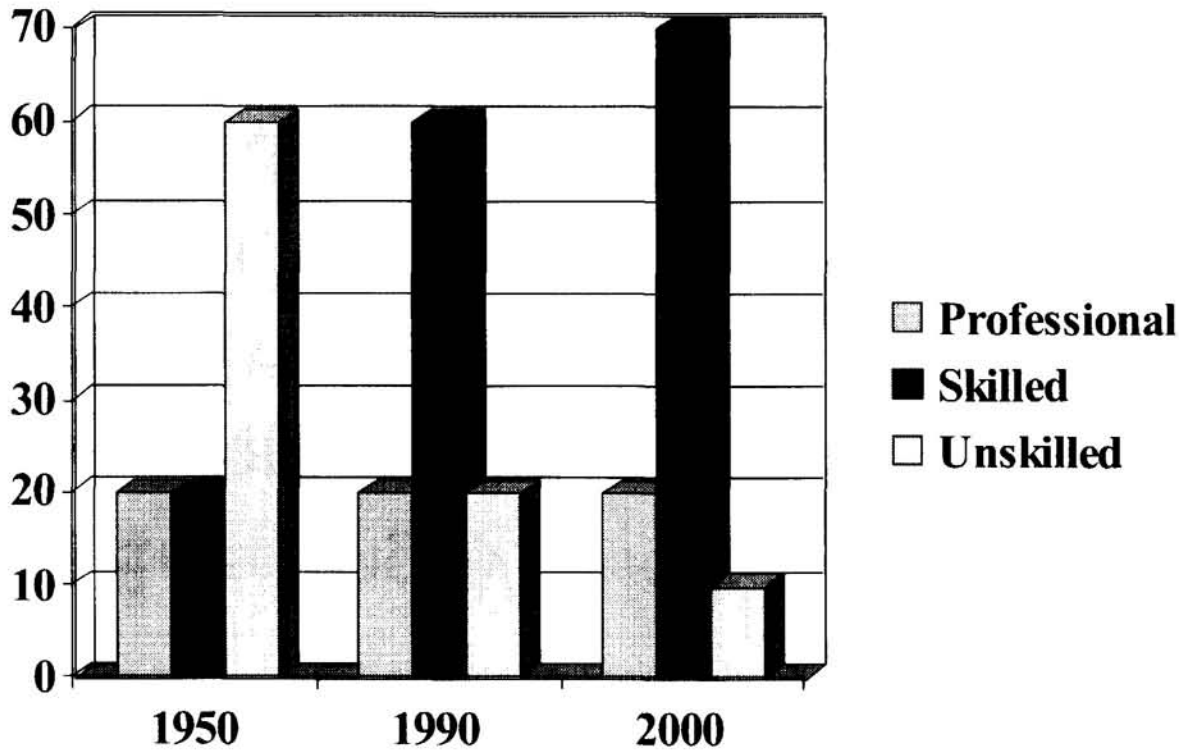

CALHOUN COMMUNITY COLLEGE

Developing the U. S. Workforce

(the path from HS to Graduate)

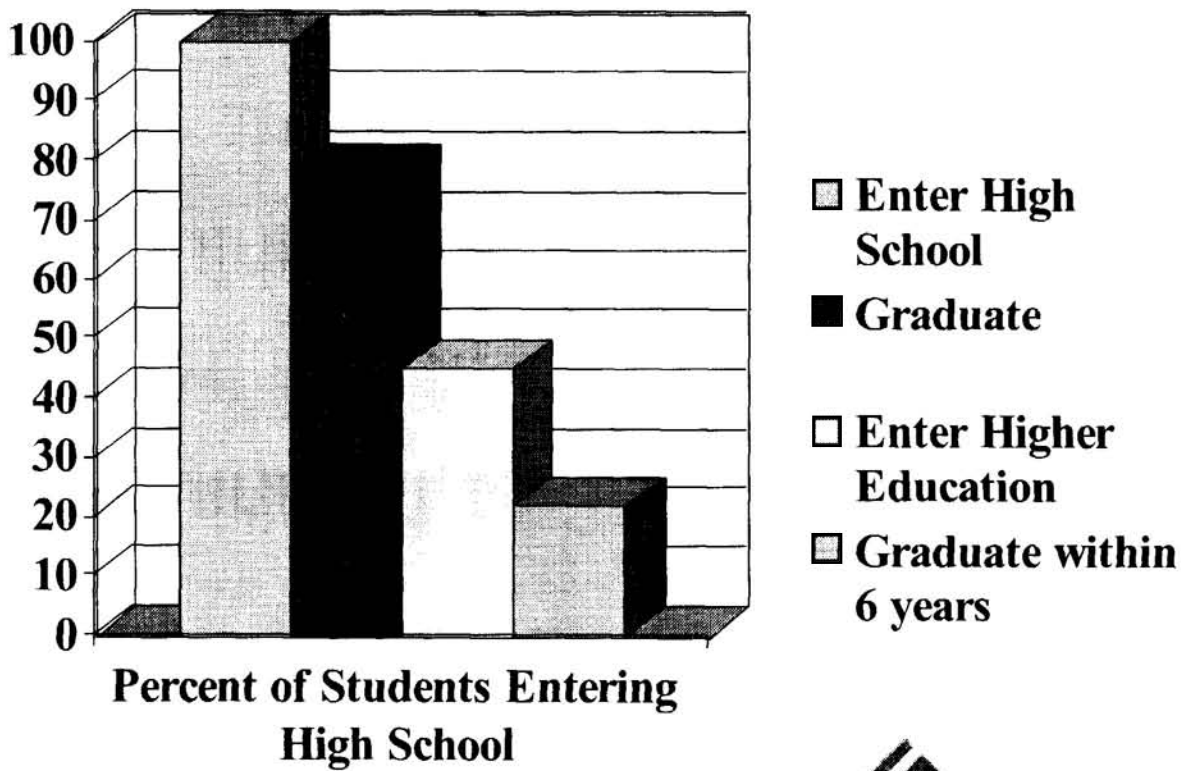

CALHOUN COMMUNITY COLLEGE

Minimum Job Requirements

the change between 1990-2000

- Jobs requiring 1 to 3 years of college

  ..... +50%

- Jobs requiring a 4 year college degree

  ..... +36%

- Jobs requiring no more than a high school education

  -20%....

CALHOUN COMMUNITY COLLEGE

Projections of New Aerospace Employees
Huntsville – Decatur Area
2001-2003

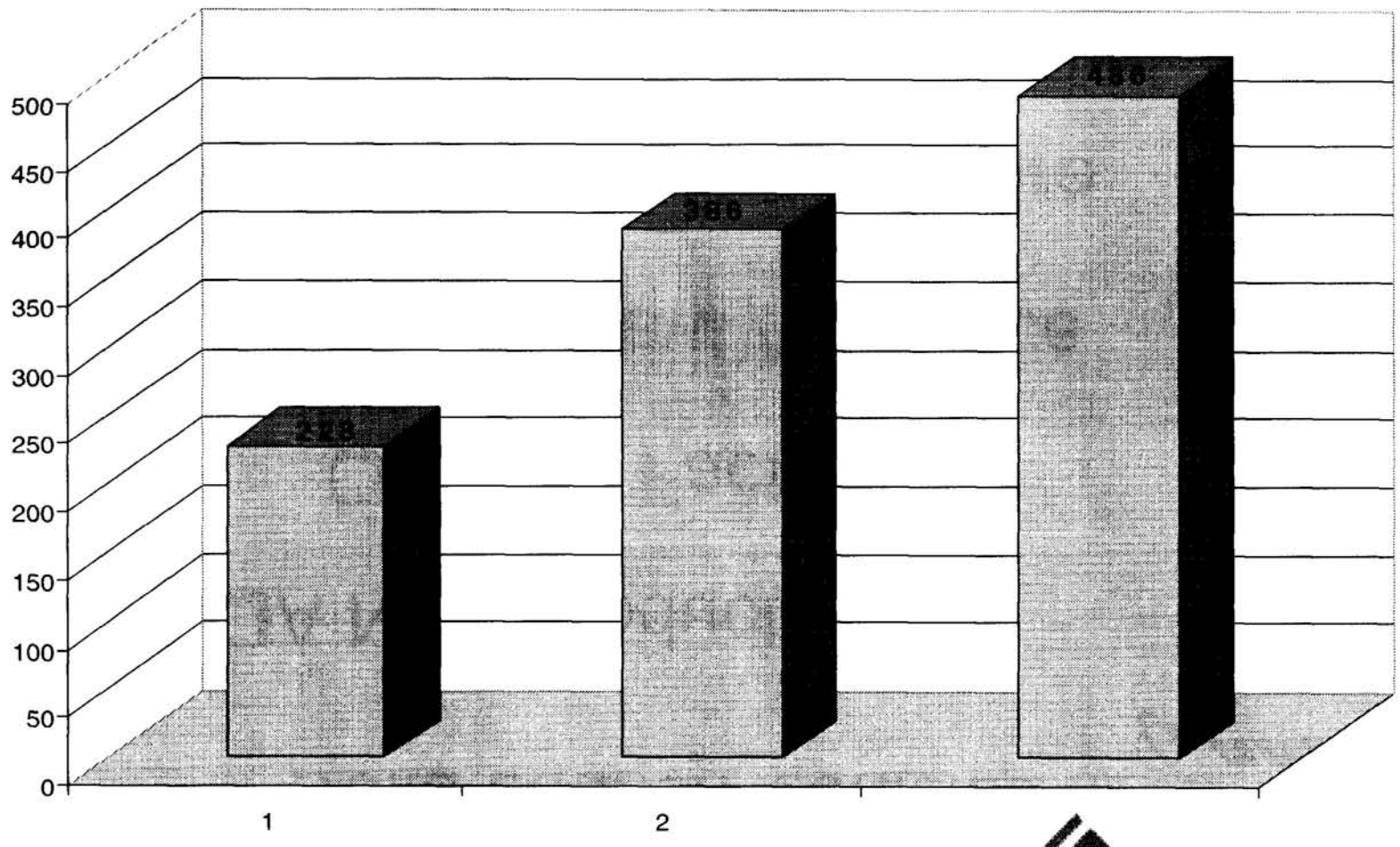

CALHOUN COMMUNITY COLLEGE

The Boeing Challenge for Delta Launch Vehicles

- ❑A New Product
- ❑A New Factory
- ❑A New Workforce
- ❑A New Culture
  - LEAN High-Performance Teams
  - Manufacturing

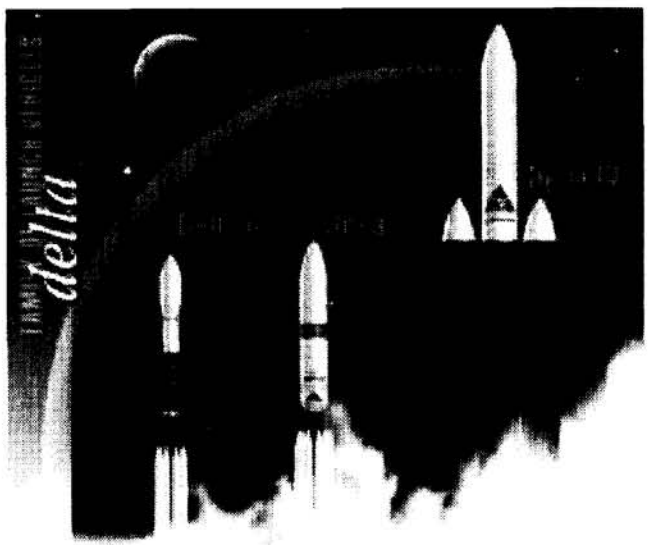

The Answer - Boeing Decatur

The Business

- Expendable Launch Systems
- Common Booster Core
- Capacity of 40 per year

The Site and Facility

- Facility 1.4 million sq. ft.
- 125 acres under roof
- Construction cost $450 M

The Key Elements

- **Partnerships**
- **Workforce Planning**

EELV / Delta

BOEING

Workforce Planning

- Staffing
  - Select for:
    - Attitude
    - Aptitude
  - Currently 525
  - Growing to 1500
- Training
  - 220 technical courses
  - 12 distinct work centers
  - Teaming skills

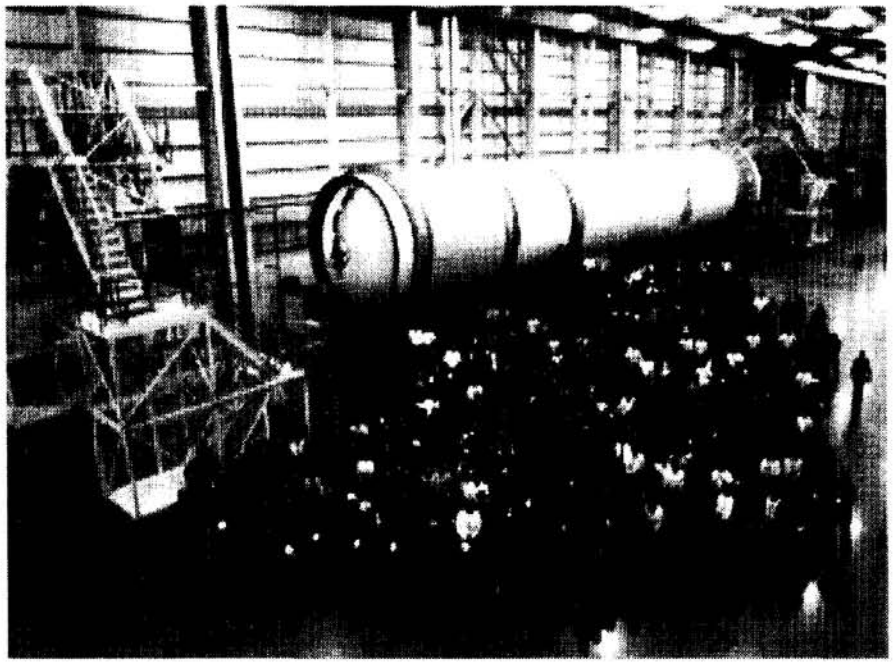

Partners in Progress

EELV / Delta

BOEING

- Alabama
  - State Employment Office
  - Industrial Development Training
  - Calhoun Community College
- Boeing
  - Decatur
  - Other Locations
  - Consultants…

    …Fluor Daniel

Partners - AIDT

EELV / Delta
BOEING

- Administers Staffing process.
- Conducts Pre-employment Training.
- Provides instructors for technical courses.
- Helps with course development.
- Provides advice and counsel.
- Provides funding.

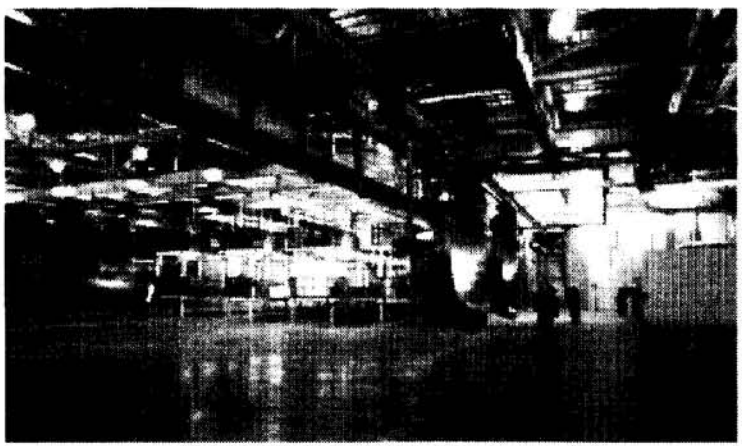

Partners – Calhoun Community College

- Provides training facilities.
- Built and staffed the Aerospace Training Center.
- Provide courses and instructor for continuing training.
- Will supply downstream candidates.

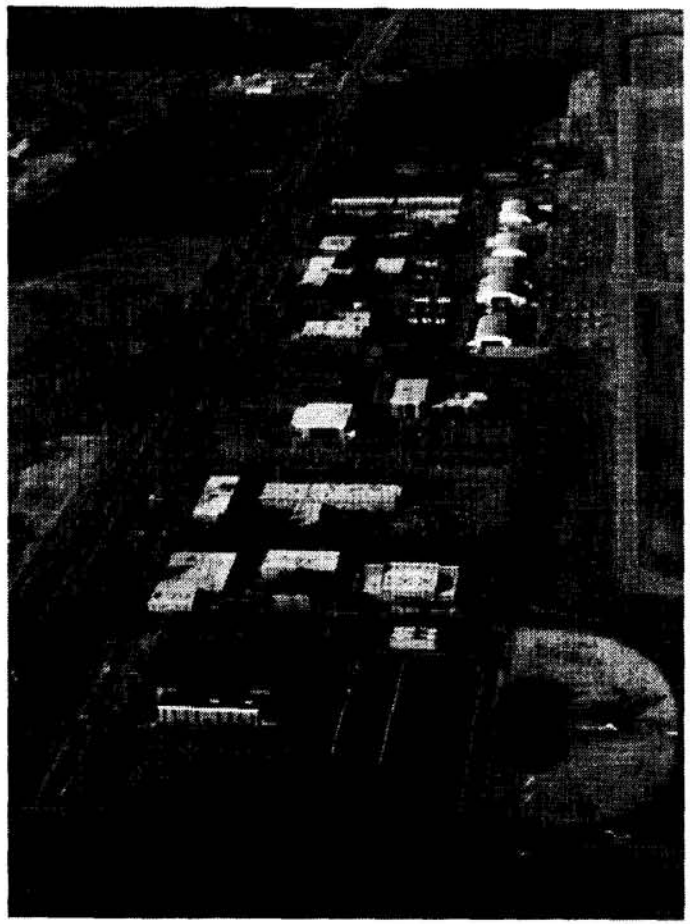

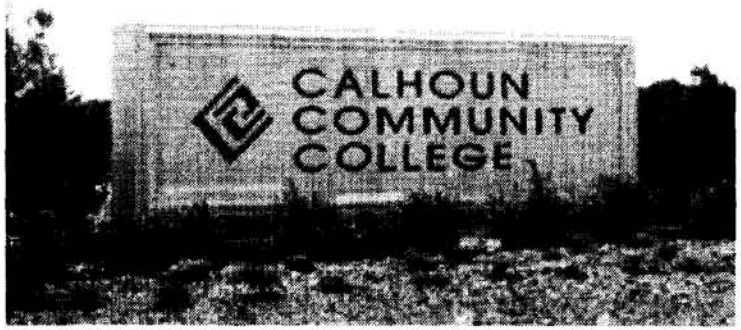

Partners - Fluor Daniel

- Skill and workforce needs assessment.
- Advice on manufacturing processes.
- Structured on-the-job training.

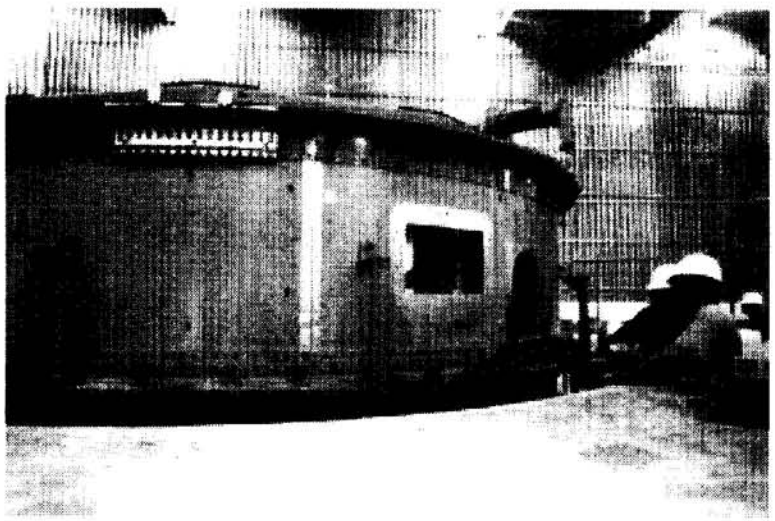

EELV / Delta

BOEING

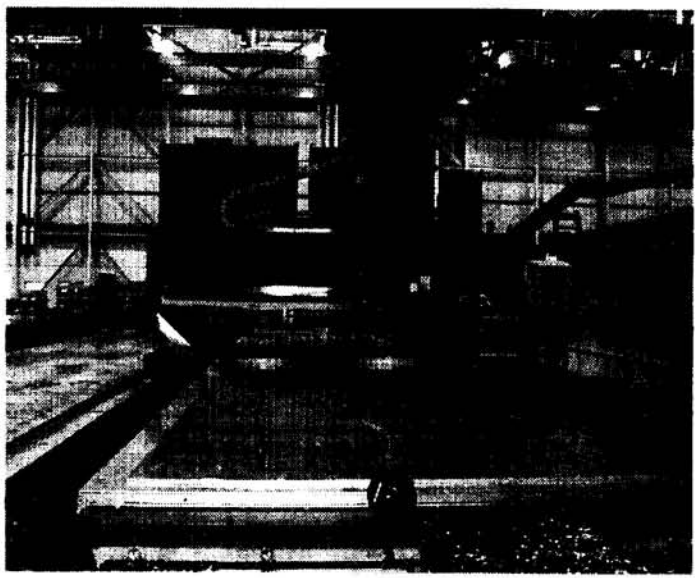

Progress to Date

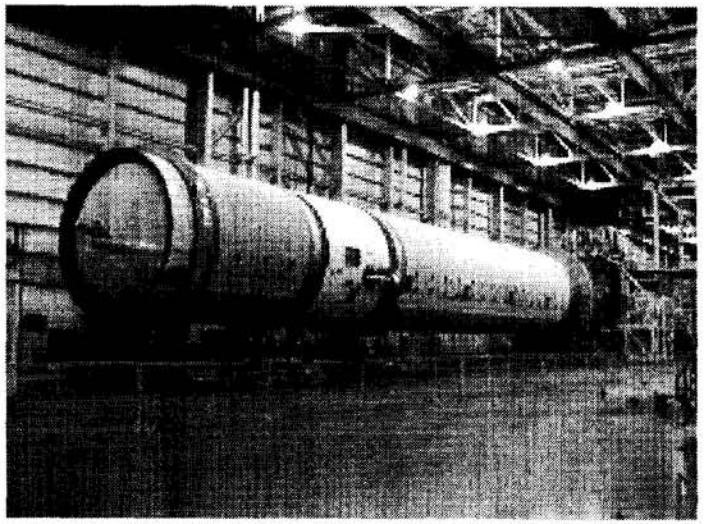

- 1200 courses taught
- 9600 student enrollments
- 56,000 student hours
- New Delta II/III work awarded
- Aerospace Training Center completed.
- AAS in Aerospace Technology being developed.

AIDT Roles in Recruitment & Training

- Recruitment
- Applicant Processing
- Testing and Skill Assessment
- Pre-Employment Training
- Startup Training

Recruiting Process

- Advertisement ... >36,000 applicants
- Application kits mailed and returned
- Application screening and banding
- Candidates entered in database
  - State Employment Service
  - AIDT

Applicant Process

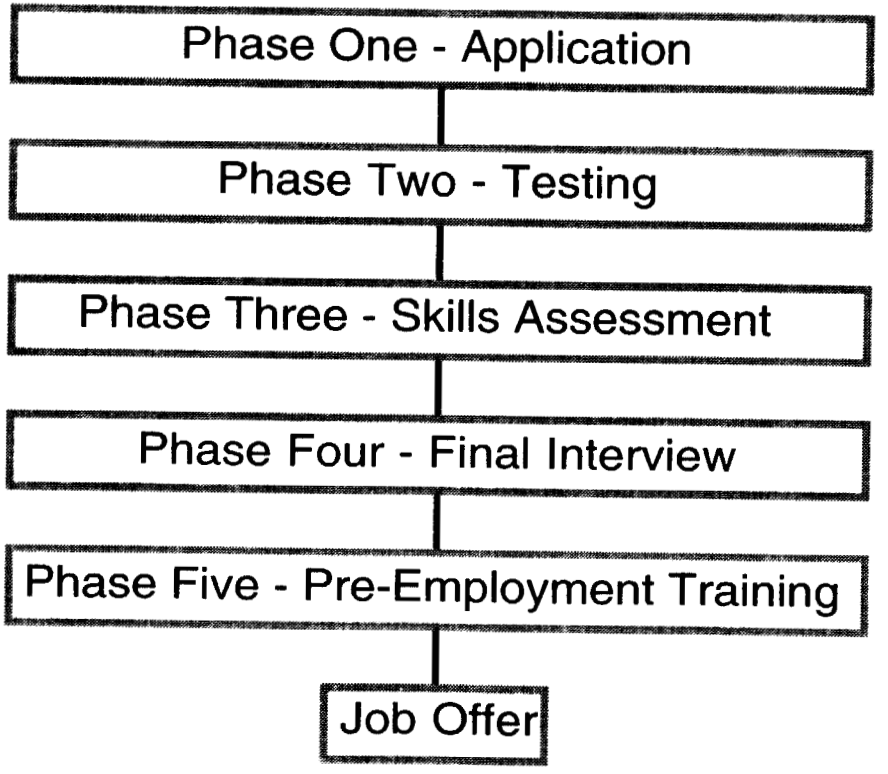

Alabama Industrial Development Training

Test and Assessment Process

TESTING

Situational Judgement Inventory (SJI)
Job Fit Inventory (JFI) - team
Purdue Pegboard - dexterity
Mechanical Reasoning - aptitude

SKILL ASSESSMENT

Individual Production Exercise
Individual Problem Solving
Group Production Exercise

Pre-Employment Orientation

Topics:

- Orientation, Diversity, Sexual Harassment
- Quality Programs, ISO 9000
- Computers
- Team Effectiveness, Communication Skills
- Team Problem Analysis, Decision Making
- Blueprint Reading, Precision Measuring, GD&T
- Lean Manufacturing
- Hazardous Materials and Safety

Continuous Improvement & Flexible Schedules

Alabama Industrial Development Training

Startup Training

- AIDT provides assistance with:
  - Instructors
  - Course development
  - Materials and equipment
  - Training

Startup Training

SAFETY COURSES

- HazCom Awareness
- Fall Protection
- Respiratory Protection
- Elevated Work Platform
- Lockout/Blockout/Tagout
- Confined Space Entry
- Corrosive Safety

PRODUCT ASSURANCE AND TESTING

- Performing Sub-Assembly Leak Checks

COMPOSITES ASSEMBLY

- Mechanical/Structural Torquing
- Mechanical Assembly
- Aerospace Electrical Assembly
- Composite Hole Drilling
- Click Bond Installation
- Wire Harness Installation

METALLIC SUB-ASSEMBLY

- Installing Propulsion and Pneumatics
- Strain Gage and Temperature Sensors

Alabama Industrial Development Training

Status Report Review

- 8,000 candidates tested
- 4,500 candidates assessed
- 225 trainees completed pre-employment
- 150 trainees have been hired

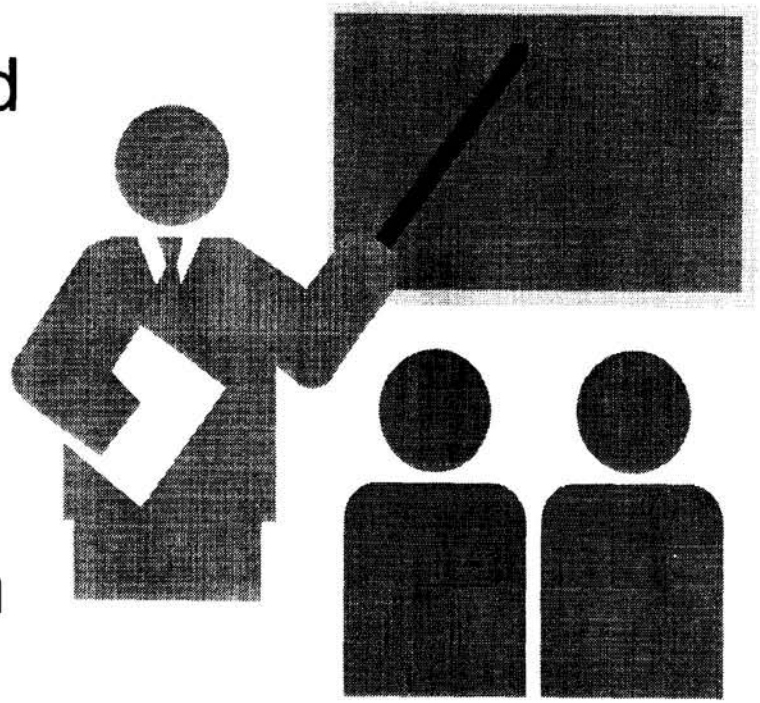

Calhoun College's Primary Role

- Design and Construct an Aerospace Training Center (ATC)
- Equip the ATC to provide high tech classroom and hands-on training for highly skilled technicians
- Design, develop and deliver an Associate Degree in Aerospace Technology
- Prepare Technicians for the Aerospace Industry

CALHOUN COMMUNITY COLLEGE

Calhoun Community College Aerospace Training Center

- 38,000 square feet
- 192 seat lecture hall
- exhibition hall
- 7 class rooms
- equipment high bay
- multi-purpose room
- conference room
- administrative areas
- stand-alone paint shop

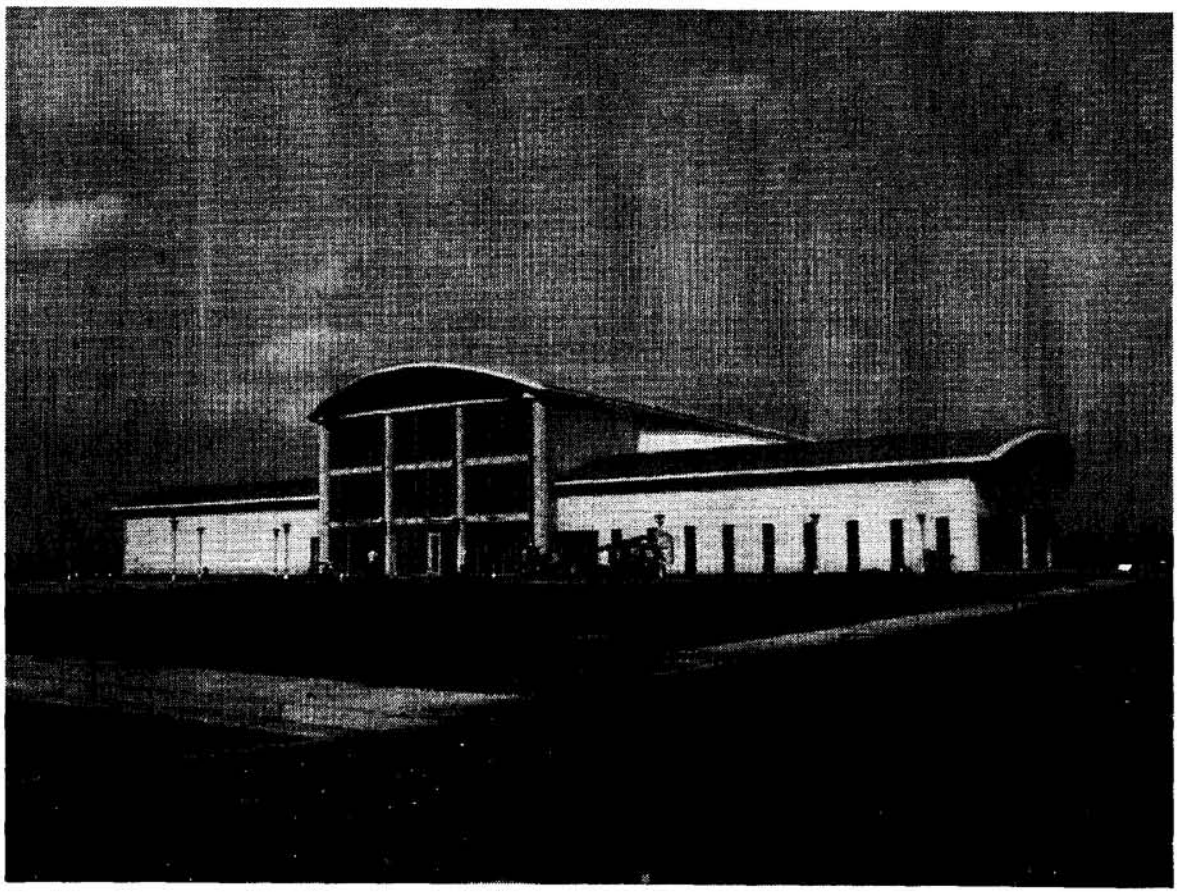

CALHOUN
COMMUNITY
COLLEGE

Multifunctional Classrooms

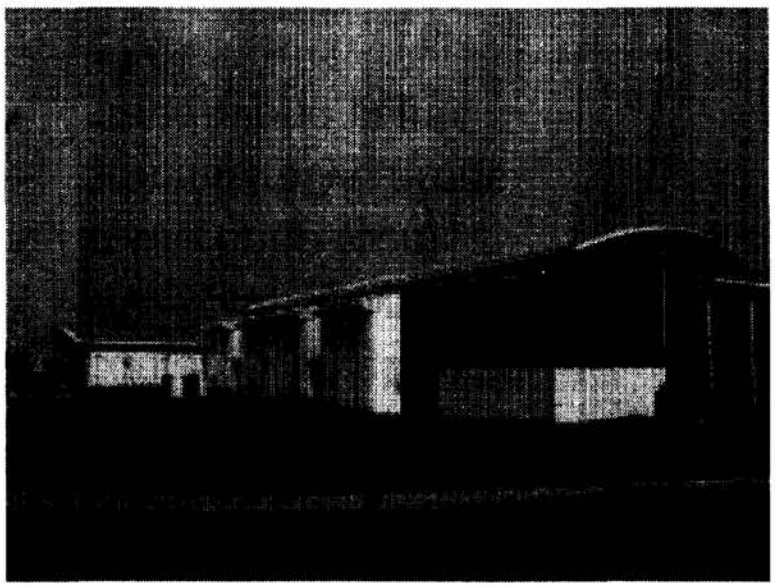

Seven classrooms including:

- Composite laboratory
- Computer laboratory
- Full multimedia presentation and communications

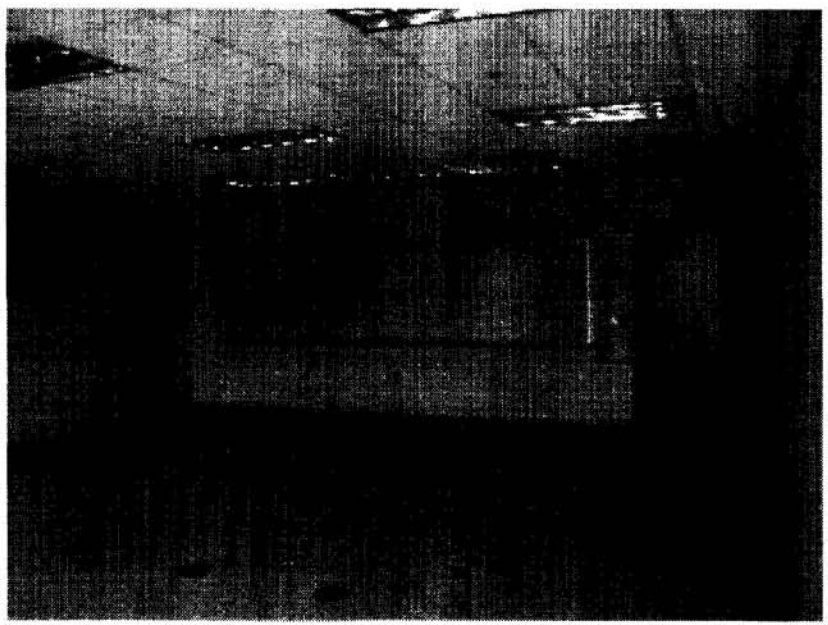

CALHOUN COMMUNITY COLLEGE

High-Bay Training Area

Machining and forming

- Five Axis Horizontal Mill
- Vertical Boring and Turning Mill
- Press Brake

Welding Room

Assembly and Test Area

Nondestructive Examination Room

Overhead Crane

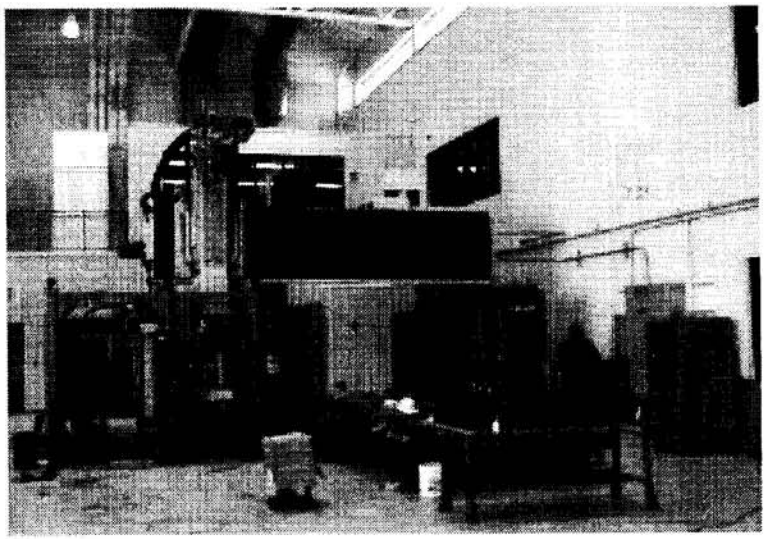

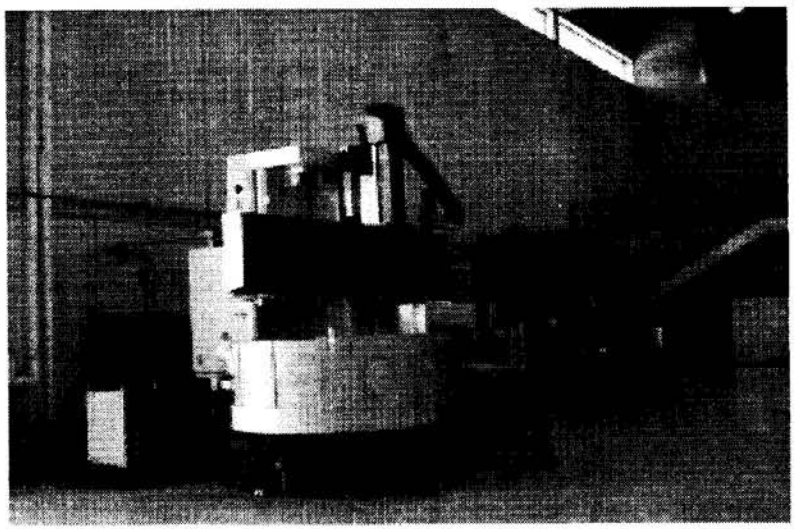

CALHOUN
COMMUNITY
COLLEGE

Associate of Applied Science Degree in Aerospace Technology

- General Education Core Requirements
- Aerospace Common Core
- Aerospace Specialties:
  - Machining and Fabrication
  - Welding and Construction
  - Structures and Assembly
  - Electronics

CALHOUN COMMUNITY COLLEGE

Progress in Program Implementation

- Degree program approved by Alabama state boards in August 2000
- Facility construction complete in August 2000
- Starting degree program in Fall 2000
- Participate in National Consortia initiatives on aerospace technician training
- All courses phased in over two years

CALHOUN COMMUNITY COLLEGE

The Year 2000 and Beyond

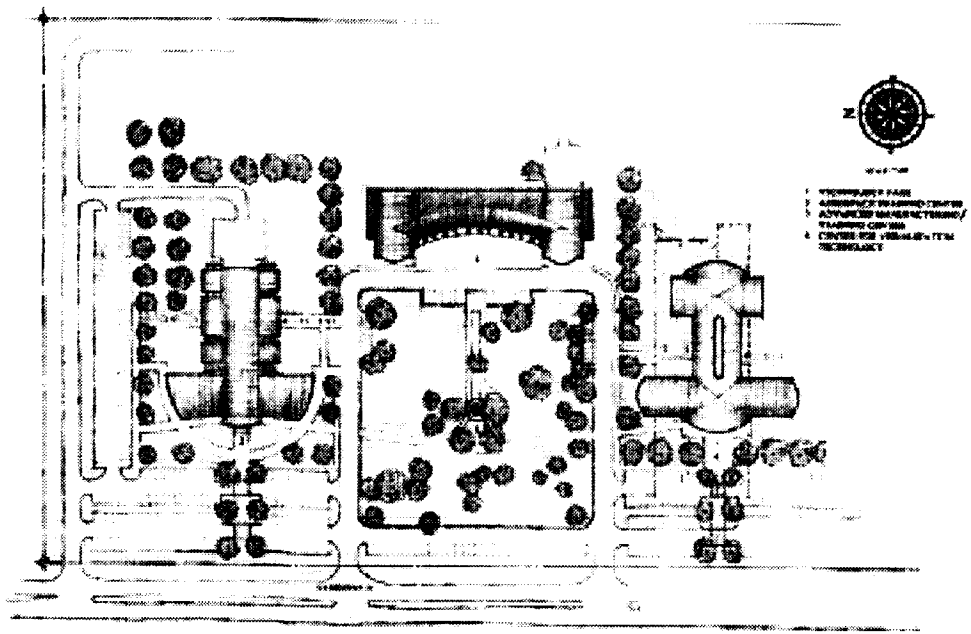

- Technology Park will expand the capacity for workforce training in aerospace, advanced manufacturing, and visualization/information technologies

CALHOUN COMMUNITY COLLEGE

Advanced Manufacturing Process Lab

- Renovation and New Construction project
- Construction to start Fall 2000
- Funded by bond and NSF funding
- Focus on Semiconductor, Modern Manufacturing and Robotic Technologies

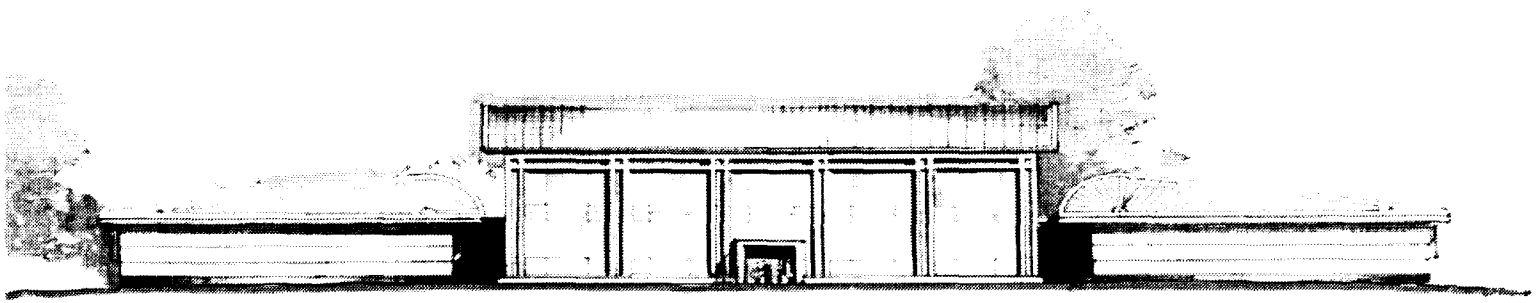

CALHOUN
COMMUNITY
COLLEGE

Visualization and Information Technology Center

- Bridge building for Technology Park
- Focus on computer-aided drafting, graphic design, image processing, virtual reality, and multimedia
- Calhoun Foundation will secure funds through *Partners in Progress* capital campaign
- Groundbreaking in Summer 2001

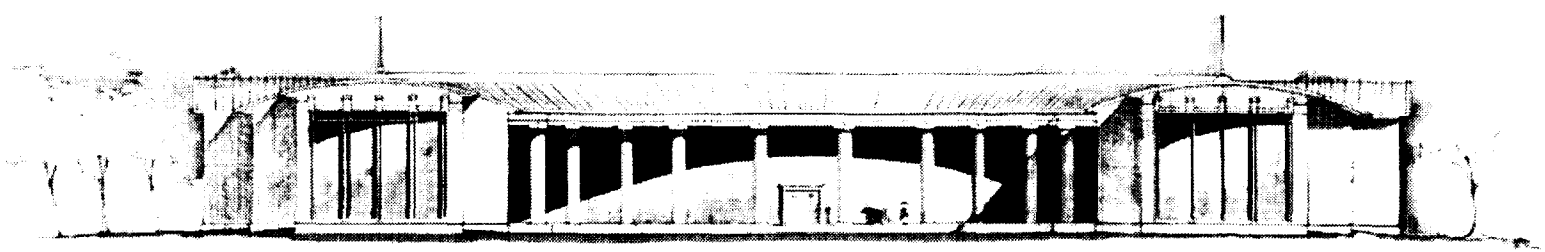

CALHOUN
COMMUNITY
COLLEGE

Why Partnerships between Industry and Education/Training?

- Clear Industry Needs
- Shortage in Critical High Tech Skills
- Critical to Continued Industry Growth
- A Key Factor in Regional Development
- Leading Edge in National Skill Standards
- Planning for the Future

AIDT

EELV / Delta

BOEING

CALHOUN COMMUNITY COLLEGE

CALHOUN
COMMUNITY
COLLEGE

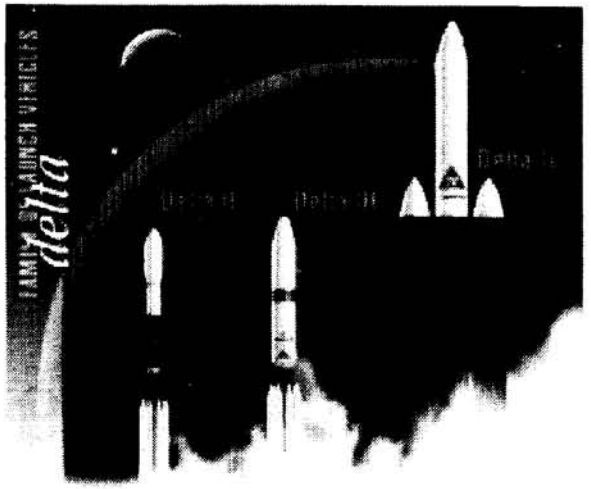

Thank You

Alabama Industrial Development Training

Composite Manufacturing for Space Launch Vehicles

DONNA Y. KNEZEVICH

Lockheed Martin Space Systems/D-4800
P.O. Box 29304
New Orleans, LA 70189 USA
Phone: 504-257-2445
E-mail: donna.y.knezevich@maf.nasa.gov

Composite materials offer a large potential for performance increase and weight reduction over metallic components for advanced launch vehicles. Building composite hardware for large high-efficiency launch vehicles is one of the most demanding engineering challenges from the aspects of materials science, structure, and manufacturing. Modern launch vehicles require robust, durable, and reliable components capable of operating in cryogenic, high-pressure, and high-temperature environments, while in contact with highly volatile oxidizers and fuels.

Lockheed Martin Space Systems Company, Michoud Operations, has developed critical technologies for this effort by building, testing, and flight qualifying composite hardware for launch vehicle applications for numerous projects, such as the Space Shuttle, X-33, X-34, and the A2100 Satellite. Composite hardware built and tested by Lockheed Martin Space Systems Company includes high-temperature vehicle fairings and nosecones, launch vehicle intertank skirts, high-pressure cryogenic helium tanks, cryogenic liquid hydrogen and liquid oxygen tanks, feedlines, and tank coverplates. Composite manufacturing for space launch vehicles will soon be enhanced by activation of the National Center for Advanced Manufacturing (NCAM). Located at Michoud, NCAM will partner government, industry, and academia and bring on line fiber placement and autoclave capabilities that are required for production of large composite structures.

Laser Cladding / Glazing as a Surface Coating Alternative

Authors

Mr. Rob Hull, Anteon Corporation, 5100 Springfield Pike, Dayton, OH 45431
Phone (937) 252-3132 x3009; Fax (937) 252-0418; e-mail: rhull@anteon.com

Dr. Dave Firsich, Inorganic Specialists, 720 Mound Ave, COS-327, Miamisburg, OH 45343
Phone (937) 865-4491; Fax (937) 865-3680; e-mail: firsich@coax.net

Dr. Chuck Woods, Global Manufacturing Solutions, 720 Mound Ave, B-3, Miamisburg, OH 45343; Phone (937) 865-5039; Fax (937) 865-4749; e-mail: cwoods@globalms.com

Mr. John Eric, AFRL/MLPJ, 3005 P Street Suite 1,Wright-Patterson AFB, OH, 45433
Phone (937) 255-2334x3165; Fax (937) 255-1128; e-mail: john.eric@ml.afrl.af.mil

Abstract

Increasing environmental regulations and rising waste disposal costs are driving the need for economic chrome plating replacement technologies. This paper summarizes one of several chrome replacement research & development programs funded by the Air Force Pollution Prevention office. This work focuses on two laser-based coating processes – laser cladding and laser glazing – for the application of a thick (5-25 mils) uniform coating with similar if not superior mechanical performance to that of hard (wet) chrome plating. All experiments were performed using a flattop continuous wave carbon dioxide laser, operating at 10.6 microns.

This paper describes the laser cladding and glazing techniques, the processing parameters developed and the mechanical performance of the resultant coatings. Emphasis will be placed on the laser glazing technique developed under this effort. The technique uses the laser's rapid surface heating effect to melt, re-flow and consolidate protective coatings deposited using any type of thermal spray technique – in this case, a flame-spray coating system. Post flame-spray treatment using laser glazing transformed an economical but porous coating into a uniform, pore-free coating with superior performance characteristics to that of chrome. Materials characterization and mechanical property test results are discussed.

Introduction

For many years, chromium plating has been an inexpensive standard Air Force (AF) processing technique for providing corrosion protection, friction reduction, wear resistance, and the ability to build-up worn surfaces. Chrome plating or electroplated chrome is an electrochemical process for depositing a bonded layer of chromium metal on aerospace parts of various base materials. The process, which involves large vats of chromium metal to deposit the coating and chemical stripping or traditional machining facilities for the removal of the chrome coating prior to rebuild and repair, produces a large stream of toxic waste. Changing emission regulations and Environmental Protection Agency (EPA) chemical reduction policies (EPA-17), along with rising disposal costs, made it necessary for the AF to develop alternative treatment methods to chrome plating. Estimates of the disposal costs associated with this process topped $16M/year in FY95. Preliminary studies indicate that laser deposition of metals or other laser-assisted surface treatments might offer acceptable replacement techniques.

Conventional chrome plating is used to apply a wide range of thicknesses, corresponding to different applications. Thin chrome coatings (1-10 mils) can be used for corrosion protection, while thick chrome coatings (10-40 mils) are often used to build up surfaces, which have worn down through extended use. The primary challenge in developing a substitute process for chrome plating was to provide most, if not all, of the desirable properties of chrome – hardness, adhesion, corrosion protection, lubricity, surface finish, and the ability to build-up

worn surfaces – with one alternative process. Providing one or two of these characteristics is relatively easy; to simultaneously provide all of these characteristics is a formidable task. The AF and other chrome platers are finding that one replacement technique for all chrome plating applications may not be practical but that a variety of application-specific solutions may be required.

The Air Force Research Laboratory Materials & Manufacturing Directorate (AFRL/ML), as part of their Pollution Prevention Special Emphasis Area, funded Anteon Corporation to investigate laser-based surface treatment techniques as possible replacement technologies for electroplated chrome. This project would expand upon laser processing activities Anteon was already performing as part of their operation and support contract for the Laser Hardened Materials Evaluation Laboratory (LHMEL), a state-of-the-art materials effects test facility housing a number of high energy lasers.

The results of laser processing work at LHMEL – both with laser cladding and with laser glazing of thermally sprayed coatings – have shown that laser processing is a viable and feasible process for producing well consolidated, corrosion and wear resistant coatings. The common feature of the two is that they each melt the coating layer, reducing its porosity and sealing the surface against air or water permeation, a critical requirement for preventing corrosion of the underlying metal. Results also showed that these laser-processed coatings could satisfy the majority of the performance requirements currently fulfilled by electro-deposited chrome plating, especially where large thickness build-up is necessary.

The laser used for these experiments was the LHMEL I device, a 15-kW continuous wave flattop carbon dioxide laser. This is a very well characterized and repeatable research & development laser used by the Air Force for a variety of materials interaction experiments. The high energy output provided by this device allowed these laser processing experiments to be performed using larger beam sizes than are typically demonstrated. Larger beam sizes will equate to faster processing speeds in actual applications. Laser glazing samples were rotated on a small lathe during laser processing while the part was translated laterally through the beam using a CNC table. Clad samples were prepared using the same CNC controlled table.

The authors wish to recognize their government sponsors, Mr. Jay Tiley and Ms. Mary Ann Phillips from AFRL/ML at Wright-Patterson AFB, OH.

Laser Glazing of Flame-Sprayed Coatings

Flame spraying is an inexpensive method of applying wear or corrosion resistant coatings. The process uses a modified acetylene-fueled torch to heat a powdered metal, which is then deposited on the substrate surface via a gas-assisted delivery system. The process, however, produces a relatively low velocity spray resulting in a slightly porous coating with limited adhesion to the substrate. The quality of a flame-sprayed coating may, however, be improved using a process called laser glazing. Laser glazing utilizes the laser's rapid surface heating effects to melt, re-flow and consolidate the flame-sprayed coatings thus reducing its porosity and improving the bonding. The remaining porosity seen in flame-sprayed/laser glazed coatings is comparable to that seen in conventional chrome electroplate. The remaining porosity also appears to be closed-cell, suggesting that the glazed coating is not permeable, and in fact, a glazed part has passed 196 hours of salt-spray testing.

Laser glazing experiments were conducted using approximately 7.5-kW of power on target, deposited in a 1.3-cm diameter beam. The samples used were cylindrical rods approximately 12" long and 1" in diameter. The rods were mounted on a small lathe bed and were rotated during the glazing process. The rotating rod was then translated through the laser beam on a CNC controlled table. Typical translation speeds of X feet per minute were used for these experiments.

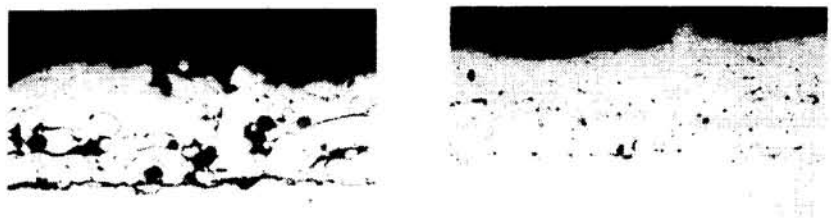

Figure 1: **Cross**-section of a flame-sprayed coating, before and after laser glazing. (200X)

Two types of coating materials were investigated under this study. The first coating was Versalloy 50; a nickel-based coating selected for corrosion resistance applications. The second coating was a mixture of Versalloy 50 with tungsten-carbide cobalt (WC-Co), selected for wear resistance applications. These two coating materials were flame sprayed on a variety of substrate materials including AISI 1030 steel, D2 tool steel and AISI 4340 alloy steel. While good results were obtained with both powders, the WC-Co/Versalloy mixture proved the most interesting.

SEM analyses of the WC-Co/Versalloy coating showed that an interdiffusion had take place between the WC particles and the surrounding Versalloy matrix or nickel (Ni) matrix, resulting in a microstructure consisting of WC particles surrounded by a transition layer, encased in the Ni rich matrix material. This interdiffusion creates a continuous transition layer from the hard WC particles to the ductile Ni rich matrix. The transition layer not only facilitates an excellent bond between the particles and substrate, but also provides a region of transition in physical properties, such as thermal expansion etc. The figures below show the results of analyses of these coatings applied to a D-2 tool steel substrate.

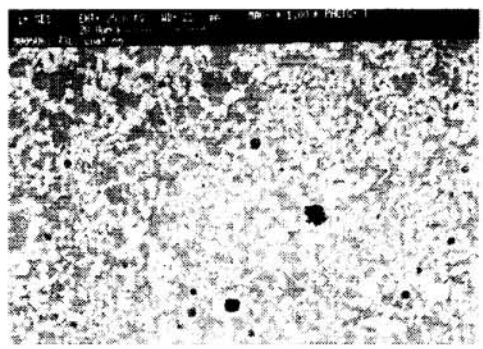

Figure 2: SEM Micrograph showing phases in WC/Co/Versalloy 50 coating. Note homogeneous coating.

Figure 3 depicts a higher magnification of the laser glazed WC-Co/Versalloy coating and shows that W-rich particles, which were once WC, have now been alloyed with the matrix material yet still retain the hard complex carbides.

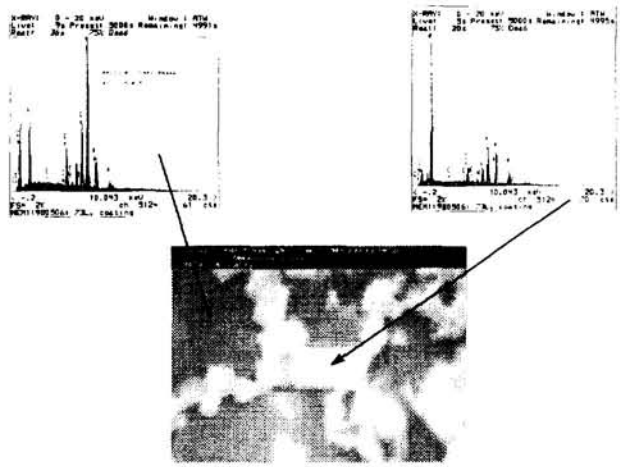

Figure 3: Higher magnification image of "altered" WC particles in Versalloy 50

Figure 4 further magnifies the WC particle that is undergoing dissolution and alloying. The carbon becomes more diffuse and there is an exchange of elements with the surrounding matrix materials. This results in a complex distribution of complex carbides that are nicely compatible with the surrounding matrix and results in a tough coating.

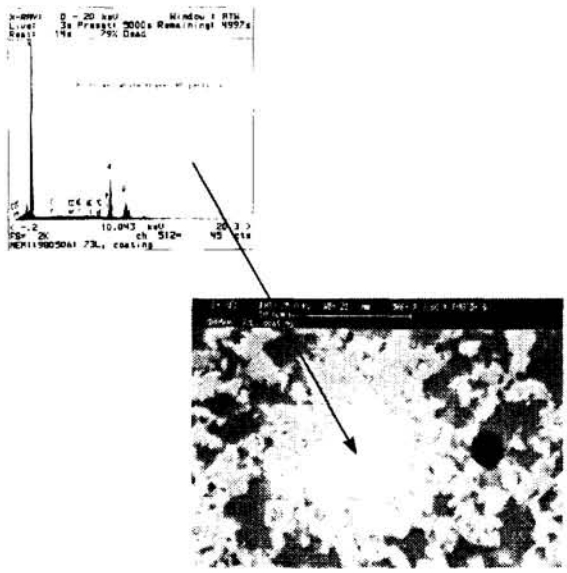

Figure 4: High magnification SEM micrograph of WC particle surrounded by Versalloy matrix. Note transition zone from particle to matrix.

After laser glazing, the WC/Co/Versalloy coating was welded to the substrate. No discrete interface layer appeared to exist between the coating and the substrate material. The welding occurs over about a 4 mil thick layer in the substrate. This is shown in the two figures below.

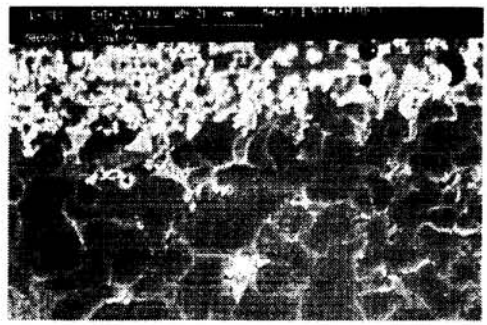

Figure 5: SEM Micrograph of interface region between the WC-Co/Versalloy coating and the D2 substrate.

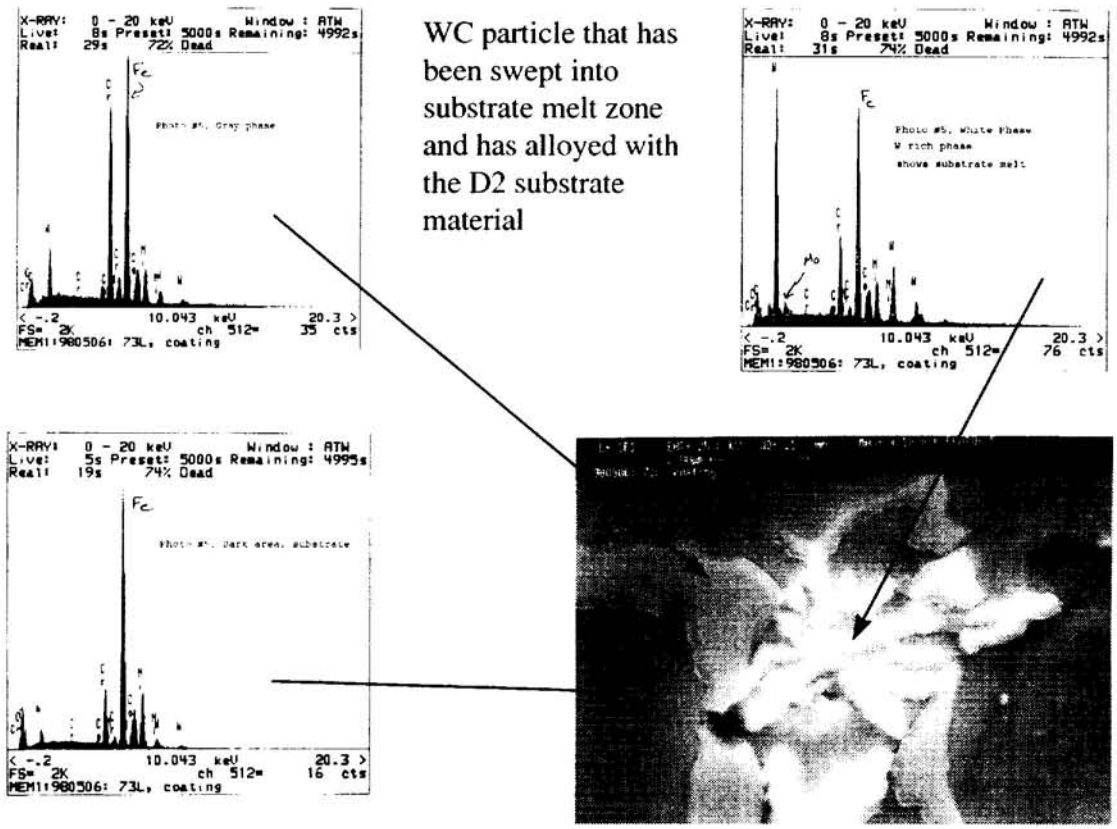

Figure 6: WC particle found 3-mils into the D2 steel substrate.

Excellent laser glazing results were obtained with both the Versalloy50 and WC-Co/Versalloy mixture. It was much more difficult to laser glaze the Versalloy 50 alone, however. This is most likely due to the difference in specular reflectivity of the powders. The WC-Co/Versalloy is less reflective than the Versalloy alone. The powder mixture allows for a wider range of laser power to achieve melting, whereas the Versalloy alone had to be taken right up to the limit of melting, where it becomes more absorbent and sometimes over-absorbed and burned through.

It should be noted that thermal spray parameters do indeed play a major role on the ability to successfully glaze a part, and effect the integrity of the glazed coating produced. It is not just adequate to have the powder

adhere to the surface. The density of the powder sprayed and the integrity of the bond between the substrate and the sprayed powder profoundly effects the glazing process. Results of this study seem to indicate that the bond integrity of the flame-sprayed coating effects the thermal conductivity of the powder/substrate combination, which in turn influenced the laser processing parameters needed to produce a sound glazed coating.

Analysis of the substrate after the laser glazing process was applied revealed that, in some cases, fresh martensite was formed in the heat-affected zone below the coating layer. This was particularly true for the WC-Co/Versalloy coatings on heat treatable substrates such as D-2 and 4340. A low temperature tempering will probably be needed after the laser glazing process to convert the fresh martensite and stabilize the mechanical properties of the substrate.

Another brief set of experiments were performed to demonstrate that damaged or worn laser glazed coatings could be repaired and returned to service without the need for costly coating removal and disposal. To demonstrate this fact, selected rods damaged in testing were flame-sprayed again and then re-glazed. The coatings produced were as uniform as the original coating with little or no noticeable transition between the original and repaired areas. This repairability factor could make laser glazing a much more appealing replacement for chrome than other candidate processes that cannot support this ability.

Laser Cladding

The second laser processing technique investigated was laser cladding. This process uses laser energy to simultaneously heat the substrate surface and melt a coating material – in powder or wire form – to produce a uniform surface coating at a variety of thicknesses.

For the LHMEL cladding experiments, a powder feed system was used to deliver the powder and laser energy simultaneously onto a flat sample. The powder was injected along the sample's axis of translation at a 15-degree angle to the surface. The samples were translated over a four pass track with overlaps of 25% to 45% between passes. The nozzle orientation provided the best powder deposition pattern but variations were seen depending on whether the nozzle was in a leading or trailing relative to the laser beam. Leading deposition seemed to produce the more uniform coating.

The large spot sizes achievable with the LHMEL I device were again utilized for these laser cladding experiments. Laser power on target was held constant at 5-kW with a beam size of 0.5" diameter. Samples were flat pieces of steel, 2" wide x 6" long x ½" thick. Typical translation speeds of 0.25" per second were used for these experiments. The samples were placed on a CNC table and were translated in both the x- and y-directions during the cladding process.

All laser cladding experiments were conducted on AISI 1018 carbon steel substrates. Powders selected for laser cladding experiments were the same as were used for the laser glazing study – the Versalloy 50 nickel-based powder and the WC-Co/Versalloy mixture. The nickel-based powder was much easier to clad and produced smooth, uniform beads of coating on each pass with good overlapping. The tungsten carbide mixture produced a rougher, less uniform coating that was clearly going to require extensive machining to produce an acceptable coating. Since funds were limited on this study and the challenge of machining the WC-Co/Versalloy mixture

seemed excessive, further cladding work concentrated on the Versalloy 50 coating alone.

Results of the tests were very promising. The laser cladding process produced a smooth uniform coating with thicknesses in the range of 10-25 mils. A representative clad sample was sectioned and examined; it appeared to have a dense and well-bonded coating as shown in Figure 7. Another item of note regarding the coatings shown in this figure is that the coating was produced by two separate 4-pass treatments. The two groups of passes were overlapping and offset by approximately 1/8". As can be seen in the micrographs and despite being formed in two separate passes, the coating appears as a single uniform layer. This fact validates the assumption that worn or damaged laser clad surfaces can be easily repaired with no impact on the coating performance.

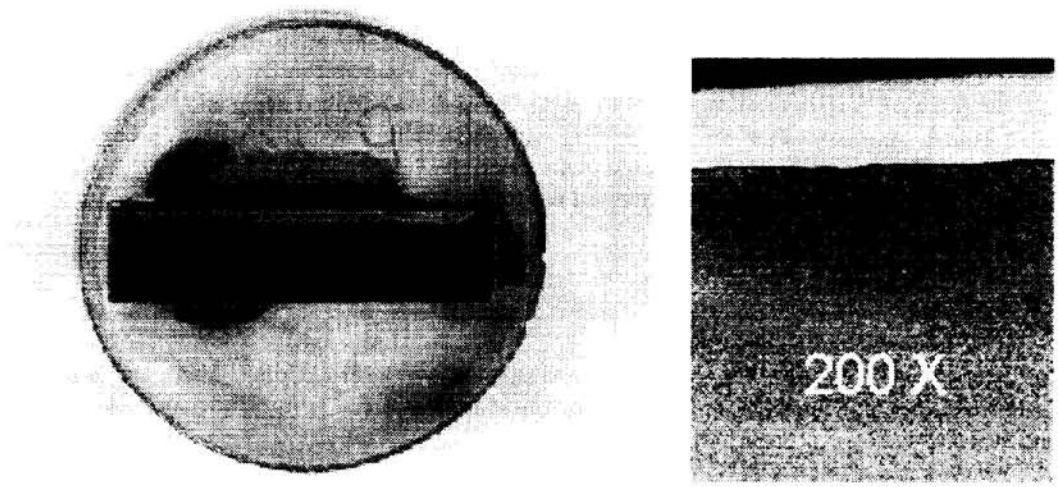

Figure 7: Micrographs of laser clad Versalloy 50 on 1018 steel

Corrosion tests also confirmed that this coating provided a pore-free protective layer that easily survived 196 hours of salt spray exposure. While additional work is required to demonstrate this process on cylindrical or other more complex shapes, the results offer great promise for a very versatile yet durable coating process.

Mechanical Testing

Mechanical property tests revealed that both the laser glazed and laser clad coatings produced durable, non-porous coatings. The laser glazed and laser clad Versalloy 50 coatings, originally selected as corrosion resistance coatings, performed well in the salt spray booth, easily surviving the standard 196 hour durability test. Unexpectedly, the laser glazed WC-Co / Versalloy 50 mix coating also survived remarkably in the salt spray tests. After surviving the initial 196-hour test, samples were left in the salt spray for an extended period until any sign of visible corrosion or pitting occurred on the sample surface. The samples survived a remarkable 2700 hours in salt spray before showing one or two small pits.

The laser clad and glazed samples were also subjected to wear tests to assess their durability and wear resistance. Flat circular samples were placed in a pin-on-disk wear fixture and tested at 300 RPM with a 200-gram load for 25,000 cycles. A similar chrome plated sample was also placed in the test to serve as a comparison to current performance. As was expected, the Versalloy 50 corrosion resistant coating wore slightly faster than the chrome plated sample. The WC-Co/Versalloy wear resistant sample's performance was roughly equivalent to that of the chrome coating.

Summary

It has been demonstrated that flame sprayed coatings can be successfully applied to a substrate then laser glazed to produce excellent high density, corrosion resistant, wear resistant coatings. Successful laser glazing was performed on rods coated with Versalloy-50 and on rods coated with a mixture of Versalloy/Tungsten Carbide Cobalt. The reproducibility of the process was far greater for the mixture, which melted at a much higher temperature and introduced more heat into the substrate. It has also been shown that the laser glazing process has very little effect on the underlying substrate microstructure and that the integrity of the flame sprayed coating plays an important role in determining the integrity of the resultant laser glazed coating. Microstructures produced by laser glazing of the WC-Co/Versalloy coating resulted in partial dissolution of the carbides into the nickel rich matrix. This creates a very strong and hermetically sealed coating that should withstand corrosion and thermal cycling environments very well.

Laser cladding has also been demonstrated as a viable chrome-plating alternative. This method can produce pore-free, well-bonded coatings of varying thicknesses on a variety of substrates. Under this study, cladding experiments gave better results with Versalloy-50 powder alone than with the WC-Co/Versalloy powder mixture. Corrosion and wear tests on the clad samples showed comparable performance to that of chrome.

This effort also demonstrated the successful repair of worn or damaged parts using either laser glazing or laser cladding. The ability to apply a second layer of coating without creating any apparent interface between it and the original suggests that cladding and/or glazing can be used to build-up or repair worn parts without the added costs of prior coating removal and the subsequent disposal of the waste stream.

Testing of Environmentally Preferable Aluminum Pretreatments and Coating Systems for Use on Space Shuttle Solid Rocket Boosters (SRB)

By
Catherine Clayton
United Space Alliance
8550 Astronaut Blvd., M/C USK-821
Cape Canaveral, Fl 32920-4304
(321) 853-0523
claytonc@usasrb.ksc.nasa.gov

Randy Raley
United Space Alliance
8550 Astronaut Blvd., M/C USK-821
Cape Canaveral, Fl 32920-4304
(321) 853-0521
raleyr@usasrb.ksc.nasa.gov

Lee Zook
United Space Alliance
8550 Astronaut Blvd., M/C USK-C52
Cape Canaveral, Fl 32920-4304
(321) 861-5611
zooklm@usano.ksc.nasa.gov

Abstract

The SRB has historically used a chromate conversion coating prior to protective finish application. After conversion coating, an organic paint system consisting of a chromated epoxy primer and polyurethane topcoat is applied. An overall systems approach was selected to reduce waste generation from the coatings application and removal processes. While the most obvious waste reduction opportunity involved elimination of the chromate conversion coating, several other coating system configurations were explored in an attempt to reduce the total waste. This paper will briefly discuss the use of a systems view to reduce waste generation from the coating process and present the results of the qualification testing of nonchromated aluminum pretreatments and alternate coating systems configurations.

Introduction

United Space Alliance – Solid Rocket Boosters (USA-SRB) refurbishes the non-motor components of the SRB. The structural components are primarily constructed of aluminum alloy (AA) 2219 or Alclad 7075. The aluminum is chromate conversion coated with MIL-C-81706 (Alodine 1200S/1201), primed with Deft primer 44-GN-7 and then topcoated with Deft topcoat 03-W-127A.

MIL-C-81706 specifies chromate-based solutions used in the formation of a conversion coating to provide a protective layer on an aluminum surface. This conversion coating is used by industry for its corrosion protection properties and to promote adhesion of paints to the aluminum. However, the high copper content in AA 2219 negates the corrosion protection properties of the chromate conversion coating. Since much of the aluminum components of the SRBs are 2219, the pretreatment is only used to promote and stabilize paint adhesion. The waste stream for this process is one of the largest at Kennedy Space Center (KSC). Anywhere from 20 to 50% of chromate conversion coatings are chromic acid. Hexavalent chromium, which is present in these solutions, has been determined to have serious acute and chronic exposure hazards. The Occupational Safety and Health Administration (OSHA) continues to move toward stricter regulations for the use of chromium in the work place. The Environmental Protection Agency is also continuing to tighten regulations related to airborne and liquid releases of these materials.

The Deft paint system is used to coat the aluminum and Corrosion Resistant Steel (CRES) alloys. Deft was chosen as the paint system on these metal surfaces for its lower volatile organic compound (VOC) content and compatibility with the thermal protection system (TPS) materials. The Deft paint system has several processing limitations which include a short pot life for both primer and topcoat, primer curing issues and topcoat catalyst moisture sensitivity. These processing problems result in process efficiency limitations that currently have no options to avoid or mitigate them. The primer also uses a hexavalent chromium corrosion inhibitor, which is under the same regulatory pressure as the pretreatment. Finally, these coatings which cover and protect 95% of the SRB hardware are sole sourced with no alternates. A fire or other disaster at the manufacturer's plant could place space shuttle schedules in jeopardy. For these reasons the Alternate SRB Aluminum Coating Project was undertaken to identify and qualify alternatives for the current coating and pretreatment system.

Experimental Design

The Alternate SRB Aluminum Coating Project consisted of three phases: down selection, qualification, and implementation. After review of vendor information, such as data sheets, and MSDSs six pretreatments and six coating systems were tested in the down selection portion of the project. Three pretreatments and three coating systems were chosen from the down selection testing for qualification. Consult "Alternative SRB Aluminum Coating System Down Select Test Report" (8) for a discussion of how the candidates were chosen. The candidate materials chosen for qualification testing are listed in Table 1*. In addition to testing new materials for a straight drop in replacements, this qualification program has also considered a new flight configuration, which consists of primer as the only coating. The goal was to certify the pretreatment/primer configuration without topcoat in areas that are stripped every flight. All coating candidates (primer and topcoats) were evaluated on each candidate pretreatment and the baseline pretreatment (Alodine 1201). Additionally, the baseline coatings (Deft 44GN7 primer and 03W0127 topcoat) were evaluated on all pretreatments. Testing included the currently used SRB coating configuration as a baseline to assist in the performance assessment of the candidate materials. The full factorial experiment design panel matrix used for each test required 104 separate conditions to be produced which, with duplication, would mean 208 test surfaces. The alloys tested included aluminum alloys 2219, 6061, and 7075; also 304 stainless steel. Where appropriate, the number of material variables was reduced to simplify testing and data analysis.

Table 1. Candidates Selected for Qualification Testing

Pretreatments	Primers	Topcoats
Alodine 1201	Deft 44GN7	Deft 03W127A
Alodine 5700	PRC-DeSoto EEAE152A/B	PRC-DeSoto EUAW098A/ EUAC082B
Chemidize 727A	Hentzen Corp. 05510WEP-X/ 05511CEH-X	Hentzen Corp. 4636WUX-3/ 4600CHA-SG
Okemcoat 4500	Lord Corp. 9929A/B	Lord Corp. A276

When a coating was found to be unsatisfactory for qualification at any point, testing of that pretreatment and/or coating system was halted. One pretreatment and one coating were dropped during the qualification testing, Okemcoat 4500 pretreatment and the PRC-DeSoto coating system.

Testing was conducted in accordance with "Alternative SRB Aluminum Coating System Qualification Test Plan," CPC-054-98MP (8) which gathered corrosion protection, bond strength, compatibility with other SRB materials, batch-to-batch consistency, and thermal environments data. A complete copy of the test data along with pertinent digital photographs has been placed on computer disk and is available upon request.

Methods

Testing conducted to qualify the candidate pretreatments and coating systems consisted of analysis in these areas: Corrosion, bond strength, compatibility with other SRB materials, batch-to-batch consistency, and thermal environments.

The corrosion protection offered by a coating system relies upon the adhesion of the coating to the metal surface, corrosion inhibition properties of the pigments within the coating and the resistance of the coating to moisture absorption/permeation. It is very difficult to formulate a single product to encompass all of these considerations. To maximize the corrosion protection, several classes of products are used. These include adhesion promoters (pretreatments), primers (incorporating corrosion inhibiting pigments) and topcoats (to minimize moisture permeation). The level of corrosion protection required for a particular component/system should be based upon the use environment and service (refurbishment cycle) requirements.

Corrosion testing of the candidate pretreatments and coating systems was conducted to determine the effectiveness of the corrosion preventative properties of the candidate materials. The evaluations included beach exposure, seawater immersion, and Electrochemical Impedance Spectroscopy (EIS). These test regimes were selected to provide an aggressive real life performance evaluation of the candidates combined with a practical laboratory evaluation technique. While the SRB uses several aluminum alloys, AA 2219 was selected for all corrosion testing due to its inherent poor corrosion resistance.

Seawater immersion testing was conducted to reflect the actual use environment of the SRB hardware. After launch, the SRB lands in the ocean and is towed back to port. The SRB normally spends 24 to 48 hours in seawater but has been immersed more than twice that long when problems were encountered in recovery. The coupons used in the seawater immersion test were then used for the beach exposure test. The coupons were placed at the Kennedy Space Center (KSC) Atmospheric Corrosion Test site within 48 hours of removal from the seawater. These coupons went through both tests scribed. The exposure times were six and twelve months.

The final corrosion test conducted was Electrical Impedance Spectroscopy (EIS). With EIS, a small amplitude AC voltage is applied to the test coupon and the coating response is measured. This process is repeated over a range of frequencies to generate a broad response spectrum. EIS technique is considered to be nondestructive to the coating, this allows the change in coating performance to be measured over time. Each electrolytic cell over the test coupon contained 200 ml of filtered seawater. Measurements were taken at 4, 168, and 672 hours.

The most critical physical property for SRB coatings is the ability to act as an adhesive base for the thermal protection system materials. Bond strength testing was conducted to ensure that the coating systems adhere to the pertinent SRB substrates and to themselves. Next the testing was expanded to look at the effects of different environments, thermal cycling, water immersion, and damage resistance or flexibility. Adhesion testing was conducted per ASTM D 4541-95 "Pull-Off Strength of Coatings Using Portable Adhesion Testers" (6). Adhesion of the coatings in high temperature environments was tested per ASTM D 1623-78 "Tensile and Tensile Adhesion Properties of Rigid Cellular Plastics" (7). A failure during a water immersion test could be an indication of a deficiency in the coating itself or inadequate surface preparation provided by the candidate pretreatment. Coatings used on the SRB need to be able to adhere under these conditions. Water resistance is not a corrosion test and there is no correlation with immersion into the Atlantic Ocean. Testing was conducted per ASTM D 870-97 "Testing Water Resistance of Coatings Using Water Immersion" (3). Flexibility testing was conducted to determine the resistances of the candidate coatings to cracking on metal substrates as those substrates are deformed. This is a measure of damage resistance. The testing was conducted per ASTM D 522-93a "Mandrel Bend Test of Attached Organic Coatings" (5).

Any coating system used on SRB surfaces must be compatible with the chemicals and materials that will come in contact with the coating system. This includes thermal protection system, sealants, cleaners and possible incidental contact with various chemical compounds. Materials applied to the coating system must be able to adhere to the coating system at flight temperatures as well as at room temperature. The testing for material adherence and chemical compatibility was conducted per ASTM D 1623 "Tensile and Tensile Adhesion Properties of Rigid Cellular Plastics" (7), ASTM D 4541-95 "Pull-Off Strength of Coatings Using Portable Adhesion Testers" (6), and ASTM F 502-93 "effect of Cleaning and Chemical Maintenance Materials on Painted Aircraft Surfaces" (4).

The candidate coatings and pretreatments must be able to withstand the thermal environments of space flight. The candidate coatings were subjected, bare and with the thermal protection system in place, to convective testing performed in the National Aeronautic Space Administration / Marshall Space Flight Center (NASA/MSFC) Improved Hot Gas Facility (IHGF). The IHGF is a nominal MACH 4.1 aerothermal tunnel that burns a lean mixture of hydrogen (GH_2) and air to produce temperatures up to 2200°F at total pressures up to 200 psia (pounds per square inch atmospheric). The coatings and pretreatments used on SRB flight hardware must not be able to support combustion. Testing for flammability of the pretreatments and coatings was conducted per. 4.1 of NHB 8060.1B "Flammability, Odor, and Off-gassing Requirements and Test Procedures for Materials in Environments that Support Combustion" (2).

To ensure that the vendors of the candidate coatings and pretreatments could supply a consistent product from lot to lot, repeatability testing was conducted. This testing consisted of EIS testing, adhesion testing, and compatibility testing to Spirit 126 (cleaner used on coated surfaces).

Results

The amount of data produced from the tests discussed above was substantial. Aluminum alloy 2219 was selected for all corrosion testing. The exposure tests conducted were more severe than tests used in past coating qualifications. The sea water immersion results showed that the Chemidize 727/Hentzen primer coating configuration was significantly worse at the end of the exposure period than the baseline coating/pretreatment system. All other coatings were considered nominal. The coupons used for the sea water immersion were then used for the beach exposure testing. After exposure, no coupons were found to have either filiform corrosion or any biological growth. The Alodine 5700 pretreatment with Lord primer and the Alodine 5700 with the Lord primer and topcoat had the least amount of corrosion other than the baseline configuration. The PRC-DeSoto primer was the poorest performing primer regardless of the pretreatment configuration. At the time of the corrosion testing the PRC-DeSoto announced that they would no longer produce the topcoat that was in the test program. Testing continued with the primer for further evaluation of the product. The results of the corrosion data showed that the PRC-DeSoto primer was not an acceptable coating for SRB use

The EIS testing showed no significant difference between the pretreatments of the primed and topcoated coupons. However, the performance of the primer-only coupons did show some differences for the Deft and Hentzen coatings. Both of these primers over Chemidize 727 pretreatment showed a decrease in performance, see Figure 1*.

The bond strength testing includes data of the pretreatments and coatings on 2219 T87 aluminum, 7075 Alclad aluminum, and 304 stainless steel. The coatings were tested on the 304 stainless steel without pretreatment. The coatings adhered to the stainless steel better than to the aluminum alloys. There was no significant difference in the coating material adhesion attributable to the pretreatment material. After the alloy and pretreatment factor is removed from the results, the Deft topcoat performance appeared to be better than the candidates by about 12 %. Still the adhesion values of the candidates are close to double the minimum requirement of 700 ponds per square inch (psi). The averages range from 1266 psi for Lord primer over Chemidize 727 on 7075 Alclad to 2469 psi for Deft topcoat on 304 stainless steel.

For repair purposes, testing was conducted to determine the strength of the candidates over each other. This included all variations of primers and topcoats. The values of the adhesion results were within expected population of the nominal values obtained from the previous adhesion tests with a majority of the values above 1400 psi. The range was 1259 psi to 2647 psi. Some high performance coatings develop very inert surface layers due to side reactions or level of cure and cross-linking. For this reason adhesion testing was conducted on double-coated coupons. The first coat was fully cured prior to application of the second coat. The results of the tests were nominal as compared with the previous adhesion test results with the average of the values being 1500 psi.

Figure 1. Magnitude for Chemidize 727 With Primer Candidates

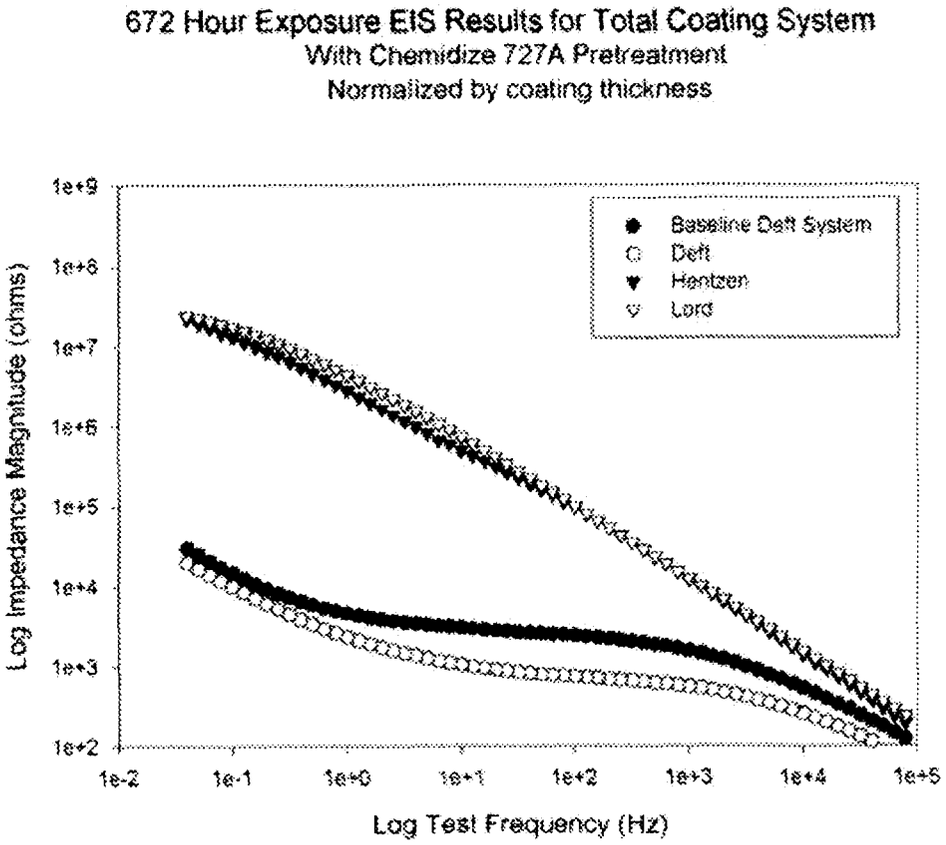

To ensure the coatings could withstand multiple flights before having to be removed, Cyclic high temperature testing was conducted. The coupons were cycled to 350°F from room temperature ten times with adhesion testing being conducted after five and ten cycles. The Hentzen and Lord primers did not show any significant change in strength throughout the cycling. This shows a stability that was expected for these materials. The baseline Deft primer showed a decrease in strength throughout the cycling. One possible explanation is that the Deft primer remains more reactive after it has dried. This would cause it to oxidize readily when exposed to a more reactive (hotter) environment. The pretreatments had no influence on the results of this test.

Flatwise-tensile testing was conducted to determine how well the pretreatments and coating systems adhere at 350°F, the worst case SRB temperature environment. One pattern emerged from the testing. The Lord coatings had a marked tendency to fail at the or near the pretreatment at the elevated temperature. This was even more pronounced when Lord coatings were over Chemidize 727 pretreatment. The lowest value of the Lord coating with the primer/pretreatment failure was 181 psi. The average of all the tests was 259 psi. This shows a drop in strength, however there is no minimum strength requirement for a paint to adhere at 350°F. Our criteria is that the coatings exceed TPS strength in the same environment. Therefore, all the paints are considered acceptable for program use.

Water immersion testing was conducted on scribed panels of the candidate coating systems per ASTM D870-97 "Testing Water Resistance of Coatings Using Water Immersion" (3). A failure during this test could be an indication of a deficiency in the coating itself or inadequate surface preparation. The principal criteria were to have no lifting of the coating and no active corrosion under the coating. Every panel, regardless of alloy, which was pretreated with Okemcoat 4500 and then coated with PRC-DeSoto failed due to blistering and flaking of the coating, both at the scribe and in the general acreage. With other pretreatments the PRC-DeSoto coatings would develop small blisters on about 46% of the panels which "healed" when the panels dried. Panels pretreated with Okemcoat 4500 developed blisters on 65% of the panel area. If the Chemidize 727 pretreatment was not completely rinsed

from the panels, the edges could flake. Some level of blistering was observed on all panels coated with Hentzen over Chemidize 727. The Alodine 1201 and Alodine 5700 had minor blistering observed at the edges. This underscored the importance of thorough rinsing and draining during the application process

The flexibility test was used to determine the resistances of the candidate coatings to cracking on metal substrates as those substrates are deformed. The results of this test showed one pretreatment, Okemcoat 4500, had significantly poorer properties. The Okemcoat 4500 did not cause the paint to crack, the pretreatment failed in shear loading along the bend leading to delamination of the coating with cracking and peeling. There are no SRB program acceptance or rejection criteria for elongation, but the failure in shear is felt to be not acceptable due to environments that the coating would see. For this reason and the results of the water immersion, Okemcoat 4500 was dropped from the qualification program. The other pretreatments did not influence the results. The coatings were all comparable with the exception of the Hentzen topcoat. It was significantly more rigid than the other coatings but still acceptable. Figure 2* shows examples of coupons that passed versus a failure of the Mandrel Bend Test.

Figure 2. Mandrel Bend Coating Failure

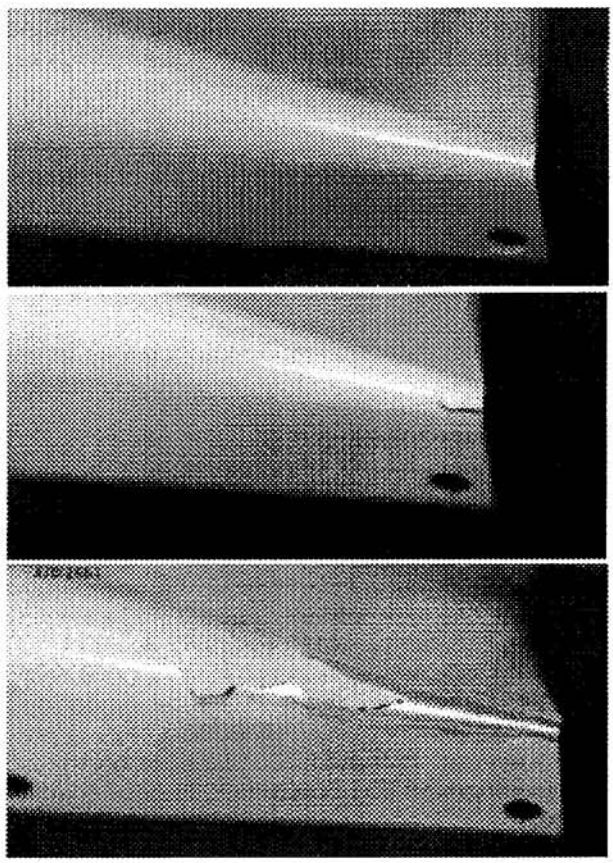

Acceptable >32% elongation

Acceptable ~20% elongation

Failure – Coating Delamination

Material compatibility testing was conducted to ensure that the materials applied over to the SRB coated surface would adhere to the candidate coating systems. The following materials were tested with the candidates:

MCC-1	PR-1422	CORK	P/S 870	BTA	RT455
Hypalon	PR-1770	Insta-Foam	RTV 133	K5NA	EA-934
VCI 368	LPS Hardcoat	DeSoto repair Primer		DeSoto Repair topcoat	

Some of the materials have minimum strength requirements. All the tensile strength requirements were met. The values were nominal as compared to the baseline and past tensile studies. The Hentzen topcoat did show a marked decrease in bond strength at room temperature with RTV 133. The drop in bond strength was about 53%. There is no minimum strength requirement for RTV 133. All failures were between the RTV 133 and the Hentzen topcoat. A change in surface preparation prior to bonding silicone sealants may be needed. The drop in bond strength for RTV 133 over Hentzen did not follow through to the high temperature testing. The values for RTV 133 over Hentzen at 350°F were nominal as compared to the other candidates and the baseline. The DeSoto repair topcoat showed a great affinity to the Hentzen and Lord primers. The average strength of the DeSoto repair compatibility testing was 1469 psi, whereas the average of the DeSoto topcoat over Hentzen and Lord primers was 2655 psi.

In addition to room temperature testing, the thermal protection system (TPS) and sealants were also tested at elevated temperature to ensure that they could adhere to the candidate coatings during flight. There is no minimum tensile strength requirement for elevated temperature adhesion, only that the material demonstrate adherence. MCC-1, K5NA, Cork, RT455, BTA, and RTV 133 were tested at 350°F. PR-1422 was tested at 275°F, PR-1770 was tested at 280°F, and P/S 870 was tested at 235°F. The polysulfide sealants were tested at a lower temperature due to their respective softening temperatures. As was seen in earlier flatwise tensile testing at elevated temperatures the Lord coatings over Chemidize 727 failed between the primer and the pretreatment. The PR-1422 with Lord primer also had failures between the primer and Okemcoat 4500, Alodine 1201, and Alodine 5700. There was significant variation within the material of the PR-1770 sealant, influencing the results of that particular test data. The rest of the test results were nominal as compared to the baseline configuration.

Chemical exposure tests were conducted to determine if contact to cleaning fluids and incidental contact to pertinent chemicals would affect the candidate coatings. A drop of 2 pencil grade is considered a failure in this test. The candidate coatings were exposed to following compounds at 95°F:

Spirit 126	Prime	PF Degreaser
14% Citric Acid	13% Sodium Hydroxide	

The exposure temperature for the following compounds was room temperature due to their flammability:

Isopropyl Alcohol (IPA)	Acetone	DS-104
Hydraulic Fluid	Toluene	Methyl Ethyl Ketone (MEK)

Spirit 126, Prime, PF Degreaser, hydraulic fluid, 13% sodium hydroxide, and 14% citric acid did not affect any of the candidate coatings. Okemcoat 4500 had been withdrawn from the test program prior to compatibility testing. IPA did affect PRC DeSoto topcoat. The other solvents, MEK, DS-104, toluene, and acetone are aggressive solvents that would affect or strip a coating. These solvents are used to remove tenacious contaminates. A drop in 2 pencil grade is not considered a failure for these solvents. Acetone did have a definite affect on PRC DeSoto and Deft topcoats. DS-104 affected Deft, PRC DeSoto, and Hentzen topcoats. DS-104 also had some effect on Hentzen primer. A second test was conducted with these solvents to more clearly determine their effect on the candidate coatings in a handwipe situation. These solvents are only used on SRB coatings in handwipe processes. A hand wipe rub test was conducted per MIL-C-85285B "Coating: Polyurethane, High Solids" (1). All candidate cleaners passed the rub test for all solvents. Okemcoat 4500 and PRC-DeSoto had been withdrawn from the test program prior to the rub test. The candidate coatings were also exposed to hydrazine. All of the candidate coating systems passed the hydrazine compatibility test.

To ensure that the candidate coatings systems are able to withstand the thermal environments of space flight, thermal testing at MSFC IHGF was conducted. All the candidates passed thermal testing with TPS applied to the surface and without TPS applied to the surface. Panels without TPS were tested at 5 BTU/ft^2 and TPS panels were tested at 7 BTU/ft^2. Okemcoat 4500 and PRC-DeSoto were dropped during the thermal testing and were not included in the results.

The coatings and pretreatments were tested to ensure that they would not be able to support combustion. All pretreatments and coatings passed the flammability tests. The burn lengths were less than 6 inches with a burn time of less than 10 minutes. There was no sparking, sputtering, or dripping. The panels that had Okemcoat 4500 pretreatment had the longest burn length with an average of 0.8 inches. The average of all the other panels was 0.25 inches.

To ensure that the vendors of the candidate coatings and pretreatments could supply a consistent product from lot to lot, repeatability testing was conducted. This testing consisted of EIS testing, adhesion testing, and compatibility testing to Spirit 126 (cleaner used on coated surfaces). The EIS testing showed very little performance difference for the candidate configurations. One notable exception is the performance of Deft primer. The spectrum for lot 2 of Deft primer was more typical of a spectrum for a coating performing as a barrier. Lots 1 and 3 were more indicative of a damaged coating. Visual examination of the Deft primer coupons showed blister on the Deft primer over Chemidize 727 lot 1 coupon and on all of the lot 3 Deft primer coupons. Despite the variation in the Deft primer performance, the second and third lots still indicate performance equal to or better than the first lot tests.

The adhesion repeatability testing showed no significant difference from the first to second lot for all the candidate configurations. Lot number three however, is significantly lower in adhesion than the previous two lots for all materials. Looking at the three charts it is possible to deduce that the drop is independent of any of the variables that were being tested. The following variables were then reviewed for a possible answer to the drop in strength: adhesive, temperature, humidity, test procedures, and personnel. Adhesive, temperature, humidity, and test procedure all turn out to be negative. However, the variation in bonding the test stubs and preparing the bond site is suspected to have been great enough from one analyst to another to cause the drop in bond strength. The results of the repeatability testing of chemical compatibility of Spirit 126 to three lots of the candidate coatings showed no variation from lot to lot.

Conclusion

The coating configurations acceptable for use on the SRB aluminum components are list in the Table 2*. Note that the pretreatment and primer only configuration is acceptable for surfaces which have the coating removed after each flight cycle. The primers and topcoats listed are also qualified for stainless steel surfaces. For further information about this test program, please refer to CPC-025-00MP "Alternate SRB Aluminum Coating System Qualification Test Report" (10).

Table 2. Coating Configurations Recommended for Use on SRB Aluminum Components

Pretreatment	Primer	Topcoat
Alodine 1201	Deft 44GN7	Deft 03W127
Alodine 1201	Hentzen 05510WEP-X/05511CEH-X	Hentzen 4636WUX-3/4600CHA-SG
Alodine 1201	Lord 9929A/B	Lord A276
Alodine 5700	Deft 44GN7	Deft 03W127
Alodine 5700	Hentzen 05510WEP-X/05511CEH-X	Hentzen 4636WUX-3/4600CHA-SG
Alodine 5700	Lord 9929A/B	Lord A276
Chemidize 727	Deft 44GN7	Deft 03W127
Chemidize 727	Lord 9929A/B	Lord A276

References

1. "Coating: Polyurethane, High-Solids," MIL-C-85285B (AS), Military Specification, 13 May 1988. *Information Handling Services*, 1999.

2. "Flammability, Odor, and Offgassing Requirements and Test Procedures for Materials in Environments That Support Combustion" NHB 8060.1B, section 4.1.

3. "Standard Practice for Testing Water Resistance of Coatings Using Water Immersion" ASTM: D 870-97, *Annual Book of ASTM Standards Section 6 Paints, Related Coatings, and Aromatics*, Vol. 06.01, ASTM, West Conshohocken, PA. 1999, pp. 84-86.

4. "Standard Test Method for Effect of Cleaning and Chemical Maintenance Materials on Painted Aircraft Surfaces" ASTM F 502-93, ASTM, *Information Handling Services*, 1999.

5. "Standard Test Method for Mandrel Bend Test of Attached Organic Coatings" ASTM D 522-93a, *Annual Book of ASTM Standards Section 6 Paints, Related Coatings, and Aromatics*, Vol. 06.01, ASTM, West Conshohocken, PA. 1999, pp. 29-32.

6. "Standard Test Method for Pull-Off Strength of Coatings Using Portable Adhesion Testers," ASTM D 4541-95, ASTM, *Information Handling Services*, 1999.

7. "Standard Test Method for Tensile and Tensile Adhesion Properties of Rigid Cellular Plastics," ASTM: D1623, *Annual Book for ASTM Standards for Plastics Section 8*, Vol. 8.01, ASTM, Philadelphia, PA. 1993, pp. 494-499.

8. *Thermal Qualification Testing of an Alternate Aluminum Coating System for the SRB*, USA SRB Report No. SA-AR-0040-2000.

9. Zook, L., *Alternative SRB Aluminum Coating System Down Select Test Report*, USBI Report No. CPC-070-98MP.

10. Zook, L., *Alternative SRB Aluminum Coating System Qualification Test Report*, USBI Report No. CPC-025-00MP.

CP/515/IN/27

Trivalent Chromium/Organically-Modified Silicate Composite Coatings for Corrosion Protection of Aluminum Alloys

Elvira Stesikova, Tammy L. Metroke, Olga Kachurina and Edward T. Knobbe*

Department of Chemistry and the Environmental Institute, Oklahoma State University, Stillwater, OK 74078

Address: 003 LSE, Stillwater, OK 74078
Phone : (405)744-9994
knobbe@okway.okstate.edu

Abstract

Deposition of either trivalent chromium, Cr(III)-based, or Cr(VI)-based, conversion coatings onto aluminum 2024-T3 alloy (AA) was followed by the deposition of hybrid silicate materials; these coatings were produced by hydrolysis and condensation of tetraethylorthosilicate/vinyltrimethoxysilane/3-(trimethoxysilyl)propyl-methacrylate. The potentiodynamic study of the Cr(VI)/silicate and Cr(III)/silicate composite coatings showed a significant shift of the polarization curves toward higher values of corrosion potential and lower values of corrosion current, relative to bare AA. Moreover, augmentation of corrosion resistance from 2.8 $k\Omega cm^2$ for bare AA, to 79-95 $k\Omega cm^2$ for the hybrid silicate coatings and further to 162-362 $k\Omega cm^2$ for the composite films was observed. The results of potentiodynamic polarization and salt spray analysis ultimately suggest that AA with the composite coatings resist corrosion much better than those with bare surface or single layer silicate coating. The impact of the Cr(III) conversion coating on corrosion resistance of the composite films is comparable to that of the Cr(VI)-based surface pretreatments. This implies that the environmentally compliant and non-toxic trivalent chromium conversion coating is a very good alternative for the hazardous and carcinogenic hexavalent chromium treatment.

Introduction

Corrosion of aluminum alloys (AA) remains a subject of intensive investigation due to the everyday importance of these materials [1-4]. To prevent interaction between the metal and the environment, protective layers such as chromate conversion coatings [5], e.g. Alodine, are currently used. Such coatings replace the native metal oxide film, e.g. alumina, with another oxide layer, thus converting the surface of the substrate to a more stable state, less susceptible to corrosion [6-7]. Despite excellent protection of the metal and inhibition of the cathodic and anodic corrosion reactions [8], Cr(VI)-containing compounds are carcinogenic, very hazardous soil and groundwater pollutants [9].

Extensive research for alternative non-toxic corrosion inhibitors resulted in a number of novel coating processes, including rare earth-based conversion coatings [10-11], Co-rich oxide layers [12], and trivalent chromium films [13]. The latter were formed in a simple one-step immersion process yielding films on aluminum alloys that are comparable in corrosion resistance to those of conventional Cr(VI)-based conversion coatings but without their toxicity [14]. This finding prompted extensive investigation of corrosion protective properties of Cr(III) conversion films on AA surfaces.

Recent studies have shown hybrid silicate films to be good corrosion protective coatings for AA surfaces [15]. These films function by providing a good barrier to the penetration of corrosion initiators. However, significant improvement of AA corrosion resistance can be achieved when a silicate coating is combined with a corrosion inhibiting conversion layer [16], yielding a composite film. In this study, two types of composite coatings, Cr(VI)/silicate and Cr(III)/silicate, were investigated using polarization curve analysis and salt spray testing. Their properties were compared to those of the silicate films coated on bare AA surface free of conversion layer. The results reveal that the presence of conversion coating, either hexavalent chromium, i.e. Alodine, or trivalent chromium, in the composite film augments the inhibition of corrosion of AA. Based on their equally good performance, the trivalent chromium conversion coating is suggested as a good alternative for the hexavalent chromium-based treatment, since it does not have Alodine s toxicity.

Experimental

Materials

Silicate precursors tetraethyl orthosilicate, TEOS, 3-(trimethoxysilyl)propyl methacrylate, MTMOS, and vinyltrimethoxysilane, VTMOS, were purchased from Aldrich and were used as received. Sodium chloride (reagent A.C.S., Spectrum) and nitric acid (NF grade, Fisher) were used without further purification. Water was purified by an ion-exchange and filtration system to produce specific resistivity 18 MΩm*cm.

ORMOSIL Preparation

A series of hybrid silicate systems was synthesized based on TEOS/VTMOS/MTMOS precursor mixture. Various amounts of 0.05 M aqueous solution of nitric acid, pH=2, were added to the mixture to achieve the desired [Si-OR]/[H_2O] molar ratios of 1:1, 1:2 or 1:4. The mixtures were allowed to stir for one hour.

Preparation of Trivalent Chromium Solution for Conversion Coatings

A trivalent chromium solution was prepared according to the procedure developed by Pearlstein and Agarwala [13]. The solution was prepared by adding 0.6 g of $Cr_4(SO_4)_5(OH)_2$ (26% Cr_2O_3 and 23-24% Na_2SO_4) and 0.8 g of K_2ZrF_6 to one liter of deionized water under continuous stirring for several hours. This solution was then allowed to stand for one week. The pH of the solution was found to decrease from 5.0 in the freshly prepared to about 3.7 in the "aged" solution.

Coating Techniques

Aluminum 2024-T3 alloy substrates used for both polarization measurements and salt spray testing were freshly degreased and deoxidized using the following cleaning process. AA substrates were, first, treated in Oakite-164 cleaner solution for 15 minutes at 65 °C, and then in Turco Smut-Go deoxidizing solution for 7-10 minutes at 25 °C under rigorous air agitation. Each one of these treatments was followed by thorough rinsing for 2 minutes using tap water at 50 °C.

AA surface pretreatment was done using either commercial Alodine 1200 solution or trivalent chromium solution. AA substrates were immersed into Alodine 1200 solution for 2 minutes to yield a uniform, golden conversion coating on the surface. In order to produce Cr(III) conversion coatings, AA substrates were sprayed with the trivalent chromium solution for 10 minutes. The synthesized hybrid silicates were subsequently applied onto bare or pretreated AA by a spray coating technique using commercial airbrush setup. The coatings were allowed to dry at ambient conditions for at least 24 hours prior to their characterization.

Polarization Measurements

Electrochemical measurements were performed using a CV-50-W unit and a three electrode cell equipped with a platinum counter electrode, a Ag/AgCl/Cl^- (3M KCl) reference electrode and an AA 2024-T3 panel as the working electrode. The latter was either coated or not coated with a film and had an exposed area of 0.36 cm^2. All measurements were conducted in an aqueous 1M NaCl working solution at 25 ± 1 °C. The reported values of potentials both shown in the polarization curves and listed in the tables are given relative to the Ag/AgCl/Cl^- reference electrode. Oxygen was removed by purging the solution with purified nitrogen during the polarization measurements.

In order to reach steady potential, the electrodes were kept in the working solution for 30 minutes prior to the measurements with the electrical circuit open. Then the acquisition of polarization curves was started from this open circuit potential, with a constant sweep of 1 mV/sec. Corrosion current values, I_{corr}, reported herein correspond to a 50 mV stretch between the cathodic and anodic parts of the polarization curve. Corrosion resistance was calculated using the equation: $R_{corr} = 50mV/ I_{corr}$. This differs from the previously described definition of the corrosion resistance,[4] however, it allows for the derivation the parameter, R_{corr}, for the entire pool of polarization curves collected in this study regardless of their shift along the abscissa. Pitting potential, E_{pit}, corresponds to the point of sharp rising of the anodic current in a linear scale.

Accelerated Salt Spray Testing

Ormosil-coated test coupons were placed in 5% salt spray at 35 ± 1.7 °C for 168 hours as per Mil-C-5541 and ASTM B117.

Results and Discussion

Comparison of Trivalent Chromium and Alodine Conversion Coatings

The impact of Alodine and trivalent chromium conversion coatings on the electrochemical and corrosion resistance behavior of 2024-T3 AA was studied using potentiodynamic polarization curves and accelerated salt spray testing, respectively. Electrochemical analysis of Alodine was hindered by the solubility of the treatment in water. Figure 1 depicts the acquired polarization curves for the bare AA (trace A) and AA substrates coated with the trivalent chromium conversion coatings by spray application (trace B). The results indicate that the presence of the Cr(III) coating shifts corrosion potentials of AA substrates to more positive values, converting the surface of the substrates to more stable states less susceptible to corrosion. This behavior is anticipated for chemical conversion coatings. Thus, within the accuracy of the experiment, ± 16 mV, the corrosion potential of bare AA was measured to be –725 mV in 1M NaCl which is in the agreement with data published by other authors [8, 17]. This value is approximately 160 mV lower than that of the Cr(III)-coated AA substrates, which for different exposure times and the deposition techniques appears in a relatively narrow range of –560 ± 22 mV.

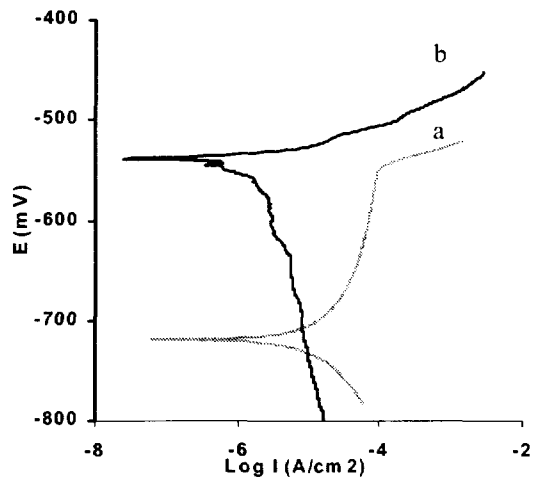

Figure 1. Potentiodynamic polarization curves measured in aqueous 1M NaCl solution at 25 °C for (a) bare 2024-T3 aluminum alloy sample and (b) aluminum alloy samples coated with Cr(III) conversion layers by spraying coating.

The corrosion resistance values for AA substrates coated with Cr(III) conversion layers were determined from the corresponding polarization curves as it described in experimental section. For the Cr(III) conversion layers produced by spray application, the resistance values were in the range 18.1 ± 2.7 kΩ*cm^2. The data indicate that Cr(III) coated substrates exhibit significant elevation of corrosion resistance, as compared to that of uncoated AA, 2.8 kΩ*cm^2. Together with the corrosion potentials, the corrosion resistance data confirms that formation of the Cr(III) conversion layer on the surface of aluminum alloy provides it with better corrosion stability.

Figure 2 shows the results of 168 hour salt spray tests for bare AA, Alodine, and Cr(III)-treated AA substrates. Both the Alodine and trivalent chromium conversion coating exhibited remarkable corrosion resistance, significantly better than that of the bare AA substrate. No pitting was observed on the Alodine-treated panels and only a few small pits were observed for the Cr(III)-treated panels. Additional specimens using hybrid coatings on

top of either Alodine or Cr (III) conversion coatings were prepared in order to determine if the presence of a conversion coating under barrier sol-gel coatings could produce composite films with improved corrosion resistance.

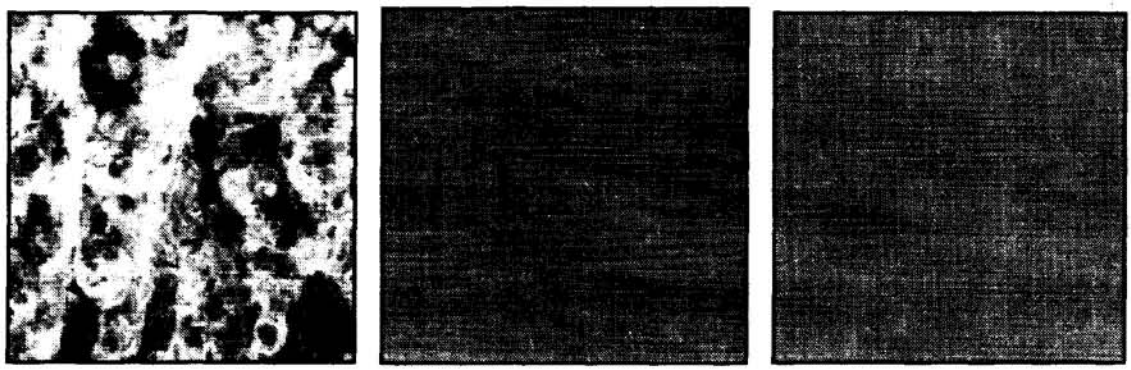

Figure 2: Results of 168 hour salt spray test for (a) Bare AA, (b) Alodine-treated AA, and (c) Cr(III)-treated AA. These photos represent approximate 2" x 2" segments from the center of a 3" x 5" coupon.

Conversion Layer/ORMOSIL Composite Films

Figure 3 shows potentiodynamic polarization curves acquired for non-coated AA (curve **a**), AA coated with hybrid silicate coatings prepared using [Si-OR]/[H_2O] molar ratios of 1:4 (**b**), composite coatings containing Cr(VI) (**c**), and Cr(III) (**d**) conversion layers, respectively. The latter was produced by spraying the trivalent chromium solution onto AA substrate for 10 minutes. The results indicate that the coatings studied in this experiment yield a significant shift of the polarization curve toward higher values of the corrosion potential and lower values of the corrosion current.

Important electrochemical characteristics assessed from the polarization curves acquired for AA substrates coated with different hybrid coatings with and without conversion layers are listed in Table 1. Thus, E_{corr} value is changed from –719 mV for a bare AA to –582 mV for the 1:4 hybrid silicate coating and further to –459 and –503 mV for the Cr(VI) and Cr(III) composite coatings, respectively. The corrosion current values decreased by two orders of magnitude for the coated aluminum alloys, when compared to the non-coated AA. It is noteworthy that corrosion resistance of the bare AA is very small, 2.8 $k\Omega*cm^2$, whereas R_{corr} values for the coated AA samples fall in the range of 80-350 $k\Omega*cm^2$. These observations provide strong evidence that corrosion of AA substrates is significantly inhibited by the presence of the composite coating.

More detailed analysis of the corrosion data implies that both composite coatings exhibit much better values of I_{corr}, and increased values of E_{corr} and R_{corr}. The latter parameter is of special importance, since it reflects a two to four-fold increment of corrosion resistance of the composite films relative to the single layer hybrid silicate coatings. Thus, for the 1:4 hybrid silicate coating, R_{corr} is changed from 79.2 $k\Omega*cm^2$ for the single layer coating to 350.0 and 281.0 $k\Omega*cm^2$ for the composite coatings containing Alodine and Cr(III) layers, respectively.

The study of composite films allows for a comparison of the corrosion characteristics of the conversion layers, which is not possible otherwise due to the solubility of the Alodine films in aqueous solutions. Analysis of the electrochemical characteristics of the AA substrates coated with composite films containing Cr(VI) and Cr(III) conversion layers indicates insignificant differences in the I_{corr}, E_{corr} and R_{corr} values between these two systems. This suggests that corrosion protection of AA furnished by either Cr(VI) or Cr(III) conversion layers are equivalent. This is a rather significant understanding, since it offers environmentally compliant Cr(III) treatment as an alternative to toxic and hazardous Cr(VI)-based protection of Alodine films.

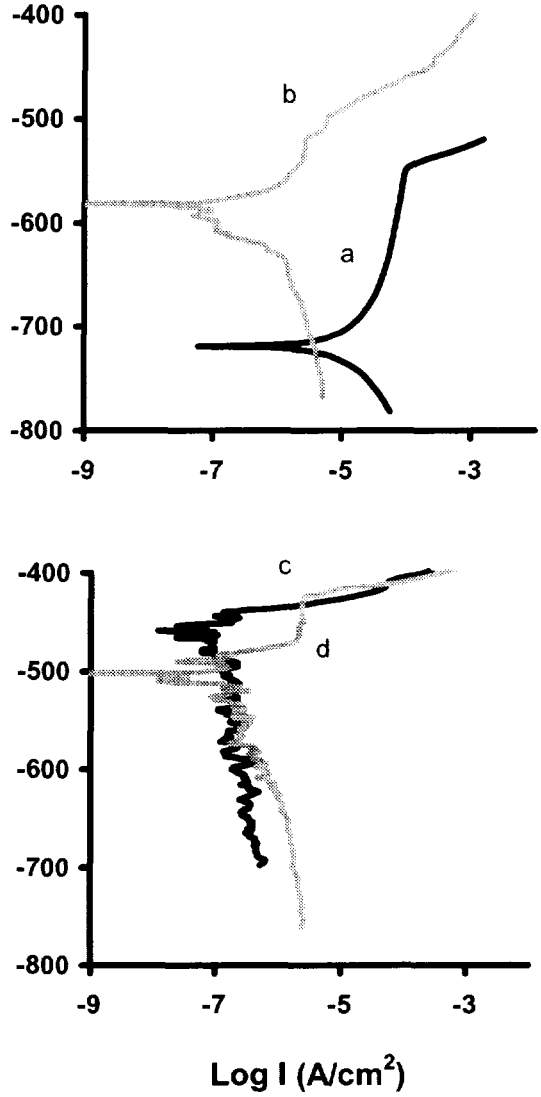

Figure 3. Potentiodynamic polarization curves measured in aqueous 1M NaCl solution at 25 °C for non-coated AA 2024-T3 (a); AA coated with: 1:4 hybrid silicate (b), composite films of Alodine and 1:4 hybrid silicate (c), composite film of Cr (III) conversion layer and hybrid 1:4 silicate (d).

Table 1. Electrochemical characteristics derived from potentiodynamic polarization curves for 2024-T3 aluminum alloy substrates coated with different hybrid coatings with and without conversion layers.

Coating/Conversion Layer	Water Ratio	$I_{corr} \cdot 10^7$, A/cm^2	E_{corr}, mV	E_{pit}, mV	R_{corr}, $k\Omega*cm^2$
None		182	-719	-540	2.8
Hybrid Silicate					
	1:1	5.89	-450	-449	84.9
	1:2	5.25	-512	-450	95.3
	1:4	6.31	-582	-475	79.2
Hybrid Silicate/Cr(VI)	1:1	1.38	-460	-453	362.0
	1:2	3.10	-507	-484	162.0
	1:4	2.00	-459	-403	350.0
Hybrid Silicate/Cr(III)	1:1	2.40	-473	-450	208.3
	1:2	1.60	-599	-439	312.5
	1:4	1.78	-503	-409	281.0

From the results of the potentiodynamic study, it can be inferred that the composite films comprised of both hybrid silicate and conversion layers provide corrosion protection of AA, which is superior to that of either one of the film components. This is further supported by the results of accelerated corrosion testing conducted for the same specimens. Figure 4 shows images of a bare AA substrate (a) and those coated with the 1:4 hybrid silicate film (b) and composite films (c,d) exposed to a corrosive salt fog atmosphere for 168 hours. Based on the amount of pitting observed on these panels, it is possible to conclude that AA with the composite coatings resists the corrosive environment in a manner superior to AA coated with the single layer silicate coating or no coating at all.

Conclusions

AA substrates coated with composite films comprising both hybrid silicate and conversion layers, trivalent or hexavalent chromium, exhibited excellent corrosion resistance. The impact of the trivalent chromium conversion coating on the corrosion resistance of the composite films is comparable to that of the Cr(VI)-based conversion coating, i.e. Alodine. This implies that the trivalent chromium conversion coating, which is an environmentally compliant and non-toxic, is a very good alternative for the hazardous and carcinogenic Cr(VI)-based surface pretreatments.

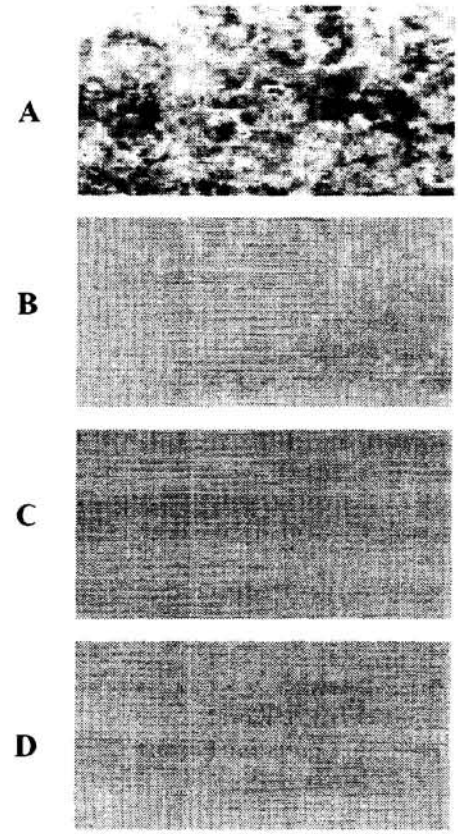

Figure 4. Aluminum 2024-T3 alloy substrates exposed to salt fog atmosphere at 35 °C for 168 hours. Coating systems: (A) bare AA, (B) AA coated with 1:4 hybrid silicate, (C) composite films of Alodine and 1:4 hybrid silicate, and (D) composite film of Cr (III) conversion layer and hybrid 1:4 silicate. These photos represent 3" x 5" coupons.

Acknowledgement

This research was supported by the U.S. Department of Defense through Prime Contract # R2CSR-98-D-SBIR with Lear-Siegler Service, Inc., subcontracted to OSU through SBIRE under subcontract number SBIRE-S98-001.

References

1. R. T Foley, Corrosion **1986**, *42*, 277.
2. L. Tomcsanyi, K. Varga, I. Batrik, G. Horayi and E. Maleczki, Electrochim.Acta. **1989**, *34*, 855.
3. C. Blank, B. Lavelle and G. Mankowski, Corros. Sci. **1997**, *39*, 495.
4. A. E. Hughes, J. D. Gorman and P. J. K. Paterson, Corros. Sci. **1996**, *38*, 1957.
5. J.K. Hawkins, Isaaks, H.S.; Heald, S.M.; Tranquada, J.; Thompson, G.E.; Wood, G.C. *Corr. Sci.* **1987**, *27*, 391.
6. R. G. King, Surface Treatment and Finishing of Aluminium, Pergamon Press, Oxford, **1988**, pg 51.
7. Ichiro Suzuki "Corrosion-Resistant Coatings Technology", Marcel Dekker, Inc. New York, **1989**, pg. 167.
8. M Kabasakaloglu.; Aydin, H.; Aydin, H.; Aksu, M.L. *Materials and Corrosion,* **1997**,*48*, 744.
9. N. I. Sax, Dangerous Properties of Industrial Materials, Fifth Edn, Van Nostrand Reinhold Company, New York, **1979**, pg. 504.
10. B.R.W. Hinton and D.R. Arnott, Microstruct. Sci., **1989**, *17*, 311.
11. D.R. Arnott, N.E. Ryan, B.R.W. Hinton, B.A. Sexton and A.E. Hughes, Appl. Surf. Sci., **1985**, *22*, 236.
12. M.P. Schriever, Non-Chromated Cobalt Conversion Coating, European Patent 0488430 A2.
13. F. Pearlstein and V.S. Agarwala, Trivalent Chromium Conversion Coatings for Aluminum, US Patent Number 5,304,257.
14. V.S. Agarwala, Trivalent Chromium Solutions for Applying Chemical Conversion Coatings to Aluminum Alloys: Naval Airfare Center, Aircraft Division, Code 434000A, MS-3, Patuxent River, MD.
15. T. Metroke, Parkhill, R.; Knobbe, E. Mater. Res. Soc. Symp. Proc. **1999,** *576*, 293.
16. E. Stesikova,.; Metroke, T.L.; Reed, P.L.; Agarwala, V.S.; Knobbe, E.T. *Proceedings paper #287 in Corrosion NACE 2000 Annual Meeting*, March 2000, Orlando, Florida.
17. W.A. Badway, Al-Kharafi,F.M,A.S. El-Azab. Corrossion Science **1999**, *41*, 709-727.

HVOF Thermal Spray Coatings as an Alternative to Hard Chrome Plating on Military Aircraft

Bruce D. Sartwell
Naval Research Laboratory
Code 6170
Washington, DC 20375
(202) 767-0722
sartwell@nrl.navy.mil

Introduction

Functional hard chrome plating is a critical process associated with manufacturing and maintenance operations on aircraft, vehicles, and ships, both in the civilian and military sectors. Since chromium is on the Environmental Protection Agency list of 17 toxic materials, fairly stringent air and wastewater emission limits have been established by the EPA. Also, hard chrome plating utilizes chromium in the hexavalent state (hex-Cr), which is a known carcinogen. As a result, the Occupational Safety and Health Administration (OSHA) has established permissible exposure limits (PEL) for hex-Cr in the workplace at a level of 0.1 mg/m^3. However, recent studies have indicated that the cancer risk is significantly increased at this level, so it is anticipated that OSHA will issue a new hex-Cr PEL that is substantially less than the current value. This would unquestionably increase the cost of plating operations that may be prohibitive in certain activities.

Compliance with increasingly stringent regulations under the broad category of environment, safety and occupational health (ESOH) is leading many organizations to investigate alternative coating processes. However, it is also found that in many instances the in-service performance of hard chrome plating is not satisfactory, so some organizations have investigated and qualified alternative processes solely on the basis of performance, but these have generally been on a piecemeal basis instead of an across-the-board qualification. As a result of these types of studies, it is apparent that as opposed to many ESOH-driven projects that seek an alternative process/material that is the "next-best thing" to the presently used process, for chrome plating replacement, it is possible to identify alternative processes that not only address ESOH issues but also improve performance. Improved performance is then translated into reduced life-cycle costs of the affected system.

In terms of identifying those technologies that are viable candidates for replacing hard chrome plating, it is essential to understand the current uses for chrome. Looking specifically at the aircraft industry, chrome plating is used in several different ways:

- As a wear-resistant coating, typically applied by OEMs to thicknesses ranging from 25 to 100 micrometers (0.001" to 0.004"), mostly for external wear areas
- As a rebuild coating, up to 0.5 mm (0.020") thick, to bring worn and/or machined components back to their specified dimensions
- As a light abrasion/corrosion barrier for many internal areas (designated as thin dense chrome or flash chrome), typically 5-10 micrometers thick.

The largest uses of hard chrome in the aerospace industry are:

- Landing gear (gas-over-fluid hydraulics) – inner cylinders, axles, and pins
- Hydraulic actuator rods
- Journals and shafts in engines
- Lugs and other wear surfaces
- Internal diameters (ID's) of hydraulic and landing gear outer cylinders (frequently thin dense chrome)

Due to the types of components and applications for which hard chrome is currently used in the aircraft industry, there are many types of coating technologies that would not be viable alternatives even though they can produce coatings with superior properties. These include chemical vapor deposition and the vacuum-based coating

technologies such as ion plating, sputtering, and cathodic arc deposition. The types of coatings that are most widely viewed as being capable of replacing hard chrome are the thermal spray technologies, especially high-velocity oxygen-fuel (HVOF) thermal spraying. With this process, the coating material, in powder form, is fed into the combustion chamber of a gun where a fuel, such as hydrogen, ethylene, or kerosene, is burned with oxygen, and the heated and softened powder is expelled as a spray with the supersonic gases. Powders deposited using HVOF include pure metals, metal alloys, cermets, and certain ceramics and polymers. The reason why HVOF is the preferred thermal spray process for chrome replacement is because it produces low-porosity (<1%), highly adherent (bond strength > 80 MPa (10,000 psi)) coatings which generally have an oxide content less than 1% even for reactive metals. As a flexible dry-coating technology it avoids high-volume waste streams and provides a choice of coating materials for each application. The use of hard chrome is so widespread that there is no single replacement technology or material, but the HVOF cobalt-cemented tungsten carbides are some of the easiest materials to spray and have shown the widest range of successful applications.

One of the clear advantages of HVOF is the high deposition rates that can be achieved. The instantaneous deposition rate is approximately 50 micrometers (0.002") per minute although in normal operation the HVOF gun is mounted on a robot or other articulating arm and the component being coated is also manipulated (e.g., a cylinder will be rotated). Figure 1 is a photograph of an HVOF WC/Co coating being applied to a Boeing 737 nose landing gear cylinder, which is approximately 0.5 meters long and 0.1 meters in diameter. It generally takes less than 20 minutes to deposit a 100-micrometer-thick (0.004") coating onto this component.

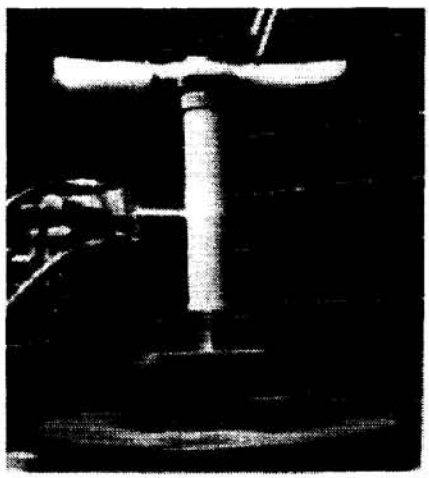

Figure 1. HVOF thermal spraying of WC/Co coating onto a nose landing gear cylinder from a Boeing 737

Establishment of DoD Program and Generic Materials Testing

Within the U.S. Department of Defense (DoD), the Hard Chrome Alternatives Team (HCAT; www.hcat.org) was formed in 1996 under the principal sponsorship of the DoD Environmental Security Technology Certification Program. Its objective is to demonstrate and validate HVOF coatings as a cost-effective and technologically superior alternative to hard chrome in most maintenance operations at Navy, Air Force, and Army aircraft overhaul and repair (O&R) depots and in manufacturing operations at DoD OEMs. The organizations that comprise the HCAT include DoD research laboratories, aircraft depots, aircraft OEMs, materials testing laboratories, an HVOF equipment manufacturer and an FAA-certified repair facility that has chrome plating and thermal spray capability.

The HCAT initially sought a more generic qualification of HVOF coatings by selecting base materials that were representative of the families of materials onto which hard chrome is deposited, applying two different HVOF coatings, and then conducting materials testing to demonstrate equivalent or superior performance. The base materials that were selected were AISI 4340 high-strength steel, 7075-T73 aluminum alloy, and PH13-8Mo stainless steel. The HVOF coatings were WC/Co (83%/17%) and Tribaloy 400, a cobalt-molybdenum-chromium alloy, deposited to a thickness of 100 micrometers (0.004"). The microhardness values for the three coatings were as follows:

- Hard chrome 10.1 GPa
- WC/Co 12.8 GPa
- Tribaloy 400 5.7 GPa

Extensive fatigue, corrosion, and abrasive wear testing was conducted on the coated materials compared to hard chrome deposited to the same thickness in accordance with standard specifications for aircraft components. The results of these studies have been reported previously.[1,2] They indicated that the fatigue performance of the HVOF coatings either met or exceeded that of the hard chrome. The cabinet corrosion testing (ASTM B117) indicated virtually no difference between the three coatings and the abrasive wear testing indicated superior performance for the HVOF WC/Co because of its higher hardness, but inferior performance for the Tribaloy 400.

Although the cabinet corrosion testing showed essentially equivalent performance for the HVOF coatings compared to hard chrome, atmospheric corrosion testing was recently completed on the various coating/substrate combinations, with the results being somewhat different. In this case, the test coupons consisted of 10 cm by 15 cm (4" x 6") flat plates onto which the three coatings were deposited to a thickness of 100 micrometers. The specimens were mounted onto atmospheric test racks near the seashore at the Navy Marine Test Facility in Key West, FL. Some of the specimens were sprayed with a salt water solution once a week to accelerate the corrosion.

It can be seen in figure 2 that both the hard chrome and the Tribaloy coatings have extensive corrosion whereas the WC/Co coatings are virtually pristine. As stated above, this result is significantly different from that of the cabinet testing, which might be a further indication that the B117 test does not accurately reflect corrosion behavior in the real world.

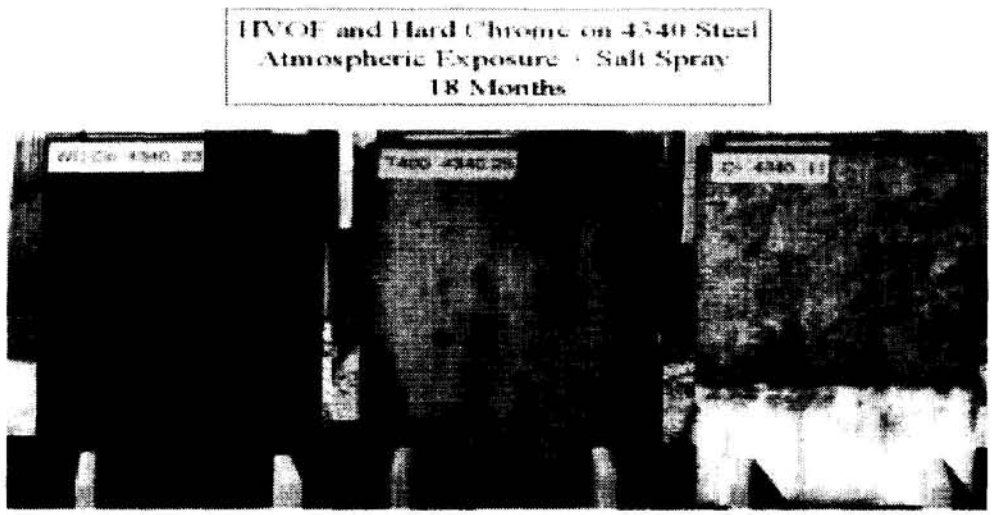

Figure 2. Representative specimens of 4340 steel plates coated with HVOF WC/Co and Tribaloy 400, and hard chrome after 18 months atmospheric exposure plus once weekly spraying with salt water

Execution of Separate Projects on Qualification of HVOF Coatings as a Hard Chrome Replacement

All of the previous studies demonstrated what might be called the technological viability of HVOF coatings as a replacement for hard chrome plating. But it was clear through discussions with individuals who make up the stakeholder community within the DoD aerospace sector (e.g., repair depot technical representatives and engineering authorities, weapons systems program managers, and structural engineers from the three services and the OEMs) that it would not be possible to have a generic qualification of HVOF for all types of aircraft components. Because hard chrome plating does in fact protect a variety of aircraft components, this means that different stakeholders would be involved in the qualification process for each type of component. As a result, the HCAT has established partnerships with two other DoD organizations that execute projects related to qualifying and inserting technologies that can have an impact related to environmental concerns (e.g., pollution prevention) and

also life-cycle costs. The first is the Joint Group on Pollution Prevention (JG-PP; www.jgpp.com) and the second is the Propulsion Environmental Working Group (PEWG; www.pewg.com).

The partnership with the JG-PP has led to the establishment of separate projects related to qualification of HVOF thermal spray coatings on the following classes of aircraft components:

- Landing Gear – inner cylinders, axles, pins, actuators (in conjunction with Boeing and the landing gear manufacturers, BF Goodrich/Menasco, Heroux and Messier-Dowty).
- Propeller Hubs (in conjunction with Hamilton Sundstrand)
- Hydraulic actuators for systems other than landing gear (OEMs to be identified)
- Helicopter Dynamic Components - including transmission and rotor head components (in conjunction with Boeing Philadelphia and Sikorsky)

The partnership with the PEWG has led to a project related to replacement of hard chrome on gas turbine engine components and is being executed in conjunction with GE Aircraft Engines, Pratt & Whitney, and Rolls-Royce Allison.

The execution plan for each project first involves the development of Joint Test Protocols (JTP) following a methodology developed by the JG-PP. The JTP defines all of the testing required for full qualification of the alternative process which generally includes both materials testing on coupons for fatigue, corrosion, wear, and other properties, and actual component testing involving installation of coated components into test rigs and into operational aircraft where performance is tracked over extended periods of time. In addition to preparation and execution of the JTPs, the projects also involve establishing production-level HVOF facilities at the appropriate military aircraft maintenance facilities, training personnel at those facilities, analyzing costs, and developing standards and specifications for application, grinding, and stripping of the HVOF coatings on the categories of aircraft components.

Execution of Project on Landing Gear

The remainder of the paper will be concerned with the execution of the project related to qualification of HVOF thermal spray coatings as a chrome replacement on landing gear since that is the one closest to completion. This is a joint project between the United States and Canada. In 1997, the Canadian Department of National Defence (DND) and Industry Canada (IC) became interested in the HCAT program because of the considerable number of military aircraft in DND and because Canadian companies manufacture more than two thirds of the landing gear on military and commercial aircraft in North America. As a result, a formal Project Arrangement was established between the two countries and a Canadian team (C-HCAT) was formed to execute some of the testing.

In July 1998 a meeting was held that involved members of the U.S. and Canadian HCAT teams and representatives from all of the DoD, DND and OEM stakeholders for the purpose of developing the JTP for landing gear. It was decided that it would be issued in two parts, with the first part describing the materials (coupon) testing and the second part describing the component (rig and flight) testing. Part I was completed and was endorsed by the stakeholders in 1999 and testing is in progress.

Only two types of HVOF coatings are being evaluated in the landing gear project on three base materials. Testing is also being conducted on hard chrome plating as a baseline. The U.S. team is evaluating WC/Co (83%/17%) and the Canadian team is evaluating WC/CoCr (86%/10%-4%) deposited onto 4340, 300M, and Aermet 100 steels. Materials testing includes fatigue, corrosion, sliding wear, impact (both particle erosion and ball drop), and hydrogen embrittlement. (The entire 50-page JTP is available at www.hcat.org).

In order to ensure reproducibility in the test results, the JTP specifically defines all aspects of the specimen preparation, coating deposition, and testing parameters. For coupon preparation, the machining, heat treatment, grinding, etching, shot peening (if applicable), and grit blasting (if applicable) are all described. Deposition of the hard chrome is specified to be in accordance with Military Standard 1501 supported by commercial standard QQ-C-320. Deposition of the HVOF coatings is specified to be in accordance with Boeing Aircraft Corporation Standard 5851, Class 2, Type I with hydrogen used as the fuel gas. Coating thicknesses are specified at either 75 micrometers (0.003") or 250 micrometers (0.010").

Because the majority of components onto which hard chrome is currently applied are fatigue-sensitive, special attention has been paid to the internal stress of the HVOF coatings. Based on the generic studies conducted earlier that showed a correlation between compressive stress and improved fatigue, it was determined that when the coatings are applied to coupons or components, they should also be simultaneously applied to almen strips (which are commonly used for measuring stress induced by shot peening). For the HVOF coatings being evaluation in the landing gear project, almen N values ranging from 3 to 12 (compressive stress) are specified.

Surface Finish

Surface finish is a critical issue, especially for items such as hydraulic rods that run against seals. For this type of application chrome plate is typically specified with a 0.2-0.4 micrometers (8-16 microinches) finish (average roughness, or Ra value). This permits the surface of the chrome to hold some hydraulic fluid in its pattern of microcracks. However, because of its higher hardness, a WC/Co surface with a finish greater than 0.2 micrometers can potentially damage the seal material. Therefore, in the JTP, the surface finish for the HVOF coatings is specified at either 0.1 or 0.2 micrometers. It is becoming clear, however, that merely defining the Ra value is inadequate and that for these types of coatings it may be necessary to adopt a more thorough specification of surface finish to better define the topography.

Fatigue

The fatigue tests are being conducted in accordance with ASTM E466-96 which specifies axial load control at constant amplitude. The number of stress levels to be evaluated is four, with five specimens tested at each stress level. In general, hourglass geometry is used for the specimens, although in a few cases smooth gage is used. Coating thicknesses are either 75 or 250 micrometers, the R values for the fatigue test are either –1 or 0.1, and the environment is either laboratory air at ambient temperature or –40° C, or immersion in a 3.5% NaCl solution at ambient temperature. More than 1300 separate fatigue tests will be conducted.

Some of the results have been obtained for the fatigue testing on the HVOF WC/Co coatings. Figure 3 provides the data on cycles to failure at different stress levels for the 75-micrometer-thick hard chrome and HVOF WC/Co coatings on 4340 steel with an R value of 0.1. The figure also shows the effect of shot peening of the base material prior to application of the coating. The results indicate superior performance for the HVOF coating and also indicate the superior performance associated with the shot peening.

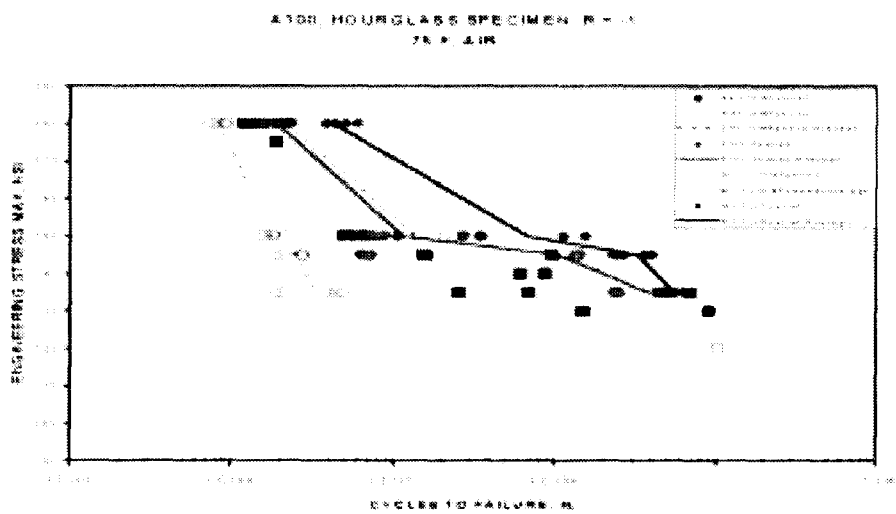

Figure 3. Results of fatigue testing for peened and un-peened 4340 steel hourglass specimens onto which hard chrome plating or HVOF WC/Co coatings had been applied

Wear Testing

Wear tests are being conducted to provide information on manufacturing variables and wear conditions including coating material, surface finish, lubrication, side loads, velocities, type of wear, and other wear environment factors. Two test methods are being employed:

- Oscillating piston/bushing at low frequency and long stroke with a load applied to the bushing perpendicular to the direction of motion of the piston (see figure 4)
- Fretting block-on-shoe test at high frequency and short stroke with a load applied to the shoe perpendicular to the direction of motion of the block (see figure 5)

The piston and bushing oscillating wear test is being used to reflect typical conditions of use under a side load. The fretting wear test is being used to reflect typical actuator piston dithering or vibration movement. The shoe and block materials correspond to the piston and bushing/seal materials. The base material for the piston and shoe is 4340 steel and the hard chrome and HVOF coatings are applied to only these components. Table 1 provides the wear material test matrix.

Because there are so many variables in the wear testing, a statistical design-of-experiments methodology is being followed. During testing of the piston/bushing, the coefficient of friction is monitored and then subsequent to the test, the coatings are examined to measure the extent of wear, if any.

Table 1. Wear test material matrix

Piston/coating material (Fretting Shoe/Coating)	**Bushing material (Fretting Block)**
4340/Hard Chrome Plate	4340 steel
4340/HVOF WC-CO	AMS 4640 (Al-Ni-bronze)
4340/HVOF WC-10Co-4Cr	Anodized aluminum
	Caron B on Al bronze
	Nitrile/PTFE T-seals in 4340

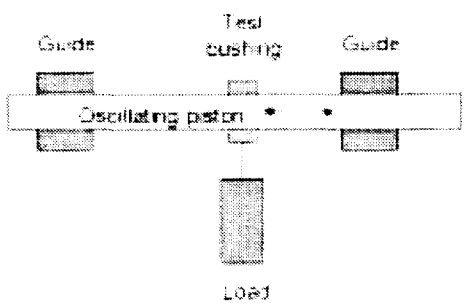

Figure 4. Cross-sectional schematic of piston and bushing oscillating wear test

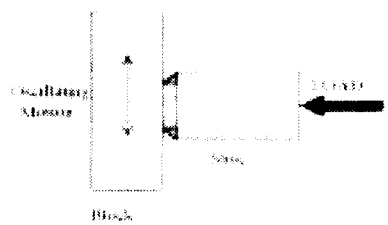

Figure 5. Cross-sectional schematic of fretting test

Flight Testing

Flight testing of HVOF-coated components which are normally chrome-plated is an essential part of the program. Several components have been coated and are either currently in flight testing or are ready to be installed on operational aircraft. Figure 6 is a photograph of a Navy P3 (four-engine turboprop) main landing gear onto which a 100-micrometer-thick WC/Co coating has been applied to the piston (center of photograph) and axle journals. These components were installed in April 1999 and were inspected in December 1999 after 241 landings. The coatings showed no signs of degradation and were still in pristine condition.

Figure 7 shows two components from a Navy EA-6B (attack jet) main landing gear piston assembly which were coated with HVOF WC/Co to a thickness of 100 micrometers. Note the multiple locations on the long L-shaped piston and also that an internal surface was coated on the collar. It is possible to deposit the coatings with a spray angle up to 45 degrees off normal such that some shallow internal surfaces can be coated. It is expected that these components will be installed on an operational aircraft sometime in June 2000.

Production, Lifetime, and Cost Issues

Several analyses have been made in recent years of the cost of HVOF coatings compared with chrome plating. Based on different types of components and different scenarios their results reflect the wide range of situations in which chrome is used. For most manufacturers, total production cost, rather than process cost alone, is the most important issue, while for most users, life-cycle cost (or cost of ownership) is the critical issue.

For aerospace OEMs the primary cost savings tend to come from elimination of the need to heat treat high strength steels to prevent hydrogen embrittlement. This reduces production time with its associated inventory and cost-of-money. This makes HVOF especially cost-effective for large items such as landing gear and hydraulics.

For users, the primary cost savings in extending time between overhauls and reducing the loss of revenue-generating time to overhaul. At Jacksonville Naval Aviation Depot there have now been several occasions when a previously-chromed item has been coated with HVOF WC-Co, with the result that it has never returned for overhaul. The permissible life of many aircraft components is often defined by fatigue limits (maximum allowable flight hours) or by repair limits (maximum number of repairs or total thickness of repair). When the repair coating life is 3-5 times that of chrome, it becomes possible to protect the component with a "lifetime coating" that will last the entire life of the item, eliminating further strip-down and repair costs.

Summary

Currently, there are several ongoing DoD/industry programs to qualify HVOF thermal spray coatings as a chrome replacement on different types of aircraft components. Testing to date has shown that HVOF WC/Co coatings generally demonstrate superior performance to hard chrome with regard to fatigue, corrosion, and wear. As more and more data is generated and the results are obtained from rig and flight testing, the qualification process should accelerate, leading to actual insertion of this technology in manufacturing operations and at military overhaul and repair depots. The higher performance of HVOF-coated components should ultimately lead to reduced maintenance, lowering the total-cost-of ownership to DoD for its aircraft.

References

1. Sartwell, B. D., Natishan, P. M., Legg, K. O., Schell, J. D. and Sauer, J. P., *Proceedings of the AESF Aerospace/Airline Plating Forum*, p. 97-105 (1998)

2. Sartwell, Bruce D., and Bretz, Philip E., *Advanced Materials and Processes*, p. 25-29 (August 1999)

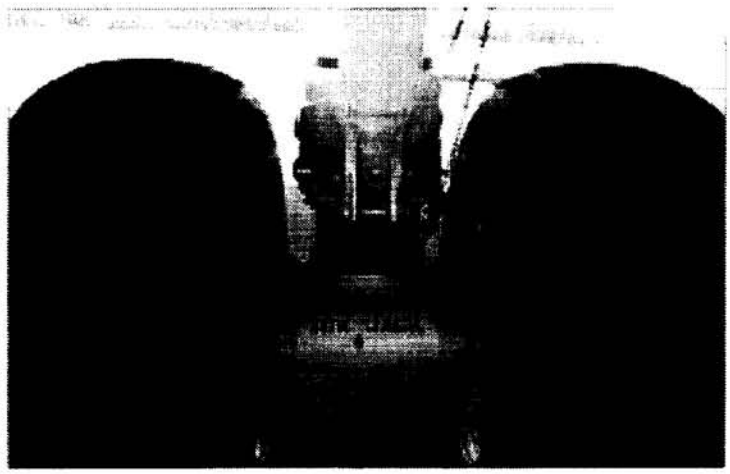

Figure 6. Photograph of Navy P3 main landing gear with the piston and axle journals coated with HVOF WC/Co

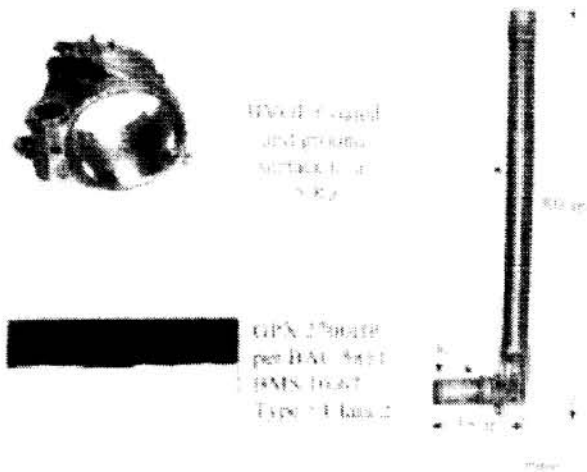

Figure 7. Photograph of Navy EA-6B main landing gear piston assembly showing the areas onto which the HVOF WC/Co coating was applied and also showing a cross-section micrograph of the coating

CP/317/IN/20

The Use of Ion Vapor Deposited (IVD) Aluminum for the Space Shuttle Solid Rocket Booster

William Imre, Howard Novak, Randy Raley

United Space Alliance
8550 Astronaut Blvd.
Cape Canaveral, FL 32920

Introduction

USA SRB Element Materials and Processes (M&P) Department had recommended the use of Ion Vapor Deposited (IVD) aluminum coating as a replacement for cadmium plating, and chromated paint primers on both Ground Support Equipment (GSE) and Solid Rocket Booster (SRB) non-insulated flight hardware. IVD aluminum provides an extremely tenacious, environmentally compatible coating, that lends itself to many items presently requiring repainting or hazardous plating removal and greasing of steel parts to prevent subsequent corrosion from seawater and seacoast environment. A Technical Directive (TD) was issued by the Marshall Space Flight Center (MSFC) SRB Program Office to evaluate the applications of IVD aluminum to SRB hardware.

Discussion

Previous to the work done on this Program, and with test samples provided by the USBI Co. M&P Dept., MSFC Corrosion Lab. performed Electrochemical Impedance Spectroscopy (EIS) testing, to confirm the excellent corrosion protection properties of IVD aluminum. The authors worked with the Kennedy Space Center - Florida Materials Science Division personnel, including Beach Corrosion Test Site, and the Seawater Immersion Facilities. The Naval Research Laboratory, located in Key West, Florida, performed unfiltered seawater immersion and alternate immersion testing of IVD aluminum coated test plates and SRB test hardware. Florida Atlantic University, Marine Engineering Division, located in Boca Raton, Florida, performed beach exposure, alternate immersion testing in filtered seawater, and electrochemical testing of IVD aluminum coatings on both steel and aluminum test plates and non-flight SRB parts. Much research involved IVD work done by the Air Force, Navy, and Army Logistics Centers at various locations within the United States.

Process Description

The IVD process is very similar to conventional plating technology, requiring surface preparation, processing and finishing operations in order to correctly process the parts to be coated. Surface preparation consists of degreasing to remove gross contaminants prior to an aluminum oxide blast treatment, which provides an anchor pattern and residual oxide free surface. Figure 1 shows the overall view of an Ion Vapor Deposition Facility. A special air suspension rack (shown at the right side of Figure 1) is used to transport the prepared parts to the IVD vacuum chamber; as shown in Figure 2 with the chamber door open and racked parts (test panels) positioned in the chamber. After the chamber door is closed, the vessel is evacuated to a pressure of 8X10–5 Torr to purge the system of residual moisture emanating from the parts and internal pressure vessel hardware. The chamber is then back-filled with low dew-point pure Argon gas to a chamber pressure of 2X10-2 Torr. At this pressure the parts are subjected to a glow discharge cleaning or sputtering operation. A high negative potential is applied between the parts being coated and the evaporation source. The Argon gas in the chamber ionizes and creates a glow discharge around the parts bombarding them with positive ions. (This ion bombardment of the part surface effects a final cleaning operation prior to coating). Pure aluminum wire is evaporated in resistance heated crucibles, and known as an "evaporator boat system". Aluminum vapors pass through the glow discharge, where it combines with the ionized Argon gas and is rapidly transported to the part surface. The IVD process provides a uniform, dense, and adherent coating. After the coating operation is complete, parts are removed from the chamber and glass bead peened to densify the coating and also to provide a quality check on coating adhesion. An optional conversion coating may then be applied to the IVD aluminum surface.

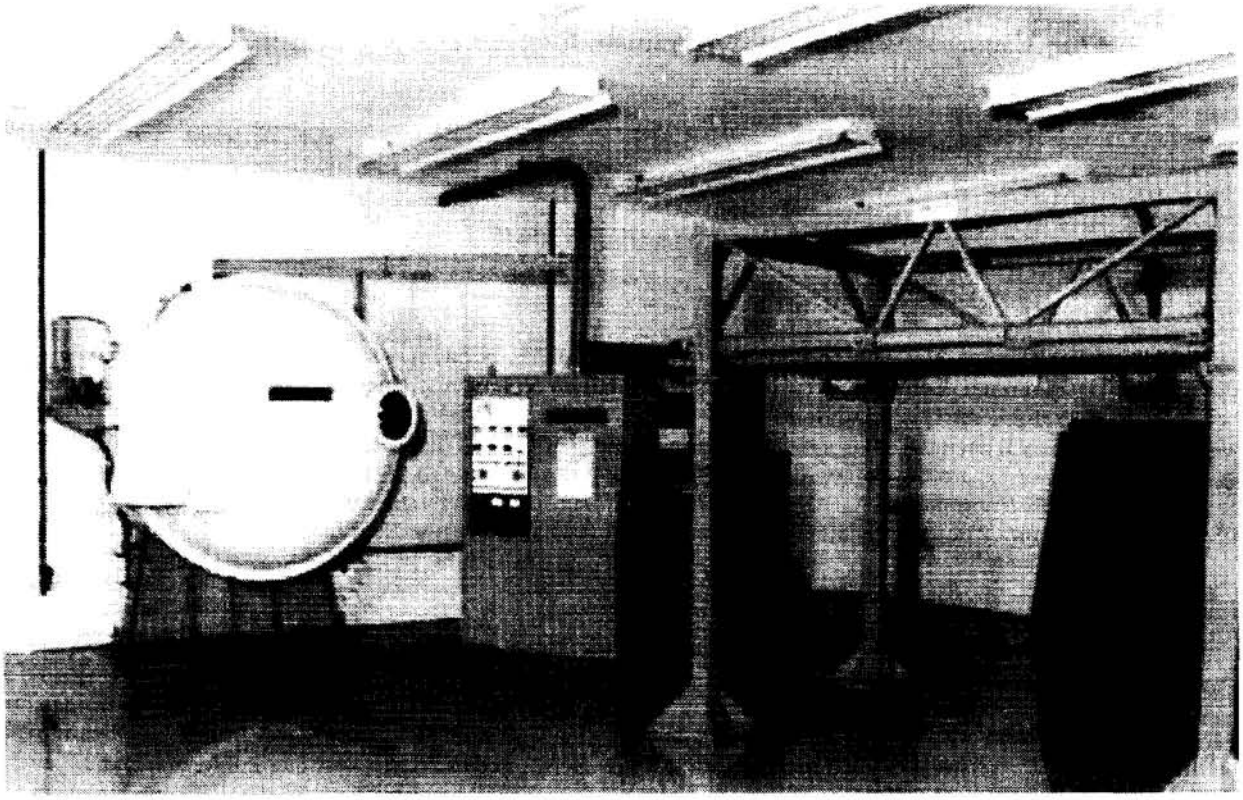

FIGURE 1. OVERALL VIEW OF AN ION VAPOR DEPOSITION FACILITY

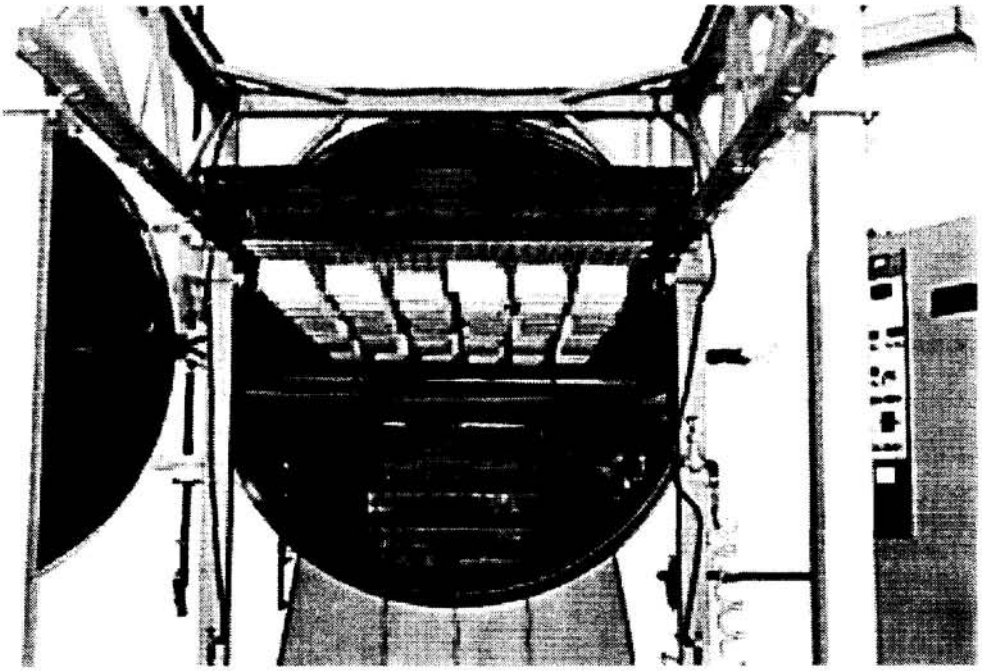

FIGURE 2. IVD CHAMBER WITH DOOR OPEN AND RACKED PANELS

Equipment Components

The Ivadizer® consists of a steel vacuum chamber, a gas pumping system, a parts racking device, an aluminum evaporation source, and a high voltage power supply as shown in Figure 3.

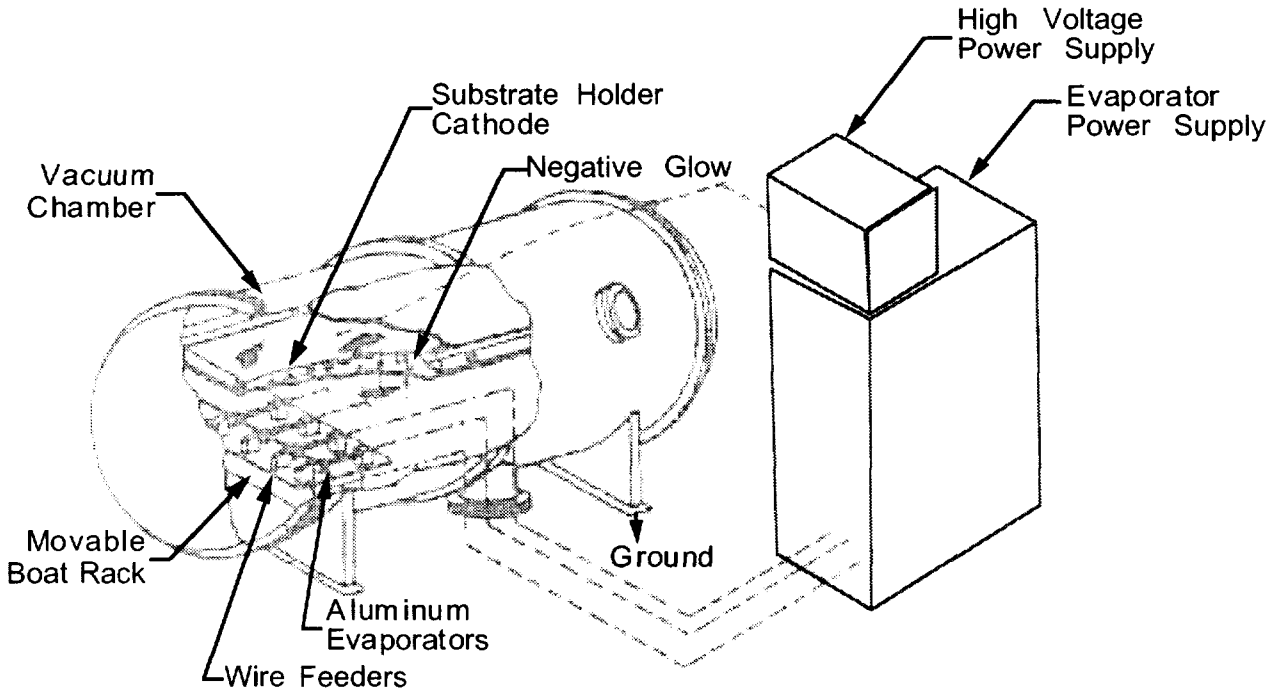

FIGURE 3. SCHEMATIC OF AN ION VAPOR DEPOSITION SYSTEM

The system utilizes conventional vacuum pumping technology components controlled by a microprocessor based control system capable of monitoring stem sequencing, system alarms, process timing, and data recording functions. A special Cryo (cryogenic cooling) Pump is an optional piece of equipment that is used during chamber pump down to help condense and freeze moisture rapidly. It significantly reduces pump down time for the oil diffusion to obtain high vacuum values of 8X10-5 Torr. As shown in Figure 1, only the front end of the vacuum chamber needs to be placed in a humidity controlled (air conditioned) environment. Parts rack and prepared parts are also kept in the air conditioned room to preclude moisture absorption prior to chamber insertion. The rear section of the chamber, vacuum pumps, Argon gas supply, and vents can be effectively kept at outside ambient conditions thereby significantly reducing air conditioning requirements. Another optional piece of equipment is known as a "Barrel Coater", that allows the coating of hundreds of small parts by utilizing a specially designed tumbling fixture that rotates inside the Ivadizer® vacuum chamber during processing.

Coating Properties

IVD aluminum coatings are very uniform and provide excellent area coverage. They are not limited to line-of-sight coverage and can produce a range of thickness' from approximately 0.0001" – 0.005"+. IVD coatings do not build up or leave holidays on sharp edges, regardless of the applied coating thickness. Figure 4 shows a typical test panel with excellent uniformity and density of IVD aluminum coating. It is possible to hard-coat anodize a portion of the relatively soft, pure aluminum IVD coating, thereby providing a very hard and durable/non-conductive surface. By leaving a soft compliant inner layer as shown in Figure 5, fracture toughness properties of a high strength aluminum or titanium alloy substrate will not be effected. IVD aluminum with supplemental treatment using MIL-C-5541, Class 3 material, meets the electrical contact resistance requirements of MIL-C-81706. Testing done on a previous program, allowed for evaluation of IVD aluminum coatings on various steel, aluminum and titanium alloy substrates. Salt fog testing per ASTM B 117, along with both beach exposure, seawater immersion and

alternate immersion testing, showed the outstanding corrosion protection afforded those substrates. NASA–MSFC M&P Laboratory evaluated various IVD coating/substrate combinations, and reported excellent results in NASA TM-108425. Electrochemical Impedance testing was also performed on uncoated steel alloy test panels and are published in NASA TP-2820 and serves as an excellent comparison of corrosion effects between coated and uncoated materials. McDonnell Aircraft Company published a 3 Phase Report No. C-87-101602 (2-1-88 to 8-31-92) for the Air Force, describing thousands of tests performed with IVD coatings used for corrosion prevention. IT Environmental Programs, Inc. published a report CETHA-TS-CR-91054, in April, 1992, for the US Army Corps of Engineers; concerning the evaluation of IVD aluminum at the Anniston Army Depot in Anniston, Alabama. In 1996, the USBI Co. Vice President's Office received a Letter of Appreciation from Lockheed Martin Corp./Johnson Controls on the recommendation of USBI Co. IR&D for using IVD Aluminum on Titan IV platform sheaves on the IUS element. Over 800 man-hours of maintenance was saved due to the superior corrosion protection of the IVD aluminum coating.

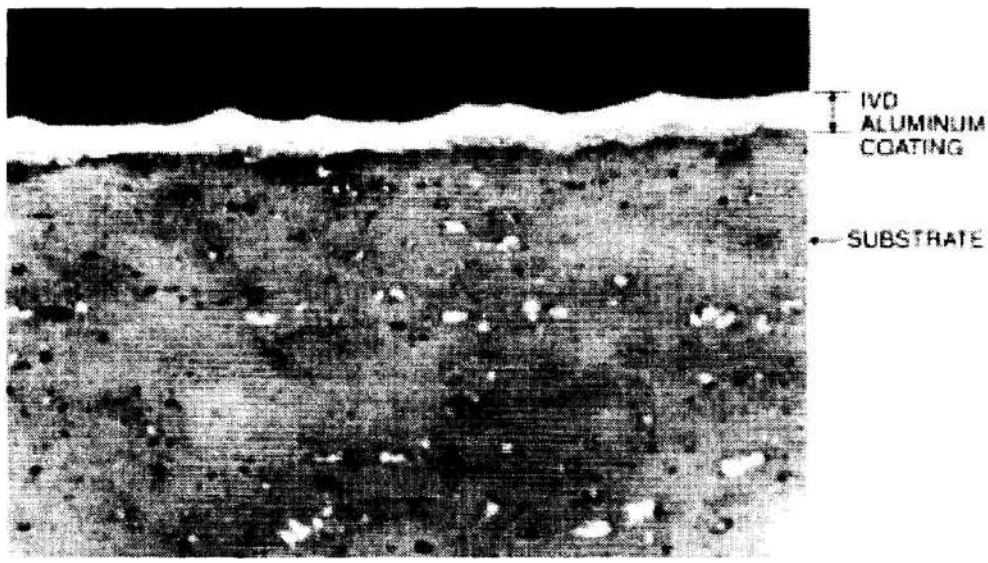

FIGURE 4. IVD ALUMINUM COATING

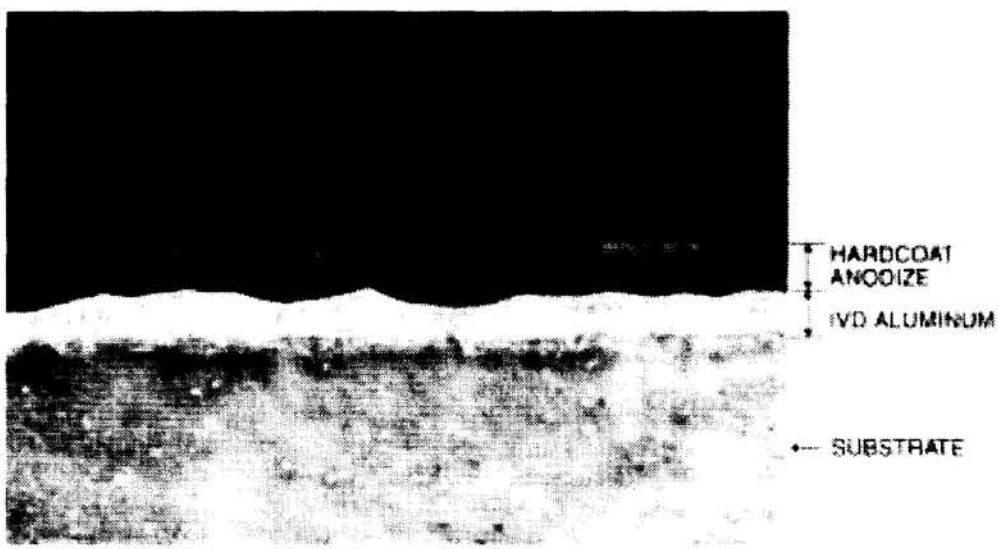

FIGURE 5. IVD ALUMINUM/HARDCOAT ANODIZE COATINGS

Selection of First SRB Flight Hardware Item for IVD Application

As a result of conversations between MSFC-SRB Program Management, USA SRB Element Mechanical Engineering, Procurement, Program Management, and M&P, it was decided to select the Drogue Ratchet Assembly for the first SRB flight hardware item IVD Aluminum coating application. One of the key reasons for selecting the Drogue Ratchet Assembly was the difficulty that Procurement encountered in obtaining new hardware. It was therefore necessary to certify the Ratchet Assemblies for multi-flight use. IVD aluminum coating is extremely tenacious, affords excellent corrosion protection and it was estimated that because of these excellent properties, will allow for multi-flight use of the Ratchet Assemblies before having to re-apply the IVD aluminum coating. Figure 6 shows the overall configuration of the Drogue/Pilot Parachute Assembly, contained by the Frustum, as part of the SRB Forward Assembly. Figure 7 shows a close-up of the Cadmium plated Drogue Ratchet Assembly.

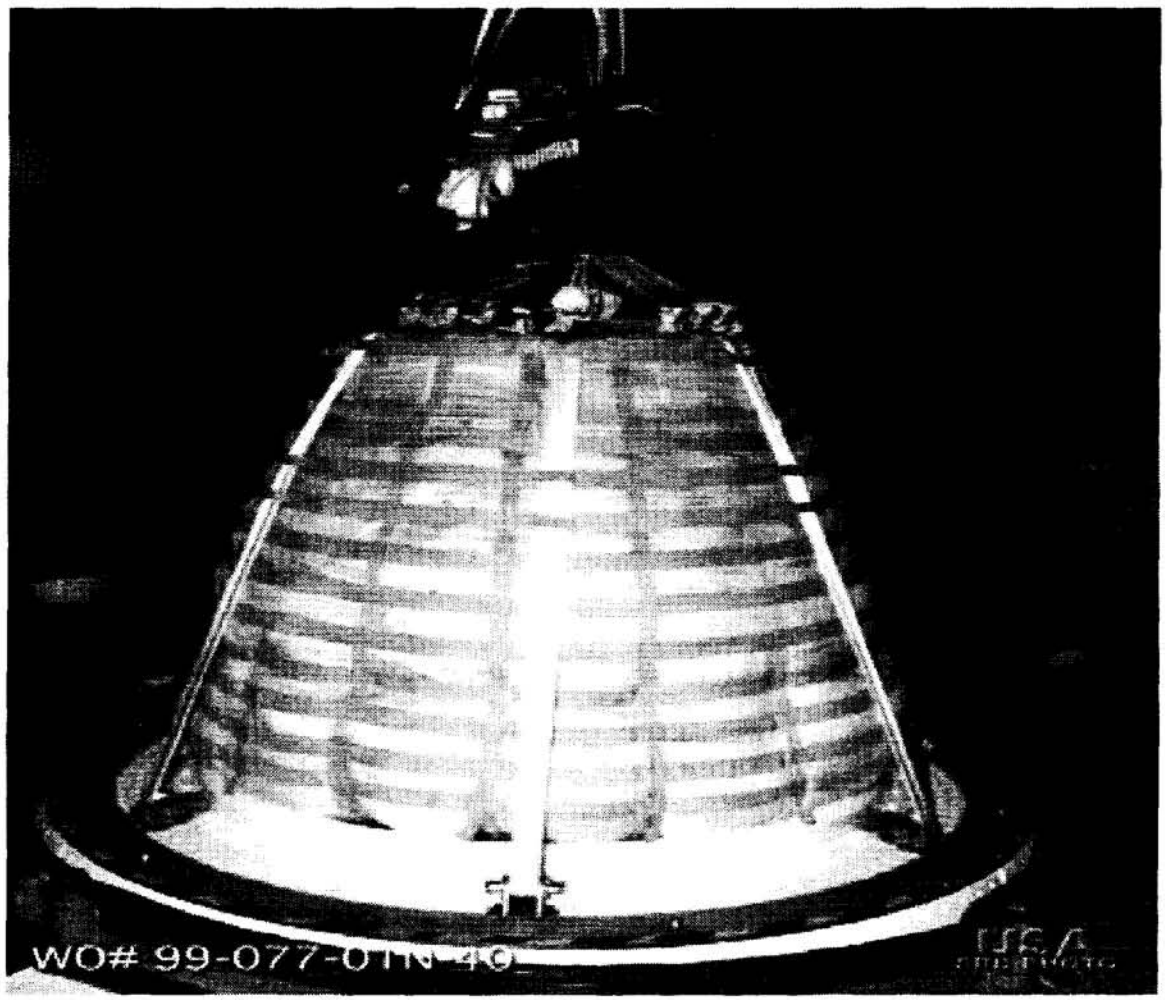

FIGURE 6. DROGUE/PILOT PARACHUTE ASSEMBLY

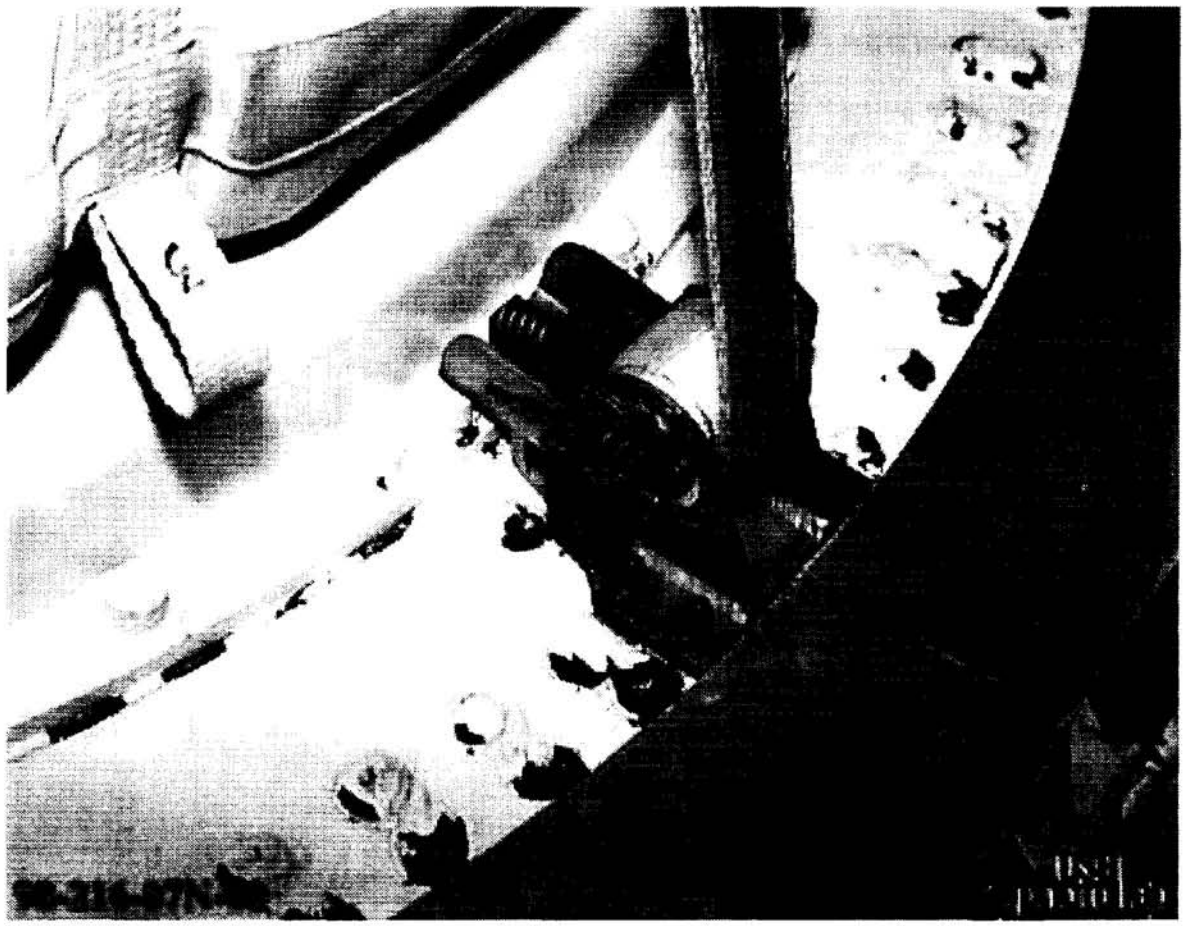

FIGURE 7. CADMIUM PLATED DROGUE PARACHUTE RATCHET ASSEMBLY

Corrosion Testing of IVD Coated Ratchet Assembly

Corrosion testing of Drogue Ratchet assemblies was performed at the KSC Beach Exposure / Seawater Immersion Corrosion sites. Ratchet assemblies were mounted to specially designed racks, facing the ocean, and located approximately 100 feet from the high tide line. Environmental effects at the Beach Exposure site are severe, and include salt fog and spray, wind driven sand, high ultra-violet exposure, solar heating, condensation of salt laden air at night, and SRB exhaust during lift-off of the Space Shuttle. For seawater immersion testing, Ratchet assemblies were first tethered, then suspended in a seawater immersion - corrosion test tank. Fresh filtered seawater was pumped from the Ocean to flow once through the tank to drain. Tanks were exposed to sunlight, so significant algae growth was experienced during the test program.

Beach Exposure Testing

It was the intent of this program to photo-document all testing at periodic intervals using a high resolution Digital Imaging Camera. Digital images were readily transferred to personal computers and inserted in report format. Rack mounted IVD coated Ratchet assemblies and disassembled sub-parts, were tested for over one year at the KSC Beach Exposure site. Figure 8 shows a typical Beach Exposure Rack with mounted parts. A general comment on Beach Exposure testing is; that all IVD aluminum coated hardware remained in the same rack locations without human interference for the extent of the test program. Periodic photo documentation helped the evaluation process. IVD coated hardware performed very consistently over the testing period, and assemblies tested did not fail the exposure criteria of visible "Red-Rust. Formal testing was completed on December 8, 1999; however, parts were allowed to remain on the racks and have not shown signs of failure to date.

FIGURE 8. IVD COATED RATCHETS MOUNTED TO BEACH EXPOSURE RACK

Seawater Immersion Testing

Over three months of seawater immersion-corrosion testing of Drogue Ratchet assemblies was completed at the KSC Seawater Immersion Facility. Because of solar radiation effects, significant algae growth was experienced on test parts. Photo documentation showed algae growth before and after wiping down at each inspection interval. There were some calcerious deposits on the base of Ratchet assembly parts shielded from the sun, and on those areas shielded from the sun, there was virtually no algae growth. Photos document the excellent resistance that IVD aluminum coating has to the seawater immersion corrosion environment. No "Red-Rust" was evident on any of the test items at the end of the test period, and to date there is no change in the appearance of the IVD aluminum coating. Figures 9 and 10 show Ratchet assemblies after 3 months of testing with algae growth and after hand wipe.

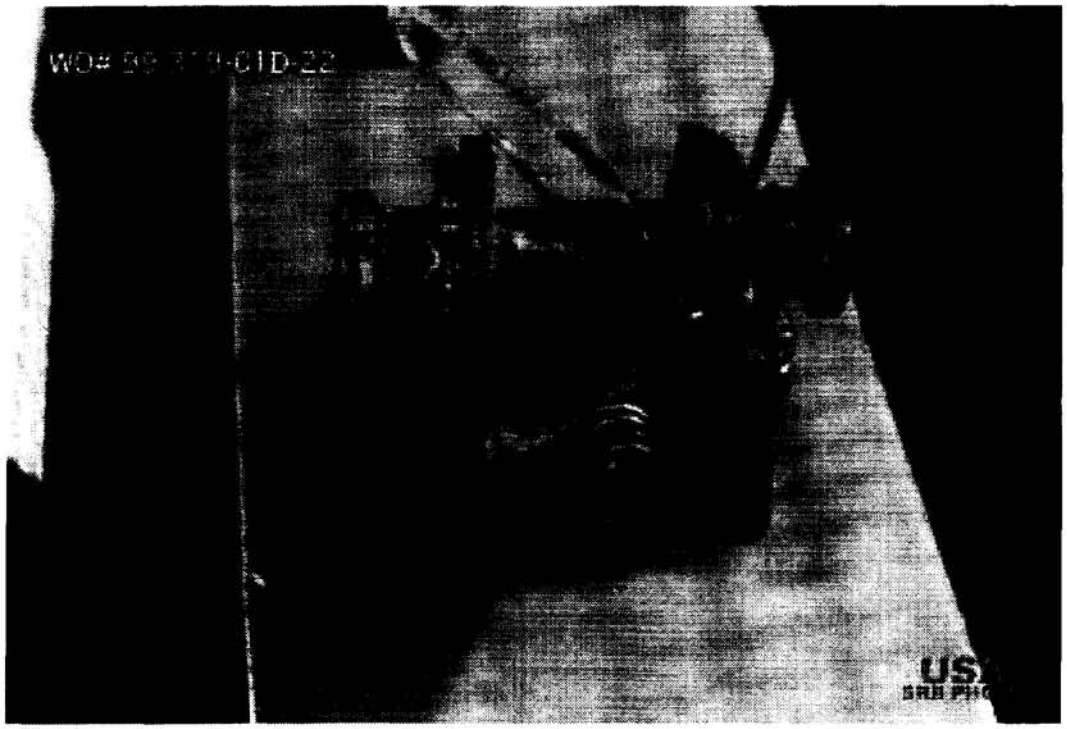

FIGURE 9. IVD COATED RATCHET AFTER SEAWATER IMMERSION /ALGAE GROWTH

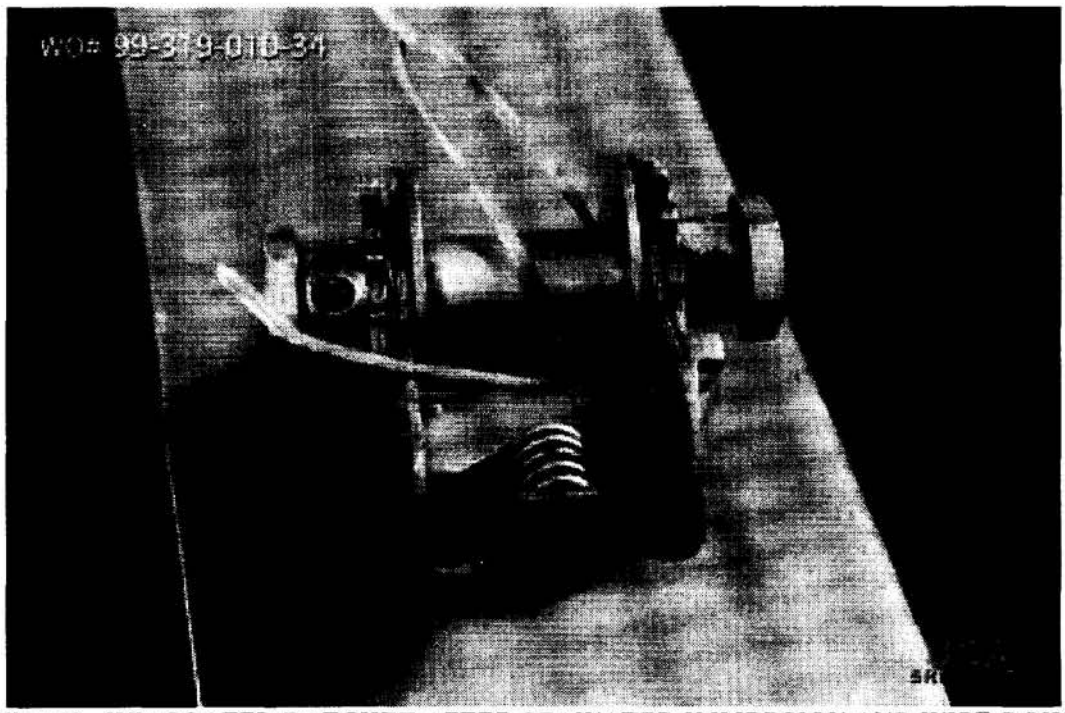

FIGURE 10. IVD COATED RATCHET AFTER SEAWATER IMMERSION AND WIPE-DOWN

Conclusions

As a result of a carefully executed and documented test program at USA SRB Florida Operations, it was found that the IVD aluminum coating process has many potential uses on SRB flight hardware and GSE. The replacement of toxic coatings such as cadmium plating, and chromate bearing paint primers with the IVD process should help mitigate or eliminate hazardous waste streams and human exposure to those materials. IVD is a very robust coating and it is visualized that it will be able to fly Multi-Missions before replacement. It is a perfect candidate material for Wash-Dry-Fly scenarios. Drogue Ratchet Assembly drawings have been changed to reflect the use of the environmentally compatible IVD aluminum coating. Flight hardware items are in process of being coated at this time.

P/S18/N/36

High Temperature Material Performance Testing Using Continuous Wave Carbon Dioxide Lasers

Timothy N. Johnson
Anteon Corporation
P. O. Box 33647
Wright Patterson AFB, Ohio 45433
Phone: (937) 252-3132 x3016; Fax: (937) 252-0418
e-mail: timothy.johnson2@ml.wpafb.af.mil

ABSTRACT

A key aspect of material development is the ability to simulate the anticipated real world application in a controlled laboratory environment. The use of continuous wave carbon dioxide lasers to simulate anticipated heat loads on high temperature materials is an efficient and cost effective tool for evaluating the performance of aerospace materials. This paper describes the use of lasers to simulate heat loads in the evaluation of aerospace material performance. Test methodology and diagnostics are described with representative data presented.

The use of continuous wave lasers as radiant heating sources have many advantages in the evaluation of high temperature materials. Thousands of material performance tests have been conducted at the Laser Hardened Material Evaluation Laboratory (LHMEL) on many of the internal ablative insulation materials used in solid rocket motors. The testing has encompassed incident heat flux rates from 25 W/cm^2 to 5000 W/cm^2, and a maximum measured surface temperature greater than 7000°F.

Analytical modeling benefits greatly from data gathered during laser material testing by correlating the transient response of mathematical material models against the high fidelity test data acquired. The lasers at the LHMEL facility can deliver up to 100 kW of power on target with a uniform spatial distribution. By providing a flat heat flux profile, simple geometric models can be used to ensure the proper physics of material response are being modeling. Historical material response data collected for modeling support includes, but is not limited to, temperature profiles, density profiles, pressure profiles, surface temperature response, and mass loss measurements. Specimens have been tested in environmental conditions ranging from a high vacuum (1x10^{-6} Torr) to high velocity flow (up to Mach 2.2) in either oxidizing or inert atmospheres.

1. Introduction

The interaction of laser irradiation with materials has been investigated extensively over the past three decades. Laser systems ranging in power from milliwatts to multi-kilowatts are used in materials processing applications such as welding, cutting and surface modification as well as in testing applications to characterize the optical and thermal response of materials. Materials processing and materials testing/characterization are two applications that require rigid controllability and temporal stability of the amount of laser energy delivered to a materials surface. For the former, a high quality beam is required to allow near-diffraction limited focal conditions to be achieved and maintained. For the latter, a uniform spatial intensity distribution is desired over the surface of the test sample. It is this last category that must be achieved in order to use a laser source as a thermal simulation tool for high-heat-flux engineering applications. In addition, the thermal conditions created at a sample surface by a laser must be matched to conditions indicative of the normal operating environment of interest. The Laser Hardened Materials Evaluation Laboratory (LHMEL), located at Wright-Patterson Air Force Base, Ohio, is a robust multi-laser test facility capable of producing extreme thermal environments in open-air, high velocity flow, and in vacuum. This paper describes the laser, environmental simulation, and diagnostics systems available at LHMEL for thermal characterization testing. A brief description of thermal response testing performed at the facility is included.

2. Thermal Simulation Using Laser Systems

For thermal response characterization of a material or system, laser energy delivered to the test surface must have high spatial uniformity and temporal stability so that precise, repeatable and controllable characteristics are produced at the target. Under ideal circumstances for the materials or systems tester, the laser should be nothing more than a well characterized and dependable tool. The following sections describe the performance capabilities of the carbon dioxide laser devices available at LHMEL. LHMEL lasers are thoroughly characterized for testing purposes with output power measurement systems calibrated on an annual basis to the National Institute of Standards and Technology (NIST) primary standard for laser measurement[1].

2.1. LHMEL Carbon Dioxide Lasers

The carbon dioxide (CO_2) laser systems available at the LHMEL facility are capable of producing output beams that have temporally stable, radially symmetric intensity distributions. Besides high performance reliability, beam spatial uniformity, and economically favorable operating characteristics, a between firing turn-around time on the order of minutes makes them very attractive for test applications. The laser systems are continuous wave CO_2 electric discharge coaxial lasers. Each laser operates at a wavelength of 10.6μm and produces a multimode output beam having a flat top spatial intensity distribution. Figure 1 shows the spatial intensity distribution measured for the output beam

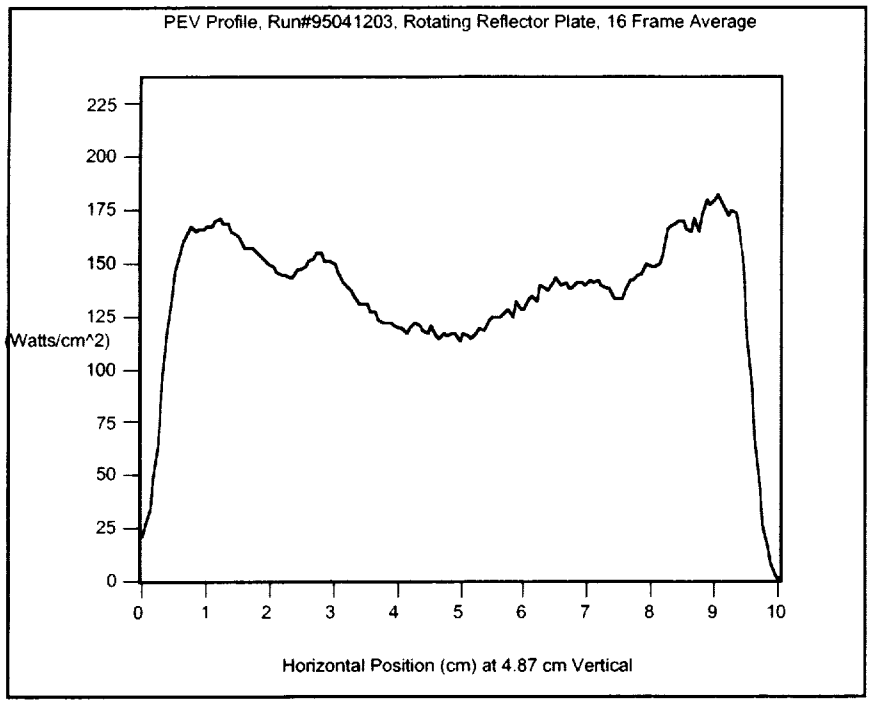

Figure 1 The spatial intensity distribution of the LHMEL I output beam varies no more than 17% from the average intensity across the beam diameter.

produced by the LHMEL I 15kW laser device. The measurement was made using the pyroelectric vidicon camera system discussed in section 4.1 of this paper. The maximum and minimum values deviate from the average intensity across the beam diameter by only ±17%. The uniformity of this spatial intensity distribution is ideal for thermal characterization testing requirements.

The LHMEL lasers can maintain power levels on target to within an average variation of ±5%. This stability is maintained over the entire target irradiation time lasting up to 80 seconds at maximum power. Longer shot durations are achieved when the lasers are operated at lower power levels. These reliable and repeatable lasers allow measurements of thermal properties to be made consistently, accurately and in a way that is easily modeled and analyzed using standard thermodynamics computer codes.

Testing applications aimed at characterizing the performance of materials and systems in high heat environments call for well defined thermal sources. These thermal sources must be capable of producing uniform heat loads over areas up to $5cm^2$ for high heat flux applications[2] and up to $300cm^2$ for applications requiring cooling for high heat load optical components[3]. LHMEL s beam transfer optics can produce beam diameters ranging from 0.6 to 100cm (0.25 to 40 inches). Figure 2 shows the maximum laser beam irradiance levels achievable for beam diameters ranging from 1 to 100cm. The lines shown correspond to the maximum output power delivered to a sample surface by the lasers listed. Each laser can be operated at lower powers allowing irradiance conditions anywhere below these maximum levels to be achieved.

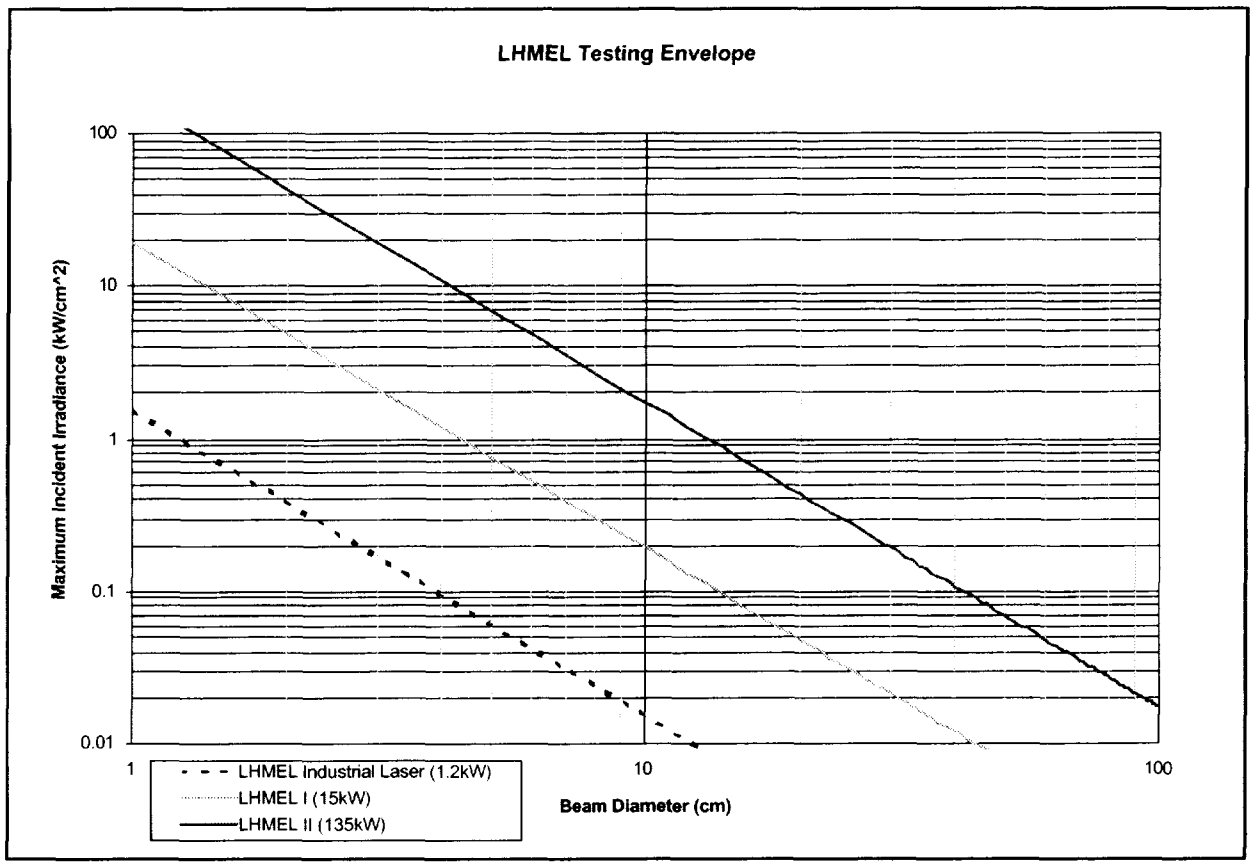

Figure 2 LHMEL carbon dioxide lasers can achieve irradiance levels up to the values shown for laser beam diameters ranging from 1 to 100 centimeters.

3. Environmental Simulation

Many testing applications investigate the response of materials or systems subjected to thermal energy input while experiencing specific environmental conditions local to the sample. The environmental simulation capability available at LHMEL consists of: 1) environmental chambers allowing specific pressure and/or gas composition conditions, 2) wind tunnel systems providing specific velocity and/or thermal transfer conditions, and, 3) dynamic mechanical loading up to 55,000 pounds.

3.1. Environmental Chambers

Two environmental chambers are available at the LHMEL facility. The operating characteristics of these environmental chambers are summarized in Table 1. These chambers are equipped with pumping capability to attain vacuum levels to 1×10^{-6} torr or can be filled with specific gases or gas compositions up to two atmospheres (30 psia). Each chamber is equipped with a window allowing laser output to be delivered to a test sample. A 30 inch diameter chamber, 40 inches in length, can accommodate a maximum test article dimension of

20cm (8 inches). The second chamber is 7 feet in diameter by 9 feet in length and can accommodate a maximum sample dimension of 120cm (47 inches).

Table 1 LHMEL environmental chambers

Chamber Dimensions (diameter x length)	**30 inches x 40 inches**	**7 feet x 9 Feet**
Routine Vacuum	$1x10^{-5}$ torr	$1x10^{-6}$ torr
Average Pumpdown time	30 min	30 min
Minimum Laser Spot Size on Target (Diameter)	1.6cm	15cm
Maximum Laser Spot Size on Target (Diameter)	16cm	100cm
Instrumentation Ports (viewing)	6 (8-1/2in. i.d.)	9 (5-1/ in. i.d.)
High Vacuum Signal Feedthrough	4 (2-3/4in. o.d.)	7 (2-3/4in. o.d.)
Maximum Number of Pumpdown Sequences per Day	10	5

3.2. LHMEL wind tunnels

Wind tunnels are available to provide air or nitrogen gas flow over material test specimens during irradiation. The wind tunnels are blow-down systems driven by a regulated high-pressure supply that exhausts into a plenum upstream of converging nozzle. The LHMEL wind tunnels can be equipped with one of two converging nozzles (5x5cm and 5x10cm) each producing subsonic flow ranging from 0.05 to 0.9 Mach. An expansion nozzle can also be attached to the 5x5cm converging nozzle allowing supersonic conditions up to Mach 2.0 to be achieved. Table 2 summarizes the performance capabilities of the wind tunnels available at the LHMEL facility. Figure 3 shows a typical test arrangement, in this case, using the supersonic nozzle configuration. Test specimens are positioned in the center of the characterized flow stream. They are held in place by thermally insulated mounts that prevent heat transfer from the test sample into the mount structure. The test sample and mounting plate are positioned with upper and lower walls to form a three-wall channel. The three-wall channel maximizes flow uniformity across the face of the test sample. A step, producing turbulence proportional to size, can be incorporated at the nozzle exit. The laser beam is directed to the sample surface through the open section of the three-wall channel. The LHMEL I wind tunnel can be rotated in 5-degree increments about the axis of symmetry of the exhaust jet if laser irradiance other than normal to the surface is desired. In addition, the optical delivery system for both lasers can be adjusted for incidence angles up to 60 degrees. Exhaust ducts are provided to remove sample debris and wind tunnel gasses.

Table 2 LHMEL wind tunnel operating characteristics

Parameter	LHMEL Wind Tunnel
Mach Number	0.05 to 2.0
Nozzle Exit Sizes	5x5cm, 5x10cm
Operating Medium	Air or Nitrogen
Operating Mode	Blow-down, Bottled Compressed Gas
Test Section Type	Free Jet, Channel or Flat Plate
Mass Transfer Coefficient	0.02 to 0.13lbm/ft^2 sec
Aerodynamic Shear Stress	0.001 to 0.04lbf/in^2

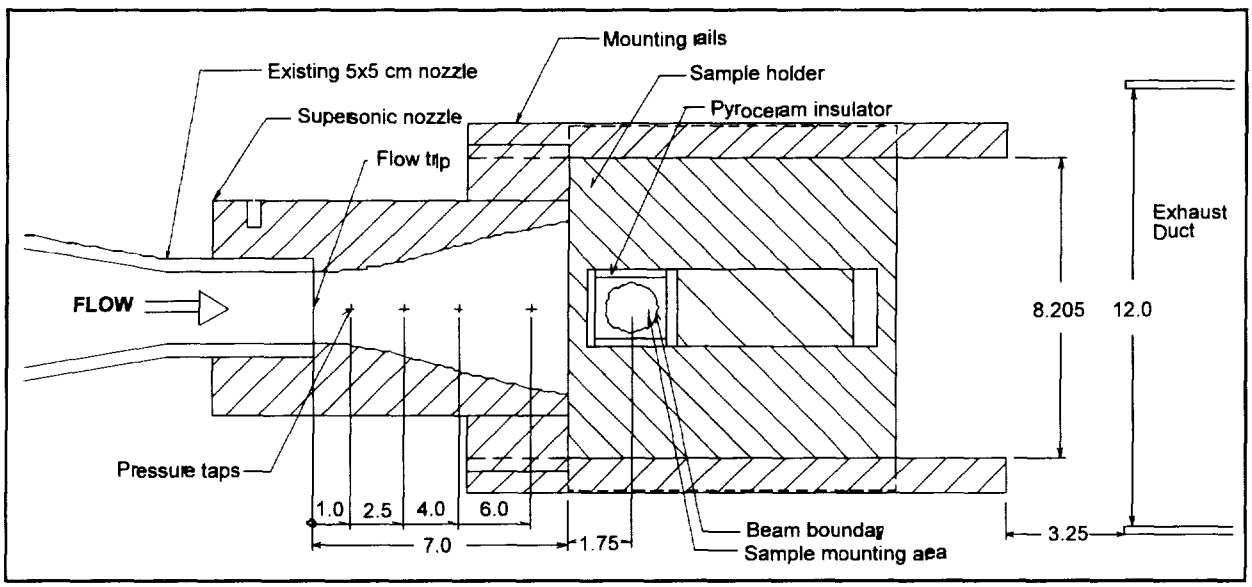

Figure 3 An expansion nozzle attached to a subsonic converging nozzle allows supersonic flow up to Mach 2.0 to be achieved. The sample mounting position is located immediately downstream of the nozzle. (Dimensions in inches)

3.3. Mechanical loading

Two tensile test machines are available to load test specimens concurrent with laser and wind tunnel operation. One is a Tinius-Olsen tensile test machine (Model Super L) with a maximum loading of 55,000lb. The second machine is an Instron model 4204 test machine with a maximum loading of 10,000lb. Both tensile test machines can be used either with LHMEL I or LHMEL II testing. Various mounting jaws are available for use with each machine to provide a wide range of testing configurations.

4. Test Diagnostics

4.1. Surface Temperature

Surface temperature is one of the most important parameters to measure during materials or systems testing. Accordingly, the LHMEL uses a variety of methods to make surface temperature measurements.

4.1.1. Thermocouples

One of the most basic and accurate ways of measuring surface temperature is through the use of thermocouples. Thermocouples make direct contact measurements of changes in temperature during a test. Type K thermocouples located outside the perimeter of the laser irradiated area can accurately measure temperatures up to 1,270°C. Thermocouples can also be embedded into the depth of a material or mounted on the back face of a sample. Calibration of thermocouples to a reference block is accomplished prior to every test ensuring signal continuity and measurement accuracy.

4.1.2. Pyrometers

Several non-contact methods of measuring surface temperature are available at LHMEL. A variety of pyrometers spanning the range of measurement from 600 to 6,000°C are used to measure surface temperatures within the irradiated area of the test sample. For absolute measurements of surface temperature using pyrometers, sample emissivity must be known. An example of this measurement is shown in Figure 4.

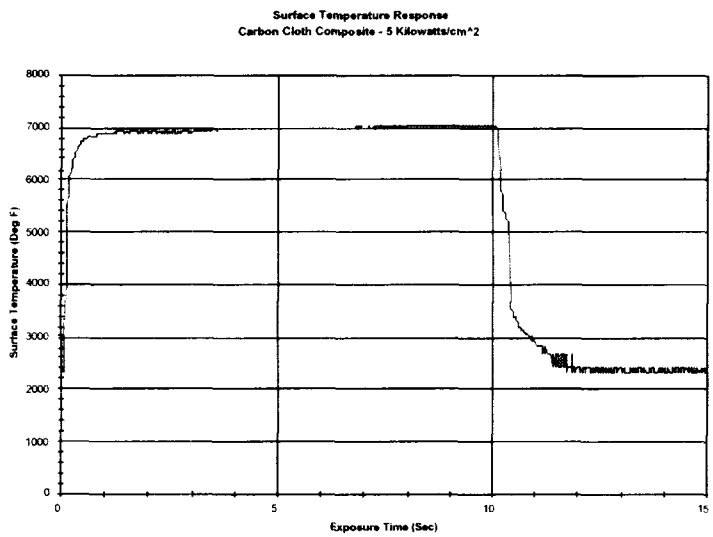

Figure 4: The measured surface temperature response of a carbon cloth composite when exposed to a laser irradiance of 5 kilowatts per square centimeter.

4.1.3. Infrared Imaging Systems

An infra-red camera system is also available for non-intrusive temperature measurements of test articles. The system presents a colored image of the imaged sample area with the different colors corresponding to different temperatures. The camera employs a 30-element mercury cadmium telluride, thermoelectrically-cooled detector sensitive to infrared radiation in the 3.2 to 5.6_m region. It can detect temperature differences in thermal patterns from 0°C to 600°C with a sensitivity of 0.1°C. The field of view is 20° in the vertical direction and 27° in the horizontal direction. Up to 128 video temperature levels can be displayed in color or black and white in 525 line/60 Hz format.

In addition to the infra-red camera, a pyroelectric vidicon camera (PEV), discussed previously in section 2.1 of this paper, is used to image the target plane. The pyroelectric vidicon camera uses a tri-glyceride-sulfide crystalline matrix, sensitive to infrared radiation in the 8 to 12μm region. The thermal sensitivity of the camera is approximately 0.2°C at 100°C and is uniform across the PEV crystal to within ±6%. The PEV camera has a RS170 format, which can be recorded on a video recorder or interfaced with a frame grabber and associated computer software. Up to 16 frames taken at pre-determined time intervals during the laser run time can be stored for later processing. The software capabilities for beam profile display include 2-D contour plots, line profile plots and 3-D surface plots. Analysis functions include the ability to locate the peak intensity, calibrate peak-to-average power ratio, and calculate distribution statistics over a defined area of interest.

4.2. Video and photographic equipment

The LHMEL facility has a variety of equipment suitable for video recording of laser/sample interactions. Black-and-white and color CCD cameras are available for use along with video cassette recorders. A variety of lenses are available for use to provide wide angle or magnified views. The LHMEL staff relies upon a broad range of experience to produce optimum visual records by selecting lenses, exposure settings and gelatin neutral density filters appropriate to materials properties and laser irradiance levels.

Still photographic coverage can also be accommodated by the LHMEL facility. An experienced photographer is on staff to advise or take 35-mm pre-test and post-test sample photographs. Camera lenses that provide wide angle or highly magnified views are available for use. Cameras may also be used to record experimental set-ups including beam trains, sample configurations, and diagnostic equipment locations.

The LHMEL facility has available two Hycam 16-mm cameras (20 to 11,000 frames per second) and one Locam II 16-mm camera (2 to 500 frames per second) along with associated optics, lighting, and mounts. IRIG timing pulses can be placed on the edge of the film by one of the Hycam cameras. The cameras can accept rolls of film up to 400ft in length. Cameras and lighting are actuated automatically in sequence with the laser.

5. Material Performance Testing

Recent tests performed at the LHMEL facility have demonstrated that CO_2 laser radiation can be used to evaluate the performance of composite ablative insulation materials at extreme temperatures and heating rates. Two primary aerospace applications of composite ablative insulation are heat shields for atmospheric reentry vehicles, and nozzle liner material used in solid rocket motors. To date, materials used for both of these applications have been successfully tested at the LHMEL facility.

The primary heat transfer mechanisms within the dynamic internal environment of an active solid rocket nozzle are convection and radiation, as compared with a primarily convective environment for heat shields. Comparatively, a laser heats a surface purely by radiative transfer of energy. Fortunately, carbon phenolic is an optically opaque material, meaning that radiation is absorbed within a few microns at the surface. This also means that the thermal response of carbon phenolic will be identical for both radiative and convective heating conditions. Therefore, the laser can simulate the equivalent heating conditions expected during rocket nozzle firing or a reentry of a heat shield by establishing irradiance conditions matching the net heat flux into the material surface and establishing the proper environmental conditions to match the rate of surface recession during exposure.

There are situations when the optimum combination of material surface heating rates and environmental boundary conditions cannot be reproduced in the laboratory. In these situations, relative material performance evaluations can be conducted by exploiting the controlled performance characteristics and the extensive instrumentation capabilities of the LHMEL facility. By conducting a short series of experiments with properly instrumented specimens, a baseline performance for that material can be obtained. A performance comparison can be obtained by repeating these experiments with other candidate materials. Although the exact conditions do not directly represent the actual flight condition, the relative performance of the materials can be evaluated in conditions representative of the flight condition.

The LHMEL facility is ideal for generating data for use in analytical model development and validation. A material test can be instrumented to such detail that a fully bounded set of response data is generated. For example, by measuring the surface temperature response of a sample with the use of an optical pyrometer, monitoring the in-depth and back face thermal response with imbedded thermocouples, the complete transient thermal profile of the specimen is obtained. This type of complete data is invaluable to the analyst, since it eliminates many of the uncertainties generally associated with other conventional means of obtaining high temperature and high heating rate material performance data. The ability to have a clear and unobstructed view of the exposed specimen surface is a great advantage to laser material response testing. This ability is usually not available when conducting full-scale flight or sub-scale static tests, or when using other laboratory convective heating sources.

5.1. Material Performance Testing of Solid Rocket Motor Nozzle Liner Materials

An extensive series of laser experiments has been performed on the carbon cloth phenolic used as a nozzle liner ablative insulation for the solid rocket motors used on the Space Shuttle. The carbon dioxide lasers and high velocity flow capabilities at LHMEL were combined to investigate the response of carbon phenolic test samples[4].

A series of experiments have been developed and conducted to obtain material performance data on carbon cloth phenolic as it is exposed to extreme heating rates. Each of these experiments was specifically designed to obtain a specific piece of material performance data for direct support of analytical material model development. If possible, the experiments were designed to measure material performance as the test specimen was being irradiated. This type of experiment is commonly referred to as a real time experiment.

The real time material performance data that has been obtained from these experiments includes, but is not limited to; flame surface, in-depth, and back face temperatures, in-depth density profiles, specimen weight loss, flame surface erosion rates, decomposition kinetics, internal pyrolysis gas pressure distributions, the kinetic energy of pyrolysis gas flow exiting the flame surface, the permeability of a forming and cooling char layer, as well as the physical swelling of a partially restrained specimen. The data obtained from these experiments, combined with existing historical material performance data have given insight into material performance issues that have been debated over the past 30 years. Figure 5 shows an example of the data generated during a series of tests in which a known incident laser intensity was delivered to the sample[5]. The samples were tested under fully characterized compressed air flow (0.5 Mach) conditions for comparison with theoretical predictions in order to validate the test method. Each of the data curves displayed in Figure 5 was gathered from an individual test specimen. Due to the consistent performance of the laser system, the data gathered from discrete tests can be treated as though it were all gathered on a single specimen.

Figure 6 shows an example of the consistency of data produced at the LHMEL facility and the repeated accuracy of the test procedures. The ability to treat the gathered data in a manner such as this greatly reduced the required complexity of test fixture design and raises the confidence associated with each of the gathered data sets. The data collected, along with other material performance thermal distribution data collected with LHMEL infrared cameras, allowed a more accurate model to be constructed predicting the thermal response for these materials.

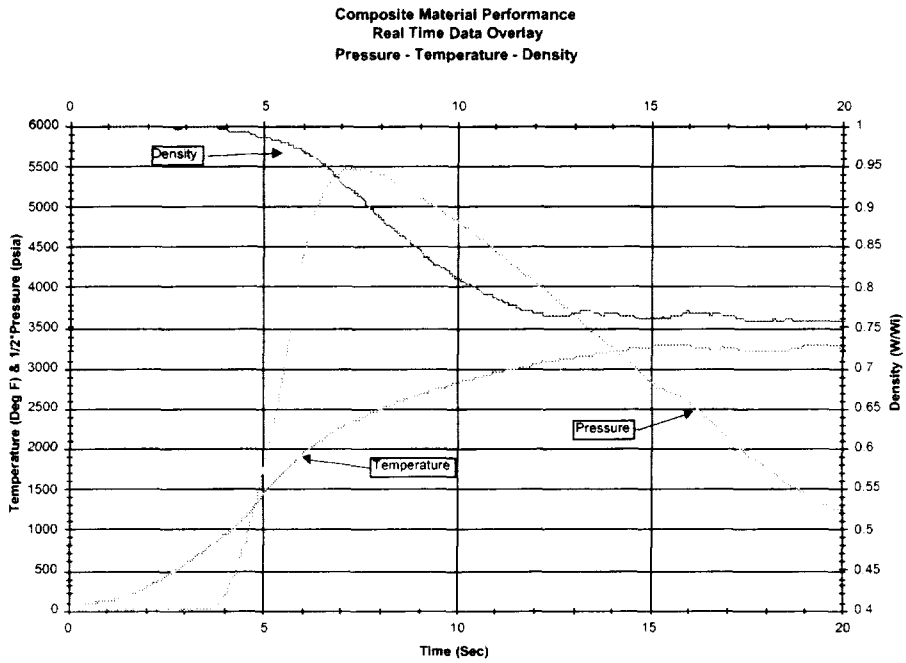

Figure 5: A more complete picture of material performance by overlaying data gathered from tests conducted with identical parameters.

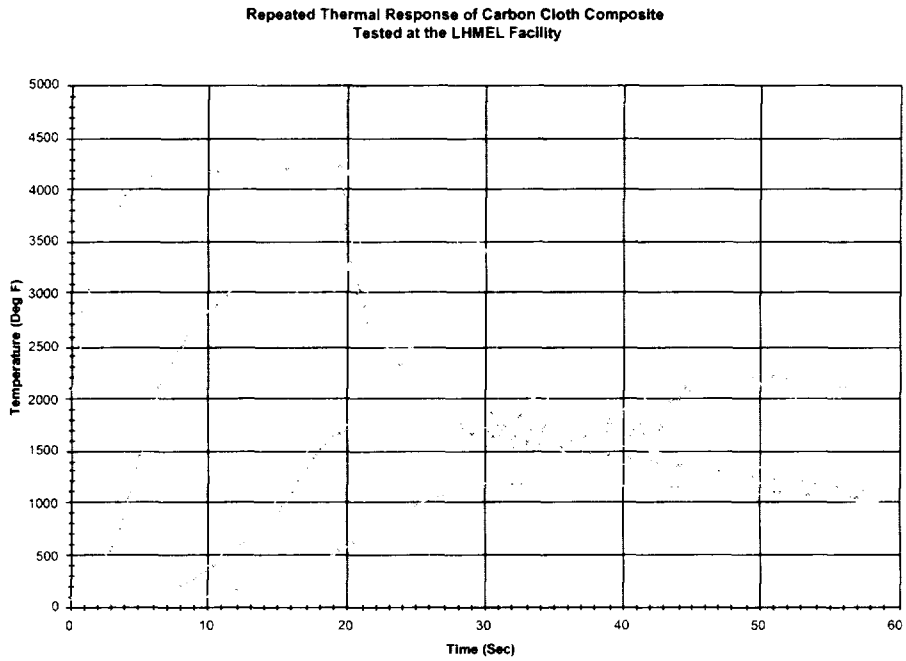

Figure 6: An example of the consistency of data generated at the LHMEL facility. Two independent temperature response tests conducted with the identical boundary conditions.

The data produced during this test series represents the first qualitative investigation of the overall response of carbon phenolic when exposed to the specific levels of thermal flux corresponding to the high heat flux environment found within an operating rocket nozzle. The test demonstrated that the use of a laser for the evaluation of rocket nozzle materials offers several advantages over alternate testing methods: 1) Lasers can simulate the thermal load experienced by rocket nozzle materials and can do so in a diagnostics-friendly environment. 2) Rocket nozzle materials can be tested under significant thermal conditions without producing the effluents and violent conditions resulting from the operation of a rocket nozzle - previously the only method used to evaluate the performance of the materials of interest. 3) The reliability and repeatability of the carbon dioxide lasers at the LHMEL facility allows a quantitative investigation of the thermal response of rocket nozzle materials where previous testing techniques provided limited meaningful data. 4) The resulting data, current and future, will allow considerable tightening in the materials tolerances relevant to designing solid rocket motor nozzles. 5) The cost of testing these materials at LHMEL is substantially lower than any other identified option.

5.2. Thermal Response Characterization Testing of Heat Shield Materials

A recent test series was conducted to evaluate the capability of the LHMEL facility to obtain high quality data to support the development and enhancement of current analytical models to predict the performance of heat shield ablative insulations. Three separate experiment test series were conducted to obtain specific material response data for the ablative insulation. Data obtained from the testing included surface and in-depth temperature response, transient mass loss, transient density profiles, and a measurement of the swell of the flame surface as the material is heated. The overall test series was completed with the successful gathering of data for each individual measurement. The experiments conducted for this series were identical to those conducted over the past three years for the nozzle liner material used in the Space Shuttle solid rocket motors. The data gathered from this test series is currently being review and processes and therefore is not available for publication in this paper.

6. Conclusion

The Laser Hardened Materials Evaluation Laboratory has applied a unique combination of high energy carbon dioxide lasers, environmental simulation and material response diagnostic capabilities to successfully simulate specific thermal conditions required for high heat flux testing applications. The highly controllable and repeatable characteristics of these high energy laser devices allow specific thermal conditions to be created at the surface of the test samples. The accuracy, repeatability and volume of data produced during these tests has been significant and has substantiated or corrected calculated predictions of material thermal and structural performance of various materials.

---

[1] M. L. Lander, J. O. Bagford, D. B. Seibert II, R. J. Hull, High power calibration of commercial power meters using an NIST-traceable secondary standard, *Journal of Laser Applications* **8**, 103-107, (1996).

[2] J. H. Rosenfeld, R. Schumaker, R. D. Watson, and J. M. McDonald, Porous media heat exchangers for high heat flux applications, *High Heat Flux Engineering, Proc. SPIE* **1997,** 53-64 (1993).
[3] F. M. Anthony, High heat load optics: an historical overview, *Opt. Eng.* **34 (2),** 313-320 (Feb. 1995).
[4] W. T. Laughlin, J. R. Koenig, Laser Analog Test Capabilities, Presented at the 1994 JANNAF Rocket Nozzle Technology Subcommittee Meeting/Seattle, WA (15-17 November 1994).
[5] T. N. Johnson, Final Test Report for PTP-0390 - Nozzle Material Integrity - High-Rate Decomposition Testing of CCP, Thiokol Wasatch Report #75979, (1998).

cp/59/IN/20

THERMOGRAPHIC NONDESTRUCTIVE EVALUATION OF THE SPACE SHUTTLE MAIN ENGINE NOZZLE

James L. Walker
Nondestructive Evaluation Team
NASA Marshall Space Flight Center
(256) 961-1784
james.l.walker@msfc.nasa.gov

Samuel S. Russell
Nondestructive Evaluation Team
NASA Marshall Space Flight Center
(256) 544-4411
sam.russell@msfc.nasa.gov

Matthew D. Lansing
Nonmetallic Materials Group
NASA Marshall Space Flight Center
(256) 544-3953
matt.lansing@msfc.nasa.gov

Paul Caraccioli
SSME Project Office
NASA Marshall Space Flight Center
(256) 544-0064
paul.caraccioli@msfc.nasa.gov

ABSTRACT

The methods and results presented in this summary address the thermographic identification of interstitial leaks in the Space Shuttle Main Engine nozzles. A highly sensitive digital infrared camera is used to record the minute cooling effects associated with a leak source, such as a crack or pinhole, hidden within the nozzle wall by observing the inner "hot wall" surface as the nozzle is pressurized. These images are enhanced by digitally subtracting a thermal reference image taken before pressurization, greatly diminishing background noise. The method provides a nonintrusive way of localizing the tube that is leaking and the exact leak source position to within a very small axial distance. Many of the factors that influence the inspectability of the nozzle are addressed; including pressure rate, peak pressure, gas type, ambient temperature and surface preparation.

INTRODUCTION

The nozzles of the Space Shuttle Main Engines (SSME) consist of over one thousand tapered Inconel coolant tubes brazed to a stainless steel structural jacket (Figure 1). Liquid hydrogen flows through the tubing under high pressure, from the aft to forward end of the nozzle, to maintain a thermal balance between the rocket exhaust and the nozzle wall. Three potential problems occur within the SSME nozzle coolant tubes as a result of manufacturing anomalies and the highly volatile service environment. These problems include poor or incomplete bonding of the tubes to the structural jacket, leaks into the interstices between the tubes and jacket, and leaks into the inner "hot wall" or "flame" side of the nozzle. Identification of hot wall leaks can be accomplished with the application of a liquid leak check solution to the inner surface of the nozzle while it is pressurized with helium gas. X-ray techniques are utilized for characterizing the condition of the braze line. The identification of interstitial leaks between the tubing and structural jacket is not as well defined and has historically been the most problematic.

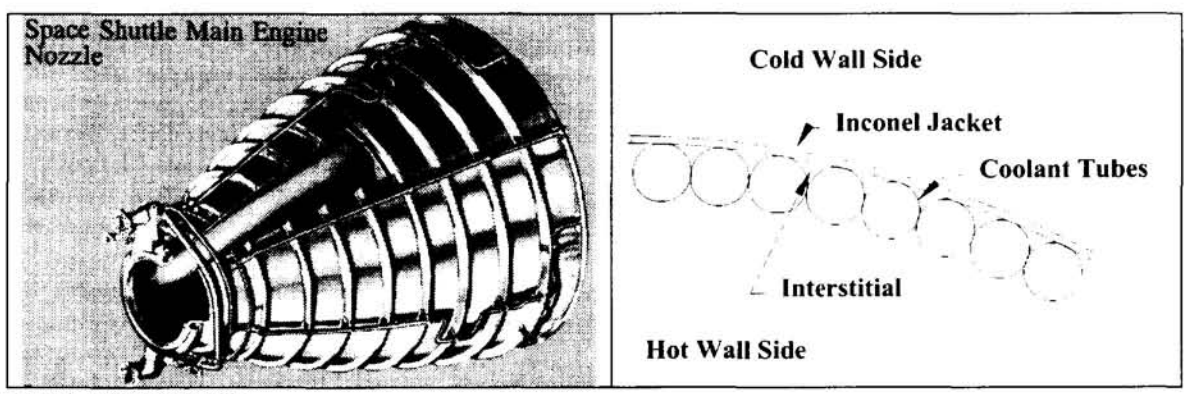

Figure 1. SSME Nozzle.

If a small leak occurs between the tubing and structural jacket the gas flows down the interstices and vents harmlessly out the aft end of the nozzle. As the leak grows though the potential exists for the nozzle to fail by

pushing a section of tubing into the hot exhaust path which in turn can cause them to rupture. If the rupture is severe enough the engine will be starved of hydrogen, and thus become oxygen rich. This at best reduces the thrust of the engine and in the worst case can endanger the launch vehicle.

Interstitial leaks are often found by first identifying which tubes are leaking by the application of a liquid leak check solution where the interstices vent at the aft end of the nozzle. Then, through a trial and error approach, tubes are cut open and an angioplasty device inserted to block off a specific region of the tube. A boroscope is then used to look at the inside of suspect tubes but leak source identification is difficult due to their typically microscopic size. With the suspect tube blocked from the pressure circuit, pressure is reapplied and the interstices leak checked again. This process is repeated until the source is located or all suspect tubes are tested. If the leak is severe enough and it cannot be found, then the nozzle must be pulled from service. Identification of which tube is leaking is difficult due to manifolding between interstices through braze line voids, resulting in the opening and inspection of many tubes that were previously undamaged. Also, when the leak originates from multiple sources it is difficult to tell if the angioplasty device has isolated a leaking tube.

BACKGROUND AND THEORY

Leaks in pressurized systems can be some of the simplest and easiest defects to identify, or they can be extremely challenging to locate. A low pressure leak check using a liquid bubble solution applied to the vessel with a brush or bottle is usually adequate if the vessel is geometrically simple and has unrestricted in access. With this method, not only can the leak be located, the leak rate can often be determined by observing the bubble formations produced in the leak check solution. Frequently though, applications exist where the leak source is inaccessible due to structural complexity. In these situations it may be possible to measure the effects of the leak on the physical condition of the structure. For example the leak may produce an audible, or ultrasonic, "hiss". For practical leak rates the magnitude of the "hiss" from the leak source may be very small making it difficult to identify over the interference from background noises. Another alternative is to record the temperature change associated with the expansion of a gas though the leak source. Here, even if the vessel has a complicated geometry, restricted assess, chemical sensitivity, or a large area, an infrared video camera may be useful for identifying, locating, and characterizing leaks. The temperature change due to a hidden leak may be observed on the outer surface of the structure provided a direct heat path is present and the structural material has an appropriate thermal conductivity. Also, infrared video cameras can inspect large areas very rapidly and with out contacting the component.

In real systems, with hidden leaks, the leak geometry is usually unknown and unpredictable making it difficult to uniquely define the physical phenomena active at the leak. The leak may act like a throttle valve, a nozzle, or a combination of both. Also, transient effects may be present including the pressurization of the gas already in the vessel, causing work on the trapped gas. For the detection of a leak, these effects do not usually need resolution or understanding. A local temperature change is simply detected. However, an understanding, or as a substitute empirical data, may be needed to locate and approximate leak rate. A discussion of some of these effects, some competing, follows.

The Joule-Thompson effect is classically exhibited in flow through a throttling restriction or valve. The flow through the restriction causes no work to be done and is considered adiabatic. For real gasses the temperature can either increase or decrease depending on the type of gas, temperature, and pressure. For each given gas there is an inversion temperature at which no temperature change occurs for the throttling process. This inversion temperature is a weak function of temperature. Below the inversion temperature the gas heats and above the gas cools upon throttling. This critical temperature is below standard conditions for hydrogen (202 K) and helium (25 K) and above standard conditions for nitrogen (621 K), air (603 K), argon (723 K), and CO_2 (1500 K).

A leak may occur in a region that has a flow cross-section that geometrically resembles a converging-diverging nozzle. An example of this is a cooling tube that has a crack, or small hole, that opens into another confined region. For the converging-diverging nozzle and compressible gasses, supersonic flow is possible if the internal pressure of the contained gas is (for air) greater than 1.893 times the absolute outside pressure[1]. Under normal atmospheric conditions this is a tank pressure of about 90 kPa (13 psig). If the flow at the opening of the pressure vessel is sonic then for air the temperature drop may be as low as -29 °C for a tank temperature of 20 °C. If the geometry acts as a converging-diverging nozzle the temperature drop away from the leak will be even larger if the flow is supersonic and will be a major factor in the detected temperature change.

The Joule-Thompson and compressible gas nozzle effects previously mentioned are usually predicated upon steady-state flow. There may be good reasons not to use a steady state condition during inspection. An example of a transient inspection will be presented later. For complex geometries during rapid pressurization, gasses contained in confined regions of the vessel may be compressed by the pressure increase. Work is then done on this confined slug of gas by the incoming gas. This causes a decrease of volume of the slug and a corresponding temperature increase.

As an illustration of how leaks behave thermally, a series of tests were performed on a single 5.08 mm (0.20 inch) diameter tube with a 0.127 mm (0.005 inch) hole. The tube was painted flat black, giving it an emissivity of approximately 0.85 and imaged with a high resolution (256 x 256 pixel) high sensitivity (0.025 °C per A/D output bit value) infrared camera. The tube was capped on one end and connected to a K-bottle containing the test gas. Four gasses in all were tested including nitrogen, argon, helium and carbon dioxide. The pressure regulator on the K-bottle was set to deliver 40 psig and was valved to provide that pressure to the tube in less than 2 seconds. The tube was purged with each test gas prior to pressurization to ensure that the tube contained only that test gas. The infrared imager was set to acquire one unpressurized reference image then one frame every 1/60 of a second for 10 seconds.

The images shown in Figure 2 demonstrate the thermal behavior of each gas as it escapes through the hole in the side of the tube. Two images are given for each gas type, the source peak temperature frame and the end frame. A time-temperature plot is also given depicting the transient thermal behavior of each gas. By referring to the time-temperature plot one can easily see how each gas has its own unique thermal response. First, and most obvious, note that when the nitrogen, argon and carbon dioxide were used an increase in temperature occurs when pressure is first applied as opposed to when the helium was used which begins to cool immediately. Secondly, notice that the nitrogen, argon and helium pressurized tubes all showed some cooling after the pressure had been applied for a long period of time, whereas the carbon dioxide pressurized tube returned to room temperature.

BUBBLE LEAK CHECK APPLICATION TO THE SSME NOZZLE

The circumferential location of interstitial leaking can be identified by the application of a liquid leak check solution in the openings where the interstices vent out the aft end of the nozzle, while the tubes are pressurized. The nozzle is pressurized with helium gas to 25 psig and the liquid solution is squirted into the interstitial vent. When the leak solution bubbles at the nozzle aft end, the leak is classified as described in Table 1, and if it is severe enough actions are taken to fix the leak. Due to cross linking of the interstices many interstitial vents may bubble when only one tube is actually leaking, making it difficult to not only locate which tube or tubes are leaking but also to determine the magnitude of the leak. If the leak is seen to manifold across several tubes it is impossible to tell if all the tubes are leaking at the degree seen at the bottom of the nozzle or if the leak is cross-linking from a single source with sufficient flow to create all the indications.

Table 1. Flow rate

Class	Flow rate (scim)	Description
1	> 2	Foaming
2	2 to 50	Bubbling
3	50 to 100	Strong bubbling that burst and re-form
4	> 100	Blowing (Bubbles cant persist)

scim = Standard cubic inch per minute

One method for isolating the defect tube and determining where along its length the leak source is located is to cut open the suspect tubes one at a time, insert an angioplasty device to close off a portion of the tube, and then repressurizing the system. In theory by using this method the leak can be isolated to a given tube by moving the angioplasty device along the length of the nozzle. Although this method requires no specialized equipment (other than the angioplasty device) many inspection induced repairs must be made to cover all the holes cut into the tubes for the angioplasty device. Also, due to the additional heating required by the hot wall repair, new cold wall "interstitial" leaks may be produced in the process of trying to find one leak.

Another method is to boroscope the inside of the tubes and to visually locate the leak. Since the boroscope can only cover a finite tube length and since it is impossible to identify which tube (to the right or left of the identified interstitial) is leaking, many extra and undesired repairs must be made to fix just one leak. Also, due to the small size of the fracture required to generate a critical leak, the defect may not be detectable through the boroscope.

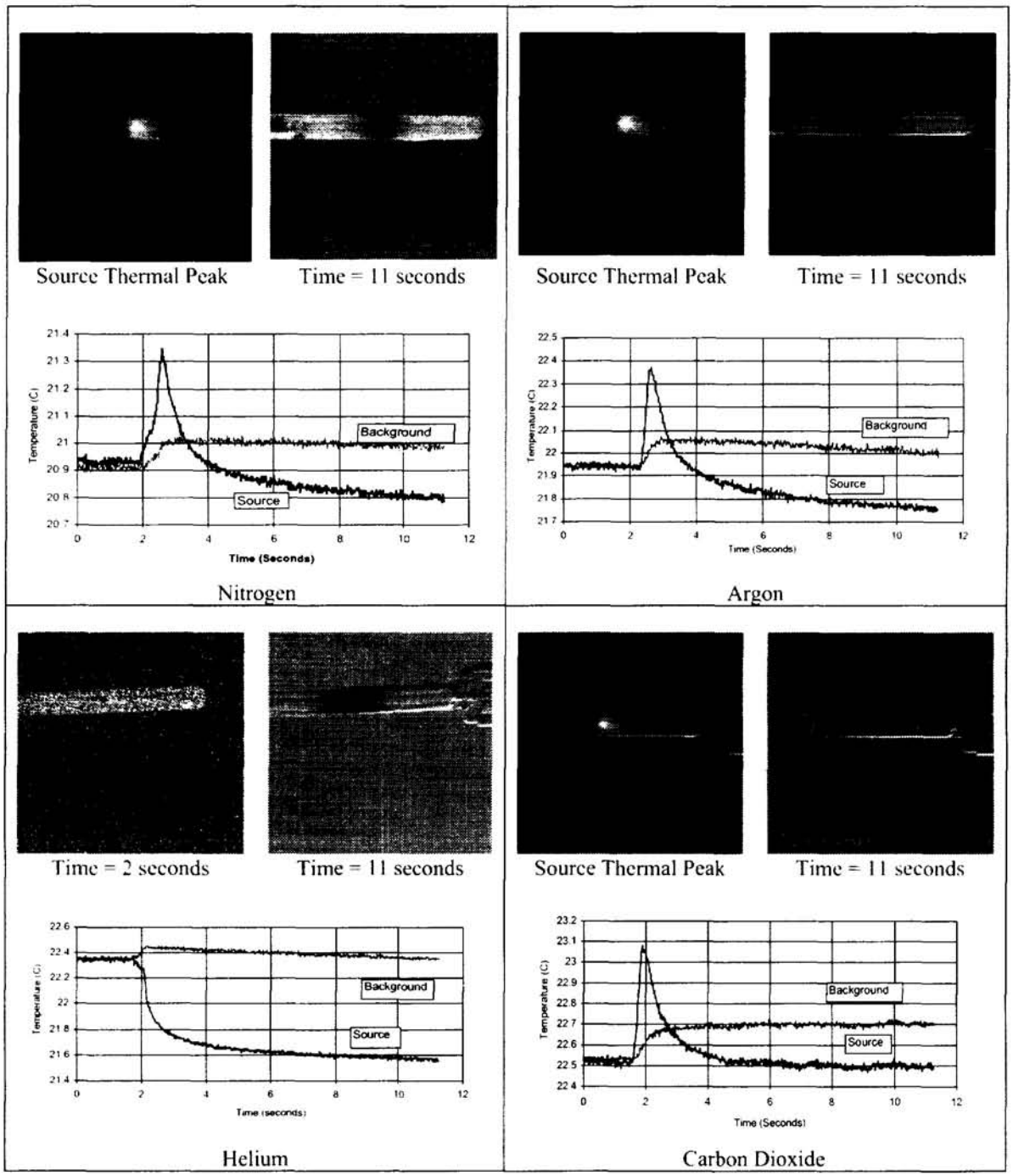

Figure 2. Thermal behavior of leaks.

THERMOGRAPHIC LEAK CHECK OF THE SSME NOZZLE

For the work described herein an Amber Radiance 1 camera with 25 mm lens controlled by Thermal Wave Imaging software was utilized. Inspections and tests were performed on sections cut from the forward and aft end of a scrap nozzle (Figure 3). The aft end section was fitted with a pressure manifold which permitted eight tubes to be pressurized simultaneously. The forward nozzle section, with its existing manifold intact was plumbed so that all the tubes were pressurized simultaneously. These sections were initially inspected using both a standard liquid leak check at the vented interstices and thermographically and determined to be free of any leaks. Artificial leaks were then manufactured in each nozzle segment to represent both class II and class III leaks. These artificial defects were fabricated by cutting open the tubing on the hot wall side of the nozzle, then puncturing the tube into the interstitial region and finally resealing the tube hot wall through a typical welding repair operation. During the reweld operation the hot wall surface of the tubes had to be cleaned with a wire brush which left the surface shiny, greatly limiting the thermographic inspection capability. Many methods were investigated to dull the surface of the nozzle, increasing the local emissivity to 0.8 or greater, without damaging the fragile nickel coating of the tubes. A water washable plat black spray paint was found to work well thermographically, but due to traces of sulfur, was deemed not acceptable from a chemical compatibility standpoint. Additional work is ongoing to find a paint that will be acceptable thermographically and chemically.

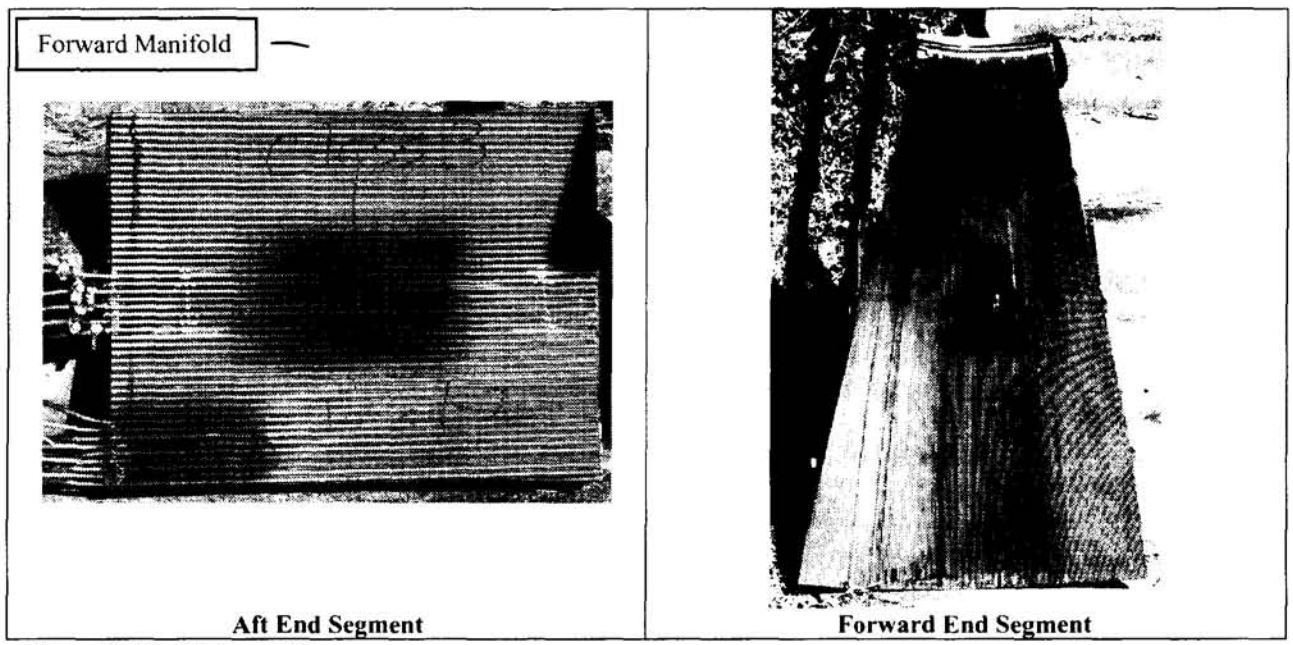

Figure 3. Nozzle segments.

The artificially damaged panels were then thermographically inspected with various flow rates, peak pressure levels, ambient temperatures, gas temperatures and with a range of gasses to bound the detection capability. The pressurization rate was found to have a strong influence on the ability to detect the leak with higher pressurization rates yielding the best thermal response for most gasses (Figure 4). When the pressurization rate is too slow the thermal signature is lost due to the highly diffusive nature of the tubing material. In general it was found that a pressure transient less than 8 seconds (>5 psi/sec) was required for adequate thermal contrast of the defect to the background. The exception to the rule was found for carbon dioxide which was unaffected by pressurization rate and could be performed with ramp times in excess of 40 seconds. The only factor limiting the ramp time for carbon dioxide being the in-plane conductivity of the nozzle itself.

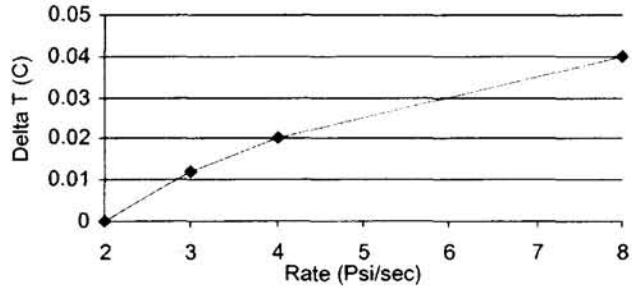

Figure 4. Thermal response as a function of pressurization rate for nitrogen.

The maximum pressure was found to have a large effect on thermal detectability of the leak. For example, as shown in Figure 5 the thermal response, as determined by computing the maximum difference between the IR camera values in the defect region and acreage region, increases nearly linearly with increasing pressure. The thermograms in Figure 6 clearly demonstrate the need for higher pressures to be able to uniquely identify the leak source. In the figure, the Class 3 leak appears as a large cool (dark) region just above the upper repair patch. The Class 2 leak is not visible at 172 kPa (25 psig) yet is clearly visible above the lower repair patch at 310 kPa (45 psig). The limiting factor for the magnitude of the pressure used was controlled by safety related issues.

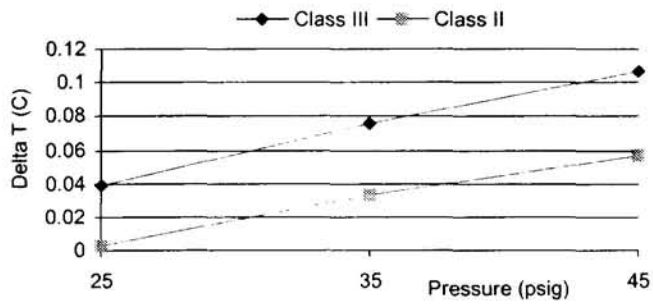

Figure 5. Thermal response at three pressures.

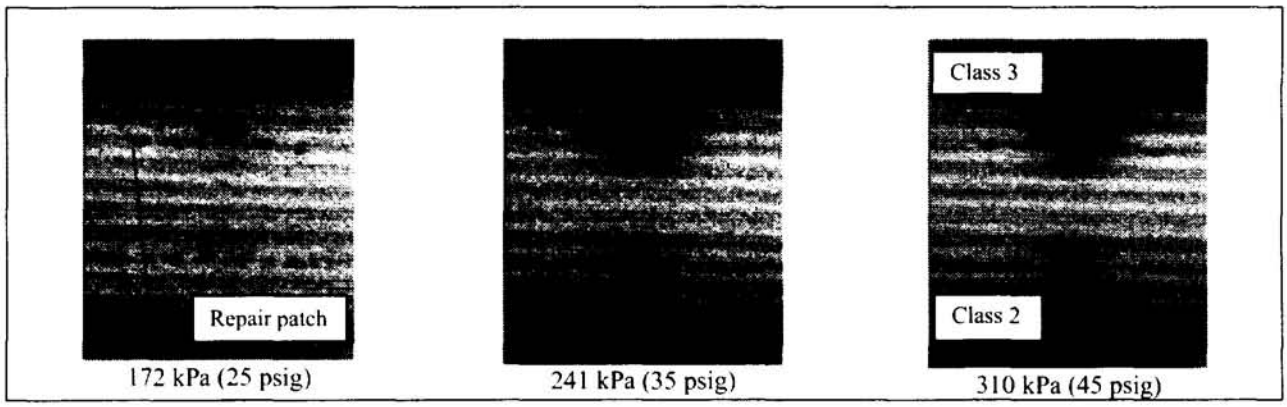

Figure 6. Thermograms at three pressure levels.

When the leaks were inspected using different pressurizing gas types it was found that the thermal response not only varied with gas type but also with the location of the leak along the nozzle length. For example, when helium was used to pressurize the aft nozzle segment no indication was present yet on the forward end of the nozzle it gave the best response (Figure 7).

Tests were also conducted to determine if the blockage associated with a repair could produce a false call for a leak. Calculations showed that the largest flow rate expected for a nozzle leak check would be below 12.2 meters/sec (40 feet per second). Two weld repair restrictions were fabricated by opening the tubing, applying braze to the bottom of the hole and then welding the tubes closed. Nitrogen gas was flowed through the tubes and its velocity measured with a hot wire anemometer at a distance of 3.175 mm (1/8 inch) from the tube opening. The tests demonstrated (Figure 8) that the flow rate threshold for thermal detection of a 50% area restriction is above 12.2 meters/sec. That is, below 12.2 meters/sec the signature of the restriction is to small for repeatable detection. Based upon these findings it is highly unlikely that a restriction alone would create a false positive signature during a thermal inspection of the nozzle.

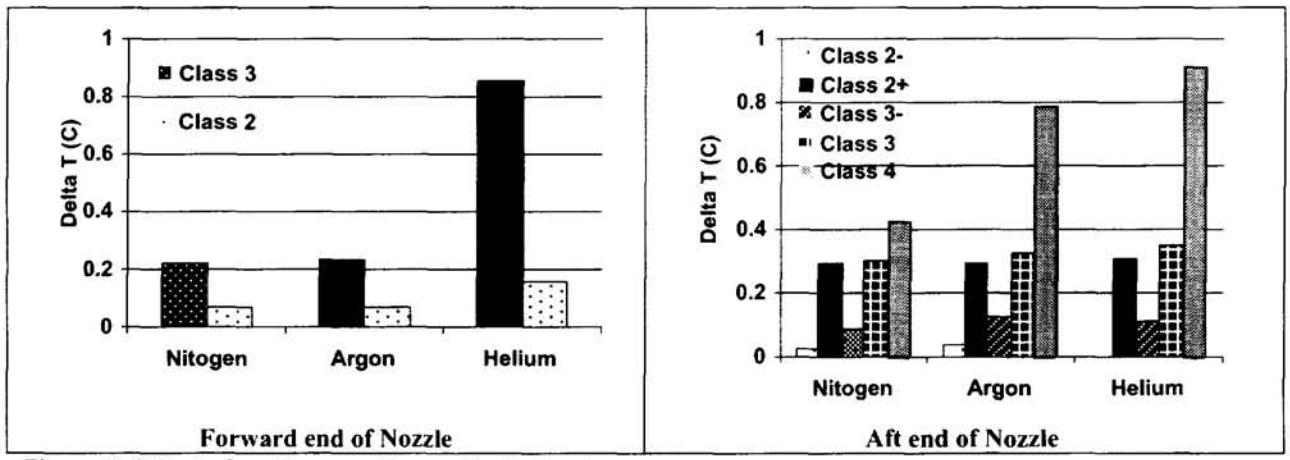

Figure 7. Effect of gas types on thermal leak signature.

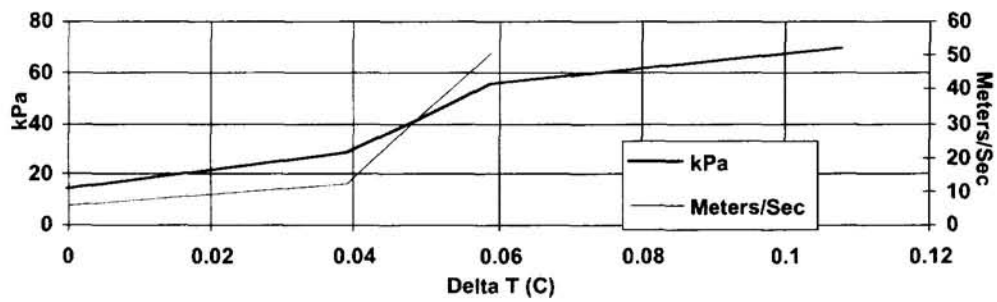

Figure 8. Flow Blockage Analysis.

APPLICATION POTENTIAL TO A FULL NOZZLE

The logistics of performing a thermographic inspection on a full nozzle were also investigated. Safety of the inspection crew and the hardware was the primary factor driving the development of the inspection procedures. To that end it was desired to limit the amount of time spent by the inspecting personnel inside the nozzle, minimize the number of pressure cycles and restrict the movement of the nozzle.

As shown in Figure 9 the nozzle is positioned vertically on three stands which support it approximately three feet off of the shop floor and a small personnel lift is placed under the nozzle cone. An initial liquid leak check is performed on the aft end of the nozzle and any leaking interstices identified. A band of tubes extending 20 tubes to either side of the leak zone is then marked at the aft end of the nozzle and reference foil markers are temporarily attached to the outermost tubes of the suspect region on six inch intervals along the length of the nozzle. A foil number is then placed next to every other marker to permit identification of camera position. Regions in the inspection area are visually inspected for hot wall leaks and prior repair work. Hot wall leaks are first repaired. Then all repairs are sprayed with an flat black paint.

The thermography camera is mounted to a pan and tilt unit on a tripod and an external focus unit is attached to the cameras lens. Starting at either end, each marked region of the nozzle is then thermographically monitored as the pressure inside the tubing is ramped and then vented. Any leak signature is marked with a foil tape and classified based upon its thermal intensity. Once the entire length of the nozzle has been inspected measures are taken to repair the defective tube and the inspection is repeated.

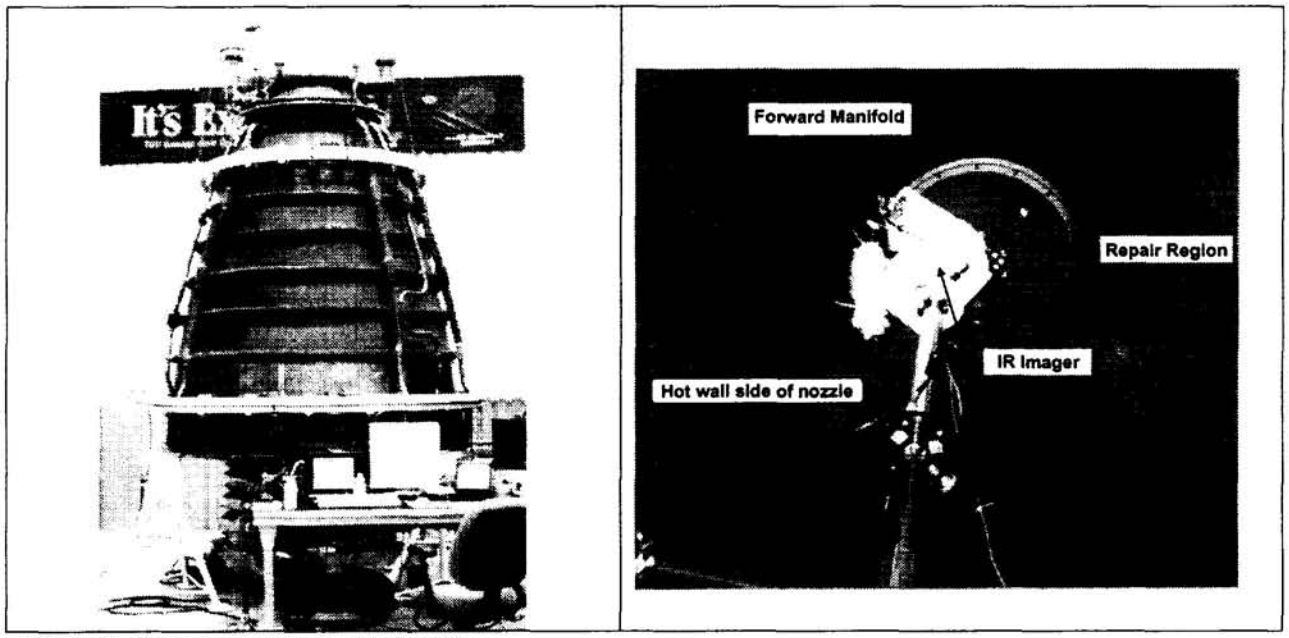

Figure 9. Thermal imager inside Nozzle.

CONCLUSIONS

The limitations and requirements for thermographic identification of interstitial leaking of the Space Shuttle Main Engine Nozzle have been addressed. With a standard thermographic test procedure established for the nozzle it should be possible to reliably locate and quantify the nature of interstitial leaking in the SSME nozzle. From these results it has been determined that the following conditions must be met to ensure adequate confidence that all critical level class II leaks are detected. First, the flow rate of gas into the nozzle must be sufficiently high to permit the transient thermal signature of the leak to be detected before it is lost to thermal conduction. Rise times to peak pressure less than 8 seconds greatly inhibit defect resolution. Next, the greater the maximum pressure reached during the pressurization the better the ability to detect a leak. Although the liquid leak check is performed at 25 psig it was found that for the best thermal response pressures of at least 40 psig were required. Carbon dioxide gas was found to give the best thermal indications of a class II or greater leak throughout the nozzle. At the forward end of the nozzle Helium was found to also work well, while at the aft end of the nozzle, either Argon or Nitrogen was found to work satisfactorily. A gas temperature slightly below ambient was required to get the desired thermal gradient and an ambient temperature between 70 °F to 90 °F was required. Optically, it was determined that the spatial resolution of the camera system must be able to uniquely identify individual tubes and the infrared imager needed to have a thermal resolution of at least 0.025 °C/Level. Finally, a surface emissivity of 0.8 or greater was required to allow measurement of the thermal gradient produced by the leak.

ACKNOWLEDGMENTS

The authors are grateful to Melvin Bryant of the NASA Marshall Space Flight Center and Ron Daniel of Boeing North American/Rocketdyne for their technical support in this investigation.

REFERENCES

1. Mechanical Engineering Reference Manual, Eighth Edition, Michael Lindeburg.

Verification of Shearography NDE Methods on Space Shuttle, X-33, and Delta IV Launch Vehicles

JOHN W. NEWMAN

Laser Technology, Inc.
105 S. Germantown Pike
Norristown, PA 19403 USA
Phone: 610-631-5043
Fax: 610-631-0934
E-mail: Jwnewman50@aol.com

Laser shearography nondestructive evaluation (NDE) was first implemented in aerospace production of the U.S.A.F. B-2 program in the 1980s. Since then, it has become widely accepted for the inspection of metal engine components, composites, honeycomb structures, and thermal protection material on launch vehicle systems. Shearography NDE images surface strain caused by the presence of subsurface anomalies when a repetitive load is applied to the structure. Very successful, high-speed inspection techniques have been developed using shearography with acoustic stress to image disbonds under sprayed-on foam insulation (SOFI) applied to aluminum cryogenic fuel tanks. Typically, 6 to 8 square feet of surface area are inspected in less than 1 second.

A large robotic shearography system has been implemented in production for the LO_2 and LH_2 tanks on the Delta IV using this technology. In addition, shearography methods were validated and implemented on the X-33 XRS-2200 aerospike rocket engine thrust ramps. Both the cooling channels and the metal honeycomb support structure were inspected. This provided rapid engineering for production engineering refinement of processes and on-site NDE in near-real time, which reduced costs and allowed inspection of braze bonds that otherwise would not have been able to be inspected.

This paper will discuss the technology and quality and cost benefits of shearography NDE as applied to rapid launch vehicle NDE and health monitoring. It will also provide specific examples of NDE verification on three programs.

THERMOGRAPHIC ANALYSIS OF COMPOSITE COBONDS ON THE X-33

Samuel S. Russell
Nondestructive Evaluation Team
NASA Marshall Space Flight Center
(256)544-4411
sam.russell@msfc.nasa.gov

James L. Walker
Nondestructive Evaluation Team
NASA Marshall Space Flight Center
(256)961-1784
james.l.walker@msfc.nasa.gov

Matthew D. Lansing
Nonmetallic Materials Group
NASA Marshall Space Flight Center
(256)544-3953
matt.lansing@msfc.nasa.gov

ABSTRACT

During the manufacture of the X-33 liquid hydrogen (LH_2) Tank 2, a total of thirty-six reinforcing caps were inspected thermographically. The cured reinforcing sheets of graphite/epoxy were bonded to the tank using a wet cobond process with vacuum bagging and low temperature curing. A foam filler material wedge separated the reinforcing caps from the outer skin of the tank. Manufacturing difficulties caused by a combination of the size of the reinforcing caps and their complex geometry lead to a potential for trapping air in the bond line. An inspection process was desired to ensure that the bond line was free of voids before it had cured so that measures could be taken to rub out the entrapped air or remove the cap and perform additional surface matching.

Infrared thermography was used to perform the precure "wet bond" inspection as well as to document the final "cured" condition of the caps. The thermal map of the bond line was acquired by heating the cap with either a flash lamp or a set of high intensity quartz lamps and then viewing it during cool down. The inspections were performed through the vacuum bag and voids were characterized by localized hot spots. In order to ensure that the cap had bonded to the tank properly, a post cure "flash heating" thermographic investigation was performed with the vacuum bag removed. Any regions that had opened up after the preliminary inspection or that were hidden during the bagging operation were marked and filled by drilling small holes in the cap and injecting resin. This process was repeated until all critical sized voids were filled.

INTRODUCTION

The X-33 reusable launch vehicle technology demonstrator was designed to store liquid hydrogen fuel in a pair of composite fuel tanks, shown in Figure 1. Each multi-lobed tank is an integral part of the vehicle's load bearing primary structure. The tanks are attached to the rest of the airframe at points around their forward and aft ends. Adjacent to each of these attachment points, a cast structural foam filler and bonded reinforcing cap are used to distribute loads to the tank skins. The general locations of these caps are shown in Figure 2, viewing one of the tanks from the aft perspective. The typical cap geometry is evident from the photographs of bonded caps shown in Figure 3.

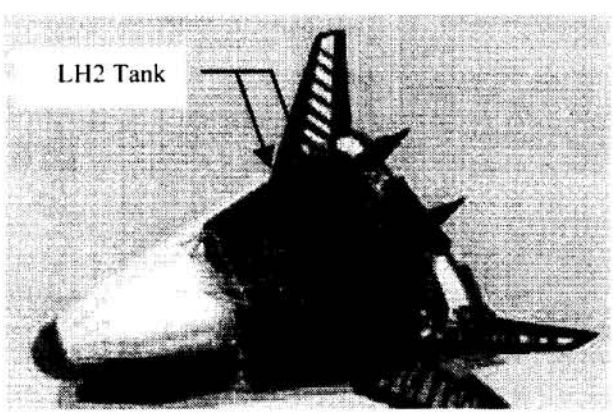

Figure 1. X-33 internal structure.

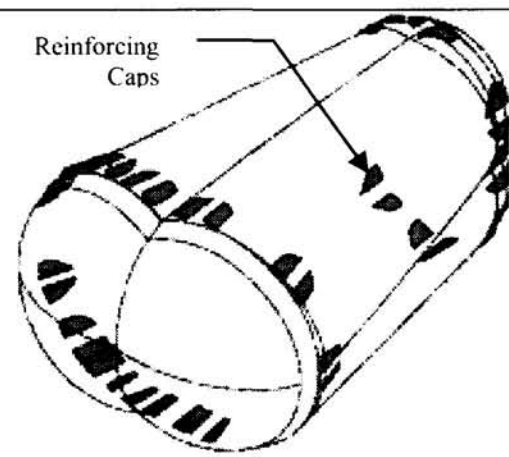

Figure 2. Locations of reinforcing caps on tank.

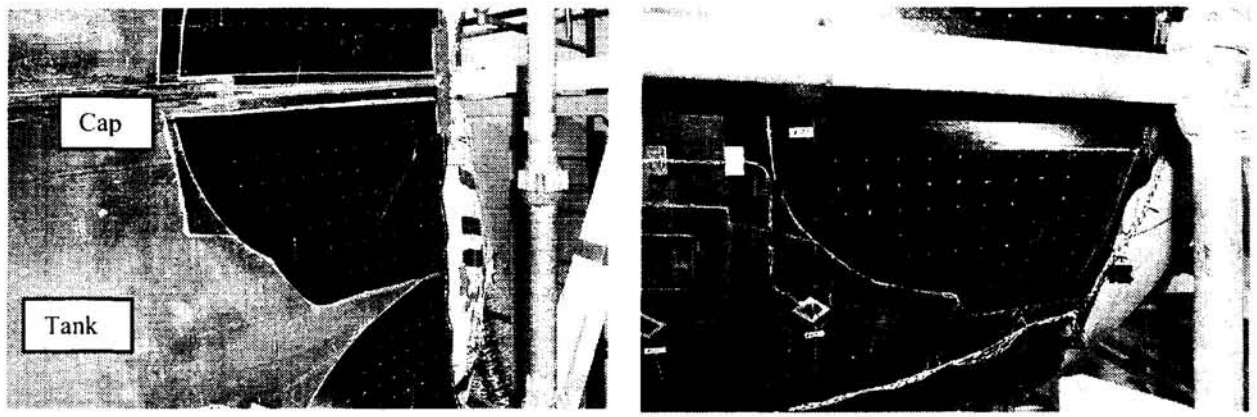

Figure 3. Photographs of reinforcing caps at various locations.

The method of thermographic inspection employed to inspect the bond lines consists of exposing the reinforcing cap surface to a rapid heat flux by pulsing a pair of high intensity flash lamps or slowly saturating the surface with heat using lower intensity hand-held quartz lamps. After the cap has been heated, an infrared camera is used to record the surface temperature as the heat transfers into the structure and the cap begins to cool. A void between the cap and underlying foam acts as an insulator, and that region of the cap will retain higher temperatures over the void than the surrounding area. Bond line voids are thus indicated as bright "hot" regions in the thermographic images.

Thermographic inspections of the wet bond line prior to curing required a novel bagging method. The thermographic imager was capable of viewing the temperature of the cap surface through the bagging and release ply material, but could not image through a traditional breather cloth, used to ensure thorough evacuation of the vacuum bag. It was also determined that when air was trapped in the bond line it was very difficult to get it to move to the edge of the cap so that it could be evacuated. The solution to this problem involved drilling a grid of vent holes over the acreage of the cap and placing a series of split, cut in half along their length, plastic tubes over the cap vent holes to facilitate evacuation. This arrangement required that minimal breather cloth only be used around the cap edges and over the tubing, allowing the camera to image most of the cap area. The region covered by the tubes, however, remained obstructed from view.

TEST APPARATUS

A digital thermography system was used to inspect most of the caps during bonding and all of the caps after the bonding process was complete and the vacuum bagging materials removed. An Amber Radiance 1T infrared camera, with a 13 mm lens and a 12" x 12" field of view, was used to image the caps after flash heating. A Thermal Wave Imaging EchoTherm data acquisition system was used to record the digital images from the camera to files on a PC hard drive. A Thermal Wave Imaging flash hood set to deliver 6.4 kJ of energy was used to rapidly heat the caps prior to image acquisition.

An analog thermography system was also used for some of the cap inspections. The analog system, although lower in sensitivity than the digital system gave real-time images of the uncured bond line and as such gave the fabrication team more time to work out any trapped air. Here, an Inframetrics SC-1000 infrared camera was used to image the caps after slow heating by way of a pair of 500W hand-held quartz shop lamps. Thermal images from the camera were recorded to VHS tape.

DEFECT STANDARDS

Reinforcing Cap Defects

Inspection of the wet bond line may have also detected defects in the reinforcing caps above the bond line. Defect standards were fabricated to simulate defects in the reinforcing caps themselves. Inserts were fabricated into sample panels between plies at various depths to simulate internal unbonds. The images shown in Figure 4 were acquired

with the digital system previously described, with the exception that a 25 mm lens (6"x6") field of view was employed. In the images the depth of the insert is given as a fraction of the panel thickness (T). Three insert diameters were used including 0.50, 0.25 and 0.125 inch.

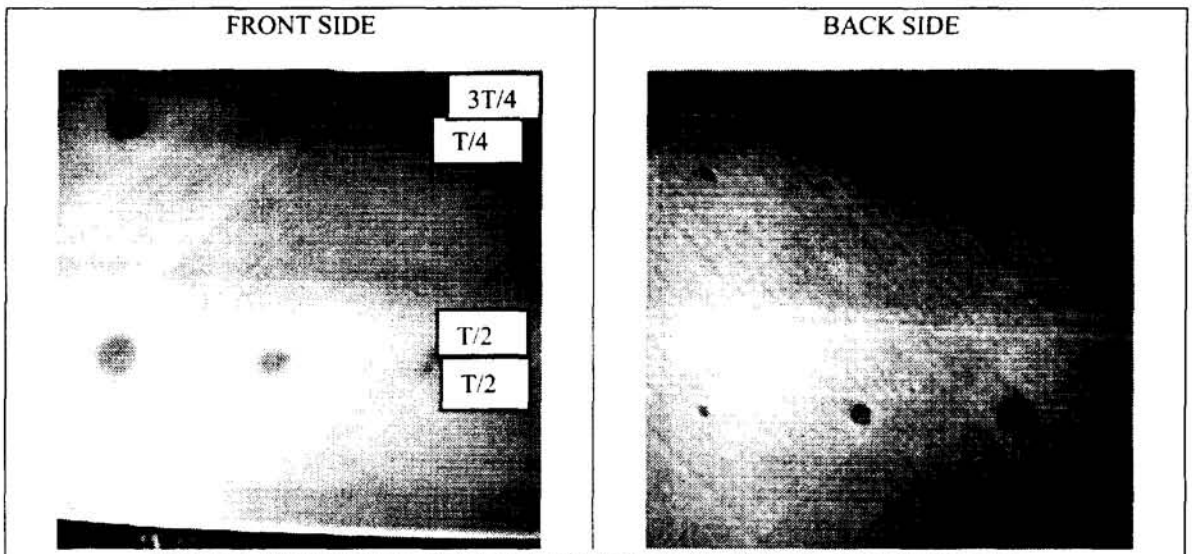

Figure 4. Thermograms of defect standard simulating disbonds in reinforcing caps.

Bond line Defects

As a method to simulate unbonds during cure a defect panel was fabricated with inserts in the wet bond line. The simulated void shown thermographically in Figure 5 was produced by inserting a 0.5 inch diameter rubber o-ring between the simulated cap and underlying material. The cap was covered with a layer of release ply and vacuum bagged. Narrow strips of breather cloth were used in this instance rather than the split plastic breather tubes. The part was then inspected by heating the surface with a pair of shop lamps for about 10 seconds. Note how the void trapped within the o-ring remains hotter than the surrounding bond line demonstrating the presence of a void.

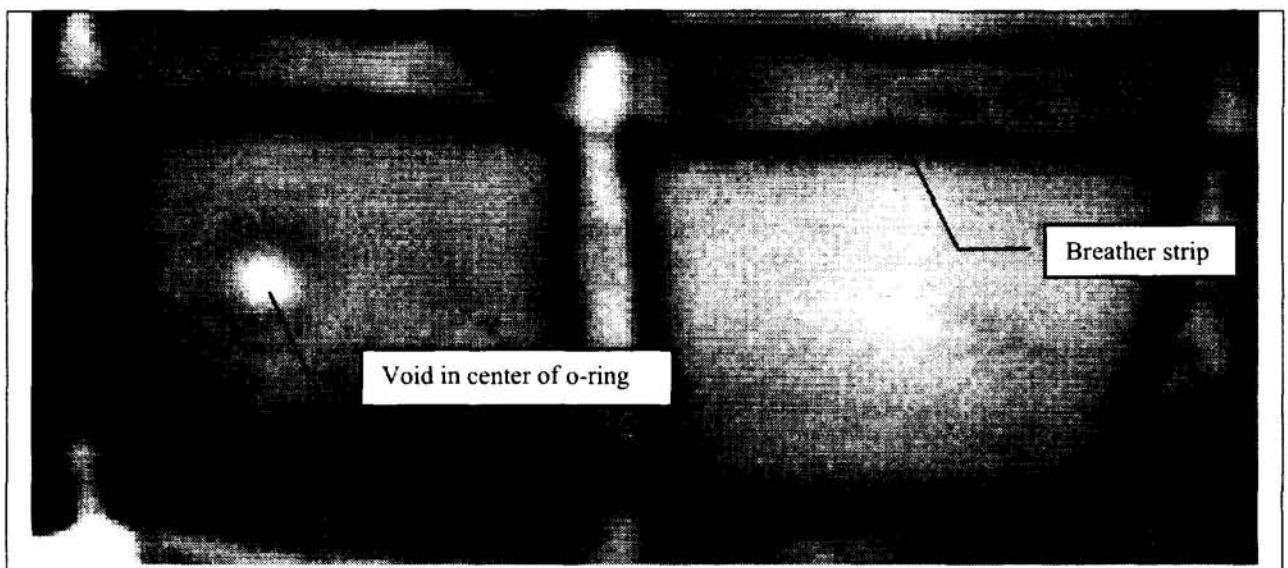

Figure 5. Thermographic detection of simulated wet bond line void.

INSPECTION RESULTS

As previously described, the initial inspections were performed when the caps were still under the vacuum bag. In this manner, voids or air pockets, trapped under the cap could be eliminated before the cure was complete or if the void was less than a previously determined critical size it could be accepted. Figure 6 demonstrates a thermogram of a cap section with two small, but acceptable, voids. When the part was cured and the bag removed a second inspection was performed (Figure 6b) revealing the first two known defects (B and C) as well as on that was hidden (A) beneath the breather ply strip.

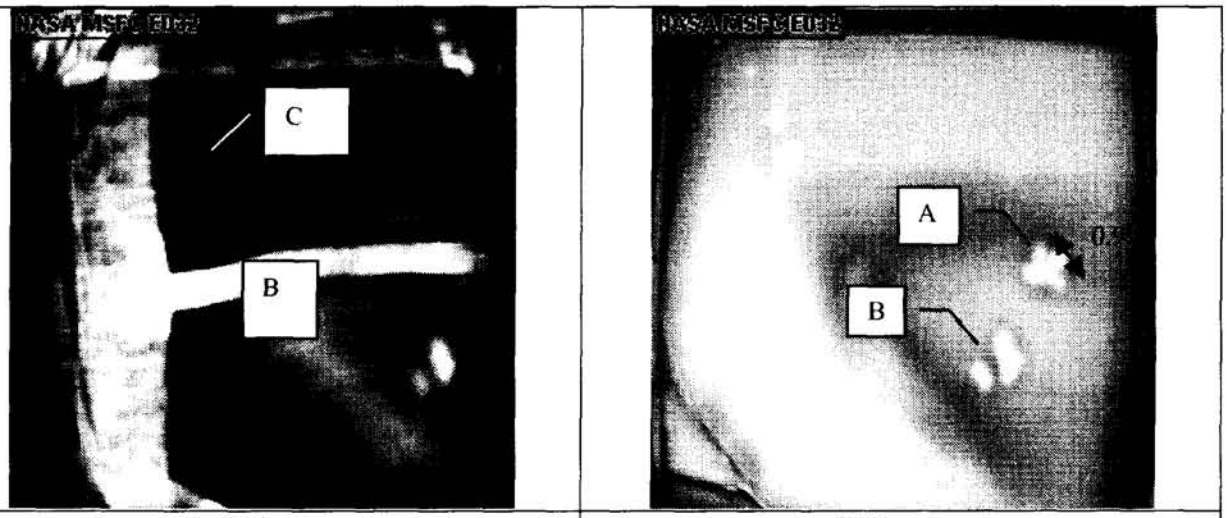

A. During cure | B. Post cure

Figure 6. Thermogram showing initially hidden void.

On average it took six image sequences to fully cover each cap. The results of thermography inspection of a reinforcing cap which did not reveal any unacceptable unbonds are shown in Figure 7. The images shown here were obtained after the bond line had cured and the vacuum bag had been removed. Minor temperature variations exist due to differences in the thickness of a foam filler material beneath the cap. A grid of hot points is visible where vent ports were drilled in the reinforcing cap to prevent the entrapment of air between the foam and the cap.

The results of thermography inspection of a reinforcing cap which revealed an unacceptable unbond are shown in Figure 8. Again, these images were obtained after the vacuum bag had been removed. A branching unbond is visible in the upper left sector with a maximum length of approximately 4.4 inches. The unbond was just barely visible in the thermograms taken before the vacuum bag was removed being all but totally obscured by breather tubes and cloth that was placed around the outer edge of the panel.

Since this defect was unacceptably large an action was taken to try to fill the void with epoxy. To aid in the repair process lead foil tape markers were placed on the cap identifying the exact location of each leg of the void and verified by re-inspecting the region. Holes were then drilled in the reinforcing cap over the void and injected with epoxy to fill it. Thermograms were taken at various stages in this process are shown in Figure 9. After the third injection of epoxy, the size of the void had been diminished sufficiently that it was deemed acceptable.

The same process of thermographically inspecting each cap during and after cure was performed for the rest of the tank. Defects found after the post cure inspections were measured and if deemed necessary filled with resin. A final post repair check was then performed to complete the inspection process.

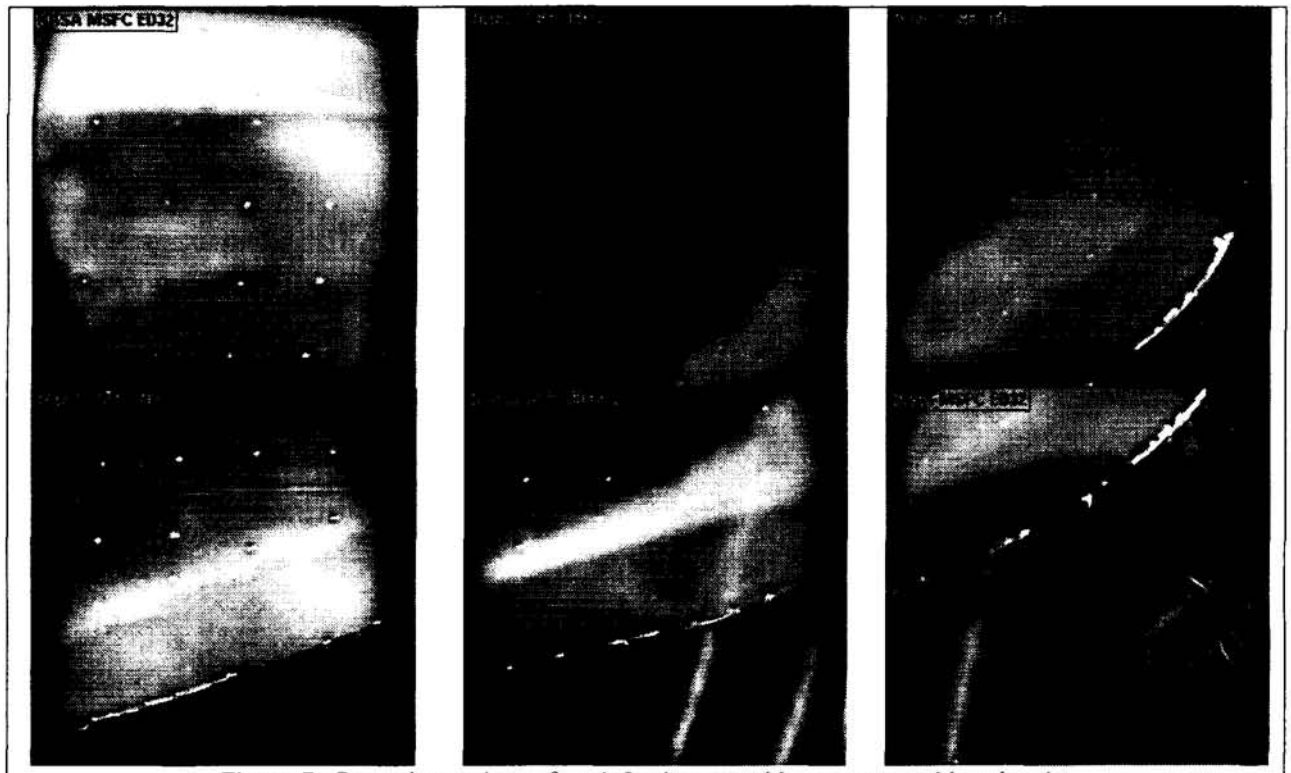

Figure 7. Sector inspections of a reinforcing cap with no unacceptable unbonds.

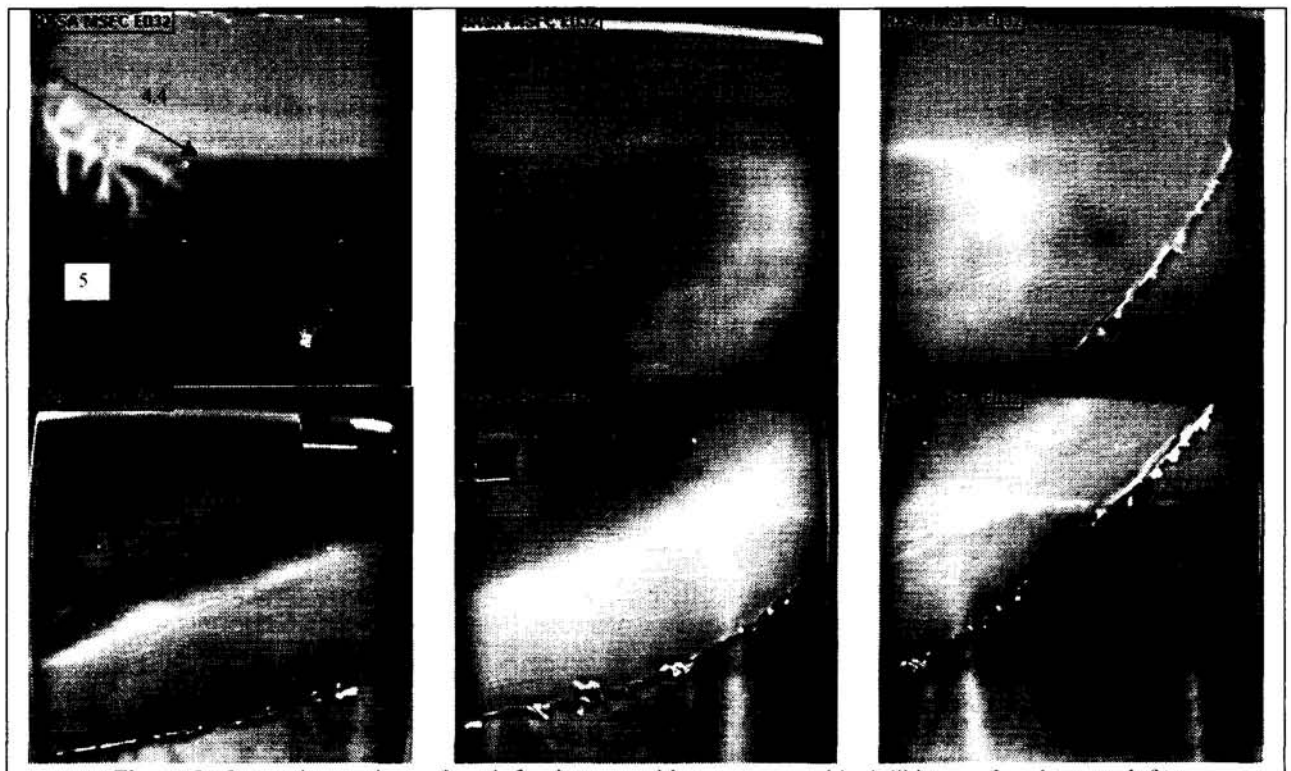

Figure 8. Sector inspections of a reinforcing cap with an unacceptable 4.4" long unbond (upper left).

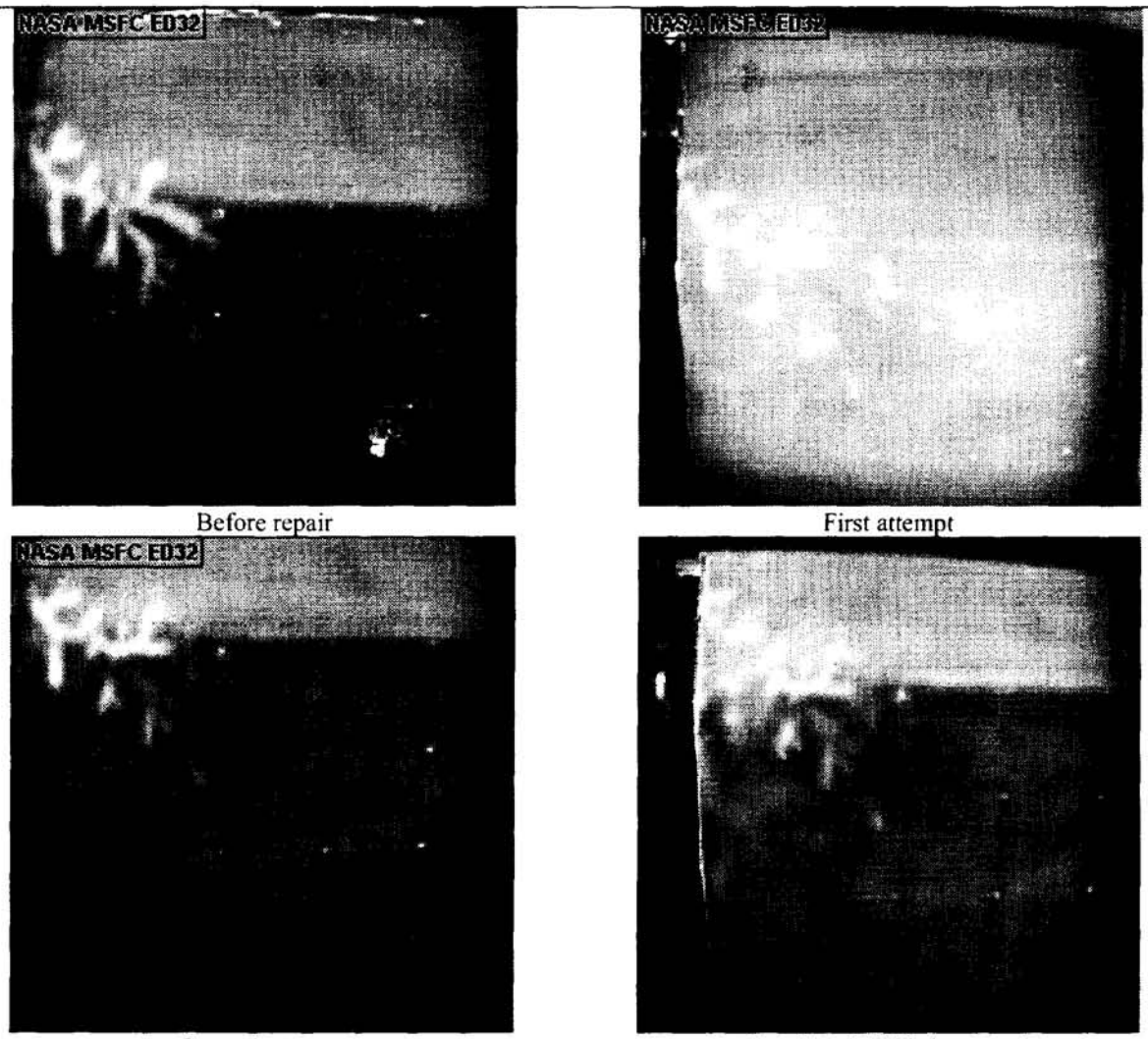

Before repair

First attempt

Second attempt

Post Repair (Third attempt)

Figure 9. Repair of a void in the wet bond line by epoxy injection.

CONCLUSIONS

Thermographic inspection proved largely successful in the detection of voids in the wet bond line between reinforcing caps and underlying foam filler on the X-33 LH_2 Tank 2. Voids that were detected precure were often eliminated by rubbing them out or removing and reshaping the cap. There were some undetected voids that had either opened up after the initial thermographic inspection or were obscured by the breather tubes used in vacuum bagging. Epoxy was injected to fill these voids, resulting in an acceptable repair.

ACKNOWLEDGEMENTS

The authors would like to acknowledge the Lockheed Martin and Alliant Techsystems composite fabrication crew and Don Bryan (NASA MSFC Thermodynamics and Heat Transfer Group) for their assistance in this effort.

Evaluation of Forces on the Welding Probe of the Automated Retractable Pin-Tool (RPT)

R. JEFFREY DING

Marshall Space Flight Center/ED33
Huntsville, AL 35812 USA
Phone: 256-544-2700
Fax: 256-544-1660
E-mail: jeff.ding@msfc.nasa.gov

The NASA invention entitled "The Hydraulic Controlled Auto-Adjustable Pin Tool for Friction Stir Welding" (U.S. Patent 5,893,507), better known as the Retractable Pin-Tool (RPT), has been instrumented with a load-detecting device allowing the forces placed on the welding probe to be measured. As the welding probe is plunged into the material, the forces placed on the probe can now be characterized. Of particular interest are those forces experienced as the welding probe comes within close proximity to the back-up anvil. For a given material, it is believed that unique forces are generated relative to the distance between the welding probe and the anvil. The forces have been measured and characterized for several materials, and correlations have been made between these forces and the pin's position relative to the backside of the weld material.

P-323 - 10/37

FRICTION STIR WELDING AT MSFC: KINEMATICS

Arthur C. Nunes, Jr.
Marshall Space Flight Center
ED33, Huntsville, AL 35812
(256) 544-2699
arthur.nunes@msfc.nasa.gov

Introduction. In 1991 The Welding Institute of the United Kingdom patented the Friction Stir Welding (FSW) process (Thomas *et al.*). In FSW a rotating pin-tool is inserted into a weld seam and literally stirs the faying surfaces together as it moves up the seam. By April 2000 the American Welding Society International Welding and Fabricating Exposition featured several exhibits of commercial FSW processes and the 81st Annual Convention devoted a technical session to the process.

The FSW process is of interest to Marshall Space Flight Center (MSFC) as a means of avoiding hot-cracking problems presented by the 2195 aluminum-lithium alloy, which is the primary constituent of the Lightweight Space Shuttle External Tank. The process has been under development at MSFC for External Tank applications since the early 1990's.

Early development of the FSW process proceeded by cut-and-try empirical methods. A substantial and complex body of data resulted. A theoretical model was wanted to deal with the complexity and reduce the data to concepts serviceable for process diagnostics, optimization, parameter selection etc.

A first step in understanding the FSW process is to determine the kinematics, i.e. the flow field, in the metal in the vicinity of the pin-tool. Given the kinematics, the dynamics, i.e. the forces, can be targeted. Given a completed model of the FSW process, attempts at rational design of tools and selection of process parameters can be made.

The dynamic anomaly. The attempts to model the FSW process at MSFC began with a cylindrical rotating flow matching the surface speed of the rotating pin-tool at the pin surface and extending out to some radius at which the flow stops. The heat generated would leak out radially into the workpiece, and the mechanical work would balance the heat loss. At steady state the moments on a ring element cut out of the swirl would balance to zero. A simple system of equations could be written to model the distribution of angular velocity throughout the deformation zone.

The stress on the outside of a ring element has the advantage over that on the inner surface. The area is bigger; the moment arm is longer. For equilibrium, then, the flow stress has to decrease with increasing radius. For metals the flow stress is not greatly affected by shearing rate, but mainly by temperature. Hence, the temperature must increase with radius. The heat generated from the plastic flow has to flow backwards down the temperature gradient into the tool! But what if the tool were insulated? With an insulated tool, backflow of heat and the required temperature rise with radius could not occur. This consequence of the plasticity of the workpiece seemed peculiar. It was dubbed a "dynamic anomaly." It led to a reevaluation of assumptions. There are several ways to alter the original assumptions to circumvent the "dynamic anomaly".

Alteration of the constitutive equation of the metal to make the metal viscous would reduce stresses at greater radii by reducing the strain rate so as to make it unnecessary for the temperature to drop. This approach was rejected because no good justification for attributing viscous behavior to a metal could be found. See Appendix 2.

Withdrawal of the assumption of steady-state flow in favor of an oscillatory flow might allow a plausible solution. Stick-slip flow is well known in friction situations. This approach was rejected because oscillations were not observed in FSW flow.

Withdrawal of the assumption of a radially distributed shear in favor of a slip discontinuity, a slip envelope, would also allow a plausible solution. Slip discontinuities are characteristic of plastic flows. This approach was adopted.

The rotating plug model. The rotating plug model superposes two flows: (1) rapid shear over an approximately discontinuous cylindrical boundary separating a plug of metal rotating with the tool from the stationary workpiece metal, and (2) a relatively slow rotating motion driven by the threads on the tool and wrapped around the tool in a ring vortex configuration. See Figure 1.

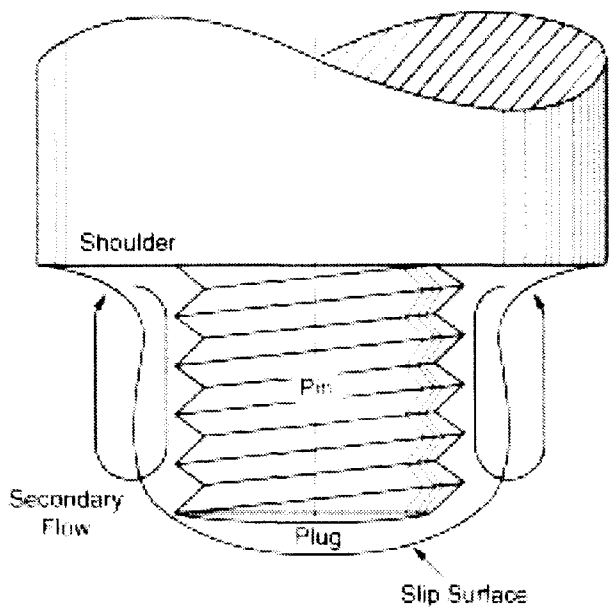

Figure 1. The rotating plug model comprises: (1) a rapidly rotating plug of metal attached to the pin-tool and slipping with respect to the workpiece on a cylindrical surface surrounding the pin-tool, and (2) a relatively slow circulation driven by the threads surrounding the pin as a vortex ring.

As the tool moves it is necessary for metal to pass from the front to the back of the tool. One way for this to occur is by a wiping motion. A wiping motion can be modeled by superposing a rotating disc velocity field

$$\vec{V} = -y\Omega\vec{i} + x\Omega\vec{j} \tag{1}$$

upon the velocity field of a uniform displacement

$$\vec{V} = -V\vec{i} \tag{2}$$

It is noted in passing that if volume is conserved ($\nabla \cdot \vec{V} = 0$) in each of the fields, it is conserved in their superposition. The velocities of the superposition field on the disc are

$$\frac{dx}{dt} = -(y\Omega + V) \tag{3}$$

and

$$\frac{dy}{dt} = x\Omega \tag{4}$$

The trajectory on the disc is computed by equating expressions for dt in the above equations.

$$xdx + \left(y + \frac{V}{\Omega}\right)d\left(y + \frac{V}{\Omega}\right) = 0 \tag{5}$$

or

$$x^2 + \left(y + \frac{V}{\Omega}\right)^2 = \text{Constant} \tag{6}$$

The resultant trajectories are circles displaced towards the forward moving side of the rotating disc (or the $\vec{V}x\vec{\Omega}$ direction). The resultant flow field is shown in Figure 2. For FSW normally $\frac{V}{\Omega} << r$, where r is the radius of the rotating plug. Hence the metal flow takes place in a thin layer on the surface of the rotating plug. Figure 2 greatly exaggerates the width of the wiping deformation layer just under the surface of the rotating plug.

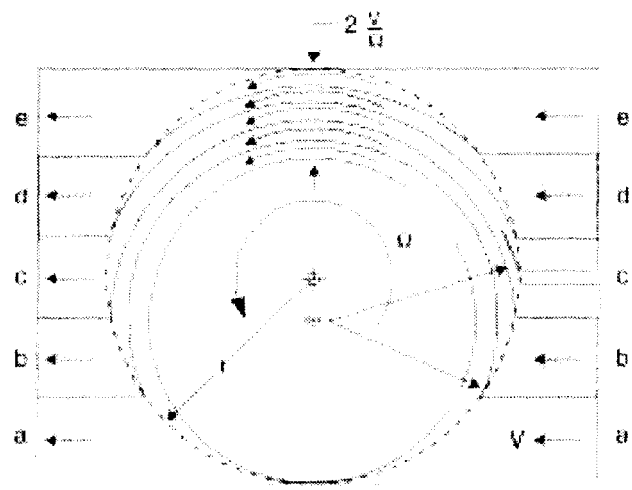

Figure 2. Wiping flow is modeled by superposing a rotating disc on a uniform translation. Trajectories on the disc are circles with radius displaced by $\frac{V}{\Omega}$ towards the advancing side of the disc. When $r\Omega >> V$, as is generally the case for FSW, flow about the central plug takes place in a thin layer ranging from zero to $2\frac{V}{\Omega}$ in thickness. Note that in this model metal exits the disc at the same position that it enters.

Because it is easy to visualize this model using people walking across a merry-go-round, it is sometimes referred to as the "merry-go-round" model. Imagine a person walking towards and stepping onto a merry-go-round. If the person continues to walk in the same direction (not an easy feat on a real merry-go-round), he moves into the rotating disc until he passes the disc center, then he moves out to the edge again in a symmetric trajectory. Because of the symmetry, he gets off at the same distance from the centerline as he gets on. That is, the rotation does not shift his ultimate y-position.

Tracer Experiments. Tracer experiments (See Figure 3) have been carried out at the University of South Carolina (Reynolds *et al*) where a FS weld is passed through a band of tracer metal of different, distinguishable composition.

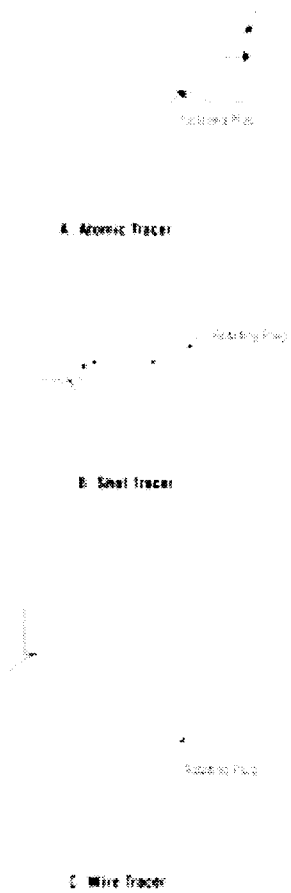

Figure 3. FSW tracer experiments.

A trailing parabolic loop of tracer metal is left behind the tool. The observed dimensions of the loop seem to agree with the rotating plug concept in that the particles appear to be displaced back from the original band by approximately the chord of the plug circle. Further, there is a forward pointing spur of tracer ahead of the original band on the forward moving side of the plug as if material being carried around the plug surface dropped off before

completing the circuit around the plug. The premature exiting of material from the rotating plug can be attributed to the secondary vortex flow.

Steel shot tracer experiments carried out at Boeing Company's Seattle, Washington, plant (Colligan) reveal a complex behavior that can be interpreted in terms of (1) the basic wiping flow characterized in Figure 2, (2) the variation in plug diameter with depth, and (3) a shifting of material with respect to the plug by the secondary flow.

For example, shot entrained by the rotating plug is not left behind at the same distance from the centerline as it entered. This is because the vortex circulation shifts the shot into an axial site where the plug radius is different. If the plug radius variation is large with respect to axial displacement along the pin close to the tool shoulder, the lateral displacement of the shot becomes more sensitive to slight variations in axial displacement. This is taken to be the reason why the shot patterns exhibit a great deal of scatter in the proximity of the tool shoulder.

At Marshall Space Flight Center the effect of the FSW tool on wire tracers (Bernstein *et al.*) was found to support the concept of the rotating plug model. Copper wires were inserted into holes drilled perpendicular to the weld interface at different plate depth levels. The wires on the forward moving side of the pin-tool were bent forward and broken. The wires on the retreating side of the pin-tool were swept backwards into a trailing curve. The shapes of the trailing curves were computed for different distributions of angular velocity around the pin-tool. The computations that agreed best with the observations were those for the sharpest drop-off of the angular velocity, i.e. the computations closest to the sharp discontinuity of the rotating plug model.

Strain Rates. The idealized wiping model presented here does not yield a strain rate. Each stream of metal approaching the rotating plug at a different lateral position receives its own instantaneous shear increment as it crosses the shear interface. The sheared metal has a certain time at the temperature of the shear zone for recovery. Then the metal receives a second shear increment as it exits from the rotating plug.

It is possible to estimate a representative shear rate, however. The metal flows into the plug of radius r over a path of width 2r. By the time it has been swept to the side of the plug, $\frac{\pi}{2\Omega}$, the stream of metal is narrowed to $2\frac{V}{\Omega}$ for a tensile strain of $\frac{r\Omega}{V}$. The strain rate $\dot{\varepsilon}$ is approximately

$$\dot{\varepsilon} \sim \frac{2}{\pi}\frac{r\Omega^2}{V} \tag{7}$$

If r = 0.22 inches, V = 5.25 inches/minute, and $\Omega = 2\pi(350\text{ RPM})$, then the resulting strain rate is 2150 sec^{-1}. This is high, in the range of metal cutting strain rates.

This strain rate estimate, more of a lower bound, perhaps, than a mean, is of interest in that it appears to have a potential for estimating the microstructure of a FS weld.

One approach is to approximate the link between mechanical strain and resulting microstructure by a dynamic recovery process. These softening processes all involve "single dislocations, which are annihilated in individual events" (McQueen and Jonas p. 438). A correlation has been published (McQueen and Jonas p. 409) between the subgrain diameter d of commercial purity aluminum and the Zener-Holloman parameter (Zener and Holloman), $Z \equiv \dot{\varepsilon} e^{\frac{37,300}{RT}}$ sec^{-1}, where $\dot{\varepsilon}$ is the applied strain rate, R, the Gas Constant, and T the absolute temperature during deformation:

$$d = \frac{1}{0.08 \log Z - 0.6} \tag{8}$$

The approximate correlation holds for Z's less than 10^{18}. The highest strain rate listed in the experimental data is 219 sec^{-1}.

An attempt (Frigaard *et al*) was made to use this relation to work backwards from measured subgrain diameters and estimate the strain rates in FS welds in AA6082 and AA7108 aluminum extrusions (conforming to 6082-T6 and 7108-T79 alloys). Rates obtained in this way were extremely low, 1 to 20 sec^{-1}. Frigaard *et al* attribute the discrepancy between their low strain rate estimates and the much higher strain rates expected from the nature of the mechanical process to melting "a liquid film at the tool/matrix interface".

An explanation more in consonance with the concept of the FSW process expressed herein would be that at the high strain rates dynamic recrystallization, "where dislocations are annihilated in large numbers through the migration of a high angle boundary" (McQueen and Jonas p.438), accounts for much of the structural transformation during mechanical deformation.

In any case a means for linking the mechanically estimated strains with the FSW microstructure does not exist at present. The understanding of the transformations that annihilate dislocations at high strain rates is not adequate.

Conclusions. The rotating plug model of the FSW process explains complex-seeming results of tracer experiments well and simply. It is thought to be fairly well substantiated.

The model permits a rudimentary estimate of the FSW strain rate. An estimation of the FSW microstructure from the strain rate, however, awaits a better understanding of recovery and recrystallization dynamics at high strain rates.

Even in its present state of development, the model is a potentially useful tool in fault diagnostics, and a correct kinematics is a prerequisite for constructing a dynamics (Nunes *et al*) of the FSW process.

References.

Backofen, Walter A. 1972. Deformation Processing. Addison-Wesley Publishing Company: Reading, MA.

Bernstein, E.L. and Nunes, A.C., Jr. 2000. The Plastic Flow Field in the Vicinity of the Pin-Tool during Friction Stir Welding. Under review by *Welding Journal*.

Colligan, K. 1999. Material Flow Behavior during Friction Stir Welding of Aluminum. *Welding Journal* 78(7): 229-s to 237-s.

Crandall, Steven H. 1956. *Engineering Analysis: A Survey of numerical procedures*. McGraw-Hill Book Company, Inc.: New York.

Frigaard, Ø., Grong, Ø., Hjelen, J., Dulbrandsen-Dahl, S. and Midling, O.T. 1999. Characterization of the subgrain structure in friction stir welded aluminium alloys using the SEM-EBSD technique. *1st International Symposium on Friction Stir Welding*, Rockwell Science Center, Thousand Oaks, CA. June 14-16.

Hill, R. 1950. *The Mathematical Theory of Plasticity*. Oxford at the Clarendon Press: New York.

McQueen, H.J. and Jonas, J.J. 1975. Recovery and Recrystallization during High Temperature Deformation. *Treatise on Materials Science and Technology, Volume 6: Plastic Deformation of Metals*, R.J. Arsenault, Ed. Academic Press: New York. 393-493.

Nunes, A.C., Jr., Bernstein, E.L. and McClure, J.C. 2000. A Rotating Plug Model for Friction Stir Welding. 81st AWS Annual Convention, Chicago, IL, April 25-28.

Reynolds, A.P., Seidel, T.U., and Simonsen, M. 1999. Visualization of Material Flow in an Autogenous Friction Stir Weld. *1st International Symposium on Friction Stir Welding*, Rockwell Science Center, Thousand Oaks, CA. June 14-16.

Thomas, W.M., *et al.*. Dec. 1991. Friction Stir Welding. U.S. Patent 5,460,317.

Zener, C. and Holloman, J.H. 1944. Effect of Strain Rate Upon Plastic Flow of Steel. *Journal of Applied Physics*. 15, January.22-32.

APPENDIX 1

Nomenclature

d	Subgrain diameter
$\vec{i}, \vec{j}$	Unit vectors in x- and y-directions respectively
t	Time
$\vec{V}$	Translational velocity of pin-tool
V	Weld speed
x	Distance from center of rotating pin in direction of movement
y	Distance from center of rotating pin perpendicular to linear movement in direction of retreating side of pin
$\dot{\varepsilon}$	Strain rate
$\vec{\Omega}$	Angular velocity of pin
Ω	Magnitude of angular velocity of pin

APPENDIX 2

Viscous theories of the FSW flow field. It is tempting to try to construct a viscous model of the FSW flow field. A viscous flow field will be continuous and distributed as initially expected. But the assumption of viscosity requires physical justification. As the apparent operating temperatures are substantially below the alloy solidus temperature, justification of the assumption of viscosity presented greater difficulties than abandonment of the expectation of a continuous, distributed FSW flow field.

Metals have flow characteristics unlike those of gases or liquids. When a layer of gas is sheared, gas molecules with speeds matched to the moving boundaries by collisions with the boundaries transfer momentum by intermolecular collisions through the layers of gas between the boundaries. The momentum transfer results in a viscous shear force on the boundaries. A rise in temperature promotes more momentum transfer so that the viscosity of gases goes up with increasing temperature.

When a layer of liquid is sheared random local structural rearrangements ease the shear force transmitted by the elastic character of the liquid. In doing so they determine the level of stress across the liquid layer. These local structural rearrangements come into play at the lowest of stress levels and in whatever direction the stress is acting. Thus liquids exhibit viscous behavior. The viscosity of liquids, unlike that of gases, goes down with increasing temperature, however, because thermal energy aids local structural rearrangements of liquids.

When a layer of metal is sheared, the metal at first deforms elastically. Only after a sufficiently high stress is imposed do the internal dislocation sources begin to emit so that plastic flow occurs. If structural changes leading to work hardening are ignored, the flow stress of a metal remains constant. Metals are not viscous. They are plastic. That is, the stress is whatever is applied up to the flow stress, but a stress higher than the flow stress cannot be applied; the metal merely flows at this point.

Because the flow stress of metals is only weakly dependent upon strain rate, the metallic stress-strain curve is more or less independent of strain rate, which is not at all the case for viscous materials. A simple dislocation mechanism of metallic flow yields a dependence of flow stress on the logarithm of the strain rate. Although metals are not viscous, the dislocation emission process is thermally activated so that the flow stress of metals depends strongly upon temperature.

This is why plasticity theory (Hill, Backofen), which amounts to the solution of a hyperbolic system of equations (Crandall), where characteristic lines exist along which there can be discontinuities, is so different from a (incompressible) viscous flow theory, which employs parabolic or elliptical systems of equations.

Aluminum Lithium Alloy 2195 Fusion Welding Improvements with New Filler Wire

AMPET 2000
Huntsville, AL

Carolyn Russell
NASA
Marshall Space Flight Center
Huntsville, AL.
256-544-2705
carolyn.russell@msfc.nasa.gov

2195 Fusion Welding Improvements with New Filler Wire

Background

- **Welding 2195 Aluminum Lithium for the Space Shuttle Super Lightweight External Tank**

NASA Space Shuttle

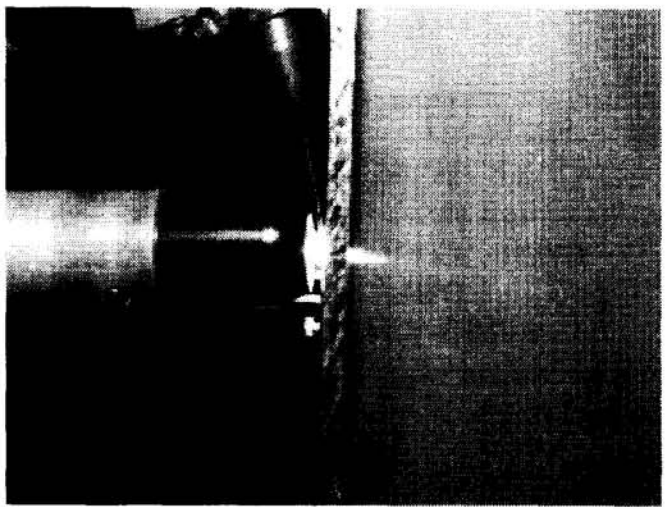

Variable Polarity Plasma Arc Welding

2195 Fusion Welding Improvements with New Filler Wire

Background

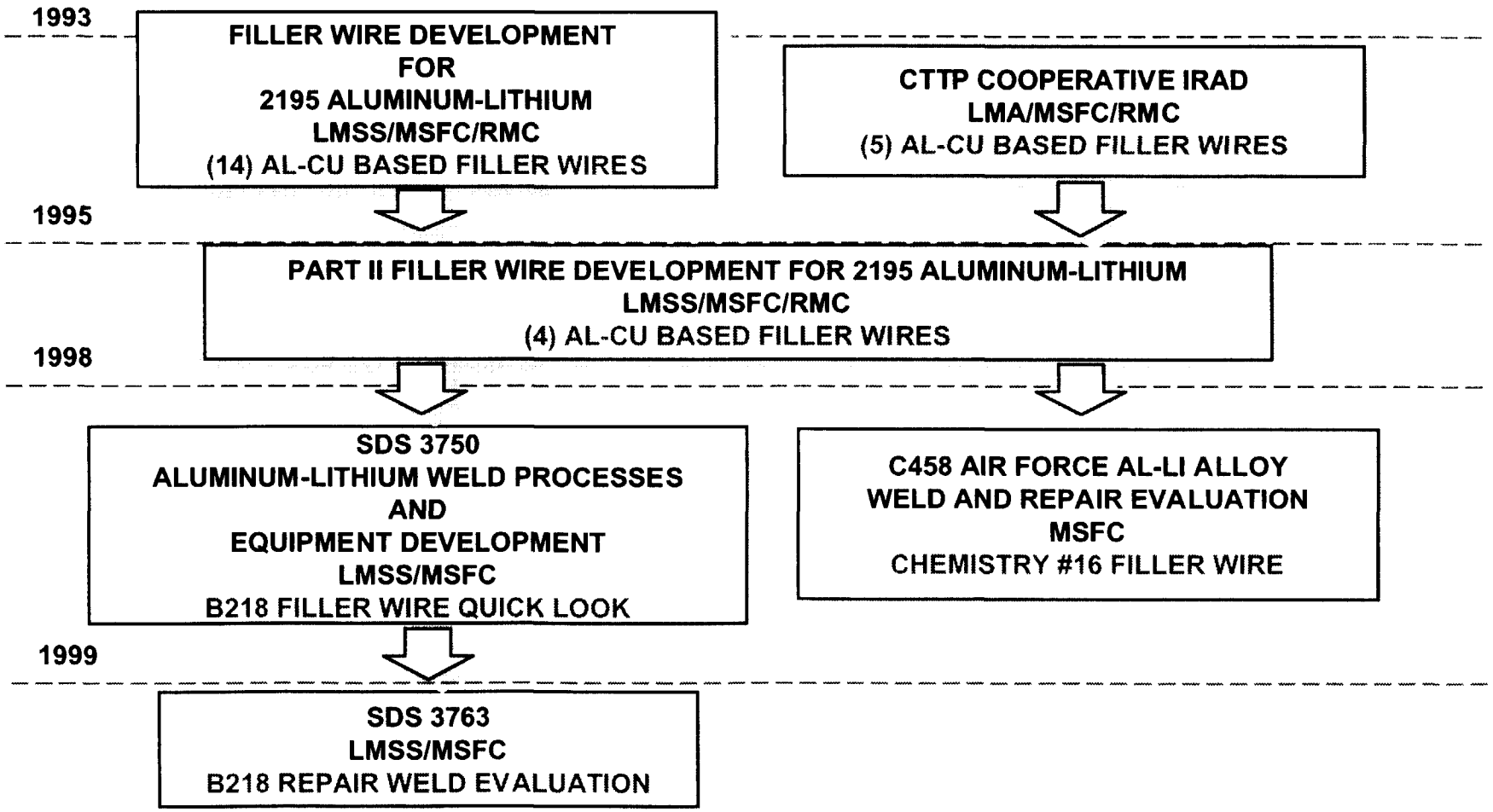

2195 Fusion Welding Improvements with New Filler Wire

2195T8M4 VPPA Weld Ultimate Tensile Strength

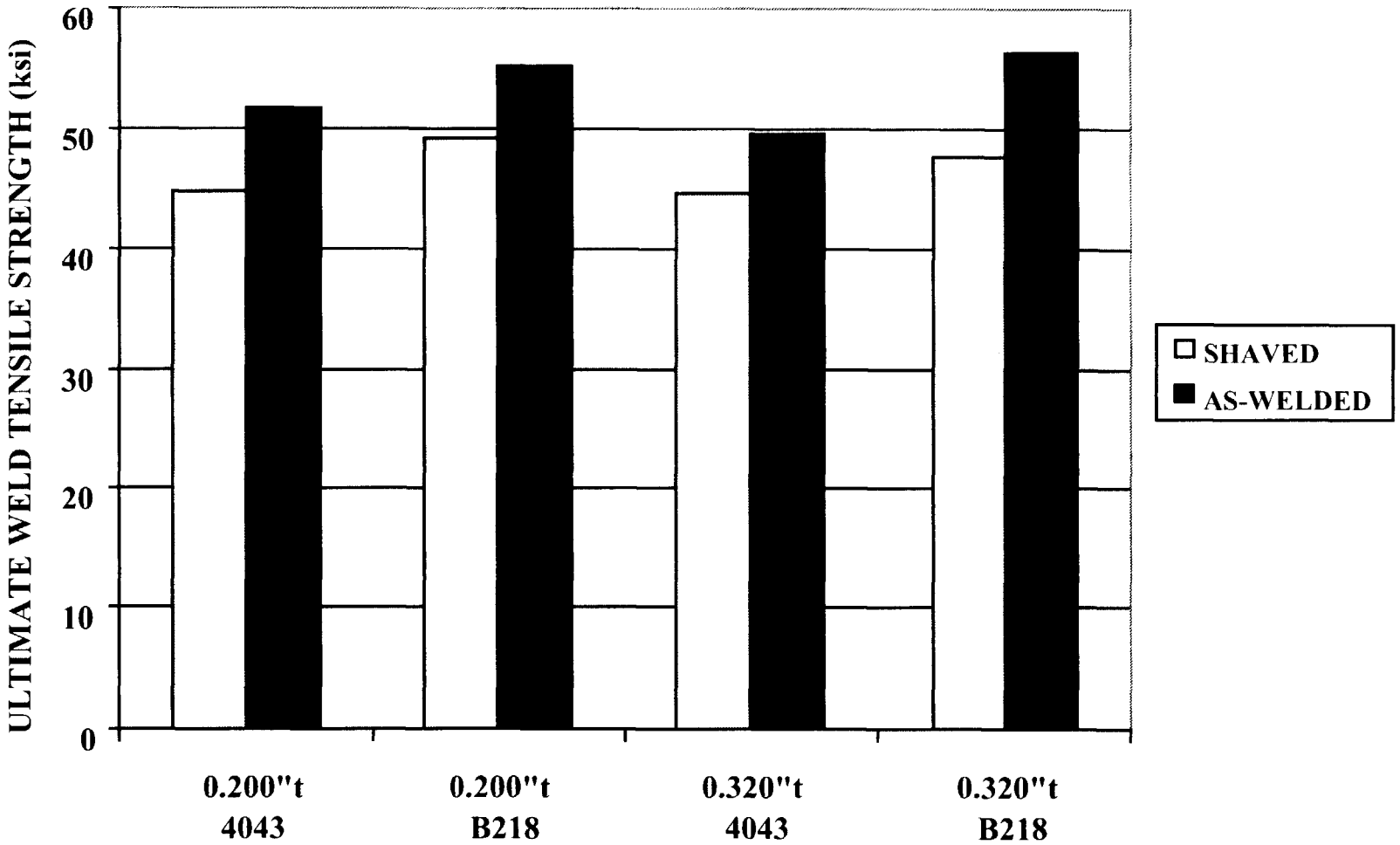

2195 Fusion Welding Improvements with New Filler Wire

2195T8M4 VPPA Weld Tensile Elongation

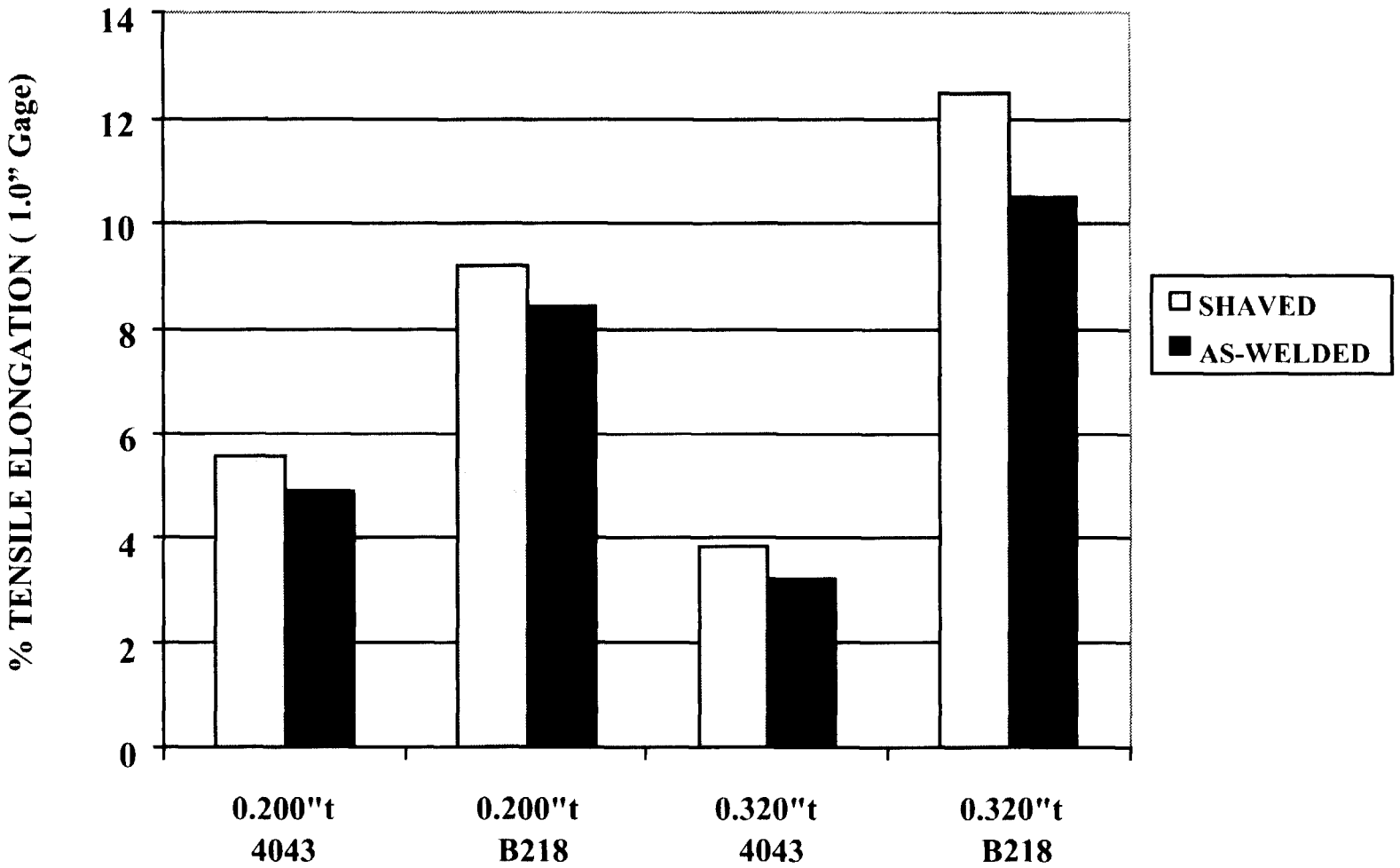

2195 Fusion Welding Improvements with New Filler Wire

VPPA Weld Grain Structure Comparison

0.320t 2195 PLATE TO 2195 PLATE VPPAW

4043 WELD FILLER WIRE

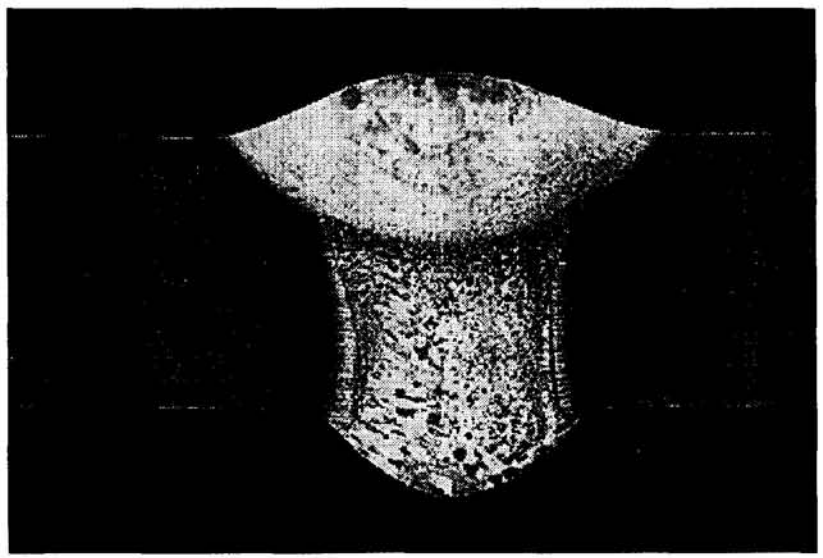

10X Original Magnification

B218 WELD FILLER WIRE

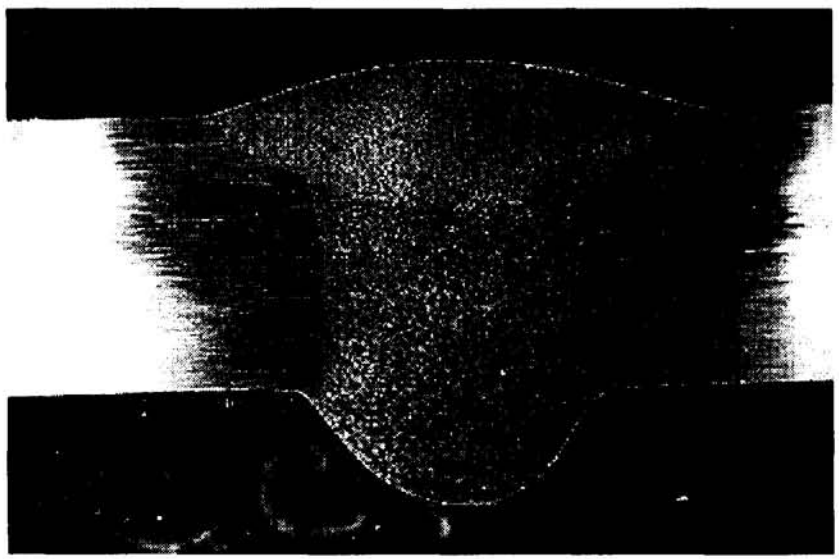

10X Original Magnification

2195 Fusion Welding Improvements with New Filler Wire

B218 VPPA Weld Grain Structure

0.200t 2195 PLATE TO 2195 PLATE VPPAW

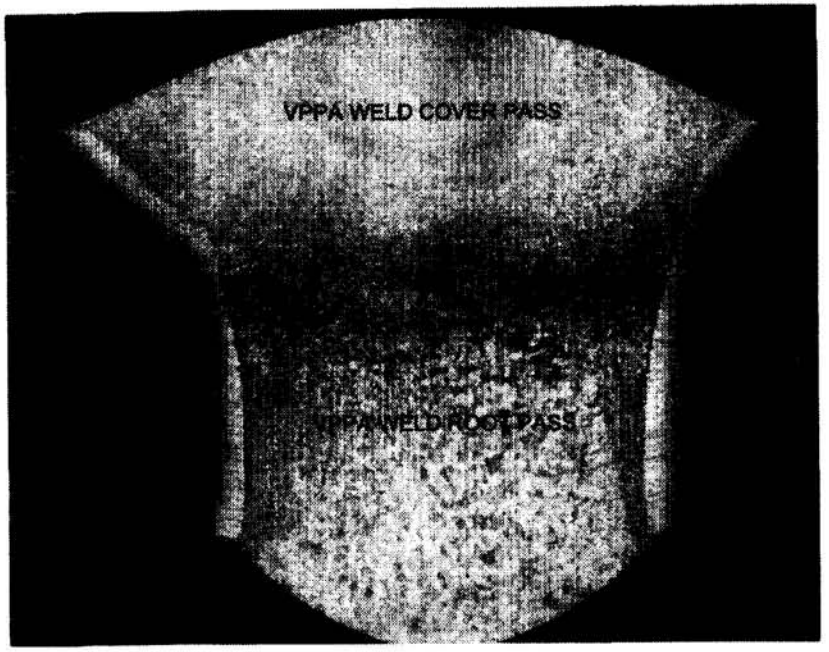

10X Original Magnification

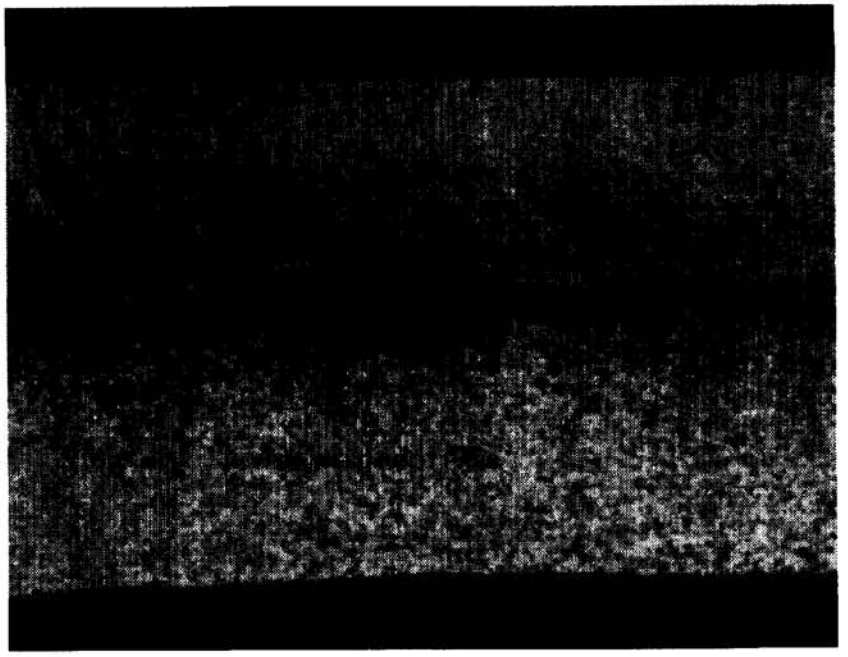

10X Original Magnification

2195 Fusion Welding Improvements with New Filler Wire

B218 GTA Repair Weld Grain Structure

R1 GTA Repair 0.200t 2195 PLATE TO 2195 PLATE VPPAW

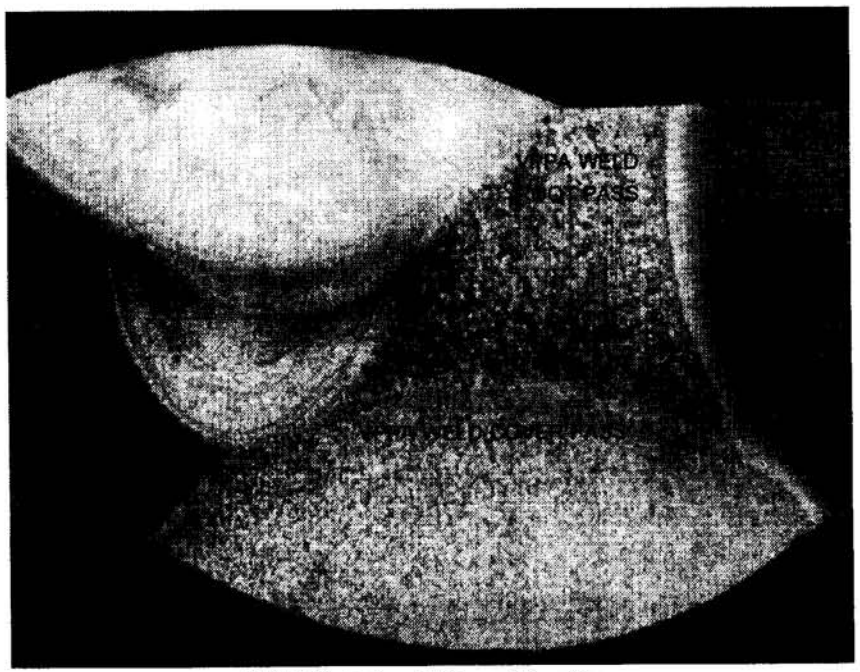

10X Original Magnification

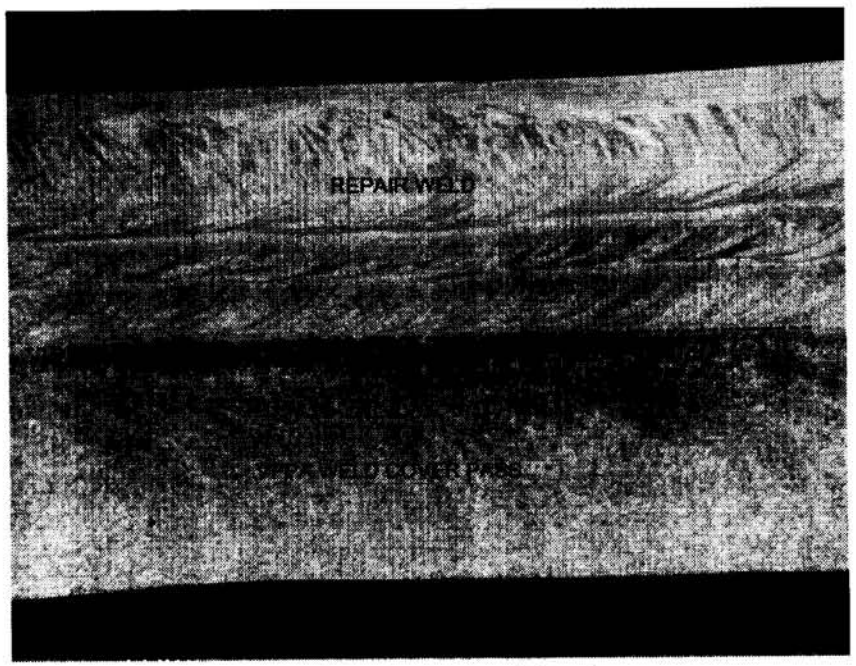

10X Original Magnification

2195 Fusion Welding Improvements with New Filler Wire

2195 Repair Weld Residual Stresses

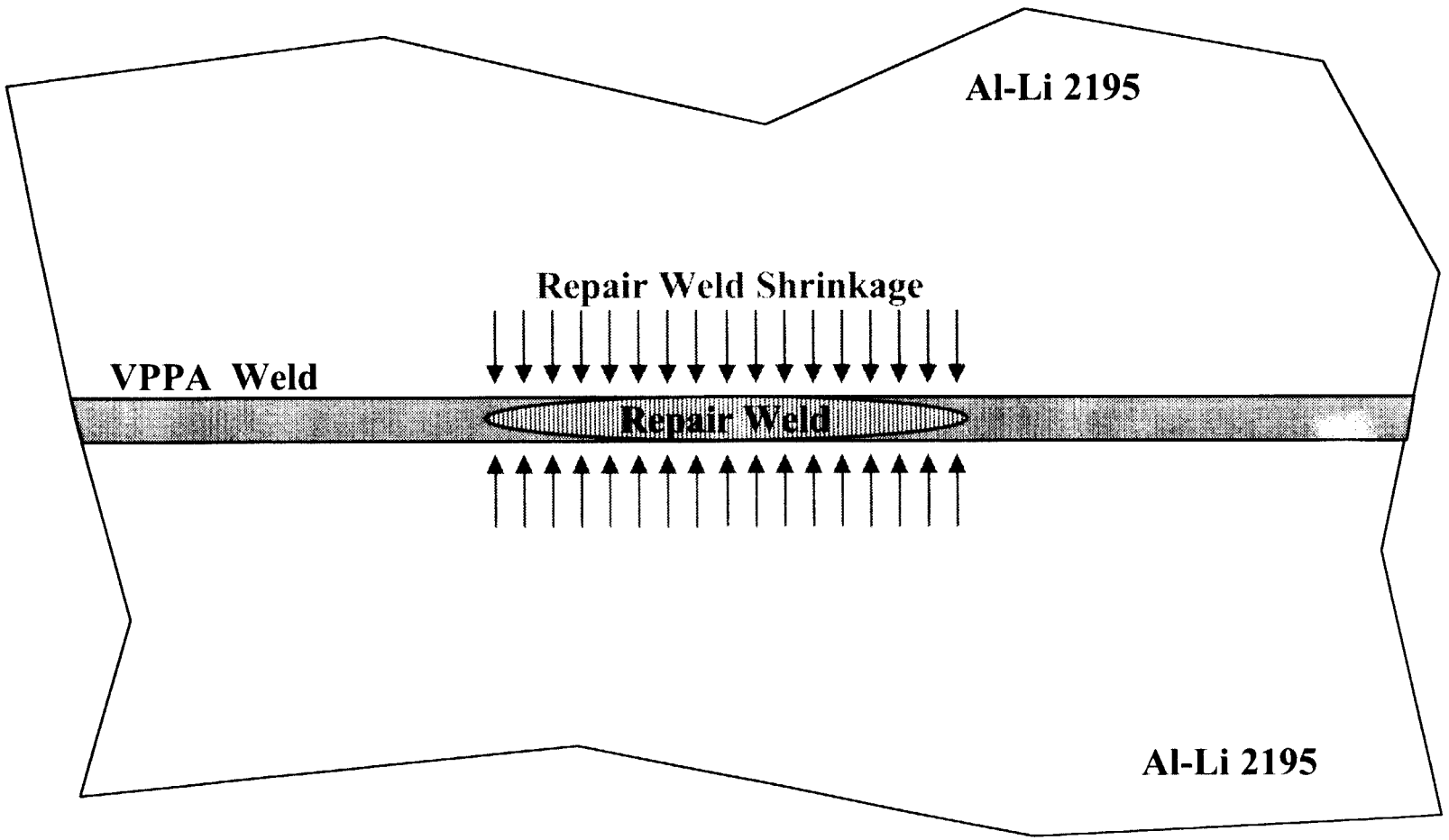

2195 Fusion Welding Improvements with New Filler Wire

2195 Repair Weld Residual Stresses

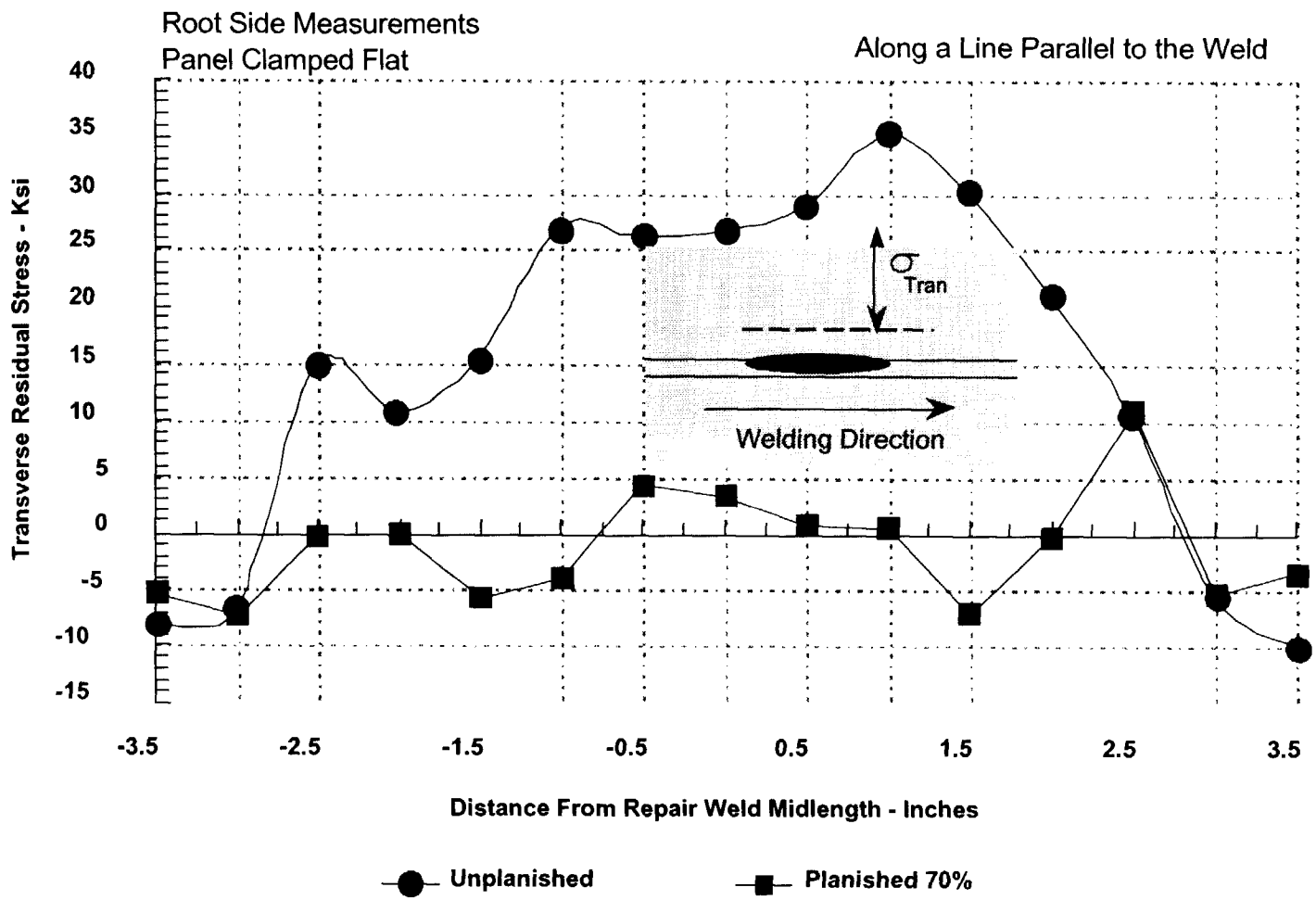

2195 Fusion Welding Improvements with New Filler Wire

2195 Repair Weld Residual Stresses

R5 GTA Repair 0.200t 2195 PLATE TO 2195 PLATE VPPAW

Photostress of Unplanished Repair Weld

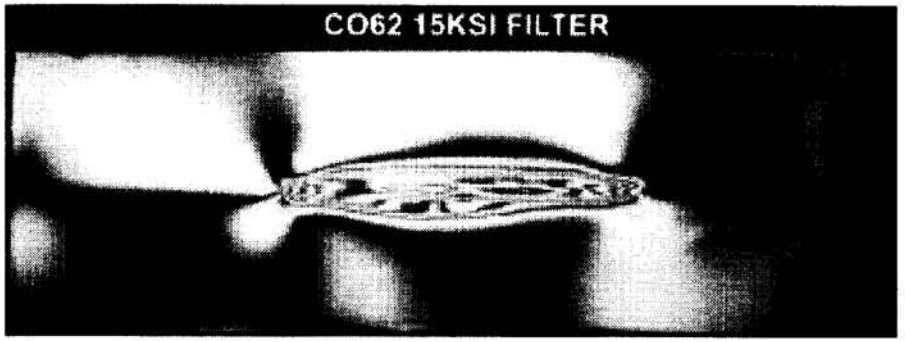

Photostress of Planished Repair Weld

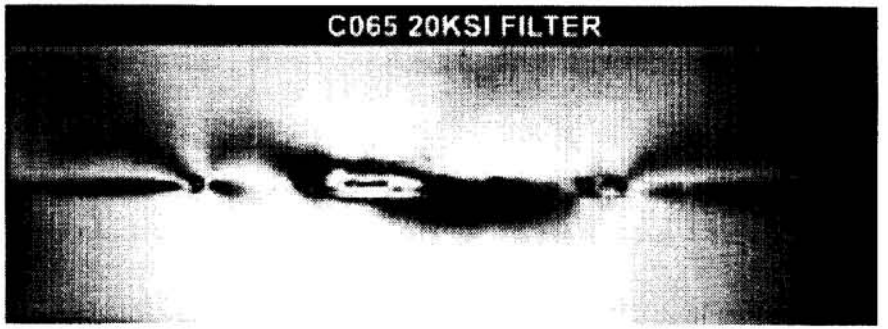

2195 Fusion Welding Improvements with New Filler Wire

Objective

- Assess B218 weld filler wire for Super Lightweight External Tank production, which could improve current production welding and repair productivity.

Approach

- Perform a repair weld quick look evaluation between 4043/B218 and B218/B218 weld filler wire combinations. Evaluate tensile properties for planished and unplanished conditions.

- Perform repair weld evaluation on structural simulation panel using 4043/B218 and B218/B218 weld filler wire combinations. Evaluate tensile and simulated service fracture properties for planished and unplanished conditions.

2195 Fusion Welding Improvements with New Filler Wire

VPPA/GTA Repair Weld Quick Look

- **14" X 24" Standard Repair Weld Panel**

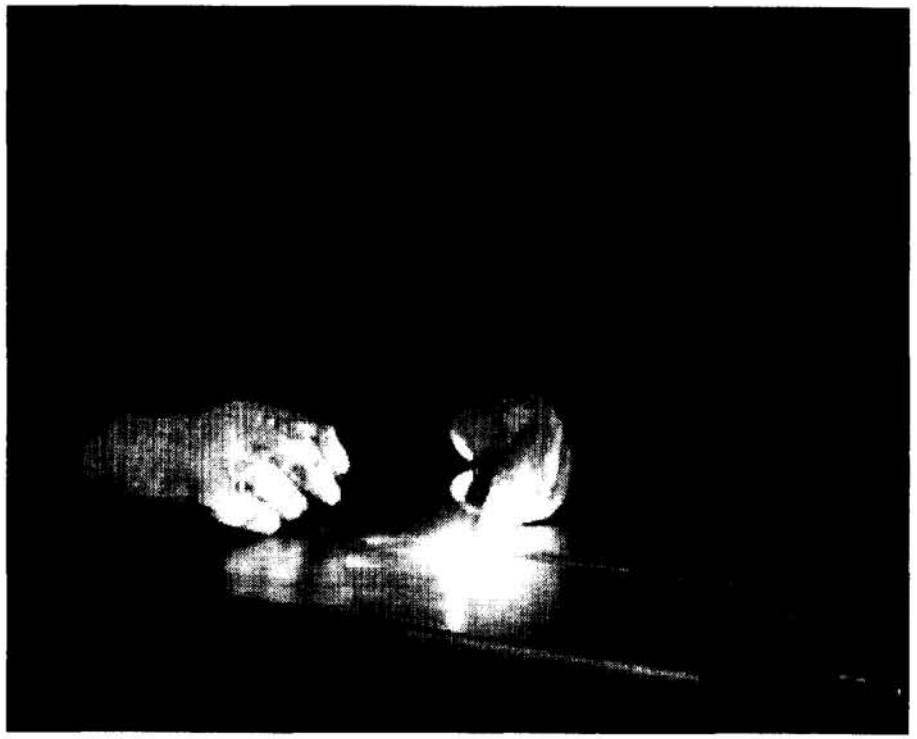

Manual GTA Repair Welding

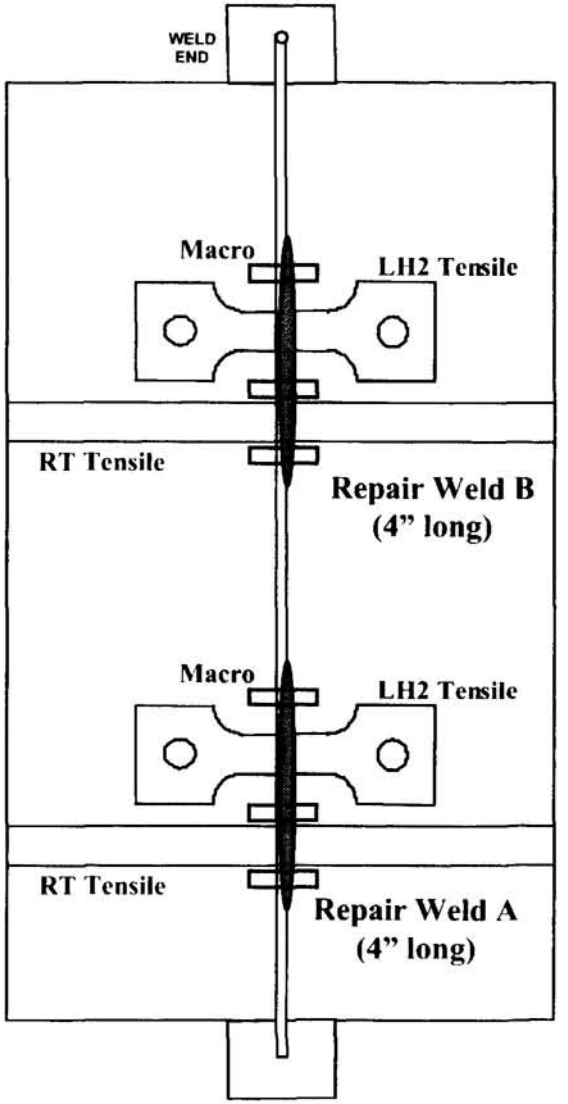

2195 Fusion Welding Improvements with New Filler Wire

0.200"t 2195T8M4 Repair Weld Ultimate Tensile Strength -Coupon Level

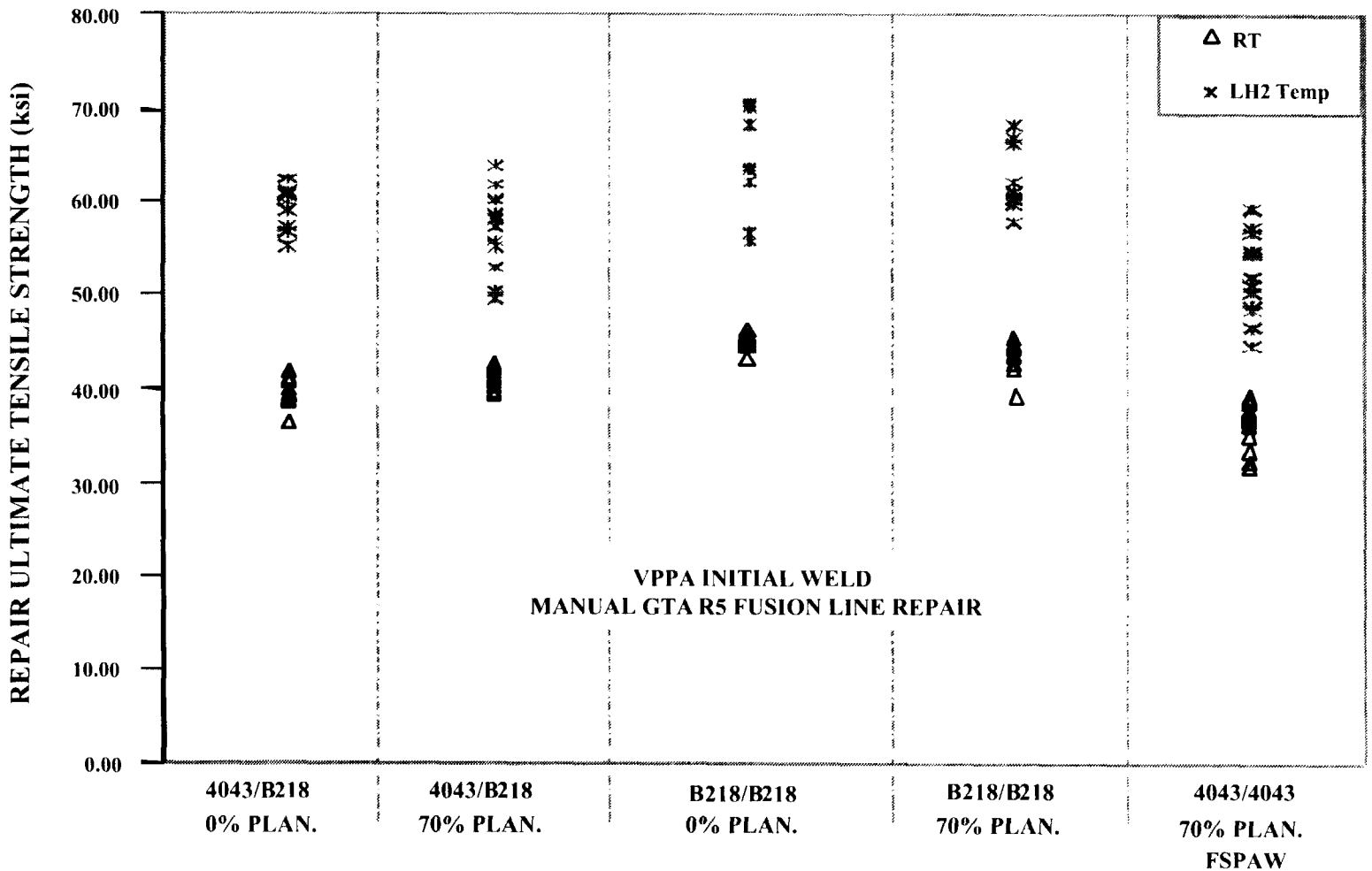

2195 Fusion Welding Improvements with New Filler Wire

0.200"t 2195T8M4 Repair Weld Ultimate Tensile Elongation - Coupon Level

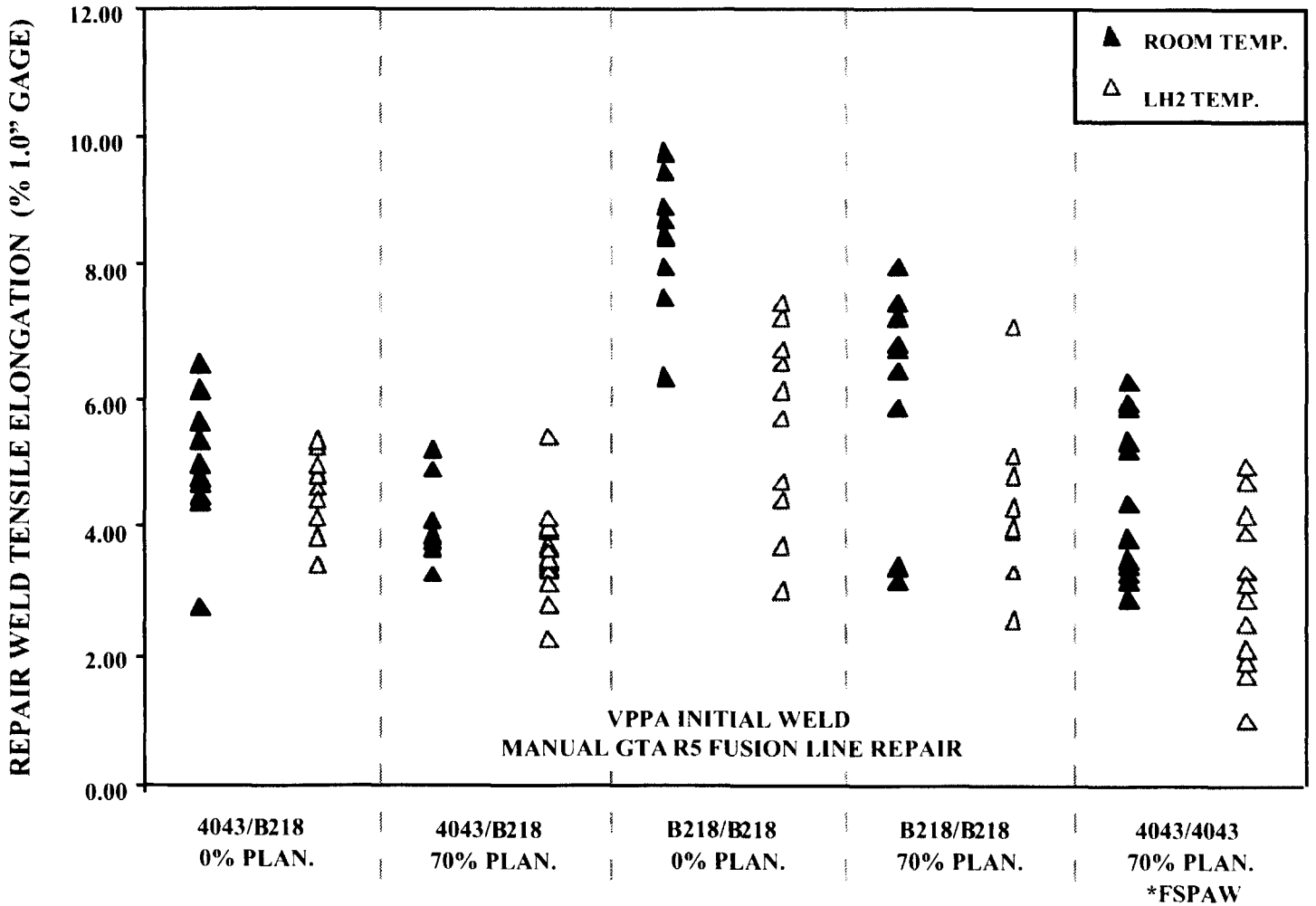

2195 Fusion Welding Improvements with New Filler Wire

0.200t 2195T8M4 VPPA/ GTA Repair Weld Metallography

- **4043/B218 0% Planished**

7X Original Magnification

C008-RT02
RT Tensile Test
36.2 ksi / 2.74%El. 1" gage

C009-CT01
LH2 Temp. Tensile Test
62.5 ksi / 3.4%El. 1" gage

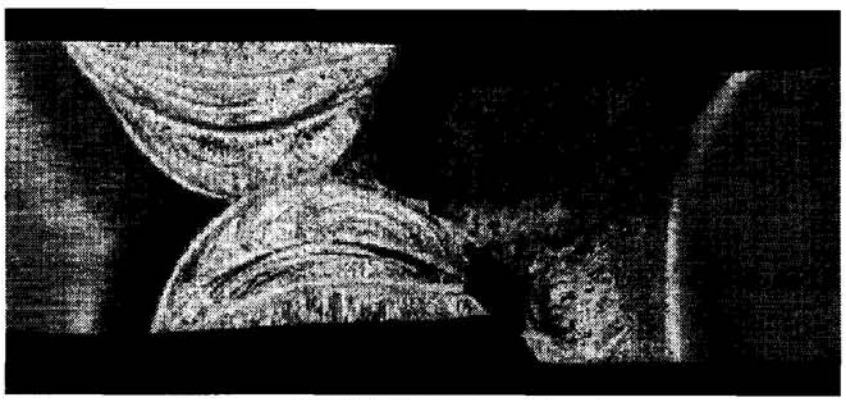

7X Original Magnification

2195 Fusion Welding Improvements with New Filler Wire

0.200t 2195T8M4 VPPA/ GTA Repair Weld Metallography

- **B218/B218 0% Planished**

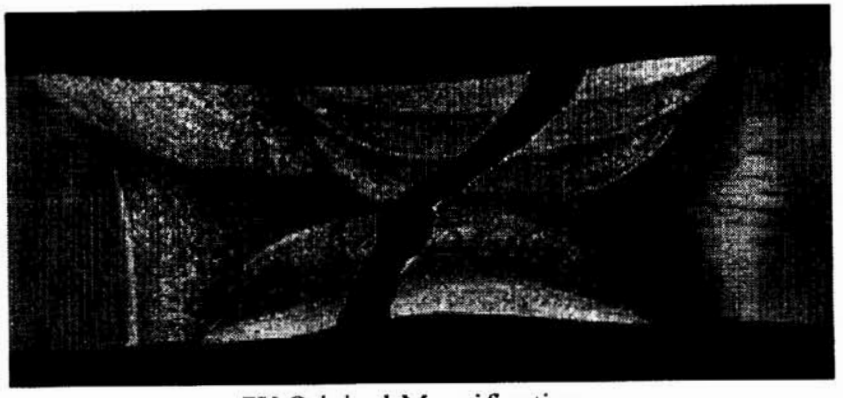

7X Original Magnification

C080-RT01
RT Tensile Test
45.2 ksi / 9.75%El. 1" gage

C080-CT01
LH2 Temp. Tensile Test
68.1 ksi / 7.40%El. 1" gage

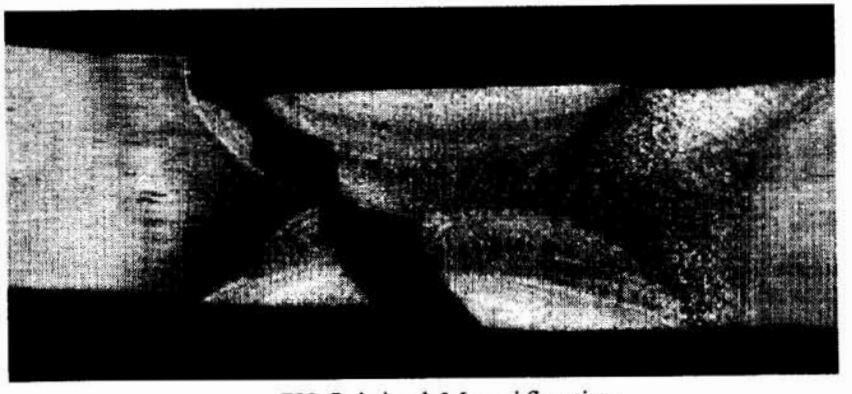

7X Original Magnification

2195 Fusion Welding Improvements with New Filler Wire

VPPA/ GTA Repair Weld Structural Simulation Panel Evaluation

- 19" X 48" Repair Weld Wide Panel

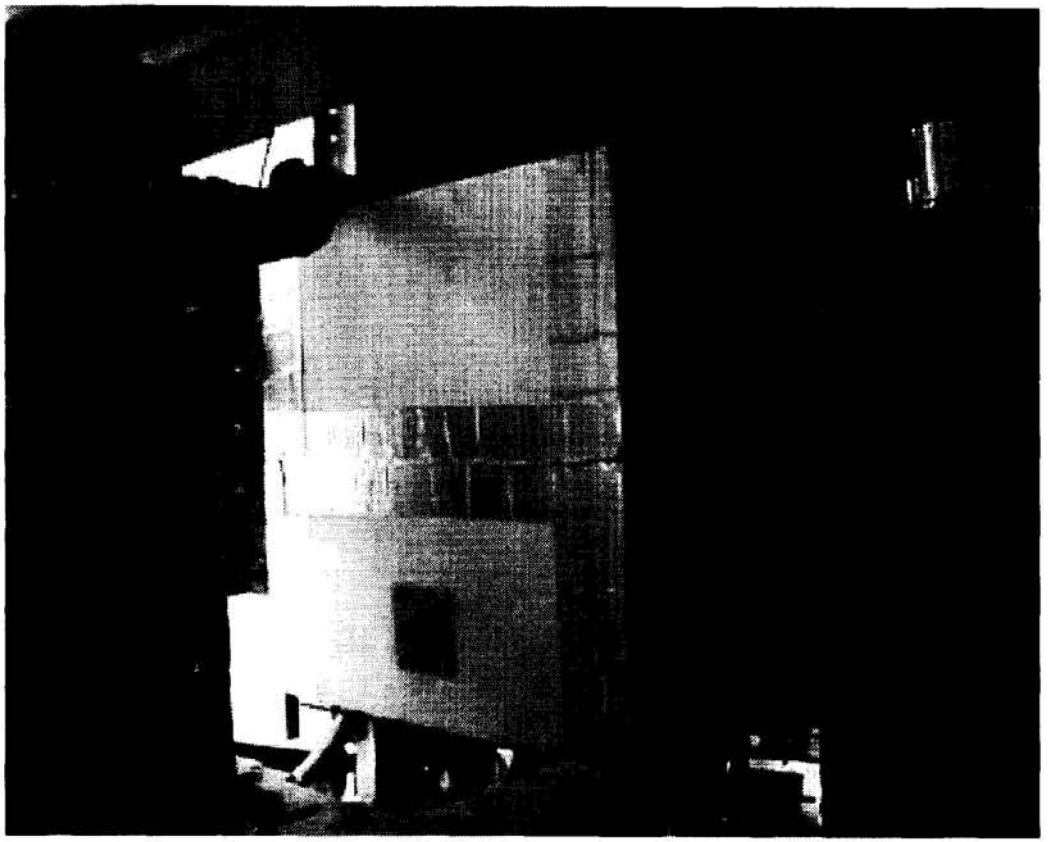

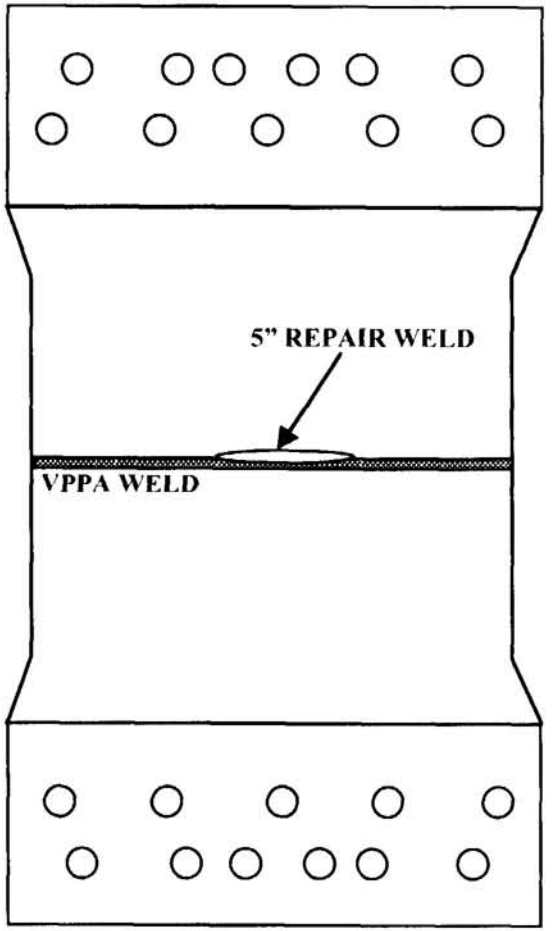

2195 Fusion Welding Improvements with New Filler Wire

0.200t 2195T8M4 Structural Simulation Panel Weld Tensile Strength (-423°F)

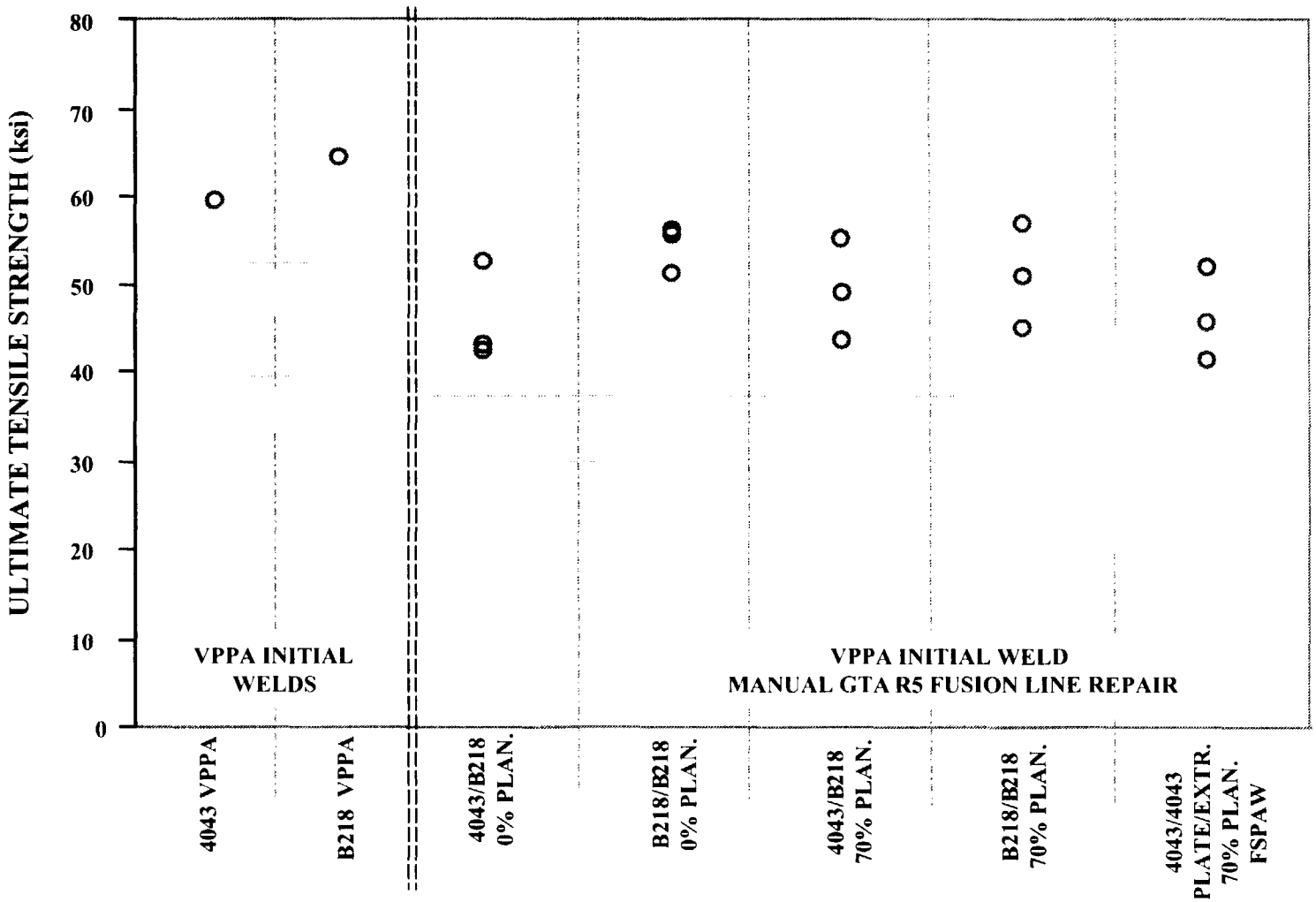

2195 Fusion Welding Improvements with New Filler Wire

0.320t 2195T8M4 Structural Simulation Panel Weld Tensile Strength (-423°F)

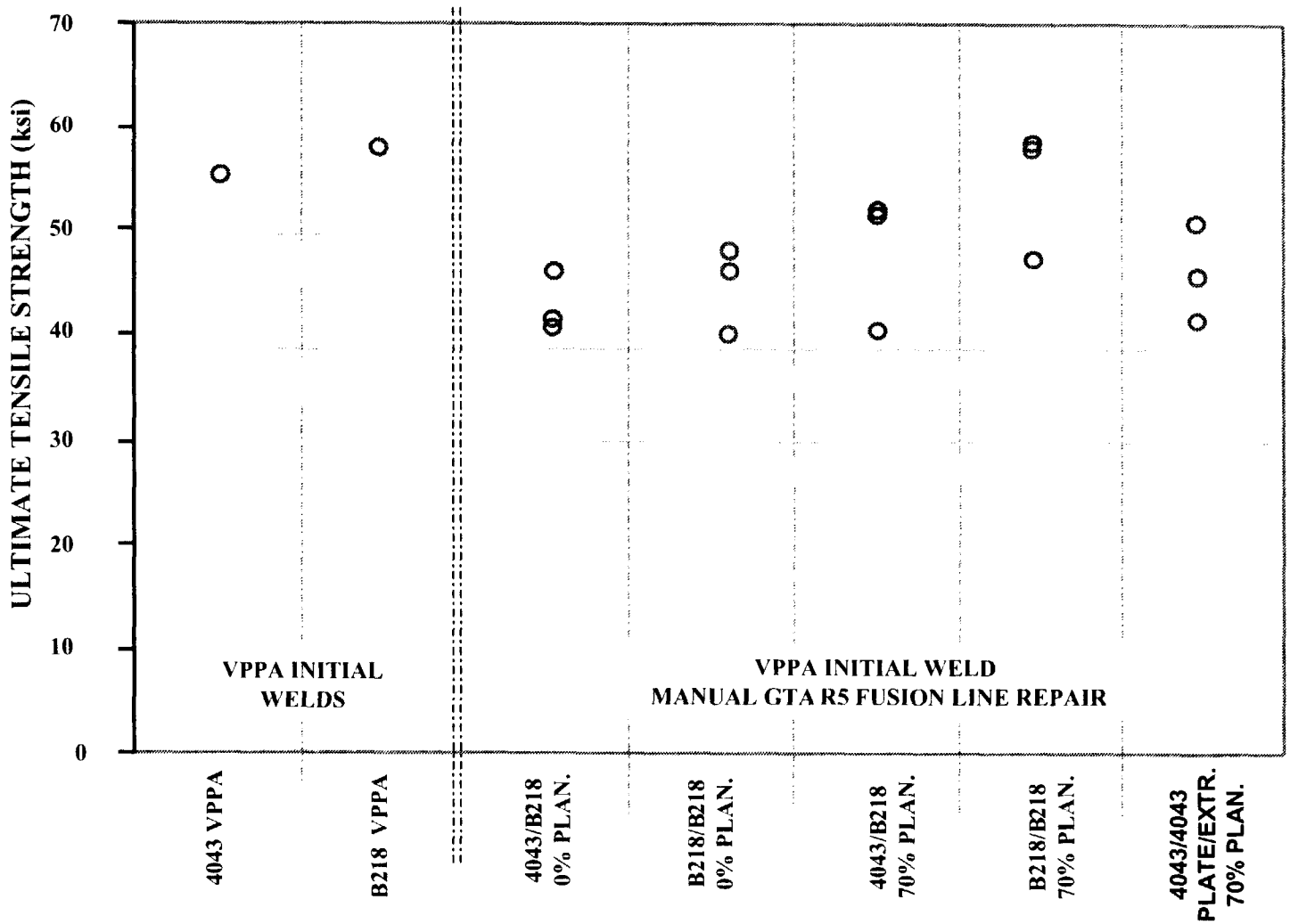

2195 Fusion Welding Improvements with New Filler Wire

0.200t 2195T8M4 VPPA/GTA Repair Weld Simulated Service Fracture Toughness

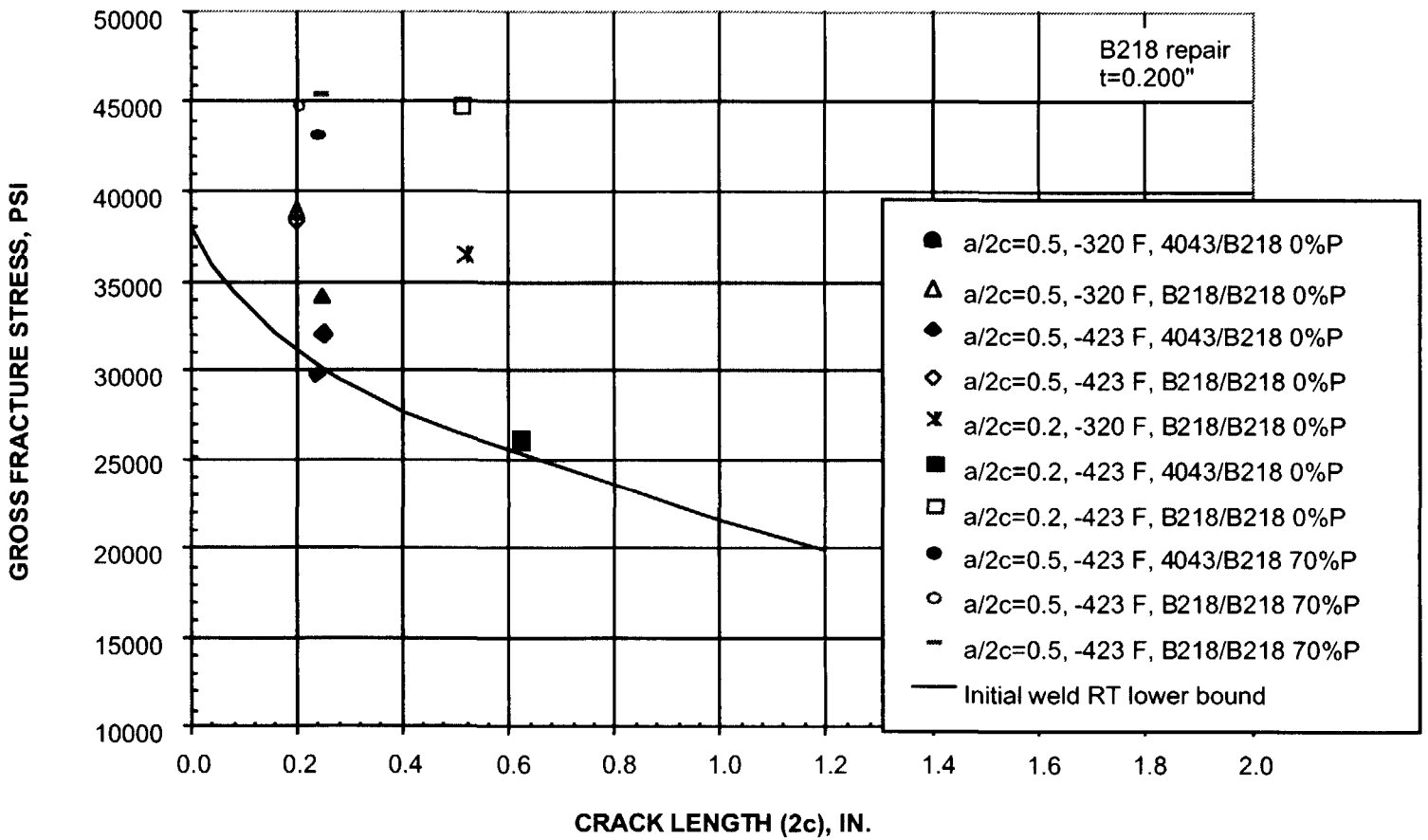

2195 Fusion Welding Improvements with New Filler Wire

0.320t 2195T8M4 VPPA/GTA Repair Weld Simulated Service Fracture Toughness

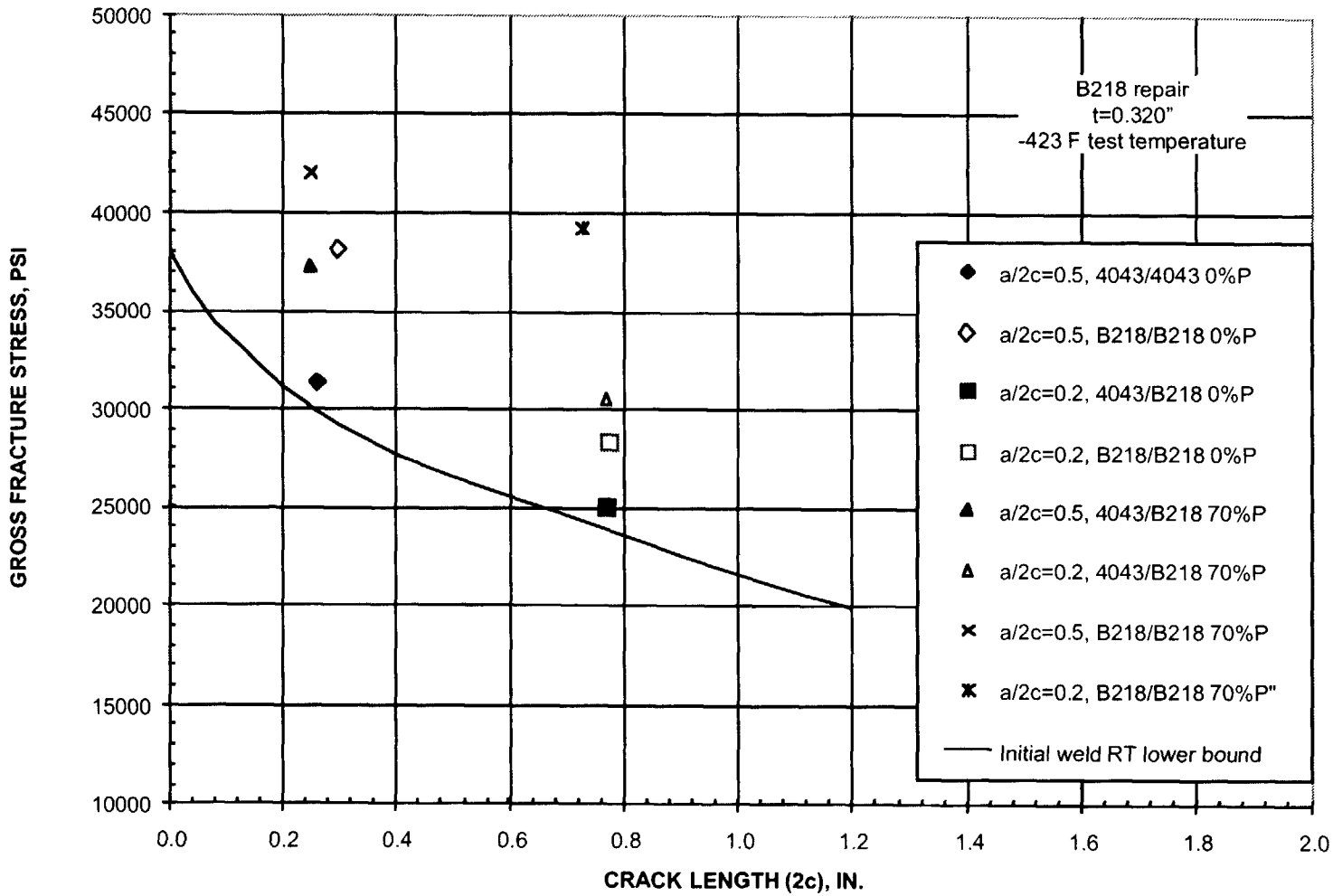

2195 Fusion Welding Improvements with New Filler Wire

Conclusions

- B218 weld filler wire displayed higher repair weld tensile strength and ductility compared to 4043.
- Unplanished and planished B218 repair welds exceeded the current SLWT 4043 repair weld tensile strength requirement.
- B218 repair weld simulated service results surpassed 4043 repair welds and were comparable to 2195 initial welds made with 4043.
- B218 displays a high potential for improving SLWT production through increased repair weldability and the reduction/elimination of planishing for the removal of repair weld residual stresses.

p/556/10/0

Fabrication of Composite Combustion Chamber/Nozzle For Fastrac Engine

T. Lawrence
Marshall Space Flight Center
Mailstop: ED34
Huntsville, AL 35812
Email: tim.lawrence@msfc.nasa.gov

R. Beshears, S. Burlingame, W. Peters, M. Prince, M. Suits, S. Tillery, Marshall Space Flight Center
L. Burns, M. Kovach, K. Roberts, Thiokol Propulsion Group

Abstract

The Fastrac Engine developed by the Marshall Space Flight Center for the X-34 vehicle began as a low cost engine development program for a small booster system. One of the key components to reducing the engine cost was the development of an inexpensive combustion chamber/nozzle. Fabrication of a regeneratively cooled thrust chamber and nozzle was considered too expensive and time consuming. In looking for an alternate design concept, the Space Shuttle's Reusable Solid Rocket Motor Project provided an extensive background with ablative composite materials in a combustion environment. An integral combustion chamber/nozzle was designed and fabricated with a silica/phenolic ablative liner and a carbon/epoxy structural overwrap. This paper describes the fabrication process and developmental hurdles overcome for the Fastrac engine one-piece composite combustion chamber/nozzle.

Introduction

The Fastrac 60,000 pound thrust engine (60K) combustion chamber/nozzle, referred to henceforth as the nozzle, began as part of a low cost technology demonstration effort. Development began at the 15 thousand pound thrust (15K) size with material performance testing and was scaled up to the 40 thousand pound thrust (40K) "flight" type demonstration size. The final 60K design has the same inner contour as the 40K with changes driven by process development and X-34 flight requirements. The technology efforts were combined into a low cost engine design under NASA's Low Cost Booster Technology project to demonstrate that a robust, low cost engine was an attainable goal.

As part of the Low Cost Booster Technology project, the engine was designed for use in an expendable booster. This significantly impacted the material selection and engine packaging. A composite liner and structural overwrap with bonded metal attach hardware were selected for development. In comparison to a regeneratively cooled thrust chamber assembly, composites were an order of magnitude cheaper and could be produced in less than one-sixth the time. With a composite design the combustion chamber and nozzle could be fabricated in a single unit, removing the complexity and weight of a joint design. The composite design also reduced the complexity of the engine since no fuel would be pumped through the component walls for cooling.

Silica/phenolic was selected as the ablative liner material and carbon/epoxy was selected as the structural overwrap. The silica/phenolic material selection was made based on knowledge and experience gained from the Space Shuttle's Reuseable Solid Rocket Motor (RSRM) and the Solid Propulsion Integrity Program. The composite processing knowledge and automated processing capabilities at the Marshall Space Flight Center (MSFC) provided the foundation to combine the materials into a single unit and to achieve the goal of low cost.

When the engine was switched from the expendable booster to the reusable X-34 the biggest problem was the packaging. Nozzle changeout was not considered a critical issue with the expendable design so easy changeout was not incorporated. The turbopump, gas generator, and thrust vector attachment were all packaged to attach to the nozzle. Had the original purpose been a reusable design all of these would have been packaged on the powerhead so the nozzle could be easily replaced.

The remainder of the paper will describe processing of the liner, overwrap, and bonding. Included will be the lessons learned in each section. The majority of the lessons learned came after the failure of 60K-01, which will be described in greater detail in the liner processing section. Nothing can replace learning by doing and this project, having been worked from initial concept to hot fire testing, has provided a tremendous learning opportunity for all those involved.

The Liner Process

The purpose of the liner is to form the flame side contour and to protect the structural overwrap and bondlines from excessive temperatures. For the 60K engine to meet its performance goal, erosion had to be almost zero. To minimize erosion, a small percentage of fuel is sprayed down the chamber wall to provide a layer of film coolant. The film coolant also helps to prevent hot spots and streaking in the chamber. Testing to date has shown no measurable erosion with an accumulated test time of up to 342 seconds. Flight requirements call for the engine to fire for 159 seconds.

Liner processing is the first step in fabrication of the Fastrac nozzle. Silica/phenolic bias tape, FM5504, is tapewrapped onto a steel mandrel using a horizontal tapewrap machine. The ply angle, the angle of the tape to the flame surface of the liner, directly affects erosion performance and stress levels of the part. Based on thermal-structural analysis, this ply angle had to be changed twice, once in the throat and once just aft of the throat (see Figures 1 & 2). This was accomplished by tapewrapping past the ply angle change and then machining a new ramp angle in the uncured silica/phenolic. Computed tomography X-ray (CT) of the overwrapped part and posttest sectioning demonstrate a well-consolidated part at the ply angle change.

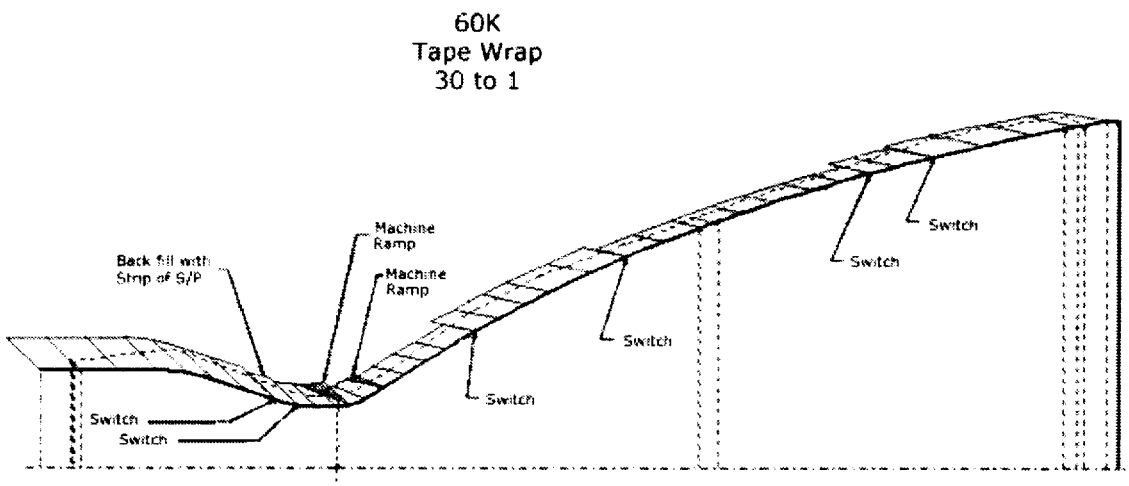

Figure1. Tapewrap Process Drawing

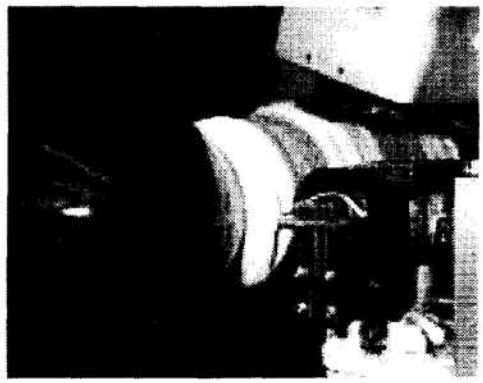

Figure 2. Machining of new ramp in uncured Si-P liner

Once the tapewrapping is complete the part is vacuum bagged and cured in an autoclave. Because of the complex shape of the nozzle and the sensitivity of silica/phenolic to cracking during cure, development of an appropriate cure cycle was critical. The cure cycle was established using data generated from instrumented panels of similar thickness and the cure model developed by the RSRM project.

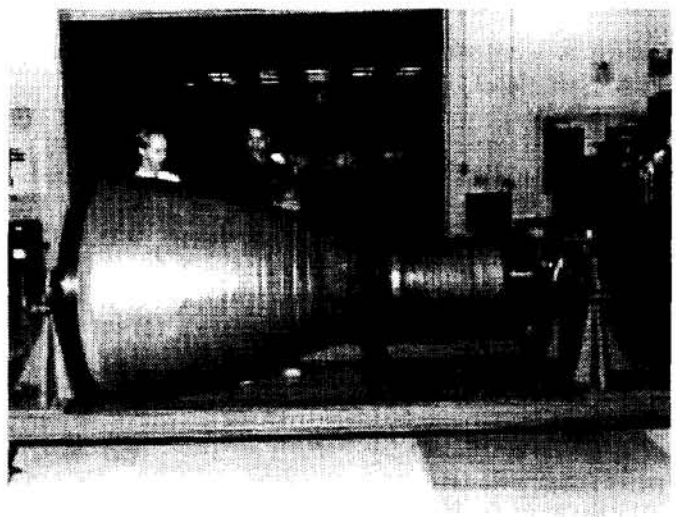

Figure 3. Cured Si-P liner billet

After liner cure the forward tag end is machined and the liner is removed from the mandrel. The liner is returned to the machine shop to have the outer diameter contoured in preparation for the overwrap process. The machined surfaces are inspected for wet line indications by alcohol wipe and then sent to the overwrap step.

Lessons Learned

As a result of lessons learned, several minor changes were made to the fabrication process and one significant change was made to the silica/phenolic tape to improve the quality of the liner. One minor change involved modification of the machining process used to cut the new ply angles in the uncured silica/phenolic. The first ply angle ramps were machined roughly and produced resin pockets visible in the post-cured computed tomography images. Once the ply angle ramp machining was improved to provide a smoother ramp, the resin pockets were essentially eliminated. Another process change was made because the 60K-03 and 04 nozzles had very poor consolidation and flow in the throat region. This problem in the throat developed because the o-ring in the throat centerline joint of the mandrel was improperly sized and leaking. Rather than reworking the mandrel, the planning was changed so that the joint was filled with

room temperature vulcanized silicone rubber (RTV) during mandrel assembly. The problem has not recurred.

During the investigation of the problem with the mandrel leakage it was determined that the part was too large for only an aft tag end. The mandrel was modified to increase the chamber length sufficiently for a forward tag end. The forward tag end is removed after liner cure and prior to the overwrap process. The data from the tag ends is charted and evaluated for any trends indicating a shift in the process or in the properties of the liner or overwrap materials.

Early in the nozzle development process, most of the cured components had dry regions because the material was overstaged during tapewrap. There were regions where the plies were rolled over on the inside surface because of significant tape to mandrel gaps. The operators performing the tapewrapping were asked to look at the cured component and once they saw how the final part looked and how their work could affect the part, significant improvement was made in the part quality.

The last minor change to be discussed involved the silica/phenolic specification for resin flow. One lot of material received had a resin flow that was on the low end of the specification. This material produced an acceptable part but was much harder to tapewrap and the resin did not flow as well during cure. The cured part resin content exceeded the upper specification limit and additional testing had to be performed. To keep the cured part within resin content specifications, the lower flow limit for the silica/phenolic was raised on subsequent material orders.

The most significant change to the liner began with the failure of nozzle 60K-01 during ignition on its third hot fire test. Prior to the third test, scheduled to be 120 seconds, 60K-01 had undergone a 20-second and 12 second test. Although the nozzle was designed for a single use, testing during the 40K test series had demonstrated that multiple short duration tests could be run on a nozzle without jeopardizing its survivability. At ignition the liner failed approximately 2 inches aft of the throat region. Since the performance of the combustion chamber was not affected, the test was continued for 59 seconds to gain needed injector performance data. The exposed structural overwrap burned, destroying data that would have been useful to the failure investigation team. Review of the high-speed video and reassembled liner pieces showed the exit cone portion of the nozzle was ejected as a single piece at ignition. The liner broke into pieces as it struck the ground and was then tumbled across the test pad by the engine exhaust plume.

The cause of the failure was determined to be a delamination that extended through the entire thickness of the liner, combined with a poor liner to overwrap bondline from the delamination point aft. Posttest CT found an axial crack in the liner which ran through the chamber and throat and ended at the delamination in the exit cone (see Figure 4). With the liner continuity broken there was nothing holding it in place. The poor bondline was caused by the inadvertent omission of a dry cycle, which is discussed in the overwrap section.

The primary cause of the liner failure turned out to be a supposedly transparent material change in the silica/phenolic. For the 40K program FM5504 silica/phenolic was used. Between the time that the 40K material was purchased and the time the material was purchased for the 60K program, Fiberite bought the producer of FM5504 and decided to phase it out and manufacture only their version of the same product, MX2600. Since both materials had been qualified for use on the RSRM and met the same specification, it was believed they would behave in a similar manner. The material change was made with no preliminary testing; a test matrix was to be performed concurrently with the fabrication and hot fire testing of the 60K components.

To evaluate the material differences, cylinders with a diameter the size of the 60K throat were made of the two materials and hoop tensile tests run at Southern Research Institute. The results, shown in Figure 5, clearly show the problem with the MX 2600. With reduced strain capability the MX 2600 could not survive the stresses put into the liner during overwrap cure. This was demonstrated when several liners made with MX 2600 and possessing good bondlines cracked axially in the chamber and throat down through the nozzle until they were stopped by a 360 degree liner delamination. With this information Fiberite agreed to supply the FM5504 and no problems have been encountered with the liners cracking.

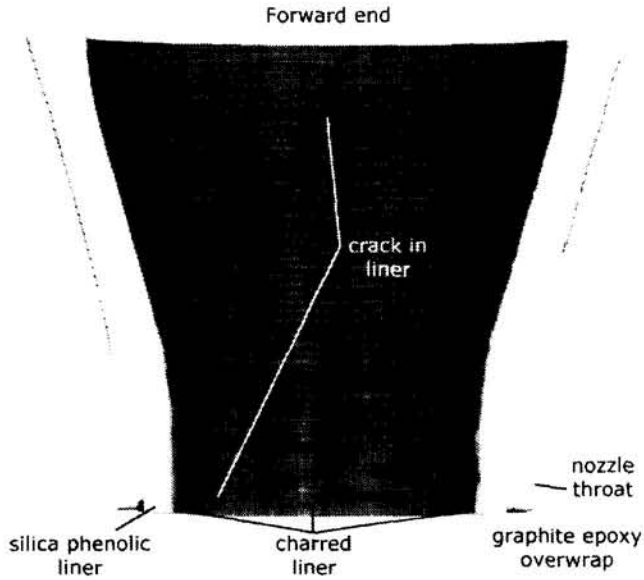

Figure 4. CT Image of Axial Crack in 60K-01 Chamber and Throat

The old FM 5504 data listed on the plot is material from the 40K development series (old) made at the original manufacturer's facility. The new FM5504 data is from material made at the Fiberite facility (new) after the original manufacturer was purchased. With the return to FM 5504, no liners have cracked in the chamber and throat regions in a total of 40 units built. The old lesson relearned many times in this industry was again demonstrated; though materials may meet the same specification, that does not guarantee that they will perform the same. The selected material must be well understood and no change should be viewed as insignificant.

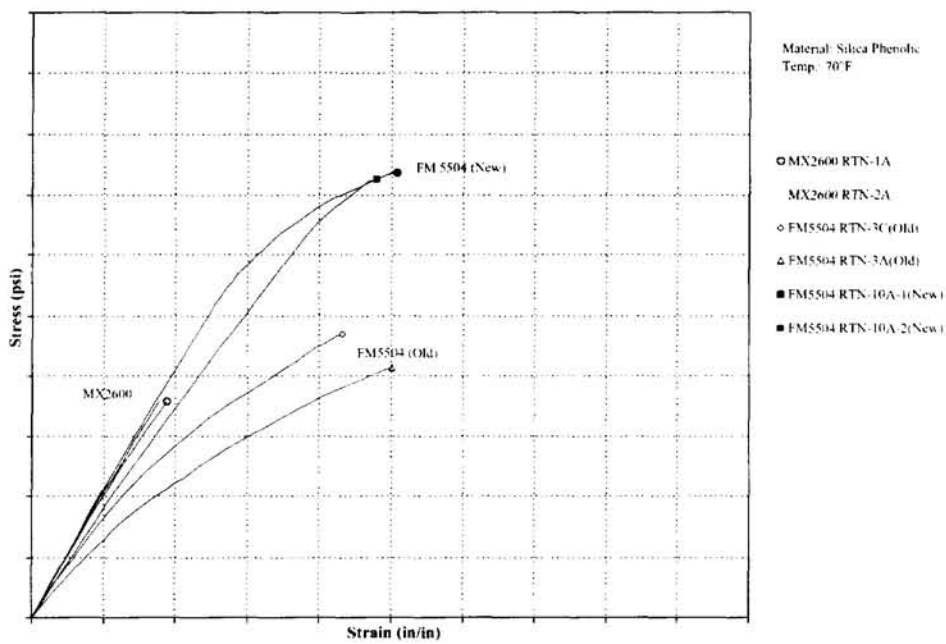

Figure 5. Ring Tensile Data for FM5504 vs. MX2600

The Overwrap Process

The purpose of the overwrap is to provide structural support to the silica/phenolic liner. The materials and processes were originally selected based on low-cost and minimized part count. Much of the process development work was done during the investigation of the 60K01 failure. The standard overwrap material is carbon/epoxy although several nozzles were overwrapped with fiberglass/epoxy. The fiberglass/epoxy was chosen as a result of the failure investigation with the intent of more closely matching the thermal expansion of the liner and overwrap materials.

The first step of the overwrap process is the liner dry cycle. The liner is subjected to high temperature to drive the moisture from the machined silica/phenolic surface. Moisture can negatively impact the bondline between the silica/phenolic and the carbon/epoxy. The temperature of the silica/phenolic must be ramped slowly to avoid potential cracking.

After the dry cycle, the liner is mounted onto the filament winding mandrel and the stainless steel flange is mated to the combustion chamber portion of the liner using Hysol® EA 9628 film adhesive. Film adhesive is applied to the entire liner surface and carbon/epoxy is then wet wound over the film adhesive (Figure 6). Thornel® T-300–12K carbon fiber and Epon® 828 resin were chosen because of their low-cost and commercial availability. Epi-Cure® W curing agent was chosen because it has an extended pot life which accommodates the time required for winding and curing of such a large part.

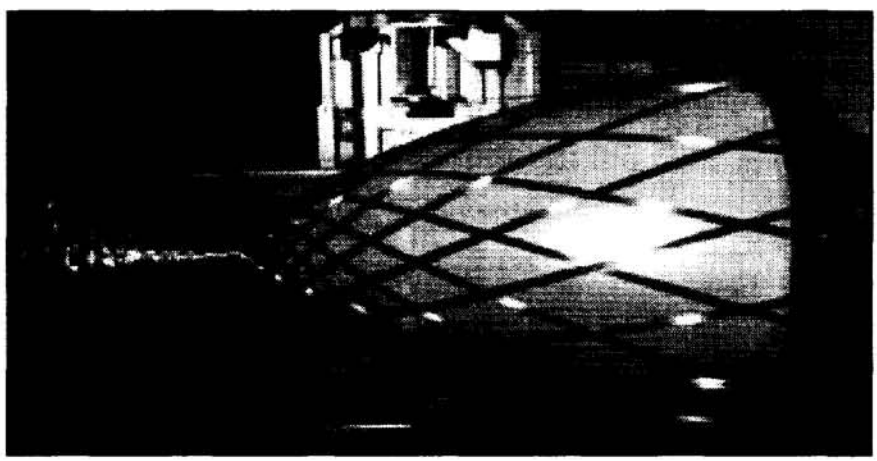

Figure 6: Wet winding of carbon/epoxy over silica/phenolic liner covered with film adhesive.

The overwrap is vacuum-bag-oven-cured with a temperature cycle that, like the dry cycle, involves a slow ramp rate to avoid cracking of the silica/phenolic. After cure, the ends of the nozzle are cut off using a grinding wheel mounted to the vertical carriage of the filament winding machine. The mandrel is then removed and the nozzle is machined in preparation for bonding of the metal hardware.

Lessons Learned

During the development of the overwrap process several challenges were overcome. Many were a result of work done during the investigation of the 60K-01 failure. Some of the most notable challenges

were wrinkling of the overwrap in the throat region after cure, bridging of the fibers in the transition regions, crack initiation in the nozzle at the very aft end and mandrel expansion during cure.

The overwrap mandrel is a "Christmas Tree" design that supports the liner in the combustion chamber area and two places in the nozzle region (Figure 7). The forward end is attached by the combustion chamber flange to a dome/pin ring. The dome/pin ring is held in place by a large nut with a spring washer. The spring washer serves to apply pressure to the flange and keep it properly seated on the combustion chamber portion of the liner as the mandrel expands during cure. During the development of the overwrap process, slippage between the mandrel and the inner liner surface was suspected. Nitrile butadiene rubber (NBR) was placed on the aluminum mandrel rings to prevent slippage.

The NBR also serves another purpose. The liner at the aft end tapered down to a fine edge that was easily chipped. The chipped area allowed cracks to initiate and propagate into the aft end of the liner. The potential for crack propagation was exacerbated by the wedge effect of the mandrel. The wedge effect is caused by the expansion of the liner during cure with the spring washer forcing the liner onto the mandrel rings. The mandrel rings act as a wedge that tries to open the nozzle portion of the liner. This problem was solved by machining the aft end of the liner to a flat edge before the overwrap process to prevent crack initiation. Application of the NBR to the mandrel rings also helped alleviate the potential for cracking by isolating the rings from the liner surface to allow relative movement during expansion and contraction.

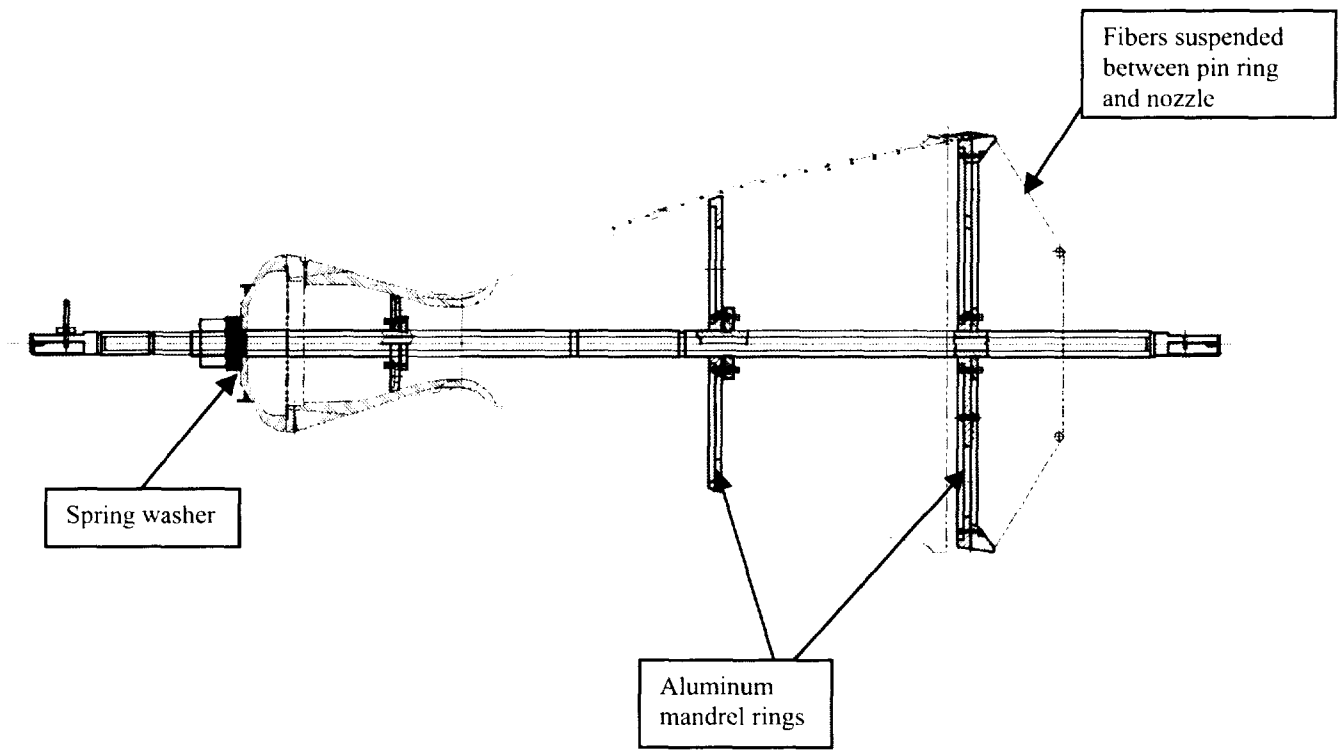

Figure 7: The filament winding mandrel is a "Christmas Tree" design. A spring washer between the forward dome and the lock nut keep the flange properly seated during cure.

Another issue that was overcome was wrinkling of the overwrap in the throat region. The bagging technique was adjusted to trap resin in the composite. This was accomplished by switching from perforated to non-perforated release film. The non-perforated release film was selectively punctured in and around the throat region to allow volatiles to escape but minimize the amount of resin lost. After several iterations the wrinkling was eliminated. This process also accomplished the task of increasing the diameter of the throat.

The throat area is machined for the application of the belly band hardware so a larger throat diameter assured that enough composite would be present for machining.

After the failure of 60K-01, the residual stress in the bondline between the overwrap and the liner became an important issue. One of the reasons for the residual stress in the bondline was the tooling and vacuum bag configuration. At the aft end, the wound fibers and vacuum bag are suspended between the pin ring and the end of the nozzle. The vacuum forces this suspended area down and increases fiber tension (see Figure 7). To minimize the impact of this effect, the first wound layer is cut flush with the aft end of the nozzle. This relieves the tension in the first layer of fibers and therefore reduces the amount of residual stress created during cure between the overwrap and the liner. Relieving the tension in the first layer also serves to reduce the potential for bridging of the wound fiber over the transition from the throat to the nozzle and the bump in the liner for the actuator attachment ring.

NonDestructive Evaluation

Once the overwrap is machined and prior to bonding on the metal attachment hardware, the nozzle is inspected by CT and ultrasonic spectroscopy (Ultraspec). These are two state of the art nondestructive evaluation (NDE) techniques that give excellent insight into the consistency of the process and the resulting part. The CT inspection looks for cracks, delaminations, and density gradients in the component which are unacceptable or out of family. The Ultraspec inspection is a technique developed by Southern Research Institute that detects debonds between the liner and the overwrap. Kissing debonds cannot be detected by CT but the Ultraspec can detect them. The Ultraspec was added to the program during the 60K-01 failure investigation. Several papers could be written on what has been learned through the use of these tools and it will be left to the appropriate experts to perform that task. Let it suffice to say that these advanced techniques have been instrumental in the success of this project.

The Bonding Process

After the overwrap is machined and NDE is performed, additional metal and composite hardware are physically bonded to the nozzle. This additional hardware facilitates attachment of the nozzle to the injector and the Thrust Vector Actuation (TVA) system. This hardware also provides mechanical support for components such as the gas generator/turbopump, igniter, exhaust duct, valve brackets, and drain lines. Figure 8 shows a nozzle with all hardware bonded and the Thermal Protection System (TPS) applied and painted.

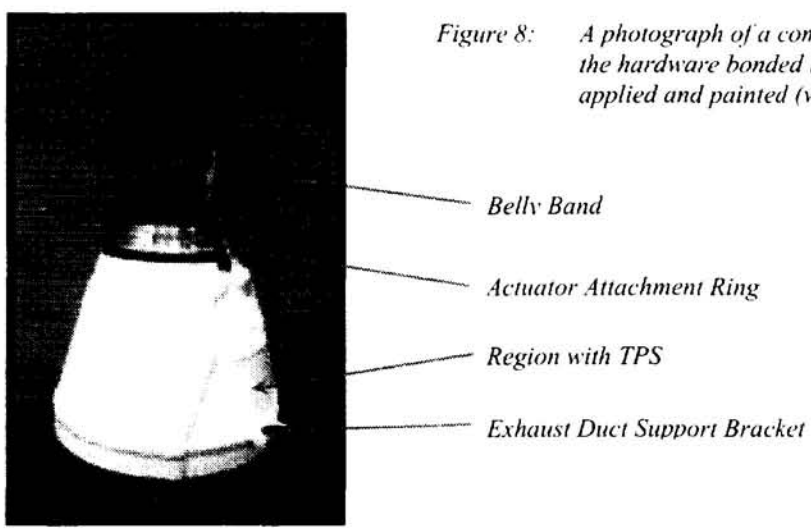

Figure 8: A photograph of a completed nozzle with all the hardware bonded (arrows) and the TPS applied and painted (white region).

The first three components bonded to the nozzle are the gas generator/turbopump/igniter support belly band, the actuator attachment ring (AAR), and the exhaust duct support bracket. These components

are machined from 300 series stainless steel. The remaining components, the valve bracket and drain line support pads, are molded from a composite sheet molding compound (SMC), Lytex™ 9063, manufactured by Quantum Composites Inc.

All of the bonding operations are performed in much the same manner. The hardware is placed in a fixture or tooling is put in place to insure accurate positioning. The hardware is then dry fitted to the nozzle to verify positioning and to determine shimming requirements. The shims aid in placement of the hardware during actual bonding and also provide a minimum bondline thickness for the adhesive. The next step is surface preparation. The exact surface preparation method is dependent on the material of the surface being bonded. Metal hardware is hand wipe cleaned, grit blasted with a zirconia or silica media, inspected by black light, and then primed with a silane-based primer. Composite hardware, and the surface of the chamber/nozzle itself, are hand wipe cleaned and grit blasted with an alumina media. Shims are then affixed to the hardware as required, and surfaces of the nozzle and hardware that are not involved in the bonding operation are masked. The adhesive used for bonding operations on the Fastrac engine is Hysol® EA 9394, a two part structural paste adhesive. The adhesive is mixed and then applied to both the hardware and the nozzle surface. Following adhesive application the hardware is positioned and held in place until a sufficient degree of cure is achieved to allow nozzle movement.

Two components, the AAR and the exhaust duct support bracket, undergo additional processing to install shear bolts following initial bonding. The shear bolts enhance the transfer of loads from the AAR and exhaust duct support bracket to the nozzle. The bolts ensure that the loads are transmitted to the entire thickness of the nozzle and not just the outer ply of the structural overwrap. Holes are machined through the metal hardware and the structural overwrap and into the silica/phenolic liner. The bolts are then installed wet with Hysol® EA 9394 adhesive and the adhesive is allowed to cure.

The TPS consists of sheet cork bonded to the exterior of the overwrap with Hysol® EA 9394 adhesive. The process is performed using standard vacuum bagging techniques. An ablative compound, RT-455 from Resin Technology Group LLC, is then applied to cover the exhaust duct support bracket and to fill in any gaps in the cork. Following cure, the cork and RT-455 are coated with an acrylic latex paint produced by Acrymax Technologies, Inc., SP130XT-LV.

Lessons Learned

Most of the challenges encountered in the evolution of the bonding process related to development of tooling and techniques to insure correct positioning of the hardware. Of necessity the initial tooling was makeshift and prone to errors and excessive variability. Over time it has matured into a very stout and reliable production system. This system includes a specialized fixture and tooling plates used to hold the metal components and the entire nozzle in place during bonding (Figures 9 and 10). Optical alignment equipment was used to set up the fixture. This assured proper leveling and parallelism. Axial adjustments are made to the components being bonded using two-piece tooling plates mounted to a drive screw system. In addition, a plumb bomb was incorporated into the fixture to aid in angular positioning of the hardware. To maximize positional accuracy, all measurements are taken relative to the combustion chamber flange and each of the bonding operations is performed independently. Lastly, hardware locations are verified following bonding using a portable coordinate measuring machine (CMM).

During process development the bonding plates underwent significant refinement. The bonding plates for the belly band were modified to more closely match the taper of the nozzle. This allowed for a better mating with the nozzle and sufficient room for the belly band plates to actuate more effectively. In addition, the thickness of the exhaust duct support bracket bonding plates was increased to eliminate unwanted flexing. The reasons for the flexing were twofold. First, the exhaust duct support bracket is mounted at the largest diameter portion of the nozzle, so the width of its bonding plates is the smallest of all the plates. Second, during bonding the adhesive provides a resistance to placement of the hardware in the form of a hydraulic pressure. Flexing also occurred with the positioning plates that support each belly band half and actuates them toward the surface of the throat. As the plates were extended toward the throat, the weight of the belly band halves caused flexing. Separate actuating supports were installed to allow the positioning plates to be supported along their full range of motion.

Tooling was also the key to sufficient accuracy and precision when bonding the composite/SMC components. The composite/SMC components are bonded to the nozzle in sets of 2-3 pieces each, using tooling that bolts to the previously used bonding plates or the previously bonded hardware. This tooling was developed based on models of the hardware to be attached to the nozzle during final assembly. Figure 11 shows the bonding of the valve bracket support pads to the nozzle.

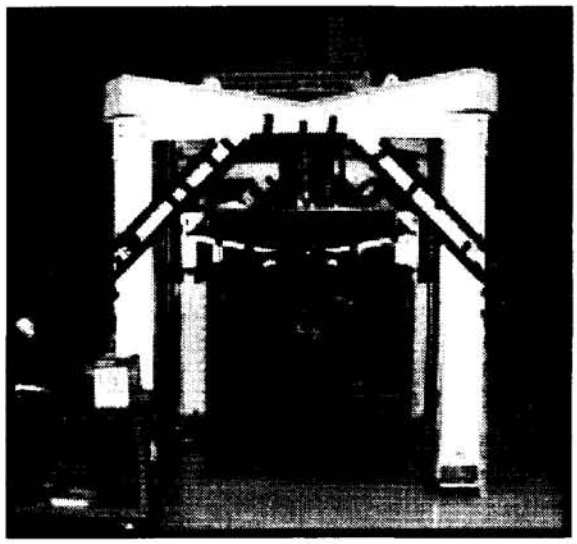

Figure 9: (left) *A photograph of a nozzle in the fixture with the belly band being bonded.*

Figure 10: (right) *A close-up of the specialized tooling plate being used to bond the belly band. The arrows point to the plumb bob used to ensure angular position.*

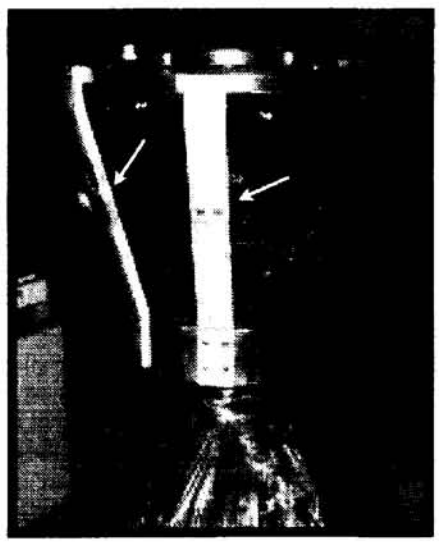

Figure 11: (left) *A photograph of the tooling used to bond the valve bracket support pads (arrows). This tooling fastens to the combustion chamber flange and the belly band to correctly position the pads.*

Summary

The development of a low cost nozzle for the 60K Fastrac Engine has been successful. The success was achieved by using well-understood material technology in a new way. Ablative, bonding and TPS technology from RSRM and structural composite technology from multiple projects provided the knowledge. With a little innovation and willingness to take some risk these materials were combined into a single unit with no joints. The manufacturing was simple, it contained a minimum number of steps and as much automation as possible. The only exception being the TPS that used old, hands-on technology due to project cost constraints at the decision point.

A significant amount of testing has been performed to evaluate the nozzle's capability to successfully meet the X-34 flight requirements. Flight requirements are for each nozzle to be used for a single, 159-second burn, and to survive intact the reentry and landing loads. To date, a shortened development nozzle has survived 4 starts and an accumulated 342 seconds of hot fire and a full-length development nozzle has survived 7 starts and an accumulated 282 seconds. In order to evaluate the capability of the bonded actuator attach ring, one nozzle actuator attach ring was loads tested and failed at 180% of the maximum expected load. The nozzle design was modified based on thermal–structural analysis and testing continues to verify the nozzle satisfies all performance requirements. Nothing has been found that would indicate future problems. The nozzle is believed to have demonstrated that it is a robust, low cost design for liquid engine applications and similar designs could be incorporated into other systems.

Acknowledgments

The success of this project is due to the many people at all levels who have taken a special pride in creating a robust component. A special thanks goes to the many technicians at Thiokol, Lockheed Martin, and ASRI whose craftsmanship and commitment were instrumental in resolving the issues faced during the development of the nozzle.

Large Composite Structures Processing Technologies for Reusable Launch Vehicles

R.G. Clinton, Jr. – NASA/MSFC
William M. McMahon - NASA/MSFC
N.J. Johnston - NASA/LaRC
H.L. Belvin – NASA/LaRC
Walter Franklin – LM/Palmdale
R.Biggs – LM/MAF
D. Ferrari – LM/MAF
John H. Vickers – NASA/MSFC
A.B. Hulcher - NASA/MSFC
R.J. Cano - NASA/LaRC
Keith McIver - Boeing
Don Sidwell – LM/Palmdale
Tod Palm – Northrop Grumman Corp.

Presented at

4th Conference on

Aerospace Materials, Processes, and Environmental Technology

September, 2000

Outline

- Second Generation RLV Goals and Technology Drivers
- Current Technology for Large Scale Polymer Matrix Composites
- Technology Scale-up Issues
- Emerging Out-of-Autoclave Processing Technologies
- NASA Development Activities
- Industry Experience
- Summary

Large Composite Structures Processing Technologies for Reusable Launch Vehicles

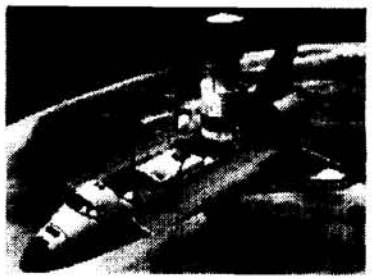

Today: Space Shuttle
1st Generation RLV
- Orbital Scientific Platform
- Satellite Retrieval and Repair
- Satellite Deployment

2010: 2nd Generation RLV
- Space Transportation
- Rendezvous, Docking, Crew Transfer
- Other on-orbit operations
- ISS Orbital Scientific Platform
- 10x Cheaper
- 100x Safer

2025: 3rd Generation RLV
- New Markets Enabled
- Multiple Platforms / Destinations
- 100x Cheaper
- 10,000x Safer

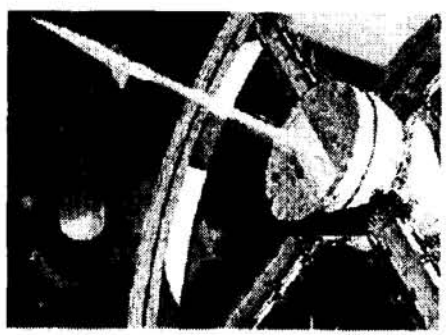

2040: 4th Generation RLV
- Routine Passenger Space Travel
- 1,000x Cheaper
- 20,000x Safer

Large Composite Structures Processing Technologies for Reusable Launch Vehicles

- **Crew Escape and Survival**
  - Detection, separation, ascent/descent
- **Operable, Long-life H_2/O_2 and RP/O_2 Engines**
  - 200 mission life, 100 missions to overhaul
- **Long life, lightweight integrated airframe**
  - Critical integrated cycle testing (500 missions)
- **Advanced TPS, IVHM, and Operations**
  - Quick turn vehicle with intelligent data analysis
- **Ejector Ramjet**
  - Improved performance margin
- **SHARP Leading Edges**
  - Global crossrange from orbit

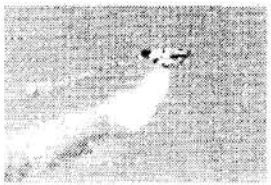

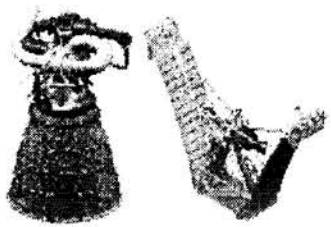

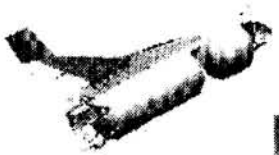

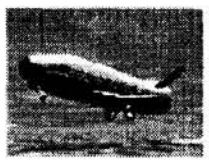

Cutting Edge for 2nd Generation

Large Composite Structures Processing Technologies for Reusable Launch Vehicles

Current Technology

- No known proven processes, tooling, or equipment to manufacture composite cryogenic tank structures over 25 ft. in diameter in the U.S.
  - Relatively small tanks built to date have been fabricated by hand, an improbable process for RLV.
  - Fiber placement and autoclave processes have been demonstrated at small scale (LMMSS X-33 10 ft. demo tank and LMSW X-33 LH_2 proto-flight tank).
- NASA/LaRC has supported substantial material and process technology development through the High Speed Research (HSR) and Advanced Composites Technology (ACT) programs for large scale vehicle structures (wing, fuselage, joints).
  - Resin film infusion-autoclave cure.
  - RTM/VARTM-oven cure.
  - Hand lay-up autoclave cure.
  - PETI-5 material and out-of-out-autoclave processing.
  - Stitched composite preform development.
- Demonstrations have hinted at feasibility of manufacturing technologies.
- Progression to RLV scale structures requires new manufacturing developments.

Large Composite Structures Processing Technologies for Reusable Launch Vehicles

Fiber Placement Machine Technology Scale-Up Issues.

- Software upgrades.
  - Accommodate effects of large scale tooling.
  - Accommodate complex (design-specific) geometries.
  - Address simulation requirements.
- Hardware upgrades.
  - Placement head/drives must accommodate complex geometries.
  - Build material delivery system (potential).
- While not a technology issue, long lead times will be required for system design, fabrication, assembly, and operational verification which must be considered in program planning.

Autoclave Technology Scale-Up Issues.

- Control of thermal field (rise rates, holds, cooldown).
- Sealing issues.
  - Lock ring assembly fabrication and installation.
  - Door seal alignment.
- Special requirements for assembly and facilitization.
- While not a technology issue, long lead times will be required for system design, fabrication, assembly, and operational verification which must be considered in program planning.

Tooling Technology Scale-Up Issues.

- Tool design and analysis.
  - Single or multi-piece construction trades.
  - Material selection: weight; CTE issues; compatibility with part fabrication and curing requirements (deformation under load, sag, thermal mass, etc.).
  - Lay-up tolerances.
  - Integration with fiber placement and curing equipment.
  - Part removal.
- Tool handling.
  - Removal from fiber placement machine.
  - Transportation to curing equipment.
  - Disassembly (if required) and storage.

Large Composite Structures Processing Technologies for Reusable Launch Vehicles

Emerging Out-of-Autoclave Processing/Manufacturing Technologies.

- Among the foremost challenges associated with fabrication and assembly of large polymer matrix composite structures is curing.
- Conventional aerospace PMC components typically require high temperature autoclave cures, and the associated tooling to achieve acceptable mechanical properties and dimensional tolerances.
- The economics of conventional curing techniques is acceptable on small scale components, however, as part sizes increase, scale-up of autoclave equipment and component tooling increases dramatically.
- Out-of-autoclave processing methods may enable significant cost savings in the fabrication of large scale composite articles.
- Currently several out-of-autoclave processing methods are under consideration for large component fabrication.
  - Thermoplastic in-situ consolidation.
  - "All at once" electron beam (E-Beam) curing.
  - In-situ e-beam cure.
  - Vacuum assisted resin transfer molding (VARTM).

Large Composite Structures Processing Technologies for Reusable Launch Vehicles

Thermoplastic In-situ Consolidation (Fiber Placement).

- Fully consolidated thermoplastic prepreg which is heated to above the resin melt temperature and bonded to the composite substrate ply by a heated compaction device.
- Advantages:
  - The process allows for simultaneous ply lay-up and consolidation while achieving 85%-100% of autoclave mechanical properties.
  - Thermoplastic materials allow for virtually infinite shelf life of the material.
- Disadvantages:
  - The technology has not been completely demonstrated for complex contoured part geometries due to the need for a conformable compaction system.
  - No commercial equipment is currently available for tape and fiber placement.
  - Elevated temperature accumulation of residual stress.
  - Process will still require expensive tooling.

Large Composite Structures Processing Technologies for Reusable Launch Vehicles

Thermoplastic In-situ Consolidation (Fiber Placement)

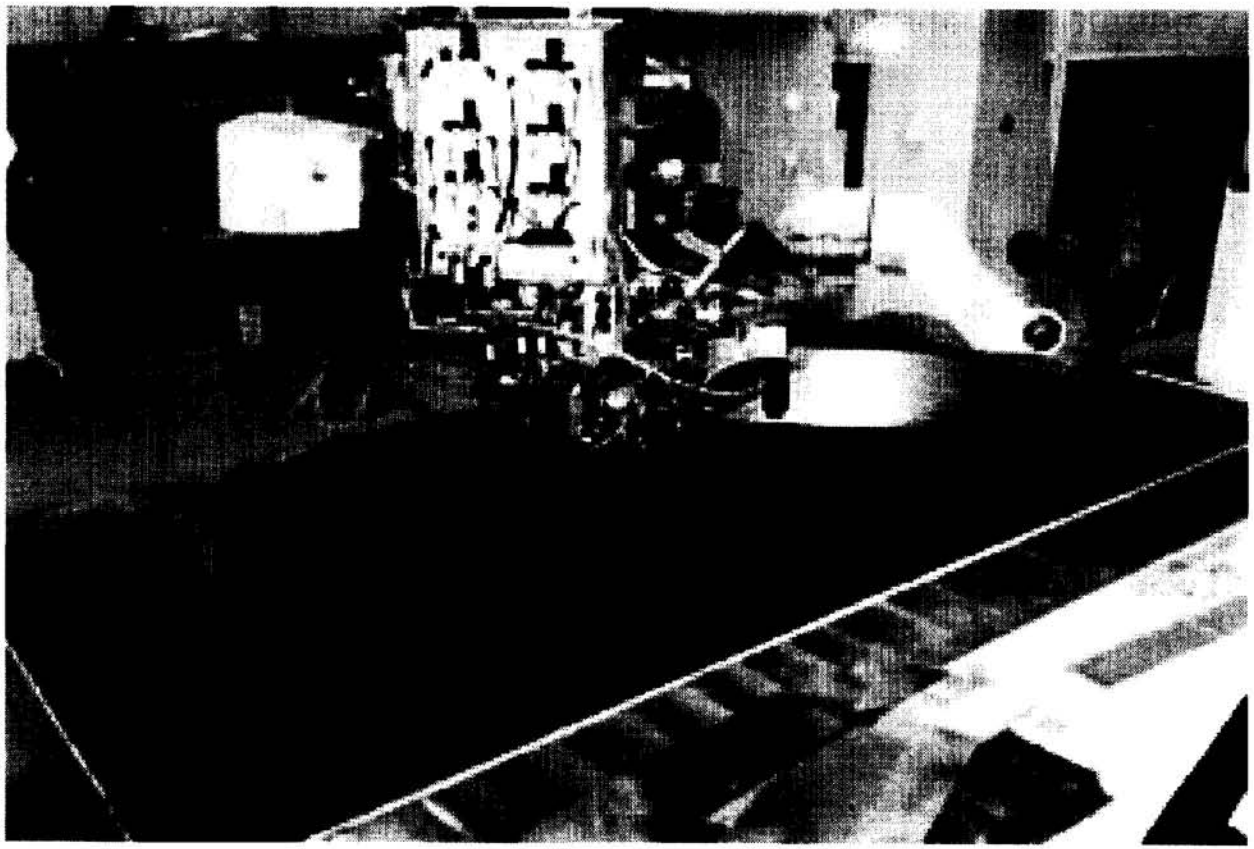

Large Composite Structures Processing Technologies for Reusable Launch Vehicles

"All-At-Once" E-beam Cure.

- Electron-beam energy is used to cure specially formulated composite resin systems.
- The composite part is typically fabricated using hand lay-up or automated techniques.
- Part is cured at ambient temperature and pressure by irradiation with a high energy electron source.
- <u>Advantages:</u>
  - Low cure temperature, generally around room temperature.
  - No thermal residual stress.
  - Substantially lower tooling cost.
  - Faster cure times.
  - Resins systems have very long out life.
- <u>Disadvantages:</u>
  - No high performance or tough e-beam resins yet available.
  - Lack of commercially available equipment.
  - No compaction force used during consolidation.
  - Little experience in fabrication of open section skins.
  - No relevant property data.
  - Radiation levels require substantial shielding.

Large Composite Structures Processing Technologies for Reusable Launch Vehicles

In-Situ E-beam Cure.

- Offers a novel approach that combines the construction sequence and cure.
- The concept is being developed for automated tape placement (ATP) processes.
- Irradiation to partial or full e-beam cure occurs as the ATP head lays each tape layer.
- The process may utilize lower energy electrons since the beam need only penetrate through a few layers of tape rather than penetrating the full part thickness.
- Advantages:
  - Low cure temperature, generally around room temperature.
    No thermal residual stress.
    Substantially lower tooling cost.
    Faster cure times.
    Resins systems have very long out life.
    Lower level radiation shielding is required.
  - Single step process (construction and cure simultaneously).
- Negative:
  - No high performance or tough e-beam resins yet available.
    No commercial equipment available.
    No compaction force used during consolidation.
    Little experience in fabrication of open section skins.
    No relevant property data.
    Significant challenges synchronizing placement processing parameters and cure kinetics.

Large Composite Structures Processing Technologies for Reusable Launch Vehicles

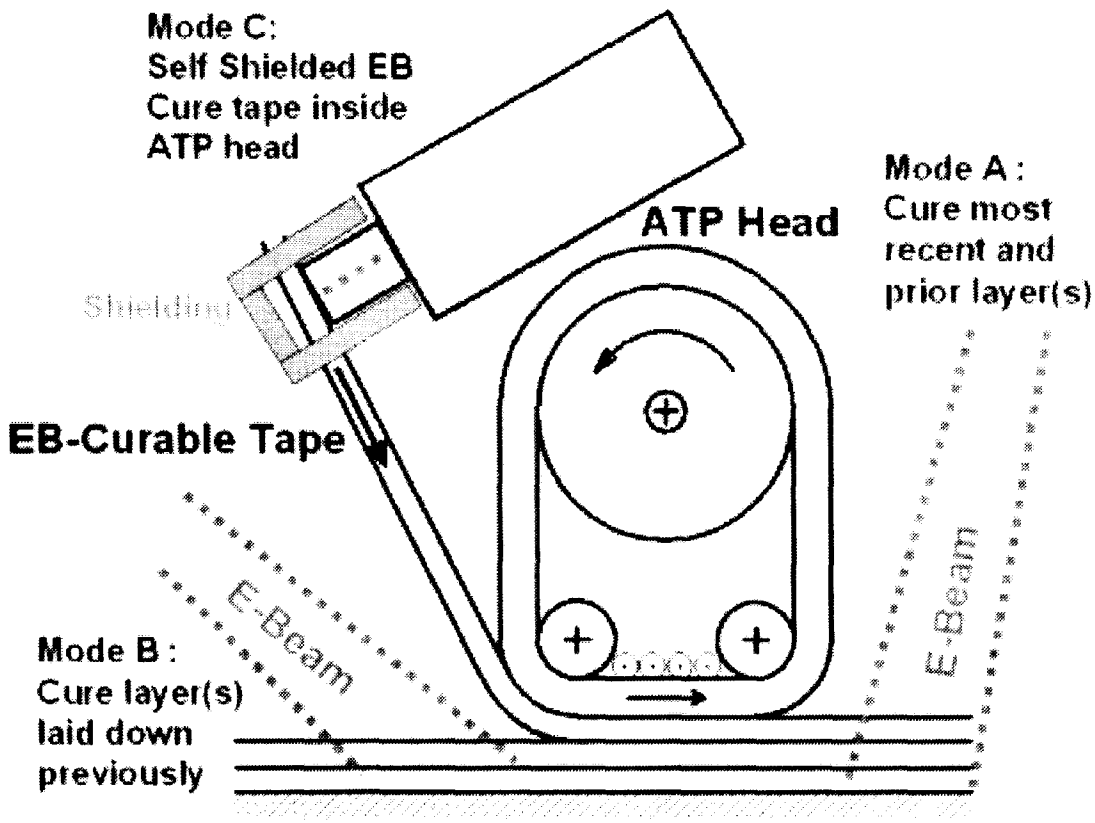

Large Composite Structures Processing Technologies for Reusable Launch Vehicles

Vacuum Assisted Resin Transfer Molding (VARTM).

- A vacuum assisted resin injection system is used to impregnate an assembled fiber preform.
- The VARTM process has been used to make large structures, however experience with large aerospace laminate fabrication is limited.
- Typically this process is used with glass fiber to manufacture products such as railroad containers, truck containers, and boat hulls.
- Advantages:
  - Low cost tooling.
  - Low cost fabrication materials.
  - Commercial availability of resins and preforms.
  - Allows for complex, very large part fabrication.
- Disadvantages:
  - Small database with carbon/epoxy composites.
  - Typically uses low temperature, thermoset resin systems.
  - Atmospheric pressure for compaction and consolidation.
  - Complex preforms can be expensive.
  - Fabric must be used with this process.

Large Composite Structures Processing Technologies for Reusable Launch Vehicles

NASA Development Activities.

- NASA seeks new and innovative technologies for materials, processes, and manufacturing that will provide safe, reliable, lightweight, and less expensive launch vehicle and spacecraft components.
- Conceptual designs for reusable space transportation systems require the manufacture of composite structures of unprecedented scale to achieve the necessary mass fraction.
- Current research has identified that advanced manufacturing processes, and the level of performance of engineering tools are not available today for production of these very complex structures.
- Toward this end NASA has established the National Center for Advanced Manufacturing (NCAM) to address the research and technology development needs for manufacturing the next generation of reusable space transportation systems.

Large Composite Structures Processing Technologies for Reusable Launch Vehicles

NASA Development Activities.

- Automated robotic placement of tow, ribbon, and tape has emerged as an important technique for fabrication of high performance fiber-reinforced composite structure.
- Production-ready equipment controlled by sophisticated computer software has been used to manufacture major portions of the Boeing 777 empennage, F18EF stabilator and inlet ducts, and V22 parts, among others.
- A fiber placement capability exists at NASA Marshall Space Flight Center's (MSFC) Productivity Enhancement Complex to provide materials and processes research and development, and to fabricate components for many of the Center's Programs.
- This equipment provides unique capabilities to build full scale and/or prototype composite parts in complex 3-D shapes with concave and other asymmetrical configurations, and localized reinforcements.
- This enabling capability assures a repeatable, controlled process that will provide government and industry a database for materials and processing development and evaluation.
- Fiber placement is projected to be next step for thermoplastic in-situ consolidation and in-situ e-beam construction as process development efforts advance.

Large Composite Structures Processing Technologies for Reusable Launch Vehicles

NASA Development Activities

- Fiber Placement Machine and Operational Schematic

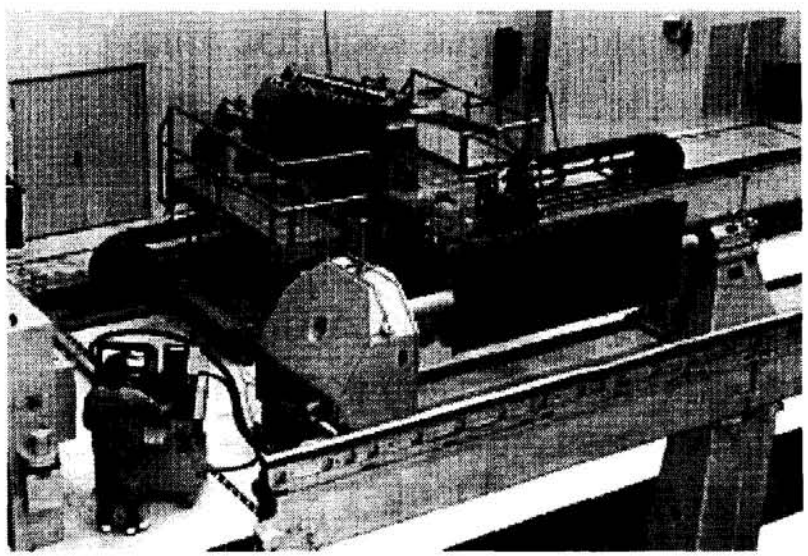

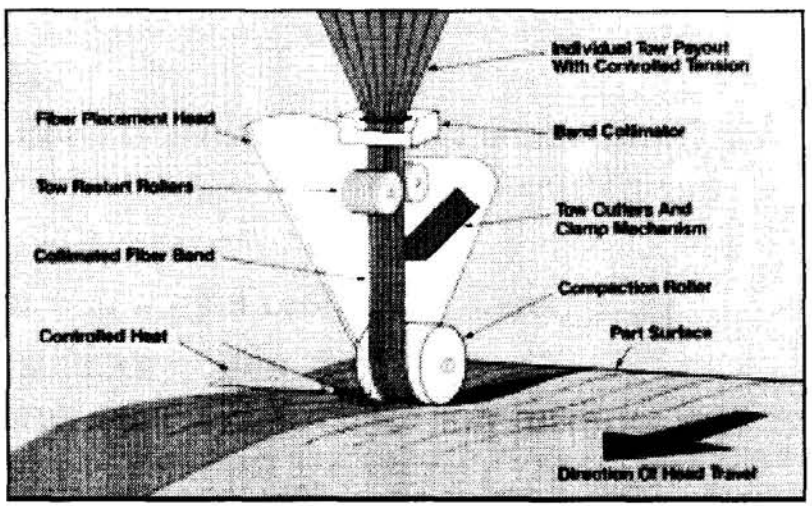

Large Composite Structures Processing Technologies for Reusable Launch Vehicles

NASA Development Activities.

- A new NASA fiber placement facility at the Langley Research Center has proved to be a valuable asset for obtaining data, experience, and insights into the automated fabrication of high performance composites.
- The facility consists of an ABB robot armed with a modified heated head capable of hot gas and focused infrared heating.
- While uncured thermoset tow and tape, e.g., epoxy and cyanate prepreg can also be placed with this equipment; its most powerful attribute is the ability to place thermoplastic material to net shape.
- Future activities will include:
  - Development of sensors for on-line part quality information and in-situ defect repair;
  - Automated placement of metal-composite hybrids using magnetic induction heating;
  - Development of conformable compactors for ply drops, ply adds, and complex geometry;
  - Development of non-autoclave processes for epoxy thermosets including net shape placement combined with ply-by-ply, cure-on-the-fly.

Large Composite Structures Processing Technologies for Reusable Launch Vehicles

NASA Langley Robotic Composite Fabrication Facility

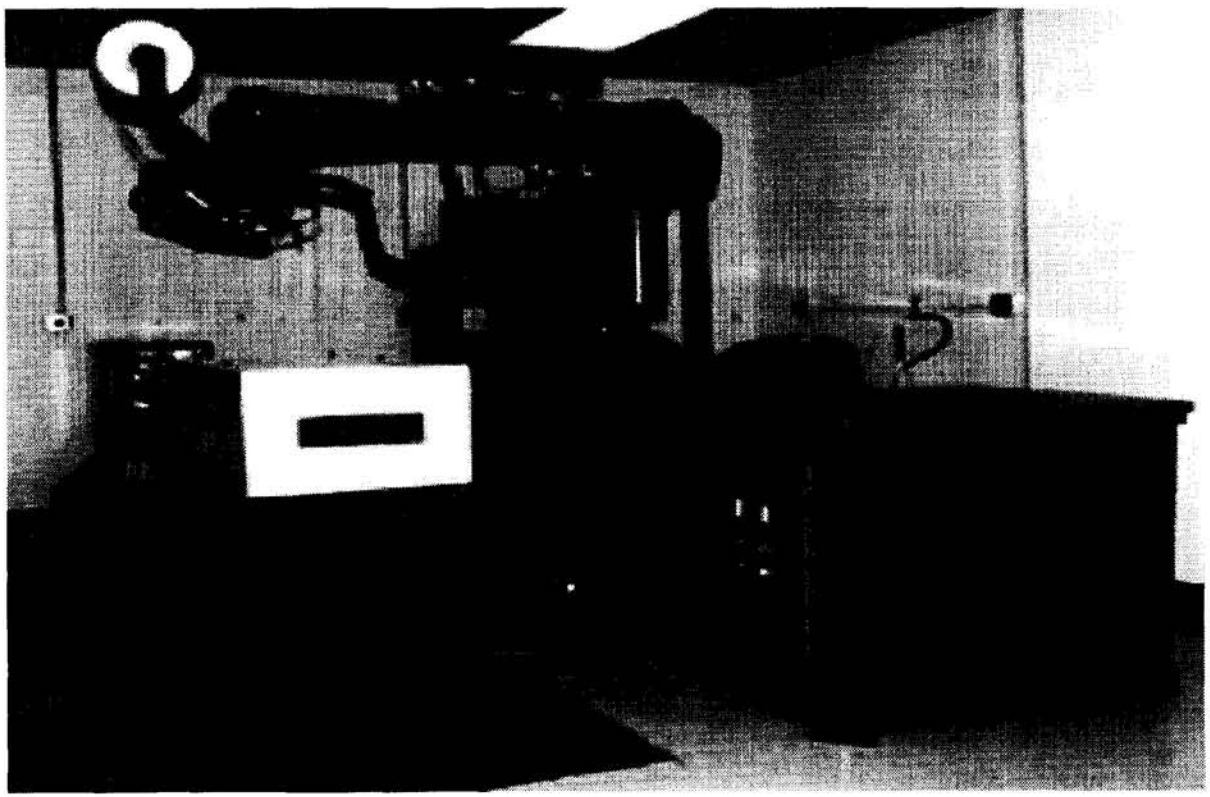

Industry Experience

Lockheed Martin - Michoud

Large Composite Structures Processing Technologies for Reusable Launch Vehicles

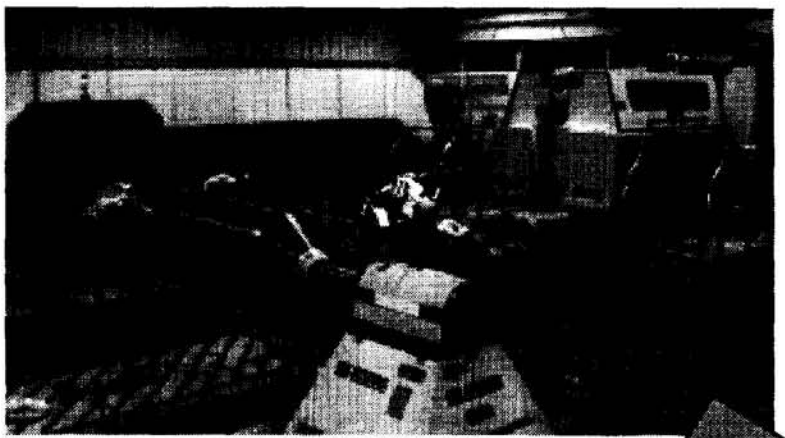

- Fiber placed toughened epoxy subscale tank demonstration.
- Autoclave grade consolidation.
- Challenges for Non-Autoclave Processes for Large Tanks.
  - Compatibility of process with toughened material systems required for cryogenic service.
  - Ability to scale up and maintain performance
  - Maintaining essentially zero defects (voids, porosity, wrinkles) for sufficient containment.
  - Maintaining adequate consolidation for optimum properties.
  - Sufficient database for implementation.

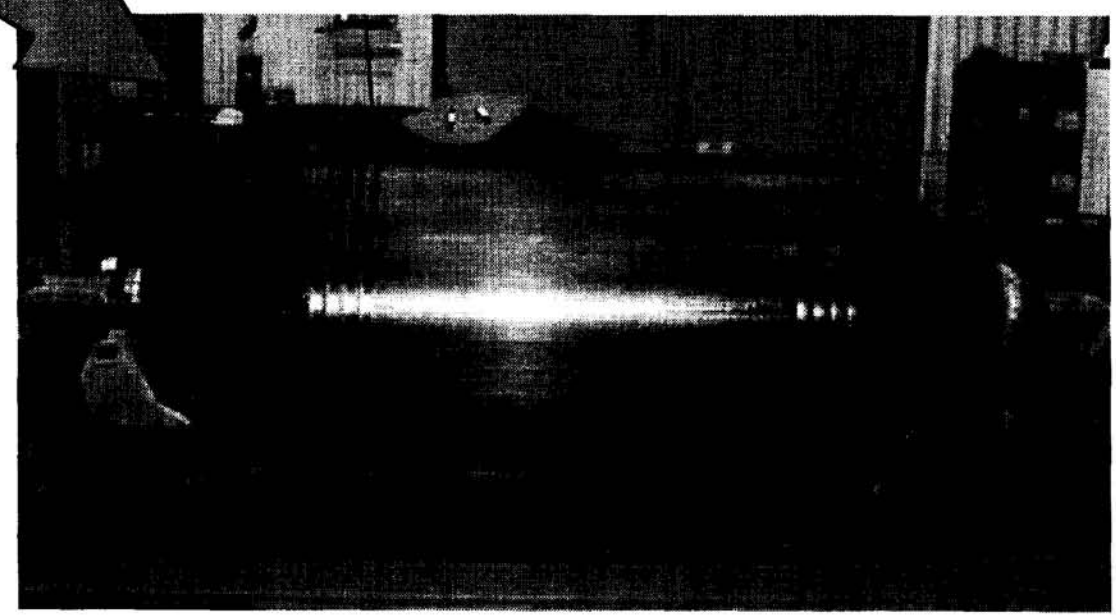

Large Composite Structures Processing Technologies for Reusable Launch Vehicles

Vacuum Assisted Resin Transfer Molding (VARTM)

- LM-Michould's patented Resin Infiltration process.
- Issues with VARTM.
  - Porosity > autoclave cure.
  - Uniformity of resin content.
  - Limited to fairly brittle resins.
- Good candidate for dry structure.

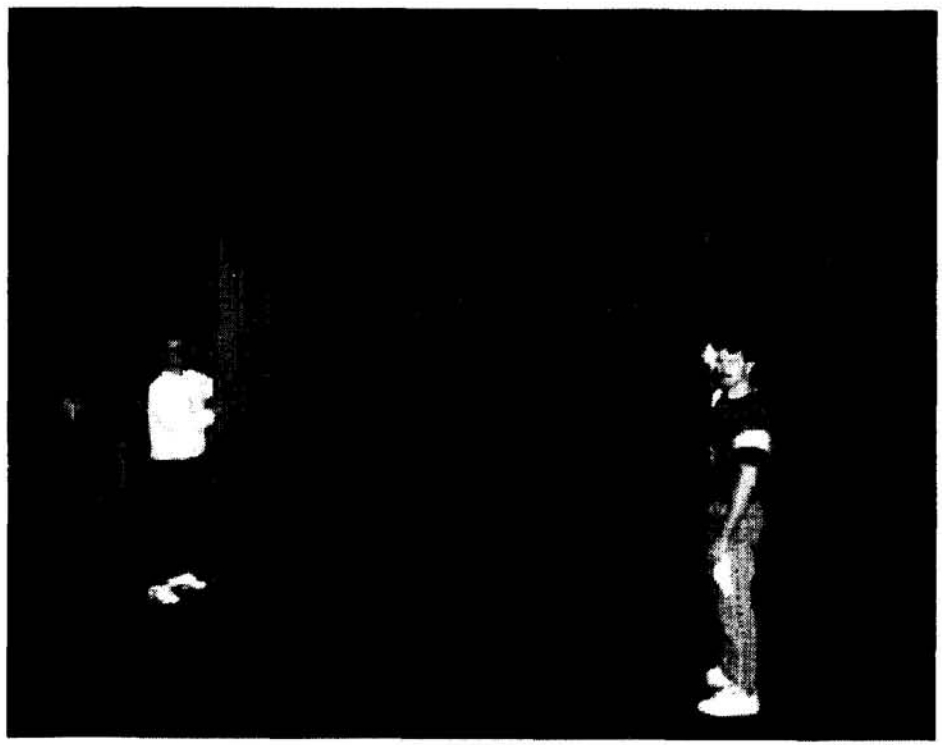

Industry Experience

Lockheed Martin Aeronautics - Palmdale

Out-Of-Autoclave Process Development

EB LH_2 Tank

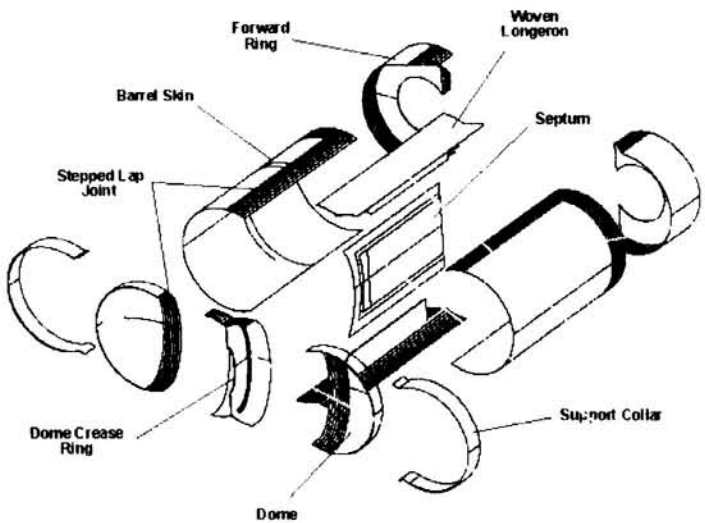

Tank Assembly

EB Barrel & FWD Ring

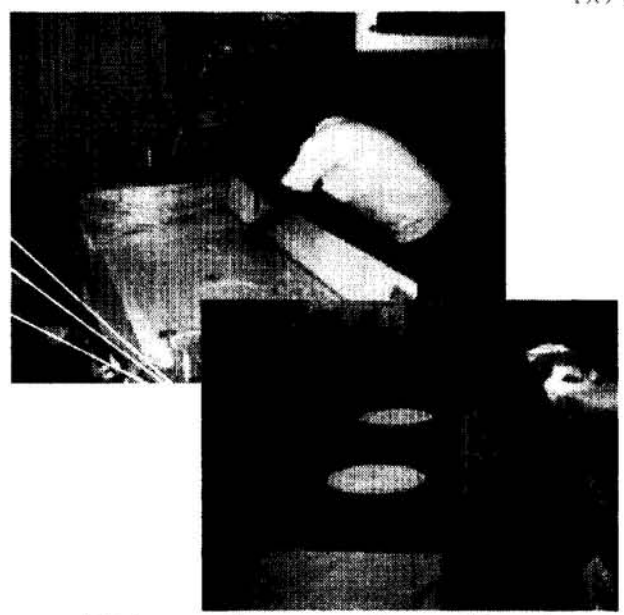

EB Septum/Longeron/Crease Ring Assy

Out-Of-Autoclave Process Development

EB LH_2 Tank - Lessons Learned

Material

- Material out-time in storage (sealed in bags) - 1 year
- Material out-time protected from UV but not sealed - 2 months
- Lay-up must be sealed & UV light protected when stored

Heat debulk

- Requires more definitive temp vs time evaluation for optimum debulk
- Multiple heat debulks may limit useful out time of material

Lead shielding

- Application of proper shielding (to allow staged curing and assembly of "green" mating surfaces) is not a trivial issue. Care must be taken in shielding design to avoid EB "leakage" and unwanted cure

Tooling

- Thin shell fiberglass/graphite tooling is sufficient for most applications
- High density foam tooling for large parts not manageable
- "Green" assembly technique is very demanding on support tooling design (tooling stiffness, tolerances, tooling "breakdown" features to allow part access, etc.)
- Minimal support tooling increases difficulty in positioning "green" joints

Design

- Tooling design must be fully integrated with component design
- Tooling requirements more demanding as structure increases in size

Air Canada - Aircraft Repair Program For Composites
EB Processing Approach

Wet Lay-up Disadvantages

Time Consuming
- 45 Hours for Simple Repair

Pot Life Constraints
Cured Properties Not Optimum
Special Storage Requirements
Special Equipment Requirements
Tooling Requirements
High Maintenance Costs

E-Beam Repair Advantages

Rapid Cure Cycle
- 1 – 3 hours for simple repair

No Pot Life Restrictions
Cure on Aircraft
No Special Storage Requirements
Multiple Repairs at Same Time
Simple Tooling
Reduction in Repair Costs

Reduction in Man-hours

- One-sided; 11% (Min.), 47% (Max.)
- Two-sided; 40% (Min.), 51% (Max.)

Queue Time for Pre-preg Thaw; 8 Hrs to 0
Freezer Cost: Reduced to 0
Material Costs: Same Price
Time-out Scrap Costs: Reduced to 0
Revisit Costs: Reduced 50%
Tool Costs: Reduced by 90%
Utilities
- Electricity; Reduced 98%
- Nitrogen; Reduced to 0

Aircraft Downtime: Reduced by 1 Day

acsion

Industry Experience

Boeing – Phantom Works
Space and Communications Group

Advanced Composite Preform Technology

Boeing/NASA Activity

Boeing/NASA ACT Wing Program

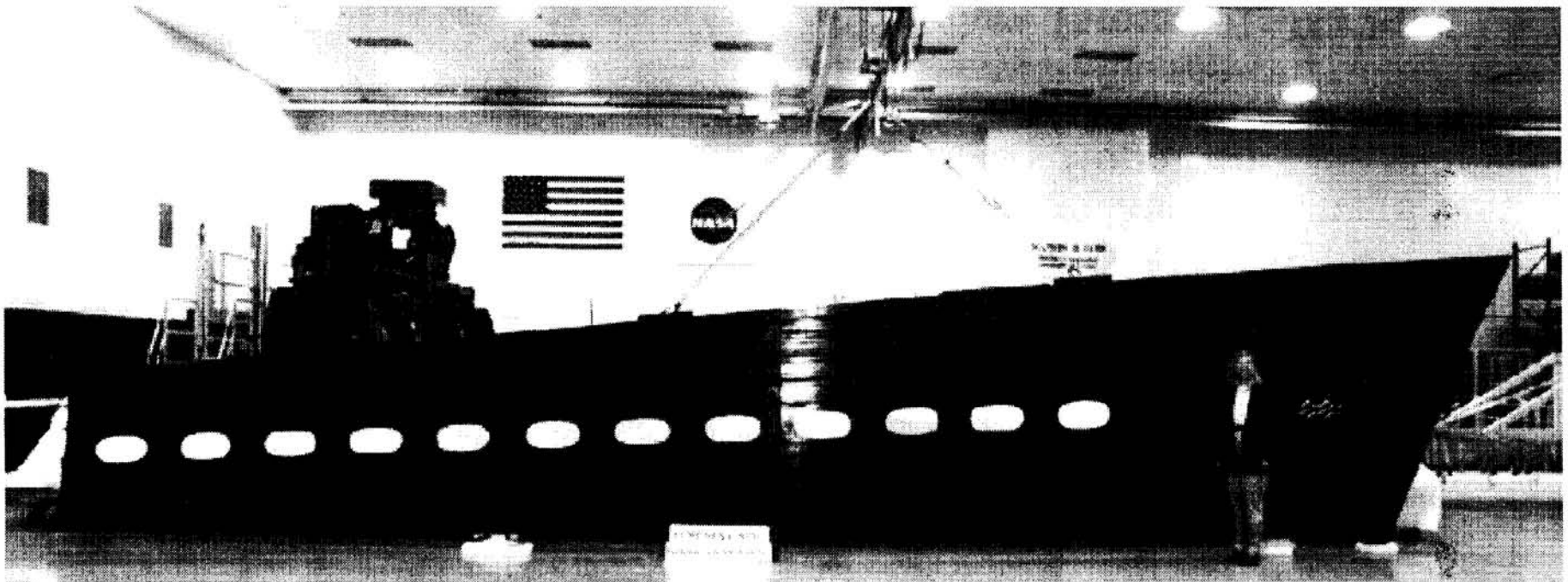

Under Contract	Infuse Panels	Ship to NASA
Jul 2000	Sep 2000	Oct 2000

Low Cost Liquid Molding Process

- Out of autoclave capable process
- Commercial Process
- Preform Technology
- New Aerospace Resins
- NASA Testing

Boeing/NASA AST Composite Wing Test

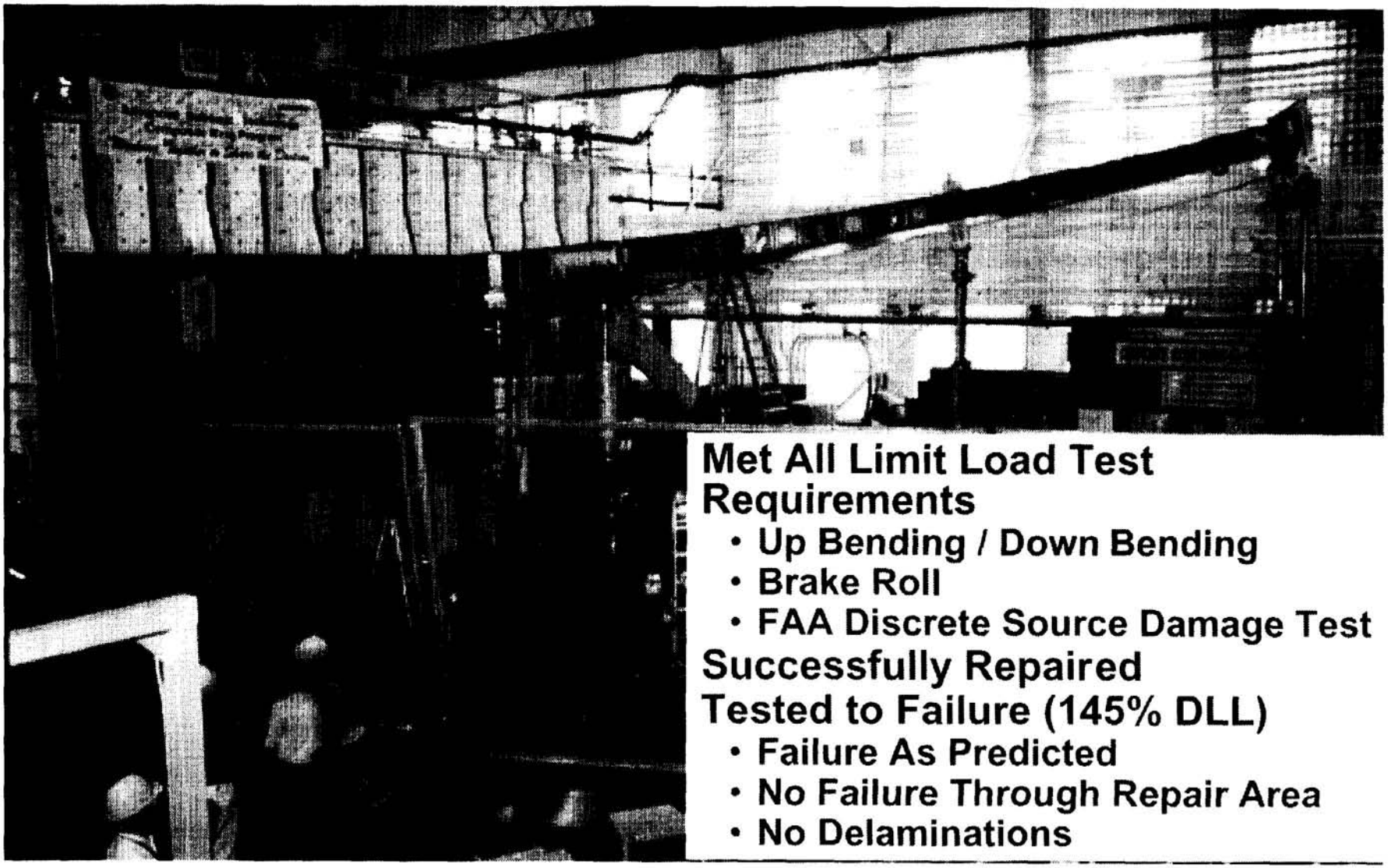

Met All Limit Load Test Requirements
- Up Bending / Down Bending
- Brake Roll
- FAA Discrete Source Damage Test

Successfully Repaired

Tested to Failure (145% DLL)
- Failure As Predicted
- No Failure Through Repair Area
- No Delaminations

... Met All Program Requirements

Vacuum Assisted Resin Transfer Molding (VARTM) Process

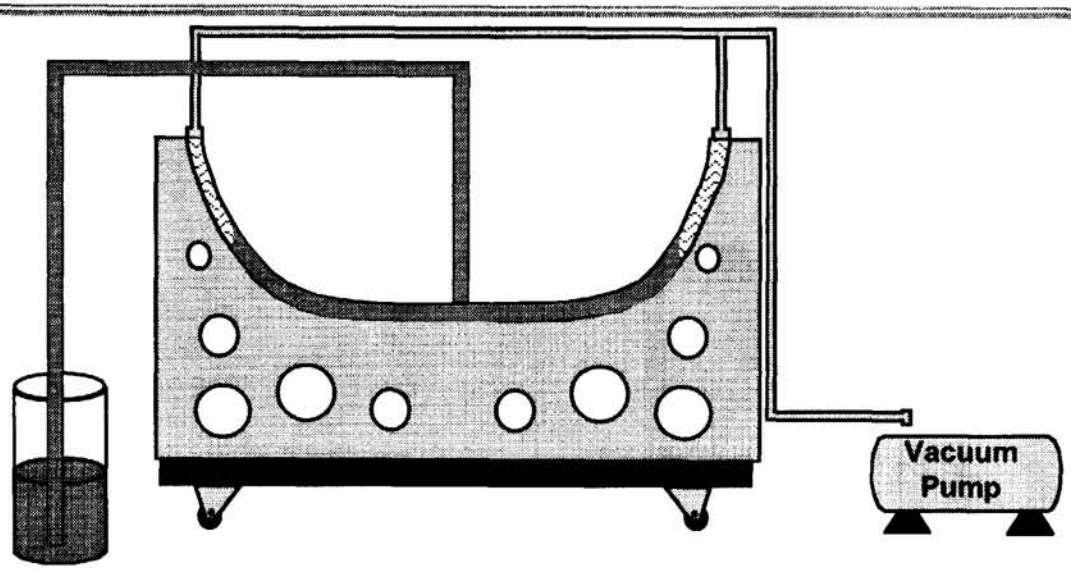

VARTM Advantages

- Low Cost/Simple Processing
- Allows Complex, Very Large Part Fabrication
- Eliminates Autoclave Requirement
- Tool One Side
- Reduced Material Storage
- Reduced Debulking

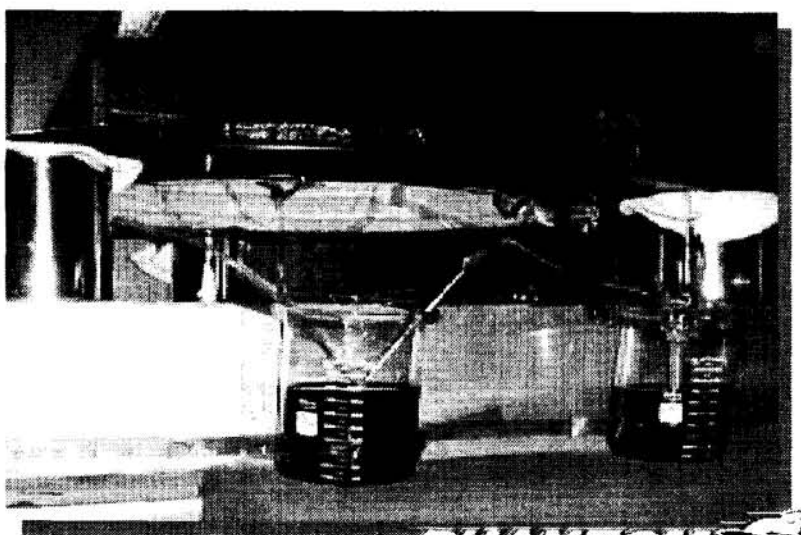

Industry Experience

Northrop Grumman

Kistler K1 RLV Fabrication

Hat Stiffened Epoxy and BMI Shell Structure

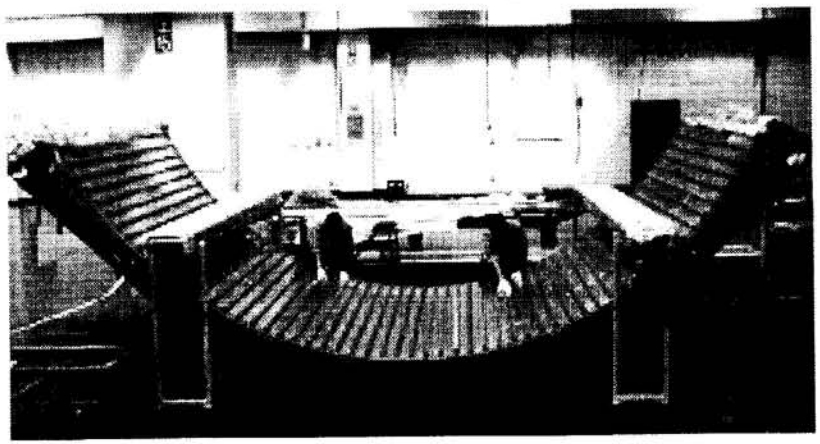

- Produced Intertanks with Cutouts and Access Details
- Applied Experience from F-18 for Local Stiffener Termination Details
- Demonstrated Fast Design and Fabrication Response to Customer

- NGC Developed Rapid Prototype Tooling and Assembly Jigs for Low Rate RLV Production on K1 Program
- Baselined Hand Lay-up Autoclave Cure due to Low Rate
- Automated Processes do not Justify Non-recurring Cost for Low Rate RLV

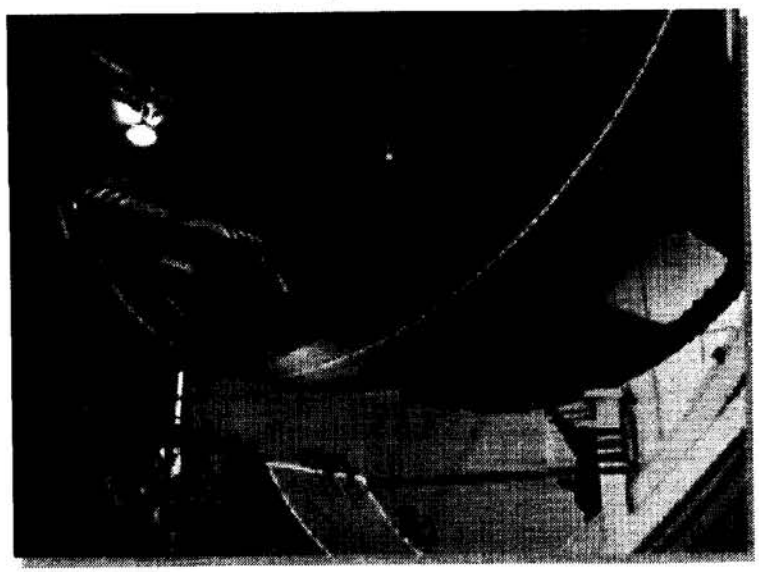

SSTO Wing Box Test

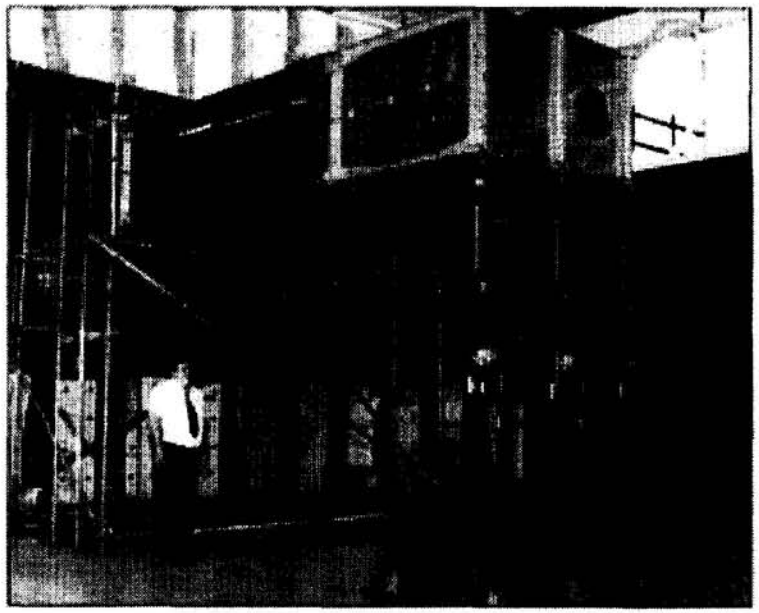

Description

- 54" x 120" x 36" Gr/BMI Wing Box
- Polyimide Core Sandwich Construction
- 4-ply 0.020" Gr/BMI Min Gauge
- Static Upward and Downward Bending Load Applied Through Metal Load Box
- 120 Channels Strain Gages
- 16 Fiberoptic/14 AE/AU Sensors for Structural Health Monitoring
- Tested at NASA LaRC 30 May 1996

Summary of Results

- **Validated NGC Design and Analysis Methods**
  - *Within 3% Predicted Failure*
- **Demonstrated NGC Lightweight Composites Mfg**
  - *Within 2% of Predicted Weight*
- **Demonstrated Integration of Structural Health Monitoring (i.e., Fiberoptic, Acoustic Sensors)**
  - *Performance Data Base on Large Test Article*

Composite Joining and Assembly

- Scaled up Innovative Joint Concepts used on Beech Starship for HSCT Aircraft
- Performed Design, Analysis, and Fabrication Activity at NGC
- Element Validation Test Program Performed at NASA LaRC
- Applied Proven Joint Concepts in Wing Box Subcomponent. Tested at LaRC to 119% Ultimate

Test Element Concept #1

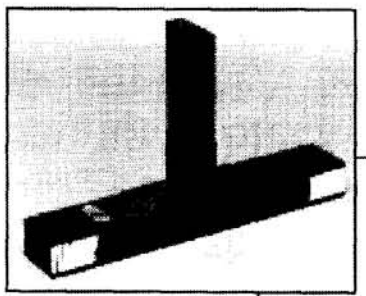

Concept #2

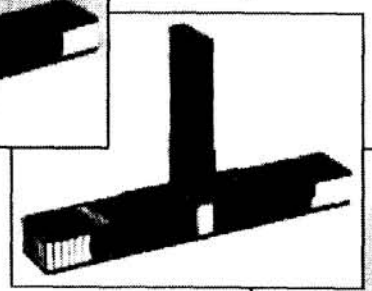

Concept #3

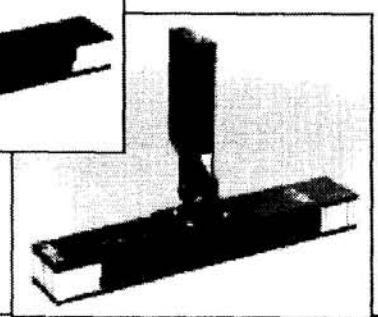

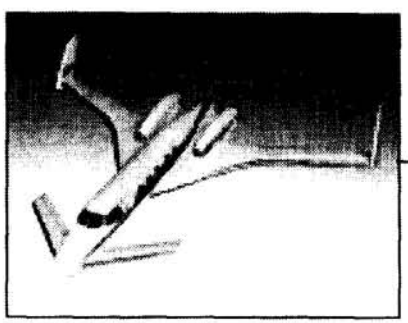

Original Application

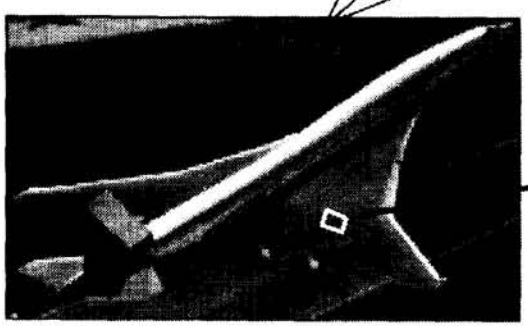

Severe Loads and Environment

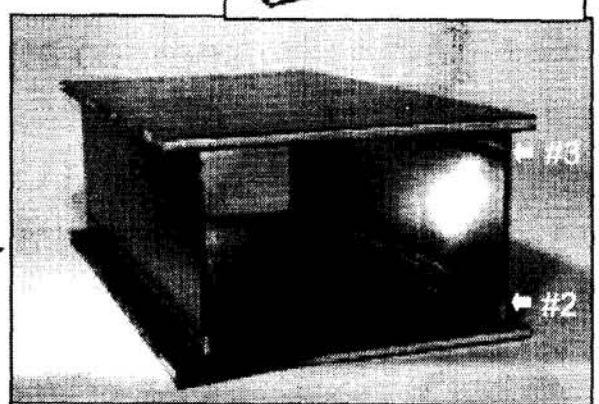

Structural Subcomponent Test

Summary

- Significant effort have been devoted to establishing the technology foundation to enable the progression to large scale composite structures fabrication.
- We are not capable today of fabricating many of the composite structures envisioned for 2nd Generation RLV.
- Conventional "aerospace" manufacturing and processing methodologies (fiber placement, autoclave, tooling) will require substantial investment and lead time to scale-up.
- Out-of-autoclave process techniques will require aggressive efforts to mature the selected technologies and to scale up.
- Focused composite processing technology development and demonstration programs utilizing the building block approach are required to enable envisioned 2nd Generation RLV large composite structures applications.
- Government/industry partnerships have demonstrated success in this area and represent best combination of skills and capabilities to achieve this goal.

CP/27 N/24
(c) 10 REPRO

Composite, Cryogenic, Conformal, Common Bulkhead, Aerogel-insulated Tank (CBAT)

Materials and Processing Methodologies

J. Keith Roberts and Michael P. Kovach

Thiokol Propulsion
SEHO Operations
P.O. Box 707, M/S 200
Brigham City, UT 84302

William M. McMahon and Jeffrey L. Finckenor

National Aeronautics and Space Administration
George C. Marshall Space Flight Center
Marshall Space Flight Center, AL 35812

ABSTRACT

The objective of the Composite, Cryogenic, Conformal, Common Bulkhead, Aerogel-insulated Tank (CBAT) Program is to evaluate the potential for using various new technologies in next generation Reusable Launch Vehicles (RLVs) through design, fabrication, and testing of a subscale system. The new technologies include polymer matrix composites (PMCs), conformal propellant storage, common bulkhead packaging, and aerogel insulation. The National Aeronautics and Space Administration (NASA) and Thiokol Propulsion from Cordant Technologies are working together to develop a design and the processing methodologies which will allow integration of these technologies into a single structural component assembly. Such integration will significantly decrease subsystem weight and reduce shape, volume, and placement restrictions, thereby enhancing overall launch system performance.

This paper/presentation focuses on the challenges related to materials and processes that were encountered and overcome during this program to date.

INTRODUCTION

One of the ongoing goals of the National Aeronautics and Space Administration (NASA) is to lower the cost of access to space. This objective is achieved through research and development into technologies that may be used to improve current and future space transportation systems. These technologies may result in improvements in safety, reliability, performance, cost, or operating efficiency. The Composite, Cryogenic, Conformal, Common Bulkhead, Aerogel-insulated Tank (CBAT) program has the potential to positively influence each of these areas.

What is CBAT? The name, CBAT or Composite, Cryogenic, Conformal, Common Bulkhead, Aerogel-insulated Tank, refers to the enabling technologies and/or the functionality desired in the end product. CBAT seeks to demonstrate and assess the potential for system improvements through the integration of various technologies. These technologies include polymer matrix composites (PMCs), conformal propellant storage, common bulkhead packaging, and aerogel insulation.

Evaluating the aspects of the system that the name suggests--Composite refers to the PMCs that will be used to fabricate the system. PMCs are the materials of choice for most of today's aerospace applications. They provide a unique combination of high strength and stiffness with low material density relative to metals. In addition, many properties of composite materials are anisotropic (directional). Therefore, these materials and their use may be tailored to a specific design. Other advantages of PMCs

© 2000 Thiokol Propulsion, a Division of Cordant Technologies Inc.

include their resistance to fracture, corrosion, and wear, ease of fabrication and assembly, ability to be fabricated to net shape, and capacity to facilitate component integration.

Cryogenic refers to the prospective propellants for use with the system. One of these propellants is liquid oxygen (LOX). LOX is a very harsh environment and hence presents many challenges to system designers. Two of its primary challenges are reactivity and low vaporization temperature. Some materials are susceptible to oxidation or combustion at standard atmospheric conditions. As oxygen concentration and pressure increases, the frequency and the severity of these reactions tend to increase, making a LOX environment very inhospitable to many materials. The other primary challenge, the low vaporization temperature of LOX (-297°F/-183°C), results in significant stresses and strains being induced simply due to thermal gradients and/or differences in coefficients of thermal expansion (CTEs). The materials have therefore been chosen with respect to the LOX environment. However, testing for this program will initially be performed using liquid nitrogen (LN_2, $T_{vap}(LN_2)$ = -320°F/-196°C) to mitigate cost and safety issues.

Conformal refers to customizing the shape of the propellant storage system to the shape of the vehicle in which it will be used. . This customization provides two significant benefits. It allows a designer to maximize the amount of propellant storage within a given space in the vehicle. It also facilitates the integration of the tank structure into the vehicle structure. Overall, this ability reduces the restrictions placed on the vehicle designer.

Common bulkhead refers to the methodology for placing or packaging the propellant storage tanks within the vehicle, in this case, one adjacent to the other with a common interface in between. This ability removes additional constraints on tank shape and placement. For previous cryogenic propellant systems this arrangement has been very difficult to accomplish. Due to the high thermal conductivity of the materials used, and the difference in temperature between the propellants, freezing of one of the propellants would invariably become a serious concern.

Lastly, aerogel-insulated refers to the use of a special class of materials, aerogels, between and around various portions of the system. Aerogels are some of the lightest solids ever produced. Highly porous and almost wispy in appearance (Figure 1), aerogels produced from such materials as silica, alumina, or zirconia can have densities as low as just three times that of air ($\rho_{aerogel} \sim 0.003$ g/cm^3). Another result of their highly porous nature is their low thermal conductivity. Aerogels can insulate almost 40X better than the best fiberglass insulations. This makes aerogels one of the best insulators available today (Figure 2).

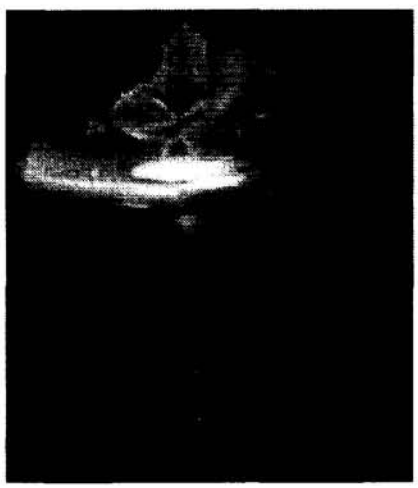

Figure 1: The wispy, fragile appearance of an aerogel shown protecting a flower from being consumed by a burner.

Figure 2: Tom Tillotson, a chemist at Lawrence Livermore, applies a flame to the top of a 1-inch-thick silica aerogel brick. Even though a thermocouple placed on the aerogel's top surface reports a temperature of 2,108°F, his hand is totally unaffected by the heat.

© 2000 Thiokol Propulsion, a Division of Cordant Technologies Inc.

Particulate/granular forms of these materials are also available. These forms trade off some of the density and thermal advantages for improvements in strength and ease of use.

The CBAT program will evaluate the potential for using and integrating these technologies through design, fabrication, and testing of a subscale system. This effort is considered critical to enabling development of the second generation of NASA RLV. The program is currently nearing the end of the design phase and the start of the fabrication phase.

The design created by NASA's George C. Marshall Space Flight Center (NASA/MSFC) and its industry partners incorporates each of the aforementioned technologies and functionality. This design is shown in Figures 3a through 3c. The design is based on a graphite/epoxy PMC. It will be fabricated by a combination of hand lay-up and filament winding, using both pre-impregnated (prepreg) fabric and tow/yarn. The system is designed for the LOX environment, and with some minor material/processing changes, may also be evaluated for use with hydrogen. The system and the tanks within the system have noncircular cross-sections. The shape is considered representative of one that would be used in conjunction with a lifting body-type RLV. The system also employs a common bulkhead between the two propellant tanks. The bulkhead functions in both structural and thermal capacities. The bulkhead utilizes graphite/epoxy and honeycomb to provide strength and aerogel-based material to provide insulation. A rapid prototype (RP) model of the system design was developed using the stereolithography apparatus (SLA) and laminated object manufacture (LOM). This model has been used to verify component form and fit.

This paper focuses on the challenges related to materials and processes that were encountered and overcome during this program to date.

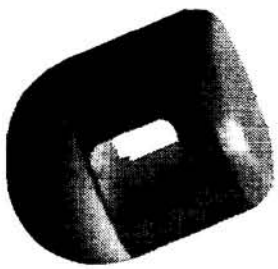

Figure 3a: CBAT propellant tank design. Cross-section is D-shaped in the plane perpendicular to the anticipated vehicle axis.

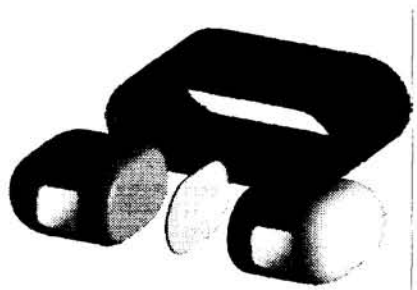

Figure 3b: Assembly of the CBAT propellant tanks around the bulkhead and insertion into the system skirt structure.

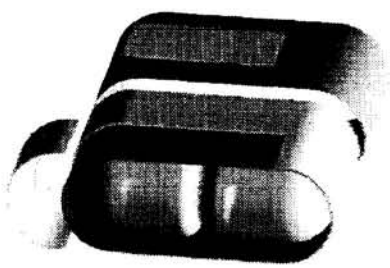

Figure 3c: Final assembly of the CBAT skirt sandwich structure. The skirt is composed of inner and outer graphite/epoxy skins bonded to a honeycomb core.

© 2000 Thiokol Propulsion, a Division of Cordant Technologies Inc.

MATERIALS AND PROCESSES

At the beginning of any composite fabrication effort, potential fabrication methods must be evaluated. After the fabrication method is determined, the tooling and types of materials must be considered. For the CBAT propellant tank, the chosen method of fabrication is a combination of polar filament winding and hand lay-up. The tank material will be IM7/977-2 pre-impregnated filament winding tow and 5 harness satin (HS) cloth. The tooling will be a removable mandrel made from a sand replacement called Macrolite™. The following sections deal with the evaluation, selection, and development of the materials and processes for the fabrication of the CBAT system.

Filament Winding

Polar winding was chosen as part of the fabrication of the CBAT propellant tanks to minimize the amount of fiber build-up in the dome regions. A 16 by 22-inch portion of the dome region will be cut out for the manhole door. Excessive build-up in this region would create mating problems for the door and the tank. Polar winding will alleviate this issue because no crossovers will occur in the filament winding pattern in the dome. Helical winding would create a greater thickness build-up in the dome region because of the crossovers that occur in a helical pattern. Polar winding creates a build-up directly adjacent to the polar boss but that area will be removed for door installation.

Since the CBAT propellant tanks have a flat portion in the common bulkhead region, filament winding will be challenging because of the changing contour. The filament winding program that controls the machine motion will be generated for a 60 inch diameter cylinder, but the tank shape creates a variation in diameter from 60 inches to 36 inches with a flat side. This will obviously lead to tow overlaps and potential tow slippage in some areas of the barrel sections of the propellant tanks. The greatest potential for tow slippage occurs in the transition from the cylindrical sections to the flat sections of the tanks.

One-fifth scale models were wound using a polar pattern to determine if these issues would be insurmountable. Both slippage and overlaps occurred in initial trials. A layer of film adhesive was then applied to the mandrel to give a tacky surface for the tow to grab. This was successful in minimizing slipping on the small-scale model. A higher resin content; i.e., tackier, version of the IM7/977-2 was also ordered for the full-scale tanks to further alleviate any problems with slipping. Issues associated with the transition regions will also be reduced upon scale-up to the full-sized tank. This effect will be due to the reduction in the size of the tow relative to the geometric features of the tank and the winding pattern. For example, overlaps will occur, but these should be less prominent on the full-scale tank because they will be spread over a larger area. To illustrate the differences between polar and helical patterns, figure 4a shows a one-fifth scale model that was wound with a polar pattern, and figure 4b shows a one-fifth scale model that was wound with a helical pattern. Notice the crossovers in the dome of the helical wound model.

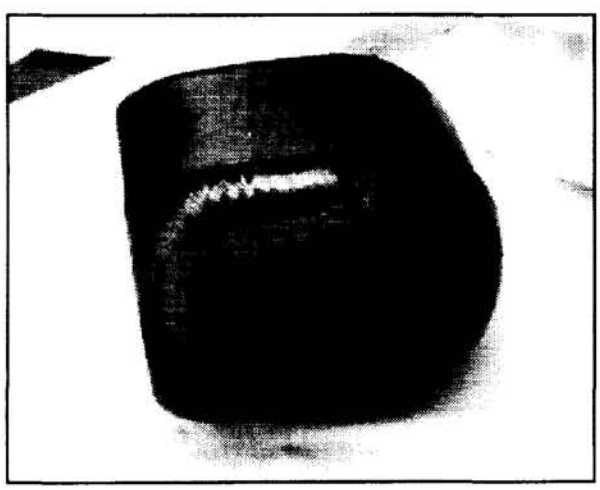

Figure 4a: Polar wound one-fifth scale model of a CBAT Propellant Tank. Polar winding minimizes build up in the domes due to fewer crossovers. The non-cylindrical shape creates fiber tow overlaps in the flat regions.

© 2000 Thiokol Propulsion, a Division of Cordant Technologies Inc.

Figure 4b: Helical wound one-fifth scale model of a CBAT Propellant Tank (before cure). Helical winding causes more build up in the domes regions because of the crossovers.

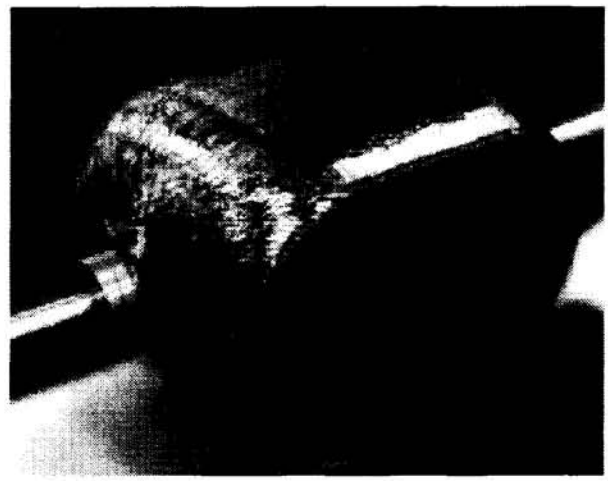

Hand Lay-up

Pre-impregnated IM7-977-2/5HS cloth will be hand laid, as the design requires, over the three regions of the propellant tanks. The hoop region will require 16 plies, the dome regions will require 10 plies and the door build-ups will require 20 plies. Laying the hoop plies and the door build-up plies should be relatively typical. The dome regions will require more attention.

The issue involved with the cloth lay-up on the domes is the challenge of getting a flat piece of cloth to conform to an 18-inch spherical surface. Obviously the fiber pattern in the cloth material will distort. NASA/MSFC Structures and Design personnel used PATRAN® Laminate Modeler to simulate how much fiber distortion would occur as the cloth was draped over the spherical dome regions. Also, a drape test was conducted with 5HS cloth to determine the degree of ply distortion that would occur. Figure 5 shows the result of the drape test. The dashed tracer lines follow individual tows within the 5HS cloth and show the distortion as the ply is wrapped around the dome. Figure 6 is the result of the modeling that was done to simulate the fiber distortion in the cloth. The model shown in Figure 6 accurately predicted the results of the actual drape test.

Figure 5: The results of the 5HS cloth drape test on a 36 inch diameter dome. The dashed tracer lines follow individual tows within the cloth. The solid line represents the centerline of the dome.

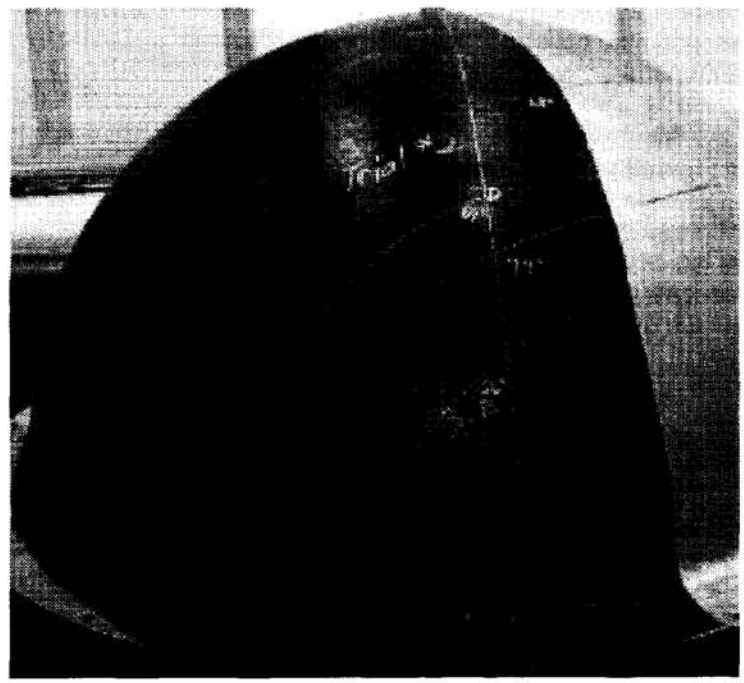

© 2000 Thiokol Propulsion, a Division of Cordant Technologies Inc.

Figure 6: PATRAN® Laminate Modeler software was used by the MSFC Structures and Design Group to predict the fiber distortion as the cloth draped on the 36 inch domes. The image shown is from Unigraphics/FiberSIM.

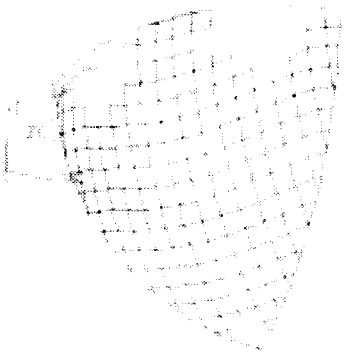

Tooling

The major parameters for selection of the mandrels for fabrication of the propellant tanks were weight, ease of removal, and dimensional stability. Sand mandrels are typically a first choice because of their ease of fabrication, ease of removal, and low cost. The mandrels for the CBAT propellant tanks will each be 48 cubic feet. A sand mandrel would weigh approximately 4000 pounds. Urethane foam was another option that was considered. Foam is lightweight and could be machined to the proper tank dimensions. Foam was eliminated as an option for the CBAT propellant tank mandrels because of the lack of dimensional stability. Since the foam has a high expansion rate and the CBAT mandrels will not be cylindrical, the expansion in the different regions of the tank would be difficult to predict. After considering the options, a lightweight ceramic material, Macrolite™, was chosen for the CBAT propellant tank mandrels.

Macrolite™ is actually a water filtration media that consists of various sizes of ceramic spheres (see Figure 7). Macrolite™ is used for tooling by some composite manufacturers including Thiokol Propulsion in Brigham City, Utah. The M&P Composites group at Thiokol-Utah researched various combinations of the different size and density Macrolite™ particles (Table 1) (Yorgason). These particles were mixed with alumina microspheres and a binder, polyvinyl alcohol (PVA). An optimized mix was used to fabricate a 97-inch diameter 110-inch long mandrel. The information from this research was used to begin the development of a Macrolite™ mandrel for the CBAT propellant tanks.

Material	Density (lbs./cu.ft.)
Macrolite™ M357	21
Macrolite™ M714	25
Macrolite™ M1430	28
Macrolite™ M3050	30
Macrolite™ M4060	56
Macrolite™ M7080	60
Sand	95

Table 1: Densities for all the Macrolite™ particles and sand. The M4060 and M7080 particles were deleted from the final mix and replaced with sand.

© 2000 Thiokol Propulsion, a Division of Cordant Technologies Inc.

The cure of the 977-2 epoxy resin used in tank fabrication will take place at 350°F (177°C). However, PVA tends to react adversely at such temperatures and produce mandrels with significantly lower solubility. For this reason sodium silicate was substituted as the binder in the CBAT program. Unfortunately, using sodium silicate as a binder with the Macrolite™ particle mix developed at Thiokol-Utah also created relatively insoluble mandrels. After discussions with the sodium silicate vendor, PQ Corporation, and many trials, a successful mixture was tested. This mixture included a reduction in the percentage of binder used from 10% to 8%, and elimination of the smallest Macrolite™ particles (M4060 and M7080) and alumina microspheres. These particles were replaced with sand. The difficulties that were encountered are thought to have been the result of the high surface area associated with the fine Macrolite™ particles. This leads to greater wetting and absorption of the binder by the Macrolite™. These fine particles also pack together better, thus eliminating porosity and preventing the water from penetrating the mandrel during washout. The addition of sand allowed the hot water to penetrate through the mandrel more readily, and therefore break down/dissolve the sodium silicate binder at a faster rate. The Macrolite™ mix reduces mandrel weight by 70% when compared to sand. The addition of the sand led to a Macrolite™ mix that was 3% heavier than the mix established by Thiokol-Utah.

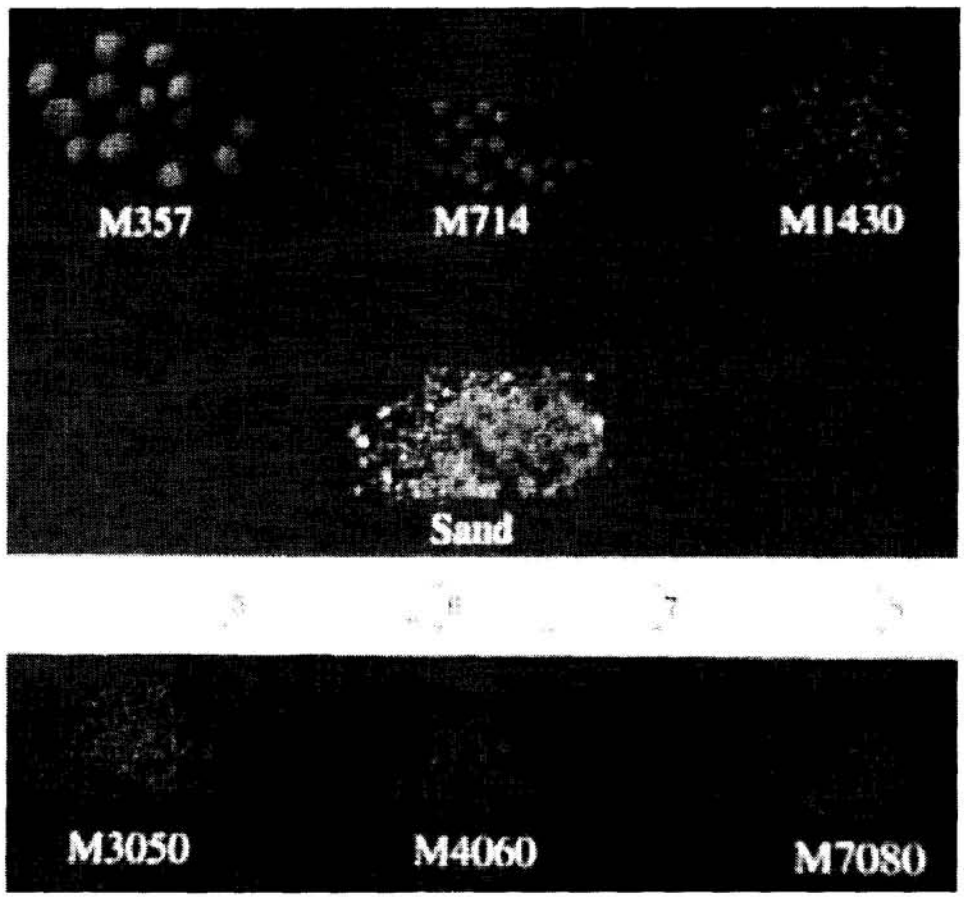

Figure 7: A photograph of the various Macrolite™ particles alongside sand. Notice the different size particles within the sand while the Macrolite™ particles are relatively consistent especially in the smaller sizes.

© 2000 Thiokol Propulsion, a Division of Cordant Technologies Inc.

SUMMARY

The CBAT program will evaluate the potential for building a conformal composite tank system that integrates a common bulkhead with aerogel insulation to reduce subsystem weight and volume, thereby enhancing the performance of future reusable launch vehicles. Although in the early stages, the CBAT fabrication effort has encountered and overcome several obstacles. The issues associated with filament winding a non-cylindrical shape, while not proven on a large scale, have been minimized through material selection and proper fabrication sequence. The hand laying of cloth onto the dome sections has been successfully tested to allow integration into the design models. Lastly, a lightweight mandrel material has been tailored to meet the specific requirements of the CBAT program.

ACKNOWLEDGEMENTS

This work is being funded under a contract with NASA's George C. Marshall Space Flight Center (NASA/MSFC). The authors would like to thank NASA/MSFC, and the following individuals who have contributed significantly to this effort:

T.W. Dillard	Thiokol Propulsion – Composite Technology
D.E. Lawrence	Thiokol Propulsion – Composite Technology
P.D. Thompson	Thiokol Propulsion – Composite Technology
G.L. Young	Thiokol Propulsion – Composite Technology

REFERENCES

1. Yorgason, James A., "LIGHTWEIGHT/LOWCOST MANDREL," Thiokol Propulsion – Science and Engineering, TR11449, November 21, 1997.

© 2000 Thiokol Propulsion, a Division of Cordant Technologies Inc.

CP/528/IN/27

Coating removal technology using starch based abrasives, a review of current Aerospace application using the Envirostrip dry stripping process.

by Denis Monette and Cameron Drake
Archer Daniels Midland

September 2000

ADM/Ogilvie

995 Mill Street Montreal, H3C1Y5
Phone: 514-846-8516

Coating removal technology using starch based abrasives, a review of current Aerospace applications using the Envirostrip dry stripping process.

Drake Cameron. Monette Denis, Archer Daniels Midland, 995 Mill St. Montreal QC, Canada, H3C1Y5. Tel: 514 846 8516

INTRODUCTION

Due to stringent environmental regulations enacted in the past 10 years, methylene chloride (MC) has been phased out in many industries because it is harmful to the environment and to the workers exposed to it. The aerospace industry, historically a large user of MC, researched and adopted many environmentally acceptable alternatives to replace methylene chloride based paint strippers. This has proved to be a very difficult task as MC chemical strippers have been very effective in removing tough polyurethane/epoxy coating systems typically found on aircraft structures

A variety of new "environmentally acceptable (EA) chemicals" were developed in the last five years to replace MC. These EA chemicals are considered safer because the chemicals are not as volatile, having very low evaporation rates. However, there are still some concerns that new EA chemicals may still pose unknown health risks to workers, as well as causing potential damage to aircraft structures due to long term ingress problems. Because MC strippers evaporate so quickly, problems associated with chemical ingress were rare. The potential for the new EA chemicals to damage and/or corrode sensitive aircraft structures is a new problem due to the low evaporation rates (low volatility) of these MC chemical substitutes.

Ten years ago, an alternative non-chemical, paint removal process was introduced to the aerospace industry. This process uses a dry abrasive media, EnviroStrip® wheat starch, projected at low pressures to remove virtually every type of organic coating from most aerospace materials. This media was considered more gentle than other dry media used at the time (e.g. plastic media). EnviroStrip® wheat starch, as the trademark implies, is manufactured from wheat starch, a biodegradable renewable resource, giving the product inherently high purity and uniformity.

Extensively tested, approved and used in production applications by Northrop Grumman, Raytheon, Cessna and Boeing, the EnviroStrip® process has been embraced for its coating removal effectiveness on metals and composite substrates. In 1998, a new sister product, EnviroStrip® XL was commercially launched (ref.4). This newer abrasive product is made from a corn hybrid polymer and offers improved water resistance. Today, EnviroStrip® XL is successfully used by major companies in the aerospace industry.

This paper will describe the methods of manufacturing these abrasive media products, the equipment used to apply the process, and the various applications for this technology in the Aerospace industry. Examples are selective stripping, metal bond adhesive removal and interior aircraft panel refurbishment. The production use of this dry stripping method on the Northrop Grumman B-2 bomber, the NASA Space Shuttle and other aircraft types will also be reviewed.

DISCUSSION – THE ENVIROSTRIP● TECHNOLOGY

The EnviroStrip● Abrasives

The starch-based media particles are irregular in shape and have sharp, angular edges (fig. 1-2). The media is amorphous in nature and semi-opaque to light. By weight the media has approximately 10-13 % moisture content. An interesting aspect of the media is the conditioning effect. After being projected several times, the media becomes more productive after each use. Two mechanism are at play: the average particle size range of the batch starts to widen to a more productive broader range (i.e. 12-100 mesh size) (ref 8) , and the media loses 1-2% of moisture which in effect sharpens the media. The principal difference between the wheat starch media and the corn polymer media is that the latter can better withstand contact with water.

The EnviroStrip® Manufacturing Process

EnviroStrip® wheat starch media and EnviroStrip® XL corn hybrid polymer are manufactured from pure native starches. A primary advantage of using a starch raw material is its purity and uniformity, and the absence of foreign particulates that are denser than the final starch abrasive product. The raw starch powder is fed to an extruder and heated in the presence of water to form a solid starch mass. Upon exiting the extruder, the starch material is formed into strands that are cut into pellets. These hard plastic-like pellets are cooled and tested for hardness. The starch pellets are then ground to various mesh sizes (e.g. 12/30 mesh).

The Process Equipment

When EnviroStrip® wheat starch was first introduced 10 years ago, it was used in dry media blast systems designed for light-abrasives such as plastic media. While EnviroStrip® media could be adequately used in these blast systems, it was found that certain design changes improved overall process efficiency. The major blast equipment manufacturers have since implemented important equipment design changes, helping to fine tune the EnviroStrip® coating removal process. Increased pressure pot angles (60+ degrees), better media flow control valves, and enhanced dust removal techniques were incorporated into the new generation of light-abrasive blast systems. These enhancements have improved EnviroStrip® coating removal rates and reduced media consumption.

There continues to be great strides in both North America and Europe in improving dry media blast systems. Flat nozzle technology, introduced recently into the light-abrasive coating removal industry, has had a significant impact on EnviroStrip® media performance. Flat nozzles have demonstrated strip rate increases of over 100% when compared to conventional round nozzles. The computational fluid dynamic programs used to design the flat nozzle revealed that media can be more uniformly distributed to the surface through a flat nozzle, minimizing media overlap and the "hot-spot" typically found in round nozzles.

Closed-cycle (dust-free) dry media blast systems have also evolved to support aerospace coating removal requirements. Historically closed-cycle systems used small nozzles designed with a 90-degree impingement angle to the working surface. These systems were difficult to use, slow to remove coatings and did not provide the operator sufficient viewing of the blast area. Major advances have been achieved with the introduction of closed-cycle systems designed for EnviroStrip® media. The new closed-cycle systems utilize the more efficient flat nozzles that are set at an optimal 45-degree angle to the working surface. In addition, a viewing window on the applicator head now allows the operator to see the blast process in progress. This helps operators to improve strip rates and, when possible, selectively strip coatings (i.e. remove top coat, leaving primer intact). Most closed-cycle systems are portable and can be used for both on and off aircraft paint and adhesive removal applications.

Benefits of Automation

The aforementioned improvements in media process equipment and nozzle design for starch media have allowed automation to yield further process benefits. High production rates on sensitive aircraft parts, providing controllable and repeatable surface finish, can now be accomplished with current automated system technology. Past work (ref 9) has shown that production strip rates increase by up to 300% when using semi and fully automated blast systems. Automated production work is presently being conducted on aerospace structures at several locations worldwide. For example, the Boeing-ASTA facility in Australia has implemented an automated starch media system for both composite coating removal and composite surface treatment. The composite surface preparation process is performed on Boeing manufactured carbon fiber parts. The system, using a large flat nozzle, has proven its ability to meet and exceed production demands without damage to the sensitive composite substrates.

Automated control of the nozzle movement allows a larger nozzle size and media flow rates to be applied. This, in turn, delivers higher strip rates and lowers material costs. Precise control can be assured, minimizing surface damage at higher production rates. Automation of the starch-based dry media process has proven to be an effective production technology in off-aircraft component stripping.

Mechanical Effects on Aerospace Materials

Most coating removal processes can induce unwanted surface effects on aerospace materials. Dry stripping causes two types of mechanical effects, residual stress and surface modifications. Residual stresses produced by dry media blasting are compressive in nature and are concentrated at the surface, similar to the effects produced by shot-peening. Within limits, compressive stresses at the surface of metals can actually be beneficial. Shot-peening studies have shown that compressive stresses can retard the onset of fatigue and corrosion in metals. However the potential of a dry stripping media to induce different compressive stress intensities(partial coverage) (ref 6) can negatively affect the fatigue life of thin skin aluminum control surfaces and fuselage sections. With such concerns in mind, the Boeing Commercial Aircraft Division issued service letters (1993, 1995) restricting the use of plastic media on Boeing civil aircraft structures. In turn, Boeing allowed EnviroStrip® wheat starch to be used an unlimited number of times on aluminum (>0.032-inch thick) as a preferred non-chemical alternative to remove coatings from thin aluminum surfaces.

The standard method used for years to gauge residual stress inducement in a substrate is the Aero Almen method. Developed by the USAF in the early 1980's, the method was borrowed from the shot-peening industry. Instead of using steel specimens, the USAF method uses 2024 T-3 aluminum strips which are 3 inches long by 0.75 wide inches and 0.032-inch thick. An Almen strip and strip holder are shown in fig 3. The higher the arc height or deflection of the Almen strip when blasted with an abrasive media, the higher the potential negative effect on the fatigue life and fatigue crack growth rate of that particular substrate. Figures 4 and 5 shows two panels 0.032-inch thick. One panel was stripped with EnviroStrip® wheat starch and had a corresponding Almen arc height of 0.003-inch, while the second panel was stripped with plastic media (Type V) and had a corresponding arc height of 0.007-inch. Note the difference in the mid plane deflection of the panels. The USAF, a long-time pioneer in researching new depaint technologies, sets a criteria that arc heights for any mechanical process not exceed 0.006 inch. Figure 6 shows typical saturation curves for EnviroStrip® wheat starch, EnviroStrip® XL and plastic media blast (Type V Acrylic) processes. Finally, aircraft components are often dry stripped prior to liquid penetrant inspections; the results of an AGARD report indicated that using starch media gave better inspection results than the more agressive media types (ref 2)

EnviroStrip® Application Overview

Adhesive Removal

Removing adhesives and sealants from sensitive substrates has always been a challenging operation. Historically, mechanical methods have utilized hand scraping or mechanical sanding. These methods are slow and often cause unacceptable damage (fig. 7). EnviroStrip® abrasives have the ideal characteristic of being able to efficiently remove various adhesives without compromising the bond primer found under the adhesive layer (fig 8)

Northrop Grumman B-2

The world's most sophisticated aircraft have been processed with EnviroStrip® wheat starch since 1994 (ref 13). After exhaustive evaluation of all alternative methods, the EnviroStrip® wheat starch was the only process found to remove special thick coating systems without affecting the carbon fiber substrate found on the B-2.

Space Shuttle

The EnviroStrip® process is used to strip the thermal protection system (TPS) adhesive from the Space Shuttle vehicles. Over 3000 ft^2 of the Shuttle vehicle's upper wings, side body, and payload bay doors were processed. (ref 7)

Selective stripping

Selective stripping is a coating removal technique where the top-coat is removed and the base primer coat is largely left intact. There are several advantages to this technique. Leaving the primer coat intact eliminates surface effects on various substrates, which is particularly beneficial for composite structures. Another advantage is a reduction in toxic metals found in the starch media waste. This occurs because the heavy metals (e.g. chromium) are predominantly found in the primer coat, and are thus not removed when selective stripping is performed. (ref 10) Airbus Aircraft recommends selectively stripping coatings from their aircraft.

Composite Structures

The most widely used media for composite stripping, EnviroStrip®, is presently used by several repair and overhaul facilities. At these locations, various coating systems are removed from commercial airliner composite structures. As an example, the following Boeing materials are approved for stripping with EnviroStrip® wheat starch.

SUBSTRATES APPROVED FOR WHEAT STARCH MEDIA BLASTING

SUBSTRATE TYPE	BOEING MATERIAL SPECIFICATION	SELECTIVE FINISH REMOVAL CYCLES	COMPLETE FINISH REMOVAL CYCLES
Fiberglass 250 F Cure	BMS 8-79	Unlimited	Two
Fiberglass 350 F Cure	BMS 8-139 BMS 8-331	Unlimited	Five
CFRP (Carbon/Epoxy) 250 F Cure	BMS 8-168	Unlimited	Two
CFRP (Carbon/Epoxy) 350 F Cure	BMS 8-212 BMS 8-256 BMS 8-276	Unlimited	Five
Aramid (Kevlar/Epoxy)	BMS 8-218 BMS 8-219	Unlimited	None
Wire Mesh Lightning Strike Protection	BMS 8-336	Unlimited	None
Aluminum Flame-Spray Coating	BAC 5056	Unlimited	None

Ref: Boeing D6-56993

Aluminum Structures

The majority of fuselage skins have a thin layer of pure aluminum, known as Alclad, that covers a high strength aluminum alloy. This clad aluminum layer provides corrosion protection for the underlying alloy, and therefore it is imperative that any alclad removal is minimal and that the resulting surface roughness is within acceptable limits. For example, the general guideline for surface roughness should not exceed 125 µinches (R_a) on 0.032-inch thick clad aluminum skins.

Today's aging aircraft have been subjected to multiple chemical paint strip cycles and some have very little clad left on their skins due to the aggressive scrubbing needed to remove residual paint. EnviroStrip® wheat starch surface roughness data, reported by Beech Aircraft in 1992 (ref 5), is shown in the table below. These results are typical and have been validated in numerous test programs worldwide. Note that clad thickness is 5% (front and back) of total thickness of skins up to 0.063 inch; above 0.063 inch , aluminum clad skins are 2.5% front and back. With increasing clad layer thickness, the resulting surface profile will become slightly rougher.

Clad Skin Thickness	Clad Layer Thickness	After blasting Roughness µinches (Ra)
0.020 inch	0.0010 (5%)	40
0.025 inch	0.0013 (5%)	70
0.032 inch	0.0016 (5%)	90
0.040 inch	0.0020 (5%)	142
0.080 inch	0.0020 (2.5%)	132

DISCUSSION – CHEMICAL STRIPPING – SOME HAZARDS STILL REMAIN

Methylene chloride, also known as Dichloromethane, is considered a very toxic chemical. It can damage the liver, heart and central nervous system (ref 14). Past studies concluded that its use was so wide spread in various industries that most of the general population was exposed to it .The main route of exposure is via inhalation.

ESTIMATED DAILY INTAKE OF DICHLOROMETHANE BY THE GENERAL POPULATION

Route of Exposure	Estimated Dichloromethane Intake (µg/kg-day) of Various Age Groups				
	0 – 6 mo	7 mo – 4 yr	5 – 11 yr	12 – 19 yr	20+ yr
Ambient Air	0.04 – 0.30	0.06 – 0.40	0.07 – 0.46	0.06 – 0.38	0.05 – 0.34
Indoor Air	3.88	5.22	6.04	5.00	4.46
Total Air	3.92 – 4.18	5.28 – 5.62	6.11 – 6.50	5.06 – 5.38	4.51 – 4.80
Drinking Water	0.01 – 0.07	0 – 0.04	0 – 0.03	0 – 0.02	0 – 0.01
Food	0.03	0.11	0.09	0.05	0.05
Total Intake	3.96 – 4.28	5.39 – 5.77	6.20 – 6.62	5.11 – 5.45	4.56 – 4.86

Source: Government of Canada 1993.

Despite its toxic nature, Dichloromethane has proven to be very effective in removing aircraft coating systems, with its main advantage being speed. When compared to the myriad of new environmentally acceptable (EA) strippers, methylene chloride (MC) is still by far the most effective. For example, if it takes MC 2-6 minutes to remove a given coating system, the EA chemical alternatives will take at least 50 times longer (i.e. 2-8 hours).

There have always been hazards to the airframe when chemical strippers are applied. One of the most severe incidents involved a commercial aircraft which lost a 5ft by 10 ft section of its rudder during a trans Atlantic flight (ref 12). The failure was attributed to residual chemical stripper coming into contact with the composite tail rudder. The chemical damaged the resin matrix allowing water to enter the composite structure. The resulting failure was a delamination of the composite skin plies from the rudder assembly. Other reported examples of chemical damage are cases where the wrong chemical was used or improper chemical application was involved, resulting in damage to various parts of the aircraft including a forward landing gear.

Environmentally Acceptable Chemical Strippers

When using the new EA chemicals one must consider the different types of products available and the potential risks involved. There are basically three types of EA chemical strippers: alkaline, acid and neutral. A neutral pH (i.e. pH 7 ± 1) chemical is preferred, provided it remains stable, while acid or alkaline strippers present different corrosion risks.

ALKALINE: "Aluminum is a reactive metal, but develops an aluminum oxide coating or film that protects it from corrosion in many environments. This film is quite stable in neutral and many acid solutions but is attacked by alkalies." (ref 1)

ACID: High Strength steel such as AISI 4340 is used on aircraft in very critical applications, they include landing gear components, engine parts and critical fasteners and bolts throughout the aircraft. If an acidic solution comes in contact with high strength steel, hydrogen embrittlement can easily occur. Hydrogen embrittlement is caused by the introduction of nascent atomic hydrogen into the steel microstructure. . Hydrogen embrittlement can occur during a plating process or exposure to an acidic agent. The only known method to remove the hydrogen is by baking the part/component at 325 - 375 °F for 12-23 hours. If and when accidental exposure occurs, there are no known non-destructive methods for determining if hydrogen was introduced. The presence of hydrogen in steel promotes a significant loss of ductility and strength, which can lead to sudden brittle failures well after hydrogen exposure (refs 3,15)

NEUTRAL: Neutral solutions are considered by far the safest to use on aircraft structures. However, a slight deviation in formulation by manufacturers may cause a neutral stripper to be slightly acidic. For example (ref 11), a solution of pH 5.7 will cause hydrogen embrittlement on AISI 4340 steel. One should also consider that the stability of a given chemical stripper. The pH of a particular solution may change with time through evaporation, or when exposed to other chemicals and/or materials.

One the most important factors in evaluating a potential chemical is exposure or dwell time, particularly in the case of ingress into aircraft structures. An argument often used when potential damage is observed with new EA chemicals is that standard test results show that it is no worse than methylene chloride. However, the question is raised as to what dwell time is appropriate in comparative tests. For example, if pure benzyl alcohol is left to evaporate in an open laboratory pan, it will still be there after 12 months. The same amount of methylene chloride completely evaporates within 7days.

Thus to assess the potential damage associated with chemical ingress into aircraft structures, the fact that EA strippers will reside and act on aircraft materials for a much longer time horizon should be taken into account. The risk of ingress occurring is also impacted by the longer application times required with the new EA chemicals. The greater potential for ingress through longer contact times suggests that the risk of damage may be underestimated.

Conclusions/ Future Work

Dry stripping with starch-based media should be considered the safest alternative to methylene chloride, now and for the future. The current popularity of EA chemical strippers does not imply that they can be used without undue risk. And with the increasing use of advanced composite materials on newer aircraft, the concerns regarding chemical stripping effects on aircraft structures will be even greater.

New starch-based media types are currently under development at ADM that will eventually offer a wider variety of media products with differing characteristics and benefits.

ADM will continue to work closely with equipment manufacturers and the aerospace community to promote and enhance the starch dry stripping process.

ADM is actively working with environmental agencies and different industries to initiate an environmentally responsible media lease/recycling program supporting customers spent media disposal needs.

FIGURE 1 NEW MEDIA

FIGURE 2 TYPICAL PRODUCTION MIX

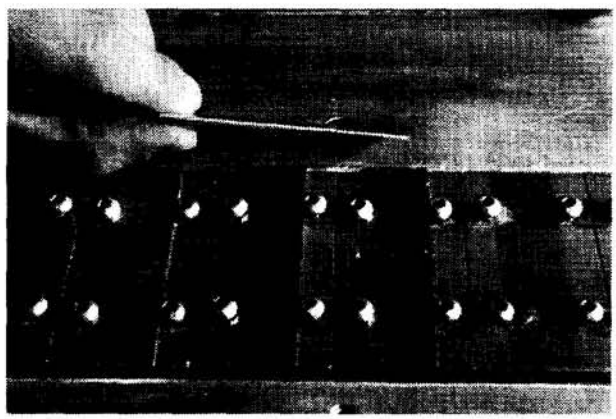

FIGURE 3 ALMEN STRIP AND HOLDER

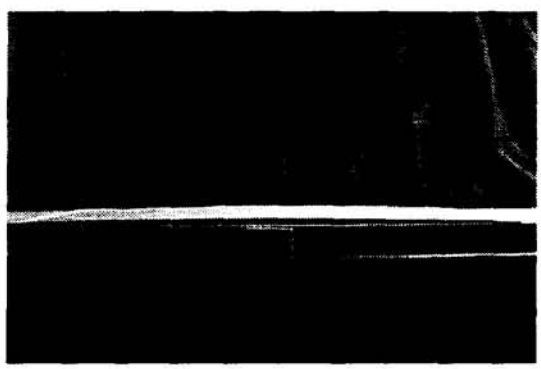

FIG 4 DEFLECTION WITH ENVIROSTRIP

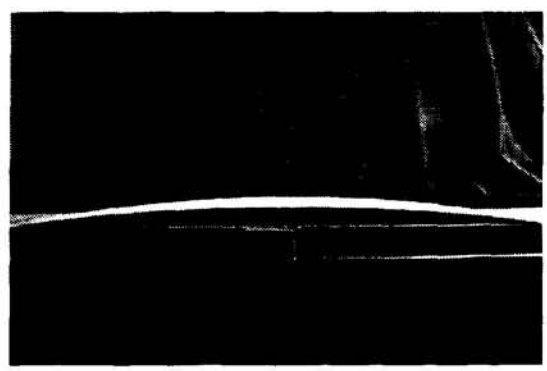

FIG.5 DEFLECTION WITH PLASTIC MEDIA

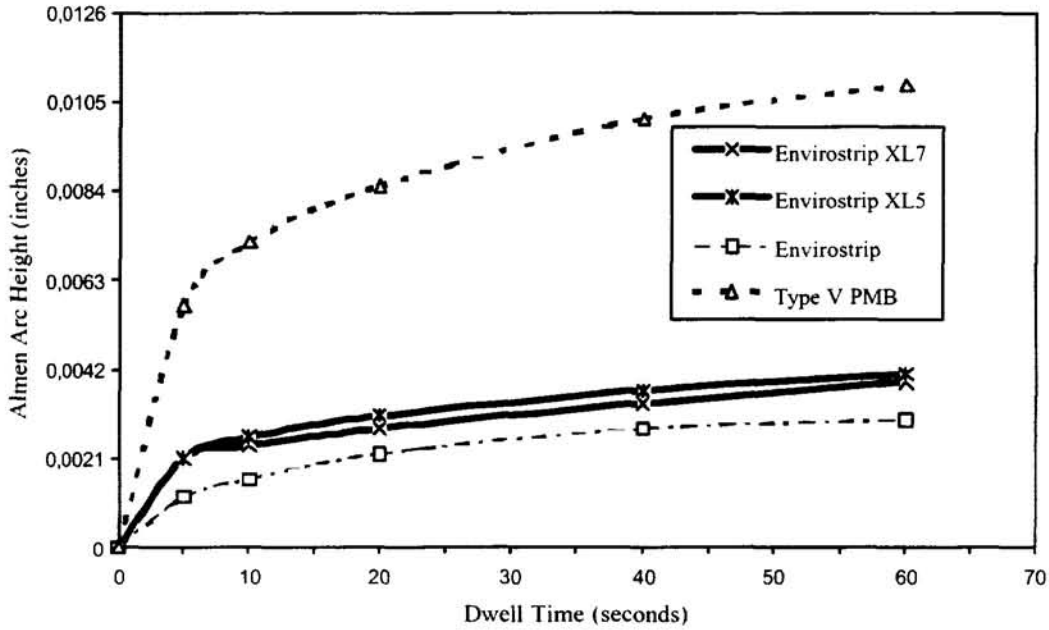

FIGURE 6 SATURATION CURVES FOR ENVIROSTRIP, XL AND PLASTIC MEDIA (TYPE V)

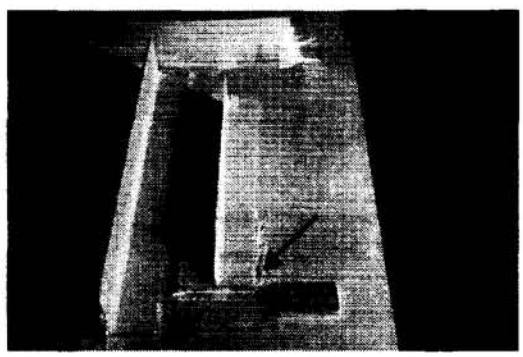

FIGURE 7 NOTE MECHANICAL DAMAGE AT ARROW

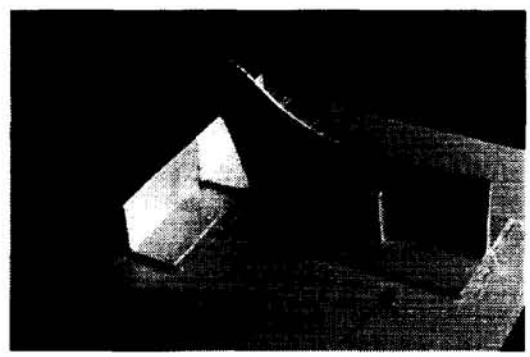

FIGURE 8 ADHESIVE REMOVED WITH ENVIROSTRIP, NO DAMAGE

CP/29/W 27

REMOVAL OF ZIRCONIA THERMAL BARRIER COATINGS AND MCrAlY BOND COATINGS FROM TURBINE BLADES: A COMPARISON OF METHODS BASED ON CHEMICAL STRIPPING, WATER JET AND SALT BATH.

A.Scrivani[1,2], U. Bardi[1], G. Ballerini[1], D. Bonacchi[1], M. Fantini[3], R. Groppetti[2], S. Ianelli[2], G. Rizzi[4]

1. Università di Firenze, Dipartimento di Chimica, Via Cavour 82, Firenze, Italy
2. Università di Parma, Dipartimento di Ingegeneria Industriale, Viale delle Scienze, Parma, Italy
3. Galvanica Parmense, Via Romagnoli 3, S.Polo di Torrile, Parma, Italy
4. Turbocoating S.p.A., Via Volta 3, Rubbiano, Parma, Italy

Abstract

In the aerospace field as well as in field of stationary gas turbines, thermal spray coatings are gaining considerable importance for the improvement the properties of Nickel-super-alloys materials surface. Thermal spray coatings are commonly used as antioxidation materials (mainly MCrAlY alloys) and as thermal barrier coatings (mainly Yttria partially stabilised Zirconia) and are applied on Nickel super-alloys (as for instance different kinds of Inconel). Coating removal is an important aspect in the production of these devices. Removal (or "decoating" or "stripping") is needed for the production of new components as well as for the reconditioning of "in service" components. The present paper is dedicated to the a comparison of different stripping methods and to the characterisation of the blades surface after removal of thermal spray coatings both of Zirconia and of MCrAlY.

The results reported here show that chemical stripping is particularly suitable for MCrAlY coating removal and does not affect the substrate. Water jet stripping can successfully be used for Zirconia-MCrAlY system removal although care is needed to avoid substrate damage. Salt bath technologies have been found to be effective for TBC removal but not for MCrAlY removal.

Introduction

Coating technologies are rapidly becoming a fundamental method in improving materials properties. In particular, thermal spray technologies are an effective and versatile method used to obtain coatings of different thickness with a good cost-quality ratio in the aerospace field as well as the in power generation sector (stationary gas turbines). In these areas, the surface proprieties of Nickel-super-alloy materials can be improved by means of antioxidation materials, such as MCrAlY (where M means Ni, Co or a combination of both), and thermal barrier coating materials, such as Yttria partially stabilized Zirconia (YPSZ). MCrAlY coating are used to improve the resistance of the component to aggressive media at high temperature (900-1000°C) while low thermal conductivity of Zirconia coatings decrease the in-service temperature of the component [Rickerby, 1991]. The system MCrAlY + Zirconia is normally called Thermal Barrier Coating (TBC), where the MCrAlY layer acts as a bonding layer between the Zirconia coating and the substrate and is normally termed "bond coat". MCrAlY coatings are normally manufactured using thermal spray technologies such as Vacuum Plasma Spray, Air Plasma Spray, High Velocity Oxygen Fuel (HVOF) depending on the specified porosity and oxides content. Zirconia coatings are almost always produced by Air Plasma Spray [Pawlowski, 1995].

In the aerospace and power generation sectors technologies of coating removal are very important. These technologies, called also "decoating" and "stripping", are used to recycle unsuccessfully coated parts and more often for reconditioning usured parts after their functional service. Stripping is used to remove damaged "in service" coatings, then, if necessary, the component can be repaired and finally re-coated with new fresh coatings.

The main characteristic of the stripping procedure is the guarantee of the complete removal of the coating without damaging the substrate. Stripping must not cause corrosion or roughening of the substrate surface and it must ensure a minimum dimensional change of its geometrical characteristics. Stripping of ceramic and MCrAlY layers remains a delicate problem in industrial production, for which the "perfect" solution has not been found yet. The aim of the present work is to discuss and compare three different stripping techniques: chemical stripping salt bath stripping and water jet stripping, to remove both MCrAlY and YPSZ.

Experimental

Stripping technologies

The stripping methodology presented is based on the combination of different techniques, usually in two subsequent steps: YPSZ removal and MCrAlY removal. The stripping of YPSZ presents two principal problems:

References:

1. Fontana M.G. Corrosion Engineering 3rd Edition , McGraw - Hill, ISBN 0-07-021463-8, 1986, 556 pp.

2. Foster T. Oestreich J., Paint removal using wheat starch blast media, Defence Research Establishment Pacific FMO Victoria, BC, Canada, 1993, AGARD Report 791

3. Jones D.A., Principles and Prevention of Corrosion, Prentice Hall, ISBN 0-13-359993-0, 1996, p334 -346,

4. Koutlakis G...LeBlanc P. Monette D., New Developments in starch based abrasive media an overview of research and development activities at Archer Daniels Midland, ADM Ogilvie, 1998 DoD/ Industry Aerospace coating conference, Batelle

5. Lott R., and Pauli.R., Dry Stripping with wheat starch, Beech Aircraft, 1992. DoD/industry Advanced Coating removal conference, Batelle.

6. Meguid S.A., Effect of partial-coverage upon the fatigue fracture behavior of peened components, Fatigue Fracture Engineering Material Structures, Vol 14 No 15, Fatigue of Engineering materials Ltd. 8756-758X, 1991, pp 515-530

7. Miller R.E Final Report for the Wheat Starch Media Blast Removal of room temperature Vulcanized RTU Silicone rubber adhesive from the Space Shuttle Orbiter Surfaces, Northrop Grumman, 1998.

8 Monette D, Envirostrip Plus Wheat Starch Dry Stripping Media, Archer Daniel Midland, DoD/Industry Aerospace Coatings Conference, 1999

9. Monette D. and Oestreich J., New Developments in Starch media applications and coating removal effects on various aerospace materials. CAE Electronics, 1996, DoD /Industry Aerospace Coatings Conference., Batelle

10 Monette D., The Environmental advantages of selective stripping, CAE Electronics, 1995, Aerospace Hazardous Materials Management Conference, GE Aircraft engines.

11. NASA (National Aeronautics and Space Administration) Joint EPA/NASA/USAF Interagency Depainting Study, Final Report, George C. Marshall Space Flight Center, Dec 1999

12. Pauli R., Alternative Processes to Methylene Chloride Chemical strippers, A Review of Progress to date, Pauli &Griffin Company, 1995 Aerospace/Airline plating and Metal Finishing Forum & Exposition, American Electroplaters and Surface Finishers Society.

13. Tracy D., and Nakahara S., Depaint Activities at Northrop's B-2 Division, Northrop Aircraft, 1994 DoD/ Industry Advanced Coating Removal Conference, Batelle

14. WHO (World Health Organization), 1984 Methylene Chloride Environmental Health Criteria 32. Published under the joint sponsorship of the United Nations Environment Programme, the International Labour Organization, and the World Health Organization, Geneva. 55 pp

15. Wulpi D.J., Understanding How Components Fail, American Society for Metals, ISBN 0-87170-189-9, 1985, PP262.

REMOVAL OF ZIRCONIA THERMAL BARRIER COATINGS AND MCrAlY BOND COATINGS FROM TURBINE BLADES: A COMPARISON OF METHODS BASED ON CHEMICAL STRIPPING, WATER JET AND SALT BATH.

A.Scrivani[1,2], U. Bardi[1], G. Ballerini[1], D. Bonacchi[1], M. Fantini[3], R. Groppetti[2], S. Ianelli[2], G. Rizzi[4]

1. Università di Firenze, Dipartimento di Chimica, Via Cavour 82, Firenze, Italy
2. Università di Parma, Dipartimento di Ingegeneria Industriale, Viale delle Scienze, Parma, Italy
3. Galvanica Parmense, Via Romagnoli 3, S.Polo di Torrile, Parma, Italy
4. Turbocoating S.p.A., Via Volta 3, Rubbiano, Parma, Italy

Abstract

In the aerospace field as well as in field of stationary gas turbines, thermal spray coatings are gaining considerable importance for the improvement the properties of Nickel-super-alloys materials surface. Thermal spray coatings are commonly used as antioxidation materials (mainly MCrAlY alloys) and as thermal barrier coatings (mainly Yttria partially stabilised Zirconia) and are applied on Nickel super-alloys (as for instance different kinds of Inconel). Coating removal is an important aspect in the production of these devices. Removal (or "decoating" or "stripping") is needed for the production of new components as well as for the reconditioning of "in service" components. The present paper is dedicated to the a comparison of different stripping methods and to the characterisation of the blades surface after removal of thermal spray coatings both of Zirconia and of MCrAlY.

The results reported here show that chemical stripping is particularly suitable for MCrAlY coating removal and does not affect the substrate. Water jet stripping can successfully be used for Zirconia-MCrAlY system removal although care is needed to avoid substrate damage. Salt bath technologies have been found to be effective for TBC removal but not for MCrAlY removal.

Introduction

Coating technologies are rapidly becoming a fundamental method in improving materials properties. In particular, thermal spray technologies are an effective and versatile method used to obtain coatings of different thickness with a good cost-quality ratio in the aerospace field as well as the in power generation sector (stationary gas turbines). In these areas, the surface proprieties of Nickel-super-alloy materials can be improved by means of antioxidation materials, such as MCrAlY (where M means Ni, Co or a combination of both), and thermal barrier coating materials, such as Yttria partially stabilized Zirconia (YPSZ). MCrAlY coating are used to improve the resistance of the component to aggressive media at high temperature (900-1000°C) while low thermal conductivity of Zirconia coatings decrease the in-service temperature of the component [Rickerby, 1991]. The system MCrAlY + Zirconia is normally called Thermal Barrier Coating (TBC), where the MCrAlY layer acts as a bonding layer between the Zirconia coating and the substrate and is normally termed "bond coat". MCrAlY coatings are normally manufactured using thermal spray technologies such as Vacuum Plasma Spray, Air Plasma Spray, High Velocity Oxygen Fuel (HVOF) depending on the specified porosity and oxides content. Zirconia coatings are almost always produced by Air Plasma Spray [Pawlowski, 1995].

In the aerospace and power generation sectors technologies of coating removal are very important. These technologies, called also "decoating" and "stripping", are used to recycle unsuccessfully coated parts and more often for reconditioning usured parts after their functional service. Stripping is used to remove damaged "in service" coatings, then, if necessary, the component can be repaired and finally re-coated with new fresh coatings.

The main characteristic of the stripping procedure is the guarantee of the complete removal of the coating without damaging the substrate. Stripping must not cause corrosion or roughening of the substrate surface and it must ensure a minimum dimensional change of its geometrical characteristics. Stripping of ceramic and MCrAlY layers remains a delicate problem in industrial production, for which the "perfect" solution has not been found yet. The aim of the present work is to discuss and compare three different stripping techniques: chemical stripping salt bath stripping and water jet stripping, to remove both MCrAlY and YPSZ.

Experimental

Stripping technologies

The stripping methodology presented is based on the combination of different techniques, usually in two subsequent steps: YPSZ removal and MCrAlY removal. The stripping of YPSZ presents two principal problems:

the YPSZ layer usually does not cover uniformly the surface of the sample, for example only some parts of gas turbine blades are covered; the layer is usured and its thickness is not the same over the covered sample.
The stripping technologies analysed in this paper are the following:

- chemical stripping performed by immersion in hydrochloric acid in various conditions of temperature and acidic concentration (proprietary method by Turbocoating SpA / Galvanica Parmense)
- molten salt stripping (Kastech Electrolytic methods by Kolene Corp.)
- standard high pressure water/abrasive jet stripping (proprietary methods by CREAS srl)

Substrates

The samples used here are parts of gas turbine components that have been coated by thermal spray. Different kinds of base materials have been used: Ni based super alloy in form of traditional casting and single crystal; all these materials contains also elements as Co, W and Mo. The coatings were manufactured as follows:

- NiCrAlY alloy coatings of thickness in the range of 300-400 μm were deposited by Vacuum Plasma Spray and diffused at temperature of about 1100°C in order to obtain a metallurgical bonding between the coating and the substrate due to the migration of atoms at the interface
- 8% Yttria Partially stabilized Zirconia deposited by Air Plasma Spray after diffusion heat treatment. The Zirconia coating thickness was 500-700 μm.

Figure 1 shows an optical macrograph of the typical microstructure of the considered coating.

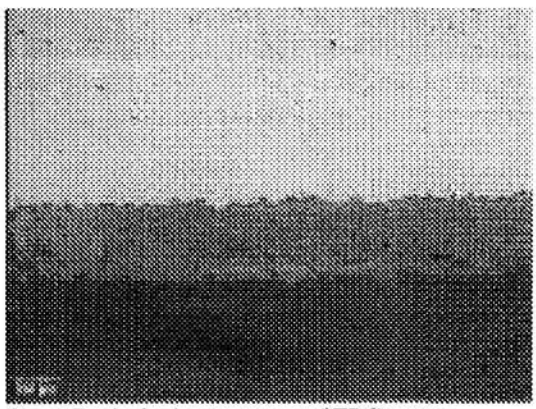

Fig. 1 Typical microstructure of TBC system

Analysis methodologies

Two types of analysis have been performed in order to investigate the roughness and the composition of the superficial layer of the stripped materials. The surface composition has been investigated with X-ray Photoelectron Spectroscopy (XPS). The measurements have been carried out using a standard UHV XPS spectrometer, conventional Al Kα and Mg Kα sources and a hemispherical analyser equipped with a single channel electron multiplier. All the XPS spectra reported in the article are normalized to the value of the most intense transition, in this case the $2p_{3/2}$ transition of Ni.

Roughness measurements have been performed by means of a Three-Dimensional Digital Stylus Profilometer (3DSP), and an off-line analysis module, that receives digitised surface data from the acquisition module and applies a series of data processing techniques to provide information and evaluate parameters to characterise surface properties. The 3D parameters obtainable by this method are based on three-dimensional extensions of 2D parameters defined in the ISO 4287 and DIN 4776 standards [Bracali, 1999]. The considered amplitude parameters have the following symbols and meaning:

S_a : Arithmetic mean deviation
S_q : Root mean square deviation
S_z : Ten point height

For metallographic investigation a metallographic microscopy (Zeiss Axiovert 100A) with an image analyser based on grey contrast has been used.

Results and discussion

Effects of stripping methods

Complete coated turbine blades have been treated by the different stripping procedures considered here. After stripping, samples for analysis have been cut from the component and prepared for examination of both the surface and the cross section. For the cross section analysis the samples have been infiltrated and mounted with epoxidic resin and polished. In addition, the root of the blade produced with the single crystal Ni-Alloy material has been submitted to a cycle of 7 hour immersion in hydrochloric acid without any protection. For each hour, roughness has been determined by means of a 3-dimensional stylus micro-topography surface analysis system and metallographic analysis have been carried out.

The sample labelled as "SB" has been stripped with molten salt to remove only the YPSZ coating; the sample labelled as "WJ" has been stripped with water jet, to remove both YPSZ and MCrAlY; the sample labelled as "HA" has been stripped with sand blasting and then with hydrochloric acid, to remove both YPSZ and MCrAlY.

Since chemical stripping has been found to be unable to remove the ceramic top coat, tests with this method have been performed after removal of the Zirconia layer by sand blasting.. In any case, the blasting operation before stripping should always performed in order to activate and clean the surface from possible pollution (grease, oil, etc.) that could stop the attack. Furthermore the acid attack is performed in order to have a "self-limiting" reaction by the use of a suitable inhibitor that reacts with the elements of the NiCrAlY coating forming a passive black layer that tend to stop the reaction and that should be removed by blasting to allow the progressing of stripping. We found that by using this procedure it is possible to avoid the attack to the substrate material.

Kolene Kastech Electrolytic solution has been trailed on the blades sections coated both with NiCrAlY and YPSZ coating. Upon removal from the molten salt, the components have been immediately ambient water quenched and rinsed to complete the cleaning cycle.

Literature shows the capability of the water jet technology in cutting, drilling or machining, while stripping with pure high-pressure water jet seems to be competitive and able to solve some environmental problem that are related to acid use [Mabrouki]. Water jet stripping was found to remove both the NiCrAlY layer and the Zirconia.

Uncoated surface analysis.

In order to understand the effects of acid attack on the substrate surface, a test has been carried out by immersing these uncoated surfaces in the acid solution for different numbers of hours. Single crystal material has been chosen for the test. These surfaces have been analysed by metallurgical microscopy to determine the presence of structural defects or cracks and by 3D Stylus Profilometer to in order to determine the roughness (this parameter is very important for the coupling with the turbine rotor). The following table shows that no substantial increase in roughness takes place for extended exposures.

Parameter/Sample	2h immersion	4h immersion	5h immersion	7h immersion
S_a [μm]	1.13	1.12	1.03	1.22
S_q [μm]	1.34	1.32	1.32	1.52
S_z [μm]	13.72	16.35	12.10	15.27

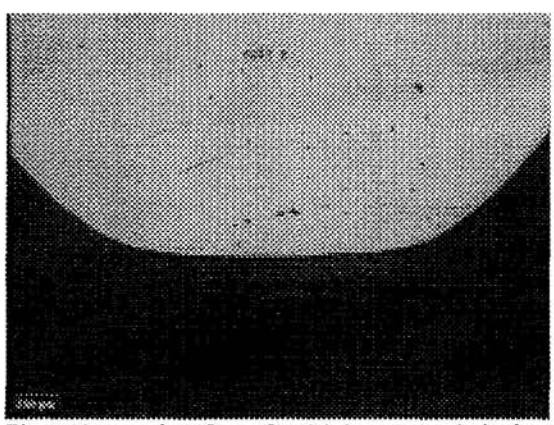

Fig. 2 Uncoated surface after 2 h immersion in hydrochloric acid - optical image

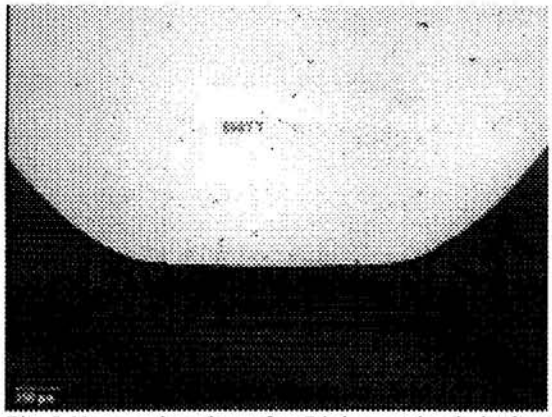

Fig. 3 Uncoated surface after 7 h immersion in hydrochloric acid –optical image

The micrographies (Fig. 2 and 3) show that no structural damage exists has been noted. We conclude that acid stripping has no substantial effect on the structure of the substrate.

XPS analysis

XPS provides a direct analysis of the surface composition with a depth resolution of a few nanometers and permits therefore to verify the coating removal without special treatments of the samples. Since Co is not present in the coating but only in the substrate, its detection by XPS can be considered as the demonstration of the complete decoating having been achieved. The main results of the XPS analysis are reported in figures 4 and 5. Figure 4 shows the spectra of the three samples for the different stripping procedures. For the SB (salt bath) sample the superficial layer of this sample presents no traces of YPSZ coating. We observe only nickel, in part present as oxide, in the outermost surface, indicating that the electrochemical treatment has leached out all the other metallic elements in the bond coating for a depth of several nanometers.

The second spectrum is related to the sample HA (acid bath) and the third spectrum is related to the water jet treated sample (WJ). In both cases, XPS shows the presence of Nickel, Chromium and Cobalt. As mentioned earlier on, the presence of cobalt indicates that both methods have completely removed the coating.

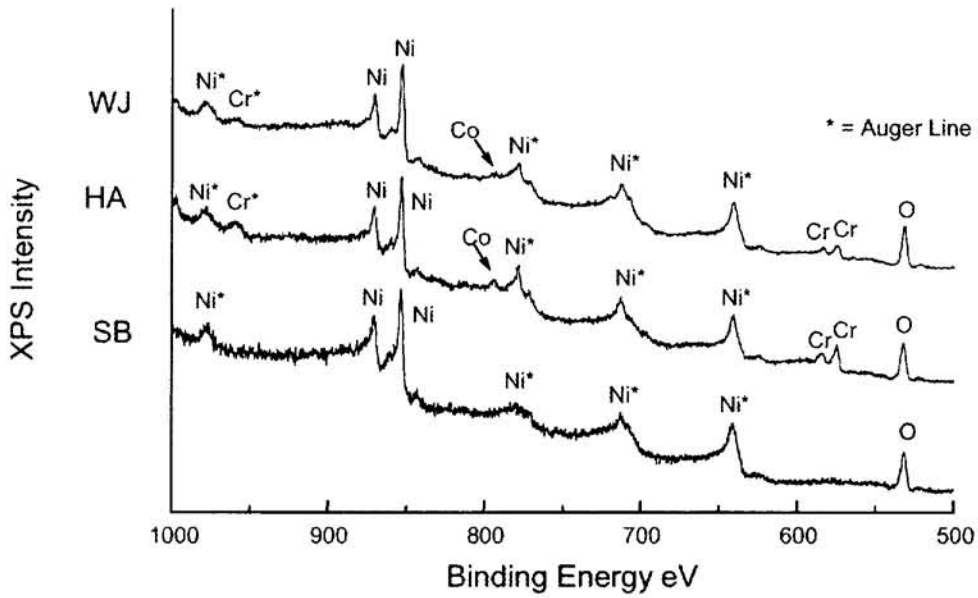

Figure 4: XPS normalized spectra of the tree stripped samples made with Al Kα transition. The spectra are normalized to the most intense line.

The Auger lines of Nickel hide partially the photoelectron lines of Cobalt. To be sure of the presence of Cobalt in the samples a XPS spectrum made with the Kα of Mg has been made, and is shown in figure 5, where the $2p_{1/2}$ and the $2p_{3/2}$ lines of Cobalt are well shown.

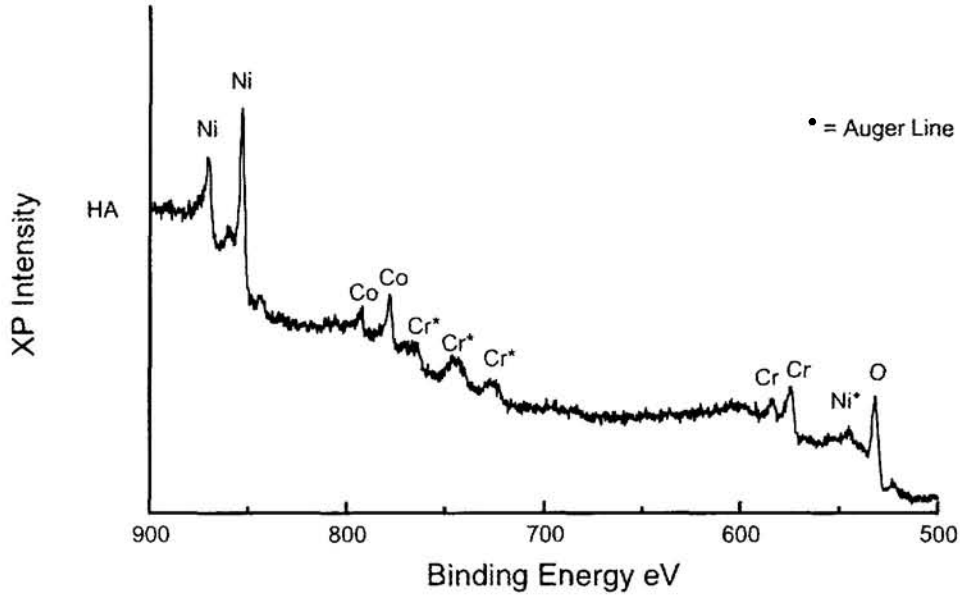

Figure 5: XPS normalized spectra of the HA stripped sample made with Mg Kα transition. The spectrum is normalized to the most intense line.

Metallographic inspection

Figure 6 shows the sample after treatment by hydrochloric acid. Confirming the XPS results, no coating is present on the surface. The same consideration holds the water jet stripped sample shown in figure 7. Figure 8 shows the sample treated by molten salt. Here it is possible to observe how the Zirconia coating has been completely removed while there remains the layer of NiCrAlY coating. On its surface it is possible to note a layer probably of oxides. Again, this result confirms the XPS data.

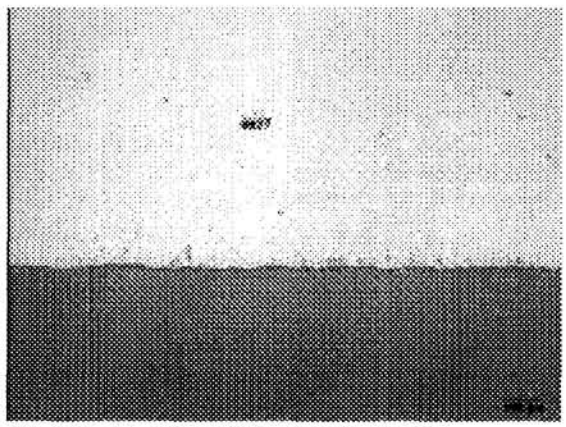

Fig. 6 Sample stripped by hydrochloric acid

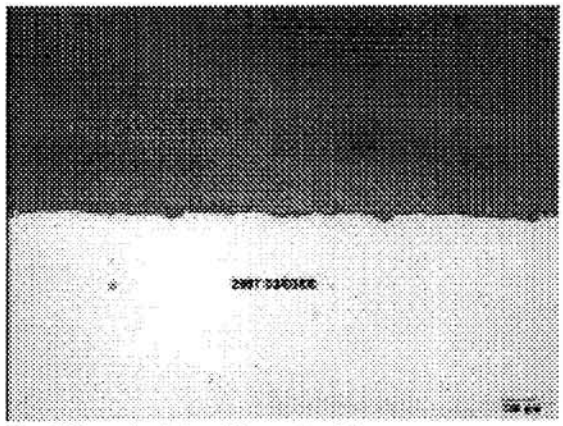

Fig. 7 Sample stripped by water jet

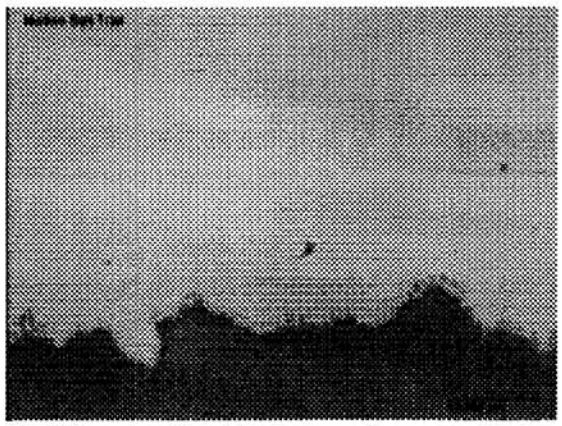

Fig. 8 Sample stripped by molten salt

Conclusion

The results show that chemical stripping is particularly suitable for MCrAlY coating removal and does not affect the substrate material. Water jet stripping can successfully be used for Zirconia-MCrAlY system removal and it seems to be the only one able to remove both the Zirconia and MCrAlY layers; although care is needed to avoid substrate damage. Molten salt methods turned out to be suitable for the removal of the Zirconia coating, but the stripping of the bond coat remains difficult and further studies will be necessary to determine the possibility of removing it.

Acknowledgements

The authors are grateful to Mr. Gordon Palmer of Kolene Corp. (Detroit, Michigan, USA) and Mr. Renato Cottica of CREAS srl (Turin, Italy) for their contribute to the development of the stripping procedures.

References

Bracali P., Groppetti R., Scrivani A.; On a micro-topographic three- dimensional acquisition and analysis system for engineering surface characterisation, Proc. AITEM99, Brescia, Italy, 1999

Mabrouki T., Raissi T., Cornier A.: Numerical simulation and experimental study of the interaction between a pure high velocity and targets: contribution to investigate the decoating process, Wear 239 (2) (2000) pp. 260-273

Pawlowski, L.; The science and engineering of thermal spray coatings, Wiley & Sons, Chichester, 1995

Rickerby D.S.; Matthews A., Advanced surface coatings: a handbook of surface engineering, Blackie & Son Ltd. London, 1991

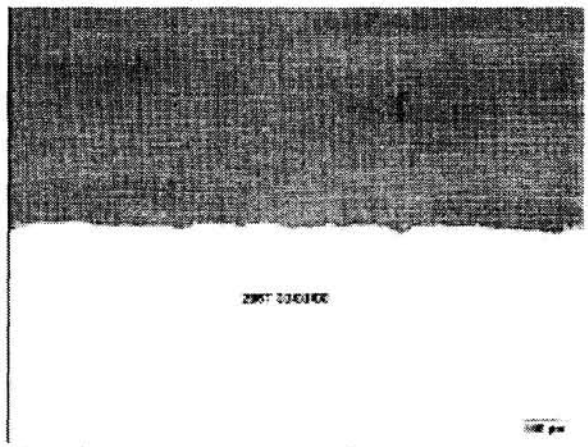

Fig. 7 Sample stripped by water jet

Fig. 8 Sample stripped by molten salt

Conclusion

The results show that chemical stripping is particularly suitable for MCrAlY coating removal and does not affect the substrate material. Water jet stripping can successfully be used for Zirconia-MCrAlY system removal and it seems to be the only one able to remove both the Zirconia and MCrAlY layers: although care is needed to avoid substrate damage. Molten salt methods turned out to be suitable for the removal of the Zirconia coating, but the stripping of the bond coat remains difficult and further studies will be necessary to determine the possibility of removing it.

Acknowledgements

The authors are grateful to Mr. Gordon Palmer of Kolene Corp. (Detroit, Michigan, USA) and Mr. Renato Cottica of CREAS srl (Turin, Italy) for their contribute to the development of the stripping procedures.

References

Bracali P., Groppetti R., Scrivani A.; On a micro-topographic three- dimensional acquisition and analysis system for engineering surface characterisation, Proc. AITEM99, Brescia, Italy, 1999

Mabrouki T., Raissi T., Cornier A.; Numerical simulation and experimental study of the interaction between a pure high velocity and targets: contribution to investigate the decoating process, Wear 239 (2) (2000) pp. 260-273

Pawlowski, L.; The science and engineering of thermal spray coatings, Wiley & Sons, Chichester, 1995

Rickerby D.S.; Matthews A., Advanced surface coatings: a handbook of surface engineering, Blackie & Son Ltd. London, 1991

Joint EPA/NASA/USAF Interagency Depainting Study

Marceia Clark-Ingram
National Aeronautics and Space Administration
NASA Operational Environment Team
ED36/MSFC
George C. Marshall Space Flight Center, AL , 35812
256-544-6229
marceia.a.clark.ingram@msfc.nasa.gov

INTRODUCTION

Environmental regulations such as National Emission Standards for Hazardous Air Pollutants (NESHAPs) are drivers for the implementation of environmentally compliant methodologies in the manufacture of aerospace hardware. In 1995, the Environmental Protection Agency (EPA) promulgated the NESHAP for the Aerospace Manufacture and Rework (Aerospace NESHAP) industry. Affected facilities were to be in compliance by September 1998. Several aerospace manufacturing operations are regulated within the Aerospace NESHAP including Depainting operations.

The National Aeronautics and Space Administration (NASA), EPA, and United States Air Force (USAF) combined resources to evaluate the performance of nine (9) alternative depainting processes. The seven alternative depainting processes were: Chemical stripping (non- methylene chloride), Carbon Dioxide Blasting, Xenon Flashlamp, Carbon Dioxide Laser Stripping, Plastic Media Blasting, Sodium Bicarbonate Wet Stripping, Waterjet Blasting and Wheat Starch Blasting. An epoxy primer and polyurethane top coat system was applied to 2024-T3 clad and non-clad aluminum test specimens.

Approximately 200 test specimens were evaluated in this study. Each coupon was subjected to three (3), four (4), or five (5) complete depainting cycles. This paper discusses the conclusions from the study including the test protocol, test parameters, and achievable strip rates for the alternative depainting processes. Test data includes immersion corrosion testing, sandwich corrosion testing and hydrogen embrittlement testing for the non-methylene chloride chemical strippers. Additionally, the cumulative effect of the alternative depainting processes on the metallurgical integrity of the test substrate is addressed with the results from tensile and fatigue evaluations.

REGULATORY BACKGROUND

Methylene Chloride was traditionally utilized for chemical stripping of coating systems. Methylene Chloride is listed as a Hazardous Air Pollutant (HAP) by the EPA. This chemical is also a suspected carcinogen.

The National Emission Standards for Hazardous Air Pollutants for Aerospace Manufacturing and Rework Facilities (Aerospace NESHAP) regulates depainting operations. The Aerospace NESHAP limits the amount of methylene chloride for coating removal operation in affected facilities. The limit is 26 gallon/craft/year for commercial operations and 50 gallons/craft/year for military operations.

The initial Aerospace NESHAP was promulgated in September 1995 however subsequent versions exist. The first substantive compliance date for existing sources is September 1998. The Occupational Safety and Health Administration (OSHA) established stringent Permissible Exposure Limits (PEL) that were effective in April 1997.

OBJECTIVE OF STUDY

The overall objective of the study was to evaluate nine (9) alternative depainting methodologies per ISO/SAE MA4872, Revision # 5 "Paint Stripping of Aircraft – Evaluation of Materials and Processes". Additionally, three (3) to five (5) cycles of panel preparation and depainting were performed for each alternative depainting methodology to determine cumulative metallurgical effects of the alternative processes on the substrate. The nine (9) alternative depainting processes are:

1 Chemical Stripping (non-methylene chloride)
2 Carbon Dioxide Blasting (Coldjet™)
3 Carbon Dioxide Blasting (TOMCO$_2$)

4 Xenon Lamp/Carbon Dioxide Blasting (Flashjet™)
5 Laser Stripping
6 Plastic Media Blasting
7 Sodium Bicarbonate Wet Stripping
8 Water Stripping
9 Wheat Starch Blasting

SCOPE OF STUDY

The specimens for evaluation were fabricated from 2024 -T3 clad and non-clad aluminum. The specimen thicknesses were 16, 32, 51, and 64 mil. The paint system utilized for the first depainting cycle contained a MIL-P-23377F , Type 1, Class 2 primer and a MIL –C-83286B urethane topcoat. The primer remained the same for all subsequent depainting cycles. The vendor discontinued the availability of the MIL-C-83286B urethane topcoat after the first depainting cycle due to the high Volatile Organic Content (VOC) of the material. The MIL-C-85285B topcoat was implemented for subsequent depainting cycles. This material contained a high solids, low VOC formulation.

SPECIMEN PROCESSING & DEPAINTING

The depainting specimens were processed per the following 9 steps:

1. Coating Application of Paint System
2. Coating thickness measurements
3. Environmental Aging
4. Depainting (Coating Removal)
5. Measurements: substrate thickness, surface roughness
6. Specimen Cleaning: Water Break Free Surface
7. Chromate Conversion (Iridite 14-2)
8. Measurements: substrate thickness and weight, surface roughness
9. Repeat for next cycle of specimen processing

SPECIMEN CLEANING

The cleaning of the test specimens (per Step 6 above) encompassed the following:

- Methyl Ethyl Ketone (MEK) handwipe
- Perchloroethylene Vapor Degreasing for 10 minutes
- Immersion in Turco 4215 for 25 minutes
- Hot Water Deionized Rinse for 5 minutes
- Immersion in Turco Smut-Go #1 for 11 minutes
- Cold Water Deionized Rinse for 5 minutes
- Water Break Free Test with Deionized Water.

ENVIRONMENTAL AGING OF SPECIMENS

The specimens were aged according to ISO/SAE MA4872. The specimen aging in cycle one required approximately 90 days. The installation of liquid nitrogen lines accelerated the aging cycle. The environmental aging consumed 35 – 50 days for the remaining cycles. The specimens were thermally cycled for 800 times. The environmental aging cycle is described below.

- Precondition : 12 hours @ 120 °F and 95% RH
- Hold at –65 °F for 1 hour
- Thermally cycle from –65 °F to 160 °F for 400x
- Return chamber to ambient temperature.
- Repeat steps 1 – 3.

MATERIAL EVALUATION TESTING

Material evaluation testing was performed on the test specimens. Sandwich corrosion testing, immersion corrosion testing and hydrogen embrittlement testing was performed on the non-methylene chloride chemical strippers. Baseline surface roughness measurements, post-cleaning surface roughness measurements, and post-stripping surface roughness measurements were taken for each test specimens. Crack Detectability measurements

were performed on all Plastic Media Blast test specimens and on non-clad test specimens for Sodium Bicarbonate Wet Stripping, High-Pressure Water Blasting, and Wheat Starch Blasting.. Tensile testing was performed on non-clad specimens that were depainted with the Xenon Flashlamp/CO_2 process, and clad/non-clad specimens depainted with the Plastic Media Blast process. Fatigue testing was performed on non-clad specimens that were depainted with the following processes: Xenon Flashlamp CO_2, Plastic Media Blasting, High Pressure Water Blasting, and Wheat Starch Blasting.

DEPAINTING STRIP RATES & OPERATING PARAMETERS

This section of the technical paper discusses the strip rates that were achieved during the evaluation of the alternative depainting methodologies.

1. Chemical Stripping

A total of five (5) depainting cycles were completed with non-methylene chloride chemical strippers. The non-methylene chloride strippers contained acid and alkaline/neutral formulations. The specimen dimensions were 12" x12" with a 64 mil thickness. Initially, low strip rates were obtained in the 1st depainting cycle prior to process optimization. Fortunately, a site visit to Raytheon in Selma, Alabama provided guidance on chemical stripping optimization.

The following operating conditions were recommended by Raytheon and implemented during the four (4) remaining depainting cycles for evaluation of the non-methylene chloride containing chemical strippers:

- Maintain environment at an RH of 34% and a temperature between 80 and 86 °F.
- Apply fine mist of stripper over panel.
- Apply heavier mist 30 minutes later.
- Check at 2 hour intervals.
- When coating is released, brush panel and reapply stripper as before.

Initially, 40 candidate strippers were evaluated for stripping efficiency. A down-selection process yielded the eight (8) chemical strippers listed in Table 1.

Table 1. Non-Methylene Chloride Chemical Strippers

Alkaline/ Neutral Chemical Strippers	*Acid Strippers*
Gage 874B	Cee-Bee-E-1004B
Turco 6813	EZE 540
Turco 6813-E	PR-2002
Turco 6840-S	Turco 6770

The aforementioned chemical strippers were highly effective and removed 100% of the topcoat and 100% of the primer from the specimens. The average "time to strip" for all eight (8) non-methylene chemical strippers is provided in Table 2. Additionally, two (2) methylene chloride containing strippers were used as controls during the evaluation.

Table 2. Strip Times for Non-Methylene Chloride Chemical Strippers and Control Chemical Strippers

Chemical Strippers	*Average Dwell Time*
Methylene Chloride Baseline for Alkaline Neutral : Cee Bee R-256	5.0 minutes
Alkaline Neutral Candidates	3.5 hours
Methylene Chloride Baseline Acid : Cee Bee A-202	5.0 minutes
Acid Candidates	3.1 hours

2. Carbon Dioxide Blasting

Two Carbon Dioxide (CO_2) Blast systems were evaluated during this study. The two systems were the COLDJET™ Model 62-250 and the TOMCO$_2$ DI-250. The COLDJET™ system caused significant deformation on 16 mil specimens. Surface damage was evident on some of the 64 mil specimens. The TOMCO$_2$ system was capable of some coating removal but the allowable pressure was ineffective for efficient stripping. The CO_2 Blast systems were removed from the study after completion of the 1st depainting cycle. The CO_2 Blast systems were effective for cleaning of specimens versus coating removal. The operating parameters for the COLDJET™ and the TOMCO$_2$ systems are provided below.

COLDJET ™

- Area Stripped : 12 in^2 - 45.5 in^2
- Angle of Attack : 75°
- Stand-Off Distance: 5 in - 6in (16 mil non-clad) & 1" to 3" (64 mil non-clad)
- Media Flow Rate: 350 lb/hr
- Nozzle: 5 in diameter
- Pressure : 120 -300 psi
- Stripping Passes : 4 maximum
- Effectiveness: 100% topcoat, 80% primer

TOMCO$_2$ System

- Area Stripped : 144 in^2 maximum
- Angle of Attack: 10 °
- Stand-Off Distance: 1in
- Media Feed Rate : 200 - 400 lb
- Nozzle : 1.5 -in diameter (fan nozzle)
- Pressure: 150 psi
- Stripping Passes: 1 to 2
- Effectiveness: 45% topcoat & 10% primer (144 in^2), 100% topcoat & 98% primer (36 in^2)

3. Xenon Flashlamp/ Carbon Dioxide (Flashjet)

A total of three (3) depainting cycles were completed for the Xenon/ Flashlamp CO_2 coating removal system. The Boeing Company in St. Louis, MO, donated generous time and effort during the evaluation of this depainting system.

The Flashjet system utilizes pulsed light and a CO_2 particle stream to remove the coating from the substrate. Boeing chose to remove 100% of the topcoat and 57-74% of the primer. Many of the Boeing customers allow a portion of the primer to remain on the craft after depainting. Typically, six (6) to twenty-two (22) passes were needed to achieve the desired coating removal.

The study team regarded data from the 3rd depainting cycle as representative of the capabilities of the Flashjet system. This data is provided in Table 3.

Table 3. Strip Rates for Flashjet System

Substrate Dimensions (in.)	Substrate Thickness (in.)	Strip Rate (in.^{2}/min)
22 x22	0.016	70.0
22 x 22	0.051	132.0
22 x 22	0.064	100.8
12 x 12	0.064	91.9

The following operating parameters were utilized to achieve the aforementioned strip rates:

Operating Parameters:

- Stand-off Distance: 2 to 3 inches
- Angle of Attack : 21 to 29°
- Media Flow Rate: 500 to 1000 lb/hr
- Input Pressure to nozzle : 90 to 180 psi CO_2
- Input Voltage : 1900 to 2300 Volts
- Repetition Rate: 3 to 5 flashes/sec
- Translational Velocity: 0.75 to 1.4 in/sec

4. Carbon Dioxide Laser Stripping

A total of three (3) depainting cycles were completed for the evaluation of the CO_2 Laser Stripping process. The first depainting cycle was performed by International Technical Associates of Santa Clara, California. A 50 watt demonstration unit was utilized to remove the coating from the specimens. The second depainting cycle was performed by Silicon Alps of Santa Clara, California. A 2kW production unit was utilized. CO_2 lasers were used for coating removal during the first and second depainting cycles. General Lasertronics Corporation of Milpitas, California, performed the 3rd depainting cycle. A Neodium –doped Yttrium Aluminum Garner laser was utilized during the 3rd depainting cycle. Processing anomalies at MSFC skewed the strip rates for the 3rd depainting cycle.

The strip rates for Laser Stripping are provided in Table 4. The stripping effectiveness is 100% removal for topcoat and 99% removal for primer. An area of 60 in^2 was stripped during the first depainting cycle and an area of 30in^2 was stripped during the second depainting cycle.

Table 4. Strip Rates for CO_2 Laser Stripping

Substrate Dimensions (in.)	Sequence	Time to Strip	Strip Rate (in^2/min)
12 x 13	1	10 min	6.0
12 x 13	2	38 sec	47.4

The following operating parameters were utilized:

- Scan Rate : 15 Hz
- Pulse Width : 6 microseconds
- Laser Power: 50 W (Sequence 1), 2kW (Sequence 2)
- Maximum Energy: 5 Joules/pulse
- Stripping Fluence: 4.5 Joules/cm
- Footprint Size: 5.5mm x 5.5mm
- Stand-off Distance : 12 inches

5. Plastic Media Blast (PMB)

A total of four (4) depainting cycles were conducted at MSFC for the evaluation of the Plastic Media Blast (PMB) process. A manual PMB system was used in the study. Strip rates from this system were not comparable to strip rates achieved by industry. Substrate thickness was 16, 32, 51 and 64 mils. Clad and non-clad specimens were evaluated. Specimen dimensions were 12" x 12" and 22" x 22". The strip rates provided in Table 5 are an average of all four depainting cycles. One stripping pass removed 100% of the primer and 80% of the topcoat.

Table 5. – Strip Rates for Plastic Media Blast Process

Substrate Thickness (inches)	Clad/ Non-Clad	Average Strip Rate (in^2/min)
0.016	Non-clad	22.4
0.016	clad	25.0
0.032	clad	26.7
0.051	Non-clad	26.4
0.064	Non-clad	22.0

The following operating parameters were implemented to achieve the strip rates provided above:

- Nozzle Diameters: 0.5 inches @ throat, 1.0 inch @ exit
- Stand-off Distance: 9 inches to 12 inches
- Angle of Attack : 30°, 30° – 45° (64mil)
- Mesh size: 20/20 (80%), 16/20 (20%)
- Media Flow Rate: 250 – 500 lb/hour
- Pressure: 30 psi – 40 psi

6. Sodium Bicarbonate Wet Stripping

A total of three (3) depainting cycles were conducted using manual and automated Sodium Bicarbonate Wet Stripping systems at the MSFC. The first cycle was performed manually and the remaining two cycles were performed with an automated system. Aquamiser and Carolina Equipment Company were the two manufacturers of the Bicarbonate of Soda System (BOSS) equipment. The substrate thickness of the clad test specimens was 16 mil and 32 mil. The substrate thicknesses of the non-clad test specimens were 51 mil and 64 mil. The specimen dimensions were 22" x 22".

The 16 mil specimens were removed from the study after the first depainting cycle. The Sikorsky Company generously donated 10 clad specimens for the 3rd depainting cycle. The data in Table 6 represents the strip rates that were obtained with the BOSS equipment. The coating removal efficiency for the 2nd and 3rd depainting cycles was 100% of the topcoat and 90% of the primer.

Table 6. BOSS Strip Rates

Substrate Thickness (inches)	Clad/ Non-Clad	Average Strip Rate (in^2/min)	Average Strip Rate (in^2/min)	Average Strip Rate (in^2/min)
		Sequence 1	Sequence 2	Sequence 3
0.016	Non-Clad	120.8	N/A	N/A
0.016	Clad	69.8	N/A	N/A
0.032	Clad	118.8	N/A	N/A
0.051	Non-Clad	96.41	170.0	162.0
0.064	Non-Clad	N/A	166.9	135.0

The following operating parameters were implemented to achieve the strip rates in Table 6. :

- Nozzle : 7° fan nozzle
- Stand-off Distance : 2 inches
- Angle of Attack: 90 °
- Media Feed Rate: 2 to 3 lb/min
- Media Flow Rate: 3.2 gallons/minute
- Pressure : 14,000 psi
- Translational Velocity: 9 to 29 in/sec

7. High Pressure Water Blast Stripping

A total of three (3) depainting cycles were conducted at MSFC utilizing the High Pressure Water Blast technology. The clad specimens were donated by Sikorsky and were 16 and 32 mils in thickness. The substrate thickness of the non-clad specimens was 16, 51 and 64 mils. The dimensions of the clad specimens were 22" x 22" and the dimensions of the non-clad specimens were 12" x 12", 12' x 13", and 22" x 22". Three depainting cycles were conducted on the non-clad specimens while one depainting cycle was conducted on the clad specimens.

The stripping effectiveness of the High Pressure Water Blast technology removed 100% of the topcoat and 100% of the primer. The aforementioned stripping efficacy was achieved with one to three stripping passes. The strip rates are provided in Table 7.

Table 7. Strip Rates for High Pressure Water Blast Stripping

Specimen Thickness (in)	Clad/ Non-Clad	Average Strip Rate (in^2/min)	Average Strip Rate (in^2/min)	Average Strip Rate (in^2/min)
		Sequence 1	Sequence 2	Sequence 3
0.016	Non-clad	85.0	173.1	
0.016	Clad	174.3	See note	See note
0.032	Clad	617.2	See note	See note
0.051	Non-clad	223.9	593.4	880.2
0.064	Non-clad	285.1	494.5	713.1

Note: Sequence 1 for clad panels occurred concurrently with sequence 3 for non-clad panels.

The operating parameters for the High Pressure Water Blast Stripping technology is as follows:

- Nozzle : Hammelmann Rotary Nozzle
- Rotational Velocity: 900 rpm
- Stand-off Distance: 2 inches
- Angle of Attack: 90^0
- Water Flow Rate: 7-11.5 gal/min
- Pressure: 20,000 – 30,000 psi
- Translational Velocity: 1.2 – 6 in/sec
- Stripping Passes: 1-3
- Overlap: 0.5 – 1.75 in

8. Wheat Starch Stripping

A total of three (3) depainting cycles were performed with the EnviroStrip Wheatstarch technology. Thirty (30) specimens were stripped with the Wheat Starch technology. Generous time and support was donated by ADM Ogilvie and CAE Electronics (Montreal, Canada). Manual and semi-automated systems were utilized. The pure wheat starch media is used with this technology. The wheat starch can be recycled a maximum of 20 times. This technology can be implemented on aluminum, composite and steel materials. The workpiece is grounded to prevent ignition of media dust.

The specimens were a thickness of 16, 51 and 64 mils. The strip rates provided in Table 8 yielded 100% removal of the topcoat and 99% removal of the primer with one pass.

Table 8. Strip Rates for Wheat Starch Stripping Technology

Specimen Thickness (in)	Manual/ Automated	Average Strip Rates (in^2/min)	Average Strip Rates (in^2/min)	Average Strip Rates (in^2/min)
		Sequence 1	Sequence 2	Sequence 3
0.016	Manual	55.2	98.0	71.0
0.051	Manual	69.2	124.6	105.3
0.064	Manual	50.0	104.9	110.0
0.016	Semi-automated	180.0	293.3	293.3
0.051	Semi-automated	382.5	484.5	535.5
0.064	Semi-automated	382.5	484.5	535.3

The following operating parameters provided the strip rates in Table 8:

- Manual Operating Parameters:
  - Area Stripped : 216 in^2
  - Nozzle : 0.5 inch double venturi

- Angle of Attack: 30 to 60 ^{0}
- Stand – Off Distance : 4 to 8 inches
- Media Flow Rate: 12 to 18 lb/min
- Pressure : 20-30 psi

- Automated Operating Parameters:
  - Area Stripped : 204 in^2, 216 in^2
  - Nozzle: 4 inch flat nozzle
  - Projection Angle: 45^0
  - Stand-Off Distance: 3 inches
  - Media Flow Rate: 12-18 lb/min
  - Pressure: 20-40 psi
  - Translational Velocity: 0.8-2.1 in/sec

SURFACE ROUGHNESS

The ISO/SAE M8472 standard requires that the cumulative surface roughness value not exceed 125 microinches after 5 (five) depainting cycles. A Giddings & Lewis profilometer and a Hommelwerke T500 profilometer were used to determine the surface roughness of the specimens. Table 9 lists the cumulative surface roughness measurements after the 3rd depainting cycles.

Table 9. – Surface Roughness Measurements

Depainting Process	Baseline (microinches)	Sequence 3 , After Cleaning (microinches)
Chemical Stripping	1.6	10.5
Xenon/Flashlamp	1.9	15.2
CO_2 Laser	2.3	-
Plastic Media Blast	2.5	16.2
Sodium Bicarbonate w Water	1.8	*28.3
High Pressure Water	1.9	*26.0
Wheat Starch Blasting	1.3	16.8

* Represents surface roughness before cleaning.

CONCLUSION

The evaluation of the alternative depainting methodologies demonstrated that all processes are viable for coating removal with the exception of CO_2 Blasting. Many factors should be taken into consideration when selecting an alternative depainting methodology. The factors are as follows:

- Capital Costs
- Operating Costs
- Specialized Training
- Facility Space
- Manual vs. Automatic
- Ease of Use
- Strip Rates
- Compatibility with Existing Systems
- Waste Generation
- Substrate Characteristics
- Hardware Characteristics
- Paint/Primer System

ACKNOWLEDGEMENTS

Thanks to the EPA, AF, Technical Advisory Committee, Aerospace Industry partners and the team at MSFC for their commitment to technical excellence and the environment.

REFERENCES

Joint EPA/NASA/AF Interagency Study – Final Report, December 1999.

Metallic Materials Division
Materials, Processes and Manufacturing Department
Marshall Space Flight Center

Fourth Conference on Aerospace Materials, Processes, and Environmental Technology

Evaluation of Various Depainting Processes on Mechanical Properties of 2024-T3 Aluminum Substrate

Preston McGill

Metallic Materials Division
Materials, Processes and Manufacturing Department
Marshall Space Flight Center

September 19, 2000

Interagency Depainting Agreement

Participants

- National Aeronautics and Space Administration
- Environmental Protection Agency
- United States Air Force
- Industry Partners

Objective

- Evaluate effects of alternative depainting technologies on aluminum substrate.

Depainting Operations

Media Stripping

- Plastic Media Blast
- Sodium Bicarbonate Wet Stripping
- High Pressure Water Blast
- Wheat Starch Blast
- Xenon Flashlamp/CO_2

Chemical Stripping

- Eight environmentally advantaged chemicals
- Two methylene chloride chemicals

Metallurgical Evaluations by Depainting Process

Depainting Process	Corrosion Potential[1]			Fatigue[2]		Crack Detectability[3]		Tensile[4]	
	Total Immersion	Sandwich Corrosion	Hydrogen Embrittlement	Clad	Non-Clad	Clad	Non-Clad	Clad	Non-Clad
Chemical Stripping	x	x	x						
Xenon Flashlamp/CO_2					x				x
CO_2 Laser Stripping[5]									
Plastic Media Blasting				x	x	x	x	x	x
Sodium Bicarbonate Wet Stripping							x		
High-Pressure Water Blasting					x		x		
Wheat Starch Blasting					x		x		

Notes:

1. Corrosion potential evaluations were conducted in accordance with ASTM F483-90, *Standard Test Method for Total Immersion Corrosion Test for Aircraft Maintenance Chemicals*; ASTM F1110-90, *Standard Test Method for Sandwich Corrosion Test*; and ASTM F519-93, *Standard Test Method for Mechanical Hydrogen Embrittlement Testing of Plating Processes and Aircraft Maintenance Chemicals*.
2. Fatigue evaluations were conducted in accordance with ISO/SAE MA4872 (draft 4).
3. Crack detectability evaluations were conducted in accordance with ISO/SAE MA4872 (draft 4).
4. Tensile evaluations were conducted in accordance with ASTM E8, *Standard Test Methods for Tension Testing of Metallic Materials*.
5. A processing anomaly during the final sequence of depainting prevented the metallurgic evaluation of the panels stripped with the CO_2 laser.

Metallic Materials Division
Materials, Processes and Manufacturing Department
Marshall Space Flight Center

Corrosion Testing

SAE MA4872
Immersion Corrosion
Sandwich Corrosion
Hydrogen Embrittlement

Total Immersion Corrosion

Test: ASTM F483-90 Standard Test Method for Total Immersion Corrosion Test for Aircraft Maintenance Chemicals

Objective: Determine corrosiveness of chemical on substrate.

Material: Clad and Non-Clad 2024-T3 Aluminum

Methodology: Immerse substrate in chemical, measure weight change and note visual change after seven days.

Metallic Materials Division
Materials, Processes and Manufacturing Department
Marshall Space Flight Center

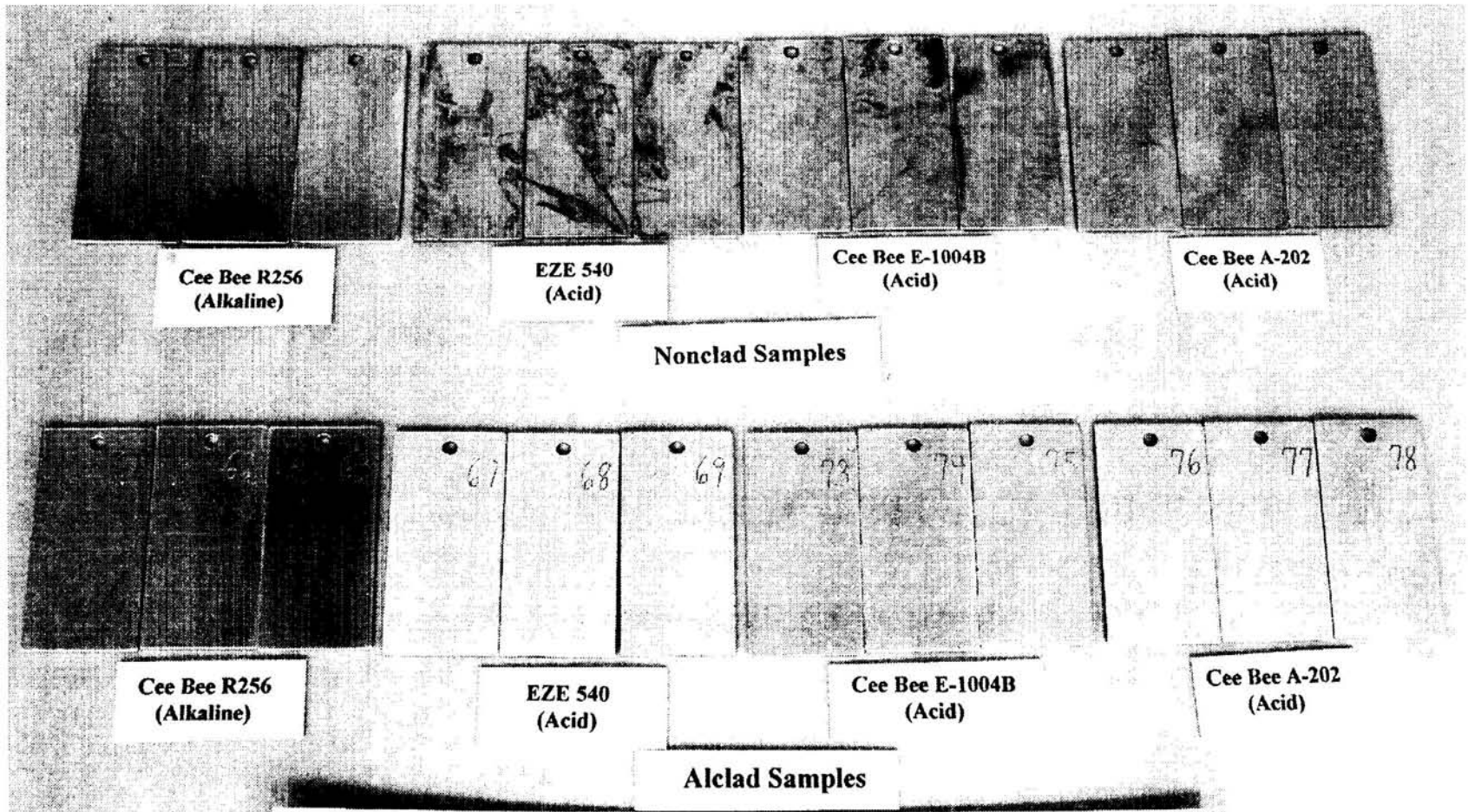

Aluminum Alloy 2024-T3 Nonclad and Alclad Samples
After 168 Hours of Total Immersion Corrosion Test per ASTM F483-90
(EPA/NASA/USAF Interagency Depainting Study)

EH22.97083.0014

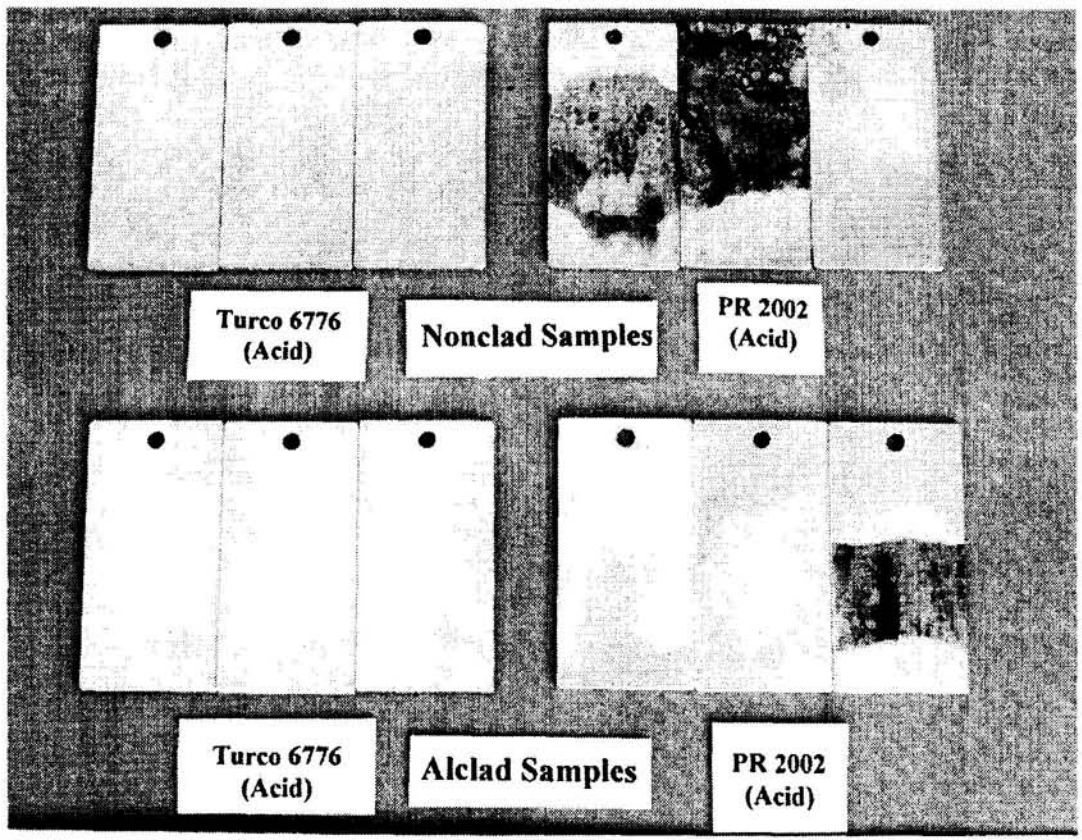

Aluminum Alloy 2024-T3 Nonclad and Alclad Samples
After 168 Hours of Total Immersion Corrosion Test per ASTM F483-90
(EPA/NASA/USAF Interagency Depainting Study)

EH22.97083.017

Metallic Materials Division
Materials, Processes and Manufacturing Department
Marshall Space Flight Center

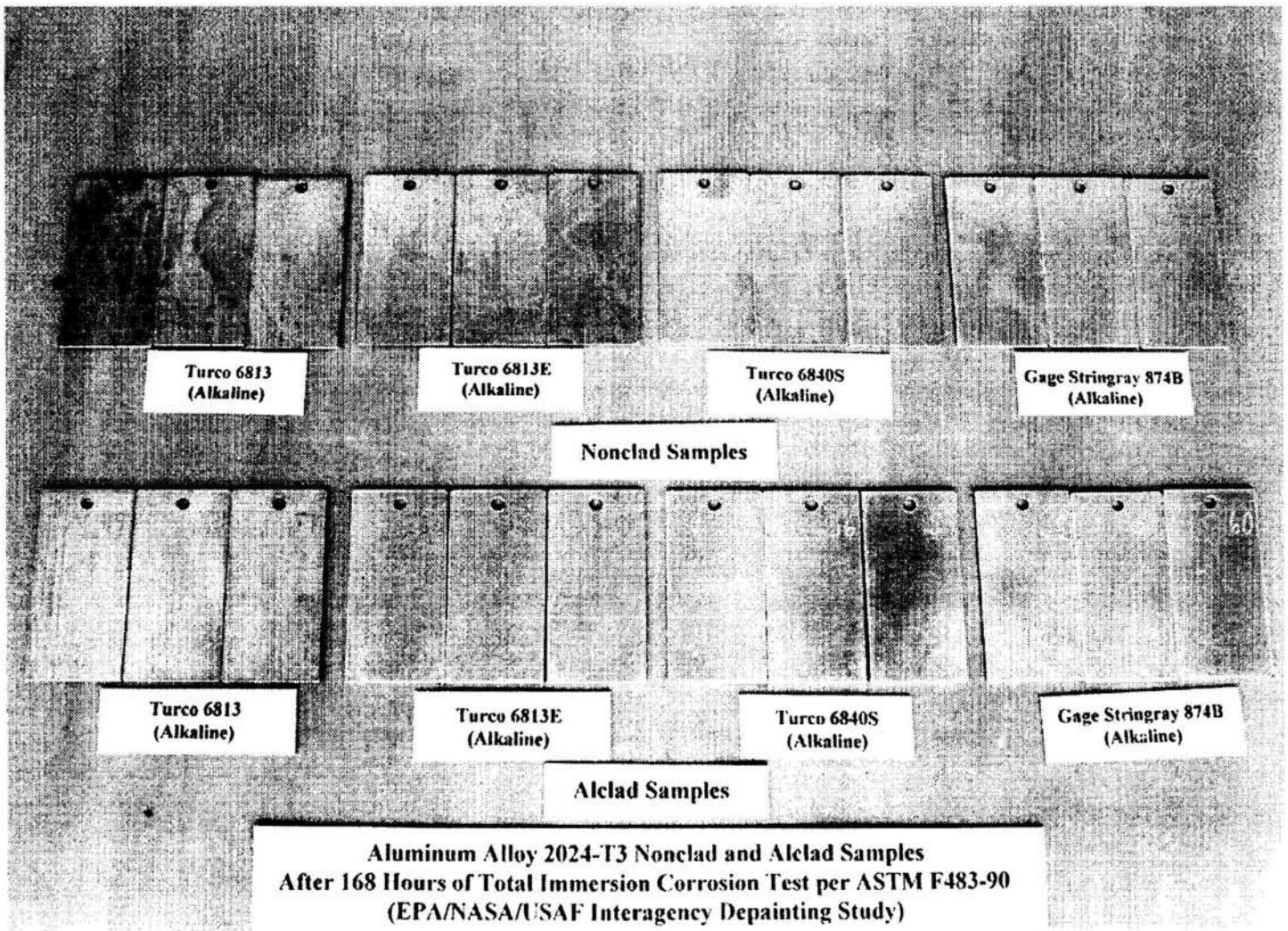

Aluminum Alloy 2024-T3 Nonclad and Alclad Samples
After 168 Hours of Total Immersion Corrosion Test per ASTM F483-90
(EPA/NASA/USAF Interagency Depainting Study)

EH22.97083.011

Total Immersion Corrosion Test Results

Chemical Tested	Weight Loss Rate ($mg/cm^2/24$ hr)			
	Non-Clad 2024-T3		Clad 2024-T3	
	24-hr Exposure	168-hr Exposure	24-hr Exposure	168-hr Exposure
Turco 6813 (Alkaline)	0.0035	-0.0005	0.0000	-0.0025
Turco 6813-E (Alkaline)	0.0071	-0.0015	0.0000	-0.0020
Turco 6840-S (Alkaline)	0.0000	-0.0010	-0.0071	-0.0020
Stingray 874B (Neutral)	0.0000	-0.0005	0.0000	-0.0010
Cee-Bee R-256 (Alkaline baseline)	0.0000	0.0015	0.0000	-0.0015
Turco 6776 (Acidic)	0.3121	0.4189	0.2092	0.3440
EZE 540 (Acidic)	0.2943	0.2771	0.2624	0.2036
PR-2002 (Acidic)	0.0319	0.0709	0.0000	0.1054
Cee-Bee E-1004B (Acidic)	0.1986	0.1717	0.1773	0.1327
Cee-Bee A-202 (Acidic baseline)	0.2979	0.2594	0.1950	0.1753

Chemical Tested	Coupon Number	Discoloration or Dulling	Etching	Accretions Present and Relative Amounts	Pitting	Selective or Localized Attack
Turco 6813 (Alkaline)	1 2 3	yes	no	no	no	no
Turco 6813-E (Alkaline)	4 5 6	yes	no	no	no	no
Turco 6840-S (Alkaline)	7 8 9	no small spots no	no	no	no	no
Stingray 874B (Neutral)	10 11 12	very little a little no	no	no	no	no
Cee-Bee R-256 (Alkaline baseline)	13 14 15	very little very little no	no	no	no	no
Turco 6776 (Acidic)	16 17 18	yes (coupons whitened)	yes	no	no	no
EZE 540 (Acidic)	19 20 21	yes	yes	no	yes	yes
PR-2002 (Acidic)	22 23 24	yes (many spots)	yes	no	yes	yes
Cee-Bee E-1004B (Acidic)	25 26 27	yes	yes	no	yes	yes
Cee-Bee A-202 (Acidic baseline)	28 29 30	yes	yes	no	yes	yes

Total Immersion Corrosion Test Conclusions

Alkaline and Neutral Chemicals -
- Little to no weight loss during exposure.
- Well below acceptable weight loss rates.
- No visible etching, pitting or accretions.

Acid Chemicals -

Non-clad - Three of five, including baseline, exhibited weight loss rates above acceptable rate (0.2mg/cm^2/24 hr).
Etching occurred from all chemicals.
No accretions on any samples.
Pitting and localized attack from all but one chemical.

Clad - One of five exhibited weight loss rates above acceptable rate (0.3 mg/cm^2/24 hr).
Etching occurred from all chemicals.
No accretions on any samples.
Pitting and localized attack from all but two chemicals.

Sandwich Corrosion Testing

Test: ASTM F1110-90 Standard Test Method for Sandwich Corrosion Test

Objective: Determine corrosiveness of chemical on substrate

Material: Clad and Non-Clad 2024-T3 Aluminum

Methodology: Immerse filter paper in chemical, sandwich filter paper between substrate panels and rate visual change per ASTM scale after seven days.

Metallic Materials Division
Materials, Processes and Manufacturing Department
Marshall Space Flight Center

Deionized Water | Turco 6813 (Alkaline) | Turco 6813E (Alkaline) | Turco 6840S (Alkaline) | Gage Stringray 874B (Alkaline) | CeeBee R256 (Alkaline) | EZE 540 (Acid) | CeeBee E-1004B (Acid) | CeeBee A-202 (Acid)

Nonclad Samples

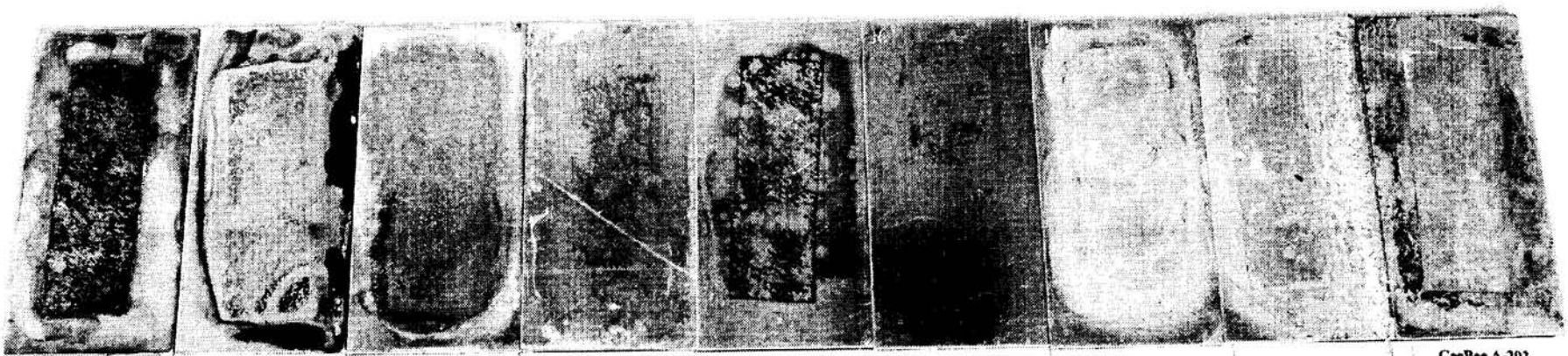

Deionized Water | Turco 6813 (Alkaline) | Turco 6813E (Alkaline) | Turco 6840S (Alkaline) | Gage Stringray 874B (Alkaline) | CeeBee R256 (Alkaline) | EZE 540 (Acid) | CeeBee E-1004B (Acid) | CeeBee A-202 (Acid)

Alclad Samples

Representative Aluminum Alloy 2024-T3 Nonclad and Alclad Samples After Sandwich Corrosion Test per ASTM F1110-90
(EPA/NASA/USAF Interagency Depainting Study)

EH22.97083.006

Rating	Condition
0	No visible corrosion
1	Very slight corrosion or discoloration (up to 5% of the surface area corroded)
2	Slight corrosion (5 to10% of the surface area corroded)
3	Moderate corrosion (10 to 25% of the surface area corroded)
4	Extensive corrosion or pitting (25% or more of the surface area corroded)

Chemical Tested	Non-Clad 2024-T3		Clad 2024-T3	
	Sandwich Number	Rating	Sandwich Number	Rating
Deionized Water (per ASTM D1193, Type IV)	1	3	121	3
	3	3	123	3
	5	3	125	3
	7	3	127	3
Turco 6813 (Alkaline)	9	1	129	3
	11	2	131	3
	13	2	133	3
	15	3	135	3
Turco 6813-E (Alkaline)	17	2	137	2
	19	2	139	3
	21	2	141	2
	23	2	143	3
Turco 6840-S (Alkaline)	25	3	145	2
	27	3	147	3
	29	2	149	2
	31	2	151	3
Stingray 874B (Neutral)	33	3	153	3
	35	3	155	3
	37	3	157	3
	39	3	159	3
Cee-Bee R-256 (Alkaline baseline)	41	2	161	1
	43	3	163	2
	45	2	165	2
	47	3	167	1
Turco 6776 (Acidic)	49	4	169	3
	51	4	171	3
	53	4	173	3
	55	4	175	3
EZE 540 (Acidic)	57	4	177	3
	59	4	179	4
	61	4	181	3
	63	4	183	3
PR-2002 (Acidic)	65	4	185	3
	67	4	187	3
	69	4	189	3
	71	4	191	3
Cee-Bee E-1004B (Acidic)	73	4	193	3
	75	4	195	2
	77	4	197	3
	79	4	199	2
Cee-Bee A-202 (Acidic baseline)	81	4	201	3
	83	4	203	2
	85	4	205	2
	87	4	207	3

Sandwich Corrosion Test Conclusions

Alkaline and Neutral Chemicals -

Non-clad -

All chemicals performed equal to or better than deionized water.

Three alkaline alternate chemicals performed equal to or better than methylene chloride baseline.

The neutral chemical did not perform as well as the methylene chloride baseline.

Clad -

All chemicals performed equal to or better than deionized water.

Methylene chloride baseline performed better than alternate chemicals.

Acid Chemicals -

Non-clad -

All chemicals performed worse than deionized water.

Alternate chemicals performed the same as the methylene chloride baseline.

Clad-

Four of five chemicals (including the baseline) performed as well or better than deionized water.

Three of four alternate chemicals performed worse than methylene chloride baseline.

Hydrogen Embrittlement Testing

Test: ASTM F519-93 Standard Test Method for Mechanical Hydrogen Embrittlement Testing of Plating Processes and Aircraft Maintenance Chemicals

Objective: Determine hydrogen embrittlement potential of chemical

Material: Cadmium plated 4340 steel

Methodology: Immerse preloaded specimen in chemical for 150 hours, check for failure of specimen

Metallic Materials Division
Materials, Processes and Manufacturing Department
Marshall Space Flight Center

Hydrogen Embrittlement Test Results

Chemical Tested	pH Values (as tested)	Failure Ratio	Time to Failure (hr or time interval)
Turco 6813 (Alkaline)	9.8	0/3	No Failures
Turco 6813-E (Alkaline)	9.9	0/3	No Failures
Turco 6840-S (Alkaline)	9.3	0/3	No Failures
Stingray 874B – Group 1 (Neutral)	5.7	2/3	98-145 128-143
Stingray 874B – Group 2 (Neutral)	5.7	1/3 (See note.)	191-198
Cee-Bee R-256 (Alkaline baseline)	8.0	0/3	No Failures
Turco 6776 (Acidic)	2.0	3/3	4.5 6 28-48
EZE 540 (Acidic)	2.5	3/3	0.5 8-24 8-24
PR-2002 (Acidic)	2.5	3/3	0.5 7-23 31-47
Cee-Bee E-1004B (Acidic)	2.4	3/3	1.75 1.75 1.75
Cee-Bee A-202 (Acidic baseline)	1.3	3/3	0.5 0.5 0.5

Note: Exposure time for the Group 2 specimens was extended to 200 hours.

Hydrogen Embrittlement Test Conclusions

Alkaline and Neutral Chemicals -

All alkaline chemicals (including the methylene chloride baseline) passed.
Failing neutral chemical exhibited two failures in six days (after 102 hours).
Failed specimens exhibited a region of intergranular fracture.
Failing neutral chemical was repeated and passed with no failures in 8 days (200 hours)
pH level of neutral chemical below levels reported by manufacturer.

Acid Chemicals -

All specimens failed within two days.
Failed specimens exhibited a region of intergranular fracture.
Methylene chloride baseline specimens failed in 0.5 hour.
Average failure times for alternative chemicals exceeded methylene chloride failure time.

Summary

Alternate alkaline and neutral chemical paint strippers have been identified that, with respect to corrosion requirements, perform as well or better then a methylene chloride baseline. These chemicals also, in general, meet corrosion acceptance criteria as specified in SAE MA 4872.

Alternate acid chemical paint strippers have been identified that, with respect to corrosion requirements, perform as well or better than a methylene chloride baseline. However, these chemicals do not generally meet corrosion acceptance criteria as specified in SAE MA 4872, especially in the areas of non-clad material performance and hydrogen embrittlement.

Metallic Materials Division
Materials, Processes and Manufacturing Department
Marshall Space Flight Center

Mechanical Testing

SAE MA4872
Tensile
Fatigue
Crack Detectability
Clad Penetration

Tensile Testing

Test: ASTM E8

Objective: Determine tensile properties of substrate

Material: Clad and Non-Clad 2024-T3 Aluminum

Metallic Materials Division
Materials, Processes and Manufacturing Department
Marshall Space Flight Center

Tensile Stress-Strain Curve for 2024-T3 Aluminum (clad)

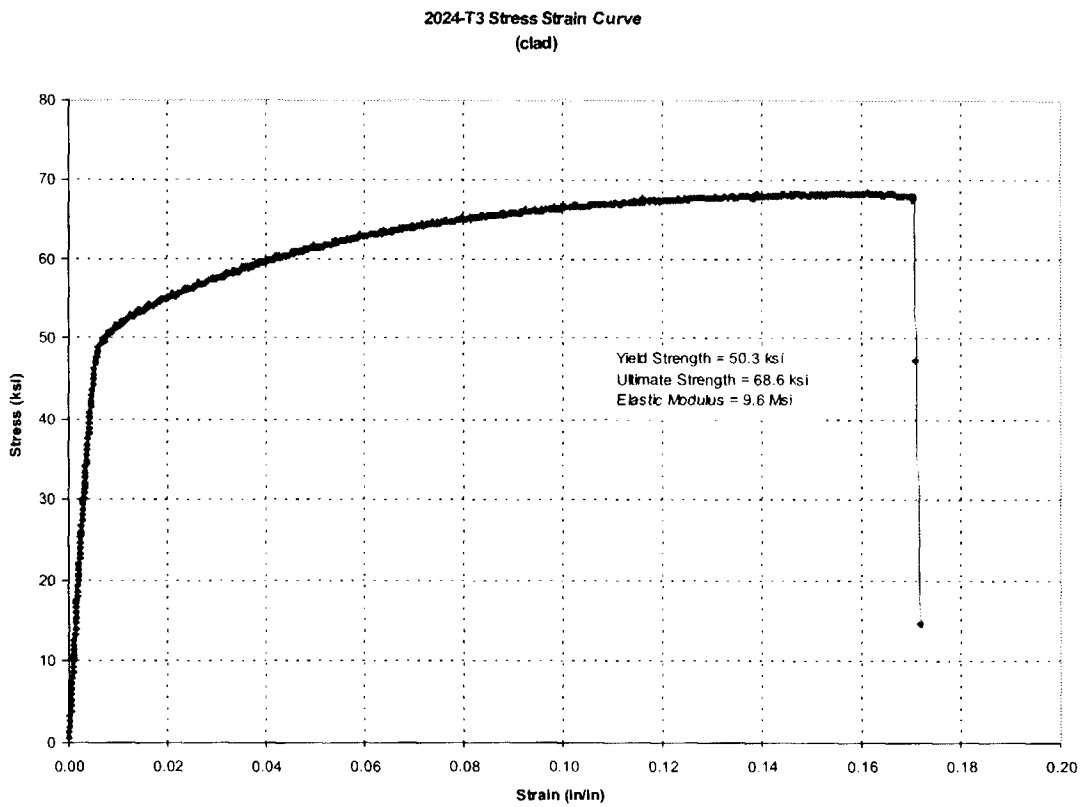

Metallic Materials Division
Materials, Processes and Manufacturing Department
Marshall Space Flight Center

Tensile Stress-Strain Curve for 2024-T3 Aluminum (non-clad)

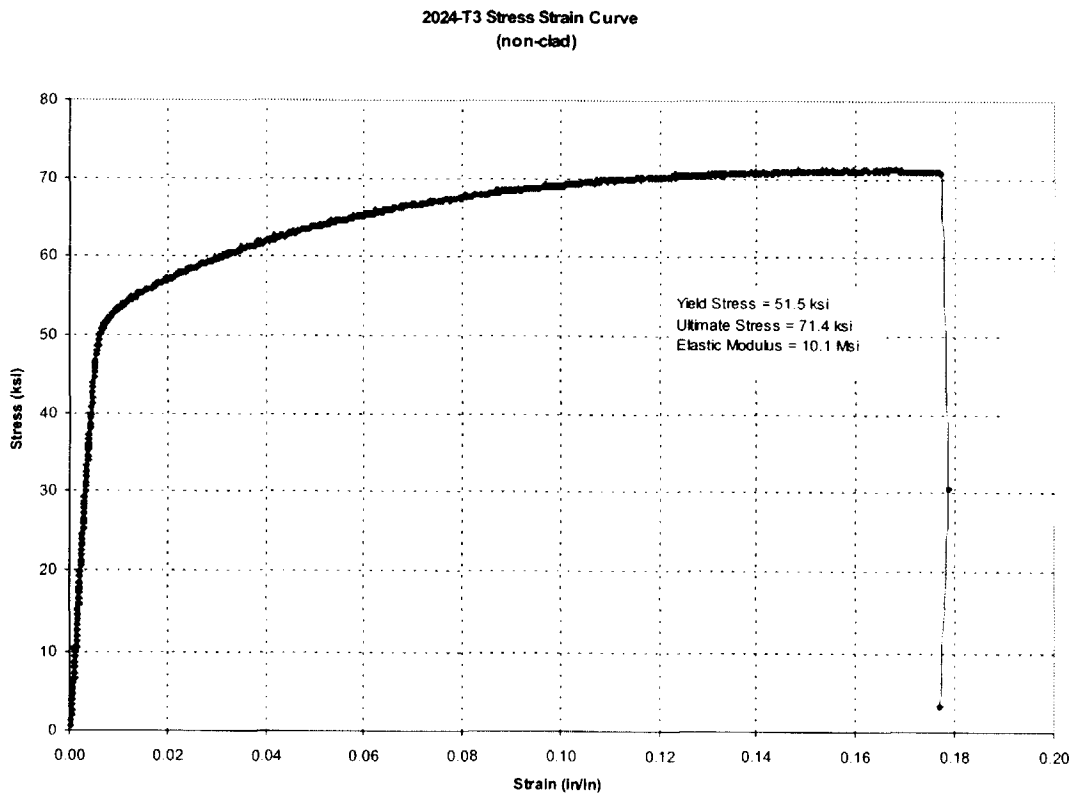

Tensile Test Data Summary (2024-T3 Aluminum, Longitudinal Direction)

Depainting Process	Clad/ Non-Clad	Ultimate Tensile Strength (ksi)	Yield Strength (ksi)	Elongation (%)
Baseline	non-clad	70.6	51.7	18.4
Xenon Flashlamp/CO_2				
Panel IV-15.7	non-clad	71.0	51.1	15.7
Panel IV-15.10	non-clad	67.3	45.6	14.7
Plastic Media Blasting				
Panel VII-VIII 29.16	non-clad	71.9	52.1	15.9
Panel VII-21.28	non-clad	71.4	51.5	17.7
MIL-HDBK-5G	non-clad	64	47	(See note.)
Baseline	clad	67.8	49.1	16.3
Plastic Media Blasting				
Panel VII-40.4	clad	68.2	49.8	16.9
Panel VII-40.2	clad	68.6	50.3	17.1
MIL-HDBK-5G	clad	60	44	(See note.)

Note: Elongation data are not provided in MIL-HDBK-5G.

Fatigue Testing

Test: SAE MA4872 (Type II Specimens)

Objective: Assess effects of depainting process on fatigue performance of substrate.

Material: Clad and Non-Clad 2024-T3 Aluminum
Baseline
Processed Panels

Methodology: Maximum stress 45 ksi
R Ratio of 0.1
Cyclic load frequency of 10 Hz.

Fatigue Test Configuration

Metallic Materials Division
Materials, Processes and Manufacturing Department
Marshall Space Flight Center

2024 T3 Baseline Fatigue Data
Cyclic Stress 45 KSI

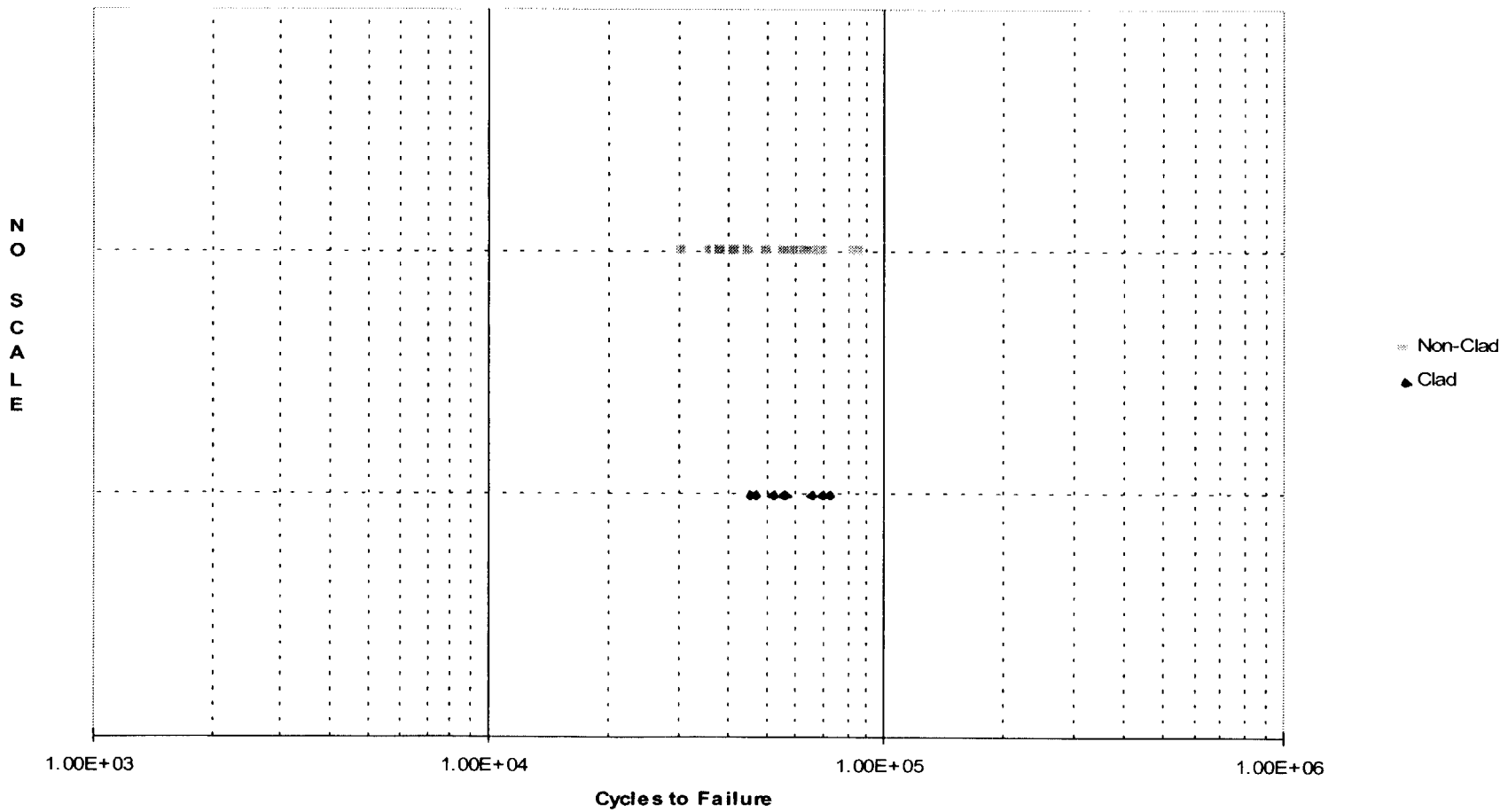

Metallic Materials Division
Materials, Processes and Manufacturing Department
Marshall Space Flight Center

2024 T3 (non-clad) Wheat Starch Fatigue
Cyclic Stress 45 KSI

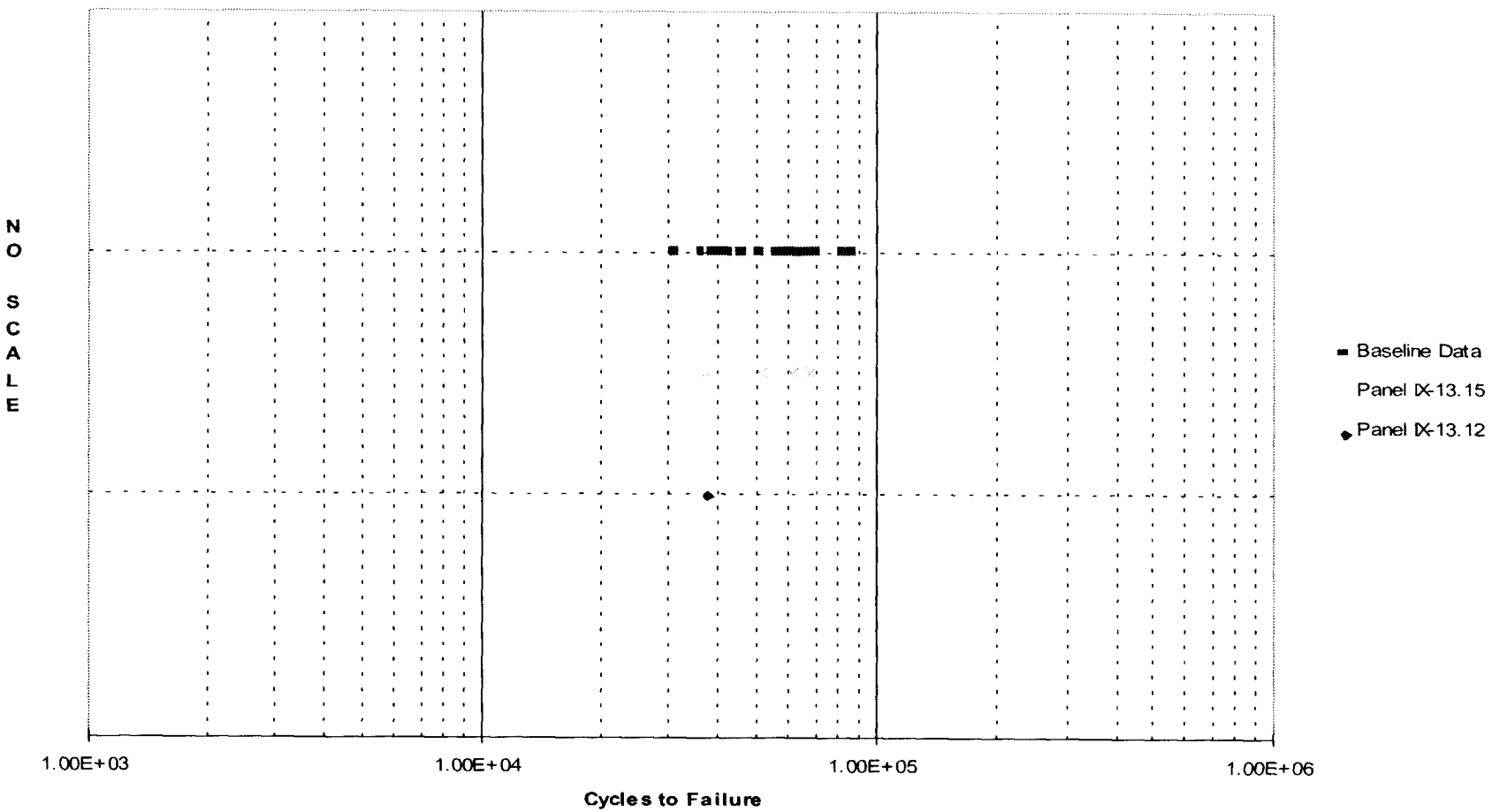

Metallic Materials Division
Materials, Processes and Manufacturing Department
Marshall Space Flight Center

2024 T3 (non-clad) Water Blast Fatigue
Cyclic Stress 45 KSI

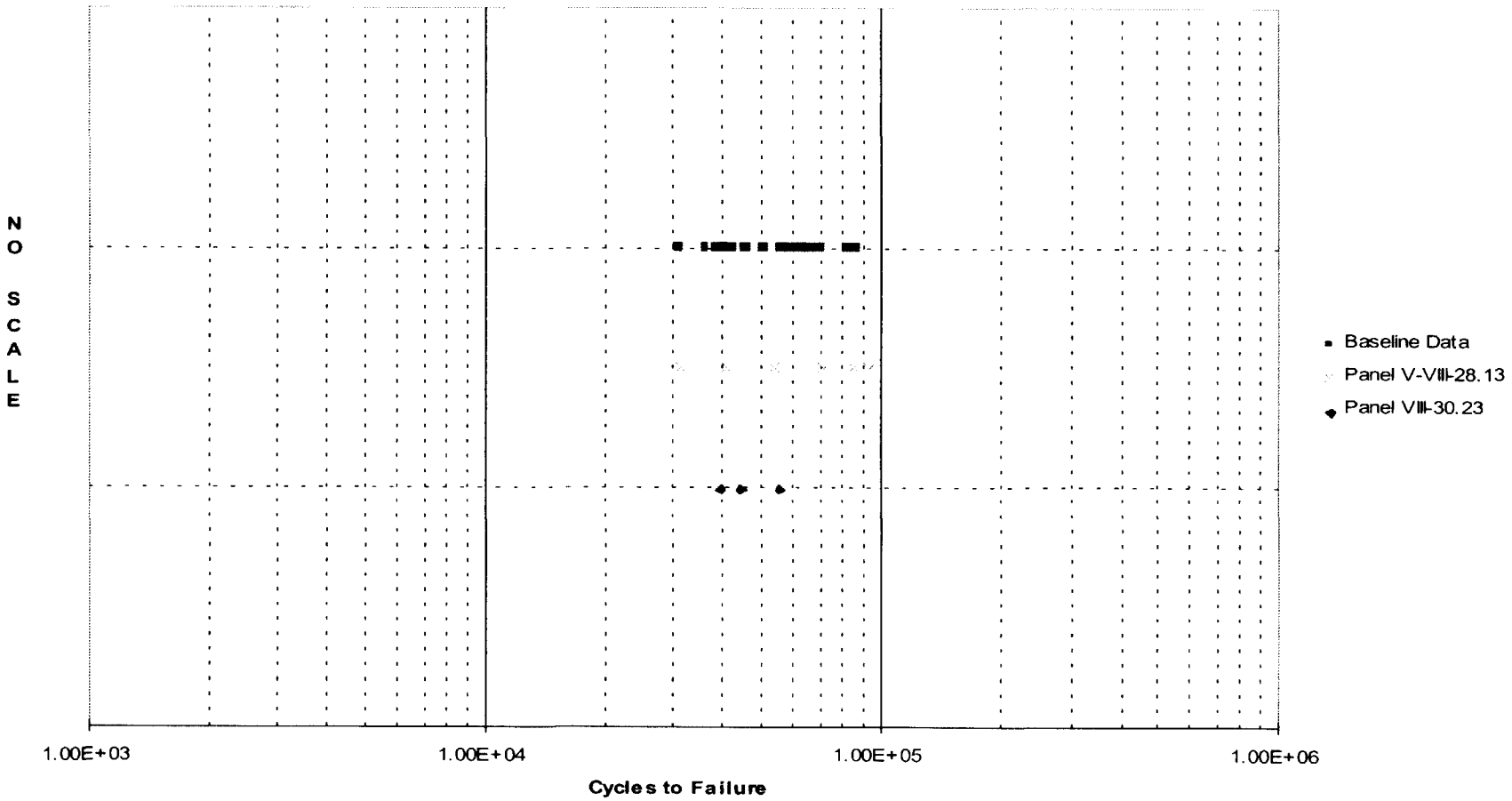

Metallic Materials Division
Materials, Processes and Manufacturing Department
Marshall Space Flight Center

2024 T3 (non-clad) Plastic Media Fatigue
Cyclic Stress 45 KSI

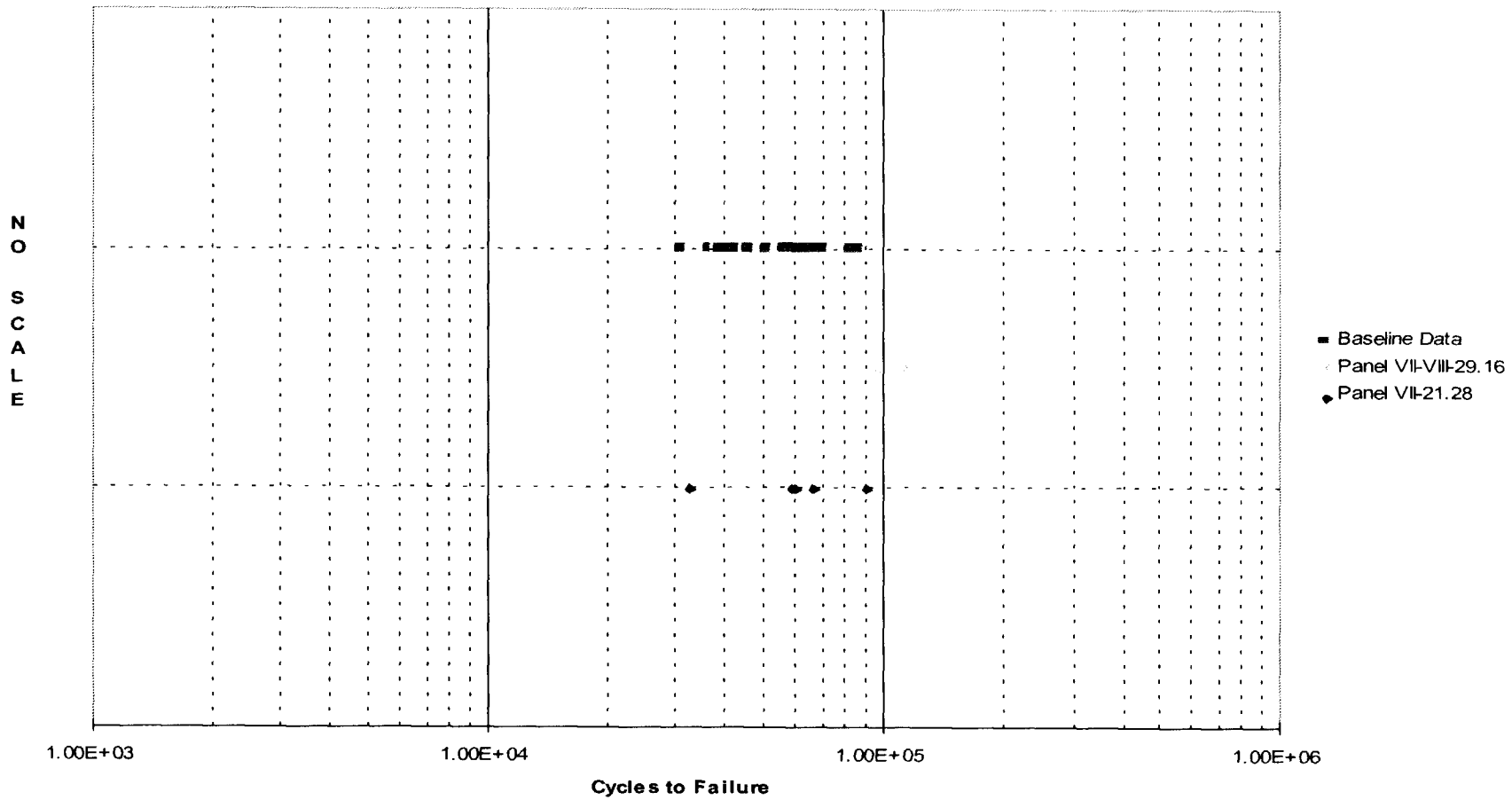

Metallic Materials Division
Materials, Processes and Manufacturing Department
Marshall Space Flight Center

2024 T3 (clad) Plastic Media Fatigue
Cyclic Stress 45 KSI

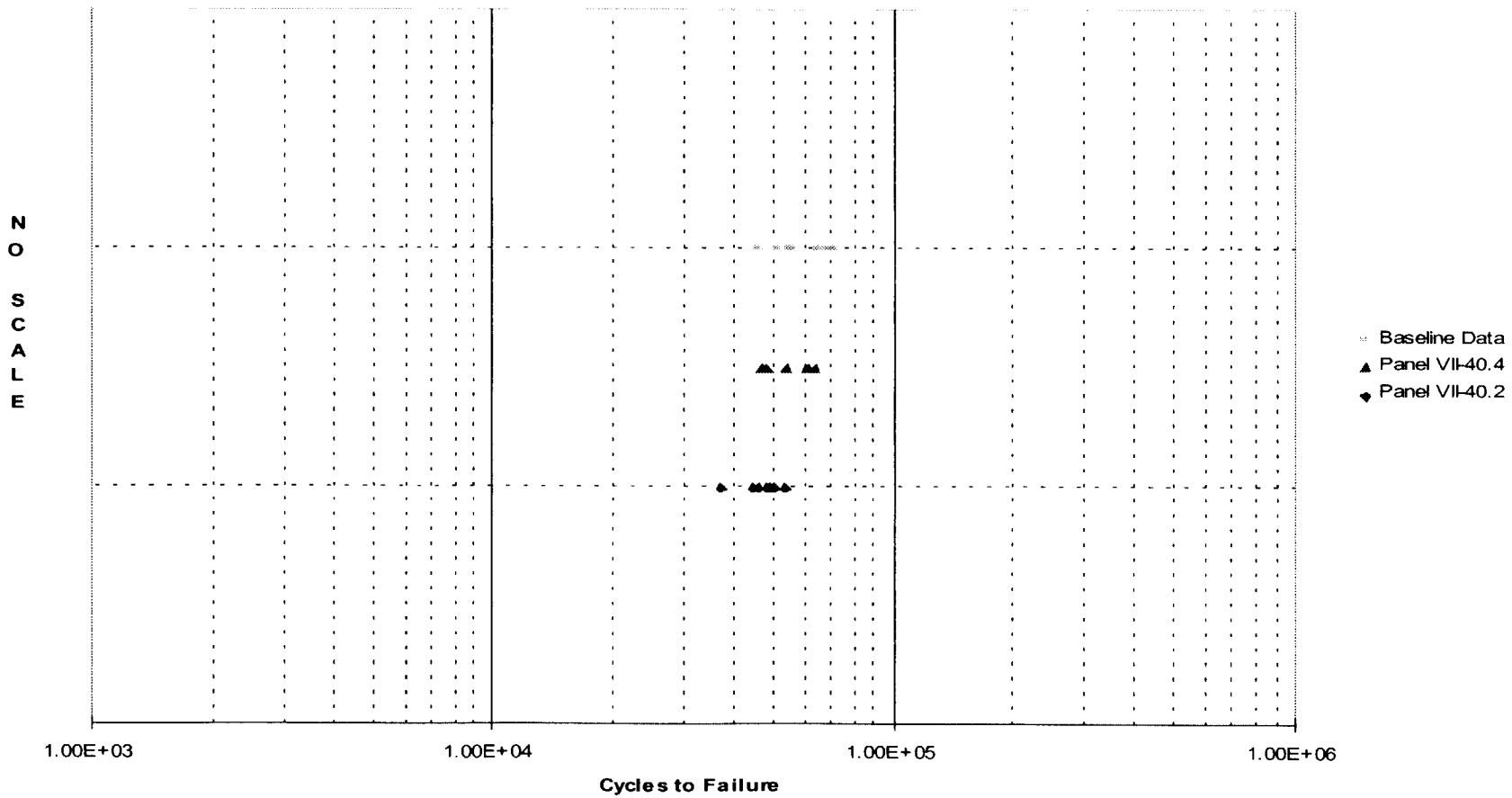

Metallic Materials Division
Materials, Processes and Manufacturing Department
Marshall Space Flight Center

2024 T3 (non-clad) Flashjet Fatigue
Cyclic Stress 45 KSI

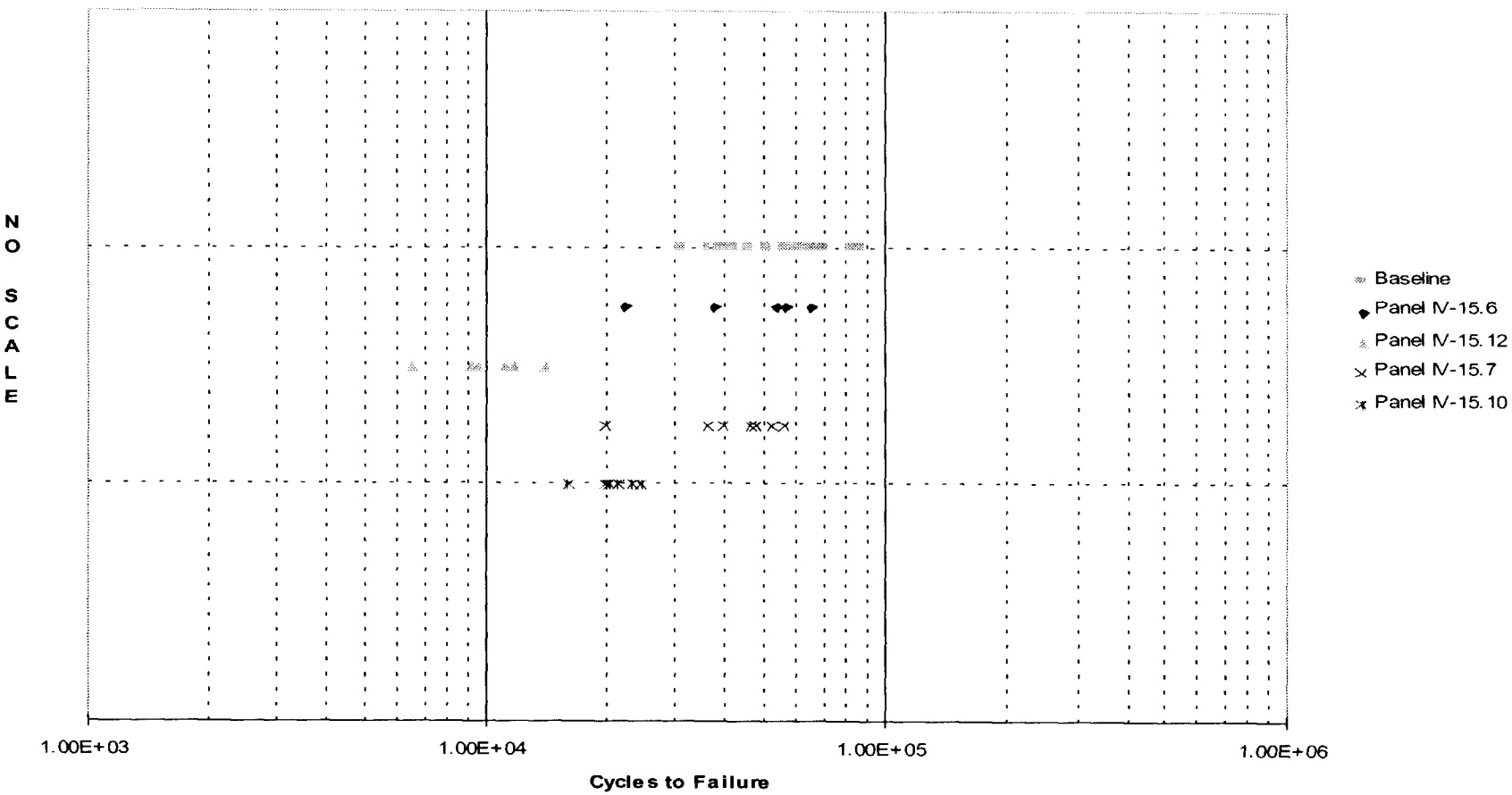

Depainting Process	Clad or Non-clad	Number of Samples	Mean Fatigue Life (cycles)	Standard Deviation (cycles)	95% Confidence Intervals for Mean Fatigue Life (cycles)	
					Lower	Higher
Baseline	Non-clad	22	54,118	15,231	47,753	60,482
Xenon Flashlamp/CO_2						
Panel IV-15.6	Non-clad	5	47,804	21,478	28,978	66,630
Panel IV-15.7	Non-clad	7	43,058	15,298	31,725	54,390
Panel IV-15.10	Non-clad	6	21,048	3,124	18,549	23,548
Panel IV-15.12	Non-clad	6	10,351	2,779	8,128	12,575
Plastic Media Blasting						
Panel VII-VIII-29.16	Non-clad	4	119,249	20,852	98,815	139,683
Panel VII-21.28	Non-clad	5	62,173	23,901	41,224	83,123
High-Pressure Water Blasting						
Panel V-VIII-28.13	Non-clad	8	79,457	42,735	49,843	109,070
Panel VIII-30.23	Non-clad	3	46,112	8,038	37,016	55,208
Wheat Starch Blasting						
Panel IX-13.12	Non-clad	1	37048[1]	Note 2	Note 2	Note 2
Panel IX-13.15	Non-clad	4	54,827	14,704	40,418	69,238
Baseline	Clad	8	57,488	9,967	50,582	64,395
Plastic Media Blasting						
Panel VII-40.4	Clad	6	55,396	7,333	49,529	61,264
Panel VII-40.2	Clad	7	46,579	5,575	42,450	50,709

Notes:
1. Only one specimen from wheat starch blasting panel IX-13.12 failed in the gauge section; this figure is the actual number of cycles performed to fatigue the specimen.
2. No data are available for these categories since only one specimen from this panel failed in the gauge section.

Fatigue Test Conclusions

Small Sample Size

Xenon Flashlamp/CO_2 (non-clad)
- Overlap in mean life for two sets of panel specimens
- Reduction in mean life for two sets of panel specimens
  - Surface condition
  - Low strength material

Plastic Media (clad and non-clad)
- Increase in mean life for one set of non-clad panel specimens
- Overlap in mean life for one set of non-clad panel specimens
- Overlap in mean life for two sets of clad panel specimens

Wheat Starch (non-clad)
- Overlap in mean life for one set of panel specimens

Water Blast (non-clad)
- Overlap in mean life for two sets of panel specimens

Crack Detectability Testing

Test: SAE MA4872 - Crack Detectability

Objective: Assess effect of depainting process on detection of substrate cracks.

Material: Clad and Non-Clad 2024-T3 Aluminum

Methodology: Painted and Cured
Notched and Precracked
Crack lengths measured (eddy current)
Depainted
Crack lengths measured (eddy current)

Crack Detectability Specimen

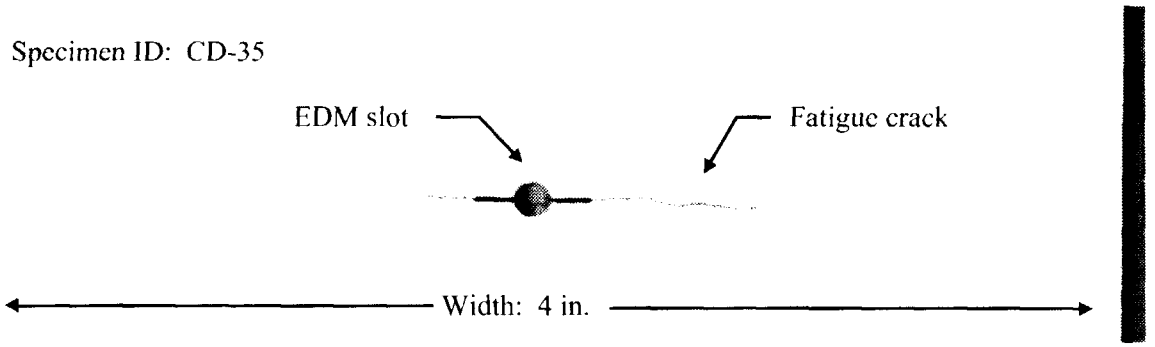

Initial vs First Cycle Crack Length Measurements
Envirostrip Wheat Starch

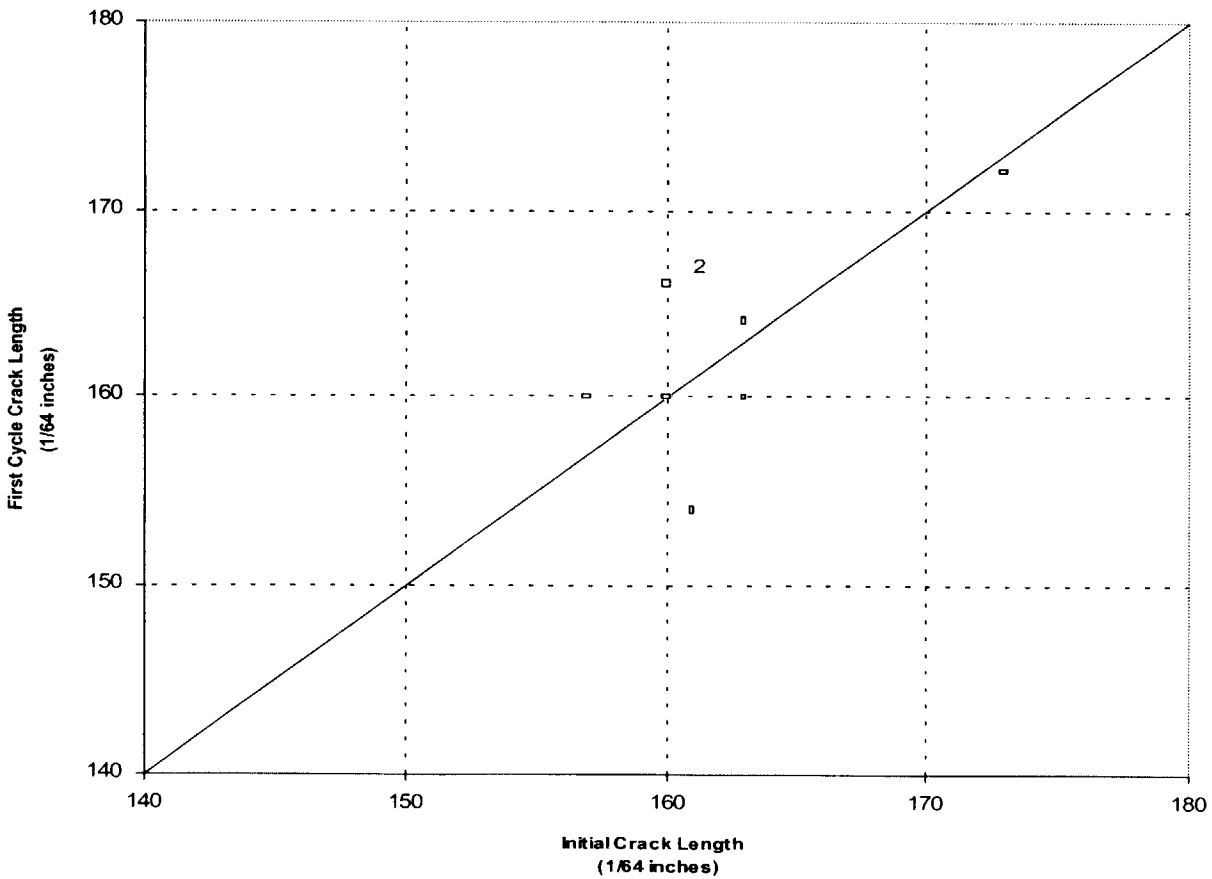

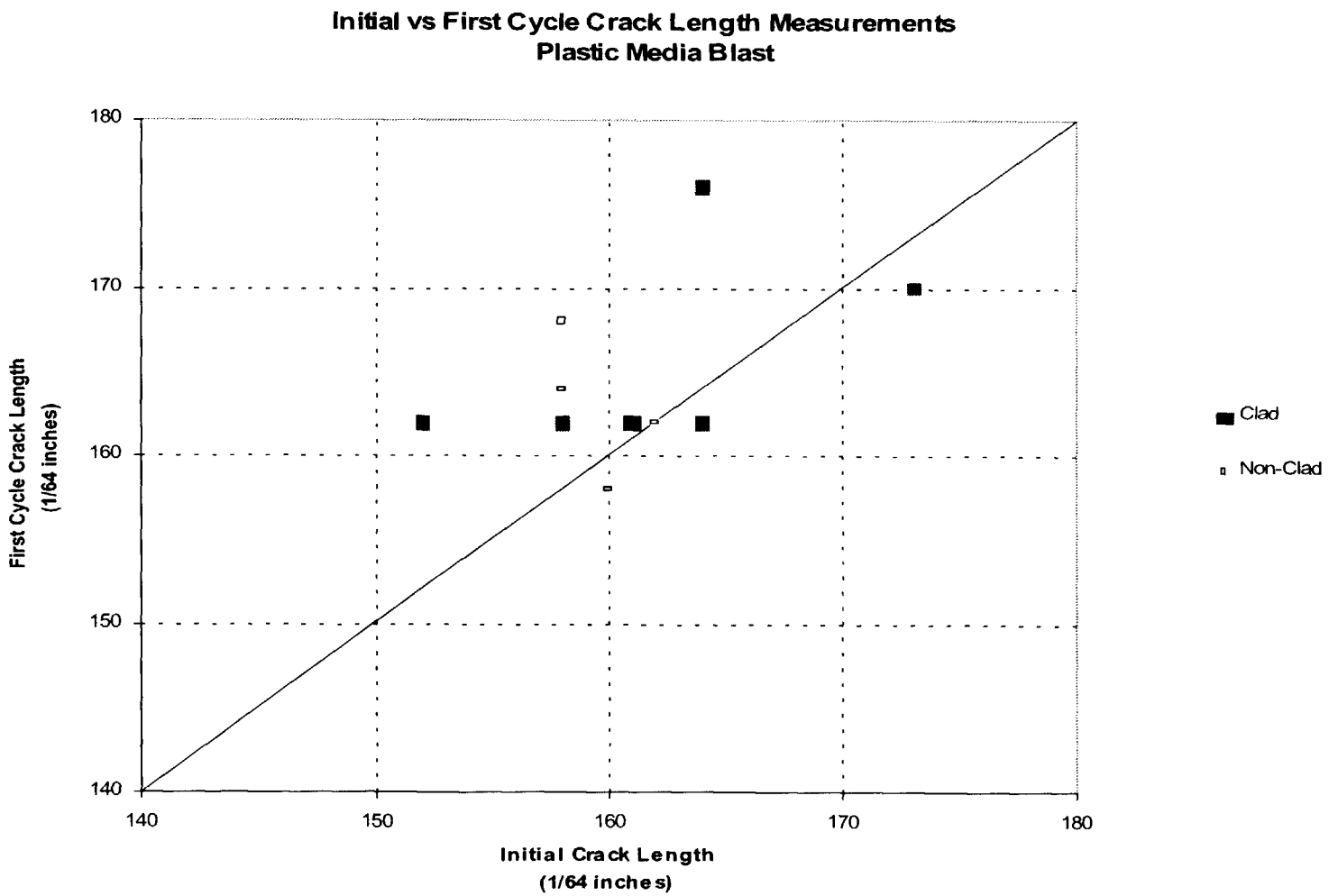
Initial vs First Cycle Crack Length Measurements
Plastic Media Blast
First Cycle Crack Length
(1/64 inches)
180
170
160
150
140
140
150
160
170
180
Initial Crack Length
(1/64 inches)
Clad
Non-Clad

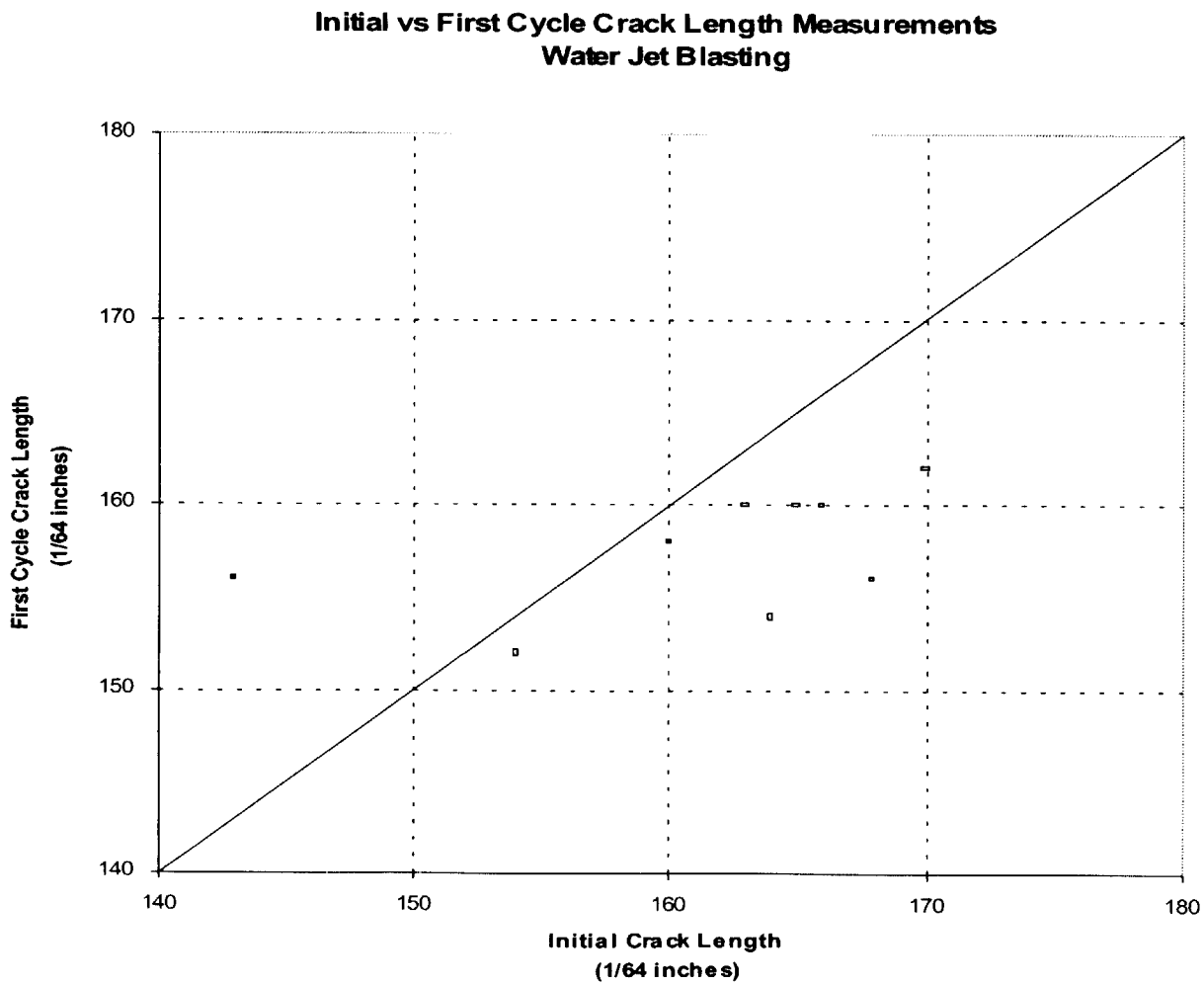
Initial vs First Cycle Crack Length Measurements
Water Jet Blasting
First Cycle Crack Length
(1/64 inches)
180
170
160
150
140
140
150
160
170
180
Initial Crack Length
(1/64 inches)

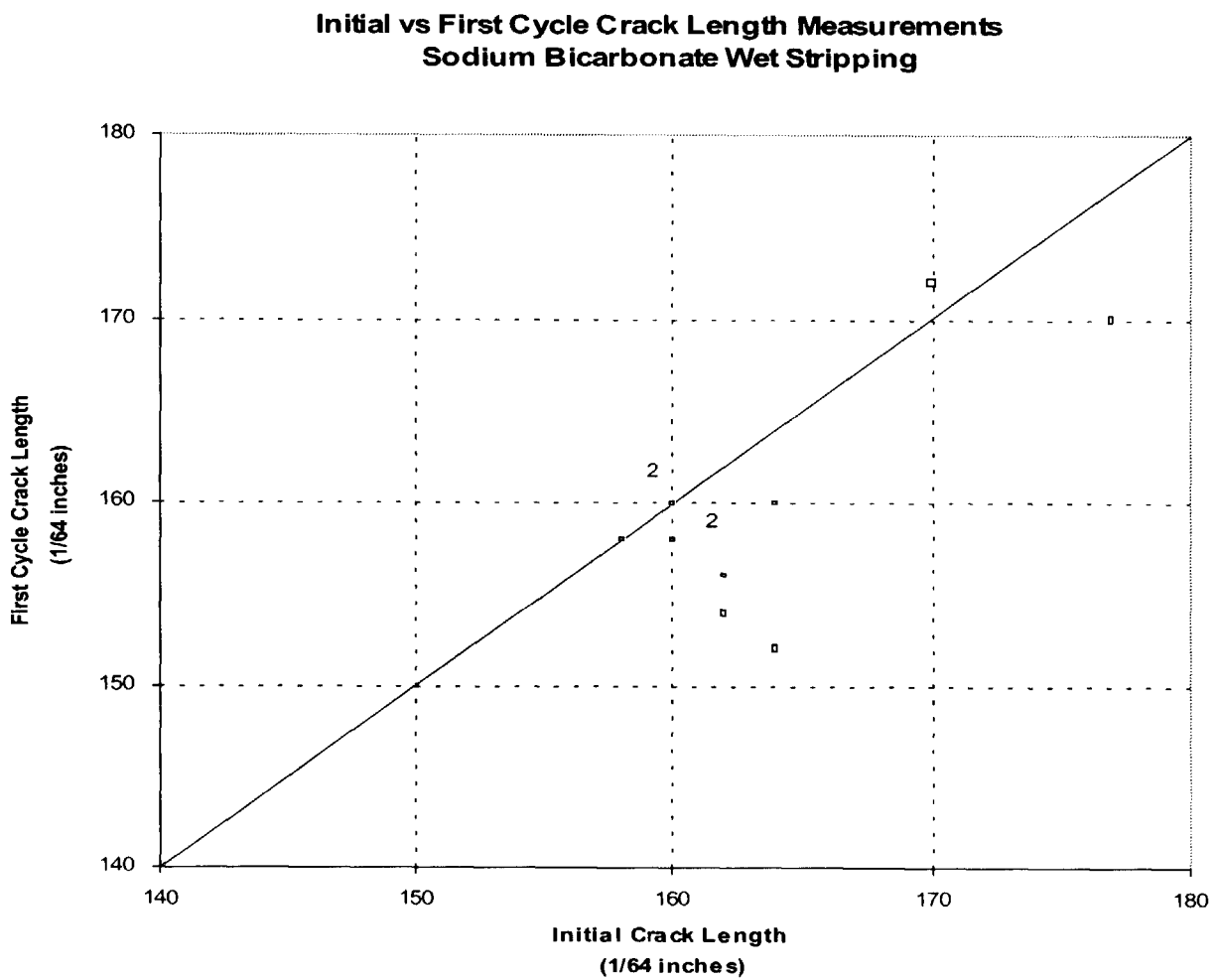
Initial vs First Cycle Crack Length Measurements
Sodium Bicarbonate Wet Stripping
First Cycle Crack Length
(1/64 inches)
Initial Crack Length
(1/64 inches)
180
170
160
150
140
140
150
160
170
180
2
2

Summary of Crack Detectability Test Results

Process	Specimen Number	Clad (y/n)	Crack Length (1/64 in.)		Process	Specimen Number	Clad (y/n)	Crack Length (1/64 in.)	
			Initial	Cycle 1				Initial	Cycle 1
Plastic Media Blasting	CD-10	n	158	164	Sodium Bicarbonate Wet Stripping	CD-2	n	162	154
	CD-11	n	158	168		CD-3	n	164	152
	CD-13	n	160	158		CD-20	n	177	170
	CD-15	n	162	162		CD-21	n	164	160
	CD-12	y	164	162		CD-22	n	160	158
	CD-14	y	164	176		CD-24	n	158	158
	CD-16	y	152	162		CD-25	n	160	160
	CD-17	y	161	162		CD-26	n	162	156
	CD-18	y	158	162		CD-27	n	160	158
	CD-19	y	173	170		CD-28	n	160	160
WaterJet Blasting	CD-30	n	166	160		CD-29	n	170	172
	CD-31	n	168	156	EnviroStrip® Wheat Starch Blasting	CD-40	n	160	166
	CD-32	n	143	156		CD-41	n	161	154
	CD-33	n	165	160		CD-42	n	160	160
	CD-34	n	170	162		CD-43	n	160	166
	CD-36	n	164	154		CD-44	n	163	164
	CD-37	n	160	158		CD-45	n	163	160
	CD-38	n	163	160		CD-46	n	157	160
	CD-39	n	154	152		CD-47	n	173	172

Summary of Pre- and Post-Processed Panel Crack Lengths

Process	Clad (y/n)	Average Difference (1/64 in.) (Cycle 1 - Initial)	Standard Deviation	Sample Size	95% Confidence Interval for Mean of the Difference	
Plastic Media Blasting	n	3.5	5.51	4	-1.9	8.9
	y	3.67	6.22	6	-1.31	8.64
Sodium Bicarbonate Wet Stripping	n	-3.55	4.27	11	-6.07	-1.02
WaterJet Blasting	n	-3.89	7.24	9	-8.62	0.84
EnviroStrip® Wheat Starch Blasting	n	0.63	4.44	8	-2.45	3.7

Crack Detectability Test Conclusions

Small Sample Size

Plastic Media (clad and non-clad)
Zero mean difference falls in 95% confidence interval.

Water Blast (non-clad)
Zero mean difference falls in 95% confidence interval.

Wheat Starch (non-clad)
Zero mean difference falls in 95% confidence interval.

Sodium Bicarbonate Wet Stripping (non-clad)
Zero mean difference does not fall in 95% confidence interval.

Metallic Materials Division
Materials, Processes and Manufacturing Department
Marshall Space Flight Center

Clad Penetration Evaluation

Baseline

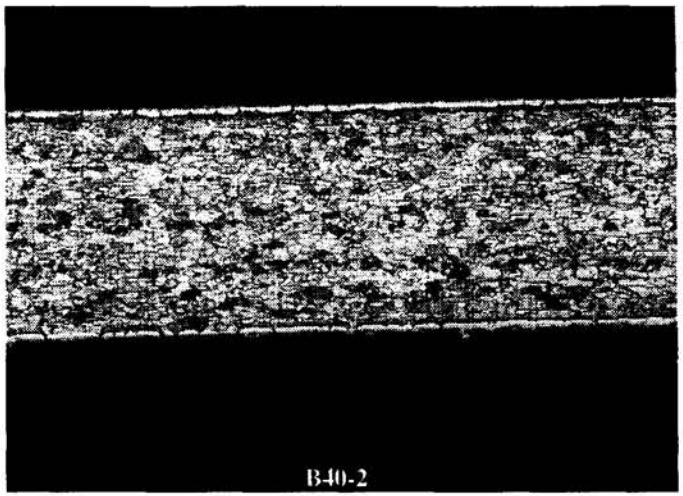

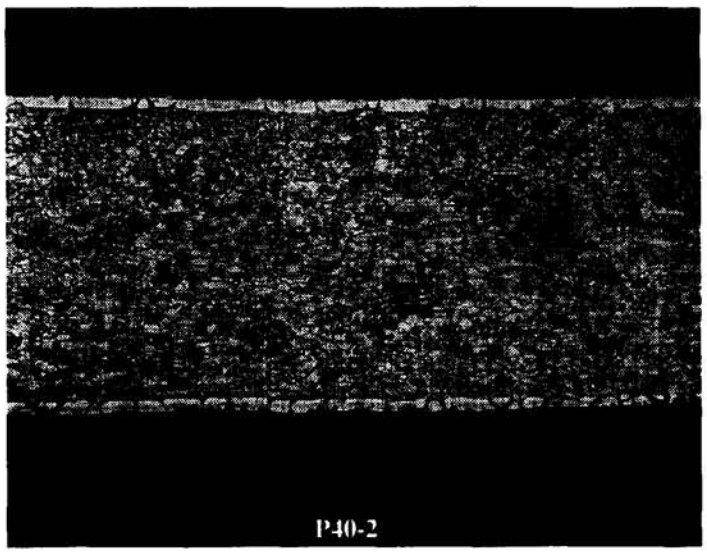

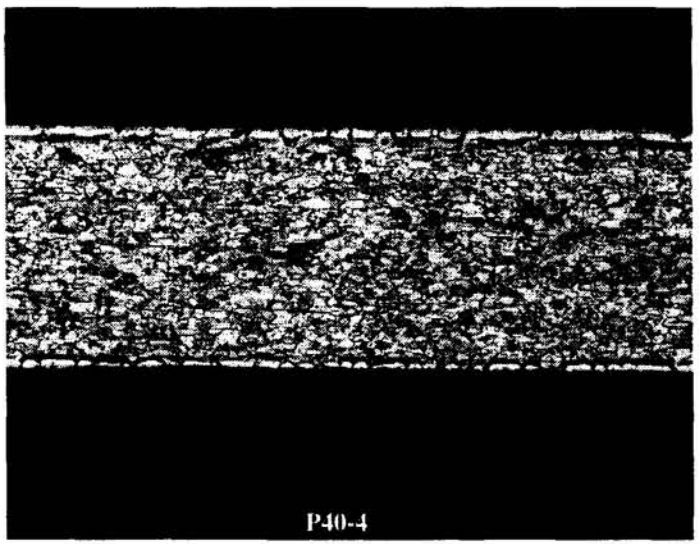

Plastic Media Blast

Summary

Alternate alkaline and neutral chemical paint strippers have been identified that, with respect to corrosion requirements, perform as well or better then a methylene chloride baseline. These chemicals also, in general, meet corrosion acceptance criteria as specified in SAE MA 4872.

Alternate acid chemical paint strippers have been identified that, with respect to corrosion requirements, perform as well or better than a methylene chloride baseline. However, these chemicals do not generally meet corrosion acceptance criteria as specified in SAE MA 4872, especially in the areas of non-clad material performance and hydrogen embrittlement.

Media blast methods reviewed in the study do not, in general, adversely affect fatigue performance or crack detectability of 2024-T3 substrate. Sodium bi-carbonate stripping exhibited a tendency towards inhibiting crack detectability. These generalizations are based on a limited sample size and additional testing should be performed to characterize the response of specific substrates to specific processes.

Flashjet Panel IV-15.12

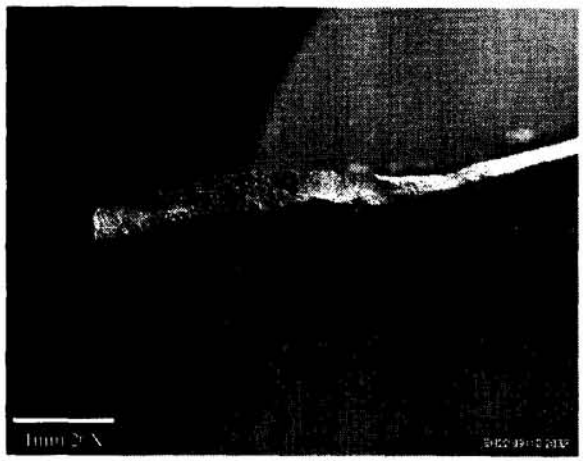

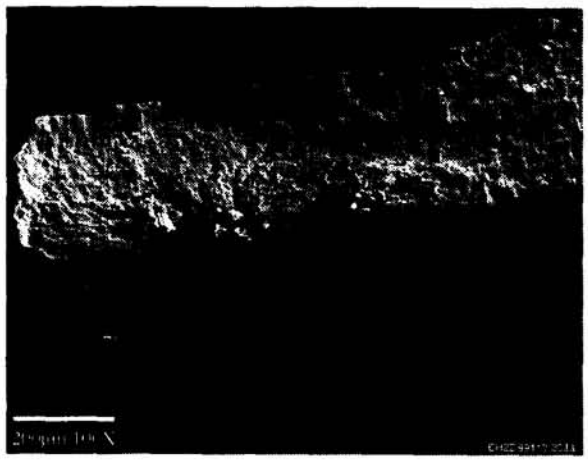

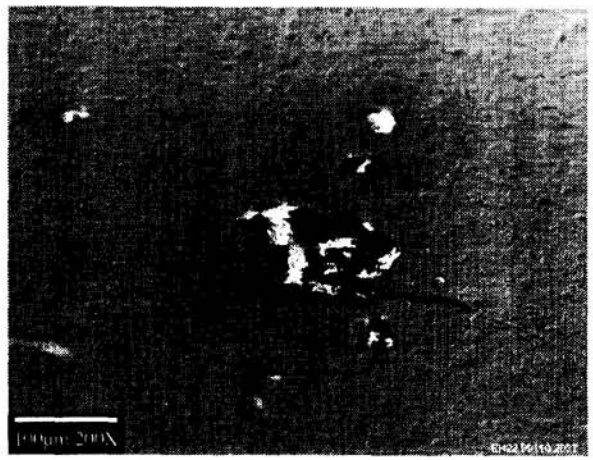

Panel IV-15.6

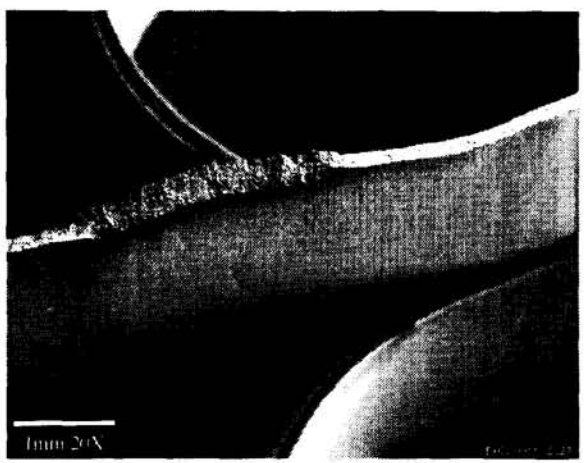

Panel IV-15.7

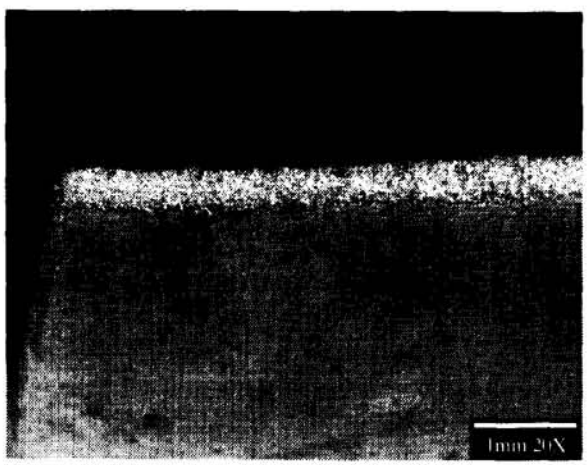

Panel IV-15.10

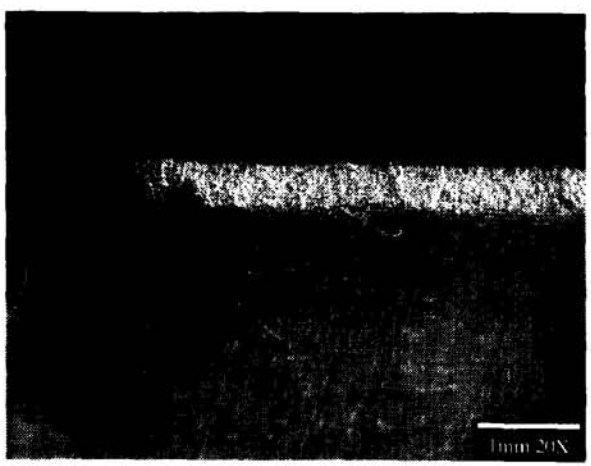

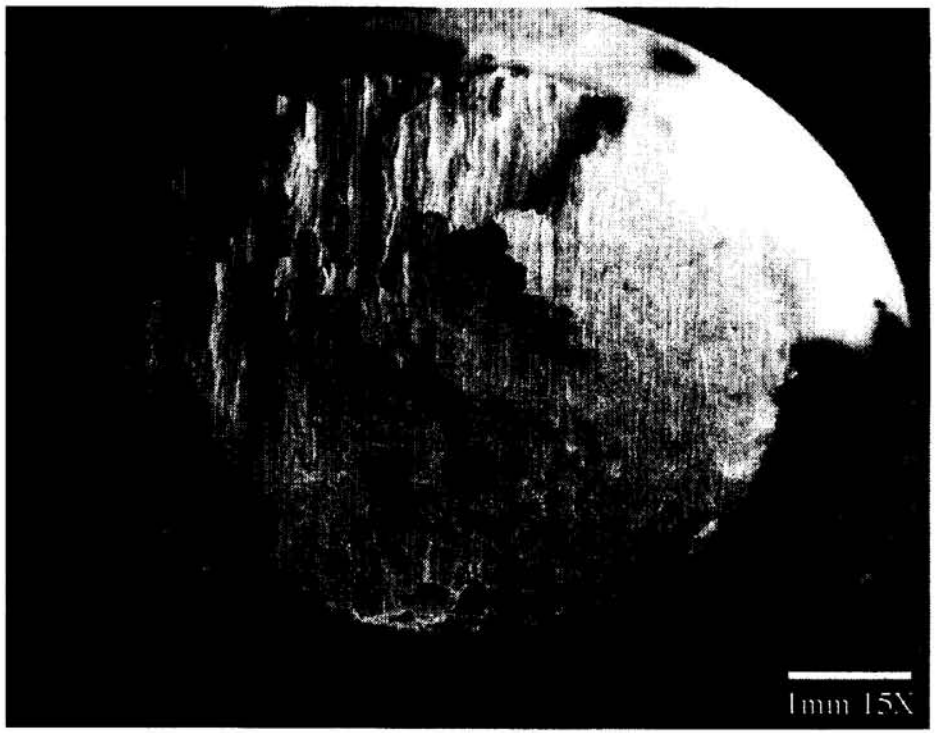
1mm 15X

Concept for Determining the Life of Ceramic Matrix Composites Using Nondestructive Characterization Techniques

Michael Effinger
NASA Marshall Space Flight Center
Bill Ellingson and Todd Spohnholtz
Argonne National Laboratory
John Koenig
Southern Research Institute

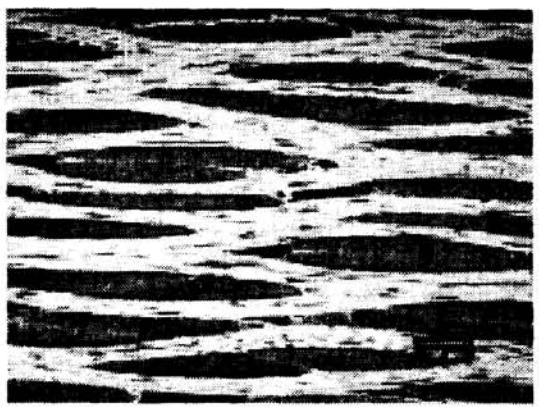

4th Conference on Aerospace Materials, Processes, and Environmental Technology
Von Braun Center, Huntsville, Alabama,
September 18-20, 2000

Agenda

- NDC Life Determination Background
  - Simplex Turbopump CMC Blisk NDC Data
  - Tensile Specimen Test Data
- General NDC Life Determination Concept
- Potential for Concept
- Case Scenario
- Challenges
- Justification
- Summary

Background

- Simplex CMC blisk program initiation in 1995
  - Two C/SiC integrally bladed disk (Blisk) architectures tested:

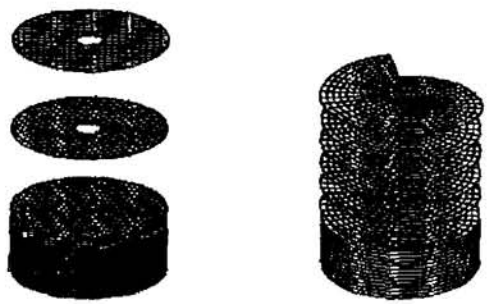

Quasi-isotropic Polar

- Thought process relative to Nondestructive Characterization (NDC) usage:
  - Try to use damping to monitor blade damage accumulation
    - Resulted in Argonne National Laboratory contracted to conduct damping and computed tomography analysis in as-received, post-proof testing, and post-turbopump testing states
    - 1998 results from as-fabricated to post-proof indicated changes were detectable
  - Formulated NDC Life Determination concept in 1999

Damping and Resonant Frequency Testing Data

- Simplex Blisk
  - Argonne National Laboratory tested:
    - As-fabricated, post-proof, and post-turbopump test conditions
  - Southern Research Institute tested:
    - Post-proof, and post-turbopump test conditions

- Coupon Specimens--establish baseline behavior for NDC C/SiC for different stresses

Blade Resonant Frequencies

Blisk -004 Blade Normalized Frequency

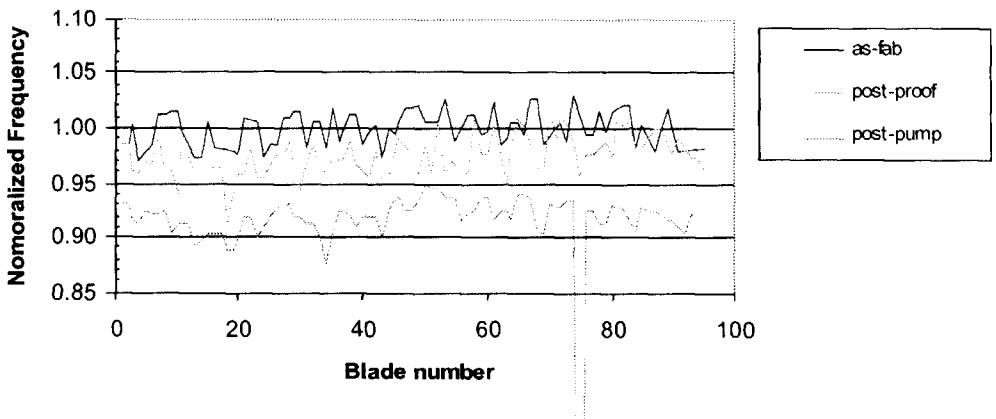

ANL Examined
Range 1

Blisk #4 Blade Frequency

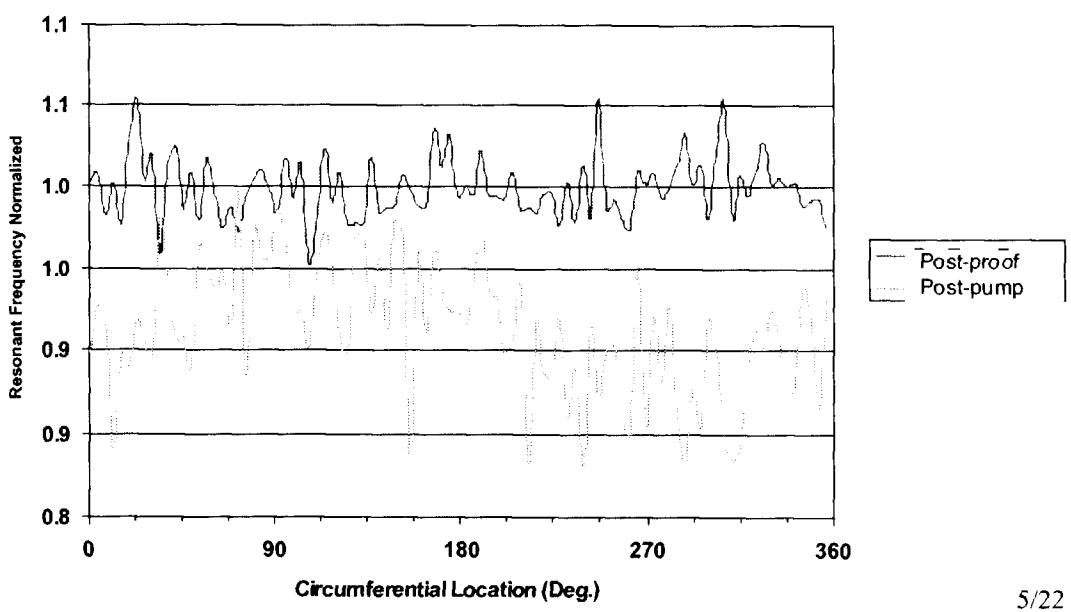

SRI Examined
Range 2

Specific Damping Capacity

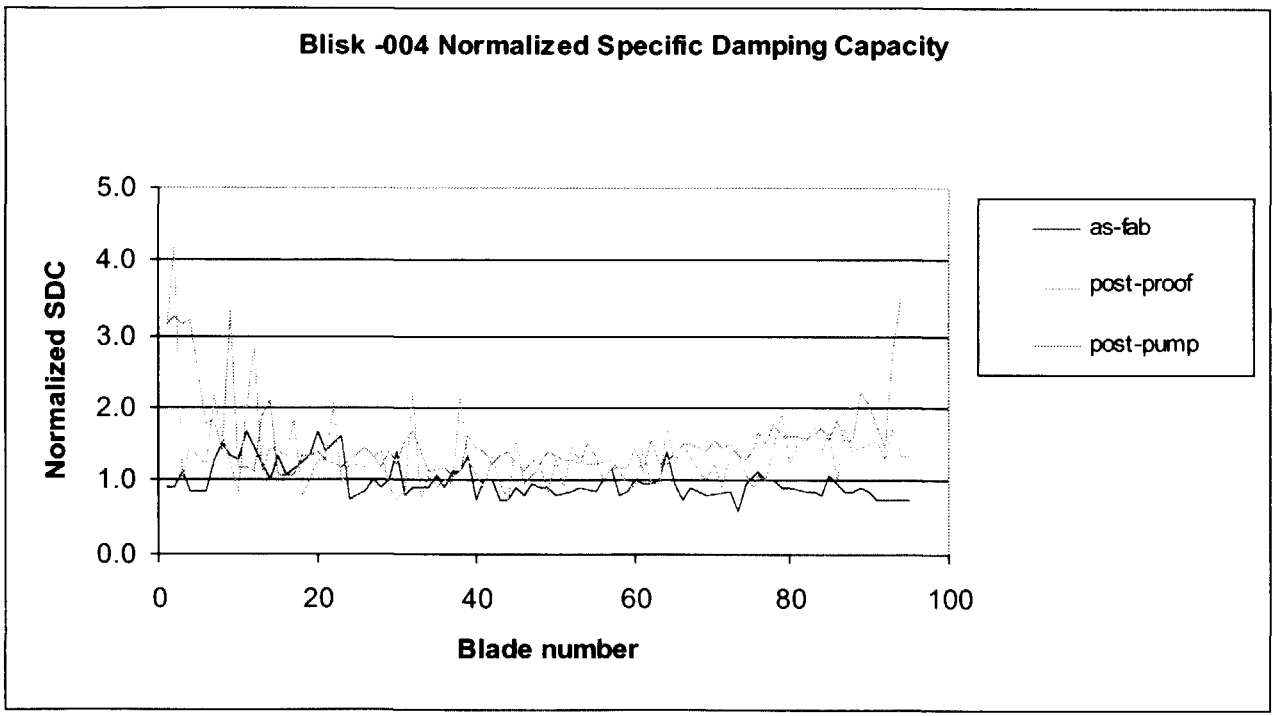

Ultrasonic Spectroscopy Coupon Data

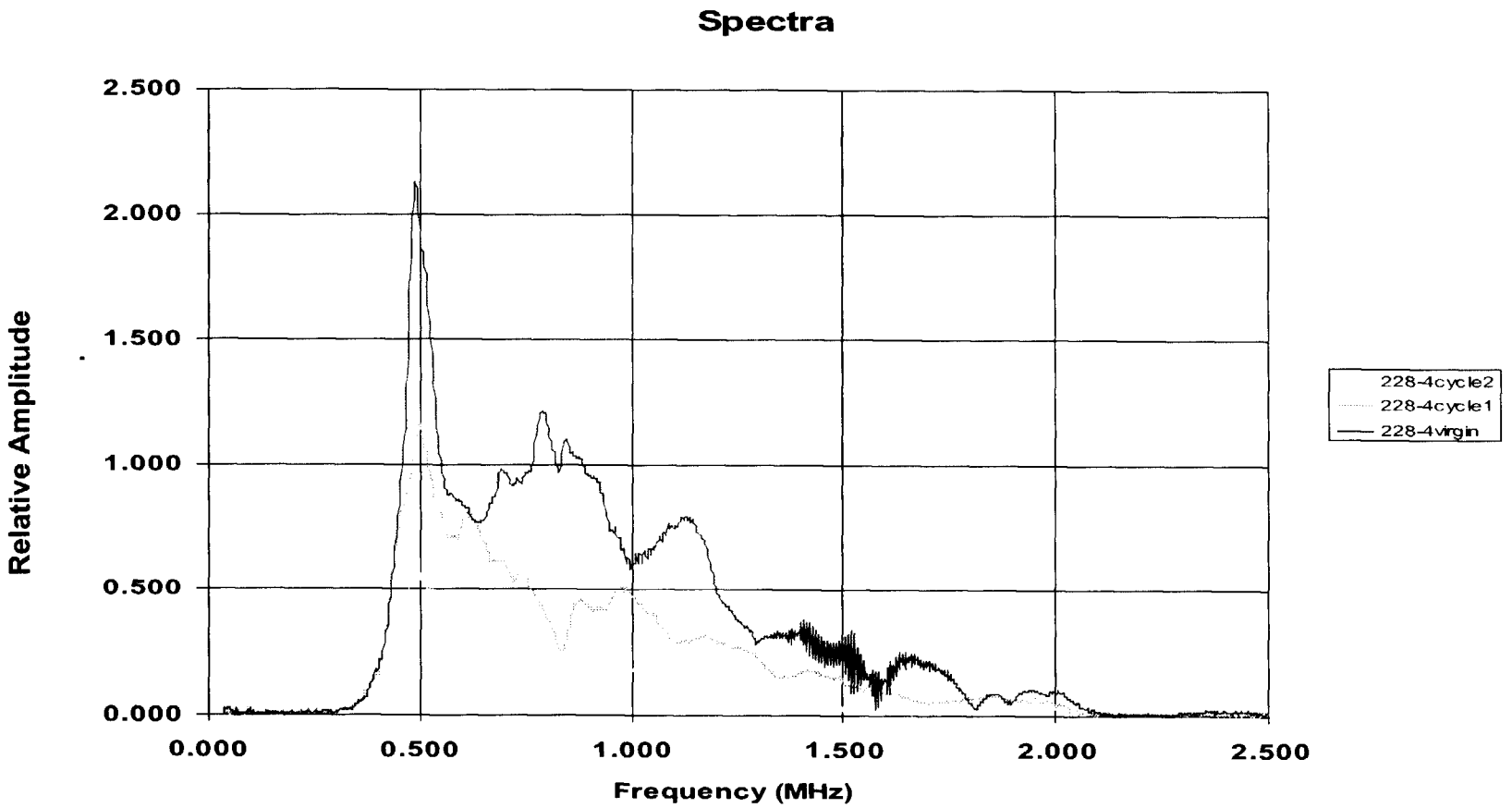

- DAMAGE MONOTORED BY SONIC VELOCITY, RESONANCE AND AND ULTRASONIC SPECTROSCOPY
- INCREASING DAMAGE SEEN WITH HIGHER LOAD LEVELS

Axial Velocity Coupon Data

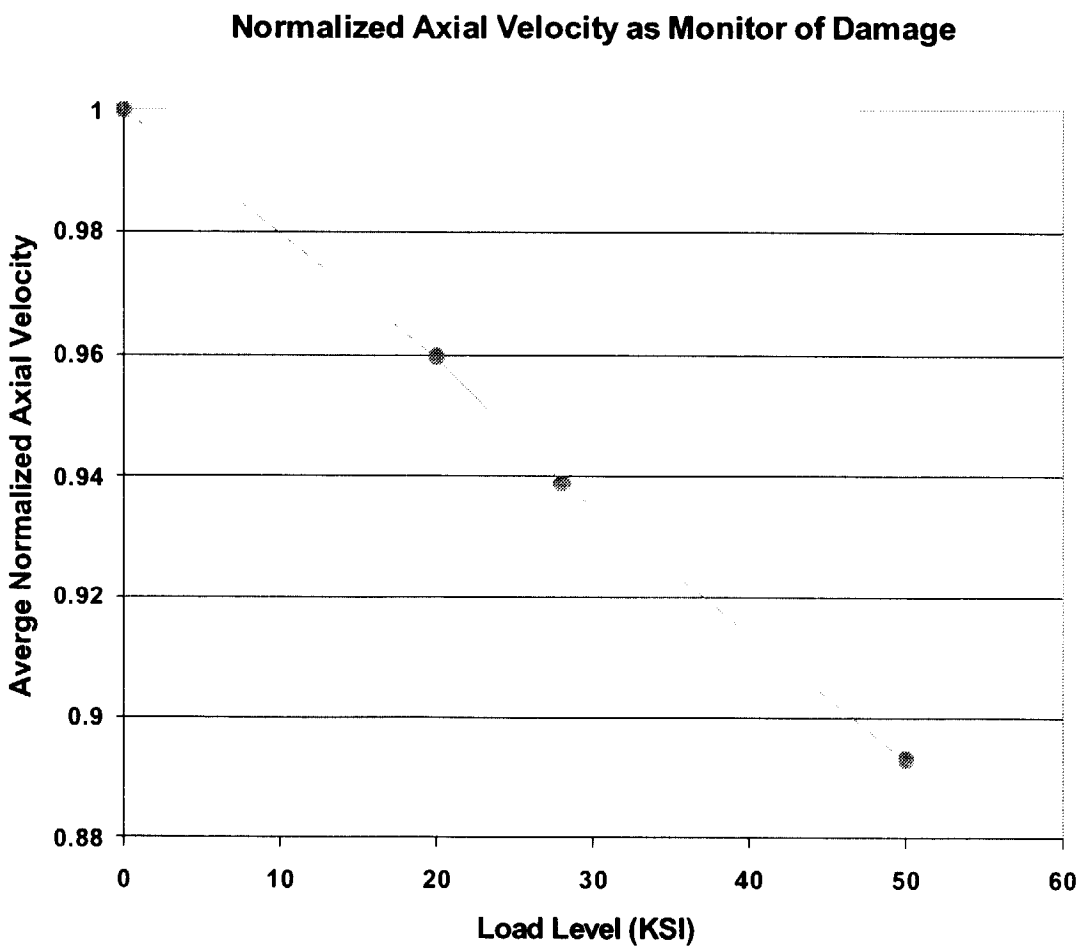

Ideal Goal

Old Way → New Way in Future

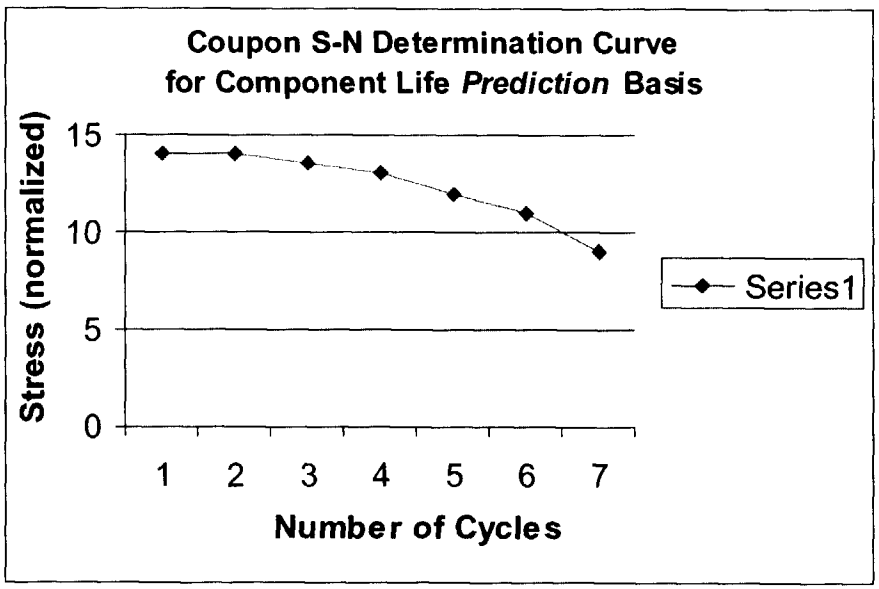

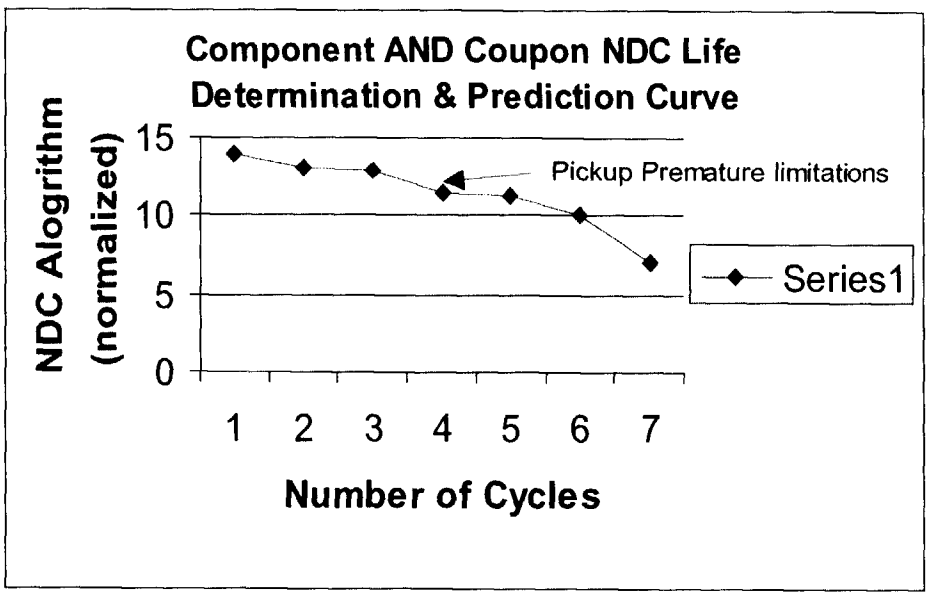

- NDC algorithm consist of:
  - Original Material Quality:
    - Computed Tomography (density/fiber architecture map), conventional coupon property baseline, NDC degrading baseline data
  - Degrading material properties and characteristics consist of:
    - Specific diffusivity, temperature capability (composition), density, strain, geometry, damping capacity, resonant frequency, modulus, etc.

Potential Payoff

- Increase Safety and Decrease Costs
  - Real-time life determination of component (not predicted)
    - Know component's integrity and health condition at any point in time.
    - React/respond real-time to FOD, overstress, and similar type events
  - Degraded residual life prediction (i.e. forecast) for component
    - Don't retire component prematurely
    - Don't conduct unnecessary disassembly inspections (thus decrease wear on other components and decrease turnaround time and cost)
    - Know that FOD & overload events may decrease life x%
  - Integrate health monitoring and control units into one control system--translates in to weight and complexity savings

Phenomena that are Necessary to be Accounted For:

- Mechanical
  - Initial inelastic strain
  - Progressive inelastic strain
  - FOD
  - Fatigue wear of fibers and matrix
  - Off nominal stress exposure
- Environmental
  - Thermal Shock
  - Oxidation
  - Erosion
  - Surface chemistry
- Combined Mechanical and Environmental Conditions
  - Creep/stress rupture (aka stressed-oxidation)
  - Thermal Mechanical Fatigue

Possible Means to Account for Real-time events

- Possible real time detection devices and quantifiable data:
  - Lasers
    - strain, emissivity, temperature, FOD events, dimension changes, off gassed particle velocity, species and amounts
  - Thermography
    - specific diffusivity, density, crack growth
  - Vibro-acoustics
    - specific damping capacity, resonant frequency, modulus
  - Optics
    - FOD events, dimensional changes, temperature
  - Sensors (strain, thermocouples, pressure, surface mount, remote, embedded, existing health monitoring data, etc.)
    - strain, modulus, temperature, on-set of corrosion, electrical resistivity

Specific Technique Data Gathering Already Demonstrated

Means of Detection	Detectable Data and Events Claimed in Abstracts	Source/Reference
Acoustic emission	Real-time CMC damage correlated to load/unload stress-strain	Luo, Jyi-Jiin, et. al. Rev, of Prog. Quant. NDE, 13A, 1994.
Acousto-ultrasonic	Real-time fatigue damage	Tiwari, Anil et. al., Nondes. Char. Of Mater., Jan 1994
Electro-optical biaxial displacement follower	Real-time displacement, velocity, acceleration	Optometrix, West Haven CT
Impact Acoustic Resonance	Specific damping capacity	Shiloh,K et. al, Trends in NDE Sci. Tech., Jan 1997
Acoustic Resonance-Modal analysis	Resonant frequency	Papazoglou, V.J., et. al., Applied Comp. Materials, 3, 1996.
Embedded Sapphire Fibers	Structure (?)	El-Sherif, Mahmound et. al, Nond. Eval. Of Mtls. and Comp. Dec. 1996
Impact Acoustic Resonance	Porosity	Shiloh,K et. al, Trends in NDE Sci. Tech., Jan 1997
Impact Acoustic Resonance	Interlayer fiber orientation	Shiloh,K et. al, Trends in NDE Sci. Tech., Jan 1997
Pulse echo ultrasonic Time-of-flight	Microstructural gradients (pore fraction, density, fiber fraction, chemical variations)	Roth, Don, Mater. Eval. 56,9, Sept, 1998.
Ultrasonic	Stress-strain curve reconstruction	Baste,Stephane, et. al. Jan 1996, J of Comp. Mtls.
Pulse-echo thermal wave	Density and disbonds	Khandelwal,P. et al, 21st Ann. Conf. Comp., Adv. Cer., Mtls. & Struct.-B, 1997
Air-coupled ultrasound & Thermography	Delaminations and density gradients	Pallai, T.A. et. al, 21st Ann. Conf. on Comp. Adv. Cer., Mtls., & Struct.—B, 1997
Laser Speckle	Strain & displacement	Dixon,G.J., Laser Focus World, June 1998

Specific Technique Data Gathering Already Demonstrated (con't)

Means of Detection	Detectable Data and Events Claimed in Abstracts	Source/Reference
X-ray Diffraction	Residual stresses	Proto Inc., Detroit MI
Resonant frequency	Bulk and shear moduli, and poison's ratio	Quatrosonics, Inc., Albuquerque, N.M. (Am. Cer. Soc. Bul, 74, 11, Nov. 1995)
Ultrasonics	9 stiffness coefficients	Baste, Stephane, Rev. of Prog. In Quant. NDE, 1995
Dynamic mechanical resonance	Thermal Shock (crack damage)	Singh, Raj, et. al. Trends in NDE Sci Tech., Jan 1997
Resonant Ultrasound Spectroscopy	Thermal Shock (crack damage)	Singh, Raj, et. al. Trends in NDE Sci Tech., Jan 1997
Laser	Emissivity	The Pyrometer Inst. Co.
Ultrasonics	Oxidation (flow rates & temps)	Chu, Ya-Cherng, et al. Am. Cerm Soc., 78,7, Jan 1995
Ultrasonics	Oxidation (time, temp, and flow)	Chu, Y et. al. Rev. of Prog in Quant. NDE, 13B, 1994.
Differential Thermography	Crack progression	Camden, M.P. et. al., 5th Inter. Conf. on Comp. Enger., July, 1998
Electrical	Electrical resistance	Maile,K. et. al, 5th Inter. Conf. on Comp. Enger., July, 1998

Modeling Using NDC data

- "Disturbed State Constitutive Modeling Based on Stress-strain and Nondestructive Behavior,"
  - Desia, Chandra et. al, Int. J of Solids and Struct. 33,11, 1996. (predict remaining life)

- "Modeling Mechanical Response of SiC/CaS-II Ceramic Composite under Quasi-Static Loads using a Real-Time Acousto-Ultrasonic NDE Technique,"
  - Tiwari, Anil et. al, J of Comp. Mtls., 29,13, 1995.

NDC Life Determination Scenario

- Baseline NDC data with laboratory coupon data.
  - Ultimate strength/strain of materials, etc./extrapolate with micromechanics
- Establish state of material with CT and thermography
  - I.e. map density, actual processed geometry (could be a little different than design), and specific diffusivity
- Overlay material properties on CT map as function of density, preform, compositional specifics, etc.
  - Could have functionally graded preform of fibers and/or matrix
- Overlay inhibited matrix requirements
- Overlay different event scenarios discretely on image
  - Failure scenarios at a turbine blade root and blade edge are different
- Use real time techniques to monitor damage accumulation progression and events.
- Couple events monitored with NDC to discrete algorithms in model to determine life and residual life of the component

Scenario

Where Computed Tomography is now calibrated to determine density, calibrate it in the future such that other NDC data, coupon property data, and degradation/damage event scenarios can be discretely mapped on to each layered image. This could be the basis of the NDC Life Determination model. As NDC properties are fed into the model real-time, then the component lifetime adjusted as appropriate.

High density indicated by C/C density blocks currently.

In future, the red could indicate mechanical fatigue of 1 million cycles after reducing NDC data on to the CT file.

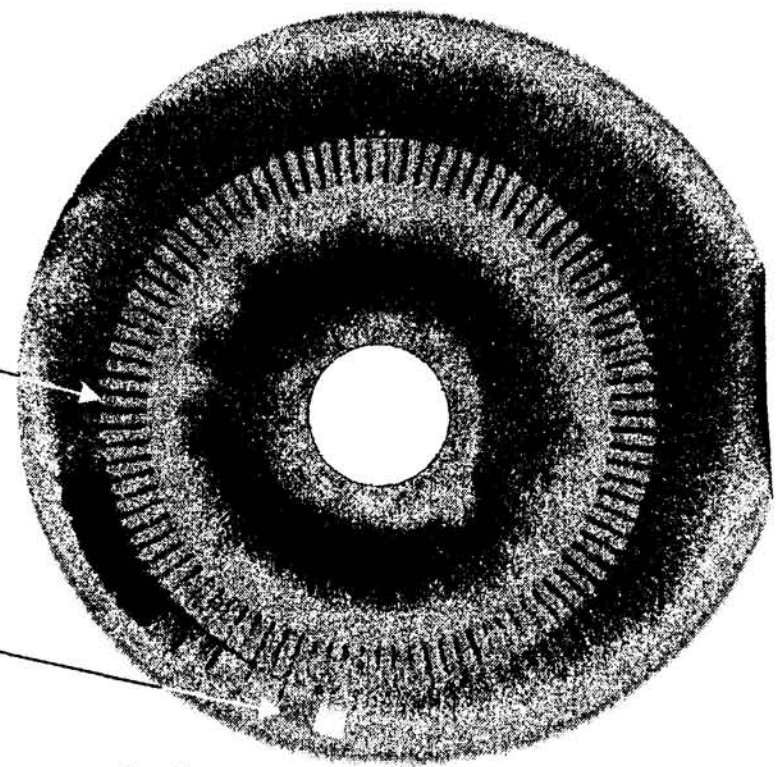

Polar C/SiC blisk prior to tubopump testing

Challenges

- Detecting all types of material degradation
  - Might not have NDC tools to detect all means of degradation
- Distinguishing between different types of degradation
  - e.g. If thermography is used, then is the change in signal from oxidation of the surface layer or microcracking
- Developing an algorithm which accurately reflect all aspects of CMC life
- Miniaturization of NDC equipment for flight hardware
  - Some equipment might not be feasible for flight
- Case, E.D. claims one property can be related to others for microcracked materials. Therefore, can different degraded material/damage states be accounted for?
  - Correlation of electrical conductivity, thermal conductivity, thermal diffusivity, and elastic modulus for microcracked materials
    - 23rd Ann. Conf. On Comp., Adv. Cer., Mtls., and Struct.: A 1999
- Formation into a design tool

NDC Life Determination and Prediction Justification (Pull)

- Models today don't always predict failure (have to go in and modify model after failure)
- Models are not run on all conditions
  - Off nominal and exact usage profiles
- Changes in design, real-time changes by mechanics, and differences in part print and part fabricated dimensions
- Parts wear out when they should not
  - If use 0% safety margin, then metal parts will fail before or after prediction--i.e. after all these years, we still can't accurately predict when metals will fail.
- Don't understand environment the parts are exposed to
  - Transient, nominal (temperature, gas composition, and their gradients, thermal & mechanical interactions, etc.), off nominal

AND this is for Metals…we have to be kidding ourselves if we expect to predict the life of CMCs using the same philosophies used in attempting to predict life for metals.

Conventional Life Prediction Success

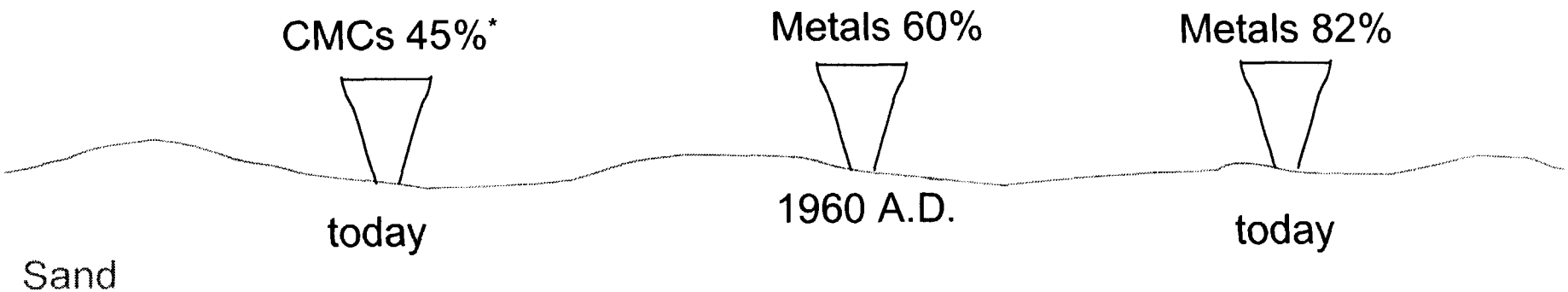

Physics based life prediction is a stake in the sand.

*Notional numbers

Life Modeling Assumptions

- Conventional Physics Based (Reactive--stake in sand)
  - Properties of coupons correlate to components
  - Know environment component is exposed to
  - Part matches print
  - No gross changes in shape with time
- Nondestructive Life Determination and Prediction (Responsive--able to change to with time and adjust to operational nuances and true exposure conditions)
  - Detect, discern, and account for all damage modes of material

Physics based life prediction is base upon:
assumption upon assumption, and assumption upon assumption--thus large safety factors required.

Summary

- Idea put forth for NDC generated Algorithm-N curve to replace a S-N curve
- A scenario for NDC life determination has been proposed
- Challenges are many for NDC Life Determination and Prediction, but could yield a grand payoff
- Justification for NDC Life Determination and Prediction documented

LOW-COST CERAMIC MATRIX COMPOSITES

W. Kowbel
MER Corporation
7960 South Kolb Rd
Tucson, AZ 85706
520-574-1980
kowbel@mercorp.com

C. Bruce, K.T. Tsou, and J.C. Withers
MER Corporation

Introduction

Despite their unique properties, ceramic matrix composite materials have found use in a very limited number of applications [1]. Current applications include rocket motor parts, turbojet parts and thermal structures for space planes and other space probes. These applications are virtually price-insensitive and are driven by the performance criteria. Numerous potential applications for continuous fiber ceramic matrix composites (CMC) have been identified including advanced heat engines, heat recovery equipment, burners and combustors, process equipment, waste incineration systems and separation and filtration equipment. However, for composites to successfully compete with other engineering materials, their cost must be substantially reduced. These costs are strongly influenced by lengthy composite processing technologies. It is expected that at least a 10 fold decrease in the CMC composite prices is needed to provide a significant penetration of commercial markets.

The processing methods for the manufacture of CMC composites are limited. The most common methods are:

i) Chemical vapor infiltration (CVI),
ii) Silicon melt impregnation and,
iii) Polymer impregnation and pyrolysis.

One major drawback of the isothermal CVI technique is that the infiltration process has to be interrupted a number of times to remove the external coating, which would otherwise prevent a complete infiltration. In summary, CVI offers a great flexibility to control the microstructure and resulting properties of CMC composites, but its application to low cost processing of CMC composites remains to be proven.

G.E. [2] and NASA Lewis [3] have developed CMC composite consisting of continuous SiC plus Si matrix produced by melt infiltration. These materials exhibit relatively good near net shape manufacturing, but poor matrix purity (due to residual silicon). The scale-up capabilities of this process compared to the established isothermal CVI method have not yet been shown. Thus, direct comparison with the CVI process is impossible. Kaiser Ceramic Composites [4] fabricated ceramic matrix composite using a polymer impregnation and pyrolysis process. Prototypes of various

structures such as gas deflection tubes, gas turbine combustors, turbine blades, fairing channels, duct sections and various engine parts were made via this process. Multiple impregnation and pyrolysis cycles are required to reduce the open porosity down to 10%. The manufacturing costs are effected by the lengthy processing and high cost of preceramic polymers. In addition, low matrix purity and crystallinity significantly limits the maximum continuous service temperature and adversely effect the through-the-thickness thermal conductivity. A direct comparison with the well-established CVI technique is not yet available.

Materials

Carbon-carbon (C-C) composites were used as a substrate. Flat C-C panels (10cm x 10cm x 0.2cm) were used. One-step fabrication process described elsewhere [5] was used to produce the C-C composites. C-C composites were fabricated using PAN-based carbon fabric and a thermoset-based resins with active fillers. A single heat treatment up to 2500°C was employed. The C-C composites were converted into C-SiC and SiC-SiC composites via Chemical Vapor Reaction (CVR) process. The CVR-SiC matrix was produced via SiO gas reaction with the carbon matrix as described elsewhere [6].

Evaluation/Characterization

SEM was used to examine the uncoated and coated composite cross section. Flexural strength was performed using a 4 point bending test with a 40:1 span-to-depth ratio. Tensile strength was obtained using dogbone shaped specimens. SEM was used to evaluate composite cross sections. Thermal diffusivity was measured with the laser flash method.

Results and Discussion

Low-Cost C-C Composites

Conventional C-C composites suffer from excessive cost ($1000 - $10,000/kg), lengthy processing time (1 - 6 months) and transverse matrix cracking. A one-step process (developed by MER [5] with a 1 day processing time) can yield C-C composites exhibiting very good mechanical properties, Table I. Very good tensile strength is obtained (280 MPa) combined with a non-brittle behavior. Virtually no transverse cracking is observed, Figure 1.

Table I. Summary of Physical and Mechanical Properties of C-C Composites

Composite Type	Density (g/cc)	Open Porosity (%)	Flexural Strength MPa (ksi)	Strain To Failure	Tensile Strength MPa (ksi)	Tensile Strain to Failure (%)	Shear Strength MPa (ksi)	KIC MPa-m$^{1/2}$
MER (C-C)	1.65	8	350(51)	0.55	280 (40)	0.3	12.5(1.8)	9
ACROSS	1.75	8	120(17)	0.2	105(15)	0.2	12.5	8
C-CAT	1.65	10	210(30)	0.2	210(30)	0.2	7(1)	5

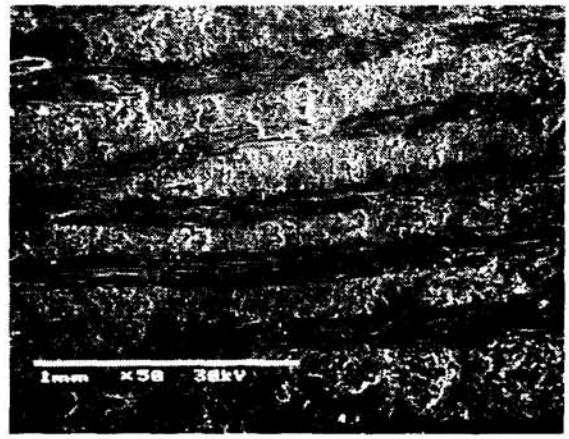

Figure 1. Cross-section of low-cost C-C composite.

CVR-SiC Fibers

Figure 2 shows the single fiber tensile strength values for single fibers extracted from T-300 1K 8HS fabric. Good strength retention (about 1.5 GPa) was attained for about 90% CVR-SiC converted fibers. A 100% CVR-SiC converted fiber was obtained, but the tensile strength was difficult to assess (increased stiffness).

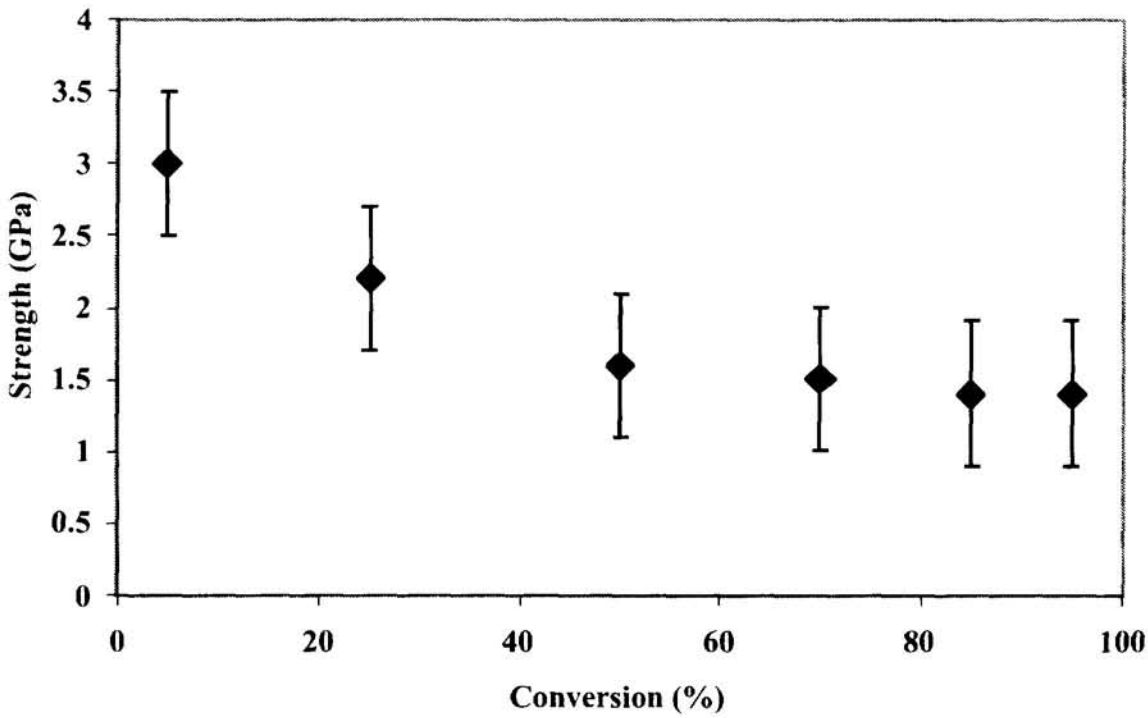

Figure 2. Single fiber strength versus SiC conversion.

The tensile strength of these fibers needs to be assessed on the basis of their heat treatment history.

The 1.5 GPa tensile strength corresponds to a heat treatment in excess of 1700∘C. Figure 3 shows the corresponding SEM micrographs (95% SiC conversion). Minimum cracking is observed at this conversion level. It is worth mentioning that for this heat treatment temperature, Nicalon S type fiber would exhibit a similar strength.

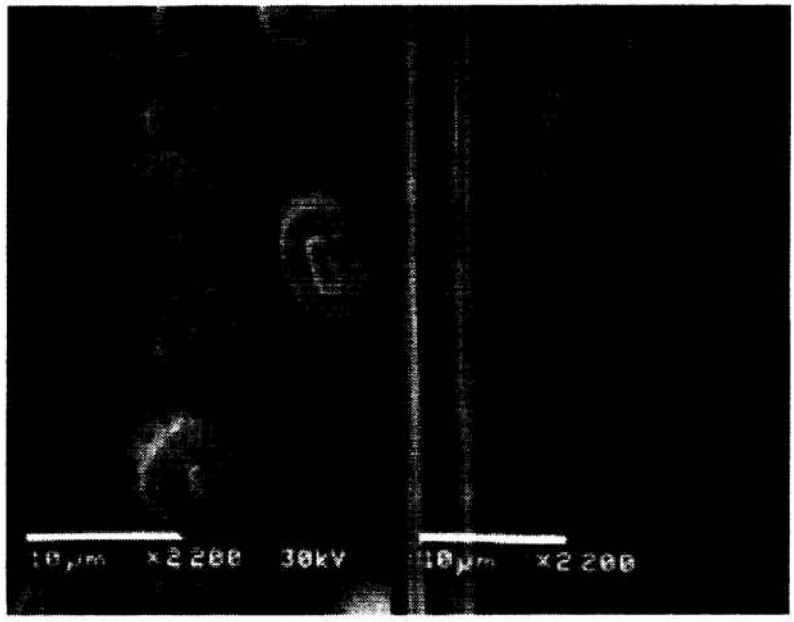

Figure 3. SEM Micrograph of 95% CVR-SiC.

This new processing scheme for C-C composites offers a potential to revolutionize low-cost processing. In principle, the processing is suitable for both fabric and fiber-tow reinforcement. The process is polymer-based (very low cost matrix precursors) and involves a single heat treatment. A combination of these factors yields a process capable of producing high quality C-C composites, at a cost below $100/kg.

CVR SiC Composites

Figure 4 shows a SEM micrograph of CVR-SiC matrix following isothermal air oxidation at 800°C. The residual carbon core of the carbon fibers was removed by oxidation. The CVR-SiC conversion is primarily confined to the matrix with limited reaction converting the graphite fiber to SiC. The CVR-process can be optimized to control the amount of the composite/matrix conversion. The ability of the CVR process to primarily convert the carbon matrix results from markedly different conversion rates exhibited between the carbon fiber and matrix. The higher porosity of the matrix and its activity results in a significantly higher conversion rate.

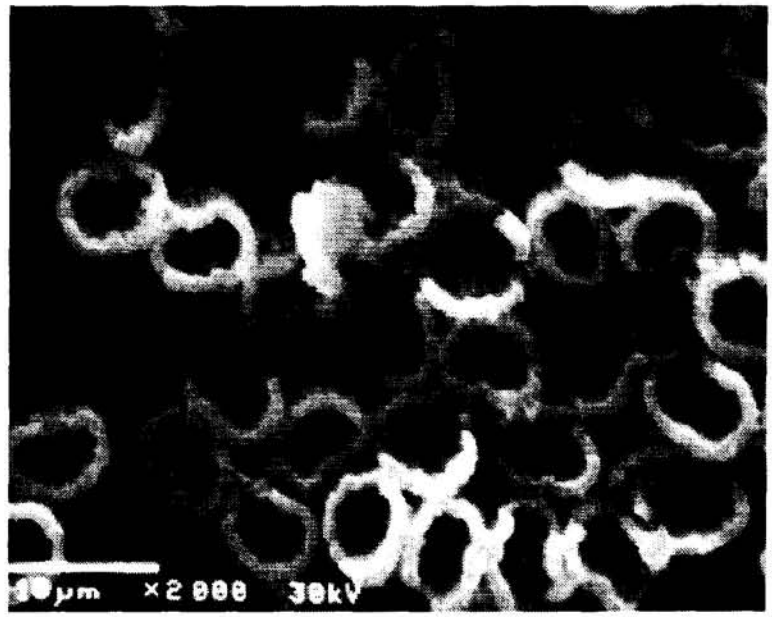

Figure 4. SEM of CVR C-SiC composite after oxidation.

Figure 5 shows the cross section of the C/CVR-SiC composite. No matrix delamination is observed.

The CVR process has several significant advantages over Si-melt infiltration, including:

i) The ability to produce pure α-SiC matrix
ii) Scaling-up capabilities
iii) Gas phase reaction
iv) Low cost
v) Minimum volume change

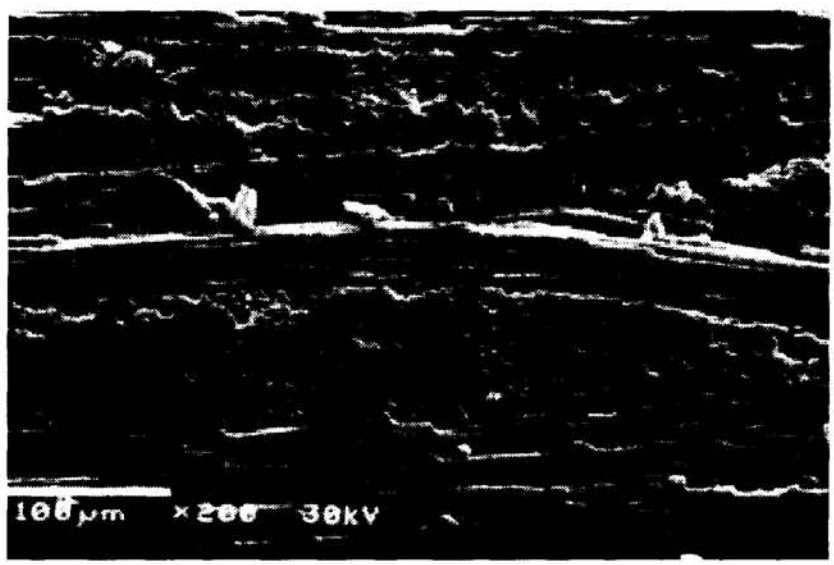

Figure 5. Cross section of a C-SiC composite.

CVR-SiC/CVR-SiC composites

Proper control of the CVR-SiC conversion can lead to the formation of CVR-SiC/CVR-SiC composites. As the conversion process progresses, the carbon fibers become converted to CVR-SiC, Figure 6. The conversion process can be controlled to obtain 100% overall conversion (both the carbon matrix and fibers are completely converted into CVR-SiC).

Figure 6. SEM of CVR SiC-SiC composite after oxidation

Figure 7 shows a cross section of the CVR-SiC/CVR-SiC composites (100% SiC conversion). No matrix delamination is observed.

Figure 7. Cross section of a SiC-SiC composite.

Interfacial Properties

The interface between the fiber and matrix plays a key role in determining the properties of the ceramic matrix composite (CMC). The sliding resistance or shear strength at the interface plays an important role in governing the rate of load transfer from the fiber to the matrix. If the fiber is bonded too well to the matrix, the load is carried into the matrix and brittle failure occurs. If the interface between the fiber and the matrix is weak, then the crack is deflected along the interface and fiber pull-out increases. If the interface is too weak, no load is transferred and the composite becomes weak. For conventional state-of-the-art SiC-SiC composites, interfacial coating such as graphite and boron nitride have been used. But these interfacial coatings oxidize easily and cause additional problems.

Figure 8 shows the fracture surface of a CVR-SiC/CVR-SiC composite. Good fiber pull out is observed combined with no apparent damage to the fiber. Thus, the CVR process conditions, up to 100% SiC conversion of the graphite fiber, can be adjusted to produce high quality SiC-SiC composites exhibiting good mechanical properties and low-cost. The key finding is that significant fiber pull out is observed at the 100% SiC conversion, Figure 8. This result represents a milestone in the area of SiC-SiC composite processing. Good fiber pull-out is observed with no interfacial coating. Thus, a 100% β-SiC/β-SiC composite was produced exhibiting good mechanical properties. In addition, no damage is observed on the 100% CVR-SiC fiber, Figure 8, converted in-situ.

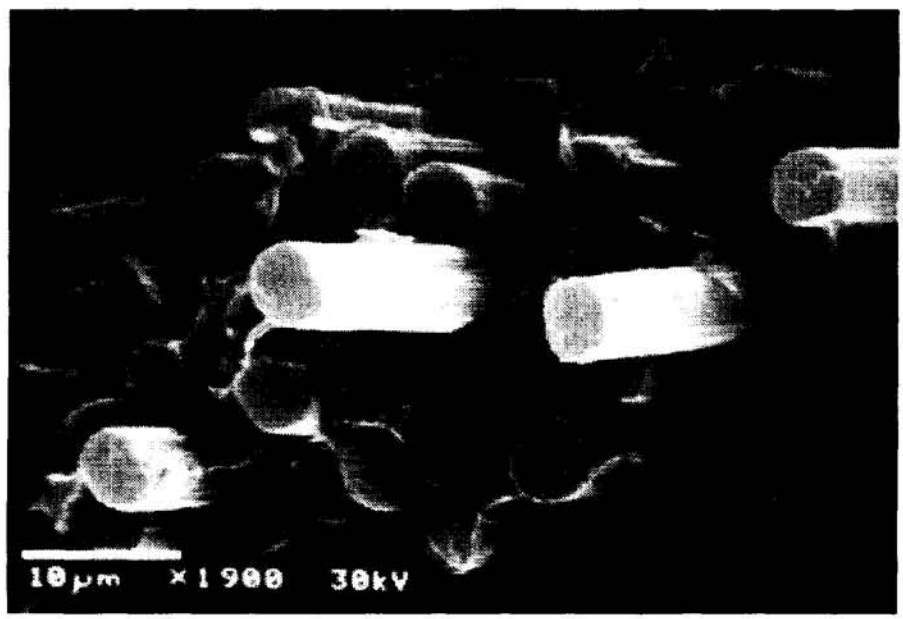

Figure 8. Fracture surface of CVR-SiC/CVR-SiC

Table II shows the properties of CVR-SiC composites as compared to CVI and PIP-based SiC composites.

Table II. Properties of different composites.

	SiC-SiC			C-SiC		
	CVR	CVI	PIP	CVR	CVI	PIP
Proportional limit (MPa)	122	95.2	108	149	149	163
UTS (MPa)	170	204	238	204	238	272
Modulus (GPa)	108	136	149	122	149	170
Shear strength (MPa)	27.2	34	34	23.8	27.2	30.6
Thermal Conductivity RT (W/mK)	80	10	15	40	10	12
CTE (ppm/K)	3.0	4.0	3.5	2.0	2.5	2.8

The key properties for structural applications of C-SiC and SiC-SiC composites is the proportional limit (at least 20 MPa comparable or better than the state-of-the-art composites) and thermal conductivity (at least 80 W/mK compared to 10 W/mK for the CVI SiC-SiC composites). The enhanced thermal conductivity offers a significant potential in engine-related applications.

Cost Analysis

Table III shows the cost analysis of the CVR-SiC/CVR-SiC composites. The cost of $200/kg is believed to be achievable at a moderate production rate. This cost analysis underscores the great market potential of this technology. Stinton [7] performed a composite cost analysis of the CVI-SiC matrix and estimated the composite cost at about $10,000/kg. Thus, this novel CVR process has a potential for a 50 times reduction in the manufacturing cost of C-SiC composites. This accomplishment could provide for significant market penetrations.

Table III. Cost Analysis

	Net Cost ($/kg) Fiber Tow Type
Raw Materials	$118.80
Supplies	$8.80
Utilities	$3.70
Labor	$44.00
Burden	$46.28
Total (without profit)	$221.58

Conclusions

Low-cost C-C composites offer potential as a precursor to fabricate C-SiC and SiC-SiC composites at greatly reduced cost. The CVR process can be controlled to convert primarily the carbon matrix leading to the formation of C-SiC composites. Adjustment of the CVR process conditions results in good mechanical properties of C-SiC. In addition, the CVR process can be adjusted to convert both the fiber and the matrix.

References

1. J.W. Finley, "Applications of High Temperature Composites," NASA CP 4552, (1993).
2. G.S. Corman, "Properties Melt-Infiltrated SiC-SiC Composites," SAMPE International Symposium, 39(1997)2300
3. A. Schweda, "Properties of PIP-Derived SiC-SiC Composites," SAMPE International Symposium, 39(1997)1781
4. M. Singh, "Effect of Carbon Preform Pore Volume and Infiltrants on the Composition of Reaction-Formed Silicon Carbide Materials," Journal of Materials Synthesis and Processing, 2 (1994)117-123.
5. W. Kowbel, V. Chellappa & J.C. Withers, "Properties of One-Step Composites," Carbon, 34(1996)819
6. W. Kowbel, et al, "Properties of CVR-Derived SiC-SiC Composites," Journal of Nuclear Materials 217(1995)2
7. D. Stinton, "Cost Analysis of CVI Processing," MRS Proceedings, 65(1995)393

Fabrication and Testing of Ceramic Matrix Composite Rocket Propulsion Components

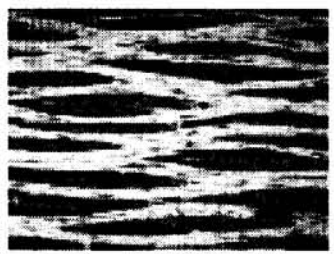

Michael R. Effinger, R.G. Clinton, Jr., Jay Dennis, Sandy Elam, and Gary Genge
NASA Marshall Space Flight Center

Andy Eckel, Martha H. Jaskowiak, J. Douglas Kiser, Jerry Lang
NASA Glenn Research Center

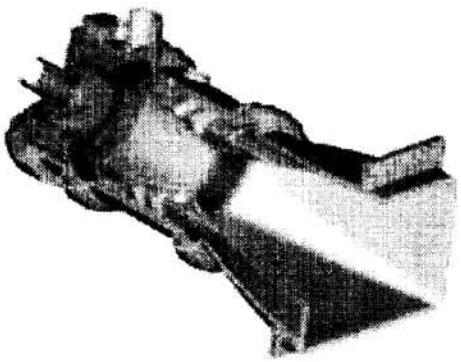

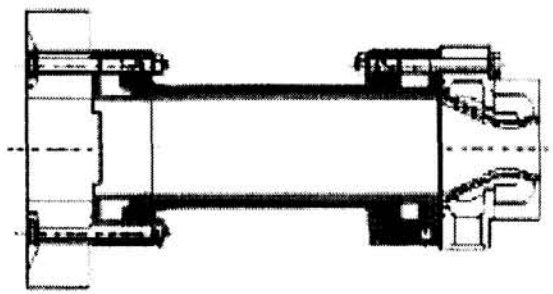

Acknowledgements

- The authors are very grateful for the outstanding expertise the following colleagues and organizations contributed to make this presentation possible:
  - CMC Blisk program members:
    - Shayne Swint (Program Manager), Kathy Mims (Program Coordinator), Eric Earhart, Wayne Gregg, Don Harris, Jose Roman, Ward Overton, Ricky Wilbanks, Ron Beshears, Mike Effinger, Gary Genge, John Forbes, Matt Marsh--all MSFC, & Doug Kiser--GRC
    - Participating Organizations: Southern Research Institute, Honeywell Advanced Composites Inc., White Sands Test Facility, Argonne National Laboratory, Oak Ridge National Laboratory, Test Devices, Lockheed Martin Corporation, University of Alabama at Huntsville, Louisiana Tech University, University of Illinois at Urbana Champaign
  - Gas Generator program members
    - Janos Borsody (Program Manager), Jerry Lang, Andy Eckel, Jay Singh, Roy Sullivan, Ted Kovacevich--GRC, Jay Dennis, Andy Hissam, Hai Nguyen, Leigh Ann Perkins, Rene Ortega, Doug Fox, Jeff Lackey--MSFC
    - Participating Organizations: Honeywell Advanced Composites Inc., Rocketdyne Division of Boeing, Materials Research and Design
  - Nozzle Ramp program members
    - Corky Clinton--MSFC, Andy Eckel--GRC, David Glass--LaRC
    - Participating Organizations: Rockwell Science Center, Honeywell Advanced Composites Inc., Refractory Composites Inc., Snecma/SEP, Rocketdyne Division of Boeing
  - Thrust Cell program members
    - Sandy Elam, Mike Effinger, Pete Valentine--MSFC, and Martha Jaskowiak, Andy Eckel--GRC
    - Participating Organizations: Rocketdyne Division of Boeing, Hyper-Therm, Inc., Ceramic Composites, Inc.

Presentation Agenda

- NASA's Goals
- Benefits of CMCs
- Simplex CMC Blisk Testing
  - Simplex CMC Blisk Follow-on
- CMC Cooled Nozzle Ramp Program
- Cooled Thrust Chambers
- C/SiC Gas Generator
- Summary

Enterprise Goals

GOALS: Earth-to-Orbit

- **Within 10 years,**
  - **Increase the safety by two orders of magnitude**
  - **Reduce the cost to NASA transportation of placing payloads in orbit by one order of magnitude.**
- **Within 25 years,**
  - **Increase the safety by four orders of magnitude.**
  - **Reduce the cost of placing payloads in orbit by two orders of magnitude.**

GOALS: In-Space Transportation

- **Within 15 years,**
  - **A factor of ten reduction in the cost of Earth orbital transportation.**
  - **A factor of two to three reduction in propulsion system mass and travel time required for planetary missions.**
- **Within 25 Years,**
  - **Enable bold new missions to the edge of the solar system and beyond by reducing travel times by one to two orders of magnitude.**

Generations of Reusable Launch Vehicles

Today: Space Shuttle
1st Generation RLV

- Orbital Scientific Platform
- Satellite Retrieval and Repair
- Satellite Deployment

2010: 2nd Generation RLV

- Space Transportation
- Rendezvous, Docking, Crew Transfer
- Other on-orbit operations
- ISS Orbital Scientific Platform
- 10x Cheaper
- 100x Safer

2025: 3rd Generation RLV

- New Markets Enabled
- Multiple Platforms / Destinations
- 100x Cheaper
- 10,000x Safer

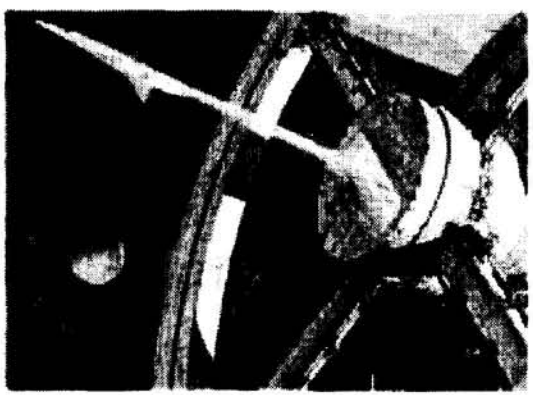

2040: 4th Generation RLV

- Routine Passenger Space Travel
- 1,000x Cheaper
- 20,000x Safer

Advanced Space Transportation Investment Areas

	Pillar 3					
			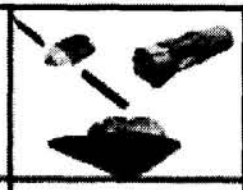	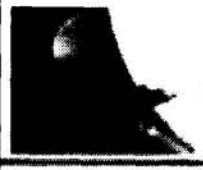	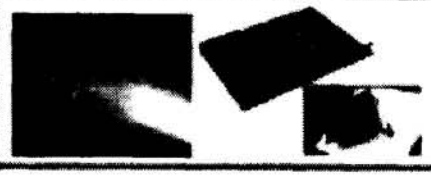	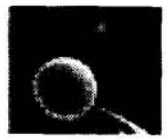
Goal	Earth-to-Orbit	Earth-to-Orbit	In-Space	In-Space	Earth-to-Orbit	Earth-to-Orbit & In-Space
Investment Area	Small Payload Focused	RLV Focused	In Space Focused	Interstellar Precursor	Space Systems Base	Space Transportation Research
Projects	Fastrac Bantam	Propulsion Airframe	Low Cost Upper Stages Electric Advanced Cryo Tehthers Non-toxic	Sails Electric	Propulsion Airframe TPS IVHM Operations & Range Vehicle Systems	4th Generation Launch Omniplanetary Interstellar

- Provide the basic building blocks of propulsion, airframe, TPS, IVHM and operations technologies to meet space transportation system goals
- Mature technologies toward flight demonstration and advanced development
- Provide technology focus for future generations of space transportation systems
- Develop breakthrough concepts to enable missions that are currently not technically or economically feasible

Benefits of CMC Components for Space Transportation Propulsion Applications

- Ceramic matrix composite (CMC) components are being developed by NASA to ***enable significant increases*** in engine performance and safety, and to reduce costs.
- CMC components provide opportunities for pursuing 'Revolutionary Propulsion Concepts,' enabling new, higher efficiency systems that can operate at higher temperatures with increased safety.
- CMC components can enable the achievement of safety and cost goals as follows:
  - CMC components can increase the safety margin due to higher temperature capability and higher damping capacity, while minimizing system complexity (e.g.--elimination of need for cooling, fewer parts) and component and system weight.
  - Low density of CMCs can allow increased thrust to weight and minimizes effects on stability when material is lost from rotating components.
  - CMC components can decrease costs via higher temperature capability, low part count (example--integrally bladed disk), and increased component life.

Potential Space Transportation Propulsion Applications of CMCs

- **Turbopump and Combustion Components:** Blisks, stator/nozzles, gas path ducting, tip seals, combustors, inserted blades, and housings

- **Actively-cooled Components:** Nozzles (ramps, bells, extensions), combustion chambers (hot gas flow path), thrust cells, manifolds, and heat exchangers.

- **Uncooled Thin Wall Structures:** Nozzles (radiation cooled), combustion chambers, and manifolds/ducts.

The use of CMC components & systems is projected to be the only way, aside from design and system engineering, to *significantly* increase safety & reduce cost simultaneously, largely due to increasing temperature margins and operational temperature at the same time, *while* decreasing weight.

No other material can do this.

Simplex Turbopump C/SiC Blisk Program

Program Description

Goals

- Identify and solve issues related to using Ceramic Matrix Composites in Rocket Turbomachinery
- Take technology to TRL Level 6
- Transfer knowledge gained from the program to industry

Challenges

- Fabricate a disk 8″ in diameter
- Demonstrate that the material could withstand the vibrational loads seen in a transonic turbine
  - Thermal issues not addressed in this program

Simplex C/SiC Blisk Images

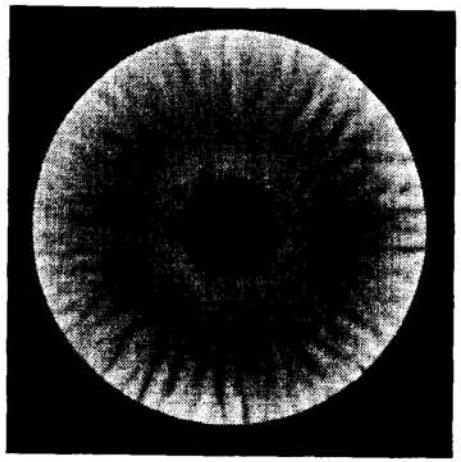

Computed Tomography image of polar CMC disk at mid-process

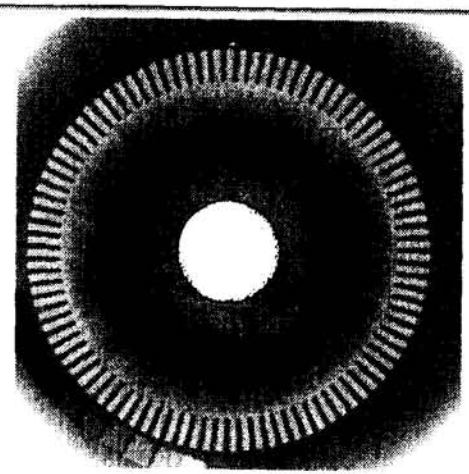

Computed Tomography image of polar CMC Simplex blisk

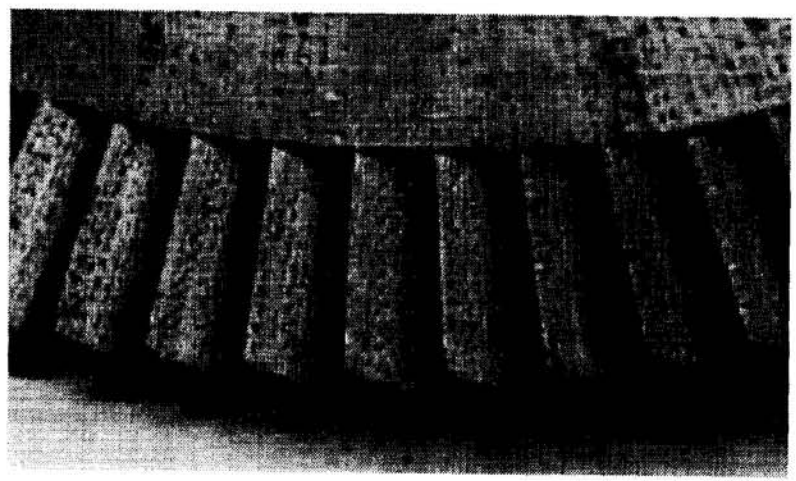

Nominal appearance of C/SiC blisk surface (Honeywell Advanced Composites, Inc.)

Simplex Turbopump C/SiC Blisk Program

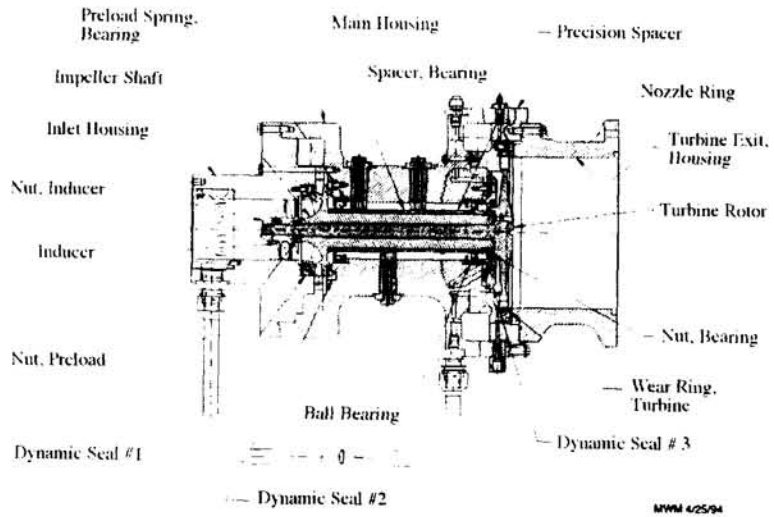

Simplex Turbopump in original baseline configuration

- Turbine Rotor replaced with C/SiC bladed disks (blisks).
- Two weave configurations tested
  - Polar Woven
  - Quasi-isotropic Lay-up

Simplex operating conditions

Parameter	Simplex Inlet
Temperature (F)	-250
Pressure (psia)	700
Flowrate (lbm/sec)	13
Speed (RPM)	25,100
Blisk Diameter (in)	7.6
Turbine Tip Speed (ft/Sec)	832

Simplex Turbopump Test Bed at NASA MSFC during chill down prior to testing.

Simplex Turbopump C/SiC Blisk Testing Results

Polar Blisk Test Summary

Test	Time (sec) > 24,000 rpm	Time (sec) > 20,000 rpm	Max Speed (rpm)
1 LN_2	0	0	0
2	0	57	20600
3	0	93	19400
4	0	136	20920
5	11	89	25390
6	169	279	25130
7	25	125	24700
8 LOX	183	297	24510
9	0	9	20140
10	197	293	24080
11	175	288	24090
12	187	285	24060
13	192	301	24100
13	1139	2252	

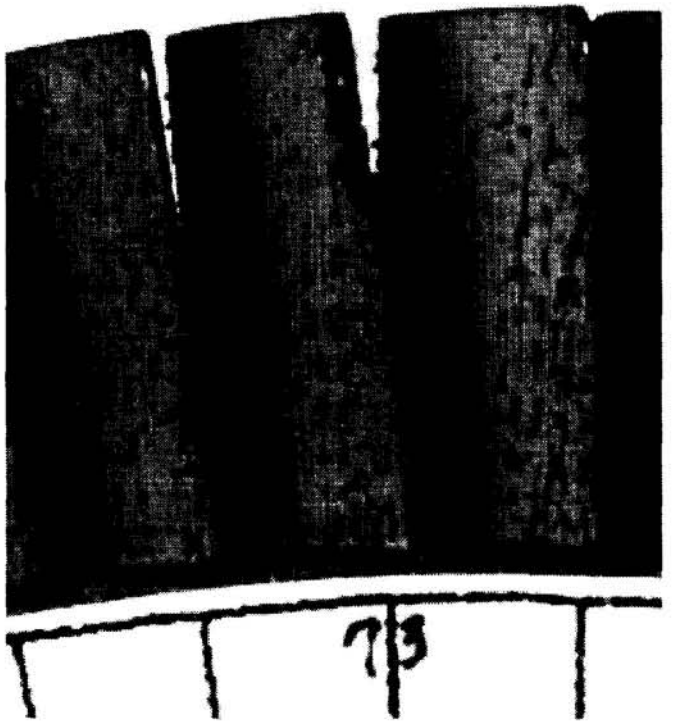

Worst Case Damage on Polar Blisk

Images of C/SiC Simplex Blisk Results

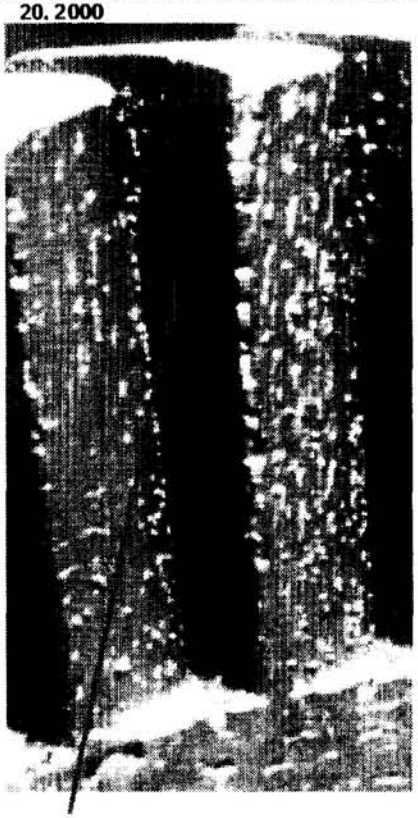

Cracked Polar Blade

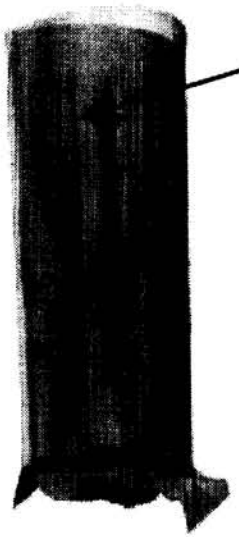

Portion of cracked polar blade discernable by computed tomography.

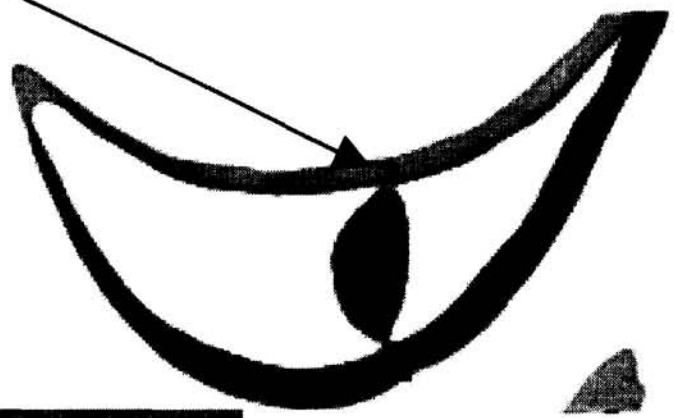

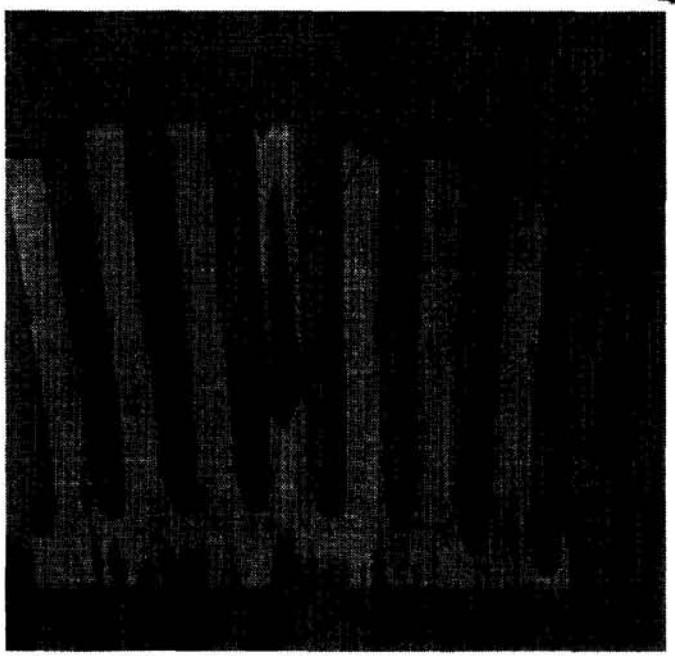

Simplex Turbopump C/SiC Blisk Testing Results

Quasi-Isotropic Blisk Test Summary

Test	Time (sec) > 24,000 rpm	Time (sec) > 20,000 rpm	Max Speed (rpm)
1 LN2	44	126.5	25490
2	169	260	25150
3	196	278	25180
4	189	266	25150
5	186	270	24920
6	199	278	25220
7 LOX	43.1	116	24690
8	226	300	24100
9	221	296	24080
10	244	309	24190
10	1717.1	2499.5	

- No through cracks found in Quasi-isotropic Blisk
- Damage to leading and trailing edges is extensive
  - 57 of 95 blades showed some damage visible by boroscope
  - Some leading edges show impact damage
  - 9 trailing edges almost completely gone

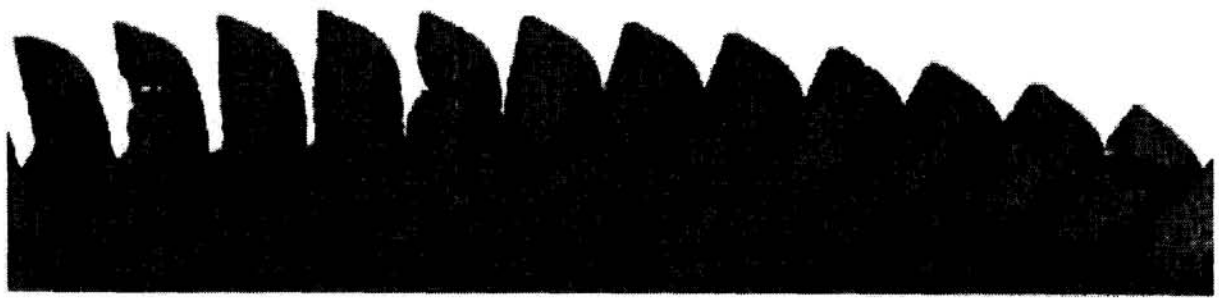

FOD impact pattern on Quasi-isotropic CMC blisk

Images of C/SiC Simplex Blisk Results

Crack

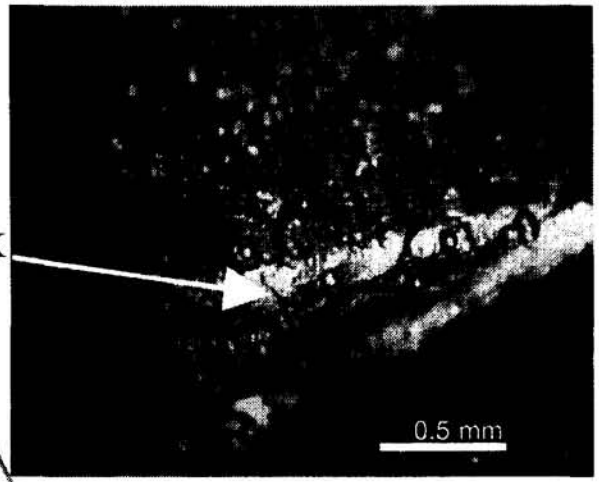

Crack at the blade root

Crack

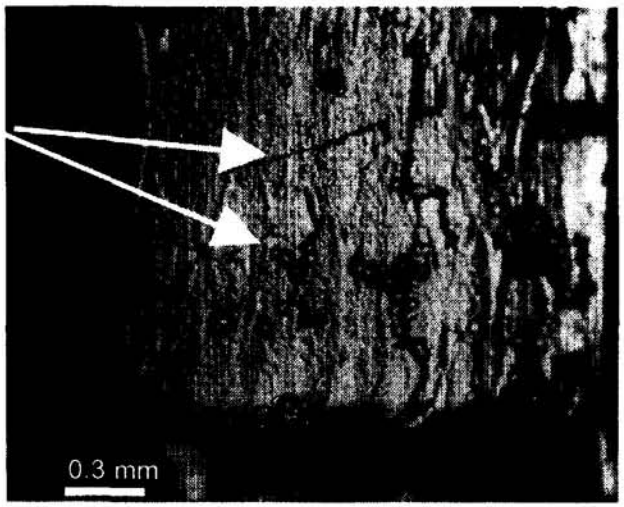

Crack on the suction side

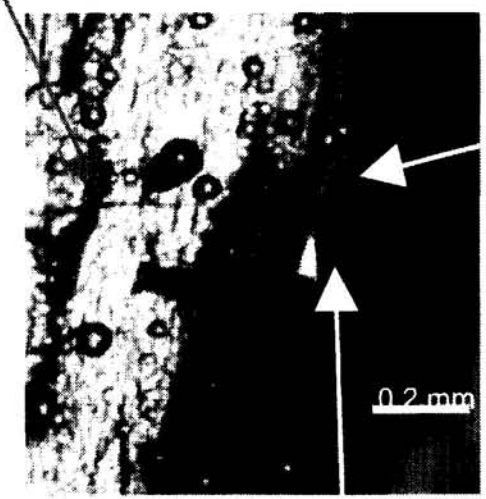

Spall edge

Typical spalling damage on the blade edges

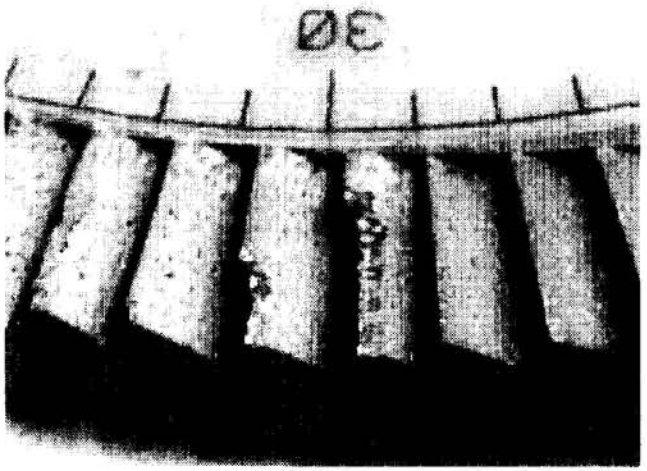

Typical trailing edge damage on the quasi-isotropic blisk

Simplex Turbopump CMC Blisk Program Accomplishments

- Manufactured 4 state-of-the-art C/SiC blisks
- 1st CMC blisk tested in a turbopump for a rocket engine
  - ~40 minutes test time and 5 million cycles for each C/SiC blisk, thus demonstrating the ability to withstand vibratory loading seen in turbopump
- CMC blisk operated nominally with loss of blade material and other less than desirable *a priori* conditions
- Successfully sustained FOD
- CMC computed tomography benchmarked at mid-process
  - Led to preforming improvements
- Blisk exposure to only mechanical and dynamic loads, and not thermal loads
  - Demonstrated value of Building Block Approach
  - Led to critical identification of mechanical and/or physical spalls and cracks which could limit lifetime
- 1st to acquire and publish CMC blisk damping data
- Nondestructive Characterization Life Prediction concept developed and established as a possibility (subject of AMPET Conference Paper in September)
- Executed an interagency cooperative effort with the Air Force through IHPRPT
- Benchmarked MSFC's structural & material analyses & component testing of a CMC component

Likely Future CMC Development Path

- Approaches to Technology development:
  - Building Block Approach (BLA)--a stepwise process for development of materials and processes based on general requirements, materials property testing, subelement testing, and then full-scale testing.
  - Build and Bust Approach (BUA)--design and build a part with a new material, test the component with little knowledge of the material that was being tested.
- Grounds for Successful CMC Technology Development: Combine the Build and Bust Approach with the Building Block Approach
  - Least costly in the long-term.
  - Most effective, efficient approach to technology development.
  - Avoids developing a material that may not be usable in the actual system configuration.
  - Avoids building and testing components and systems that fail, with little or no knowledge of what was actually being tested.
  - Apparent down side to **Combined Approach**: Need up front, long-term and substantial commitment (**8 to 10 years**) from Congress, management, and engineers.
    - Greater than the 2-6 year terms of Politicians and longer than most managers and engineers want to spend in one job nowadays.
  - Actual up side to Combined Approach: **Avoid** most likely what would happen is a BUA (2-4 yrs), followed by a 1.5 BLA (12-15 yrs) in series to yield a total (**14-19 year effort**).

Simplex Follow-On

- Objectives
  - Obtain additional data for correlation of natural frequency and damping changes to material degradation.
    - Coupon tests to be subjected to known load and cycles followed by Damping/Natural Frequency testing and subsequent tensile testing / microscopic inspection
    - Polar blisk to be run in the Simplex Turbopump for approximately 26 more tests. At midpoint of testing and at the completion of testing, Damping/Natural Frequency testing will be performed.
    - Blisk to be sectioned to determine damage accumulated and for comparison to tensile test coupon baseline material for correlation of NDE to material condition.
  - Demonstrate that the C/SiC blisk is capable of surviving the turbine conditions for the planned cycles.
  - Determine the impact on rotor stability of having material damping in the rotating system

NASA's High Risk, High Payoff Cooled Composite Nozzle Ramp

- **Objective:** Develop and demonstrate lightweight actively cooled composite material systems for potential use as nozzle ramps for the Aerospike engine.
- **Benefits**
  - Reduced weight relative to cooled metallic designs.
  - Higher operating temperature capability minimizes or may eliminate re-entry cooling requirements offering potential for additional weight reduction.
- **Schedule** -- 44 month project
  - 1st 12 months - Concept Development/Definition; 4 vendors.
  - Months 13-44 - single vendor to produce increasingly larger, more complex structures subjected to battery of thermal, mechanical, aeroconvective and acoustic tests.
  - Culminates in test of ~30"x60" test article in an aerospike test stand.

NASA's High Risk, High Payoff Cooled Composite Nozzle Ramp

Baseline Requirements and Environments

◆ **Cold Wall Heat Flux (optional arrangement)**	**Hot Wall (3000°F) heat flux**
✦ Maximum: 15 Btu/in^2-sec	• Maximum: 7 Btu/in^2-sec
✦ Average: 7 Btu/in^2-sec	• Average: 4 Btu/in^2-sec
◆ **Stagnation Gas Temperature**	**6000°F**
◆ **Maximum static gas pressure**	**50 psia**
◆ **Maximum shear load**	**5 psi**
◆ **LH_2 Coolant Inlet Pressure**	**Above 4000 psi**
◆ **Coolant Inlet to Exit Pressure Drop**	**Approximately 350 psid**
◆ **LH_2 Coolant Inlet Temperature**	**Below -300°F**
◆ **Coolant Flow Rate**	**0.8 lbm/sec per linear inch of width**
◆ **Inside ramp surface operating temperature**	**Thermal insulation may be required**

NASA's High Risk, High Payoff Cooled Composite Nozzle Ramp

- **Key technology challenges**
  - Heat exchanger weight:
    - Project Requirement is 2.0 lb/ft^2 (Project Goal is 1.5 lb/ft^2)
  - Manifolding of coolant channels
  - Hermeticity of coolant channels
  - Severe thermal gradients and thermal strain mismatches between hot surface and cryogenic coolant tubes
  - Lightweight attachment schemes for panels to support structure
  - Manufacturing scale-up to Large Scale Test Article (LSTA) 30" x 60" size
  - Subsequent scale-up to full scale Aerospike engine nozzle (beyond project scope)
    - Baseline ramp length: ~180"
    - Baseline ramp width: ~90"
    - Radius of curvature: 90" maximum

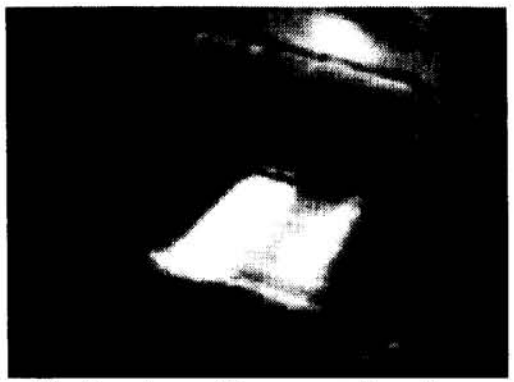

Refractory Composites Inc.

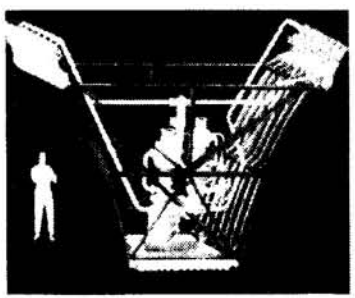

NASA's High Risk, High Payoff Cooled Composite Nozzle Ramp

- **Selected Vendors/Concepts**
  - Honeywell Advanced Composites

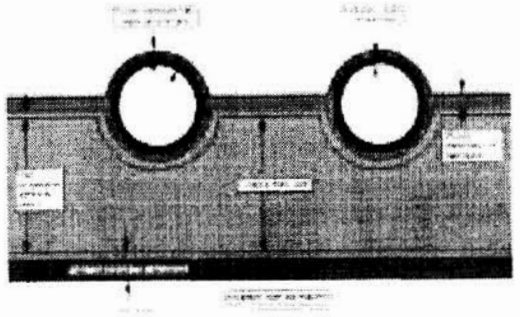

  - Refractory Composites Inc.

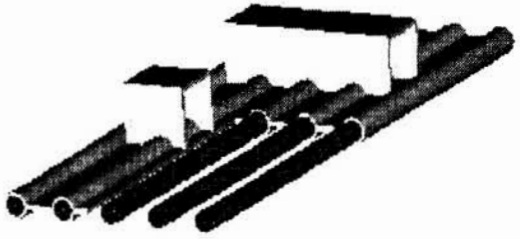

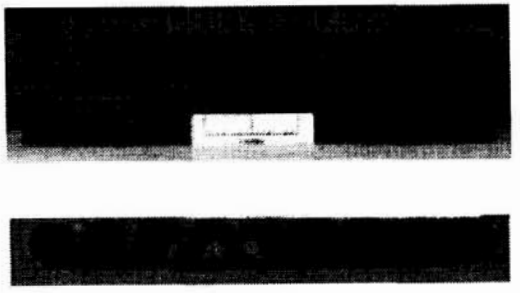

  - Rockwell Science Center
  - Snecma/SEP

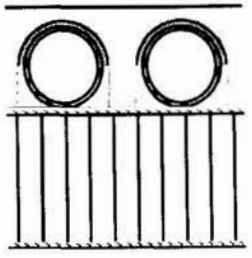

Actively Cooled Thrust Chambers

- **Objective:** Reduce weight, increase operating temperatures of current thrust chamber designs

- **Approach**
  - Address material & fabrication issues for baseline design
  - Develop potential actively cooled CMC materials with small fabrication units
  - Test each CMC unit in appropriate conditions Hot-fire testing planned at NASA-GRC:
    - GOX/GH_2 at Pc = 1000 psi (MR=6)
    - Durations = 5-250 sec
    - Coolant = LH_2

Baseline Design: X33 Thrust Cell

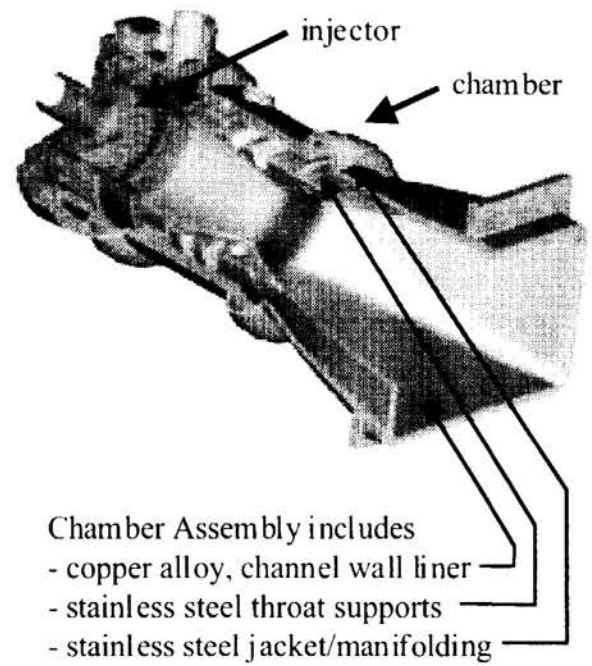

- **Challenges**
  - Acceptable permeability to contain hydrogen coolant
  - Appropriate manifolding for coolant supply
  - Oxidation resistance in hot thermal environment
- **CMC has Highest Weight, Cost, and Safety Payoff**
  - Replaces liner, throat supports, AND jacket/manifolds

Actively Cooled Thrust Chambers

- **Status**
  - Hyper-Therm, Inc.: SiC/SiC chamber with annular ring of woven coolant channels
    - Work initiated: July '99
    - Est. Completion Date: Sept '00
    - 3 complete preforms densified
    - Permeability testing planned
    - Leak checks & proof testing will be performed before delivery

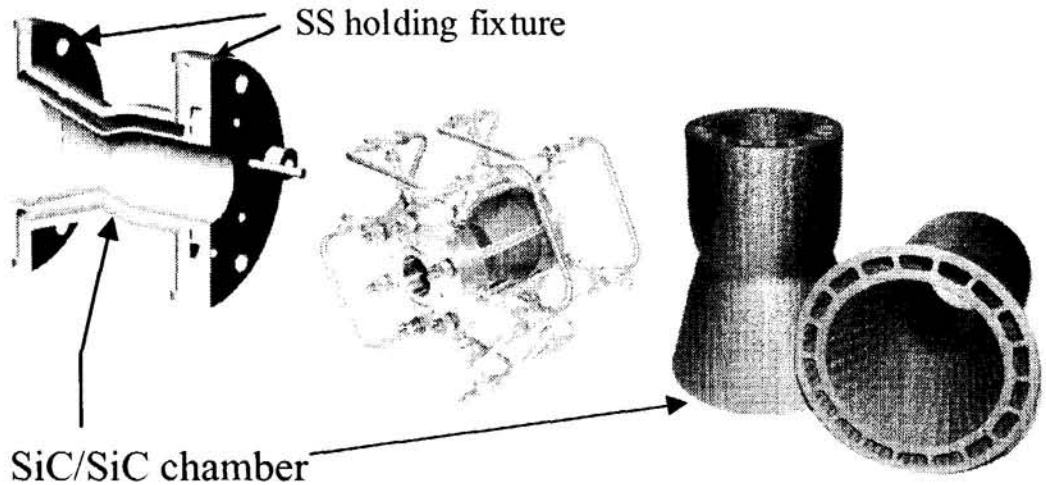

  - Ceramic Composites, Inc.: C/C chamber surrounded by copper tubing
    - Work initiated: July '99
    - Delivery Date: Sept '00
    - 3 chambers delivered
    - Oxidation protection coatings
      - HfC/SiC coatings
    - Copper tubing for LH_2 coolant relieves permeability concerns

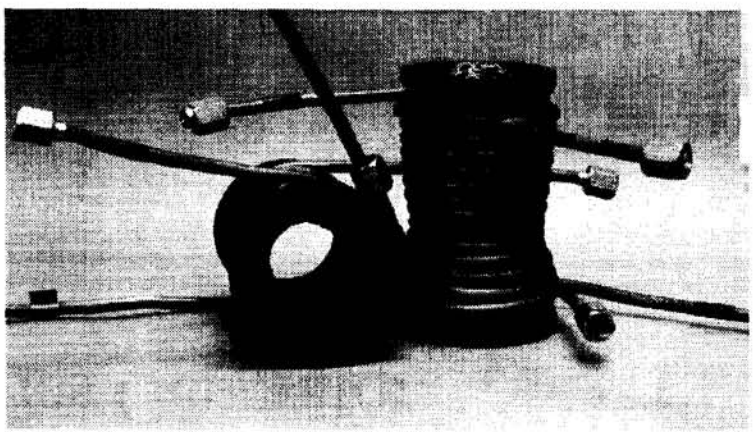

Light-Weight Gas Generator

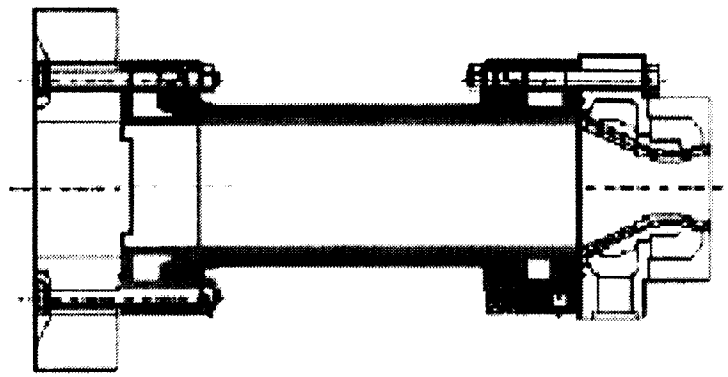

- **Objective:** Develop and demonstrate uncooled, hot gas impermeable ceramic composite structure
- **Approach:** Hot-Fire testing of sub-element
- **Challenges:**
  - CMC Architecture / Metal-Ceramic joint integrity
  - Gas impermeability
- **Status**:
  - Conceptual design selected - 8/99
  - Sub-element defined - 2/00 (Fabrication - 50% completion)
  - Hot-Fire testing target date - 12/00

Summary

- NASA has established goals for Second and Third Generation Reusable Launch Vehicles. Emphasis has been placed on significantly improving safety and decreasing the cost of transporting payloads to orbit.
- CMC components are being developed by NASA to ***enable significant*** increases in safety and engine performance, while reducing costs.
- The development of the following CMC components is being pursued by NASA: Simplex CMC Blisk, Cooled CMC Nozzle Ramps, Cooled CMC Thrust Chambers, and CMC Gas Generator.
- These development efforts are application oriented, but have a strong underpinning of fundamental understanding of processing-microstructure-property relationships relative to structural analyses, nondestructive characterization, and material behavior analysis at the coupon and component and system operation levels.
- As each effort matures, emphasis will be placed on optimizing and demonstrating material/component durability, ideally using a combined Building Block Approach and Build and Bust Approach.

Web Addresses

- NASA's Space Transportation: http://std.msfc.nasa.gov/
- NASA MSFC's Materials, Processes, & Manufacturing Department: http://mpm.msfc.nasa.gov/
- NASA GRC's Materials Division: http://www.lerc.nasa.gov/WWW/MDWeb/
- AMPET Home Page (4th Conference on Aerospace Materials, Processes, and Environmental Technology): http://AMPET.MSFC.NASA.GOV/

CP/535/IV/27

Rapid Fabrication of monolithic ceramic parts reinforced with Fibrous Monoliths for aerospace applications

R. Vaidyanathan, J. Walish, J. L. Lombardi, M.Fox, M. Rigali and M. Sutaria
Advanced Ceramics Research, Inc., 3292 E. Hemisphere Loop, Tucson, AZ 85706
Email: r.vaidyanathan@acrtucson.com Tel: 520-434-6392

INTRODUCTION

High-temperature, structural ceramics are finding increasing applications for use as components in gas turbine engines and rocket motors. A particular advantage of utilizing ceramic components over those fabricated from superalloy materials is that the former exhibit significantly greater strength and thermal stability at elevated temperatures. This enables the engines to operate at high temperatures and thus achieve greater efficiency. The reduced weight afforded by replacement of superalloy with ceramic turbine components has also been shown to increase the thrust efficiency of these engines [1]. Furthermore, conventional turbine engines fabricated from aerospace alloys require elaborate cooling schemes in order to maintain their integrity when operating at elevated temperatures. These cooling systems are unattractive since they add extra weight, cost and complexity to the turbine engine assembly. These problems could be eliminated if higher melting temperature materials, such as ceramics, were used in the manufacture of its engine components.

Although the ceramics have many attractive properties, their low fracture toughness limits their use in highly loaded structural applications such as turbine and compressor blades. It is well known that monolithic ceramics lack the fracture toughness necessary to be considered for aerospace applications. To be used for such applications, materials must possess low density, high elastic modulus, a low thermal-expansion coefficient, high thermal conductivity, excellent erosion and oxidation/corrosion resistance, and flaw-insensitivity. They will in many cases also be required to possess the ability to be joined, to survive thermal cycling and multi-axial stress states, and for reusable applications the materials must maintain the above attributes after prolonged exposure to extremely harsh chemical environments. The final and possibly most important attributes for these materials are the need to be of low cost and readily available in large quantities.

Fracture toughness of such materials could be improved by embedding continuous fibers into a ceramic matrix. This engineered material is called a ceramic matrix composite or CMC [2]. However, current state of the art methods for the fabrication of CMC materials such as chemical vapor infiltration (CVI) or polymer impregnation and pyrolysis (PIP) are expensive and time-consuming. Additionally, these processes cannot be easily adapted to rapid prototyping techniques, which would effectively reduce costs and fabrication times.

Fibrous monoliths (FMs) are a new class of structural ceramics [3-5]. They have mechanical properties similar to CFCCs, including very high fracture energies, damage tolerance, and graceful failures but can be produced at a significantly lower cost. Since they are monolithic ceramics, FMs are manufactured by conventional powder processing techniques using inexpensive raw materials. This combination of high performance and low cost enables FMs to wider applications of ceramics in energy and defense related applications. FMs are either sintered or hot pressed to various fibrous textures. The two phases that make up the macroarchitecture of a FM are a primary phase in the form of elongated polycrystalline cells, separated by a thin secondary phase in the form of cell boundaries, as shown in **Figure 1**. Typical volume fractions of the two phases are 80 to 95 % for the primary phase (polycrystalline cell), and 5 to 20 % for the interpenetrating phase (cell boundary). The cell phase is typically a structural ceramic, such as ZrC, HfC, Si_3N_4, or SiC, while the cell boundary phase is typically either a weakly-bonded, low-shear-strength material such as graphite or hexagonal BN.

Advanced Ceramics Research, Inc. (ACR) and the University of Michigan have produced fibrous monolithic ceramics from a variety of materials using a simple process for converting ordinary ceramic powder into 'green' fiber consisting of the powder and a thermoplastic polymer binder. These fibers can be compacted into the 'green' state to create the fabric of polycrystalline cells after sintering. The process is widely applicable, allowing cell/cell boundary bi-component fiber to be made from any thermodynamically compatible set of materials available as sinterable powders. The scale of the microstructure is determined by the green fiber diameter (cell size) and coating thickness (cell boundary). More details of the FM process as well as the different FM systems currently available may be seen in references 3-5.

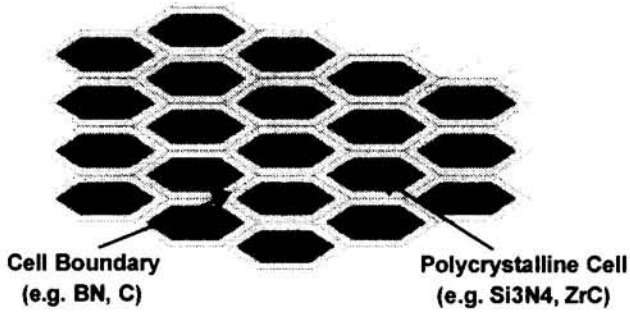

Figure 1. Schematic of a typical uniaxial Fibrous Monolith microstructure.

At present, most commercial monolithic or composite ceramic-fabrication processes do not fabricate net shape parts and require extensive finish machining. ACR has developed an efficient, cost effective ceramic prototyping process termed Wax Dip Molding (WDM) to address these issues. Figure 2 is a schematic of the process, while Figure 3 shows the ACR gelcasting technique schematic. WDM is a new ceramic fabrication technique involving CNC-machining a model of the desired component from a block of special water soluble polymer blend material developed at ACR followed by casting/solidifying molten wax around the machined model. The model is then removed from the wax merely by washing with water; leaving a core behind in a wax mold. High solids-loaded ceramic slurry is subsequently cast and thermally gelled within the mold. The gelled green ceramic part is then removed from the mold by melting the wax away. The green part is then subjected to typical binder burn out and sintering operations commonly encountered in conventional ceramic processing.

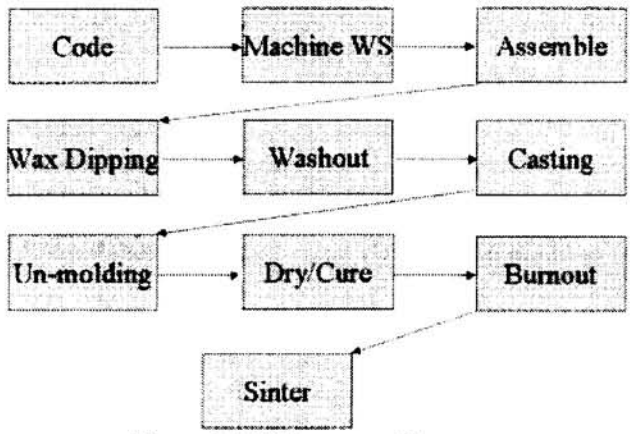

Figure 2. WDM process diagram.

A significant advantage of the WDM process is that it is reasonably simple and can rapidly turn out complex shaped ceramic articles in short order compared to other ceramic prototyping and other low volume manufacturing techniques. A photograph of a typical turbine part made by this process is shown in Figure 4. Parts made using this technique also exhibit mechanical properties that are generally better than conventionally processed materials and the technique does not require complex manufacturing equipment or extensive labor. In order to further improve the fracture toughness of the components that could be used in aerospace applications, ACR investigated the possibility of combining the WDM and FM processes to fabricate gelcast ceramic parts that are reinforced with FM fibers. There are several advantages to the development of such a process.

- Net-shape ceramic-composite parts could be fabricated directly from CAD designs.
- These parts would possess higher fracture toughness than monolithic ceramic parts.
- Since both the fibers and the monolithic ceramic matrix are mixed with thermoplastic or thermoset binder systems, they would both shrink at approximately the same rate during binder burnout and sintering, thus providing a fully dense part.

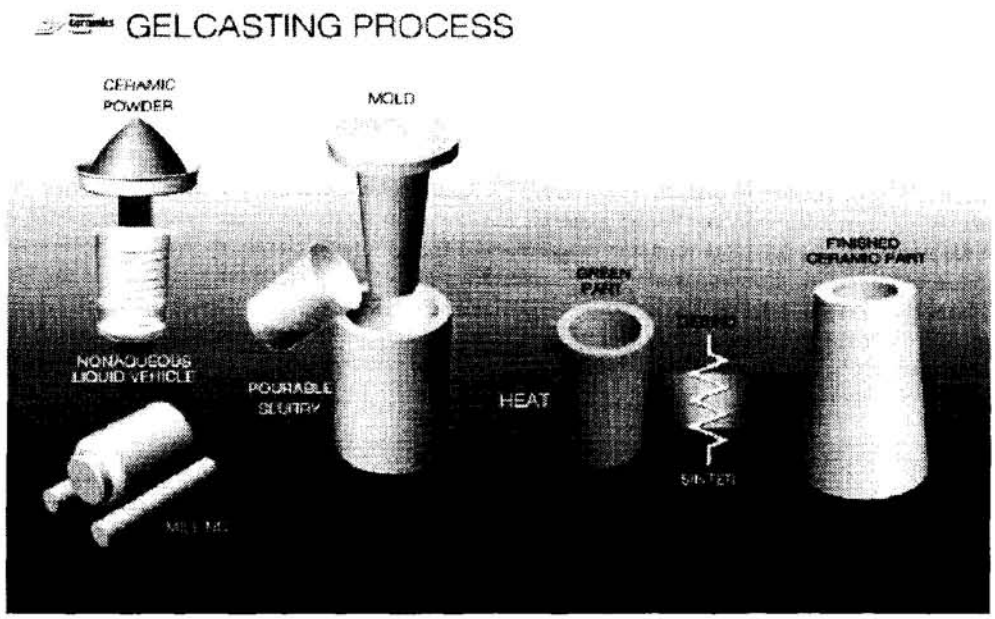

Figure 3. A schematic of the ACR gel-casting process.

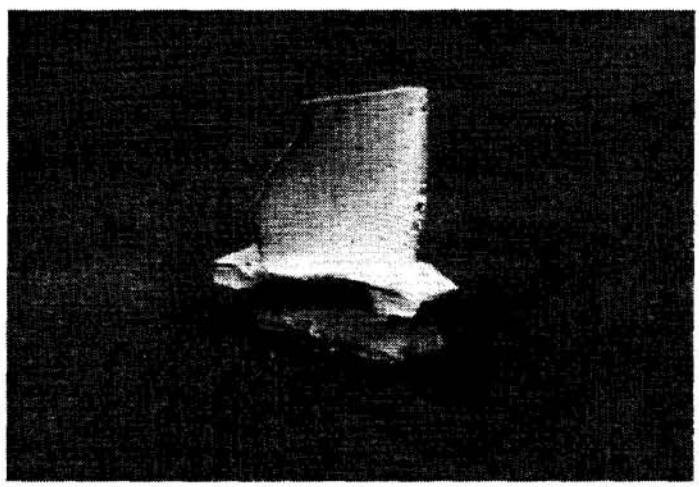

Figure 4. A sintered silicon nitride microturbine blade fabricated via WDM technique.

ACR has successfully developed gel-casting formulations of Si_3N_4, SiC, Sialons, and ZrC so far. Since the FM systems and the gel casting system would be thermodynamically compatible, the ceramic composite system would be less prone to environmental degradation. Additionally, since the components would be fully dense, the fibers and the matrix would be less prone to oxidation and loss of critical propertues. ACR's gel casting-Fibrous Monolith system capabilities are shown in Table I. Additional systems are currently in development. This paper presents the preliminary results with the Si_3N_4/BN fibers reinforced with a Si_3N_4 gel casting slurry.

Table I: Possible Composite Systems

Gel Casting System	Fibrous Monolith System
Si_3N_4	Si_3N_4 /BN
ZrC	ZrB2/BN
SiC	SiC/BN
SiC	Si_3N_4 /BN

EXPERIMENTAL PROCEDURES

A schematic describing the fabrication process is shown in Figure 5. Green Si_3N_4/BN FM feedrods were fabricated and extruded into a fiber preform using ACR's Extrusion Freeform Fabrication (EFF) equipment. More details of the EFF process are given in reference 6. The extrusion of the fibers could be achieved with the help of a high-pressure extrusion head that is retrofitted into a commercially available Stratasys rapid prototyping machine or a CNC machine. The fabrication of a mold will involve CNC-machining a model of the desired component from a block of special water soluble polymer blend material developed at ACR followed by casting/solidifying molten wax around the machined model. The model is then removed from the wax merely by washing with water; leaving a core behind in a wax mold. It is important to note that this mold will be in two halves, to assist the placement of the fibrous monolith preform into the mold. High solids-loaded ceramic slurry is subsequently cast and thermally gelled within the mold. The gelled green ceramic part is then removed from the mold by melting the wax away. The green part is then subjected to typical binder burn out and sintering operations commonly encountered in conventional ceramic processing.

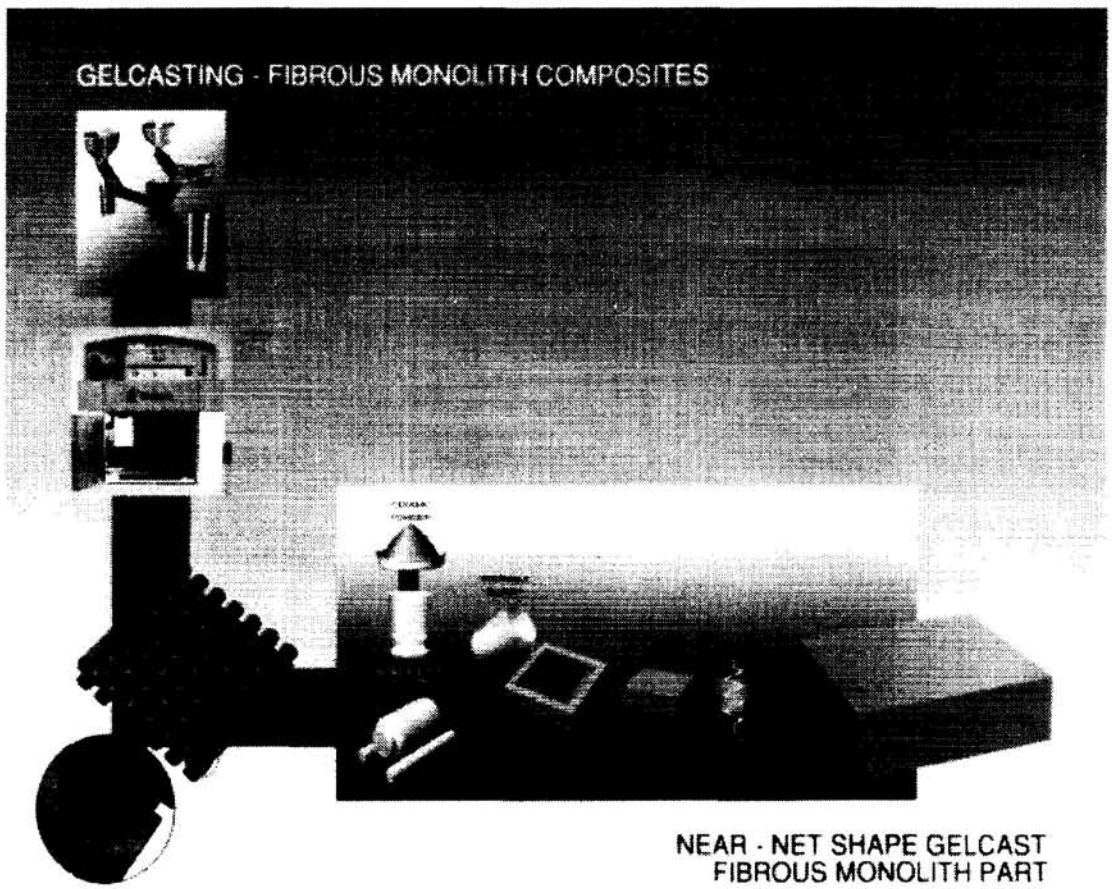

Figure 5: A schematic of the gel cast fibrous monolith ceramic composite process.

The major consideration for a successful slurry include reproducible rheology, rapid gelling characteristics, facile wetting behavior upon the fibrous monolith surface, and ultimately its ability to be pyrolyzed and sintered to produce a high-strength ceramic component. The importance of reproducible slurry rheology should not be underestimated since commercially attractive slurries should not exhibit batch to batch variability in their viscosities and possess a reasonable shelf life. Silicon nitride slurries were formulated in a non-aqueous vehicle. The silicon nitride used in slurries was a bimodal mixture of Ube SN E-10 and E-05 powders. The overall solids content of the slurries was 52 volume percent. The slurries exhibited a reproducible rheology and enhanced shelf life as can be seen in Figure 6. It can clearly be seen that the slurry has a thixotropic rheology. ACR has successfully developed highly loaded ceramic slurries with shelf lives exceeding 3 months.

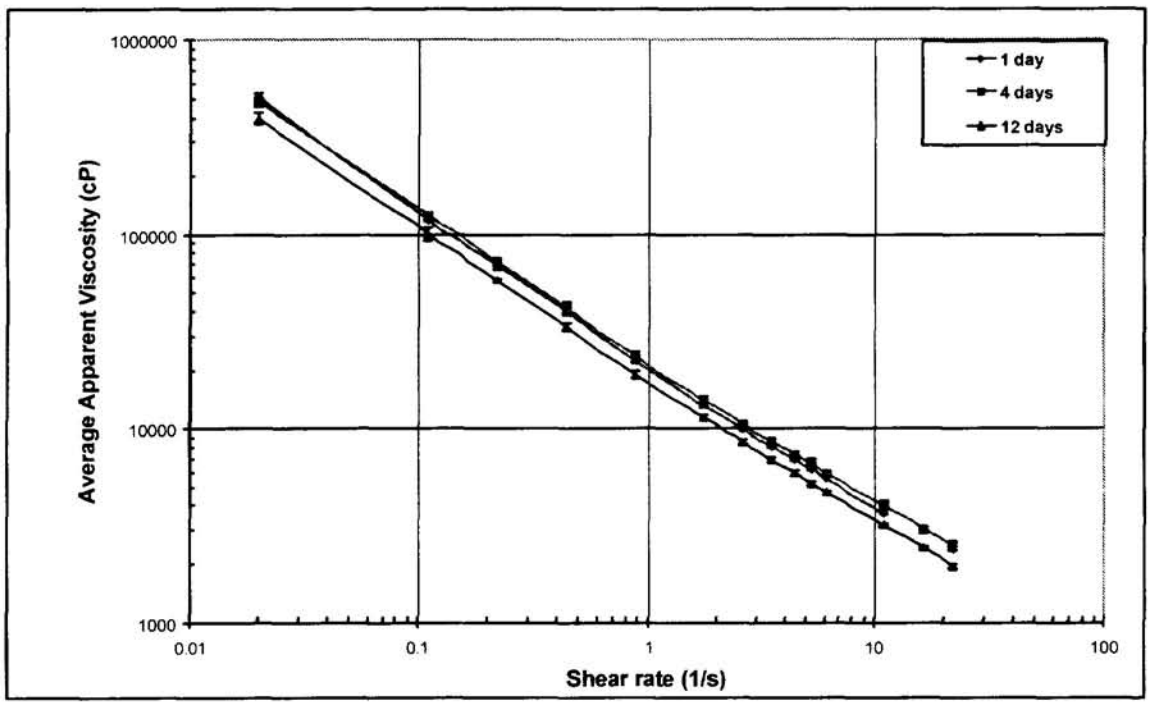

Figure 6: Viscosity plot of silicon nitride slurry formulated in a non-aqueous vehicle and aged for various amounts of time.

For demonstrating the process itself, fibrous monolith filaments were extruded and chopped into two-inch lengths. These were subsequently laid-up in alternating 0 and 90 degree orientations. The fibers were laid into a mold. The preforms were then infiltrated with the ceramic slurry. Vacuum was applied to remove any entrapped air. The samples were subsequently cured. The samples were cut into 2"x2"x0.25" billets and hot pressed. An image of the billet after hot pressing is shown in Figure 7. These billets had an average density of 3.25 g/cc, which is approximately 98% of the theoretical density. After hot pressing, the billets were cut into mechanical test bars for four point bend testing.

Figure 7. Hot pressed FM Gelcast composite billet

Mechanical testing was performed according to ASTM C 1161-90 for flexural strength of ceramics at ambient temperatures. An average strength of 460 ± 53 MPa. A typical load displacement curve is shown in Figure 8. An optical micrograph of the fracture surface of a typical sample is shown in Figure 9. The results obtained from

the mechanical testing show no load transfer to the reinforcing fibrous monolith fibers. Additionally, few fibers were found on the fracture surface, as seen in Figure 9. There could be several reasons for these results.

- Insufficient fiber volume fraction. It was estimated that the fiber volume fraction was 10-15%.
- The fibers may not have stayed in place during the casting of the gel casting slurry and could have created a sample with fiber volume gradients through the thickness.
- Insufficient control of the interfacial bond strength between the FM fibers and the gel casting matrix.

Future experiments will emphasize the optimization of the interfacial bond strength, improving the fiber volume ratio, as well as maintaining the fiber placement during the casting process. The ultimate goal would be the development of a manufacturing process that can create a CMC component directly from its CAD design.

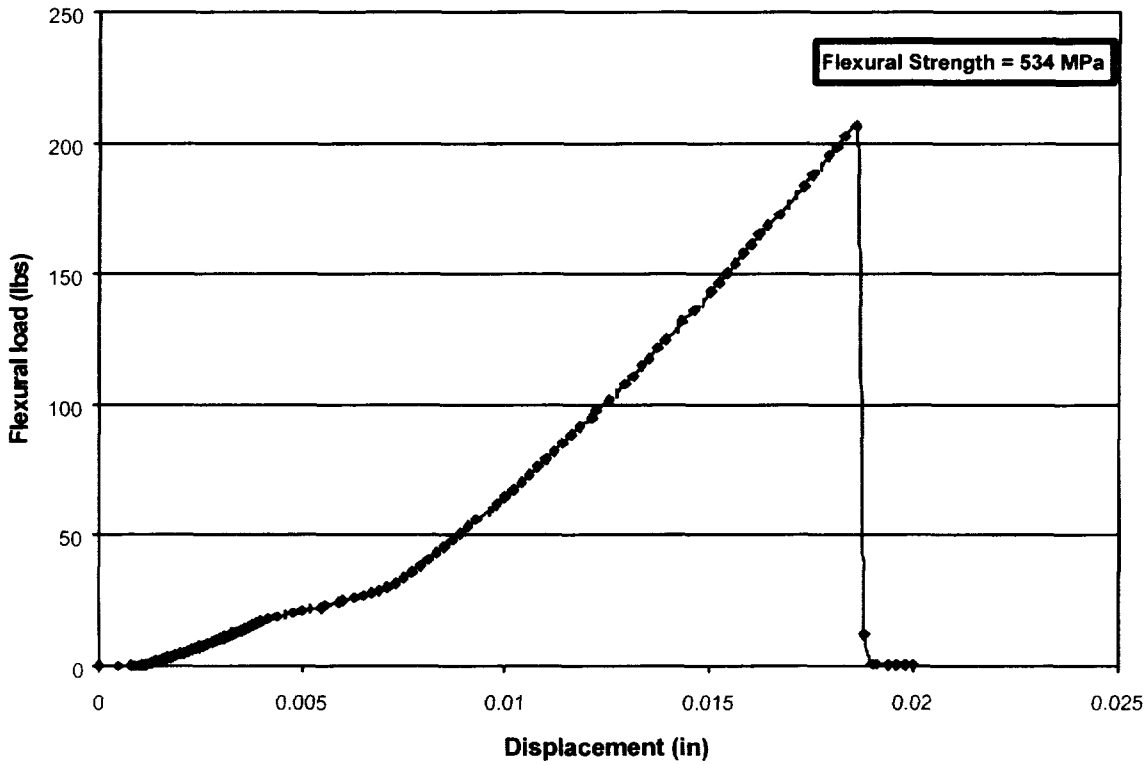

Figure 8. Typical room temperature load-displacement curve for a Si_3N_4/BN Fibrous Monolith reinforced Si_3N_4 gelcasting ceramic matrix composite.

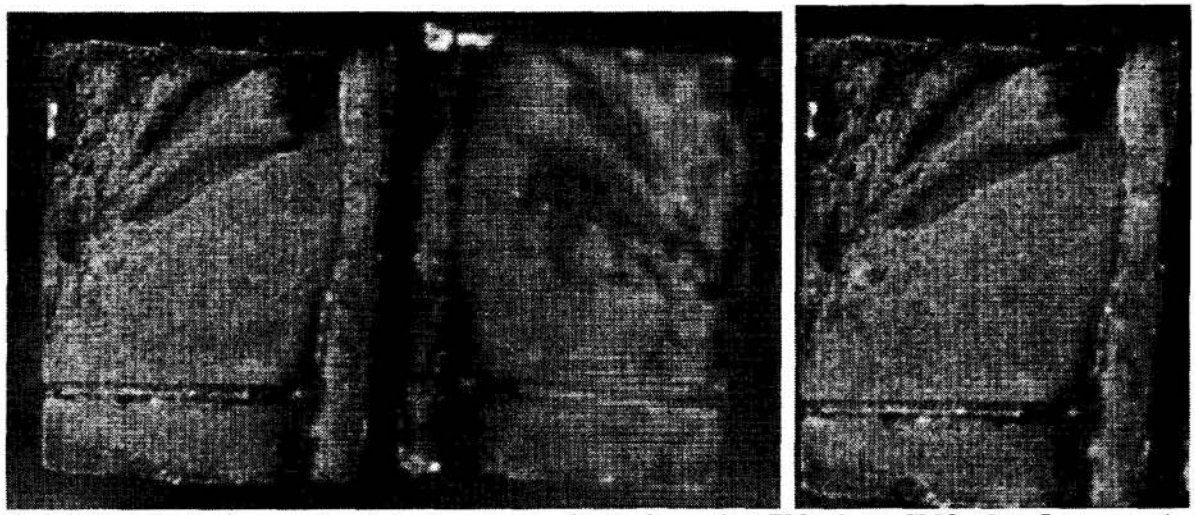

Figure 9. Optical micrographs of the fracture surfaces of a typical FM-gelcast CMC after flexure testing (Both surfaces side by side – 10X; one surface – 15X)

ACKNOWLEDGMENTS

The authors appreciate the support and advice of Dr. William Coblenz at DARPA in conceiving and executing the experimental idea.

REFERENCES

1. Richerson, D.W., "Ceramics for Turbine Engines," Mechanical Engineering, pp. 80-83, September 1997.
2. Effinger, M. R., Genge, G. G., Kiser, J. D., "Ceramic composite turbine disks for rocket engines," *Advanced Materials and Processes*, **157** [6], pp. 69-73, (2000).
3. D. Kovar, B.H. King, R.W. Trice, and J.W. Halloran, "Fibrous Monolithic Ceramics" J. Am. Ceram. Soc., **80**, [10] 2471-2487, 1997
4. G.E. Hilmas, A. Brady, U. Abdali, G. Zywicki and J.W. Halloran, "Fibrous Monoliths: Non-Brittle Fracture from Powder Processed Ceramics," *Mat. Sci. & Eng. A.*, **195**, 263-268 1995.
5. G.E. Hilmas, A. Brady and J.W. Halloran, "SiC and Si_3N_4 Fibrous Monoliths: Non-Brittle Fracture From Powder Processed Ceramics Produced by Coextrusion,"; pp. 609-614 in Ceramic Transactions-Vol. 51 *Ceramic Processing Science and Technology*. Edited by H. Hausner and G. Messing. American Ceramic Society Westerville, OH, 1993.
6. Vaidyanathan, R., Lombardi, J. L., Walish, J., Kasichainula, S., Calvert, P., and Cooper, K., "Extrusion Freeform Fabrication of Functional Ceramic Prototypes," *Ceramic Engineering and Science Proceedings*, **21** [4], pp. 121-128, (2000).

CP/536 1.N.24

Solid Freeform Fabrication of Continuous Fiber Reinforced Composites for Propulsion Applications

R. Vaidyanathan, M. Fox, J. Walish, M. Rigali and R. Cipriani
Advanced Ceramics Research, Inc., 3292 E. Hemisphere Dr.
Tucson, AZ 85706-5013
Tel: 520-434-6392 ; email: r.vaidyanathan@acrtucson.com

J. Gillespie and S. Yarlagadda
Center for Composite Materials
University of Delaware, Newark DE 19719-3144

M. Effinger
NASA Marshall Space Flight Center
George C. Marshall Space Flight Center
Huntsville, Al 35812

INTRODUCTION

Monolithic ceramics lack the fracture toughness necessary to be considered for propulsion related applications. To be used for such applications, materials must possess low density, high elastic modulus, a low thermal-expansion coefficient, high thermal conductivity, excellent erosion and oxidation/corrosion resistance, and flaw-insensitivity. They will in many cases also be required to possess the ability to be joined, to survive thermal cycling and multi-axial stress states, and for reusable applications the materials must maintain the above attributes after prolonged exposure to extremely harsh chemical environments. The final and possibly most important attributes for these materials are the need to be of low cost and readily available in large quantities.

Fracture toughness of such materials could be improved by embedding continuous fibers into a ceramic matrix. This engineered material is called a ceramic matrix composite or CMC [1]. However, current state of the art methods for the fabrication of CMC materials such as chemical vapor infiltration (CVI) or polymer impregnation and pyrolysis (PIP) are expensive and time-consuming. Additionally, these processes cannot be easily adapted to rapid prototyping techniques, which would effectively reduce costs and fabrication times.

Recently, Advanced Ceramics Research, Inc. (ACR) has developed a low cost, flexible-manufacturing processes for ceramic based continuous fiber reinforced composites. This process, called Continuous Composite Co-extrusion (C^3), incorporates fiber tows into a ceramic matrix to fabricate ceramic-matrix/ceramic fiber composites. The C^3 process is the continuous extrusion of matrix material around a fiber tow. A flow chart illustrating the C^3 process is shown in figure 1. An interface material such as graphite is introduced between the fibers and the matrix to minimize the thermal expansion mismatch between the fibers and the matrix during the final consolidation step. The process is simple, robust and is widely applicable to a number of ceramic composite material systems such as Cf/SiC, Cf/ZrC, SiC/SiC etc.

The process begins by mixing the ceramic and graphite powders individually with thermoplastic binders and additives in a high shear mixer. The resulting ceramic powder/thermoplastic blend is pressed into a "green" rod. Next, the graphite powder/thermoplastic blend is pressed into a small diameter "green" rod. A hole of equal diameter to the graphite rod is drilled into the center of the rod and the graphite/thermoplastic rod is inserted. This green composite feedrod is then re-pressed and a hole is drilled in the center of the ZrC/graphite composite feedrod allowing the carbon fiber tow to pass through the center. Since the matrix and the interface are monolithic powders, the cost of the final composite could be lower than CVI and PIP based CMC's by at least an order of magnitude.

Recently, an innovative manufacturing technique called Advanced Tow Placement (ATP) has been developed Gillespie and co-workers [2] for thermoplastic and thermoset based polymer composite components at the University of Delaware Center for Composite Materials (UD-CCM). The ATP process is an enabling technology, developed originally for thermoset composites and more recently for in-situ non-autoclave consolidation of large-scale thermoplastic composite materials for High Speed Civil Transport (HSCT) applications. In this process, consolidation of the thermoplastic composite tows is achieved by the concurrent use of localized heat and

pressure so that bonding is achieved at the newly formed interface and consolidation is achieved within the material. Figure 2 shows the schematic of the automated thermoplastic tow-placement process at UD-CCM.

Since thermoplastic binders are used in the fabrication of ACR's C^3 green CMC filaments, the ATP process originally developed for thermoplastic prepreg tows could be adapted to ceramic composites. The knowledge base of the ATP process for thermoplastic prepregs can be utilized to lay down ceramic tows reinforced with continuous fibers in the desired configuration. This allows the use of a proven technology for low cost, rapid fabrication of large complex ceramic parts. This process also allows the possibility to create complicated parts directly from a CAD drawing without human intervention. This process is called Ceramic Composite Advanced Tow Placement or CCATP process. In this paper, initial results with the CCATP process are presented.

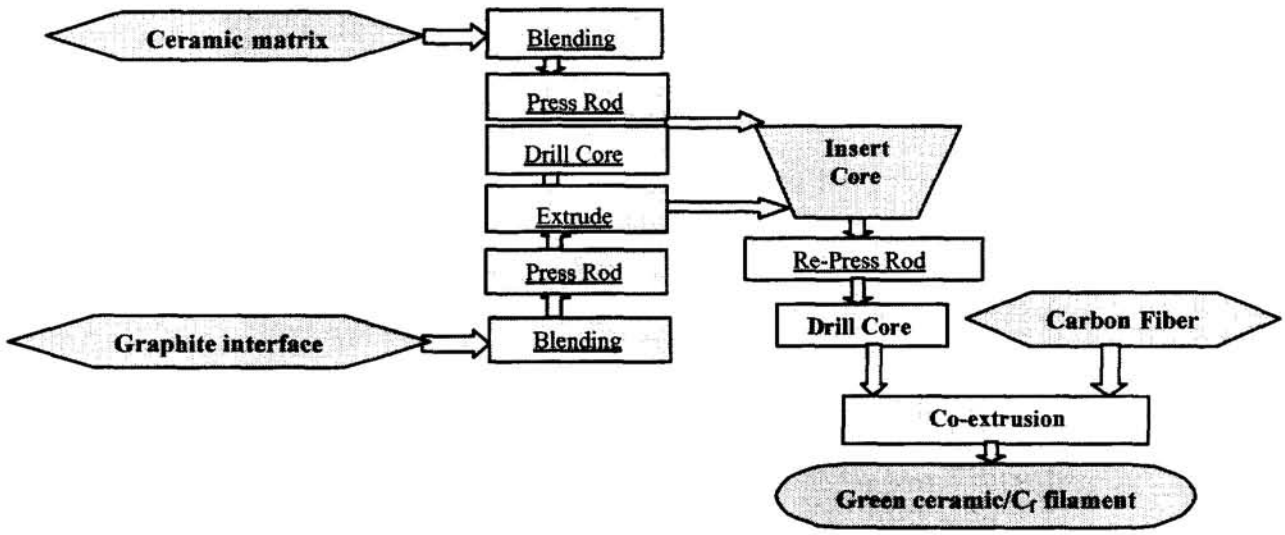

Figure 1. Flow Chart Illustrating the C^3 Process.

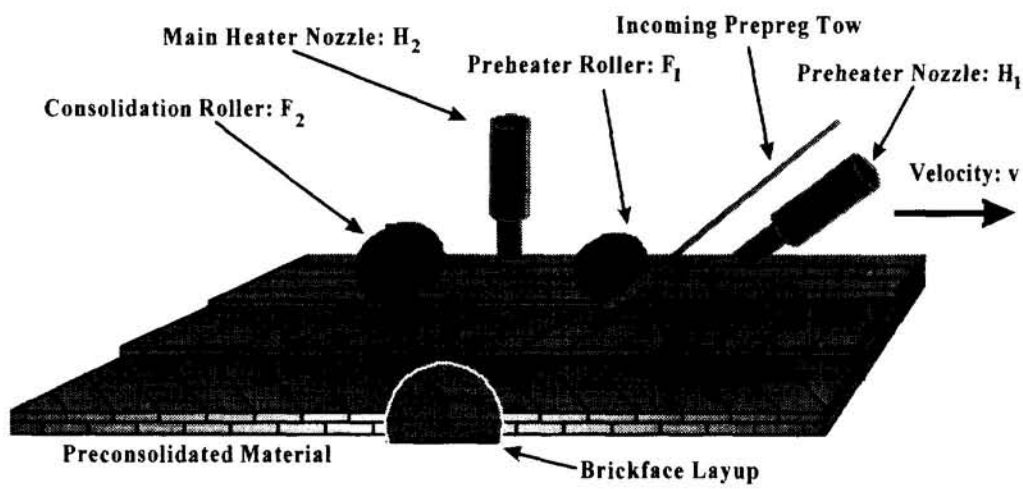

Figure 2. Schematic of the ATP process

EQUIPMENT AND EXPERIMENTAL PROCEDURES

EQUIPMENT

The automated tow placement system at the University of Delaware Center for Composite Materials was developed for rapid, low cost fabrication of fiber reinforced thermoplastic parts, and is shown in Figure 3. It employs the use of two hot-gas nitrogen torches to heat the material and two rollers to provide the pressures required for consolidation, as shown in Figure 2. The purpose of the first torch and roller is to preheat the composite surface

and incoming tow together. The material is thus "tacked" to the surface with this roller. This tacking procedure is useful in that the fed material is carefully bonded to the surface and not pulled with the main consolidation roller. This tacking approach also aids in improving the efficiency of the cut and refeed mechanism. The second torch (main heater) provides supplemental through thickness heating to facilitate consolidation and bonding of the tow and substrate under the consolidation roller. These rollers provide the necessary forces to achieve complete intimate contact across the tow interface, and as a boundary pressure for preventing any internal void development.

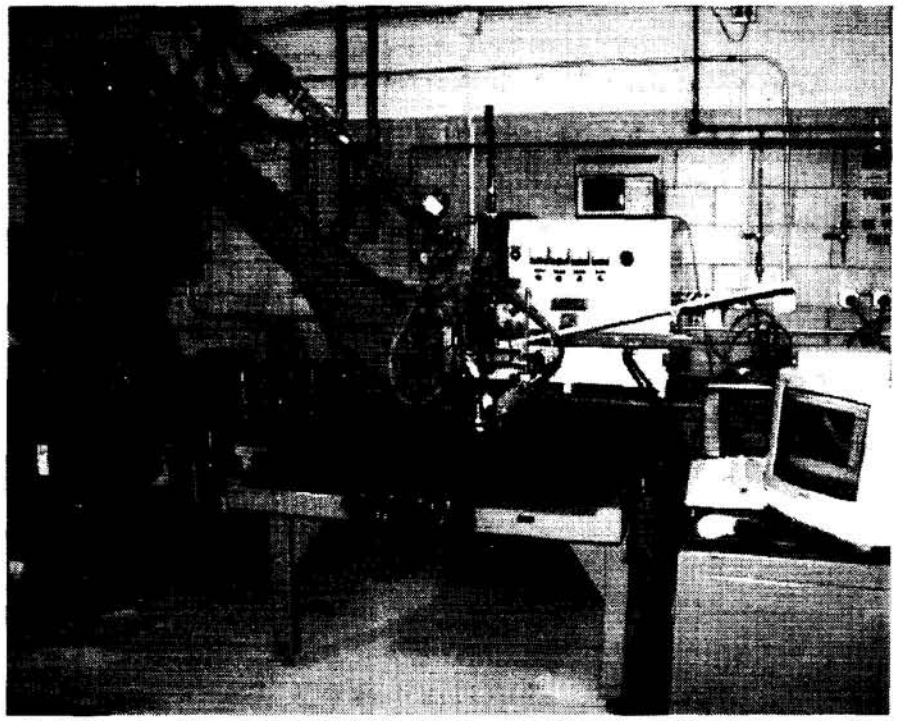

Figure 3. ATP assembly at the UD/CCM Composites Manufacturing Science Laboratory.

The forces applied to both rollers are controlled independently using a series of pneumatic actuators. The composite tows can be placed in a regular repeating pattern or with brick-face symmetry. The brick-face geometry has the advantage that more homogeneity is achieved throughout the composite structure. All the processing inputs are controlled either manually or through a PID control scheme from a LabVIEW™ interface. An ABB IRB 6400 Robotic Work cell, shown in Figure 3, is used to control the motion of the placement head. This robot is capable of carrying a 120kg payload at automated speeds up to 7m/s and is accurate to 0.01mm. A computer-controlled nitrogen hot gas torch control system (not shown) is used to monitor and control gas flow rate and temperatures within both torches. The composite surface temperatures can be adjusted by either increasing the process velocity or by independent change of the nozzle heights. This novel temperature control method shows promise as an adaptive method for rapid control of surface temperatures and was recently patented by the UD-CCM [U.S. Patent No. 5,626,472]. The temperatures are measured and controlled with an AGEMA Thermal Imaging camera with a neural network based PID control system. The camera measures the viewable peak temperatures on the laminate surface and adjusts the nozzle heights accordingly to compensate for any deviation in set point temperatures. A Labview™ interface is used to input number of layers, ply orientation, surface temperatures, panel geometry, and process velocity. This interface can also be used in conjunction with a laser displacement unit to measure warpage during processing.

Test Materials

The ATP process for thermoplastics lays down prepreg tows, typically 0.125 – 0.2 mm in thickness, with the tow width depending on the hardware. The ATP head at UD-CCM can lay down 6.25-mm wide tows, while industrial machines, such as Cincinnati Milacron's Gantry System can lay down tows as wide as 150 mm.

Fiber reinforced ceramic materials for this study were supplied by ACR and were in the form of green tows. The reinforcing fiber was carbon and the matrix was zirconium carbide based, in a low temperature thermoplastic binder. The tows were thicker than the thermoplastic tows for polymer matrix composites.

Initial tests with the ceramic tows revealed several important issues:

- The matrix was somewhat brittle and fractured easily under tension. This can pose a problem during tow placement as the tow is under tension to achieve good quality.
- Cut and re-feed mechanism on the head did not function consistently. This is due to the difference in thermoplastic (for which it was designed) and ceramic tows. Ceramic tows were manually cut to specific lengths and manually placed to simulate this.
- Adhesion between the tows and the matrix was not good. While this is not required at the green stage, fractures in the matrix result in exposure of bare fibers (in tension), causing inconsistent loading. This may not be an issue, as the actual fiber wet-out occurs during the sintering phase and can alleviate it. Further optimization of the interface thickness and type that is being carried out.
- The process temperature of the thermoplastic binder was low. Typical thermoplastic tows have process temperatures in the 300°C range. Therefore, lower torch temperatures were used.
- Over time, the matrix started adhering to the rollers. This occurred due to the rollers heating up past the melt temperature of the thermoplastic binder and resulted in the rollers peeling away the matrix from the tows. Solutions to overcome this problem are being devised.
- Minimal force was required for consolidation.

ATP Process Modification for Ceramic Tow Placement

Several process modifications were performed to obtain better quality material. These process modifications resulted in good material quality as shown in Figure 4 and 5. Note that, the tows were cut and placed manually to simulate the cut/refeed mechanism of the ATP head (Figure 6). Once the tows were placed, the robot performs the entire tow placement sequence to heat and consolidate tows.

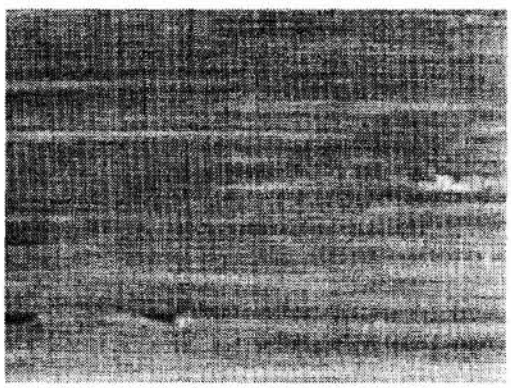

Figure 4. Good material quality was obtained with modifications to the ATP head

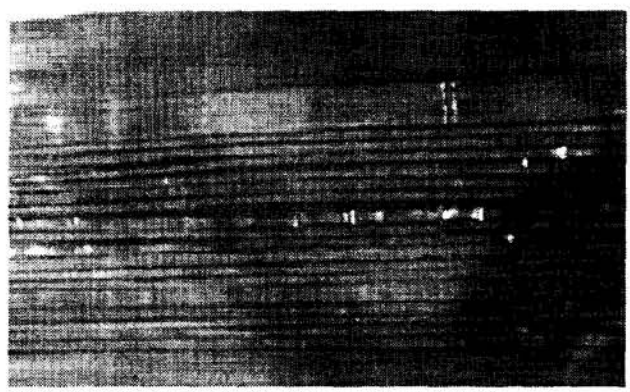

Figure 5. Photograph of ceramic tows placed manually. Upper half of the photograph shows tows consolidated by the modified ATP head

CMC Laminate Fabrication by Ceramic Tow Placement

Two green laminates were fabricated with the ceramic tows:

- 225 mm long x 75 mm wide [0/0] (9" long x 3" wide)
- 150 mm long x 75 mm wide [0/90/0] (6" long x 3" wide)

Figure 6 shows the ATP head in action during fabrication of both laminates. Typical microstructures are shown in figures 7 and 8 respectively. For both cases, the entire robot movement sequence is setup by computer programs developed for the ATP thermoplastic tow placement experiments. The torch parameters (temperatures, heights, and gas flow rates), consolidation force and head velocity can be controlled on the fly as inputs to the computer program. Final panel dimensions and lay-up sequences are also inputs to the program. Once these inputs are given to the program, it operates the robot in automatic mode and lays down the tows as specified. Green ceramic matrix laminates of any size (within limits of the robotic workcell), fiber orientation and material system

can be fabricated by this technique. The current effort has not focused on optimizing process parameters, but on demonstrating the feasibility of rapid, low cost fabrication of fiber reinforced green ceramic composites.

Both laminates were successfully fabricated, though the tows were hand-placed due to the inconsistent operation of the cut and refeed mechanism. This did not allow for a through study of the overlaps and gaps during the automatic placement of tows. In addition, tension is necessary to maintain fiber straightness during consolidation and this was not possible at laminate edges due to hand placement of tows. Consequently, movement of tows during consolidation was seen. With automatic feed from a spool with tension, cut and refeed can overcome all these issues and identify correct level of overlap for consistent quality during consolidation.

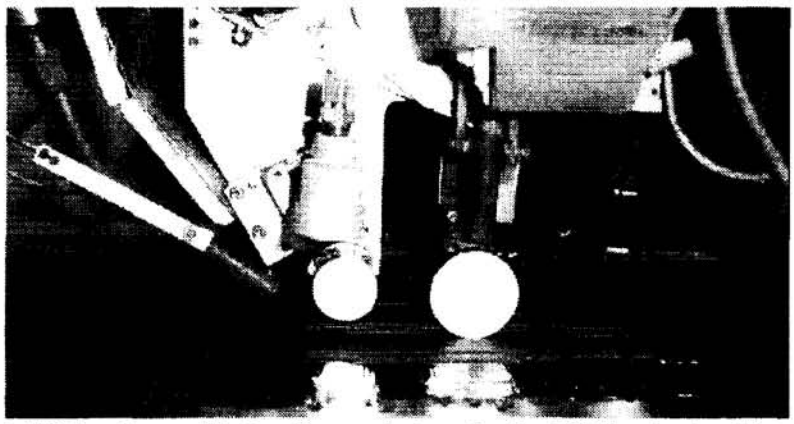

Figure 6. Modified ATP head consolidating 0 ceramic tows for the [0/0] laminate with top 0 layer showing

Figure 7. Typical cross-sections of rapid prototyped [0] Cf/ZrC panels

Figure 8. Typical cross-section of rapid prototyped [0/90/0] Cf/ZrC panel

Other components

Figure 9 shows a 6-inch diameter cylinder that was fabricated using the ATP equipment. This clearly shows the potential and capability of the process to fabricate complicated, full-scale components. This tube contains only three wraps of material.

Scale-Up Potential

Figure 10 shows the scale-up of thermoplastic ATP process developed in a DARPA RAPTECH (Rapid Technology) program led by UD-CCM with DuPont, Hercules/Alliant and Cincinnati Milacron. In this effort, UD-CCM demonstrated lab-scale viability and developed optimal process conditions for scale-up. Infrastructure for large-scale fabrication using gantry/robotic system exists.

Mechanical property and microstructural characterization of panels

Billets were hot pressed. The hot pressed panels were not entirely crack-free which indicated that the thermal stresses were not completely eliminated. An estimated fiber volume fraction of 35-40% was achieved after sintering. Specimens were tested in tension at a displacement rate of 0.2 mm/min using a load cell of 2500 lbs. at the University of Arizona. Representative samples were cut from the billets for testing. All the specimens exhibited good composite behavior, clear fiber pullout and in some cases, a stable loading pattern, with the load being taken

up entirely by the fibers. It appears that the graphite interface thickness was too large for the composite to exhibit a high enough strength and good composite behavior at the same time. However, it is believed that these issues related to materials processing, though major, can be addressed and corrected. Typical tensile stress-displacement curve is shown in Figure 11 and 12, which shows good load transfer and the ability of the fibers to carry the load after the initial matrix has cracked. In many cases, the composite did not fail entirely and the fibers continued to carry the load. The test had to be discontinued at this point.

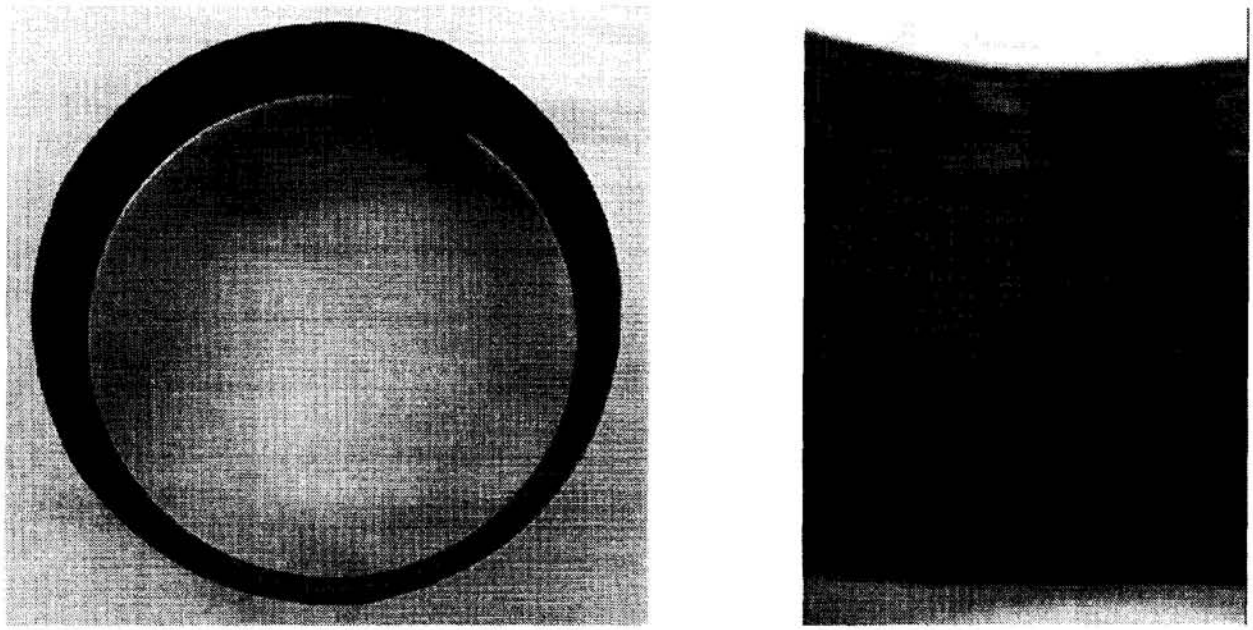

Figure 9. A six inch ZrC/Cf cylinder fabricated using the ATP equipment

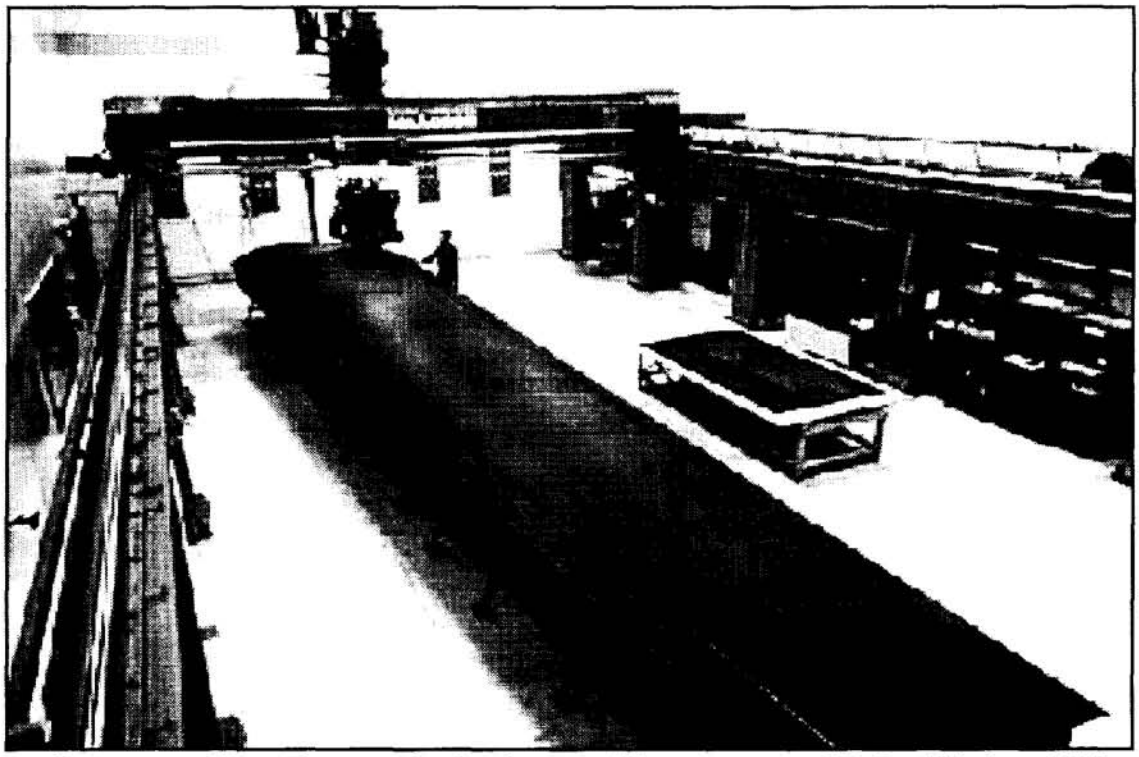

Figure 10. Automated Tape Placement head and gantry. (Picture courtesy of DuPont/Cincinnati-Milacron)

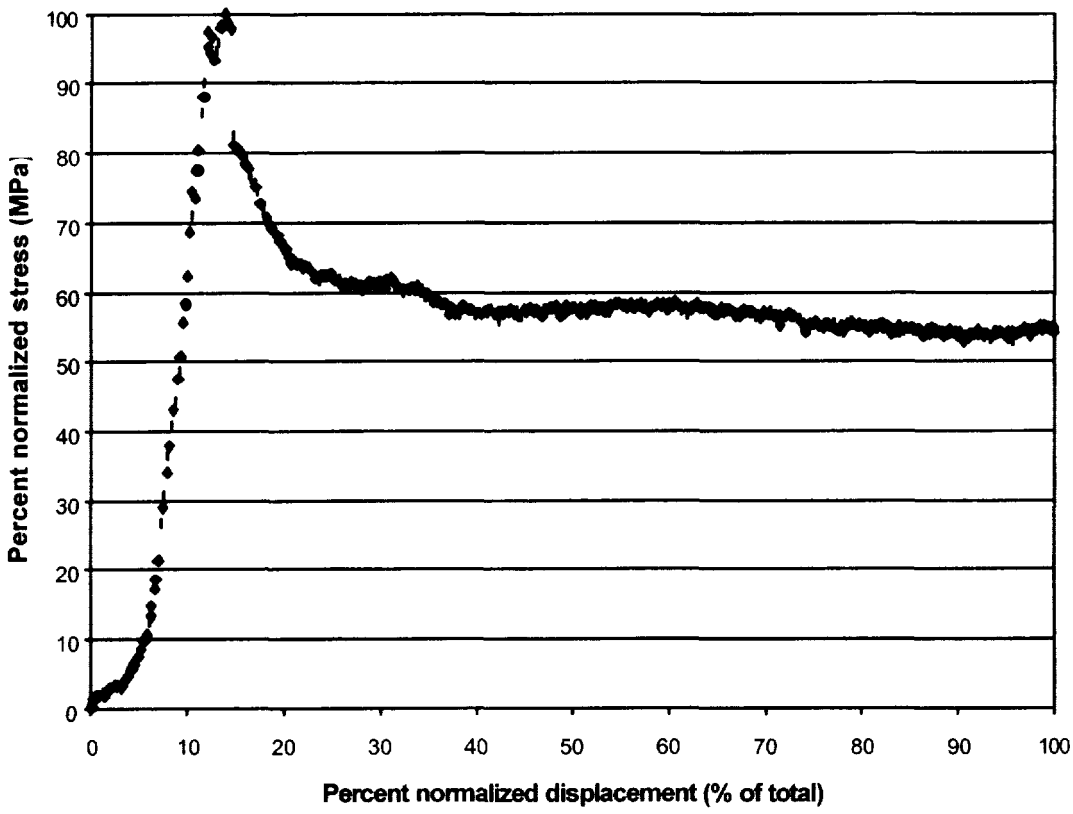

Figure 11. A typical tensile stress-strain curve for the rapid prototyped 0/90/0 panel.

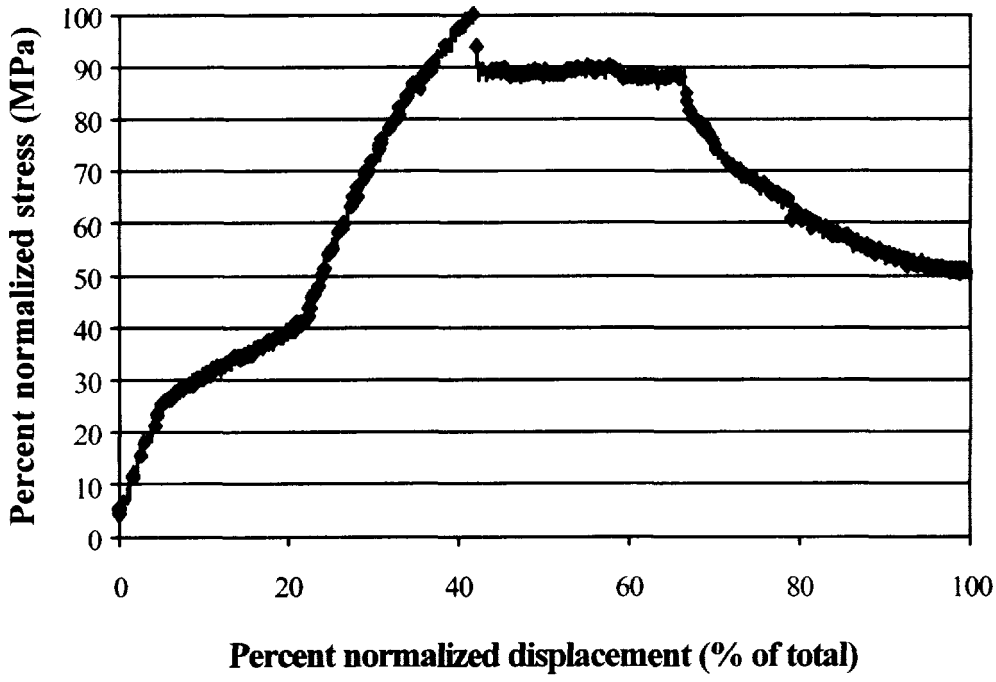

Figure 12. Typical stress-strain curve for a rapid prototyped Cf/ZrC composite specimen showing load transfer and the ability of the fibers to carry the load.

CONCLUSIONS

1. An innovative rapid prototyping technology to freeform fabricate continuous fiber reinforced ceramic matrix composites was successfully developed.
2. The feasibility of using the ATP process, with some modifications, for rapid fabrication of green ceramic composites has been demonstrated. [0/0] and [0/90/0] laminates were fabricated using the computer-controlled ATP head. Critical process parameters were torch parameters, consolidation force and process velocity. Several issues that need to be addressed are the automated cut and refeed system, parametric studies, optimization of process parameters and binder optimization.
3. 2D panels were rapidly prototyped using a fiber placement system similar to commercially available fiber placement equipment. A 6-inch diameter cylinder was also fabricated.
4. An estimated fiber volume fraction of 35-40% was obtained in the composites after sintering.
5. The composite exhibited good fiber pull-out and load-transfer from the matrix to the fibers, although further optimization of the interfacial properties are required to obtain satisfactory mechanical properties.

ACKNOWLEDGMENTS

This manuscript contains work performed as part of the "Rapid prototyping of continuous fiber reinforced ceramic composites," SBIR phase I program funded by NASA Marshall Space Flight Center under contract number NAS8-00084.

REFERENCES

1. Effinger, M. R., Genge, G. G., Kiser, J. D., "Ceramic composite turbine disks for rocket engines," *Advanced Materials and Processes*, **157** [6], pp. 69-73, (2000).
2. Don, R. C., J. W. Gillespie Jr., and S. H. McKnight, "Bonding Techniques for High-Performance Thermoplastic Compositions," U. S. Patent No. 5643390, issued July 1, 1997.

AN EXAMPLE OF ECONOMIC VALUE IN RAPID PROTOTYPING

ROBERT L. HAUER
EDWARD P. BRAUNSCHEIDEL
JOHN H. GLENN RESEARCH CENTER

SINTERSTATION 2500plus

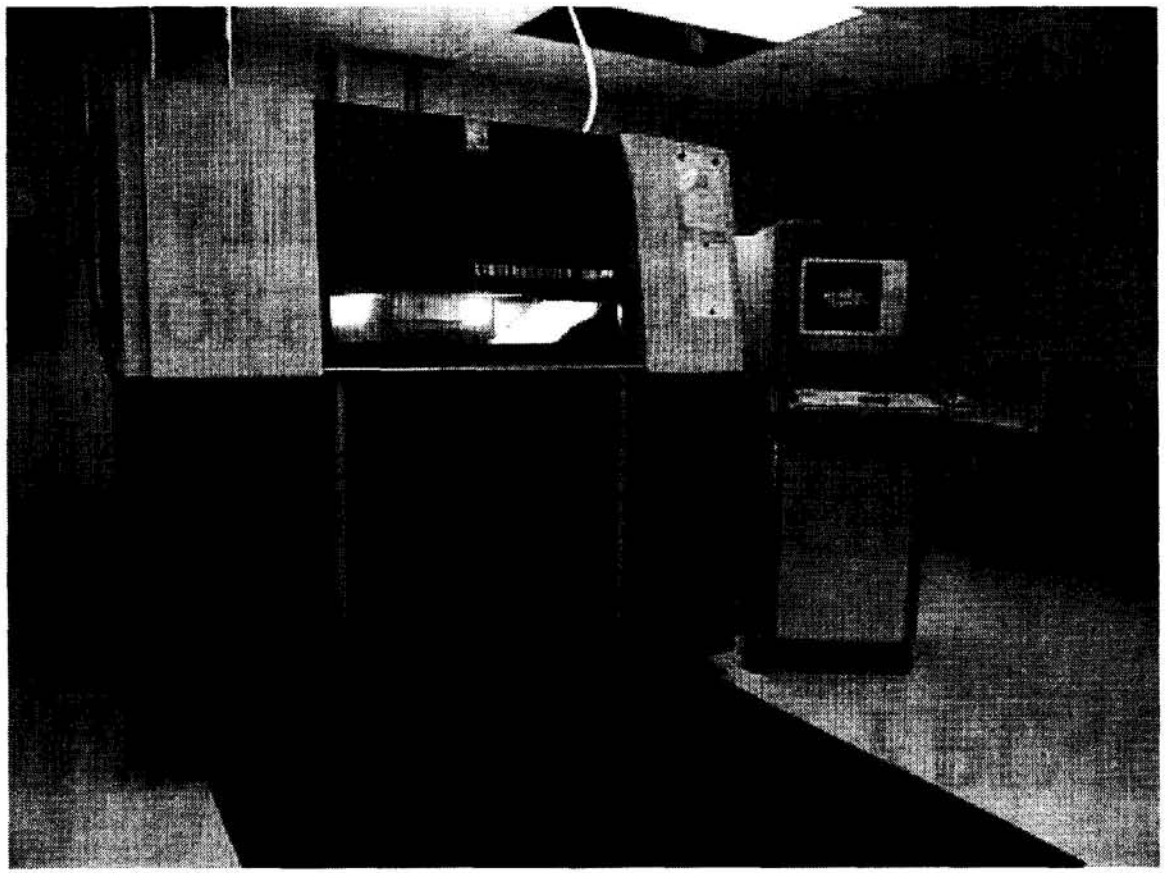

RAPID PROTOTYPING

- TODAY'S MODERN MACHINING PROJECTS ARE COMPOSED OF MORE AND MORE COMPLICATED AND INTRICATE STRUCTURE DUE TO A VARIETY OF REASONS INCLUDING THE ABILITY TO COMPUTER MODEL COMPLEX SURFACES AND FORMS

RAPID PROTOTYPING

- THE COST OF PRODUCING THESE FORMS CAN BE EXTREMELY HIGH NOT ONLY DOLLARS BUT IN TIME TO COMPLETE.
- CHANGES ARE EVEN MORE DIFFICULT TO INCORPORATE

RAPID PROTOTYPING

- PICTURE OF THE SUBJECT BLADE

RAPID PROTOTYPING

- THE BLADE SHOWN IN THE PREVIOUS SLIDE IS AN EXCELLENT EXAMPLE
- ITS COMPLEX FORM WOULD HAVE REQUIRED HUNDREDS OF HOURS IN FABRICATION FOR JUST A SIMPLE PROTOTYPED

RAPID PROTOTYPING

- AFTER A SERIES OF COMPLEX DRAWINGS WERE ASSEMBLED A PROCUREMENT WOULD HAVE BEEN INITIATED TO MACHINE A PROTOTYPE BLADE OR TO BUILD A COMPLEX DIE FOR THE PRODUCTION OF WAX FORMS FOR THE CASTING PROCESS.

RAPID PROTOTYPING

- THE PROCUREMENT WOULD HAVE TAKEN IN THE NEIGHBORHOOD OF 6 WEEKS TO COMPLETE
- THE ACTUAL FABRICATION WOULD HAVE BEEN AN EQUAL AMOUNT OF TIME TO COMPLETE

RAPID PROTOTYPING

- AN ALTERNATIVE TO THIS PROCESS WOULD HAVE BEEN A WOOD MODEL ALTHOUGH CHEAPER THAN A METAL FABRICATION IT WOULD BE EXTREMELY TIME INTENSIVE AND REQUIRE IN THE NEIGHBORHOOD OF A MONTH TO PRODUCE IN-HOUSE

RAPID PROTOTYPING

- JUST A ROUGH ESTIMATE WOULD PUT COSTS AT NEAR $32,000 RANGE WITH 2 TO 3 MONTHS TO PRODUCE A USEABLE PRODUCT

RAPID PROTOTYPING

- WITH THE SINTERSTATION 2500 PLUS ALL THAT WAS REQUIRE WAS TO:
  - A SOLID MODEL FROM A CAD/CAM SYSTEM DOWNLOADED AS A STL FILE
  - LOAD THE FILE TO THE MACHINE
  - 2 TO 3 HOURS OF SET UP TIME
  - 16 HOURS OF UNATTENDED RUNNING
- TOLERANCES OBTAINED ARE TYPICALLY 0.005 TO 0.010

RAPID PROTOTYPING

- THE BUILD CHAMBER IS ABOUT 12” X 13” X 17”
  - THE CHAMBER IS FILLED WITH DURAFORM POWDER
  - A NITROGEN BLANKET IS APPLIED
  - POWDER BECOMES SELF-SUPPORTING

RAPID PROTOTYPING

- A 100 WATT CO2 LASER IS SCANNED ON THE SURFACE OF THE POWDER
  - EACH PASS OF THE LASER ADDS 0.004" LAYER TO THE MODEL
  - THE PART IS BUILT FROM THE BOTTOM UP IN AN INCREMENTAL FASHION

RAPID PROTOTYPING

- UPON COMPLETION THE PART IS SIMPLY SEPARATED FROM THE SURROUNDING POWDER BY A SIMPLE SHAKEOUT
- THE PROCESS IS NEAT, CLEAN, SAFE, AND ENVIRONMENTALLY FRIENDLY
- COST TO PRODUCE < $7000!

RAPID PROTOTYPING

- HERE ARE SOME OTHER SUCCESS STORIES

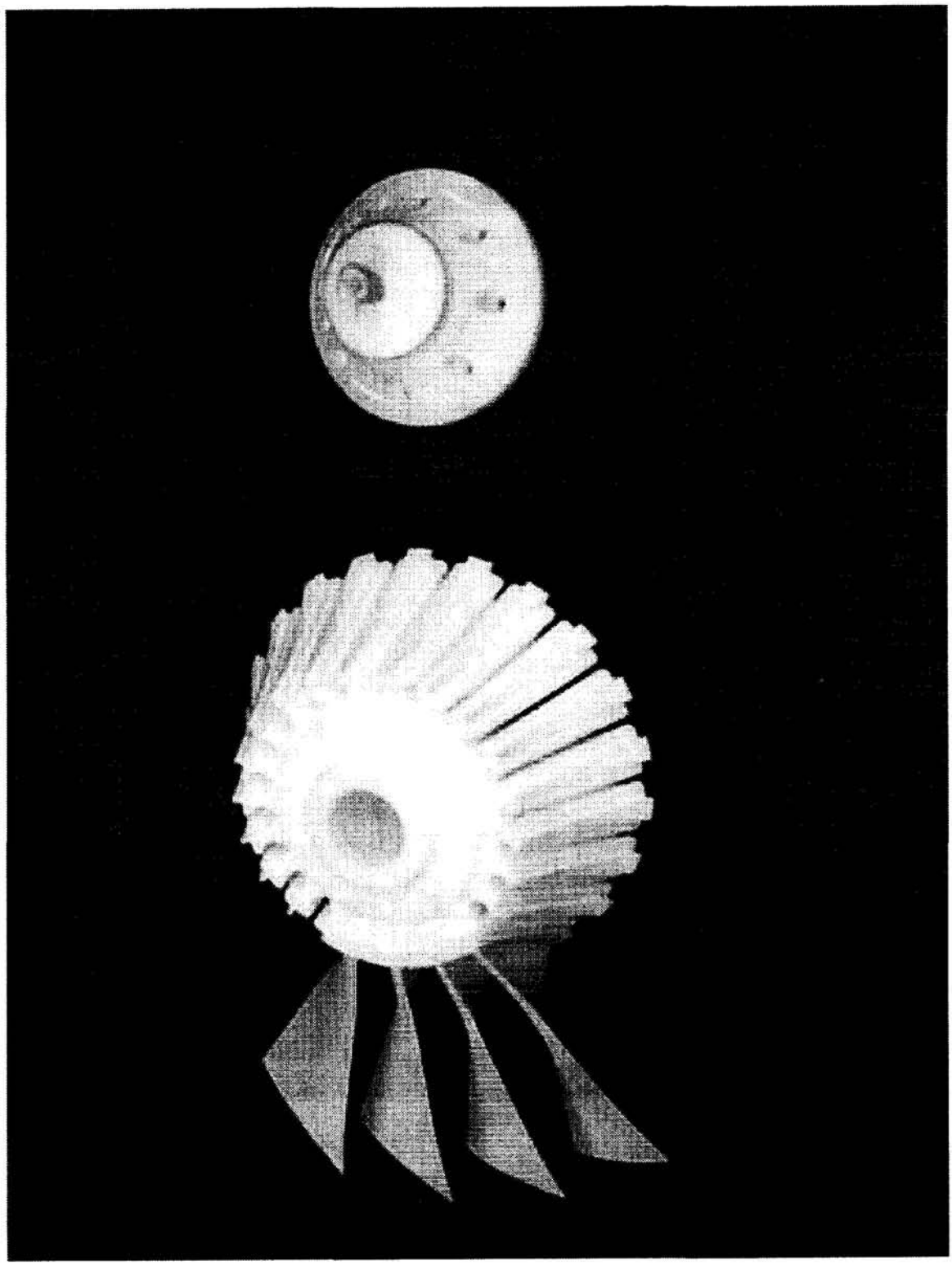

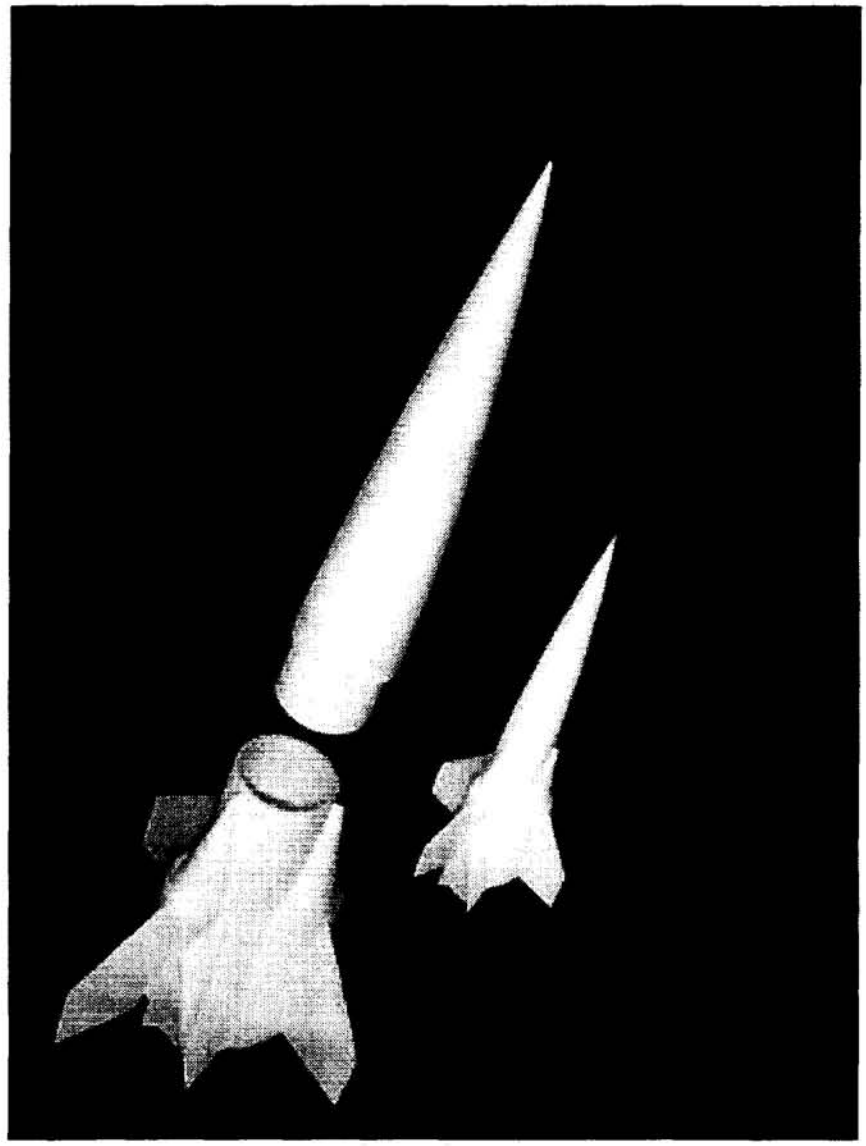

RAPID PROTOTYPING

- THE BENEFITS ARE IMMEDIATE
  - THE PARTS ARE VISUALLY CLEAR TO ALL
  - ANY NEEDED MODIFICATION CAN BE SEEN IN DETAIL
  - TIME CONSUMPTION IS MINIMAL
  - EXTENDED PROCUREMENT PROCESSES ARE AVOIDED

RAPID PROTOTYPING

- GLENN RESEARCH CENTER HAS RECENTLY ORDERED AND WILL HAVE AVAILABLE LATER THIS YEAR A DMDS LENS TECHNOLOGY THAT WILL GIVE US A DIRECT METAL SINTERING CAPABILITY

CP/538/IN/26
ABS. ONLY

High-Efficiency Monolithic Lightweight Aluminum Cast Structure

JOHN BOWKETT

Nu-Cast, Inc.
29 Grenier Field Road
Londonderry, NH 03053 USA
Phone: 603-432-1600
Fax: 603-432-0724
E-mail: nci@grolen.com

Nu-Cast, Inc., is manufacturing highly efficient, low-cost truss-like platforms/structures using the investment casting process developed at Nu-Cast, Inc., and the current rapid prototyping capabilities of steriolithography (SLA). This integrated production process allows for direct transfer of the computer design into hardware with a minimum of compromising fabrication restrictions. In the monolithic 3D-truss approach, control of structural integrity and thermal homogeneity is significantly improved over conventional multipart assemblies because of the elimination of most joint problems and their analytical uncertainties. For example, preliminary analysis of a typical 3D-truss-based instrument platform indicates a potential increase in stiffness up to 130X when compared to a plate of equal mass and area. Localized high-stress areas can be eliminated easily using this approach; additional material can be added locally during normal detailed design to satisfy the part's system requirement and to allow an efficient structural design to become a reality. Additionally, there can be a significant cost reduction for this monolith, compared to multipart assemblies, especially where tight tolerances are not system-functional but are only required for individual piece-part assembly/interface. The improved component performance achievable at a given weight with reduced resource expenditure will clearly support the NASA mandate to "do more with less."

p 29 pw 01

Preliminary Component Integration Utilizing Rapid Prototyping Techniques

Ken Cooper, NASA Marshall Space Flight Center
Pat Salvail, IITRI

Abstract

One of the most costly errors committed during the development of an element to be used in the space industry is the lack of communication between design and manufacturing engineers. A very important tool that should be utilized in the development stages by both design and manufacturing disciplines is rapid prototyping. Communication levels are intensified with the injection of functional models that are generated from a drawing.

At the Marshall Space Flight Center, this discipline is utilized on a more frequent basis as a manner by which hardware may be tested for design and material compatibility.

Background

Rapid prototyping in this text refers to a collective set of solid freeform fabrication technologies, which build physical models directly from computer aided design (CAD) data. The fixtureless processes operate in an additive fashion, whereas each model is built from the bottom upwards by adding thin horizontal layers of material.

The MSFC maintains a unique rapid prototyping laboratory, equipped extensively with each domestically available rapid prototyping technology; a total of seven processes in all. These include the following:

1. Stereolithography, a liquid-resin based technology which employs an ultraviolet laser to selectively cure the epoxy into the shape desired.
2. Selective Laser Sintering, a powder-based process which uses a laser to melt cross sections of polymer or semi-metallic powders into the shape desired.
3. Laminated Object Manufacturing, a solid-based process which adheres layers of paper, plastic or composite and cuts each cross section with a laser.
4. Fused Deposition Modeling, another solid-based process which extrudes a semi-molten thermoplastic through a moving XY orifice to form the necessary shape.
5. Multi Jet Modeling builds solid wax patterns by printing layers of hot wax directly through standard print jets.
6. Three Dimensional Printing prints layers of binder into a polymer powder matrix.
7. Laser Engineered Net Shaping deposits a thin bead of metal powder into the focal point of a high-powered laser, while the part is moved in the XY plane underneath to form the cross sections properly.

These processes are employed at the MSFC for a variety of concurrent engineering tasks, including concept modeling, assembly verification, fit-check analysis, flow functionality testing and investment casting pattern making.

Applications at the MSFC

Shooting Star Experiment

During the initial stages of the Shooting Star Experiment, rapidly produced absorbers were cast of a superalloy to be used in thermal experiments, prior to the procurement of the rhenium hardware.

Early designs of the solar thermal engine housing and absorber inserts were rapid prototyped in an investment casting wax in a matter of days, and the parts were investment shelled and cast on-site within four weeks.

These hardware castings have been, and continue to be, tested extensively by thermal elevation and cycling in the MSFC Test Stand Area. Data from these inexpensive models allowed for early analysis of the functionality of the engine design, as well as saving the project just under $300,000 and six to twelve months of lead time. (See Figures 1 and 2)

Simplex TurboPump

Another application involved the Simplex TurboPump, a high pressure experimental turbomachinery design. The application of rapid prototyping prevented a costly mistake in the manufacturing of the pump's complex impeller.

Five of the components were set to be machined, at an individual cost of $60,000 each. The drawings had already been delivered to the machine shop and tooling-up had begun when a rapid prototyped model was fabricated using MSFC's stereolithography apparatus.

The resulting plastic model verified that the blueprints designated the impeller blades the exact reverse of what the final part needed to be, and hence production was altered to make the final correct designs. Approximately $300,000 again was saved by a simple plastic model which cost about $1,000 to prototype.

Additional savings in time and cost were then added throughout the life of the Simplex program by the application of rapid prototyping and investment casting to provide castability verification of candidate materials, fabrication planning and continuous auditing with functional models and hardware. (Figure 3)

Space Shuttle Main Engine Fuel Ducts

During a redesign of the Space Shuttle Main Engine, it was determined that replacement of existing supply and drain fuel lines would reduce weight and increase safety and reliability.

The previously used lines were fabricated by welding various shaped sections of steel line together in order to access all of the required inlet/outlet ports of the engine.

The new design called for continous feedlines to be custom-formed from tubing to reduce the weight of the welds, optimize flow and decrease the probability of fuel leakage.

Unfortunately, the first hot gas duct to be fabricated didn't integrate properly after additional hardware was attached to the engine during assembly. The process to correct the problem was costly and time consuming, and it was determined that rapid prototyping patterns be fabricated for the remaining five ducts for fit verification.

Each duct was approximately seven feet in length and six inches in diameter, with a complex three-dimensional curvature and precisely placed junctions. The prototypes were fabricated in twelve-inch sections using the laminated object manufacturing process at MSFC, and it took two to three weeks to fabricate the entire set. The engine contractor designed each section having dissimilar boss-and-socket alignments for proper assembly.

These prototyped lines were shipped to the engine contractor facility, where they were assembled and mounted to an actual main engine to verify the designs prior to manufacturing the remainder of the required lines. A potential cost saving of approximately $35,000 per line was recognized by the application of the rapid prototyping models, resulting in an overall potential savings of about $175,000 and several months of lead-time. (Figures 4)

Meteorite Patch Kits

One continuous application of rapid prototyping at MSFC involves a project that applies meteorite patch kits. The process requires precise mixing of a two-part solution to obtain the adhesive properties required for composite material bonding.

A special funnel was designed which allows for accurate delivery of each component of the adhesive mixture. Due to the low number of these funnels that are required, approximately two to four every year, it is not cost effective to have them mass-produced.

The solution is to directly fabricate the funnels using rapid prototyping. The materials used are compatible and provide adequate strength and density to prevent permeation or breakage. The funnels are even chemically cleaned and reused several times prior to disposal.(Figure 5)

Space Shuttle Main Engine Fuel Seals

Another shuttle engine application of rapid prototyping occurred recently when, after a design change, it was found that a particular fuel line didn't match up properly with a pump.

The result was a need for a flexible seal, which consisted of a 270-degree rotation of an eccentric nature. The overall part required was about nine inches in diameter.

The contractor for the pump received several solid prototypes of the flange from the MSFC rapid prototyping lab. These parts were used to make molds, which in turn produced the final products required to satisfy the needs of the engine.

Summary

The application of rapid prototyping technologies at the MSFC continues to yield significant cost and timesavings to NASA projects. Increased use of these technologies is anticipated in order to cater to a concurrent engineering environment that has been realized due to decreased funding allocations and project time constraints mandated throughout the agency.

Similar applications and successes are seen throughout the private manufacturing industry, as well, where profit margins and a highly competitive market drive companies to deliver products quickly and efficiently.

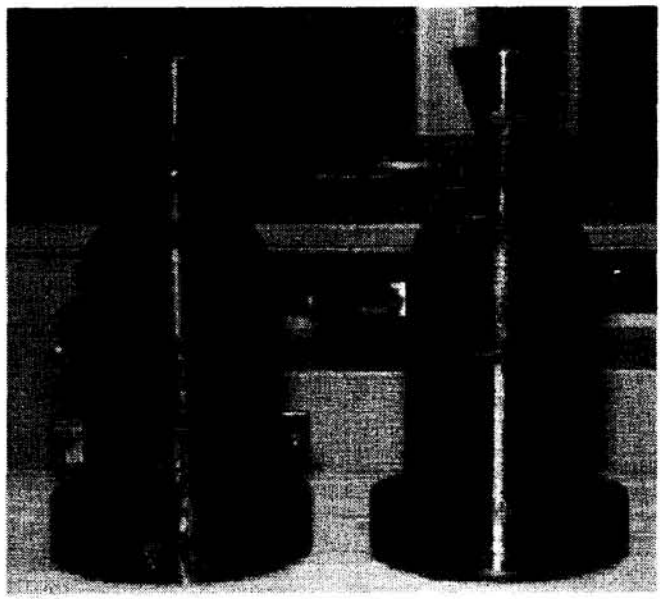

Figure 1

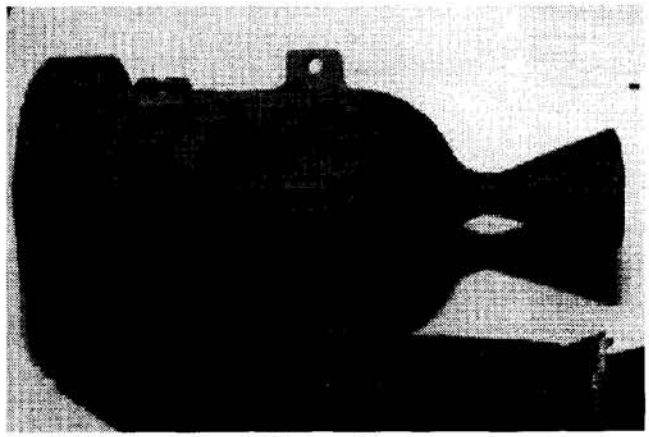

Figure 2

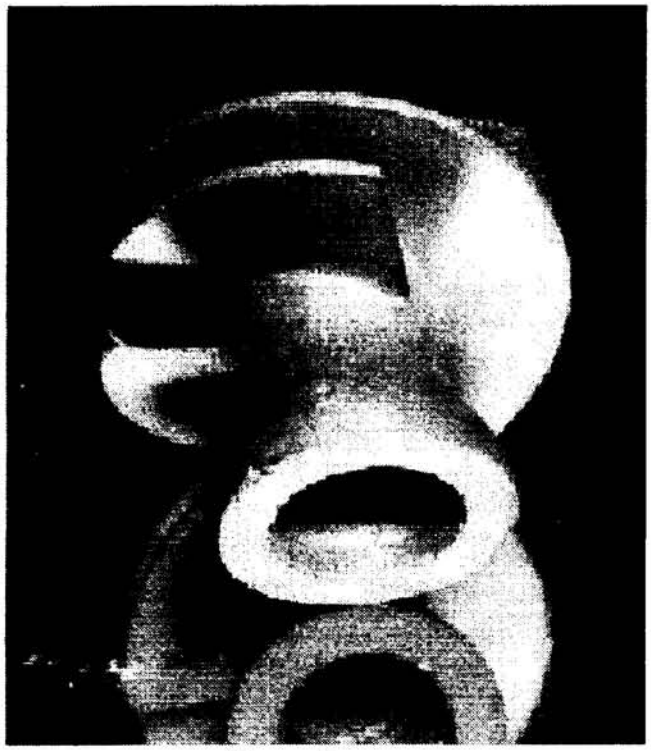

Figure 3

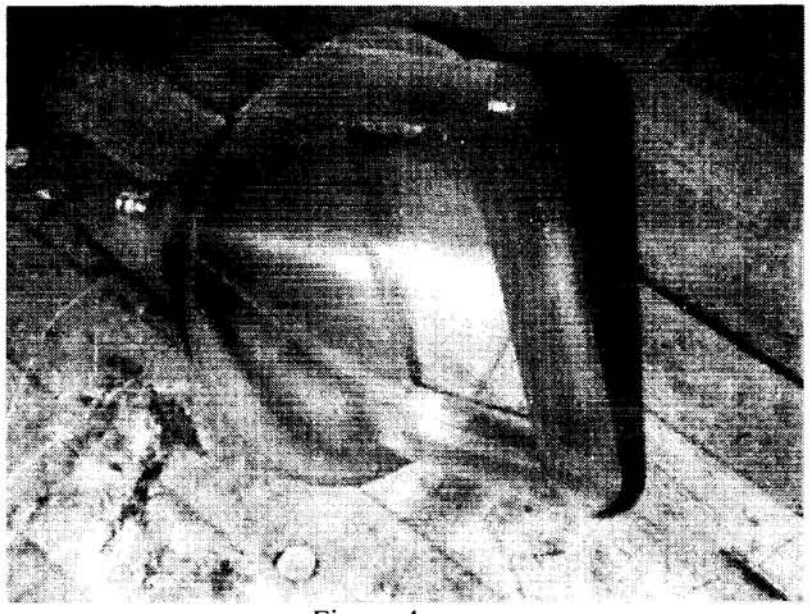

Figure 4

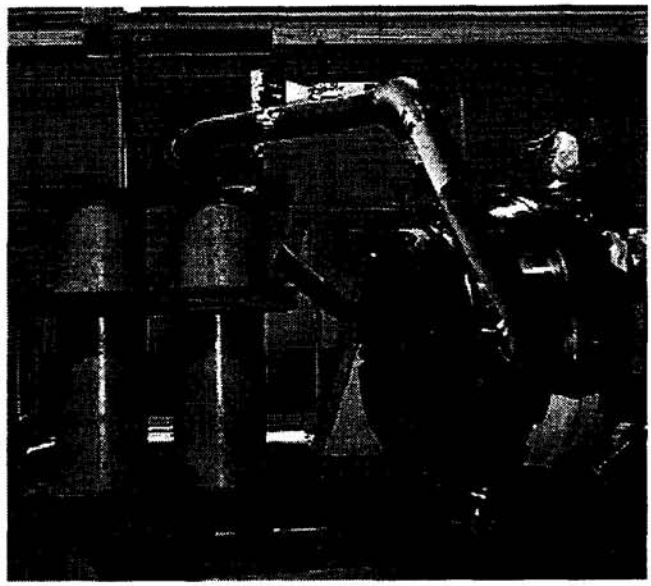

Figure 5

Multifunctional Carbon Foams for Aerospace Applications

DARREN K. ROGERS and Janusz Plucinski

Touchstone Research Laboratory, Ltd.
Triadelphia, WV 26059 USA
Phone: 304-547-5800
Fax: 304-547-5764
E-mail: dkr@gold.trl.com

Carbon foams produced by the controlled thermal decomposition of inexpensive coal extracts exhibit a combination of structural and thermal properties that make them attractive for aerospace applications. Their thermal conductivity can be tailored between 0.5 and 100 W/mK through precursor selection/modification and heat treatment conditions; thus, they can serve in either thermal protection or heat transfer systems such as heat exchangers. Because their structure is essentially a 3D random network of graphite-like members, they also can be considered low-cost, easily fabricated replacements for multi-directional structural carbon fiber preforms. Strengths of over 4000 psi in compression are common. Their density can be designed between 0.1 and 0.8 g/cm^3, and they can be impregnated with a variety of matrices or used, unfilled, in sandwich structures. These foams also exhibit intriguing electrochemical properties that offer potential in high-efficiency fuel cell and battery applications, mandrels and tooling for composite manufacture, ablative performance, and fire resistance.

This paper presents the results of research conducted under NASA SBIR Topic 99.04.01, General Aviation Technology, supported from Langley Research Center. The potential of foam design through precursor selection, cell size and density control, density grading, and heat treatment is demonstrated.

Polymer Matrix Composite Material Oxygen Compatibility

Marshall Combustion Research Facility
Materials and Processes Laboratory
Marshall Space Flight Center

Tom Owens
Materials and Processes Laboratory

Materials Combustion Research Facility

- Problem Statement:
  - New Launch Vehicles require lightweight structures to achieve design goals
  - Polymeric Composite materials are being used in applications where lightweight structures are needed
    - Composite materials have been used successfully in many times:
      - Liquid Hydrogen Tank
      - Propellant Feedlines
      - Shroud Structures
      - Intertank Structures
  - Potentials weight savings for use of composite materials for Liquid Oxygen (LOX) tank structures is on the order of 25% weight reduction when compared to AL2219

Materials Combustion Research Facility

- All materials must be evaluated for oxygen compatibility
- Materials exposed to elevated oxygen concentration and pressure possess and increased combustion hazard
- **Oxygen Compatibility**: The ability of a material to coexist with oxygen and potential ignition sources with an acceptable degree of risk.
- **Fire Triangle** - Combustion to occur, three factors must be present:
  - Fuel
  - Oxidizer
  - Ignition Source

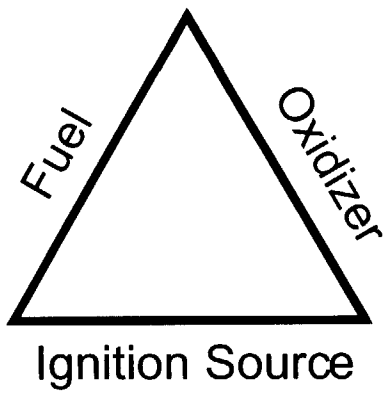

Materials Combustion Research Facility

- Materials Testing
  - Because of the present difficulties in analysis for oxygen compatibility, we rely on testing to determine the oxygen compatibility of a material
  - Credible ignition sources are tested to determine the sensitivity of the material to ignition
- Two Standard Tests for Oxygen Compatibility
    - Per the requirements of NHB 8060.1C, Flammability,Odor, Offgassing, and Compatibility Requirements and Test Procedures for Materials in Environments that Support Combustion
  - Mechanical Impact (Test 13)
  - Upward Propagation (Test 17) also known as "Promoted Combustion"

Materials Combustion Research Facility

- Mechanical Impact (Test 13)
  - Striker pin transfers energy from 20 lb plummet dropped from 43.3 inches
  - Success criteria, 0 reactions out of 20, or if one reaction occurs, 40 additional tests with no reaction, 72 ft-lbs (98J)
  - Composite materials generally fail
  - Advantages:
    - Large Database
    - History of application
    - Fast
    - Inexpensive
    - Small amount of material required
    - Can be used as a relative ranking method

Materials Combustion Research Facility

- Example of a typical composite material failure following mechanical impact in LOX
- Failure criteria includes:
  - Audible report
  - Flash
  - Visible charring of sample cup, striker pin, or sample
- Test is conservative, 72 ft-lbs is a large amount of energy
- IM7/8552 has been tested for damage tolerance, and energies greater than about 2 ft-lbs caused cracking that was significantly permeable

Materials Combustion Research Facility

- Promoted Combustion Test (Test 17)
  - Test determines the relative flammability of a material in 100% GOX.
    - Samples are 12" x 1/8"dia. "rods"
    - Materials burning less than 6" at the maximum use pressure are given an "A" rating
    - Samples are ignited by aluminum "promoter" and pyrofuse wire (aluminum-palladium)
    - A minimum of 5 samples are tested

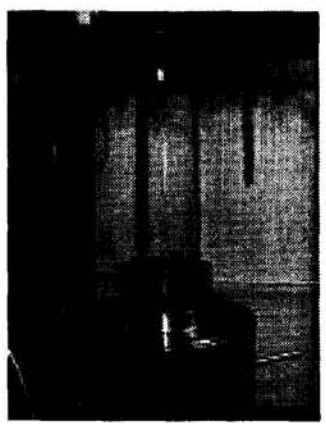

Materials Combustion Research Facility

- Mechanical Impact results
  - Many composites readily fail the mechanical impact test, often failing at low impact energy levels of 10-20 ft-lbs
  - Some materials are passing at higher energy levels, even as high as the 72 ft-lb requirement, however these results are from a limited amount of data
- Promoted Combustion results (Test 17)
  - Test 17 determines the relative flammability of materials in GOX at ambient temperature at a specified pressure
  - All composite materials fail this test readily at their intended use pressures
  - The consequence of failure (ignition), the tank would be fully consumed, and fail catastrophically
- Alternate Approach
  - Evaluate component design, relative risks and potential ignitions sources
  - Test composite materials for relative risk

Materials Combustion Research Facility

- External Puncture Test
  - Punctures a disk of material 2.36" dia.
  - Punctures Outside to Inside
  - Liquid Oxygen on top of sample
    - LN2 jacket maintains -320°F
  - Pressures up to 100 psia
- Performance
  - Titanium, severe reactions
    - Samples Combust, Audible Report
  - Polymer matrix composite materials
    - No reactions to date

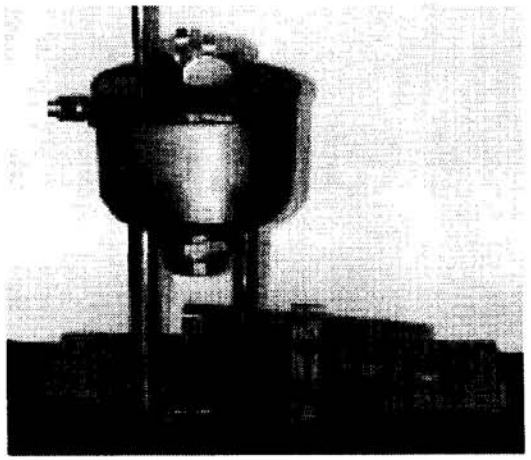

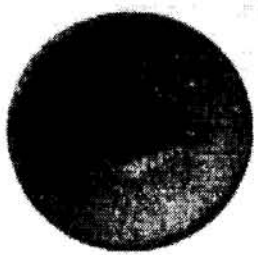

Punctured Composite

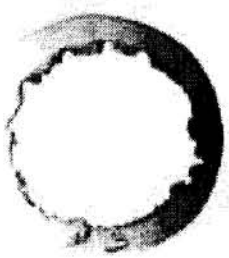

Punctured Titanium

Materials Combustion Research Facility

- Internal Puncture Test
  - Punctures a disk of material 2.35" dia.
  - Punctures Inside to Outside
  - Liquid Oxygen on top of sample
    - LN2 jacket maintains -320°F
  - Pressures greater than 100 psia
- Performance
  - Titanium, severe reactions
    - Samples Combust, Audible Report
  - Polymer matrix composite materials
    - No reaction to date
- Results are the same as External Puncture

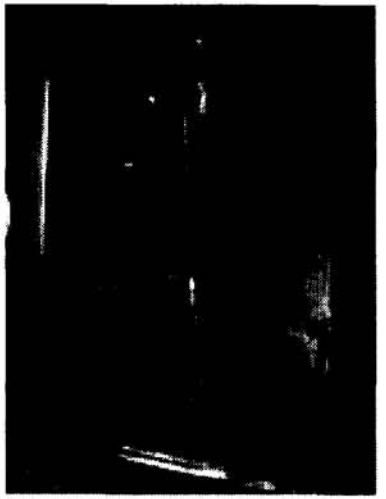

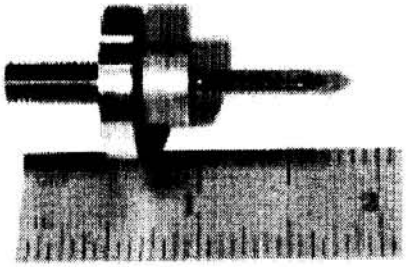

Materials Combustion Research Facility

- Electrostatic Discharge
  - Test Determines whether a spark is a credible ignition source
  - The system is capable of delivering a spark of 5000V, with an energy of 112.5J
  - Samples were tested of various thickness, ranging from 0.006" to 0.125"
  - Only one composite material has failed this test
  - Currently only ambient pressure tests

Materials Combustion Research Facility

- Friction (Low Speed Friction)
  - Test determines the relative ignitability of composite materials when heated by friction while immersed in LOX
  - Well over 100 tests have been completed to date in both LOX and GOX, using a modified drill press
  - One sample is held stationary, and one sample is rotated in sample holder placed in the drill chuck, data measured included axial load (lbs) and stationary sample temperature using an embedded thermocouple
  - Samples reached maximum temperatures exceeding 600°F, this exceeds the maximum use temperature of the composite (~350°F), the composite samples disintegrated during the test
  - Samples showed no signs of reacting with the liquid oxygen, faint burn smell existed after the test

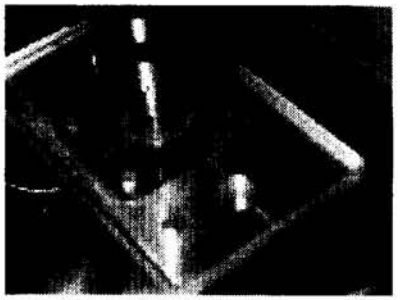

Materials Combustion Research Facility

- Pyroshock Sensitivity

Materials Combustion Research Facility

Test Method	Titanium	AL 2219	Composites
Reaction Frequency at 72 ft-lbs	19-60%	<10%	~85%
Impact Energy Threshold (ft-lbs)	15-20	72	10-40
Upward Propagation Threshold Pressure	<1 psi	<30 psi	<14.7 psi
Shock Sensitivity	Very High	Very Slight	Very Slight
Puncture Sensitivity	Very High	Unreactive	Unreactive *
Spark Sensitivity	Reactive	Unreactive	Very Low
Vibration Sensitivity	Slight	Slight	Low **
Frictional Heating Sensitivity	High	Low	Low *

* Limited number of tests

** Per testing performed by McDonnell Douglas

Materials Combustion Research Facility

- Results
  - Titanium (found to be unsuitable for LOX tank applications)
    - High sensitivity to mechanical impact
    - Sensitivity to pyroshock
    - High sensitivity to puncture
    - Low pressure for sustained combustion
  - Aluminum (the standard LOX tank material)
    - Performs well on most tests with the exception of Promoted Combustion
  - Polymer Matrix Composites (better than Titanium, and worse than Aluminum)
    - Mechanical Impact - wide variability (10 ft-lbs to 72 ft-lbs)
    - Puncture Acceptable (External and Internal)
    - Electrostatic Discharge Acceptable
    - Friction Acceptable
    - Pyroshock Acceptable
    - Particle Impact Acceptable (WSTF)
    - Adhesive Failure hasn't caused ignition (WSTF)

Materials Combustion Research Facility

- Future Work
  - Continue to refine Hazard Analysis
  - Test new credible ignition sources
  - Additional Coupon Tests
    - Elevated Pressure ESD
    - Elevated Pressure Friction
    - Electrical Overload
  - Push Oxygen Compatibility Testing beyond "Coupon Level"
    - Vibration testing of small bottles
      - Boeing (McDonnell Douglas) has demonstrated this on one bottle
    - Burst Tests with small bottles

- LOX Tank Design Recommendations
  - Goal is to lower the risk by management of the "Fire Triangle"
    - Fuel
      - Choose the most compatible materials that are suitable
      - Keep the composite cold
      - Liners?
    - Oxygen
      - Keep the oxygen as cold as possible
      - Inert gas pressurant system, such as helium
    - Ignition Sources
      - Avoid objects in the tank that can cause mechanical impact
      - Design to minimize other potential ignition sources

- Conclusions
  - Carbon Fiber / Polymer Matrix Composite Materials look promising as a material to construct LOX tanks
  - Based on mechanical impact tests the risk will be greater than aluminum, however the risk can probably be managed to an acceptable level
  - Proper tank design and operation can minimize risk
  - A risk assessment (Hazard Analysis) will be used to determine the overall acceptability for using polymer matrix composite materials
    - Note: A individual Hazard Analysis must be performed on each and ever LOX tank design to evaluate the relative safety of design and operation

CP 2021 N 26

Low Density Monolithic Metal Honeycombs by Thermal Chemical Processing

PI's: Joe Cochran, Jim K. J. Lee*, Dave McDowell, Tom Sanders
GRA's: B. Church, J. Clark, B. Dempsey, 'Le Hayes, K. Hurysz, T. McCoy,
J. Nadler, R. Oh, W. Seay, B. Shapiro

Schools of Materials Science and Engineering & Mechanical Engineering
Georgia Institute of Technology
(*:presenting: jki.lee@mse.gatech.edu)
(Main Contact: joe.cochran@mse.gatech.edu)

Fourth Conference on Aerospace Materials, Processes and Environmental Technology
September 18-20, 2000, Huntsville, Alabama

A technology developed at Georgia Tech allows fabrication of thin-walled metal articles. Using conventional powder processing techniques, precise shapes were formed with non-metal precursors and subsequently converted to the metal state by a direct reduction process. The metal articles can be formed via powder forming techniques including extrusion, slurry coating of sacrificial cores, slurry casting methods (slip, pressure, centrifugal, tape, and gel casting), and dry pressing. By using fine powders in the micron and sub-micron range, articles that have small dimensions (i.e., micro- to milli-meter) may be formed. Practical experience has shown that maximum particle sizes of 1/50 of the feature dimension are necessary for producing features with good precision. Through a properly controlled conversion process, the articles formed from brittle powder precursors (principally oxides) are chemically converted into a metal article with structural integrity and substantially the original shape. A variety of shapes have been formed by (1) Honeycomb Extrusion, (2) Spray Coating, (3) Dry Pressing, (4) Slip Casting, and (5) Tape Casting. Demonstrated alloys include stainless steel, maraging steel, Inconel 617 and 718, Super Invar, and copper alloys. Demonstrated strength and specific energy absorption of a maraging honeycomb at 1.5 gm/cc were approximately 400 MPa and 100 Joules/gm respectively.

Low Density Metal Structures

There are basically five types of metal foams or cellular metal structures that are either being used or under development as promising low density structures. These structure types (Fig.1) are closed cell foam (e.g., ALPORAS by Shinko Wire, Ltd.), open cell foam (e.g., reticulated foams by ERG, Inc. and INCO, Ltd.), hollow sphere foam (Georgia Tech and Fraunhofer), honeycomb (Hexcel and Georgia Tech), and lattice structure (Molecular Geodesic, Inc. and JAMCORP.). The first three types are stochastic in nature, the honeycomb and lattice structure are ordered or periodic structures. For each type of architectures, a variety of fabrication methods are possible. For further details on these foams, readers are referred to Metal Foams: A Design Guide by M. Ashby et al. [1], in which the production methods and properties are described.

The characteristics of a low density structure can be best described by its dominant geometry, relative density (ρ^*/ρ_s), and solid material properties. Defects and anisotropy, which most often are present, play a very important role in behavior of the low density structure. Above all, the relative density (ρ^*/ρ_s), a ratio of foam density (ρ^*) to solid material density (ρ_s), is the single most important parameter. Various mechanical, thermal, and physical properties are a function of ρ^*/ρ_s. The scaling relationship takes the form of

$$P^*/P_s = \alpha(\rho^*/\rho_s)^n \qquad (1)$$

where P is a property, α is a constant and n is an exponent. (Note: the superscript * means property of the foam and the subscript s means property of the solid.).

Using foam geometry as an example, when P represents the thermal conductivity of a metal foam, λ, the equation becomes

$$\lambda^*/\lambda_s = (\rho^*/\rho_s)^{1.65\sim1.80} \tag{2}$$

for both the open and closed cell type, with α being one. When P represents the electric resistively of a metal foam, R, the equation becomes

$$R^*/R_s = (\rho^*/\rho_s)^{-1.60\sim-1.85} \tag{3}$$

for both the open and closed cell type, with α being one.

For compressive strengths of foams, the global scaling relationships are

$$\sigma^*/\sigma_s = (0.1\sim1.0)(\rho^*/\rho_s)^{1.5} \tag{4}$$

for open cell type and

$$\sigma^*/\sigma_s = (0.1\sim1.0)[0.5(\rho^*/\rho_s)^{0.67} + 0.3(\rho^*/\rho_s)] \tag{5}$$

for closed cell type, where σ is the compressive strength. Specifically, the most widely accepted strength to relative density relationships are

$$\sigma^*/\sigma_s = 0.3(\rho^*/\rho_s)^{1.5} \tag{6}$$

for the open cell foam, and

$$\sigma^*/\sigma_s = 0.35(\rho^*/\rho_s) \tag{7}$$

for the closed cell foam. [2]

For honeycombs of all cell shapes (square, triangular, or hexagonal), the compressive strength in the cell axial direction (i.e., tested in the out of plane direction) scales linearly with relative density,

$$\sigma^*/\sigma_s = (\rho^*/\rho_s)\,. \tag{8}$$

When loaded off axis or tested in plane, cell walls are subjected to bending and transverse strengths are lower by a certain amount depending on cell shape and angle of force loading.

Figure 2 contains plots of strength behavior of open and closed cell structures in comparison to honeycomb for stainless steel, titanium, and aluminum alloys according to Eq. (6), (7), and (8). The experimental properties of both open and closed cell foams sometimes fall short of the expected value by a factor of 2 to 100. [3] The experimental properties of hollow sphere foams fall between the theoretical closed cell and open cell foam curves. In general, hollow sphere foam is equal to or slightly better than the mechanical properties of closed cell foams.

Honeycomb vs. Foam

Current status of foam properties indicates major improvement in processing and alloy development are necessary before these foam structures to become competitive with ordered or periodic geometries. Based on Fig. 2, honeycomb geometry clearly excels among these low density structures, when structural application is the first order of consideration. Conclusive test results are rapidly becoming available to substantiate that honeycomb is the geometry-of-choice for better strength and stiffness, as compared to its stochastic counterparts.

Among low density structures, honeycombs are manufactured and used in commercial quantities. There are two basic honeycomb manufacturing methods. Traditionally, the aerospace industries use Al, Ti and Ni based superalloy honeycombs, along with other non-metal composites, for weight reduction. They are made with thin sheet or foil of the alloys, crimped into a corrugated profile and joined to form a hexagonal cell. The automotive industry uses ceramic honeycomb made of cordierite as catalyst supports for emission control. These structures are fabricated by extruding plastic paste of ceramic powders with a binder. After extrusion the product is dried and sintered to strengthen the webs.

To maximize the value of a low density structure, one needs to adopt the best possible geometry, to select a composition that has the suitable bulk properties, and to have it made with a process that is most economical. A geometry which is ideal for improved strength in transverse direction

is the triangular honeycomb shown in Fig. 3. Triangular cell honeycomb can be made by the extrusion process as easy as the square cell honeycomb. The same can not be said about the crimped sheet process. About cost, honeycomb by powder paste extrusion is also more economical. On the mass production scale, such as for the auto industries, finished parts are approximate at ~$5.00 per pound for the cordierite honeycomb. Therefore, extruded honeycomb should be the best candidate for meeting the above criteria.

Metal Honeycombs Made by Extrusion and Direct Reduction

An extruded square cell honeycomb, similar in composition to Inconel 617, is shown in Fig. 4. This thin-walled honeycomb, at 18% relative density, is made with a two step process. The first step is the shape fabrication and the next step is the conversion of non-metallic precursors to the corresponding alloy (Fig. 5). Shape fabrication is primarily done by powder paste extrusion at ambient temperatures. Other fine powder shape forming processes can also be employed. Conversion is carried out in solid state at elevated temperatures very similar to the direct reduction process (DR). Direct reduction is a process for the production of metal directly from metal bearing ores or oxides by removing the associated oxygen at temperature below the melting point of materials involved. Reducing agent can be a gas (e.g., hydrogen or carbon monoxide) or other solids (e.g., carbon). During the reduction process, hydrogen reacts with the oxygen and forms water vapor, which is then removed from the system. The open structure of the honeycomb provides an efficient path for hydrogen and water vapor transport.

In addition to honeycombs and hollow spheres, metal parts of a variety of geometries, such as rod, ribbon, tape, disk, and hollow ware have been fabricated with this process. They are used as test samples for the extraction of bulk material properties.

Process Capability and Composition Limit

Since the oxide particle sizes suitable for extrusion are small, on the average at ~5 microns, thin-walled (e.g., 50 to 300 microns) honeycomb webs are feasible. A number of transition metal oxides and their mixtures for a wide range of engineering alloys have been successfully processed. The list of oxides includes Fe, Ni, Co, Cr, N Cu, Mo, W, Mn, Nb, etc. Specific engineering alloys made so far include Fe12Cr SS, Cu30Ni, Fe18Ni10Co4Mo (maraging steel), Ni22Cr12.5Co9Mo (Inconel) and Fe32Ni5.5Co (Super Invar). For most oxide mixtures, complete reduction and 95 % densification of the walls of the honeycomb occurred in a hydrogen atmosphere at less than1350° C. Above 1350° C, melting and collapse of the low density structure can occur. For better conversion efficiency, one would like to conduct the reduction at high homologous temperatures (T/T_{mp}) of the resultant alloy when feasible.

Like the gaseous reducing agents, carburizing gases can be forced to flow through the honeycomb channels easily. Being able to add carbon to the alloy increases the composition flexibility greatly. Furthermore, honeycombs are better suited to survive the large shrinkage that occurs during the reduction process. Unlike other porous materials with random distribution of materials, the materials in honeycombs are uniformly and orderly distributed. The constant web thickness insures an equal coercion force to keep the material from separating or cracking, a phenomenon often observed where two neighboring unit cells were joined with a substantially smaller cross section.

A critical issue related to the direct reduction process is the reducibility of the constituents involved. Elements such as Ti and Al, whose oxides are stable at these temperatures with pO_2 level in the range of ~10^{-16} atm or higher, can not be introduced into the alloy as oxide. When needed, Ti and Al must be added by secondary processes such as pack bed cementation, chemical vapor deposition, or in the form of other compounds. These methods for introducing Ti and Al are being investigated.

Reduction of oxides to the metallic state results in a large density increase, translating to a shrinkage typically on the order of 30 to 70 % by volume. Shrinkage can be an advantage for producing finer geometric features that would otherwise difficult or expensive to fabricate. For example, the cell density of a square cell honeycomb with 400 cell per square inch (csi) in the green (oxide) state increased to 900 csi after reduction and sintering (Fig. 6). State-of-the-art extrusion technology is capable of producing web thickness at around 100 microns, which translates to ~70 micron web after reduction. Similarly cell size of 500 microns is projected to be feasible with this technology. Bulk density achievable controllably with this process can approach 8% of theoretical on the low end.

Other Process Issues

The direct reduction process can be coupled with various fine powder fabrication techniques such as casting, coating, pressing to make other complex shapes. Direct reduction by hydrogen can also be replaced with thermal decomposition when metal carbides and hydrides are used as the precursors. For example, Ti hollow sphere foams were made using TiH_2 as the raw material which was converted to Ti by thermal decomposition in an inert or vacuum environment.

Another important feature of the honeycombs made by extrusion is the connectivity of the honeycomb with the outer surface. It is therefore quite feasible to include an integral skin layer on the structure. Hermeticity of the structure can be obtained by capping off the open ends to prevent water vapor or other elements from entering the structure.

The ability to manufacture metal honeycombs from their oxides has cost advantages as well. Most oxides of transition elements are colorful and hence have been used as pigments, colorants, or inorganic dyes. Fine oxide powder of these oxides is readily available at very low cost. The cost differential between a metal oxide powder and its metal counterpart, if and when it is available, is usually better than a 1-to-10 ratio.

Metallurgy of Alloys via Direct Reduction

The mechanical performance of honeycomb structures is directly related to the properties of the bulk material according to the Gibson-Ashby model. Therefore it is necessary to study the bulk material processed via the same route. Samples in the form of 1.8 mm diameter rods and 10 mm X 0.5 mm ribbons were fabricated for bulk property measurements. The important measurements of the bulk material are density/porosity, pore size/morphology, grain size/microstructure, yield strength, and modulus. Properties of two popular engineering alloys (Maraging 350 for high strength and Inconel 617 for high temperature applications) were tabulated in Table I. Square cell honeycombs of the same compositions at 18% relative density were tested for mechanical properties reported in the next section. Other properties in the transient state such as compositional homogeneity, oxide–metal interface and presence of intermediate reaction compounds were also studied for better understanding of the conversion process.

On the average, the porosity value derived from density measurement of the maraging steel composition was 5-7% and the Inconel 617 composition 7-15%. The higher porosity of the Inconel is associated with the high content of the hard-to-reduce Cr_2O_3 in the starting composition. First, the high vapor pressure of CrO_x at high temperatures (e.g., >1200C) can lead to voids resulted from vapor phase transport. With a large amount of Cr_2O_3, reduction and subsequent sintering would require longer time to complete. Longer soaking at peak temperatures should lead to lower porosities [4], assuming no abnormal grain growth to occur.

A sizable gap existed for both compositions in terms of their mechanical properties, comparing the direct reduction alloy with the regular alloy. First of all, porosity was believed to play a significant role. The low elongation at failure (e.g., 1-2% for the Maraging steel) was a good indication of brittle behavior of the alloy. For material to fail by brittle fracture, its strength decays as a function of porosity according to the following equation,

$$\sigma_p / \sigma_o = \exp(-nP) \qquad (9)$$

where σ_p and σ_o is the strength with and without pore, P is porosity and n is a constant with a typical value of 4 to 6.[5] Figure 7 shows a plot of the equation, showing porosity as a strong strength decay factor. A second cause was composition limitation of the process, leading to the absence of either Al or Ti from the chemical makeup. In the case of Maraging steel where minor constituent like Ti participates in age hardening by forming precipitates of Ni_3Ti, the effect on strength when it is missing from the composition is obvious (Fig. 8). [6] The magnitude of strength decay was believed to be confounded by the two variables described above.

Compression Testing of Monolithic Metal Honeycombs

Compression experiments were conducted on honeycombs with 3x3, 5x5 7x7 and 10x10 cell arrays at two orientations (in-plane and out-of-plane) under both quasistatic and dynamic conditions. All experiments were conducted at room temperature. Quasistatic experiments were performed by compressing between planar parallel platens at an engineering strain rate on the order of 10^{-4} s^{-1}.

Dynamic experiments were performed using a split Hopkinson assembly at engineering strain rates on the order of 10^3 s^{-1}. In all cases, simple measures of nominal stress and strain were employed to reduce the data. The nominal stress is defined as current load divided by original cross-sectional area, and the nominal strain is defined as the magnitude of the change of length divided by the original length. Use of nominal measures is sufficient since the honeycomb is a structural rather than material element. These measures are also labeled as normalized load and displacement in plots.

Honeycomb samples were prepared by extrusion and hydrogen direct reduction as described earlier in this paper. A typical 10x10 in-plane array of cells is shown in Fig. 9. For these honeycombs, the cell size d is approximately 1.5 mm. The relative density is about 0.18. Several types of defects arise from the extrusion process, including corrugation or waviness of cell walls with a period on the order of the cell diameter, separation of cell walls, and skew cells.

Sample preparation included cutting sections of uniform length from extrusions in either the green state or after reduction. Green state machining was used to extract specimens of smaller dimension (e.g. 3x3 or 5x5 cells) to examine constraint and scale effects. Samples were placed between two flat and parallel compression platens, either loosely or bonded with epoxy to explore effects of end fixity. Tests were performed at room temperature using displacement control. Samples were compressed under quasistatic loading until the densification strain was exceeded.

Mechanical Properties of Extruded Honeycombs

In Fig. 10, both out-of-plane and in-plane compression behavior of the Inconel 617 honeycomb are shown. The first minimum after initial buckling instability in the out-of-plane case is due to classical wall wrinkling near the platen that extends across the entire lateral dimension. In the in-plane case, each local minima of load owes to a collapse of a row of cells, and hence the marked undulations of load versus displacement, a progressive crush band type of behavior. Quasistatic collapse is highly inhomogeneous for the relatively ductile Ni-alloy walls, although cell wall fracture is observed in the post-buckling behavior of some of the walls. In contrast, Fig. 11 compares the significantly higher plateau stress of a honeycomb made with Fe18Ni Maraging steel composition, aging tempered to result in a precipitation hardened structure. This steel has much higher yield strength but lower ductility than the in situ Ni walls, producing a remarkable initial normalized buckling load (engineering stress) in the range of 300-400 MPa, and a plateau stress level of about 200 MPa.

Cell wall fracture dominates the compressive response of the Maraging steel honeycombs. These fractures occur in rather random, distributed fashion, likely contributing to the excellent capacity for energy absorption. Typical plateau stress values for the out-of-plane case are much higher than Al open or closed cell foams. Although the behavior of these honeycombs is highly anisotropic, the energy absorption (area under nominal stress-strain curve up to the point of densification strain) is considerably higher than these random Al foams, even for in-plane loading conditions.

Furthermore, the in-plane behavior of the Maraging steel exhibits less variation of the plateau stress level. It was found in quasistatic experiments that there is a certain dimension below the results become specimen size dependent; this dimension appears to require more than about seven cells to achieve. For smaller arrays, the plateau stress decreases, possibly due to a lack of constraint on the propagation of crush or localization bands that emanate from isolated defects. Figure 12 compares the energy absorption for both in-plane and out-of-plane compression of Maraging steel honeycomb relative to other low density metal foams; the out-of-plane energy absorption is orders of magnitude higher than common low density metal foams with comparable relative density. Figure 13 compares the dynamic (10^3 s^{-1}) compressive response of Ni-alloy honeycombs loaded out-of-plane with the quasistatic behavior. An increase of impact energy absorption of approximately 40% is observed, depending on aspect ratio. It appears that more uniform compaction is achieved in the dynamic case.

Concluding Remarks

Low density metal honeycomb is a highly functional geometry in terms of its density adjusted property. This technology has the advantage over conventional metal fabrication techniques for making monolithic honeycomb. The direct reduction process is proven feasible for making quality alloys with good mechanical properties. Specific energy absorption at orders of magnitude higher than common low density metal foams is achieved. It is made possible with the combination of honeycomb geometry, high strength alloy (maraging steel) composition and powder paste extrusion. Three processing issues are

identified for further improvement. There are, namely, reduction of processing induced defects, full densification of wall material, and addition of essential trace elements. The projected strength is 660 MPa for a maraging steel (Maraging 350) at a density of 1.5 gm/cc once improvement agenda Is fully implemented.

Acknowledgement

This work is sponsored by DSO of DARPA (N00014-99-1-1016) and ONR (N0014-99-1-0852) and monitored by Dr. L. Christodoulou of DARPA and Dr. S. Fishman of ONR. The assistance by Prof. Min Zhou of ME/Georgia Tech in Hopkinson bar testing is appreciated.

References

1. Ashby, M.F., Evans, A., Fleck, N.A., Gibson, L.J., Hutchinson, J.W. and Wadley, H.N.G., Metal Foams: A Design Guide, Butterworth-Heinemann, Boston, 2000.
2. Gibson, L., Ashby, M.F., Cellular Solids: Structures and Properties, 2nd Ed. Camnbridge University Press, Cambridge, UK, 1997.
3. Bart-Smith, H., Bastawros, A.F., Mumm, D.R., Evans, A.G., Sypeck, D.J., Wadley, H.N.G., "Compressive Deformation and Yielding Mechanisms in Cellular Al Alloys Determined Using X-ray Tomography and Surface Strain Mapping", in Porous and Cellular Materials for Structural Applications, Edited by Schwartz, D.S., Shih, D.S., Evans, A.G., Wadley, H.NG., MRS Symp. Proc. V. 521, Warrendale, Pa, 1998.
4. Hurysz, K.M., Clark, J.L., Nagel, A.R., Hardwicke, C.U., Lee, K.J., Cochran, J.K., Sanders, T,H., "Steel and Titanium Hollow Sphere Foams", in Porous and Cellular Materials for Structural Applications, Edited by Schwartz, D.S., Shih, D.S., Evans, A.G., Wadley, H.NG., MRS Symp. Proc. V. 521, Warrendale, Pa, 1998.
5. Kingery, W.D., Bowen, H.K., Uhlmann, D.r., Introductin to Ceramics, 2nd Ed. John Wiley & Sons, Inc. 1976.

Table I. Comparison Between Conventionally Processed And Direct Reduction Alloys

Composition Comparison				
Maraging Steel 350		**Element (%)**	**Inconel 617**	
Regular Alloy	**Direct Reduction**		**Regular Alloy**	**Direct Reduction**
Balance	Balance	**Fe**	-	-
18.0	18.0	**Ni**	Balance	Balance
-	-	**Cr**	22.0	22.0
12.5	10.0	**Co**	12.5	12.5
4.2	4.0	**Mo**	9.0	9.0
1.6	-	**Ti**	0.5	
0.1	-	**Al**	1.0	-
-	-	**C**	0.1	-
Bulk Property Comparison				
8.0	7.61-7.73	**Density (gm/cc)**	8.27	6.99
2450	1250	**UTS (MPa)**		
2400	1200	**Tensile Strength (MPa)**	760	350
186	160	**Modulus of Elasticity (GPa)**	211	80
6.0	1-2	**Strain at Failure (%)**	56	15
480 C for 3-6 hrs	480 C for 5 hrs	**Heat Treatment**	1200 C	1175 C

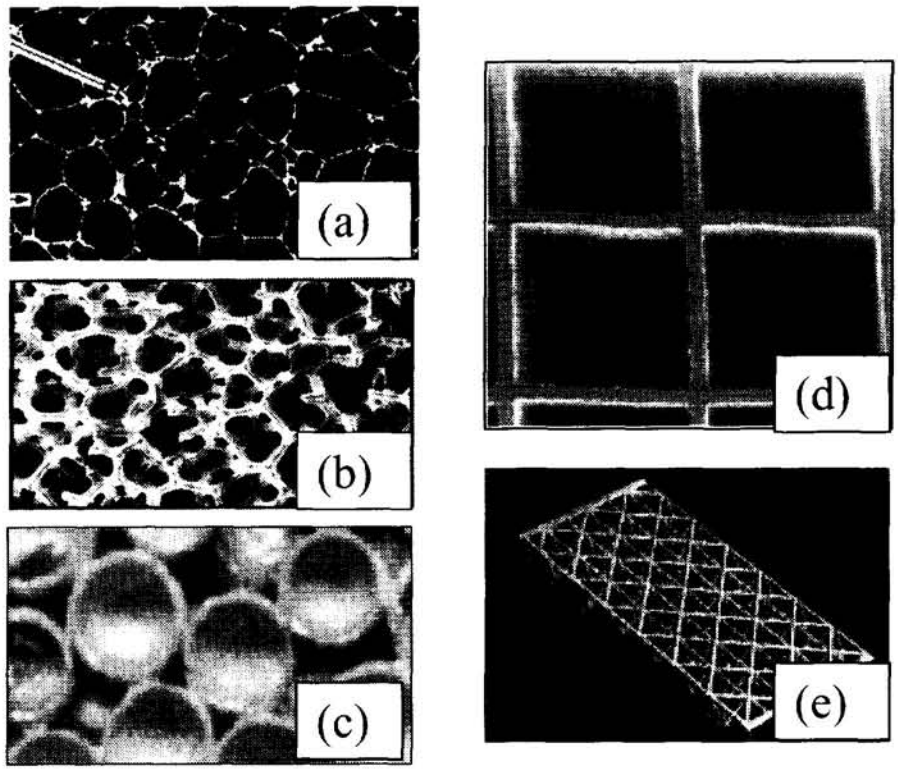

Fig. 1. Examples of Metallic Low Density Structures: (a) Closed Cell Al Foams-ALPORAS by Shinko Wire, (b) Reticulated Al Foams by ERG, Inc., (c) Inconel Hollow Sphere Foam By Georgia Tech, (d) Maraging Steel Honeycomb by Georgia Tech, (e) Lattice Block Material by JAMCORP.

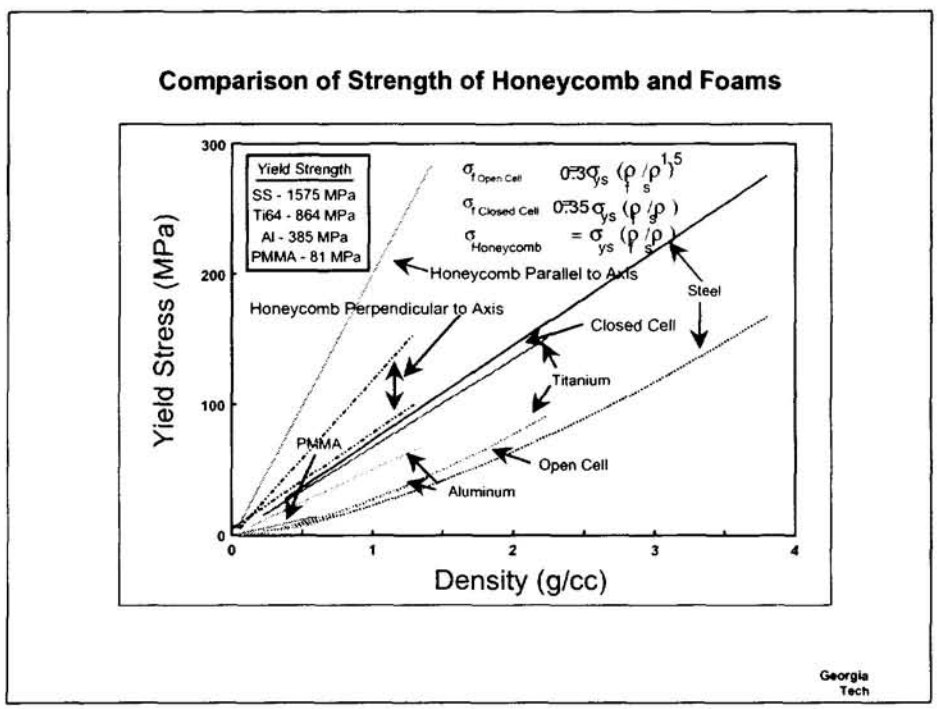

Fig. 2. Comparison of Compressive Strength of Open and Closed Cell Foams to Honeycomb for SS, Ti64, and AL as a Function of Material Density

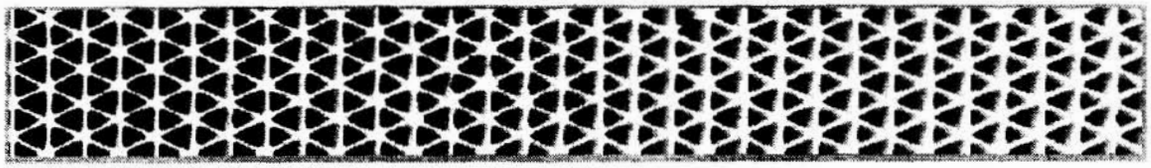

Fig. 3. Triangular Cell Honeycomb for Improved Properties in the Transverse Direction

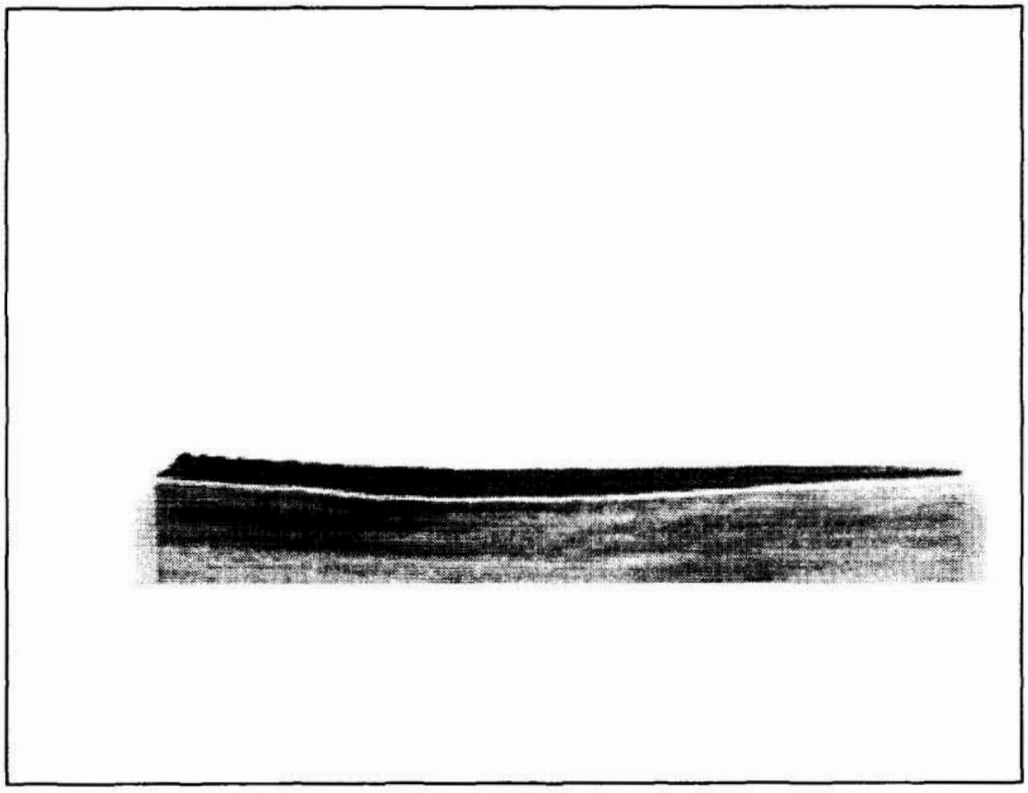

Fig. 4. Inconel 617 Honeycomb at 18% Relative Density, Featuring 150 μ Web Thickness and 1500 μ Cell to Cell Spacing

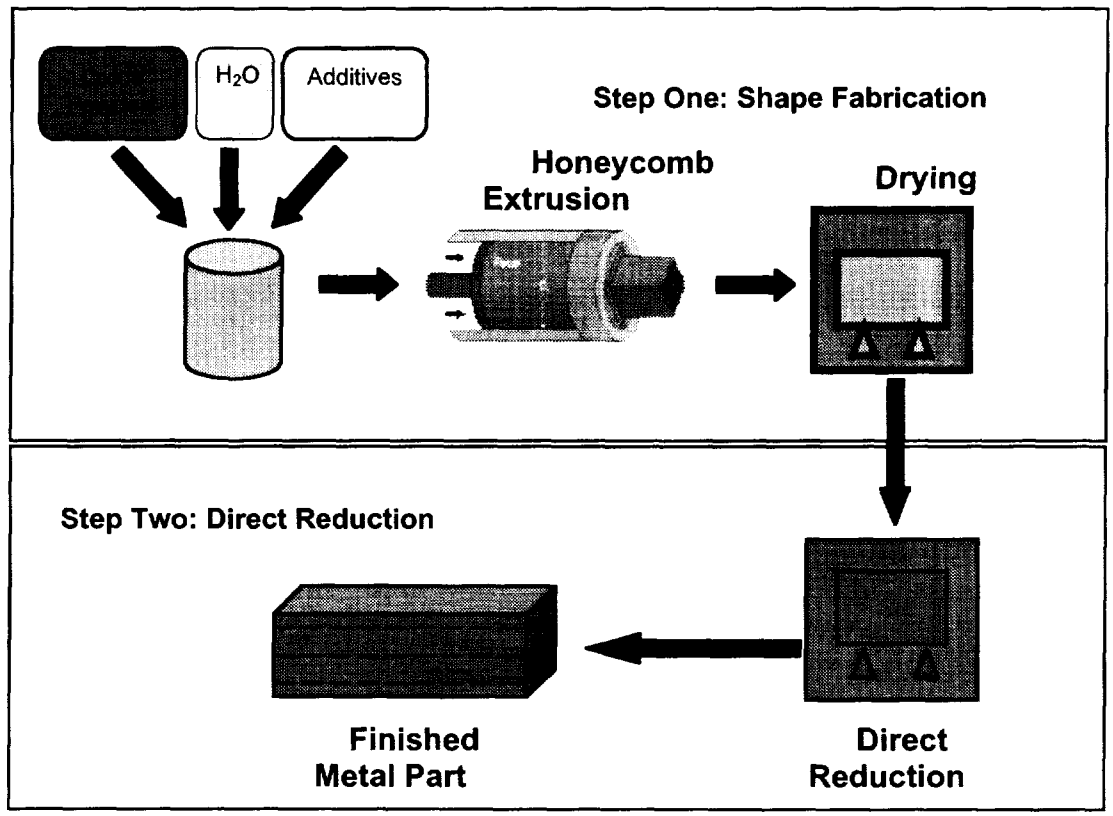

Fig. 5. Oxide Powders to Monolithic Metal Honeycomb

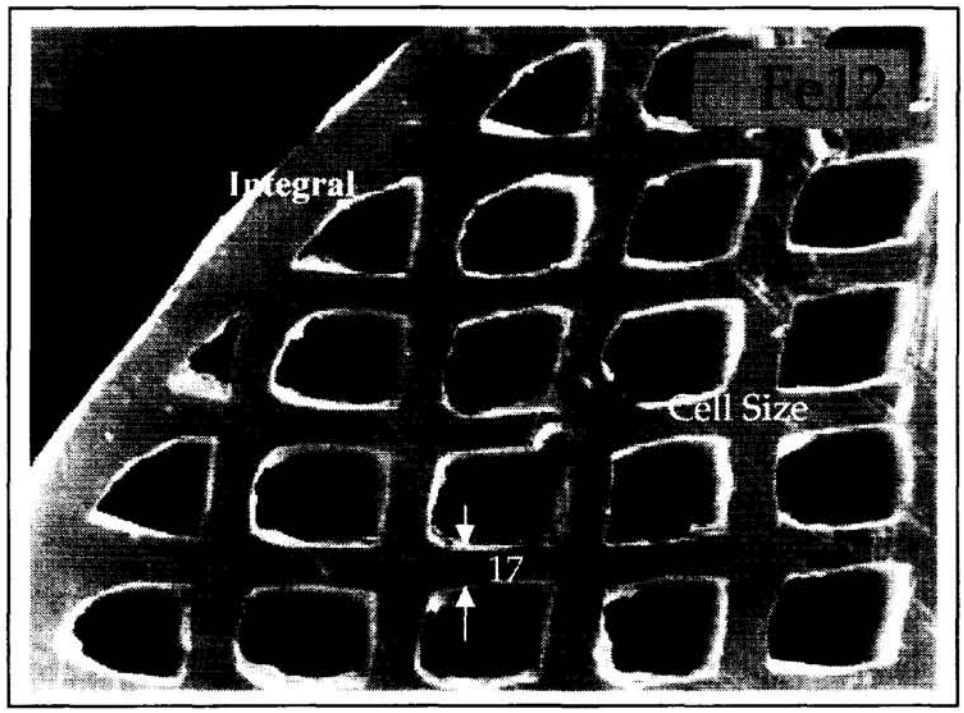

Fig. 6. Fe12Cr Honeycomb at 900 Cells per Square Inch

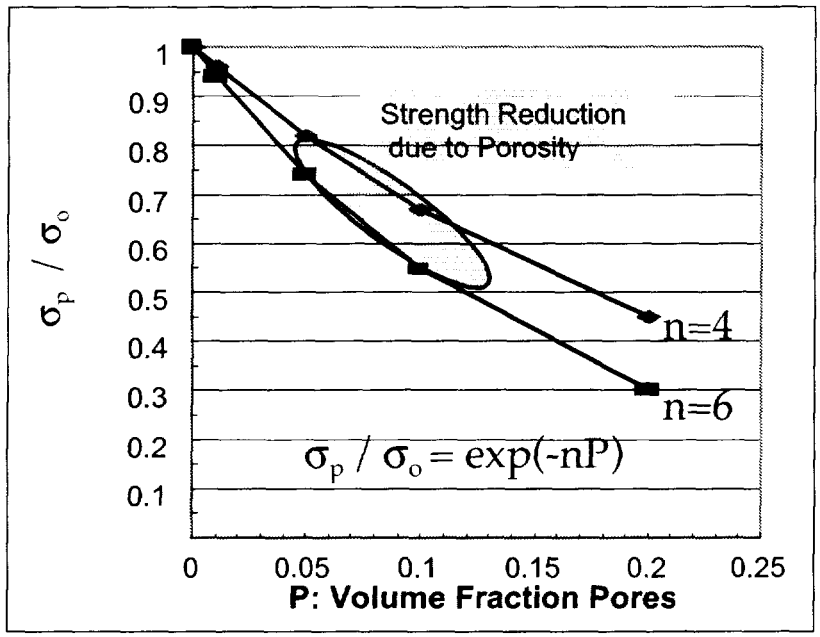

Fig. 7. Effect of Porosity on Strength

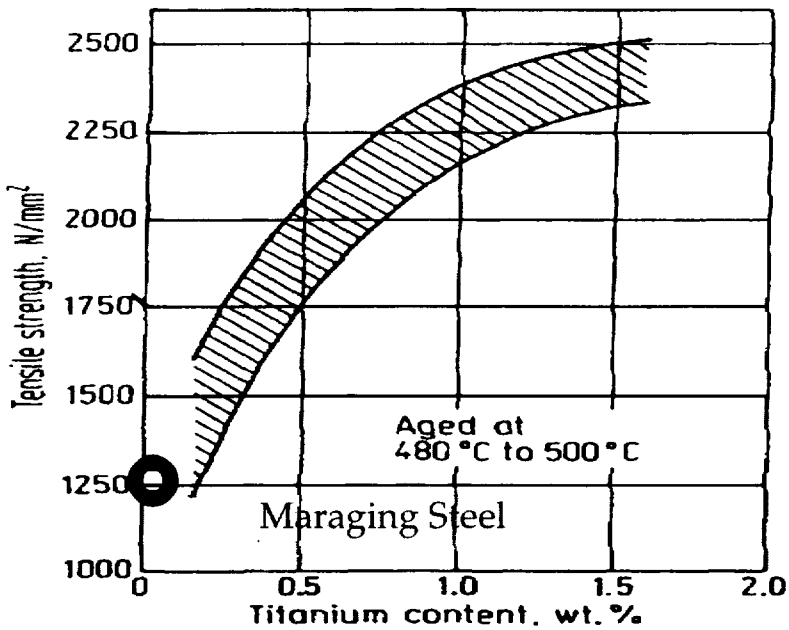

Fig. 8. Effect of Ti Content on Tensile Strength of Maraging Steels Containing 18% Ni, 8 to 12% Co, and 4 to 5% Mo

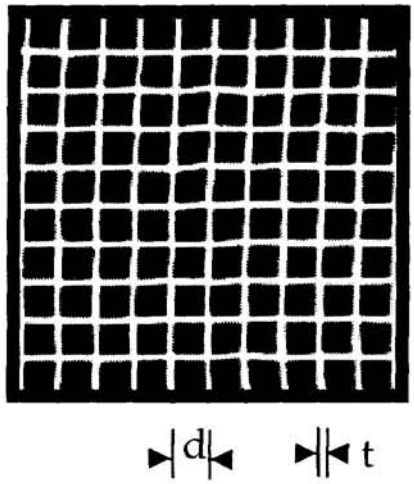

Relative Density: $\rho^* / \rho_s = 2t/d - (t/d)^2$
t = web thickness
d = cell size

Fig. 9. Representative In-Plane Cross Section of Extruded and Reduced Honeycomb

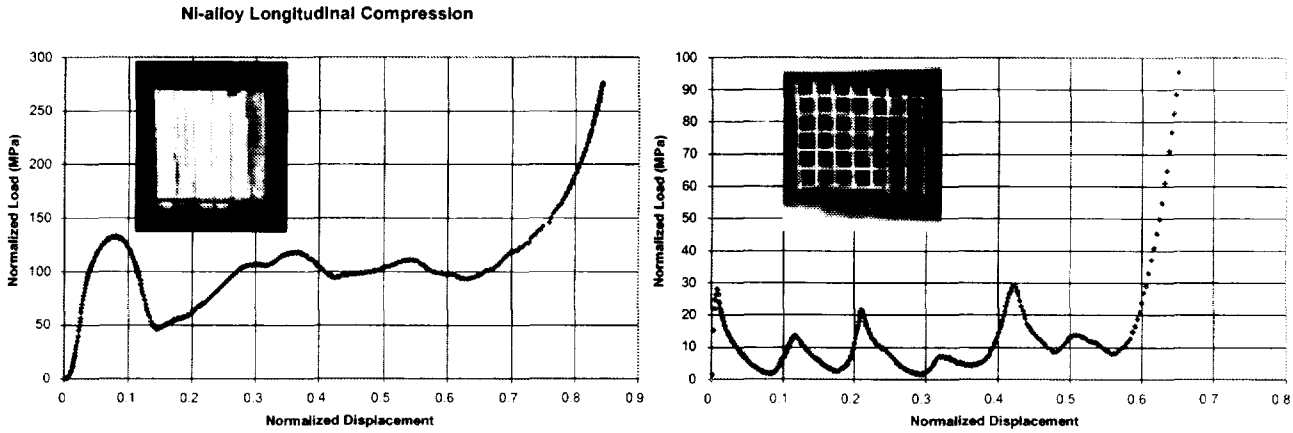

Fig. 10. Out-Of-Plane Compression Of 1:1 Aspect Ratio 6x6 Cell Ni-Alloy Honeycomb Specimen (Left), And (Right) In-Plane Compression Of A 7x7 Square Array Honeycomb

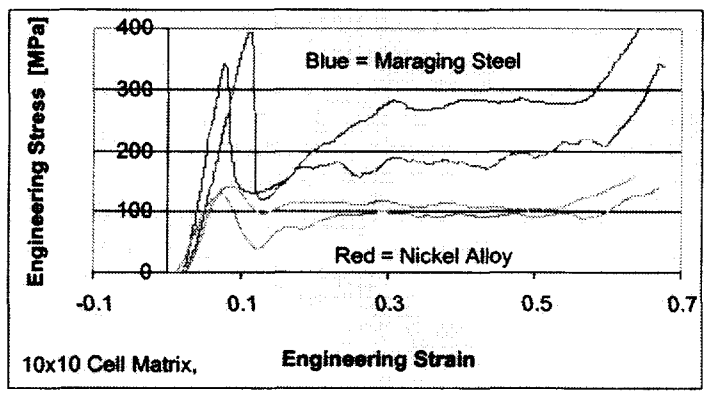

Fig. 11. Relative Compression Behavior For A Maraging Steel Square Cell Honeycomb With An In Situ Wall Yield Strength Of About 1.1 Gpa And Ni-Alloy Honeycomb.

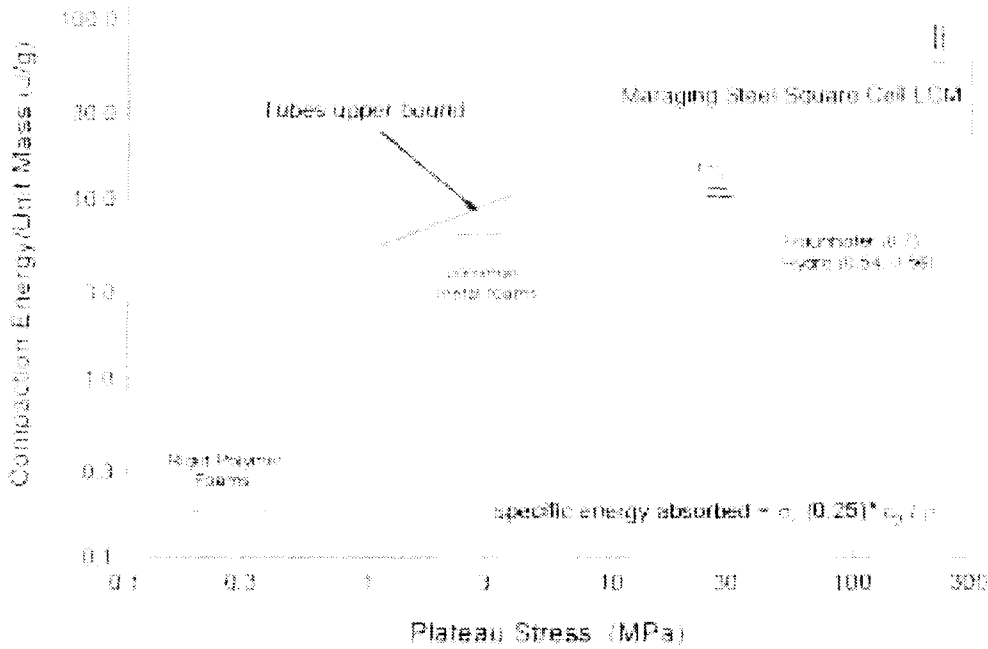

Fig. 12. Comparison Of Energy Absorption Per Unit Mass Versus Plateau Stress For A Range Of Low Density Foams For Quasistatic Loading. The Out-Of-Plane Crushing Of Maraging Steel Honeycombs Essentially Lies On The Extrapolated Line Representing The Upper Bound Solution For Energy Absorption Based On Collapse Of Thin-Walled Tubes (Ashby et al., 2000).

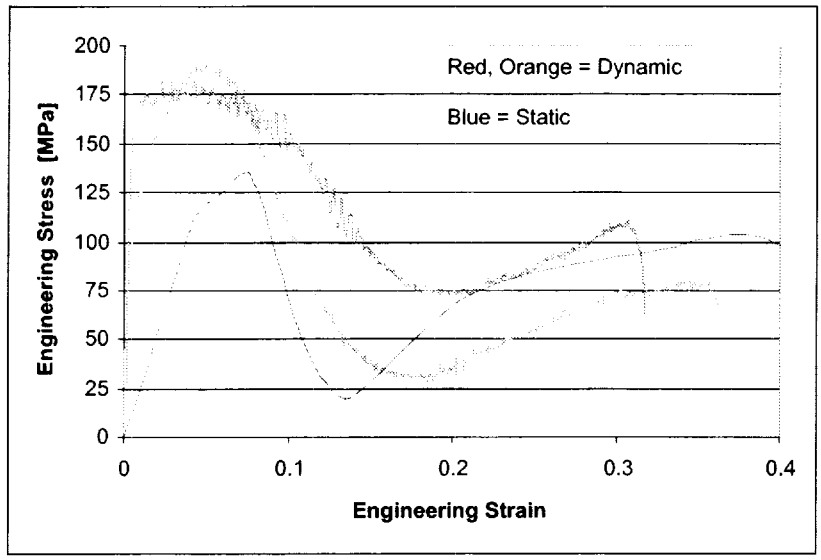

Fig. 13. Comparison Of Dynamic (Hopkinson Bar) Versus Quasistatic Out-Of-Plane Compression For 1:1 Aspect Ratio Ni-Alloy Honeycombs. The Orange And Red Curves (Dynamic) Represent Specimens With 1:1 And 1:2 Aspect Ratios, Respectively

AMPET Aerospace Materials, Processes, & Environmental Technology

Session 4: Innovative Materials Applications

TransHab Materials Selection

Michael D. Pedley, Brian Mayeaux

NASA-Johnson Space Center
Manufacturing, Materials, and Process Technology Division

TransHab Materials Selection

crew habitation

crew support

environmental control

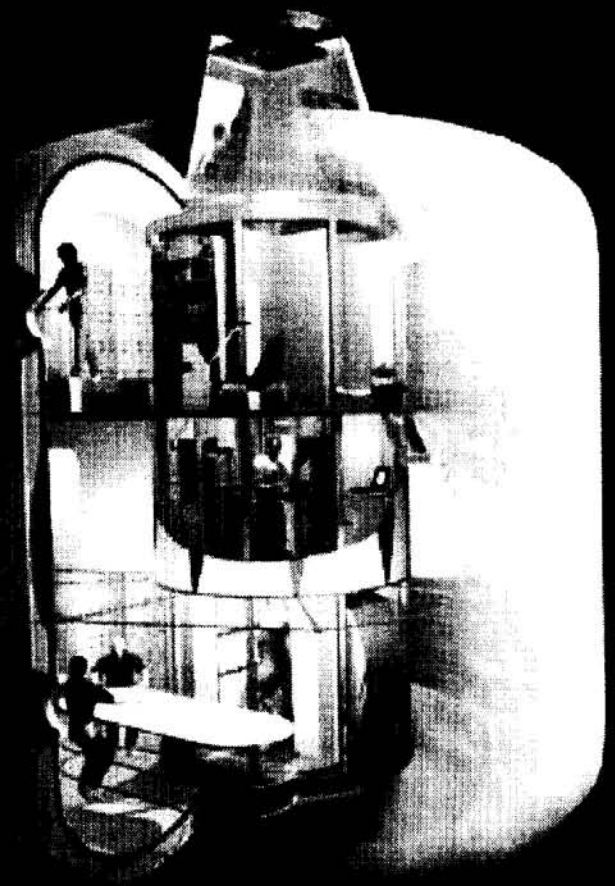

Micrometeroid/orbital debris protection

radiation protection

Acknowledgments: Tim Burns, Joe Lovoula, Benny Ewing, Jeremy Jacobs, Rajib Dasgupta

Mike Pedley, Brian Mayeaux

Location of TransHab on the ISS

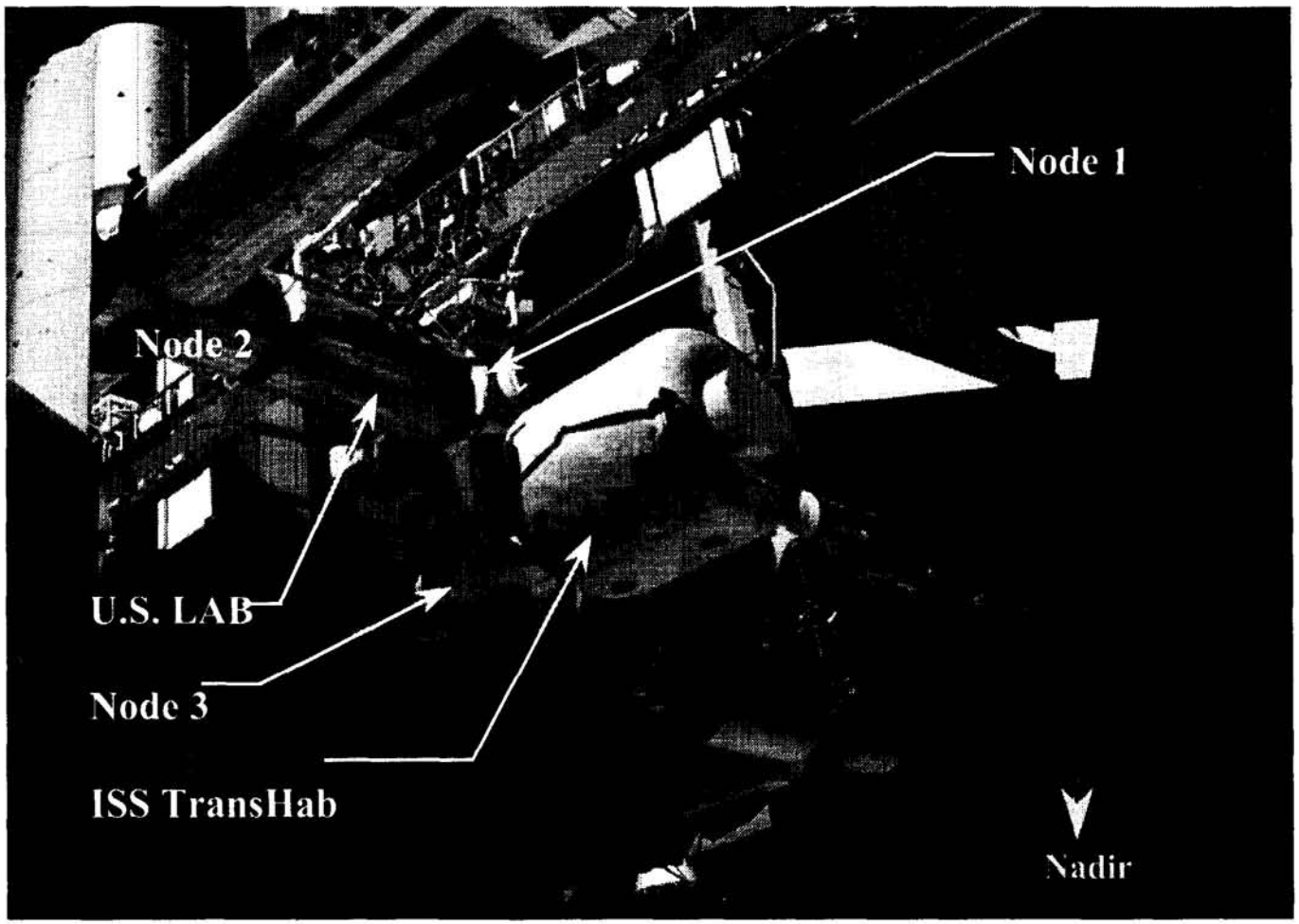

Mike Pedley, Brian Mayeaux
September 19, 2000

Multi-Layer Inflatable Shell

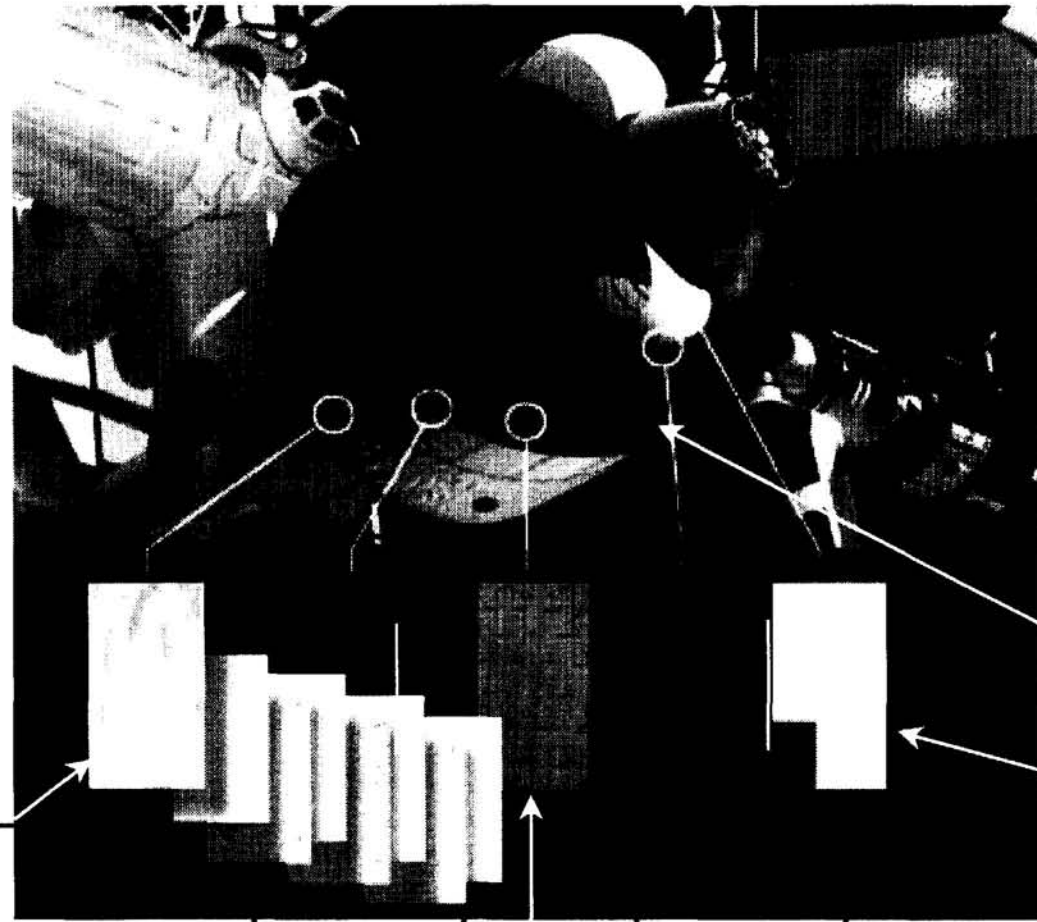

Window

External Thermal Blanket

Internal Scuff Barrier

Meteoroid/debris Shielding

Bladder Restraint Layer

Redundant Bladders

Mike Pedley, Brian Mayeaux
September 19, 2000

Multi-Layer Inflatable Shell

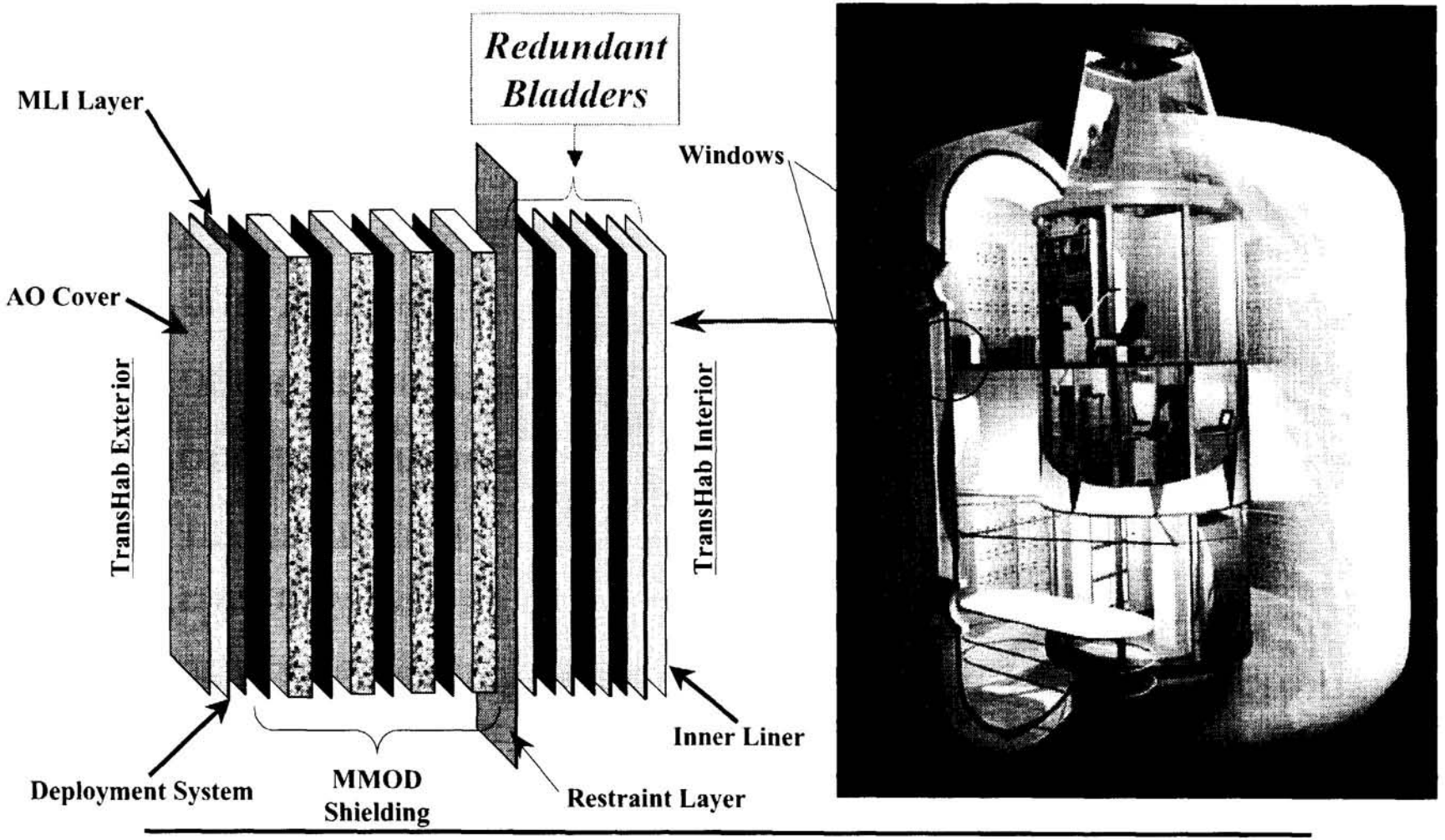

Mike Pedley, Brian Mayeaux
September 19, 2000

TransHab Functions

- **Crew Habitation Functions:**
  - Private Sleeping Compartments
  - Food Preparation
  - Food Consumption
  - Food Stowage
  - Full Body Cleansing
  - Earth Viewing
  - Stowage (Personal, Food, Water)

- **Crew Support Functions:**
  - Social Gathering
  - Meeting Area
  - Private Gathering
  - Crew Health Care
  - Exercise
  - Housekeeping
  - Stowage
  - Radiation Protection

TransHab Materials Requirements

- Structural integrity
  - Hold 1 atm pressure differential
- Deployment in various thermal conditions
- LEO environment compatibility
  - Atomic oxygen
  - Ionizing Radiation
  - Plasma
  - meteoroids and debris
- Material properties/inflatable compartments
  - nonflammable
  - low offgassing
  - resistant to fungus and microbial growth

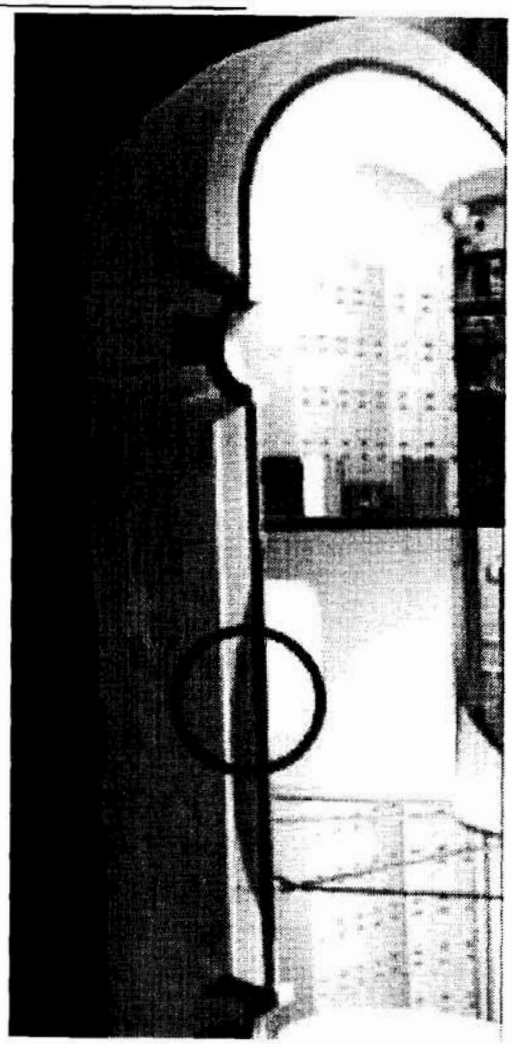

Expected Thermal Environment

- In Shuttle payload bay:
  - Approximately 20 °F average "bulk" temperature
    - Assuming no internal heat source
    - Based on engineering judgement, thermal analysis not yet performed
- At time of deployment:
  - Approximately 0 °F average "bulk" temperature
    - Assuming no internal heat source
    - Some local temperatures may be as low as -20 °F
    - Based on engineering judgement, thermal analysis not yet performed
- -20 °F expected material temperature spec. (-30 °F cold temperature limit for non-silicone mat'ls)
  - Heaters in seal region and core will be implemented if thermal analysis shows temperatures < -20 °F at deployment

Materials Selection Challenges

- Materials currently baselined or under consideration require further development, and their structural integrity must be sustained in a variety of environments.
- The finished shell, with multiple layered elements and a unique shape, requires the development of unique fabrication techniques for bladder seals and bonding.
- Progressive testing program will develop fabrication techniques and provide correction for currently unforeseen fabrication problems.
- An integral water tank is a new technology that requires further laboratory testing and engineering development.

Bladder Restraint Layer Materials

- Kevlar (Aramid) fibers
  - Bladder reinforcement
  - degradation/embrittlement at cryogenic temps.
  - Aerozid/Debris shielding

Mike Pedley, Brian Mayeaux
September 19, 2000

Bladder Assembly

- Three bladders, separated by bleeder cloth and sealed to the interface at the bulkhead
- Each bladder gore cut out from (Polyurethane/Saran film) and heat sealed together
- Bladders indexed to each other; tabs provided for indexing to restraint and inner layers

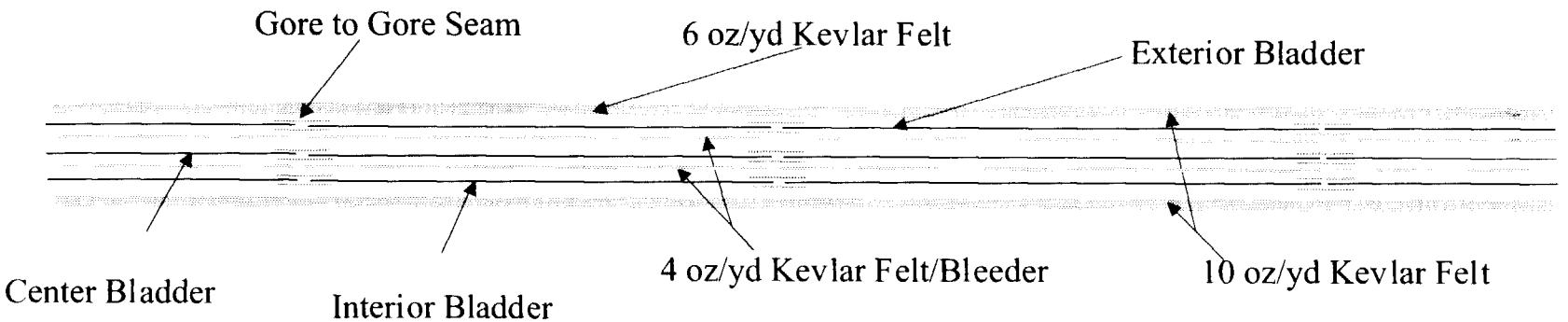

Mike Pedley, Brian Mayeaux

Bladder Materials Requirements

- Evaluation Criteria
  - Must exhibit cold temperature ductility
    - % elongation @ -50 °F and -30 °F relative to Ambient Temperature.
    - No delamination between gas barrier and polyurethane
  - Must pass toxic offgassing
  - Must pass permeation
    - Leak rate not to exceed 2 cc/100 sq.in./24hr/atm
  - Must exhibit flex cracking resistance
    - Use Permeation testing to verify defect free samples
  - Must pass puncture test

Bladder Materials Testing

- Puncture resistance at -30 °F & 0 °F
- Triple point fold test at -30 °F & 0 °F
- Cut slit method tensile tests
- Permeability testing of 50% elongation at break samples
- Cold temperature bally flex testing
- SEM analysis of cold temperature tensile fracture surfaces and component layers

Bladder Materials Selection

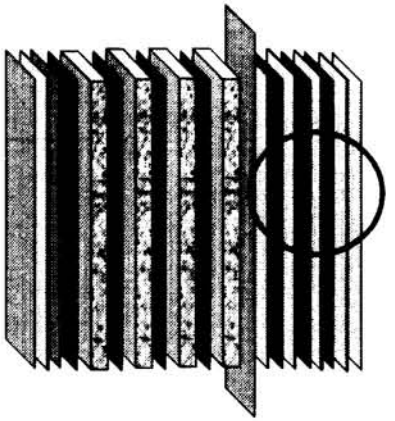

- **Polyethylene/ethyl vinyl alcohol/nylon laminate**
  - light weight, low density
  - good offgassing/toxicity
  - low permeability (0.07cc/100in^2*day*atm)*
  - very brittle at cold temperatures (flex cycling, puncture tests)
- **Polyurethane/Saran laminate**
  - higher permeability (0.32cc/100in^2*day*atm)*
  - adequate mechanical integrity at cold temperatures (flex cycling, puncture tests)
- **Tedlar-Mylar-Polyurethane-Polyester Scrim**
  - higher permeability (barely meets requirement)*
  - poor mechanical integrity at ambient temperature(flex cycling, puncture tests)

* 2.0cc/100in^2*day*atm requirement

Bladder Materials Selection

- -30 °F & -50 °F testing to characterize mechanical properties
  - Material Properties at Room Temperature after 100% Elongation of Peak Load
  - Material Properties at Room Temperature after 50% Elongation of Break

-30 °F Typical Tensile Stress Curve

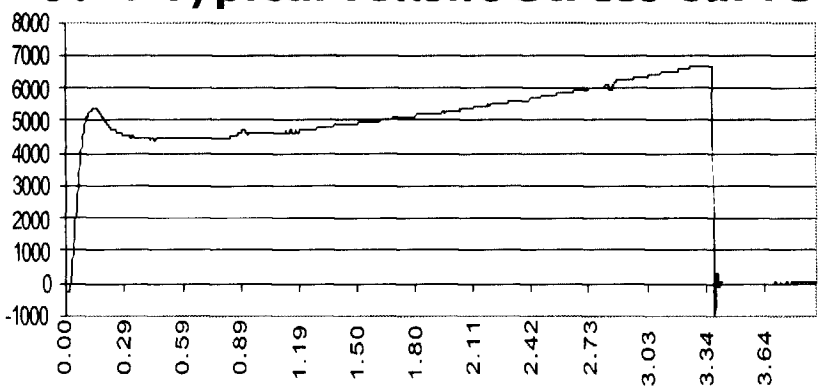

Stress(PSI) vs. Elongation(in)

-50 °F Typical Tensile Stress Curve

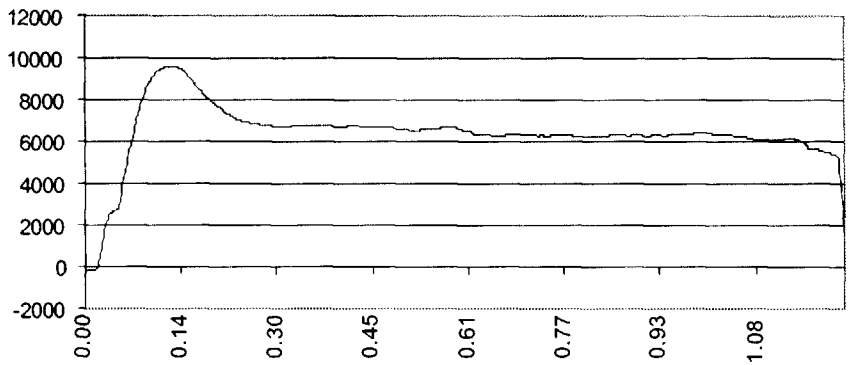

Stress(PSI) vs. Elongation(in)

Mike Pedley, Brian Mayeaux
September 19, 2000

Bladder Materials Selection (Polyurethane/Saran)

50% Loading of Break Elongation at –50 °F

- Cracking in the polyurethane only
- Verified that these cracks are not thermally induced by examining unloaded samples
- Cracks in the polyurethane suppressed by thin saran layer

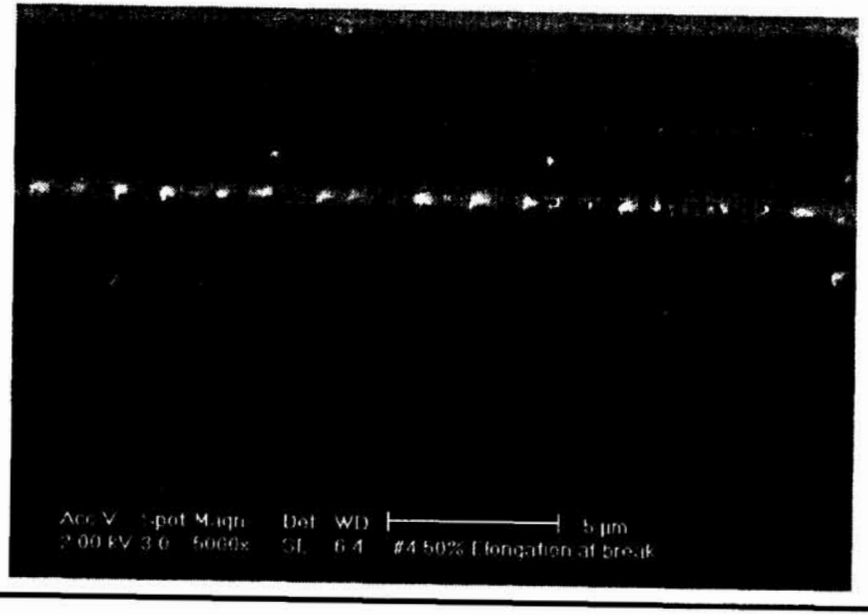

Mike Pedley, Brian Mayeaux
September 19, 2000

Bladder Materials – Future Testing

- Polyurethane/Saran
  - Thickness (4.75mil, 6.75mil, 12.75mil)
  - Seam Testing of Heat Seals
    - Tensile, Permeation and Bally Flex Testing
  - Adhesive Testing and Evaluation
  - S-Flex Testing of Bladder Layup
  - Testing to Determine Elongation Properties of Two Individual Components Saran and Polyurethane
  - Bally Flex Testing will continue past the 3000 cycles currently completed
  - Cold Temperature Laminate Failure Without Loading

Meteoroid/Debris (MMOD) Shielding

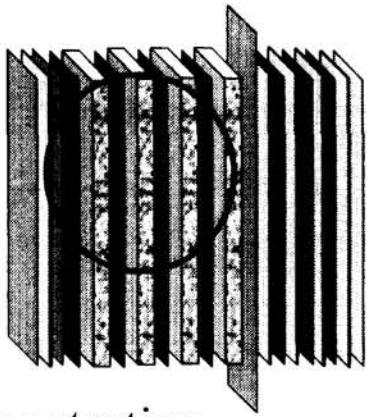

- Shield Requirements
  - meet or exceed ISS requirement for probability of no penetration
- Design
  - based on ISS multishock shield (Kevlar/Nextel)
  - shield layers separated by foam spacers
  - manufactured in gores similar to bladder
  - gaps in foam allow MMOD to fold
  - vacuum-packed to minimize folded volume, foam expands during deployment/inflation
  - all fabric system
  - state of the art in hypervelocity impact protection

Meteroid/Debris Protection Materials

- Test Matrix
  - Large historical data base on ceramic based bumper shields
  - Over 50 shots completed by TransHab Program at JSC/WSTF (6.5 km/sec.)
    - Sub Scale
    - Full Scale
    - Variety of Configurations
  - Current design viable solution to meet ISS requirements
  - 12 Full scale shots underway to determine ballistic limit curve

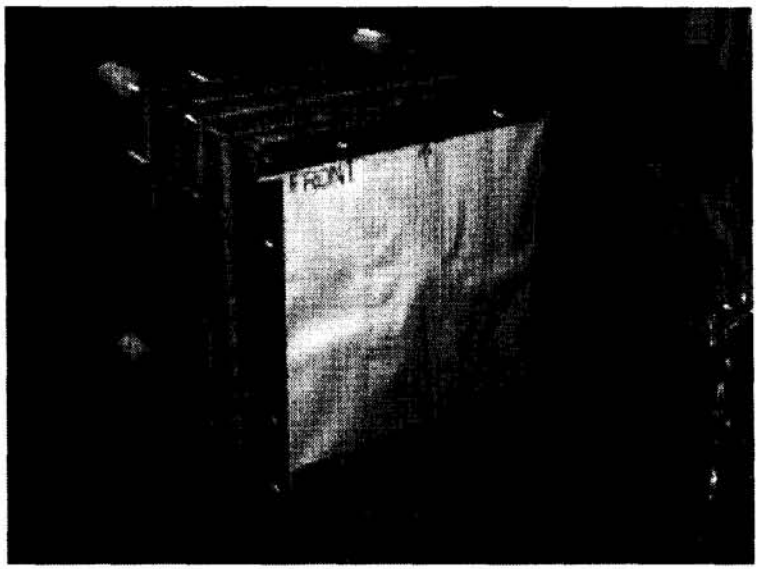

Multilayer Insulation (MLI)

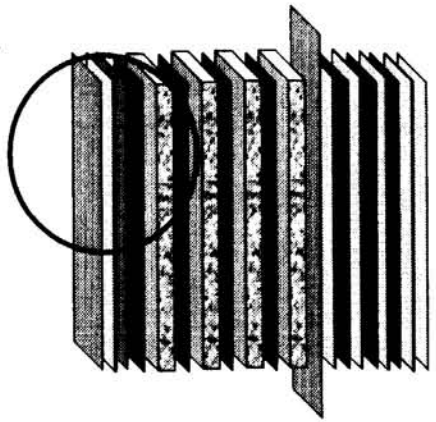

- **Requirements**
  - Provide Thermal Insulation
  - Atomic oxygen protection
  - Electrically grounded
  - Foldable for launch packaging
  - Vented
  - Not load bearing
- **Design**
  - Based on ISS standard MLI design
  - Beta Cloth outer layer protects against atomic oxygen attack (aluminized on inside to block light transmission)
  - 20 layers of reinforced double aluminized Mylar with inner and outer cover of reinforced double aluminized Kapton
  - Atomic oxygen protection and MLI split into two separate layers
  - Deployment system on separate load bearing layer between MLI and Beta Cloth

Manufacturing Processes

- **Key Special Processes**
  - Adhesive bonding to bladder materials
  - Sewing, weaving
  - Folding, packing
  - Control of foreign materials in-and-around shell and bladder
    - bladder damage (sewing equipment, fasteners, sharp objects)
    - contamination control

- **Key Controlled Materials**
  - Bladder material
  - Adhesives
  - Kevlar restraint layer material

Project Status

- Remains candidate for ISS Habitation Module

- In competition with aluminum Habitation Module (shell fabricated at MSFC several years ago, not outfitted)
  - Transhab provides higher potential for long-term applications, higher volume
  - Aluminum Hab provides lower risk, lower cost

SP/544/N/31

Identification of High Performance, Low Environmental Impact Materials and Processes Using Systematic Substitution (SyS)

Patrick M. Dhooge and Jonathan S. Nimitz
Environmental Technology and Education Center (ETEC)
4500-B Hawkins St. NE
Albuquerque, NM 87109-4517
Phone: (505) 345-2707
http://www.etec-nm.com
pdhooge@etec-nm.com jnimitz@etec-nm.com

INTRODUCTION

Process analysis can identify opportunities for efficiency improvement including cost reduction, increased safety, improved quality, and decreased environmental impact. A thorough, systematic approach to materials and process selection is valuable in any analysis. New operations and facilities design offer the best opportunities for proactive cost reduction and environmental improvement, but existing operations and facilities can also benefit greatly. Materials and processes that have been used for many years may be sources of excessive resource use, waste generation, pollution, and cost burden that should be replaced. Operational and purchasing personnel may not recognize some materials and processes as problems. Reasons for materials or process replacement may include quality and efficiency improvements, excessive resource use and waste generation, materials and operational costs, safety (flammability or toxicity), pollution prevention, compatibility with new processes or materials, and new or anticipated regulations.

Very often, material and process substitution is performed in a nonsystematic manner. While a material or process may be identified as a problem, often the substitution decision is made "on the fly." Personnel may rely on vendor recommendations and specify substitute materials and processes without a systematic analysis of alternatives. Such decisions may lead to sub-optimal performance, increased waste generation, higher life cycle costs, and increased risks. The authors cannot stress too greatly the need for a thorough, systematic evaluation of an operation's materials and processes with the goal of decreased cost, waste, and pollution. If replacements are to be made, it is logical to identify the best possible replacements systematically to minimize life cycle cost, risk, and the need for future replacements or modifications. The so-called "rule of ten" applies to this situation. That is, if a change made at the design stage costs $1, that change at prototype stage costs $10, and the change at operational stage $100.

Many factors must be considered in most materials and process substitutions. The number of alternatives and their different characteristics can be overwhelming if a methodical system of evaluation is not used. Additionally, it is uncommon that one or two personnel will be able to understand all the implications of alternatives' characteristics. There should be involvement from team members with good knowledge of the material or process use, materials properties, engineering, health and safety, operations management, and waste management. Involvement of these personnel also helps ensure acceptance of the new material or process.

The net result of a systematic evaluation, as described below, is a small set of top-ranking alternatives to evaluate in the laboratory and, after further downselection, prototype or pilot testing. Candidates should be tested against the current material or process before final selection is made, to eliminate alternatives that have unanticipated disadvantages, and to identify the best option from those with similar evaluation scores. Again in the evaluation phase, personnel from a number of disciplines, including the operations personnel, should be involved to obtain the widest possible input on the advantages and disadvantages of the selections. Once sufficient testing is completed, the team makes the final choice.

Properly evaluating substitute materials and processes should be part of a larger process for achieving high quality and environmental excellence. Quality and environmental management tools include process mapping; life cycle cost analysis; an effective employee involvement program; identification of opportunities for improvement; action plan development and implementation, including use of evaluation methods such as SyS; quantitation of results, management by fact; and a continuous improvement program. Achievement of quality and environmental excellence, and associated goals such as energy efficiency are being recognized through state and federal programs such as Energy Star, Climate Protection, and New Mexico's Green Zia. Such recognition motivates organizations to additional achievement and is good publicity, but more importantly the programs instituted result in improved efficiency and cost savings.

DESCRIPTION

The authors have developed a systematic substitution (SyS) process applicable to a wide variety of materials and processes. SyS incorporates a refinement of a technique reported previously (Nimitz a). While SyS is certainly not unique, and the weighted ranking matrix for scoring candidates has been used for many years, we have found the overall SyS process highly effective in identifying high performance substitutes without being overly complex and costly.

The logical, methodical SyS process identifies and ranks candidate materials and processes for given applications. The process has been used successfully in several projects for a variety of applications (Kuchar, et al.; Nimitz b-g, Shell, et al., Toohey, et al.). The steps of the SyS process have been given in a previous paper (Nimitz h) but are listed here in somewhat more detail and for completeness.

(1) Determine all requirements, including performance; compatibility; stability; regulations; cost sensitivity; safety (toxicity and flammability); and maximum allowable environmental impact. Establish the advantages and disadvantages of the current material or process versus the requirements. The extremes of the requirements define the limits of acceptable properties for a candidate replacement. Team members (e.g., floor personnel, production engineers, ES&H, waste management, and operations management) should be included in this process for their valuable input and "buy-in" to ensure acceptance of the ultimate results.

(2) Develop a list of evaluation criteria based on the requirements. In SyS, criteria are often grouped under the main headings of physical properties, performance, toxicity, compatibility, environmental effects, and cost, all of which may be further subdivided as desired. There are obviously some differences between evaluating a process versus a material. For a process,

the toxicity heading may have grouped under it the toxicities of all the materials involved in the process. Performance criteria may include estimated energy efficiency, throughput, product quality, ease of use, and any existing test data for similar applications. Physical data may include (for process equipment) dimensions and weight, and (for materials) molecular weight, density, strength, ductility, wear resistance, vapor pressure, viscosity, heat capacity, thermal stability, electrical resistivity, etc. Compatibility and other chemical data for materials may include flammability and compatibility with metals, plastics and elastomers, and other chemicals. Environmental criteria for materials may include factors such as atmospheric lifetime, ozone-depletion potential (ODP), global warming potential (GWP), total equivalent warming impact (TEWI), volatile organic compounds (VOCs), regulatory status, waste disposal, and air and aquatic toxicity of materials and wastes. Environmental criteria for processes may include materials criteria plus waste generation, resource use (including utilities), emissions, and potential severity of accidental spills and releases. Toxicity criteria for materials may include exposure limits, carcinogenicity, teratogenicity, odor, and sensitization.

(3) Develop an initial list of candidates for consideration. Sources for candidate materials may include chemical databases (e.g., Chemical Abstracts Service, Beilstein, Gmelin), relevant literature, and vendor information. Sources for candidate processes may include personnel knowledge; scientific and technical journals; vendor literature; U.S. and international patents; government laboratories and publications; and information on competitors and benchmark organizations. If possible, include known competitors' and benchmark organizations' current materials or processes for comparison.

(4) Assign relative weights to evaluation criteria on a scale of one to ten points based on which are judged more important and more accurately known. Other factors being equal, higher uncertainty means lower confidence in data values and assignment of a lower relative weight. This step can be one of the most involved parts of the SyS process. The working team must reach consensus on the weightings before the evaluation process proceeds, and this consensus should be documented. If the weightings are later found not to reflect the true requirements for some unanticipated reason, they can be changed by consensus, although such changes should be made only when necessary.

(5) Collect and tabulate properties of reference materials or processes, and the candidate replacements. Reference materials or processes include the material or process to be replaced and corresponding materials or processes used by competitors or benchmark organizations. Estimate unreported properties as needed, and assign realistic uncertainties to the estimations. Estimation of unreported properties involves some uncertainty. The actual properties could be better or worse than estimated. Using the worst possible value may eliminate a good candidate. Using the estimate may overestimate the value of the property. It has been our experience that at this stage it is better to keep a marginal candidate than to eliminate a good candidate, so the estimate is typically used as is. The uncertainty should be listed with the value.

(6) If reasonably accurate numerical values are available for the data, develop a point scale of 0-10 for data values for each criterion, where 0 is least attractive and 10 is most attractive, and

assign scores for each candidate for each criterion. If numerical values are not appropriate or not available, assign subjective descriptions to the value of each criterion for each candidate (e.g., very high, high, moderately high, moderate, moderately low, low, or very low), then assign numerical values to the subjective descriptions (e.g., very high = 10, high = 8 etc.). First-time SyS users should probably use a linear mapping of points to criteria values. However, in this step experienced SyS users can add a certain amount of sophistication. The mapping of numerical values to the point scale need not be linear. As an example, assume a substitute cleaning solvent is being sought. For the substitute cleaning solvent the allowable viscosity range is 0.5 to 5.5 centiPoise (cP). On a linear scale, a solvent with a viscosity of 2 cP will get a 7 score and a solvent with a viscosity of 3 cP will get a 5. However, because low viscosity is valued for both good penetration and effective draining, the solvent with a viscosity of 2 cP should get a proportionately higher score because low viscosity is important for two reasons. The scoring function can be a polynomial function, an exponential function, some other type of function, or even values chosen manually. In this example, the function should result in a value of 0 at 5.5 and a value of 10 at 0.5, and it should have higher values than a linear mapping when viscosity is low. What function is used to map point scores depends on the relative importance of individual values within the allowable value range. This is different from the weightings assigned in Step 4 above. The weightings reflect the importance of the criteria against each other. Score mapping curves are used to adjust the scores of values within a criterion. Score mapping is an intracriterial process.

(7) Sum the products of the criteria weights times the individual scores for each candidate to give weighted rankings. Any spreadsheet program can be used for this step. Table 1 shows the type of table used for property tabulation and scoring.

(8) Evaluate several of the highest-ranking candidates in the laboratory and at pilot scale, then test the highest-ranked candidate in the facility.

Table 1. Sample Table for Property Tabulation and Scoring

Category	Evaluation Parameters	Weight	Candidate 1 data	Candidate 1 score	Candidate 2 data	Candidate 2 score
Physical	Freezing point					
	Liquid density					
	Molecular Weight					
	Viscosity					
	Etc.					
Performance	(vary with application)					
Compatibility	With metals					
	With polymers					
Toxicity	Acute inhalation					
	Ames					
	Chromosomal damage					
	Etc.					
Environmental	Atmospheric lifetime					
	GWP					
	ODP					
	Partition coefficient					
	Etc.					
Weighted total score						

RESULTS AND DISCUSSION

The SyS process has identified good substitute materials and processes in a variety of applications. Several examples are discussed below.

Space Shuttle Heat Transfer Fluid

The hydrochlorofluorocarbon (HCFC)-21 is used as a heat transfer fluid in the Space Shuttle. However, HCFC-21 is a Class 2 ozone-depleting substance whose production has been halted under the Montreal Protocol and HCFC-21 has relatively high toxicity with a Threshold Limit Value (TLV) of 10 ppmv in air. Its high toxicity complicates Space Shuttle maintenance operations. An environmentally friendly, nonflammable, low toxicity, inexpensive heat transfer fluid for potential use in the Space Shuttle and other applications was desired. Ideally, the replacement should be a drop in or near-drop in replacement for HCFC-21.

Working with NASA and contractor personnel, ETEC identified the requirements for the replacement fluid, screened over 100 candidates, downselected to the best ten candidates, and finally selected the three best candidates. NASA and contractor personnel eliminated one of the three best candidates because, although it was not flammable and would have saved significant launch weight, it was combustible at high temperature. The heat transfer rates of the two remaining candidates, HFC-245fa and HFE-7100, were calculated for the Space Shuttle system and HFC-245fa was identified as the best candidate. HFC-245fa was estimated to transfer heat about 8 % better than HCFC-21 under typical Space Shuttle cooling loop conditions. HFC-245fa is considerably less toxic than HCFC-21. Although exposure limits have not yet been officially set, HFC-245fa is expected to have a Permissible Exposure Limit (PEL) of 500 to 1000 ppmv in air. HFC-245fa is compatible with all Space Shuttle cooling loop materials, and it would save about 8 kg launch weight versus HCFC-21. HFC-245fa will also soon be in bulk production by Honeywell (formerly AlliedSignal) as a replacement for HCFC blowing agents in the manufacture of rigid, closed cell polymer insulating foams, and its cost is expected to be $8 - $10 per kilogram.

Following identification of HFC-245fa as the top candidate, ETEC evaluated its heat transfer rate versus HCFC-21 at bench scale in a circulating heat transfer loop with tubing size, linear flow rate, pressurization, and warm and cold side temperatures matched to the Space Shuttle cooling loop conditions. Multiple runs were made with HCFC-21 and HFC-245fa. Relative standard deviations were 1.2% or less, and the results showed a heat transfer rate for HFC-245fa that was 12 - 13% greater than HCFC-21's heat transfer rate.

Cleaning

In a project for the U.S. Air Force, ETEC worked with BDM Federal, Inc. to review use of a large vapor degreaser used to clean aluminum honeycomb for aircraft wing repair. The vapor degreaser used 1,1,1-trichloroethane (TCA). Because TCA is being phased out under the Montreal Protocol as a Category 2 ozone-depleting substance, a new cleaning method was desired. The new method had to be environmentally friendly, use a nonflammable, low toxicity cleaning agent, leave no corrosive residues, and clean aluminum honeycomb adequately to give a surface that would bond strongly with epoxy. A review and evaluation of possible cleaning methods (nonaqueous, semi-aqueous, and aqueous) showed the attractiveness of aqueous cleaning. Approximately 50 aqueous cleaners were evaluated. Note that in this project there were

two phases to the evaluation, the evaluation of types of cleaning (i.e., nonaqueous, semi-aqueous, and aqueous) then the evaluation of cleaners (50 aqueous cleaners). This project involved evaluation of both a process and a material, and such evaluations can often be logically divided in this manner. The top three aqueous cleaner candidates were evaluated in the laboratory. Laboratory evaluation involved tests of cleaning abilities, adequate penetration of the honeycomb, corrosion during cleaning, corrosive residues as revealed by accelerated aging, and compatibility with nondestructive crack-detection methods (no residues left in cracks to interfere with dye penetrant). An aqueous spray cleaning system was identified as the most attractive alternative to vapor degreasing for aluminum aircraft honeycomb. This custom system was designed and built, and is now in place at the National Defense Center for Environmental Excellence (NDCEE).

In a project for the U.S. Air Force Research Laboratory, a new group of nonaqueous, nonflammable, low atmospheric impact solvents was evaluated for aircraft maintenance critical cleaning operations. The solvents were perfluoro-n-propyl iodide (1-C_3F_7I), perfluoro-n-butyl iodide (1-C_4F_9I), and perfluoro-n-hexyl iodide (1-$C_6F_{13}I$) and their blends with conventional solvents. Evaluation of physical properties, stability, compatibility, toxicity, and cleaning abilities identified perfluoro-n-butyl iodide, given the trade name Ikon® Solvent P, as the top-ranking iodofluorocarbon (IFC) solvent. Perfluoro-n-butyl iodide has physical properties and cleaning abilities very similar to CFC-113, and is superior to CFC-113 for removing perfluorinated greases. Its rat 4-hr LC_{50} of 14,000 ppmv is considerably higher than that of 1,1,2-trichloroethane (2,000 ppmv) and approximately the same as 1,1,1-trichloroethane and trichloroethylene (18,400 and 12,500 ppmv, respectively). Perfluoro-n-butyl iodide is Ames-negative and is not clastogenic by the human lymphocyte test. Because IFCs photolyze quickly in sunlight to simple, natural products, perfluoro-n-butyl iodide has an atmospheric lifetime of only about 2 days, giving it essentially zero (<0.0025) ozone-depletion potential (ODP) and an extremely low global warming potential (GWP) of less than 2 (relative to CO_2 = 1) for a 100 year horizon. NASA Kennedy Space Center (KSC) sponsored an additional effort to determine perfluoro-n-butyl iodide's potential suitability as a cleaner for oxygen systems. The new solvent was found to be quite compatible with oxygen and an excellent candidate for oxygen system cleaning, particularly as it is even more effective than CFC-113 at removing fluorinated greases. The project sponsored by the Air Force Research Laboratory also investigated thirty-six conventional flammable solvents to blend with IFCs. The conventional flammable solvents were also evaluated using SyS, and were scored on physical properties, flammability, thermal stability, estimated fractionation from the IFCs, environmental impact, toxicity, and cost. The result of the SyS evaluation was a list of 19 high ranked potential blends. When these potential blends were evaluated in the laboratory two nonflammable near-azeotropes were discovered, one of which was practical as a solvent blend. The blend has been given the trade name Ikon® Solvent M. Ikon® Solvent M's cleaning effectiveness is not quite as good as Ikon® Solvent P for some soils, but it is less expensive and will have a higher exposure limit.

Thrust Vector Control Fluid

The Minuteman Stage II rocket was designed to use Halon 2402 (1,2-dibromotetrafluoroethane) as a liquid injection thrust vector control (LITVC) fluid. This fluid is injected into the exhaust stream, where it decomposes to form a large volume of gas that deflects the exhaust stream to steer the missile. Because of the phaseout of production of Halon 2402 as a Category 1 ozone-depleting substance under the Montreal Protocol, a replacement had to be found. It was most desirable that the replacement use the existing hardware to avoid expensive redesign and testing. ETEC worked with GenCorp AeroJet to identify the required properties, examine an initial list of over 1000 candidate replacements, model performance, downselect the candidates, and choose the most attractive candidate for performance testing. The material selected was perfluorohexane, which has excellent stability and compatibility, low toxicity, and acceptable performance. Although in some applications perfluorocarbons are released to the atmosphere and cause concern about global warming, in this application they undergo combustion and are not released to the atmosphere.

Refrigerants

In a project for NASA KSC, SyS was used to identify top-ranking components for new high performance, nonflammable, zero ODP, stable, compatible, azeotropic or near-azeotropic refrigerant blends to replace ozone-depleting chlorofluorocarbon (CFC) and HCFC refrigerants phased out or facing phaseout under the Montreal Protocol. Ozone-depleting refrigerants that could be replaced include R-12, R-22, R-500, R-502, and R-123. R-12's production has already been phased out in developed countries, R-22's phaseout will start in 2003, and R-123 will shortly follow R-22. R-500 is a blend that contains R-12 and R-152a. R-502 is a blend that contains R-22 and R-115. Available substitutes such as R-134a, R-404A, and R-410A do not have as high innate energy efficiency and performance as desired.

Approximately 100 possible refrigerant components were screened and ranked. Fractionation and performance of potential blends were modeled using ETEC's proprietary AZEO and COOLS computer programs and the National Institutes of Standards and Technology (NIST)'s Refprop® refrigerant properties database. From the screening a set of attractive candidate components were selected. The candidate components were then blended, tested for flammability and performance, and developed into Ikon® Refrigerants A, B, and C. These refrigerants have attractive physical properties, zero ODPs, and low total equivalent warming impacts (TEWIs). They appear suitable to replace R-12, R-22, R-500, R-502, R-123, R-134a, R-404A, R-407C, and R-410A in residential refrigerators, residential and commercial air conditioners, commercial and industrial water chillers, commercial and industrial refrigeration, industrial process coolers, and other cooling and refrigeration equipment that has relatively low leak rates. From all data known so far, the three refrigerants appear superior in performance and environmental properties to any other available alternatives.

Performance tests on Ikon® A and Ikon® B in a 1.75 ton water chiller test bed at ETEC, a compressor calorimeter at Oak Ridge National Laboratories, a 20 ton air conditioning unit at NASA Kennedy Space Center, and a residential refrigerator have shown that both have 10-15% higher energy efficiency and 10-15% greater volumetric cooling capacity than R-12 and R-134a. Ikon® A and Ikon® B also have a total of over five years run time in several refrigerated transports ("reefers") at Dole Fresh Fruit with no indications of incompatibility. Both Ikon® A and Ikon® B

have been approved under the U.S. Environmental Protection Agency's Significant New Alternatives Policy (SNAP) program as ozone-depleting refrigerant replacements in multiple applications including residential refrigerators, air conditioning, refrigerated display cases, and water chillers. Initial performance tests on Ikon® C in ETEC's 1.75 ton water chiller test bed show that it has about 95% of the capacity of R-22, and 4-5% higher energy efficiency than R-404A, R-407C, or R-410A. Ikon® C has a low evaporator temperature glide and operating pressures almost identical to R-22. Ikon® C may be usable as a direct replacement in R-22 equipment with an oil change, and can definitely be used as a replacement with a compressor change. A SNAP application has been prepared for Ikon® C.

Firefighting

In a project for the U.S. Air Force, trifluoromethyl iodide (CF_3I) was identified as an effective replacement for Halon 1301 for fire suppression in unoccupied areas. Subsequent testing showed excellent performance and environmental properties, and this chemical was approved as a halon replacement for use in unoccupied areas under the SNAP program. CF_3I is being installed in a variety of facilities in Australia and the Far East, and has recently been named the preferred choice as a substitute fire suppression agent for the F-16 fuel tanks.

CONCLUSIONS

A systematic approach to materials and process substitution is valuable for product quality improvement, process efficiency improvement, cost reduction, increased safety, waste and resource use reduction, and pollution prevention. The SyS process has proven successful in identifying high performance, energy-efficient, low life cycle cost, safe, and environmentally friendly replacement materials and processes for both highly specific and more general applications.

ACKNOWLEDGEMENTS

The funding for the material and process development work described in this paper was provided by the U.S. Air Force, the U.S. Air Force Research Laboratory, BDM Federal, Gencorp Aerojet, NASA Kennedy Space Center, and the U.S. Environmental Protection Agency. We would like to thank Dr. Carl E. Snyder of the U.S. Air Force Research Laboratory, John Carroz of the U.S. Air Force, Tony Harrison of Gencorp Aerojet, Wayne Kuchar and John Toohey of BDM Federal, Dr. Jacqueline Quinn of NASA KSC, and Michael Bender of the U.S. EPA for their valuable technical support during the efforts. The Ikon® refrigerants and solvents are patented products of the Ikon Corporation.

REFERENCES

Kuchar, W., Gordon, B., Bennett, D., and Nimitz, J., "Aqueous Cleaning of Aluminum Honeycomb," Fifth International Workshop on Solvent Substitution, Phoenix, AZ, Dec. 6-9, 1994.

Nimitz a: Nimitz, J. S., and Shell, V., "How to Find Safe, Effective, Environmentally Sound Alternative Chemicals," Proceedings of the 5th Annual New Mexico Air and Waste Management Technical Meeting, Albuquerque, NM, October 31, 1991.

Nimitz b: Nimitz, J. S., and Lankford, L. H., "A New Class of Nonflammable, Environmentally Safe Solvents," Fourth Annual International Workshop on Solvent Substitution, Phoenix, AZ, Dec. 7-10, 1993.

Nimitz c: Nimitz, J. S., High-Performance, Environmentally Sound Replacements for Halon 1301, Prepared for McClellan AFB under contract F04699-93-C-0004, December 1993, ETEC 93-3

Nimitz d: Nimitz, J. S., "Trifluoromethyl Iodide and its Blends as High-Performance, Environmentally Sound Halon 1301 Replacements," Halon Options Technical Working Conference, University of New Mexico, Albuquerque, NM, May, 1994.

Nimitz e: Nimitz, J. S., Olsen, K., Glass, S. M., Dhooge, P. M., and McCullough, E. T., Development of Nonflammable, Environmentally Compliant Fluoroiodocarbon Solvents: Phase II Final Report, prepared for Wright Laboratories under U.S. Air Force Contract Number F33615-95-C-5026, December 1999.

Nimitz f: Nimitz, J. S., Glass, S. M., McCullough, E. T., and Dhooge, P. M., "Applications Tests of Energy Efficient, Environmentally Friendly Refrigerants," 21st National Industrial Energy Technology Conference, May 12 - 13, 1999, Houston, Texas, available through Texas A&M University Energy Systems Laboratory, College Station, Texas.

Nimitz g: Nimitz, J. S, Dhooge, P. M., Waldrop, S. D., McCullough, E. T., and Glass, S. M., "High-Performance Environmentally Safe Refrigerants: Phase II Final Report," Environmental Technology and Education Center, prepared for NASA Kennedy Space Center under contract NAS10-98028, March, 2000.

Nimitz h: Nimitz, J. S., Dhooge, P. D., and Glass, S. M., "Successful Environmentally Friendly, High Performance Substitute Materials for Manufacturing and Facilities," Proceedings of the SAE Aerospace Manufacturing Technology Conference, June 2-4, 1998, Long Beach, California, available through SAE International, Warrendale, PA.

Shell, V., Harrison, A., and Nimitz, J., "Finding an Environmentally Acceptable Replacement for Freon 114B2 (Halon 2402) That Meets Minuteman LITVC Performance Criteria," Proceedings of the 1994 NATO Advisory Group for Aerospace Research and Development, Norway, August 29, 1994.

Toohey, J. A., Kuchar, W. E., and Nimitz, J., Final Technical Report: Alternative Process for Cleaning Aircraft Honeycomb, prepared for U.S.A.F. Wright Laboratory WL/MTX under contract F42600-90-D-1140/RZ01, BDM/ABQ-95-AQ-0445-TR, August 1995.

SELECTION CRITERIA FOR ALTERNATE TECHNOLOGIES, AS A METHOD OF HAZARDOUS WASTE MINIMIZATION

Authored by: Eric Lethe
Inland Technology Inc.
401 East 27th Street
Tacoma, WA 98421
(253) 383-1177
inland@inlandtech.com

The need for environmentally compliant processes and materials in the Aerospace Industry grows more pressing every day. As the need for these processes grows, so grows the confusion regarding the selection and implementation of these new methods and materials.

In the past, price and traditional procedure were the only criteria by which a material was procured. Speed and compliance with OEM specification governed how things were done on the shop floor. With the advent of the environmental regulations, processes are being examined all across the globe. In many of the larger Aerospace companies, the chief environmental officer has as important a role as the comptroller or CFO. Environmental managers are often not chemists or aerospace line mechanics, as typically, the environmental manager is skilled in the policies of waste disposal, spill clean up, or remediation.

The methods whereby a company can minimize the generation of hazardous waste remain less known. Often the examination of possible alternate techniques and materials are left for the last minute, or are conducted by personnel who are unfamiliar with how to make changes work. This is usually a recipe for failure in the implementing of anything new.

This paper will suggest methods for selection of alternative products and processes in a clear and organized manner. Salient points will be:

1. Process Examination
2. Material Selection
3. Steps For Successful Implementation
4. Possible Impediments
5. How to Avoid Risky Alternatives

It will focus on procedures that will assist in the decision making process, and hopefully be of use in the choosing of environmentally sound equipment, chemicals, and methodologies.

In the past, price per gallon and traditional procedure were the only criteria by which a material was procured. Speed of delivery and compliance with OEM specification governed how and what was procured. Hazardous chemicals were used traditionally because they WORKED. However, with the advent of environmental regulations, the Environmental Affairs Director, the shop manager, and the floor personnel are often at odds with the Regulations on one side, and the standard operating procedures called out in the technical manuals on the other. This condition causes a sense of desperation or hopelessness, which is counter productive to any examination of new technology. It is critically important that an organized method of examination be in place before any discussion of the testing of alternative materials. Each process, which uses hazardous chemical, needs to be examined to determine if that process itself, is necessary. This examination affords the Environmental Officer an intimate knowledge of the processes for which that officer will be making recommendations. In that way, the problem of changes to standard procedure can be addressed with less resistance.

When the environmental concerns are being addressed, the engineers who would like to introduce an alternative are thwarted by a need for a substitute, which must perform "identically" to the original material. The "chemical physics" stand against any legitimate candidate material being identical.

As a rule, the faster a chemical evaporates the greater the potential for there to be a hazard associated with that chemical's use, whether the hazard is ozone depletion potential, toxicity, smog formation potential, or flammability. In the very greatest of likelihood, the alternative candidate material will be slower in evaporation. This is an important concern when selecting candidate materials, since it is quite possible to be in a situation where one hazard is substituted for one that is even greater or more expensive to deal with. In the search for successful solvent substitutes, it is critically important to select a course of action based upon each process, as opposed to the focus of attention being each chemical.

MEK for example, is a solvent used in so many applications that to say "I want a replacement for MEK" is far too ambiguous to begin a concerted effort to examine candidate replacements. Is the MEK used for surface cleaning prior to painting, prior to welding, cleaning of painting equipment, removal of adhesive, or thinning and diluting paints or shoe polish? A metaphor I often use to describe this situation is the consideration of a combination lock. Randomly selecting numbers seldom achieves the opening of the lock. A skilled locksmith, armed with the knowledge of the make, model, year of manufacture, and other pertinent data will have a far easier time opening that lock.

Using the premise that a substitute will behave differently, and not for all of the applications of the original material, will facilitate an examination of the processes that use this material. The resulting "needs assessment" will evaluate what will work on a process-by-process basis. There are occasions when the application differences are subtle, and the substitute materials are not needed to be absolutely specific for each application. The bulk of this substitution effort will be on an application specific basis. There is no single answer. I f there were, the hazardous solvents would have been phased out years ago.

What is called for is an organized method for determining the applicability of candidate materials, based on a "needs assessment" of the affected processes. Part of the initial assessment must be a determination of whether a material is needed for that application. The alternative may be a change of process that eliminates the need for cleaning of the candidate part altogether.

Steps for Successful Solvent Substitution:

1. **Identify target solvent:** Make a priorities list of those solvents that are a hazardous waste source, or health and safety concern. For each of those solvents on your list, proceed through the steps.

2. **Orient workers and supervisors:** Let the staff know the importance of this substitution effort. The shop personnel will be able to help you.

3. **Identify and describe** all processes using target solvent.

4. **Examine all upstream conditions**: Identify the source of the contaminants that the solvent is called upon to remove. Perhaps a modification to the upstream process will eliminate the need for cleaning, or solvent cleaning.

5. **Examine all the downstream requirements:** How clean does that component part need to be once it has been cleaned. Does that part need to be cleaned at all?

6. **Identify substitution candidates:** Request of current vendors as to the availability of environmentally responsible substitutes for the target solvents. Requests should be application specific! Review MSD Sheets, if the MSDS does not show contents of the candidate material, contact manufacturer for that information. If you receive a "this stuff is safe, and we're not telling what's in it" response, do not use this product. As soon as a chemical crosses your threshold, you are responsible for handling, worker protection, and proper disposal. This applies to "free" samples as well.

7. **Evaluate the candidate materials:** Determine if there are going to be requirements for extraordinary worker protection. Will there be extensive training requirements? Will the vendor assume the task of training, and will that training be billed to you? Create a testing protocol that will give an accurate example of the candidate material performance. Does your OEM specify the candidate materials?

Does the vendor supply a list of customers with a track record of success using this candidate material for the same application? Do any of these references have a history of usage in the cleaning of similar substrates, and of similar contaminants? Can the vendor supply an estimate of cost per application or time weighted usage?

8. **Conduct off-line tests:** While this may seem an obvious course of action; it cannot be stressed enough. Often when there is a real push to have an alternative in place, having an ineffective alternative, or worse an alternative that is not compatible with the substrate, is simply not an acceptable risk. Always select test coupons that represent all of the substrate materials that the cleaner will contact. Select contaminant samples that represent a realistic working scenario, i.e. neither too easy to remove, nor unrealistically difficult.

9. **Train employees:** This phase of alternative material substitution is probably the most difficult. The difficulty comes from the basic resistance we all feel toward any new process. It is imperative that a clearly defined method for application of the substitute material be developed using data gathered from the previous steps in the evaluation and testing process. If it is possible to use the expertise of the vendor in the training process, so much the better. If this is not possible, I would recommend asking the vendor of the candidate material to supply references. If there are other companies that are using this product, how did they develop a usage method for that product? How long did this "breaking in" program take, and how much impact did the transition have to the manufacturing or maintenance process? During the training period, make sure there is opportunity to integrate suggestions from the line personnel who will be using the product, often this is the best way to develop the most efficient methods for use of a new material.

10. **Implement:** Utilizing the methods learned in Steps 8 & 9, bring the new cleaner on-line. I would suggest using the new material in a limited and controlled area at first. It may be possible to rotate into this area of usage, other workers for an opportunity to use the new material first hand. This is also the time for the quality assurance engineers to be involved in the first stages of implementation.

11. **Evaluate:** Establish a time frame for the primary implementation. At the end of this time frame, call in representatives of each step of the usage process.

If all of the user groups report satisfactory results from the preliminary implementation, set a new time frame for plant-wide usage. The revised time frame should be long enough to project cost savings as well as effects on overall production.

There is a twelfth step to this process. With all apologies to self-help groups, this is a "Twelve-Step Program". The last step is to review the final results after the plant wide usage trial. If the material seems unsatisfactory, or overly costly, the option still exists to go back to Step 7 and begin again.

The Twelve-Step Program is not a guarantee that all will be smooth and seamless in transition. There will be impediments on the way to successful material substitution. Impediments to making a successful transition typically fall into two categories: The first should have been eliminated by the testing step included in the program, and occurs when the candidate material fails to perform chemically, the contaminant is not removed, or the test coupon dissolves, explodes, or otherwise is damaged by the candidate cleaner. The second category of impediment is that the personnel are not willing to make the changes in method necessary to accommodate the new material.

The key to overcoming this unwillingness to look at process changes is communication. It is a normal human reaction to resist a new behavior when it is ordered upon the individual without their input. That is why the process development phase depends on the communication between the environmental staff, engineering staff and representatives of the floor personnel. This reaction to new processes or products is at the root of the failure of otherwise acceptable environmentally responsible alternatives.

How often has the Environmental Director heard the phrase, "We've tried that before. It didn't work". It is important to ask the question, "Was the problem that the chemical did not work, or was the problem that the personnel would not work with the chemical?" This stresses the need for an organized method for testing and

implementing new materials. This problem also refers back to the need for involvement of the line worker. While the Environmental Director may have an intimate knowledge of the regulations that are driving the process of change on the shop floor, the shop floor personnel are the people who will be using the new material daily, and it is they who will determine the success of the project. The shop workers have intimate knowledge of the overall processes that help make the company run, so it is imperative that we draw on the knowledge base represented by these line workers in a cooperative effort.

Communication is the key to overcoming the impediments. Making the substitution effort common knowledge should be a win-win situation for the Environmental Engineer. By drawing on all available expertise, the project can progress without fear of unknown effects of new materials or equipment. If the above Twelve-Step Program is followed, and all affected divisions within the company share the test results, the resistance to "surprises" will be eliminated. Uncomfortable as the subject may be, this information sharing process does leave the door open to worker-management conflict issues, even when the safety of the worker is the primary motivation of the proposed changes. In any organization of some size, there will be some resistant personnel.

However small that percentage may be, this presents a significant impediment to programs which could benefit the company as a whole. Communication is again the key to overcoming this problem. There must be the backing of the upper management even before the Twelve-Step process begins. In order to assure those engineers working on the program that the new processes decided upon will be implemented without exception and in order to make that process become part of the standard operating procedure, management must have the courage to say, "we welcome input from the line personnel, but this will be an ongoing program of change". Without management courage, and the backing of the company, there will never be a successful transition into the future. That future requires a low or no hazardous waste generating industry.

What has not been discussed in depth, as yet, is cost. Traditionally, cleaning chemicals have been regarded as a commodity, whatever was least expensive per gallon or pound, and still met the specification, was what was ordered. When hazardous waste handling, hauling, and storage became an issue, many companies simply budgeted for the disposal costs without concern for minimization or elimination of these products. In a large organization, it is often one individual, or department that oversees the budget for cleaner procurement. A totally separate individual or department oversees the budget for disposal of hazardous waste, often generated by the first group's procured material. While the hazardous material price remains stable incoming, the cost for hazardous waste disposal continues to go up. If there is no communication between these entities, there is very little incentive for reducing or eliminating the hazardous waste at the source? Additionally, there are concerns when using a hazardous material for cleaning that are never reflected in the per-gallon price. Insurance companies are increasingly interested in the volume of hazardous materials used on a site. The cost of worker illness or chemical related injury is never calculated into the price of an "inexpensive" hazardous cleaner. The potential for contamination of the property, soil, or ground water exists wherever a hazardous chemical is used. The costs for such a clean-up will far exceed any savings from years of traditional cheap solvent use. With respect to the overall usage, recall my statement about evaporation rates. Most hazardous solvents typically evaporate rapidly, which makes them effective at cleaning and leaving a prepared surface in a short amount of time. In point of fact, a major portion of this fast evaporating solvent is consumed in evaporative loss. In the case of MEK, more than 60%. With acetone the figure is closer to 80%! The actual cleaning is done with only 20 to 40% of the material. The other percentage of the cost of the cleaner is wasted into the air and into the bodies of the personnel using this cleaner when they breathe.

In the event of a spill or other incident which attracts media attention, a company can expect to lose customers if the company is a commercial enterprise. Do you remember the incident with the big French water bottler? Five years later they still had not regained market share. Conversely, many companies are advertising the new "green" aspects of their business. People will go out of their way to do business with a company who cares about the environment and their workers. This can more than compensate for any new expenses in the implementation of environmentally responsible materials.

Joint Group on Pollution Prevention

Chartered by Joint Logistics Commanders

JG-PP
Partnering for Progress

Aerospace Materials, Processes, and Environmental Technology (AMPET) Conference

Mr. Robert Hill
321-867-8795

Overview

Who is JG-PP?

What does JG-PP do for you?

What has JG-PP achieved?

Where is JG-PP going?

Who is JG-PP

DoD/NASA flag officer group

- Originally created in 1995 at industry request
- Chartered by Joint Logistics Commanders/NASA HQ

Chartered to

- Reduce or eliminate system hazardous material requirements – **Project Benefits**
- Avoid duplication of effort – **Consensus Building**
- Reduce technical risk – **Stakeholder Ownership**
- Transfer technology **- Documentation**
- Leverage opportunities -- reduce costs – **Cost Control**

Dual focus on uniform implementation

- Acquisition (Contractor design) and sustainment community (Depot) needs
- Manufacturing and maintenance processes

JG-PP Leadership

Joint Logistics Commanders

General John G. Coburn
Commander
Army Materiel Command

Vice Admiral James F. Amerault
Deputy Chief of Naval Operations, (Logistics)

General Lester L. Lyles
Commander
Air Force Materiel Command

Major General Paul M. Lee
Commander
Marine Corps Materiel Command

Lt.. General Henry T. Glisson
Director
Defense Logistics Agency

JG-PP Principals

Major General David R. Gust
Deputy Chief of Staff for Research, Development and Acquisition
HQ, Army Materiel Command

Rear Admiral Larry C. Baucom
Director, Environmental Protection, Safety and Occupational Health
Chief of Naval Operations (N45)

Major General Paul Bielowicz
Director of Logistics
HQ Air Force Materiel Command

Mr. Ken Trammell
Deputy Commander, Logistics Operations
Marine Corps Logistics Bases

Major Gen. Timothy P. Malishenko
Commander
Defense Contract Management Agency

Ms. Olga Dominquez
Director, Environmental Management
National Aeronautics and Space Administration

Working Group (JASPPA)

Mr. George Terrell
AAPPSO
HQ Army Materiel Command

Mr. Winston deMonsabert
Pollution Prevention Branch
Chief of Naval Operations (N451W)

Ms. Debora Meredith
Chief, Logistics Environmental Office
HQ, Air Force Materiel Command

Mr. John Wolfe
Marine Corps Logistics Bases

Mr. Dave James
Defense Contract Management Agency

Mr. Robert Hill
Kennedy Space Center
National Aeronautics and Space Administration

What can JG-PP do for you

Proven Methodology

Coordinate/facilitate project management

Advocate funding

Reduce individual participant's costs

Reduce alternative technical risk

Assist in qualified alternative implementation

Right People, Right Place,
Right Time For Decisive Action

Joint NASA/DOD P2 Needs Integration

Common Problems, Joint Solutions, Shared Efforts

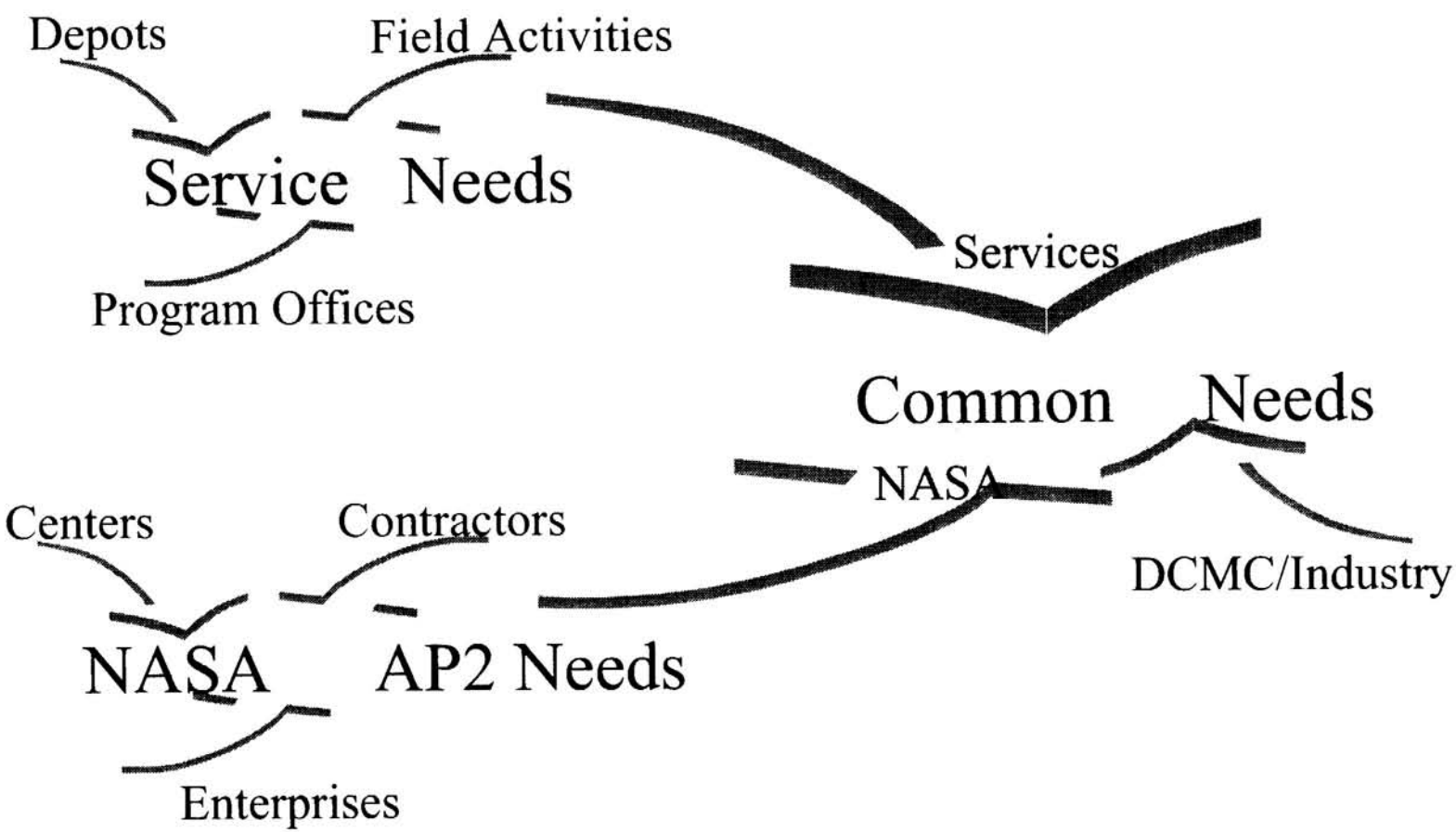

Technology Pull and Technology Push

JG-PP Proven Methodology

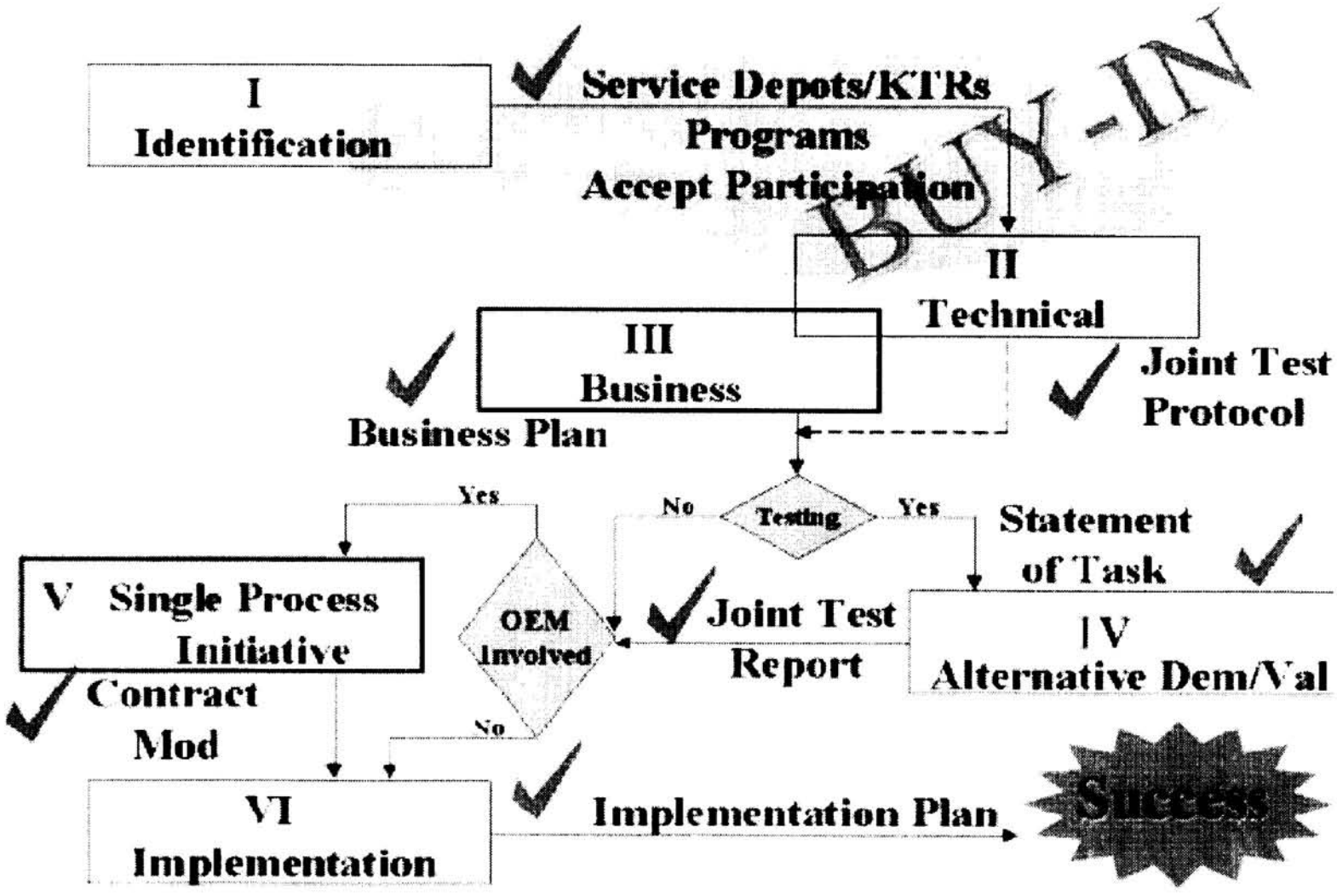

Harmonized projects, leveraged resources

JG-PP Projects

Project	Locations
Coating Systems (11)	
Non chrome conversion coating	Hughes Missile-Tucson
Non chromate aircraft primer	Boeing-St. Louis
Low VOC topcoat & primer	Raytheon Texas (incl. Dallas)
Low VOC - ID marking	LM-Orlando, WR-ALC, NADEPCP
VOC ballast tank coatings	NAVSEA
VOC non skid (Type I & II)	NAVSEA
VOC paint med. cal. munitions	Three OEMs, Army, USN, OO-ALC
VOC topcoat support equipment	USAF, USN, Army, NASA
Non chromate alum. pretreatment	Four OEMs, USAF, USN, Army, NASA
Non chromate conversion coat	NCMS
Joint Org. Coatings & Surf. Trmt.	N/A
Metal Finishing (7)	
Chrome free fasteners	P&W West Palm
Cadmium free electroplating	Boeing-Seattle, Phila., St Louis
Cr free - landing gear (HVOF)	Four OEMs, NADEPJAX/CP, OO-ALC
Cr free - prop hubs (HVOF)	HSD, NADEPCP, WR-ALC
Cr free - actuators (HVOF)	OO-ALC, OC-ALC, all NADEPs
Cr free - helo rotor parts (HVOF)	Three OEMs, NADEP-JAX, CCAD
Joint Cd Alternatives Team	Four OEMs, USAF, USN, Army, NASA
Cleaning (2)	
Oxygen line cleaning (ODS free)	OC-ALC, NASA, NAVAIR, Northrop-Grumman
Hand wipe prepaint cleaner	TBD
Coating Removal (1)	
Hand held LASER-de-coat	Selected depots and field units
Electronics Mfg. (1)	
Lead & VOC free- printed circuits	CCAMTF
Special Projects (1)	
Lead free, dry film lube- jet engines	Five OEMs, PEWG
Total Projects: 23	

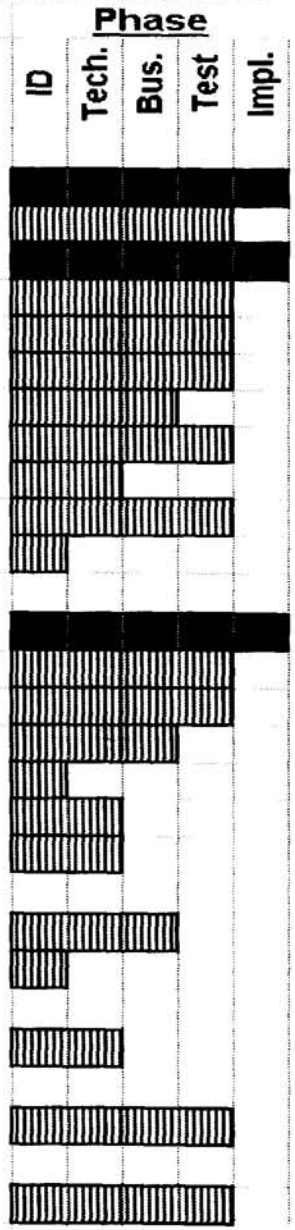

JG-PP Completed Project

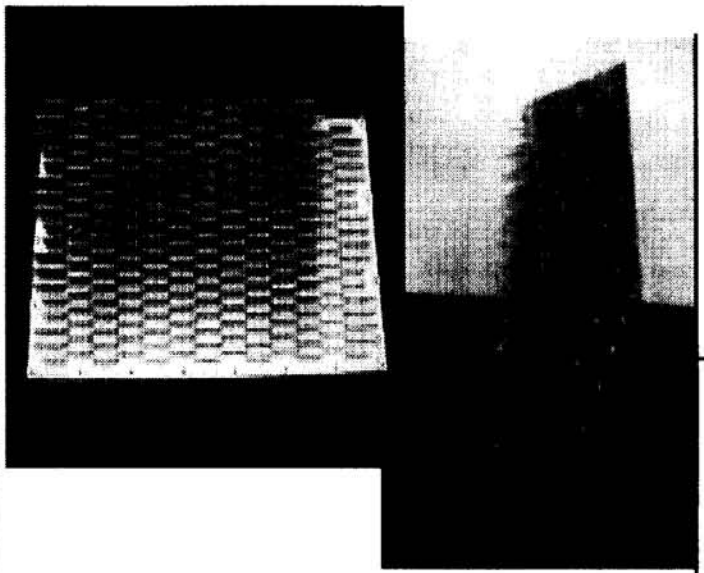

Deliverables:

- Potential Alternative Report
- Joint Test Protocol
- Joint Test Report
- Qualified Alternatives

Benefit/Impact:

- Initial reduction 40 to 88%
- Cost avoidance - $9M in reduced contract change
- Reduce VOC emissions 100%
- Cost avoidance >$5M/Yr manufacturing
- Material cost savings of $1.20/square foot
- Eliminates masking/de masking operations.
- Labor savings for parts 3 hours
- 10 weapon systems - all services

Description:

- Eliminate VOCs in topcoats and primers
  - Toluene, Xylene, Methyl Ethyl Ketone
- Provides a non-VOC, non-hazardous alternate material for applications using MIL-C-46168, Urethane, Camouflage, Infrared and CARC qualified

Milestones:

- Project began Aug 95
- First block change in DoD Apr 96
- Second block change completed Jul 97

Costs: $700K **ROI** <.3 year

Raytheon Corporate-wide SPI

Leveraging JG-PP Successes

- Former Raytheon Systems Co. (RSC) Customer Council MOU signed in Feb 00
  - Established corporate-wide Joint Test Protocol (JTP) for validating low VOC replacement topcoats & primers
  - Builds on legacy SPIs, especially legacy Texas Instruments (TI) JTP developed by JG-PP
    - Substantial VOC reduction
    - $680K DCAA audited 5 year avoidance at TI legacy plant
    - "Spin-off" SPI at Raytheon Electronic Systems, Bedford, MA provided additional $87K 5 year avoidance
- Potential for implementation at over 60 plants

Raytheon Corporate-wide SPI

Leveraging JG-PP Successes

- Implementation in formative stage
  - SPI mandates that each program has to be briefed on JTP and agree to its use in validating substitution candidates
  - Currently being implemented on 40 contracts at two locations: Dallas (legacy TI) and Tucson (partial implementation)
  - Tucson Cost savings/avoidances
    - Contractor estimated 5 year direct cost savings is $37K on following programs: AIM9X, AMRAAM, MAVERICK, STD MSL

Boeing Aircraft And Missiles Non-Hexavalent Chromate Primers

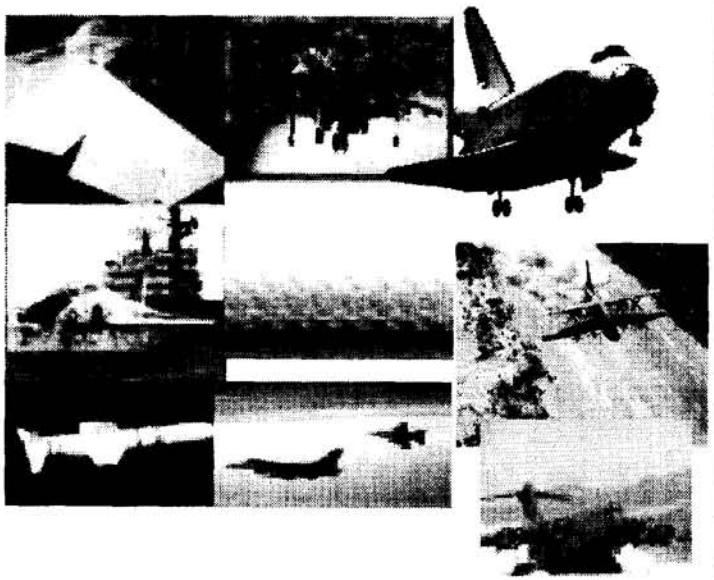

Description:

- Eliminate Cr^{+6} and reduce VOCs in primer used on aircraft outer mold line for F-15, C-17, F-18, T-45, Harpoon/SLAM, AV-8B
- Lockheed Martin conducting same tests on F-16, collaborative with Boeing

Benefit/Impact:

- Reduce chrome releases by 60% for this process
- 72% AFMC primer reduction of Cr^{+6} (7,000 lbs)
- Cost Avoidance >$250K/Yr manufacturing
- Affects 7 weapon systems - all services
- DoD depot cost avoidance $31.3M/20 yrs

Migration:

- NASA Columbia Space Shuttle
- Flipper doors (every other one)
- C-130

Milestones:

- Lab testing complete Dec 1997
- Flight testing Feb 1998 - Jan 2002
  - F-15, F-18, AV-8A, T-45, Harpoon
  - Added C-17, C-130, two more F-15s
- F-16 testing primers, coordinating

What has JG-PP achieved

Pioneered workable joint partnering

- Created pragmatic, stakeholder driven 6 step method

Acquisition reform in action

- First technical block change at Raytheon-TI
- Results establishing performance specs

Created partnerships on 23 active projects

- Affecting over 150 systems
- 17 original equipment manufacturer locations/10 depots
- Coordination with over 800 technical and business stakeholders

Created cost/benefit analyses process

- Meets DCAA requirements, when required

Where is JG-PP going next

International Partners

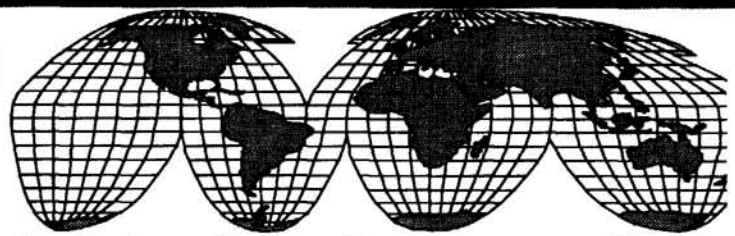

- **Leverage environmental technology and resources when found**
  - "Engagement is warranted" Mr. Gary Vest, PADUSD(ES), JG-PP Principals' Mtg Dec 99
- **JG-PP open to International P2 partners**
  - U.S. Law 10 USC 2530a(e) and SECDEF MEMO
    - Cooperative RDT&E of defense systems
    - DoD procurement of foreign technology and logistics support
- **Success partnering with Canadians on High Velocity Oxygen Fuel Project through Navy**

JG-PP Keys to Success

Proactive Involvement

- Partnership
- Technical confidence
- Communication
- Risk Reduction
- Reduced costs

JG-PP Web Page

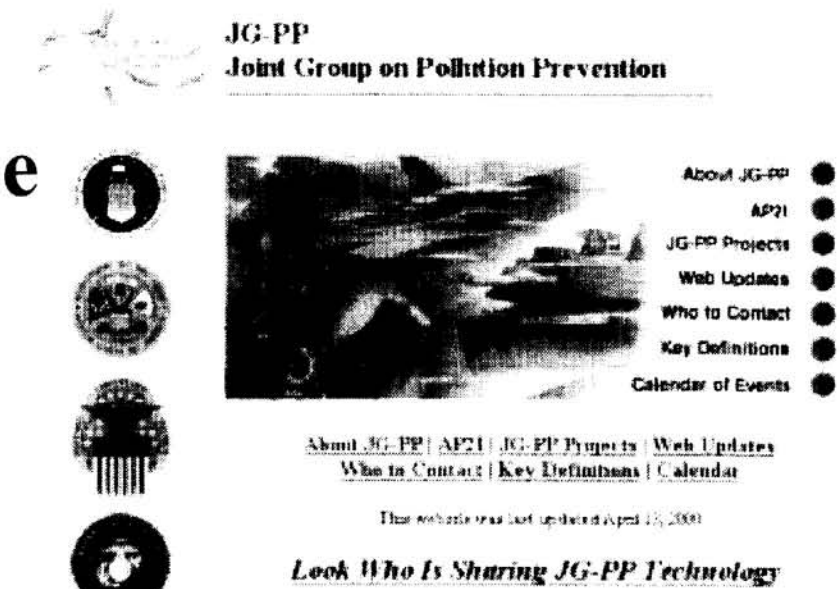

http://www.jgpp.com

7 11 31

Liquid Filtration for Component Reliability and Waste Minimization

By

Edward Kanegsberg and Barbara Kanegsberg

BFK Solutions

16924 Livorno Dr., Pacific Palisades, CA 90272

(310)-459-3614, Ed@Bfksolutions or Barbara@Bfksolutions

Introduction

Liquid filtration is an important tool for the component manufacturer for increasing the performance of the component, to reduce manufacturing costs and to minimize waste streams. The type of filter to be used depends on its function and degree of effectiveness required. Using a filter not matched to the requirement can, at the least, increase costs and, at the worst, result in component failure.

The principles of liquid filtration are applicable to both aqueous and non-aqueous solvent cleaning but much of the terminology is grounded in aqueous cleaning.

Performance is the most important driver

Performance is probably the most important driver in a manufacturing process. If the part doesn't function, yield drops, and the costs can become non-competitive. A part will not function properly if it is not clean. A part can not be free of contamination if the cleaning solution isn't pure and clean. Filtration may be needed to increase the cleanliness of the cleaning agent at the beginning of its use cycle or to restore previously used agent by removing soil build up. It is necessary to adequately remove soils, without redeposition, and with no substantial residue (spotting) by soils or cleaning agents.

Pollution Prevention and Cost Reduction

Minimizing the waste stream goes far beyond "Doing what it takes to comply with environmental regulations". Cost is always a driver and very frequently, if waste streams can be reduced, so can costs. Waste streams are not only what is left to be disposed of at the end of the whole process; it can be thought of as what is, in its present state, unusable at the end of any part of the process. If, by filtration or other means, the cleaning or rinsing agent can be restored to a usable state, the life of the cleaning solution can be prolonged and the cost of the cleaning chemicals will be reduced. In this age of low Ozone Depleting Chemicals (ODCs) and low Volatile Organic Compounds (VOCs), sometimes the alternatives are costly. Even at the end of the process, disposal of waste streams can be an extremely large portion of the overall cleaning process cost (Kanegsberg and LeBlanc). In some cases, by concentrating waste into easily disposed filters, a company may be able to reduce its classification as a waste generator.

When to filter?

Filtration requirements are different at each stage of the cleaning cycle. In many cleaning processes, the flow of cleaning agents is reversed from that of the parts to be cleaned so it is important to realize that beginning, middle, and end of cleaning agent use does not refer to the cleaning flow. The purest (input) chemicals are used for the final rinse, and most of the soils that need to be processed as waste (output) will enter the cleaning agents in early wash stages.

Even with high-purity water and other solvents, filtration may be desirable to remove contaminates at the point of use. Water for precision cleaning processes must frequently be cleaner than clean enough to drink. It may contain contaminants such as particles, dissolved salts, organic material, chlorine, or fluorine which, even in small concentrations, can interfere with its ability to clean or will leave residues on the part.

Not only before use or before disposal, but also in the middle of the cycle, especially for precision cleaning applications, soil build up and redeposition must be avoided. Filtration can be a critical part of the "keep it clean at all times" philosophy. Further, when water or other solvent used at the beginning of the cleaning agent cycle is the recycled output from another stage, contaminants must be removed without substantially altering the cleaning agent itself.

The Perfect Filtration System

Those of us involved in manufacturing precision components have exacting, idealized expectations for filtration systems. For example, in an ideal aqueous filtration system, the in-process filter would separate particulate, inorganic, and organic contamination from the cleaning agent, leaving the cleaning agent pristine and totally unaltered from its original state. The filter would be readily regenerated so that it could last for months, perhaps years. The filtrating system for regenerating rinse water would remove particles, separate process oil for recycling, separate and concentrate the cleaning agent surfactant package in its original concentration, and provide a source of regenerated 18 megaohm water.

In the real world, there is no universal filter; and there is no perfect filtration system, just as there is no universal cleaning agent or cleaning system. However, we can optimize the filtration system by understanding the types of filters, their benefits, and their limitations.

Choosing the filter

There are four basic types: bulk, membrane, adsorption, and replacement. Filters are frequently used in combination with each different filter dealing with a separate part of the process.

Bulk granular media filters are called for to remove large particles or heavy contaminant loads. Even in critical cleaning applications, some early parts of the process may have large particles and heavy loading of contaminants.

If the particulate size is small and the soil loading is low, membrane microfilters or ultrafilters might be needed. Sometimes the material is not particulate. For dissolved materials, a de-ionization or reverse osmosis process will be called for.

For organic molecule removal, adsorptive filtration can frequently be used.

In any event filter selection should be accomplished from a cooperative effort involving equipment and cleaning agent vendors and of course the user.

Mechanical Filters

Both bulk and membrane filters are **Mechanical filters.** They depend on a physical barrier for contamination removal. In manufacturing applications, small objects, such as the cleaning agent molecules, can pass through the filter but larger objects, the particulate contaminants, can not. Mechanical filtration is one of the most common methods used to remove particles from cleaning agents.

For larger particles, 20 μm in diameter or larger, **granular media filters,** composed of sand and other minerals, can be used. For somewhat smaller particles, **Cartridge Filters,** made from synthetic and natural fibers, and **Bag Filters**, with felt-like materials, can be employed. Cartridge filters are most often used for lower flow rates and higher efficiency applications and bag filters for high flow rate and lower efficiency applications (Russo). All of these are **flow-through or bulk filters**, as the entire fluid stream is passed through the filtering media and the particles are trapped inside the bulk of the media. With flow-through filters, the particles are harder to dislodge because they penetrate more to the center of the filter. It is usually more cost effective to dispose of the filter and replace with a new one than to attempt to regenerate it.

Membrane Filters are designed to remove very small particles and organic molecules from a liquid stream. The particle entrapment is a surface phenomenon; therefore the capacity is lower than that for bulk filters. On the other hand, because particles are retained on the surface, they can generally be purged by flushing and recycled. **Microfilters** remove all particles down to 0.05 to 1.0 μm. **Ultrafilters** remove particles and large molecules down to .005 μm. No industry wide terminology distinguishes microfilters from ultrafilters; the terms can overlap (Russo). Contaminants are in general not spherical. If the filter pore size lies between the minimum and maximum dimensions of the particle, there can be incomplete filtering. It is therefore imperative to monitor the process and confirm, via particle counters, resistance measurement, or other methods, that the desired level of purity is being achieved.

When used for recycling, microfilters and ultrafilters have limitations in that they can alter cleaning agent composition. Dirt and oil must be retained while allowing the cleaning agent to pass through the membrane (Bahr and Gaydos). With water/surfactant solution, some filters may only minimally affect the cleaning agents (Quitmeyer). However, with microfilters of pore size less than 0.2 μm, the filter may remove not only the contaminant but also much of the surfactant itself. This is due to properties of the chemistry, which cause surfactant molecules to clump into micelles (Peterson). This limits the lifetime of the cleaning agent and the lifetime of the filter.

Self-emulsifying oils are difficult to treat to prevent redeposition (Brockhurst et al.). These lubricants contain surfactants, which form stable emulsions. In general, aqueous cleaners can not break these emulsions without being consumed in the process. Microfilters (0.1 – 0.5 μm) can be used to remove some or most of the emulsion but generally results in some loss of cleaner constituents. Monitoring and adjusting of the tank becomes cumbersome and may not be an economically viable option. Some recent work (Ventura and Dahanayake) may lead to development of surfactants that are more amenable to microfiltration.

Other important parameters are the pH and temperature of the solution. Cleaning efficiency is better at elevated temperatures and aqueous cleaners are usually high pH (alkaline). Both the component to be cleaned and the cleaning equipment, including filters, must withstand these conditions. Of two types of membrane filters, inorganic/ceramic membranes have greater tolerance to both heat and alkalinity than do organic polymer membranes (Rajagopalan et al.) although, as will be discussed later, there are newer polymer filters in development with improved heat and alkalinity tolerance.

Filter life can be extended with appropriate flushing techniques. Because membrane filters trap the particles on the source side, it is possible to flush the filter by reversing the flow direction (backwash). Many membrane filters feature a crossflow, in which most of the fluid travels tangentially to the surface to sweep the contaminants away and avoid fouling the filter. Only a small portion (approximately 10%) of the fluid passes through the filter as the cleaned permeate.

When a variety of particle sizes are present, it is wise to consider a tandem arrangement of filters starting with granular, bag or cartridge filters to remove the larger particles, then microfilters, and finally ultrafilters. Just as several rinses are more effective than one, several filters may be more cost effective than one.

The contaminant does not need to be a particulate to be removed by a filter process. Water is different from most other solvents due to its polarity. The high polarity allows a large number of substances, particularly ionic salts, to dissolve. Removal of these ionic substances can be challenging. **Reverse Osmosis (RO)** is a mechanical filtration membrane process used to separate a solvent, usually water, from a solution of dissolved solids. When solvent and solution are on opposite sides of a semi-permeable membrane, so called because it allows some molecules to pass through more easily than others, the chemical energy of the solution favors the solvent flowing (osmosis) through the membrane to dilute the solution. A differential pressure will build up; the height of the fluid column on the solution side can be greater than on the solvent side. If pressure is applied to the solution, this typical direction of flow can be reversed (reverse osmosis) and purer solvent can be extracted from the solution.

Since the membrane also is a mechanical filter, it also retains larger molecules, such as organic dyes, cleaners, oils, and metal complexes. Therefore, RO membrane systems frequently feature crossflow filtration to allow the concentrate stream to sweep away retained molecules and prevent the membrane surface from clogging.

While the membrane removes essentially all non-dissolved particles including microorganisms to the limit of the filter pore size, the rejection of dissolved substances is a percentage of the concentration in the incoming stream. The weight, shape and amount of ionic charge determine the degree of rejection. Higher purity can be attained if more than one RO unit is used in series. Cartridge filters are frequently used to remove particulates from the feed solution that would otherwise clog the units.

In the past, RO applications were primarily limited to final treatment of combined wastewater streams. More recent cleaning applications involve RO units in specific process operations (such as cleaning agent or rinse water maintenance), allowing return of the concentrate to the process bath and reuse of permeate as fresh rinse water.

Adsorptive Filters

Adsorptive filters use large surface areas to remove contamination. Adsorption is a physical process in which attractive force fields at the solid surfaces pull contaminants from the liquid phase and bind them to the surface. The difference in strength of interaction between a solid surface and different contaminant molecules is the basis of adsorption separation. In general, the amount of adsorbate that can be attracted by an adsorbent is a function of available surface area and the strength of the force fields at the surface. Therefore, increasing the surface area in combination with increasing the attraction force fields increases the adsorption capacity. One way to increase the force fields is by generating small micropores in the adsorbent materials (Lordgooei et al.), (see discussion of Activated Carbon Fiber below). The overlap of the force fields from the opposite pore walls strongly enhances the adsorption in the micropores.

Activated Carbon is the most commonly used absorbent and is generally a granular media made by heating carbon-containing materials in the absence of air, producing a porous material with a large surface area. This large surface area allows the attachment of large organic molecules. Typically, it is used as a pretreatment method to remove chlorine and long-chain organic molecules. It is also used to remove low levels of oils and greases.

A relatively new carbon filter, with the micropore structure mentioned above, is **Activated carbon fiber (ACF)** which is made from viscose rayon or polyacrylonitrile fiber through the process of carbonization and activation (Zhu). It is chemically stable in high acid or alkali condition, light weight, and has good adsorption at low soil concentration. The narrow diameter of the fibrous form (normally around 20μm) allows much more rapid rates of ad-sorption, desorption and reaction than is possible over larger (mm size) granular forms (Jagtoyen et al.). The incorporation of activated carbon fibers (ACF) into permeable monoliths provides a connectivity between individual fibers allowing, for the first time, their pore structure and other characteristics to be combined with a pathway for electrical and thermal conduction (Kimber et al.). One of the most interesting, and to date unexplored, aspects of these systems lies in the ability to control the electrical potential of the adsorbent surface. This introduces a parameter by which to investigate the fundamental mechanisms of adsorption and catalysis, and raises the prospect of being able to develop methods to monitor and/or control the physical and chemical changes that take place. In particular, the adjustment of surface potential can provide a technique for promoting or inhibiting the adsorption of certain compounds or reactants. In adsorption, it offers a means to enhance the removal of selected species in order to purify a bulk fluid stream, to recover chemicals, or even to effect the separation or fractionation of gas or liquid phase constituents (Univ. of Ky. CAER).

Replacement Filters

A replacement filter replaces an undesirable material with a more desirable one. **Deionization (DI)** is the most common replacement filter process and removes dissolved ionized materials from water. Technically, DI water is any water from which dissolved ionic salts are removed. There is no specific water purity that defines the term "deionized" but it usually refers to a resistivity of greater than 1 megohm-cm (pure water has a resistivity of 18 megohm-cm)[2]. Deionization removes ions, positively charged cations and negatively charged anions, by replacement using ion-exchange resins. The net result is that a salt is replaced by pure water. A two-bed deionizer consists of a tank with cation resin followed by a second tank with anion resin. A mixed-bed deionizer has both cation and anion resins intimately mixed in one tank.

DI water will remain only as pure as the equipment containing it. It may readily pick up ions from the process equipment, especially when heated. Also, as an example of "be careful what you wish for", ultra pure water may undesirably alter product surfaces by removal of ions.

The used resin may be used once and discarded, sent back to a vendor to be regenerated or regenerated on-site inside the actual tanks. However, regeneration involves strong acids and caustic chemicals and if performed on-site, the user may have to treat the waste produced by the regeneration process for pH imbalance and/or heavy metals before disposal. Resin cannot be regenerated *ad infinitum*. The capacity decrease rate is usually greater for waste applications than for source pre-treatment due to higher contamination levels.

Deionization and reverse osmosis often are found sequentially in the same system. DI is necessary as a post-treatment process to RO whenever the user requires a higher water purity than one megohm-cm resistivity. Sometimes the only way to make DI economical is to use an RO membrane as pretreatment for the deionizer to reduce the ionic percentage and therefore prolong the ion exchange resin in the deionization unit.

The challenge of specialized filtration development

To those of us involved in critical cleaning, development of advanced filters may be paramount. Unfortunately, the materials used in filters are often developed by large petroleum companies, with what might be described as an oil-company mentality. That is, they develop a plastic with the idea of selling immense quantities, but they may be unaware or unconcerned about high-value, niche markets.

Serving the niche applications of the future is likely to involve an ability to respond to the subtle requirements of each micro-niche market by surveying and perhaps modifying the physical and chemical characteristics of the overall product line. Mike Beeks technical director, research and development, at The Brulin Corporation, Indianapolis, IN explains that the filter must remove soils and particles, sometimes to fractions of a micron, while having minimal impact on the cleaning chemistry. It must be able to withstand a wide range of organic and inorganic materials. In the general scheme of the plastics industry, filters are a tiny application; but a properly engineered filter could provide an invaluable pivotal solution for the components industry (Beeks)

Let us examine, for example, one class of polymers, polysulfones, which have unrealized potential in membrane filter manufacture. Polysulfones are strong, clear, and they have temperature stability and chemical resistance which is superior to other plastics. Polysulfone, polyether sulfone and polyphenyl sulfone currently find uses in areas ranging from biomedical/diagnostic products to filters. However, the role of polysulfones in improving filtration performance could be greatly increased.

Roger Jones, president of Franklin Polymers sees the desirability of a paradigm shift. "Polysulfones represent a significant, profitable business. Unfortunately, the niche doesn't fit the current business template of consolidation and size. Many companies are trying to get bigger, faster - they are trying to be first or

second. It's a flawed template. You don't have to be first or second to be a success. Let's take for example the use of polyethersulfones for filters. Filters are a polyethersulfone market rather than a polysulfone market, because polyethersulfone has better heat and chemical resistance. You have the producer, the compounder, then the distributor. From the producers' viewpoint, filters are a miniscule market, so people in those areas may get little support from the polymer producer. If the managers considered the impact of smaller niche markets, they could provide more product support, charge more, and make more money. This is counter to a bulk chemical mentality." (Jones)

There is progress in development of more specific products for filtration. One example is ACF, described previously. Developmental work is also proceeding which may lead to improvements in plastics-based filters. Dr. Ryan Giedd at Southwest Missouri State University sees applications for secondary modification of polysulfones to produce narrow-niche products of high value. He describes his work in ion implantation as a tool in expanding applications for polysulfones. "When you ion implant, hydrogen is removed from the polymer structure, making it a hard carbon-based material. The implanted segment may be only 700 Angstroms. The softer, less resistant material can then be removed, resulting in three dimensional micro-machined structures. The structure is electrically-conducting, providing potentially utility for high-value resistors."

Dr. Giedd notes that this is a secondary process on the finished polymer. He sees applications for such modified polymers where there are requirements for a material that is thin, hard, strong, and with a high surface area, such as in high value small geometry resisters and microstrain gauges, and bolometers (specialized heat measuring sensors used to detect infrared radiation) (Giedd).

Conclusion

Filtration, like the rest of the critical cleaning industry, is an evolving science. Cleanliness demands keep increasing, especially in electronics and biomedical applications, and cost and environmental pressures favor recycling of cleaning chemicals and extending the useful lifetime of filters. Developments are continually being made to advance the utility of filters of all types, and such developments are likely to continue due to performance and environmental drivers. There is no one-size-fits-all solution and users, cleaning agent and cleaning equipment suppliers must continue to work closely with each other to achieve affordable, effective processes.

References

1. M. Bahr and S. Gaydos, "Effects of Microfiltration on Aqueous Degreasing Solutions", CleanTech '98 Proceedings, pp. 321-330.

2. M. Beeks, Technical Director, The Brulin Corporation, personal communication.

3. R. Brockhurst, M. Beeks, and D. Keller, " Aqueous Cleaning Essentials", in "Handbook For Critical Cleaning", Barbara Kanegsberg, ed. , CRC Press (in press),.

4. R. Giedd, Department Head, Material Science, Southwest Missouri State University, personal communication.

5. Jagtoyen et al, 1994, Materials Res. Soc. Symp. Proceedings,344, 77-81; as referenced by the Univ. of Kentucky Center for Applied Energy research (CAER), at http://www.mrsec.uky.edu/research/research.htm

6. R. Jones, President, Franklin Polymers, personal communication.

7. B. Kanegsberg and C. LeBlanc, "The Cost of Process Conversion", CleanTech '99 Proceedings, pp. 12-29, 1999.

8. Kimber et al, 1996, Gas. Sep. Purif., 10 (2), 131 136; as referenced by the Univ. of Kentucky Center for Applied Energy research (CAER), at http://www.mrsec.uky.edu/research/research.htm

9. M. Lordgooei, K. R. Carmichael, M. J. Rood and S. Larson, "Development of an Activated Carbon Fiber Cloth Adsorption/Regeneration System to Recover and Reuse Toxic Volatile Organic Compounds", Illinois Waste Management Research Center (WMRC), report RR-081 available from WMRC through library@wmrc.uiuc.edu

10. J. Quitmeyer, "Aqueous Cleaning Filtration Study", CleanTech '98 Proceedings, pp 20-25.

11. D. Peterson, "Limits of Microfiltration", Plating and Surface Finishing, May 1995, p82-86.

12. N. Rajagopalan, T. Lindsey, and J. Sparks, "Recycling Aqueous Cleaning Solutions", Products Finishing, Vol 63, No. 10, July 1999.

13. J. Russo, "Selecting the Best Waste Water Treatment for Aqueous Operations", in "Handbook For Critical Cleaning", Barbara Kanegsberg, ed. , CRC Press (in press).

14. Univ. of Kentucky Center for Applied Energy research (CAER), at http://www.mrsec.uky.edu/research/research.htm

15. M. Ventura and M. Dahanayake, "Filterable Surfactant Class Resolves Separation Anxiety", Precision Cleaning Magazine, July 1998.

16. H. Zhu, Shanghai No. 1 Carbon Fiber Co., Ltd., personal communication.

About the authors

Ed Kanegsberg, Ph.D., is a physicist with BFK Solutions and a member of the technical staff at Litton Guidance and Control (Woodland Hills, CA). He has over 30 years of experience in precision instrument development and productionization. He addresses production yield issues through both process improvement and component modification.

Barbara Kanegsberg, President of BFK Solutions, works with components and parts manufacturers to resolve cleaning, contamination control, and environmental issues. Barbara is a recipient of the U.S. EPA Stratospheric Ozone Protection Award for her achievements in implementing effective, environmentally-preferred processes. She is also a member of the Editorial Advisory Board of Precision Cleaning Magazine.

CP/248/N 27

Chemical Aging of Environmentally Friendly Cleaners[1]

L.L. Biegert, K.B. Evans, B.D. Olsen, B.L. Weber
Cordant Technology: Thiokol Propulsion
P.O. Box 707
Brigham City, Utah 84302-0707
(435)-863-3958
Biegell@Thiokol.com

ABSTRACT

Use of cleaners in the manufacturing area demands bottles that will hold a sufficient amount of material and allow for easy and controlled dispensing by the operator without contamination or material leaching from the bottle. The manufacturing storage conditions are also a factor that may affect cleaner chemical integrity and its potential to leave a residue on the part.

A variety of squeeze bottles stored in mild (72 °F, 10% R.H., dark) and harsh (105 °F, 50% R.H., fluorescent lighting) conditions were evaluated to determine the effect of environment and bottle exposure on ODC cleaners chemical composition. Low Density Polyethylene (LDPE) bottles were found to be quite permeable to all the cleaners evaluated in this study indicating this bottle type should not be used in the manufacturing area. Fluorinated Polyethylene (FLPE) bottles showed little cleaner loss and change in cleaner chemical composition over time suggesting these bottles would be acceptable for use.

Chemical analysis indicates limonene containing cleaners show increased non-volatile residue (NVR) content with storage under harsh conditions. Some cleaners use BHT (butylated hydroxytoluene) as stabilizer and to protect against limonene oxidation. Under harsh conditions, BHT was quickly depleted resulting in higher NVR levels.

INTRODUCTION

The vendors of environmentally friendly cleaners have established shelf life times for each of the cleaners based on containment within the manufacturer's sealed container. In the manufacturing area, these cleaners will be removed from the vendor container and placed in dispensers that will make hand wipe operations convenient. To ensure the exposure to the dispensing unit (squeeze bottles) and the manufacturing environmental conditions (temperature, humidity, light, and time) do not impose any adverse chemical aging on the cleaners, an aging study was initiated.

Many of the cleaners currently being evaluated for hand wipe operations in the manufacturing area contain the terpene hydrocarbon, limonene. It is well known that limonene readily oxidizes upon environmental exposure forming less volatile compounds. Conditions in this study were selected to not only mimic manufacturing conditions but also be of a sufficient harsh environment to produce oxidized limonene compounds.

© 2000 Thiokol Propulsion, a Division of Cordant Technologies

[1] This work was performed under contract NAS8-38100 as part of NASA's ODC Cleaner TCA Replacement Program.

PLAN

CLEANERS, BOTTLES AND ENVIROMENTAL CONDITIONS

Six cleaners were selected from the candidates that are currently considered as acceptable alternative cleaners to TCA for hand wipe cleaning RSRM production components. These cleaners are listed in Table I along with a chemical description. Most of the cleaners contain the hydrocarbon limonene that has two sites of unsaturation. BHT (butylated hydroxytoluene) is found in three of the cleaners containing limonene and is used as a stabilizer. DPGME (dipropylene glycol methylether) is reported in two of the cleaners. 1TB2P (1-t-butoxy-2-propanol) is also found in two cleaners and like DPGME would expect to be hydrophilic. Eventhough hydrocarbons are found in both PFD and BA4 cleaners the types of hydrocarbons are different for these two cleaners.

Table1: Cleaners and Their Composition

Cleaners***	Abbreviation	Limonene (%)	BHT (ppm)	DPGME (%)	HC (%)	MP (%)	1TB2P (%)
BIOACT® PCG	PCG	100					
RE-ENTRY® PREPSOLV	PRP	100	278				
RE-ENTRY® PLUS4 SOLVENT	PL4	75	198	9		5	11
BIOACT® 113	BA1	36					64
PF™ Solvent	PFD	8	17		92*		
BIOACT® 145	BA4			27	73**		

* = C_{10} to C_{14} hydrocarbons
** = mixed aliphatic hydrocarbons (C_9 to C_{13} branched and cyclic).
*** = all cleaners are manufactured by Petroferm except for PF™ Solvent that is manufactured by PT Technologies

Four bottles were evaluated in this study. LDPE (low density polyethylene) and FLPE (Fluorinated High Density Polyethylene) bottles were evaluated. The FLPE bottles are currently used to contain TCA in the manufacturing area. Silgan bottles (manufactured by Silgan Plastic Corporation) were also evaluated. These bottles are composed of a HDPE (high density polyethylene) outer layer and a Nylon inner layer. Glass bottles were used as a baseline. Glass Qorpak bottles (Fisher Catalogy #03-320-11J) were fitted with Teflon closures and spouts so the cleaner would be exposed to the atmosphere to simulate exposure that cleaners in the squeeze bottles would see.

The storage conditions were selected to not only represent typical and worse case conditions found in the manufacturing areas but also in the worse case condition be of a sufficiently harsh environment to induce high levels of non-volatile residue (NVR). The mild (typical normal manufacturing area) environment was selected as 72 ± 5°F, less than 10 % R.H. and samples stored in the dark. For harsh conditions the bottles were stored at 105 ± 5°F, 50 % R.H. and under constant exposure to fluorescent lighting.

CHEMICAL ANALYSIS

Several methods of chemical analysis were conducted to monitor the effect that aging has on the chemical properties of the cleaners. The methods used in this study include non-volatile residue, and moisture.

The NVR testing conducted on cleaners containing limonene is not an absolute evaluation of the non-volatile residues that will be seen on a production part. Instead the NVR results should only be used to evaluate the purity of the material. Non-volatile residue is an empirical measurement defined by the evaporation conditions. NVR, as determined by this method, is defined as any material that does not evaporate after four hours in a forced draft oven at 105°C.

The water present in the cleaners was determined by a Karl Fischer titration method using pyridine-free reagents. The method measures water content by quantitatively titrating the water with a base-iodine-sulfur dioxide complex. Water consumption is determined by amperometric endpoint detection using a dual platinum wire electrode.

DISCUSSION

To ensure the NVR testing method would produce results that would be consistent throughout the study, a correlation between NVR and test conditions was made. A newly manufactured lot of PCG was compared with cleaner that had been stored in the manufacturing area for 6 months. Seven to ten milliliters were placed in a 75-ml aluminum dish and allowed to evaporate under temperatures ranging from ambient (20°C) to 130°C.

Figure 1 shows the effect of test temperature on NVR level. For the aged PCG, the ambient dried samples had a higher NVR percentage most likely due to low molecular weight oxidized limonene products. These low molecular weight compounds are present when the evaporation temperature is near ambient while at higher temperatures they evaporate. The NVR content for the aged PCG appears to stabilize between 100 and 110°C.

The time that the samples were dried was also investigated during the development of the NVR test method. Figure 2 shows the NVR levels of the newly manufactured PCG and 6 months aged PCG ranging from a dry time of 10 minutes to 6 hours at 105°C. The fresh PCG NVR levels become stable after 2 hours while the aged PCG continues to lose weight. The weight loss over time is most likely due to a continued loss of semi-volatile oxidized compounds. From this preliminary testing, the NVR test method was selected as evaporation of a 10 milliliter sample of cleaner at 105°C for four hours in a forced draft oven.

The NVR content of the cleaners stored under harsh conditions in glass bottles over time readily correlated with limonene content and BHT depletion. Both cleaners that contain limonene and no stabilizer (PCG and PRP) show initial higher levels of NVR compared to the other cleaners. Those cleaners that contain limonene and stabilizer show increased NVR levels as soon as the stabilizer is depleted. Stabilizer depletion for PFD was 3 weeks, for PRP four weeks and for PL4 the stabilizer was depleted by 9 weeks. The time to stabilizer depletion was dependent on both the stabilizer amount and limonene percentage in the cleaner.

The NVR content of the cleaners in glass bottles under mild is shown in Figure 4. As expected, only those cleaners with limonene and without stabilizer show any increase in NVR content. The NVR content for cleaners stored under mild conditions is lower than when stored under the harsh environment.

A comparison of bottle NVR content is shown for PCG under harsh conditions in Figure 5. The LDPE bottles appear to be more permeable. Under the harsh conditions, water not only diffuses into the bottle, cleaner also diffuses out. The NVR difference between glass and FLPE bottles may be attributed to the glass bottle larger spout opening or also the transparency of the glass.

The moisture content of the cleaners in glass bottles stored under harsh conditions is shown in Figure 6. The cleaners with the higher moisture content (BA1, BA4 and PL4) all contain chemical components that are hydrophilic in nature (DPGME and 1TB2P). Over time and 50% relative humidity, these cleaners continue to pick up moisture.

Figure 7 shows the cleaner moisture content stored under mild conditions (less than 10% relative humidity) in glass bottles. Those cleaners with hydrophilic components have higher levels of initial moisture and will gain more moisture over time with exposure to the atmosphere.

Like the NVR levels, moisture in cleaners stored in LDPE bottles is higher compared to the other containers evaluated in this study. Figure 8 shows the moisture content of PL4 stored in the various bottles under harsh conditions. The glass bottles also have higher moisture content compared to the FLPE bottles and may be explained by the larger spout in the glass bottle allowing for an increased exposure to the atmospheric moisture.

SUMMARY/CONCLUSIONS

The NVR content as measured by evaporation of ten milliliters at 105°C for 2 hours in a convection air oven is a method that can be used to monitor the purity of a cleaner and is not an absolute evaluation of non-volatile residues that will be seen on a production part. The NVR content is dependent not only on the amount of limonene present in the cleaner but also on the presence of a stabilizer (BHT). The storage of cleaners in high humidity, high temperature and fluorescent lighting also contributes to the oxidation of limonene.

Cleaners that contain moisture sensitive compounds (1TB2P and DPGME) initially have higher levels of water. The moisture content continues to increase as samples are stored under high humidity conditions. If stored in a mild environment there is little change in moisture content over 4 months.

A cleaner's susceptibility to moisture and NVR formation is also dependent on the type of storage bottle. The permeability of LDPE bottles to moisture prohibits their use in a manufacturing environment. FLPE bottles are less susceptible to moisture and thus are a good candidate.

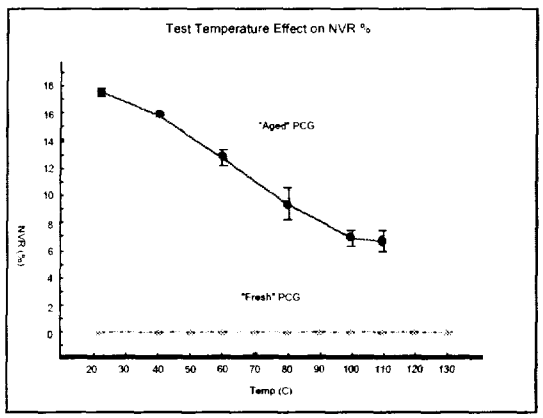

Figure 1: Percent NVR as a Function of Evaporation Temperature.

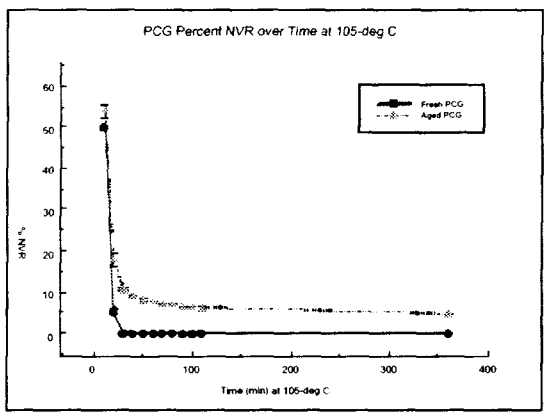

Figure 2: Percent NVR as a Function of Time at 105 °F.

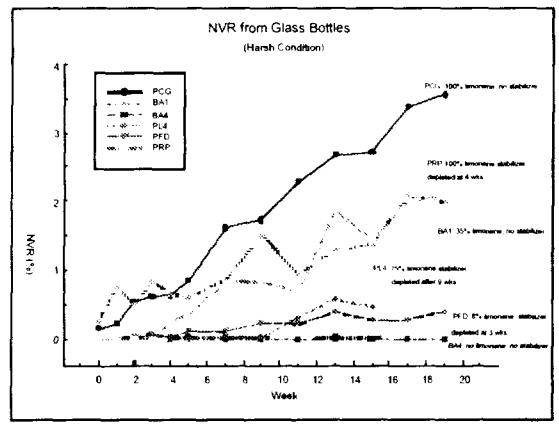

Figure 3: Percent NVR as a Function of Time under Harsh Conditions

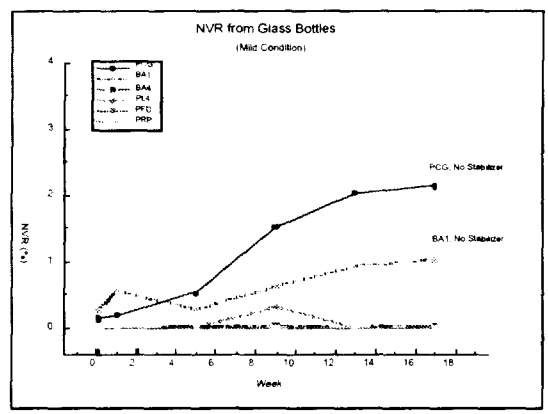

Figure 4: Percent NVR as a Function of Time under Mild Conditions.

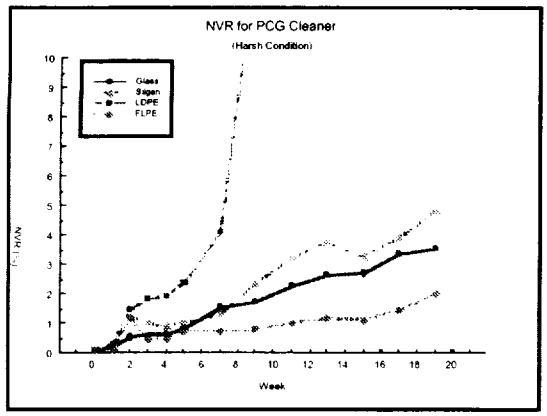

Figure 5: Percent NVR in PCG as a Function of Bottle Type

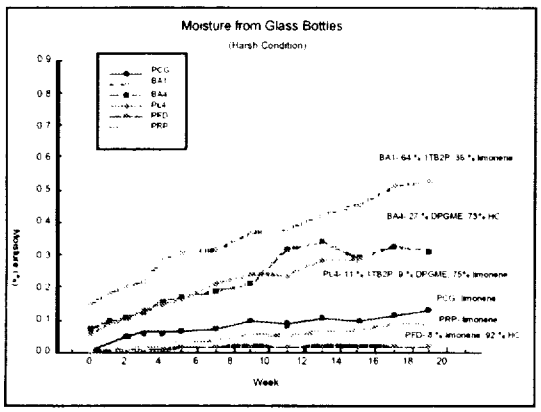

Figure 6: Percent Moisture under Harsh Conditions

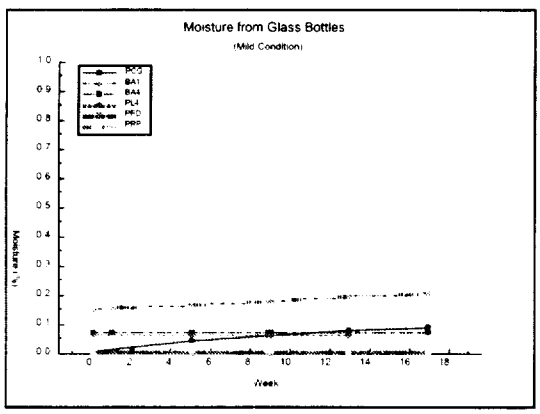

Figure 7: Percent Moisture under Mild Conditions

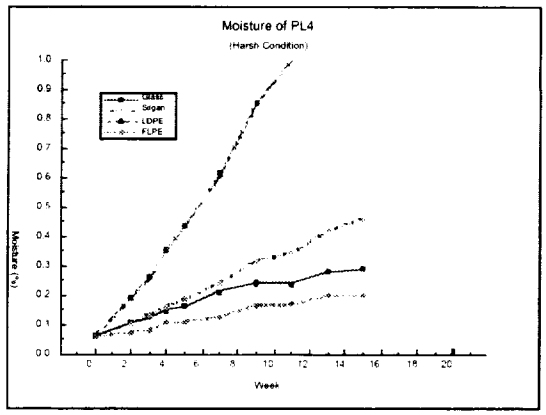

Figure 8: Percent Moisture in PL4 as a Function of Bottle Type.

CP/549 IN/82

NAtional Materials Information System

Jeff Guthrie
AMPTIAC
201 Mill St
Rome, NY 13440
Phone #: (315) 339-7058
Fax #: (315) 339-7107
E-mail: jguthrie@iitri.org
Web: http://amptiac.iitri.org/

Abstract

The following paper describes the NAtional Materials Information System (NAMIS) developed by the Advanced Materials and Processes Technology Information Analysis Center (AMPTIAC).

NAMIS preserves the DoD materials and process knowledge base making it readily available to the materials community. Inside NAMIS, users will find several database modules of interest space and launch vehicles communities. Two searchable bibliographic database containing all past High Temple Workshop and the Cocoa Beach Conference proceedings have individual paper citations linked viewable electronic documents. The third database module, NASP, contains a virtual library of all the NASP (National AeroSpace Plane) final reports from the materials and structures augmentation program.

Although it never came to fruition, many breakthroughs in high temperature materials and processes owe their success to the NASP program. Since NASP was never fielded, these breakthroughs in materials never fully transitioned and eventually the technical heritage and expertise dissipated. Both government and industry personnel moved away from high temperature materials problems and often their personal libraries were lost.

Today, many proposed new systems present similar technical challenges and require this same expertise. For example, NASA's X33, X34, Reusable Launch Vehicle (RLV), Hyper X, and Future X will need advanced Thermal Protection Systems (TPS), hot structures, and huge liquid hydrogen (LH) and liquid oxygen (LOX) tanks. In the military, Military Space Plane (MSP) will require these same technologies. Additionally, multiple new missile concepts such as the Common Aero Vehicle (CAV), the Hypersonic Technology program (HyTech), and High Speed Strike program (HST), demand innovative hot structure and TPS.

AMPTIAC will demonstrate the features of these web-based databases found at the following URL: http://NAMIS.iitri.org/

Introduction

Continuing advancements in high temperature materials require a sound database of material properties and an understanding of past technology development. The Advanced Materials and Processing Technology Information Analysis Center (AMPTIAC) operated by IIT Research Institute (IITRI), function as the caretaker of materials information for DOD. As part of its caretaker role, AMPTIAC populates and maintains high temperature materials databases with evolving technology. These databases, in-turn, helps fulfill an AMPTIAC'S role of disseminating DoD materials data.

About AMPTIAC

AMPTIAC, is the culmination of 13 other materials information analysis centers dating back to 1955 at Battelle Memorial Institute and 1960 at Purdue University. The AMPTIAC library contains nearly 210,000 technical reports and books addressing a broad spectrum of engineering materials. This library is continuously updated in an attempt to collect the latest technology advancements in material applications, properties and processing techniques. As part of its mission for DOD, AMPTIAC is applying this resource to construct an integrated material and process database - labeled the NAtional Materials Information System (NAMIS).

Making this database possible requires a fusion of materials and software expertise to achieve the desired functionality and aesthetics. Additionally, rigorous data evaluation ensures pedigreed data through strict criteria mapped out by both the American Society for Testing and Materials (ASTM) and the National Institute of Standards and Technology (NIST). Evaluated data is critical since the exploding availability of technical data from handbooks, electronic databases, on-line libraries and the World Wide Web, require the user to examine the quality of data. The performance of manufactured products depends on the reliability of the materials data used to design and plan the manufacture of the product.

Legacy Materials Data

Future high performance hypersonic vehicles will require many advanced materials. Fortunately, there is an abundance of data from past programs and conferences available for use. Unfortunately, this data is scattered throughout a sea of documents. Furthermore, the past bow waves in funding for hypersonic activities have ensured that very few people have remained active in this technical arena. Consequently, our heritage and core competency has diminished. To make matters worse, as organizations and people moved, whole libraries were discarded. AMPTIAC is actively collecting this data and depositing it in easily manipulated databases to ensure the survival of our technical legacy.

Today, hypersonic applications are re-asserting themselves and high temperature materials are once again a lead interest item. These new systems present similar technical challenges and require this same expertise. For example, NASA's X33, X34, Reusable Launch Vehicle (RLV), Hyper X, and Future X will need advanced Thermal Protection Systems (TPS), hot structures, and huge liquid hydrogen (LH) and liquid oxygen (LOX) tanks. In the military, Military Space Plane (MSP) will require these same technologies. Additionally, multiple new missile concepts such as the Common Aero Vehicle (CAV), the Hypersonic Technology program (HyTech), and High Speed Strike program (HST), demand innovative hot structure and TPS.

NAMIS

Without electronic materials databases, engineers resort to looking up data by hand using databooks and property sheets. Finding data via this method is both inefficient and time consuming – much like finding a needle in a haystack. Most importantly, the lost opportunity, which results from excess data retrieval time, often prevents the designer from being able to fully perform their duties. Electronic materials databases allow efficient access to the materials properties and characteristics by organizing large quantities of data - often searchable through automated procedures. Databases also preserve corporate expertise making past work available at an engineer's fingertips and allow for swift updates to the knowledge base.

NAMIS Architecture

NAMIS is an ongoing effort to develop and field an information system to be used by design engineers involved with selecting materials for component designs. In addition, NAMIS facilitates materials engineers who are trying to disseminate data. The information contained in this system will include numerical material properties, life cycle information, and graphical information such as images of material microstructures, and phase diagrams. Additionally, NAMIS will house electronic documents from which the numerical data were extracted. The electronic documents are derived from AMPTIAC library holdings as well as selected reports and documents from various sources including specific conferences and workshops.

NAMIS is a web-based information system, which will include many different types of materials classes. Web-based systems don't require the stringent hardware requirements that software resident on a personal computer does. For example, a disclaimer usually accompanies commercial software listing minimum microprocessor, RAM, and disk space needed for installation. Moreover, web-based systems work well across many platforms be it a Macintosh, Pentium III, or even a 386 because all machines will use a standard browser to interface with the database resident on a server. Additionally, the browser (either Netscape or Internet Explorer) can be downloaded on the Internet for free.

To cover the breadth of materials classes, AMPTIAC is building this database in a modular fashion with each module functioning either as a stand-alone database or an integral piece of the larger database. NAMIS functions as the umbrella that binds the individual modules together. The database will contain materials descriptors, test techniques, evaluation criteria, electronic supporting documents, and all the accompanying property data.

Upon entering NAMIS, you will note that NAMIS is funded by components of the Army, Navy, Air Force, DoD, and NASA. You will also see that NAMIS is composed of three main sectors of information: Conference/Workshop Proceedings, Numerical Material Property Databases, and Virtual Libraries. A couple other items are immediately apparent. First, NAMIS provides current and topical information about what is going on through out the modules via pop-up menus. Second, NAMIS provides information about how to use the site, how to contact AMPTIAC, and provides a site search option. See Figure 1 for a depiction of the overarching NAMIS features.

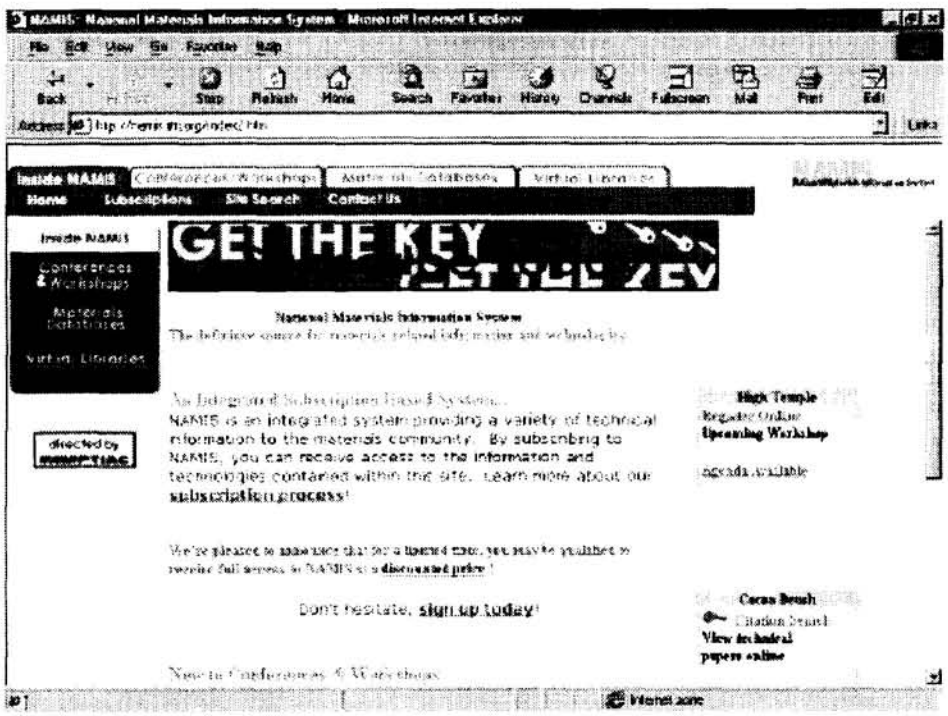

Figure 1: Main Navigation Screen.

Security

Given the sensitive nature of the data, NAMIS must first ensure that adequate security measures are employed to preclude unauthorized users from gaining access to the system and tampering with the data. AMPTIAC is focusing on sensitive hard to get materials and process data for NAMIS. Currently, most of the data is either Export Controlled, ITAR restricted, or For-Official-Use-Only. AMPTIAC will ensure adequate security measures are employed to preclude unauthorized users from gaining access to the system and tampering with the data. AMPTIAC uses authentication, encryption, firewalls, and other technologies in a system that incorporates features specified in the emerging Public Key Infrastructure (PKI).

PKI is a comprehensive system that provides public-key encryption and digital signature services. The purpose of a PKI is to manage electronic keys and to maintain a trustworthy networking networking environment. PKI will be the standard for all DoD sensitive information placed on the web. Additionally, the DoD plans to fully adopt and implement PKI by FY02.

The elements of PKI include encryption, which provides confidentiality and access control while digital signatures provides for authentication, data integrity, and non-repudiation. These elements are combined to effectively 'sign and seal' any electronic communication, and the signing is done in a way that the user who signed the data cannot later successfully deny signing that data.

Currently, NAMIS is encrypted, access controlled through user names and passwords, and resides behind the IITRI firewall. NAMIS users can apply for access to the sensitive areas of NAMIS through a link on the main navigation screen (Figure 1) to a subscription page. Once in the subscription area, users will be asked to supply a DD form 2345, a letter from their company security office stating that they are an employee and a U.S. citizen, and a subscription form.

When PKI is fully adopted by the DoD, all NAMIS users will have a registered identity stored in a digital format known as a public-key certificate. The certificate will specify the validity period (or lifetime). These certificates are inherently secure and can conveniently be distributed in a completely public manner. To reduce cost and ensure a secure environment, AMPTIAC will select a qualified third party to issue certificates to users and act as the certificate authority.

Conferences/Workshops

The Conference/Workshop Proceedings represent a unique opportunity to capture the evolution of whole technical communities and define the current state-of-the-art with-in those technical communities.

Cocoa Beach

The Annual Conference on Ceramic, Metal, and Carbon Composites, Materials and Structures (commonly referred to as the Cocoa Beach Conference) has a wealth of high temperature composites data. The Cocoa Beach Conference is organized by representatives from the U.S. Navy, U.S. Army, U.S. Air Force, the Defense Advanced Research Projects Agency (DARPA), the Department of Commerce/National Institute for Standards and Technology (DoC/NIST), the National Space Aeronautics and Space Administration (NASA), and the Department of Energy (DOE). AMPTIAC is responsible for publishing the proceedings. The 1998 proceedings are currently available as an information system with a virtual library. Also, this database is available as a standalone product on CD. In the near future, AMPTIAC will expand the web site to include he 1996, 1997, 1999, and 2000 proceedings. AMPTIAC's plans to ultimately convert all the past meeting's paper presentations to electronic documents.

The Cocoa Beach module of NAMIS is really a dynamic virtual library. Since it grows every year, a software virtual librarian helps organize the data. Navigating within the Cocoa Beach module is straightforward. Each paper has a bibliographic citation linked to a PDF file of the paper or briefing. The fields in the bibliographic database consist of Title, Author, Abstract, and Keywords. See Figure 2 for a depiction of the module.

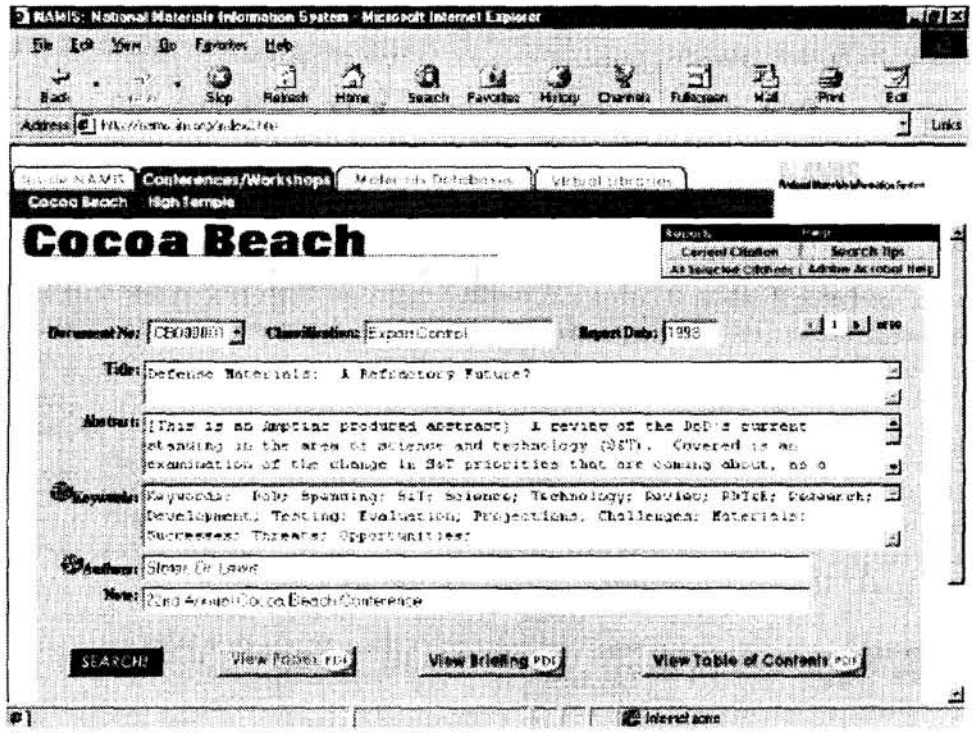

Figure 2: Main Screen Cocoa Beach Module

The search engine searches any or all of these fields. Moreover the user has the option of viewing and printing the bibliographic results either for a single citation or for all of them via the reports section. The following figure shows the results of a bibliographic search.

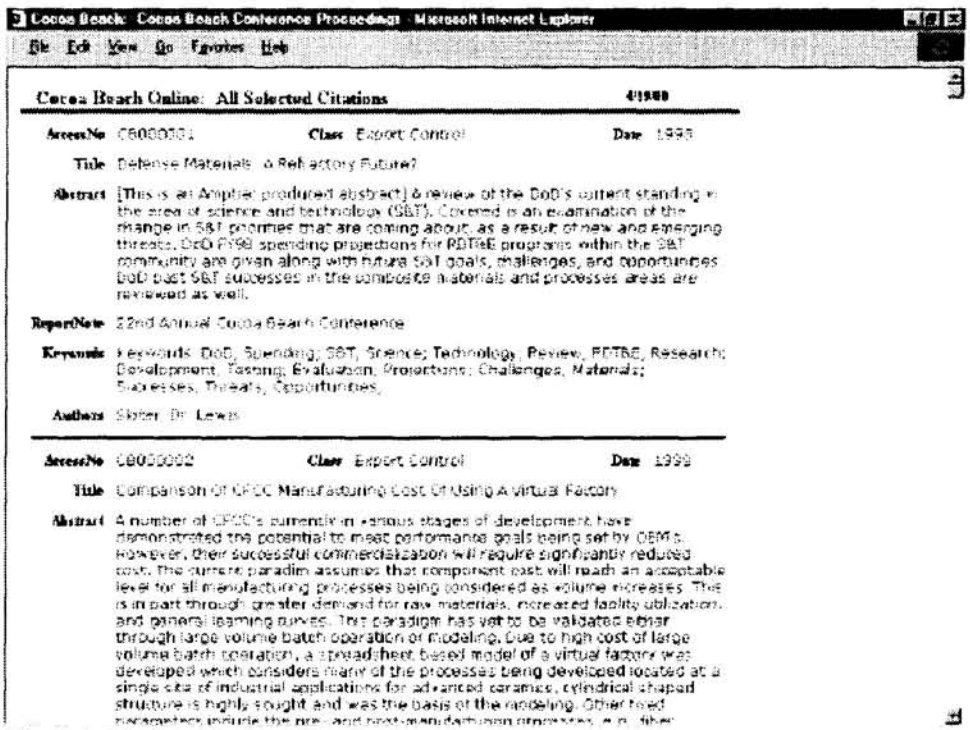

Figure 3: Bibliographic Search Results

Users can also scroll through the search results to view either the briefing presented or the paper if one was submitted. If the user decides to view a presentation by clicking the View Briefing link, the database brings-up Adobe Acrobat within the browser. The first item visible is a proviso concerning the export control restrictions on the document. Subsequent pages of the presentation are all marked top and bottom with "Document is Subject to Export Control" to ensure that when printed the document restrictions are clear. Within the Acrobat frame, users can search using the find feature characterized by the binocular icon. Optical character recognition was performed upon all the documents that reside within NAMIS to enable the Acrobat text string search.

One final search strategy the Cocoa Beach module features, employs the "View Table of Contents" icon to link to an index of the conference by year. Once inside the index, papers are viewable by further clicking the "View" icon to the right of the index.

High Temple

High Temple Workshops are a series of workshops covering the areas of design, development, and application of high temperature reinforced polymeric composites. Structural applications of interest typically see time-temperature relations measured from hours at 500°F-700°F to seconds at 1,400°F. A Tri-Service/NASA steering group initiated the High Temple Workshops. Workshops were held from 1982 to the present. Over the years, hardcopy proceedings were generated for each workshop.

The High Temple Workshop information system serves a dual purpose. First, this module helps to administer the conference. Second, High Temple has a dynamic virtual library component much like Cocoa Beach. Figure 4 illustrates the layout of High Temple.

Figure 4: High Temple Navigation Screen

Functionally, the site is split into several sections for administrative purposes and a section for the virtual library. A secure forum section for year round information dissemination and technical interchange is available. Note, the key next to this section denotes that this section is protected and encrypted.

The "Inside High Temple" section is open to everyone and serves to help advertise the workshops. This section contains background information about the workshops, a pictorial history of the workshops, and information on how to contact the key steering group members.

The "Upcoming Workshop" section of course describes information about the next workshop including a calendar, an agenda, hotel directions with a link to the hotel web site, and an online registration tool. (Note this section is also open.) The registration tool asks users to complete a form, which generates an email to the workshop administrator. The data from the form populates a database of attendee information that the workshop administrator could then access for later mailings.

The "@The Workshop" section contains the virtual library; as such, it is all export controlled and restricted to only properly registered users. Much like Cocoa Beach, users can sift through the papers by year and by paper title via the "Workshop Listing" and "Papers" links. However, thanks in large part to the High Temple Index Committee of 1996, the virtual library searches using key words in addition to title and author. AMPTIAC generated detailed keywords for papers from 1996 to 2000 and converted the 1996 paper index to an electronic format for searching. Keywords represent the most powerful search mechanism. Using keywords allows the user to quickly search large amounts of data by cutting it into successively finer and finer pieces. NAMIS has eight major keyword categories, which are comprised of material type, property, process, application, testing technique, funding organization, and analytical tools. The search tool permits the user to use any conceivable combination of the keywords. The search results represent only those papers which have all the keywords selected for searching. The following figure shows that searching for the glass transition temperature of AFR700B yields 24 papers.

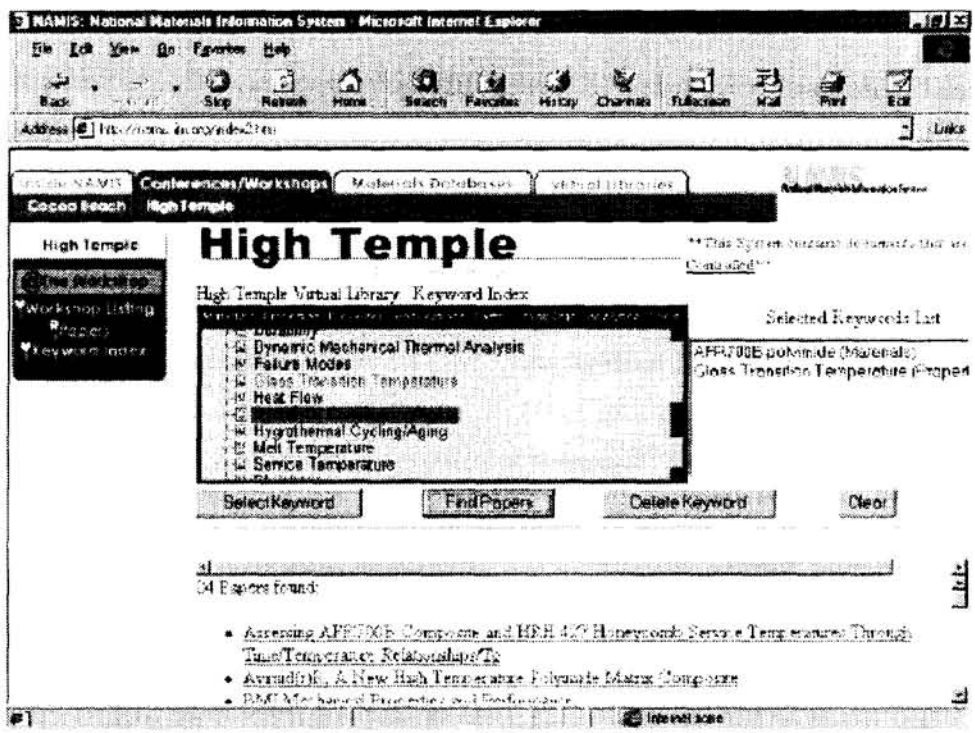

Figure 5: Keyword Search Tool

The papers listed are each linked to the pdf image of that paper. Once again, users can use Acrobat to search for text. In this case, searching for Tg will display the property. A final benefit to using key words involves the ability to identify missing data. If a search yields no results then it is fairly certain that no work has been done in the past given that the High Temple Workshops encompass nearly all the work performed on high temperature polymers. For example, to date, the glass transition temperature hasn't been measured on resin transfer molded LARC-13. This feature not only helps the community reduce duplication of effort but it also helps the community work in a synergistic manner on new problems.

Virtual Libraries

Virtual libraries differ from conferences and workshops in that they are static – no new materials are added on a year-to-year basis. Virtual libraries also do not perform an administrative function for the conference. NAMIS virtual library modules are intended to capture legacy DoD generated data.

NASP

The materials development under NASP was extensive with between 100 to 200 million spent on the Materials and Structures Augmentation Program and accompanying laboratory programs. This development was spread over a wide variety of materials classes including Titanium Aluminides, Ceramic Matrix Composites, and Carbon-Carbon Composites. This valuable data was never collected and focused in a fashion that made it available to the whole high temperature community.

Currently, the NASP module functions like the Cocoa Beach module. Each paper has a bibliographic citation linked to a PDF file of the paper or briefing. The fields in the bibliographic database consist of Title, Author, Abstract, Keywords, and a NASP Joint Program Office report number. The same reporting and viewing option in the Cocoa Beach module are available to NASP. The NASP library contains 638 bibliographic citations and 468 electronic reports. (170 reports are classified - as such they are not included but they have pointers to the controlling authority.) This represents well over 80,000 pages of dedicated materials and structures information.

Within a month of the time of this paper, the NASP virtual library will feature a keyword tool like the one found in the High Temple Module.

IHPTET

The Integrated High Performance Turbine Engine Technology (IHPTET) program is an ongoing National program focused upon doubling the US military's 1988-propulsion capability. A consortium of high level Government and propulsion industry managers, known as the IHPTET Steering Committee, provides oversight and guidance for the IHPTET Program. The Army, Navy, Air Force, NASA, DARPA, and six major US turbine engine manufacturers are involved in the IHPTET Program.

Materials development is a very important piece to IHPTET success. Like NASP many materials breakthroughs owe their success to the IHPTET program. At the time of this paper, AMPTIAC is nearing completion of an IHPTET module to NAMIS. When completed, the IHPTET virtual library will function like the NASP module with over 70 digitized materials related IHPTET reports in its library.

Numerical Databases

AMPTIAC wants to provide designers with a reliable source of data to assist in making materials selection, risk reduction, and life extension decisions. As such, AMPTIAC is developing numerical databases that will eventually feed design packages. Presently, the numerical databases contain property data and metadata which describes processing history, test type and conditions, physical form, composition and source data. A complete description of all metadata supplies the pedigree that should always accompany property data. In order to make materials selection easier, the numeric databases will utilize software tools that allow a variety of display methods including transparent unit conversion, display of multiple plots, scalable plot axis and both linear and logarithmic axes.

Infrared Window and Domes

AMPTIAC is developing an infrared window and dome materials numerical database complete with descriptions of processing history, test type and conditions, physical form, composition and source of data. A complete description of all the metadata is important to prevent misuse of data and to interpret the fidelity of the data. AMPTIAC actively participates in the ASTM E49 committee for materials databases to make sure NAMIS accurately captures a materials pedigree. This database will have a host of optical, dielectric, thermophysical, mechanical, rain erosion, and laser damage properties. See Table 1 for a complete list of properties contained in this module.

Table 1: MATERIAL PROPERTIES

OPTICAL	MECHANICAL
Transmission	Compressive Strength
Absorption	Flexural Strength
Reflectance	Elastic Compliance
Refractive Index	Hardness
Laser Damage Threshold	Shear Strength
Scattering	Fracture Toughness
Dielectric Constant	Young's Modulus
	Poisson Ratio
THERMOPHYSICAL	RAIN EROSION
Emissivity	Velocity Damage Threshold
Heat Of Fusion	Damage Site Density
Thermal Conductivity	Degraded Transmittance
Thermal Expansion Coefficient	Scatter
Thermo-Optic Coefficient	Failure Time
Melting Point	
Thermal Diffusivity	

The database module contains over 1800 data sets compiled from over 300 reports extracted from six major window materials. These six materials are germanium, zinc sulfide, zinc selenide, having long wave IR applications and sapphire, spinel and yttria, finding applications in the midwave IR band. Moreover the database will utilize software tools that allow a variety of display methods including transparent unit conversion, display of multiple plots, scaleable plot axis, and both linear and logarithmic axis.

The InfraRed Window and Dome Database (IRDB) is intended to aid designers for materials selection. A designer must typically select a window/dome material by identifying bounds on material properties that cannot be exceed if reliable performance is to be achieved. An initial consideration is the passband and flexural strength, which quickly eliminates materials. Next, relative advantages and disadvantages may be applied to narrow the selection. The selection is further narrowed as other requirements are identified.

Structural metals

The final NAMIIS numeric module in development will cover the three most common structural metals and their alloys (Aluminum, Steel, and Titanium). It will act in a similar fashion to IRDB; however, it will contain different property sets. To date, the database module contains over 1000 data sets compiled from over 150 reports. The same software tools present in the IRDB will be used for Structural metals.

Summary

Through NAMIS, AMPTIAC is trying to save the DoD materials and process knowledge base making it readily available to the materials community. This will reduce duplication of effort and help transition the technology. Additionally, NAMIS will cut the time and cost of materials selection by giving designers a source for reliable and pedigreed materials data.

AMPTIAC is boldly entering uncharted waters with a web-based database, which has the proper security precautions to handle export-controlled data. Lastly, unrestricted portions of NAMIS are viewable at the following URL: http://namis.iitri.org/

Acknowledgements

I would like to thank Beth Kinman and the other members of the High Temple index committee listed below for providing the kernel for our keyword index.

Ray Adsit
Glenn Anderson
Michael Brunner
Mike Holl
Lew Lineberger
Wanda Sigur
Brian Wilson
Bob Acree

I would also like to thank Ron Kuhbander, Jim Folk and Daniel McCray for supplying early High Temple Workshop proceedings and Brett Bolan (AFRL/MLS), John Russell (AFRL/MLB) and Jim Sutter (NASA-Glenn) for sponsoring the High Temple Module.

I would like to thank Michael Stropki (AFRL/MLO) who sponsored the NASP module and Jack Rike (DTIC-O) who provided electronic copies of the reports to AMPTIAC.

I would like to thank Mark Opeka (NSWC Code 681) for sponsoring and providing materials for the Cocoa Beach Module.

Finally, I would like to thank our core sponsor and program manager Mr. Ron E. Hale at the Defense Technical Information Center and his technical representative Dr. Lewis E. Sloter II at the Office of the Director Defense Research and Engineering (Weapons Systems).

I would also like to thank Dr. Sloter's associate technical representatives as follows:

Ceramics, Ceramic Composites	Dr. S. Carlos Sanday Naval Research Laboratory
Organic Structures Materials & Organic Matrix Composites	Mr. Roger Griswold Air Force Research Laboratory
Metals, Metal Matrix Composites	Dr. Joe Wells Army Research Laboratory
Electronics, Optical, & Photonics	Mr. Robert L. Denison Air Force Research Laboratory
Environmental Protection & Special Function Materials	Dr. James Murday Naval Research Laboratory

p/550 N/27
11B5 2024

Durability Characterization of Advanced Polymeric Composites at Cryogenic Temperatures

THOMAS S. GATES

Mechanics and Durability Branch/Mail Stop 188E
Langley Research Center
Hampton, VA 23681 USA
Phone: 757-864-3400
Fax: 757-864-7729
E-mail: T.S.Gates@larc.nasa.gov

The next generation of reusable launch vehicles will require technology development in several key areas. Of these key areas, the development of polymeric composite cryogenic fuel tanks promises to present one of the most difficult technical challenges. It is envisioned that a polymer matrix composite (PMC) tank would be a large shell structure capable of containing cryogenic fuels and carrying a range of structural loads. The criteria that will be imposed on such a design include reduced weight, conformal geometry, and impermeability. It is this last criterion, impermeability, that will provide the focus of this paper.

The essence of the impermeability criterion is that the tank remains leak free throughout its design lifetime. To address this criterion, one of the first steps is to conduct a complete durability assessment of the PMC materials. At Langley Research Center, a durability assessment of promising new polyimide-based PMCs is underway. This durability program has focused on designing a set of critical laboratory experiments that will determine fundamental material properties under combined thermal-mechanical loading at cryogenic temperatures. The test program provides measurements of lamina and laminate properties, including strength, stiffness, and fracture toughness. The performance of the PMC materials is monitored as a function of exposure conditions and aging time. Residual properties after exposure are measured at cryogenic temperatures and provide quantitative values of residual strength and stiffness. Primary degradation mechanisms and the associated damage modes are measured with both destructive and nondestructive techniques. In addition to mechanical properties, a range of physical properties, such as weight, glass transition, and crack density, are measured and correlated with the test conditions. This paper will report on the progress of this research program and present critical results and illustrative examples of current findings.

DEVELOPMENT OF METAL MATRIX COMPOSITES FOR NASA'S ADVANCED PROPULSION SYSTEMS

Jonathan Lee and Sandy Elam

National Aeronautics and Space Administration (NASA)
Marshall Space Flight Center (MSFC)
Mail Code ED33
Huntsville, AL 35812
Jonathan.Lee@msfc.nasa.gov

ABSTRACT

The state-of-the-art development of several Metal Matrix Composites (MMC) for NASA's advanced propulsion systems will be presented. The goal is to provide an overview of NASA-Marshall Space Flight Center's on-going activities in MMC components for advanced liquid rocket engines such as the X-33 vehicle's Aerospike engine and X-34's Fastrac engine. The focus will be on lightweight, low cost and environmental compatibility with oxygen and hydrogen of key MMC materials, within each of NASA's new propulsion application, that will provide a high payoff for NASA's Reusable Launch Vehicles and space access vehicles. In order to fabricate structures from MMC, effective joining methods must be developed to join MMC to the same or to different monolithic alloys. Therefore, a qualitative assessment of MMC's welding and joining techniques will be outlined.

INTRODUCTION

In this paper, the state-of-the-art development of Metal Matrix Composites (MMC) for NASA's advanced propulsion systems will be presented. The focusing theme will be on lightweight, affordable and environmental compatibility with oxygen and hydrogen of key MMC materials that will provide a high payoff for NASA's reusable launch vehicle systems and space access vehicles. Historically, MMC has been used for NASA's flight hardware such as boron fibers reinforced aluminum struts for the Space Shuttle's mid-fuselage in 1982, and graphite fibers reinforced aluminum antenna for the Hubble Space Telescope in 1990 (ref. 1). However, these types of MMC were costly to produce and were not developed specifically for propulsion systems.

In recent years, Marshall Space Flight Center (MSFC) has been focusing on the development of low cost and lightweight components using net shape casting for advanced propulsion systems, which commonly have high density copper alloys and superalloys. In order to improve the engine thrust-to-weight ratio for advanced launch vehicles, lighter materials with new fabricating methods must be developed using concurrent engineering method (ref. 2). MMC are often valued for their "tailor-ability" property, which dictates a specific MMC formation for a specific application. For this reason, complexity and cost for the development of an MMC property database can often be more than for a conventional alloy database, which favors a "commodity" approach. In the commodity approach, the conventional practice is based on one single alloy formulation to be used for many structural applications. For MMC, material specialists and engine's designers must work closely during the early phases of the program to develop a specific MMC property database for a specific application. As part of the planning stage, the Technology Readiness Level (TRL) for material, joining processes and the cost affordability factor have become important development issues for MSFC's material selection strategy.

MATERIAL AND PROCESS SELECTIONS

Material Selections

Technology assessment has shown that Discontinuously Reinforced Aluminum (DRA) MMC can become viable candidate materials for propulsion applications in cryogenic and near ambient temperatures. Evidently, the development cost for DRA is affordable and the TRL is relatively high such that production of complex DRA components have been applied for the auto industry with high dimensional tolerance and minimal machining requirements (ref. 3, 4, 5). Figure 1 shows the comparison for the specific stiffness (modulus/density) of DRA, which is better than most conventional superalloys being used in propulsion hardware. DRA also acquire its toughness and ductility from the aluminum and will behave more like conventional aluminum alloys due to its isotropic properties (ref. 6, 7). On the other hand, isotropic property also means that DRA would tend to have lower specific strength value (strength/density) as compared with Continuously Reinforced Aluminum (CRA) with fibers such as silicon carbide, aluminum oxide, etc. Therefore, the selection strategy is to substitute DRA for stiffness-driven applications and CRA for strength-driven and unidirectional loading applications at cryogenic and near ambient temperatures.

Similarly, copper MMC can become viable candidate materials for oxygen-rich environment at relatively high temperatures and pressures. However, copper MMC have not been extensively used for commercial applications as compared with aluminum MMC. Technology assessment of nickel and copper MMC programs, funded by the DoD and NASA in recent years, indicated that these high temperature MMC are not as "mature" as aluminum MMC (ref. 8, 9). However, the current development for Discontinuously Reinforced Copper (DRC) appears to be more viable technology than Continuously Reinforced Copper (CRC) for certain types of stiffness-driven applications in oxygen-rich environment.

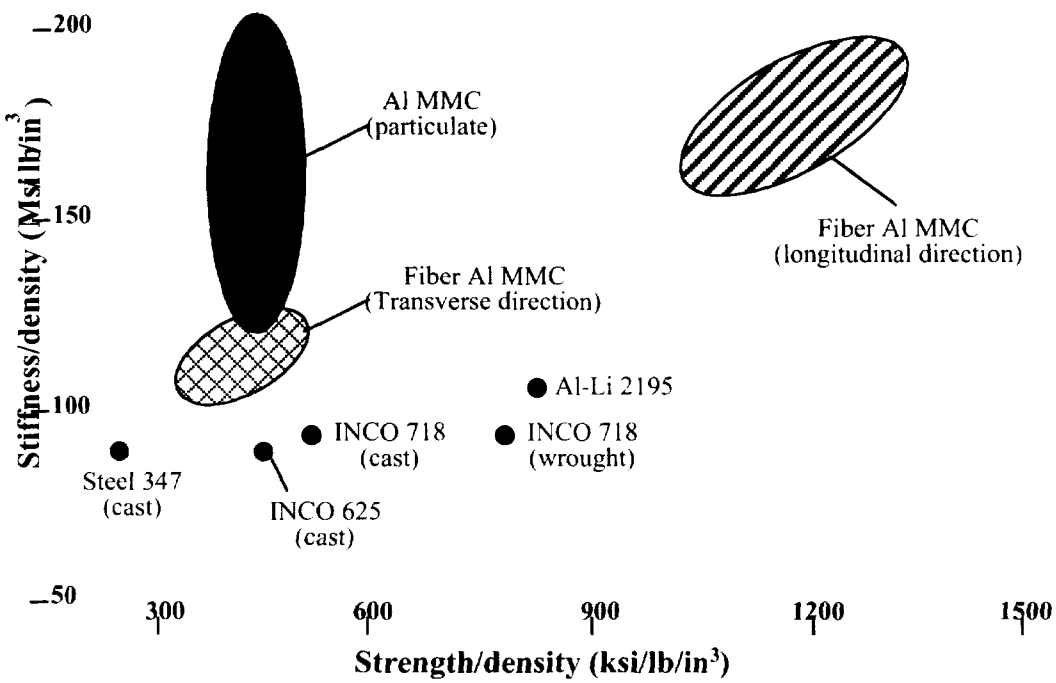

Figure 1. Plot of specific stiffness versus specific strength for Al MMC.

Process Selections

Similar to material selection, the strategy for process selection is based on low cost and capability for net shape fabrication with minimal machining and welding requirements. In order to evaluate these fabricating processes as a function of component applications, forms (shapes) and materials, a ranking matrix is developed for the fabricating processes, which can be classified into 7 classes as shown in Figure 2. Each of these techniques consists of unique features that are grouped in terms of applications, product forms and materials. For example, diffusion bonding is a choice method for continuous fibers MMC, which is applicable for unidirectional loading applications such landing gear, struts, beam, etc. Historically, diffusion bonding has been used for NASA's flight hardware such as MMC struts for the Space Shuttle's mid-fuselage and antenna for the Hubble Space Telescope. However, these types of MMC were costly to produce and not directly applicable for making complex near net shapes such as turbopump housings. In summary, pressure infiltration and gravity casting were selected as primary level processes because they are the most versatile for producing complex net shape components with relatively low processing cost. Secondary processing level would be selected as spray deposition and centrifugal casting for fabricating of simple net shape components. Finally, powder metallurgy and laser 3D deposition processes are selected as a third level for wrought products for airframe applications with near isotropic properties. In some instances, powder metallurgy can be used to produce simple net shaped components. Currently, Laser 3D deposition is an emerging technology with limited data for MMC assessment.

Relative Cost: High ← Low

MMC's Fabricating Methods

	REQUIREMENTS	Diffusion bonding	Powder metallurgy	Laser 3D deposition	Spray deposition	Pressureless infiltration	Pressure infiltration	Gravity Casting
Applications	Ultra-high strength	●					●	
	Ultra-high stiffness	●	●		●		●	
	Moderate strength	●	●	●	●	●	●	●
	Moderate stiffness	●	●	●	●	●	●	●
	Isotropic properties		●	●	●	●	●	●
	Wear resistance		●	●	●	●	●	●
Product Forms	Thick plates & blocks		●		●		●	●
	Thin plates & sheets	●	●	●	●	●	●	
	Large cylindrical shells	●			●			
	Tubes, rods & beams	●	●		●	●	●	●
	Simple near net shapes	●	●	●	●	●	●	●
	Complex near net shapes			●			●	●
Materials	Continuous fibers & tapes	●					●	
	Chopped & short fibers				●		●	●
	Particulate & whiskers		●	●	●	●	●	●
	Hybrid systems				●		●	●

Figure 2. Qualitative assessment for MMC fabricating methods.

ENVIRONMENTAL COMPATIBILITY

The material compatibility with oxygen and hydrogen environment has always been an important issue for rocket propulsion systems (ref. 10). Preliminary assessment has shown that aluminum alloys and aluminum MMC are considered to be compatible with oxygen environment only at low pressure (<1500 psi) and cryogenic temperature. Therefore, aluminum MMC can be used for ducts, flanges and turbopump housings that operate at cryogenic temperature and low pressure. From near ambient temperature up to about 900 F, copper-based MMC are compatible with high pressure oxygen-rich environment. The development of copper alloys reinforced with aluminum-oxide particulate and/or fibers, have shown to be compatible with oxygen environment. On-going efforts are under way at MSFC to characterize the material compatibility issues in an oxygen-rich environment for aluminum and copper based MMC. Currently, titanium based MMC are not recommended for oxygen environment even at cryogenic temperature. For hydrogen environment, aluminum and copper-based MMC are shown to be compatible in a wide range of operating temperatures and pressures. However, some titanium MMC are compatible with hydrogen only at cryogenic temperatures. In contrast with polymer matrix composites, the hydrogen permeation is not an issue for most metals and MMC. This is an important compatibility factor for MMC in the design consideration of ducts, flanges and pressure vessels for hydrogen containment applications.

COMPONENT SELECTION FOR DEMONSTRATION

Flanges for Fuel Line

There is a significant amount of mass associated with the usage of superalloy's ducts and flanges for the fuel feed lines of the X-33's Aerospike engine. The ducts are identified as strength-driven components, which will be made from lightweight nanophase aluminum or aluminum-lithium alloys in the future. The flanges are stiffness-driven components, which are ideal targets for weight reduction using particulate reinforced aluminum MMC such as boron carbide (B_4C), silicon carbide (SiC) or aluminum oxide (Al_2O_3). With SiC reinforced aluminum MMC, a 55% mass reduction over conventional IN 625 can be expected for each of the flanges. Significant total weight reduction can be expected since there are approximately 36 flanges for the combined oxygen and hydrogen side for the feed lines of the Aerospike engine. The potential technical issue is to develop appropriate techniques for joining the aluminum-lithium, aluminum alloys or nanophase aluminum ducts to Al MMC flanges. Figure 3 shows several prototype aluminum MMC flanges that were produced by Metal Matrix Cast Composites (MMCC) Inc. using advanced pressure infiltrated casting.

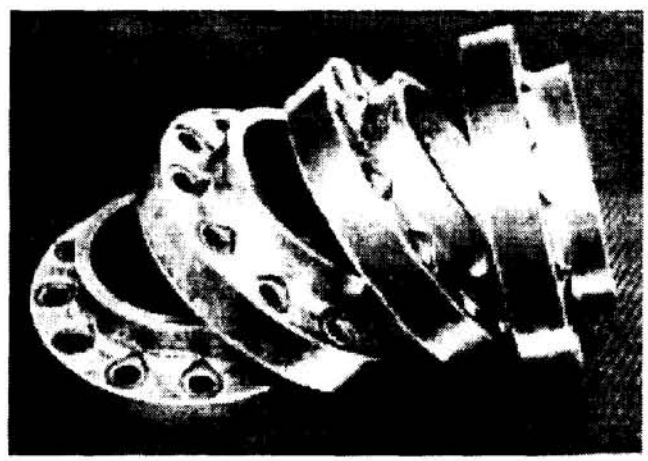

Figure 3. Al MMC prototype flanges for X-33's fuel line ducts.

X-33 Engine's Thrustcell

The X33's aerospike engine consists of several thrust cells which can comprise as much as 25% of the engine weight. The interior wall of the thrust cell chamber is exposed to high temperature combustion products and must be cooled by using liquid hydrogen. Currently, the structural jacket and manifolding of the thrust cell chamber is made of stainless steel (SS) 347, which can potentially be replaced with a lighter material by using aluminum MMC. Up to 50% mass reduction over conventional SS 347 can be expected for each of the thrust cell chambers using MMC. To demonstrate the level of maturity for aluminum MMC technology, several MMC chambers have been produced using gravity casting and plasma spray deposition process. In addition to MMC, a new copper alloy (Cu-8Cr-4Nb), that has higher strength than the traditional copper alloy of NARloy-Z for chamber liners, is also being investigated in this program. Currently, several thrust chamber design concepts are being worked to resolve the potential technical issue of bonding or brazing the liquid hydrogen cooled Cu-Cr-Nb liner to the surrounding MMC jacket. For instance, Figure 4 shows an MMC chamber, made from an Al/SiC MMC jacket, which is cast around a copper liner in a "one-step" brazing-casting process under gravity casting by MSE Technology Applications, Inc.

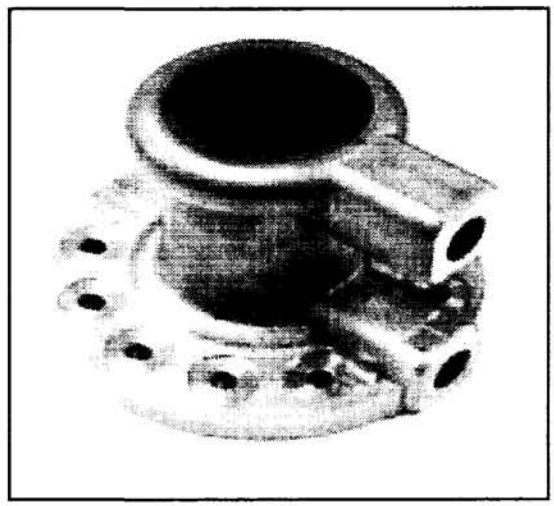

Figure 4. Al MMC prototype "lightweight" thrust chamber for thrust cell applications.

X-34's Turbopump Housing

Preliminary analysis has shown that up to 40% mass reduction over conventional cast INCO 718 superalloy can be expected for the X-34's Fastrac engine turbopump housing. The candidate material under consideration is a hybrid aluminum MMC system that consists of a mixture of aluminum oxide (Al_2O_3) continuous fibers and Al_2O_3 particulate. For this reason, the key material challenge is to develop a capability to manufacture hybrid MMC, with selectively reinforced fibers for high strength in proper high stress locations, using pressure infiltrated casting. This Al MMC technology is targeted for new hydrogen or hydrocarbon turbopumps and is also applicable to low-pressure oxygen turbopump at cryogenic temperature. If successful, many rocket systems such as the Venture Star, Long Life Bantam engine variations and rocket based combined cycle systems will benefit by the weight reduction achieved from this Al MMC for the X-34's turbopump housing demonstration program. Figure 5 shows a half-scale X-34's turbopump housing which was produced by MMCC, Inc. using advanced pressure infiltration casting of aluminum alloy reinforced with 50% by volume of aluminum oxide particulate.

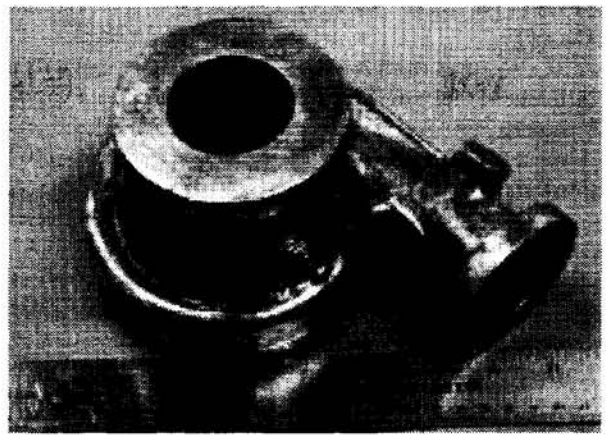

Figure 5. Half-scale Al MMC turbopump housing for X-34's Fastrac Engine.

Al MMC ducts

Preliminary analysis of cryogenic feedlines and ducts has indicated that up to 30% weight redution can be achieved by using MMC reinforced with continuous alumina fibers. This is based primarily on the hoop strength of such a brazed aluminum composite relative to the strength of an Inconel feedline as used on the X-34 vehicle technology demonstrator. Under NASA sponsorship, this novel MMC material tape concept has been developed by Touchstone Research Laboratory (TRL), for making lightweight MMC ducts from prepreg unidirectional tape produced by 3M. This unique MMC prepreg unidirectional tape form can be laid-up as plies with the plies oriented to meet the component performance requirements in an analogous manner to polymer matrix composites. These plies can then be consolidated using TRL's patented brazing process. Theoretically, TRL's solution incorporates a very thin MMC tape with an automated brazing technique that combines the ability to produce propellant feedlines with inherent low cost of polymer manufacturing technique but it could achieve a better interlaminar strength than polymer composites. This technology demonstration of brazed continuous aluminum MMC tape for propellant feedlines and ducts could have direct application to cryogenic tanks and airframe structure as well. Figure 6 shows a small section of a cryogenic duct that is produced by using a continuous in-situ brazing process for a 2-ply hoop wound cylindrical section with a diameter of 5 inches.

Figure 6. A small section of a cryogenic duct produced by brazing MMC tape.

QUALITATIVE ASSESSMENT FOR JOINING TECHNOLOGIES

In order to fabricate structures from MMC, effective joining methods must be developed to join MMC to the same or to different monolithic alloys. Since MMC utilize a variety of non-metallic reinforcements, they will naturally impose limitations for joining using conventional methods from monolithic metals. As a general rule, the adaptability of any joining techniques for MMC will depend on the combination of the following factors: (1) the volume percent amount and types of reinforcements, (2) metal matrix melting point, and (3) the thermal energy management from the selected joining process. Discontinuously reinforced MMC are easier to join than continuously reinforced using fibers, which are prone to matrix-fiber de-bonding, de-lamination, non-uniform fiber packing density and migration of fiber bundles into the weld regions. The prolonged contact time between a molten metal matrix and a reinforcement can lead to undesirable chemical reactions, which are accelerated as the molten metal temperature increases. Although high thermal energy is required for most conventional joining processes, excessive thermal energy input is undesirable. For this reason, the higher the metal matrix melting temperature the less likely for most of the fusion techniques to be applicable for MMC. A qualitative assessment of the adaptability of 17 monolithic joining techniques to MMC is summarized in Figure 7 (ref. 11). It is important to realize that MMC joining is not a mature technology and many important joining technical details are still lacking. Consequently, the adaptability for a specific joining method is a specific material and process factor which must be determined experimentally (ref. 12, 13).

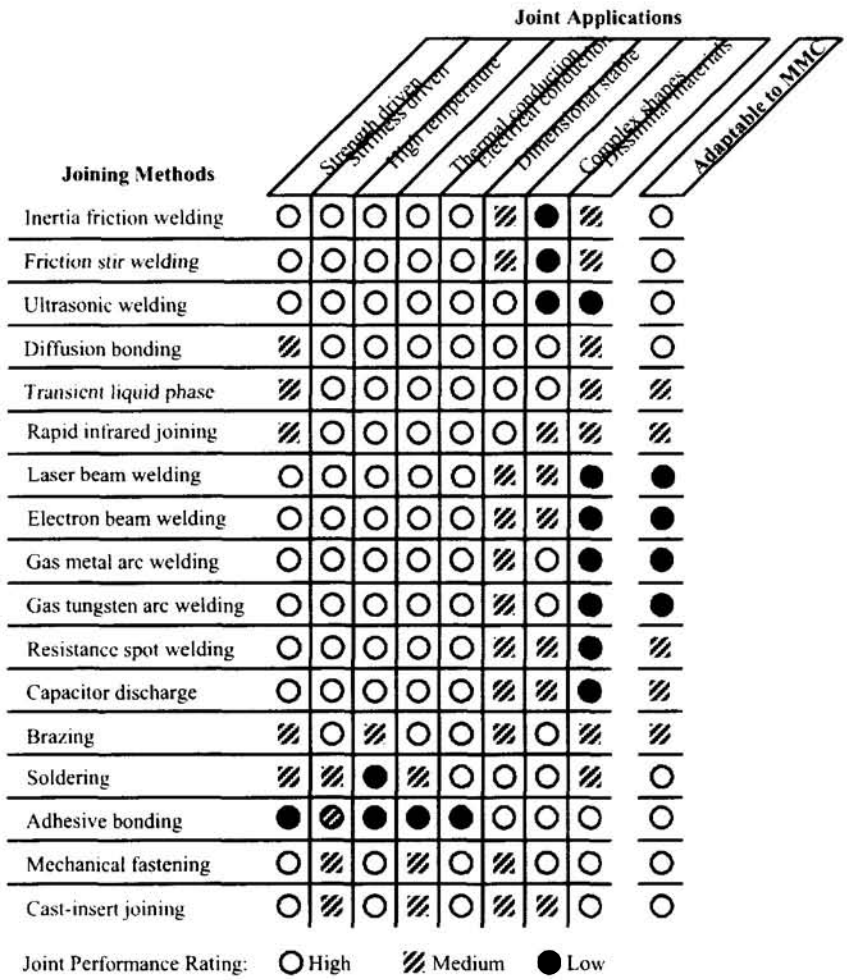

Figure 7. Qualitative assessment rating for MMC joining methods.

CONCLUSIONS

Technology readiness level for materials, joining processes and the cost affordability have become important issues for NASA in developing MMC for advanced propulsion systems. Discontinuously reinforced aluminum (DRA) are viable candidate materials for propulsion applications and they can be substituted for component with stiffness-driven applications at cryogenic and near ambient temperatures. Similarly, copper MMC are viable candidate materials for in oxygen-rich environment at relatively high temperature and pressure. A qualitative assessment for joining methods has shown that the use of solid state and low temperature processes are often more adaptable for joining of MMC than the use of high temperature fusion processes.

REFERENCES

1. Reinhart, J. J.: "Engineered Materials Handbook. Volume 1: Composites," ASM International, Metal Park, OH, p. 856, 1987.

2. Waterman, N. A.; Ashby, M. F.: "The Materials Selector," 2nd edition, Chapman-Hill, NY, 1997.

3. Rohatgi, P.: "Cast Aluminum Matrix Composites for Automotive Applications." Journal of Metals, pp. 10-15, April 1991.

4. Mangin, G. E.; Isaacs, J. A.: "MMC for Automotive Engine Applications." J. Metals, p. 49, Feb. 1996.

5. Hammond, D.E.: "Castable Composites Target New Applications," Modern Casting, p. 27, 9/1990.

6. Lee, J. A.: "High Strength Aluminum Casting Alloy for High Temperature Applications," MSFC, NASA/TM-1998-209004, December 1998.

7. Lee, J. A.: "Low cost Al-Si Casting Alloy as In-situ Composites for High Temp. Applications," 24th Conf. Composites, Structural. & Mat., Jan. 23, 2000, Cape Canaveral, FL

8. Lee, J. A.; Mykkanen, D.: "Metal and Polymer Matrix Composites," Noyes Data Publisher, Park Ridge, New Jersey, 1987.

9. Lee, J. A.: "Tungsten Fiber Reinforced Superalloy Metal Composites," 23rd Conf. on Composites, Structures & Materials, Jan. 23-28, 1999, Cocoa Beach , FL

10. Lee, J. A.: "A Theory for Hydrogen Embrittlement of Metals and Alloys," In: Hydrogen Effects in Materials, A. W. Thompson (eds.), TMS publication, 1995.

11. Lee, J. A.: "Qualitative Assessment for MMC Joining Methods," Mil-Hdbk-17-4, V4, Sept 21, 1999.

12. Lee, J. A.; Carter, R. and Ding, J.: "Friction Stir Welding for Aluminum Metal Matrix Composites," MSFC, NASA/TM-1999-209876, December 1999.

13. Lee, J. A.; Kashalika, U.: "Casting of Weldable Graphite/Magnesium MMC with Built-in Metal Inserts," NASA Conf. 3249, V1, p. 371, Dec. 7, 1993, Anaheim, CA.

INORGANIC-ORGANIC HYBRID POLYMERS FOR HIGH TEMPERATURE AEROSPACE APPLICATIONS

Teddy M. Keller

Advanced Materials Section, Code 6127
Chemistry Division
Naval Research Laboratory
Washington, DC 20375-5320
Tel: 202-767-3095
E-Mail: keller1@ccf.nrl.navy.mil

Introduction

Our current interest in inorganic-organic linear hybrid polymers as precursors to high temperature thermosets and ceramics has led us to investigate the synthesis of novel materials containing silicon, carborane, and acetylenic segments. Several poly(carborane-siloxane-acetylene)s **1** (1) and **2** (2) and poly(siloxane-acetylene)s **3** (3) are being evaluated as high temperature matrix materials for composites and as precursor materials to ceramics for applications under extreme environmental conditions.

The major advantage of our approach is that the desirable features of inorganics and organics such as high thermal and oxidative stability and processability are incorporated into the same polymeric chain. The siloxane units provide thermal stability and chain flexibility to polymeric materials. Siloxane-acetylenic polymers have also been made but lack the thermal and oxidative stability that the carborane units possess. The chemistry involved in synthesizing poly(siloxane) and poly(carborane-siloxane) has been modified to accommodate the inclusion of an acetylenic unit in the backbone. The novel linear polymers have the advantage of being extremely easy to process and convert into thermosets or ceramics since they are either liquids at room temperature or low melting solids and are soluble in most organic solvents. They are designed as thermoset polymeric precursors. The cross-linking density of the thermosets is easily controlled as a function of the quantity of reactants used in the synthesis. The acetylenic functionality provides many attractive advantages relative to other cross-linking centers. The acetylene group remains inactive during processing at lower temperatures and reacts either thermally or photochemically to form conjugated polymeric cross-links without the evolution of volatiles.

This paper is concerned with the processability and thermo-oxidative properties of **1**, **2** and the blending of **1** and **3** in an attempt to arrive at similar thermoset and ceramic compositions as found for copolymer **2** upon thermal treatment. Thermal analysis studies were performed on thermosets and ceramics obtained from **1**, **2** and various blends from **1** and **3a**.

Results and Discussion

The synthesis of inorganic-organic linear hybrid polymers **1**, **2** and **3** have been reported previously (1-3). Several molar mixtures (50/50, 25/75 and 10/90) of **1** and **3a** were prepared for cure and thermal analysis studies. Homogenous mixtures were obtained by dissolving the linear polymers **1** and **3a** in THF. After thorough mixing, the solvent was removed by distillation at reduced pressure. The resulting mixtures as prepared were viscous compositions. However, gummy, semicrystalline compositions formed after several days. Upon heating to 100 °C, the mixtures existed as viscous liquids.

DSC Studies. The thermal cure behaviors of the linear polymers **1** and **3** were examined using DSC analysis (see Figure 1). Large exotherms peaking at 350 and 289 °C were observed for **1** and **3**, respectively. Copolymers **2** have large exotherms peaking between 289 and 350 °C. The exact position depends on the amount of **1** and **3** units present in the copolymer. For example, copolymer **2c** shows a similar DSC thermogram with a strong exotherm at approximately 300 °C (4). These peaks were atttibuted to the acetylene crosslinking reaction. A small broad exotherm was also apparent from about 150-225 °C due to the presence of a small amount of primary terminated acetylenic units. DSC analyses of blends of **1** and **3a** show a homogeneous reaction initially to a thermoset. The DSC scans to 400 °C of the blends exhibit only one cure exotherm for each of the compositions studied (see Figures 2). For example, mole percent mixtures (10/90, 25/75 and 50/50) of **1** and **3a** display exotherms (polymerization reaction) peaking at 296, 298 and 328 °C, respectively. It is apparent from the observed cure temperature for the

blends that **3a** being more reactive initially forms radicals that are not selective in the chain propagation reaction with the acetylenic units of both **1**and **3a** (5). Samples that have been heat treated to 400 °C do not exhibit characteristic exothermic transitions.

Thermal and Oxidative Stability. The thermal and oxidative stability of **1**, **2** and **3a** was determined by heating at 10 °C/min to 1000 °C by simultaneous TGA/DTA analysis. Pyrolysis of **1** to 1000 °C under a flow of nitrogen resulted in a ceramic yield of 85%. Further heat treatment of the ceramic at 1000 °C for 12 hours resulted in no additional weight loss. When the ceramic material was cooled back to 50 °C and rescanned to 1000 °C in air, the sample gained weight (~2%) attributed to surface oxidation. Further TGA aging studies of the ceramic in air revealed that additional weight loss did not occur and that the sample actually increased in weight as observed previously. When heated in air to 1000 °C, the chars from **2a-c** lose no mass. The char from **2d** displayed only a 7% weight loss under the same conditions. No weight loss was observed on heating the char from **3c** at 700°C and 900°C for 16 hr and for 7 hr, respectively. Thus, this study demonstrated that the char from **2c**, containing only one-tenth the amount of carborane found in **1**, exhibited the same outstanding thermo-oxidative stability. Thermal treatment of **3a** to 1000 °C under inert conditions resulted in a char yield of 74%. The char retained the original shape without cracking. When heated to 1000 °C in an oxidizing environment, the char remained stable to ~600 °C, before a gradual weight loss was observed resulting in an overall weight loss of 15% at 1000 °C. Moreover, an oxidative aging study on a charred sample showed a 28% weight loss after 15 hours at 500 °C.

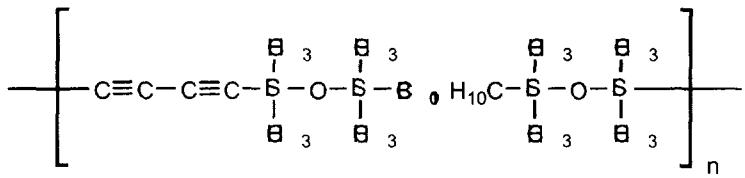

1

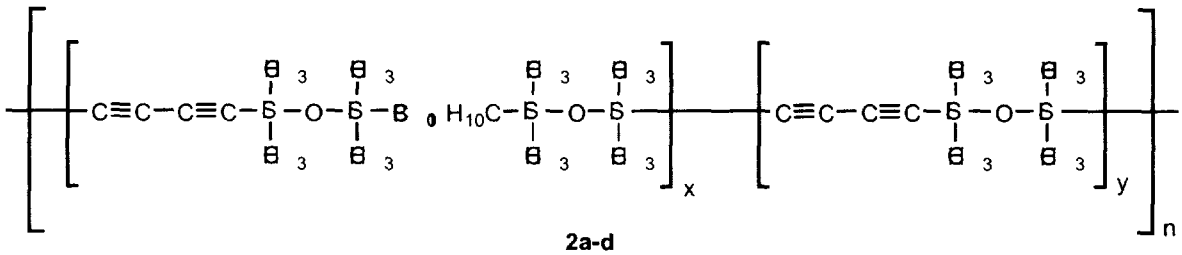

2a-d
a, x/y = 50/50
b, x/y = 25/75
c, x/y = 10/90
d, x/y = 5/95

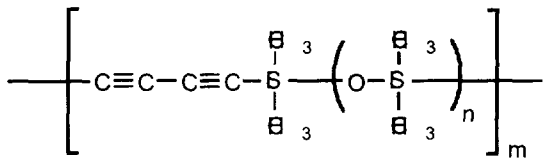

3a, n=1
3b, n=2

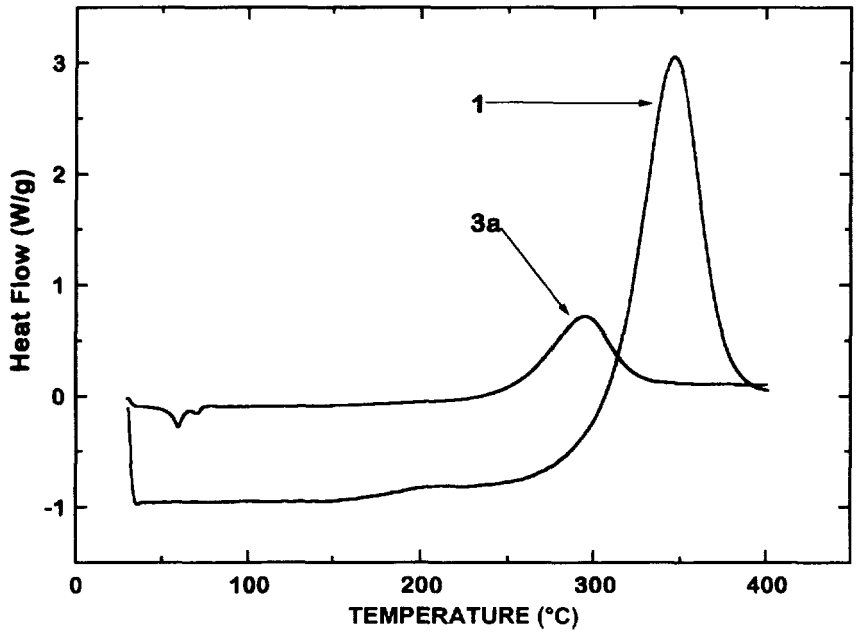

Figure 1. DSC thermograms of **1** and **3a**

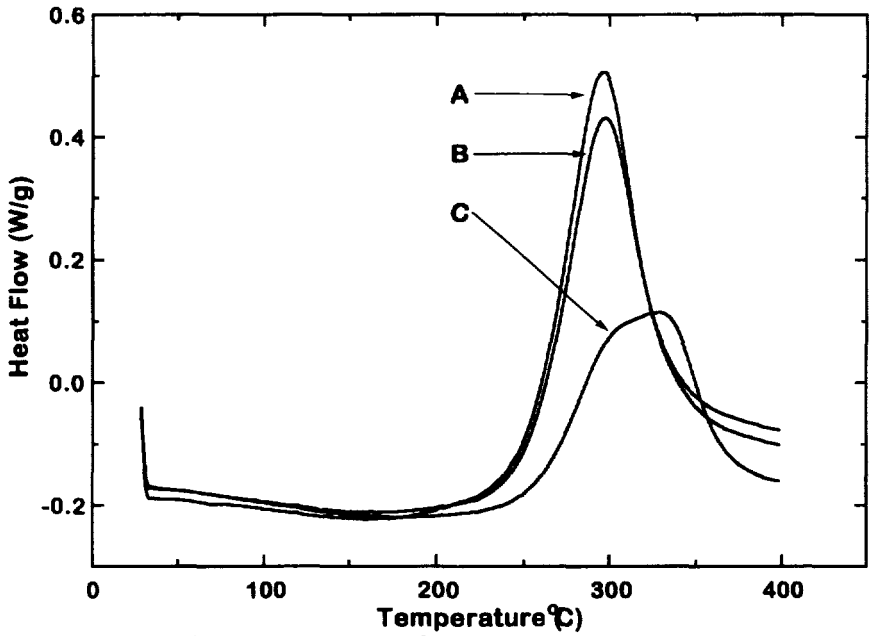

Figure 2. DSC thermograms of various mixtures of **1/3a**: (A) 10/90, (B) 25/75, and (C) 50/50

The thermal and oxidative stability of various mixtures of **1** and **3a** was determined to 1000 °C and 1500 °C. When heated to 1000 °C and 1500 °C under inert conditions, the various mixtures containing **1** and **3a** afforded char yields of 79-80 and 77-78%, respectively. During the heat treatment, similar exothermic transitions (DTA) as found during the DSC scans were observed. Moreover, above 1000 °C, an exothermic transition is observed which is attributed to the formation of crystalline ceramic components such as SiC and B_4C. Upon cooling, the carbon/ceramic masses were reheated to 1500 °C in air. The oxidative stability of the charred mass was found to be a function of the amount of **1** present and the initial heat treatment. Charred samples obtained from heat treatment to 1000 °C and 1500 °C of 10/90, 25/75 and 50/50 molar weight percent of **1** to **3a** showed charred residues of 98, 98, 99% and 90, 97, 98% respectively, when reheated in air.

Oxidative Aging Studies. The stabilizing effect of the carborane unit on the thermo-oxidative properties of the cured polymeric compositions is apparent from oxidative aging studies at elevated temperatures. The aging studies were performed by TGA analyses on small samples of the thermosets. Conversion to the thermosets of the carborane-siloxane-acetylene linear polymers **1** and **2a** and siloxane-acetylene polymer **3a** were achieved by thermal treatment at various temperatures in an inert atmosphere. Aging of the thermosets from **1** and **2a** was performed by heating the individual sample in sequence for 4 hr at 300, 350, 400, 450 and 510 °C in air. The thermoset from **3a** commenced to lose weight during the 350 °C heat treatment in air and was only aged to 450 °C. All of the samples gained weight during the oxidative exposure up to 350 °C. Extreme heat treatment of the carborane-containing thermosets at 400-510 °C showed an enhancement in oxidative stability relative to a similar sample from **3a** (see Figure 3). The thermosets from **1** and the 50/50 copolymer **2a** exhibited outstanding oxidative performance during the entire heat exposure. When **3** was cured and aged under identical environmental conditions, the sample gained almost 5.5 % weight during the heat exposure at 300 °C. Further heat treatment at 350 °C resulted in a small weight loss (1.6 %). When aged at 400 and 450 °C, an acceleration in the degradation process was observed. The heat treatment between 350 and 450 °C resulted in a weight loss of about 28 %. These results show the importance of boron at enhancing the oxidative stability of a polymeric material through the formation of a passive protective layer that protects the interior against oxidation.

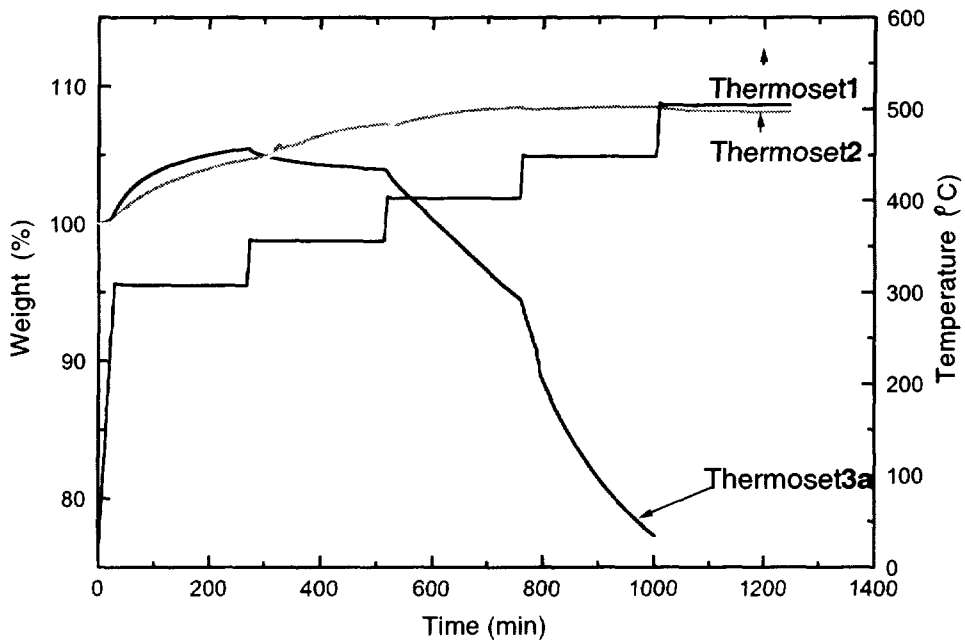

Figure 3. Oxidative Aging Studies on Thermosets from **1**, **2**, and **3a**

Isothermal studies were performed on the thermosets derived from various blending compositions of **1** and **3a**. The compositions were cured by heating at 200, 250, 350 and 450 °C for 4 hr at each temperature under a nitrogen atmosphere. Aging of the thermoset was studied by heating the sample in air for 5 hr in sequence at 250, 300, 350 and 400 °C followed by 15 hr at 450 °C. Copolymer **2c** and the 10/90 composition showed similar thermo-oxidative stability upon conversion into a thermoset. The stabilizing effect of the carborane unit was apparent. All of the samples gained weight during the oxidative exposure up to 350 °C. Moreover, less oxidation occurred on the surface as the amount of **1** increased. More extreme heat treatment at 400 and 450 °C showed an enhancement in oxidative stability with greater amounts of carborane (see Figure 4). The 50/50 mixture exhibited outstanding oxidative performance during the entire heat exposure. When **3a** was cured and aged under identical conditions, the sample gained almost 7% during the heat exposures from 200 to 300 °C. While at 350 and 400 °C, the sample had lost about 14% weight. Upon exposure at 450 °C for 5 hours, the sample lost another 25% weight. These results show that boron enhanced the long-term oxidative stability of the polymeric materials.

Long-term oxidative studies were also performed on the chars obtained from blending compositions of **1** and **3a**. A ceramic composition prepared from the 10/90 mixture was initially processed to 1000 °C under a nitrogen atmosphere. Upon cooling, the char was aged in sequence at 400, 500, 600 and 700 °C in a flow of air for 5 hours at each temperature (see Figure 5). While at 500 °C, the char gained about 0.3% weight. During the entire heat treatment, the ceramic sample lost less than 1% weight. This weight loss occurred between 500 and 600 °C. At 700 °C, no weight changes were observed. Similar results had been observed previously for the copolymer **2c** (6). A charred sample that had been processed from **3a** in an identical manner as the blended mixture showed a 28% weight loss after 15 hours in air at 500 °C. The outer surface of the sample was coated with a white flaky residue attributed to silicon oxide. The outer surface of the chars formed from the blended mixtures upon exposure to air at elevated temperatures remained black. This observation indicates that a different outer oxidized surface forms with structural integrity when boron is present.

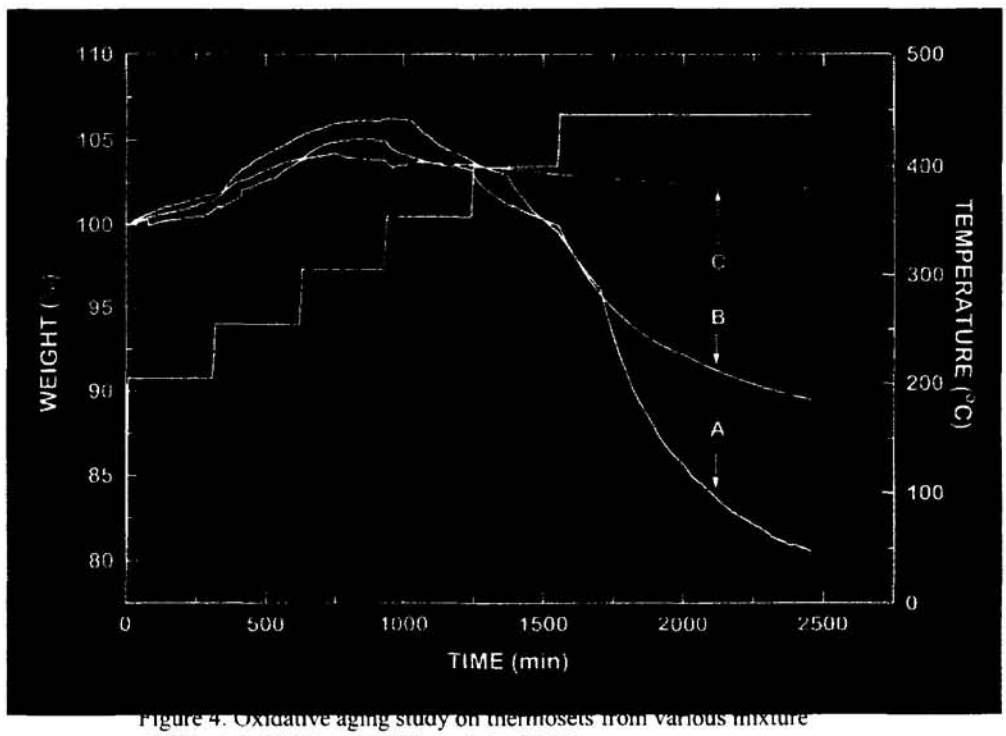

Figure 4. Oxidative aging study on thermosets from various mixture of **1/3a**: (A) 10/90, (B) 25/75, and (C) 50/50

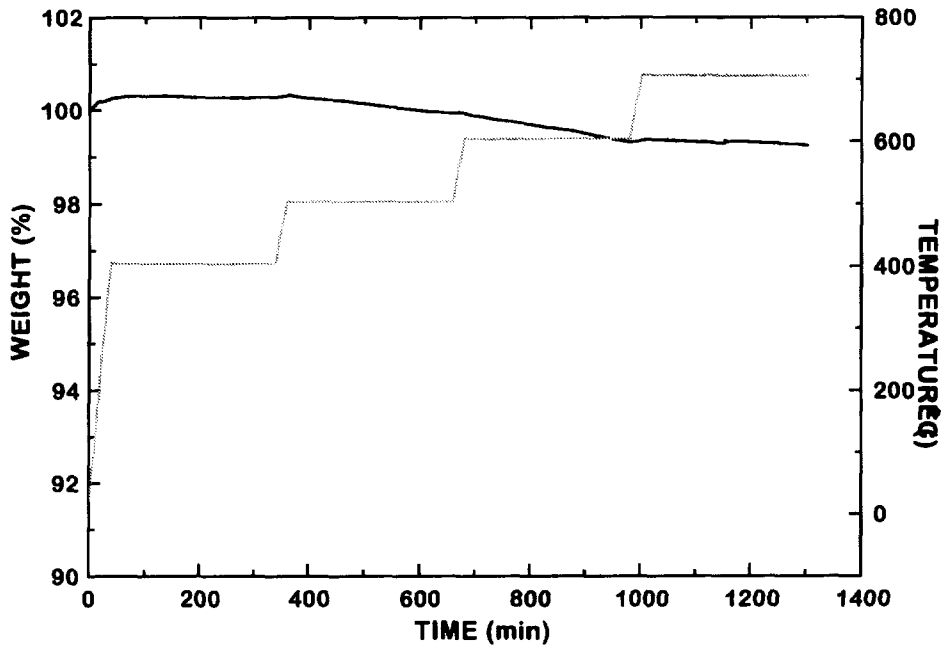

Figure 5. Oxidative aging study on char from 10/90 molar amount of **1/3a**

Conclusions

Extreme aging conditions show the importance of silicon and boron in the protection of carbon-based systems against oxidation. Thermoset and ceramic compositions formed from **1**, **2** and mixtures of **1** and **3a** show outstanding oxidative stability up to 510 °C. The precursor linear compounds contain acetylenic units for thermal conversion to network polymers. The resistance to oxidation of the thermosets and ceramics in **2** and mixtures of **1** and **3a** was a function of the amount of **1** present in the polymeric mixtures. The studies show that carbon can be protected from oxidation at various temperatures by proper incorporation of silicon and boron units into a carbon precursor material. The observations indicate that a protective outer layer forms, when boron is present, and insulates the interior against further oxidation. The ceramic compositions obtained from **2** itself and mixture of **1** and **3a** show similar oxidative stabilities. Further studies are underway to evaluate and exploit the polymeric thermosetting and ceramic compositions as matrix materials for high temperature composites.

Acknowledgment is made to the Office of Naval Research for financial support of this work.

Reference

1. Henderson, L. J.; Keller, T. M. *Macromolecules* **1994**, *27*, 1660
2. Son, D. Y.; Keller, T. M. *J. Polym.Sci.: Part A: Polym. Chem.* **1995**, *33*, 2969
3. Son, D. Y.; Keller, T. M. *Macromolecules* **1995**, *28*, 399
4. Son, D. Y.; Keller, T. M., *Fire and Polymers II*; Gordon L. Nelson; ACS Symposium Series 599, American Chemical Society, 1995 edition, Chapter 19, p. 280
5. Sastri, S. B.; Keller, T. M.; Jones, K. M.; Armistead, J. P. *Macromolecules*, **1993**, *26(23)*,6171
6. Keller, T. M.; Son, D. Y., *Polymeric Materials Encyclopedia*; Joseph C. Salamone; CRC Press: New York 1996; Vol. 5(H-L), p. 3262

Integrated High Payoff Rocket Propulsion Technologies Program Material Development Plan

R.G. Clinton Jr., NASA/MSFC
Dan Cleyrat, AFRL/ML/Anteon
Shawn Phillips, AFRL/PR
Michael Stropki, AFRL/ML
Brian Stucke, AFRL/ML
Brian Reed, NASA/GRC

4th Conference on
Aerospace Materials, Processes, and Environmental Technology
September, 2000

OUTLINE

- IHPRPT Goals
- IHPRPT Materials Working Group (IMWG)
- Materials Plan Development
- IMWG PRDA Status
- National Materials Plan for Rocket Propulsion
- Summary

IHPRPT Is . . . .

A DoD / NASA / Industry Initiative Which Will "Double" Rocket Propulsion Capability by 2010

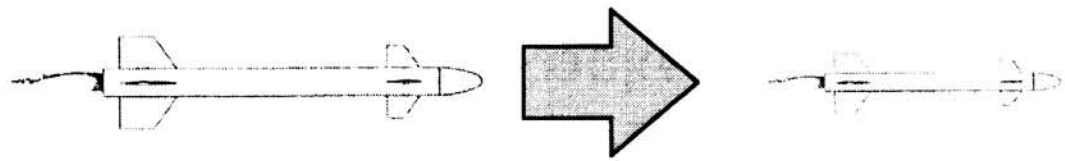

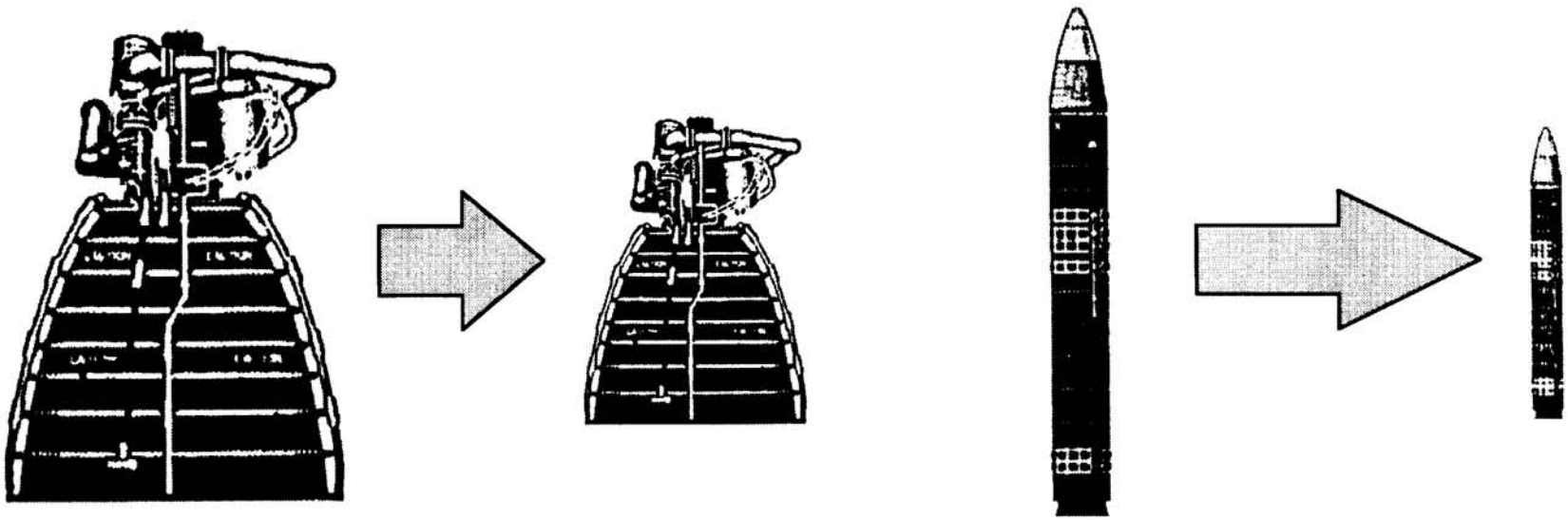

September, 2000

IHPRPT Goals

	Phase I	Phase II	Phase III
Boost and Orbit Transfer Propulsion	**2000**	**2005**	**2010**
▪ Reduce Stage Failure Rate 75%		25%	50%
▪ Improve Mass Fraction (Solids)	15%	25%	35%
▪ Improve ISP (sec)	14	21	26
▪ Reduce Hardware Costs	15%	25%	35%
▪ Reduce Support Costs	15%	25%	35%
▪ Improve Thrust to Weight (Liquids)	30%	60%	100%
▪ Mean Time Between Removal (Mission Life-Reusable)	20	40	100
Spacecraft Propulsion			
▪ Improve I_{tot}/Mass $_{(wet)}$ (Electrostatic/Electromagnetic)	20%/200%	35%/500%	75%/1250%
▪ Improve Isp (Bipropellant/Solar Thermal)	5%/10%	10%/15%	20%/20%
▪ Improve Density-Isp (Monopropellant)	30%	50%	70%
▪ Improve Mass Fraction (Solar Thermal)	15%	25%	35%
Tactical Propulsion			
▪ Improve Delivered Energy	3%	7%	15%
▪ Improve Mass Fraction (Without TVC/Throttling)	2%	5%	10%
▪ Improve Mass Fraction (With TVC/Throttling)	10%	20%	30%

IHPRPT GOALS

Benefits from Achieving Goals [1]

- Payoffs in increased capability, increased reliability and reduced cost are enormous.
- Achievement of the technology goals would provide the following possibilities for system performance improvements:
  - Increase from 25k pounds payload to 65k pounds on a reusable launch vehicle.
  - 92% increase in payload on an expendable launch vehicle.
  - Average annual savings of $648M per year for space launch (based on the National Mission Model over 20 years with Atlas, Delta, Titan IV and Shuttle and including operations cost, hardware costs and cost of failure).
  - 45% increase in satellite life (approximately $240M/satellite savings).
  - 500% increase in satellite repositioning.
  - 100% increase in range/payload capability for a tactical missile.

[1] Information from IHPRPT Point Paper by Dr. Robert C. Corley.

IHPRPT Materials Working Group (IMWG) Activities

Feb 97 **Materials Working Chartered by IHPRPT Steering Committee**

Mar 97 Working Group Membership Established

Apr 97 Status Brief to ODDRE

May 97 **Inaugural Meeting of IMWG**

Jun-Sep 97 Review/Analysis of ARPP's & 48 SBIR Evaluations

Aug 97 IHPRPT Materials DTO MP.29.01 Established

Oct 97 NASP Lessons Learned Workshop & 2nd Meeting of IMWG

Jan 98 3rd IMWG Meeting & Status Brief to ODDRE

Feb 98 DTO Briefing at Reliance Meeting

Feb 98 Brief to IHPRPT Steering Committee

May 98 4th IMWG Meeting

Jun 98 Status Brief to ODDRE

Jul 98 Brief to IHPRPT Steering Committee

Nov 98 IMWG Chair Meetings at Industry Sites

Dec 98 DTO Briefing at Reliance Meeting

Jan 99 Status Brief to ODDRE

Feb 99 Brief to IHPRPT Steering Committee & Reliance

Jun 99 IMWG Weekly Telcons

Jul 99 Brief to IHPRPT Steering Committee

Oct 99 IMWG - Component Lead Meeting

Feb 00 Brief to IHPRPT Steering Committee

Mar 00 Execution/PRDA Development Meeting

May 00 **Materials PRDA Released**

Liquids B&OT Plan

Solid B&OT Plan

Solids Tactical Plan

Spacecraft Plan

Materials Execution Plan

IHPRPT Materials Working Group

Process

- Evaluate Requirements and Develop Materials Plan for IHPRPT Liquid, Solid, and Spacecraft Propulsion Goals
- Co-Chairs: AFRL- Michael Stropki; & NASA-MSFC- Corky Clinton

Team

Government

USAF: AFRL Materials & Manufacturing Directorate (ML); Propulsion Directorate (PR)

Army: ARL, MCOM

Navy: NAWC, NSWC

NASA: MSFC, GRC, LaRC

Industry

ARC	Primex
Aerojet	Thiokol
Alliant	TRW
Boeing/Rocketdyne	UT Chemical Systems
Kaiser-Marquardt	UT Pratt & Whitney

Considering Addition of Materials Suppliers

Product - Materials Plan

Materials Weight , Durability, & Performance Improvements For

Liquid B&OT

- **PMD**
  - Turbopump Housing
  - Ducts, Line, Valves
- **C&ECD**
  - Thrust Chamber
  - Nozzles

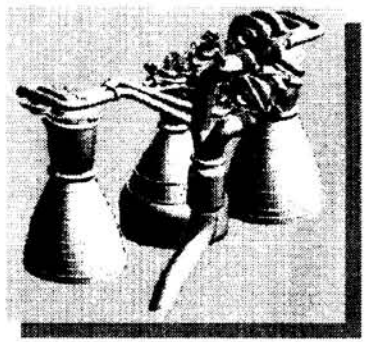

Chamber

Catalyst/ Thermal Bed

Optics(Grids)

Spacecraft

Case / Insulation

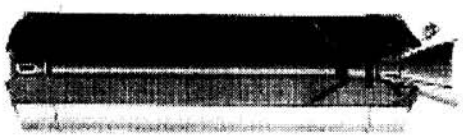

Exit Cone

Nozzle

Throat

Solids: B&OT/Tactical

Materials Plan Development

- Materials Plan for IHPRPT Developed
  - Developed by IHPRPT Materials Working Group (IMWG)
  - Addresses Liquids, Solids, Spacecraft, Tactical Components
  - Category Prioritization Developed with Industry and Government Representatives - Continuing Iterative Process
- Air Force Funding Allocated for Materials Development
- Formula for Program Execution (Iterative Process)
  - Materials Execution/Funding Allocation per IMWG Plan
  - Coordinate with IHPRPT Component Leads
  - Coordinated with NASA Plans in Materials Technology for Integrated Space Transportation Plan (ISTP) (Currently part of IMWG process)
  - IHPRPT Steering Committee Approval
  - Execute Plan Through AFRL/ML PRDA Process

Materials Plan Development

- Materials and Processes Science & Technology Program (Not Component Development)
  - Up to sub-scale development as required
  - Component development *not* part of this M&P program
- IMWG Materials Program Has Transition Path to Component Program (Traceability) Through IHPRPT Component Leads
- Materials Vendors /Propulsion Primes to Be Contractually Connected Through PRDA
- Program Maintains Flexibility to Allow for :
  - New developments in materials and processes
  - Adjustments to materials and processes maturation
  - Phase III initiatives (i.e., new starts)

Materials Plan Development
IHPRPT M&P Program Progression

Critical Component Requirements

- Determine/Coordinate on Key Components
- Assess Materials Requirements
- Combined DOD, NASA, Industry Activities
- Use ARPP, Tech. Leads, IMWG

Pre-TRL

M & P Dev/Subscale Demonstration

- Develop/Characterize Materials Based on the Assessment
  - Process Development/Evaluation
  - Preliminary Configuration Assessment
  - Measure Preliminary Thermal and Mechanical Properties
  - Conduct Environmental Assessment
  - Assembly Considerations
- Subscale Component Demonstration/Validation

TRL 3/4

Scale-up, Property Verification, Component Dev

- Take THE Best Materials Approach; Scale-up Process to Verify
  - Material Uniformity
  - Thermal, Physical and Mechanical Properties
  - Process Reproducibility
  - Failure Mechanisms

TRL 5/6

- IHPRPT Scale Up
  - Refine Design
  - Produce Full Scale Components
  - Further Define Component Failure Mechanisms
  - Provide Component for Demonstration Testing
- Validate Demonstration Exit Criteria for Demo Testing

Component Verification

- The M& P Technology Transition to IHPRPT Demo Team
  - Process
  - Properties
  - Subcomponent Performance
  - Failure Mechanisms
- Participate in Component Demo Phase ATD Development

Demo of New Material

September, 2000

IHPRPT Materials Plan

2000

Examples from Plan Development Process

September, 2000

IMWG Program Support To Propellant Management Devices (PMD)

	COMPONENT	CANDIDATE MATERIALS PROGRAMS
HIGH	HOUSING - Ox Compatible	
	HOUSING - LH2 Compatible	
	LINES, DUCTS & VALVES	
MED	ROTATING ELEMENTS	

Other M&P Critical Needs May Emerge for Phase II & III Based on Iterative Process

Oxygen-Rich Turbopump Housing

Component Objectives	Material Candidates
Oper. Temp Ultimate Strength (Long./Trans) Shear Strength TBD (Long/Trans) Elastic Modulus (Long/Trans) Shear Modulus Poisson's Ratio Fracture Toughness Thermal Shock Density CTE (Long/Trans)	• Candidate A • Candidate B

EXAMPLE

Cryo Boost Phase II PMD

LOX Turbopump Housing

Candidate Material A

Current Properties	Technical Issues / Risks
▪ Very little data developed to date ▪ Demonstrated oxidation resistance ▪ Limited matrix strength and ductility data available	▪ Demonstrate oxidation resistance and promoted combustion resistance; mech properties, characterization ▪ Establish design and analysis methodology; data ▪ Develop interfaces and attachment approaches ▪ Fabricate sub scale components ▪ Validate life/performance

Current Tasks	Total($K)	ORG	FY99	FY00	FY01	FY02	FY03	FY04	FY05
Metal Matrix Composite - Turbopump Demo	XXX	NASA	XXX	XXX					
		IRAD	XX →						
NASA-SBIR	XXX	NASA	XXX	XXX					
Total Current									

* - M&P portion of total task
** - leveraging of Al Based LH2 MMC Program

Planned M&P Programs

-D&A to Est. Requirements.
-Develop Interfaces and attachments
-Examine alternative approaches/ materials
Validate life/performance

PRDA Task TBD

September, 2000

IMWG PROGRAM SUPPORT TO Combustion and Energy Conversion Devices (C&ECD)

	COMPONENT	CANDIDATE MATERIALS PROGRAMS
HIGH	LT WGT THRUST CHAMBER (Ph II & III)	
MED	HI TEMP COMPOSITE TECHNOLOGY (NOZZLE)	

Other M&P Critical Needs May Emerge for Phase II & III Based on Iterative Process

IMWG Program Support To SRM (B&OT and Tactical)

COMPONENT	CANDIDATE MATERIALS PROGRAMS
HIGH	
NOZZLE - Low-Eroding Throats	
INSULATION	
CASE	
NOZZLE - Low Cost Components	
CASE	
NOZZLE - Exit Cone Ablative	

*Programs that will apply to Tactical and to B/OT

IMWG Program Support To Spacecraft

COMPONENT	CANDIDATE MATERIALS PROGRAMS
HIGH	
CATALYSTS	
ION ENGINE OPTICS	
CHAMBER MATLS	

IMWG PRDA Status

September, 2000

IHPRPT Materials PRDA Schedule

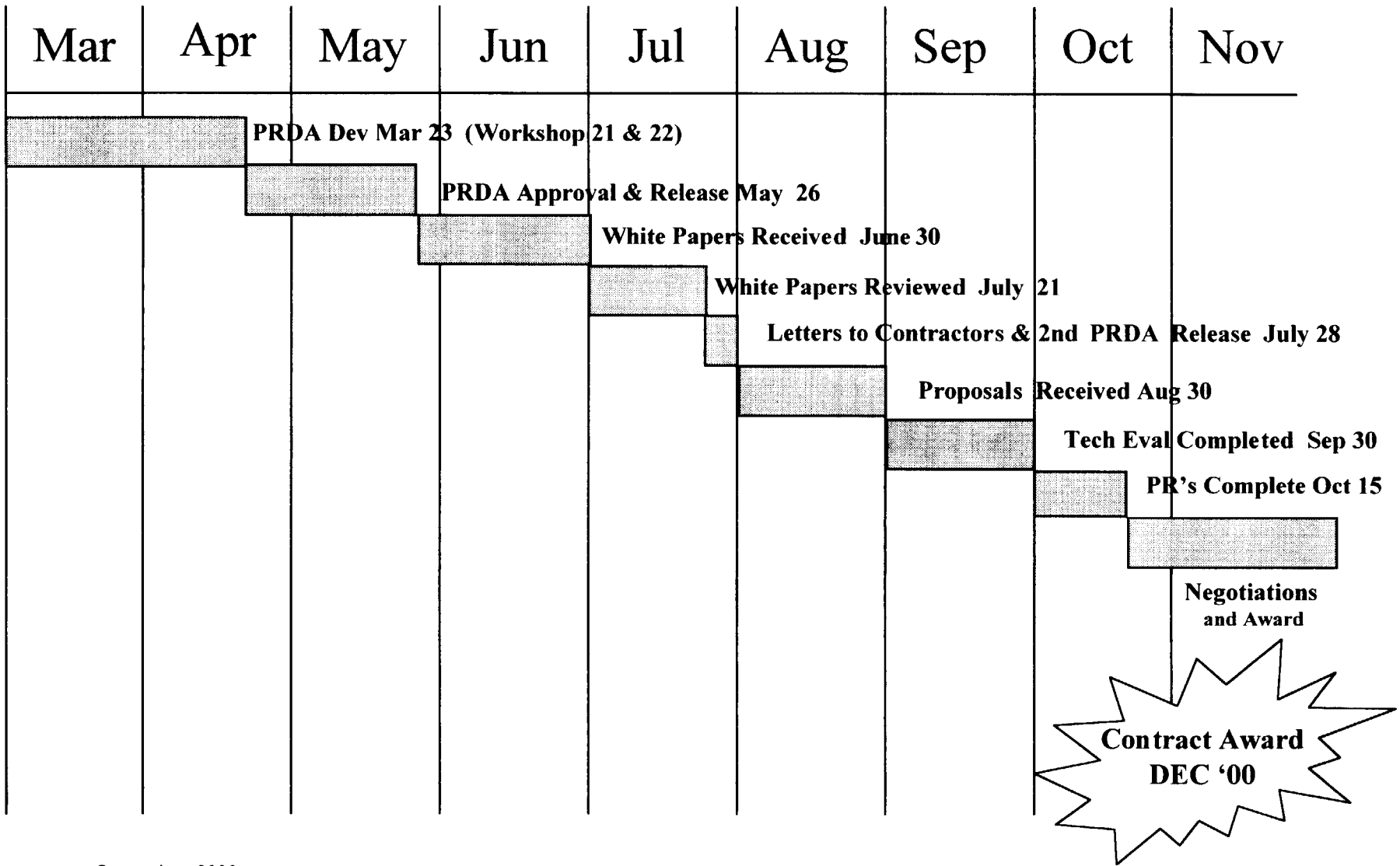

September, 2000

imwg PRDA Topics

Liquid Boost and Orbit Transfer

Topic	Team	Topic Lead
1. LOX Turbopump Housing	AFRL/ML/PR, NASA MSFC, NASA LaRC, NASA GRC	Benji Maruyama
2. LH2 Turbopump Housing	AFRL/ML/PR, NASA MSFC, NASA LaRC, NASA GRC	Benji Maruyama
3. Lines, Ducts, Valves	AFRL/ML/PR, NASA MSFC, NASA LaRC, NASA GRC	Kumar Jata
4. Thrust Chamber Jacket	AFRL/ML/PR, NASA MSFC, LaRC, GRC	Dan Miracle
5. Nozzle and Coatings	AFRL/ML/PR, NASA MSFC, NASA LaRC, NASA GRC	Steve Steel

IMWG PRDA Topics

Solid Rocket Motor Boost & Orbit Transfer/Tactical

Topic	Team	Topic Lead
6. Nozzles and Inserts	AFRL/ML/PR, NASA MSFC, Aerospace Corp.	Scott Theibert
7. Insulation and Case	AFRL/ML/PR, NASA MSFC, Aerospace Corp.	Derek Linco

Spacecraft

Topic	Team	Topic Lead
8. Catalyst/Thermal Bed	AFRL/ML/PR, NASA GRC	Steve Steel
9. Optic Grid	AFRL/ML/PR, NASA GRC	Kristen Kearns
10. Oxidation Resistant Chamber Mat.	AFRL/ML/PR, NASA GRC	Kumar Jata

IMWG PRDA Status
OMC Study for Phase III Applications

- OBJECTIVES:
  - Assess OMC technology for feasibility of application to Liquid Propulsion Components. (LH2 turbopump housings, lines, ducts, valves and a thrust chamber structural jacket identified in materials plan for Phase III development).
  - Provide assistance in determining scope and direction to future DOD and NASA investment in OMC's for liquid propulsion components.

- Performed by a "Blue Ribbon" materials and processes group including propulsion expertise with no affiliations to an organization that could bid on topics in a future IHPRPT Materials OMC PRDA.
- Posture for timely Materials PRDA II (6 month duration).
- Present findings at appropriate space materials or propulsion conference (e.g. NSMMS).

National Materials Plan for Rocket Propulsion

September, 2000

National Materials Plan for Rocket Propulsion

- Under IMWG Initiative, Developing Strategy and Process for Coordinating IHPRPT Materials Plan with NASA Materials Planning for ISTP.
- Product will be a Joint IHPRPT - ISTP Materials Development Roadmap.
- Will Provide for a Combined IHPRPT-NASA Strategy for Materials Development (National Plan).
  - Maximize use of resources (avoid duplication).
  - Provide opportunities for cooperative programs.
  - Rebuild National leadership in propulsion technology.

National Materials Plan for Rocket Propulsion

- Coordination of IMWG and NASA ISTP efforts towards development of the National Rocket Propulsion Materials Plan is in progress.
  - Key NASA materials experts participation on IMWG Technical Teams for PRDA drafting and white paper evaluation.
  - NASA/MSFC has assigned specific responsibility for 2nd Gen/3rd Gen RLV synergistic technologies coordination to the RLV Focused Technology Project.
  - Dissemination of 3rd Generation RLV Program planning results to IMWG PRDA Technical Teams supporting white paper evaluation (in progress).
  - NASA-led 2nd Generation RLV proposals will be assessed for potential overlap with IMWG white papers (in progress).
  - Industry-led 2nd Generation RLV proposals will be assessed for potential overlap with IMWG proposals.

National Materials Plan for Rocket Propulsion
NASA ISTP - IMWG
Merging Common Space Propulsion Materials Efforts

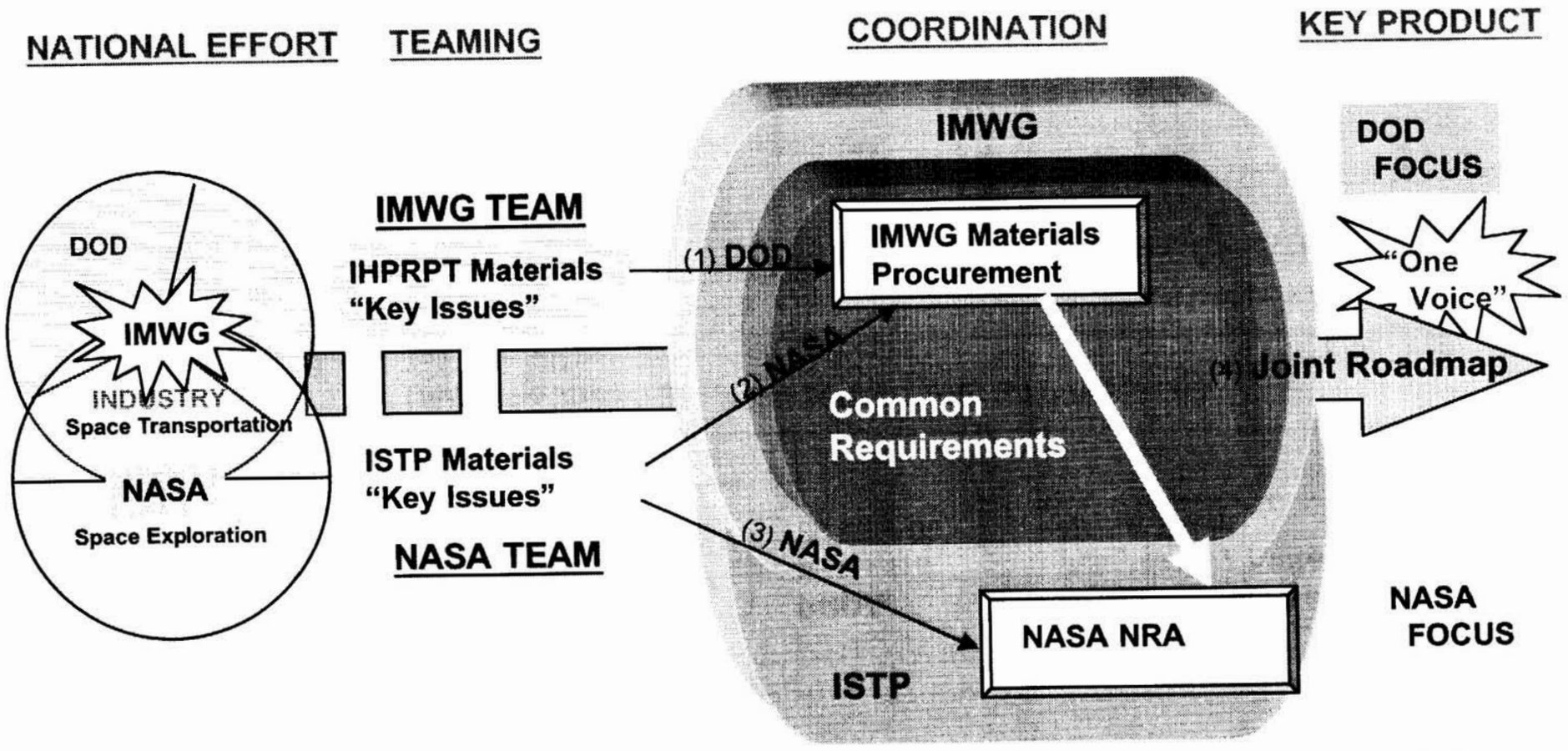

1. DOD (AF) Funds IMWG PRDA for IHPRPT Materials Requirements
2. NASA Augments Funding or Specific Tasks for Increased NASA Materials Requirements
3. NASA Funds NRA for ISTP Unique Requirements (Focused on 2nd & 3rd generation goals)
4. IMWG Develops Joint Materials Roadmap as Part of IMWG Plan

September, 2000

National Materials Plan for Rocket Propulsion
NASA ISTP - IMWG
Current Activity

IHPRPT Materials Plan

PRDA Developed by AF/Navy - NASA Team

PRDA Released 29 May 00

Final Proposal Review in Progress by AF/Navy - NASA Team

Under the Auspices of the IHPRPT and ISTP Programs

Strategy

Utilizing AF/Navy - NASA Engineers to Develop Plans, Prepare Solicitations, and Evaluate Proposals

Review Requirements and Approaches for Areas of Commonality

NASA ISTP Planning

Third Generation RLV Planning May 00

NASA-Led Second Generation RLV Proposals July 00

Industry-Led Second Generation RLV Proposals Fall 00

September, 2000

National Materials Plan for Rocket Propulsion
NASA ISTP - IMWG
Next Steps

IHPRPT Materials Plan

Recommendations Addressing Opportunities and Development of Joint Roadmaps Led by the DOD-NASA IHPRPT Materials Working Group

Develop Joint Roadmaps that Reflect:
- Joint opportunities
- Funding
- Milestones
- Transition

Leveraging - thru industry contracts
Collaboration - information sharing
Joint Projects - Joint funds on project
Project Enhancement - applying funds to existing contract

"National Materials Plan" for Rocket Propulsion

NASA ISTP Plan

Linkage/Input to Joint Roadmap Development/National Plan through NASA IMWG Representative(s)

Summary

- IMWG Government and Industry Members, Together With the IHPRPT National Component Leads, Have Developed a Materials Plan to Address the Critical Needs of the IHPRPT Community.
  - Liquids Boost and Orbit Transfer.
  - Solids Boost and Orbit Transfer.
  - Tactical.
  - Spacecraft.
- Criticality of Materials' Role in Achieving IHPRPT Goals Evidenced by the Significant Investment Over the Next 5 Years.
- Materials Plan Is a "Living" Document to Assure Appropriate Focus and Progress.
- Excellent Response to IMWG PRDA With 50 White Paper Proposals Received for the 10 Topic Areas.
  - Final Reviews in Progress.
  - On Schedule for December 2000 Awards.
- National Rocket Propulsion Materials Plan, Coordinating IHPRPT and NASA Activities, Being Developed by IMWG.

X-33 LH_2 Tank Failure Investigation Findings

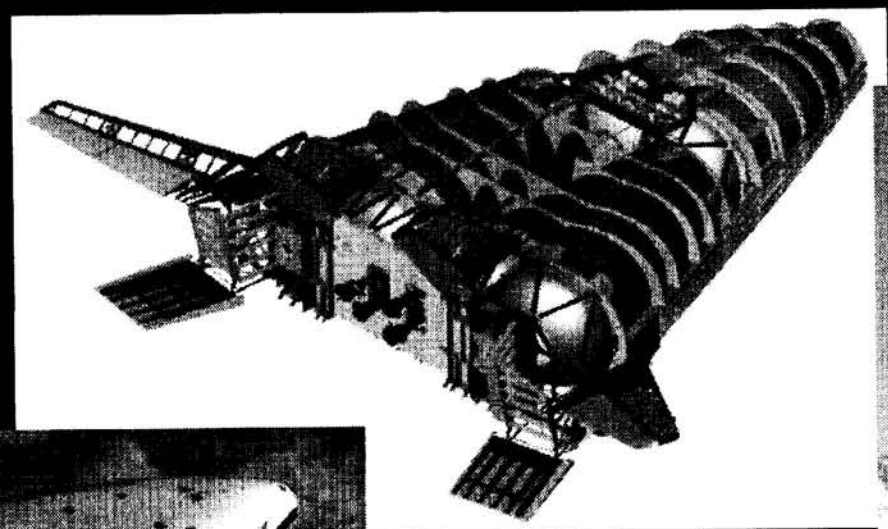

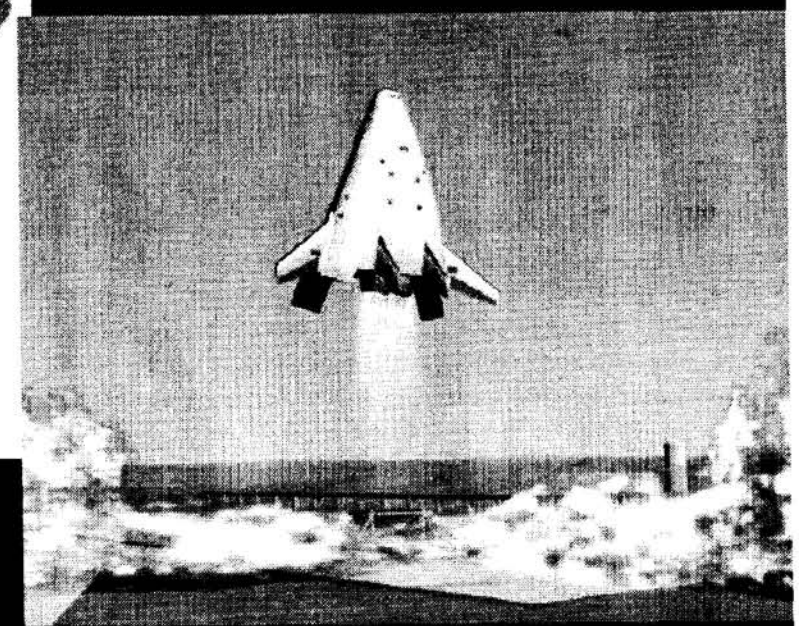

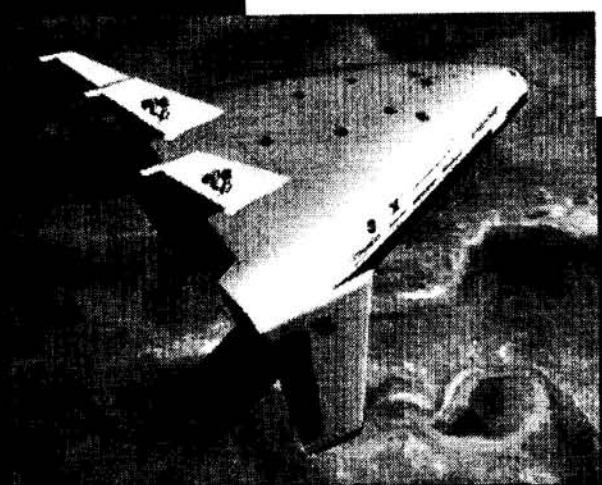

Presented by
Mindy Niedermeyer
MSFC

Aerospace Materials, Processes, and Environmental Technology Conference

September 18 - 20, 2000

X-33 LH_2 Tank Failure Investigation Findings

X-33 LH_2 Tank Failure Investigation Findings

X-33 LH_2 Tank Failure Investigation Findings

Introduction

- Tank History and Test Objectives
- Failure Description
- Investigation
- Conclusions

X-33 LH_2 Tank Failure Investigation Findings

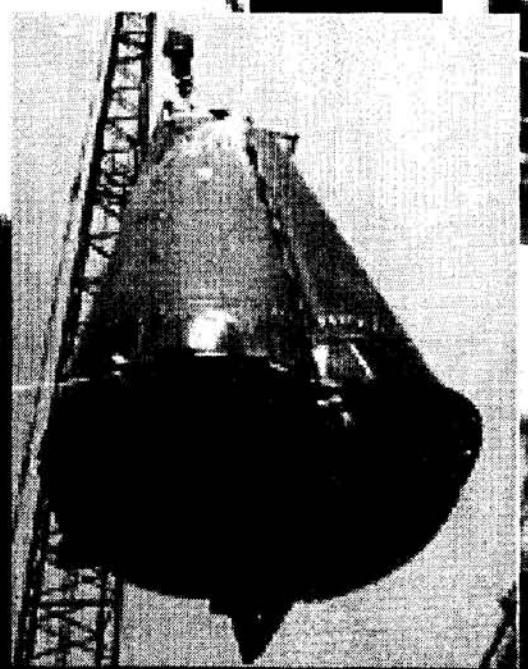

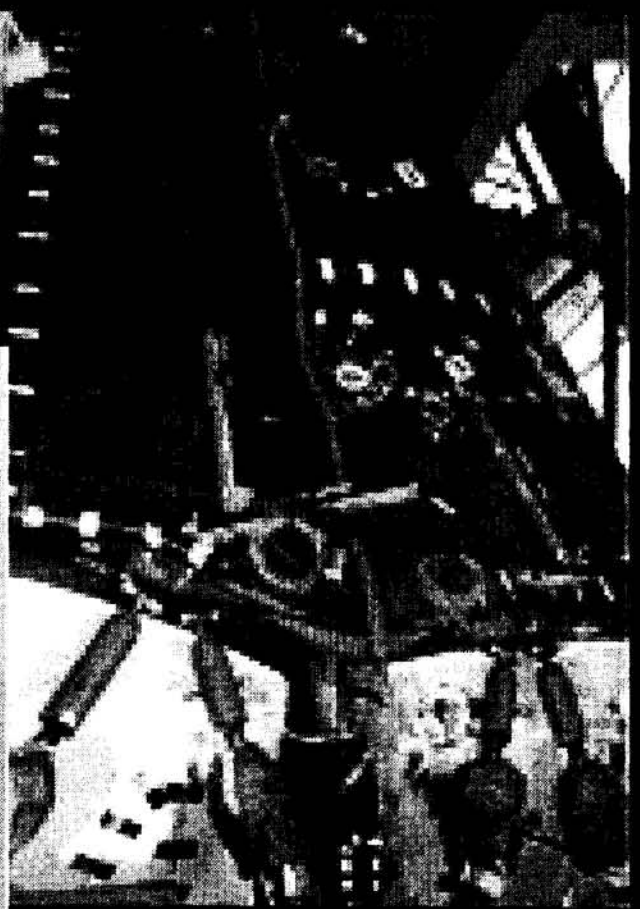

X-33 LH_2 Tank Failure Investigation Findings

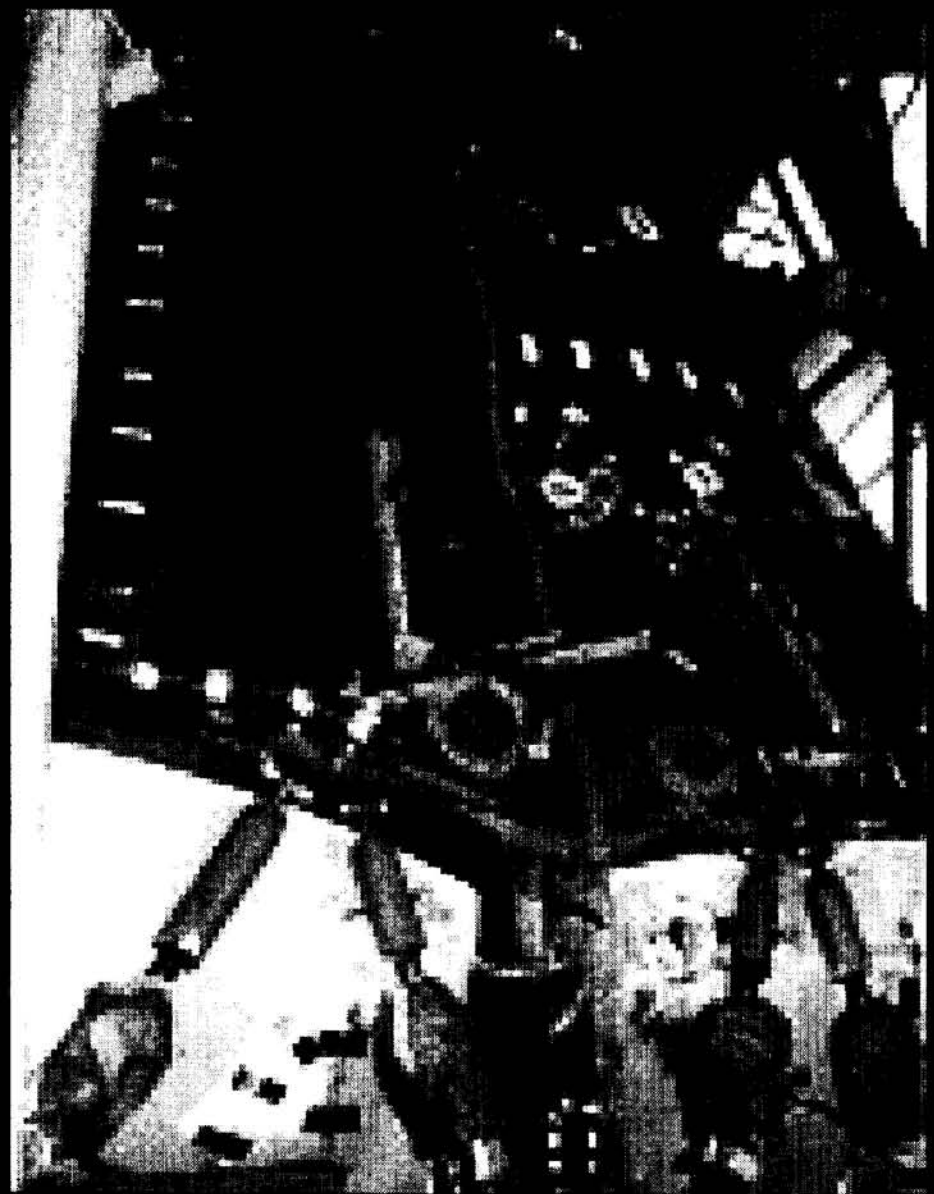

X-33 LH_2 Tank Failure Investigation Findings

Tank Description

- Structural component of the aft body
- Quad-lobe design
- Sandwich - honeycomb graphite epoxy construction

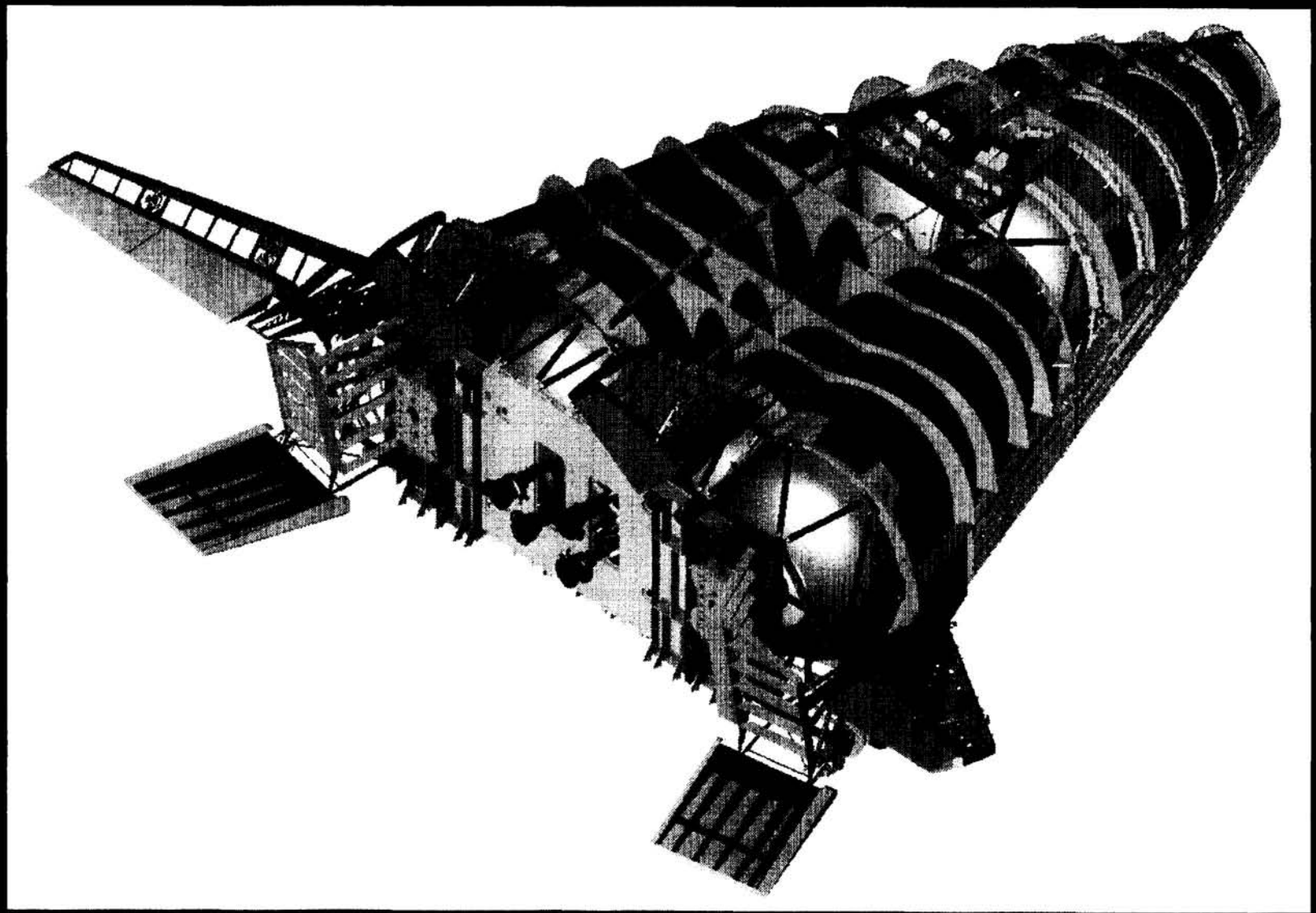

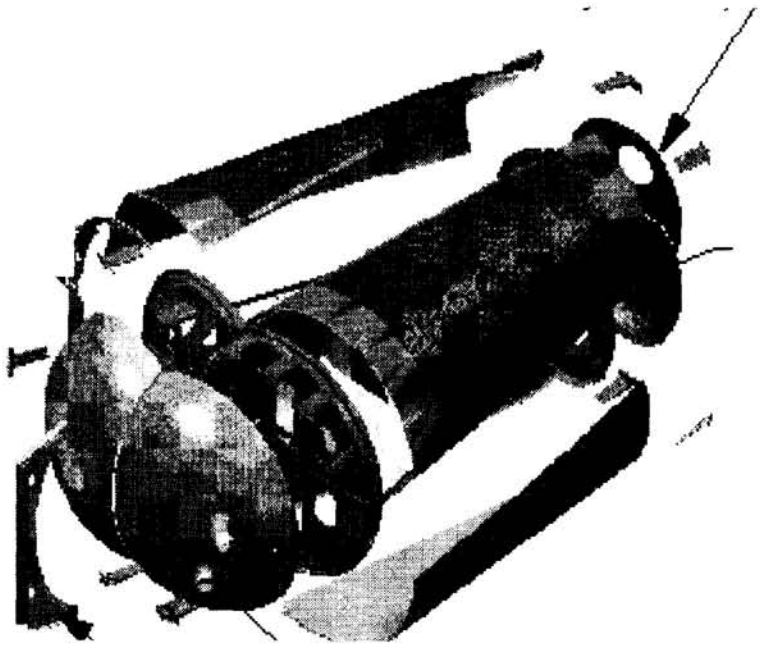

External View

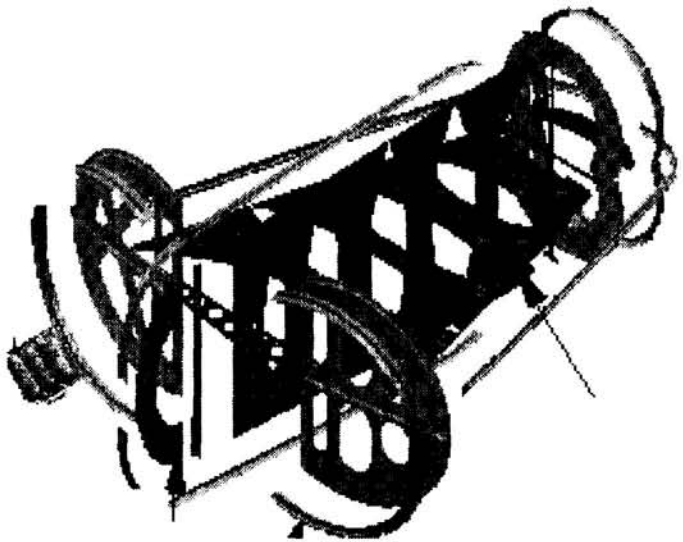

Internal View

X-33 LH_2 Tank Failure Investigation Findings

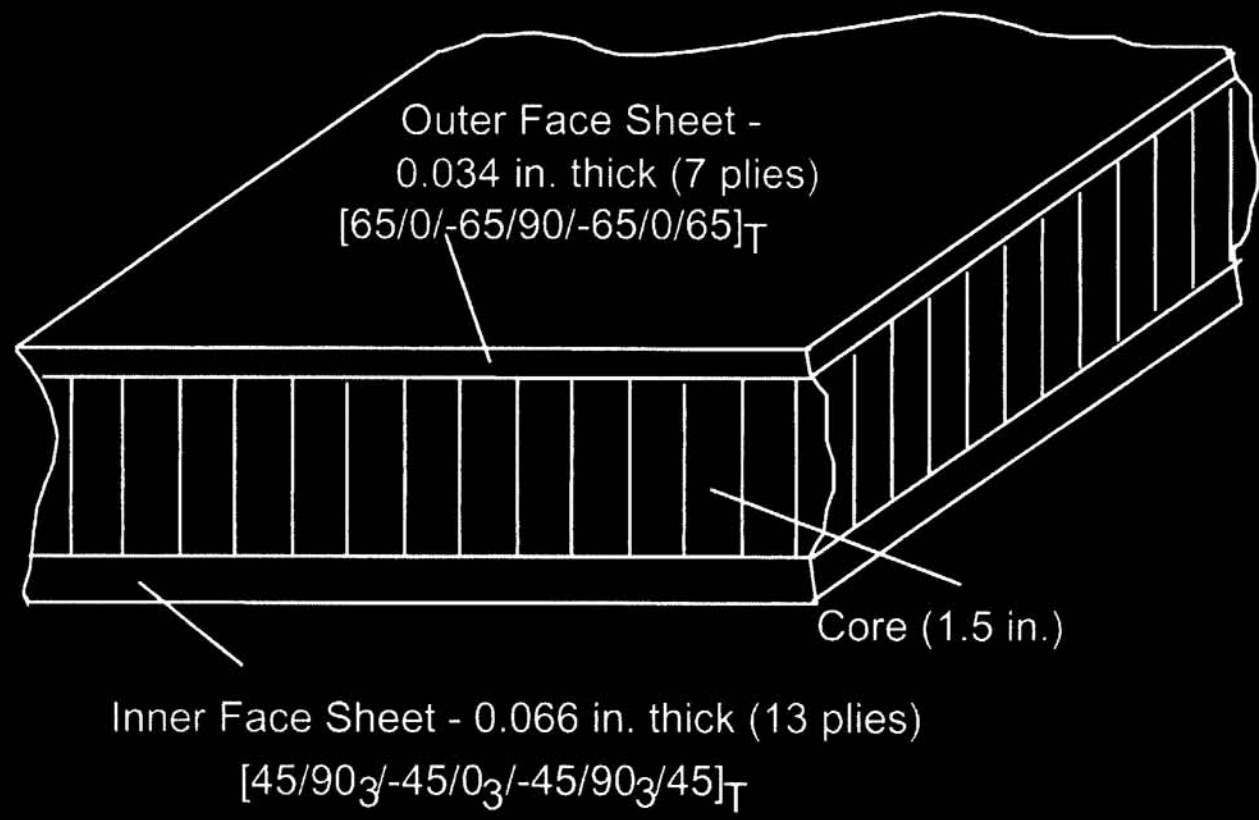

Geometry of sandwich structure

X-33 LH_2 Tank Failure Investigation Findings

Test Objectives

- Verify structural integrity at 105% expected flight load limit varying the following parameters
  - Cryogenic temperature
  - Internal pressure
  - Mechanical loading

X-33 LH_2 Tank Failure Investigation Findings

- **September 21, 1999 test aborted due to hydrogen leaks**
  - **100% cryogen fill (LH2)**
  - **20 psig internal pressure**

- **November 3, 1999 test completed**
  - **100% cryogen fill (LH2) at 42 psig internal pressure**
  - **Load case 5 applied at 5 psig internal pressure**
  - **Tank drained of cryogen**

X-33 LH_2 Tank Failure Investigation Findings

Timeline

- Tank filled,12:30 PM
- Tank pressurized to 42 psig, 2:00 PM
- Tank vented to 2 psig, 3:00 PM
- Loads applied, pressure increased to 5 psig, 4:40 PM
- Tank drained, 6:00 PM
- Lobe 1 failure, 6:24 PM

X-33 LH_2 Tank Failure Investigation Findings

X-33 LH2 Proto-Flight Tank Test

Camera 14 : Lobe 1 and Lobe 4
Longeron

X-33 LH_2 Tank Failure Investigation Findings

Initial Findings

- Peel Failure
  - Outer skin and core peeled away from inner skin
- Core Failure
  - Core is 'mangled'
- Hydraulic fluid on test article
- Foreign Object Debris (FOD)
- Poor bondlines
- Pressure in core above ambient 13 hours after failure

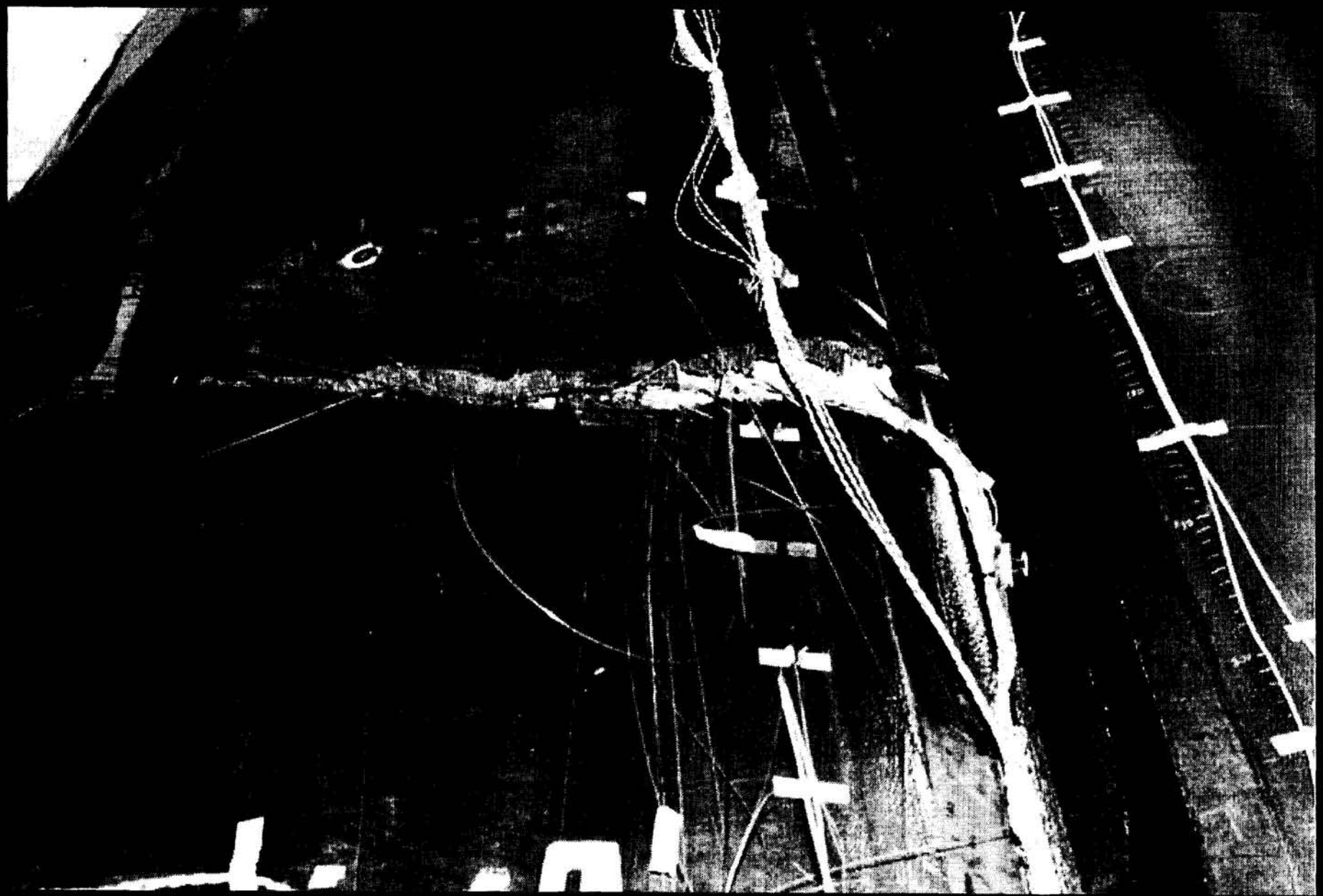

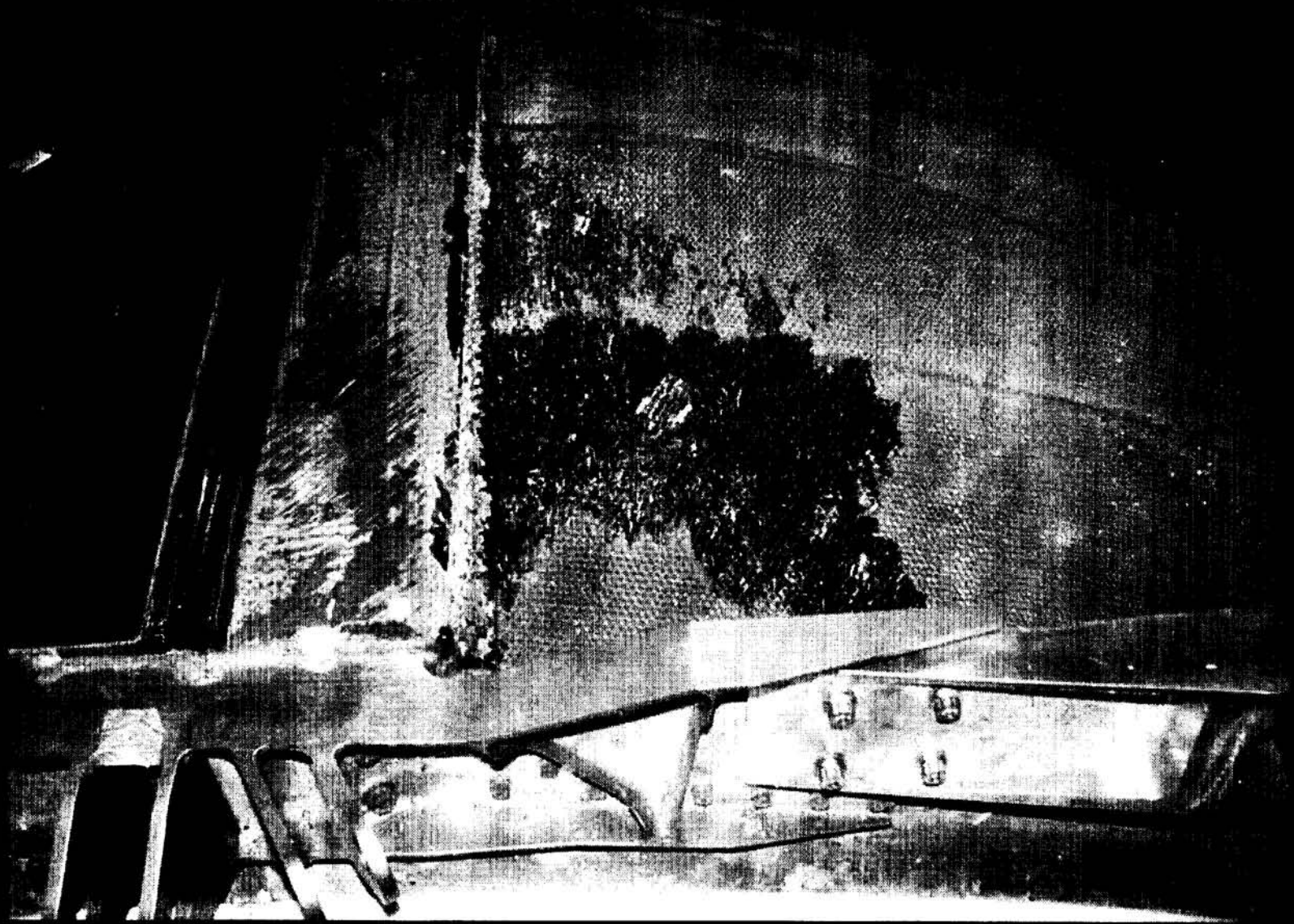

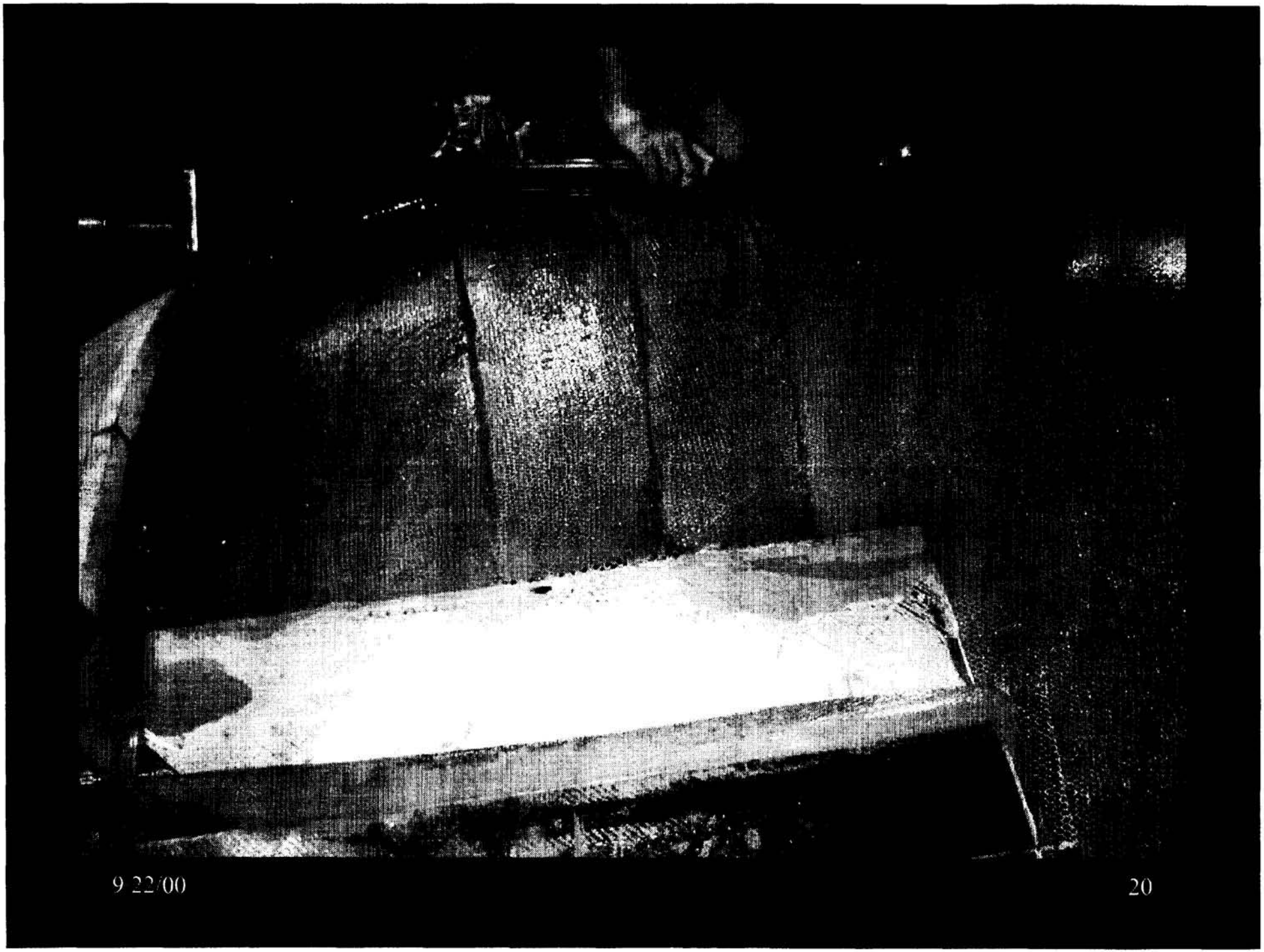

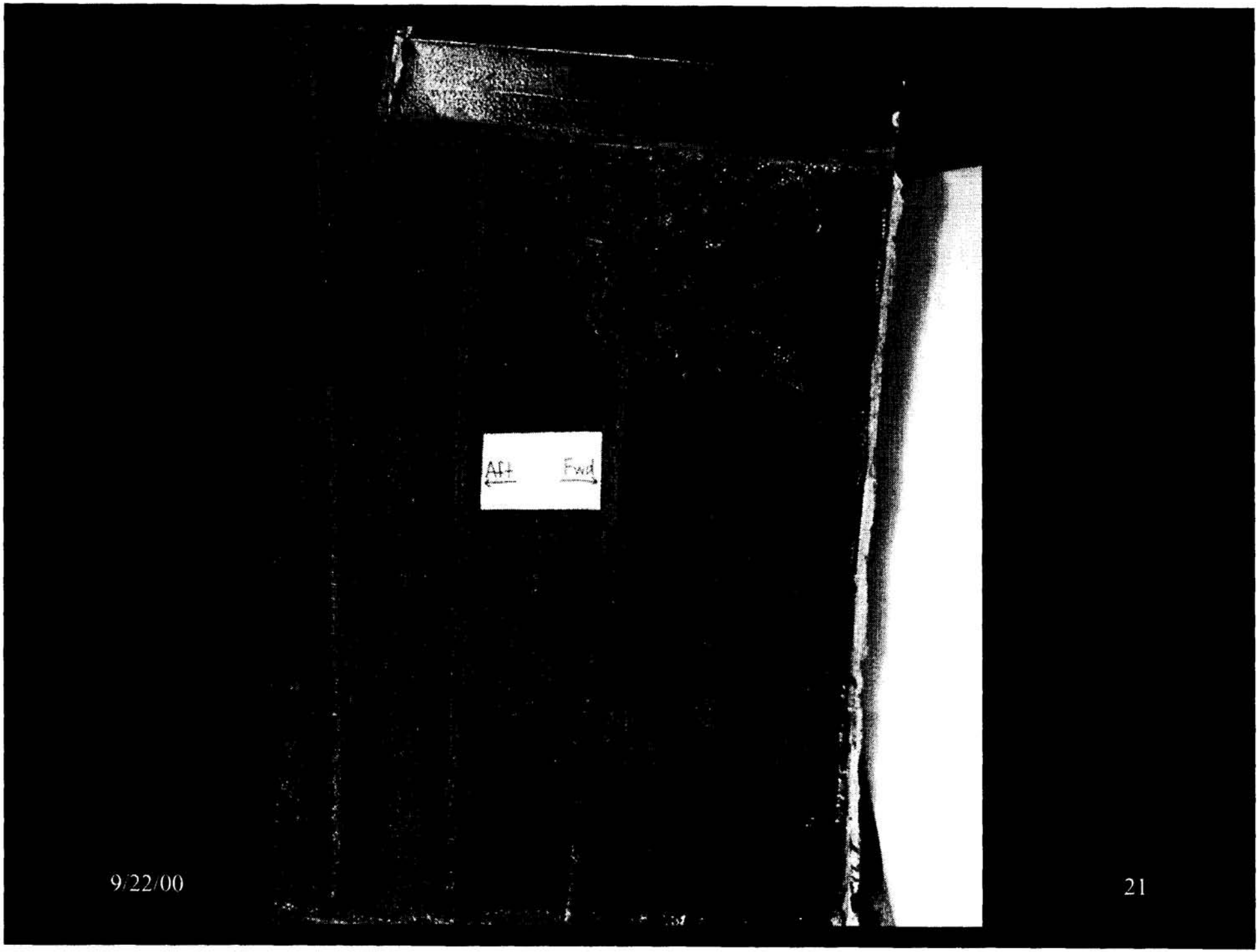
Aft
Fwd

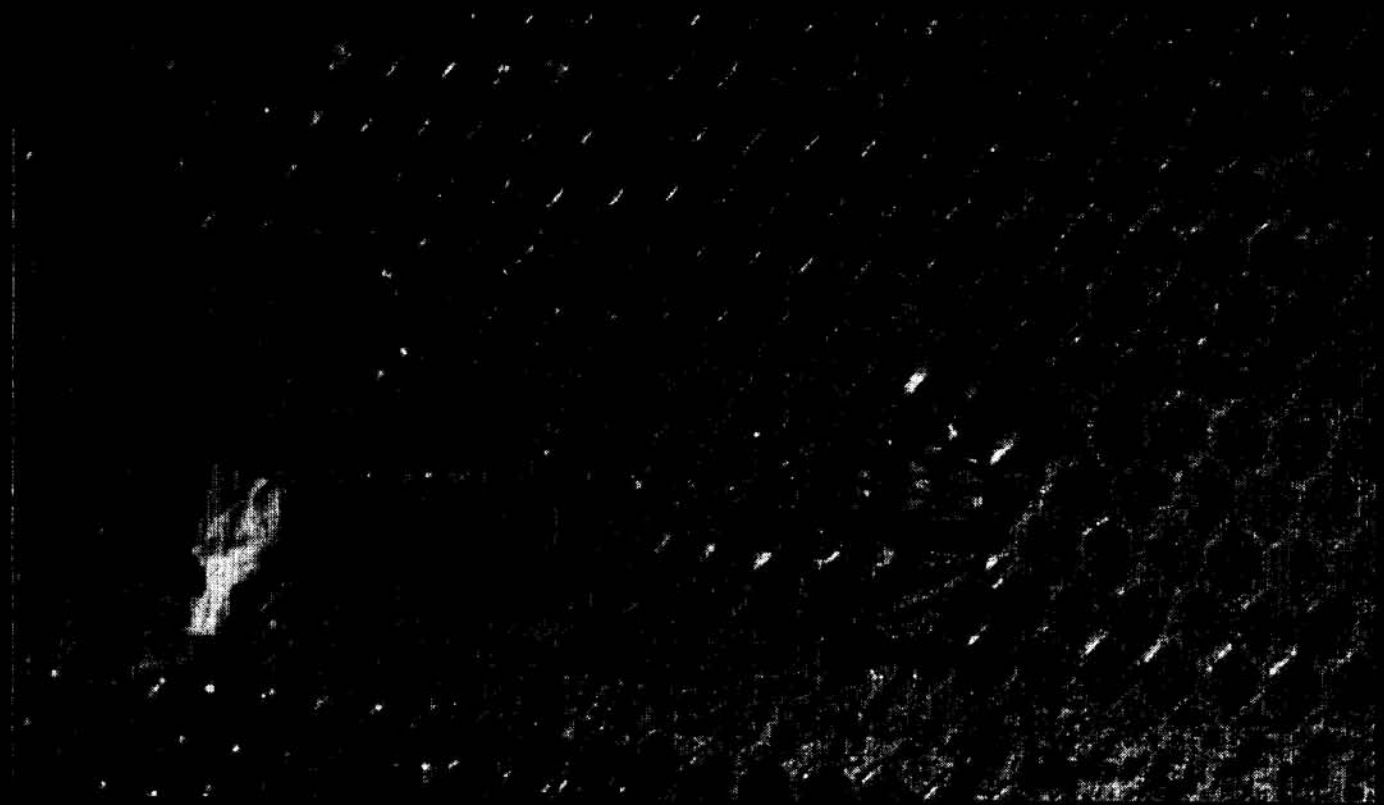

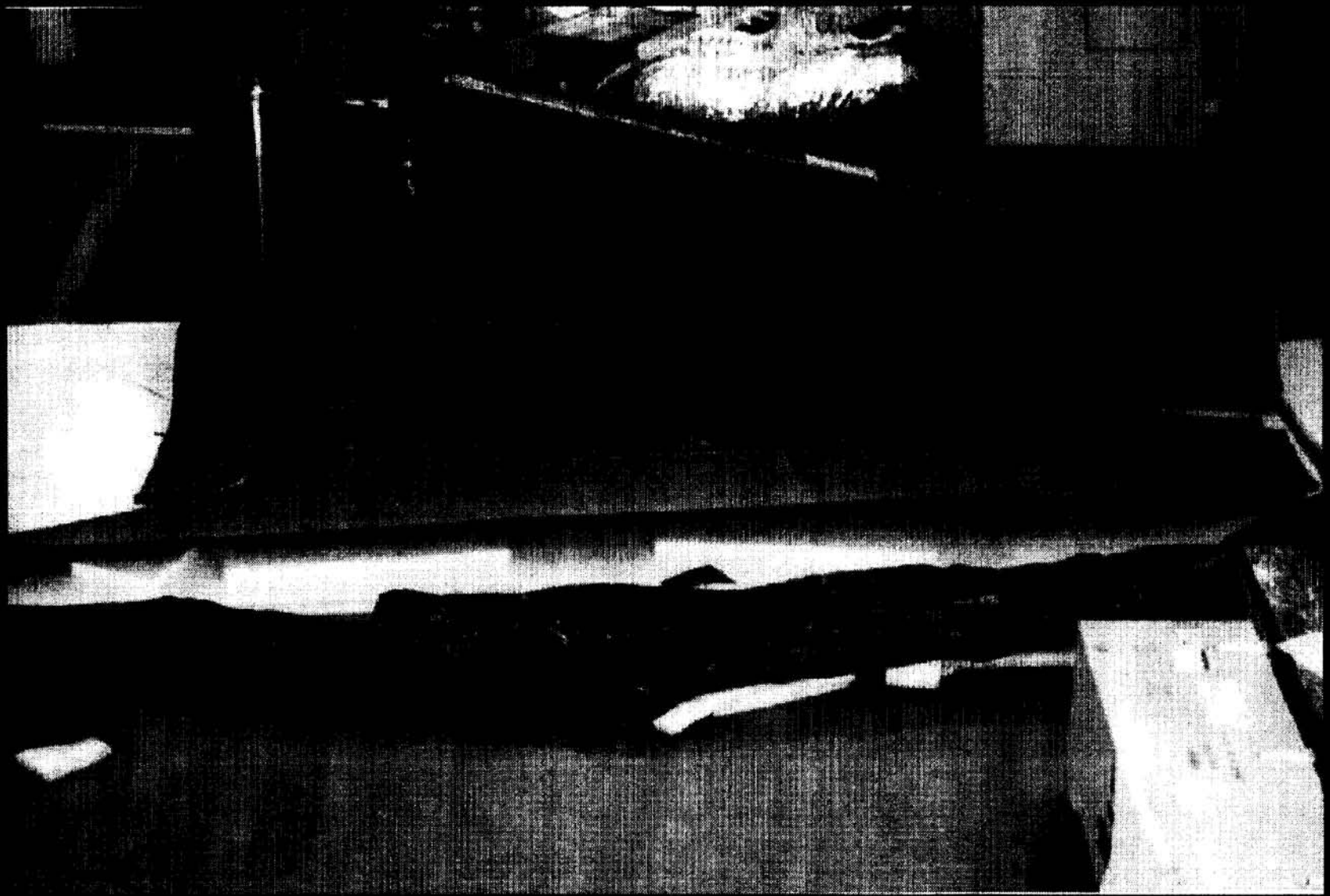

X-33 LH_2 Tank Failure Investigation Findings

Subsequent Findings

- Core pressures behaved unexpectedly
- Microcracking

Core Pressure vs Time

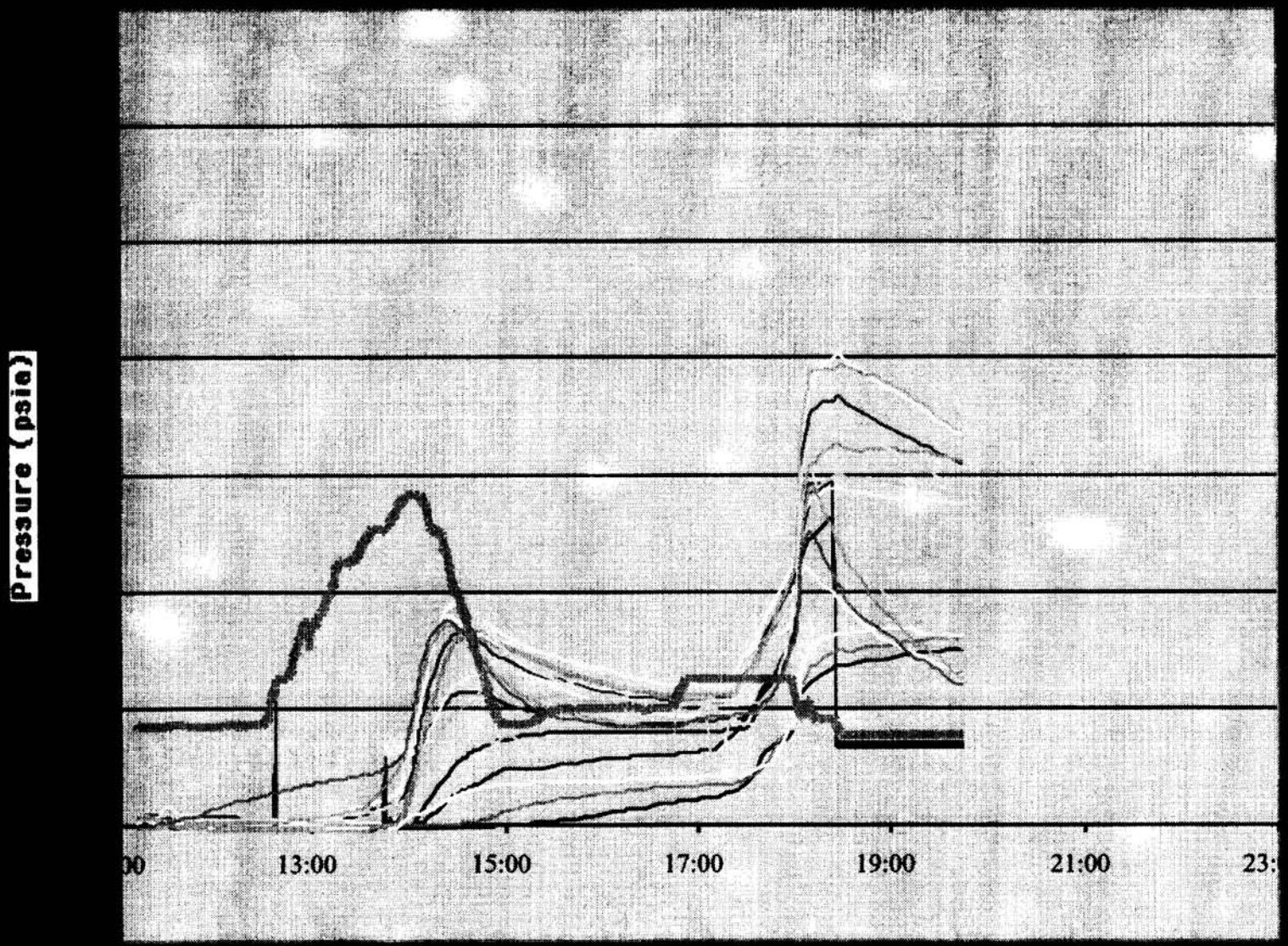

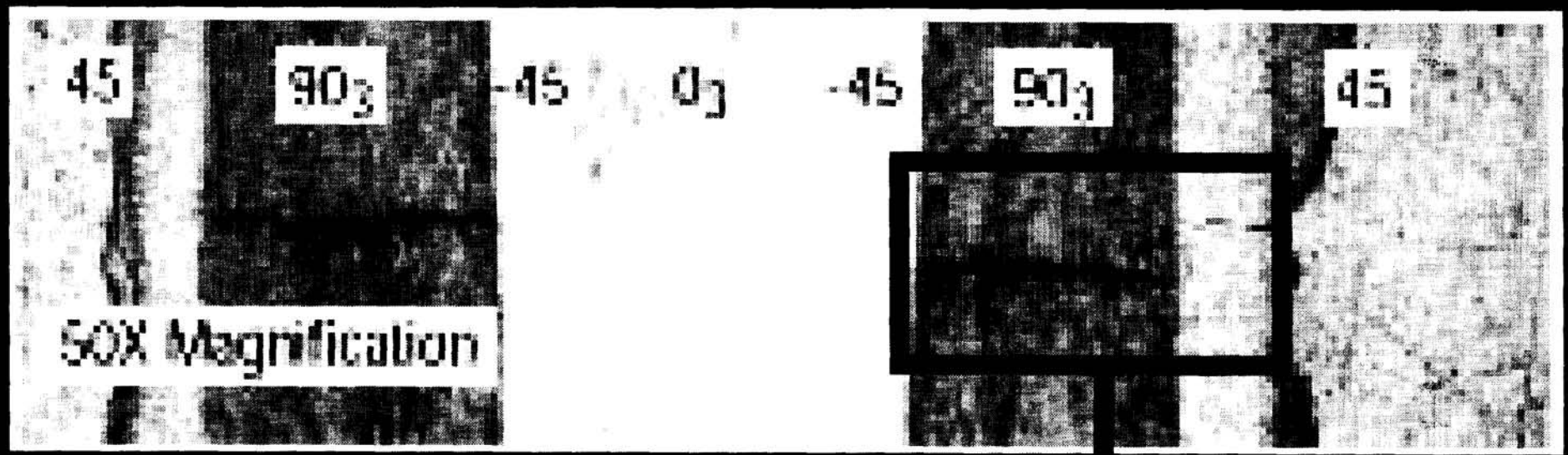
45
90$_3$
-45
0$_3$
-45
90$_3$
45
50X Magnification

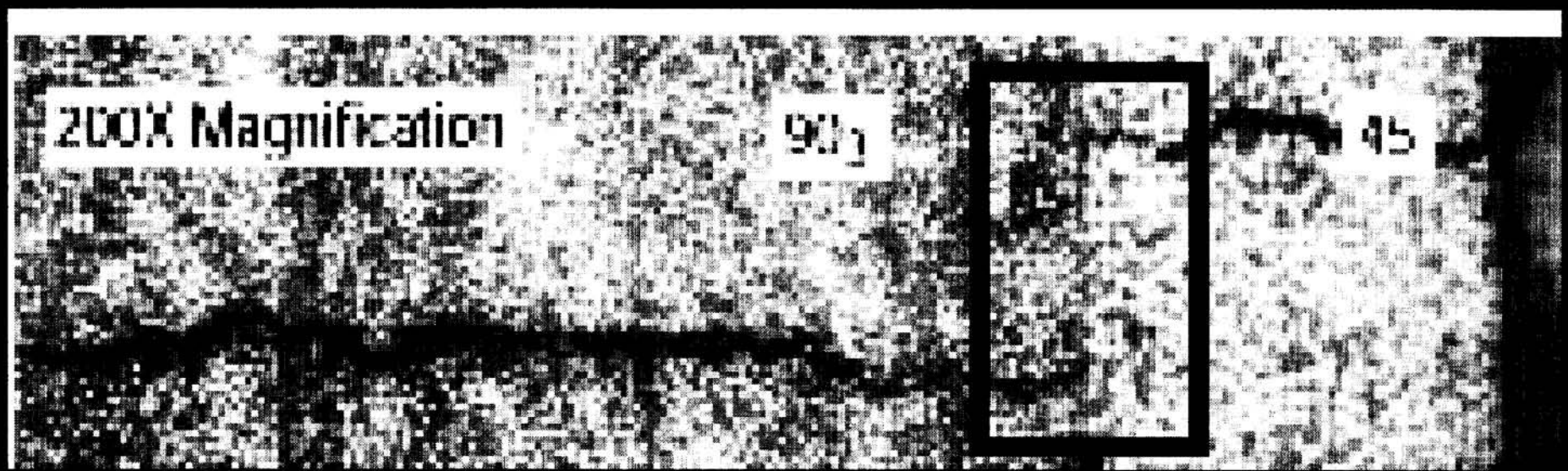
200X Magnification
90
45

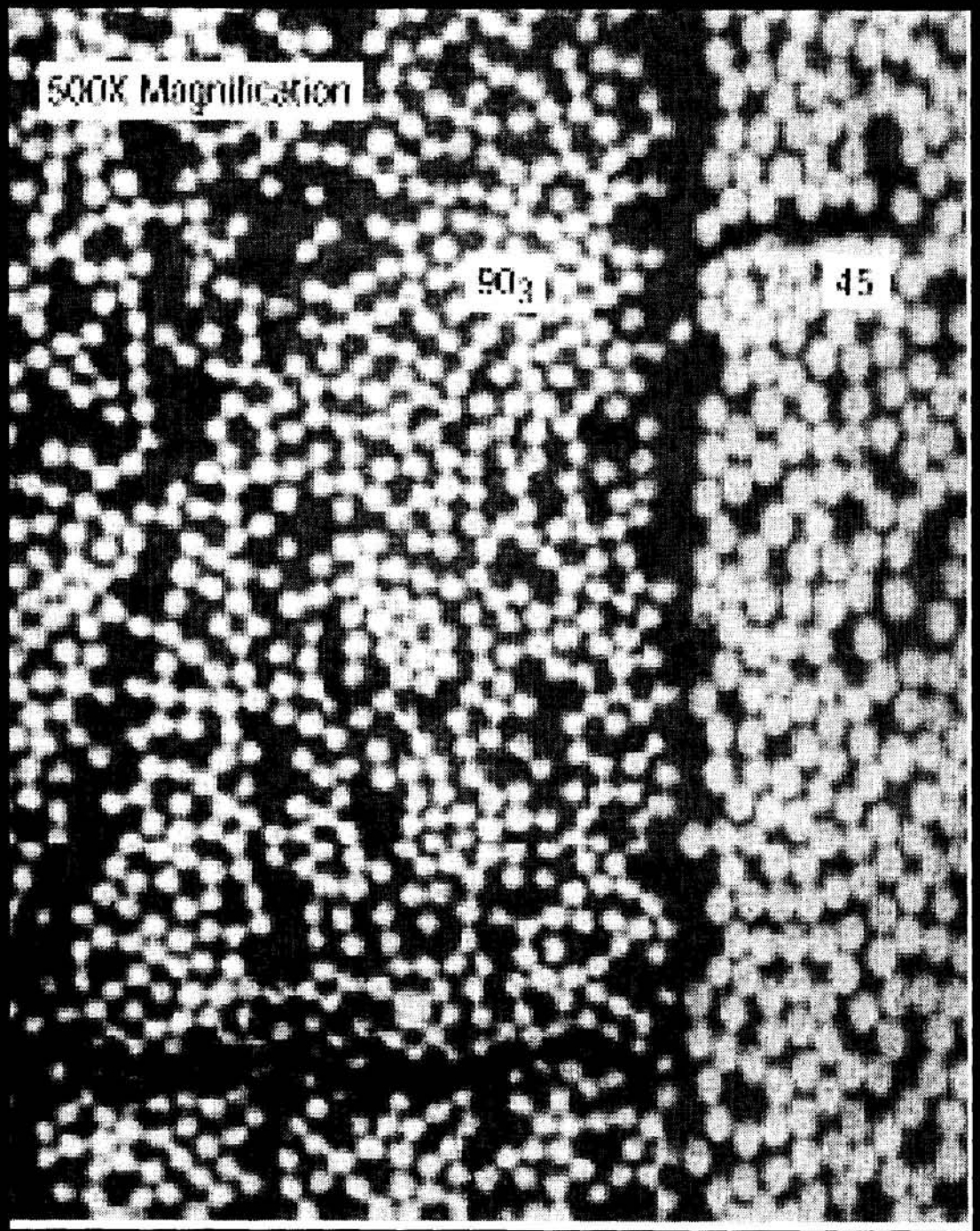
500X Magnification
90
45

X-33 LH_2 Tank Failure Investigation Findings

Conclusions

- The inner skin microcracked and hydrogen infiltrated
- The cracks grew larger under pressure
- When pressure was removed cracks closed slightly
- When tank was drained and warmed, cracks closed and blocked leak path
- FOD and debond areas provided an opportunity for a leak path
- There is still hydrogen in the other 3 lobes today

Assessment of the State-of-the-Art in the Design and Manufacturing of Large Composite Structure

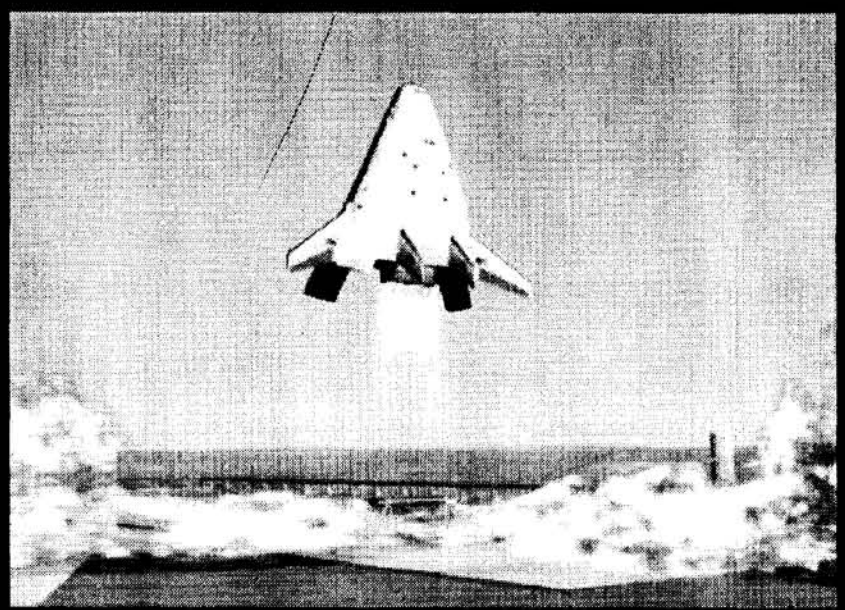

presented by
Dr. Charles E. Harris
NASA Langley Research Center

at the
4th conference on Aerospace Materials, Processes, and Environmental Technology
Von Braun Center, Huntsville, AL
September 20, 2000

03/3RD
95/N/55/05

Outline of Presentation

- Applications in Commercial and Military Aircraft
- Applications in Space Launch Vehicles
- Assessment of the State-of-the-Art
- Concluding Remarks

Scope of the Assessment

Continuous Fiber Reinforced, Polymer matrix composites (CFRP) in vehicle structure

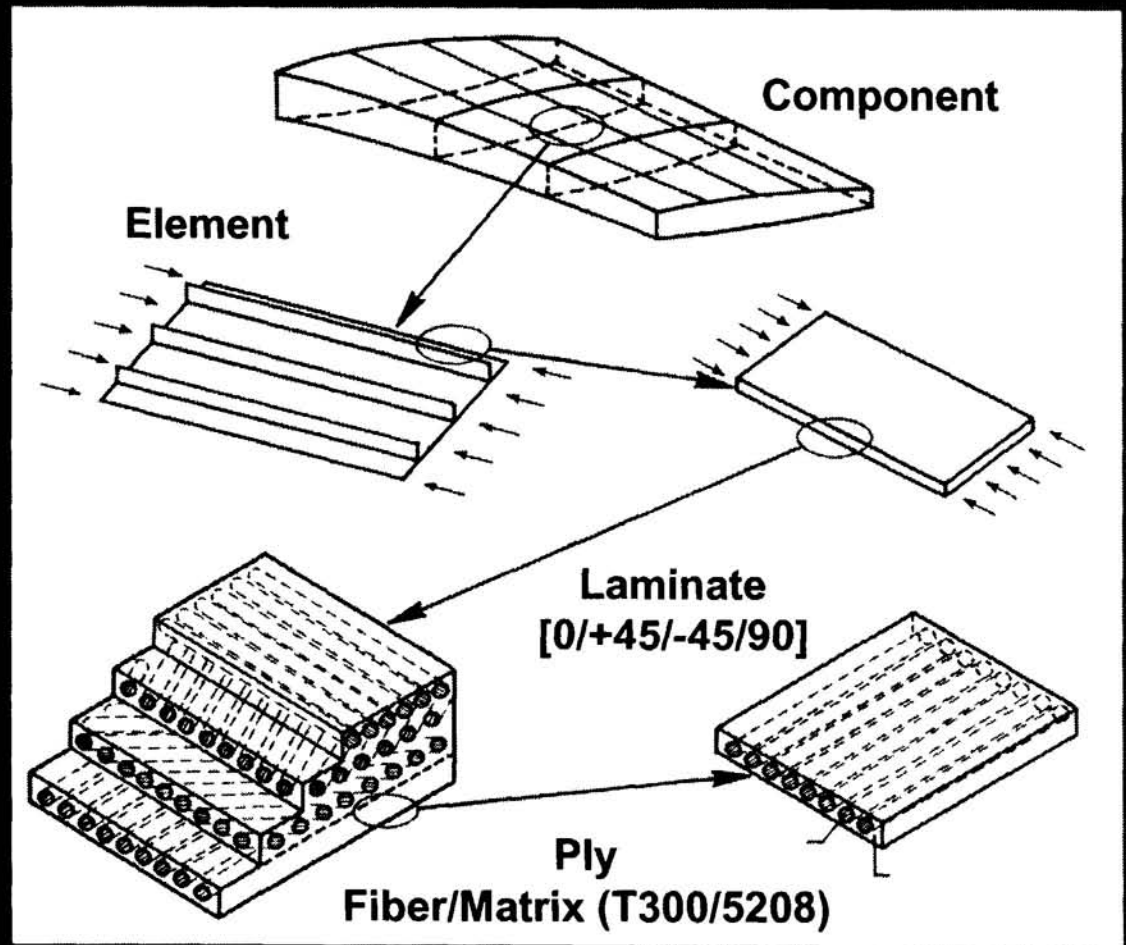

Assessment Team

Raymond G. Clinton, MSFC
H. Benson Dexter, LARC
Charles E. Harris, LARC
Norman J. Johnston, LARC
Eric I. Madaras, LARC
Charles A. Meyers, MSFC
J. Wayne Sawyer, LARC
James H. Starnes, Jr., LARC

Historical Development of Structural Composites

- Applications in Commercial Aircraft
- Applications in Military Aircraft

Composites in Commercial Transport Aircraft

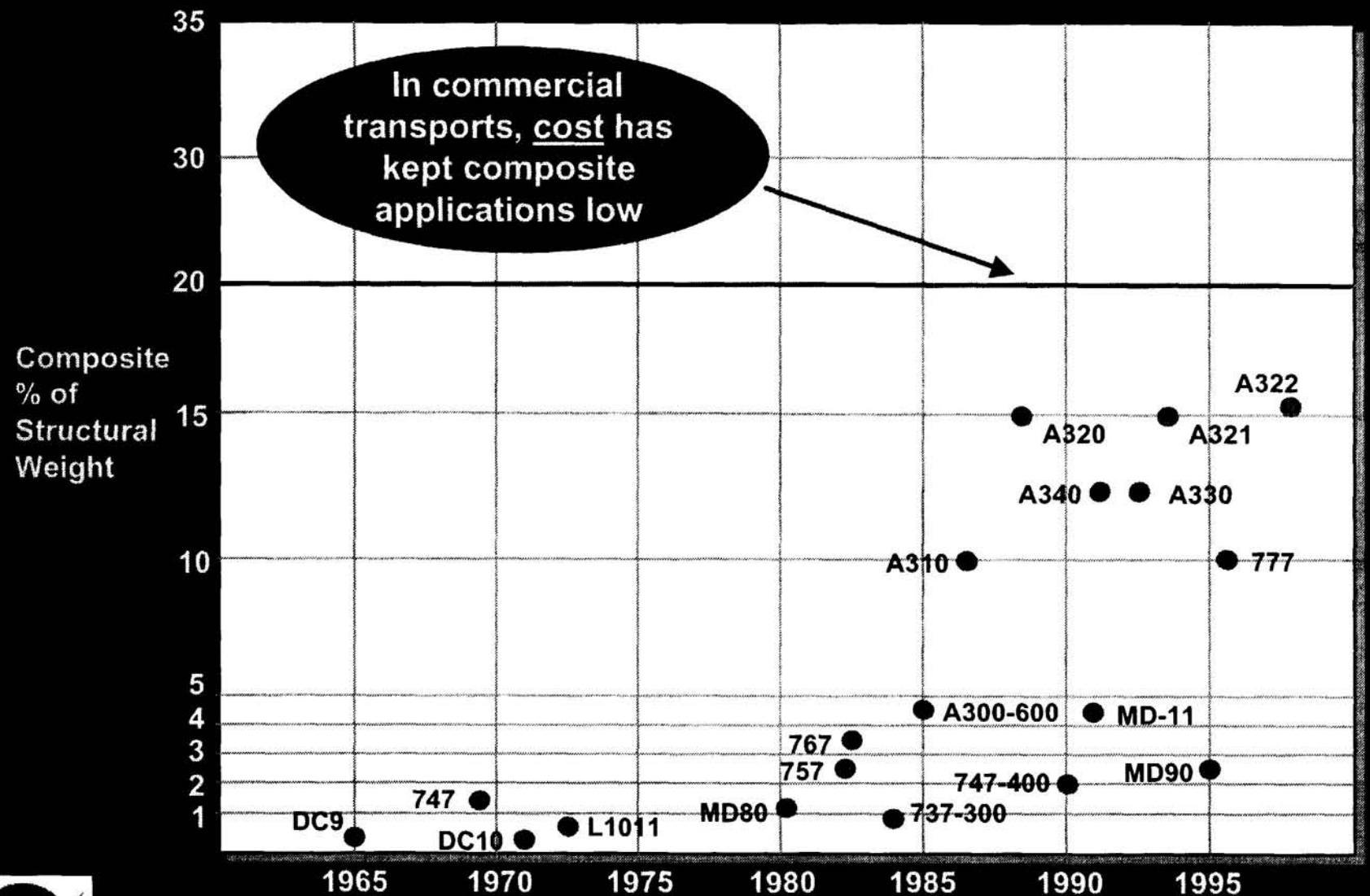

General Aviation Aircraft and Rotorcraft

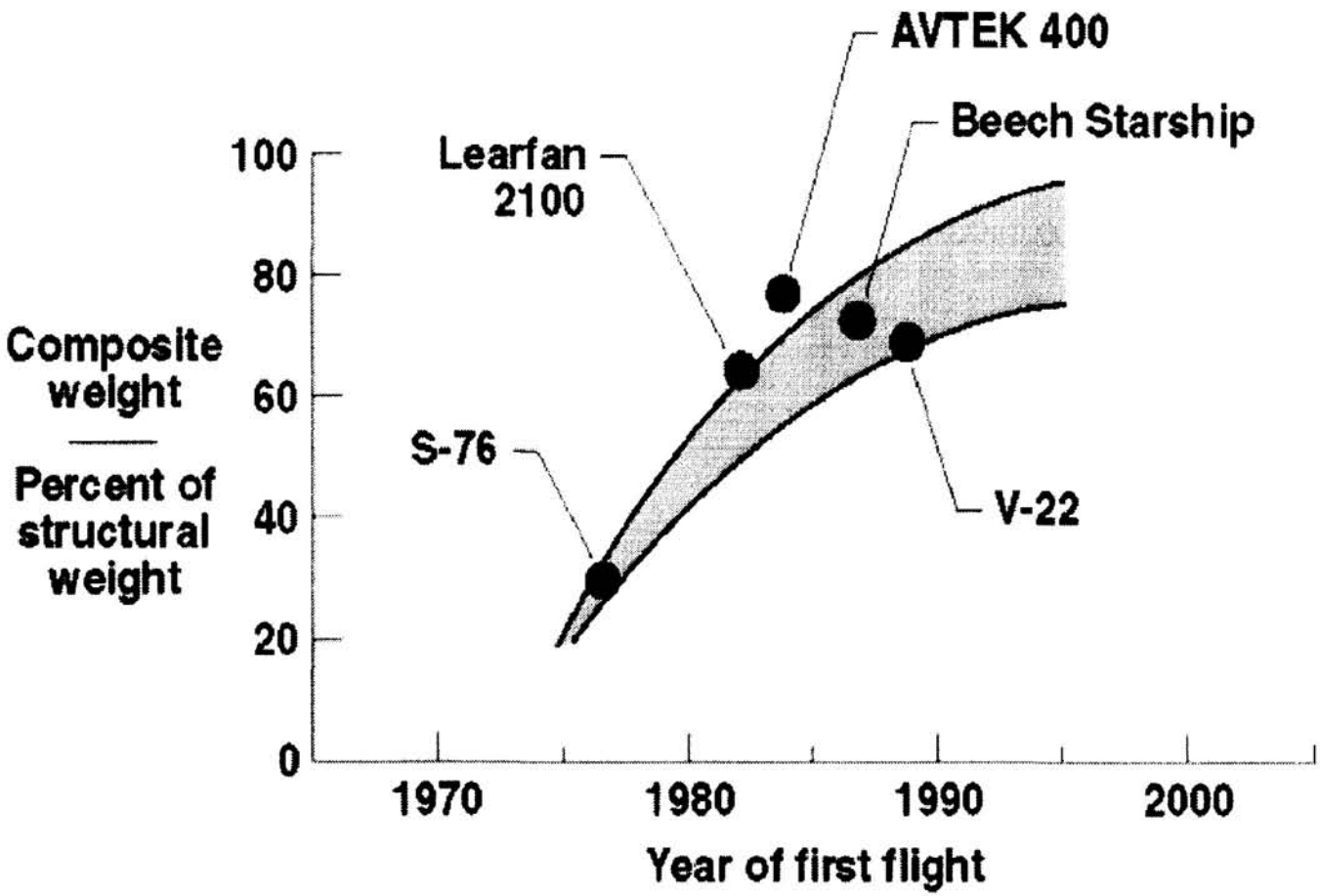

Composite Applications in Military Fighter Aircraft

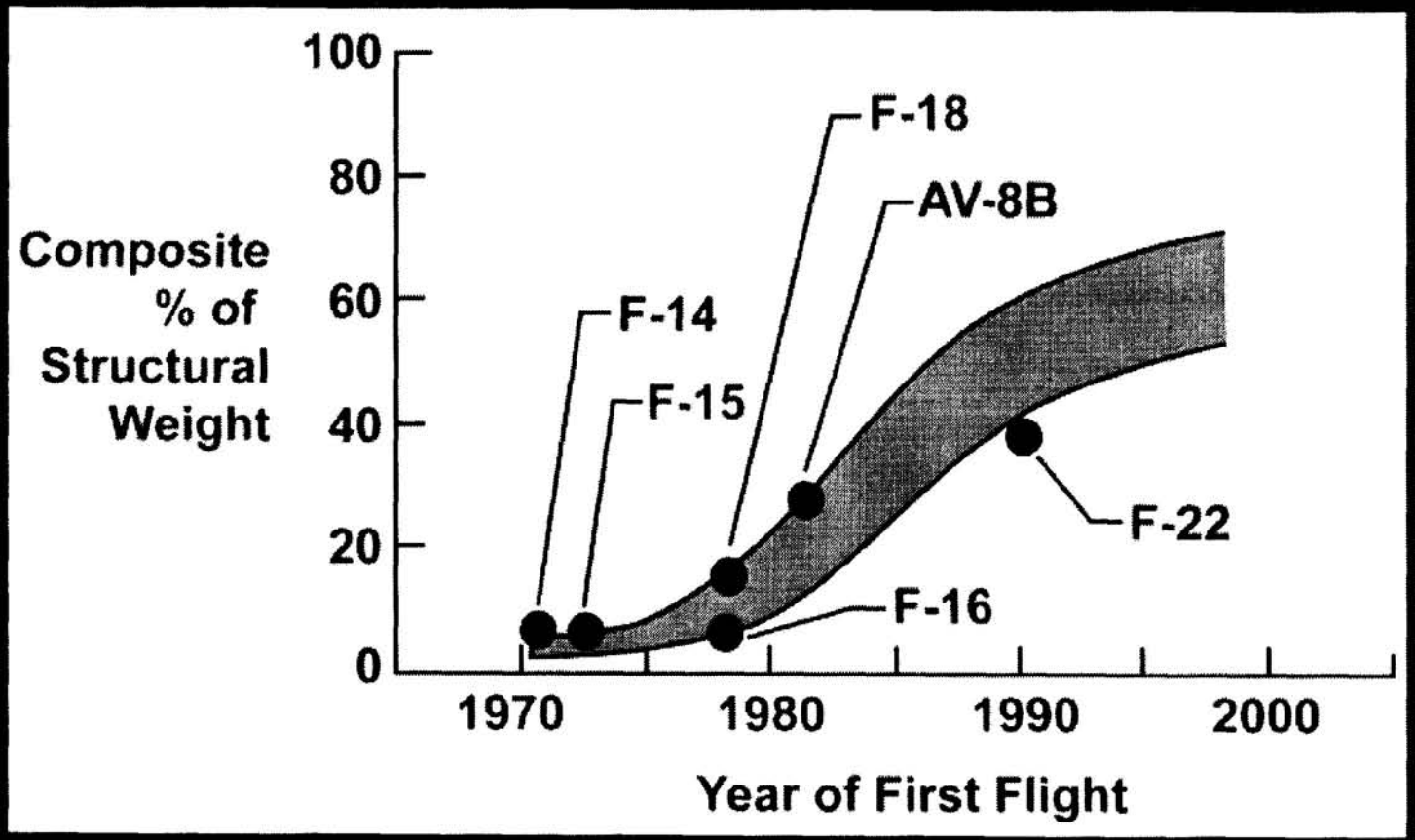

Performance and weight drivers have led to significant levels of composite application

Structural Composites on the B-777

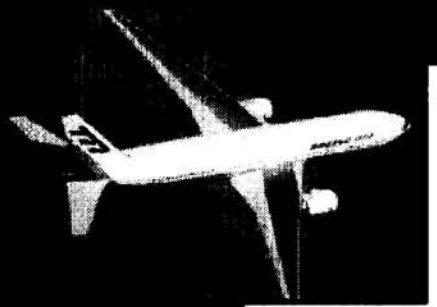

777 composite structure:

- Toughened materials for improved damage resistance and damage tolerance
- Designed for simple, low-temperature bolted repairs
- Corrosion and fatigue resistant
- Weighs less (composite empennage saves over 1,500 lb compared with prior aluminum structure)

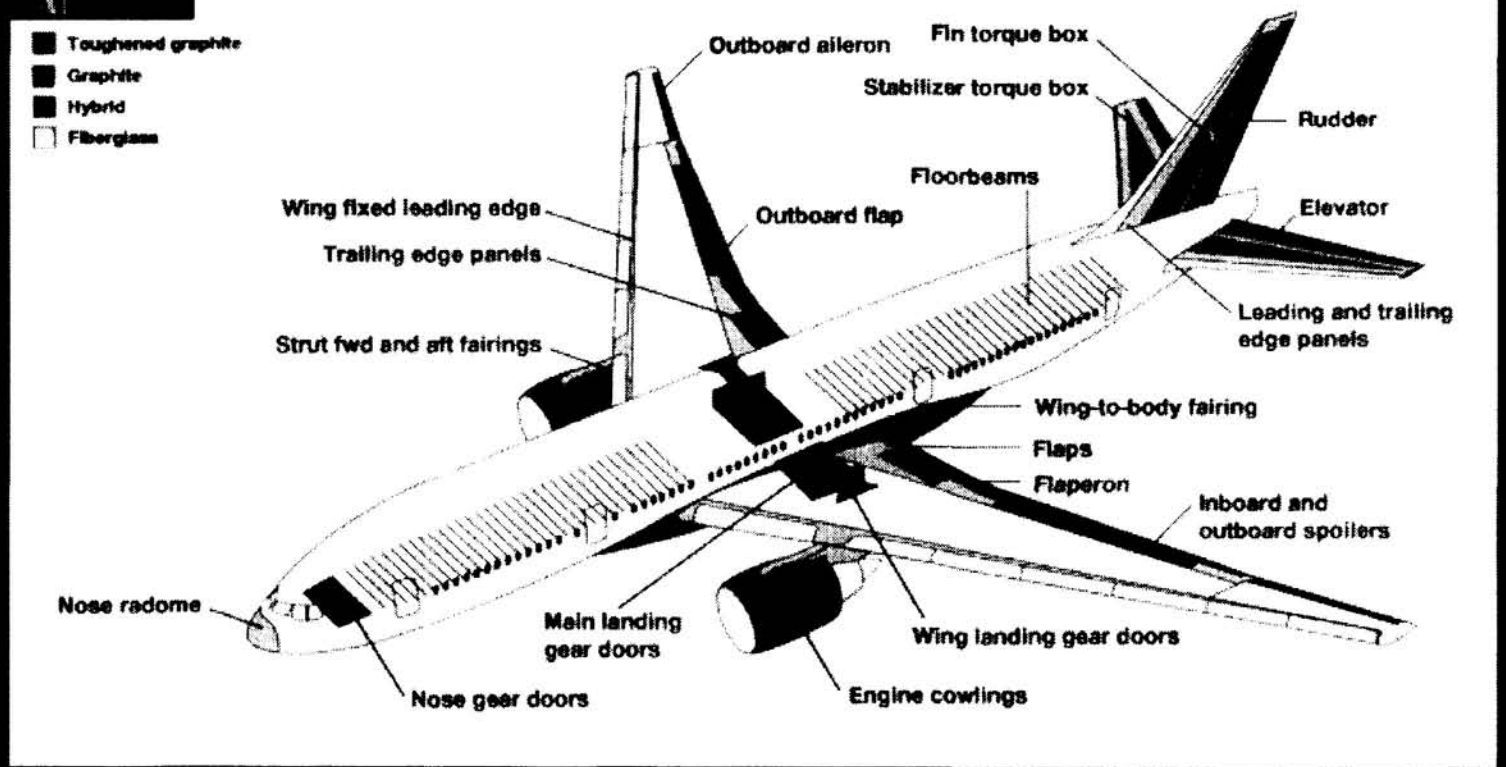

Applications of Composites on the V-22 Tiltrotor Aircraft

- Approximately 41% of the airframe is composites
- Wing is IM6 / epoxy and the fuselage and tail is AS4 / epoxy

F-22 Structural Materials is about 25% CFRP Composites

- Wing skins are monolithic graphite / bismaleimide
- Horizontal and vertical stabilizers are graphite / bismaleimide

B-2 Primary Structure Is Almost All Composites

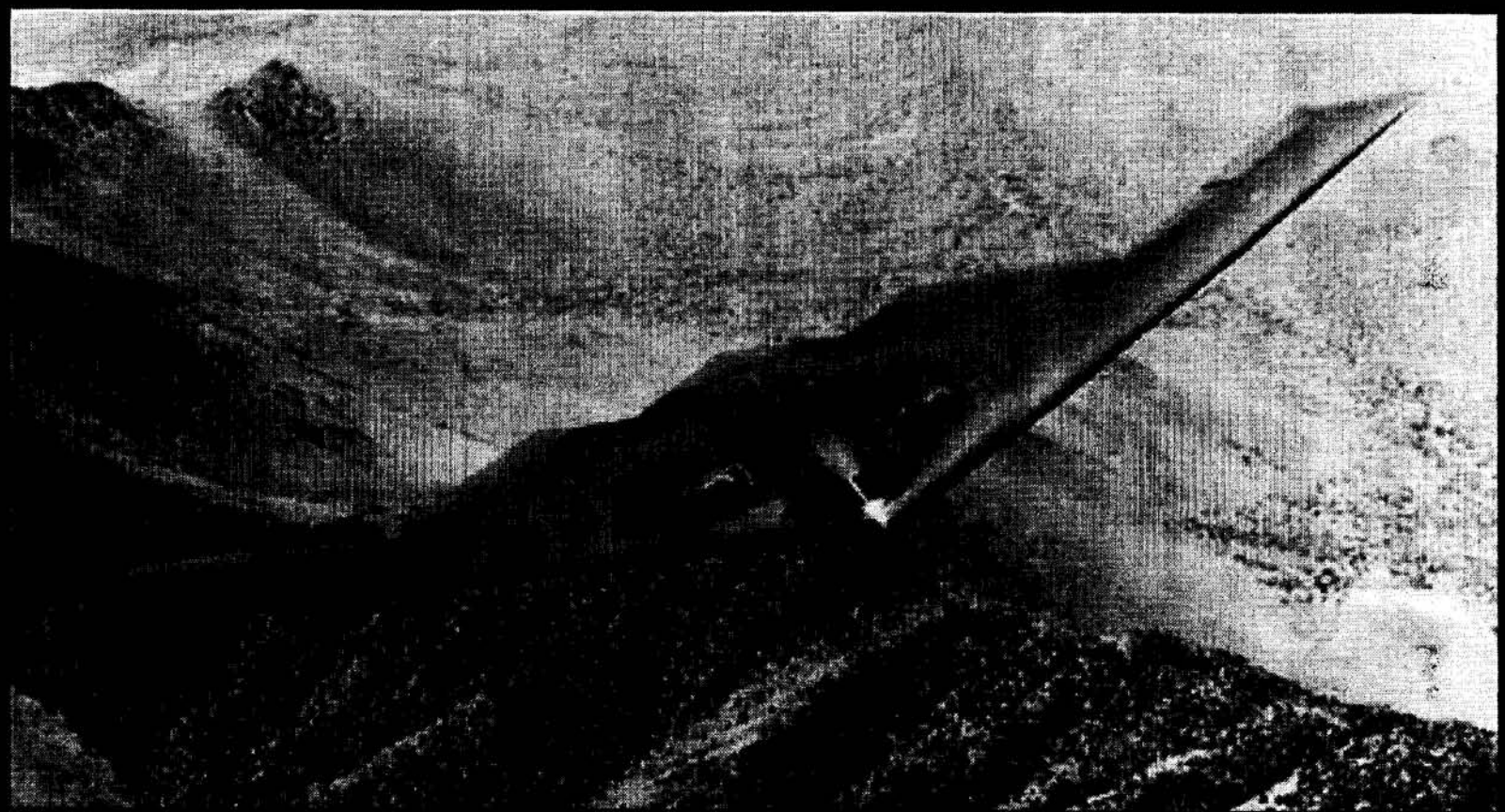

- First flight test was July 17, 1989
- Wing is almost as large as B-747 (span of 172 ft and 5,140 ft^2)
- Wing Box: composite covers and substructure
- Fuselage: composite forward, mid, rear, and internal members

Applications in Space Transportation Vehicles

- Structural Composites on Delta Launch Vehicles
- DC-XA Technology Components
- X-33 Liquid Hydrogen Tank

Structural Composites on Delta Launch Vehicles

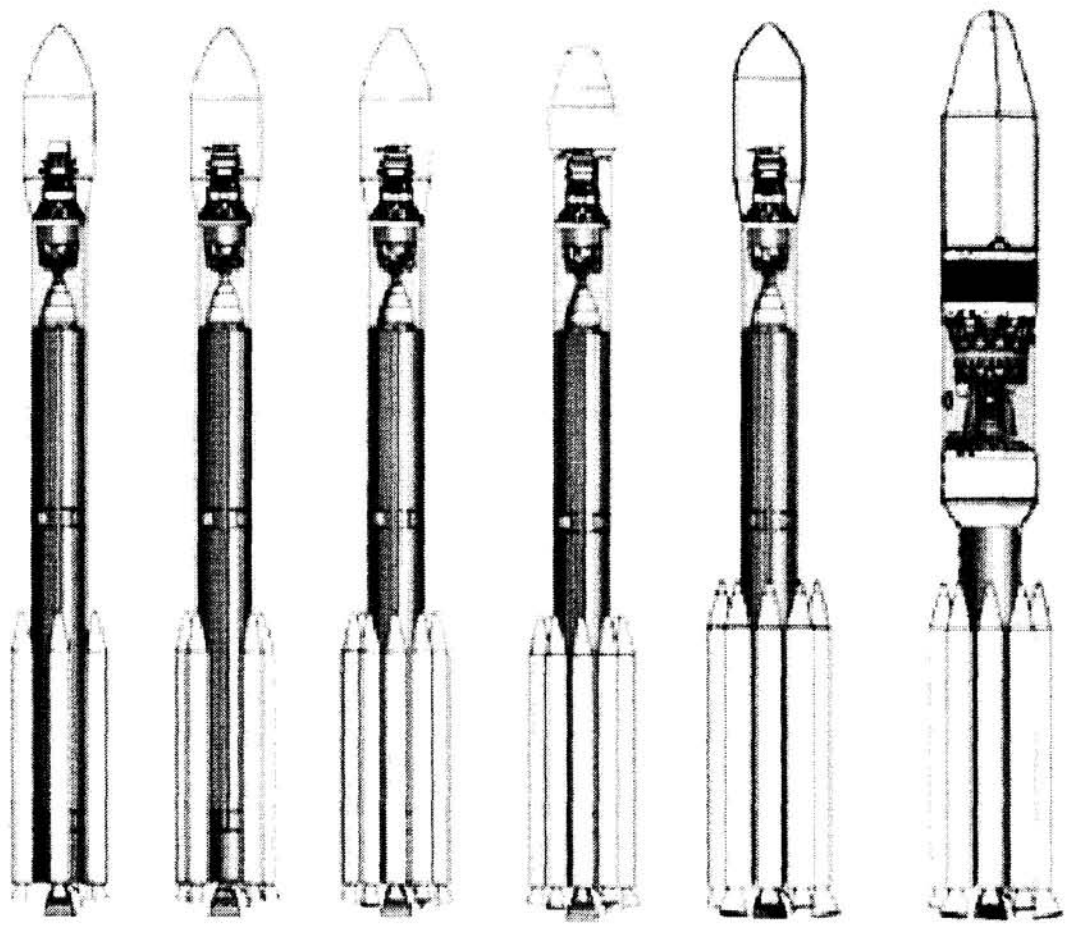

Delta II (7326-10) | Delta II (7425-10) | Delta II (7925-10) | Delta II (7925) | Delta II (7925 H10) | Delta III

DC-XA Technology Components

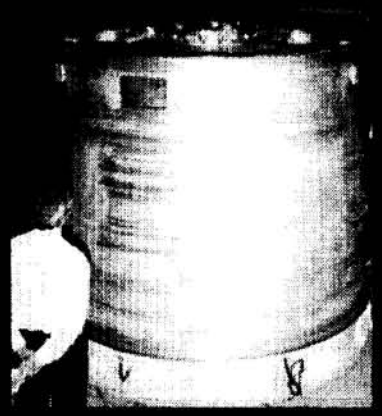

Aluminum-Lithium
LO_2 Tank

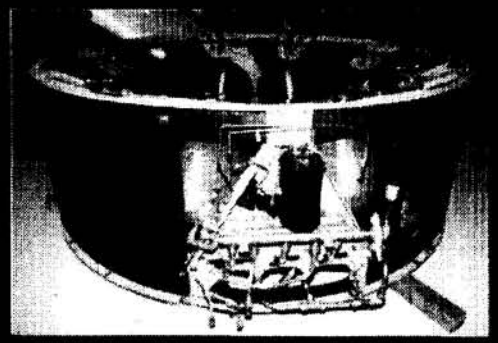

Composite Intertank

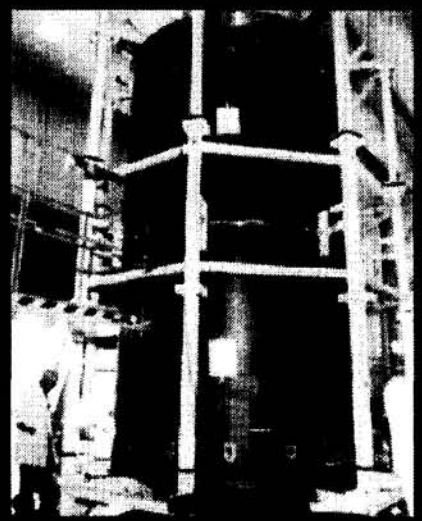

Composite LH_2 Tank

DC-XA Composite Intertank

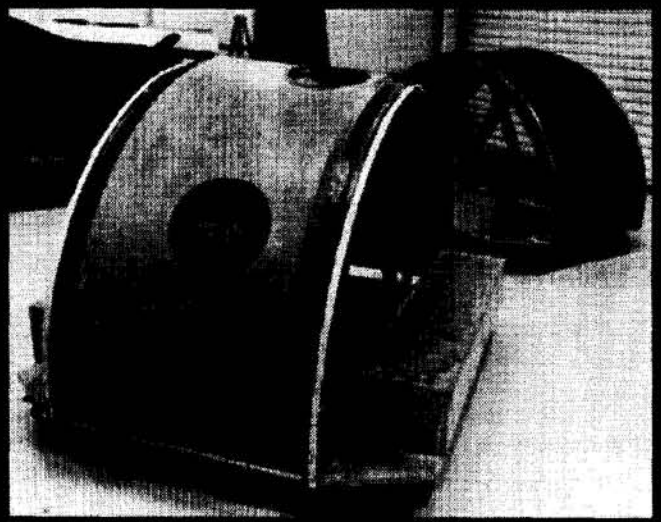

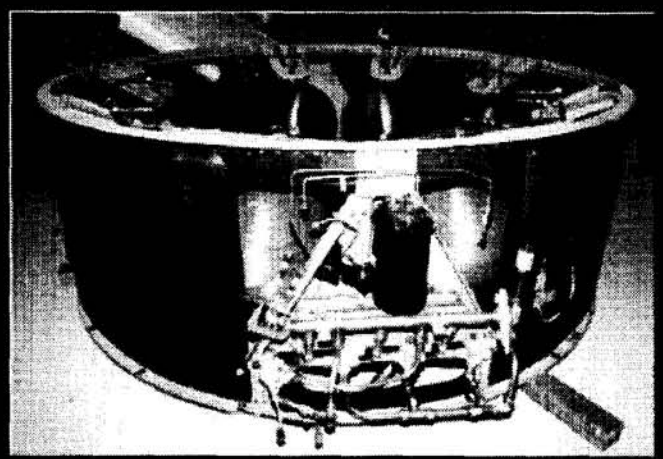

Design and Fabrication

- 2 semi-circular pieces bolted together
- IM7/5250-4 graphite / bismaleimide
- Aluminum honeycomb core
- 44% weight savings over DC-X

Development History

- First semi-circular part failed during fabrication due to rupture of the core
- Process changed by lowering post-cure temperature that avoided outgassing
- Successful ground tested at MSFC

Flight Test History

- 3 DC-XA flight tests

DC-XA Composite Liquid Hydrogen Cryotank

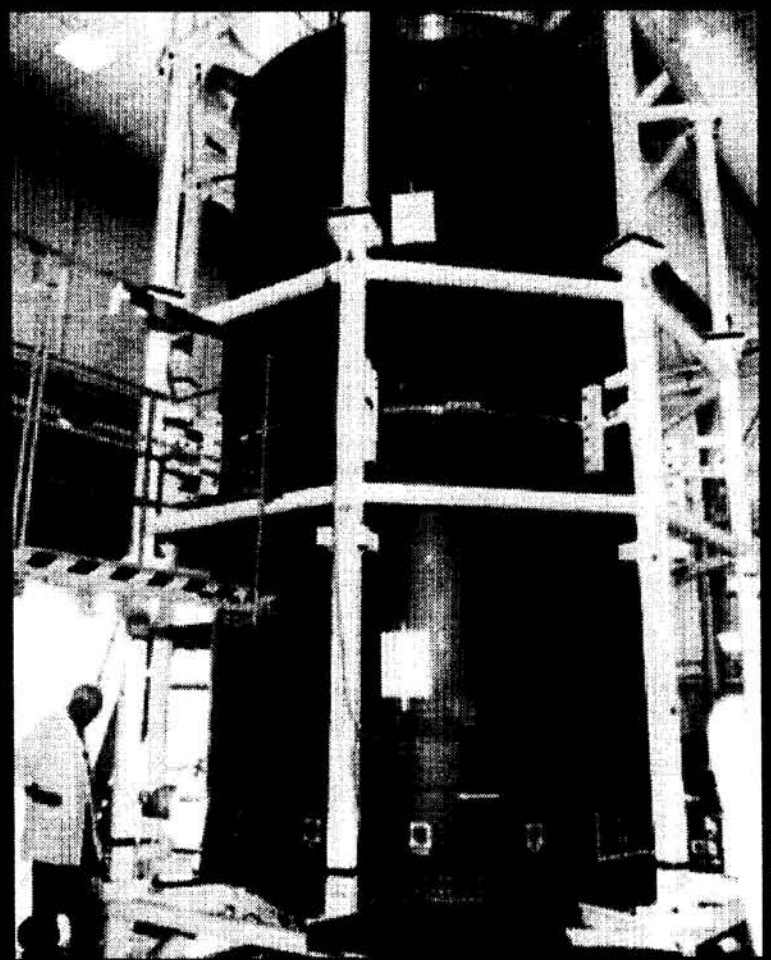

Design and Fabrication

- 2 cylindrical pieces, bonded splice joint
- 24-ply IM7/8552 graphite / epoxy
- Internal 3-D reinforcement urethane foam insulation
- 34% weight savings over DC-X tank

Development History

- Repaired damage from shop accident
- Insulation separated from tank wall
- Successfully ground tested at MSFC

Flight Test History

- 3 DC-XA flight tests

X-33 Composite Liquid Hydrogen Tank

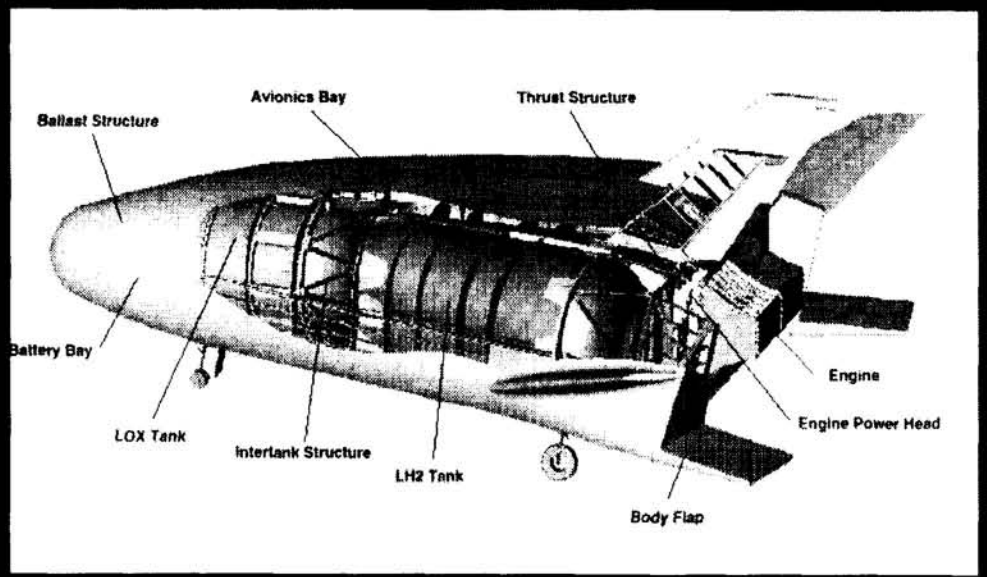

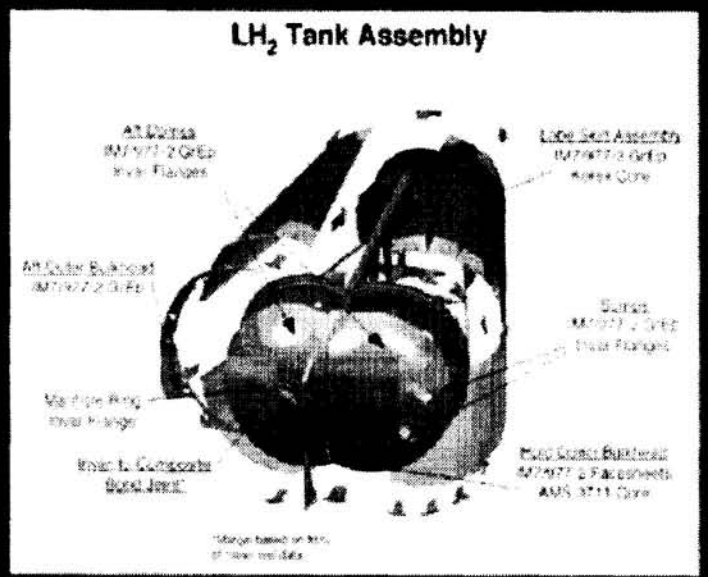

- Composite structural design was the highest risk concept
- Project recovery plan addressed as-fabricated tank weaknesses
- Tank failed in the ground test as a result of several causal factors

Assessment of the State-of-the-Art

- Lessons learned
- Assessment of the technology readiness
- The current state-of-the-art

Technology Readiness Levels (TRL)

1 - 3 Research
4 - 6 Technology Development
7 - 9 Advanced Vehicle Development

Materials, Processes, and Manufacturing

Lessons Learned

1. Materials development in conjunction with product development creates undue risks.

2. Experienced materials and processing engineers should be included in the design phase and must be readily available to correct problems in production processes.

3. Manufacturing process scale-up development tests should be conducted to optimize the production processes.

4. Co-curing and co-bonding are preferred over secondary bonding which requires near perfect interface fit-up.

5. Mechanically fastened joints require close tolerance fit-up and shimming to assure a good fit and to avoid damage to the composite parts during assembly.

6. Dimensional tolerances are more critical in composites than in metals to avoid damage to parts during assembly. Quality tools are essential to the production of quality parts.

7. Selection of the tool material depends on part size, configuration, production rate, quantity, and company experience.

8. Tool designers should anticipate the need to modify tools to adjust for part springback, ease of removal, or maintain dimensional control of critical interfaces.

Evolution of Composite Materials (Matrix) Development

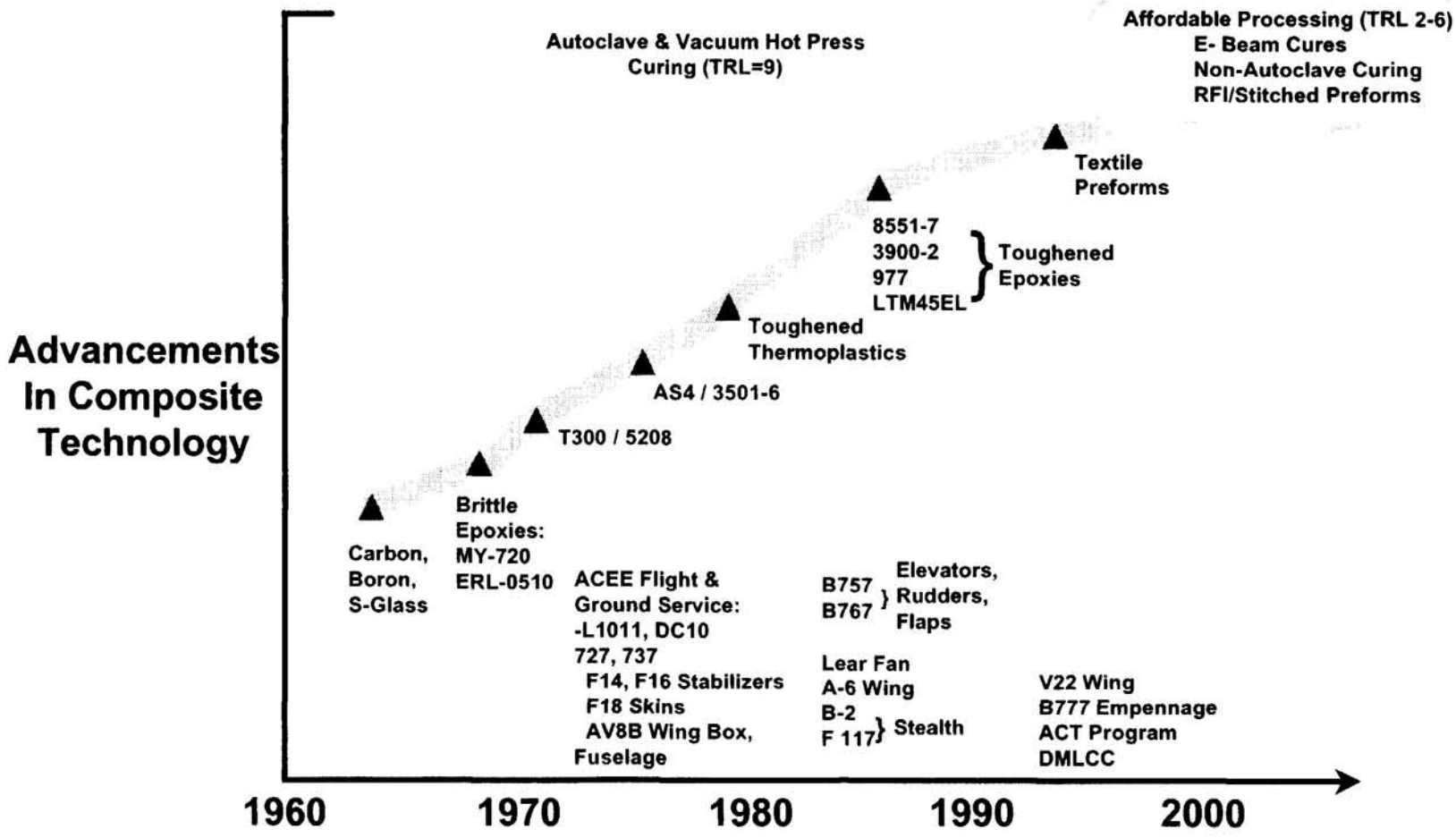

Structural Design, Analysis, and Testing

Lessons Learned

1. Design and certification requirements for composite structure are generally more complex and conservative than for metal structure.

2. Successful programs have used the building-block approach with a realistic schedule that allows for a systematic development effort.

3. The use of basic laminates containing 0/90/+45/-45 plies with a minimum of 10% of the plies in each direction is well suited to most applications.

4. Mechanical joints should be restricted to attachment of metal fittings and situations where assembly or access is impractical using alternative approaches.

5. Large, co-cured assemblies reduce part count and assembly costs but may require complex tooling.

6. Structural designs and the associated tooling should be able to accommodate design changes associated with the inevitable increases in design loads.

7. Understanding and properly characterizing impact damage would eliminate confusion in the design process and permit direct comparison of test data.

Current Practice: Test-Based Building-Block Approach

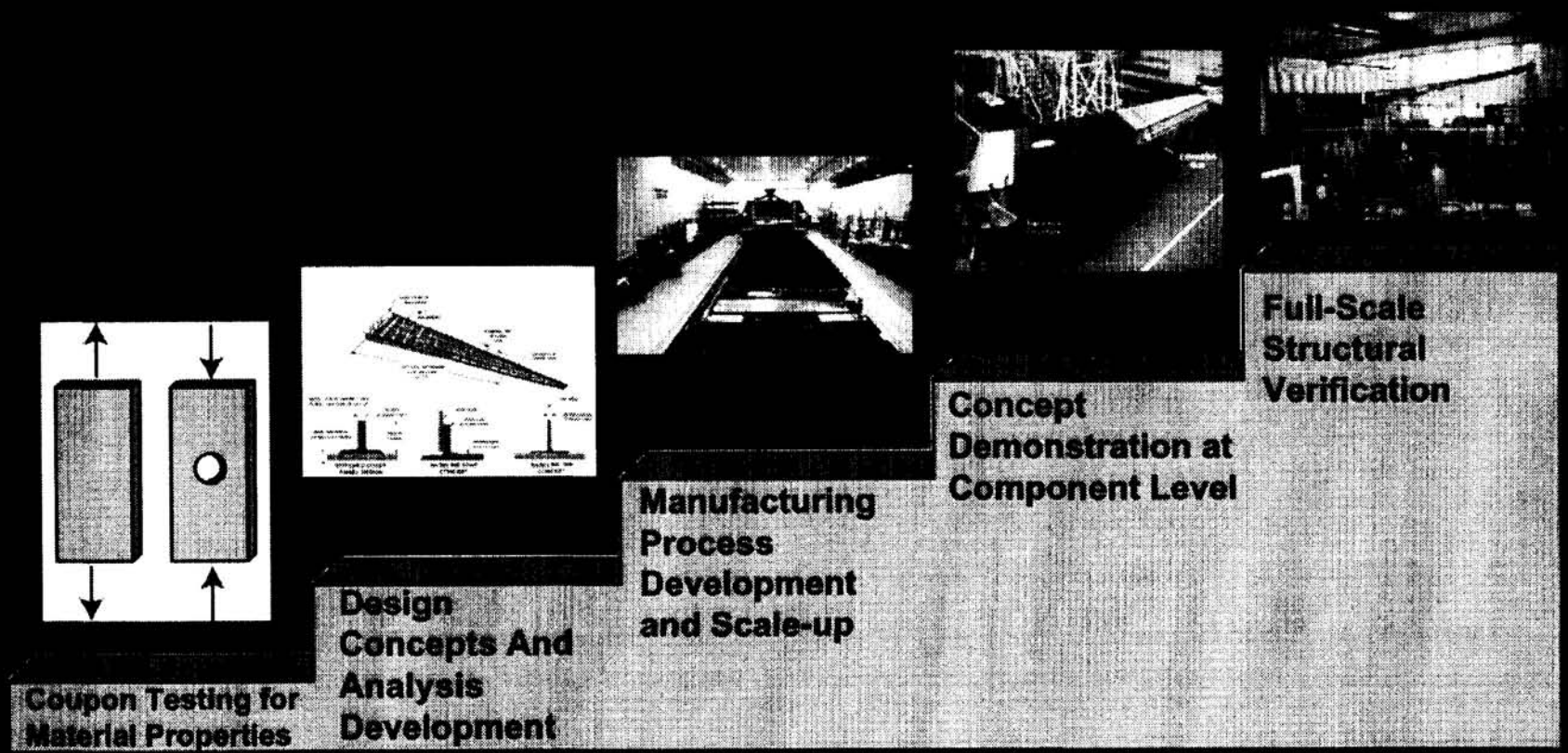

R&D Goals: Physics-based computational methods (TRL = 4-6) and reliability-based design methods (TRL = 3)

Quality Control, Inspection, and Supportability

Lessons Learned

1. Automated processes can help to reduce QC costs.
2. Inspection and quality control should focus on aspects of the process and part that have a direct bearing on part performance.
3. Determine and understand the effects of defects on part performance.
4. **Supportability should be addressed during design so that composite structures are inspectable, maintainable and repairable.**
5. Most damage to composite structure occurs during assembly or routine maintenance of the aircraft.
6. Repair costs are much higher than for metal structures.
7. Improved Standard Repair Manuals are needed for in-service maintenance and repair.
8. Special long-life and low-temperature curing repair materials are required.
9. Moisture ingestion and aluminum core corrosion are recurring supportability problems for honeycomb structures.

Development of Nondestructive Inspection (NDI) Methods

Detection of damage using nondestructive inspection

- Porosity, Fiber Orientation
- Disbonds, Delaminations, Cracks
- Processing Quality Control

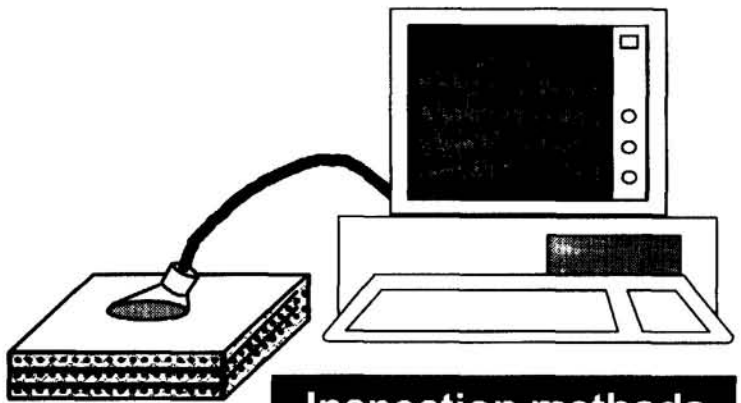

Inspection methods

- X-Ray
- Ultrasonic
- Thermal
- Electromagnetic
- Optical

Evolution of NDI Technology

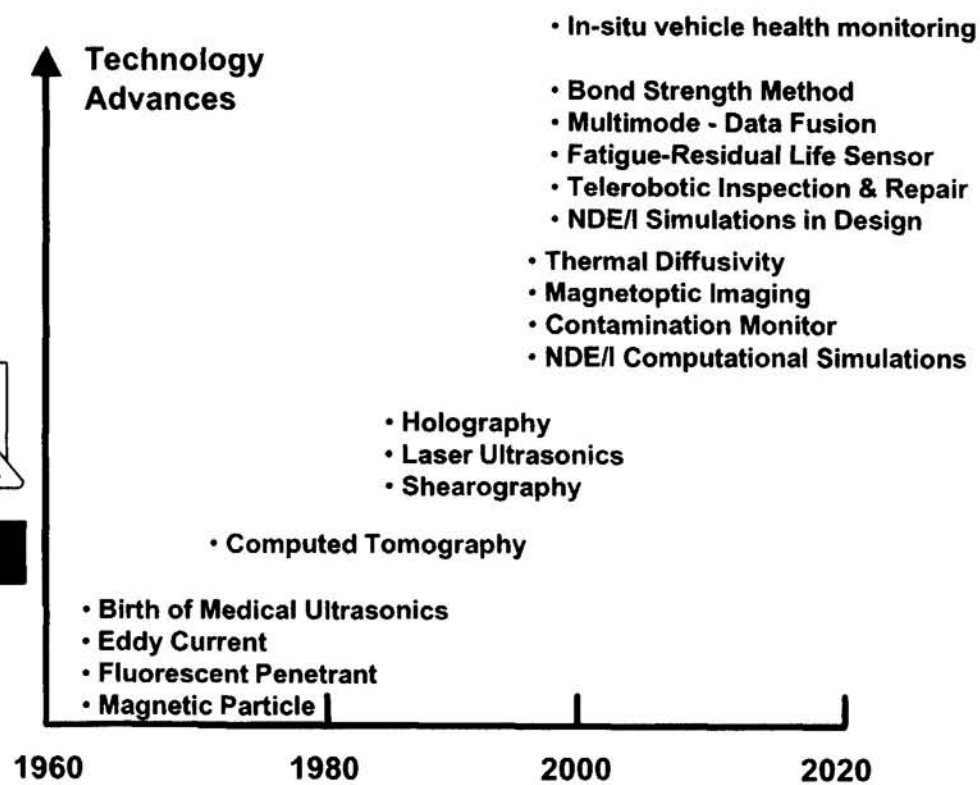

TRLs vary from 3 to 9, depending on detection objective

Summary of The Current State-Of-The-Art

- Designing a composite structure is not the same as designing a metallic structure
- A composite material must be "designed" for each specific structural application
- Composite materials exhibit brittle failure mechanisms that are not well understood
- Fabrication processes are still evolving and fabrication costs are not accurately predictable
- The industrial infrastructure for engineering design and manufacturing of composites is not fully developed

Engineering Infrastructure is Created Through Design Development Experiences

Engineer Career Length Vs. New Designs By Decade

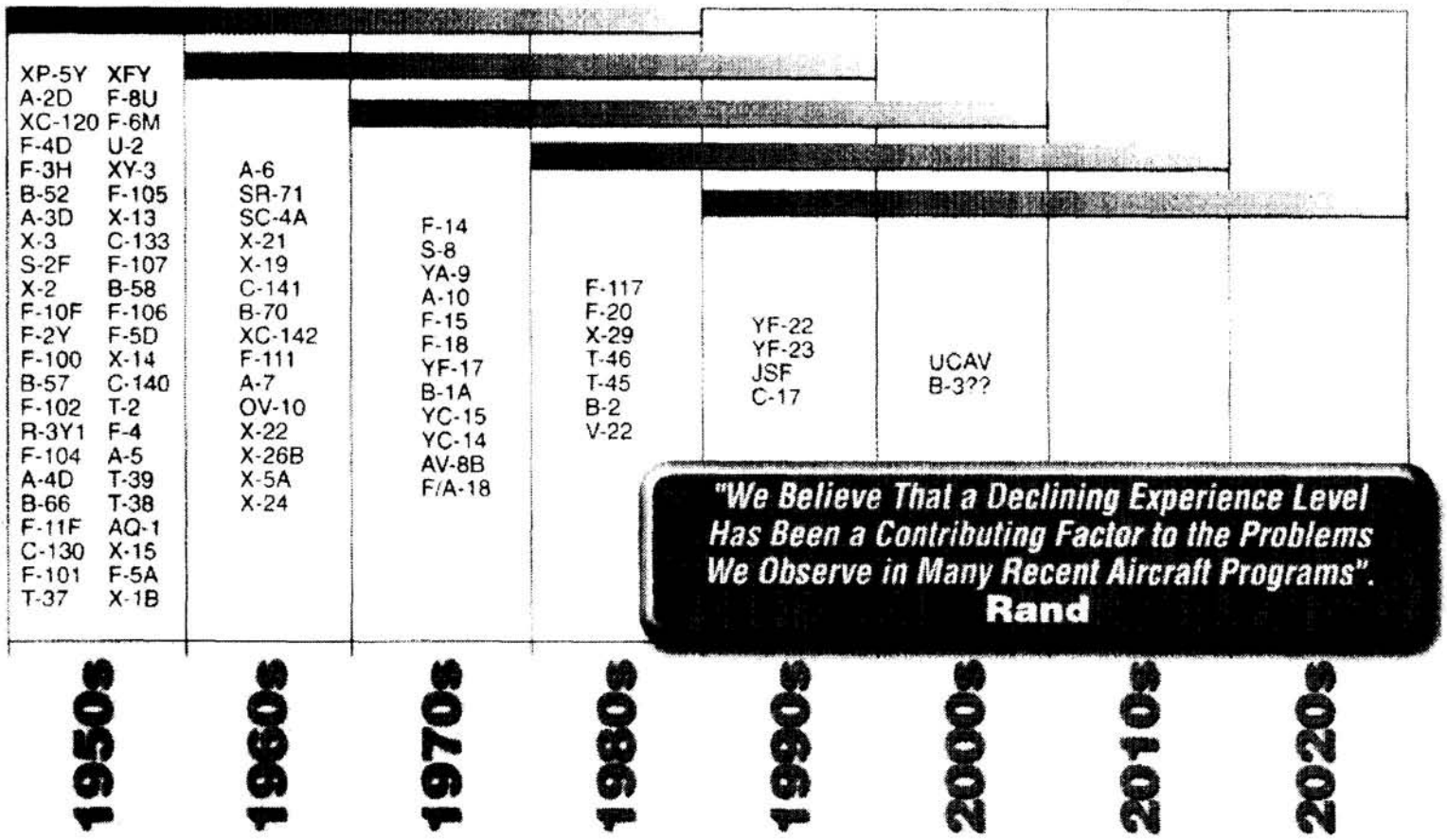

"We Believe That a Declining Experience Level Has Been a Contributing Factor to the Problems We Observe in Many Recent Aircraft Programs".
Rand

Note: Rand study assumes 40-year career length

Concluding Remarks

- Project **risk mitigation plans** must include a building- block test approach to structural design development, manufacturing process scale-up development tests, and pre-flight ground test to verify structural integrity.

- **Stay the course!** The potential benefits of composite structures justifies the Agency investment in developing the technology. Advanced composite structures technology is enabling to virtually every Aero-Space Technology Enterprise Goal.

A Mass Spectrometer-Based Tool for In-Process Analysis of RSRM Components

MICHAEL MELTZER

Lawrence Livermore National Laboratory/L-627
7000 East Avenue
Livermore, CA 94550-9234 USA
Phone: 925-424-6923
Fax: 925-422-4038
E-mail: meltzer1@llnl.gov

Carolyn Koester
Lawrence Livermore National Laboratory/L-542
7000 East Avenue
Livermore, CA 94550-9234 USA
Phone: 925-422-6888
Fax: 925-423-7998
E-mail: koester1@llnl.gov

Neil Sagers
Thiokol Propulsion
231 N. Burns
Ogden, UT 84404 USA
Phone: 435-863-6116
Fax: 435-863-5509

Work to date is reported for a project testing the capabilities of a mass spectrometer-based system for analyzing *in-situ* organic compounds on a variety of substrates. The system, which was built at Lawrence Livermore National Laboratory, is termed a Contamination Analysis Unit (CAU) and employs vacuum and thermal desorption of surface residues, followed by ionization and analysis with a Leybold Inficon Transpector mass spectrometer. The CAU was employed in this study to examine soils, cleaner residues, and substrates on Space Shuttle Reusable Solid Rocket Motor (RSRM) components. Project work was supported by Thiokol Propulsion. Major project objectives include:

1. Determine if the CAU can detect solvent that has soaked into NBR insulation material
2. Test the capabilities of the CAU for analyzing non-flat surfaces on the inside and outside surfaces of the RSRM and nozzle throat housing
3. Determine if solvent extraction and gas chromatography approaches are able to enhance the surface analysis data available through use of the mass spectrometer-based CAU
4. Determine the CAU's detection limit for various RSRM soils and cleaners
5. Determine if contact of either Viton® or silicon O-rings with critical substrates will result in any visual evidence of the contact, when observed under black light.
6. Demonstrate CAU viability during routine RSRM manufacturing operations.

CP/587/IN/27

P4/2N7

Effects and Detection of Silicone and HD2 Grease Contaminants

J. W. Blanks
Thiokol Propulsion
SEHO Operations
P.O. Box 707, M/S 200
Brigham City, Utah 84302

ABSTRACT

The bond integrity of RSRM bond systems can influence the overall system safety. The minimum level of different contaminants, especially silicone oils, present before various bond systems are weakened was evaluated. Application of an infrared spectrometer was used to detect and quantify sets of contaminants on selected composites and metal substrates. Techniques for applying the contaminants are discussed. Changes occurring with time at the contaminant/substrate interface were monitored. Use was made of these techniques to prepare bond specimens for determining the lowest level of common contaminants that are detrimental to selected bond systems.

INTRODUCTION

Concern first and foremost for the safety of human life, and also the high cost of flight system hardware and payloads, has supported efforts to make the RSRM a dependable component in the Space Shuttle system. Although no major system failure has occurred because of contamination scenarios, specific bond failures do occur in laboratory prepared specimens from time to time. A search of eight years of computer archived reports on laboratory bond failure anomalies revealed the following information.

1992 – Apparent failure mode shift at bonding interfaces of flexible boot assembly (phenolic/CL-220/NBR).
Analysis results: Failure influence by thin portion of NBR. Failure mode was determined cohesive in phenolic material. No contaminants such as silicone or hydrocarbons detected.

1992 – sandblasted aluminum plate/silica filled EPDM rubber bond failure.
Analysis results: No contaminants detected known to degrade these adhesive bonds.

1992 – Adhesive failure of paint chips at Chemlok to metal case bond.
Analysis results: No detected silicone or hydrocarbon contaminant.

1994 – Monel wire mesh unbond in polysulfide peel tabs.
Analysis results: exposed wire mesh exhibited traces of hydrocarbon, which may have acted as mold release.

1994 – Failed tensile adhesion buttons, EA913/primer/metal interface.
Analysis results: Examined to verify presence of primer. Primer not detected. Examination revealed thin layer of EA913 on metal surface therefore cohesive failure.

1995 – RTV/RTV unbond where voids were backfilled.
Analysis results: CONOCO HD-2 grease present on surface of cured RTV.

1995 – Adhesive failure of cork to zinc rich primer.
Analysis results – Primer solvents detected. Perhaps not enough primer drying time.

Copyright 2000 Thiokol Propulsion, a division of Cordant Technologies, Inc., All rights reserved.
Approved for public release; distribution is unlimited.

1996 – Weak bond strength within Chemlok 236.
Analysis results: No obvious chemical reason revealed for the failure.

1996 – Liner to liner separation, TL-H755/TL-H770
Analysis results: Adhesive mixes noted as not being mixed uniformly evidenced by pockets of uncured adhesive in bulk of material. No contaminants detected.

1998 – Bond study - 0.5 mg/ft^2 silicone can weaken EA-913/D6AC steel bond system to an unacceptable level.

Processing errors, such as insufficient drying time or abnormal component thickness caused several of the above anomalies. Contaminants are only seldom detected. The most common surface sampling technique consists of chloroform wipe followed by infrared analysis of extracted material. Common contaminants requested for detection include various tape adhesive residues, silicone, hydrocarbon oils and greases, HD-2 grease, dirt, vacuum putty, and poorly mixed materials. Improvements in instrumentation now allow direct spectra collection on the suspect surface and much lower detection limits, especially on grit blasted metal surfaces.

The standard surface preparation for all bonded metal surfaces includes solvent cleaning and grit blasting steps. Examination of these surfaces before bonding shows only microscopic traces of grit blast media. Composite surfaces are solvent cleaned before bonding.

Although the initial intent of this paper was to report results from a broad bond study to correlate silicone contaminant levels on numerous RSRM bond interfaces, that program was delayed while various other contamination issues were resolved. Therefore, this paper now entails discussion and results of several contamination issues.

Composites

After years of evaluating various analytical tools to detect and quantify contaminants on metal surfaces, an infrared spectrometer, model SOC400, was selected as the primary choice. Other tools examined included near infrared spectrometers, Flash UV Imaging system, OSEE, and black light. The Flask UV Imaging system is applicable to fluorescing contaminants. Since contaminants occasionally appear on composite surfaces, experiments were performed to determine the best tool for this type problem. Composites evaluated included surfaces of silica glass phenolic (SGP), carbon cloth phenolic (CCP), fiberglass phenolic (FGP), and graphite epoxy (GE). A set of D6AC steel coupons was contaminated at the same level.

Standards

Calibration standards were prepared using an ultrasonic sprayer made by Sono-Tek Corporation. A solution of HD-2 grease dissolved in methyl chloroform was sprayed onto 2x3 inch composite coupons. The quantity of applied contaminant was determined by simultaneously spraying a tared foil specimen, weighing the foil after drying and assuming the concentration of contaminant on the coupon and foil were identical. The target levels were 1, 5, 10, and 20 mg/sqft. The measured levels are displayed in Table 1.

SOC400 Infrared Spectrometer Data

Spectra were collected on the SOC400 Fourier transform infrared spectrophotometer, 50 scans, 4 cm^{-1} resolution, 4000 to 650 cm^{-1} spectral width, at a non-contact head distance of 0.04-0.06 inches. The 2x3 inch coupons were examined at 9 equally spaced locations to obtain an average contaminant value. A background or reference spectrum was taken on clean grit blasted D6AC steel. Spectra were initially taken on specimens of each clean composite. Significant variation was detected in the spectra at different locations depending on the relative ratios of binder to filler in the field of vision. The spectral energy reflected from the composites containing carbon and graphite was quite low compared to the energy from the other type composites containing no carbon polymorphs. The model for HD2 grease on the D6AC steel is presented in Figure 1 showing a linear relationship

between HD2 grease and absorption at two selected wavelengths. The infrared peak at 2922 cm^{-1} is due to the hydrocarbon in HD2 grease, while the peak at 1409 cm^{-1} is from a carbonate constituent. Past calibration models for HD2 grease on steel and aluminum have chosen the 1409 cm^{-1} peak for most accurate quantification. However when one looks for this peak in the spectra of the HD2 grease contaminated composites, no peak is detected. Either the carbonate reacts with some component on the composite surface or it is hiding in holes on the surface. Figure 2 displays the models for the composites using the peak at 2922 cm^{-1}. Even this peak is not observed in the spectra of some of the composites. The constituents of the composites exhibit major infrared peaks. To actually detect and measure the HD2 grease peak requires subtracting the average clean composite spectrum from each HD2 contaminated same type composite spectrum. Ideally this subtraction removes all the composite peaks leaving only HD2 absorption.

Flash UV Fluorescence

Application of the Flash UV Fluorescence Imaging system to the composite standards with HD2 grease produced the models displayed in Figure 3. The fluorescence data shows a valid correlation of HD2 fluorescence with concentration down to about 5 mg/sqft for all four types of composites. As with the infrared data the composites containing carbon absorb much of the energy, from either the flash UV and/or the fluorescence.

Contec Wipes Issue

A recent issue at KSC involved the observation that certain batches of Contec wipe cloths exhibited abnormal fluorescence under black light. Some fluoresced only at the seamed edge, others fluoresced everywhere, while some showed spots and streaks. Because the Flash UV source is high intensity, examination of the wipes with the Flash UV Imaging system indicates all the wipes fluoresce to some degree. Initial investigation found the yarn used to serge the cloth edge contained silicone. Immediate silicone panic lead to numerous tests. Was silicone transferred to wiped surfaces?

Grit blasted steel panels were wiped with Contec wipes using a standard wipe procedure. First with wipe wet with the Reveille solvent followed by a dry wipe. Two lots of wipes were tested. Diffuse reflectance spectra were collected by SOC400 FTIR.

Panel One

A wipe from the first lot fluoresced under black light only at the serged edge. A panel wiped with the first lot was examined at nine locations. A typical spectrum is displayed in Figure 4. Similar spectra were observed at each location indicating uniform transfer of cloth components. The spectra exhibited major cellulose peaks, an ester peak from the serge yarn, and a doublet peak near 1250 cm^{-1}. No conclusive indication of silicone could be made from the reflective spectra.

The panel surface was extracted with chloroform, the extract dried and diluted to a specific volume, and a spectrum collected on this solution in a 1 mm sealed cell. Using a previously prepared calibration curve the silicone present on the panel was calculated to be ~0.1 milligrams per square foot.

Panel Two

Another panel was wiped with Contec wipes that fluoresced all over. The reflectance spectra were similar to those from panel one. The panel was extracted with chloroform, dried, diluted to specific volume, and a spectrum collected in a 1mm cell. This initial extraction found 0.7 mg/sqft silicone on the panel. A second and third extraction found 0.08 and 0.016 mg/sqft silicone respectfully. A fourth extraction found no detectable silicone. There was little change in reflectance spectral features, shown in the bottom spectrum of Figure 4, of residue on the panel before and after each chloroform extraction. The Flash UV image of panel two indicated high fluorescence before and after each chloroform extraction. This observation indicates the fluorescing components are not soluble in chloroform. Microscopic examination of the residue on the panel revealed fibrous material.

Experiments to extract fluorescing component

Samples of Contec wipes that fluoresce were extracted with various solvents attempting to remove the fluorescing components. Comparison of solvent effectiveness indicated water>ethyl alcohol>acetone>chloroform. Examination of material removed indicated discrete fluorescing particles. This observation supports the conclusion that the solvents are only dislodging particles of the brightening agent but not really dissolving them.

Silane Adhesive Promoter

Enhancement of epoxy bonds to steel was achieved years ago by use of silane bond promoters. Theoretically the silane forms a covalent chemical bond with oxides or hydroxide on the steel surface and ties into the crosslinking structure of the epoxy. The silane is applied in solution, which helps the penetration of the silane into the pores of the steel. Bond data supports the conclusion that silanes can overcome the bond inhibiting presence of trace amounts of many contaminants. Experiments are in progress to better understand the action and chemistry of the silane adhesive promoter.

Questions of concern

How much time at ambient conditions after applying the silane is required before bonds are formed between the silane and steel? The SOC400 can readily detect and quantify silane on grit blasted steel surfaces. Calibration was obtained by applying silane over a range of concentrations on steel coupons, collecting spectra at numerous locations on each coupon using the SOC400, washing the silane from the coupons with chloroform, diluting to specific volume, and analyzing for silane by classical infrared in a sealed 1 mm cell. Calibration of silane in the 1mm cell was accomplished using solution of known silane content, Figure 5. A model was prepared correlating silane absorbance versus concentration using diffuse reflectance spectra collected on the SOC400 FTIR, also Figure 5.

Silane in the 10-50 mg/sqft range was allowed to remain on four grit blasted steel coupons for three days, washed from the surfaces multiple times with chloroform and the dried surfaces examined by SOC400. Silane still remained on the surface at 1.2 to 1.5 mg/sqft. The standard procedure is to apply silane for 1 to 3 hours before applying epoxy. An experiment in which silane was washed off after 3 hours found no silane detected on the dried surface. So how long is really best? The application for 1 to 3 hours seems to enhance the bond. More experiments are planned to answer this question. How much silane should be applied? A range of silane was applied to a set of tapered double cantilever beams, the amount of silane measured by SOC400 and bond samples prepared. The bond data was similar for each silane concentration except the very lowest level; however, the silane remained on the beams two days before bond sample preparation due to analysis time and bond scheduling. More experiments need to be performed to quantify rates of silane/steel bonding.

Cleaning of Silicone from Grit Blasted Steel

One of the problems holding up the test plan originally intended for this paper is the ability to remove silicone from tested bond specimens so they can be recycled to prepare more specimens. When silicone is applied to grit blasted steel it seems, over a period of contact time, to either diffuse deep into the pores of the steel or to bond to the surface such that washing with solvent does not remove all of it. If steel panels contaminated with even a small amount of silicone are grit blasted, the grit blasting apparatus will become silicone contaminated. Numerous solvents and cleaners were evaluated to find one effective in removing the silicone.

DS104 Cleaner

A recent candidate includes DS104, a brew of saturated hydrocarbons and acetates manufacture by Dynamold Solvent, Inc. Three steel plates were contaminated with greater than 100 milligrams per square foot of Dow 200 silicone oil and aged for one week. The plates were soaked for 15 minutes in the DS104 solvent, flushed

with this solvent, then washed with hot water. After drying 24 hours the plates were examined for silicone with the SOC400. Silicone was detected at approximately 0.4 to 0.6 mg/sqft. Re-examination after placing in storage for several weeks found the silicone observable on the surface had increased to 0.7 to 0.9 mg/sqft. Steel coupons contaminated with silicone oil and previously cleaned with DS104 solvent were subjected to ultrasonic cleaning using the same type solvent, DS104. Examination using the SOC400 FTIR revealed two coupons still exhibit traces of silicone, 0.3 mg/sqft. A third contaminated coupon and control coupon did not show silicone but had rust or stains on the surface.

Wasatch cleaning solution

Another candidate cleaner consists of a solution of 2-methylethanol, mineral spirits, and sodium hydroxide. The alkaline nature of this solution will, supposedly, break down the silicone structure. Grit blasted steel 2x3 inch coupons (3) were coated with silicone, greater than 100 mg/sqft, aged one week, soaked in the candidate cleaner for 15 minutes, flushed with the solution, washed with hot water, and dried. Examination by SOC400 found silicone on each coupon at about 1 mg/sqft. Examination after a week of storage found essentially the same silicone level.

A successful solvent to remove all the silicone has at present not been found. Other candidates are under evaluation.

SUMMARY AND CONCLUSIONS

Composites

Composites containing carbon polymorphs, carbon and graphite absorb essentially all the infrared energy and preclude valid models. The contaminant HD2 grease can be detected by infrared spectroscopy on composites not containing carbon and quantified down to approximately 5 mg/sqft. The data manipulation, spectral subtraction, etc., to perform this task is tedious. Flash UV Fluorescence Imaging can quantify HD2 grease on composites even those containing carbon to approximately 5 mg/sqft.

Contec Wipes

The silicone content of the Contec wipes that fluoresce all over is an order of magnitude higher than in those that fluoresce only at their serged edge. The major portion of residue transferred from wiping cloths to the steel grit blasted surface, whether fluorescing or non-fluorescing Contec, are similar. The composition is mostly the bulk cellulose cloth along with binder or sizing. During standard panel wipe procedure some of the bulk cellulose cloth and serge yarn (polyester in Contec) are transferred with traces of silicone. The total silicone transferred in the worst case is less than 1 milligram per square foot. The major transfer mechanism is the very abrasive nature of the grit blasted surface and solubility of silicone in Reveille solvent. Reveille solvent dissolves the silicone from the serge yarn. Reveille solvent does not dissolve the cloth yarn, binders, sizing, or the fluorescing component present in the wipes. The fluorescing component on the Contec wipes is an inorganic fluorescing brightening agent.

Silane Adhesive Promoter

Silane adhesive promoters enhance the bond of epoxy to steel. Many questions remain unanswered as to what the chemistry is, how much to use for optimum results, and how long to wait before applying the epoxy for optimum bond formation.

Cleaning of Silicone from Grit Blasted Steel

Obviously silicone is difficult to remove from grit blasted steel after a few days of contact. The mechanism by which the silicone is retained on the surface is not really defined.

Table 1. Gravimetric levels of HD2 grease applied to composite specimens.

Target, mg/sqft	Level Determined Gravimetrically, mg/sqft				
	SGP	CCP	FGP	GE	D6AC
1	1.18	1.18	1.18	1.18	1.18
5	5.3	5.3	5.3	5.3	5.3
10	9.9	9.9	9.9	9.9	9.9
20	21.6	21.6	21.6	21.6	21.6

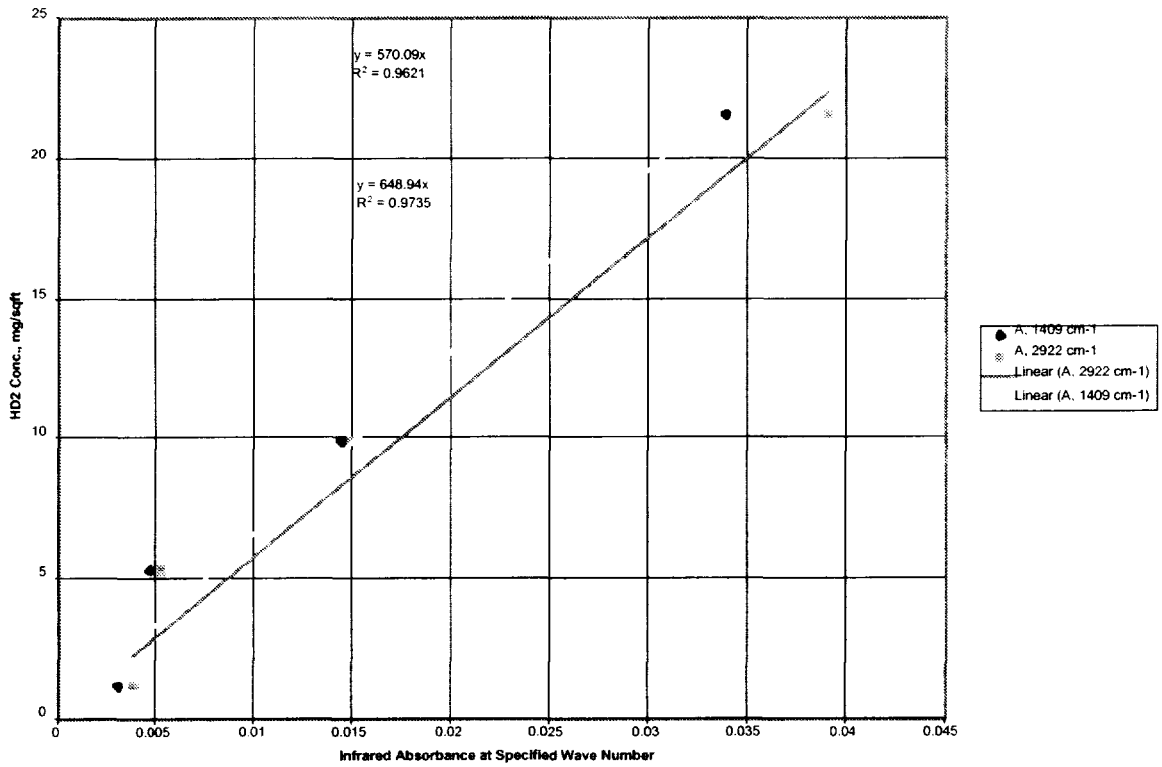

Figure 1. Calibration models for HD2 grease on grit blasted steel at two different wavelengths exhibiting linear correlation of absorbance versus concentration.

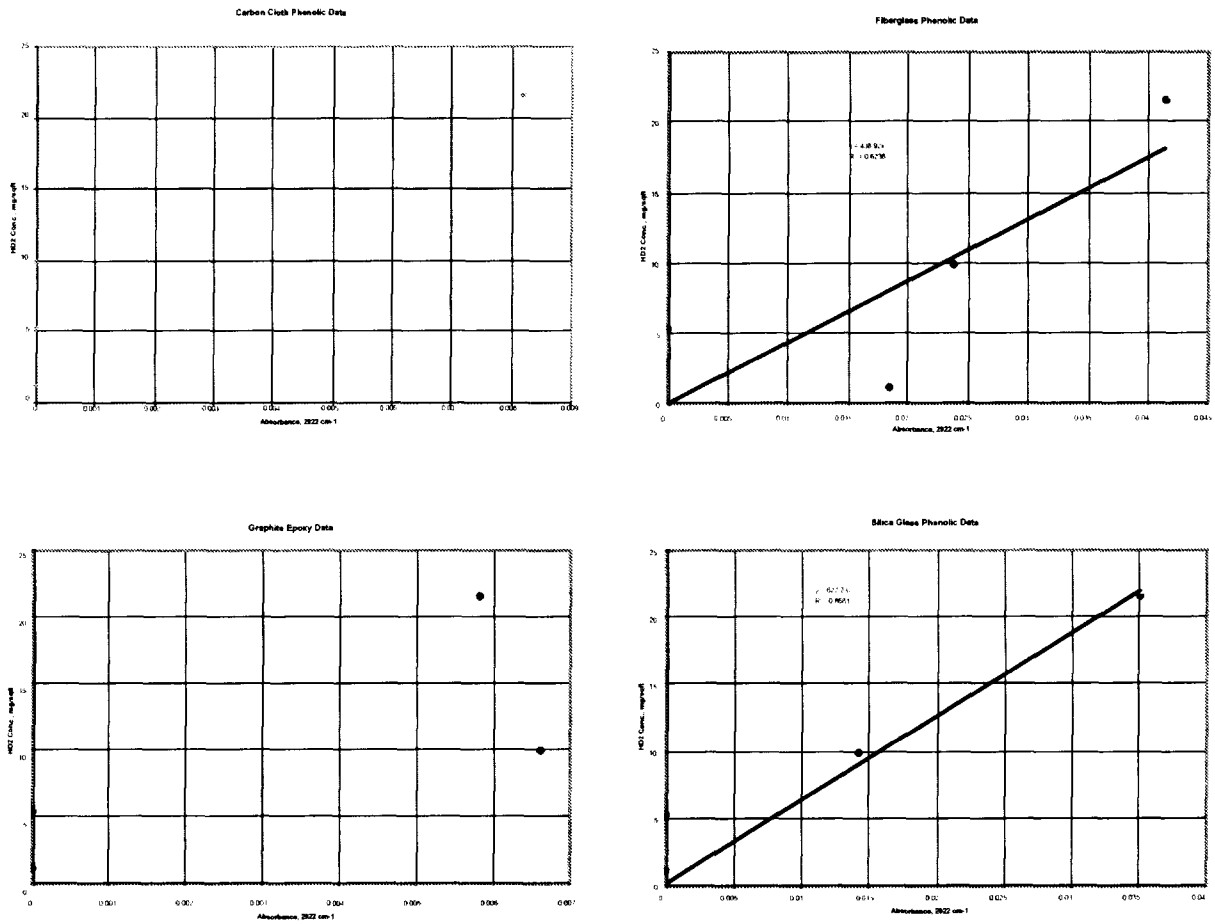

Figure 2. Calibration models for HD2 grease on four types of composites. Composites containing carbon polymorphs, carbon and graphite absorb essentially all the infrared energy and preclude valid models.

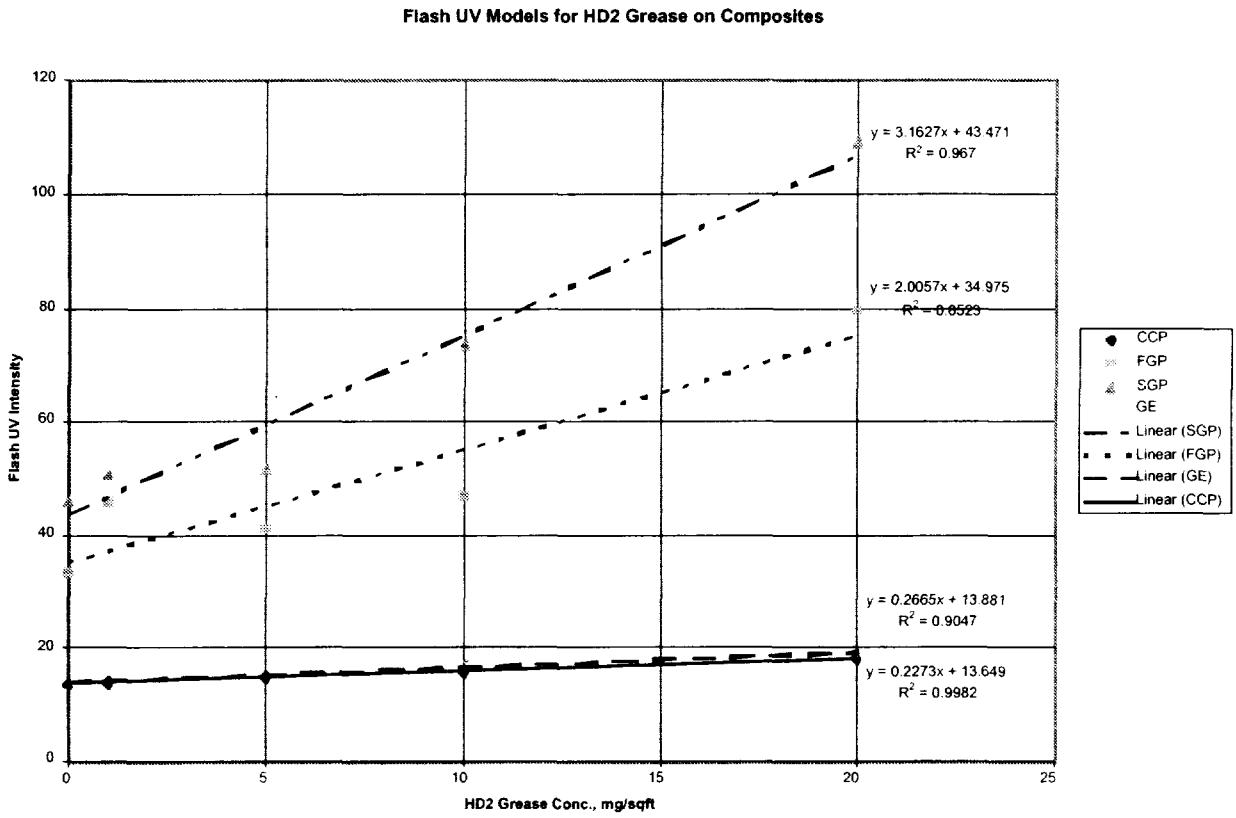

Figure 3. Flash UV Fluorescence Imaging calibration models for HD2 grease on four types of composites exhibit good correlation. Composites containing carbon polymorphs, carbon and graphite absorb much of the fluorescent energy but still exhibit linear correlation of fluorescence versus concentration.

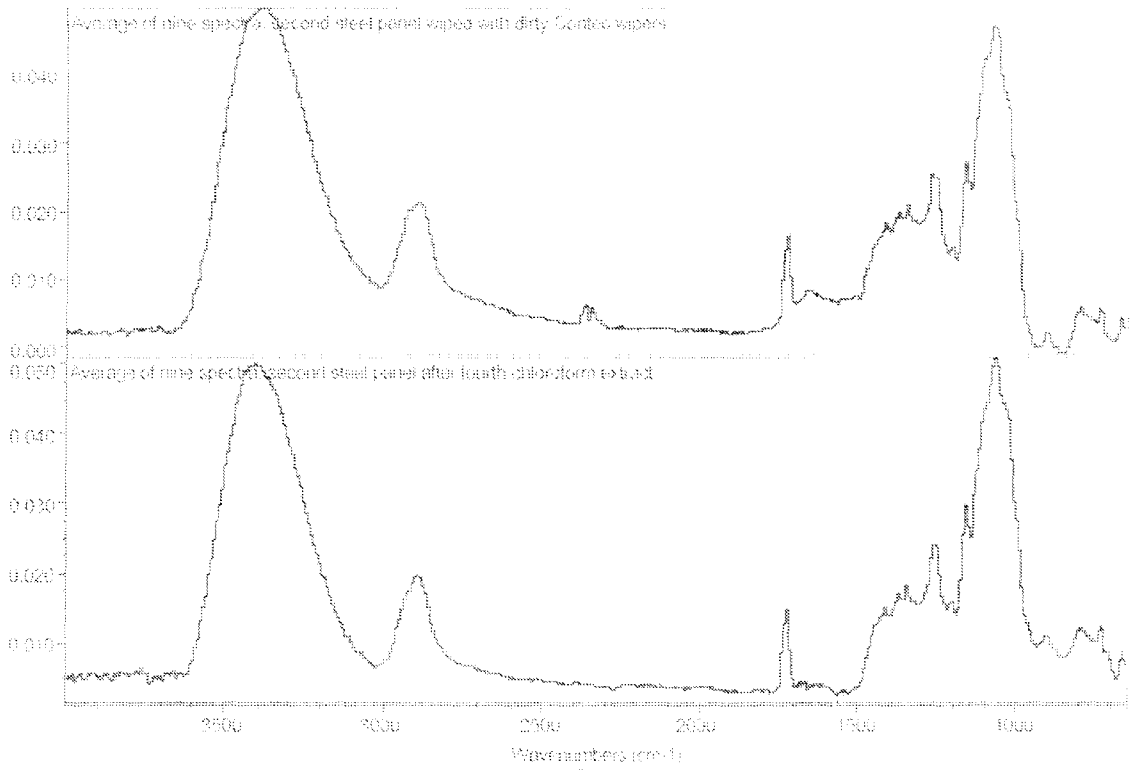

Figure 4. SOC 400 infrared spectrum (Top) of steel panel after wiping with Contec wipe considered dirty with fluorescence over entire surface. Bottom spectrum is on the same panel after being extracted four times with chloroform.

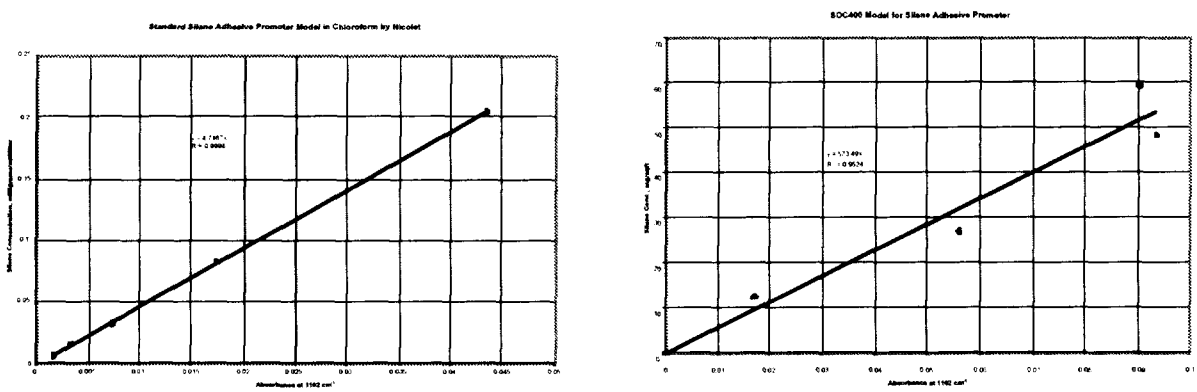

Figure 5. Calibration model, left, for silane adhesive promoter in chloroform using Nicolet FTIR and 1 mm sealed cell showing very linear correlation. Calibration model, right, for silane adhesive promoter on grit blasted steel using SOC400 diffuse reflectance spectra.

Physical Evaluation of Cleaning Performance – We Are Only Fooling Ourselves

EARL PRATZ

D4/3

Lockheed Martin Michoud Space Systems
P.O. Box 29304, M/S 4710
Michoud Assembly Facility
New Orleans, LA 70189 USA
Phone: 504-257-1761
Fax: 504-257-4438
E-mail: Earl.H.Pratz@maf.nasa.gov

Surface cleaning processes are normally evaluated using visual physical properties, such as streaking, staining, and water-break-free conditions. There is the assumption that these physical methods will evaluate all surfaces all the time for all operations. We have found that these physical methods are lacking in sensitivity and selectivity with regard to surface residues and subsequent process performance. We will report several conditions where evaluations using visual physical properties are lacking. We will identify possible alternative methods and future needs for surface evaluations.

CP/559/IN/27

E1/15T

Low Environmental Impact, High Performance Foam Blowing Agents Based on Iodofluorocarbons

Patrick M. Dhooge, Suzanne M. Glass, and Jonathan S. Nimitz
Environmental Technology and Education Center (ETEC)
4500-B Hawkins St. NE
Albuquerque, NM 87109-4517
Phone: (505) 345-2707
http://www.etec-nm.com
pdhooge@etec-nm.com jnimitz@etec-nm.com

INTRODUCTION

Chlorofluorocarbons (CFCs) and hydrochlorofluorocarbons (HCFCs), including CFC-11, CFC-12, HCFC-141b, and HCFC-142b, have been used as high performance polymer foam blowing agents because of their physical properties, stability, relatively high molecular weight, and low toxicity. However, these blowing agents deplete stratospheric ozone, and have been or will soon be phased out of production in developed countries under the provisions of the Montreal Protocol and its amendments. CFC-11 and CFC-12 have already been phased out of production and replaced with HCFC-141b and HCFC-142b. Although HCFC-141b has been widely used as an interim blowing agent, its production is scheduled to cease in 2003. HCFC-142b production is scheduled to cease in 2010.

In general, the blowing agent in insulating foam provides from 50% to 80% of the foam's insulating value. Substitute blowing agents such as hydrocarbons and CO_2 have low insulating value and diffuse out of the foam much more quickly than the CFCs and HCFCs, further reducing the insulating value of the foam as it ages. Hydrocarbon blowing agents introduce complications in manufacturing processes because they are flammable and they produce more flammable foam. Hydrofluorocarbon (HFC) blowing agents such as HFC-245fa, planned as the next standard blowing agents, have significantly higher vapor thermal conductivities than HCFC-141b or CFC-11. In addition, HFCs have moderate global warming potentials (GWPs).

In the aerospace sector, where weight and volume are highly valued, there is a strong need for a rigid closed-cell polymer foam blowing agent that is non-ozone-depleting, nonflammable, relatively nontoxic, thermally stable, compatible with polymer materials, reasonably priced, and will produce foams with superior insulating value and superior insulation aging characteristics. The same is true in applications such as refrigerator and freezer insulation, where insulation value in a fixed size appliance is highly valued. A third high value application is refrigerated transport units, where weight and volume are also highly valued due to fuel use per weight.

Iodofluorocarbons (IFCs) were identified by Jon Nimitz and Lance Lankford as potentially attractive nonflammable foam blowing agents that would address the need for high performance, low atmospheric impact foam blowing agents. IFCs have attractive physical properties (similar to CFCs), high molecular weights, and because they undergo photolysis within two days when released into the atmosphere they never reach the stratosphere and thus have negligible ozone-depletion potential (ODP) (Solomon a and Solomon b). Their short atmospheric lifetimes also give them very low GWPs. The high molecular weights are expected

to make these compounds outstanding insulating gases and to reduce permeation, thus improving retention of insulating performance on aging. Theory and previous experimental results with other foam blowing agents indicate that, if properly formulated, foams blown with an IFC such as CF_3I should have 15-20% better insulating ability than foams blown with HCFC-141b and HCFC-142b. In addition, because CF_3I has a significantly greater molecular weight than HCFC-141b or HCFC-142b, it will diffuse out of the foam more slowly, giving foams blown with CF_3I better aging characteristics. Because of their superior insulating ability, polymer foams blown with IFC-based agents should allow lighter weight and lower volume insulation, significantly improving performance in a variety of applications.

ETEC's initial investigation of IFCs as foam blowing agents was sponsored by the U.S. Department of Energy's Energy-Related Inventions Program (ERIP). IFCs considered in this investigation included CF_3I, 1-C_3F_7I and 2- C_3F_7I. Blends of CF_3I with hydrofluorocarbons (HFCs) and with carbon dioxide were also investigated.

RESULTS AND DISCUSSION

Predicted Performance

The high molecular weights of IFCs made it appear highly probable that they would provide substantially better insulation than CFC-11 or any of the currently available alternatives (CARIERS, Center for Emissions Control, Chemical Marketing Reporter, DuPont, EPA, Jeffs, Kirk-Othmer a and b, Recktenwald, Smits, and Ullman). Reasoning for this statement follows immediately below.

Heat transfer in foams is by conductive, convective, and radiative processes. For most insulating foam, by far the greatest contribution is from conductive heat transfer. With small cell size, convective processes are limited and radiative transfer at typical temperature differentials is small. The thermal conductivity of the foam cell gas is the major contributor to the thermal conductivity of the foam.

The relative insulating value of a gas is inversely proportional to its thermal conductivity. The measured vapor thermal conductivity of CF_3I at 10°C and 1.0 atmosphere is 6.7mW/m-K. CF_3I has low thermal conductivity and low diffusion rate principally because of its high molecular weight and good infrared absorption. In general, the diffusion rate and thermal conductivity of gases varies with the inverse of the square root of their molecular weights. If heat transfer occurs entirely by conduction, the ratio of thermal conductivity for CF_3I relative to HCFC-142b is given by Equation [1].

$$6.7/12 = 0.558 \qquad [1]$$

Insulating foam can be considered to have two heat flow paths: one for the polymer matrix and one for the gas. If the polymer matrix does not change, that portion of the heat flow will not change. However, if the gas is changed, its contribution to the heat flow changes. Depending on the density and nature of the foam, anywhere from 50% to 80% of the insulating ability of rigid, closed cell polymer foam is due to the thermal conductivity of the gas in its cells (Glicksman). CF_3I vapor is a better insulator than HCFC-142b vapor by about 44%. The estimated improvements from CF_3I versus CFC, HCFC, HFC, hydrocarbon, carbon dioxide, and

blowing agents are shown in Table 1, assuming a conservative value of 50% of the insulating value of the foam is attributable to the blowing agent.

Table 1. Predicted Improvements in Insulating Abilities and Diffusion Rate for CF_3I Versus Other Foam Blowing Agents

	Predicted improvement in gas insulating ability and diffusion rate, %	Predicted improvement in insulating ability of foam, %[a]
CFC-11	27	13
CFC-12	27	13
HCFC-22	31	15
HCFC-141b	25	12
HCFC-142b	44	22
HFC-245fa	52	26
HFC-356mffm	54	27
cyclopentane	36	18
CO_2	56	28

[a]These values assume complete vaporization that occurs only above their boiling points. At lower temperatures, some of these agents condense and create partial vacuums in the cells, which will tend to diminish the insulating effect of the gas.

The results in Table 1 show that replacement of HCFCs and alternative agents with CF_3I is estimated to lead to an improvement in the insulating ability and diffusion rate of the gas of 25% to 56%, and a conservatively estimated increase in the insulating ability of the rigid, closed-cell polymer insulating foams of 12% to 28%. If the contribution of the blowing agent to the total foam thermal conductivity is more than 50%, the predicted insulating improvements in the right hand column of Table 1 will be greater. Thus, calculations show that CF_3I should increase the insulating performance of rigid polymer foams by 10% to 30% over CFCs and other common blowing agents. The increased insulating value of rigid polymer foams prepared with this blowing agent and its blends will give it very low Total Equivalent Warming Impact (TEWI).

Stability and Compatibility of CF_3I

Although iodinated organic compounds are *in general* more reactive, more toxic, and less stable chemically than other halogenated organic compounds, the presence of fluorine atoms bonded to the iodinated carbon atom provides substantial additional stability and greatly decreased toxicity. The presence of strongly bonded, highly electron-withdrawing fluorine atoms on the iodinated carbon atom greatly inhibits both common mechanisms of reaction for iodocarbons. Steric hindrance (physical blocking by the fluorine atoms) prevents back-side attack by nucleophiles (S_N2 or substitution, nucleophilic, bimolecular mechanism) and the increased C-I bond strength inhibits unimolecular bond-breaking (S_N1 or substitution, nucleophilic, unimolecular mechanism). For toxicity and stability considerations, IFCs containing a terminal iododifluoro group ($-CF_2I$) are preferred over other molecular arrangements. By having three fluorine atoms on the same carbon atom as the iodine the C-I bond in CF_3I is further strengthened and reactions are greatly inhibited.

Published studies on thermal decomposition of CF_3I indicate that the compound is quite thermally stable (Nimitz a). In one study it is reported that CF_3I is stable in contact with metals up to 443 K (170°C or 340°F). Recent work indicates that it is stable when heated to 355 K (82°C or 180°F) for at least 60 days (Dierdorf).

In testing by Dr. N. Dean Smith at EPA's Risk Management Laboratory and by Spauschus and Associates, CF_3I blends have been shown to have good thermal stability and good compatibility with common materials of construction (Smith and Spauschus). In testing by Dr. Smith's group, a blend containing CF_3I was sealed in evacuated vials containing Vespel®, Buna-N®, silicone rubber, Teflon®, Viton®, stainless steel, aluminum, brass, or bronze, in the presence and absence of POE oil, and aged for two weeks at 448 K (175°C). Only Buna-N® was found to be unacceptable, having 11% swelling and becoming approximately 23% harder. The blend showed no significant degradation ($\leq$0.05%) by itself or in the presence of any of the materials. From decomposition rate studies performed by Spauschus and Associates, it has been shown that CF_3I would undergo less than 0.1% decomposition in twenty years under typical ambient temperature conditions.

Flammability

CF_3I is an outstanding fire extinguishant, comparable in effectiveness to Halon 1301. CF_3I has been shown to prevent combustion of hydrocarbon fuels when present at about 3% concentration by volume in air (Nimitz b). Thus, it will not contribute to the flammability of foams. In a fire environment, the cells in most foams rupture long before the polymer starts to burn. This rupture is caused by softening of the polymer and thermally induced pressure. The gas in the cell is released and carried away. Polyurethane polymer matrixes are often highly flammable (although flame retardants can be added to decrease this flammability); polyisocyanurates are more flame-resistant. Although CF_3I is not expected to make otherwise flammable foams nonflammable, the blowing agent will not contribute to foam flammability.

Atmospheric Lifetime, ODP, and GWP of CF_3I

CF_3I has negligible ODP because it undergoes photolysis within about two days when exposed to solar ultraviolet radiation in the atmosphere, and thus never reaches the stratosphere (Ikon). This short atmospheric lifetime also gives CF_3I very low GWP. Dr. Don Wuebbles of the Department of Atmospheric Sciences at the University of Illinois (Urbana-Champaign), one of the world's foremost experts on ODP and GWP, has concluded that the ODPs of IFCs such as CF_3I are less than or equal to 0.0025, "much less than is of concern within the U.S. and international guidelines." The GWP of CF_3I is also extremely small, less than 2 relative to CO_2 for a 100 year time horizon. Dr. Wuebbles concluded that "these results imply essentially a negligible effect on future climate" from IFCs (Wuebbles, et al.).

Blends

Blends of conventional agents with IFCs can provide the advantages of lower cost and customized performance. Very little solubility data have been reported in the literature on IFCs. Because of their chemical structures, however, they were expected to have similar solubility characteristics to CFCs. In other projects, we have found that IFCs can be blended with a wide variety of common chemicals from the classes of hydrocarbons and HFCs.

In published work on the solvent cleaning agent abilities of IFCs, the IFCs tested (C_4F_9I and $C_6F_{13}I$) were found to be miscible in all proportions with all other common solvents tested, including isopropyl alcohol, ethanol, ethyl acetate, acetone, methyl ethyl ketone, hexanes, toluene, naphtha, and limonene (Nimitz c). In general, addition of 20% to 50% of the IFC by volume was found to render blends nonflammable when an open flame was touched to the surface. These results encouraged us that CF_3I would be miscible with other foam blowing agents and could serve to inert flammable agents.

Azeotropic blends are particularly attractive because they do not change composition on evaporation. Thus, an azeotropic or near-azeotropic foam blowing agent would not tend to lose the more volatile component if exposed to air. In the work reported here, we used two nonflammable near-azeotropic blends containing CF_3I to produce polyurethane foams. These blends were Ikon® A and Ikon® B, which we had previously developed as refrigerants. Ikon® A is a blend of CF_3I and HFC-152a, while Ikon® B contains these two components plus HFC-134a.

Toxicity of CF_3I

There has been a significant amount of misunderstanding regarding the characteristics of CF_3I. The main concerns regarding this compound have been its toxicity, stability, and compatibility.

Recent results of CF_3I toxicity studies at Wright-Patterson Air Force Base show that CF_3I has very low acute toxicity (Jepson). Mice exposed continuously to 6% CF_3I for 3 days showed no lethalities. The lethal concentration by inhalation for 50% of a mouse population in 15 minutes (mouse 15-minute LC_{50}) has been measured at 27.4%. These are reassuringly high values, indicating very low acute toxicity. Additional older toxicity information on CF_3I has been reviewed (Nimitz a and Skaggs). Dodd and Vinegar have recently presented a review of CF_3I toxicity in comparison to common firefighting agents (Dodd). Their conclusion was that CF_3I's toxicity data profile fits within the range of toxicity data profiles of currently used fire extinguishants, to which personnel are exposed routinely.

The one major toxicological disadvantage of CF_3I is its relatively low threshold cardiac sensitization level. Many gaseous hydrocarbons and halocarbons sensitize animal hearts to adrenalin. The possibility of death from heart fibrillation after exposure to a halocarbon was first realized in the 1960s. A standard test was developed at that time to measure the relative cardiac sensitization of compounds. The test uses Beagle dogs that are injected with enough ephinephrine (adrenalin) to be barely under the amount that would cause that dogs' heart to go into fibrillation (this dosage is determined for each individual dog in the test group). After injection, the dogs are exposed to concentrations of the test compound in air. The minimum amount of the compound found to induce heart irregularities is the LOAEL, or Lowest Observable Affect (sic) Exposure Limit. The NOAEL, or No Observable Affect (sic) Exposure Limit, is the maximum concentration the dog can be exposed to with no affect. This test is quite rigorous, since the dogs are already just below the point of fibrillation due to the very high ephinephrine level, and the test was not originally intended to established exposure limits. It has been estimated that the ephinephrine levels used in this test may be 100 times or more higher than would be seen in a very frightened test subject (Vinegar). It is worthwhile to note that no cardiac problems have been seen in normally stressed animals and humans exposed to high concentrations of CF_3I, as evidenced by the high concentrations tolerated by rats in the acute

inhalation toxicity tests. The cardiac sensitization test's relevance is being questioned, but it remains the standard at this time. CF_3I's cardiac sensitization NOAEL is 0.2% by volume, or 2,000 ppmv in air (Kenny, et al.). With appropriate precautions, personnel will never be exposed to a CF_3I concentration this high.

After a review of all available toxicity data on CF_3I by toxicologists at Environ and Dr. Reva Rubenstein of the U.S. EPA Significant New Alternatives Policy (SNAP) program office, a recommended 8-hour time-weighted average exposure level for CF_3I was established at 150 ppm (Ikon). This value is higher than the value for many common industrial chemicals, including R-123, and the solvents methylene chloride, trichloroethylene, and perchloroethylene, indicating that CF_3I is in general safer than these materials. The recommended short-term exposure limit (STEL) for CF_3I is 2000 ppm.

Synthesis, Price, and Availability of CF_3I

CF_3I is in pilot scale production and is a commercial product, sold in relatively small amounts as a total flooding fire suppression agent for normally unoccupied areas. Current production is capable of supplying 50,000 kg/yr of CF_3I. The price has decreased significantly over the last six years, but is still much higher than it will eventually be in bulk production. The current best price for CF_3I is about $50/kg. Tosoh (F-Tech), a Japanese company, has announced a new continuous process that should be able to produce CF_3I from catalytic gas-phase iodination of trifluoromethane at an estimated cost of $29/kg assuming the current high iodine price of about $22/kg. If iodine price drops back to near its historic level of about $11/kg and economics of scale decrease overhead and trifluoromethane costs, the estimated cost of CF_3I produced by the Tosoh process should be about $12/kg.

The available data indicate that iodine supply for producing CF_3I and other IFCs as replacements for CFCs, HCFCs, and halons will not be a problem. Present world production of iodine is approximately 15 million kg per year. Currently, iodine prices are near a modern all time high due to China's decision several years ago to iodize their table salt. This decision caught iodine producers by surprise and raised iodine prices. New iodine production facilities are being built. Iodine price should return closer to its historic level of about $11/kg. Proven worldwide reserves of iodine recoverable at less than $15/kg are about 6.4 billion kg (Bureau of Mines). If the need for iodine increases, it is almost certain that more reserves will be proven. In addition, the oceans contain an estimated 34 billion kg of iodine, part of which can be recovered directly during extraction of chlorine, bromine, or magnesium from seawater, or indirectly by collecting and processing kelp. Seaweeds of the Laminaria family accumulate up to 0.45% iodine on a dry weight basis; before 1959 seaweed was a major source of iodine. At least one company in China is now producing iodine extracted from seaweed at a quoted price of $23.50/kg. The price of iodine recovered from seaweed should decrease as production volume increases. Cultivation and harvesting of seaweed for iodine and food products such as alginates can create an alternative source of income for coastal peoples, reducing economic pressure to over-fish and providing marine habitat.

Test Foam Results

Polyurethane and polystyrene foams were prepared with CF_3I and blends containing CF_3I. The foam formulations were not optimized for the CF_3I blowing agents, and the

polyurethane foams in particular had large voids indicating insufficient solubility of the CF_3I-based blowing agents in the polymer formulation components. The limited solubility also made the foams denser that desired. The data that could be acquired from the foam samples was therefore limited, but what results were obtained were encouraging.

Table 2 gives a comparison of thermal conductivity of polyurethane foam samples as prepared and after 30 day aging by ASTM C-518. Although the R-12 blowing agent formed a foam with better cell structure (no voids), and thus better insulating value, the foam blown with CF_3I is losing almost no insulating value on aging, and has significantly better dimensional stability. The slower loss of insulating value for the foam blown with CF_3I would be expected from its lower diffusion rate and thus slower loss from the foam cells. All foams blown with CF_3I in these studies had the excellent aging properties shown here.

Table 2. Properties of Polyurethane Test Foams Blown with R-12 and CF_3I

Property	R-12 Blowing Agent	CF_3I Blowing Agent
Approximate blowing agent concentration by weight %	20	20
Density, pcf	2.97	2.79
Dim. Stability, % change @158 oF/97% RH		
Length	3.01	2.17
Width	2.73	1.90
Thickness	-1.13	-0.95
K-factor, mW/m-K		
As received	23.2	41.0
+ 30 days	26.1	41.0

Trial production runs of extruded polystyrene (XPS) foam blown with CF_3I/CO_2 mixtures were prepared at Owens-Corning. The trial foams were compared to the same polystyrene formulation blown with HCFC-142b. Table 3 shows selected results from these foams. The same problem was encountered with this polymer formulation as with the polyurethane formulation in that it was not optimized for the CF_3I blowing agent, which is reflected by the significantly greater densities for the foams blown with the CF_3I blends. The foams blown with CF_3I blends are more fire-resistant as demonstrated by their higher oxygen index numbers, and their strengths, when adjusted for density, were the same as for the HCFC-blown foams.

Normalized for density, the thermal conductivities of the XPS foams blown with the different agents were all identical within experimental error. Thermal conductivity was linearly dependent on foam density to 99.5% confidence level. These results imply that there was no effect from the blowing agent gas, which is counter to the known thermal conductivity of CF_3I and previous theory and experiment with other foam blowing agents. The reasoning for why the XPS foams blown with CF_3I should have had lower thermal conductivity is as follows. The relative density of insulating foam reflects the fraction volume occupied by the polymer. For example, bulk polystyrene has a density of about 1050 kg/m^3. The polystyrene in foams prepared for this project had densities of about 30 to 40 kg/m^3. The fraction of polymer is therefore about

0.03 to 0.04. Taking a midrange value of 0.035 multiplied by the thermal conductivity of polystyrene (150 mW/m-K) times the efficiency gives the contribution to thermal conductivity of the polymer.

$$0.035 \times 150 \times 0.67 = 3.5 \text{ mW/m-K} \quad [4]$$

Compared to the measured thermal conductivities of the foams, this contribution is about 12% of the total thermal conductivity. Some contribution to thermal conductivity is due to radiative transfer, and it is estimated that about 60% of the thermal conductivity of these foams is expected to be determined by the thermal conductivity of the cell gas. Thus, there should have been a measurable decrease in thermal conductivity of the foam blown with 11 wt% CF_3I/1 wt% CO_2, when corrected for density.

Table 3. Data from Extruded Polystyrene Foams Blown with HCFC-142b and CF_3I/CO_2

Property	Foam blown with HCFC-142b	Foam blown with 11 wt% CF_3I and 1 wt% CO_2	Foam blown with 5 wt% CF_3I and 4 wt% CO_2
Density, kg/m^3	29	37.7	42
Cell diameter, mm	0.25	0.31	0.19
k-factor normalized to HCFC-142b foam density, mW/m-K	28.8	29.7	28.8
Compressive Strength, kPa	276	not measured	638
Oxygen Index, %	24	35	31

CONCLUSIONS

CF_3I and its blends appear to be excellent replacements for the CFC and HCFC insulating foam blowing agents. However, at least two major developmental tasks remain to be accomplished.

First, formulations for preparing polyurethane and polystyrene insulating foams need to be optimized for use with CF_3I blends. This will require solubility studies to identify polymer-forming components that dissolve significant amounts of CF_3I.

Second, foams need to be prepared with candidate optimized formulations and foam properties including density, cell size, strength, thermal conductivity, and aging characteristics thoroughly determined. Optimized formulations will be identified for application.

ACKNOWLEDGEMENTS

The funding for the work described in this paper was provided by the U.S. Department of Energy's Energy-Related Inventions Program. We would like to thank David Crouch of DOE, our Invention Coordinator, for his valuable technical support during the effort. ETEC would also like to thank Owens Corning, and particularly Ms. Barbara Fabian, for her support in preparing the test runs of foams and the properties testing provided.

REFERENCES

Bureau of Mines, Mineral Commodity Summaries 1993, U.S. Department of the Interior, Washington, DC, 1993, pp. 86-87.

CARIERS (Conservation and Renewable Energy Inquiry and Referral Service), "Foam Insulation," Merrifield, VA, 1994.

Center for Emissions Control, Flexible Polyurethane Foam Manufacture: An Assessment of Emission Control Options, October 1991, 1225 19th St. NW, Suite 300, Washington, DC, 20036-2411.

Chemical Marketing Reporter, "New Urethane Foams," Nov. 19, 1990, p. 7.

Dierdorf, D., New Mexico Engineering Research Institute, Albuquerque, NM, personal communication to Dr. Jon Nimitz, ETEC, Albuquerque, NM.

Dodd, D. E. and Vinegar, A., "Toxicity Data Comparison of CF_3I with Currently Used Fire-Extinguishing Agents and Refrigerants of Interest to the Military," Proceedings of the Halon Options Technical Working Conference, Albuquerque, New Mexico, April, 1999, available from New Mexico Engineering Research Institute, The University of New Mexico, Albuquerque, New Mexico.

Du Pont de Nemours, E. I., and Company, "Properties of Rigid Urethane Foams," Publication BA13, 1984.

Environmental Protection Agency, Handbook for Reducing and Eliminating Chlorofluorocarbons in Flexible Polyurethane Foams, Report 21A-4002, April 1991.

Glicksman, L. R., "Heat Transfer in Foams," in Low Density Cellular Plastics: Physical Basis of Behavior (Chapter 5), Edited by Hilyard, N. C. and Cunningham, A., Chapman and Hall, London, 1994.

Ikon Corporation, "Significant New Alternatives Policy (SNAP) Program Submission to the U.S. Environmental Protection Agency on Ikon B Refrigerant," April 1998.

Jeffs, M. "Phasing out CFCs in Polyurethane Rigid Foams - Technology Transfer" ICI Polyurethanes, Luxembourg, Belgium, 1993.

Jepson, G., Wright-Patterson AFB, OH, personal communication to Dr. Jon Nimitz, ETEC, Albuquerque, NM, 1994.

Kenny, T. J., Shepherd, C. K., and Hardy, C. J., "Iodotrifluoromethane and Iodoheptafluoropropane Assessment of Cardiac Sensitization Potential in Dogs," report AL/OE-TR-1995-0031 published by Occupational and Environmental Health Directorate, Toxicology Division, Wright-Patterson AFB, OH, 1995.

Kirk-Othmer Encyclopedia of Chemical Technology, The, "Insulation, Thermal," Vol. 13, Wiley, 1991, pp. 591-605.

Kirk-Othmer Encyclopedia of Chemical Technology, The, "Foamed Plastics," Vol. 11, pp. 82-123, Wiley, 1991.

Nimitz a: Nimitz, J. S., "High-Performance, Environmentally Sound Replacements for Halon 1301,"Prepared by ETEC for McClellan AFB under contract F04699-93-C-0004, December 1993.

Nimitz b: Nimitz, J. S., Glass, S. M., and Dhooge, P. M., "Gas Phase Combustion Suppression of Various Fuels by CF_3I," Proceedings of the 1999 Halon Options Technical Working Conference, Albuquerque, New Mexico, April 27-29, 1999, The University of New Mexico, New Mexico Engineering Research Institute, Albuquerque, NM, USA.

Nimitz c: Nimitz, J. S., Development of Nonflammable, Environmentally Compliant Fluoroiodocarbon Solvents: Phase I Final Report, Prepared for U.S.A.F. Wright Laboratories under contract F33615-94-C-5003, ETEC 95-1, January 1995.
Recktenwald, G. W., and Andrews, W. R., "Rigid Urethane Foams" in Bruins, P. F., ed., Polyurethane Technology, Interscience, New York, 1969, pp. 67-93.
Skaggs, S. R., Dierdorf, D. S., and Tapscott, R. E., "Update on Iodides as Fire Extinguishing Agents," *Proceedings of the 1993 CFC and Halon Alternatives Conference*, Washington, DC, October 20-22, 1993, pp. 800-809.
Smith, N. D., "Materials Compatibility with Ikon-B: Final Report," prepared for the Environmental Technology and Education Center by the National Risk Management Laboratory, U. S. EPA, Research Triangle Park, NC, September 1997.
Smits, G. F. and Thoen, J. A. "Mathematical Modeling Techniques to Predict Important Aspects of k-Factor Aging of CFC-11 Free Rigid Insulation," *Journal of Cellular Plastics*, Vol. 29, Jan 1993, p. 57.
Spauschus and Associates, "Results of CF_3I Stability and Compatibility Tests," confidential report prepared for Ikon Corporation.
Ullman's Encyclopedia of Industrial Chemistry, "Foamed Plastics," Vol. A11, Verlag, 1984, pp. 435-463.
Vinegar, A. and Jepson, G. W., "Epinephrine Challenge for Cardiac Sensitization Testing vs. Endogenous Epinephrine: A Perspective," Proceedings of the Halon Options Technical Working Conference, Albuquerque, New Mexico, April, 1999, available from New Mexico Engineering Research Institute, The University of New Mexico, Albuquerque, New Mexico.
Wuebbles, D. J., Li, Z., and Patten, K. O., "Estimated Ozone Depletion Potentials and Global Warming Potentials for 1-C_3F_7I, 1-C_4F_7I, and 1-$C_6F_{13}I$," 1996 report included as an appendix in EPA Significant New Alternatives Policy (SNAP) Program submission for Ikon B refrigerant, 1998.

CP/560/IN/27

E1/2ND

Update: HFC 245fa Blown Foam Development with External Tank Spray Foams

SIMON DAVIS

Lockheed Martin Manned Space Systems
Marshall Space Flight Center/Bldg. 4739
Huntsville, AL 35812 USA
Phone: 256-544-6482
Fax: 256-544-2774
E-mail: Simon.Davis@msfc.nasa.gov

The MSFC Thermal Protection Systems (TPS) Materials Research Laboratory is currently investigating environmentally friendly blowing agents for use in the insulations of the Space Shuttle's External Tank. The original TPS foam materials of the External Tank were blown with chlorofluorocarbon 11, which is now regulated because of its high Ozone Depletion Potential (ODP). Hydrochlorofluorocarbons (HCFCs), with an ODP that is one tenth that of CFCs, have been widely adopted as an interim blowing agent in urethane insulations. In FY96, Lockheed Martin completed the production qualification and validation of HCFC 141b blown insulations. Because of the expected limited commercial lifetime of HCFC 141b, research efforts are underway to identify and develop alternatives with zero ODP. HFC 245fa (1,1,1,3,3 pentaflouropropane) has been chosen by the manufacturer as a third-generation blowing agent to be marketed commercially. Preliminary work evaluating this third-generation candidate has demonstrated promising material mechanical property data. Favorable results from small-scale spray activities have justified evaluations using production foam processing spray parameters. With the scale-up of the spray equipment, however, additional processing issues have been identified. This paper will present data collected to date regarding the use of this blowing agent in External Tank spray foams.

High-Performance, Low Environmental Impact Refrigerants

Edward T. McCullough, Patrick M. Dhooge, Suzanne M. Glass, and Jonathan S. Nimitz
Environmental Technology and Education Center (ETEC)
4500-B Hawkins St. NE
Albuquerque, NM 87109-4517
Phone: (505) 345-2707
www.etec-nm.com
pdhooge@etec-nm.com jnimitz@etec-nm.com

INTRODUCTION

Refrigerants used in process and facilities systems in the U.S. include R-12, R-22, R-123, R-134a, R-404A, R-410A, R-500, and R-502. All but R-134a, R-404A, and R-410A contain ozone-depleting substances that will be phased out under the Montreal Protocol. Some of the substitutes do not perform as well as the refrigerants they are replacing, require new equipment, and have relatively high global warming potentials (GWPs). New refrigerants are needed that addresses environmental, safety, and performance issues simultaneously.

In efforts sponsored by Ikon Corporation, NASA Kennedy Space Center (KSC), and the U.S. Environmental Protection Agency (EPA), ETEC has developed and tested a new class of refrigerants, the Ikon® refrigerants, based on iodofluorocarbons (IFCs). These refrigerants are nonflammable, have essentially zero ozone-depletion potential (ODP), low GWP, high performance (energy efficiency and capacity), and can be dropped into much existing equipment.

Current Refrigerants

Although its production is now banned in the U.S. and other developed countries, R-12 is still used extensively. It was estimated by the American Refrigeration Institute (ARI) that at the end of 1999 approximately 50% of the R-12 equipment in the U.S. had not yet been converted to newer equipment or the R-12 replaced. R-500 is a blend of R-12 and R-152a.

R-134a, an HFC, will not be phased out under the Montreal Protocol. R-134a has replaced R-12 in many applications. As a low cost refrigerant it is cost effective for some applications, but it requires new or modified equipment. Carrier manufactures R-134a water chillers, and U.S. producers of residential refrigerators and automobile air conditioners now use R-134a. However, the performance of R-134a cooling systems tends to degrade at high ambient temperatures because of R-134a's relatively rapid decrease in cooling capacity at higher temperatures. International concern about greenhouse gases may limit R-134a applications in the future.

R-123 use in water chillers is increasing despite the fact that it is an HCFC and subject to phaseout as a Category 2 ozone-depleting substance under the Montreal Protocol. Trane is converting many existing R-12 systems to R-123, and manufacturing new R-123 systems. The attraction of R-123 is its inherent energy efficiency. R-123 water chillers are the most energy-efficient on the market. However, R-123 is relatively toxic, with a permissible exposure limit of only 50 ppmv in air, which means that air monitors must be installed around R-123 equipment and liability risk is increased. It also means that R-123 has only limited application and cannot be used in smaller commercial and residential systems.

R-22 has been used extensively in systems where rapid cooling is needed, including almost all window air conditioners, central air conditioners, and ice-making machines. R-22 is also used in many water chilling and process cooling systems. R-502, a blend of R-22 and R-115 with slightly higher capacity than R-22, has been used in many supermarket refrigerated display case systems. It has been difficult to find good replacements for R-22 and R-502 because of their high capacity combined with reasonably good energy efficiency. Many new R-22 systems are still being installed. However, because of continuing concerns over ozone depletion, R-22 phaseout has been accelerated and may be accelerated again. Phaseout of R-22 in the U.S. will begin with a 35% reduction in production starting in 2003, and then a 65% reduction in production starting in 2006. The price of R-22 is likely to increase significantly when its phaseout begins, similar to R-12 when it was phased out of production.

R-404A, R-407C, and R-410A, replacements for R-22, are inherently less energy efficient than R-22 according to the National Institutes of Standards and Technology (NIST)'s Refprop® refrigerant properties program. R-404A and R-410A have higher operating pressures than R-22 and require new equipment. R-407C has a high temperature glide in the evaporator and is not suitable to replace R-22 in many applications. Like R-134a, these refrigerants are not miscible with mineral oil and require polyol ester (POE) oil or some other synthetic lubricant in the compressor.

It is important to note that new refrigeration and cooling equipment is considerably more energy efficient than older equipment because of improvements in design and in the efficiencies of motors and compressors, not because new refrigerants are more energy-efficient (with the notable exception of R-123). In addition, in some applications additional energy efficiency gains have been obtained in new systems using ice making, liquid refrigerant pressurization, groundwater heat exchange, and other engineering advances. While these engineering advances are all of significant value, they do not reflect the inherent energy efficiency of the refrigerant, which is determined by its thermodynamic properties. A more energy-efficient refrigerant will add to the gains achieved through engineering changes.

It has been stated that replacing an old refrigerated cooling unit with a new unit is a "no-brainer" because the improvement in energy efficiency will repay the cost of the new unit in three years or less. This is not true for many units, however, and not every facility has the investment capital, desire, or time to replace entire units and systems. An alternative solution that can be much more cost-effective is to use more energy-efficient refrigerants in these units and perhaps install new, more energy-efficient compressors.

Ikon® A

Ikon® A (previously called Ikon®-12), a near-azeotropic blend of R-152a and trifluoroiodomethane (CF_3I), was the first of the new refrigerants developed, and was originally developed as a near-drop-in replacement for R-12. Ikon® A is fully miscible with mineral oil and so can be used directly in R-12 and R-500 systems. It can also replace R-134a. Ikon® A's evaporator temperature glide in air conditioning and refrigeration applications is about 0.10 – 0.15 K, which makes it highly suitable for critically flooded evaporators. Ikon® A also has a very low global warming potential (GWP) of about 30 versus CO_2 = 1 for a 100 year horizon. EPA has tested Ikon® A in automotive air conditioners with good results (Jetter). Dole Fresh Fruit ran

Ikon® A in an R-12 refrigerated transport (a "reefer") for two years with no indications of incompatibility or refrigerant decomposition. Although Ikon® A has superior cooling capacity and energy efficiency versus R-12 and R-134a, it was soon realized that automobile manufacturers were too heavily committed to R-134a. In addition, the added energy efficiency of Ikon® A would be reflected in at most a few tenths of a mile per gallon average fuel efficiency increase, which most motorists would not notice or value. Finally, the relatively high average leak rates for automotive air conditioning systems make an inexpensive refrigerant such as R-134a more desirable for these systems.

Further applications analysis indicated that Ikon® A might have a good application as an energy-efficient refrigerant in residential refrigerators and freezers, as these devices have high energy use per weight of refrigerant and very low leak rates. In a subsequent effort sponsored by EPA, ETEC measured Ikon® A's performance versus R-134a in an instrumented R-134a domestic refrigerator and had Ikon® A's thermodynamic properties measured. Ikon® A has been approved for a variety of cooling applications under the U.S. Environmental Protection Agency's Significant New Alternatives Policy (SNAP) program.

Ikon® B

NASA KSC's interest in the IFC-based refrigerants is for replacement of ozone-depleting refrigerants in their facility equipment to minimize operational and life cycle costs. Ikon® B, the second of the IFC-based refrigerants, was developed in the initial effort with assistance from N. Dean Smith at EPA's Risk Management Laboratory. Ikon® B is a near-azeotropic blend containing R-152a, R-134a, and CF_3I. Ikon® B is also highly suitable for systems with critically flooded evaporators, with an evaporator temperature glide of about 0.15 – 0.2 K in air conditioning and refrigeration applications. It has slightly better performance and lower cost than Ikon® A at the expense of a somewhat higher GWP and the need for POE compressor lubricating oil. Ikon® B is suitable for replacing R-12, R-134a, and R-500 in a variety of applications including water chillers, process coolers, air conditioners, refrigerators, and freezers. Performance tests of Ikon® B versus R-12 and R-134a were conducted in ETEC's instrumented 1.75 ton water chiller test bed and in an instrumented 20 ton air conditioner at NASA KSC. In addition, Ikon® B's performance has been measured versus R-22 in the Vapor Compression Test Loop (a type of compressor calorimeter) at Oak Ridge National Laboratories, its performance was measured versus R-134a in an instrumented R-134a domestic refrigerator at ETEC, and it has been used in a Dole Foods R-134a reefer for over two years. Ikon® B's thermodynamic properties have been measured. Ikon® B has been approved for a variety of cooling applications under the U.S. Environmental Protection Agency's Significant New Alternatives Policy (SNAP) program.

Ikon® C

NASA KSC was also interested in a zero ODP, energy-efficient replacement for R-22. In the effort for NASA KSC, ETEC developed Ikon® C as an energy-efficient R-22 and R-502 replacement. Ikon® C is a proprietary, near-azeotropic blend containing CF_3I. Ikon® C's operating pressures are almost an exact match for R-22. Ikon® C's performance has been measured versus R-22 in ETEC's instrumented 1.75 ton water chiller test bed. Ikon® C is significantly less expensive than Ikon® B. Ikon® C's thermodynamic properties have been measured, and a SNAP application has been prepared.

RESULTS AND DISCUSSION

Toxicity of CF_3I

There has been a significant amount of misunderstanding regarding the characteristics of CF_3I. The main concerns regarding this compound have been its toxicity, stability, and compatibility.

Recent results of CF_3I toxicity studies at Wright-Patterson Air Force Base show that CF_3I has very low acute toxicity (Jepson). Mice exposed continuously to 6% CF_3I for 3 days showed no lethalities. The lethal concentration by inhalation for 50% of a mouse population in 15 minutes (mouse 15-minute LC_{50}) has been measured at 27.4%. These are reassuringly high values, indicating very low acute toxicity. Additional older toxicity information on CF_3I has been reviewed (Nimitz; Skaggs, et al.). Dodd and Vinegar have recently presented a review of CF_3I toxicity in comparison to common firefighting agents (Dodd and Vinegar). Their conclusion was that CF_3I's toxicity data profile fits within the range of toxicity data profiles of currently used fire extinguishants, to which personnel are exposed routinely.

The one major toxicological disadvantage of CF_3I is its relatively low threshold cardiac sensitization level. Many gaseous hydrocarbons and halocarbons sensitize animal hearts to adrenalin. The possibility of death from heart fibrillation after exposure to a halocarbon was first realized in the 1960s. A standard test was developed at that time to measure the relative cardiac sensitization of compounds. The test uses Beagle dogs that are injected with enough ephinephrine (adrenalin) to be barely under the amount that would cause that dogs' heart to go into fibrillation (this dosage is determined for each individual dog in the test group). After injection, the dogs are exposed to concentrations of the test compound in air. The minimum amount of the compound found to induce heart irregularities is the LOAEL, or Lowest Observable Affect Exposure Limit. The NOAEL, or No Observable Affect Exposure Limit, is the maximum concentration the dog can be exposed to with no affect. This test is quite rigorous, since the dogs are already just below the point of fibrillation due to the very high ephinephrine level, and the test was not originally intended to established exposure limits. It has been estimated that the ephinephrine levels used in this test may be 100 times or more higher than would be seen in a very frightened test subject (Vinegar and Jepson). It is worthwhile to note that no cardiac problems have been seen in normally stressed animals and humans exposed to high concentrations of CF_3I, as evidenced by the high concentrations tolerated by rats in the acute inhalation toxicity tests. The cardiac sensitization test's relevance is being questioned, but it remains the standard at this time. CF_3I's cardiac sensitization NOAEL is 0.2% by volume, or 2000 ppmv in air. With appropriate precautions, operations personnel will never be exposed to a CF_3I concentration this high.

After a review of all available toxicity data on CF_3I by toxicologists at Environ and Dr. Reva Rubenstein of the U.S. EPA Significant New Alternatives Policy (SNAP) program office, a recommended 8-hour time-weighted average exposure level for CF_3I was established at 150 ppm (Ikon). This value is higher than the value for many common industrial chemicals, including R-123, and the solvents methylene chloride, trichloroethylene, and perchloroethylene, indicating that CF_3I is in general safer than these materials. The recommended short-term exposure limit (STEL) for CF_3I is 2000 ppm.

Stability and Compatibility of CF_3I

Although iodinated organic compounds are *in general* more reactive, more toxic, and less stable chemically than other halogenated organic compounds, the presence of fluorine atoms bonded to the iodinated carbon atom provides substantial additional stability and greatly decreased toxicity. The presence of strongly bonded, highly electron-withdrawing fluorine atoms on the iodinated carbon atom greatly inhibits both common mechanisms of reaction for iodocarbons. Steric hindrance (physical blocking by the fluorine atoms) prevents back-side attack by nucleophiles (S_N2 or substitution, nucleophilic, bimolecular mechanism) and the increased C-I bond strength inhibits unimolecular bond-breaking (S_N1 or substitution, nucleophilic, unimolecular mechanism). For toxicity and stability considerations, IFCs containing a terminal iododifluoro group ($-CF_2I$) are preferred over other molecular arrangements. By having three fluorine atoms on the same carbon atom as the iodine the C-I bond in CF_3I is further strengthened and reactions are greatly inhibited.

Published studies on thermal decomposition of CF_3I indicate that the compound is quite thermally stable (Nimitz). In one study it is reported that CF_3I is stable in contact with metals up to 443 K (170°C or 340°F). Recent work indicates that it is stable when heated to 355 K (82°C or 180°F) for at least 60 days (Dierdorf). An additional indication of stability is that many IFCs can be purchased from vendors and stored without unusual precautions such as refrigeration.

In testing by Dr. N. Dean Smith at EPA's Risk Management Laboratory and by Spauschus and Associates, CF_3I blends have been shown to have good thermal stability and good compatibility with common materials of construction (Smith; Spauschus). In testing by Dr. Smith's group, a refrigerant blend containing CF_3I was sealed in evacuated vials containing itself, Vespel®, Buna-N®, silicone rubber, Teflon®, Viton®, stainless steel, aluminum, brass, and bronze, in the presence and absence of POE oil, and aged for two weeks at 448 K (175°C). Only Buna-N® was found to be unacceptable, having 11% swelling and becoming approximately 23% harder. The refrigerant showed no significant degradation ($\leq$0.05%) by itself or in the presence of any of the materials. The kinetics testing by Spauschus and Associates gave a decomposition rate for CF_3I about 5 times greater than that of R-12. However, R-12 is extremely stable. Under typical air-cooled refrigerated cooling system operating conditions, it is estimated that the decomposition rate of CF_3I would be about 1% in twenty years. A refrigerant blend containing CF_3I has been used for over two years in a Dole Fresh Fruit refrigerated transport with no detectable decomposition.

Atmospheric Lifetime, ODP, and GWP of CF_3I

CF_3I has negligible ODP because it undergoes photolysis within about two days when exposed to solar ultraviolet radiation in the atmosphere, and thus never reaches the stratosphere (Ikon). This short atmospheric lifetime also gives CF_3I very low GWP. Dr. Don Wuebbles of the Department of Atmospheric Sciences at the University of Illinois (Urbana-Champaign), one of the world's foremost experts on ODP and GWP, has concluded that the ODPs of IFCs such as CF_3I are less than or equal to 0.0025, "much less than is of concern within the U.S. and international guidelines." The GWP of CF_3I is also extremely small, about 6 relative to CO_2 for a 100 year time horizon. Dr. Wuebbles concluded that "these results imply essentially a negligible effect on future climate" from IFCs.

Synthesis, Price, and Availability of CF_3I

CF_3I is in pilot scale production and is a commercial product, sold in relatively small amounts as a total flooding fire suppression agent for normally unoccupied areas. Current production is capable of supplying 100,000 to 150,000 kg/yr of Ikon® refrigerants. CF_3I's price has decreased significantly over the last six years, but is still much higher than it will eventually be in bulk production. The current best price for CF_3I is about $50/kg. Tosoh (F-Tech), a Japanese company, has announced a new continuous process that should be able to produce CF_3I from catalytic gas-phase iodination of trifluoromethane at an estimated cost of $29/kg assuming the current high iodine price of about $22/kg. If iodine price drops back to near its historic level of about $11/kg and economics of scale decrease overhead and trifluoromethane costs, the estimated cost of CF_3I produced by the Tosoh process should be about $12/kg.

The available data indicate that iodine supply for producing CF_3I and other IFCs as replacements for CFCs, HCFCs, and halons will not be a problem. Present world production of iodine is approximately 15 million kg per year. Currently, iodine prices are near a modern all time high due to China's decision several years ago to iodize their table salt. This decision caught iodine producers by surprise and raised iodine prices. New iodine production facilities are being built. Iodine price should return closer to its historic level of about $11/kg. Proven worldwide reserves of iodine recoverable at less than $15/kg are about 6.4 billion kg (Bureau of Mines). If the need for iodine increases, it is almost certain that more reserves will be proven. In addition, the oceans contain an estimated 34 billion kg of iodine, part of which can be recovered directly during extraction of chlorine, bromine, or magnesium from seawater, or indirectly by collecting and processing kelp. Seaweeds of the Laminaria family accumulate up to 0.45% iodine on a dry weight basis; before 1959 seaweed was a major source of iodine. At least one company in China is now producing iodine extracted from seaweed at a quoted price of $23.50/kg. The price of iodine recovered from seaweed should decrease as production volume increases. Cultivation and harvesting of seaweed for iodine and food products such as alginates can create an alternative source of income for coastal peoples, reducing economic pressure to over-fish and providing marine habitat.

Performance Tests and Demonstrations

<u>Ikon® B vs. R-12 and R-134a in ETEC's Instrumented Chiller Test Bed</u>

At ETEC, Ikon® B performance was measured versus R-12 and R-134a in an instrumented 1.75 ton (20,000 Btu/hr) air-cooled water chiller with a semi-hermetic reciprocating compressor. A 565 L water reservoir equipped with heaters was used as a heat load and thermal mass for the water chiller. Water was continuously circulated from the reservoir through the water chiller evaporator heat exchanger and back to the reservoir. The chiller was operated to keep the water reservoir at a constant temperature of about 290 K as measured by triplicate temperature sensors. The reservoir heaters' amperages and voltages were measured to determine heat input. Refrigerant loading was adjusted to give a flooded evaporator. Multiple runs were conducted with each refrigerant to confirm consistency of the results and obtain a standard deviation. In runs with R-134a, an R-134a expansion device was used. R-12 and Ikon® B runs used an R-12 expansion device. Ikon® B gave approximately 2% higher COP and 16% greater volumetric cooling capacity than R-12, and about 17% higher COP and 2% greater volumetric cooling capacity than R-134a in this piece of equipment.

Ikon® B vs R-12 in a 20 ton Air Conditioner at NASA KSC

Ikon® B was used to replace R-12 in a 20 ton (240,000 Btu/hr) air conditioning unit at NASA KSC. This unit, a backup for the unit used to provide pre-launch cooling of the Space Shuttle cabin, is diesel-powered with a semi-hermetic reciprocating compressor. The unit was instrumented and multiple runs were conducted with its standard R-12 charge and mineral oil lubricant to measure baseline performance. The unit was then charged with Ikon® B and POE lubricant. No other changes or adjustments were made. In multiple runs with Ikon® B, diesel fuel use was 8 – 10% less, and Ikon® B had approximately 15% greater cooling capacity versus R-12. Figure 1 shows why Ikon® B had greater cooling capacity. Pressure and temperature data, combined with the compressor displacement and thermodynamic properties for R-12 and Ikon® B, allow calculation of the mass flow of each refrigerant. Ikon® B's cooling capacity per pound is almost exactly equal to that of R-12, but the mass flow of Ikon® B is about 15% greater than R-12's mass flow, giving Ikon® B about 15% greater volumetric cooling capacity than R-12. Note that the effect increases as ambient temperature, and thus the unit's operating temperature, increases. In this unit, a significant fraction of Ikon® B's extra cooling capacity resulted in operating energy savings because although the compressor operates continuously, it is equipped with compressor cylinder unloader solenoids that reduce the work load on the compressor when capacity is in excess of that needed. The full 15% was not realized because the diesel engine also provides power to drive the unit's fans, and because of mechanical inefficiencies.

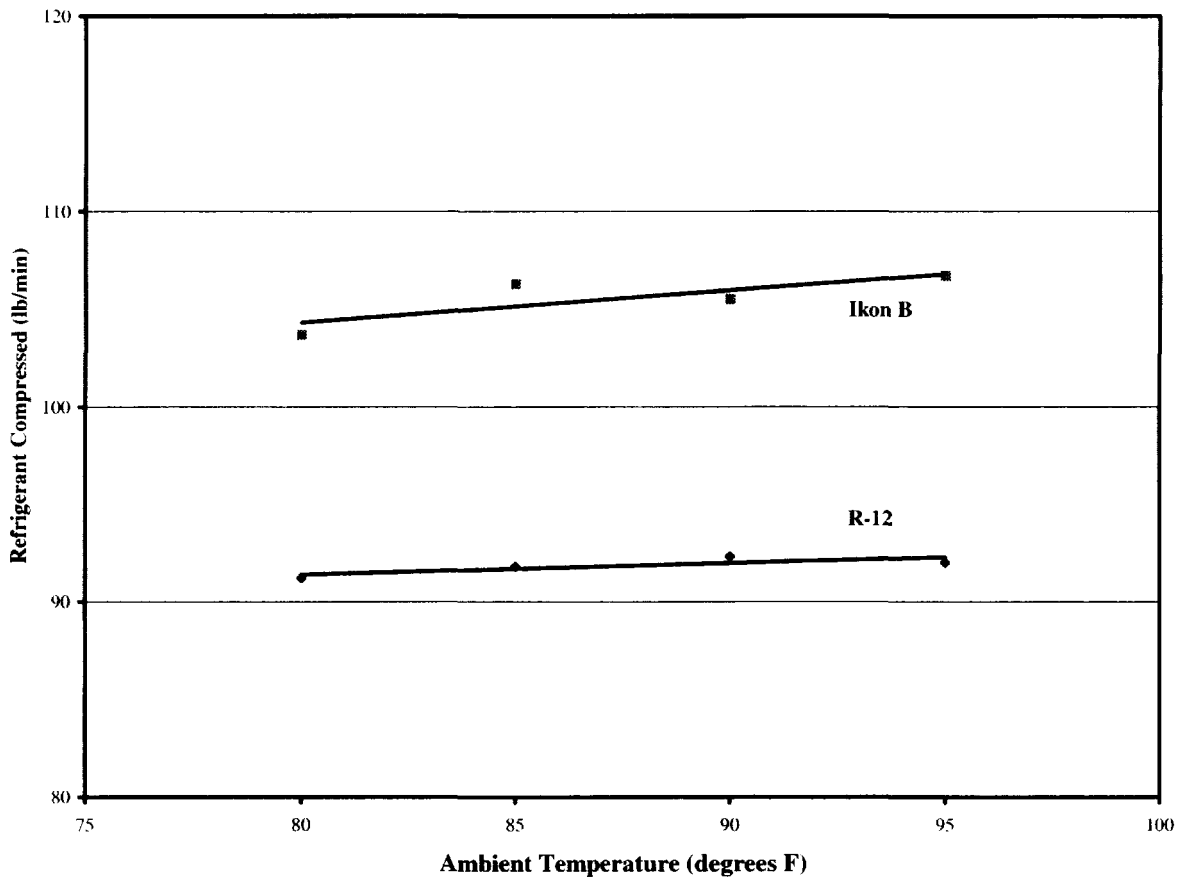

Figure 1. Refrigerant Flow Rate versus Ambient Temperature for 20 Ton AC Unit

Ikon® B vs. R-22 in the Vapor Compression Test Loop at ORNL

The performance of Ikon® B versus R-22 was tested under the direction of Van Baxter in the Vapor Compression Test Loop (VCTL) at ORNL. The VCTL is a sophisticated type of compressor calorimeter where the speed of the compressor can be varied to equalize cooling capacity. The efficiency of the compressor and compressor motor at different speeds are known and test results can be corrected accordingly. The conditions used were a 250 K evaporator and a 305 K condenser. The corrected results showed that the Energy Efficiency Ratio (EER) for Ikon® B is 20-25% higher than that of R-22 under these conditions. The capacity of Ikon® B tested 40-50% less than that of R-22 in this system under these operating conditions. Because R-22 is a refrigerant with much greater capacity but somewhat lower energy efficiency than R-12 or R-134a, these data are in agreement with the other performance data.

Ikon® A and Ikon® B vs R-12 and R-134a in Refrigerated Transports at Dole Fresh Fruit

At Dole Fresh Fruit Ikon® A and Ikon® B have been run in refrigerated transport units. Ikon® A was run for over two years in an R-12 system. For the first six months of operation, the compressor oil was tested periodically for total acid number, viscosity, and content of a variety of metals, to determine whether any significant breakdown of the refrigerant or oil, or any significant corrosion, was occurring. No decomposition products were seen. Tests of the oil after six months showed identical results to the zero time results. No operational problems or damage to the compressor were seen. The test was terminated to put the units back into shipping service with their standard refrigerants. Ikon® B has been run in two R-134a refrigerated transport units at Dole Fresh Fruit with no indication of incompatibility.

Ikon® A and Ikon® B vs R-134a in a Residential Refrigerator

Ikon® A and Ikon® B were tested versus R-134a in a new R-134a residential refrigerator. Tests were conducted in a walk-in environmental chamber capable of maintaining the exacting temperature conditions specified in energy use and performance tests of residential refrigerators and similar equipment. Initial tests were based on the ANSI/ASHRAE Standard 117-1992 and ANSI/AHAM HRF-1-1988 test methods for refrigerators. Both Ikon® A and Ikon® B showed about 13% greater volumetric cooling capacity than R-134a during pulldown. Energy use during pulldown was about 13% lower for Ikon® A and 10% lower for Ikon® B versus R-134a. Residential refrigerators have cooling capacity far in excess of that used in low temperature maintenance (i.e., steady state operation), so the extra energy efficiency of Ikon® A and Ikon® B could not be exploited in this unit during temperature maintenance because considerably more refrigerant is cycled than is used in cooling.

Therefore, the Embraco EMI60HER compressor in the test refrigerator was replaced with the next size down, an Embraco EMI50HER. The EMI50HER has about 15% less cooling capacity rating (and thus about 15% less volumetric displacement) than the EMI60HER, and has no higher EER than the EMI60HER. Refrigerant charges were always adjusted to give a just-flooded evaporator in the refrigerator. The DOE energy efficiency test at 305 K (90°F) ambient and the ANSI/AHAM pulldown test at 316 K (110°F) ambient were performed on both the baseline refrigerator configuration and the modified refrigerator. The baseline DOE energy efficiency result we obtained was 693 KWh/y, identical within experimental error and manufacturing variations to the refrigerator's official energy use rating of 691 KWh/y. The

pulldown time using Ikon® B and the EMI50HER was 6% faster than R-134a and the EMI60HER (the baseline refrigerator configuration). Energy use in the DOE energy efficiency test with Ikon® B and the EMI50HER was 9% less than with R-134a and the EMI60HER. These results indicate that Ikon® B is a significant improvement over R-134a in residential refrigerators and other applications. Ikon® B is still pulling down 6% faster with a 15% smaller volumetric displacement compressor, indicating that its cooling capacity is about 20% greater than R-134a under these conditions. If the compressor can be sized to take advantage of all of Ikon® B's capacity, an energy efficiency increase of over 10% should be obtained. The estimated cost per refrigerator of using Ikon® B instead of R-134a in new refrigerators is about $6, with estimated cost savings of $4.15 per year at 10% efficiency increase. The estimated payback time is just over 17 months.

Ikon® C vs. R-22 in ETEC's Instrumented Chiller Test Bed

ETEC's instrumented water chiller (described above) was outfitted with an appropriately sized R-22 compressor and expansion valve. The water chiller's performance was then measured with R-22 and Ikon® C. Ikon® C had about 94% of the cooling capacity and 98% of the COP of R-22. In comparison, the COPs of R-404A and R-407C under these operating conditions, according to the National Institute of Standards and Technology (NIST)'s Refprop® program, are 93 - 94% of R-22's. The temperature difference across the evaporator with Ikon® C was 1.1 K (2°F) greater than R-22, much less glide than that of R-407C. Ikon® C's operating pressures of 68 psia on the low side and 244 psia on the high side were an excellent match to R-22's 70 psia and 249 psia. We believe that, with a change to POE oil, Ikon® C can be a direct replacement for R-22 in most equipment. A change to POE oil may require a change of compressor if the existing R-22 compressor is not rated for POE oil, but this can be an opportunity to install one of the new, highly energy-efficient compressors in the system to obtain energy savings. One impressive aspect of Ikon® C was that the compressor outlet temperature with Ikon® C was only 341 K versus 362 K for R-22. The lower compressor outlet temperature means the compressor is running cooler with Ikon® C, which should significantly extend compressor life.

CONCLUSIONS

Ikon® A and B refrigerants have significantly greater performance than R-12 and R-134a. Their relative improvement over R-12 and R-134a increases with increasing operating temperatures, giving additional energy savings when most needed. It is estimated that in many applications their increased energy efficiency will pay back their extra cost within 1 – 3 years.

Ikon® A can be used to directly replace R-12 in R-12 equipment. Ikon® B can be used to replace R-12 in R-12 equipment with a change of compressor lubricating oil. For R-12 water chiller retrofits with Ikon® B, a new, energy-efficient compressor can be installed and the evaporator and condenser thoroughly de-scaled to obtain perhaps 30% or more reduction in energy use. Replacing R-134a in R-134a equipment with Ikon® B should give 10-15% reduction in energy use and about 15-20% additional cooling capacity in the equipment.

Ikon® C can be a direct replacement for R-22 in R-22 equipment if the compressor can tolerate POE oil. In older R-22 equipment, it may be desirable to replace the compressor with a new, more energy-efficient one rated for use with POE oil if a change to Ikon® C is made. The lower compressor operating temperature with Ikon® C should extend compressor life vs R-22.

ACKNOWLEDGEMENTS

Funding for the work described in this paper was provided by NASA Kennedy Space Center and the U.S. Environmental Protection Agency. We would like to thank Dr. Jacqueline Quinn of NASA KSC and Michael Bender of the U.S. EPA for their valuable technical support during the efforts. The Ikon® refrigerants and solvents are patented products of the Ikon Corporation.

REFERENCES

Bureau of Mines, Mineral Commodity Summaries 1993, U.S. Department of the Interior, Washington, DC, 1993, pp. 86-87.

Dierdorf, Douglas, New Mexico Engineering Research Institute, Albuquerque, NM, personal communication to Dr. Jon Nimitz, ETEC.

Dodd, D. E. and Vinegar, A., "Toxicity Data Comparison of CF_3I with Currently Used Fire-Extinguishing Agents and Refrigerants of Interest to the Military," Proceedings of the Halon Options Technical Working Conference, Albuquerque, New Mexico, April, 1999, available from New Mexico Engineering Research Institute, The University of New Mexico, Albuquerque, New Mexico.

Ikon Corporation, "Significant New Alternatives Policy (SNAP) Program Submission to the U.S. Environmental Protection Agency on Ikon B Refrigerant," April 1998.

Jepson, Major (rank) Gary, Wright-Patterson AFB, OH, personal communication to Dr. Jon Nimitz, ETEC, Albuquerque, NM, 1994.

Jetter, J. J., et al., "Evaluation of Ikon®-12 Refrigerant for Motor Vehicle Air Conditioning," available in the Proceedings of the SAE International Congress and Exposition, February, 1997, published by SAE International, Warrendale, PA.

Nimitz, J. S., High-Performance, Environmentally Sound Replacements for Halon 1301, Prepared for McClellan AFB under contract F04699-93-C-0004, December 1993, ETEC 93-3.

Skaggs, S. R., Dierdorf, D. S., and Tapscott, R. E., "Update on Iodides as Fire Extinguishing Agents," Proceedings of the 1993 CFC and Halon Alternatives Conference, Washington, DC, October 20-22, 1993, pp. 800-809.

Vinegar, A. and Jepson, G. W., "Epinephrine Challenge for Cardiac Sensitization Testing vs. Endogenous Epinephrine: A Perspective," Proceedings of the Halon Options Technical Working Conference, Albuquerque, New Mexico, April, 1999, available from New Mexico Engineering Research Institute, The University of New Mexico, Albuquerque, New Mexico.

Smith, N. D., "Materials Compatibility with Ikon-B: Final Report," prepared for the Environmental Technology and Education Center, September 8, 1997, by the National Risk Management Laboratory, U. S. EPA, Research Triangle Park, NC.

Spauschus and Associates, "Results of CF_3I Stability and Compatibility Tests," confidential report prepared for Ikon Corporation.

CP/72 IN/27

E.14

VOC Compliant Wax Removal Process

Alan Brown, David Grimmett, Margarite Sylvia
The Boeing Company
Rocketdyne Propulsion & Power
6633 Canoga Ave.
Canoga Park, California

Abstract

Wax is often used as a maskant during plating operations to protect against unwanted deposits on hardware details. Historically, perchloroethylene was used to remove this wax at the completion of the plating operation. In 1994, perchloroethylene was eliminated from this process at Rocketdyne, and was replaced by a high temperature oil and a cleaning process based on a semi-aqueous cleaner. This semi-aqueous cleaner has a volatile organic content of 768 g/l and environmental management of this material has limited the location of the operation. It was therefore desirable to identify a replacement cleaner, which is not subject to these limitations and enable the process to be located in closer proximity to the other manufacturing areas processing the hardware. This would result in the elimination of transportation of the hardware, the schedule impact of moving it, and the risk associated with additional handling. A cleaner was identified which satisfied these requirements and Taguchi methodology was used to optimize the process using this material.

Background

Rigidax[1] is a high melting point wax which is melted and poured into a variety of components including MCC channels to serve as a maskant for plating operations or to mask off parts prior to machining operations. After the wax has served its purpose as a maskant, it must be removed to allow subsequent processing and to open the channels for cooling during engine operation. Up until the early 1990's wax removal was accomplished through use of perchloroethylene. In 1992- 1993, a hot oil process was developed to eliminate the use of perchloroethylene and is outlined below in Figure 1.

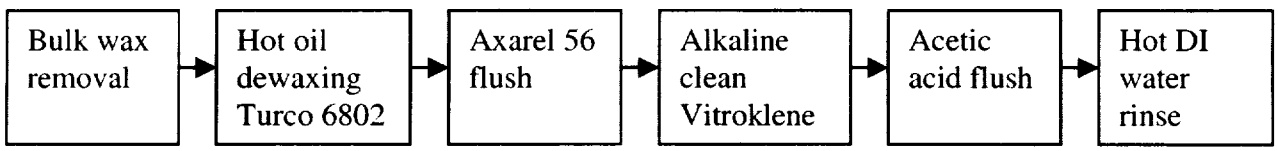

Figure 1. Current Dewax process.

The initial step of the process consists of bulk melting of most of the wax in an oven. The subsequent cleaning steps include immersion/flushing in a hot oil (Turco 6802)[2] tank, immersion/flushing in an Axarel 56[3] tank, immersion/flushing in a alkaline cleaner such as Vitro-klene[2], flushing with acetic acid and a final rinsing in a tank of hot DI water.

The above process has been successfully used, but the volatile organic content (VOC) of the Axarel 56 is 768 grams per liter. In order to meet more stringent emission requirements which would allow the process to be relocated, a VOC limit of less than 50 grams per liter must be met. Enabling the process to be relocated minimizes handling and eliminates shipping, significantly reducing cycle time. For this reason, laboratory and full scale process tests were performed to define and demonstrate a process to remove Rigidax wax from MCC liners and other hardware. In addition to eliminating the Axarel 56, it was desirable to meet certain other goals as defined below:

- Dewaxed parts shall meet a final surface cleanliness less than 1 mg/ft^2 of residual hydrocarbons.
- The process should be repeatable, robust, and not operator dependent.
- The process can be used for all items requiring dewaxing.

---

[1] Argueso, M., & Co., Inc., Mamaroneck, NY.
[2] Elf Atochem North America, Inc., Philadelphia, PA.
[3] Petroferm, Inc., Fernandina Beach, FL.

Process Evaluation – Laboratory Scale

Potential cleaning agents were identified through a vendor survey and previous experience. These cleaning agents were reviewed and subjected to rinsability and embrittlement tests. These tests measure the ability of a cleaner to rinse freely from a surface and measure whether a cleaner may cause sulfur embrittlement. Based on successful results from these tests, the cleaners were used in several different types of processes for removing wax from slotted coupons. The goal was to reduce cycle time by finding a more effective cleaner, eliminating an immersion step or otherwise optimizing the process. The processes tested included:

- Bulk Dewax / 1 Cleaner / Steam clean
- Bulk Dewax / Turco 6802 (hot oil) / 1 cleaner
- Bulk Dewax / Turco 6802 (hot oil) / 1 cleaner / Vitro-klene
- Bulk Dewax / Turco 6802 (hot oil) / Steam Rinse / 1 cleaner

The laboratory scale tests were performed with slotted coupons to simulate slotted MCC liners. Most of the dewaxing tests were performed using 3 x 5 inch copper coupons 0.5 inch thick containing 15 slots typical of liner geometry. (See Figure 2)

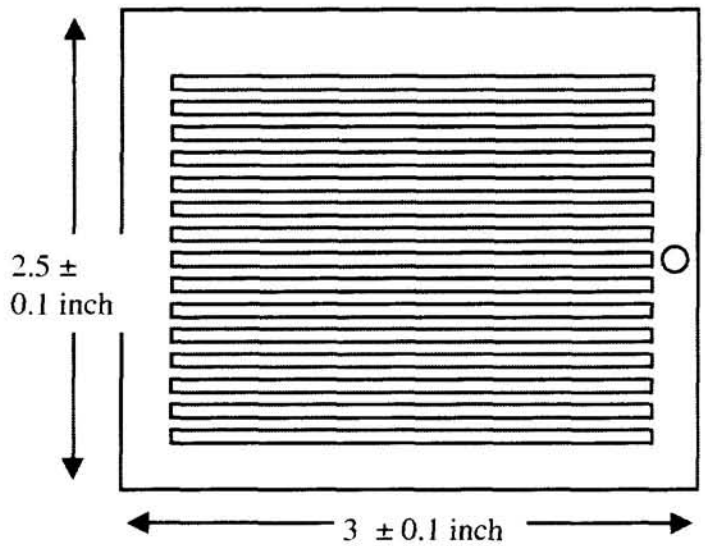

Figure 2. Test coupon used in most small scale testing.

The bulk dewaxing step in this process initially melts off most of the wax, permitting fluid to flow in the channels, and was maintained. After the bulk dewax step was simulated, the slotted coupons were suspended with the slots aligned vertically in the test fluid that was contained in a glass beaker. The test fluids were preheated to the desired temperature on a hot plate stirrer prior to immersion of the coupon. Stirring was accomplished with a Teflon coated magnetic stirring bar. Coupons were generally weighed to 0.1 mg before waxing, after waxing, after all dewaxing steps were complete, and after residual hydrocarbon analysis. A DI water rinse was used after each immersion cleaning. As a result of these tests, Turco 6849[2] was selected as the most promising cleaner.

Residual hydrocarbon analysis was performed by first suspending the cleaned coupon vertically in a beaker and then rinsing the coupon slots with cyclohexane. After evaporation of the cyclohexane, FTIR analysis was used to quantify the amount of residual hydrocarbons. Only the coupon slots were rinsed and analyzed for hydrocarbons. The flat sides and back of the coupon were not subjected to hydrocarbon analysis. The amount of residual hydrocarbons detected was used as the basis for determining how well the coupons were cleaned.

Use of steam cleaning and use of a single cleaner following the Turco 6802 did not yield acceptable levels of cleanliness. Use of Turco 6802 followed by a steam rinse followed by Vitro-klene did result in acceptable cleanliness levels. However, since one goal is to have a process that is not operator dependent, the use of steam cleaning, which is operator dependent, was only considered as a secondary process choice.

X-ray Photoelectron Spectroscopy was used to analyze the surface of two small slotted copper coupons that had been dewaxed with the Turco 6802 / Turco 6849 / Vitro-klene sequence. The purpose was to determine the nature of the residual material on the surface of a cleaned coupon. Both coupons had Rigidax wax placed in the small slots. One coupon was only heated in the oven and not subjected to any further cleaning. This coupon only had a coating of residual wax. The other coupon underwent the full cleaning sequence. The coupon that only had a layer of wax on it contained only carbon and oxygen species. The coupon that was subjected to the cleaning sequence contained a residue greater than 100A in thickness which contained carbon, oxygen, and nitrogen. This indicates that the residue is at least partially composed of some of the cleaning agents. This demonstrates the need for thorough rinsing.

In addition to the flat coupons, testing was performed using slotted cylinders. These cylinders represent a scaled up and somewhat more realistic test piece than the rectangular coupons. The cylinders, shown below in Figure 3, were approximately 3 inches in diameter, 5 inches long and contained 64 slots of typical geometry. The total internal area of the 64 slots was calculated to be about 1.87 ft^2. This number was used in calculations of surface cleanliness. The total surface area of the cylinders including the slots, area between slots, and the two circular ends was about 2.14 ft^2.

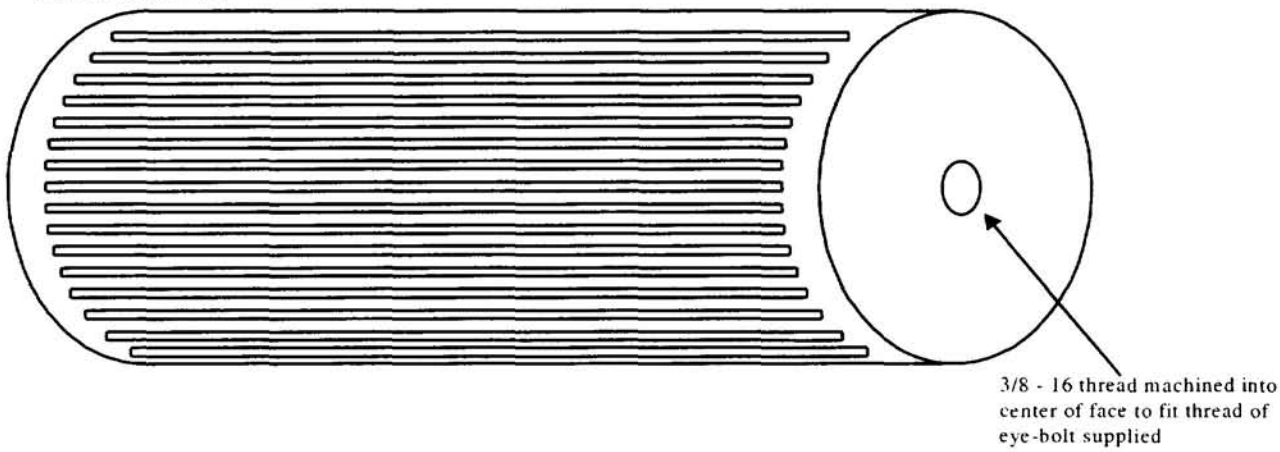

Figure 3: Sketch of slotted cylinder.

Dewaxing of these cylinders was performed in a manner similar to that used for the rectangular coupons, but with somewhat larger containers for the cleaning solutions. The cleaning sequence and results for tests with the slotted cylinders are shown in Table 1. As before, all coupons were placed in an oven for bulk wax melting. Rinsing steps were performed after all the cleaning sequences listed. An initial test of the new dewaxing sequence (#1), where all the cleaning steps were performed in the lab, gave a final cleanliness result of 1.2 mg/ft^2, higher than that observed with flat coupons or with the scrap liner.

#	Cleaning sequence	mg/ft^2
1	Turco 6802, 230F, 3 hours (in lab) 20% Turco 6849, 175F, 2 hours (in lab) 8 oz/gal Vitro-klene + 2% Turco 4215, 185F, 2 hours (in lab)	1.2
2	Turco 6802, 230F, 3 hours (in lab) 20% Turco 6849, 145F, 2 hours (in tank P-6, Auburn, WA) 8 oz/gal Vitro-klene + 2% Turco 4215, 185F, 2 hours (in lab)	1.6
3	Turco 6802, 230F, 3 hours (in lab) 20% Turco 6849, 145F, 1 hours (in tank P-6, Auburn, WA) 8 oz/gal Vitro-klene + 2% Turco 4215, 185F, 2 hours (in lab)	0.70
4	Turco 6802, 230F, 3 hours (in lab) 20% Turco 6849, 145F, 1 hours (in tank P-6, Auburn, WA) 8 oz/gal Vitro-klene + 2% Turco 4215, 185F, 2 hours (in lab) 50% Acetic acid, ambient temperature, 2 hours	0.53
5	Turco 6802, 230F, 2 hours (in dewax area at SSFL) 20% Turco 6849, 150F, 2 hours (in lab with better stirring) 8 oz/gal Vitro-klene + 2% Turco 4215, 185F, 2 hours (in dewax area)	0.68, 0.97

Table 1: Results for slotted cylinders.

In the next three tests with the slotted cylinders (#2-4), the cleaning step with Turco 6849 was performed in a large process tank. The other cleaning steps were performed in the lab. The cylinder treated for only 1 hour in the Turco 6849 was significantly cleaner than the cylinder treated for 2 hours. At this point, it was suspected that the agitation of the solution in the lab, which consisted of suspending the slotted cylinder in a beaker stirred with a magnetic stirring bar, may not have been vigorous enough to get sufficient cleaning. For the last test with the slotted cylinders (#5), two slotted cylinders were used. To achieve better stirring, the hot oil and Vitro-klene steps were carried out in actual process tanks at SSFL. Also, in the Turco 6849 cleaning step, a more powerful mechanical stirrer was used. Both of these cylinders were cleaned to levels below 1 mg/ft^2. The stronger agitation in all the cleaning steps had a significant beneficial effect on final surface cleanliness. Analysis of these cylinders was performed by soaking them in cyclohexane followed by FTIR analysis of the evaporated residue.

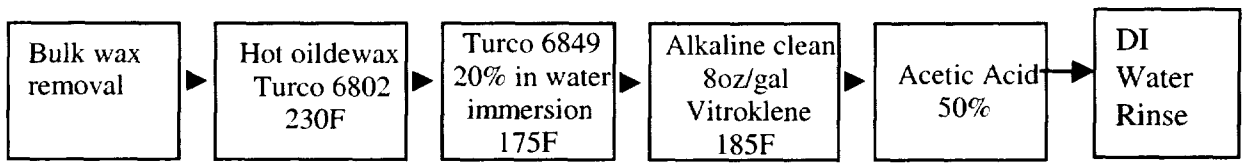

Figure 4. New Dewax Process.

The Bulk Dewax / Turco 6802 (hot oil) / Turco 6849 / Vitro-klene process shown in Figure 4 was selected as the new process. Turco 6849 also has a high loading capacity. Tanks of Turco 6849 at Boeing facilities in Auburn, WA can typically be used up to contaminant loadings of 7%. The cleanliness level achieved on a lab scale with this process was 0.5 ± 0.2 mg/ft^2 based on six replicate tests. The base line process was also performed on a lab scale for comparison purposes and achieved a final cleanliness of 0.2 ± 0.2 mg/ft^2 based on four replicate samples. Thus, the new dewax process was demonstrated to remove wax to a final surface cleanliness of $< 1 mg/ft^2$. The remainder of the work focused on materials corrosion tests, optimization of process parameters on a small scale, and demonstration of the process on a full scale part.

In addition to cleanliness tests, corrosion tests were performed to ensure compatibility of the new cleaner with materials of construction. This resulted in Turco 6849 being tested with 12 different materials associated with a typical MCC. These included copper, Narloy-Z, Hastelloy W, Alloy 625, Alloy 718, 321 CRES, 347 CRES, 21-6-9, Incoloy 903, A286 and electrodeposited Nickel. The test solution was at 20-wt% in water, the highest concentration recommended for use. Corrosion tests were performed at both 175F and 145F. Following preliminary abrasive cleaning with Scotch-Brite and DI water, the specimens were dried and weighed. They were then immersed for 20 minutes in the heated solution while it was stirred. The samples were removed from the solution and allowed to cool

for 24 hours to ambient temperature, rinsed, dried, weighed and evaluated. None of the materials were affected by contact with Turco 6849 at 145 F. There were some affects observed at 175F, but they were less than a 0.01% weight change and the intent is to operate at the lower temperature.

Process Optimization with Taguchi Matrix Tests

Process variables for this process with three cleaning steps include cleaner temperature, concentration, cleaning time, and rinsing characteristics. In an effort to optimize these process variables, a Taguchi type test matrix was developed. Taguchi methods can be used to optimize several process variables with a minimum of testing. The goal of this type of testing is to minimize both the residual hydrocarbons present on the cleaned parts and to achieve consistent results from test to test. The following control factors (process variables) and levels were selected for analysis in an L8 type matrix.

Control factor	Level 1	Level 2
Turco 6849 temperature	150F	175F
Vitro-klene temperature	185F	170F
Oil immersion time	3 hours	2 hours
Turco 6849 immersion time	2 hours	1 hour
Vitro-klene immersion time	2 hours	1 hour
Turco 6849 concentration	20%	10%
Vitro-klene concentration	16 oz/gal	8 oz/gal

Table 2: Control factors and levels used in optimization.

The temperature of the Turco 6802 oil was not selected as a factor to be studied in the Taguchi analysis. Since the hot oil dissolves wax, it is expected that the higher the temperature of the oil, the better the wax dissolution (wax removal). The oil is now operated at 230 ± 20 F which is the highest temperature allowed due to safety concerns. For this reason, the temperature of the oil was not included in the Taguchi analysis.

In the testing, three replicate coupons were used for each trial. The average of the results (mg/ft^2) residual hydrocarbons) on each set of coupons and the average of the signal to noise ratio for each three replicate tests were used in further calculations. The signal to noise ratio S/N was calculated as $-10 \log\{[(result1)^2 + (result2)^2 + (result3)^2]/3\}$. A higher S/N indicates more reproducibility in the results. Coupons for all tests were initially waxed with Rigidax wax.

Prior to the full Taguchi matrix tests, a set of three coupons were cleaned with the assumed best set of levels for each of the control factors. Also another set of three coupons was cleaned under the assumed worst set of control factors. Results are listed Table 3. The large difference between the best and worst conditions indicates that the control factor levels chosen are capable of showing some effect of process variables with Taguchi matrix testing.

Control factor	Initially assumed "Best" Conditions	Initially assumed "Worst" Conditions
Turco 6849 temperature	150F	175F
Vitro-klene temperature	185F	170F
Oil immersion time	3 hours	2 hours
Turco 6849 immersion time	2 hours	1 hour
Vitro-klene immersion time	2 hours	1 hour
Turco 6849 concentration	20%	10%
Vitro-klene concentration	16 oz/gal	8 oz/gal
Residual HCs	0.12 mg/ft^2	1.5 mg/ft^2
S/N	18.5	-3.9

Table 3: Initial best and worst conditions.

	Control factor	Level 1	Level 2	Average Level 1	Average Level 2	S/N Level 1	S/N Level 2
A	Turco 6849 temperature	150F	175F	0.71	1.36	5.30	2.42
B	Vitro-klene temperature	185F	170F	0.88	1.19	9.66	-1.94
C	Oil immersion time	3 hours	2 hours	0.82	1.25	4.30	3.42
D	Turco 6849 immersion time	2 hours	1 hour	1.39	0.68	0.79	6.93
E	Vitro-klene immersion time	2 hours	1 hour	0.83	1.24	8.69	-0.97
F	Turco 6849 concentration	20%	10%	1.24	0.83	2.04	5.68
G	Vitro-klene concentration	16 oz/gal	8 oz/gal	0.45	1.62	10.91	-3.19

Table 4: Results of Taguchi matrix testing.

	L8 orthogonal array							Residual wax, mg			Residual wax, mg/ sq. Ft.				
Trial	A	B	C	D	E	F	G	Panel 1	Panel 2	Panel 3	Panel 1	Panel 2	Panel 3	Avg	S/N
1	1	1	1	1	1	1	1	0.02	0.02	0.02	0.12	0.12	0.12	0.12	18.54
2	1	1	1	2	2	2	2	0.12	0.11	0.06	0.71	0.65	0.36	0.57	4.54
3	1	2	2	1	1	2	2	0.26	0.2	0.36	1.54	1.18	2.13	1.62	-4.42
4	1	2	2	2	2	1	1	0.01	0.06	0.21	0.06	0.36	1.24	0.55	2.53
5	2	1	2	1	2	1	2	0.47	0.58	0.35	2.78	3.43	2.07	2.76	-8.99
6	2	1	2	2	1	2	1	0.01	0.01	0.01	0.06	0.06	0.06	0.06	24.56
7	2	2	1	1	2	2	1	0.33	0.15	0.06	1.95	0.89	0.36	1.07	-1.97
8	2	2	1	2	1	1	2	0.22	0.23	0.33	1.30	1.36	1.95	1.54	-3.90

Table 5: L8 orthogonal array used and raw data.

Results of the Taguchi matrix testing are indicated in Figures 5 and 6. From Figure 5, the conditions that favor the least amount of residual hydrocarbons (cleanest surface) are:

- Turco 6802 oil; 3 hours immersion time.
- Turco 6849; 10% concentration, 150F, 1 hour immersion.
- Vitro-klene; 16 oz/gal concentration, 185F, 2 hour immersion.

The conditions that favor the cleanest surface are also the conditions that yield the highest (best) S/N. This last result is normal in a "least is best" type of Taguchi analysis. For the Turco 6802 and the Vitro-klene solutions, all results are as expected; a higher concentration, higher temperature and longer immersion time are beneficial. The effect of a higher Vitro-klene concentration is especially evident. For the Turco 6849, results are the opposite of what was first expected. For Turco 6849, a lower temperature and shorter immersion time were better. A lower concentration was also beneficial, but the effect of concentration was somewhat less than other factors.

One final confirmation test was performed using all the optimized conditions listed above. Results from the three coupons tested under the optimized conditions were 0.06, 0.06, and 0.06 mg/ft^2. This gives a S/N of 25. These results are better than what was originally obtained with the initially assumed "best" conditions. It can also be seen from the raw data that for trial #6 all the optimum conditions were used except that the Turco 6849 was operated at 175F and the Turco 6802 was operated for only 2 hours. This set of conditions also gave the same results as the optimum conditions. From this testing, the effects of process parameters were determined with optimized conditions as listed above. Using the predictive equations, the effect of any combination of the levels tested can be predicted. This may be valuable for an initial estimate of any trade off between cost, cycle time and process quality.

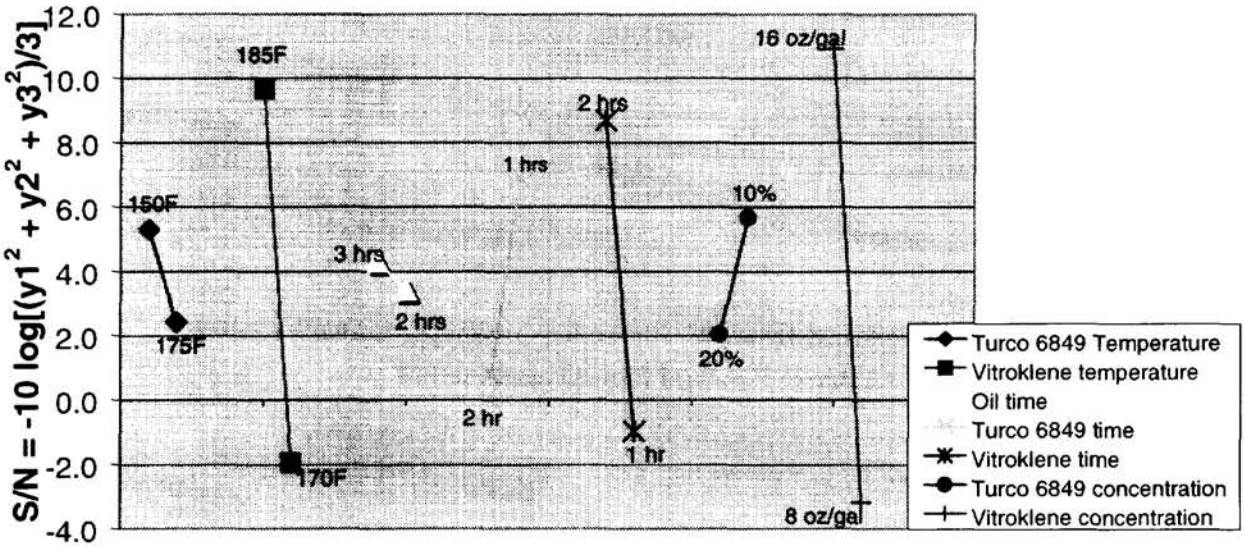

Figure 5: Results of Taguchi matrix testing.
Average values of residual hydrocarbons.

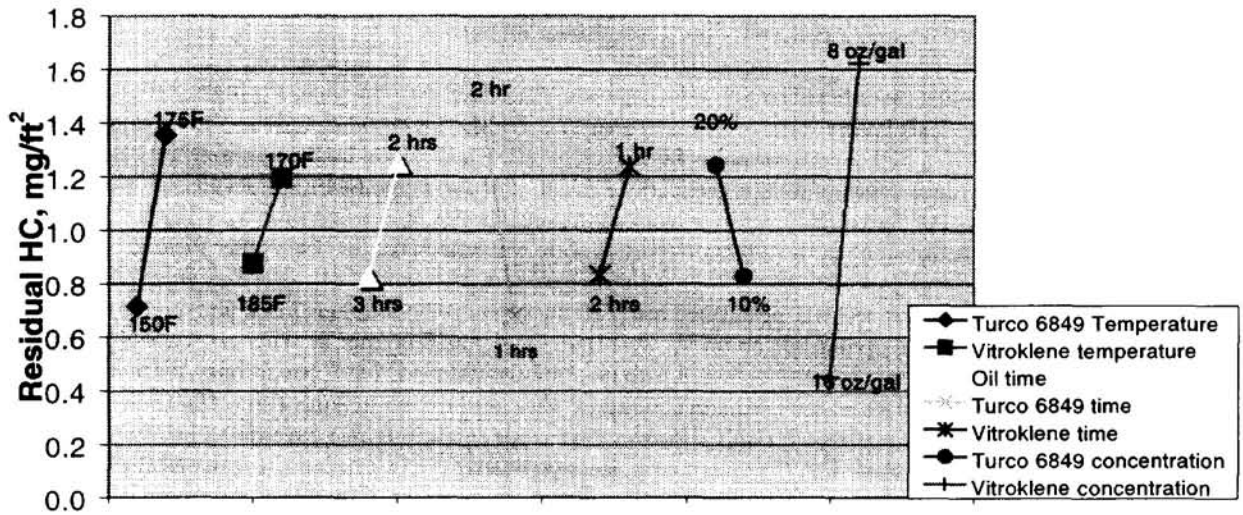

Figure 6: S/N results for Taguchi matrix testing.

Full Scale Process Demonstration

Demonstration of the immersion process on a full-scale test article was performed with a scrap SSME large throat MCC liner. This liner, shown in Figure 5 below, was 24 inches OD at the widest point, 29 inches tall and contained open channels. Each channel has an internal surface area of about 0.064 ft^2.

Figure 7. Scrap SSME large throat MCC liner.

All operations except immersion in the Turco 6849 were performed at Rocketdyne. Tank P-6 at Boeing facilities in Auburn Washington contains Turco 6849 at a concentration of about 18% and was used for the immersion step. This tank is commonly used for cleaning aluminum, titanium, stainless steels and Inconel alloys. The tank is fitted with two turbulators for agitation and is typically operated at 140F to 150F. The liner was placed in a basket which was lowered into the Turco 6849 tank. After cleaning, rinsing, and drying, the liner was wrapped in Aclar sheet prior to shipment. The following sequence of process steps were performed:

1. Channels filled with Rigidax Wax (Canoga)
2. Liner heated in oven for bulk wax removal (Canoga)
3. Immersion in Turco 6802 oil at 230F for 2 hours (SSFL dewax area)
4. Rinse and GN2 dry (SSFL dewax area)
5. Immersion in 18% Turco 6849 at 145F for 2 hours (Auburn, WA)
6. Part soaked briefly in 140F rinse water (tank P4A in Auburn, WA)
7. Part soaked briefly in 103F rinse water (tank P4B in Auburn, WA)
8. Liner placed in hot air drier (tank P-7 in Auburn, WA)
9. Immersion in Vitro-klene tank, 8oz/gal, 185F, 2 hours (SSFL dewax area)
10. Rinse and GN2 dry (SSFL dewax area)

After all the cleaning steps were complete, the residual hydrocarbon content in the slots was measured. Each of ten adjacent slots was rinsed with cyclohexane. The cyclohexane was collected, combined for a total of about 300 ml and evaporated. FTIR analysis was used to quantify the amount of residual hydrocarbons. Duplicate analyses were performed on five different sections of the liner which resulted in an overall average of 0.33 ± 0.28 mg/ft^2 ,with the highest value being 0.70, all at a final cleanliness level less than 1mg/ft^2.

Conclusions

Conclusions from the study on Dewax development include:

- A robust process has been demonstrated on small slotted coupons and on a scrap SSME MCC liner that is capable of wax removal to less than 1 mg/ft^2
- The new cleaner passes embrittlement, rinsability, and corrosion tests and has a VOC content < 50 grams per liter.
- Process optimization through Taguchi matrix analysis has allowed process parameter selection to reproducibly yield coupons cleaned to the levels of analytical capability (< 0.1 mg/ft^2)

Acknowledgments

The authors would like to thank Dr. Carl Schack and Mr. Larry Hill (Boeing Canoga Park) for supporting this effort by conducting these laboratory experiments in their usual excellent manner.

Highly Effective, Low Toxicity, Low Environmental Impact Total Flooding Fire Suppressants

Suzanne M. Glass, Patrick M. Dhooge, and Jonathan S. Nimitz
Environmental Technology and Education Center (ETEC)
4500-B Hawkins St. NE
Albuquerque, NM 87109-4517
Phone: (505) 345-2707
http://www.etec-nm.com
pdhooge@etec-nm.com jnimitz@etec-nm.com

INTRODUCTION

Halon 1301 (CF_3Br) has been used for decades as the primary fire suppression agent for areas where powder agents cannot be used because of concerns for sensitive equipment. Halon 1301 is an excellent extinguishing agent, effective at about 3% in air and quite non-toxic. It has an effective exposure limit much greater than its extinguishing concentration, so it can be used in normally occupied areas.

The ability of a chemical to destroy stratospheric ozone is its ozone-depletion potential (ODP). ODP is the amount of ozone destroyed per pound of a chemical, relative to the standard CFC-11 with an ODP = 1.0. Because halons have been implicated in stratospheric ozone depletion, their production was stopped at the end of 1995 under the provisions of the Montreal Protocol plus later amendments (Environmental policy and law; Grey; International Lawyer; Zurer). In the U.S., the Clean Air Act Amendments of 1990, Presidential directives, and DoD Directive 6050.9 implemented this phaseout (United States a; United States b). These regulations and penalties have provided strong incentives for U.S. businesses to decrease CFC use. The Omnibus Budget Reconciliation Act of 1989 mandates high Federal taxes on CFCs and halons, designed to price them out of the market. The taxes also capture for the government the windfall profits that would otherwise go to producers as scarcity drives up prices.

Several replacements have been developed for Halon 1301. One is carbon dioxide, which has been used as a firefighting agent for many years. However, a high concentration of carbon dioxide is necessary to inert fuels. The effective concentration for inerting with carbon dioxide is approximately 29%, which is above the concentration lethal to humans. HFC-227ea is being used extensively to replace Halon 1301 systems in normally occupied areas and some normally unoccupied areas. However, since the effective concentration of HFC-227ea is about three to four times that of Halon 1301 the extinguishing systems have to be larger and new extinguishing systems have to be installed. HFC-125 is also being sold as an extinguishing agent (Nimitz). It has problems similar to HFC-227ea, with a greater concentration needed for effectiveness and the need to use a larger system. This is a particularly onerous penalty in aircraft and spacecraft, where weight and space are extremely important, and substitution is often impossible in existing aircraft due to space limitations.

Several research groups have conducted extensive and productive studies on the inerting concentrations and combustion chemistry of halons and candidate halon replacements. These groups have included, among others, researchers at NIST, NMERI, and the Naval Research Laboratory (Brabson, et al.; Clay, et al.; Fleming, et al.; Grosshandler, et al. a; Grosshandler, et

al. b; Hamins; Heinonen; Maranghides, et al.; Moore, et al.; Paige; et al.). Intensive investigations have been conducted to find a general replacement for Halon 1301, thus far to no avail. Some very effective agents such as $Fe(CO)_5$ and other organometallics, PBr_3, and phosphonitriles have been discovered, but they are either unstable, highly toxic, produce highly toxic byproducts in flames, or would be expensive to manufacture.

ETEC has performed studies on a number of alternative fire suppression agents, including iodofluorocarbons (IFCs), and in particular CF_3I. Iodofluorocarbons (IFCs) have been shown to have excellent physical properties, zero ozone-depletion potential (ODP), extremely low global warming potential (GWP), good thermal stability, and relatively low toxicity. Previous work by the proposed PI determined that CF_3I could provide an effective, long-term Halon 1301 replacement. CF_3I is almost exactly as effective as Halon 1301. Subsequently, CF_3I has been approved under the U.S. EPA's Significant New Alternatives Policy (SNAP) for use as a Halon 1301 replacement in unoccupied areas. CF_3I has also recently been recommended as a Halon 1301 replacement for inerting the fuel tanks in the F-16 (Vitali).

The one major disadvantage of CF_3I is its relatively low threshold cardiac sensitization level. Many gaseous hydrocarbons and halocarbons sensitize animal hearts to adrenalin. The possibility of death from heart fibrillation after exposure to a halocarbon was first realized in the 1960s. A standard test was developed at that time to determine the relative cardiac sensitization of compounds. The test uses Beagle dogs that are injected with enough ephinephrine (adrenalin) to be barely under the amount that would cause that dogs' heart to go into fibrillation (this dosage is determined for each individual dog in the test group). After injection, the dogs are exposed to concentrations of the test compound in air. The minimum amount of the compound found to induce heart irregularities is the LOAEL, or Lowest Observable Affect Exposure Limit. The NOAEL, or No Observable Affect Exposure Limit, is the maximum concentration the dog can be exposed to with no affect. This test is quite rigorous, since the dogs are already just below the point of fibrillation due to the very high ephinephrine level. It has been estimated that the levels used in these tests may be 100 times or more higher than would be seen in a highly frightened test subject (Vinegar). This test's relevance is being questioned, but it remains the standard at this time. CF_3I's NOAEL of 0.2% is well below its effective concentration for total flooding applications, and therefore it is not approved for use in normally occupied areas.

As part of its effort to develop low atmospheric impact, high capacity, energy-efficient refrigerant blends for NASA Kennedy Space Center, ETEC investigated several gaseous combustion suppression agents. The rationale for this was to inert flammable compounds that are otherwise excellent refrigerants. Examples of such compounds are R-152a, R-161, and propane. If a gaseous combustion suppressant could inert the flammability of a good refrigerant compound at a low enough concentration that the good refrigerant properties of the flammable compound could be retained, the result would be a desirable new refrigerant blend. There is precedent for this approach in refrigerant blends such as R-500, a blend of R-152a and R-12 where R-152a's flammability is suppressed by R-12.

In the course of our studies, some interesting results were obtained, including some unexpected results involving the flammability suppression effectiveness of CF_3I and identification of a new suppression agent that appears to be considerably more effective than

Halon 1301 or CF_3I. The new agent has promise of having acceptably low toxicity to be used as a total flooding fire suppression agent in normally occupied areas.

In addition, development work for the U.S. Air Force Research Laboratory on new IFC-based solvents produced data on their flammability suppression effectiveness and flammability. The results of these studies included here because they are also of potential interest for fire suppression applications.

RESULTS AND DISCUSSION

Flammability Suppression of Solvents by Selected IFCs

The definition of flammability for liquid compounds is a flash point less than or equal to 333.5 K (60.5°C or 141°F). A combustible liquid is defined as having a flash point between 333.5 K and 366 K (93°C or 200°F) (United States c). A liquid with a flash point above 366 K is often described as nonflammable or noncombustible, but we prefer to use the term fire-resistant. Any material that can oxidize can be made to combust under severe enough conditions (for example, in high pressure oxygen).

The studies done to support alternative solvent development concentrated on near-azeotropic blends of IFCs with flammable solvents. Near-azeotropic blends were identified by computer modeling to narrow the range of candidate blends followed by distillations of mixtures to identify near-azeotropic, i.e., constant-boiling, compositions. In distillation studies, nine (9) near-azeotropic blends of IFCs with flammable solvents were identified. These blends were tested for flammability using Setaflash® open and closed cup (ASTM D 4206-89 and ASTM D 3828-93), wick (ASTM D 4207-91), aerosol spray (ASTM D 3065-72), and vapor phase (ASTM Method E-681) tests.

Three of the nine near-azeotropic blends proved to be nonflammable. It was found that, in general, 40 – 60% by volume of the IFC was needed in the blend to render it nonflammable. Some of the variation appeared to be dependent on the chemical nature of the flammable compound. For instance, hydrocarbons such as pentane and cyclohexane required 55 – 60% by volume IFC for inertion, while alcohols such as ethanol and isobutanol required 40 – 45% by volume IFC.

The Vapor-Phase Flammability of Selected IFCs

Vapor-phase flammability tests produced some interesting results. The ASTM E-681 testing reported in this section was conducted based on the older version of this test (5 L test flask). ASTM E-681 is a very severe test of flammability in air that is normally used for gases such as gaseous fuels and refrigerants. This is not a standard test for solvent flammability. In this test, the compound (or mixture of compounds) at the desired test concentration in air containing 50% relative humidity is introduced into a 5 L spherical flask maintained at 373 K, allowed to equilibrate, and sparked repeatedly with a 15 KV, 30 mA spark between two platinum electrodes. Desired concentrations are prepared by pressure measurements. The compound or mixture of compounds is flammable if a resulting flame exceeds the extent of a 45° cone marked on the flask. It is not one of the standard tests used for solvents, and is not mandated for solvent flammability testing. All of the near-azeotropic blends were found to be flammable by this test, but this test also gives flammability limits in air for the normally nonflammable solvents 1,1,1-

trichloroethane (TCA) and trichloroethylene (TCE). When we tested the pure IFCs, they also gave flammability limits by this test method. The results for the IFCs are shown in Table 1, along with values for several other compounds of interest for comparison purposes. CF_3I does not combust by this test, and it is interesting that the higher IFCs we tested combust at all, since the similar fully halogenated compounds CFC-113 and perchloroethylene do not combust in this test. Visual observations during the testing indicate that elemental iodine is released in the higher IFC combustion process. It must be noted, however, that 1-C_4F_9I, perfluoro-n-butyl iodide, was extremely resistant to oxidation by oxygen in other test methods. Perfluoro-n-butyl iodide tested only slightly less stable than CFC-113 in the liquid oxygen compatibility test. CFC-113 passes this test at 72 ft-lbs striking force. Only two out of seventeen samples of perfluoro-n-butyl iodide reacted at 72 ft-lbs, and none out of 20 samples at 65 ft-lbs. Perfluoro-n-butyl iodide's autoignition temperature in 100% oxygen at 13.8 Mpa (2000 psia) was measured as 444 – 448 K (171 - 175°C).

Table 1. Flammability Limits of Pure IFCs and Comparison Compounds in Air by ASTM E-681

Compound	Lower Flammability Limit (mole % in air)	Upper Flammability Limit (mole % in air)
CFC-113	none	none
TCA	6.5	15.5
TCE	8	10.5
perchloroethylene	none	none
CF_3I	none	none
1-C_3F_7I	13.5	34.5
1-C_4F_9I	8.2	33.1
1-$C_6F_{13}I$	7.5	25.2

Flammability Suppression Effectiveness of CF_3I on Selected Fuels

Results of some of the studies we had conducted indicated that there might be an effect from fuel type on the combustion suppression effectiveness of IFCs. Of particular interest to us in our refrigerant development studies was CF_3I.

In order to determine some of the effects of the fuel type on the inerting concentration of CF_3I, a set of simple fuels and a gas phase test apparatus was used. A gas flammability apparatus based on ASTM E-681 was used to obtain homogeneous inertion concentrations not dependent on flow rates, position of suppressant injection, or mixing efficiency. The test apparatus used in this testing was the updated apparatus specified in the recently revised E-681 test procedure. The revised version of the test uses a 12 L spherical glass flask maintained at 60^0C.

Fuels consisting of a single chemical with small molecules were used to keep complex combustion intermediates to a minimum and to determine whether any trends with chemical structure were apparent. The fuels were propane, cyclopropane, isobutane, dimethyl ether, and fluoroethane. The flammability results, over a range of concentrations, were used to prepare flammability diagrams and determine the ratios of CF_3I to fuel vapor required for inertion.

Figure 1 shows an example of an inertion diagram for one of the fuels tested with CF_3I. The data were examined in two ways. In the standard approach, the concentration of CF_3I needed

to inert any concentration of air in the fuel was determined by drawing a tangent line to the flammable region perpendicular to the CF_3I axis. We also determined the ratios of CF_3I to fuel needed to give nonflammable compositions in air. To achieve this a tangent line was drawn from the origin through the lower borderline of the flammable region. The slope of this line gave the minimum ratio of CF_3I to the flammable component necessary to inert the blend at any concentration in air. We refer to this line as the dilution line because it represents all possible dilutions of the borderline nonflammable composition in air. Both of these tangent lines are shown in Figure 1.

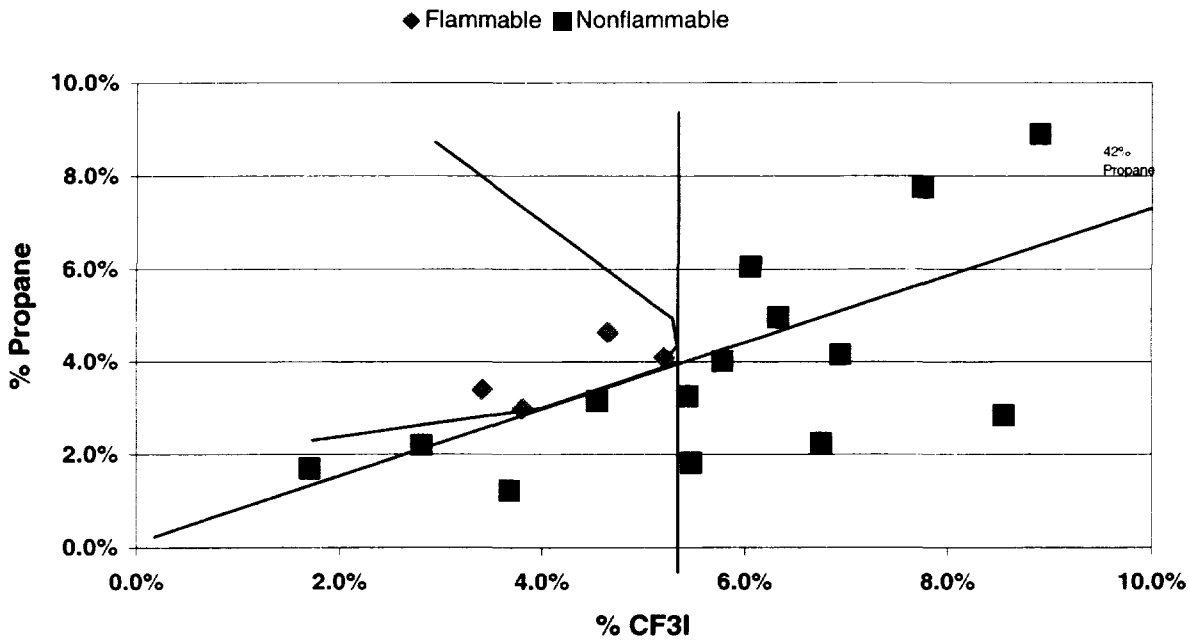

Figure 1. Inertion Diagram for Propane and CF_3I Flammability by ASTM E-681

Table 2 shows the percentages of CF_3I needed to inert the five fuels tested and the ratios of CF_3I to fuel needed for inertion. All percentages are given by moles. The absolute percents of CF_3I needed to inert the fuel have a relatively high uncertainty (±0.5%) because we were primarily interested in the ratios of extinguishant to fuel.

Table 2. Mole Percentages and Ratios of CF_3I Needed to Inert Selected Fuels in ASTM E-681

Flammable Gas	Absolute Mole Percent CF_3I to Inert Fuel	Mole % CF_3I in Blend with Fuel Needed to Inert	Mole Ratio CF_3I/Fuel Needed to Inert
fluoroethane (R-161)	4.8	45	0.82
propane	5.4	57	1.38
isobutane	5.2	62	1.63
dimethyl ether	57	>95	>20
cyclopropane	44	>95	>20

The results obtained are consistent with known previous data for combustion suppression effectiveness of CF_3I. Previous work has shown that CF_3I and Halon 1301 have very similar inerting concentrations for propane in the explosion sphere, 6-7 mole percent absolute or 54-58 mole percent in fuel blends (Moore, et al.; Heinonen). Although the apparatus used in the previous studies was somewhat different from ours, the results for propane are in good agreement. The results for isobutane are in excellent agreement with the results of an EPA study which found the flammability borderline to be at a ratio of 62 mole percent CF_3I to 38 mole percent isobutane (Baskin, et al.).

The unanticipated finding was that CF_3I was extremely ineffective at inerting dimethyl ether and cyclopropane, requiring over 40 mole percent absolute or over 95 mole percent in the fuel blend. To attempt to understand the somewhat surprising ineffectiveness of CF_3I in inerting dimethyl ether and cyclopropane, we considered the fuels' chemical structures and heats of combustion. Table 3 lists heats of combustion for the fuels. No differences are apparent that explain the results obtained. Chemically, the differences between these fuels and the hydrocarbons or hydrofluorocarbons are that one of the fuels contains an oxygen atom and the other has a highly strained ring, both of which may significantly affect chemical reactivity. Clearly, these fuels are either increasing the rate of flame radical propagation or heat generated, or decreasing inhibitory species. It is also possible that exothermic chemical reactions are occurring between CF_3I and dimethyl ether or cyclopropane. However, our data set is very limited and studies with additional fuels would be needed to determine what is occurring. In any event, the results obtained here should not affect the large majority of proposed uses of CF_3I as a total flooding fire suppressant, since fuels of concern rarely contain ethers or cyclopropanes.

Table 3. Heats of Combustion of Selected Fuels

Fuel	$-\Delta H_c°$, kcal/mole	$-\Delta H_c°$ per carbon atom, kcal/mole
ethane (for comparison)	373	186
propane	530	177
isobutane	685	171
cyclopropane	500	167
dimethyl ether	348	174
fluoroethane (R-161)	308	154

Flammability Suppression Effectiveness of ETEC Agent A

In the course of our investigations into combustion suppressant agents for flammable refrigerants, several other known combustion suppressant agents and several experimental combustion suppressant agents were tested. One agent proved to be particularly effective in inerting gaseous fuels. The new agent, given the temporary name ETEC Agent A, is in general a better combustion suppressant than CF_3I, HFC-125, or HFC-227ea, and, from the toxicity data that is known, has promise to be acceptable for use in normally occupied areas. ETEC Agent A is proprietary at this time, but the results of combustion suppression testing with it can be shown.

Figures 2 through 4 show some combustion suppression results for ETEC Agent A compared to CF_3I and HFC-227ea. As shown in the previous section, CF_3I was found to be very ineffective in suppressing the combustion of cyclopropane and dimethyl ether. HFC-227ea is

somewhat effective on these fuels, but still requires a large amount to inert. ETEC Agent A is significantly better than both CF_3I and HFC-227ea on these fuels that are very difficult to inert. CF_3I is very effective in inerting isobutane and other hydrocarbons. HFC-227ea is considerably less effective than CF_3I with respect to hydrocarbons, the source of HFC-227ea's needed extra volume and weight compared to Halon 1301. ETEC Agent A is almost as effective as CF_3I and Halon 1301 on isobutane, a typical hydrocarbon fuel.

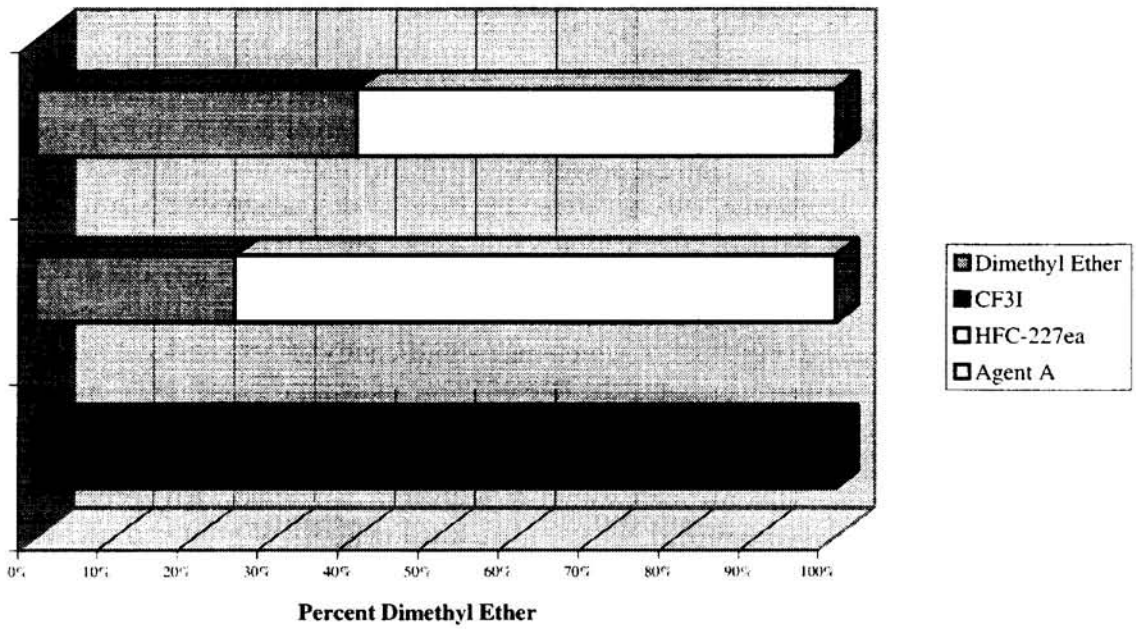

Figure 2. Flammability Suppression of Dimethyl Ether by CF_3I, HFC-227ea, and ETEC Agent A (note: CF_3I totally ineffective, 100% needed to inert)

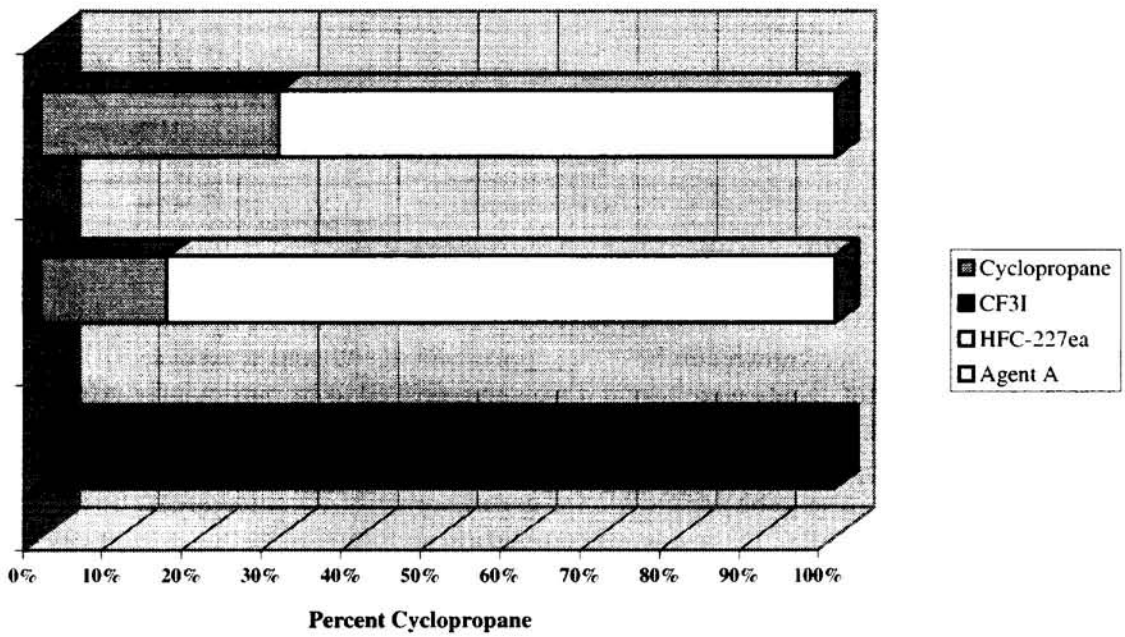

Figure 3. Flammability Suppression of Cyclopropane by CF_3I, HFC-227ea, and ETEC Agent A (note: CF_3I totally ineffective, 100% needed to inert)

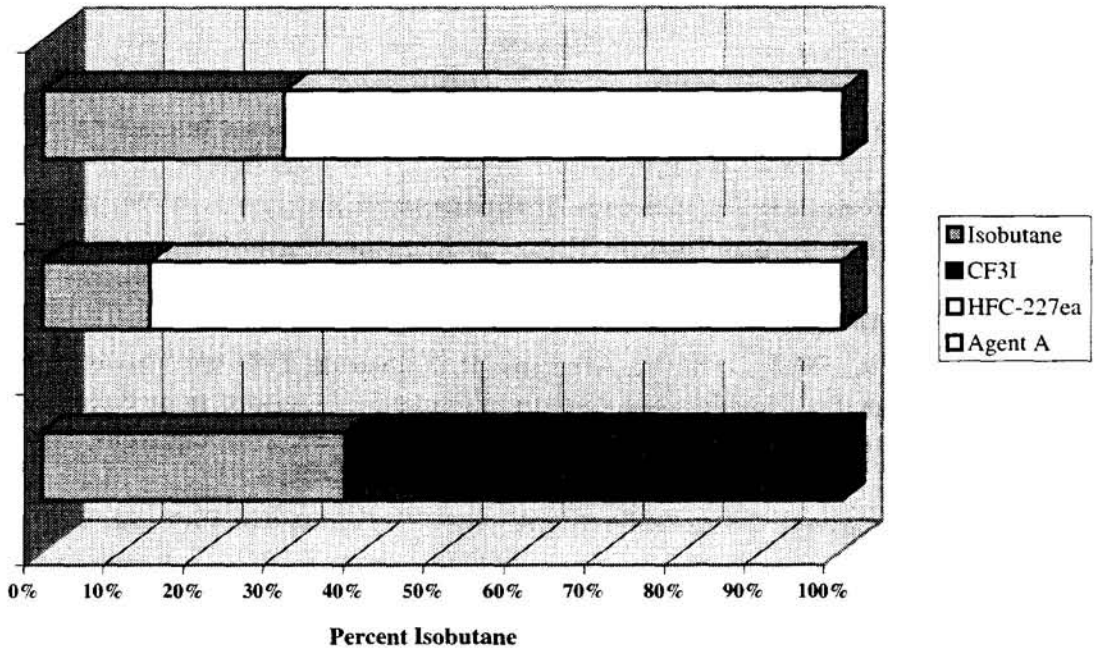

Figure 4. Flammability Suppression of Isobutane by CF_3I, HFC-227ea, and ETEC Agent A

Table 4 gives absolute mole percentages needed to inert the three fuels shown in Figures 2 through 4.

Table 4. Absolute Mole Percentages of CF_3I, HFC-227ea, and ETEC Agent A to Suppress the Flammability of Dimethyl Ether, Cyclopropane, and Isobutane by ASTM E-681

Fuel	Absolute Mole % CF_3I to Inert	Absolute Mole % HFC-227ea to Inert	Absolute Mole % ETEC Agent A to Inert
dimethyl ether	57	11	7.1
cyclopropane	44	12	8.3
isobutane	5.2	11.5	6.5

CONCLUSIONS

A new combustion suppression agent, ETEC Agent A, has been identified that has promise of being an effect Halon 1301 replacement in total flooding fire suppression applications for normally occupied areas. The new agent appears to be particularly effective on fuels whose flammability is difficult to suppress. More extensive flammability suppression studies need to be done, and the toxicity of the new agent needs to be established in detail. A retrofitable Halon 1301 replacement that could be used in the same size and weight systems would save millions of dollars in fire suppression system replacement costs, and would be particularly valuable on aircraft.

ACKNOWLEDGEMENTS

We are grateful for support of the work described here by NASA Kennedy Space Center and the U.S. Air Force Research Laboratory. We would like to thank Dr. Jacqueline Quinn of NASA Kennedy Space Center and Dr. Edward Snyder of the U.S. Air Force Research Laboratory for their valuable technical support during the efforts.

REFERENCES

Baskin, E., Smith, N. D., and Perry, R., "Flame Suppression and Lubricant Interaction of Hydrocarbon Mixtures for Household Refrigerators/Freezers," Proceedings of the International Conference on Ozone Protection Technologies, Washington, DC,Oct. 24-26, 1994, pp. 32-37.

Brabson, G. D., Walters, E. A., and Tapscott, R. E., "Insights into Extinguishment Mechanisms from Heat Extraction Experiments," abstract only in Proceedings of the Halon Options Technical Working Conference, Albuquerque, NM, May 6-8, 1997.

Clay, J. T., Walters, E. A., Willcox, M. V., Arneberg, D. L., Nimitz, J. S., and Grover, J. R., "Fundamental Studies on the Chemical Mechanism of Flame Extinguishment by Halons," Proceedings of the Halon Alternatives Technical Working Conference, Albuquerque, NM, April 30-May 1, 1991.

Environmental policy and law, "Montreal Protocol," Vol. 29, February 1, 1999, pg. 9.

Fleming, J.W., L'Esperance, D., Williams, B.A., and Sheinson, R. S., "Halon Replacement Research at the Naval Research Laboratory: Laboratory Studies," Proceedings of the International Conference on Ozone Protection Technologies, Washington, DC, October 21-23, 1996, pp. 659-668.

Grey, K. R., "Decision in the Desert: Report on the 10th Meeting of the Parties to the Montreal Protocol in Cairo," *Review of European community & international env.*, Vol. 8, 1999, pg. 160.

Grosshandler a: Grosshandler, W. L., and Gmurczyk, G. W., "Interaction of HFC-125, FC-218, and CF_3I with High Speed Combustion Waves," Proceedings of the 1995 International CFC and Halon Alternatives Conference, Washington, DC, Oct. 21-23, 1995, pp. 635-643.

Grosshandler, W. L., Presser, C., and Gmurczyk, G. W., "Effectiveness of Halon Alternatives in Suppressing Dynamic Combustion Processes," Proceedings of the American Chemical Society 208th National Meeting, ACS Symposium Series 611, Chapter 18, Aug 21-25, 1996, Washington, DC, Miziolek, A. W. and Tsang, W., Eds, pp. 204-224.

Hamins, A., "Flame Suppression by Halon Alternatives," U.S./Japan Government Cooperative Program on Natural Resources UUJNR). Fire Research and Safety, 13th Joint Panel Meeting, Vol. 2, Mar 13-20, 1996, Gaithersburg, MD, Beall, K.A., ed., pp. 119-127, 1997.

Heinonen, E. W., "The Effect of Ignition Source and Strength on Sphere Inertion Results", Halon Alternatives Technical Working Conference 1993, Albuquerque, NM, pages 565-576.

International Lawyer, The, "Montreal Protocol," Vol. 26, no. 1, pp. 148-179, 1992.

Maranghides, A., Sheinson, R.S., and Wentworth, B., "Flammable Liquid Storerooms: Halon 1301 Replacement Program," in Beall, K.A., ed., National Institute of Standards and Technology. Annual Conference on Fire Research: Book of Abstracts, Nov 2-5, 1998, Baithersburg, MD, pp. 131-132.

Moore, T. A., Skaggs, S. R., Corbitt, M. R., and Tapscott, R. E., Dierdorf, D. S., and Kibert, C. J., "The Development of CF3I As A Halon Replacement" report NMERI 1994/40, prepared under contract S-5007.7 from Applied Research Associates, October 1994.

Nimitz: Jon Nimitz and colleagues discovered and patented use of HFC-125 for firefighting. The patent is licensed to DuPont.

Paige, H.L., Berry, R.J., Schwartz, M., Marshall, P., Burgess, D. R. F., and Nyden, M.N.F., "Ab Initio Calculations and Kinetic Modeling of Halon And Halon Replacements, Proceedings of the Halon Options Technical Working Conference, May 7-9, 1996, Albuquerque, NM, pp. 1-12.

Vinegar, A. and Jepson, G. W., "Epinephrine Challenge for Cardiac Sensitization Testing vs. Endogenous Epinephrine: A Perspective," Proceedings of the Halon Options Technical Working Conference, Albuquerque, New Mexico, April, 1999, available from New Mexico Engineering Research Institute, The University of New Mexico, Albuquerque, New Mexico.

Vitali, J., Tyndall AFB, FL, personal communication to Dr. Jon Nimitz, ETEC, Albuquerque, NM, April 1999.

United States a: "Omnibus Budget Reconciliation Act of 1989," Public Law 101-189 (H.R. 2461). November 29, 1989 (103 Stat. pp. 1425-1426).

United States b: "Clean Air Act Amendments of 1990: Conference Report to Accompany S. 1630," report 101-952, U.S. Government Printing Office, Washington, DC 20402.

United States c: Code of Federal Regulations 173.120, "Hazardous Materials Guide," May 1995.

Zurer, P., "Ozone Treaty Tightened, CFC Substitutes Controlled," *Chemical & Engineering News*, December 7, 1992, p. 5. (Montreal Protocol 1992 Copenhagen amendments)

Promoted Combustion of Metals in a High-Pressure, Flowing Oxygen Environment

Miguel J. Maes
NASA Johnson Space Center
White Sands Test Facility
Las Cruces, New Mexico
(505) 524-5677
mmaes@wstf.nasa.gov

Joel M. Stoltzfus
NASA Johnson Space Center
White Sands Test Facility
Las Cruces, New Mexico
(505) 524-5731
jstoltzf@wstf.nasa.gov

ABSTRACT

Traditional promoted combustion testing has used 0.125 in. dia samples that are ignited in a pressurized, oxygen-enriched environment. Many years of testing this sample size have yielded useful data regarding threshold pressure, or the minimum oxygen pressure required to support self-sustained combustion. However, when a material is tested in a flowing system, the threshold pressure changes. White Sands Test Facility has developed a test system to burn samples in flowing gaseous oxygen. Current sample configurations are 0.5 in. dia rods and 1.25 in. dia pipes with pressures ranging up to 2000 psi and gas velocities reaching 200 ft/s. This paper describes the test apparatus, modifications made as the result of a fire, and a description of the tests currently being performed.

INTRODUCTION

In oxygen systems, metals selection is very important to ensure compatible materials are used for the system's operating conditions. Much data have been collected regarding material flammability versus pressure [1]. Typically, materials burn better as pressure increases. These data provide a good basis for choosing materials based on their flammability. However, these data are based on a material's flammability in a static oxygen environment. When the oxygen is flowing, material flammability can be enhanced or reduced depending on the flow velocity. The NASA White Sands Test Facility (WSTF) has developed a test system that can perform promoted combustion tests in flowing oxygen conditions while controlling pressure and velocity past the test sample. This paper describes the test apparatus, modifications made as the result of a fire, and a description of the tests currently being performed.

BACKGROUND

For years it has been known that materials burn much better at higher oxygen concentrations. As the demand of increased operating pressure in oxygen systems became more acute, particularly in the aerospace industry but also in industrial applications, the incidence of oxygen system fires increased because the normally inflammable metals were flammable at the higher operating pressures. This prompted the area of study known as promoted combustion. The purpose of the present study was to characterize the fire propagation properties of various metals and alloys [1]. Benz, Shaw, and Homa have outlined two major considerations that must be addressed when determining the fire hazards of metals or alloys. "First it must be determined whether the material will ignite, which requires knowledge of the minimum energy rate and temperature for ignition. Second, it must be determined whether the material will support combustion after the stimulus of the ignition source has terminated" [1]. Previous promoted combustion testing typically occurred with 0.125 in. rod configurations that were supported at either the top or bottom of the sample and ignited at the opposite end. The ignition source consisted of a magnesium cylindrical sleeve, or promoter, that was press-fit onto the sample. The promoter was wrapped with nickel-chrome or similar-type wire and ignited electrically. This "kindling chain" was effective for consistently igniting the samples, which could be tested over a wide range of pressures, depending on the chamber design. All

chamber designs shared a common feature in that they were capable of producing only static conditions of oxygen before the test and had no way to flow the oxygen at controlled velocities.

Importance of Understanding Velocity

The importance of fluid velocity affecting material flammability is particularly evident when building a campfire, for which the kindling chain of the leaves, twigs, and dead grass catches fire first and in turn ignites sticks, which ignite split logs, and so on. Suppose that the kindling wasn't burning as much as one would like. The usual response is to blow onto the embers. The normally unexcited embers now become more energetic due to the dynamics of the situation. The driving mechanism creating this apparent increase in flammability is the flow velocity. If the velocity is too high, the flames can be blown out. However, gas velocities below this range can increase the potential for fire. Flowing gas produces a forced convection effect that increases the availability of oxygen for consumption at the burning interface. The flowing oxygen also decreases the concentration of inflammable combustion products around the burning interface simply by blowing them away.

Test System Description

The test system is modeled after the static pressure promoted combustion apparatus. It consists of a cylindrical chamber that can be pressurized to 4500psi (Figure 1). The chamber body is made from 304 stainless steel, and the interior is lined with copper to protect it from the burning metal samples. Near the inlet, there is a flow-straightening device made from K500 Monel[1], and directly below it is a copper sample holder. Welded on either side of the chamber are vent ports lined with copper, which protects them from molten debris.

The system is designed so that it is very difficult for debris to make it outside the chamber. A copper slag filter separates the burning sample from the vent outlets. A series of 0.125 in. dia holes has been drilled through the side of the filter at a 15 degree downward angle to minimize slag escape. This filters out any debris larger than 0.125 in. dia. Although debris smaller than this can fit through the holes, the particles must change their direction to travel up the 15 degree incline. Specifically sized orifices can be placed on these vents to control the mass flow rate of oxygen out of the chamber. Below the slag filter is a copper catch cup whose mass is sufficient to conduct the heat from the molten slag away without damage to the cup or chamber body. Two copper terminals that extend down from the top exterior of the chamber ignite the samples. Each terminal is attached to a Kemlon®[2] electrical feedthrough. The terminals have adapters that can be mated with banana-plug type connectors. The pyrofuse wire used to ignite the promoters is attached to the banana plugs. A sapphire crystal view window is mounted onto the chamber wall, with copper crush washers providing the sealing surfaces. The window is housed in a Monel viewport boss flange. A borescope connected to a video camera is mounted to this viewport flange to view and record the burning sample. The chamber is located downstream of a heat exchanger capable of heating the oxygen to 1000 °F. The system supplying the oxygen is capable of producing 6000 psi at a mass flow rate of 8 lb_m/s.

Three pressure transducers and one thermocouple record the test data. One transducer is tapped into the chamber wall opposite the view window to record the chamber pressure, which is also the test article pressure. The other two transducers and thermocouple are located in a four-way block that is connected directly upstream of the chamber inlet. One of these transducers is used as a report-back channel to a pressure control valve, which is computer controlled and regulates itself to achieve the desired pressure.

Test Configuration

Test samples are held vertically and supported at the top from the copper sample holder with setscrews. Oxygen flows into the chamber from top to bottom, and the test samples are ignited at the bottom. Therefore, this testing evaluates material flammability in a counterflow environment.

Currently WSTF is testing two different sample configurations. One configuration is flow in a pipe. Pipes ranging up to 1.25 in. dia schedule XX can be tested at pressures up to 1500 psi, with velocities of 50 ft/s, 100 ft/s, and 200 ft/s. The samples are 5.5 in. long, and the oxygen flows inside the pipe. Depending on the pipe thickness, the promoter is counterbored and either sunk into the wall thickness or attached to the exterior of the pipe.

---

[1] Monel® is a registered trademark of Inco Alloys International, Inc.
[2] Kemlon® is a registered trademark of Kemlon Products.

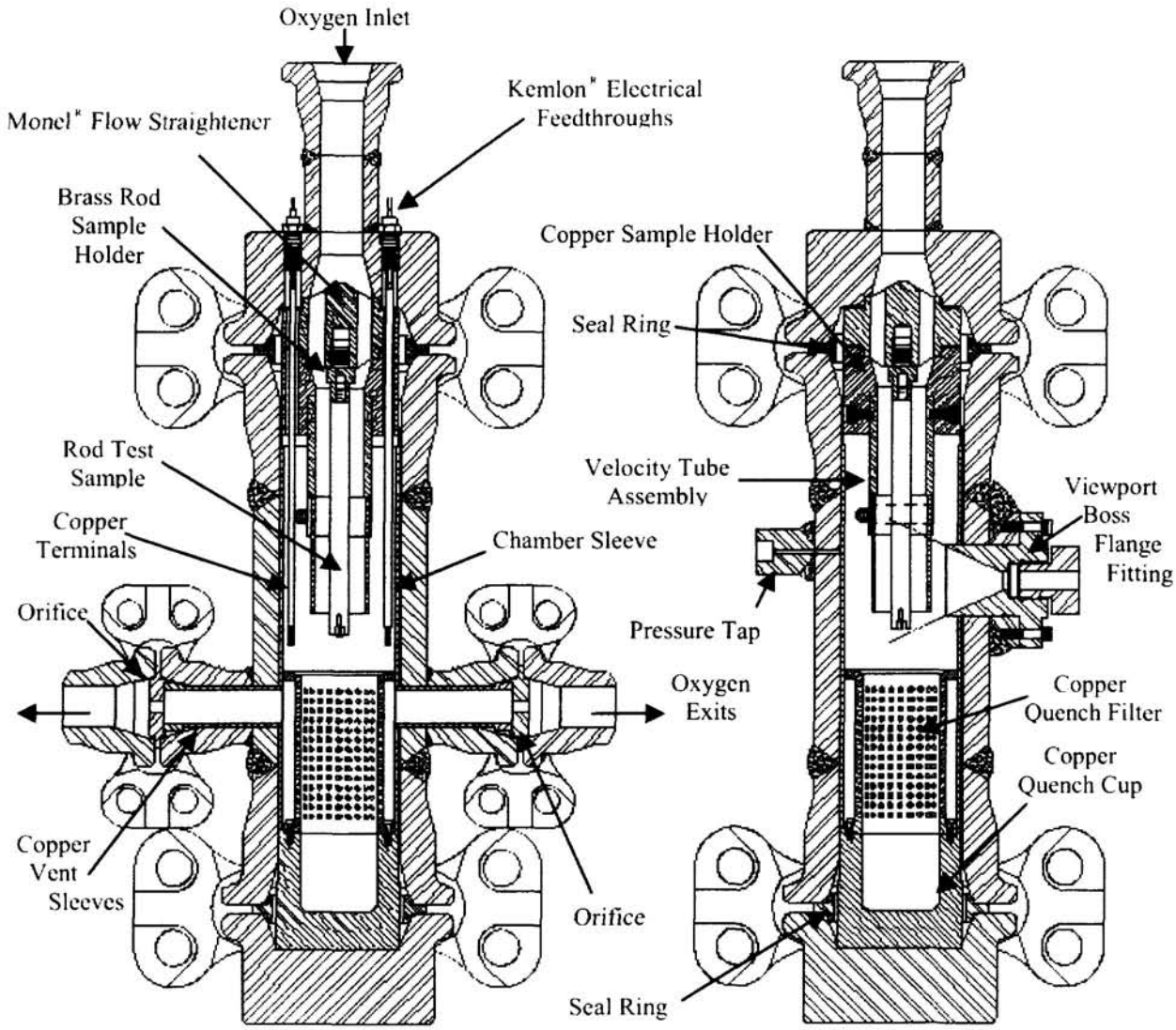

Figure 1
First Test Apparatus, Front View (left) and Side View (right)

The other configuration is a 0.5 in. dia rod. A 1.378 in. ID mock pipe called the velocity tube, consisting of a copper upper section and a quartz lower section, is clamped into the sample holder. The quartz tube slides into a countersunk region in the copper tube, and the two are connected by a worm clamp that compresses petals on the copper tube against the exterior of the quartz tube. Quartz is used because of its extremely low coefficient of thermal expansion, which keeps it from cracking or breaking if it comes into contact with molten metal; the molten metal simply quenches onto the quartz. The 0.5 in. rod is screwed onto a brass sample holder, and the test article assembly is then screwed into the bottom of the Monel flow straightener. Similar to the pipes, the rods have been tested at pressures ranging up to 1500 psi at velocities of 50 ft/s, 100 ft/s, and 200 ft/s. Flowing oxygen passes over the sample but within the velocity tube. By knowing the cross-sectional flow areas and the mass flow rate, gas velocity can be calculated.

RESULTS

The original intent of this paper was to present combustion data for 0.5 in. dia aluminum, carbon steel, and 304 stainless rod samples. However, during testing of a 1.25 in. dia schedule XX pipe sample at a 500 psi, 200 ft/s flow velocity, an event occurred that resulted in destruction the test chamber. Therefore, no test data were collected.

The remainder of this paper will discuss the results of the fire and modifications that have been performed to rebuild a better chamber.

After test sample ignition, a larger fire began on the right side of the chamber. Most of the right vent port (Figure 2, front view) was consumed during the fire. The chamber fire was extinguished by shutting off the oxygen flow. A 3 in. dia hole remained where the vent hub was welded to the chamber, and 75 to 90 percent of the clamp and right exterior hub were consumed in the fire. Internally, the thinnest sections of the copper quench filter and most of the chamber sleeve were melted or eroded away on the right side. This was the first test conducted on schedule XX pipes in this chamber at this flow velocity. Schedule XX pipes had been tested in this chamber at higher pressures and slower velocities of up to 1500 psi and 50 ft/s. After investigation of this incident, it was determined that a dimensioning tolerance exposed a 0.04 in. annular ring of chamber wall around each copper vent sleeve. The vent sleeves and the Monel viewport boss flange protruded through the copper chamber sleeve as a means of eliminating exposure of molten metal to the chamber wall. This of course was dependent on machining tolerances being tight enough to seal around the protruding pieces. Recall that the chamber was made of 304 stainless steel, for which data show the lower flammability threshold to be around 500 psi. It is believed the 200 ft/s flow was more efficient at distributing molten slag into crevices leading to the chamber wall. The conditions between the copper liner and the chamber wall produced a condition favorable to combustion of a nominal 4.5 in. dia stainless steel pipe with a wall thickness of 0.674 in.

Figure 2
Burnthrough of First Test Apparatus, Right Vent Port

Test Apparatus Modifications

The test apparatus has since been modified and rebuilt (Figure 3), which does not show the entire assembly as in Figure 1. Instead, it shows the major modifications which includes enlarging the inner diameter of the chamber to increase the thickness of the copper liner. This increased thickness allows for a sufficient counterbore to be drilled to accommodate the vent sleeves. The sleeves no longer protrude into the flow; instead, they extend just to the inner diameter of the chamber sleeve. The sleeves now have a recessed lip that exactly fits the counterbore depth. Also, the vent sleeves have been made thicker to provide more protection to the vent walls. Another modification was to eliminate the protruding edge of the viewport flange. The overall length of flange was shortened, and one end was "fishmouthed" to the exact radius of the outer diameter of the inner sleeve. When bolted down, the edge of this fishmouth cuts into the chamber sleeve, thereby producing a sealing surface. To protect the resulting cavity, another modification was made to the chamber sleeve. The top 4 in. of the sleeve now has a counterbore to fit large quartz sleeves. The inner diameter of these quartz sleeves matches the inner diameter of the lower portion of the chamber sleeve. Once again, quartz is used because the molten metal quenches onto the quartz sleeve without any damage to the chamber. In addition to the modifications made, another component was added to further fireproof this new chamber. A quench ring that is press-fit into the inner diameter of the chamber sleeve directly above the quench filter has been added. This quench ring is simply a thick ring of copper to act as a heat sink to protect the upper lip of the quench filter.

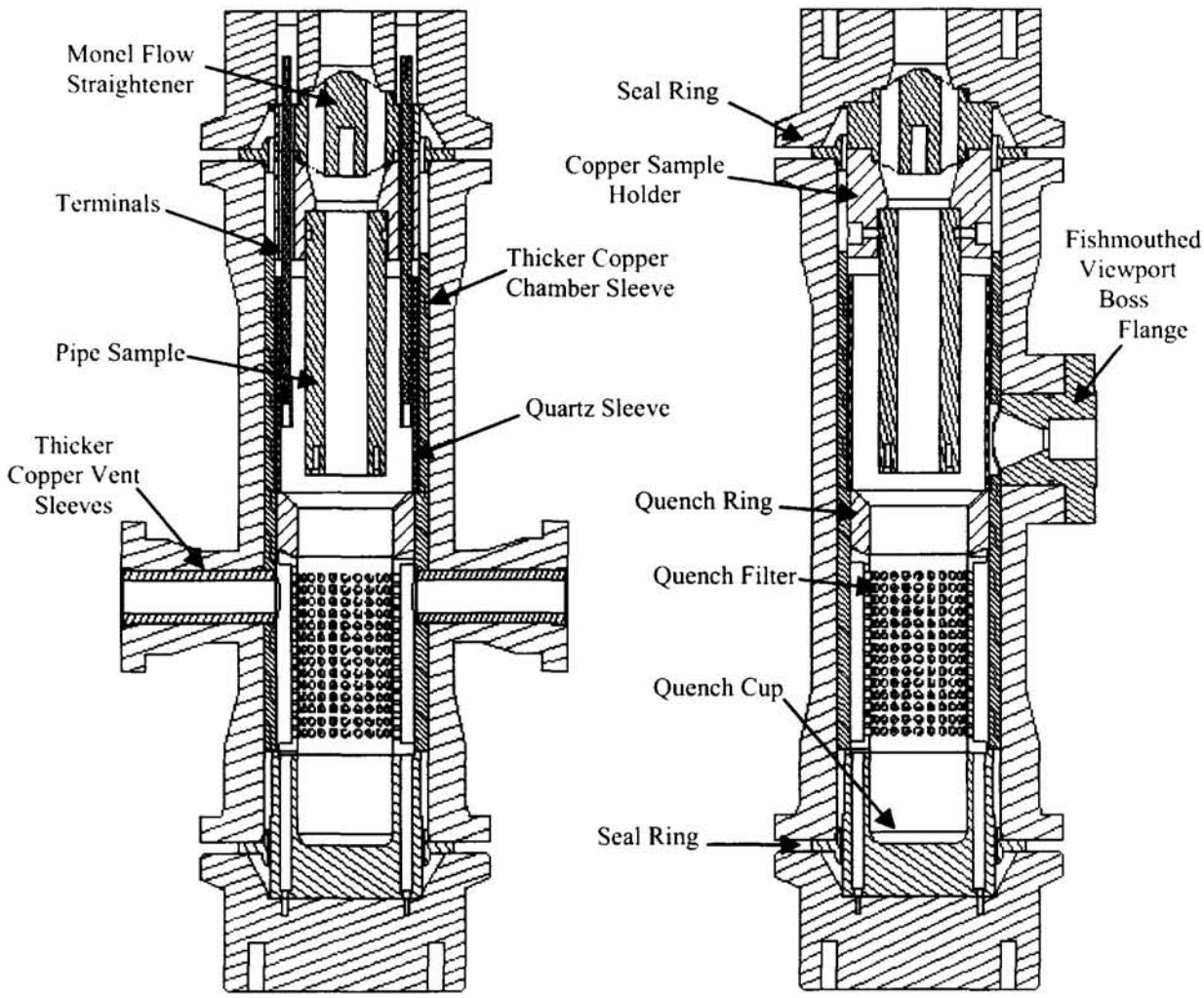

Figure 3
Second Test Apparatus after Improvements, Front View (left) and Side View (right)

CONCLUSIONS

The remaining 1.25 in. dia samples have been tested at the same flow velocities that destroyed the first chamber. The modifications performed have proved to be effective in eliminating the problems that existed in the first test chamber. Tests that have been performed to date include 0.5 in. dia rods and 1.25 in. dia pipes at 500 psi, 1000 psi, and 1500 psi with velocities 50 ft/s, 100 ft/s, and 200 ft/s. Flammabilities are increased with flow velocity, but there exists a point at which the velocity is too great for a material to sustain combustion. WSTF now has the capability to test metals flammability in flowing conditions. A new realm of data can and should be obtained for materials in flowing oxygen. Perhaps there are conditions that materials exhibit increased flammability with pressures lower than current threshold data shows when the oxygen is flowing. To a systems engineer, this type of data would be very useful to improve the design of oxygen systems.

REFERENCES

[*1*] Benz, F. J., Shaw, R. C., Homa, J. M. "Burn Propagation Rates of Metals and Alloys in Gaseous Oxygen," *Flammability and Sensitivity of Materials in Oxygen-Enriched Atmospheres: Second Volume*, ASTM STP 910, M. A. Benning, Ed., American Society for Testing and Materials, Philadelphia, PA, 1986, pp. 135-152.

/P/ 565 IN/82

52/2ND

PROBLEM SOLVING APPLICATIONS OF CHEMICAL FINGERPRINTING

MICHAEL O. KILLPACK, DENNIS J. FIFE, CHAD R. SAUNDERS, CHARLES R. WHITWORTH, AND WILLIAM H. MCCLENNEN, Thiokol Propulsion, Analytical Laboratories, P.O. Box 707 M/S 245, Brigham City UT 84302-0707

Good manufacturing processes are dependent on the ability to foresee, reduce, or quickly resolve problems critical to the quality and consistency of the end product. Thiokol has initiated a chemical fingerprinting program in conjunction with NASA, designed to identify and mitigate such manufacturing problems through a better understanding of the base materials. A historical database with real-time access maintained by a core of material specialists is an essential problem-solving tool. This "fingerprinting process" will be discussed in terms of identification of critical materials and analysis techniques, development of a comprehensive database, coordination and concerns of vendors, and actual examples where fingerprinting has been used to reduce and resolve problems.

PROBLEM SOLVING APPLICATIONS OF CHEMICAL FINGERPRINTING

MICHAEL O. KILLPACK, DENNIS J. FIFE, CHAD R. SAUNDERS, CHARLES R. WHITWORTH, AND WILLIAM H. MCCLENNEN, Thiokol Propulsion, Analytical Laboratories, P.O. Box 707 M/S 245, Brigham City UT 84302-0707

Good manufacturing processes are dependent on the ability to foresee, reduce, or quickly resolve problems. Thiokol has initiated a chemical fingerprinting program in conjunction with NASA, designed to identify and mitigate such manufacturing problems through a better understanding of the base materials as provided by the vendor as well as their interaction with other materials used in the manufacturing process. The major objectives of the fingerprinting program is to develop a comprehensive data base on critical materials, reduce the probability of unexpected or unrecognized changes, enhance the ability to detect and resolve material compatibility and environmental issues as well as understand how a material ages/degrades.

The fingerprinting process starts with the identification of critical materials and assigning of a materials specialist from the analytical labs. Along with the materials specialist, a team of personnel from manufacturing, design engineering, and quality meet and outline a plan for fingerprinting actions. One of the first actions is to review the literature and past studies performed on the material. The team then obtains several samples of the material and submits them for chemical analysis. This involves method development as well as verification of techniques previously used. Examples of analytical techniques include FTIR, NMR, HPLC, GPC, ICP, IC, TGA, DSC, GCMS, as well as a variety of other methods including mechanical properties.

Throughout the fingerprinting process a relationship with the material vendor is cultivated. An initial contact is made at the start of the fingerprinting process to inform them of the goals and purpose of fingerprinting the material. In many cases they have been apprehensive about the degree to which their product is analyzed. Often, proprietary agreements are required before they will participate. To facilitate good relations as well as to see the manufacturing process, the material specialist will visit the manufacturing facility. He normally presents the initial fingerprinting data and discusses the availability as well as the security of our database. Another goal of the visit is to inform the vendor of the plans for acceptance testing and discuss their ability to run appropriate tests prior to shipping. In addition, discussion of sub-vendors and acceptance criteria of raw materials can be reviewed to insure that even subtle changes in the end product will be detected and reported to Thiokol Propulsion.

The next major hurdle is to organize the data and information gained during the fingerprinting process in a user friendly, ready access database. This has been accomplished using several off-the-shelf computer programs linked together with a custom PowerBuilder application. It coordinates the fingerprinting information and serves as the systems main viewer. There are six interactive pages on the main viewer that include Executive View, Method Information, Component Information, Method QC, View Comparison, and Lab Notebook.

The Executive View Page is the most widely used and gives access to most of the information obtained during the fingerprinting process. As can be seen in Figure 1, the Executive View page is broken down into several different areas. A pull down tab allows you to select the material you wish to look at and once selected a description of the material shows up in the second box. The third box lists the material components and as seen in Figure 2, a double click on a component brings up the structure and a few characteristics of the compound. The reference data of the material and its component parts can be viewed by clicking on the appropriate reference button. Galactic's GRAMS/32 software package is used to handle the raw analytical data and is used to show pre-built workbooks containing data from the material itself as well as data of its component parts (see Figure 3). Double clicking on the appropriate document title in the Reference Material block will access the fingerprinting final report as well as other previous studies. Where proprietary information is contained on the Executive Viewer page, only those who have been given access rights can open the component structures, GRAMS/32 workbooks, or reference data.

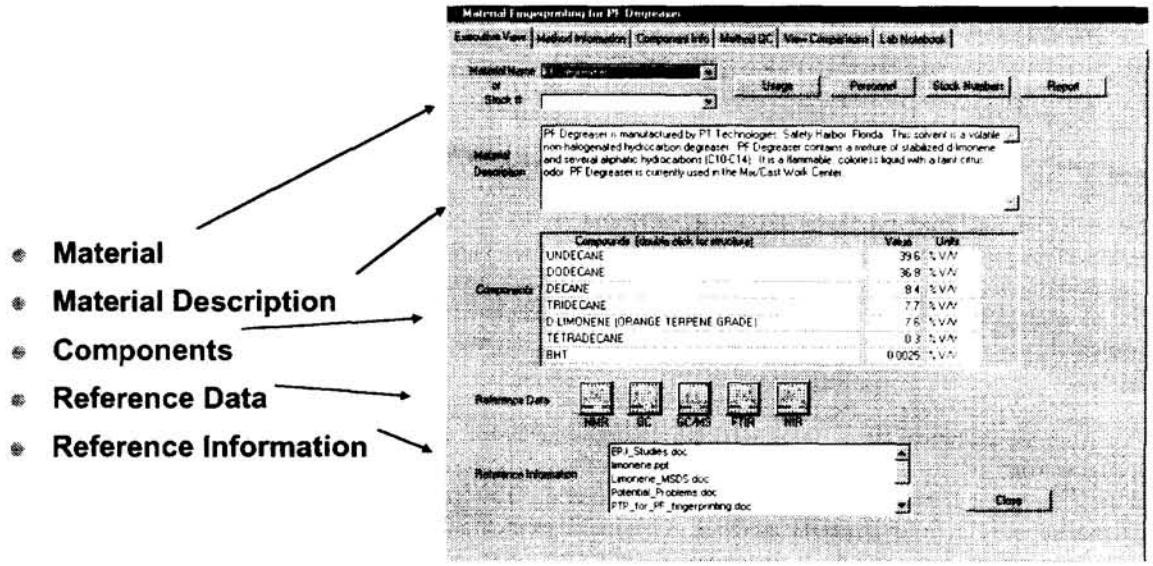

Figure 1. Executive Viewer

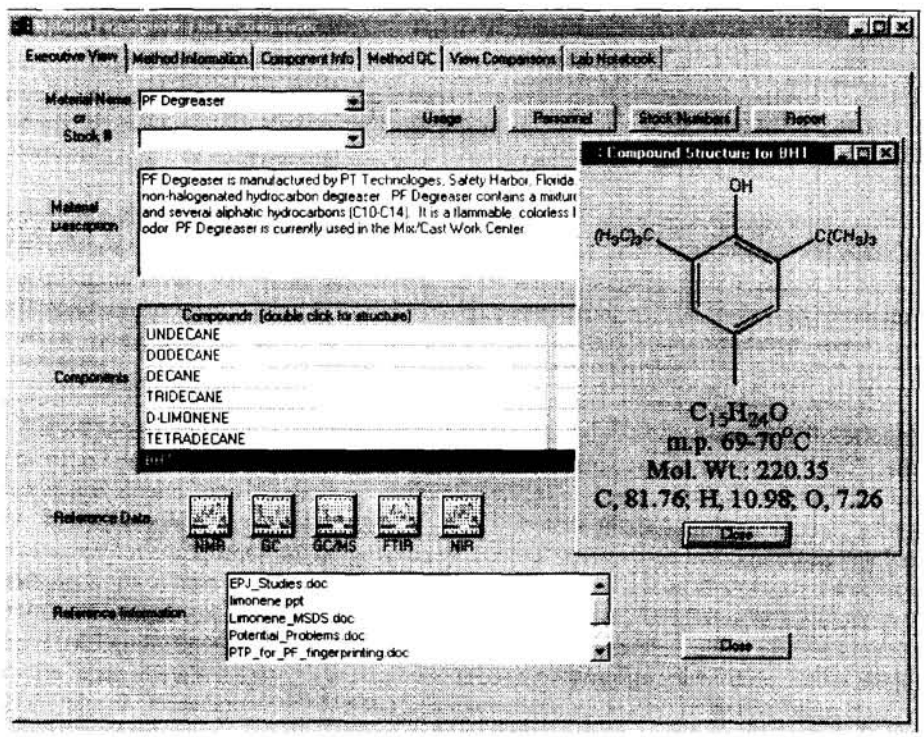

Figure 2. Component Structure

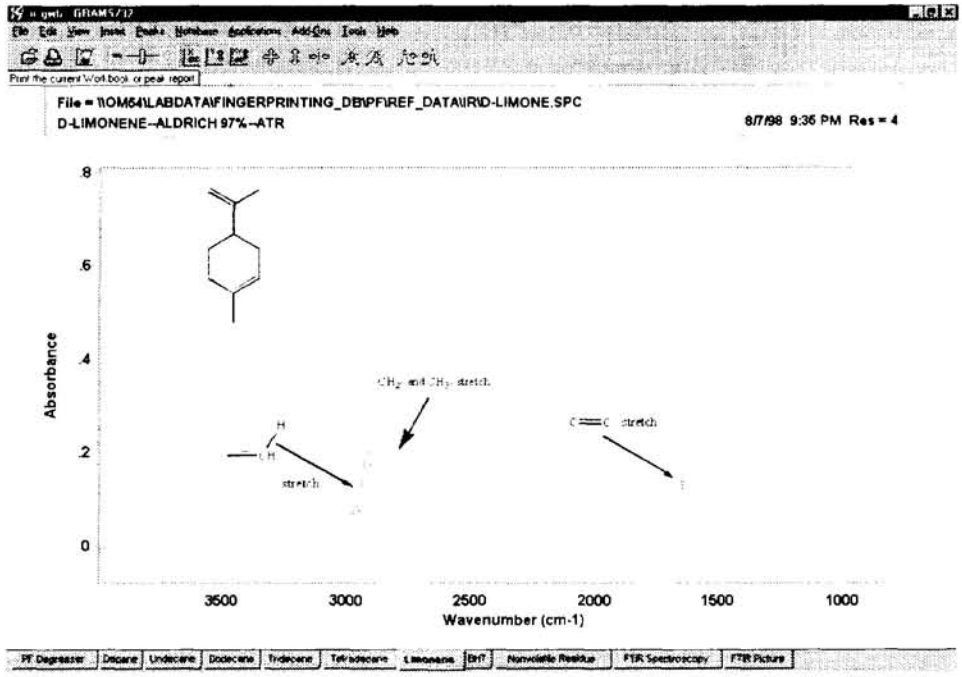

Figure 3. Grams Workbook of PF Degreasor

The method information page lists the analytical methods developed during the fingerprinting process and references written procedures that can be used to duplicate the analysis if future problems should occur. It also highlights those procedures that have been selected for acceptance testing in the process control lab. The component information page allows our technical personnel to view data on specific tests (see Figure 4). Pull down tabs enable the selection of the lab that performed the analysis, the test method of interest as well as the analyte when more than one is available per test method. Analytical data is represented graphically and gives the average as well as the two and three standard deviation boundaries. Referencing "Display Values" will bring up the list of numerical values used to generate the graph along with sample details such as lot number, etc. The Method QC page enables trend analysis of quality control parameters.

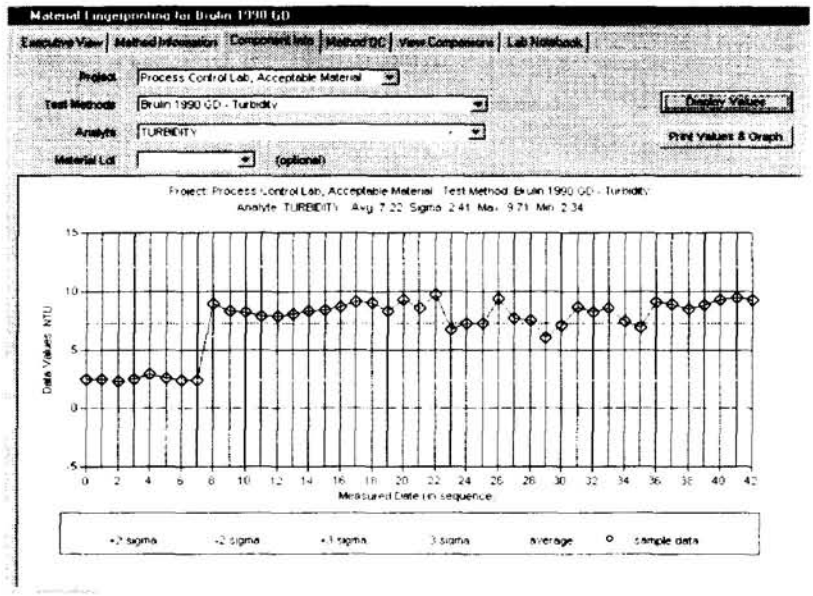

Figure 4. Component Information Page

The View Comparison page accesses five categories of sample analysis including aging studies, acceptable and unacceptable material as well as developmental data. Grams/32 workbooks enable users to manipulate and overlay data with reference material for direct comparisons. An example of overlaid FTIR data is shown in Figure 5.

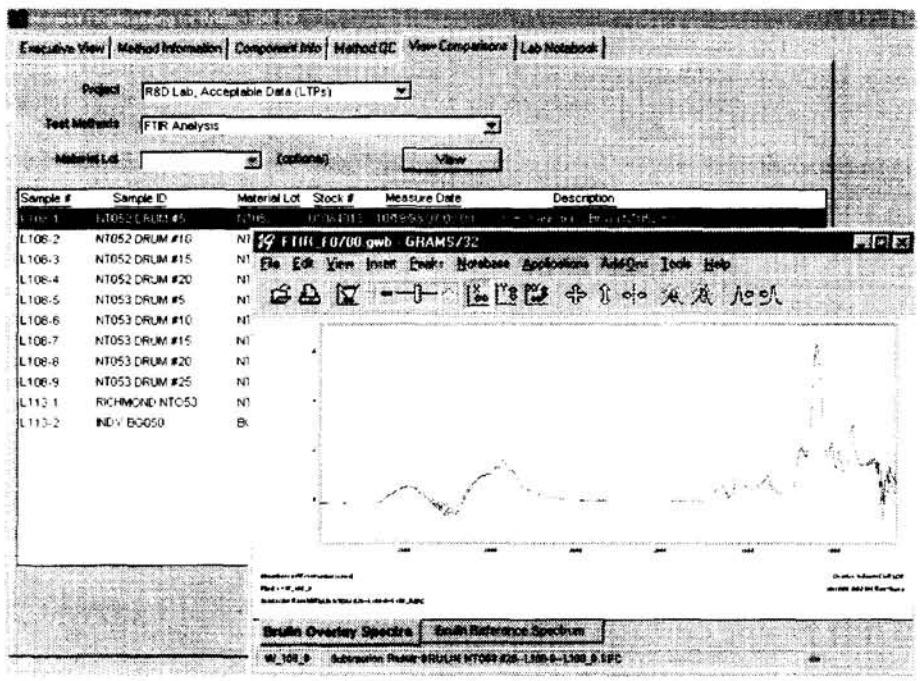

Figure 5. View Comparison Page

At Thiokol Propulsion, the fingerprinting database with real-time access has become a valuable problem-solving tool. In the first two years of the program we have completed or are currently fingerprinting 37 separate

critical materials. As the database has expanded it has been increasingly useful to resolve manufacturing and material down-selection issues. Examples include aging of stockpiled materials, shelf-life discrepancies, manufacturing changes, down-selection of new materials, and incompatibility issues.

An excellent example of how fingerprinting has been used to resolve issues is the work done to correct solubility problems and extend the in-use life of Brulin 1990 GD. Since 1997, Brulin 1990 GD has been used as a concentrate for our Spray-In-Air degreasing facility. The concentrate was selected as one of the first materials to be fingerprinted. During acceptance testing of the fourth production lot of Brulin 1990 GD, problems of increased turbidity and a low pH were identified. This resulted in the rejection of 400 gallons of Brulin 1990 GD. A white precipitate, identified as insoluble silicates, was found in the solution. This accounted for the increased turbidity and the result was a loss of corrosion inhibitor. It was also noted that the solution had a pH much lower than the specification. Based on literature studies it was found the solubility of silicates is directly related to the pH of the solution (see Figure 6). As is noted, the Brulin 1990 GD will form a precipitate when the pH falls close to 11. The vendor had verified the pH was between 11.8 and 12.2 prior to shipping but our testing showed the pH to be well below 11.

To resolve the problem, the vendor was contacted and the problem was defined. Initial studies indicated that the solutions pH gradually changed over time when exposed to the atmosphere (see Figure 7). To show it was caused by the formation and subsequent reaction with carbonic acid, the solution was sampled to correlate with the pH measurement over time. The samples were tested for carbonate by sampling for CO_2 under acidic conditions and as shown there was a direct correlation between CO_2 concentration and pH.

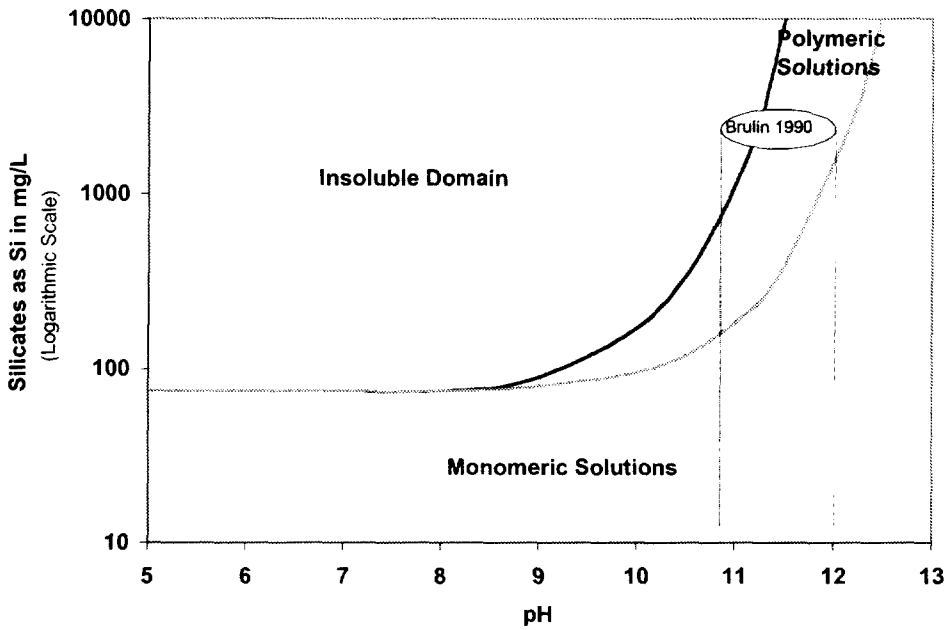

Figure 6. Silicate Solubility

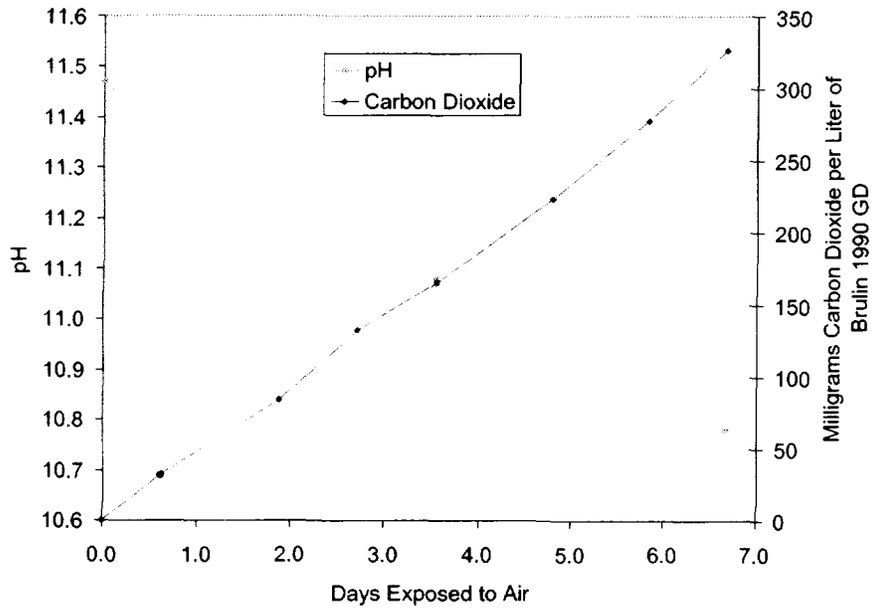

Figure 7. pH of Brulin 1990 GD with Exposure to Air

A team of material specialists was then sent to the manufacturer to present our findings and work out methods to stabilize the product. Production was observed at two different facilities followed by open discussions to develop methods that would improve the as received product. Several refinements were made to include the use of additional caustic to give the solution a final pH of 11.5 and the introduction of techniques to insure mix kettle cleanliness. Based on these recommendations and implementation of changes to the manufacturing process, we have since received five 3000 gallon lots that have met acceptance criteria and no insoluble material has been observed.

Based on the lessons learned from this experience we were able to resolve additional production issues related to the use of Brulin 1990 GD. Over a period of eight days at operating temperatures the pH of the solution would decrease to levels where the silicates would again begin to precipitate. This created an obvious burden on production to replace the 2200 gallons of cleaning solution after such a short period of time. The material specialists resolved this problem by developing a KOH add-back method that maintains the pH at levels that give a reliable cleaning solution. This has extended the useful bath life to 90 days.

The chemical fingerprinting program has been a success story at Thiokol Propulsion. The information gained has drastically improved our knowledge of the chemistry and baseline profiles of the materials in use. Acceptance testing has been updated to use modern and efficient methods and enable better lot-to-lot monitoring. When issues do arise, material specialists with technical ownership have a variety of analytical methods in place for evaluation and assessment. Resolution is done in minimal time and with increased accuracy. The relationships developed with vendors has improved data sharing as well as increased the understanding of the acceptance requirements in place for each material. Where possible, testing is transferred directly to the vendor.

CP/566/IN/27

RESOURCES AVAILABLE FOR HAZARDS ANALYSIS OF AEROSPACE FLUIDS*

Stephen S. Woods
Honeywell Technology Solutions Inc.
P.O. Box 20
Las Cruces, NM 88004
(505) 524-5607
swoods@wstf.nasa.gov

Walter F. Stewart
L & M Technologies
Las Cruces, NM

David L. Baker
Harold D. Beeson
NASA Johnson Space Center White Sands Test Facility
Las Cruces, NM

E2/3RD

INTRODUCTION

In recent years, the legislative and executive branches of the federal government have pushed to make government more efficient and responsive to the needs of the marketplace. One of these initiatives, Public Law 104-113, also known as the National Technology Transfer and Advancement Act of 1995 (NTTAA), is designed to accelerate technology transfer to industry and promote government-industry partnership. Summarized, NTTAA states that "... all Federal agencies and departments shall use technical standards that are developed or adopted by voluntary consensus standards bodies, using such technical standards as a means to carry out policy objectives or activities determined by the agencies and departments."[1] Government agencies must now determine if their in-house requirement-setting activities are sufficiently unique that no public interest is served by having them adopted by a voluntary consensus organization (VCO), or if not, to use or develop voluntary consensus standards. The Office of Management and Budget (OMB) is chartered by the law to monitor federal agency progress and report the results to Congress.

In response to NTTAA, agency-wide oxygen[2] and hydrogen[3] safety standards sponsored by the NASA Headquarters (HQ) Office of Safety and Mission Assurance (OSMA) were obvious choices for early adoption by VCOs. In 1996, HQ sought assistance from the Johnson Space Center (JSC) White Sands Test Facility (WSTF), the technical lead for development of these safety standards, to evaluate their adoption by VCOs. At that time, WSTF-developed propellant hazards manuals were likewise identified for possible VCO adoption. Subsequently, WSTF was asked to represent NASA for development of an international ISO safety standard for hydrogen use. Concurrent with these WSTF standards activities are related efforts to develop and publish propellant hazards analysis protocols and safety courses for the industrial, propellant use of oxygen, hydrogen, and hypergols.

This paper reports on these efforts and describes WSTF's overall voluntary consensus standards program to coordinate the interchange of NASA's propellant hazards and safety information with industry.

WSTF VOLUNTARY CONSENSUS STANDARDS DEVELOPMENT AND TECHNOLOGY TRANSFER PROGRAM

WSTF has been involved with testing of hazardous fluids, components, and materials for over 30 years and with the development of hazards manuals during the last 15 years. With this new emphasis in direction prompted by NTTAA, the relationship among research and development, hazards analysis

---

* Approved for public release; distribution is unlimited.

protocols, safety course development, voluntary consensus standards activities, and industry communications has become apparent.

A New Environment for Cooperation

The rapid pace of transfer of government activities to the aerospace industry, along with the increasing incidence of aerospace corporate mergers, have the potential for disrupting coordination and flow of vital propellant safety and hazards information among personnel involved in design, operations, and safety. Within this milieu exist the risks associated with employees' potential exposure to hazardous chemicals in governmental and industrial work environments. The latter has led to detailed regulations that specify a highly trained work force, the use of hazards review methodologies, hazards communications with employees and the surrounding community, and adequate emergency preparedness. How can the effects of these potentially opposed forces be countered?

One response is for government and industry to cooperate within the framework provided by a VCO, which acts as a clearing house for critical information, helps identify top expertise, and offers training. The democratic structure of VCOs enables them to develop voluntary consensus standards that meet the needs of both government and industry.

By design, NTTAA has prompted a new, more cooperative environment between government and industry that accelerates technology transfer to industry and promotes government-industry partnership. But technology transfer from government to industry involves more than simply relaying scientific data and technology development. It also involves sharing hazards review and training expertise and making the information and techniques used by government laboratories more accessible to industry and the public. Technology transfer activities also drive government efforts to be more attuned to industry needs.

An Engine for Focused Technological Advancement

One of WSTF's primary goals is to support NASA's propellant safety efforts, which involve testing, research and development, and hazards analysis of cryogenic and hypergolic propellants. These activities are organized to support queries from industry and the public, to provide training to those who need it, and to collaborate with VCOs to develop voluntary consensus standards. Important insights into the role hazards analyses can play in the overall direction and planning of safety research have become apparent. WSTF is recognized throughout NASA and by the aerospace community for its formalized approach to oxygen hazards analysis and has designed protocols for application to hydrogen, hydrazine fuels, and nitrogen tetroxide.

WSTF Hazards Analysis Protocol

The protocol works by examining in detail all components exposed to a particular propellant, analyzing likely failure modes, determining the consequence(s) of a particular failure to the system, and qualitatively assessing the risk for the system owners. The general hazards analysis procedure is depicted in Figure 1. Protocols for oxygen and hydrogen have been established, and protocols for hypergols are near completion. The protocols address primarily combustion hazards.

Preliminary activities are to adequately define the application and the scope of the investigation. Once defined, an analysis team with expertise in mechanical design, materials, ignition and combustion, safety, and component testing as it pertains to the propellant is assembled. Before convening for the analysis, detailed information on the components and the system in question is compiled as a skeleton report draft that the team fleshes out during the analysis. Thorough preparation at this point cannot be overemphasized, for it directly influences the productivity of the analysis.

The team begins by reviewing the hazards analysis protocol objectives and methodology. An overview of system design and operation is then established through review of system and component drawings, materials lists, and a failure modes and effects analysis. Operating and worst-case conditions are then identified. Component design and function are examined to see if grouping them by failure type,

failure effect, or subsystem can streamline the analysis. The analysis proceeds for each component or subsystem in a given operational mode by identifying the nature of the failure, type of combustible mixture formed, potential ignition mechanisms, and whether a flash, fire, or explosion can occur. Also considered are design features and administrative controls that may be used. Occurrence probabilities are assessed for each of these categories. The scenario posed by a given failure and its potential to result in combustion are evaluated to see what secondary effects may result. Assessing the overall risk to the actual system or to its intended purpose completes the analysis at this level. The results are documented in a summary chart for each component. When necessary, supporting rationale is noted. An example summary chart from the hydrogen hazards analysis procedures is shown in Figure 2.

Analysis scores are determined by team consensus and are tallied through a qualitative rating scheme that relies heavily on existing databases. Where data are insufficient to define the hazards, then a recommendation for testing is made. Quantitative analysis, personal experience, and intuition are also a vital part of the decision-making process.

The rating scheme, used in the assessment of the probability of failure, formation of combustible mixtures, potential for ignition, and the resulting consequences, is based on a qualitative probability rating of 0 through 4, with the following identification:

- Almost impossible (0),
- Remotely possible (1),
- Possible (2),
- Probable (3), or
- Highly probable (4).

The secondary effects category is assigned an "R" when additional analysis is required; otherwise "N" for "No further analysis required" is noted. To describe the overall risk arising from component failure, the reaction effects category is scored as:

- Negligible (A),
- Marginal (B),
- Critical (C), or
- Catastrophic (D).

The results tabulated in each step are read as independent assessments of probability rather than as interrelated. Analysis places failure of an individual component not only in the context of its function in the subsystem or system but also its functional environment. When necessary, the interaction among components may be evaluated in a matrix fashion. Analysis may also be driven by fault-level requirements. The final risk assessment given for reaction effects is not read as a result derived by "multiplying" the probabilities assessed in Steps 2 through 5 of Figure 2. Rather, it is an assessment of the overall effect on personnel, the system, or its mission caused by the particular failure mode of the component under consideration, regardless of the probability.

The analysis proceeds through all the components. Recommendations are recorded as they become apparent from the analysis. During team deliberations the analysis, supporting rationale, and recommendations are recorded into the skeleton draft report by a team member acting as "secretary," with the objective of having a draft report when the team is finished. After review of this draft report, a final report is prepared for the system owners. Where needed, the report provides recommendations for testing, component redesign, materials replacement, and the identification of procedural controls. The risks identified in the hazards analysis are then available for appropriate upper management review teams.

The Hazards Analysis Protocol as the Engine for Technology Transfer

Successful technology transfer requires placing critical information where it is needed. While this sounds obvious, the challenge is in identifying what information is critical and then knowing how to get it to those who need it.

In its traditional role, the hazards analysis protocol is used by project- and program-oriented groups as a means of identifying and remediating potential component and system inadequacies. But sometimes during the course of an analysis, a need arises for data that do not exist. For example, in the assessment of propellant hazards, this may involve the need for combustion or materials data that are not currently available but can be gained through testing. But if the team determines that testing is too difficult or expensive, the analysis might prompt a system redesign, the acceptance of greater risk, or a new method for assessing the hazards.

Unfortunately, the information obtained from the hazards analysis and how to apply it is often perceived as so specialized that little is done other than basic documentation of the analysis. End-users perceive that only those involved could promote further use of the data, which may or may not be true. Given this, how can hazards analysis protocols figure both in the promotion of technology transfer and technology development?

The hazards analysis process is by nature dynamic and points out what is known and what is not. The results of this process can be used to identify new research, problem areas, operational issues, or training requirements and should be considered prime information for technology transfer. When this knowledge is acted upon, perhaps by obtaining new data through testing, the results are state-of-the-art information. Typically the information is efficiently obtained because it results from the already-funded process of the hazards analysis. In a proactive environment, hazards analysis information can be used to propose new research to cover the deficits of data uncovered by the process. This information can prompt a refinement of hazards analysis techniques, which can then point toward improvements of the protocols. Another benefit is that the information is developed by industry expertise and can be applied directly to industry development as specific solutions and recommendations. Finally, publishing the information in the open literature makes it accessible to a wide audience that may be able to take advantage of it without "reinventing the wheel" and incurring the cost of unnecessary testing.

There are implications for use of this information beyond immediate aerospace applications. Such information is not only important in the technical development of a system; it can also be critical in the acceptance of the technology. For example, systems developed by the commercial sector that will be used by the public must be perceived as safe before investors can obtain the insurance to cover venture capital. One area of current development in which this is true is the application of hydrogen fuel cells to everyday applications. Also, it is acknowledged that the use and protection of proprietary information will always be a sensitive issue.

How might hazards analysis information be gathered and distributed? There are "lessons learned" databases and compilations of data on accident investigations currently available, but they appear to be static compilations that are periodically updated. It is hoped that the information gathered through hazards analyses would be the focus of an established group. WSTF currently serves that function, but given the current emphasis on VCOs, the activity could be managed by a VCO as well, with appropriate input from industry and government. The VCO's objective would be to compile and analyze the findings of recently completed hazards analyses, then help distribute the results.

Consensus as a Means of Communication

Easily leveled criticisms of standards efforts conducted within government agencies are that the results are inadequate, one-sided, and inaccessible. The NTTAA has forced government to reevaluate its standards efforts. But for NASA, an agency that has always been proactive with regard to public outreach and technology transfer, NTTAA provides the basis for even greater interaction with industry and the public.

Aside from the primary goal of managing standards through a VCO, other positive attributes should arise from pursuit of the law. These include improved communication within government agencies and between industrial entities as well as interagency/interindustry connections. This has the potential to bring different interests together and lead to the establishment of a common ground in which research and development can take root. But it is likely that VCOs will continue to be a focal point for general information related to voluntary consensus standards, such as identifying where particular expertise can be found.

NASA's interest in participation with VCOs in the safety arena includes transfer of hazards manuals and the development of voluntary consensus standards. In theory, hazards information is better distributed by VCOs, with the cost being covered by the program interests that need the information rather than subsidized by the government. One goal is to promote the creation of general safety standards for propellant use that can be applied in government-industry contract negotiations.

For agencies that are not proactive in response to NTTAA, it will be interesting to see how the law will work in the future. The OMB requires federal agencies to report on the status of their efforts to meet the law. Already the mobile home construction industry has brought a legal challenge[4] against legislation pending in Congress, the American Homeownership and Opportunity Act, H.R. 1776, citing conflicts with NTTAA. Here industry is claiming that preexisting law directs them through VCOs to keep standards for manufactured homes up-to-date and the new law is not needed.

Interrelationship Among Hazards Analysis, Consensus Communications, and Research

The hazards analysis process is depicted at the center of the technology transfer process shown in Figure 3. The information gained by hazards analyses can serve as input to VCOs, for research, and for training. Conversely, VCO committees, research groups, and trainers can have influence on hazards analysis protocols. For this scheme to function effectively, some group in industry or government must have a vested interest in tracking, documenting, and communicating key information obtained from the use of hazards analysis protocols. At present WSTF is funded to do this work. A logical extension of who performs this sort of work would include the VCOs themselves.

SPECIFIC ACHIEVEMENTS

WSTF's parallel efforts to promote safety research and safety standards development are a vital part of its mission. The next section outlines the specific achievements by these efforts.

Propellant Oxygen

Research into propellant oxygen hazards has been ongoing at WSTF since the mid-1970s and is its most mature expression of the interrelationship among research, hazards analysis, and VCO participation. Technical communications and technology transfer with industry are achieved through a long-standing participation with ASTM Committee G4 on Compatibility and Sensitivity of Materials in Oxygen Enriched Atmospheres and the National Fire Protection Association's committees on Health Standards and Hyperbaric Standards. The oxygen hazards analysis protocol has been in use for over a decade. WSTF researchers have developed an oxygen safety training course, "Fire Hazards in Oxygen Systems,"[5] that is offered through ASTM. At the request of the NASA HQ/OSMA, WSTF developed a safety standard for oxygen and subsequently collaborated with ASTM to publish it as Manual 36, "Safe Use of Oxygen and Oxygen Systems."[6] WSTF's progress in the oxygen arena serves as a model for its development of hydrogen and hypergol propellant programs. The following documents and courses are available for oxygen safety assessment:

- NASA Safety Standard 1740.15, "Safety Standard for Oxygen and Oxygen Systems"
- ASTM MNL36, "Safe Use of Oxygen and Oxygen Systems"
- NASA Technical Memorandum 104823,[7] Guide for Oxygen Hazards Analyses on Components and Systems"
- ASTM G63, "Guide for Evaluating Nonmetallic Materials for Oxygen"[8]
- ASTM G88, "Guide for Designing Systems for Oxygen Service"[9]

- ASTM G94, "Guide for Evaluating Metals for Oxygen Service"[10]
- NFPA 53, "Recommended Practice in Oxygen-Enriched Atmospheres"[11]
- ASTM Technical and Professional Training Course, "Fire Hazards in Oxygen Systems" (several versions exist that are tailored to particular audiences, such as design engineers, technicians, and the scuba community)
- ASTM Technical and Professional Training Course, "Oxygen Systems: Operation and Maintenance"

Propellant Hydrogen

Progress in the hydrogen safety arena includes development of the NASA Safety Standard for Hydrogen and Hydrogen Systems and collaboration with the American Institute of Aeronautics and Astronautics (AIAA) toward the formation of an aerospace hydrogen safety committee. This hydrogen safety committee will oversee the development of a consensus guide based on the NASA hydrogen safety standard and ultimately the development of a national standard. NASA has been invited to help represent U.S. interests in the international hydrogen safety community. In parallel with the AIAA effort, WSTF supports ISO Technical Committee 197, Working Group 7 on general hydrogen safety. Following the model of oxygen activities, a hydrogen hazards analysis protocol and a hydrogen safety training course have been developed. The hydrogen safety training course is available through the NASA Safety Training Center. The hydrogen hazards analysis protocol is available from WSTF. The following documents and courses are available for hydrogen safety assessment:

- NASA Safety Standard 1740.16, "Safety Standard for Hydrogen and Hydrogen Systems"
- TP-WSTF-937,[12] "Guide for Hydrogen Hazards Analysis on Components and Systems"
- RD-WSTF-0001,[13] "Ignition and Thermal Hazards of Selected Aerospace Fluids"
- NASA Safety Training Center, Course 037, "Hydrogen Safety"

Hypergolic Fuels and Oxidizers

Progress in the hypergol safety arena parallels WSTF's oxygen and hydrogen efforts in that several manuals covering the hazards of hypergolic propellants have been developed. This is just the kind of information that could better serve the aerospace community if it was managed by a VCO. In collaboration with AIAA, WSTF has promoted the formation of the recently initiated AIAA Liquid Propellant Committee on Standards to serve as a forum for discussion of hypergolic and related propellant safety issues. This committee has an agenda to oversee the development of voluntary consensus standards covering hydrazine, monomethylhydrazine, dinitrogen tetroxide, and other aerospace fluids of interest. WSTF hypergolic hazards manuals have been transferred to AIAA for distribution as AIAA Special Projects. The agreement stipulates that needed updates of hypergolic hazards information will be published through AIAA Special Projects or Guides. In addition to the AIAA committee work, JSC has funded development of a hazards analysis protocol for hypergolic propellants. Also, NASA HQ/OSMA has funded WSTF for development of a hypergol safety training course. Both these efforts are in progress and the results will be available in fiscal year 2001. The following documents and courses are available for hypergolic safety assessment:

- RD-WSTF-0001, "Ignition and Thermal Hazards of Selected Aerospace Fluids"
- RD-WSTF-0002,[14] "Fire, Explosion, Compatibility, and Safety Hazards of Hydrazine"
- RD-WSTF-0003,[15] "Fire, Explosion, Compatibility, and Safety Hazards of Monomethylhydrazine"
- RD-WSTF-0017,[16] "Fire, Explosion, Compatibility, and Safety Hazards of Nitrogen Tetroxide"
- AIAA SP-084-1999,[17] "Fire, Explosion, Compatibility, and Safety Hazards of Hypergols – Hydrazine"
- AIAA SP-085-1999,[18] "Fire, Explosion, Compatibility, and Safety Hazards of Hypergols – Monomethylhydrazine"
- TP-WSTF-953,[19] "Guide for Hydrazine Hazards Analysis on Components and Systems"
- TP-WSTF-959,[20] "Guide for Nitrogen Tetroxide Hazards Analysis on Components and Systems"

- NASA Safety Training Center, Course 040, "Hypergolic Propellant Safety"

SUMMARY AND CONCLUSIONS

The goal of the paper has been to inform aerospace researchers and engineers of new resources and an improved way of approaching and communicating propellant safety concerns and to raise awareness regarding NTTAA. The nexus of propellant activities for oxygen, hydrogen, and hypergol safety underway at WSTF can aid researchers with locating critical information, expertise, testing services, and training. The authors encourage those who have a stake in making this kind of information available to their own organization to participate in VCO activities, such as the ASTM Committee G4 and the AIAA Liquid Propellant Committee on Standards. For hydrogen, readers are encouraged to contact AIAA and/or the WSTF propellant hazards program for further information.

Another goal of this paper is to recommend that the aerospace community reevaluate how the results of hazards analyses are conveyed beyond an immediate project or program. It is important that a mechanism exist to organize and convey this information. Specific recommendations for oxygen, hydrogen, and hypergol safety are:

- Examine how your own organization treats the results of hazards analyses after specific project or program needs have been satisfied.
- Consult the WSTF propellant hazards programs, which have a strong history as contact points for coordinating and organizing hazards information.
- Seek participation in an appropriate VCO to organize and disseminate hazards analysis results.

The NTTAA has pointed the way for a reconsideration in the way government and industry interact. For the maximum benefit to accrue in the propellant safety arena, industry and government representatives must participate through the technical committees of the VCOs chartered to manage this information.

REFERENCES

1. Public Law 104-113 (104th Congress). *National Technology Transfer and Advancement Act of 1995.* 15 USC 3701. Washington, D.C. Signed by the President, March 7, 1996.

2. NASA Office of Safety and Mission Assurance. *Safety Standard for Oxygen and Oxygen Systems (Guidelines for Oxygen System Design, Materials Selection, Operation, Storage, and Transportation).* NSS 1740.15, Office of Safety and Mission Assurance, Washington, D.C., January 1996.

3. NASA Office of Safety and Mission Assurance. *Safety Standard for Hydrogen and Hydrogen Systems (Guidelines for Hydrogen System Design, Materials Selection, Operations, Storage, and Transportation).* NSS 1740.16, Office of Safety and Mission Assurance, Washington, D.C., February 1997.

4. ASME. *ASME Letter to the Honorable Constance A. Morella Regarding the Proposed Manufactured Housing Improvement Act.* American Society of Mechanical Engineers, New York, NY, Feb. 11, 2000. http://www.asme.org/gric/00-02.html.

5. "Fire Hazards in Oxygen Systems," Technical & Professional Training Course, American Society for Testing and Materials, West Conshohocken, PA, latest version.

6. Beeson, H. D., W. F. Stewart, and S. S. Woods, Eds., "Safe Use of Oxygen and Oxygen Systems: Guidelines for Oxygen System Design, Materials Selection, Operations, Storage, and Transportation," ASTM MNL36, American Society for Testing and Materials, West Conshohocken, PA, January 2000.

7. Stoltzfus, J. M., J. Dees, and R. F. Poe. *Guide for Oxygen Hazards Analyses on Components and Systems*. NASA Technical Memorandum 104823, Johnson Space Center, Houston, TX, October 1996.

8. ASTM G 63. *Standard Guide for Evaluating Nonmetallic Materials for Oxygen Service*. Annual Book of ASTM Standards, American Society for Testing Materials, Philadelphia, PA (1992, or latest revision).

9. ASTM G 88. *Standard Guide for Designing Systems for Oxygen Service*. Annual Book of ASTM Standards, American Society for Testing Materials, Philadelphia, PA (1990, or latest revision).

10. ASTM G 94. *Standard Guide for Evaluating Metals for Oxygen Service*. Annual Book of ASTM Standards, American Society for Testing Materials, Philadelphia, PA (1992, or latest revision).

11. NFPA 53. *Recommended Practice on Materials, Equipment, and Systems Used in Oxygen-Enriched Atmospheres*. National Fire Protection Association, Quincy, MA (1999, or latest revision).

12. Woods, S. S., G. Packard, and H. D. Beeson. *Guide for Hydrogen Hazards Analysis on Components and Systems*. TP-WSTF-937, NASA Johnson Space Center White Sands Test Facility, Las Cruces, NM, August 19, 1998.

13. Benz, F. J., C. V. Bishop, and M. D. Pedley. *Ignition and Thermal Hazards of Selected Aerospace Fluids*. RD-WSTF-0001, NASA Johnson Space Center White Sands Test Facility, Las Cruces, NM, October 14, 1988.

14 Pedley, M. D., D. L. Baker, H. D. Beeson, R. C. Wedlich, F. J. Benz, R. L. Bunker, and N. B. Martin. *Fire, Explosion, Compatibility, and Safety Hazards of Hydrazine*. RD-WSTF-0002, NASA Johnson Space Center White Sands Test Facility, Las Cruces, NM, February 20, 1990.

15. Woods, S. S., D. B. Wilson, R. L. Bunker, D. L. Baker, and N. B. Martin. *Fire, Explosion, Compatibility, and Safety Hazards of Monomethylhydrazine*. RD-WSTF-0003, NASA Johnson Space Center White Sands Test Facility, Las Cruces, NM, May 5, 1993.

16. Davis, D. D., D. L. Baker, L. A. Dee, B. Greene, C. H. Hart, and S. S. Woods. *Fire, Explosion, Compatibility, and Safety Hazards of Nitrogen Tetroxide*. RD-WSTF-0017, NASA Johnson Space Center White Sands Test Facility, Las Cruces, NM, November 15, 1999.

17. AIAA SP-084-1999. *Fire, Explosion, Compatibility, and Safety Hazards of Hypergols – Hydrazine*. American Institute of Aeronautics and Astronautics, Reston, VA, 1999.

18. AIAA SP-085-1999. *Fire, Explosion, Compatibility, and Safety Hazards of Hypergols – Monomethylhydrazine*. American Institute of Aeronautics and Astronautics, Reston, VA, 1999.

19. Rathgeber, K. A., L. J. Bamford, and D. L. Baker. *Guide for Hydrazine Hazards Analysis on Components and Systems*. TP-WSTF-953, NASA Johnson Space Center White Sands Test Facility, Las Cruces, NM, May 4, 2000.

20. Rathgeber, K. A., L. J. Bamford, and D. L. Baker. *Guide for Nitrogen Tetroxide Hazards Analysis on Components and Systems*. TP-WSTF-959, NASA Johnson Space Center White Sands Test Facility, Las Cruces, NM, publication in process.

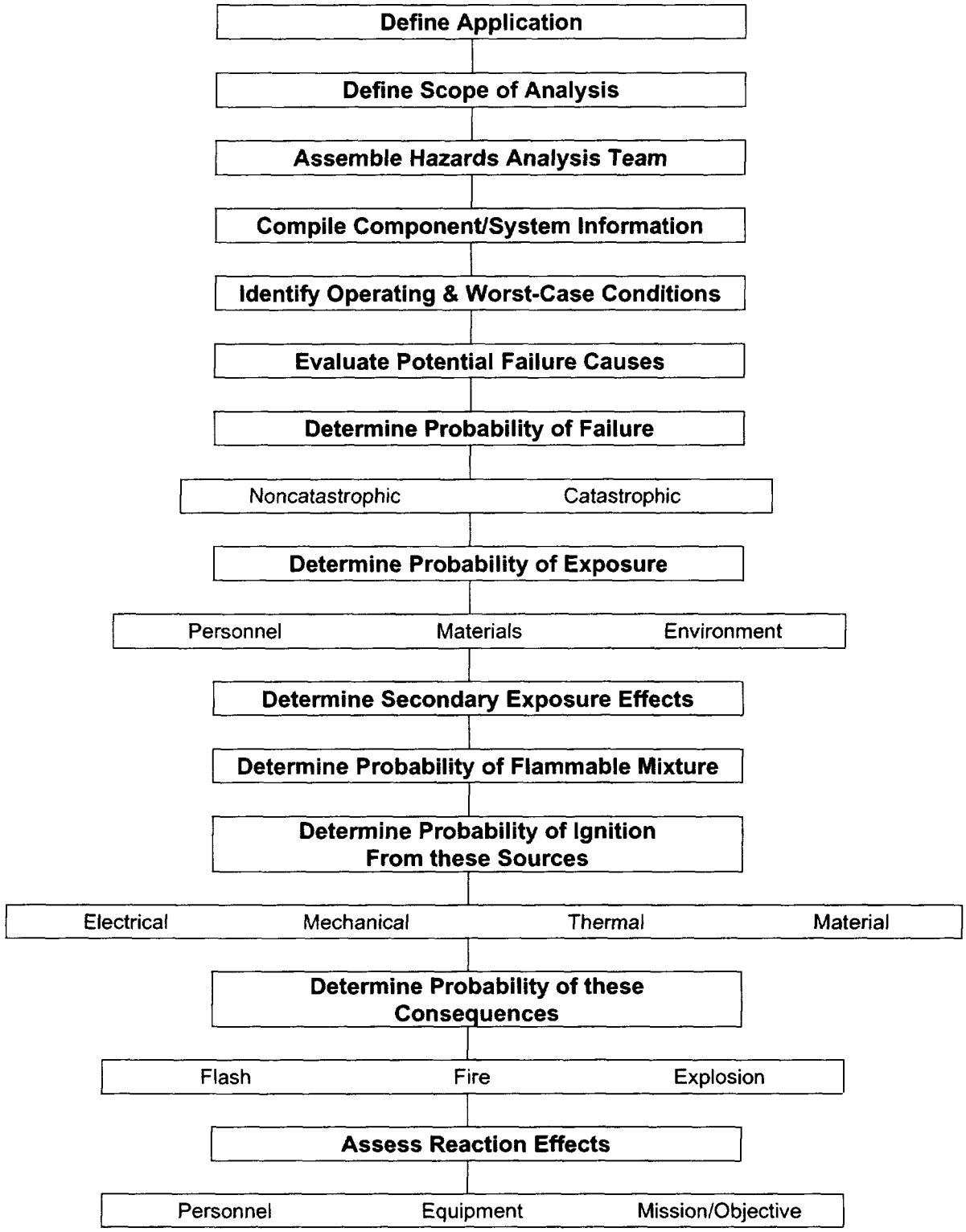

Figure 1. Procedure for General Hazards Analysis

CP/F67/IN/27

E2/4T

Chemical Fingerprinting of Materials Developed Due to Environmental Issues

Doris A. Smith, Lockheed Martin Space Systems, P.O. Box 29304, New Orleans, LA 70189, (504) 257-0228
doris.smith@maf.nasa.gov

Abstract

Instrumental chemical analysis methods are developed and used to chemically fingerprint new and modified External Tank materials made necessary by changing environmental requirements. Chemical fingerprinting can detect and diagnose variations in material composition. To chemically characterize each material, fingerprint methods are selected from an extensive toolbox based on the material's chemistry and the ability of the specific methods to detect the material's critical ingredients. Fingerprint methods have been developed for a variety of materials including Thermal Protection System foams, adhesives, primers, and composites.

Introduction

Some of the materials used in the Space Shuttle External Tank have been or will be replaced or modified due to environmental restrictions impacting the availability of raw materials. For example, External Tank Thermal Protection System (TPS) urethane foams originally containing CFC-11 blowing agent have been replaced with foams containing HCFC-141b blowing agent. Materials such as the TPS foams are critical to the performance of External Tank and, therefore, must be adequately tested to ensure that materials variations are detected before the material is used. Material variations can be due to a number of occurrences such as formulation changes, ingredient substitutions, material degradation, contamination, and mislabeling. A material can be simple such as a solvent, or complex such as a urethane foam that contains multiple ingredients (blowing agent, polyols, flame retardants, catalysts, surfactant) that in turn contain multiple ingredients.

Traditional tests used to characterize materials can be grouped into several categories. Traditional wet chemical tests are based on titrimetric or gravimetric procedures and include tests such the hydroxyl number test for reactive polyol and the amine equivalent test for reactive isocyanate groups in urethane foam formulations. Physical property tests include viscosity, specific gravity, color, haze, and particle size measurements. Mechanical property tests include compressive strength, tensile strength, and hardness measurements. Although the traditional tests are extremely valuable and may indicate the presence of material variations, traditional tests alone cannot identify the exact nature and origin of the variation. Instrumental chemical analysis or chemical fingerprinting can both detect and diagnostically identify variations in chemical composition.

Chemical Fingerprinting Techniques

Chemical fingerprinting techniques most frequently used to characterize materials used on the External Tank program are identified in Table 1. These techniques are used to qualitatively (What's there?) or quantitatively (How much is there?) characterize materials.

Spectroscopic techniques are based on the interaction between light (electromagnetic radiation) and matter and are used to obtain information about elemental or molecular composition. Elements or compounds within a sample absorb or emit light of specific energy and intensity. The energy of the emitted or absorbed light (measured as a frequency or wavelength) is used to identify the elements or compounds present. The intensity of the emitted or absorbed light is related to the amount or concentration of the detected component. Spectroscopic techniques most commonly used are of two types: techniques that are used to identify elements present (examples: atomic emission, atomic absorption, and x-ray fluorescence spectroscopy) and techniques that are used to identify molecular compounds present (examples: infrared and Raman spectroscopy, mass spectrometry).

In a chromatographic procedure, the sample is dissolved or dispersed in a mobile phase, then passed through a column containing a stationary phase. Components within the sample are separated from one another based on the relative affinity of the components for the stationary phase. The mobile phase is either a gas (gas chromatography) or a liquid (high performance liquid chromatography, ion chromatography, gel permeation chromatography). In gas chromatography separated components are most often detected as changes in thermal conductivity or flame ionization current, whereas in liquid chromatography the separated components are usually detected as changes in ultraviolet absorption, refractive index, or conductivity.

Table 1. Fingerprint Techniques

Technique (Acronym)	Applications/Advantages	Limitations/Disadvantages
Atomic Absorption Spectroscopy (AA)	Elemental quantitative analysis Rapid analysis of single element High sensitivity for some elements Inexpensive	Not applicable to most nonmetal elements Small linear response range High matrix interference Solution usually required Sample preparation time consuming Special accessory required for solids
Inductively Coupled Plasma Atomic Emission Spectroscopy (ICP/AES)	Simultaneous multi-element analysis Large linear response range Better than AA for refractory mat's	Limited sensitivity to non-metals Solution usually required Sample preparation time consuming Special accessory required for solids Expensive
X-ray Fluorescence Spectroscopy (XRF)	All elements of atomic number ≥ 11 Minimal sample preparation Applicable to solids and liquids Inexpensive	Not applicable to elements of atomic number < 11 without modifications
Infrared Spectroscopy (IR or FTIR)	Molecular identification Functional group identification Applicable to solids, liquids, gases Minimal sample preparation Extensive reference spectra libraries Inexpensive	Minor components masked by major Molecule must undergo dipole moment change during vibration
Raman Spectroscopy	Molecular identification Functional group identification Applicable to solids, liquids Applicable to aqueous solutions Minimal sample preparation	Not applicable to highly colored samples and samples that fluorescence Limited reference spectra libraries Molecule must undergo polarizability change during vibration Expensive
Mass Spectrometry (MS)	Identification of organic compounds Widely applicable to volatiles Extensive reference spectra libraries	Special sample introduction required for non-volatile samples Expensive
Gas Chromatography (GC)	Separation of multi-component mixtures of volatile compounds for quantitative analysis or for identification by tandem techniques Selectivity general or specific Inexpensive	Not applicable to non-volatile compounds without derivatization Not applicable to thermally unstable materials
High Performance Liquid Chromatography (HPLC)	Separation of multi-component mixtures of soluble compounds for quantitative analysis or for identification by tandem techniques	Method development time-consuming Sample must be soluble in suitable solvent Large volume of waste solvent Moderately expensive
Ion Chromatography (IC)	Separation of complex mixtures of ionic species for quantitative analysis Applicable to organic and inorganic More sensitive than wet methods	Method development time-consuming Moderately expensive
Gel Permeation Chromatography (GPC)	Separation of complex mixtures based on molecular size Determination of molecular weight	Sample must be soluble in suitable solvent Large volume of waste solvent GPC columns expensive

Applications of Chemical Fingerprinting to Simple and Complex Materials

The chemical fingerprint techniques listed in Table 1 are not all used for each material. Instead, a combination of techniques is selected based on the material's chemical composition and its physical properties. One or two techniques may be sufficient to adequately identify and monitor the composition of a relatively simple material, while a combination of several techniques may be required for more complex materials.

An example of a simple material is the solvent HCFC-225, which is a mixture of two isomers, HCFC-225ca and HCFC-225cb. Gas chromatography readily separates the two isomers from one another and from low concentration impurities. This technique is used to measure the percent purity of the HCFC-225 and to measure the ratio of the two isomers. Gas chromatography is also used to measure the percent purity of HCFC-225G, which is composed predominantly of the HCFC-225cb isomer.

Urethane foams comprising the External Tank Thermal Protection System (TPS) are examples of complex materials that cannot be totally characterized by a single fingerprint technique. Several TPS foam materials containing CFC-11 as blowing agent were modified or replaced by materials containing HCFC-141b. These materials are received as two liquid components. One of the components contains methylene diphenylene diisocyanate (MDI) and its oligomers and is frequently referred to as Component A. The other component, frequently called Component B, may be a complex mixture of polymeric alcohol (polyols), flame retarding ingredients, blowing agents, catalysts, and surfactants. Ingredients may be in the formulation at widely different concentrations ranging from less than one percent to up to nearly seventy percent by weight. More than one of each type of ingredient may be present, and ingredients themselves may be multi-component. In addition, the ingredients are very different from one another chemically and therefore require the use of different fingerprinting techniques. To completely characterize the material, a combination of techniques capable of detecting each key ingredient in the formulated material must be identified

The combination of fingerprinting techniques that may be required to characterize a complex urethane formulation is presented in Table 2. The goal of the fingerprinting program is to identify and develop a group of techniques that adequately and efficiently characterizes the material. Often, a single procedure can target several ingredients. For example, an inductively coupled plasma atomic emission spectroscopic (ICP/AES) procedure can be used to measure concentrations of elements such as phosphorus present in flame retardants, silicon present in silicone surfactants, and metals such as tin, lead, or potassium present in catalysts. On the other hand, an ingredient that is both present at a low concentration and inherently difficult to detect due to its chemistry may necessitate the development of a procedure that targets that ingredient alone. Examples include a low concentration amine catalyst that requires a gas chromatographic procedure with a specialized nitrogen-phosphorus detector (NPD) or low concentration bromine-containing flame retarding compound that requires a special high performance liquid chromatographic (HPLC) procedure.

Table 2. Fingerprinting Techniques to Characterize Generic Foam Formulation, Component B

Generic Ingredient	Typical Concentration	Fingerprint Techniques	Chemistry Measured
Polyols	5 – 70%	FTIR GPC HPLC GC	Functional Groups (Polyol Identification) Polymer Molecular Weight, Concentration Concentration Based on Detected Components Concentration Based on Volatile Components
HCFC Blowing Agent	15 – 35	GC FTIR	Concentration of Volatile HCFC Functional Groups (Blowing Agent Identification)
Amine Catalysts	0.2 – 3.0	GC	Concentration of Volatile Amines
Organo-metallic Catalysts	0.2 - 0.6	ICP/AES	Elemental Concentration Related to Catalyst Conc.
Silicone Surfactant	1 - 2	ICP/AES	Silicon Concentration Related to Surfactant Conc.
Phosphorus-Containing Flame Retardants	2 - 20	GC ICP/AES	Concentration of Volatile Flame Retardant Phosphorus Concentration Related to Fl. Ret. Conc.
Halogen-Containing Flame Retardants	1 - 10	GC HPLC	Concentration Based on Volatile Components Concentration of Halogen Compound

Supplier Partnership

Partnership with our suppliers is a key component in our fingerprinting program. Important steps in developing fingerprint methods for a given material are identifying the formulation ingredients and understanding each ingredient's role in the formulation. In some cases, ingredients are identified in the Material Safety Data Sheet or in other easily obtained documents. When the material is a simple mixture of relatively simple ingredients, fingerprint analysis may readily identify ingredients. However, in most cases, especially when materials are composed of complex mixtures of complex ingredients, the supplier's cooperation is needed. For the most part, our suppliers have been willing to identify the ingredients in their materials, to disclose ingredient concentrations, and to provide samples of ingredients. This cooperation has greatly expedited fingerprint method development. By fingerprinting a material's ingredients, the peaks in the material's chromatograms and spectra can be assigned to individual ingredients, and changes in the material's fingerprint can be readily attributed to specific ingredients. When material problems arise, fingerprinting data can be relayed back to the supplier in order to expedite resolution of the problem. Supplier partnership is based on the understanding that formulation information will be used only to better understand the material's chemistry and to develop methods to ensure material consistency, and that proprietary information will not be disclosed without the supplier's agreement.

Fingerprint Databases

Fingerprinting of a material yields data that is compiled into a quantitative database for that material. Fingerprint databases provide a baseline reference that are used to detect and identify lot-to-lot variations in composition that may be due to formulation changes, material degradation, or contamination. When a sufficient number of lots have been fingerprinted, the database is used to select fingerprint methods for implementation as receiving/acceptance tests and to establish receiving/acceptance ranges. Fingerprint methods and databases are also used to support material failure investigations, new material development, alternate material qualification, new supplier qualification, new manufacturing location qualification, and material shelf-life investigations.

Fingerprint databases provide a reservoir of data that can be used to generate control charts. Through the use of control charts, shifts or trends in material parameters can be detected early, before the material fails to meet specification.

Acknowledgements

Tammy Bourgeois, Mary Capezza, Emile Evans, Debbie Pierce, Laurie Rando, and Lance Spiers have made major contributions to the chemical fingerprinting program. Mary Capezza's support with this presentation is greatly appreciated.

Use of GC/MS and Microtome Techniques as Methods to Evaluate ODC Free Cleaner Diffusion and Evaporation in Insulation and Phenolic Case Material [1]

L.L. Biegert
Cordant Technology: Thiokol Propulsion
P.O. Box 707
Brigham City, Utah 84302-0707
(435)-863-3958
Biegell@Thiokol.com

5

ABSTRACT

Because of the 1990 Clean Air Act Amendment (CAAA) many chlorinated solvents used in the aerospace industry are being phased out. Replacement of the ODC (ozone-depleting chemicals) with less volatile, non-ozone depleting cleaners has been extensively studied over the past seven years at Thiokol Propulsion, a Division of Cordant Technologies, Inc.

The down selection of ODC replacement cleaners has been based on several factors including the diffusion/ evaporation of the cleaners in selected substrates. Methodologies were developed to evaluate the cleaner content in substrates. Methods of cutting thin slices of material (microtoming) were combined with GC/MS (gas chromatography/ mass spectroscopy) analysis.

Substrates evaluated in this study include potential solid rocket motor materials: ASNBR (asbestos-filled nitrile butadiene rubber) and CFEPDM (carbon-filled ethylene propylene dimonomer) insulation and glass (GCP), carbon (CCP) and silica (SCP) cloth phenolic substrates with fibers either parallel (0°) or perpendicular (90°) to the surface. Residue profiles indicate both cleaner and substrate composition affect the diffusion and subsequent evaporation of the cleaner from the substrate surface.

INTRODUCTION

Federal air regulations under the 1990 Clean Air Act Amendment (CAAA) has presented a big challenge and cost impact to the aerospace industry by phasing out the use of Class I and II ozone-depleting chemicals and substances. TCA (1,1,1-trichloroethane), a chlorinated solvent used at Thiokol Propulsion a division of Cordant Technology, is targeted by this clean air amendment. Alternate cleaners must be qualified before depletion of the TCA stockpile and/or before the TCA "essential use" waiver expires.

Over the past seven years ODC replacement cleaners have been evaluated for safety, solubility, compatibility, cleaning efficiency, effects on subsequent bond strength and substrate integrity. Development of discriminating methods to screen cleaners has been an important feature in the selection process to replace TCA. The combined use of GC/MS analysis and microtome cutting has been developed to obtain cleaner residue profiles in substrates that will be hand cleaned with the new cleaner. This information can be further combined with mechanical properties (tensile and shear information) to determine the detrimental effect of the cleaner on substrate properties or subsequent bonding.

© 2000 Thiokol Propulsion, a Division of Cordant Technologies, Inc.

[1] This work was performed under contract NAS8-38100 as part of NASA's ODC Cleaner TCA Replacement Program.

EXPERIMENTAL

Six types of cloth phenolic coupons (1-inch by 2-inches) were used in this study. They include glass cloth phenolic (GCP), silica cloth phenolic (SCP) and carbon cloth phenolic (CCP). Fibers in these coupons were wound either perpendicular (90°) or parallel (0°) to the cleaner exposed surface. Two types of motor insulation coupons were also evaluated and include the ASNBR (asbestos-filled nitrile butadiene rubber) and the CFEPDM (carbon-filled ethylene propylene dimonomer) rubbers.

Coupons (one- by two- inch) of either cloth phenolic or cured insulation were secondarily bonded onto a stage that was clamped into the microtome apparatus. For the insulation, a manual microtome instrument was used to cut slices from the surface at approximately 0.4-mm. The hardness of the cloth phenolic prevented manual microtoming and the samples were cut automatically using an instrument that cuts slices approximately 0.1-mm thick from the surface.

Three cleaners were evaluated in this study. The baseline solvent, 1,1,1-trichloroethane (TCA) was included to compare with the new cleaners under evaluation. Bioact PCG has been extensively evaluated in several of the work areas and represents a cleaner that contains limonene. Many of the other cleaners evaluated at Thiokol also contain limonene and thus the diffusion and evaporation of this component from motor substrates is important. The cleaner PFD was also included since this material not only contained limonene but also a mixture of hydrocarbons. Table I lists the cleaners evaluated in this study and their components.

Table I
Cleaners and Their Components

Cleaner	Abbreviation	Chemical Description
Trichloroethane	TCA	1,1,1-trichloroethane
Bioact PCG	PCG	Limonene (> 98%)
PF Degreaser	PFD	Limonene (8%), BHT (inhibitor), Hydrocarbons (92%)

Rymple cloth was saturated with the appropriate cleaner and the coupon hand wiped with the wet cloth. After several passes of the wet cloth on the surface, a dry rymple cloth was used to remove any excess cleaner. The coupons were allowed to dry at ambient conditions for a selected number of minutes (15, 30, 45 and 60) prior to removing three slices from the surface.

Slices of cloth phenolic or cured insulation were placed in glass bottles with rubber septum for GC/MS headspace analysis. Each sample was heated to 110°C for approximately twenty minutes then a 250-µl aliquot of headspace gas was removed for cleaner residue analysis.

DISCUSSION

Cured Insulation Substrates

The diffusion/evaporation profiles of the three cleaners in cured ASNBR insulation are shown in Figure 1. The TCA residue cleaner profile shows the chlorinated solvent is readily absorbed into the ASNBR rubber substrate. Even after 60 minutes dry time the levels of TCA remain relatively high at the substrate surface. High values of TCA are also observed at 0.5 mm into the sample. Over time the surface levels of TCA remain the same and the levels at 0.5 mm decrease. Two processes are contributing to this cleaner profile: evaporation from the surface and diffusion from the bulk substrate.

The PCG cleaner profile in ASNBR insulation shows a significant loss in substrate cleaner levels from 15 minutes to 30 minutes. Relatively little change in cleaner surface levels is observed between 30 and 60 minutes. The PFD hydrocarbon levels in ASNBR cleaner show this component of the cleaner does not penetrate very deep into the substrate and does not evaporate readily from the surface. Nitrile butadiene rubber is specifically formulated to resist oil and hydrocarbons and the cleaner profiles that were generated in this study support this chemical feature.

Cleaner profiles in CFEPDM are shown in Figure 2. Similar levels of TCA are found in CFEPDM in comparison with ASNBR insulation. A significant loss in cleaner surface levels is noted between 15 and 30 minutes. Once again the cleaner is observed at fairly significant levels at 0.6 mm into the bulk substrate.

The PCG profile in CFEPDM is significantly different than that observed for ASNBR insulation. In CFEPDM, limonene is readily absorbed into the rubber. Limonene levels are almost as high 0.6 mm in the substrate as they are on the surface. There is a significant decrease in limonene between 15 and 30 minutes of ambient drying, however, there is little change in cleaner levels up to 60 minutes.

The PFD cleaner profiles in CFEPDM are also significantly different in comparison with ASNBR insulation profiles. Like PCG, the hydrocarbons in PFD are readily absorbed into the CFEPDM. Very high levels of cleaner are observed at 0.6 mm even after a 60 minutes ambient temperature dry.

Cloth Phenolic Substrates

The cleaner evaporation/diffusion profiles in carbon cloth phenolic (CCP) coupons are shown in Figure 3. Very little cleaner (TCA or PCG) is observed on the surface with no sequential decrease in cleaner residue observed over a 60 minute dry. Variability due to hand wiping appears to be greater than the evaporation of the cleaner.

PFD has the highest surface residue of the three cleaners evaluated in this study with little penetration into the bulk substrate and a decrease in surface residue observed over time. The 90-degree wound fiber coupons were selected for evaluation since the fibers are perpendicular to the surface and if cleaner is wicked by the fiber a deeper cleaner diffusion into the bulk would be observed.

The cleaner profiles with glass fiber phenolic (GCP) coupons are shown in Figure 4. Like the carbon fiber profiles very little cleaner is observed on the surface of the substrate with almost no penetration into the bulk substrate. Trends between the cleaners indicate TCA is absorbed less into the bulk compared to PCG and with PFD demonstrating a deeper penetration.

The silica cloth (SCP) coupons demonstrate a higher absorption of cleaner (PCG and PFD) into the bulk compared to the other types of fiber-filled coupons (carbon and glass). Figure 5 shows the cleaner profiles in the SCP substrate with fibers perpendicular to the substrate. Higher levels of limonene (PCG) are actually observed deeper into the substrate compared to the surface. Eventhough the SCP substrate demonstrates the highest levels of cleaner, the cloth phenolic substrates demonstrate significantly reduced levels of cleaner on the surface and into the bulk compared to the insulation substrates.

The effect of fiber direction is readily observed with the SCP coupons and the PCG cleaner. Figure 6 shows the difference in depth of hydrocarbon penetration for the fibers perpendicular to the surface (90-degree) compared to the fibers parallel to the surface (0-degree).

SUMMARY/CONCLUSIONS

The diffusion of cleaner into rubber is dependent on the type of compounds found in the cleaner and the type of rubber. NBR insulation is normally known for its resistance to petroleum-based fluids, and thus, the dramatic difference in PFD (hydrocarbon-based cleaner) diffusion into CFEPDM compared to ASNBR is not surprising. The limonene-based cleaner PCG is also more similar in structure to the CFEPDM compared to ASNBR and deeper penetration into CFEPDM is observed.

The diffusion of TCA into both rubber substrates shows similar absorption. Evaporation of TCA takes place at the surface of the substrates however because of the depth of penetration, there is a reservoir of TCA in the substrate bulk that even after 60 minutes of drying allows a significant level of TCA to remain on the rubber surface.

As would be expected cleaner diffusion into the cloth phenolic coupons occurs less readily than diffusion into the more porous insulations. The type of fiber also influences the penetration of cleaner as noted by the SCP coupons absorbing more limonene- (PCG) and hydrocarbon- based (PFD) cleaner compared to the glass and carbon cloth coupons. The depth of penetration is not only dependent on the type of fiber in the phenolic but also on the fiber orientation. Fiber that is perpendicular to the surface can wick the cleaner deeper into the substrate compared to fibers that are wound parallel to the surface.

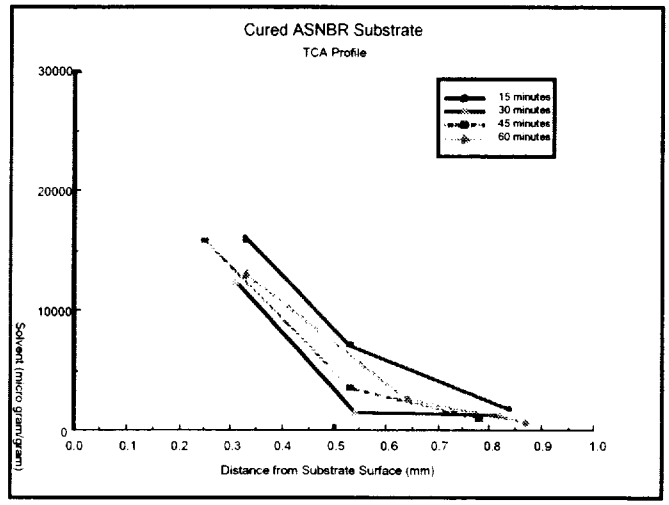

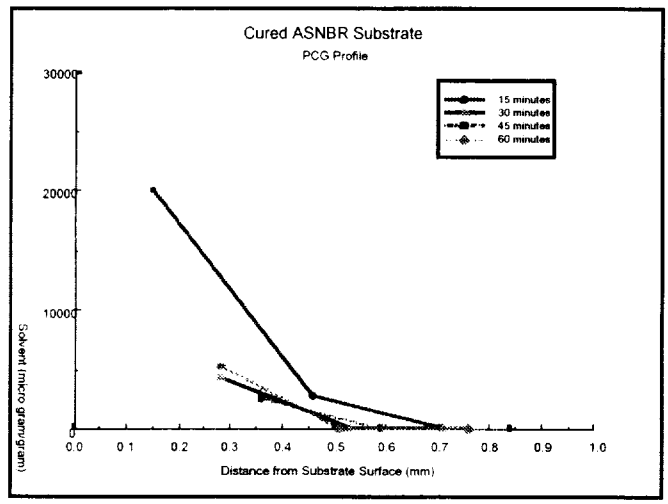

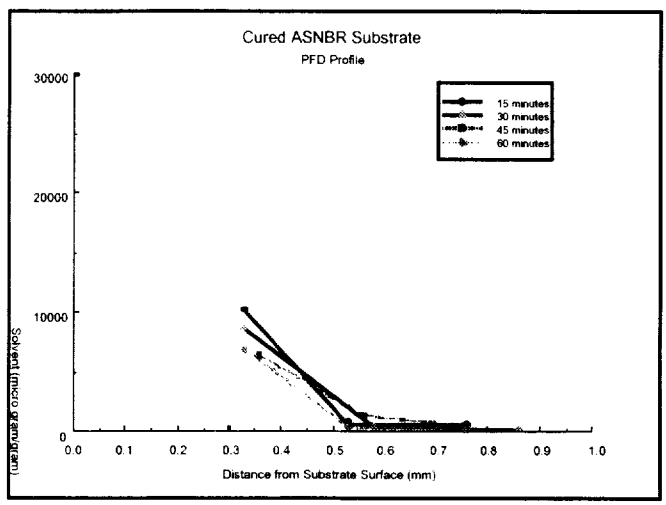

Figure 1: Cleaner Profiles in ASNBR Insulation

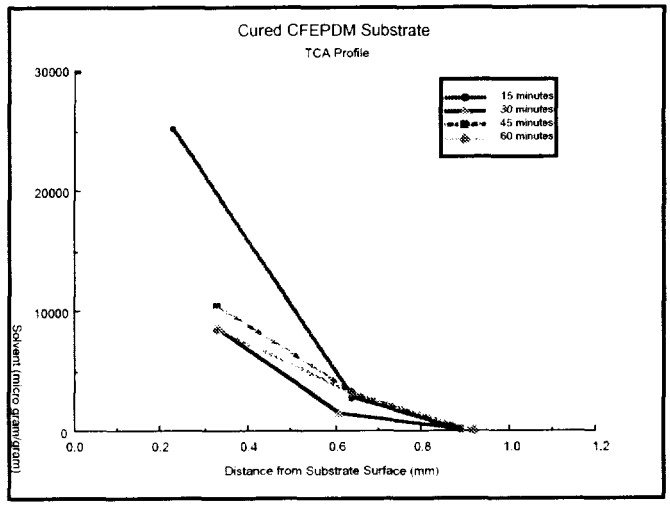

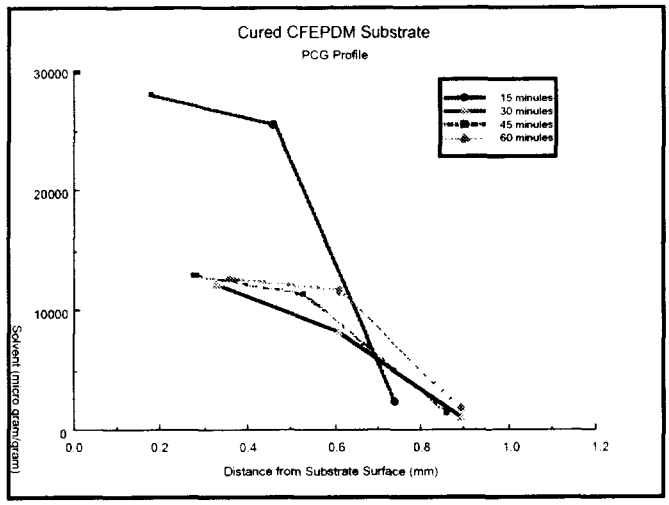

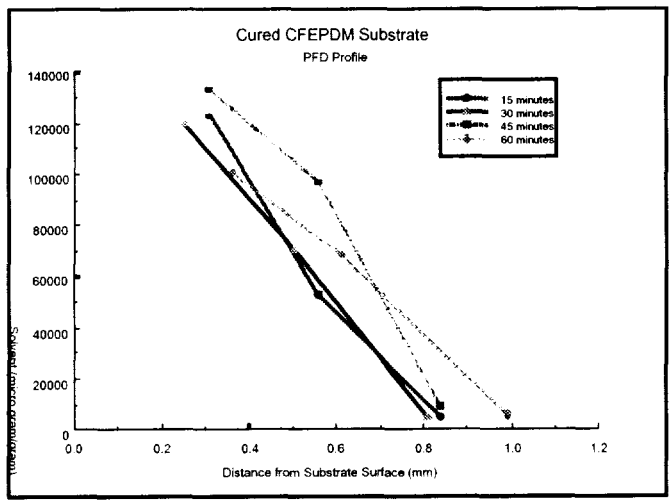

Figure 2: Cleaner Profiles in CFEPDM Insulation

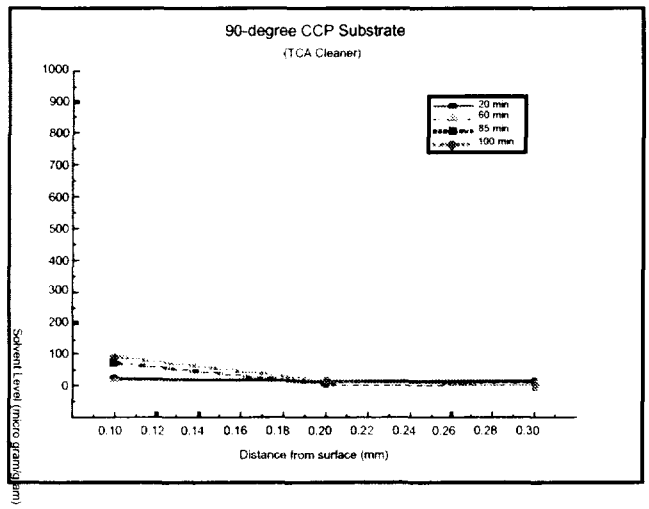

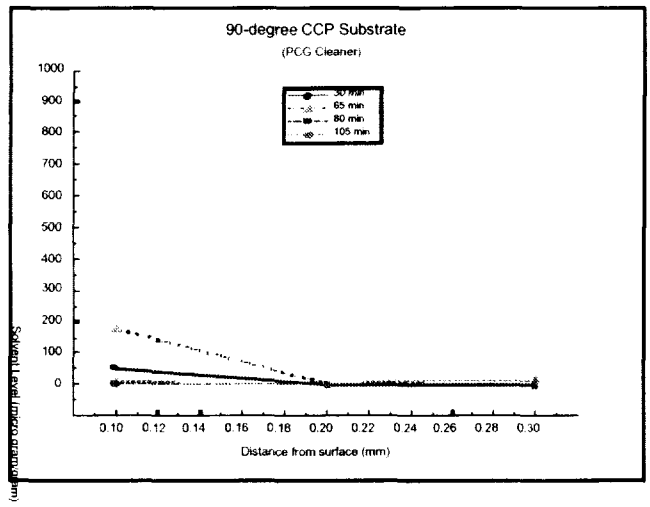

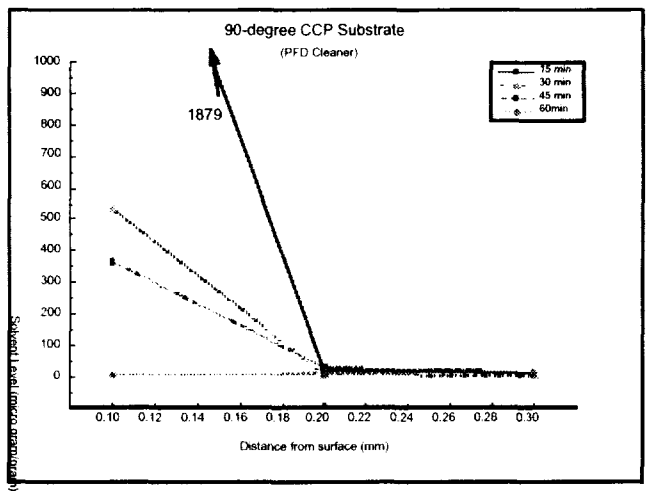

Figure 3: Cleaner Profiles in CCP Substrate

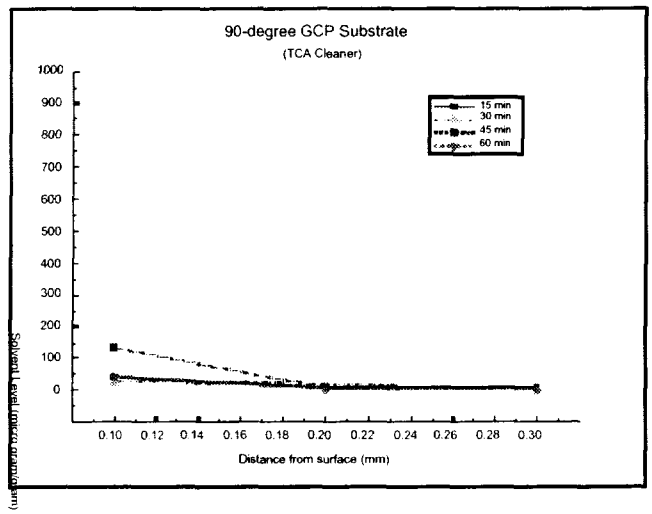

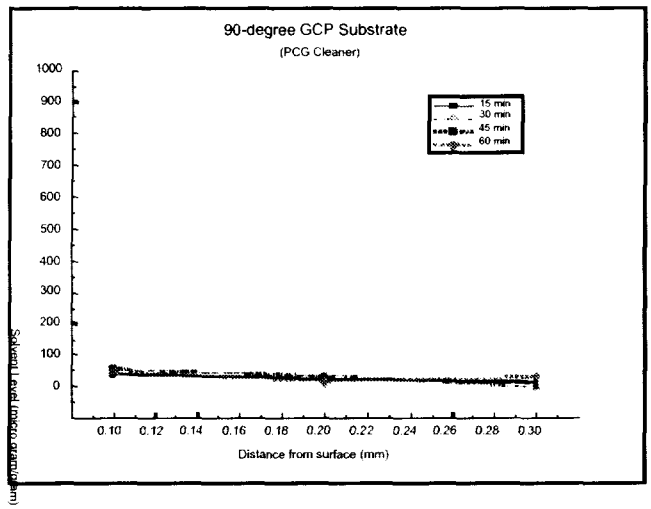

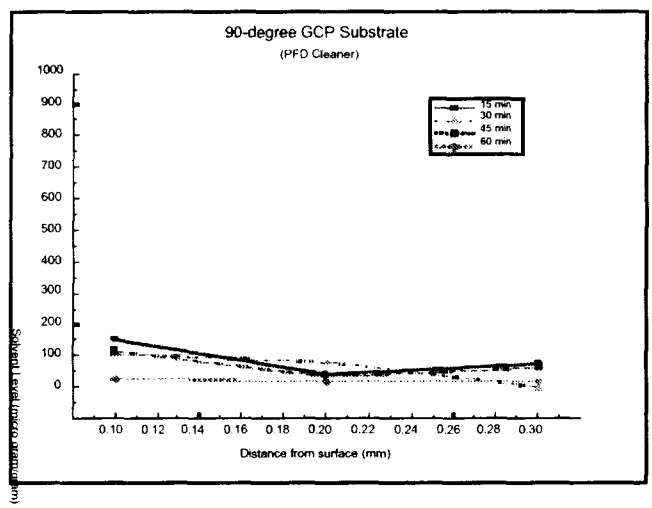

Figure 4: Cleaner Profiles in GCP Substrate

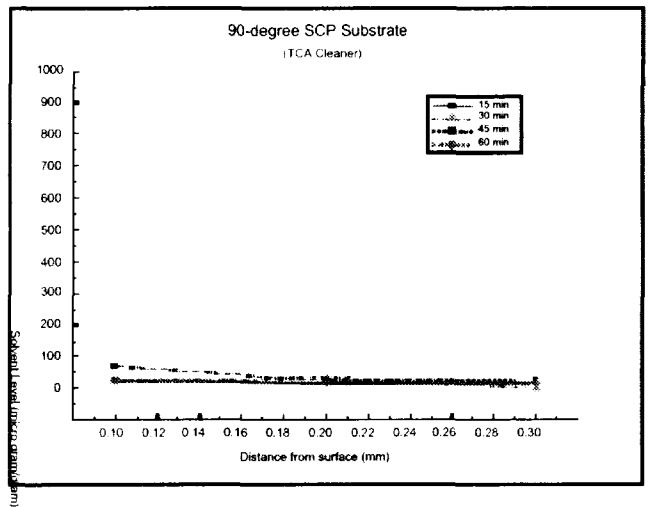

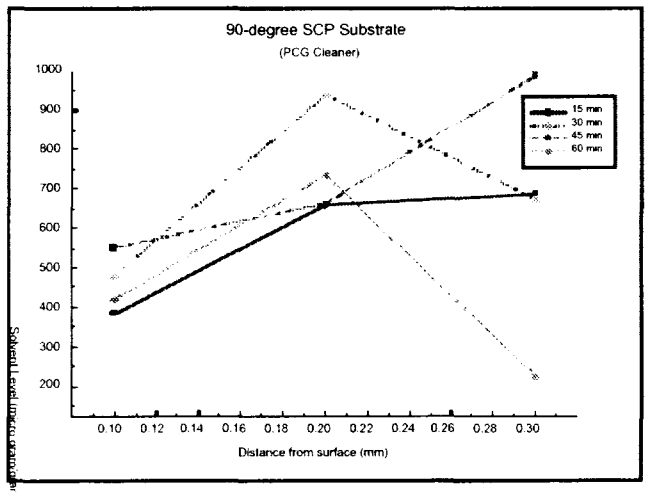

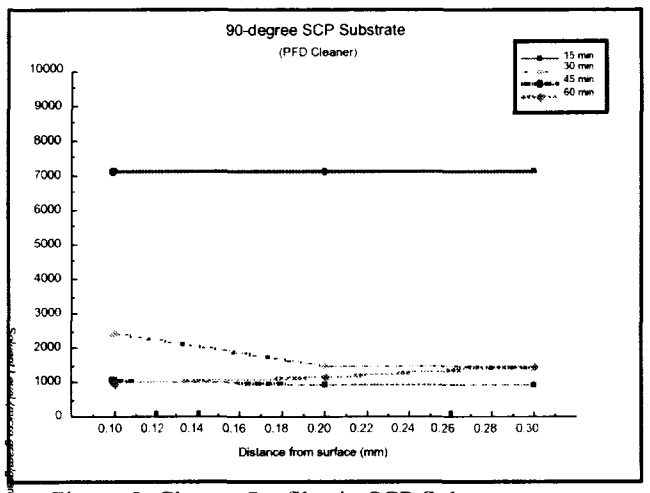

Figure 5: Cleaner Profiles in SCP Substrate

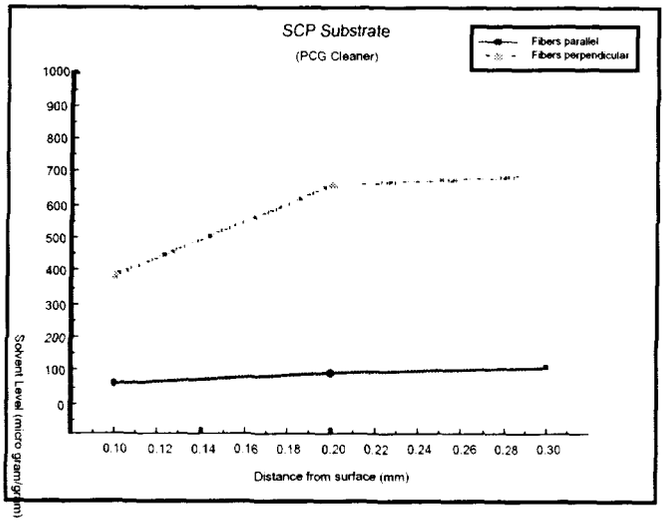

Figure 6: Cloth Fiber Direction Influence on Absorption

Electron Beam-Cure Polymer Matrix Composites: Processing and Properties

GEORGE WRENN and Barbara Frame

E3/1

Oak Ridge National Laboratory
One Bethel Valley Road
P.O. Box 2009
Oak Ridge, TN 37831 USA
Phone: 423-241-2521 (Wrenn), 423-576-1892 (Frame)
Fax: 423-574-8257
E-mail: wrenngejr@y12.doe.gov
framebj@y12.doe.gov

Brian Jensen
Langley Research Center/Mail Stop 226
Hampton, VA 23681-2199 USA
Phone: 757-864-4271
Fax: 757-864-8312
E-mail: B.J.Jensen@larc.nasa.gov

Alan Nettles
Marshall Space Flight Center/ED34
Huntsville, AL 35812 USA
Phone: 256-544-6109
Fax: 256-544-7255
E-mail: Alan.Nettles@msfc.nasa.gov

Researchers from NASA and Oak Ridge National Laboratory are evaluating a series of electron beam curable composites for application in reusable launch vehicle airframe and propulsion systems. Objectives are to develop electron beam curable composites that are useful at cryogenic to elevated temperatures (-217 °C to 200 °C), validate key mechanical properties of these composites, and demonstrate cost-saving fabrication methods at the subcomponent level. Electron beam curing of polymer matrix composites is an enabling capability for production of aerospace structures in a non-autoclave process. Payoffs of this technology will be fabrication of composite structures at room temperature, reduced tooling cost and cure time, and improvements in component durability.

This presentation covers the results of material property evaluations for electron beam-cured composites made with either unidirectional tape or woven fabric architectures. Resin systems have been evaluated for performance in ambient, cryogenic, and elevated temperature conditions. Results for electron beam composites and similar composites cured in conventional processes are reviewed for comparison. Fabrication demonstrations were also performed for electron beam-cured composite airframe and propulsion piping subcomponents. These parts have been built to validate manufacturing methods with electron beam composite materials, to evaluate electron beam curing processing parameters, and to demonstrate lightweight, low-cost tooling options.

CP 570/N/27

F3/2

MANUFACTURE OF POROUS CERAMIC MATERIALS BY COMBUSTION SYNTHESIS

H.C. Yi, L.A. Whelan, and J.Y. Guigné

Guigné International Ltd, 685 St. Thomas Line, Paradise, NF, Canada A1L 1C1

ABSTRACT

Porous ceramic materials are suitable for a wide variety of applications. By creating a porous ceramic, the properties of both porous materials and ceramic materials can be combined and utilised. The ideal applications for porous ceramic materials would include use in corrosive environments, thermal insulation, catalyst support, highly-efficient engine filters, pre-forms for composite materials, and implants into which body tissue could easily attach and grow.

Experiments have been carried out to produce a series of porous ceramic materials using the combustion synthesis technique. These porous materials have such ceramic matrices as Al_2O_3, MgO, Al_2O_3-MgO and TiC-Al_2O_3. Studies were done to investigate and characterize the ignition and combustion characteristics of these systems as well as to control the porosity and pore distribution of the final products. The combustion wave velocity ranged from 1-5 mm/s and the combustion temperatures ranged from 1500-2000°C, depending on the chemistries.

All materials exhibited a large degree of linear expansion (100-200%) during the combustion reactions. Typical apparent porosity (open and interconnected pores) for the materials was >70% and the overall porosity was >80%. Successful attempts were made to control the apparent and overall porosity of the products. This was done through the addition of a diluent and by physically confining the samples. As a result, the porosity can be made to vary controllably over a large range (42-83% apparent porosity).

A technique has also been developed to increase the quality of the high porosity samples by improving the pore size and distribution. As a result, both the strength and modulus of these samples were increased substantially.

1.0 INTRODUCTION

The unique characteristics of porous ceramic materials such as high hardness and resistance to heat and chemical attack make them suitable for a wide variety of applications. These materials can operate at high temperatures and do not degrade significantly due to oxygen, however, they are brittle. The brittleness is associated with voids, cracks, and impurities in the material. Several important properties of porous ceramic media include their lightweight, thermal insulation, filtration ability, and absorbency.

Combustion Synthesis or Self-propagating High Temperature Synthesis (SHS) is a novel technique and a proven effective method of producing various advanced, porous, high-temperature ceramic and composite materials [1-3]. It involves the reaction of solid state powders initiated by an external energy source and combines the principles of chemical reaction engineering and materials science. Once a sample is ignited, the highly exothermic reaction would ignite the next adjacent reactant layer by itself thereby generating a self-sustaining combustion wave propagating through the material.

The SHS method has many advantages over traditional synthesis techniques. It saves energy since no high-temperature furnace is required, it allows for faster production since the typical combustion velocity is from a few millimetres to a few centimetres per second, it produces a relatively high purity of the final product since high combustion temperature vaporises most impurities, it requires simple equipment, and it allows simplicity of the whole process. Owing to these advantages, it is likely that materials produced by SHS have a lower overall cost compared to the conventional melting-casting route.

A SHS reaction is defined by three main parameters. They are: 1) an ignition temperature at which the reaction becomes appreciable and self-sustaining, 2) a combustion temperature (maximum temperature achieved),

and 3) a combustion wave velocity which is the overall combustion rate. However, other parameters such as green density, particle size, and the reaction environment may have a profound influence on the combustion reaction.

2.0 METHODOLOGY

2.1 Materials

Combustion experiments were carried out using various reaction systems to produce a wide range of porous ceramic materials having a matrix of Al_2O_3, MgO, or a combination of the two (Al_2O_3-MgO). The systems are represented by the following reactions:

$$2\ B_2O_3 + 6\ Mg + C = B_4C + 6\ MgO \quad (2.1)$$

$$4\ B_2O_3 + 6\ Al + 2C + 3\ Mg = 2\ B_4C + 3\ Al_2O_3 + 3\ MgO \quad (2.2)$$

$$2\ B_2O_3 + 4\ Al + C = B_4C + 2\ Al_2O_3 \quad (2.3)$$

$$2\ B_2O_3 + TiH_2 + 4\ Al + 2C = TiC + B_4C + 2Al_2O_3 + H_2(g) \quad (2.4)$$

$$2\ B_2O_3 + 4\ Al + C + x\ CaO = B_4C + 2Al_2O_3 + x\ CaO \quad (2.5)$$

The reactions are designed such that at least one substance boils at a temperature lower than the combustion temperature of the reaction to assist pore formation. The evaporation of that substance at the combustion front releases gases, thus help generating pores in the product. Some physical data for the reactant powders are shown in Table 1. The gasifying substance in equation (2.1) is Mg, in (2.2) is Mg and B_2O_3, in (2.3) is B_2O_3, in (2.4) is B_2O_3 and H_2.

Table 1: Data for Reactant Powders

Powder	Molar Weight	Melting Temp. (°C)	Boiling Temp. (°C)
Al	26.98	660	2467
Al_2O_3	101.96	2015	2980
B_2O_3	69.62	450	1860
C	12.01	3727	4830
CaO	56.08	2614	2850
Mg	24.31	650	1107
MgO	40.31	2852	3600
SiO_2	60.09	1710	2230
TiH_2	49.92	400	600

2.2 Experimental Methods

Calculated masses of reactant powders were mixed to produce the desired composition, according to the reactions shown in (2.1)-(2.5). The powders were thoroughly mixed by ball milling using ceramic balls. To form the 0.5-inch diameter pellet to be used for experimentation, a known mass of this mixed powder was measured out on a balance and then pressed using a tool steel die and a hydraulic press to 60 ± 3% theoretical. Lower density pellets (~30-35%) were also fabricated using a technique developed in our laboratory.

Once the sample was prepared, it was placed in a fume hood and ignited in air using an oxygen-propane torch. The reaction of the sample was recorded using a high-resolution colour video camera and VCR system to allow determination of the velocity of the wave propagation and the analysis of its behaviour. To determine the temperature profiles, samples were ignited inside a chamber in an inert atmosphere by applying high power through

a tungsten ignition coil. Temperature profiles were measured using Type C thermocouples and a data acquisition system.

3.0 RESULTS AND DISCUSSION

3.1 Combustion Characteristics and Porosity

A typical temperature profile during the combustion synthesis process is shown in Figure 1 for a pellet with 60% density from Reaction (2.3). The maximum temperature, i.e., the combustion temperature for this particular sample was 1900°C and the wave velocity was 1.7 mm/s. Combustion wave velocities for other reactions are also shown in Table 2, along with the adiabatic temperatures of these reactions.

Figure 1: A Typical Temperature Profile

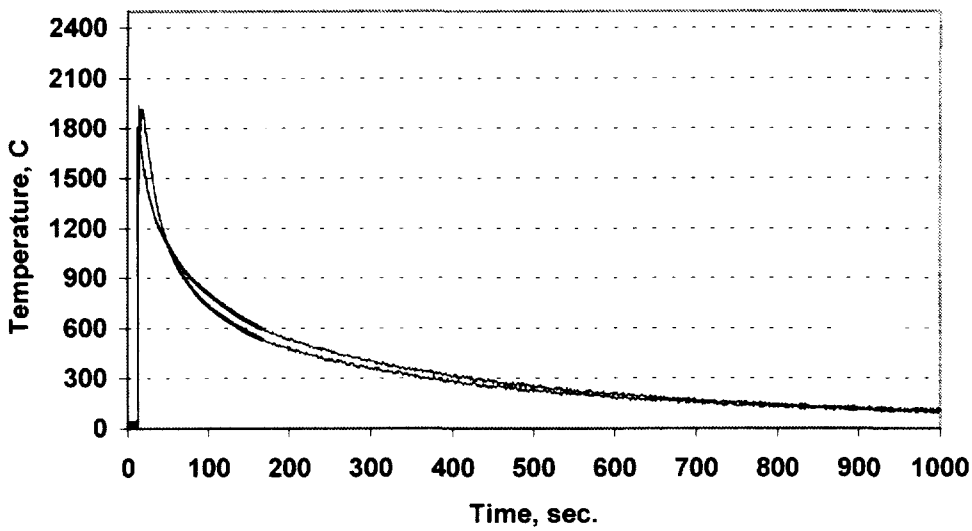

Table 2: Combustion Characteristics and Porosity of Selected Materials

Reaction	Wave Velocity mm/sec	Tad °C	Porosity (%)		
			Apparent	Overall	Ratio
(2.1)	1.7	2470	73	82	89%
(2.2)	3.7	2054	71.3	82.5	86%
(2.3)	1.5	2054	71.5	84.3	85%
(2.4)	1.3	2040	77.0	84.5	91%

For reactions (2.1) and (2.3), the pellets were easily ignited and the combustion wave velocities were around 1.5 to 1.7 mm/s. The combustion waves were unstable due to two factors. Firstly, the high thermal conductivity lead to a large heat loss by conduction and, secondly, the large expansion during combustion decreased the continuity of the material and made it difficult to react the next adjacent layer. Reaction (2.1) was particularly violent and unstable and the wave propagated in a helical pattern. These factors were responsible for the low

velocity of these samples and several did not complete the combustion process. Reaction (2.2) is a combination of reactions (2.1) and (2.3) and produces a ceramic composite with matrices of Al_2O_3 and MgO. This reaction had a higher wave velocity because of the high exothermicity. Reactions (2.4) was also easily ignited and produced a relatively high wave velocity. Reacted samples contained higher apparent porosities due to the generation of hydrogen gas at the combustion front. All samples showed large expansion, some as much as 300%, and the porosity tended to be non-uniform as will be shown later.

3.2 Porosity Control

The materials produced by the above reactions were very porous and because of that, they were also very fragile. In some circumstances, lower porosity might be desired. Two techniques were used to control the porosity of these materials: 1) by adding a diluent to the combustion reaction and 2) by physical confinements to limit expansions.

3.2.1 Effect of the Diluent

One method of controlling the product porosity was to reduce the exothermicity of the chemical reactions by addition of one or more diluents. For instance, by adding an oxide, such as CaO, to the reaction to act as a chemical diluent as shown in Reaction (2.5). This diluent decreased the combustion temperature and, therefore, decreased the amount of expansion of the sample. Both the apparent and overall porosity decreased drastically as the amount of diluent increased, as shown in Figure 2.

Figure 2: Effect of Diluent on Porosity

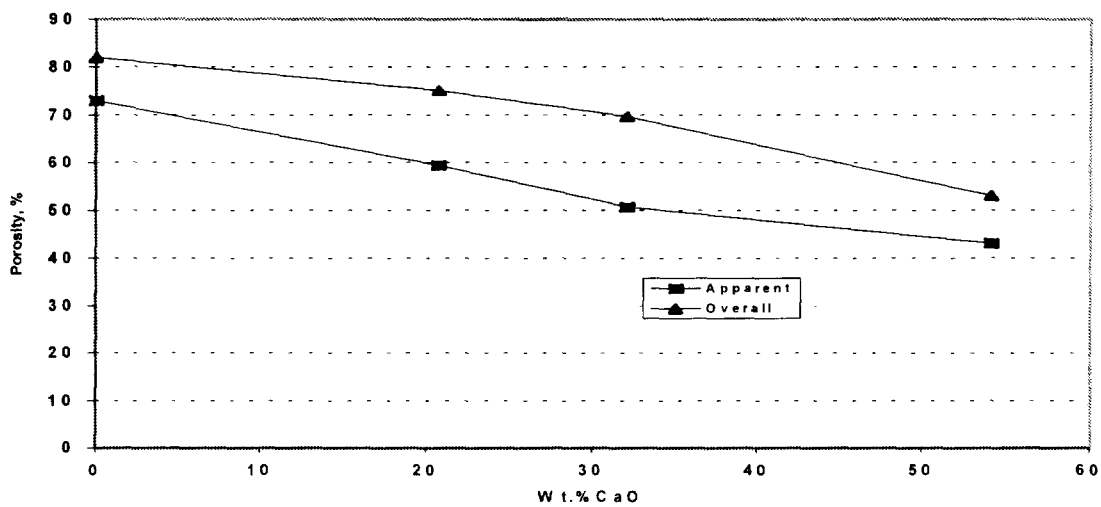

3.2.2 Physical Confinements

Confining the samples inside a cylinder made of stainless steel also controlled porosity of the materials. A rod was inserted into the end of the cylinder through a hole and could be fixed at a desired location, depending on the length (and thus porosity) desired for the samples. A sample could be completely confined and not permitted to expand at all or a specified distance could be left for the sample to expand, thus creating different porosity

Table 3 shows the average apparent and overall porosity and also some measured velocities for some confined samples. As clearly shown in the table, the apparent and overall porosity (as well as the velocity) increases with decreasing confinement. The highest porosity occurs in the samples that were permitted to undergo free

expansion. The velocity increases with decreasing confinement due to the fact that less heat is being conducted away from the sample.

Table 3: Average Porosity and Velocity Results for Confined Samples (Density=60%)

Confinement Condition (Total length once reacted)	Apparent Porosity: P(%)	Overall Porosity: Po (%)	Average Velocity (mm/s)
Free expansion	75.8	82.3	-
30 mm	72.6	79.5	9.11
25 mm	68.5	75.4	-
20 mm	62.9	70.5	5.85
Completely confined	56.5	65.2	4.53

Although the degree of porosity could be controlled, there seemed to be a porosity gradient in those materials. During combustion, a sample that was not completely confined would expand in length until it reached the rod. A higher density (and thus lower porosity) would be created at the end that was pressing against the rod therefore creating an uneven pore distribution throughout the sample. To produce samples without porosity gradient, low-density cylindrical samples were prepared before placing it in the confinement cylinder. The sample was made to a specified length, depending on the desired porosity and, consequently, the samples also contained various densities. This method did not require the sample to expand during combustion and, since the powder was loose and evenly distributed before combustion, the product also contained a uniform pore distribution. Figure 3 shows the average apparent and overall porosity and also some measured velocities for the samples of different densities. As can be seen from the figure, the apparent and overall porosity increases with decreasing density.

Figure 3: Effect of Confinement on Porosity

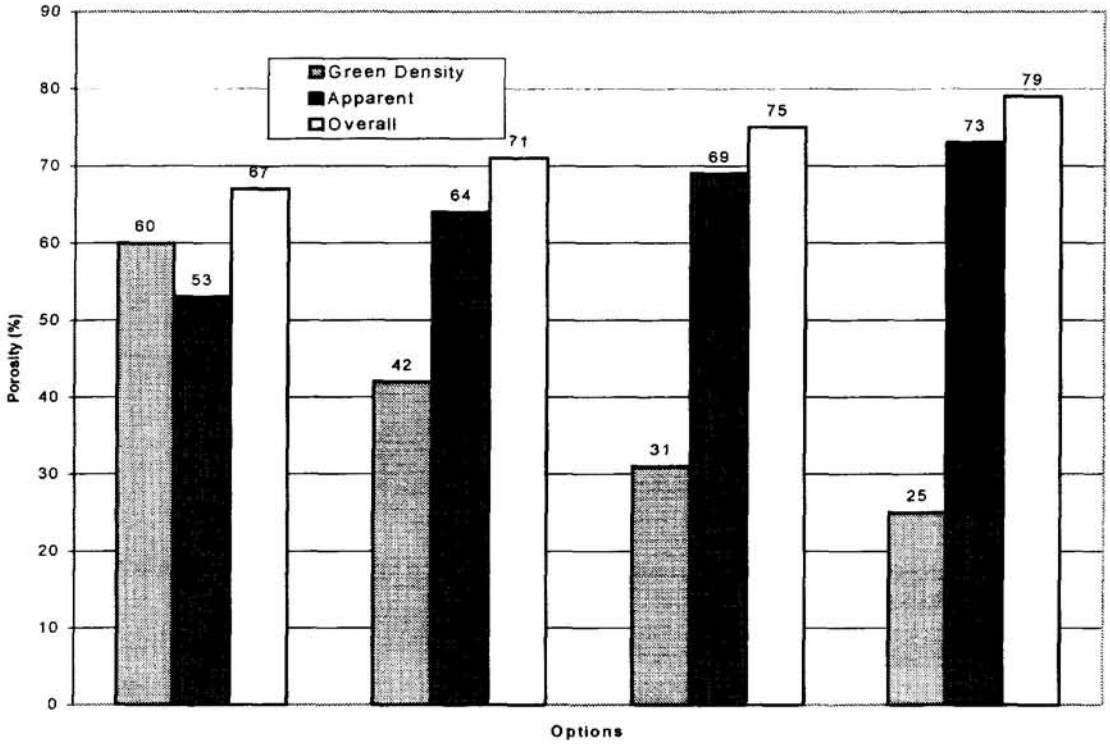

3.3 Improvement of Pore Structure

When sample produced from igniting relatively high-density pellet (~60%) of the reaction (2.3) with free expansion, they often contain macro-pores in the order of 1mm in size. A typical photomicrograph of such a sample is shown in Figure 4. Such samples had very low strength and were somewhat fragile. Figure 5 shows a typical stress-strain curve for such a sample during a compression test. The strength of the sample was 298 psi. To increase the strength of these materials, green pellet with about 35% density was prepared and ignited. Figure 6 shows a photomicrograph of the same reaction. Apparently, the surface of the sample is much smoother and no macropores existed. The compression test of such a sample is shown in Figure 7. The strength of the sample was 740psi, much higher than the sample produced from a green pellet with 60% theoretical density. The average mechanical properties from samples produced by the two approaches are shown in Table 4.

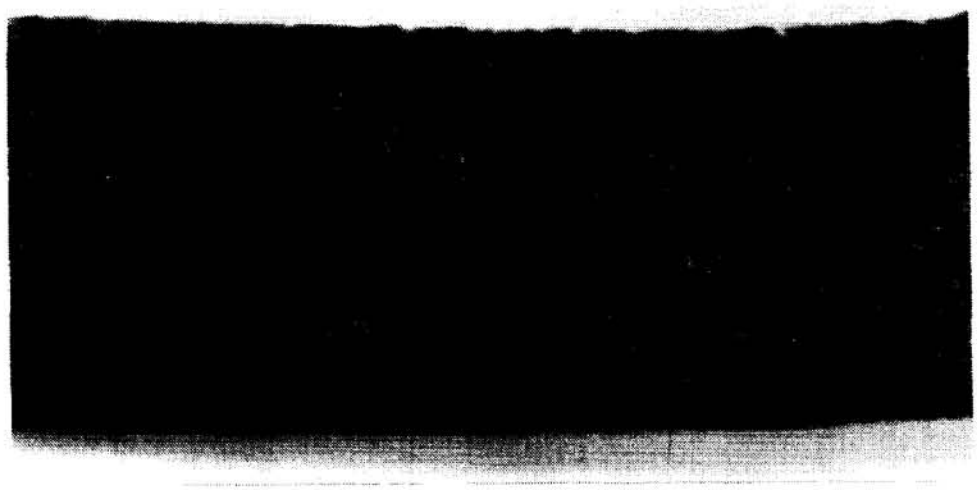

Figure 4: An optical photograph showing macropores on surface for a sample reacted from a pellet with a green density of 60% by Reaction (2.3).

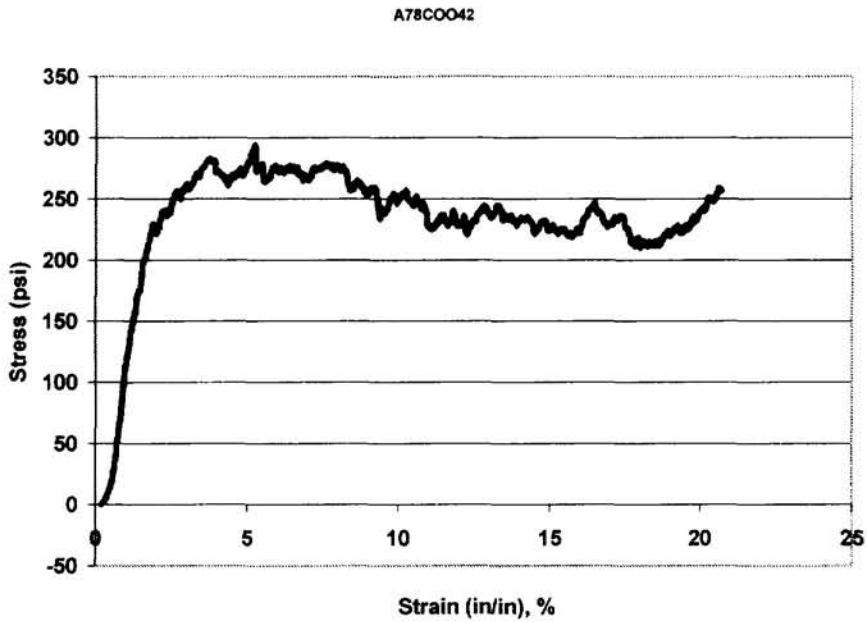

Figure 5: A Typical Stress-Strain Curve During Compression for a sample reacted from a pellet with a green density of 60% by Reaction (2.3).

Figure 6: An optical photograph showing no macropores formation on surface for a sample reacted from a pellet with a green density of 35% by Reaction (2.3).

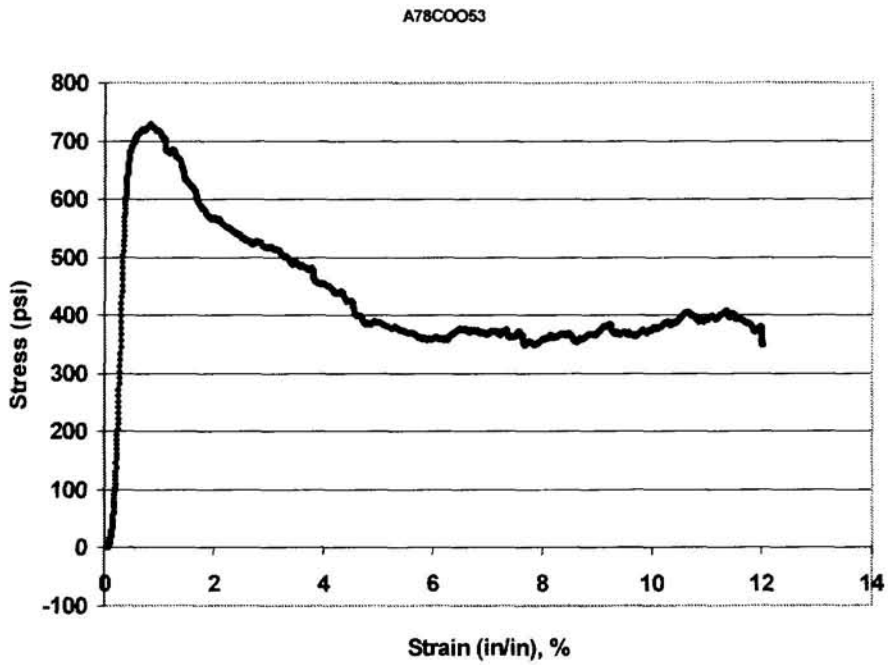

Figure 7: A Typical Stress-Strain Curve During Compression for a sample reacted from a pellet with a green density of 35% by Reaction (2.3).

Table 4: Average Mechanical Property Data

Samples Produced From	Strength, MPa	Modulus, MPa
60% Pellets	1.05	2.06
35% Pellets	5.47	4.43

4.0 CONCLUSIONS

Highly porous ceramics have been produced by the combustion synthesis technique. Large expansion is the characteristic of most systems, therefore creating large porosity. However, porosity of the products could be controlled. This was achieved by adding a diluent and physically confining the samples.

Highly porous samples produced from relatively high green density pellets exhibit poor mechanical properties due to macropores formation in the samples. An improved fabrication technique has been employed to produce higher quality, uniform distributed pores. As a result, both the compression strength and Young's modulus increased substantially.

REFERENCES

1. Munir, Z.A. and Anselmi-Tamburini, U., 1989, "Self-propagating exothermic reactions: the synthesis of high temperature materials by combustion", *Mater. Sci. Rep.*, 3, 227-365.

2. Yi, H.C. and Moore, J.J., 1990, "Review: Self-propagating high temperature (Combustion) synthesis (SHS) of powder-compacted materials", *J. Mater. Sci*, 25, 1159-1168.

3. Moore, J.J., and Feng, H.J., *Prog. In Mater. SCI.*, **39**, 243-316 (1995).

The Composites Affordability Initiative

JOHN MISTRETTA

Materials & Manufacturing Directorate
Air Force Research Laboratory
2977 P Street, Room 121
Wright-Patterson Air Force Base, OH 45433-7739 USA
Phone: 937-904-4597
E-mail: john.mistretta@wpafb.af.mil

The Composites Affordability Initiative (CAI) is a multi-service and aerospace industry collaborative effort. This long-range initiative has the goal of developing the technologies and tools necessary to reduce the acquisition cost of composite structures by an order of magnitude. The current phase of CAI includes Joint Strike Fighter-related transition programs at Boeing and Lockheed Martin, plus a cooperative pervasive technology program. This is the second phase of a four-phase effort.

To provide sufficient depth, all relevant areas including design, fabrication, assembly, analysis, quality, and cost models, must be advanced. In the past year, several large producibility articles have been developed to focus the fabrication and assembly technology development process under the pervasive technology program. In addition, cost, analysis, and quality tools have been developed and enhanced.

CP/572 IN/57

E3/4AST

Title: **Advanced Ceramic Matrix Composites for Aerospace Applications**

Co-Authors: Bill Patterson, Bob Klacka, John Garnier, Paul Gray,

Company: Honeywell Advanced Composites Inc., Newark, Delaware USA

Abstract:

Advanced ceramic matrix composites (CMCs) are an enabling technology for hypersonic trans-aerospace, missile and turbine engine applications demanding high performance utility. Honeywell Advanced Composites has developed a palette of CMCs in limited commercial production and in various stages of evaluation for aerospace related programs. CMCs include carbon fiber reinforced silicon carbide (C/SiC) and Enhanced silicon carbide fiber reinforced silicon carbide (E-SiCf/SiC). Hardware fabrication can use chemical vapor infiltration (CVI), silicon melt infiltration (MI) and chemical conversion processing techniques. C/SiC is a leading thermal heatshield protection material for several heat shield structural designs (RLV/SOV/SMV) and has demonstrated excellent low erosion hypersonic leading edge performance. Because of materials attributes of low density, high strength and very high temperature capability, C/SiC has been in development for linear Aero-spike engine applications including ramp and pump. SiCf/SiC MI CMC is qualified as the only 2200 F, 20 Ksi, long duration materials for NASA high-speed civil transport advanced turbine engines. Commercial accomplishments also include more than 10,000 hours of field time in stationary power turbine engines (DOE-CFCC). Open literature C/SiC, E-SiC/SiC and SiC/SiC MI CMC thermal, mechanical data will be presented including customer approved hardware and test results. The following are selected viewgraphs from the presentation, which contains more detailed information.

- **Material challenges for Aerospace**

Material Challenges for AeroSpace

* Weight is always a premium commodity
  Utilizing CMCs will lighten existing metal systems
* Next-generation performance goals impose very high temperatures on existing metal components
  Utilizing CMCs will greatly extend performance capabilities
* Cooling, in any form, greatly increases weight
  CMCs can be run hotter, reducing cooling
* Strength of metals drops off rapidly with temperature
  CMCs retain or increase strength up to as high as 3000F

Honeywell
Advanced Composites Inc

- **Palette of C/SiC and SiC/SiC ceramic matrix composite materials**

Honeywell ACI's CMC Materials

Fiber	Interface	Matrix	Trade Name/Comments
T-300	PyC	CVI SiC	C/SiC
Needled PAN	PyC	CVI SiC	Novoltex/SiC
T-300	PyC	Melt Infiltration	MI C/SiC

SiC	C or BN	CVI SiC	CVI SiC/SiC
SiC	BN	Melt Infiltration	MI SiC/SiC

* SiC Fibers: Hi-Nicalon, Type S, Tyranno, ZMI, Type SA, Sylramic

* Anti-oxidants are added for the "enhanced" versions: E-SiC/SiC and E-C/SiC

Honeywell
Advanced Composites Inc

Honeywell ACI: CMC Manufacturing/Processing Options

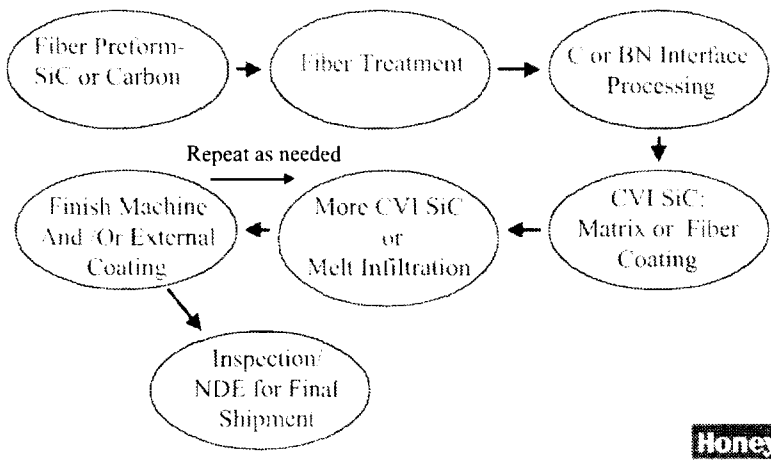

Honeywell
Advanced Composites Inc

Demonstrated Materials Applications

Substrate	Application	Comments
CVI C/SiC (T-300 carbon fiber)	Re-entry heat shields, Turbo-pump rotors/stators	Low recession rates in high aerothermal heating.
Braided C/SiC (T-300 carbon fiber)	Thrusters, fins	Very high strength and low recession properties.
Novoltex/SiC	Thrusters, Leading edge components, vanes	Low recession rates in rocket exhaust.
MI C/SiC (T-300 carbon fiber)	Combustion chambers and vanes	Thermal shock resistant and high strength, low perm.
CVI SiC/SiC CVI E-SiC/SiC	Turbine engine exhaust structures, combustion chambers, leading edges.	Demonstrated stress rupture performance to 2200F/15 ksi.
MI SiC/SiC	Heat shields, mirrors turbine eng. combustors, blades and vanes.	Demonstrated stress rupture performance to 2200F/15 ksi.

Honeywell
Advanced Composites Inc.

- **Overview C/SiC thermo-mechanical properties.**

C/SiC Material Properties Overview

Property	2D C/SiC (CVI)	Novoltex/SiC (CVI)	MI C/SiC (MI)
RT Tensile, ksi	76	7-10	59
2200 F Tensile, ksi	77	9-12	69
RT Compression, ksi	75	73	56
Cross-Ply Tensile, psi	1900	n.d.	2200
Iosipescu Shear, ksi	n.d.	15	16.5
Interlaminar Shear,Ksi	3.7	n.d.	4.1
Ther.Cond. Btu/HrFtF	3.8	7.4	6.1

* C/SiC properties depend highly on fiber type, weave and processing.
* C/SiC attributes are high temperature strength, low areal weight and recession resistance over carbon-carbon

Honeywell
Advanced Composites Inc.

Other Properties of MI C/SiC

Property	Value	Comments
Density	2.1-2.2 gm/cc	Almost theoretical density.
Porosity	2 - 4 volume %	Isolated, closed porosity in tows.
Thermal Expansion	2.0-3.6 ppm per deg C	Linear increase from 200-1200 C
Thermal Conductivity	6 - 7 BTU/hr ft2-Deg F/ft	Value almost **"2 x"** above CVI C/SiC
Permeability (~150 psi)	0.080 lb/ Ft2-min	Value is "far lower" than all CVI SiC. (measured on surface-ground MI C/SiC disks with no "seal coat")

Honeywell
Advanced Composites Inc.

- **Summarize of MI C /SiC thermo-mechanical properties.**

Summary and Conclusions

* A lower cost process for producing C/SiC materials having properties "similar" to an all-CVI SiC matrix has been developed.
* The higher density MI matrix increased the thermal conductivity and matrix dominated substrate properties over a CVI SiC matrix.
* The MI process for producing C/SiC can reduce manufacturing times from 30-50 percent.
* The MI processed developed may be useful for rendering complex fiber preforms " impermeable".

Honeywell
Advanced Composites Inc.

- **Overview SiC/SiC thermo-mechanical properties.**

SiC/SiC Material Properties Summary

Property	2D SiC/SiC (a) (CVI)	2D MI SiC/SiC (b) (MI)
RT Tensile, ksi	47	52
2200 F Tensile, ksi	38	48
RT Compression, ksi	84	85
Cross-Ply Tensile, psi	1200	1400
Iosipescu Shear, ksi	n.d.	15
Interlaminar Shear,Ksi	5.5	5.0
Ther.Cond. Btu/HrFtF	2-4	9.0

(a) Utilizes Hi-Nicalon Fibers, enhanced version
(b) Utilizes Sylramic Fibers

---

* SiC/SiC properties depend highly on fiber type, weave and processing
* SiC/SiC attributes are high temperature strength for extended times over C/SiC. Both CVI SiC/SiC and MI SiC/SiC materials provide optical quality surface for mirrors.

Honeywell
Advanced Composites Inc.

E-SiC/SiC and Melt Infiltrated SiC/SiC CMC Materials

- **E-SiC/SiC attributes**
  - NASA HSCT Engine Propulsion Material Qualified
  - Performance Utility capable: 2200 F extended life (>2000 hours)
  - Static stress up to 20 Ksi
  - Low Cycle Fatigue runout: 10(+6) cycles @ 10Ksi, 2200 F)
- **Melt Infiltrated SiC/SiC attributes**
  - Field demonstration up to 15,000 hours in stationary power testing (2200 F)
  - Joining by Melt Infiltration
  - Materials in development under AF IHPTET 2400 F for extended life (>2000 hours)
  - Static stress up to 20 Ksi. LCF in progress at 2400 F.
- **Applications**
  - Advanced turbine engine hot section components
  - Turbine engine afterburner flaps and seals
  - Hypersonic applications with mission cycles > 100, T < 2500 F
  - Mirror panels/support for optical concentrators and high energy beam deflection

Honeywell
Advanced Composites Inc.

- **Typical uses and applications for C/SiC and SiC/SiC CMCs**

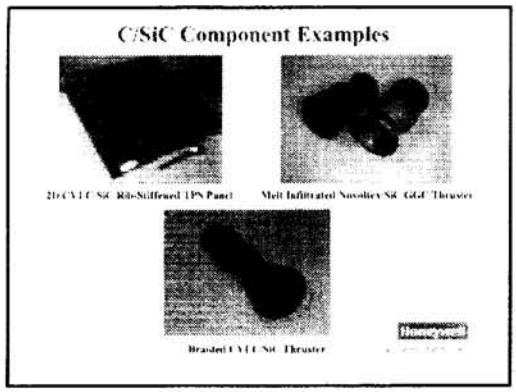

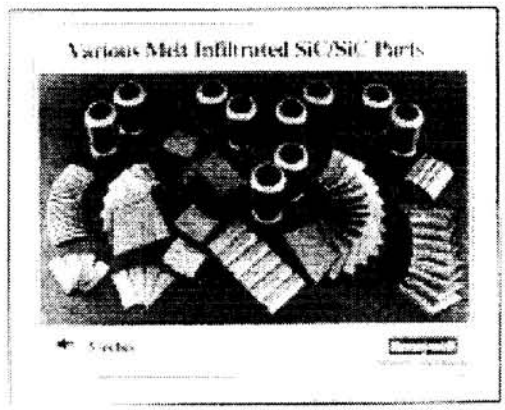

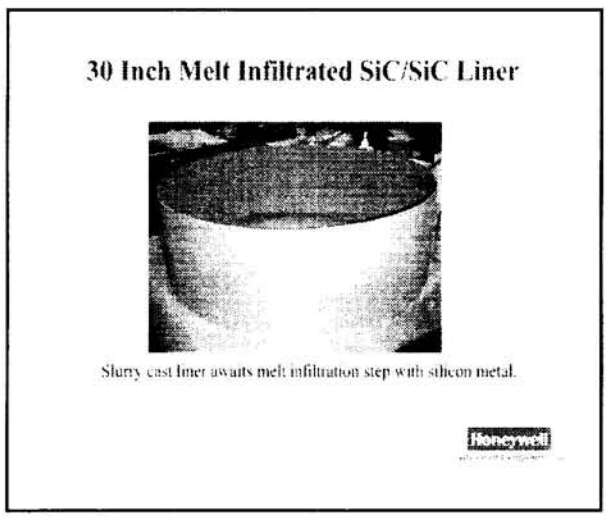

- **Summary**

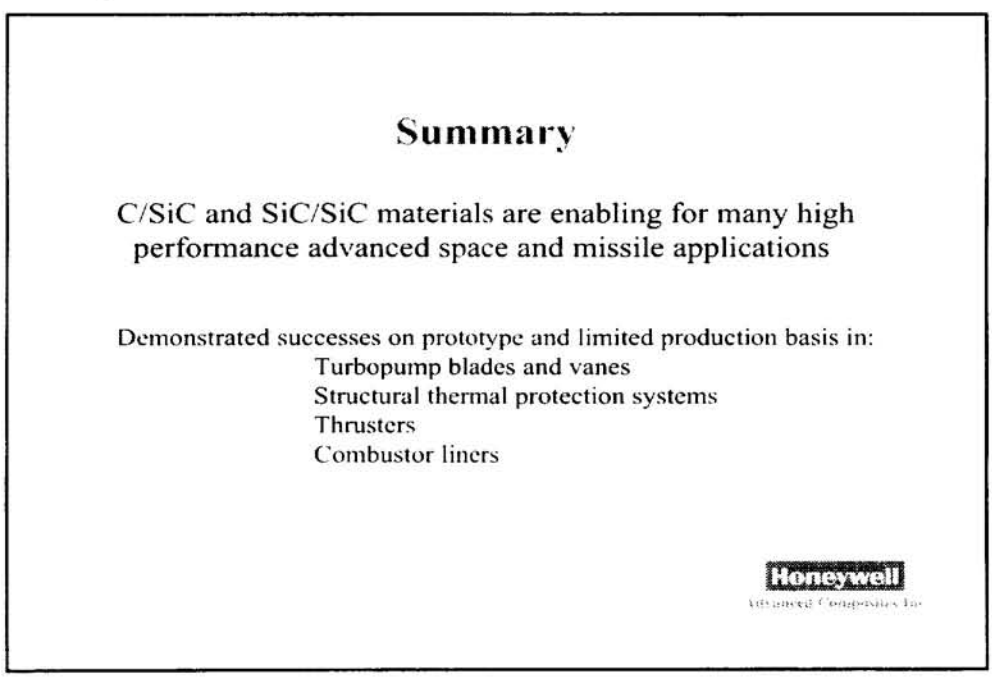

Aluminum Investment Cast Spacecraft and Aerospace Structures

JOHN BOWKETT

Nu-Cast, Inc.
29 Grenier Field Road
Londonderry, NH 03053 USA
Phone: 603-432-1600
Fax: 603-432-0724
E-mail: nci@grolen.com

The mandate for "better, faster, cheaper" has had a profound effect on aerospace projects. Project personnel, budgets, and development time have been compressed. Coupled with this mandate has been the threat to cancel projects that exceed their budgets. Projects perceived to be grandiose or padding their cost estimates are eliminated or not even considered for selection, regardless of their technical or scientific merit. There is no single solution for this situation. To work effectively in this environment requires an end-to-end approach that reduces project engineering, analysis, drafting, checking, manufacturing, testing, and integration. This approach, above all, must include the desire to depart from standard aerospace engineering practices.

Engineers at Goddard Space Flight Center addressed this changing environment with investment casting technology. Previously, casting had been used for electronic enclosures and some secondary structures; it required production rates of 100 units before being considered. Expanding the technology to primary load path spacecraft structures had been perceived to be costly and of marginal benefit. NASA engineers designed and successfully flew a low-risk investment cast spacecraft and then progressed to a larger, complex monolithic spacecraft for Pegasus-class expendable launch vehicles and primary load path payload structures for the Space Shuttle.

Significant and surprising cost savings have been realized end to end on projects employing this technology. The presentation will showcase advanced applications with aluminum investment casting, the evolutionary approach taken, cost savings realized, technical and political complications encountered, lessons learned, and future work.

Vacuum Plasma Spray of Cu-8Cr-4Nb for Advanced Liquid-Fuel Combustion Chambers

Marshall Space Flight Center, AL
Glenn Research Center, OH
Plasma Processes Inc., AL

Frank Zimmerman - MSFC
Sandra Elam - MSFC
David Ellis - GRC
Heather Miller - Boeing/RKDN
Timothy McKechnie - PPI
Robert Hickman - PPI

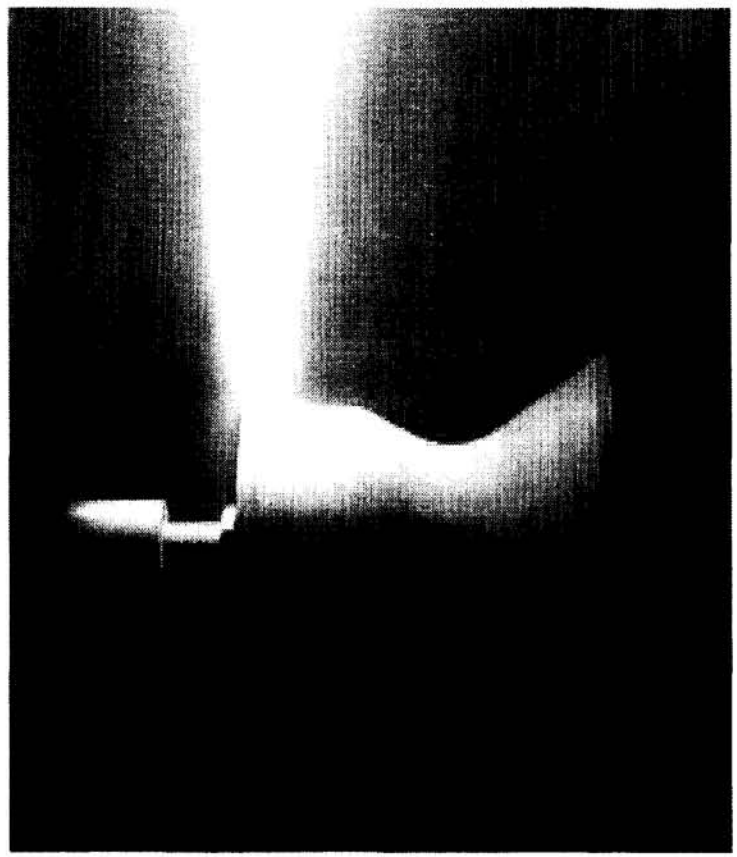

Introduction

- Cu-8Cr-4Nb alloy developed by GRC
  - Intended for use in liquid engine combustion chambers
  - Improved high temp. properties over NARloy-Z
  - Strengthened by fine Cr_2Nb precipitates in Cu matrix

- Vacuum Plasma Spray (VPS) forming advantages
  - Can form near net shape structures vs HIP & extruded
  - Incorporate integral thermal/oxidation barrier, hot wall

Process

- Cu-8Cr-4Nb powder purchased- Crucible Research

Powder	Cr (wt.% / at.%)	Nb (wt.% / at.%)	O (ppm)
MSFC Lot 1	6.45 / 8.00	5.61 / 3.90	1355
MSFC Lot 2	6.79 / 8.33	5.99 / 4.11	805
Special Metals Lot 2	6.35 / 7.79	5.75 / 3.95	468

Process

- Cu-8Cr-4Nb deposited onto mandrels via VPS
- Four post spray processes evaluated
  - As sprayed
  - Four hour vacuum anneal @ 954° C
  - Four hour HIP @ 954° C, 2000 atm
  - Four hour vacuum anneal + one hour HIP
- Measured hardness (Rockwell B) & density

Process

Condition	Hardness (R_B)	Density (g/cm^3)
As-Sprayed	62.6	8.48
Vacuum Anneal 4hrs @ 954°C	72.3	8.60
HIP 4hrs @ 954°C, 1000 atm	69.3	8.73
Vac. Anneal 4hrs @ 954°C + HIP 1hr/954°C, 1000 atm	76.8	8.73

Note: theoretical density = 8.4 g/cm^3

Process

- Tensile test at room temp. & 538° C
- Evaluate effects of oxygen, post processing
- Compare to GRC data for HIP and extruded

Vacuum Plasma Spray of Cu-8Cr-4Nb for Advanced Liquid-Fuel Combustion Chambers

Test Data

Processing		0.2% Yield (MPa)	UTS (MPa)	Reduction In Area (%)
VPS + 4 hr HIP @ 954°C	Avg.	179.4	197.1	26.8
	σ	2.8	1.4	1.7
LeRC - Extruded	Avg.	165.6	183.5	44.2
	σ	1.8	2.5	3.9

Room Temperature Strength for VPS + HIP and Extruded Cu-8Cr-4Nb Material

Test Data

Material	Density (lb_m/ft^3)	Thermal Cond'ty (BTU/in-s-^{0}F) 10^{-3}	Yield Strength @ 1000 ^{0}F (ksi)	Ultimate Strength @ 1000 ^{0}F (ksi)
NARloy-Z	570	4.7	13	17
Cu-8Cr-4Nb (extruded)	543	4.0	17	22
Cu-8Cr-4Nb (VPS formed)	545	4.0	23	27

Vacuum Plasma Spray of Cu-8Cr-4Nb for Advanced Liquid-Fuel Combustion Chambers

Test Data

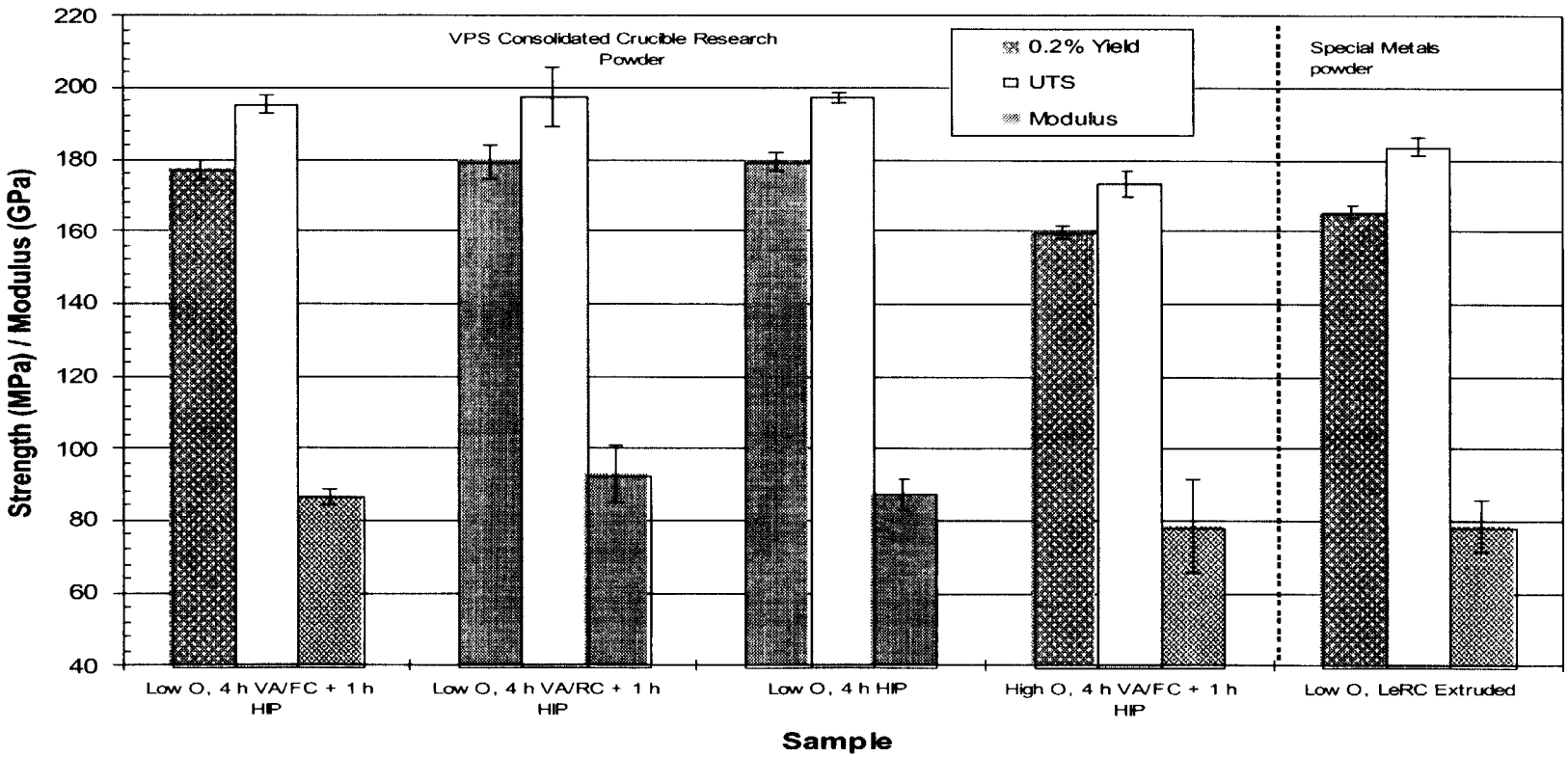

Effect of Processing and Oxygen on Strength and Modulus @ 538° C

Vacuum Plasma Spray of Cu-8Cr-4Nb for Advanced Liquid-Fuel Combustion Chambers

Test Data

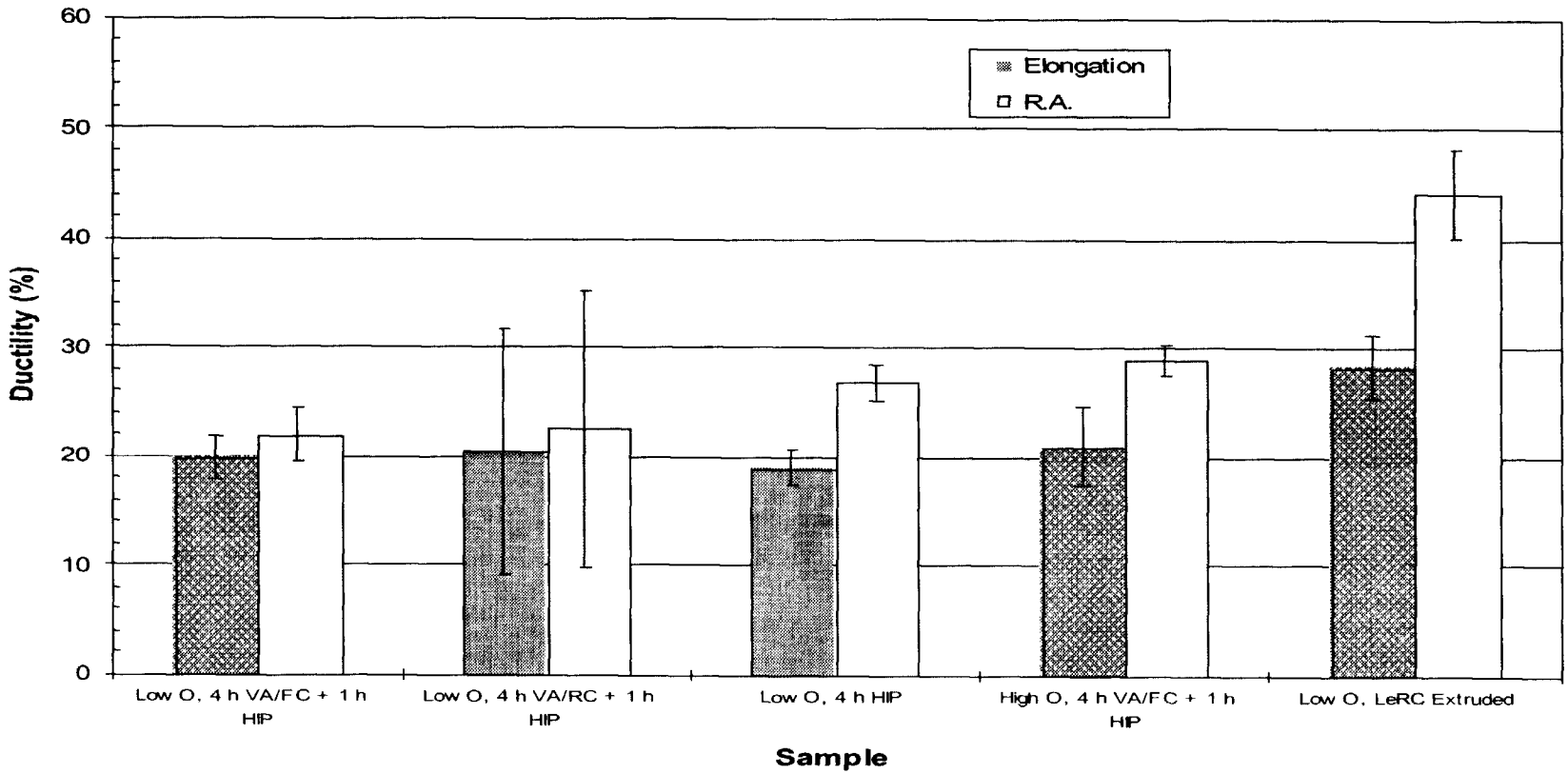

Effect of Processing and Oxygen on Ductility @ 538° C

Vacuum Plasma Spray of Cu-8Cr-4Nb for Advanced Liquid-Fuel Combustion Chambers

Test Data

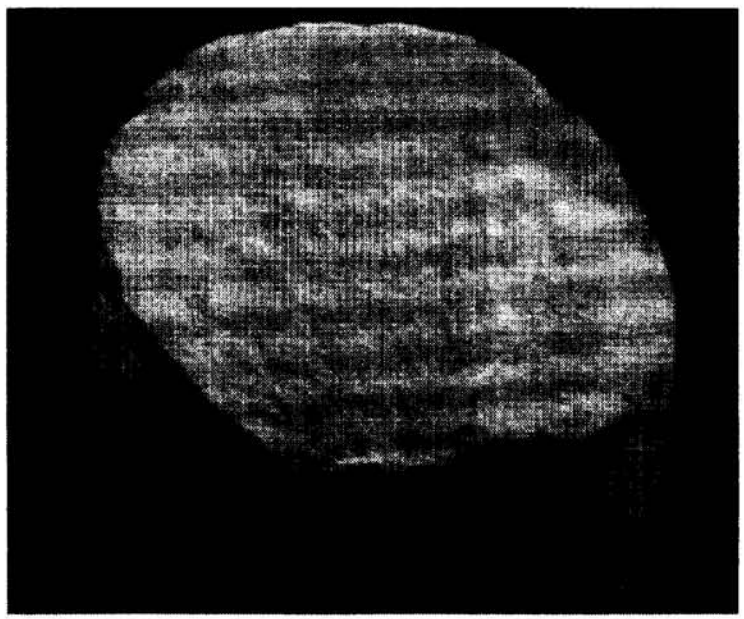

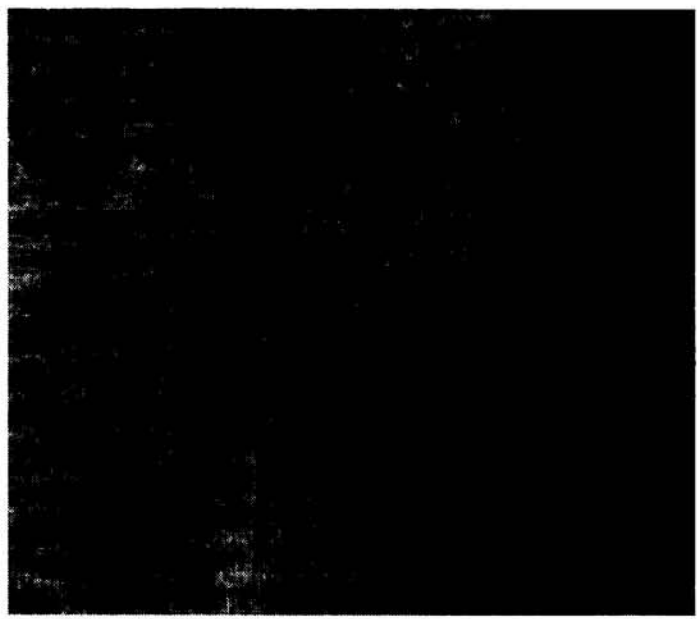

SEM micrograph of a fracture surface from low oxygen VPS formed Cu-8Cr-4Nb tensile specimens.

15x (left) **1000x (right)**

Applications

- Straight-wall calorimeter spool
  - integral thermal/oxidation coating
  - hot fired at GRC last spring
- Liners for Light Weight Thrust Cells
  - supports NRA work for non-metallic structural jackets
  - novel technique for coolant channel close out

Vacuum Plasma Spray of Cu-8Cr-4Nb for Advanced Liquid-Fuel Combustion Chambers

Applications

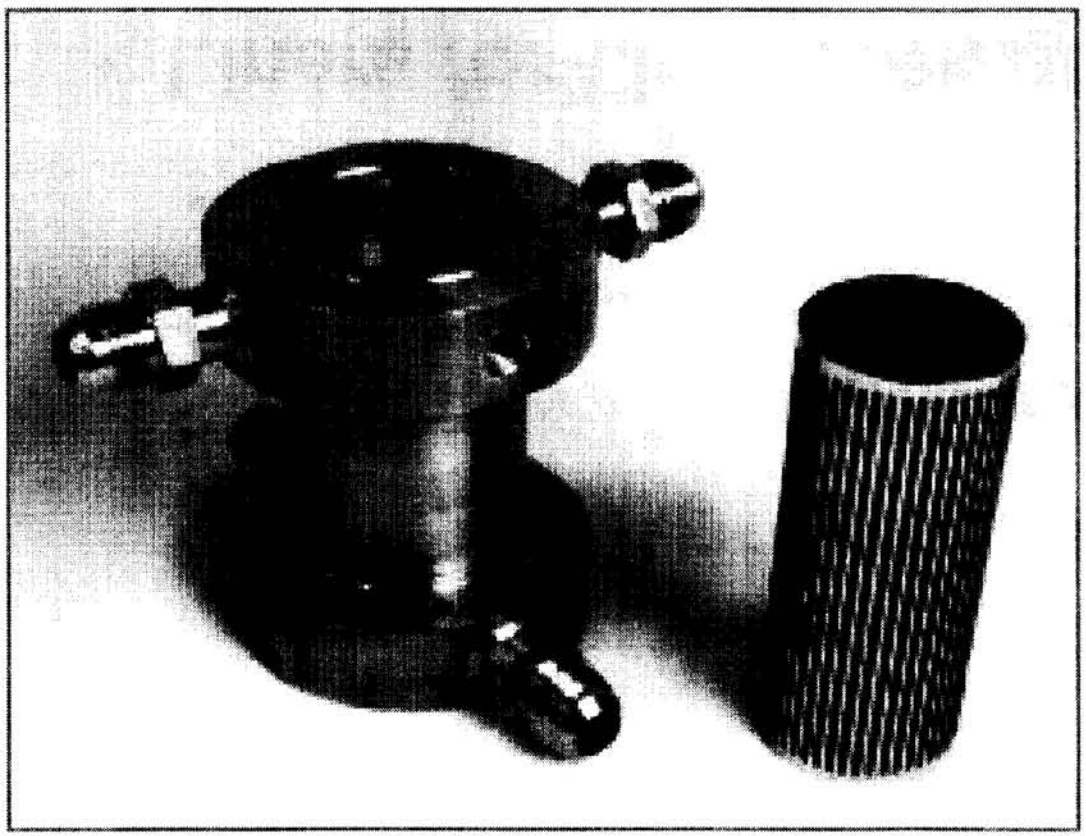

VPS formed liner with integral thermal/oxidation barrier coating on hot wall

Applications

- Hot Fire Testing at GRC
  - Chamber pressure = 750 psia
  - Oxygen/Hydrogen ratio = 7.0
  - 15 cycles and 450 seconds
  - Test article hot wall condition rated excellent
  - First demonstration of VPS coating through multiple hot fire cycles

Applications

- Two Liners for Light Weight Thrust Cell
  - PPI formed hot wall portion with CuCrNb
  - Boeing/RKDN closed out cooling channels at MSFC facility
  - Demonstrated water-leached filler for cooling channels
  - Finished liners provided to contractors for application of light weight jacket

Vacuum Plasma Spray of Cu-8Cr-4Nb for Advanced Liquid-Fuel Combustion Chambers

Applications

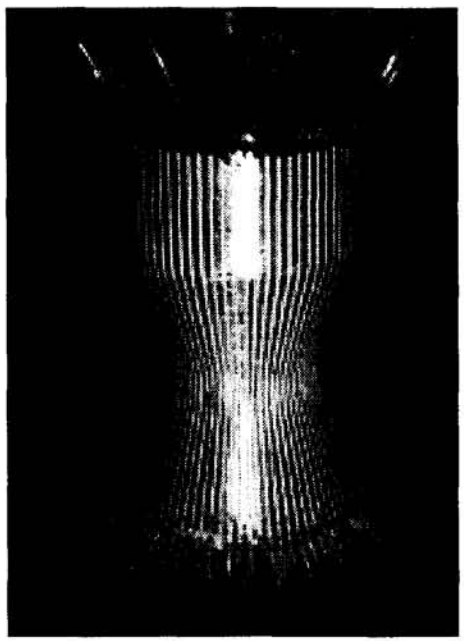

With filler & ceramic string

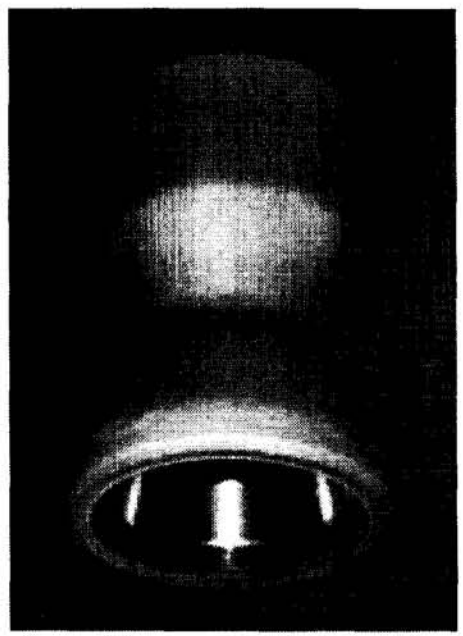

After close out

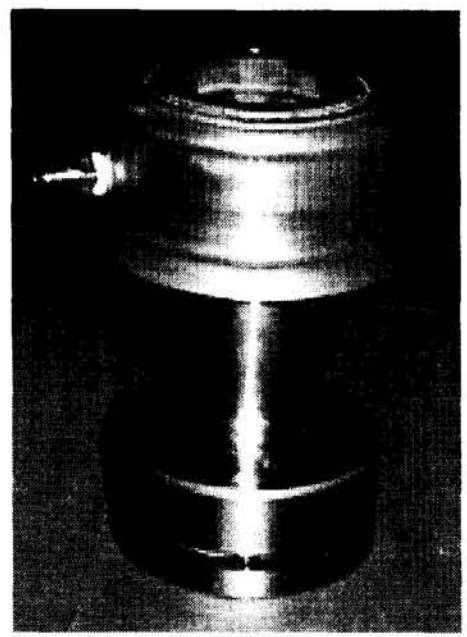

Final machine and leaching

Vacuum Plasma Spray of Cu-8Cr-4Nb for Advanced Liquid-Fuel Combustion Chambers

Applications

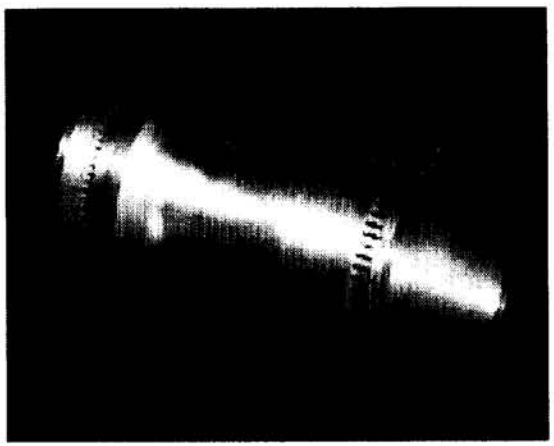

Two liners have been provided to contractors for application of graphite fiber and epoxy structural jackets

Cryogenic flow testing complete on first unit (5 cycles LN_2). Hot fire testing to begin end of this year.

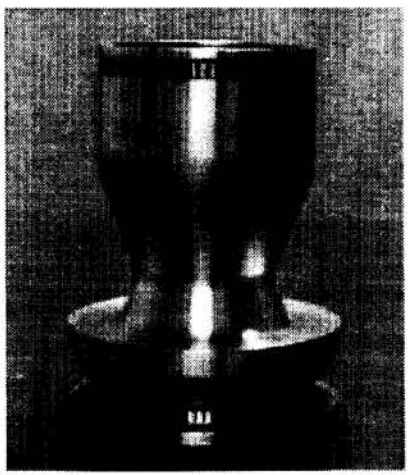

Discussion

- Vacuum anneal increased hardness and density
- Argon quench vs furnace cool showed no effect
- Add'l HIP further increased hardness & density
- HIPing longer that 1hr showed no add'l benefit
- HIPing alone more effective than vacuum anneal

Discussion

- High oxygen reduces strength, may increase ductility

- Vacuum anneal not effective in abating oxygen effect, as seen in NARloy-Z alloy

Conclusions

VPS formed Cu-8Cr-4Nb alloy, with low oxygen, exhibits higher strength at room and elevated temperature than material formed by extrusion.

The VPS formed material exhibits slightly lower ductility than the extruded material.

VPS forming of Cu-8Cr-4Nb can be used to produce near net structures with mechanical properties comparable to current extruded mat'l

Acknowledgments

The authors would like to thank the Center Director's Discretionary Fund and the Advanced Propulsion Development Office at NASA's Marshall Space Flight Center for their support of this effort.

W/SP5/IN/75 E4/3

DYNAMIC OXIDATION OF A PLASMA-SPRAYED Cu-Cr COATING

K. T. Chiang

The Boeing Company
Rocketdyne Propulsion & Power
6633 Canoga Avenue, Canoga Park, CA 91309-7922
(818) 586-1211
kuang-tsan.k.chiang@boeing.com

Abstract

The dynamic oxidation of a plasma-sprayed Cu-30 vol.% Cr coating was investigated in an electric arc-heated wind tunnel. The wind tunnel generated high velocity, fully dissociated air containing atomic oxygen. The metal surface temperature was maintained at 650°C for up to 5 hours (h). The high velocity atomic oxygen enhanced oxidative evaporation of Cr metal resulted in rapid metal weight loss. The high temperature atomic oxygen caused rapid oxide formation on Cu. The scale cracked and spalled severely during cooling to room temperature. The plasma-sprayed Cu-Cr coating provided good oxidation protection for the copper alloy substrate under a dynamic environment. The oxidation mechanism involved four steps. First, oxidative evaporation of elemental Cr resulted in a Cu-enriched surface with increased nucleation sites. Second, rapid whisker formation resulted in a mushroom-like Cu-oxide scale morphology. Scale formation involved a combination of surface diffusion, short circuit diffusion, lattice diffusion and evaporation. Third, inward migration of oxygen atom formed mixed oxides of CuO and $CuCrO_2$. Fourth, formation of a continuous Cr_2O_3 layer beneath the external Cu, Cr mixed oxides. The scale morphology and oxidation mechanisms will be compared with those of static laboratory furnace oxidation.

Introduction

Copper-based alloys and composites are candidate materials for high heat flux structural applications in hypersonic vehicles because of their combined properties of high-thermal conductivity and high-temperature strength (Refs. 1 and 2). A major limitation to using copper-based materials is their rapid oxidation at elevated temperatures. Protective coatings that shield these materials from oxidation must be employed to enable their use at temperatures up to 650°C.

One approach to a protective coating for copper-based alloys uses chromia scales, like those formed on M-Cr alloys (where M is Fe, Ni, or Co), which impart oxidation resistance when formed on the alloy. One practical requirement of such coatings is that the chromium concentration at the surface must be high enough to form a continuous Cr_2O_3 scale, which must be stable in the service environment. Reference 3 showed that Cu-30 vol.% Cr coatings produced by vacuum plasma spray (VPS) form a protective scale on Cu-Nb alloy in static air at high temperatures. However, Ref. 4 showed that oxidative vaporization of Cr_2O_3 in oxygen is enhanced by about 10 at 550°C by the presence of 2.5% atomic oxygen. Therefore, a concern is that the plasma-sprayed Cu-30 vol.% Cr coating will not protect copper-based alloys employed in hypersonic vehicle applications where atomic oxygen may be present.

The objective of this study was to examine the performance of plasma-sprayed Cu-30 vol.% Cr coating under dynamic oxidation conditions containing atomic oxygen. The paper presents results from dynamic oxidation tests of Cu-15 vol.% Nb substrate with a VPS Cu-30 vol.% Cr coating. The tests were conducted at 650°C in an electric arc-heated wind tunnel. Data for weight change during static and dynamic oxidation and metallurgical analysis results are presented for coated and uncoated specimens.

Experimental

Specimens were 2.5-cm-diameter discs cut from a 0.76-mm-thick Cu-15 vol.% Nb sheet. The specimens were coated on all surfaces with Cu-30 vol.% Cr coating. Details of the coating deposition process were described elsewhere (Ref. 3).

Coated specimens were tested under dynamic oxidation conditions (Mach 4.2, 1.5 torr pressure, and 2.9 MJ/kg enthalpy) at 650°C for times to 5 h in the Hypersonic Materials Environmental Test System (HYMETS) at the NASA Langley Research Center (Ref. 5). The HYMETS is a 100-kW constrictor-arc-heated wind tunnel that uses air plus nitrogen and oxygen in ratios equivalent to air to produce the test environment. Specimens under test are held on a pneumatic strut so that gas flow is normal to the surface. The temperature of a specimen is monitored during exposure by a thermocouple attached to its back surface or by a radiation pyrometer focused on its front surface. The test conditions attainable in the HYMETS are not equivalent to the environment associated with high heat flux structural applications of hypersonic vehicles. However, the environment does contain high-speed flowing gas with atomic and molecular oxygen, which is of critical concern to using copper-based materials in hypersonic vehicle applications.

Tests consisted of exposure of specimens for half-hour periods at 650°C for an accumulated exposure of up to 5 h. The specimen temperature was maintained at 650°C by adjusting the power input to the HYMETS. Specimens were periodically removed from the test facility for weighing and examination.

The morphology and chemical composition of the surface of the coated specimens were characterized, before and after oxidation exposure, by scanning electron microscopy (SEM) with energy dispersive x-ray analysis (EDXA), and x-ray diffraction (XRD). Selected specimens were cross-sectioned and examined by SEM with EDXA.

Results and Discussion

The weight change history of Cu-30 vol.% Cr coated Cu-15 vol.% Nb specimens under dynamic oxidation conditions at 650°C in the HYMETS facility is shown in Figure 1. Data are included for coated specimens and

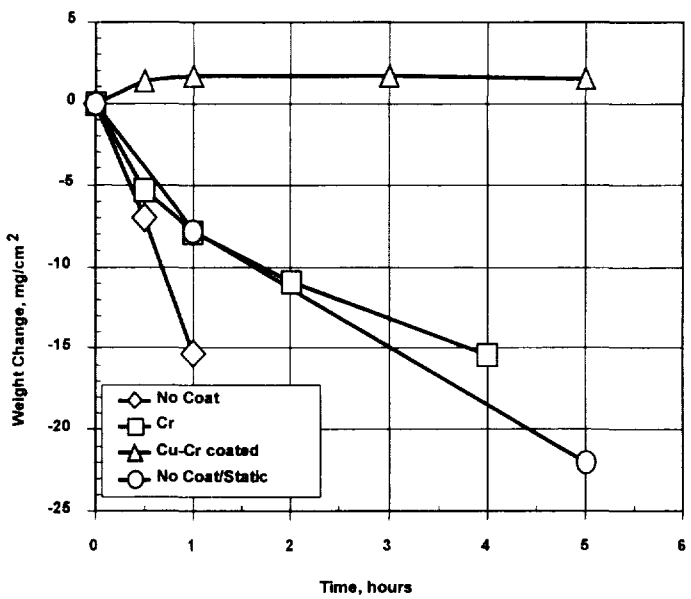

Figure 1. Oxidation weight change history of Cu-15 vol.% Nb with Cu-30 vol.% Cr coating under dynamic conditions at 650°C

uncoated Cu-Nb specimens oxidized under static and dynamic oxidation conditions. The test data for a pure chromium specimen under dynamic oxidation condition are also included because chromium is a major constituent of the Cu-Cr coating. The chromium samples experienced a slight increase in weight with exposure to static oxidation in air at 650°C, but showed a severe weight loss under dynamic oxidation conditions. XRD data show Cr and Cr_2O_3 as the only phases present on the surface after exposure to either static or dynamic oxidation. These results confirm that the conditions present in HYMETS are sufficient to accelerate the oxidative evaporation of chromium or Cr_2O_3, as described by Fryburg et al. (Ref. 4). The plasma-sprayed Cu-30 vol.% Cr coating provided good oxidation protection to the Cu-Nb substrate during exposure to dynamic oxidation condition. The overall weight change over the 5-h test was less than 2 mg/cm^2. The specimen showed a rapid weight increase during the initial 1 h of dynamic oxidation exposure, followed by a slow rate of weight decrease. Uncoated Cu-Nb alloy specimens experienced a severe loss of weight with oxidation exposure under both static and dynamic oxidation conditions. Under both conditions, the uncoated specimens form heavy oxide layers, which are not protective. Upon cool-down, the oxides on the surface spall from the specimen exposing bare alloy.

Scanning electron micrographs of the specimen surface of as-coated, as well as after static and dynamic oxidation exposures, are compared in Figure 2. The as-coated surface exhibits a "splat" structure typical of the VPS process (Figure 2a). Semi-quantitative EDXA showed that the coating composition was Cu-26 wt.% Cr, which was within 1% of the nominal composition. After static oxidation in air at 650°C, the coating surface formed fine-grained crystalline oxides (Figure 2b). EDX analysis showed the surface contained elements of Cu, Cr, and oxygen indicating the formation of Cu-oxide and chromium oxide. The oxide morphologies of the coating under dynamic conditions were distinct from those of static oxidation. Figure 2c shows the coating surface morphology after 3 h of

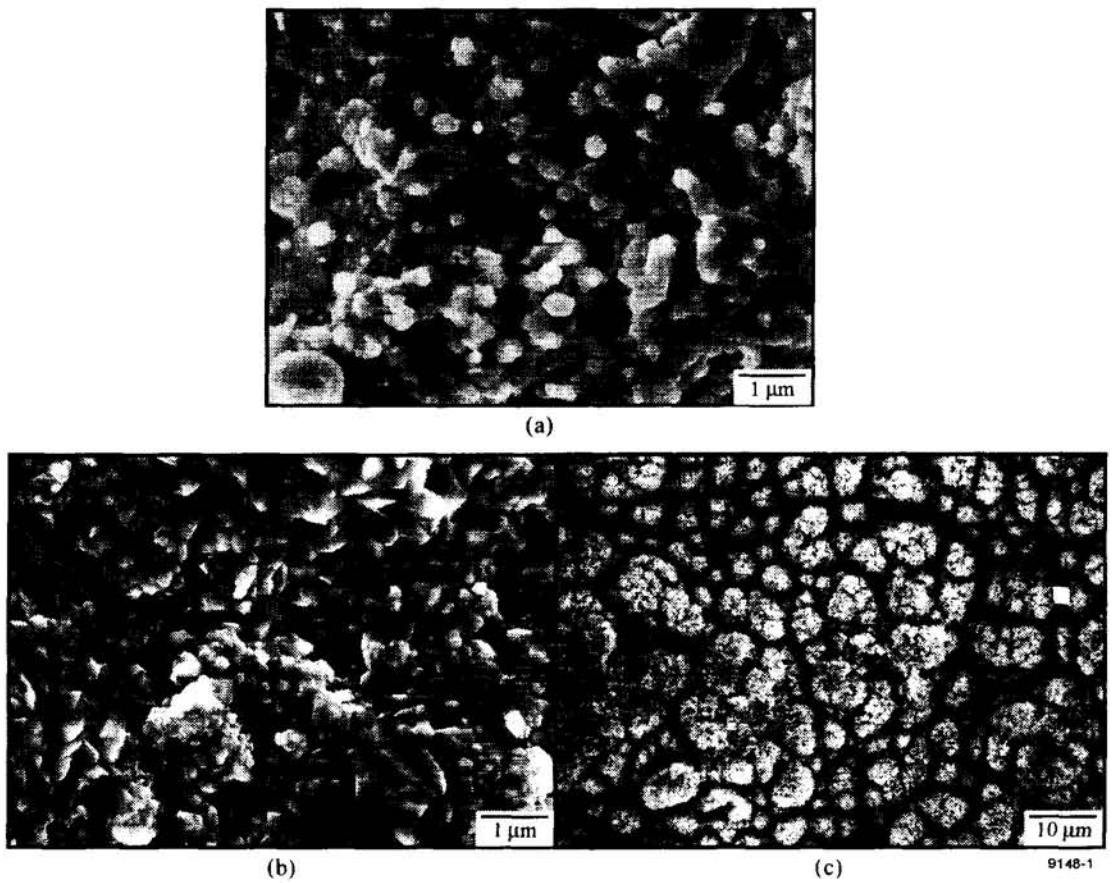

Figure 2. Scanning electron micrographs of plasma-sprayed Cu-30 vol.% Cr coating surfaces. (a). as-coated, (b) after static oxidation in air for 22 h, (c) after dynamic oxidation for 3 h.

dynamic oxidation. The surface is covered by porous, spherical oxide deposits, which are typical of oxides formed by Ni and Cr containing alloys under dynamic oxidation conditions (Ref. 6). The porous mushroom-like structure was formed because of rapid evaporation of chromium element through interaction of chromium with atomic oxygen, and rapid formation of whiskers of copper-oxides through surface diffusion, lattice diffusion, and evaporation. The EDXA of the coating surface showed strong peaks of Cu and oxygen indicating that the outer surface layer was covered predominantly by Cu-oxides.

The XRD data in Table 1 demonstrate variance in the phase composition of the surface region of the Cu-30 vol.% Cr coating with oxidation exposure time at 650°C. The coating in the as-coated condition consists of only face-centered-cubic (fcc) Cu and body-centered-cubic (bcc) Cr with no evidence of compound or solution. When exposed to static or dynamic oxidation conditions, the coating oxidizes to form mixed oxides of Cu and Cr. The surface of coated specimens tested under dynamic oxidation conditions at 650°C consists of Cu, Cr, CuO, Cr_2O_3, and $CuCrO_2$. The primary oxide phase identified for coated specimens after exposure to dynamic oxidation condition is CuO with lesser phases of Cr_2O_3, and $CuCrO_2$. The ratio of metallic Cu and Cr is greater for the exposed specimens than for the as-coated specimen. The amount of Cr oxides detected by XRD in the surface region decreases with time of exposure to dynamic oxidation at 650°C.

Table 1. XRD Results for Cu-30 vol.% Cr Coating

Exposure Condition*	**Cu**	**Cr**	**CuO**	**Cr_2O_3**	**$CuCrO_2$**
As coated	vs	s	–	–	–
1 h at 650°C	w	w	s	m	w
5 h at 650°C	w	w	s	vw	vw

* Specimens exposed to dynamic oxidation in arc jet (HYMETS facility at NASA Langley Research Center)
XRD Signals : vs – very strong; s – strong; m – medium; w- weak; vw – very weak

Cross-section views of Cu-Cr coated Cu-Nb substrate, in the as-deposition condition and after 3 h of dynamic oxidation, are shown in Figures 3 (a) and (b). The coating consists of heterogeneous of Cu and Cr phases. After dynamic oxidation, a multilayered-oxide structure was formed. The oxides consist of an approximately 15-μm-thick, mushroom-like external oxide layer. The EDX analysis [Figure 3 (c)] shows that the oxide contained only elements of Cu and oxygen indicating the oxide was CuO. Underneath the porous Cu-oxide, a region of solid CuO approximately 20 μm thick was observed. Underneath the external oxides, a mixed Cu-Cr oxide layer was clearly seen. The thickness of the mixed oxide layer was not uniform ranging from 1 to 25 μm. Beneath the mixed oxide layer and near the unreacted coating/oxide interface, a layer enriched in Cr and oxygen was observed [Figure 3 (d)], indicating formation of Cr_2O_3 scale.

The results presented here with the results from Refs. 3 and 4 suggest the following mechanism of protection by the Cu-30 vol.% Cr coating. When the plasma-sprayed Cu-Cr coated Cu-Nb specimen is exposed to a dynamic oxidation condition, the oxidation mechanism involved four steps. First, oxidative evaporation of elemental Cr resulted in a Cu-enriched surface with increased nucleation sites. Second, rapid evaporation and whisker formation resulted in a mushroom-like Cu-oxide scale morphology. Scale formation involved a combination of surface diffusion, short circuit diffusion, lattice diffusion, and evaporation. Third, inward migration of oxygen atom formed a mixed oxide of CuO and $CuCrO_2$. Fourth, beneath the external Cu, Cr mixed oxides, the oxygen partial pressure was reduced. Because the Cr particles in the plasma-sprayed Cu-Cr coating were finely dispersed (Ref. 3), the flux of Cr was sufficient to form a continuous Cr_2O_3 scale under the external Cu-oxides and Cu, Cr mixed oxides. As the Cr_2O_3 scale developed, it acts as a barrier for outward diffusion of Cu ions and inward penetration of oxygen

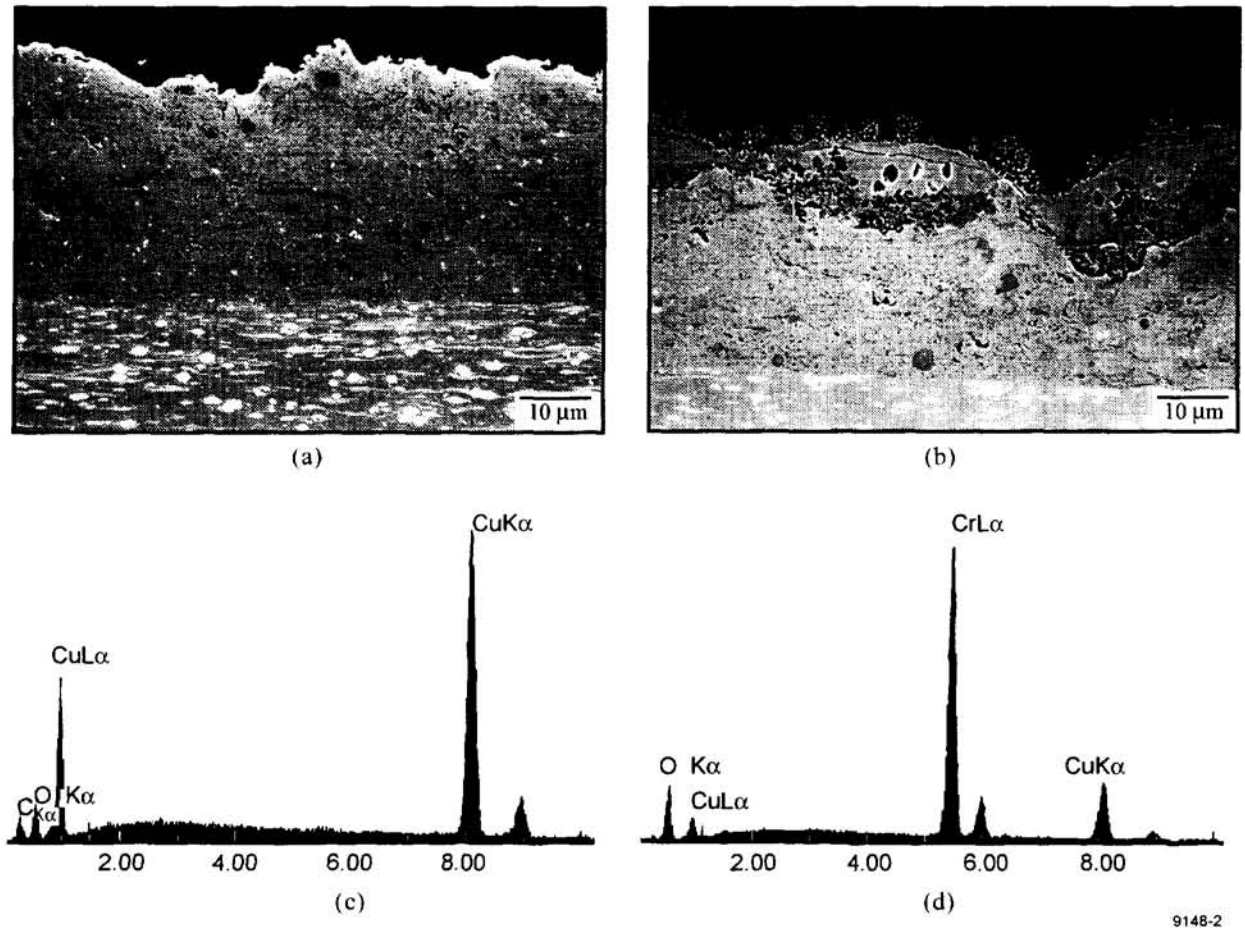

Figure 3. Scanning electron micrographs of Cu-Cr coated Cu-Nb alloys. (a) as-coated, (b) after 3-h dynamic exposure, (c) EDX of external oxides, and (d) EDX of oxide/coating interface.

ions. The Cr_2O_3 was shielded from atomic oxygen attack by the external Cu-oxides, and mixed Cu, Cr oxides. With the coating, the Cu-Nb substrate was protected against the degradation caused by atomic oxygen-containing hot gas.

Summary and Conclusion

Cu-Nb specimens coated with plasma-sprayed Cu-30 vol.% Cr coating were tested under dynamic oxidation conditions at 650°C for up to 5 h. Uncoated specimens were tested for comparison. The coating protects the alloy under dynamic oxidation conditions, with specimens gaining less than 2 mg/cm^2 over a 5-h exposure period. Uncoated specimens tested under static and dynamic conditions experienced severe weight loss because of spalling of the oxides formed at the surface.

The examination of coated specimens using SEM, EDXA, and XRD showed that Cu and Cr exist in the as-coated specimen as a heterogeneous mixture. When oxidized, the coating is transformed to a mixed oxide containing the phases CuO, $CuCrO_2$, and Cr_2O_3. A proposed mechanism for protecting the alloy is that a continuous layer of Cr_2O_3 forms underneath the external Cu-oxides and $CuCrO_2$. The Cr_2O_3 acts as a barrier for outward diffusion of Cu ions and inward penetration of oxygen ions, while the external CuO, Cu-Cr mixed oxides shield the Cr_2O_3 from the hostile atomic oxygen environment.

Acknowledgements

This work was supported by US Air Force Contract No. F33657-91-C-2012. Contributions from R. K. Clark and T. A. Wallace of NASA Langley Research Center in directing the dynamic oxidation tests and analyses are gratefully acknowledged.

References

1. Tenney, D. R.; Kisagor, W. B.; Dixon, S. C., Materials and Structures for Hypersonic Vehicles, in *The 1988 ICAS Proceedings*, American Institute of Aeronautics and Astronautics, Inc. Washington, DC, vol. 1, 1988, pp. 398-415.

2. Ronald, T. M. F., NASP Launches New Materials, *Advanced Materials and Processes*, vol. 144, September 1993, pp. 24-27.

3. Chiang, K. T., Krotz, P. D., Yuen, J. L., Blanching Resistant Cu-Cr Coating by Vacuum Plasma Spray. *Surface and Coatings Technology*, vol. 76-77, 1995, pp. 14-19.

4. Fryburg, G. C., Kohl, F. J., and Stearns, C. A., Enhanced Oxidation Vaporization of Cr_2O_3 and Chromium by Oxygen Atoms. *J. Electrochemical Society: Solid-State Science and Technology*, vol. 121, no. 7, July 1974, pp. 952-959.

5. Schaefer, J. W., Tong, H., Clark, K. J., Suchsland, K. E., and Neuner, G. J., Analytic and Experimental Evaluation of Flowing Air Test Conditions for Selected Metallics in a Shuttle TPS Applications, NASA CR-2531, 1975.

6. Tenney, D. R., Young, C. T., and Herring, H. W., Oxidation Behavior of TD-NiCr in a Dynamic Oxidation High Temperature Environment. *Metallurgical Transactions*, vol. 5, May 1974, pp. 1001-1023.

4th Conference on Aerospace Materials, Processes, and Environmental Technology

Manufacturing Challenges Implementing Material Changes for the Super Light Weight External Tank

A Welding Process Perspective

Kirby Lawless and Chip Jones

Super Lightweight External Tank

Al-Li Weight Savings

1791 Oxygen Tank

[illegible]

3283 Hydrogen Tank

8003 Pounds Total

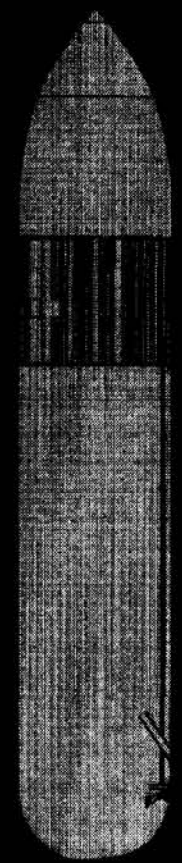

External Tank Configuration

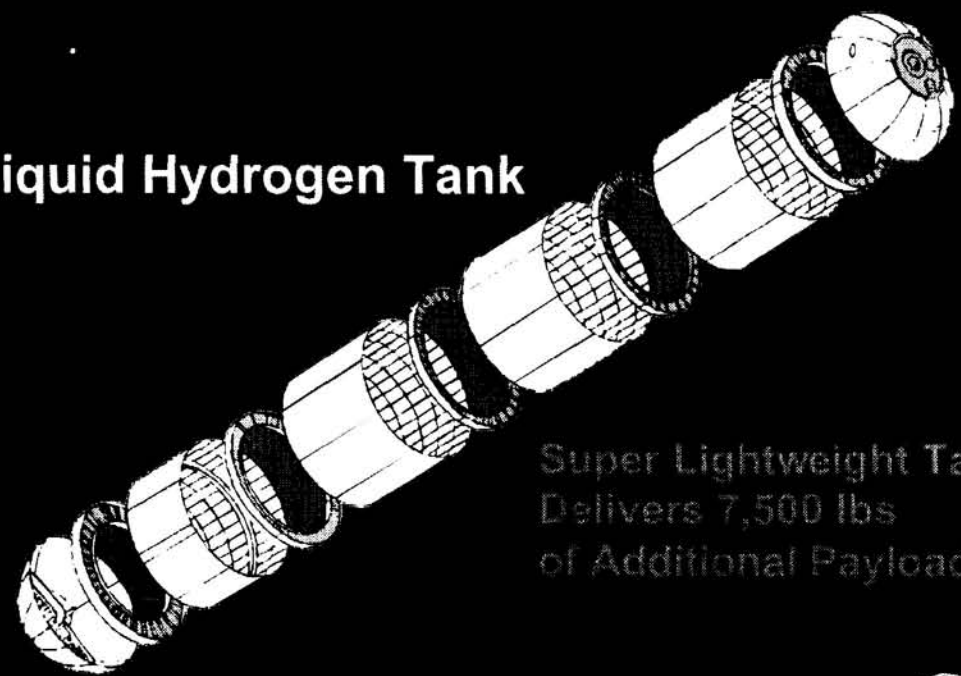

Liquid Hydrogen Tank

- Substitute Al 2195 for Al 2219
- Redesign to Orthogrid Waffle
- Optimize TPS Application
- Weight Savings - 4,200 lbs

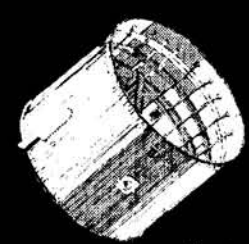

Intertank

- Substitute Al 2090 for Al 2024 and Al 7075
- Machine TPS After Application
- Weight Savings - 750 lbs

Super Lightweight Tank
Delivers 7,500 lbs
of Additional Payload

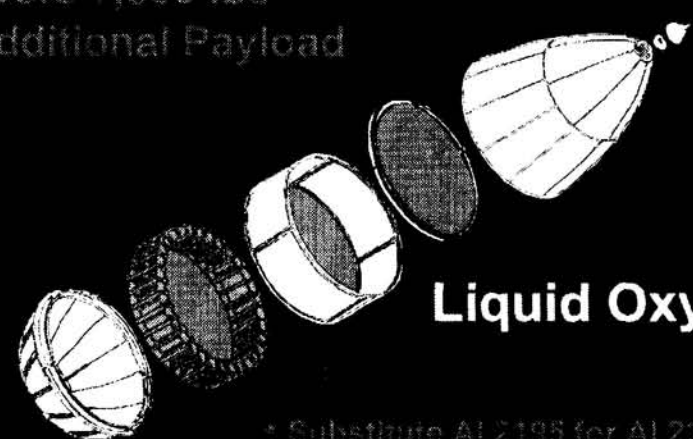

Liquid Oxygen Tank

- Substitute Al 2195 for Al 2219
- Resize Panel Thickness
- Optimize TPS Application
- Weight Savings - 1,620 lbs

= Al Li 2090, 2195

= Other Redesigned Parts

= No Change

Super Lightweight Tank

- One-Half Mile of Weld Joints per Tank
  - Thickness ranges from 0.140" to 0.991"
  - Plate,Extrusion, Forging Product Forms
- Initial Automated 3-Pass Weld Process
  - Four basic geometries:
    - Dome Gores, Ojives
    - Longitudinal
    - Circumferential
    - Circular Caps and Fittings
  - Repair Welds Manual GTA Process
  - Inspected with Visual, Radiography, Penetrant

Weld Purging Equipment

- Inert gas purge required on both sides of weld joint for 2195 alloy
  - Existing tooling retrofitted
  - Narrow tooling gaps provided major challenges
  - Circumferential weld tools required very complex devices
- Mixture of Helium and Argon purge gas required on root side shield
- Pre-weld test developed for gas coverage adequacy

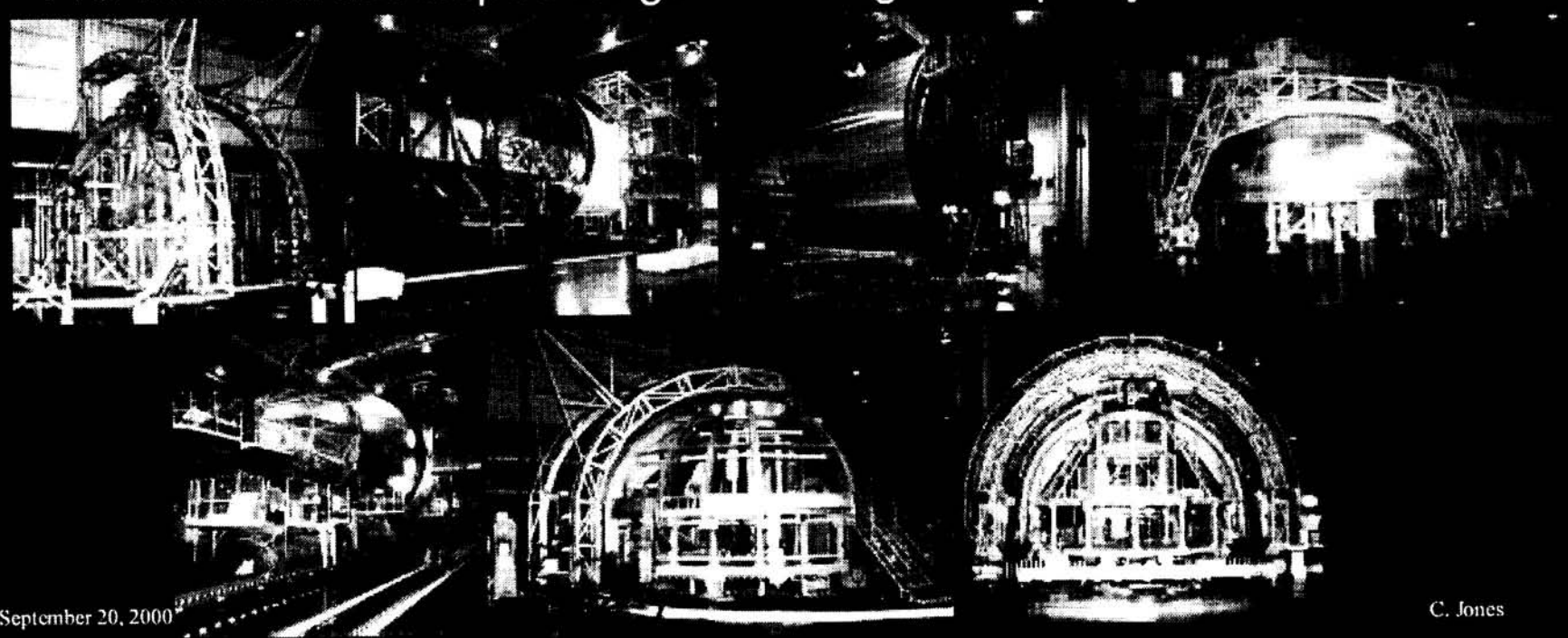

Selection of Weld Filler Wire Alloy

- Baseline 2319 Aluminum Filler until repair cracking discovered
- Survey/Testing conducted of Commercial Alloys
- 4043 Selected
  - Adequate Weld Strengths
  - Liquation Cracking Backfill/Healing Properties
  - Consistent Properties at Cryo Temperatures after significant cold work
- New NASA/LMC/McCook alloy B218 with higher ductility nearing maturity for implementation

Initial Weld Microstructure

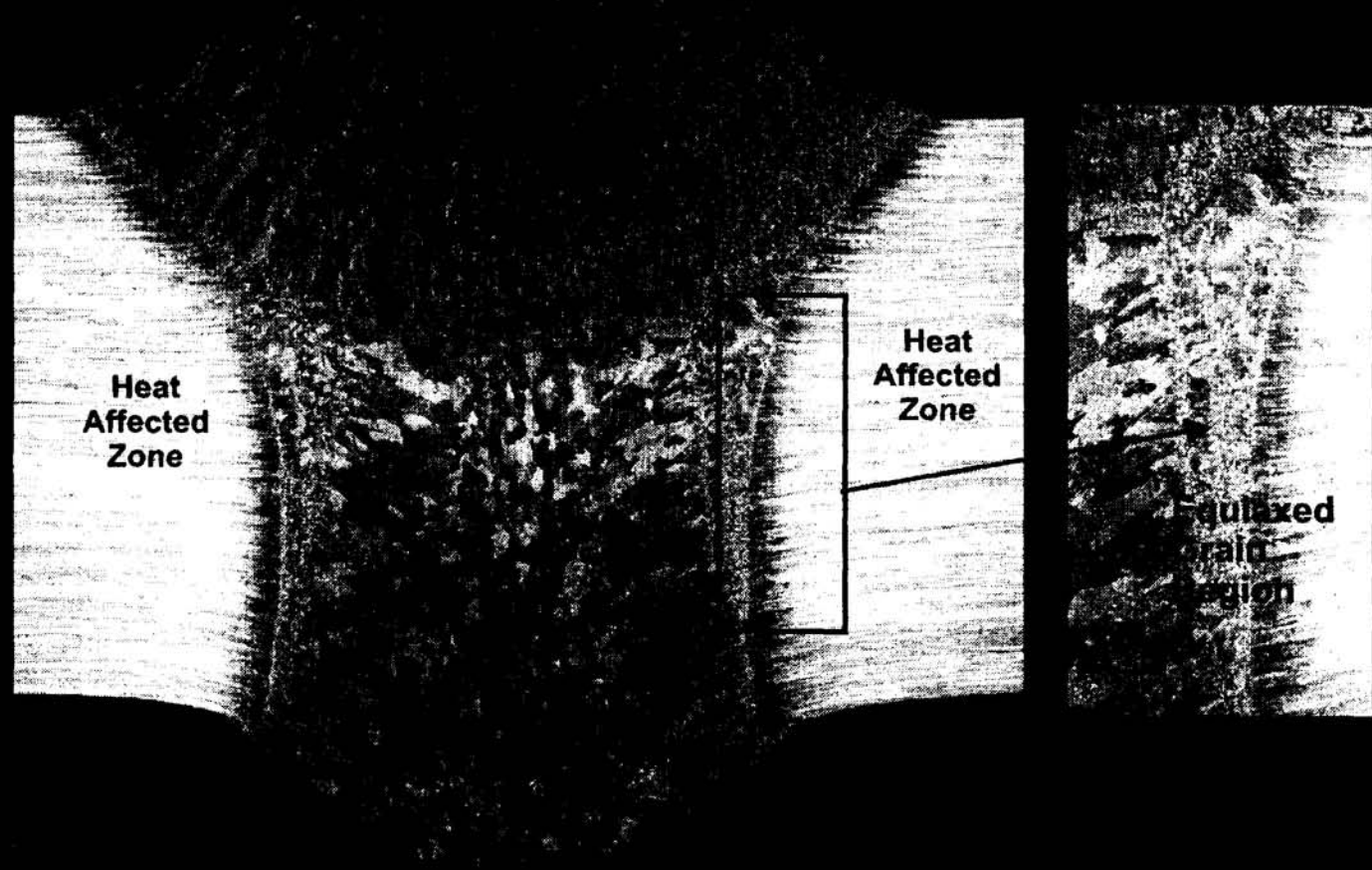

Repair Weld Microstructure

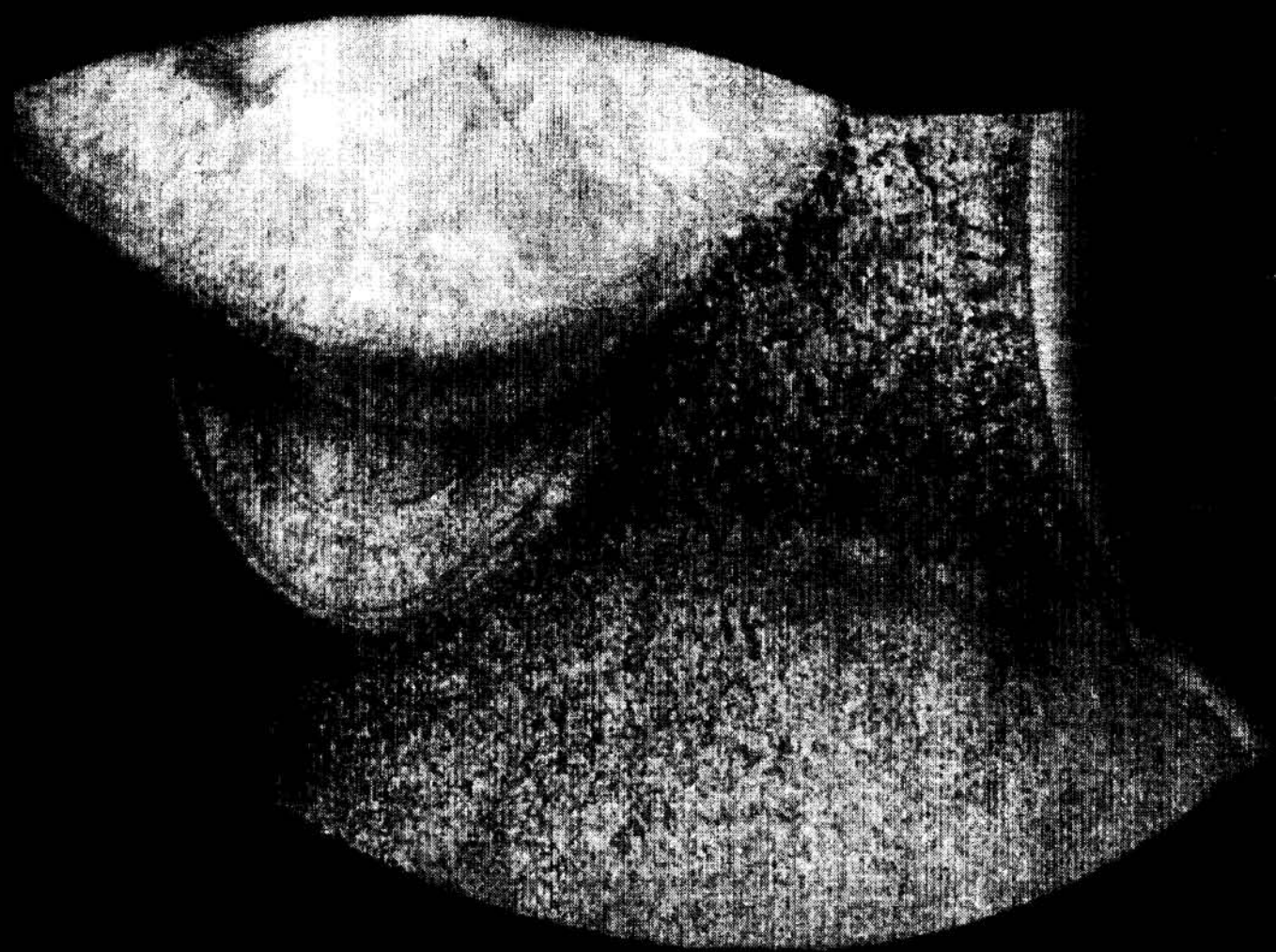

Fault Tree Approach to Resolution

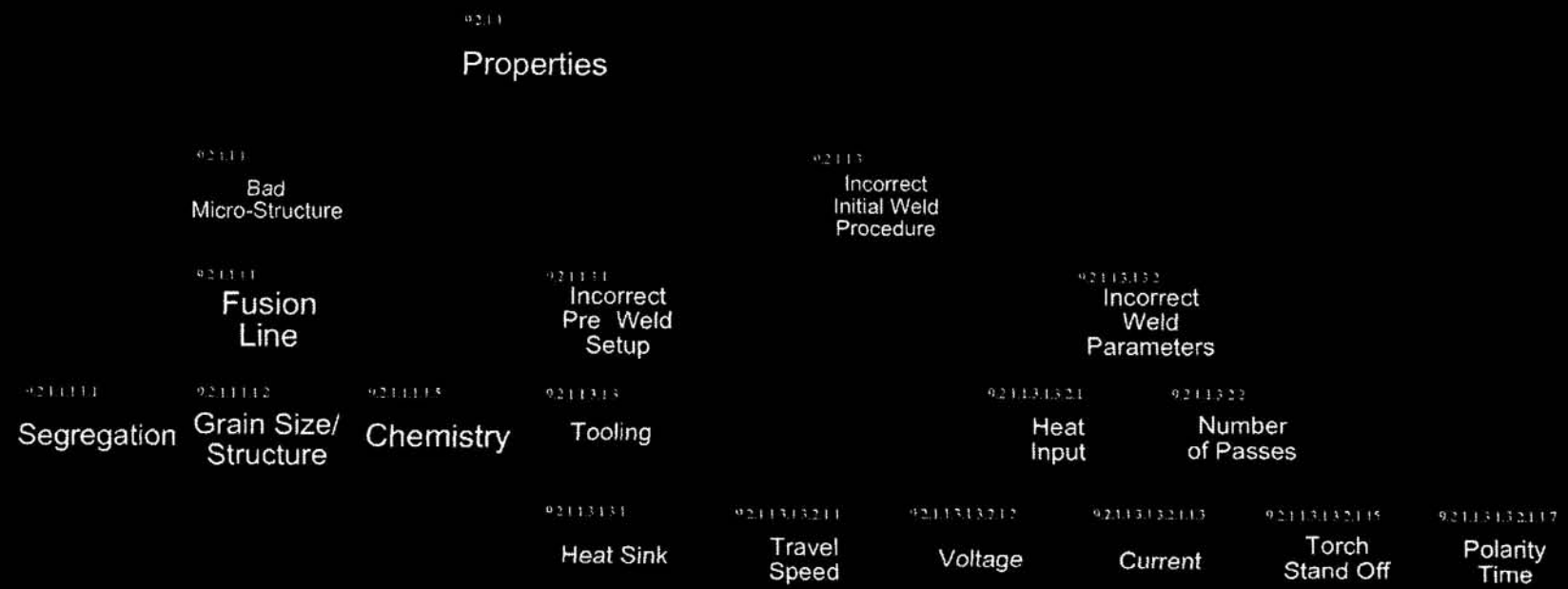

Fault Tree Approach to Resolution

Wide Panel Tensile Testing

- Small Structural Article developed to reveal stress distribution around repairs
- Instrumented with strain gauges and photoelastic material
- Results indicate residual stresses too high in repair for adequate load redistribution
- Some Wide Panel Tensile Testing data is now required for all 2195 weld repair development

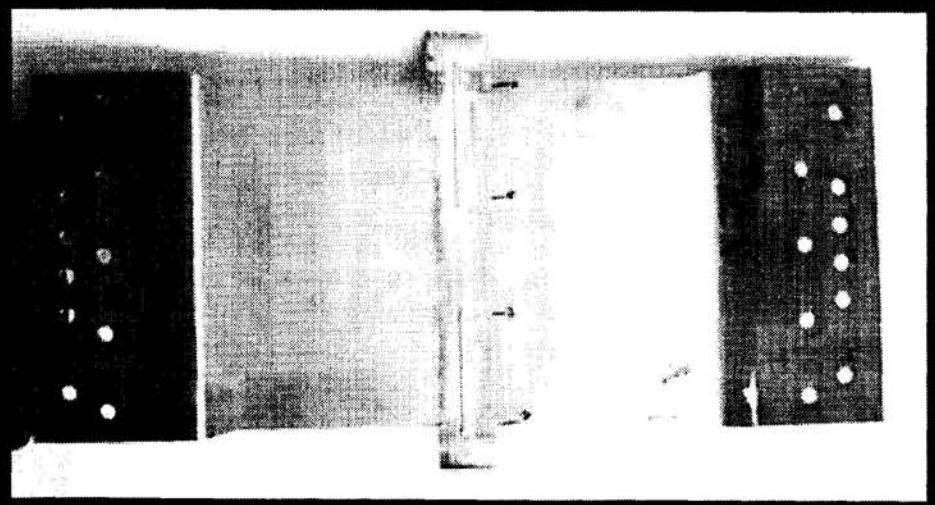

Wide Panel Tensile Specimen

Planishing

- Planishing Required for all 2195 weld repairs
- Relieves Tensile residual stresses
- Drives Compressive stresses into repair
- Allows for stress redistribution around repair

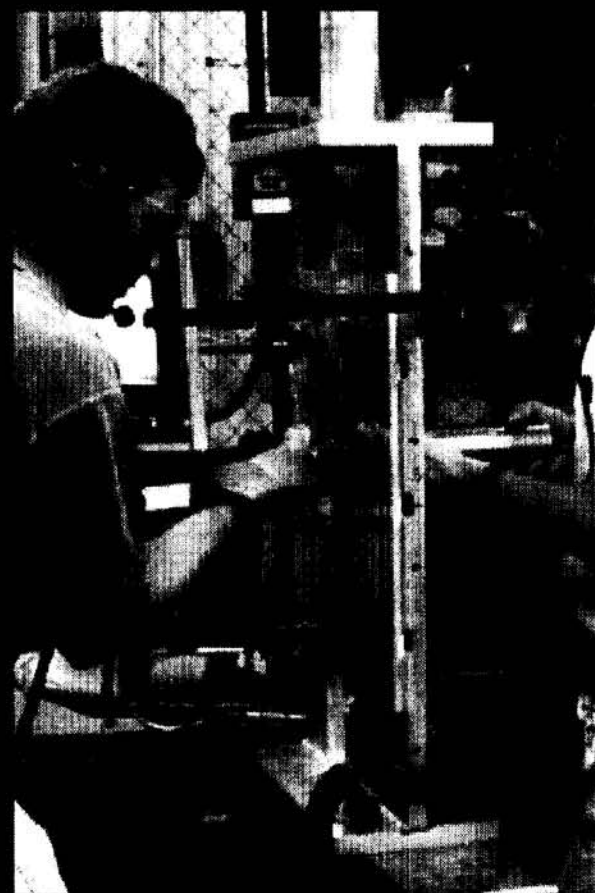

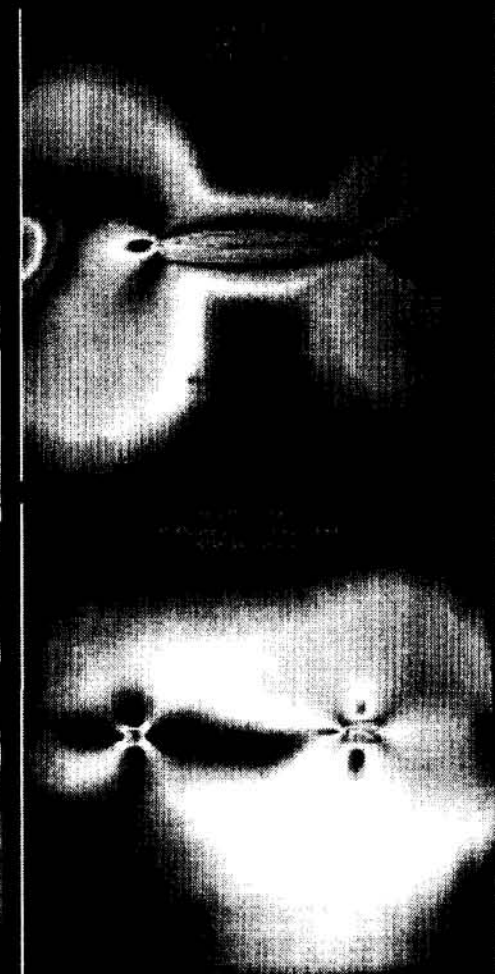

New Metrics Developed for Planishing

- Planishing originally used on ET for distortion removal
- No metric existed other than removal of distortion
- Transverse Shrinkage Reduction Became new metric
- Adequate Strengths developed with 70% to 110% recovery

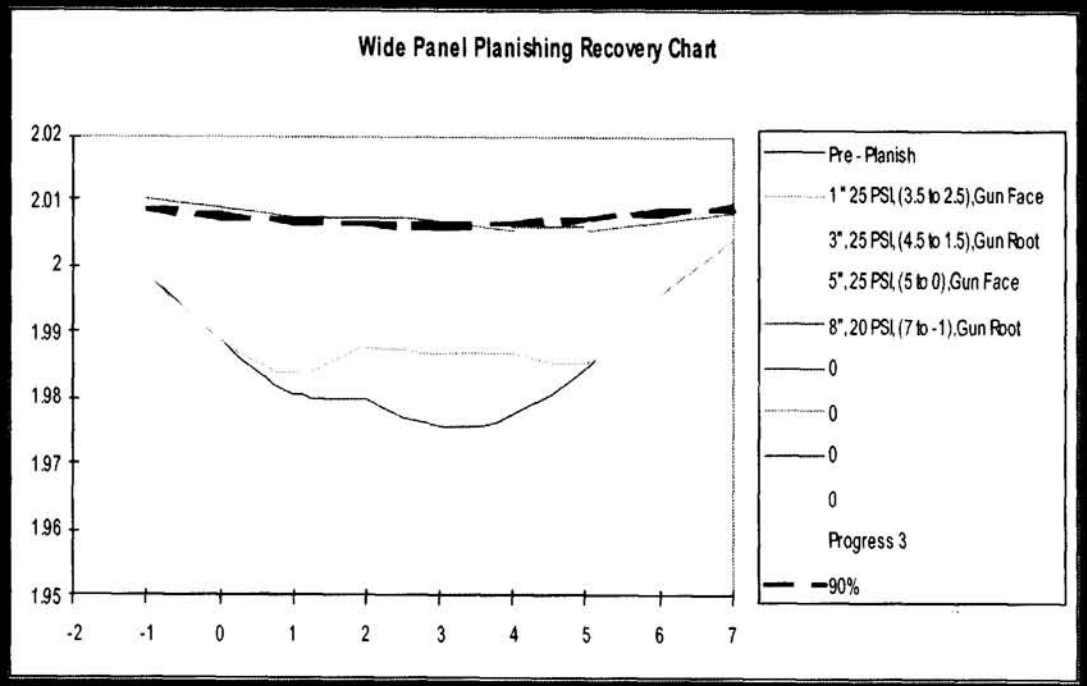

Manual Welder Training

- Smaller Grinds
- "Fast Hand" Technique
- Continuous wire feed
- Special Start/Stop Technique

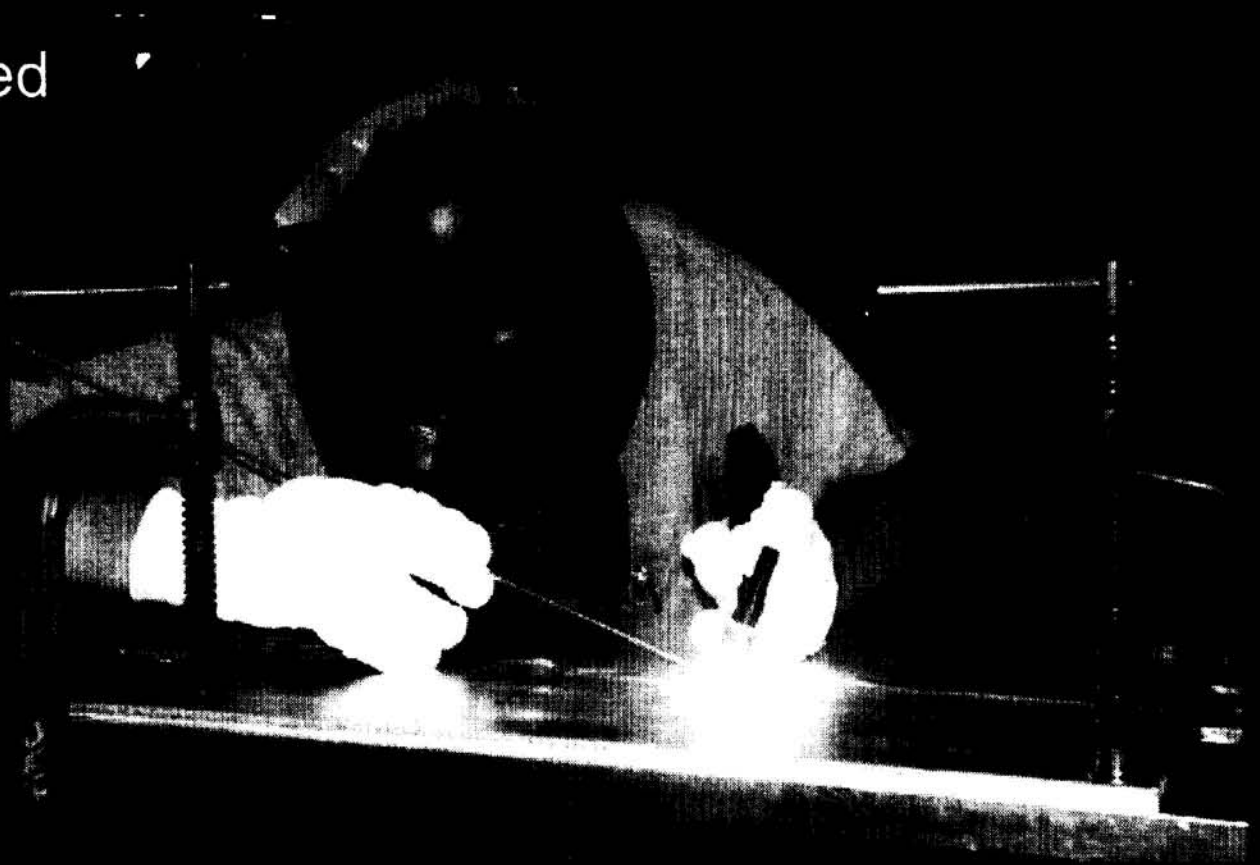

Special Tooling for Weld Repairs

- Flat Position Determined Optimal Repair Position
- Vertical Position as a maximum case without defects

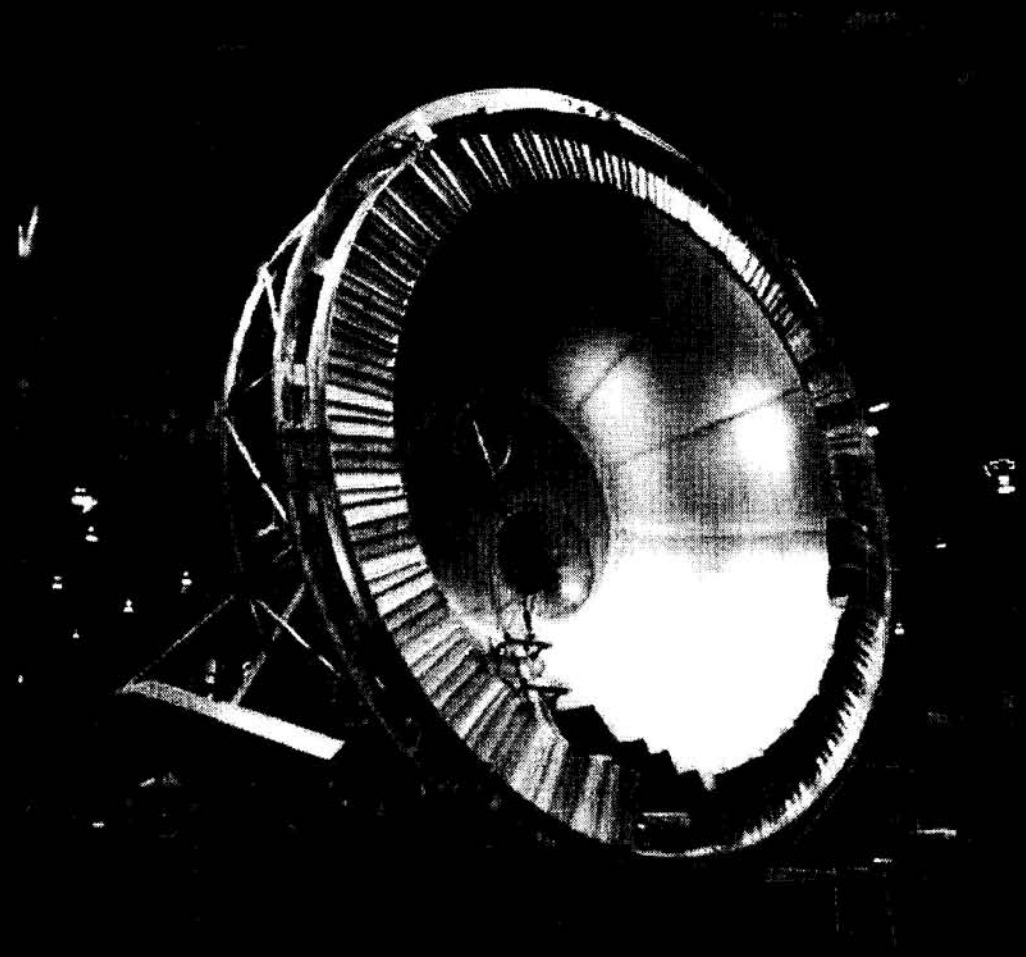

Sensor Technology Implemented

Optical/Laser based sensor system

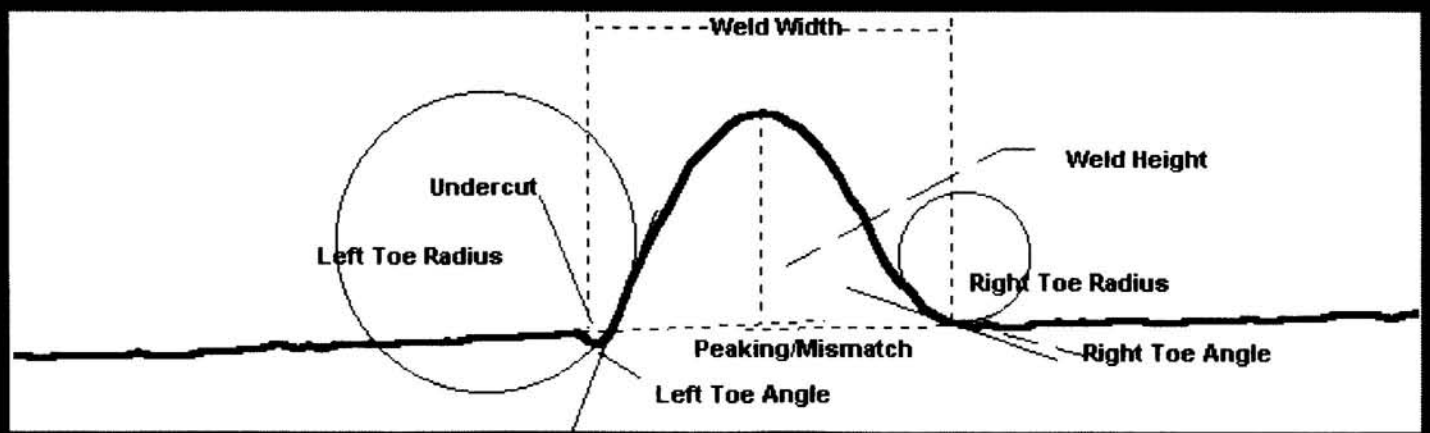

Intersection Cracks

Crack Location

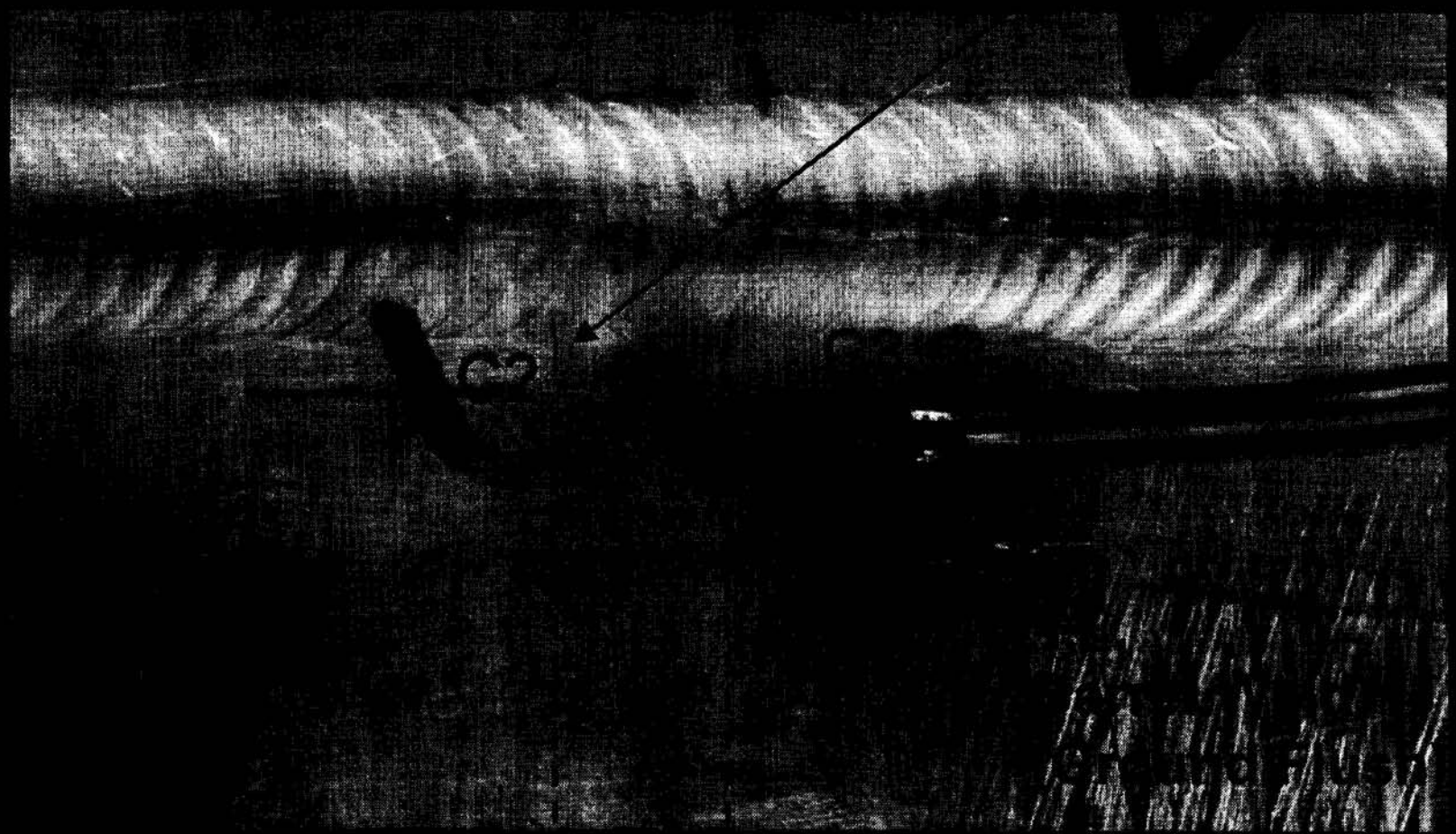

Intersection Crack Affected Tools

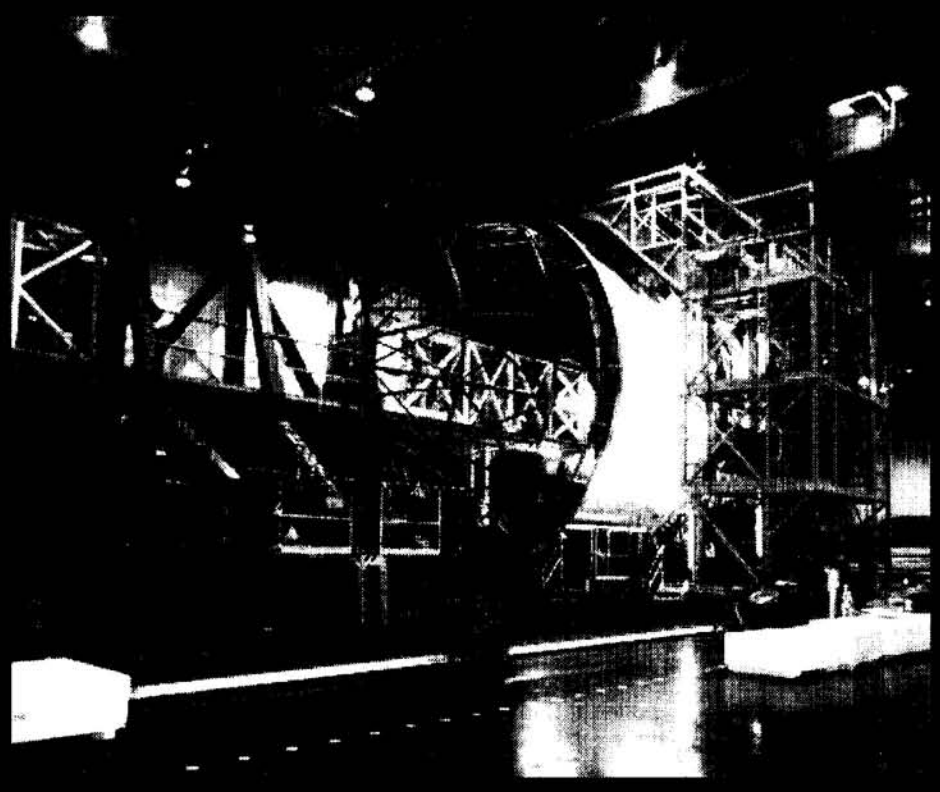

Hydrogen Tank Final Assembly Tool

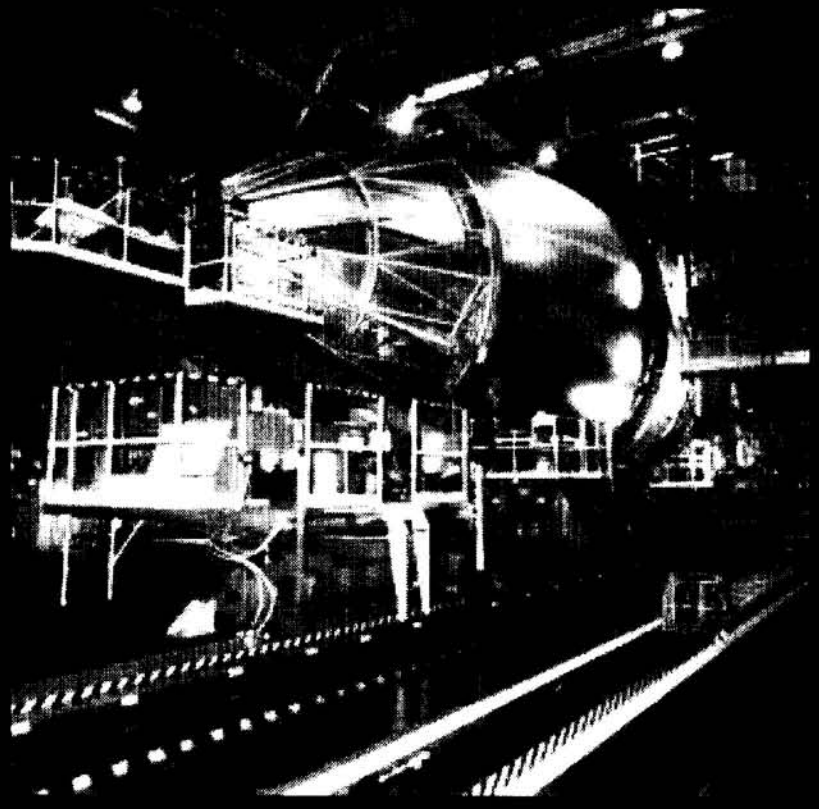

Oxygen Tank Final Assembly Tool

Photomicrograph of Dual Cover Pass

Crack Susceptible Region Setup by Intersection

97B324 M-8

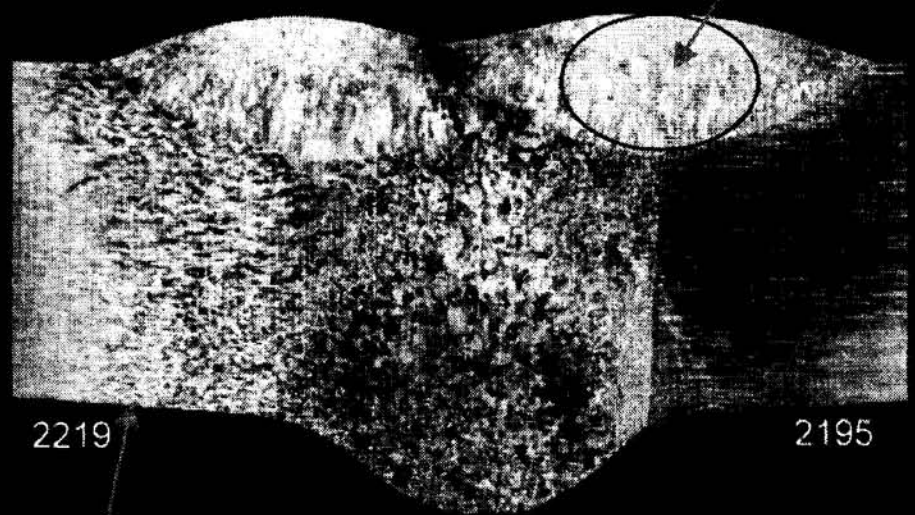

.320" Thick

2219 Material
No Problem on
Frame side

Weld Lack of Penetration Issue

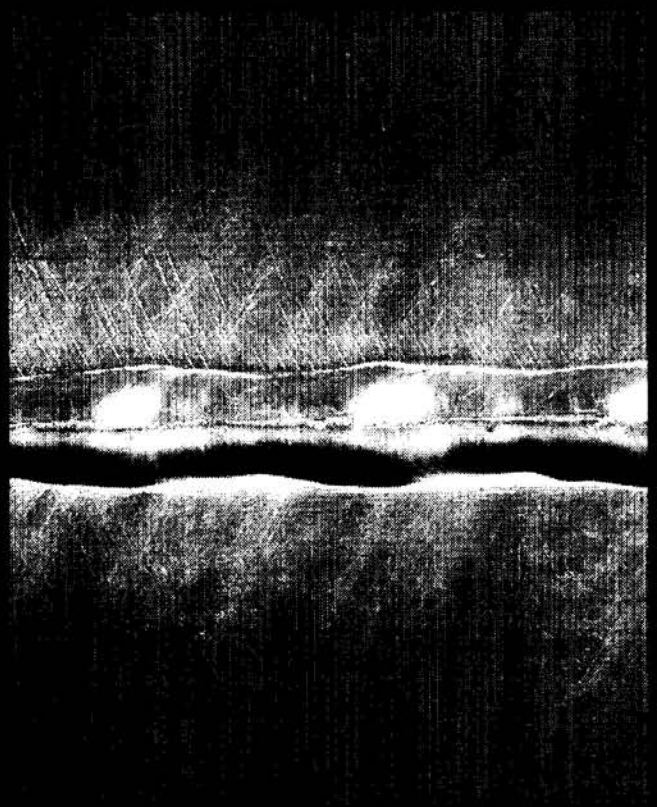

Weld Root

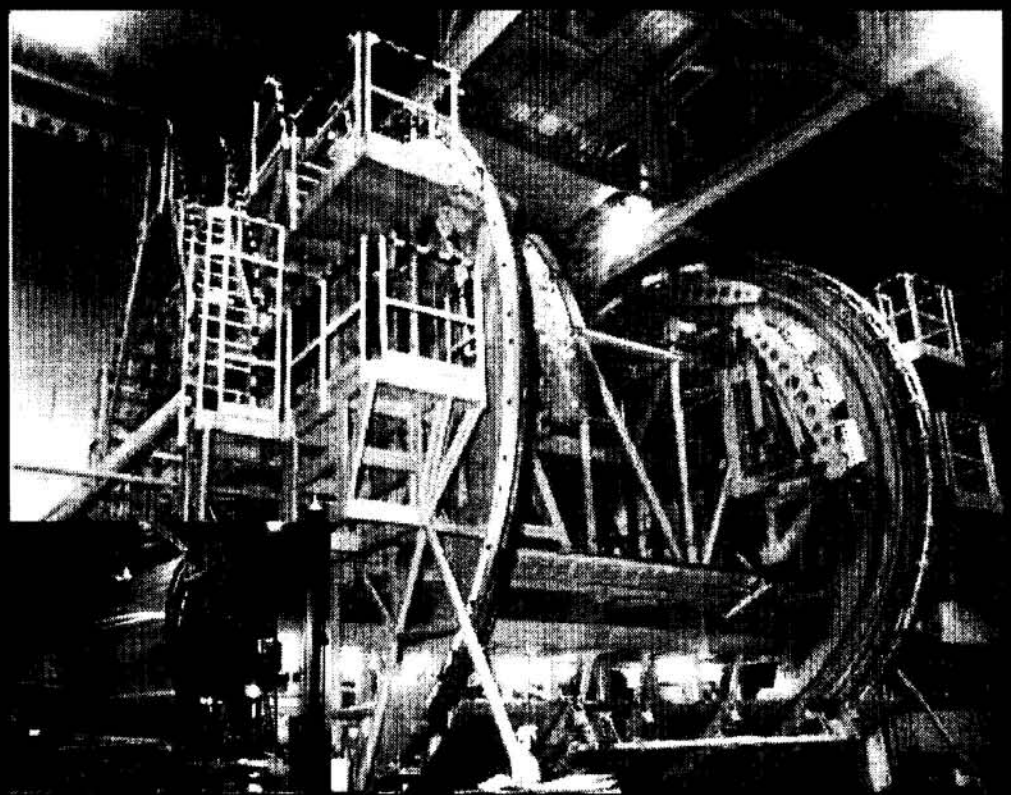

Hydrogen Tank Barrel Weld Tool

Development of Standoff Control

Spring Loaded VPPA Torch
with SPAW Tungsten and Orifice Configuration

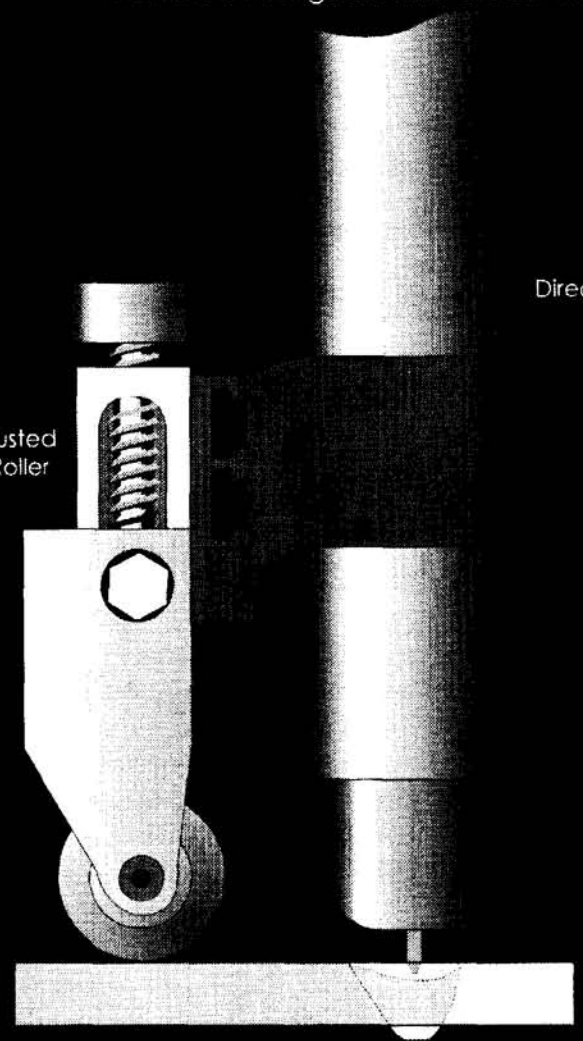

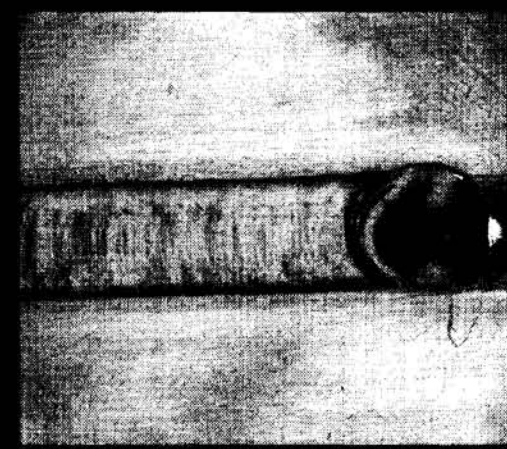

Downhand SPAW with
Trailing Wheel Mechanical
Standoff
5016 Barrel Tool
Configuration for SLWT

.025" Tungsten "Stick-in"

Toe Cracks Investigation

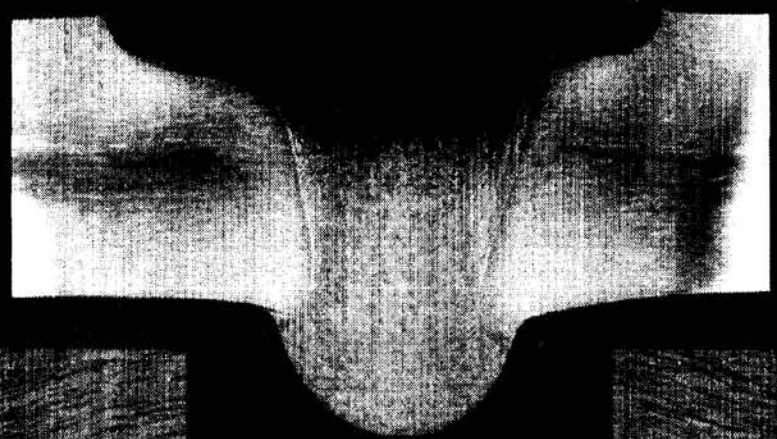

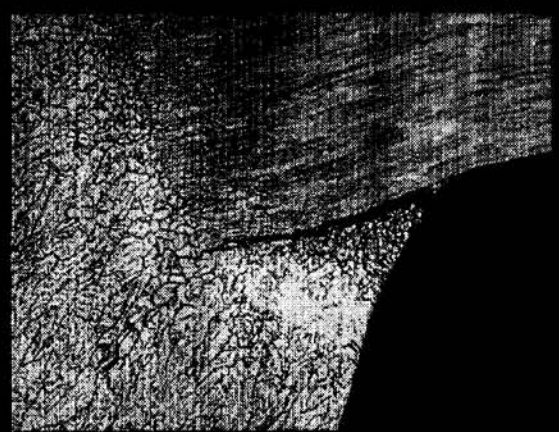

ROOT TOE 50X ORIGINAL MAG.

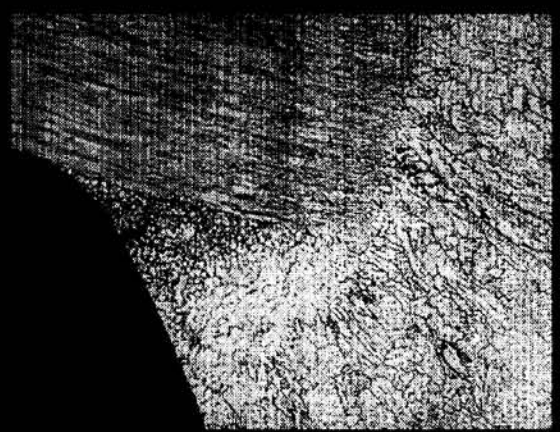

ROOT TOE 50X ORIGINAL MAG.

Forward Ogive Welding

0.190" –0.220" thick tapered welds

- VPPA power supply has inconsistent reverse current
- Repairs require even faster manual repair travel speeds and narrow grinds

5012 Forward Ogive tool

Dome Cap Welding

- Oxygen Tank Dome Cap most challenging weld
- Hydrogen Dome Cap a close second.
- Peaking at intersections creates welding challenge

Dome Cap to Body Weld Tool

First SLWT Launched June 2, 1998

STS 91

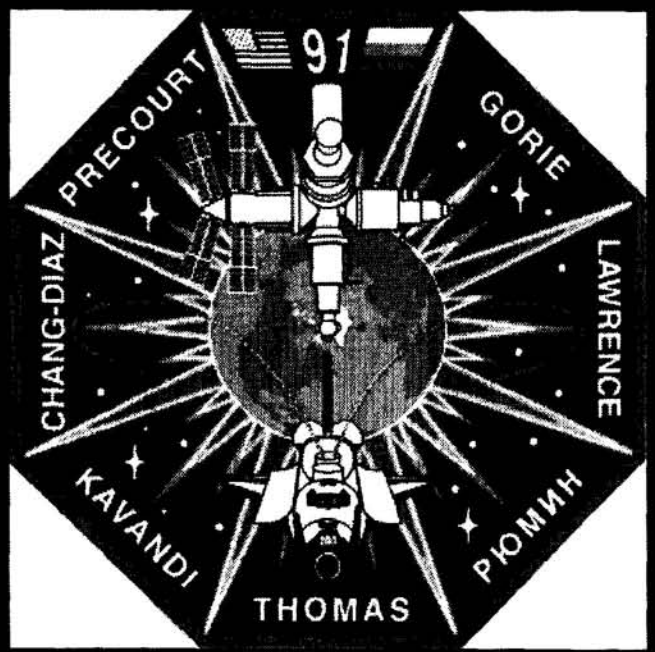

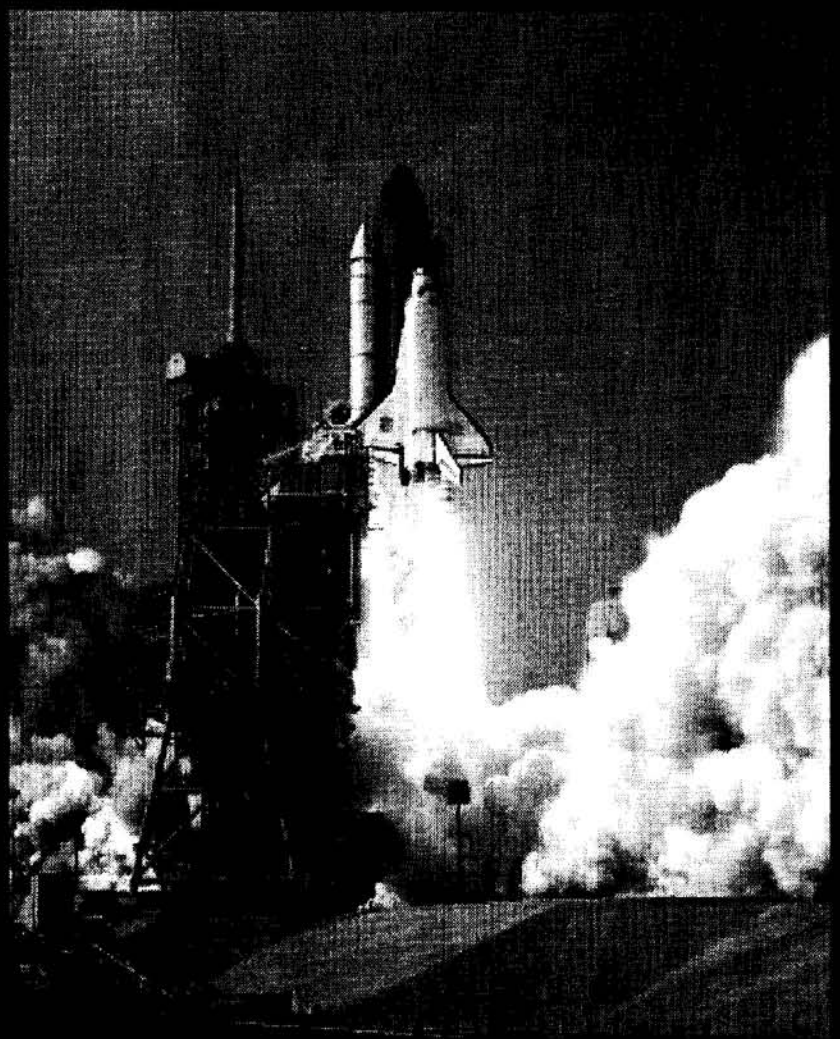

- Eight Super Lightweight Tanks have flown

Al 2195 Welding Summary

- Alloy Is More Reactive
  - Root-side Inert Gas Purging Required
  - Improved Cleanliness Helpful
  - Automatic Arc Voltage Control More Sensitive
- Alloy Is Crack Sensitive
  - Reduced Heat Input Beneficial
  - Filler Alloy Critical
- Minimize Repair Grindouts
- Planishing Required If Filler Alloy Strength Is Mismatched

CRYOGENIC TANK TECHNOLOGY PROGRAM (CTTP)

- CONCLUSIONS
  - NEAR NET SHAPE HARDWARE CAN BE COST EFFECTIVE FOR HIGHER PRODUCTION RATE CRYOTANK HARDWARE
  - LARGE SCALE-FLIGHT QUALITY HARDWARE CAN BE MANUFACTURED USING NEAR NET SHAPE PROCESSES
  - FRICTION STIR WELDING SUCCESSFULLY DEMONSTRATED

CRYOGENIC TANK TECHNOLOGY PROGRAM (CTTP)

- PROGRAM STATUS
  - ADAPTERS, BARREL PANELS, AND DOMES HAVE BEEN COMPLETED
  - FRICTION STIR WELD TOOLING IN PLACE ON CIRCUMFERENTIAL TOOL
  - BARREL PANEL WELDS COMPLETED
  - EXCESSIVE POROSITY IN BARREL TO ADAPTER WELDMENTS PLACED TANK FABRICATION ON HOLD STATUS

CRYOGENIC TANK TECHNOLOGY PROGRAM (CTTP)

- NEAR NET SHAPE TECHNOLOGIES
  - EXTRUDED BARREL PANELS
  - ROLL FORGED Y-RING ADAPTERS
  - ONE PIECE SPIN FORMED DOMES
- OTHER TECHNOLOGIES
  - LOW PROFILE, NON-TANGENT NET SHAPE SPIN FORMED BULKHEADS
  - FRICTION STIR WELDING

CRYOGENIC TANK TECHNOLOGY PROGRAM (CTTP)

- OBJECTIVES
  - DETERMINE FEASIBILITY AND COST EFFECTIVENESS OF NEAR NET SHAPE HARDWARE
  - DEMONSTRATE NEAR NET SHAPE PROCESSES BY FABRICATING LARGE SCALE-FLIGHT QUALITY HARDWARE
  - ADVANCE STATE OF CURRENT WELD PROCESSING TECHNOLOGIES FOR ALUMINUM LITHIUM ALLOYS

CRYOGENIC TANK TECHNOLOGY PROGRAM (CTTP)

Timothy P. Vaughn
Marshall Space Flight Center
September 20, 2000

Developments to Improve Productivity

- Domes & Ogives return to 2219
- Friction Stir Welding to be implemented on Barrels
  - Lower Manufacturing Cost
  - Higher Weld Strength Margins/Less Variability
  - Lower defect rate
- Friction Plug Repairs
  - Higher Strength
  - Automated
- New Filler Alloy Developed
  - Improved Strength
  - Planishing Not Required

CP/578/IN/25

F1/15T

Elimination of Carbon Tetrachloride for Quantitative Hydrocarbon Analysis

Vonnie M. Douglas
The Boeing Company
Rocketdyne Propulsion & Power
6633 Canoga Avenue
Canoga Park, CA 91309-7922

ABSTRACT

The elimination of ozone depleting substances, such as carbon tetrachloride, has resulted in the use of new analytical techniques for cleanliness verification and contamination sampling. The last remaining application at Boeing Rocketdyne which required a replacement technique was the quantitative analysis of hydrocarbons by infrared spectrometry. This technique, which previously utilized carbon tetrachloride, was successfully modified using the SOC-400, a compact portable FTIR manufactured by Surface Optics Corporation[1]. This instrument can quantitatively measure and identify hydrocarbons from solvent flushing of hardware as well as directly analyze the surface of metallic components without the use of ozone depleting chemicals. Several sampling accessories were evaluated to perform hydrocarbon analysis for various applications.

BACKGROUND

Prior to 1996 carbon tetrachloride was used in the laboratory for extractions and for standard preparation, sample dilutions and as a pick up solvent for Fourier transform infrared (FTIR) techniques. It was also utilized as a flush solvent for hardware cleanliness verification procedures, including non-volatile residue (NVR), handwipe applications and particle count determinations. Cyclohexane gravimetric NVR and Total Organic Carbon (TOC) analysis replaced many of the cleanliness verification techniques which utilized carbon tetrachloride. Cyclohexane and Soxhlet extractions utilizing CO_2 were used as alternatives to many laboratory applications.

Cleanliness verification of smaller sized hardware and wipe/swab analysis still utilized carbon tetrachloride for hydrocarbon determination. Certain hardware was incompatible with the TOC technique due to the electrical connectors and other parts did not contain a large enough surface area to be used with gravimetric methods. Wipes and swabs were extracted with cyclohexane, but still required quantitative techniques that could attain the low detection limit provided by FTIR methods. During these analyses, an aliquot of the final flush solvent was collected and evaporated to dryness. The remaining residue was taken up in a known quantity of carbon tetrachloride and was subsequently analyzed on an infrared spectrometer. A technique was required to achieve the required detection limit of 1.0 mg/ft^2 without the use of ozone depleting chemicals.

An analytical procedure was investigated which involved evaporating cyclohexane directly onto a sampling device followed by subsequent analysis of the residue using a FTIR spectrometer. This would eliminate the need for carbon tetrachloride as a pick-up solvent. New programs, new cleaning facilities and the goal to reduce cycle time also led to the investigation of surface analysis techniques for cleanliness verification. The same instrument evaluated for quantitative hydrocarbon analysis was also evaluated as a surface analysis tool for several applications, including wax removal and cleanliness verification of specific hardware.

INTRODUCTION

Historically, quantitative analysis using FTIR techniques involved the following steps.

1) Cyclohexane was obtained from hardware by flushing or from wipe extractions.
2) The solvent was evaporated to residue.
3) Remaining residue was picked up in carbon tetrachloride.
4) The carbon tetrachloride solution was transferred into a quartz cell.
5) Hydrocarbon analysis by FTIR was performed on the carbon tetrachloride solution.

The proposed FTIR method utilized a portable spectrometer, Model SOC-400, manufactured by Surface Optics Corporation. The unit contains an integrating spherical adapter, referred to as a V-sphere, designed specifically for this application. The V-sphere is a hemispherical gold plated container, which attaches directly to a matching hemispherical part on the main unit. When the two hemispheres are attached by threaded closures a complete sphere is formed. The infrared beam enters through a small hole from the detector side of the sphere and is reflected off of the sampling hemisphere, which contains the sample residue. The beam is reflected many times within the sphere, which amplifies the signal and increases sensitivity before reaching the detector. The instrument measures data collected over the entire hemispherical area for any set of incident or reflected angles.

The portability of the unit is an added feature, but was not deemed as important as the sampling devices available for analysis. The advantage of the V-sphere accessory is that the solvent can be directly evaporated into the sample holder. The sampling device has a capacity of 5 ml, which allows easy transfer of the solvent. This minimizes sample loss and decreases analysis time when compared to other methods.

The SOC-400 also has the capability of detecting organic contaminants directly on metallic surfaces using specular, diffuse and grazing angle measurement heads. The IR beam from the unit illuminates the sample outside the instrument. The incident beam from the FTIR is reflected into specular and diffuse beams which are then focused onto the detector, collected and analyzed. The beam of infrared light penetrates a thin layer of a contaminant on the inspected surface and part of the beam is absorbed by the molecules of the contaminant. The amount of absorbed energy changes with illuminating energy and each polyatomic molecule produces its own characteristic infrared spectrum. Therefore this technique has the ability to identify as well as quantify a given contaminant. A feasibility study was conducted on the capability of this technique using the three measurement heads on various surface finishes.

V-SPHERE TESTING

Qualification testing was performed utilizing the SOC-400 with the gold plated integrating spherical sampling accessory (V-sphere). This technique involved evaporating solvent onto the V-sphere and analyzing the remaining residue with an SOC-400 FTIR spectrometer. Mineral oil standards were prepared in cyclohexane and evaporated directly onto the sampler. A calibration curve was obtained from 0.01 mg to 0.5 mg. See Figure 1. An infrared absorption spectrum was obtained between 3000 cm-1 and 2800 cm-1 wavenumbers. Sixty four (64) scans at 8 cm-1 resolution were obtained.

Figure 1.

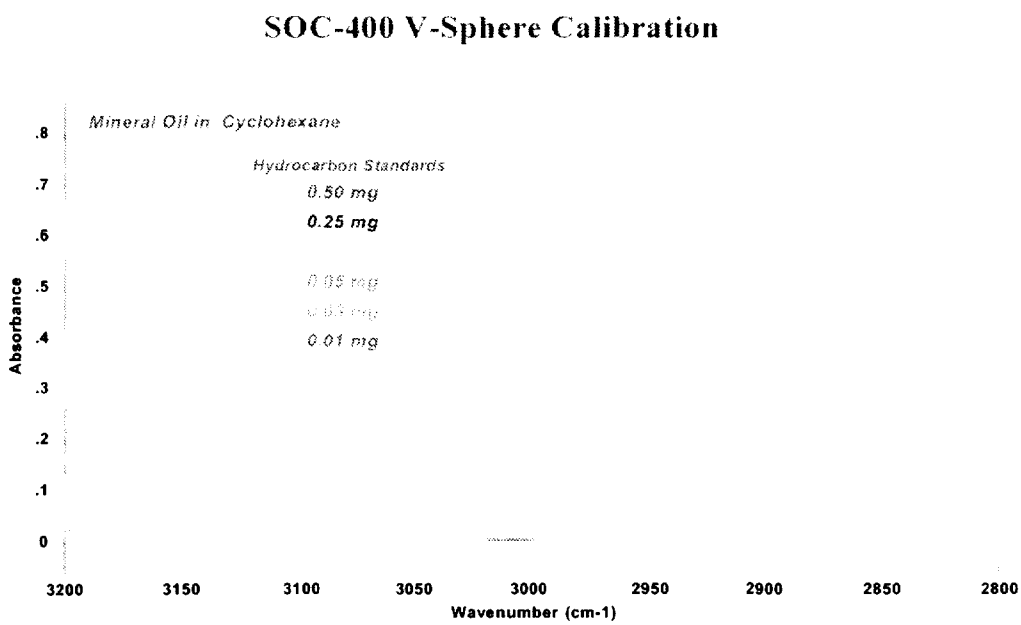

Initial calibration results indicated that two sets of calibration data were required to cover the needed range of 0.01 to 1.0 mg. This was demonstrated by high recoveries (200 percent) in the lower concentration range. See Table 1. Each set of calibration data consisted of 5 points, the lower ranging from 0.01 to 0.25 mg and the higher from 0.05 to 1.0 mg. With the two sets of calibration data, the lower concentration recoveries decreased to an acceptable range. See Table 2.

A know volume and concentration of contaminant in cyclohexane was placed in the V-sphere and allowed to evaporate. After the solvent was evaporated to residue the V-sphere surface was analyzed. The contaminants and contaminant mixture are described in Tables 3 and 4. See Table 5 for results.

Hydrocarbon standards were concentrated in a small area of the spherical V-sphere surface and compared to hydrocarbons spread evenly over the entire surface. The goal was to determine if the recovery would vary with the thickness of the residue remaining in the V-sphere. Mineral oil standards in cyclohexane were evaporated into the V-sphere such that 0.1 mg residue would remain in the V-sphere, while the volume, and thus the area covered by contaminant, varied from 0.1 to 5.0 ml. The results indicate thickness of the residue does not significantly effect recoveries. See Table 6 for results.

Table 1.
Mineral Oil Recovery
Obtained using One Set of Calibration Data

Recovery (Percent)	Amount Applied (mg)	Recovery (Percent)
0.01	0.02	200
0.01	0.02	200
0.01	0.02	200
0.01	0.02	200
0.03	0.03	100
0.03	0.02	80
0.03	0.03	100
0.05	0.05	100
0.13	0.11	85
0.13	0.10	77
0.25	0.27	108
0.25	0.23	82
0.50	0.49	98
0.50	0.40	80

Table 2.
Repeatability Test Results Using Two
Sets of Calibration Data

Mineral Oil														
Amt.Applied (mg)	0.01		0.02		0.05		0.10		0.25		0.5		1.0	
	Amt. Detected	% Rec.	Amt. Detected	% Rec.	Amt. Detected	% Rec.	Amt. Detected	% Rec.	Amt. Detected	% Rec.	Amt. Detected	% Rec.	Amt. Detected	% Rec.
	0.012	120	0.018	90	0.049	98	0.103	103	0.242	97	0.507	101	1.061	106
	0.012	120	0.020	100	0.050	100	0.105	105	0.239	96	0.529	106	1.049	105
	0.012	120	0.020	100	0.050	100	0.102	102	0.238	95	0.511	102	1.039	104
	0.013	130	0.020	100	0.050	100	0.100	100	0.239	96	0.498	100	0.998	100
	0.010	100	0.020	100	0.049	98	0.100	100	0.239	96	0.487	97	0.938	94
	0.011	110	0.019	95	0.051	102	0.100	100	0.249	100	0.511	102	0.912	91
Average		117		98		100		102		96		101		100
Std. dev.		10.3		4.2		1.5		2.1		1.7		2.8		6.2

Table 3.
Contaminant Description

Contaminant	Description
Mineral Oil	Light paraffin oil
Mil-H-83282 Hydraulic Fluid	Synthetic hydrocarbon fluid containing triphenyl phosphate
Spinnestic 22 Oil	Petroleum lubricating oil
Paraffin Wax	Low melting wax
Rigidax	High melting wax

Table 4
Mixture composition

Contaminant	Percent by Weight	Manufacturer	Description
Rapid Tap	43.7	Relton	Lubricant, containing mineral oil, paraffin and soybean oil
Mil-H-83282 Hydraulic Fluid	3.9	Bray Oil Co.	Synthetic hydrocarbon fluid containing triphenyl phosphate
LS-10	3.7	ITW Fluid Products Group	Fatty alcohol based lubricant
Bio-Pen P6F-4	3.5	Ardox Inc.	Fluorescent, water-soluble dye penetrant
Turco 4215 Additive	5.2	Elf Atochem, Turco Products	Non-ionic detergent, containing diethylene glycol monobutyl ether and nonnylphenoxypoly (ethyleneoxy) ethanol

Table 5.
V-Sphere Qualification Data

Contaminant	Concentration (mg)	Amount Detected (mg)	Recovery (Percent)
Mixture	0.07	0.060	86
	0.07	0.060	86
	0.07	0.061	87
	0.07	0.061	87
	0.07	0.061	87
	0.07	0.061	87
Hydraulic Fluid Mil-H-83282	1.0	0.992	99
	1.0	1.116	112
	1.0	1.059	106
	1.0	1.069	107
	1.0	0.997	100
	1.0	1.099	110
	0.50	0.40	80
	0.5	0.42	84
Spinnestic Oil	0.25	0.23	92
Parrafin Wax	0.035	0.03	86

Table 6.
Effect of Residue Thickness

Solvent Volume (ml)	Contaminant (mg)	Amount Detected (mg)	Recovery (Percent)
0.1	0.10	0.105	105
0.5	0.10	0.113	113
1	0.10	0.095	95
2	0.10	0.091	91
4	0.10	0.101	101
5	0.10	0.090	90

SURFACE ANALYSIS APLICATIONS

The SOC-400 was used in a feasibility study to detect organic contaminants directly on metallic surfaces. Three types of measurement heads were utilized on various surface finishes. This technique, if proven effective, could provide a rapid method of verifying surface cleanliness on precision cleaned hardware. The goal was to determine the feasibility of using SOC-400 surface analysis techniques for cleanliness verification.

A test plan was developed, but prior to implementation, the following tasks were required:

1. Identify test coupon substrates which would be consistent with production hardware surfaces
2. Fabricate test coupons
3. Determine method of contaminant application

Coupons were fabricated from 0.016" thick 718 Alloy. The coupons were 4.8" x 3.0 " (0.1 sq. ft). Four surface finishes representative of production hardware were obtained as follows in Table 7.

Table 7.
Coupon Description

Coupon Set	Surface Treatment	Visual Appearance
1	Untreated material	Light color, smooth surface
2	Glass bead, grit blasted	Light color, rough surface
3	Heat treated in air, then grit blasted	Dark color, rough surface
4	Heat treated in vacuum	Dark color, smooth surface

Initially contaminants were applied to the coupons using a cleaned syringe. A known volume of a known concentration was applied to a one sq. cm surface area. However it was observed visually and analytically the technique was not providing a uniform layer of contaminant. Since the FTIR only analyzes a 2 mm surface area, large variations in the results were observed when analyzing different locations within the contaminated area. A more precise technique of applying contaminant was required.

An air brush sprayer was then utilized to apply the contaminant. The contaminant was diluted in cyclohexane and sprayed onto a coupon. The amount applied was determined by weight difference. This technique resulted in a much more uniform coupon and was also being used by other industries for similar applications. A limited amount of variation was still observed on the coupons. This was overcome by taking more samples on each coupon. Initially only 3-5 areas on each coupon were analyzed. It was determined that by averaging 10 spots on each coupon, more reliable results could be obtained.

SURFACE ANALYSIS TEST RESULTS

A calibration curve was run using mineral oil in cyclohexane with the diffuse reflectance head on coupon Set 2 (grit blasted, no heat treat). See Figure 2. The calibration curve was used for quantitative comparison of the various surfaces. See Table 8 and Figures 3-6. The recoveries appear much higher on the more reflective surfaces due to high background noise. Average percent recoveries for 5 to 10 mg/sq. ft coupons on the various surface types were 220, 90, 55 and 210 percent on coupon Sets 1, 2, 3 and 4 respectively. This indicates good recovery on the coupons used for the calibration curve, low recoveries on the most diffuse surface and high recoveries on the most reflective surfaces. The difference in recoveries indicate that the SOC-400 is more sensitive to certain surface finishes and implies that surface finish plays a large role in the detection capabilities of the instrument.

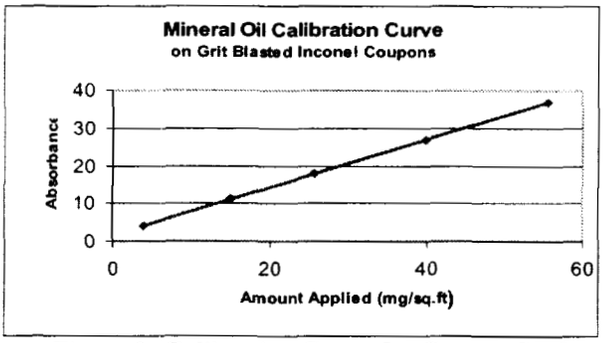

Figure 2. Calibration Curve for Coupon Set 2

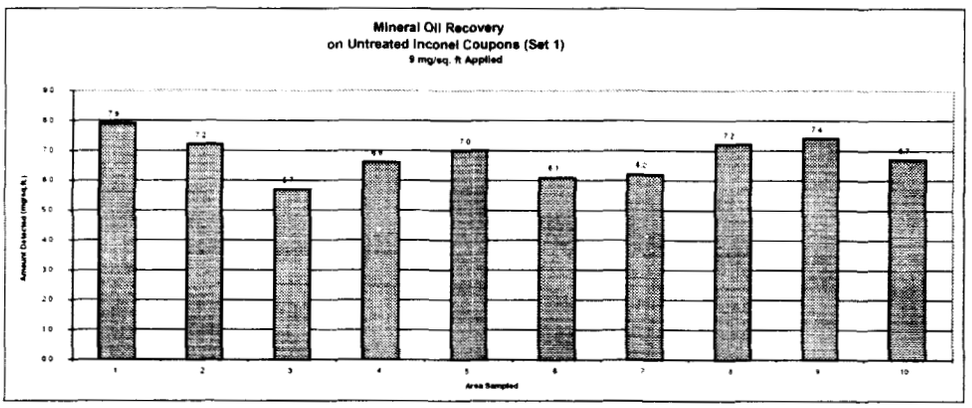

Figure 3. Mineral Oil Recovery on Coupon Set 1

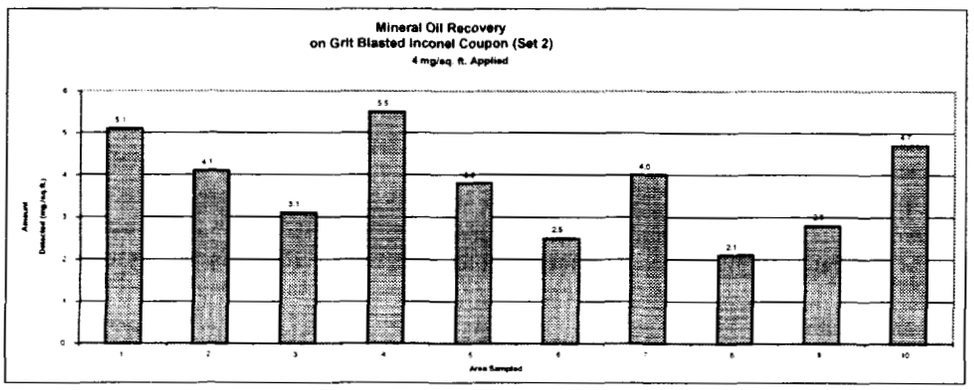

Figure 4. Mineral Oil Recovery on Coupon Set 2

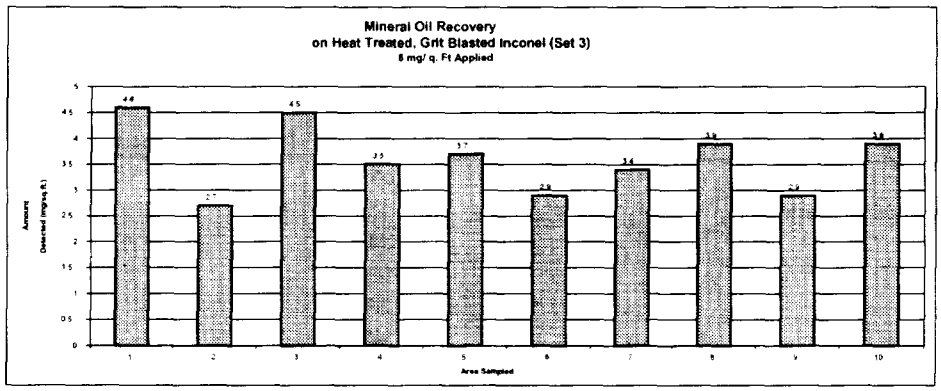

Figure 5. Mineral Oil Recovery on Coupon Set 3

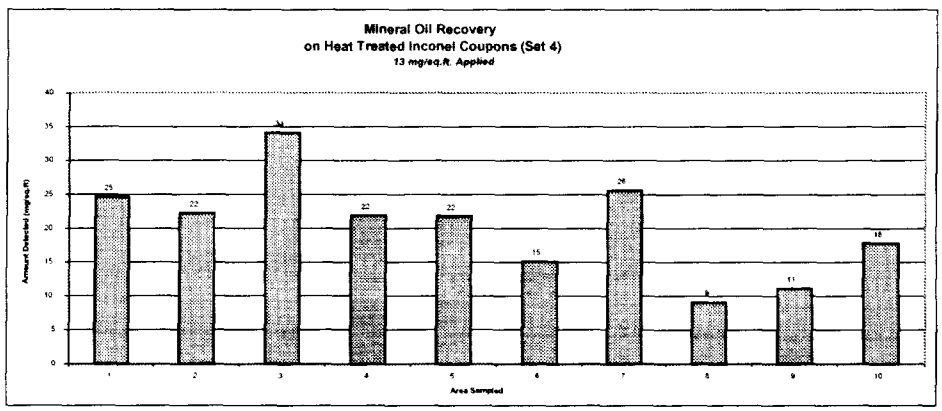

Figure 6. Mineral Oil Recovery on Coupon Set 4

FTIR Accessories

A grazing angle measurement head has just recently become available from the SOC-400 manufacturer. The purpose of the grazing angle is to enhance the detection capability of the instrument on more specular substrates. This is done by simply changing the angle of the incident beam coming from the IR source. An added benefit with the grazing angle accessory is that a larger spot size is analyzed. An elliptical area approximately with major and minor axes of 1 and 0.25 inches is analyzed as opposed to the 2 sq. mm area using the diffuse or reflectance head accessories.

Coupons were analyzed using grazing angle, diffuse head and reflectance head accessories. The diffuse head gave the highest peak intensities. The specular head had a comparatively lower intensity and a higher noise level. The grazing angle had lower intensity, but also lower noise. The fact that the noise level was lower with the grazing angle proved to be an added benefit for lowering detection limits.

Table 8.
Diffuse Measurement Surface Analysis Results

Coupon/Surface Treatment	Amount Applied (mg/sq. ft.)	Amount Detected (mg/sq. ft.)	Percent Recovery	Amount Applied (mg/sq. ft.)	Amount Detected (mg/sq. ft.)	Percent Recovery
1	6	19.1	318	8	30.7	341
Untreated material		20.2	337		24.9	277
		20.6	343		33.8	376
		9.9	164		35.3	392
		14.4	240		33.0	367
		18.4	307		32.0	356
		26.5	442		26.6	296
		20.1	335		23.2	258
		21.5	358		25.6	284
		20.9	348		31.0	344
Average		**19**	**319**		**30**	**329**
2	4	5.1	128	9	7.3	81
Grit blasted material		4.1	103		5.4	60
		3.1	78		7.9	88
		5.5	138		8.1	90
		3.8	95		9.2	102
		2.5	63		7.8	87
		4.0	100		5.6	62
		2.1	53		4.9	54
		2.8	70		10.9	121
		4.7	118		8.2	91
Average		**3.8**	**94**		**7.5**	**83.7**
3	6	4.6	115	8	4.4	55
Heat treated in air, then grit blasted		2.7	45		7.7	96
		4.5	75		7.5	94
		3.5	58		4.8	60
		3.7	62		4.1	51
		2.9	48		5.2	65
		3.4	57		4.7	59
		3.9	65		6.9	86
		2.9	48		3.9	49
		3.9	65		5.7	71
Average		**2.8**	**47**		**5.5**	**68.6**
4	7	13.5	193	13	25	189
Heat treated in vacuum		21.7	310		22	171
		13.3	190		34	262
		17.2	246		22	168
		20.0	286		22	168
		7.04	101		15	116
		11.1	159		26	197
		9.3	133		9	70
		11.9	170		11	85
		14.6	209		18	137
Average		**14**	**199**		**20**	**156**

A set of twelve coupons contaminated with 0.5 to 2.0 mg/ft^2 of mineral oil was analyzed by grazing angle, diffuse and specular FTIR . The diffuse and specular measurements could only detect contaminants at the highest concentration, 2 mg/ft^2. The grazing angle was much more sensitive and could detect hydrocarbons at 0.5 mg/ft^2 on all but one surface. The grazing angle could not detect hydrocarbons on the most diffuse surface, coupon Set 3-heat treated in air, then grit blasted material.

Other manufacturers have developed FTIR units with a grazing angle accessory in conjunction with fiber optics. Remspec * makes a unit which contains a detector connected at the end of the fibers which is in direct contact with the surface being analyzed. This increases the sensitivity without losing signal through the fibers. One disadvantage to that unit is the grazing angle accessory is approximately 5 x 6 inches and is rather bulky to be used on many hardware configurations. The advantage is this unit can analyze a spot size approximately 6 sq. in., which can reduce the problems associated with analyzing inhomogeneous contamination.

WAX REMOVAL APPLICATION

The SOC-400 was evaluated for surface cleanliness verification of the SSME Main Combustion Chamber (MCC) after wax removal operations. The MCC contains many slotted channels which were considered the most likely areas to trap contamination. Slotted channel coupons and an actual (scrap) SSME MCC liner were utilized to evaluate the portable FTIR for detection of residual hydrocarbons. Tests were performed using 3 x 5 inch copper coupons 0.5 inch thick containing 15 slots each of width 0.065 inch and depth 0.45 inch. See Figure 7.

The SOC 400 was modified by placing a raised slot 0.040 inches wide in the plastic faceplate. This slot aligned the instrument to be able to analyze hydrocarbons in the slotted channels. This arrangement was used for the rectangular coupons and for the scrap MCC. About half the channels in each slotted coupon was contaminated with wax by rinsing channels with a solution of yellow Rigidax in cyclohexane. The SOC-400 was easily able to distinguish between the contaminated and uncontaminated slots.

Efforts to produce a calibration curve for wax in the slotted coupons have thus far been unsuccessful, primarily to the difficulty of applying a uniform coating of hydrocarbons on the inner surface of a slot. Both soaking and spraying of a cyclohexane solution of Rigidax yellow wax into the slots were tried with limited success.

Analyzing a clean MCC was also performed. The SOC-400 was placed on an adjustable tripod as shown in Figure 8. Data collection took about 30 seconds per location and those results were compared to conventional cyclohexane rinsing of the slots. Conventional cyclohexane rinsing of the slots followed by FTIR analysis indicated the level of cleanliness was less than 1.0 mg/ft^2 within the slots. Qualitatively, use of the SOC-400 FTIR detected the presence of small amounts of hydrocarbons within the slots as well as other contaminants, possibly cleaning agents. This was confirmed by X-ray Photoelectron Spectroscopy (XPS) analysis of the coupons. More work is needed to confirm that a quantitative assessment of cleanliness within a slotted channel can be reliably made.

CONCLUSIONS

The V-sphere technique was shown to be an acceptable method for the hydrocarbon analysis and the process has been implemented successfully at Rocketdyne. Because the new method utilized similar analytical techniques as the previously used method (both used FTIR techniques), the implementation and qualification was much easier than that of an entirely new analytical technique.

[2]More work is required to determine if surface analysis is a viable technique at Rocketdyne. Preliminary results indicate that the required detection limit can be achieved using a grazing angle accessory, but sensitivity is dependent on surface finish. A determination of how many areas must be analyzed to confirm cleanliness of an entire part will also be required and will most likely be part specific. Because the surface finish varies from part to part, it is doubtful this technique will be widely used for cleanliness verification. However, it may be a useful tool for select hardware applications and contamination analysis. The SOC 400 FTIR is being used successfully at other Boeing locations for various surface analysis techniques.

---

[2] Remspec Corporation, Charleston, MA. See http://www.remspec.com

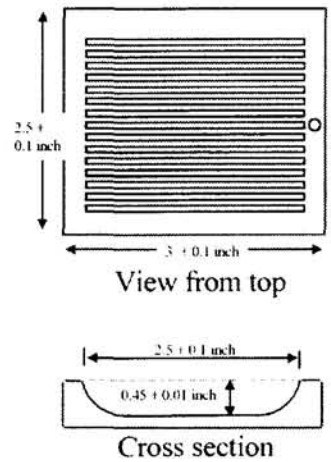

Figure 7. Slotted Coupon

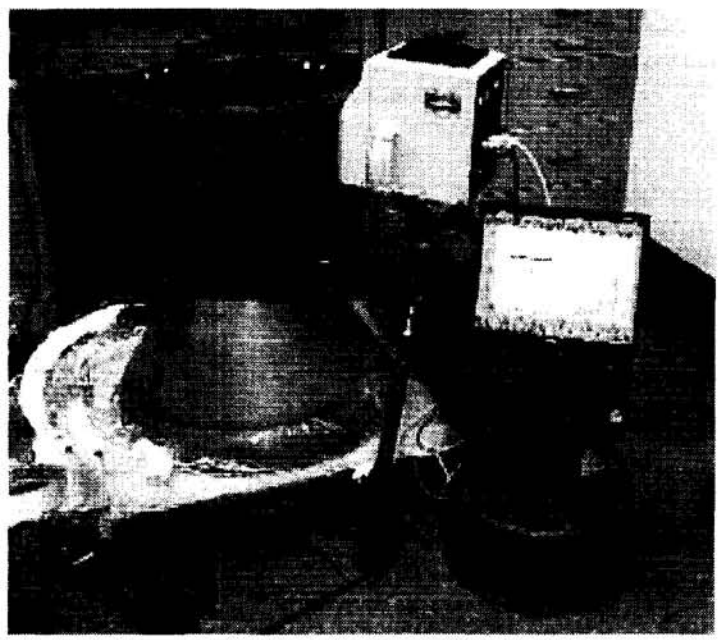

Figure 8. Surface Analysis of SSME MCC

ACKNOWLEDGEMENTS

The author would like to recognize Larry Hill for his contributions in the development of the infrared techniques and also expresses gratitude to Sarah Kipp for performing laboratory analysis in support of this project. Special thanks to Martin Szczesniak at Surface Optics and Paul Shelly from Boeing Seattle for performing additional analyses and providing technical support.

CP 379 N/27

ELLIPSOMETRIC VERIFICATION AND EVALUATION OF CLEAN SURFACES

F1/2ND

Wayne Thompson
The University of Alabama in Huntsville
Center for Automation and Robotics
NASA Surface Contamination Analysis Technology Team
UAH, R.I. Room M-62A
Huntsville, Alabama 35899
256-890-6281
Thompsg@email.uah.edu

Introduction

As precision cleaning techniques become more critical to the Aerospace Industry, good methods of verifying and evaluating those techniques become more important. Precision cleaning can often mean contamination thickness on the order of molecular diameters. Therefore, inspection instrumentation must be extremely precise. Ellipsometers provide the measurement capability necessary to determine the contamination of "clean" surfaces to within a few molecular diameters.

This paper is an introduction to how ellipsometry plays a vital role in the verification and evaluation of "clean" surfaces for NASA's Surface Contamination Analysis Technology (SCAT) Team.

Clean Surfaces

To those in the field of non-contact measurement, a "clean" surface implies that no other molecules can be present on a surface other than the surface's material itself, or that material's native oxide. Of course this also means that very few surfaces are actually "clean". Ellipsometry is one of the main tools used by NASA's Surface Contamination Analysis Technology Team verify that a surface is indeed clean or not.

The Ellipsometer

The ellipsometer is a non-contact measurement instrument that measures electromagnetic properties of light to derive optical constants for materials or to derive the thickness of thin films, or in this case, contamination layers. The physical aspects of the ellipsometer's measurements are shown in figure 1.

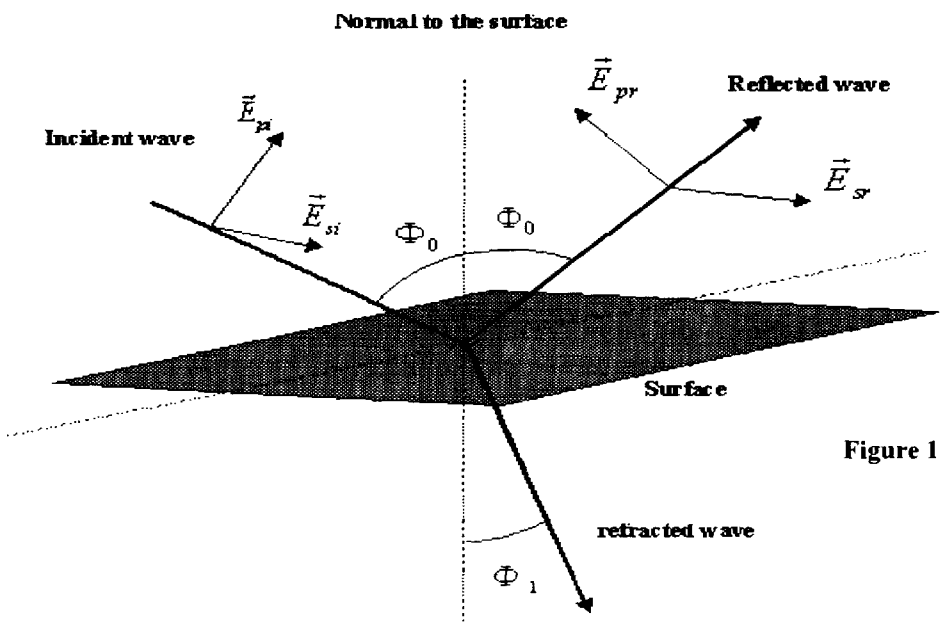

Figure 1

The $\mathbf{E_P}$ and $\mathbf{E_S}$ light polarization vectors correspond conceptually to the **E** and **B** fields of a propagating electromagnetic wave. The $\mathbf{E_P}$ and $\mathbf{E_S}$ wave components are always perpendicular to one another and have varying lengths or amplitudes. At any instantaneous moment the ratio of their amplitudes geometrically describes the form of an ellipse, hence the term "ellipsometer". Most light is elliptically polarized. In circularly polarized light (a special case of elliptically polarized light), the $\mathbf{E_P}$ and $\mathbf{E_S}$ wave components have equal amplitudes.

The ellipsometer uses the detection of these $\mathbf{E_P}$ and $\mathbf{E_S}$ wave component amplitudes through the equation:

$$(1) \qquad \rho = \frac{r_p}{r_s} = \tan\psi * \exp(i\Delta)$$

where Psi (ψ) and Delta (Δ) are the amplitude ratio and phase shift, respectively, of the P and S components of the light wave. $\mathbf{r_P}$ and $\mathbf{r_S}$, the amplitudes of the reflected wave components, are the actual quantities measured by the ellipsometer. From the Psi and Delta data, the index of refraction, the coefficient of extinction, and/or the thickness of a thin film can be derived.

The ellipsometer used by NASA's SCAT team is a J.A. Woollam VASE system as shown below in figure 2.

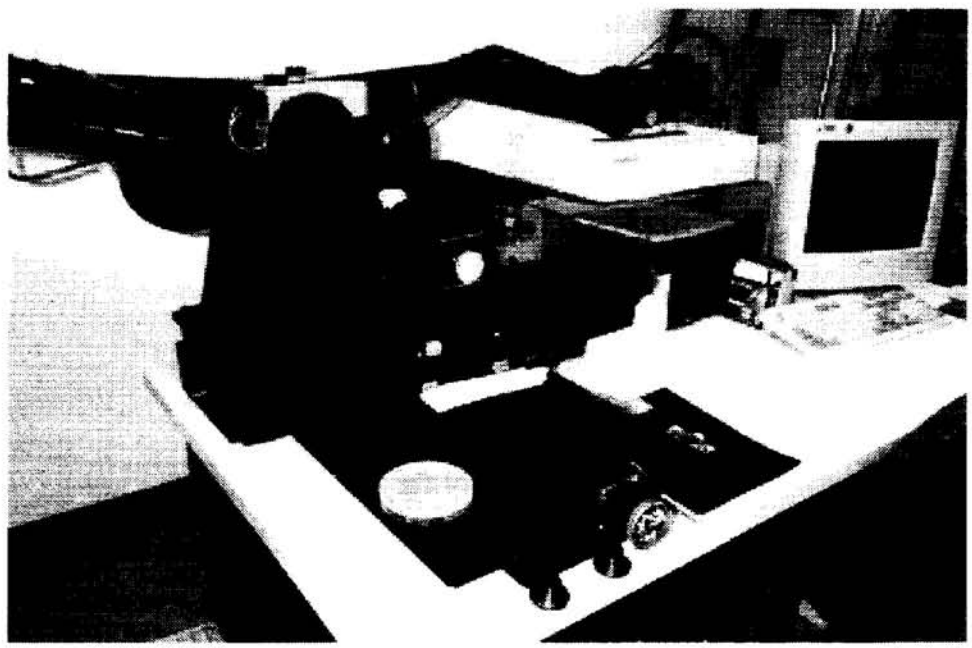

Figure 2

VASE stands for Variable Angle Spectroscopic Ellipsometer. By varying the incident angle and the wavelength of light, the system is able to generate very precise measurements. The J.A. Woollam company states that the tolerance (or noise level, as it is often referred to) is $\pm$ 5 Angstroms ($\pm 5 \times 10^{-10}$ m). However, in house variance measurements on a typical silicon wafer show even better performance of less than $\pm$ 3 Angstroms. Three Angstroms is actually less than the molecular diameter of an H_2O molecule. This allows for the detection of monolayer contaminants like H_2O.

Verification of Clean Surfaces

Many of NASA's scientific endeavors depend upon the absolute highest quality of fabrication for its space flight optics. This entails detailed clean assembly procedures within stringent clean rooms. One of the ways that NASA verifies the cleanliness of its procedures is via a "witness mirror". This type of verification is achieved by placing a standard electronics industry silicon wafer, the "mirror", in close proximity to the fabrication to be "witnessed". Periodically these witness mirrors will be sent to NASA's Surface Contamination Laboratory for verification

Examples of this are the witness mirrors that were used in NASA's XRCF project (X-ray Calibration Facility). The witness mirrors are base-lined on the SCAT team's J.A. Woollam VASE ellipsometer before it is placed within the XRCF chamber. At pre-determined intervals those mirrors come back for comparison with their baselines. If there is little change in the Psi and Delta data, then it may be concluded that the mirror is clean implying that the assembly area is free from airborne contaminants that could deposit on critical optics. However, if there is substantial difference between the baseline data and the verification data, then the critical space flight optics could be in danger of contamination and measures must be taken to ensure a clean environment for the hardware assembly.

The following data shows particular cases when a monolayer of contamination was indicated on XRCF witness mirrors. Baseline data is shown below (figures 3 and 4).

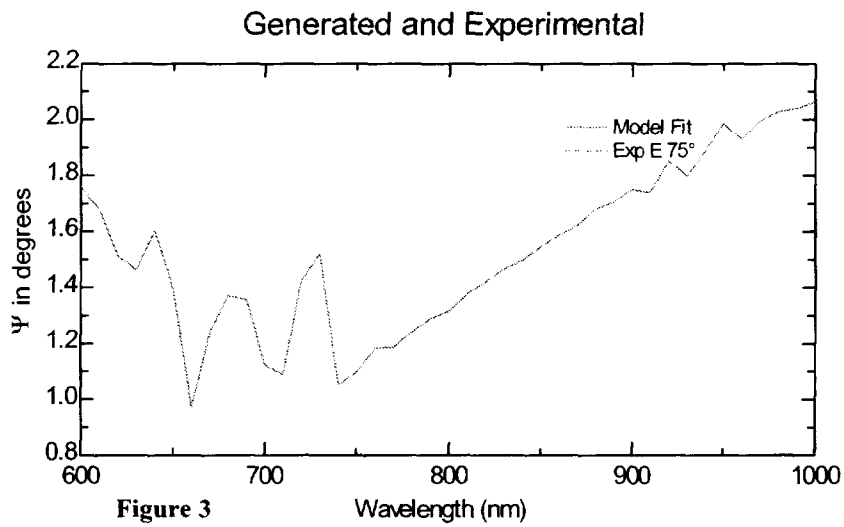

Figure 3

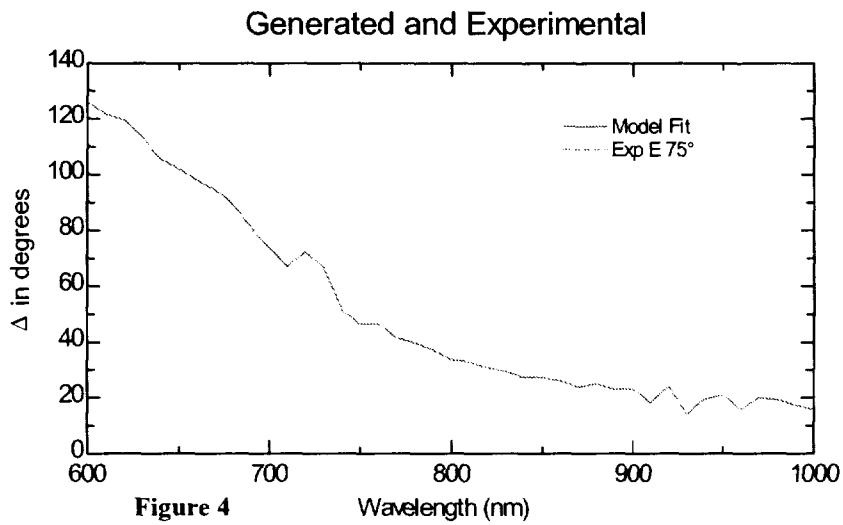

Figure 4

The next plots show Psi and Delta data for the same wafer after a time in the XRCF chamber. Also on the plot is a fitted model for the baseline data that shows how the data sets differ, indicating the possibility of contamination (figures 5 and 6).

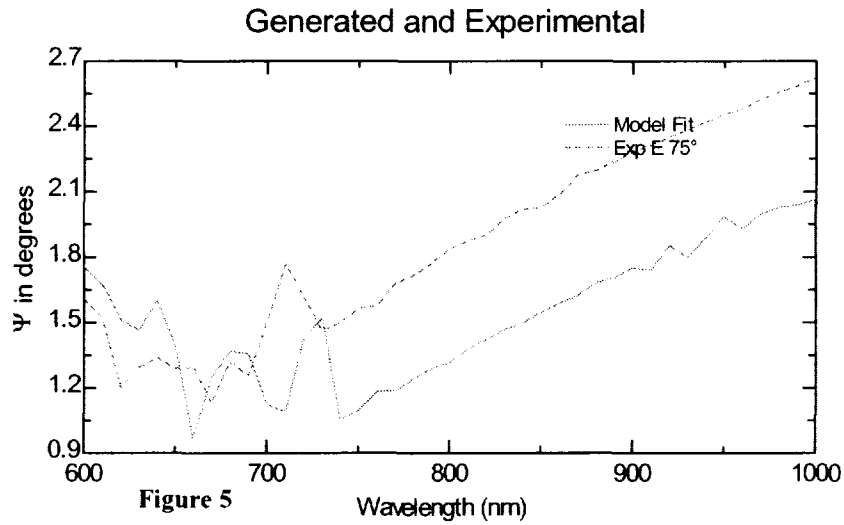

Figure 5

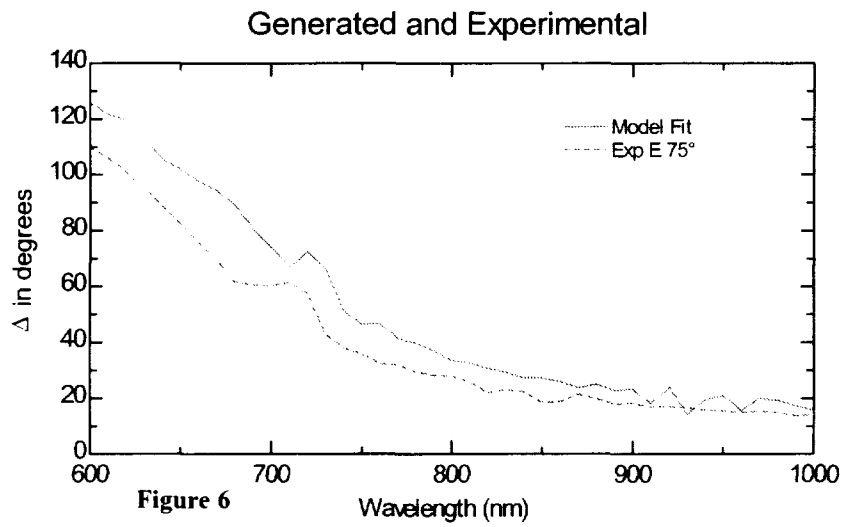

Figure 6

By adding an additional layer of SiO_2 to the baseline model and fitting the layer's thickness and optical constants, an estimation of the possible contamination layer's thickness is achieved (table 1).

2	sio2	5.8678 Å
1	sio2	41.507 Å
0	si	1 mm

Table 1

The following plots show how this solution now fits the data that indicates a contaminant on the wafer (figures 7 and 8).

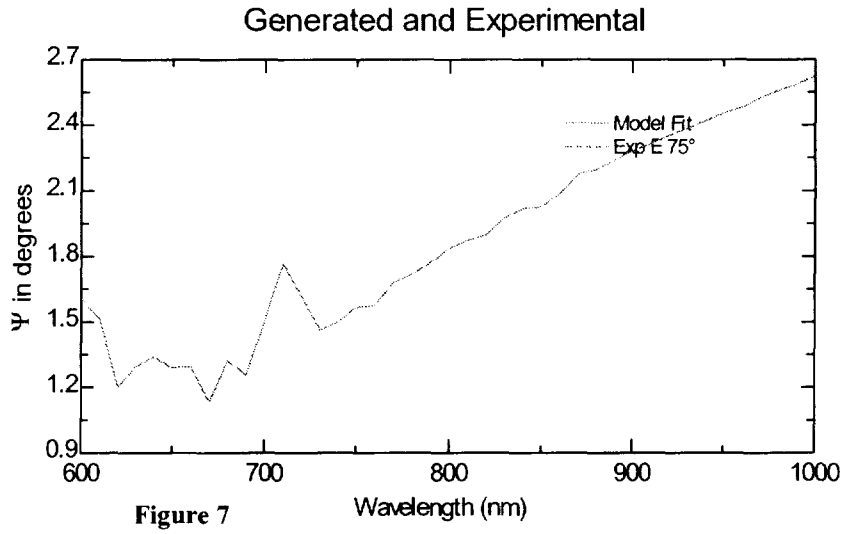

Figure 7

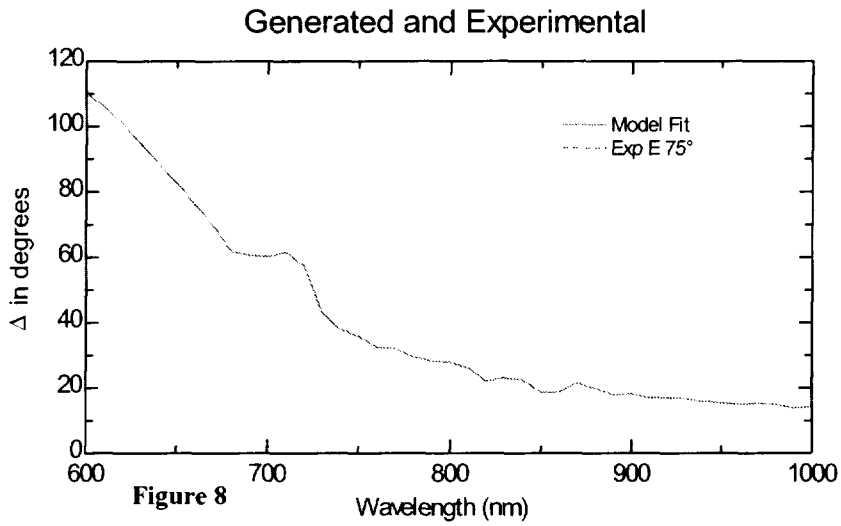

Figure 8

Another example of this (using just the Psi data) shows another indication of a possible layer of contamination on an XRCF witness mirror (figure 9).

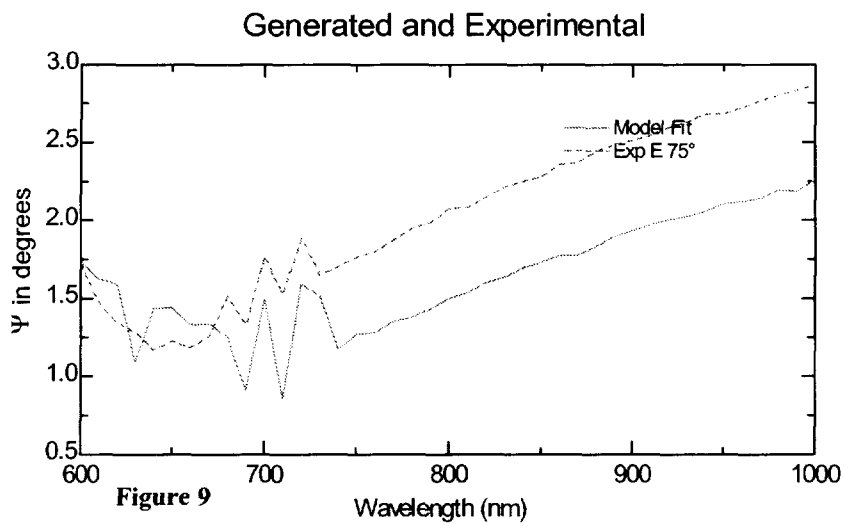

Figure 9

Once again the figure shows a few degrees discrepancy with the baseline data, indicating the possibility of contamination. Adding a contamination layer to the baseline model and fitting it gives an indication of a possible contamination layer (figure 10).

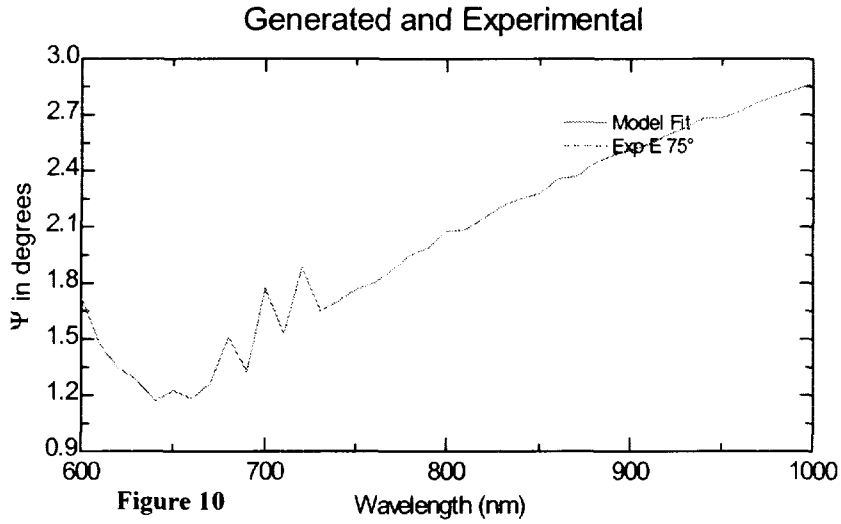

Figure 10

2	sio2	7.4504 Å
1	sio2	20.719 Å
0	si	1 mm

Table 2

So here again we have indication of a very thin layer of contamination on the witness mirror (table 2).

This type of cleanliness verification is very valuable to NASA's optical fabrication efforts. And, with the VASE ellipsometer, it is easy.

Evaluation of Cleaned Surfaces

Another service that ellipsometry has provided in the realm of precision cleaning, is an assessment of cleaning methods. Considering the instrument's precision, it may be one of the best methods available for this type of assessment.

The general procedure for a precision cleaning assessment is to baseline a set of sample surfaces (in this case, standard silicon wafers), then clean them normally with the cleaning methods of interest, and then use the ellipsometer to solve for any residue thickness. The residue thickness results from modeling the cleaned samples will allow for a comparison between methods, and the method that leaves the least amount of residue can be chosen for a particular application.

NASA's SCAT team performed a cleaned surface evaluation on several common laboratory solvents including some standard laboratory wipes and gloves. The solvents used for the study were acetone, ethanol, isopropanol, methyl-chloroform, and 1-1-2 trichloroethane.

All of the 2-inch standard silicon wafers were base-lined from a new, pristine state and then contaminated according to four types of contamination: solvent flush, solvent soak, solvent wipe, and solvent rinsed glove print. Once contaminated and stored in a new, sealed container, the samples were transferred to the ellipsometer for scanning. After scanning, the "cleaned" sample data was modeled and residue thickness was derived. A set of three wafers was averaged for each sample set.

The solvent flush contamination consisted of using three wafers per solvent and placing them on vacuum wands at roughly a 45° incline to allow for solvent run-off. Each wafer was then flushed with approximately 20-ml of solvent and allowed to dry before scanning. The following chart shows the results of the flush test after averaging (figure 11).

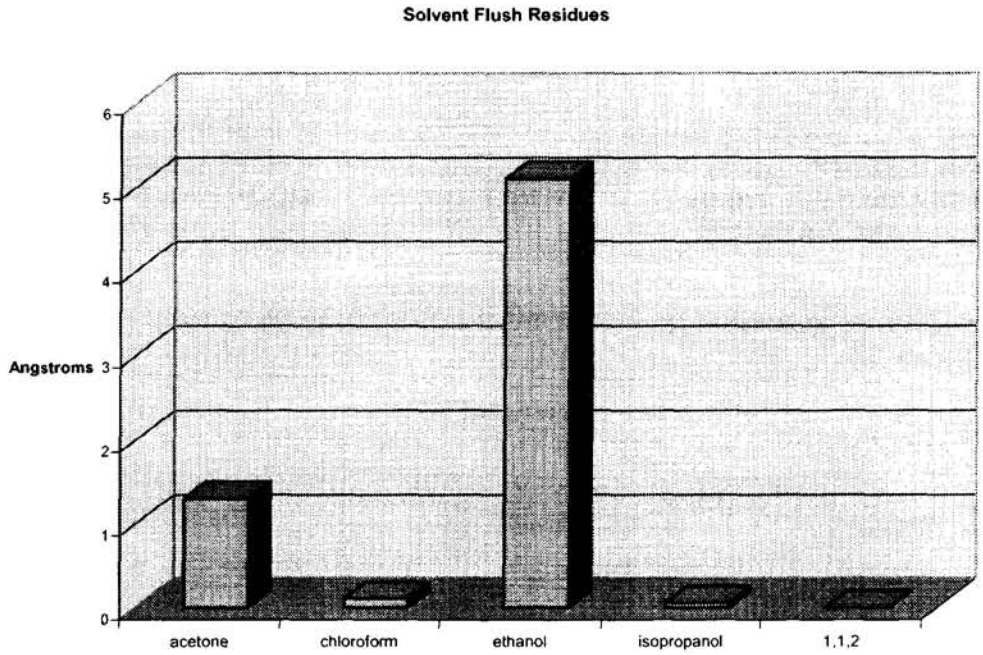

Figure 11

It is clear from the chart that ethanol leaves the greatest residue in this flush–type cleaning operation.

A similar test was used to investigate the residuals left by a soaking-type operation where the wafers were left horizontal on the vacuum wands and the solvents were allowed to evaporate after covering the wafers with solvent. The following chart illustrates these results after averaging (figure 12).

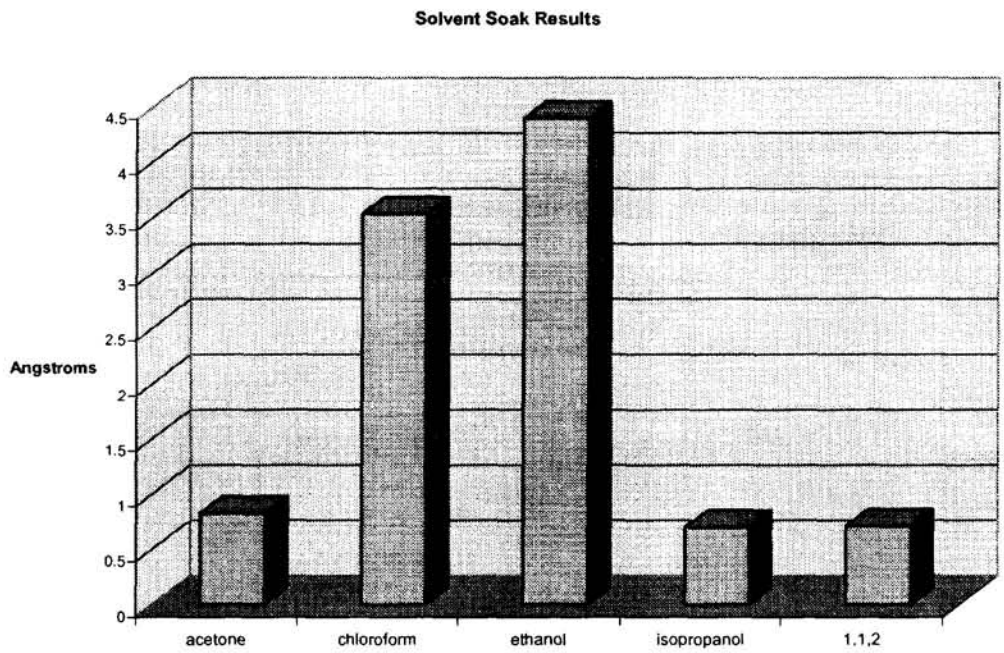

Figure 12

Here again, ethanol leaves the most residue. This is likely due to its hydroscopic nature. It is important to notice the scale of residual thickness here: Angstroms. The residues left are very thin. Residues indicating a contamination thickness of less than 3 Angstroms are more likely to actually be a change of surface quality rather than a contamination layer. However, this can still be helpful in choosing precision cleaning techniques by indicating which solvent or procedure has the least effect on the surface.

Quite frequently a laboratory or manufacturing cleaning issue needs to involve the use of a wipe. The SCAT team's study extended the investigation of the solvents to include five of the wipes that were easily found around the laboratory. The wafers were once again mounted on the vacuum wands horizontally and then wiped with a solvent impregnated wipe. The following chart shows the results of the solvents as averaged over the five wipes (figure 13).

The averages of the ellipsometric results show that, from this data, for wipe-cleaning operations in general, acetone may be the best bet.

Figure 13

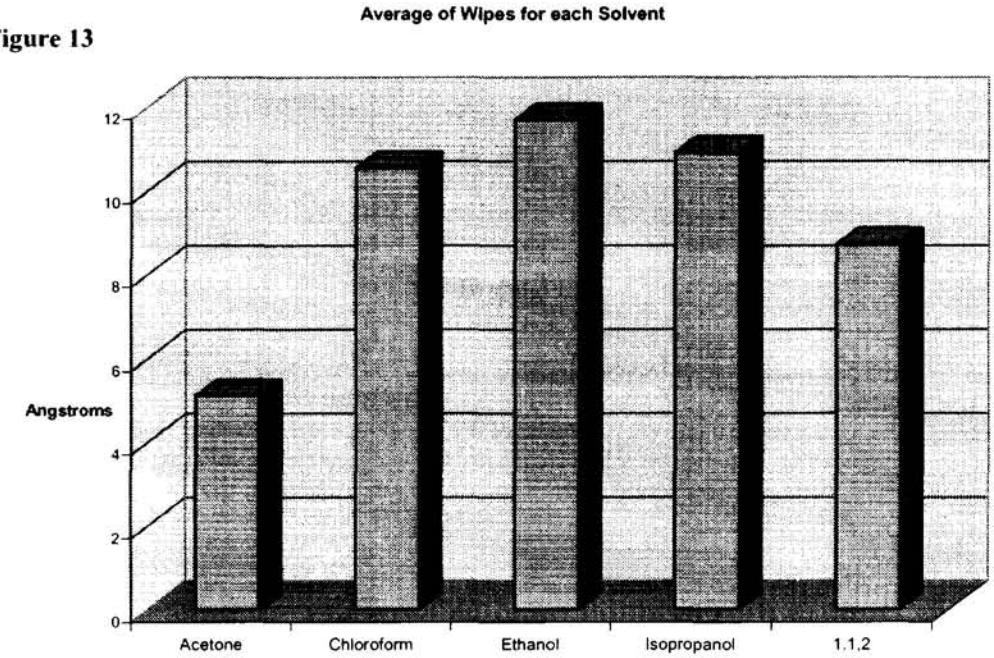

The same procedure was performed for a solvent-use-with-gloves scenario. Wherein, the gloves were rinsed with solvent for approximately 10 seconds and then a side-to-side print was applied to each wafer. Again, three wafers were averaged to obtain a single result. The following chart shows the results of the solvents when averaged over the gloves (figure 14).

From the glove results it can be seen that, if a cleaning operation is necessary where gloves are in sustained

Figure 14

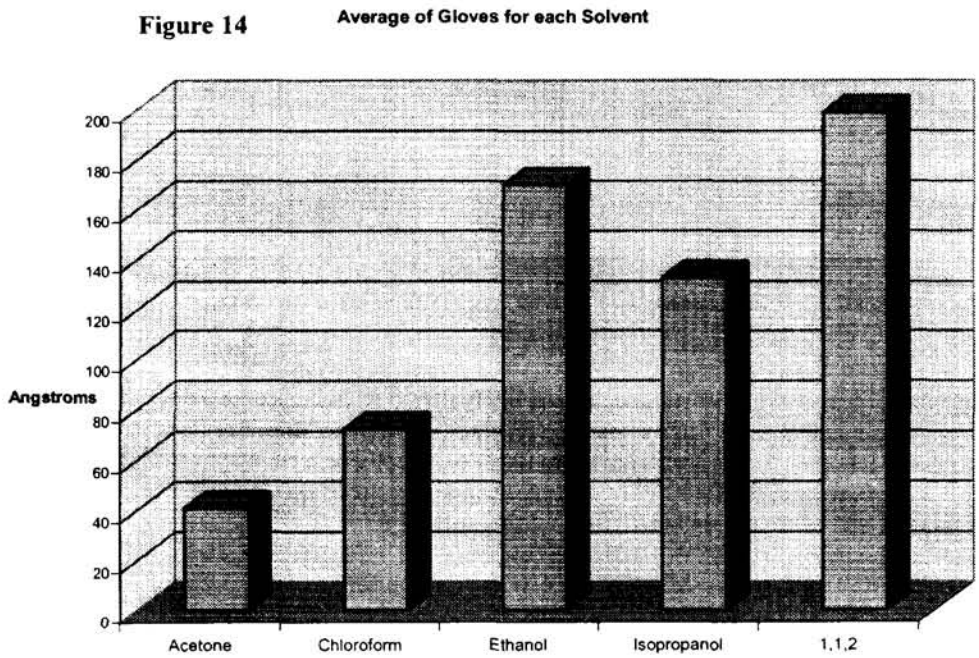

contact with solvents, then this data indicates that acetone may be the best choice again.

Conclusion

Currently in use at NASA's Marshall Space Flight Center, Space Environmental Effects Group – Surface Contamination Analysis Technology Team, Variable Angle Spectroscopic Ellipsometry offers one of the better ways to verify and evaluate surface cleanliness. It is one of the few methods that can resolve monolayer contaminants with a non-contact measurement.

P-80 / N 27

F1/3

Improved Detection Technique for Solvent Rinse Cleanliness Verification

Steven D. Hornung
Honeywell Technology Solutions Inc.
NASA Johnson Space Center
White Sands Test Facility
Las Cruces, New Mexico
(505) 524-5647
shornung@wstf.nasa.gov

Harold D. Beeson
NASA Johnson Space Center
White Sands Test Facility
Las Cruces, New Mexico
(505) 524-5542
hbeeson@wstf.nasa.gov

INTRODUCTION

The NASA White Sands Test Facility (WSTF) has an ongoing effort to reduce or eliminate usage of cleaning solvents such as CFC-113 and its replacements. These solvents are used in the final clean and cleanliness verification processes for flight and ground support hardware, especially for oxygen systems where organic contaminants can pose an ignition hazard. For the final cleanliness verification in the standard process, the equivalent of one square foot of surface area of parts is rinsed with the solvent, and the final 100 mL of the rinse is captured. The amount of nonvolatile residue (NVR) in the solvent is determined by weight after the evaporation of the solvent. An improved process of sampling this rinse, developed at WSTF, requires evaporation of less than 2 mL of the solvent to make the cleanliness verification. Small amounts of the solvent are evaporated in a clean stainless steel cup, and the cleanliness of the stainless steel cup is measured using a commercially available surface quality monitor.

The effectiveness of this new cleanliness verification technique was compared to the accepted NVR sampling procedures. Testing with known contaminants in solution, such as hydraulic fluid, fluorinated lubricants, and cutting and lubricating oils, was performed to establish a correlation between amount in solution and the process response. This report presents the approach and results and discusses the issues in establishing the surface quality monitor-based cleanliness verification.

BACKGROUND

Cleaning operations at WSTF encompass support for materials, components, propulsion test systems, and a sizeable shuttle depot activity. As part of these operations, components and piece parts are cleaned for a variety of services including oxygen, hydrogen, hydrazines, and nitrogen tetroxide. Most of these parts are constructed of stainless steel and are resistant to corrosion in aqueous media. For precision cleaned parts, the standard cleaning process consists of two major elements: an aqueous precleaning process and a solvent-based final cleaning and cleanliness verification. Cleanliness levels are specified by a number that has an associated number of particles at this maximum size in micrometers followed by a letter to specify the maximum residue allowed on 1 ft^2 of surface area. The letters A, B, C, and D refer to 1, 2, 3, and 4 mg of residue, respectively. Cleanliness levels to 50A are required for high-pressure oxygen service. Following the aqueous precleaning, the parts are dried, visually inspected, and if passed, are transferred to the Class 100 clean room. The accepted process for solvent-based final cleaning and NVR determination using HFE 7100 is shown in Figure 1. The components to be cleaned are rinsed with HFE 7100 in the vapor degreaser followed immediately by a sampling rinse of approximately 100 mL/ft^2 of component surface area. This rinse is then filtered for a particulate count and then submitted for NVR determination. The components are then blown dry with nitrogen, packaged, and labeled for use.

Figure 2 shows the steps in obtaining the NVR from the solvent rinse. First the solvent is transferred to a boiling flask, and the volume of the solvent is reduced to 10 to 15 mL by distillation. The solvent trapped in the distillation by a condenser is recycled. The remaining 10 to 15 mL is transferred to a tared weighing pan and placed in a 100 °C oven for 30 min to complete the drying. The weighing pan is allowed to cool in a desiccator before weighing again to determine the NVR. For HFE 7100, the process takes approximately 40 min. It should also be noted that some of the more volatile contaminants could be volatilized, especially during the 30 min drying in the oven. Light hydrocarbons can show 40 percent NVR recovery or less from spiked solvent samples.

An improved cleanliness verification process that replaces the current NVR procedure makes use of a commercially available surface quality monitor. This monitor measures the photocurrent produced from a sample when it is exposed to ultraviolet light. The photocurrent magnitude depends on surface characteristics. A clean metal surface will give a high photocurrent while an organic compound will give a much lower photocurrent or photoelectron yield. For example, a clean stainless steel surface will give up to 10 times the photocurrent of an organic compound. And because photoelectrons can escape from only the top few atomic layers, this measurement technique is very sensitive to thin layers of organic contaminants on metals. A photograph of the surface quality monitor (SQM) is shown in Figure 3.

APPROACH

The testing used to certify the SQM cleanliness verification process was divided into two phases: proof-of-concept testing and process validation. In the proof-of-concept phase, the feasibility of the technique was evaluated, and variables such as aliquot size, evaporation temperature, and distance from the probe were investigated to determine the optimum setting for a production test. Several different contaminants were also tested with concentrations ranging from 0.5 to 2 mg per 100 mL of solvent to determine the sensitivity and detection limit of the technique. These 100 mL solutions are analogous to the 100 mL solvent verification rinse, and it is assumed that all contaminant on a surface would be taken into solution by the solvent rinse. These solutions were mixed well upon preparation and were assumed to be a true solution rather than an emulsion. No homogenization of the solution was made before sampling with the SQM.

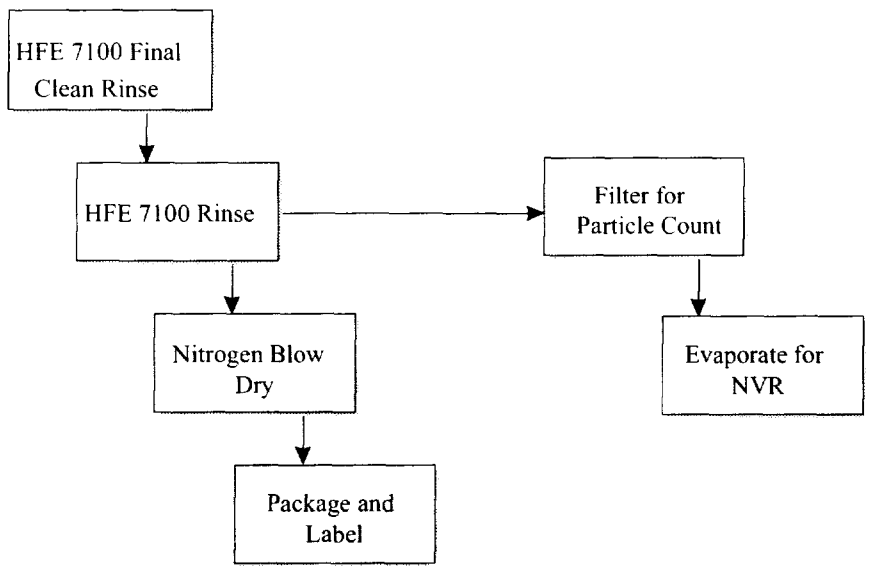

Figure 1
Solvent Final Cleaning and Verification Process

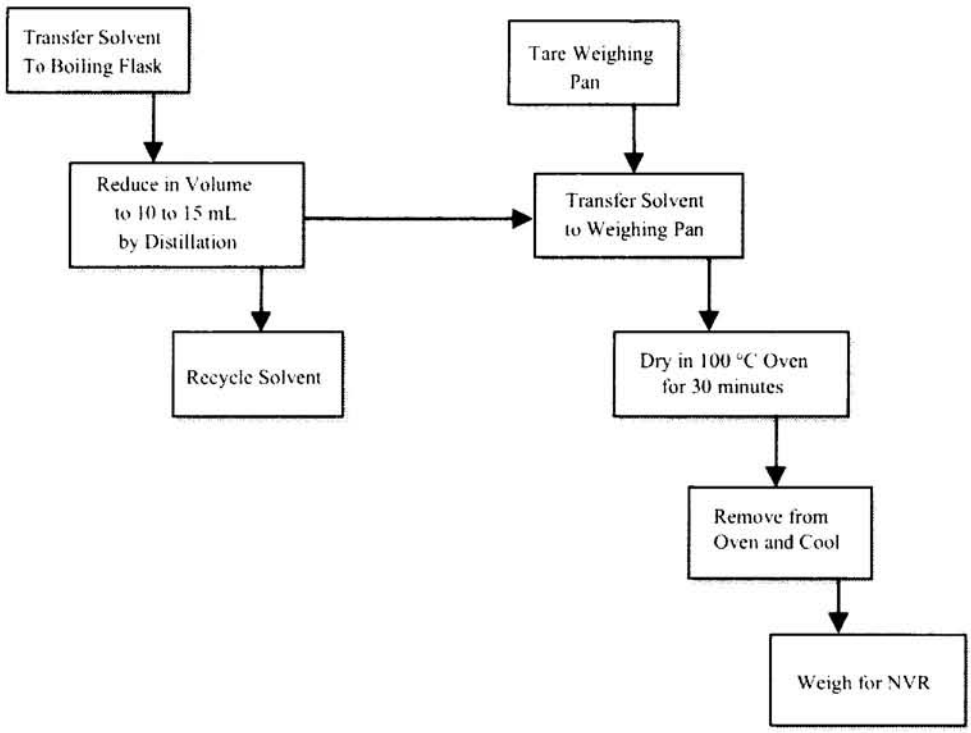

Figure 2
NVR Process for Cleanliness Verification

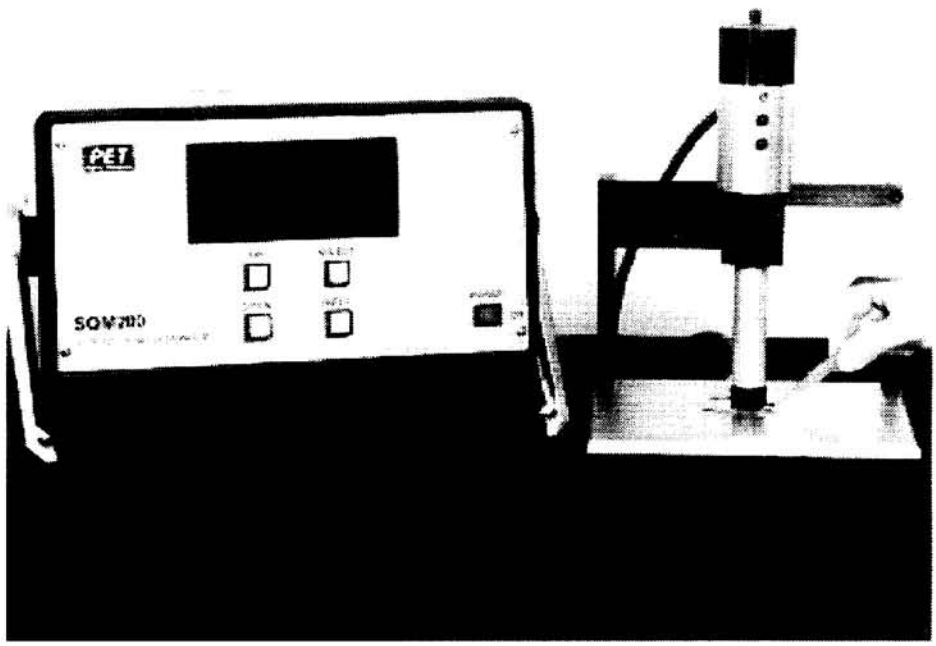

Figure 3
SQM 200 Surface Quality Monitor

Process validation was performed to determine the reliability of the process on a production scale and the frequency of false pass or false failure as compared with the standard HFE 7100 NVR. Sampling was performed on

actual cleanliness verification rinses from WSTF cleaning processes. In this parallel sampling, 2.2 mL of the 100 mL for the standard HFE 7100 NVR was removed for testing with the SQM-based technique, and the remainder was evaporated by the standard NVR technique. In addition, 40 samples of HFE 7100, spiked with selected contaminants at concentrations ranging from 0.25 to 2.0 mg/100 mL, were submitted for parallel sampling. Results from the SQM-based cleanliness verification were compared with the results from the standard NVR method.

Proof-of-Concept Testing

Proof-of-concept testing was performed to determine the response of the technique to varying levels of contaminants dissolved in HFE 7100. Test solutions were prepared by dissolving 2 mg of Krytox 240 AC or Duo Seal oil contaminant in 100 mL of HFE 7100. At least 10 tests were performed for each contaminant and concentration. First, the photocurrent was measured from a clean cup; a reading of at least 400 was required before the test could proceed. Using the same cup, a 0.3 mL aliquot of the contaminated solvent was placed in the cup. The cup was then heated to 40 °C on a hot plate until the solvent evaporated, approximately 1 min. After the cup was allowed to cool for 3 to 5 s, another measurement was taken. This process was repeated for a total of 5 doses of the contaminated HFE 7100. An illustrated procedure is shown in Appendix A.

Process Validation

Process validation was performed in parallel with the standard HFE 7100 NVR technique. The parallel sampling included 74 work orders sampled over a period of two months. When solvent rinses were submitted for the NVR determination, four doses of 0.5 mL were removed for sampling by the SQM method. The remainder of the solvent was processed by the standard NVR method.

In order to obtain a statistically significant number of samplings that produce an NVR in the measurable range, it was necessary to submit solvent samples spiked with contaminants. This was accomplished by spiking the submitted NVR with 5 mL of solvent containing 0.5 mg of a five-component contaminant mix consisting of equal amounts of Krytox, Sebacate, DC 190 silicone oil, hydraulic fluid, and Tap Magic. These were processed in the same way as the other NVR samples.

EQUIPMENT AND REAGENTS

The following equipment and reagents were used in this study. **Trademark holders are listed on the trademarks page at the front of this document.**

- Photoemission Technology, Inc., Model SQM 200 with 0.25-in. aperture
- Stainless steel sample cup, 1.9 cm diameter (0.75 in.) with 0.6 cm (0.25 in.) indentation
- 3M Brand HFE 7100
- Contaminants: Tap Magic, DC 190 silicone oil, Duo Seal pump oil, hydraulic fluid, Amflo lubricating oil, Krytox 240 AC, and di-2-ethylhexyl sebacate calibration fluid.

RESULTS AND DISCUSSION

Proof-of-Concept Testing

When HFE 7100 containing Krytox 240 AC at a concentration of 2 mg in 100 mL is used in this process, the plot shown in Figure 4 results. This is a Tukey box plot in which the box represents the range of the 25th to 75th percentiles of the data and the 10th and 90th percentiles as error bars. The mean is shown as a horizontal line in the box. The photocurrent values reported are the direct readout from the instrument and are dependent on the gain settings in the instrument. This plot of photocurrent as a function of solvent dosage shows a large initial drop followed by sequentially smaller drops in the photocurrent for a leveling off effect. This is attributed to the coverage of the clean metal surface by the contaminant, which has a lower photoelectron yield than the clean metal.

As additional doses of contaminant are added, the photocurrent drops from the high values for clean stainless steel and approaches the photocurrent for a thick film of the contaminant. Table 1 gives the measured photocurrent for very thick films of the contaminants applied to the stainless steel cups. These contaminants have much lower photoelectron yields than does clean stainless steel, making it advantageous for the detection of small amounts of these contaminants. Also, the photoelectron yields of the contaminants are all of the same order of magnitude, making the technique relatively insensitive to contaminant makeup. Regardless of the contaminant, the photocurrent will follow the same relationship. Figures 5 and 6 show a similar photocurrent versus dose curve for DuoSeal oil and DC 190 silicone oil.

For comparison, results of a set of tests using clean HFE 7100 are shown in Figure 7. This figure shows that the photocurrent drops with each sequential addition of HFE 7100. The means of the distributions show a nearly linear drop in photocurrent with successive solvent doses. This drop is still readily differentiated from those for HFE 7100 containing a contaminant. The mechanism of the photocurrent reduction by the clean solvent is unknown and will require further study.

Using Krytox and Duo Seal oils, operational parameters were optimized to produce the maximum change in signal between the clean cup and the initial dose. The volume and shape of the stainless steel cup was adjusted to hold 0.5 mL with a 0.25 in. central depression to concentrate the solution at the center of the cup as the solvent evaporates. A 0.25 in. aperture was chosen to match the central depression in the stainless steel cup where the contaminant should be concentrated upon solvent evaporation. The working distance is the closest distance that can be achieved given the variation in the height from one cup to the next. A hot plate temperature of 40 °C gave acceptable drying times, minimal contaminant loss, and is a safe temperature in case of accidental contact by the operator.

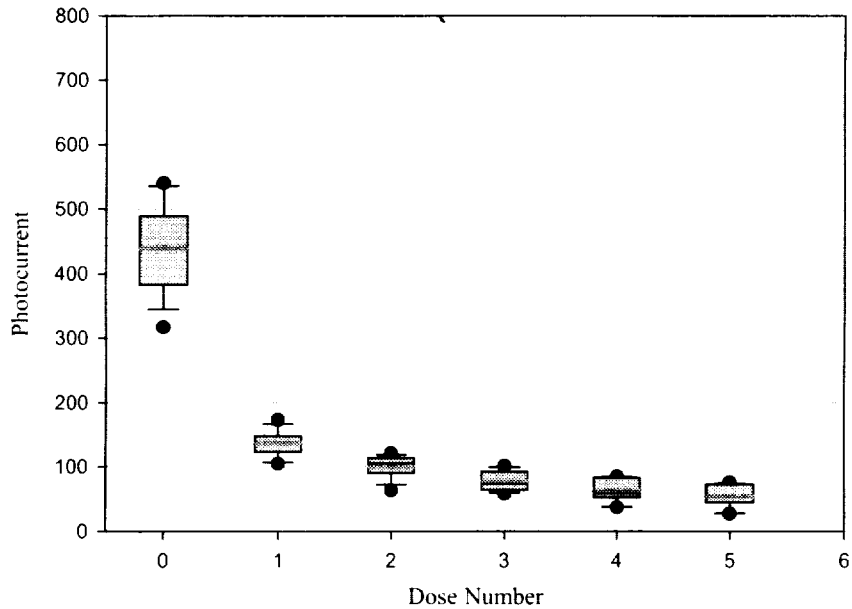

Figure 4
Photocurrent as a Function of Dose with HFE 7100 Containing 2 mg Krytox® in 100 mL

Table 1
Measured Photocurrent for Thick Films

Material	Photocurrent
WSTF Cleaned Stainless Steel 304	> 500
Duo Seal®	80
Amflo® Oil	105
DC 190® Silicone Oil	40
Hydraulic Fluid	100
Houghto Draw®	40
Tap Magic®	100
Krytox® 240 AC	60
NOTE: Instrument gain set at 1, probe gain set at 7	

Process Validation

The process validation results are shown in the box plot in Figure 8. It shows the same behavior as in the Figure 7 results from the proof-of-concept testing. Much of the range (spread, distribution) in the data is due to the variability in photocurrent in the set of clean coupons. For each cup tested, a ratio was obtained by dividing the photocurrent from a clean cup by the photocurrent from the same cup after each dose. This resulted in a tighter distribution of data for the first three doses. The resulting plot is shown in Figure 9. All 74 samples passed the standard NVR cleanliness verification with a residue of less than 0.2 mg.

The results as photocurrent and photocurrent ratio for spiked samples are shown in Figures 10 and 11. Comparing Figures 9 and 11, it is possible to distinguish between clean and spiked solvent with no overlap in the distributions by the second dose of solvent. Based on the need for no more than three doses of solvent to detect contaminants, the improved cleanliness verification process is shown in Figure 12.

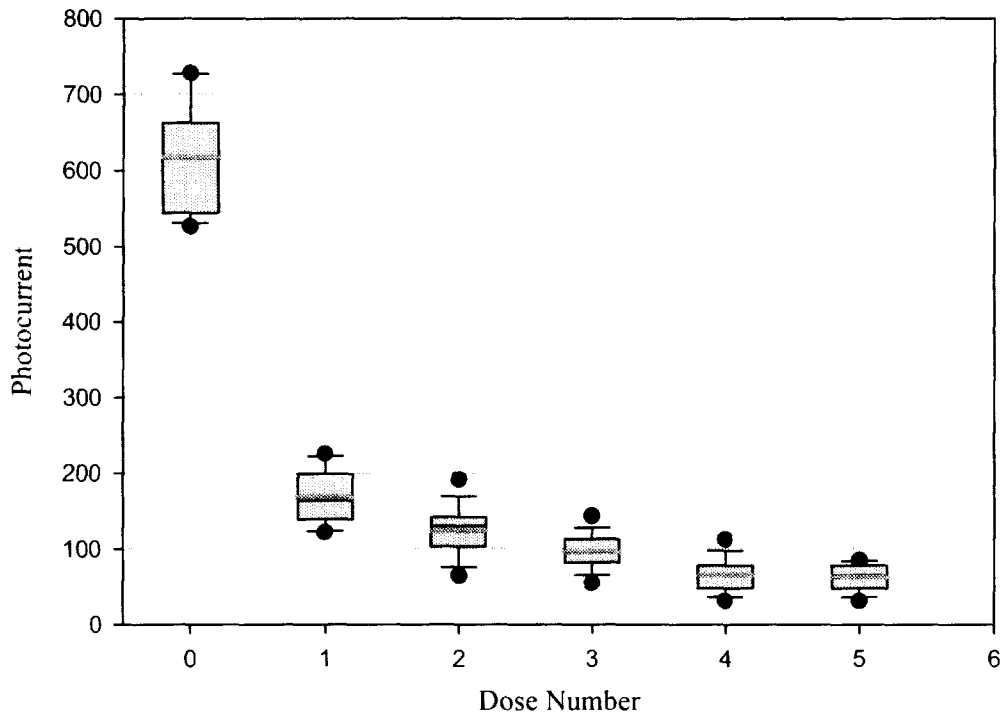

Figure 5
Photocurrent as a Function of Dose with HFE 7100 Containing 2 mg Duo Seal® in 100 mL

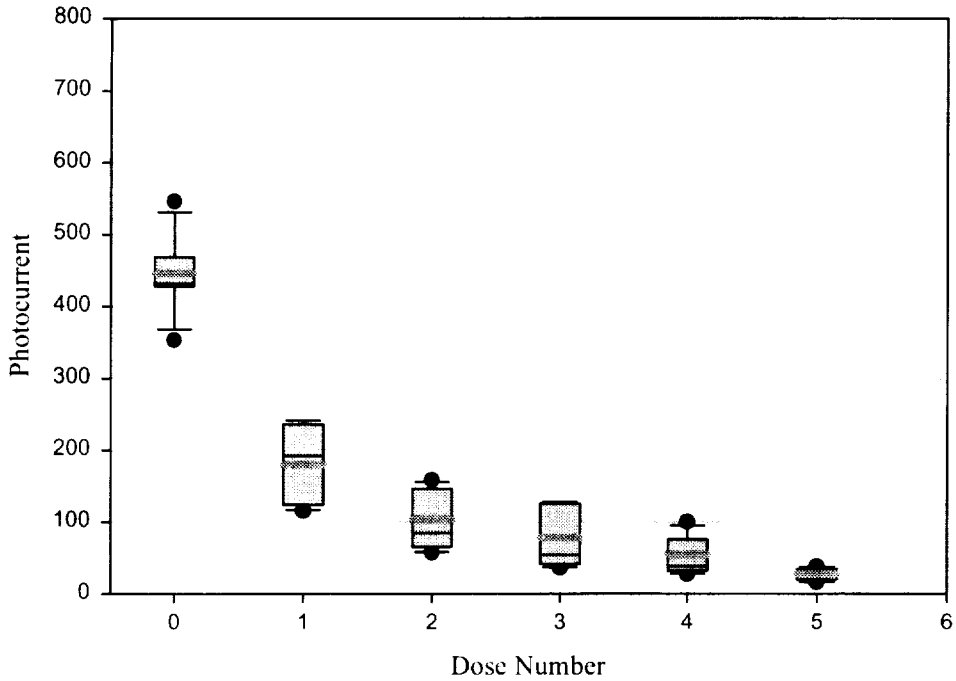

Figure 6
Photocurrent as a Function of Dose for HFE 7100
Containing 1 mg DC 190® Silicone Oil in 100 mL

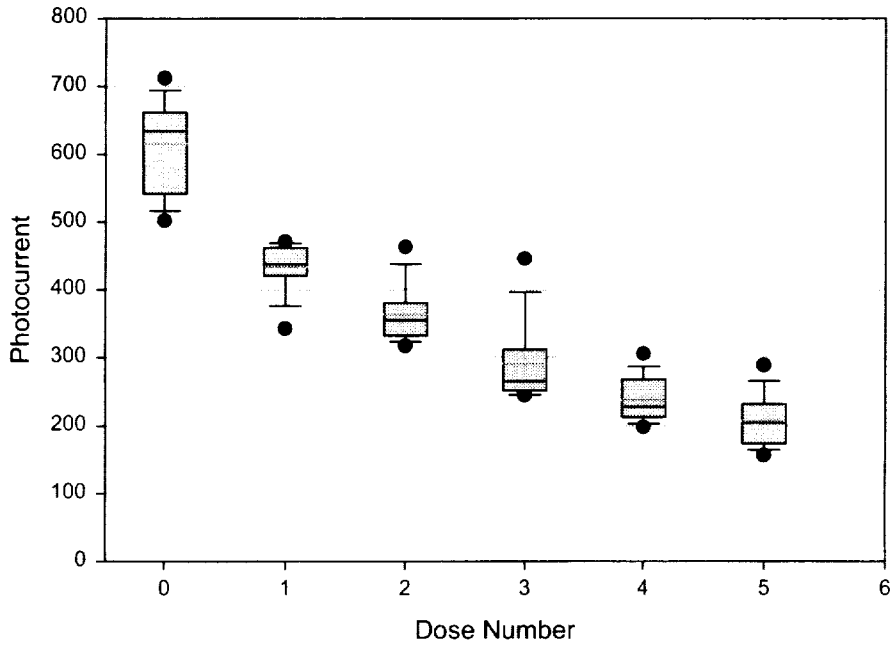

Figure 7
Photocurrent as a Function of Dose with Clean HFE 7100

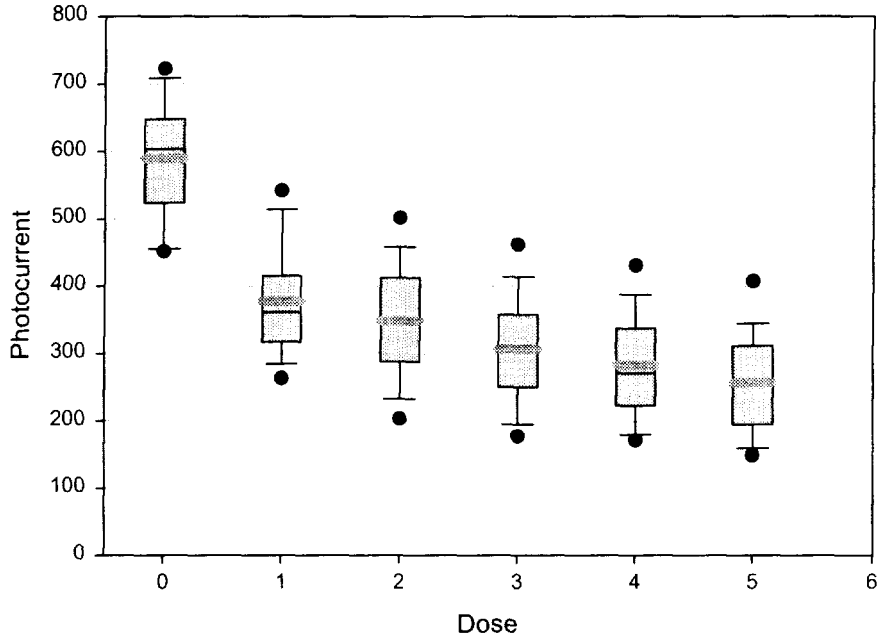

Figure 8
Photocurrent as a Function of Dose for Parallel Sampled Work Orders

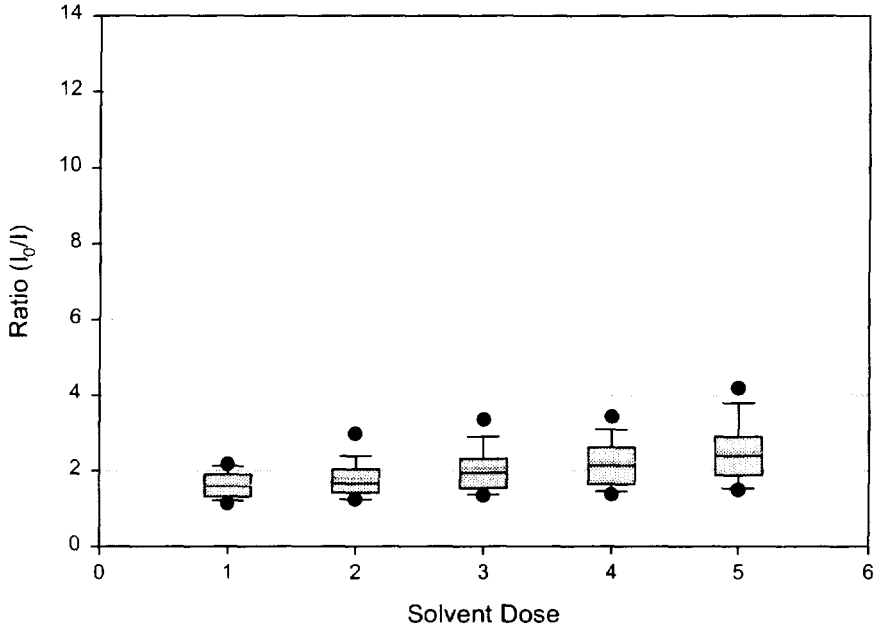

Figure 9
Photocurrent Ratio as a Function of Dose Number for Parallel Sampled Work Orders

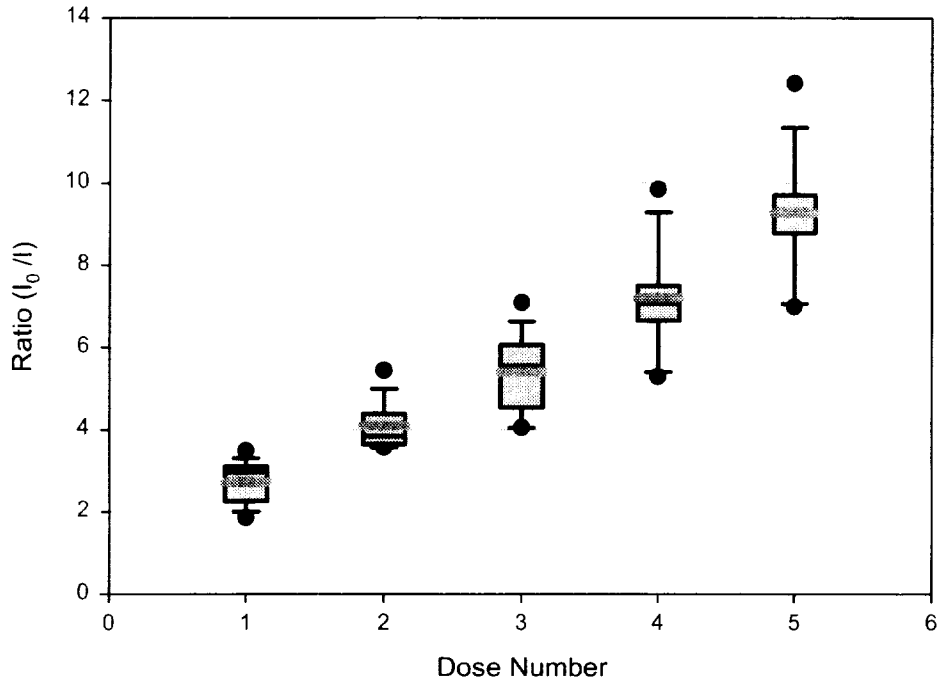

Figure 10
Photocurrent as a Function of Dose Number for HFE 7100 Samples Spiked with 0.5 mg Five-Component Mix

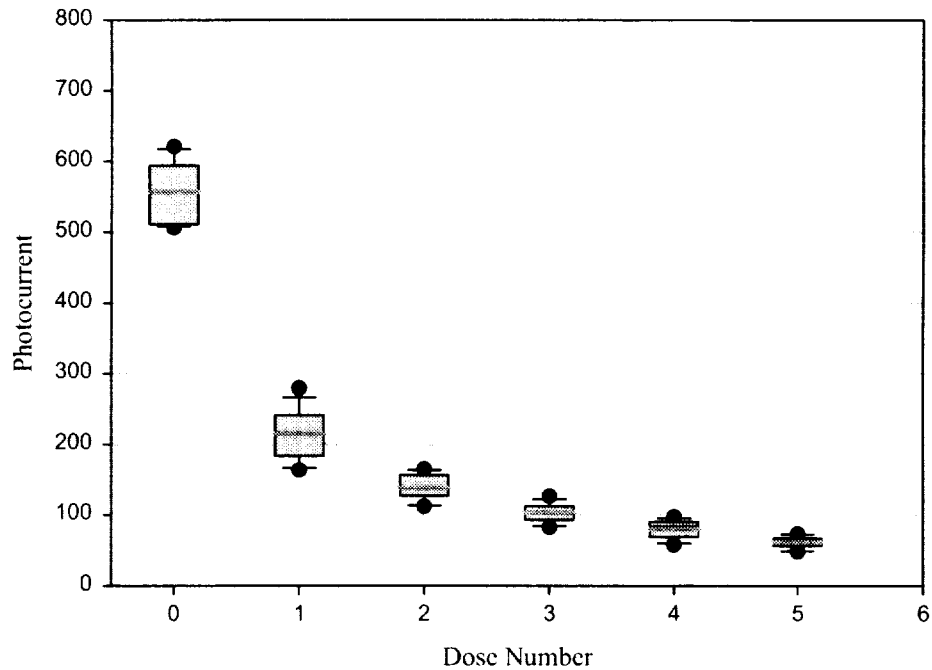

Figure 11
Photocurrent Ratio as a Function of Dose Number for HFE 7100 Samples Spiked with 0.5 mg Five-Component Mix

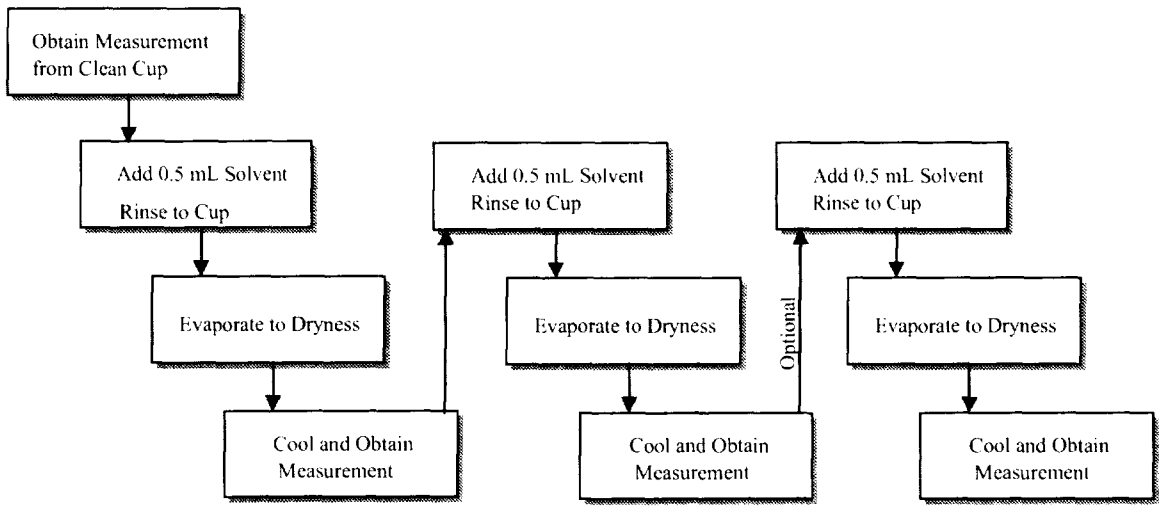

Figure 12
SQM Cleanliness Verification Process

In operation, the SQM is connected to a computer for data logging and computation. First a baseline photocurrent measurement is taken from a clean cup. The signal is averaged for 10 s. From the 100 mL rinse acquired for the NVR, a 0.5 mL aliquot is placed in the cup. The cup is then heated to 40 °C until the solvent evaporates, approximately 1 min. After the cup is allowed to cool, another measurement is taken. Using the same cup, a second sample of the HFE 7100 rinse is then processed in the same way. An optional third evaporation and measurement of the solvent can be taken if further confirmation is required.

Setting the Pass-Fail Threshold

A set of response curves for three doses of clean HFE 7100 and HFE 7100 contaminated with 0.25, 0.5, 1.0, 1.5, and 2.0 mg of the five-component mix was generated from the average of 10 replicate samplings at each concentration. These response curves are shown in Figure 13 where the average photocurrent and linear regressions are plotted for the first three doses. Figure 14 is a plot of the photocurrent ratio as a function of dose number from the same data set. These curves can be used to set a pass-fail threshold for a particular cleanliness requirement. The data may also be used to construct a calibration curve for each dose from which the contaminant amount can be determined for a given photocurrent or photocurrent ratio.

SUMMARY

- A method for cleanliness verification has been developed using the SQM 200.
- A number of contaminant responses were measured and the reponses were very nearly equal.
- By sampling the rinse solvent two or more times, the confidence in the measurement is increased.
- Because of the small amount of solvent used, retests are possible.

CONCLUSIONS

- The SQM and NVR methods are equivalent in measuring surface cleanliness.
- The SQM offers significant savings in the time required to process the NVR.
- In handling and evaporating less solvent, significant solvent savings can be realized.

REFERENCES

NASA. *Contamination Control Requirements Manual.* JHB 5322, Revision C, NASA Johnson Space Center, Houston, TX (February 1994 or latest revision).

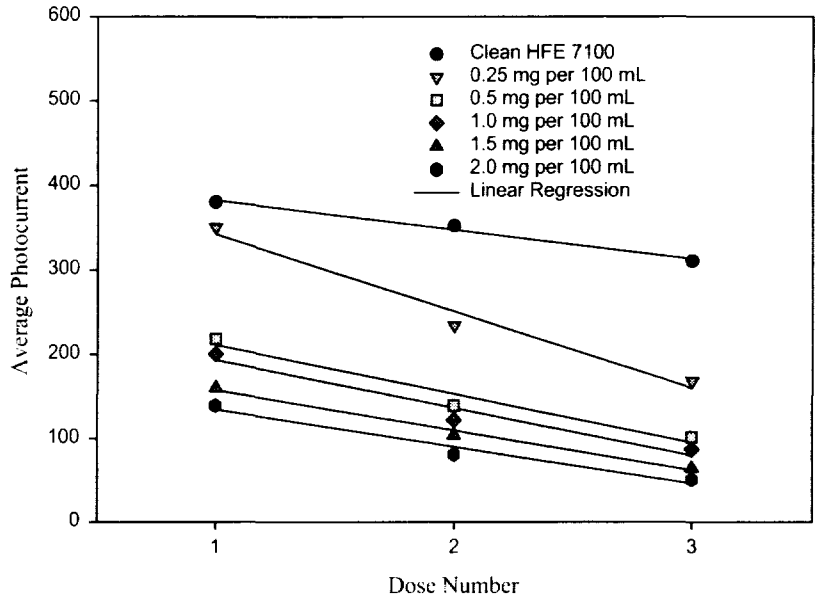

Figure 13
Average Photocurrent versus Dose Number for Clean and Spiked HFE 7100

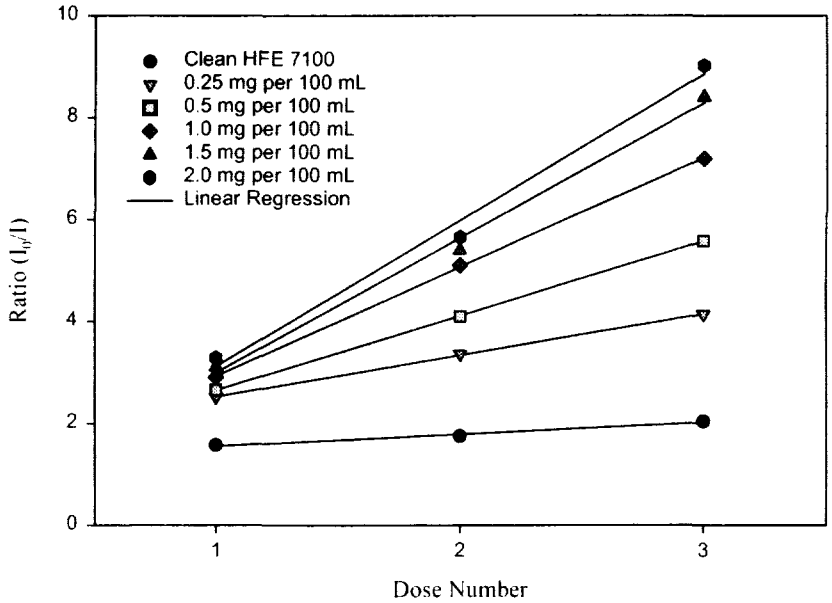

Figure 14
Photocurrent Ratio versus Dose Number for Clean and Spiked HFE 7100

Criteria for NVR Solvent Replacement

Dianne J. Coleman, Kenneth T. Luey and Joseph C. Uht
Space Materials Laboratory

and

Graham S. Arnold
Office of Research and Technology Applications
The Aerospace Corporation
El Segundo, CA 90009

Abstract

Molecular film contamination is detected and monitored using a gravimetric laboratory process described in ASTM standard methods. These processes currently specify the use of methylene chloride, an organic solvent targeted for reduction by the Environmental Protection Agency. In this paper, we describe a request for a change in the solvent specified. We briefly review the criteria for the suggested replacement, ethyl acetate. The solubility criteria assembled for the replacement of methylene chloride are then used to evaluate the replacement of methlyene chloride-based paint removers.

1.0 Introduction

The most typical and important contaminants affecting space hardware are microscopic particles and molecular films. Contamination by particles is removed using precision vacuuming or wiping with benign solvents. The cleanliness of critical surfaces can be verified by the microscopic inspection of tape lifts or witness plates. The quantitative detection of molecular films, however, involves a gravimetric laboratory process. For the measurement and diagnosis of spacecraft processing facilities, the procedure uses the exposure of witness plates and subsequent rinsing with solvents[1]. To measure nonvolatile residue (NVR) directly on surfaces, the process involves wiping with solvent-soaked cloths[2].

In ASTM E1235-95. a stainless steel witness plate is exposed to a facility environment for an extended time. In a laboratory, the plate is then rinsed with solvent. The solvent is filtered and deposited in a beaker of known tare. The solvent is then evaporated away, leaving the non-volatile residue or NVR. Initially, the solvent used for rinsing the NVR from the witness plates or from the wiping clothes was a mixture of ethyl alcohol and 1,1,1 trichloroethane. 1,1,1 trichloroethane has since been categorized a Class I Ozone Depleting Chemical (ODC). As currently written, ASTM E1235-95 specifies the use of methylene chloride (dichloromethane) as the rinsing solvent. Methylene chloride is targeted for reduction by the US Air Force under Section 313 of the federal Emergency Planning and Community Right-To-Know Act (EPCRA). EPCRA 313 requires facilities to report releases of 650 toxic chemicals to the air, water and land, as well as the quantities recycled, treated, burned or otherwise disposed of. ASTM E1235-95 itself notes:

> *Methylene chloride is toxic and is being phased out for many applications. Replacement solvents are under study and will be substituted when available. Use methylene chloride only in an exhausting work station.*

This paper is composed of three parts.

I. We document and describe an official request for a change of solvents in the ASTM E1235-95 standard process in Section 2.0.

II. We review the rationale for the choice of the replacement solvent, ethyl acetate, in Section 3.0.

III. We discuss the extension of the methylene chloride replacement criteria to the operation of paint removal in Section 4.0.

2.0 ASTM E1235-95 Request for Change

ASTM E1235-95 was due for reconsideration in the year 2000 by the Subcommittee E21.05 on Contamination. Subcommittee E21.05 is part of the ASTM Committee E-21 on Space Simulation and Application of Space Technology. The process for consideration is outlined below:

1. *ASTM subcommittee receives request, proposal and supporting data.*

   This request was made in November 1999. The supporting data and reports are summarized in the following section.

2. *Proposal and data are discussed by the committee members.*

   For ASTM E1235-95, the committee members were in general agreement that the standard solvent was in need of change. Basic agreement was obtained in this meeting of the 21.05 subcommittee.

3. *Develop a proposal for a rewritten standard.*

The proposed rewriting of the standard was developed and submitted to the E21.05 subcommittee chairman on 28 April 2000. The proposed rewrite is presented below.

TABLE 1. Proposed rewrite of ASTM E1235-95 with respect to the usage of methylene chloride and its replacement by ethyl acetate.

LINE NUMBER	CURRENT TEXT READS	PROPOSED REVISION
4.2	The plate is rinsed with a high purity methylene chloride solvent.	The plate is rinsed with high purity ethyl acetate solvent.
7.6	NVR *Solvent* consisting of HPLC (high-purity liquid chromatography) grade methylene chloride (dichloromethane). The solvent shall be certified to contain <1 ppm (<1 mg/L) NVR using the procedure in Section 10.	NVR *Solvent* consisting of HPLC (high-purity liquid chromatography) grade ethyl acetate. The solvent shall be certified to contain <1 ppm (<1 mg/L) NVR using the procedure in Section 10. Note: Burdick & Jackson cat. No. 100, B&J Brand Ethyl Acetate has been found to be satisfactory
NOTE 5	Methylene chloride is toxic[17] and is being phased out for many applications. Replacement solvents are under study and will be substituted when available. Use methylene chloride only in the exhausting work station (6.3).	Ethyl acetate[17] is an organic solvent, and as such, presents some degree of physical and health hazard. Use of ethyl acetate should be according to the recommendations provided in the Material Safety Data Sheet
Footnote 17	Material Safety Data Sheet No. 310, Genium Publishing Corp., 145 Catalyn St., Schenectady, N.Y. 12303.	Material Safety Data Sheet No. 437, Genium Publishing Corp., 145 Catalyn St., Schenectady, N.Y. 12303.
10.2	The NVR of each bottle shall be determined upon opening in accordance with **10.3**.	*Typo*: The NVR of each bottle shall be determined upon opening in accordance with **10.7**.
10.4.1	Methylene chloride can be toxic. Handle with caution and observe appropriate precautions.	Handle ethyl acetate with caution and observe appropriate precautions.
11.2.1	Methylene chloride can be toxic. Handle with caution and observe appropriate precautions.	Handle ethyl acetate with caution and observe appropriate precautions.

Note the typo in the current standard in Section 10.2, erroneously referring to Section 10.3.

4. *This proposal will be reformatted as needed by the E21.05 subcommittee chairman.*
The proposal is currently at this point in the process.

5. *A final vote will conclude the process.*

We note here as well that ASTM E1560M-95 "Standard Test Method for Gravimetric Determination of Nonvolatile Residue from Cleanroom Wipers" specifies an NVR solvent consisting of three parts 1,1,1 trichloroethane and one part ethanol, by volume. As noted earlier, 1,1,1 trichloroethane has been denoted a Class 1 ODC. The NVR solvent designated in E1560 will also have to be modified at a future time.

3.0 Replacement Rationale

In this section we briefly review the rationale for the replacement of methylene chloride.

In work performed by Arnold and Uht[3], potential solvent replacements were evaluated using a literature review of solvent properties together with a laboratory testing approach. The goal of the effort was not to find the best solvent for removing a particular NVR, but rather to maintain a connection with heritage results. A suitable "drop in" replacement therefore would have properties closely matched to methylene chloride and the NVR mixture of 1,1,1 trichloroethane and ethanol. In addition, certain other properties would also play a key role in the evaluation. The vapor pressure would play a key role since the solvent needs to remain on the surface long enough to perform an effective wiping test. However, one would not want a solvent with too low a vapor pressure such that the evaporation step in the NVR tests would take an unreasonably long time. The results of most NVR tests are desired in 24 – 48 hours. The replacement solvent would need to be readily available from more than one source. Ideally, it would be available routinely having a low level of impurities. It would have suitable safety, toxicity and flammability properties and, of course, would be environmentally acceptable. All of these properties were evaluated to develop a "score" for a large number of replacement candidates.

In this paper, we focus on the solvent properties. Solvent properties are described successfully beginning with the cohesive energy density, c, given by

$$c = -U/V \qquad (1)$$

where U is the molar cohesive energy and V is the molar volume and where the units of c are the same as pressure. The Hildebrand parameter is given by

$$\delta = c^{1/2} \qquad (2)$$

δ has units of $(MPa)^{1/2}$. According to Barton [4], two materials with similar values of δ gain energy on mutual dispersion to permit mixing. On the other hand, a material with a high value of δ requires higher energy for dispersal than can be obtained from a material with smaller δ and immiscibility results. These statements are similar to the rule-of-thumb often stated that "like dissolves like."

Solvent properties are now successfully described using multi-component parameters such as the three-component Hansen parameters shown in Equation 3.

$$\delta^2_t = \delta^2_d + \delta^2_p + \delta^2_h \qquad (3)$$

where δ_d describes dispersion forces, δ_p describes the polar forces and δ_h corresponds to hydrogen bonding. The total Hansen parameter, δ_t, is equivalent to the Hildebrand parameter.

The replacement of methylene chloride or 1,1,1 trichloroethane begins by identifying those solvents with a similar δ_t. The results of that study are shown in Figure 1. Note in Figure 1 that several solvents have very large δ_t values, among them the solvents Freon 113 and methanol. However, the key is to identify those solvents that have the greatest similarity to methylene chloride and 1,1,1 trichloroethane, whose values of δ_t are between 18.5 and 20.5.

The suitable candidates are methyl isobutyl ketone, n-butyl acetate, methyl acetate, ethyl acetate, and tetrahydrofuran.

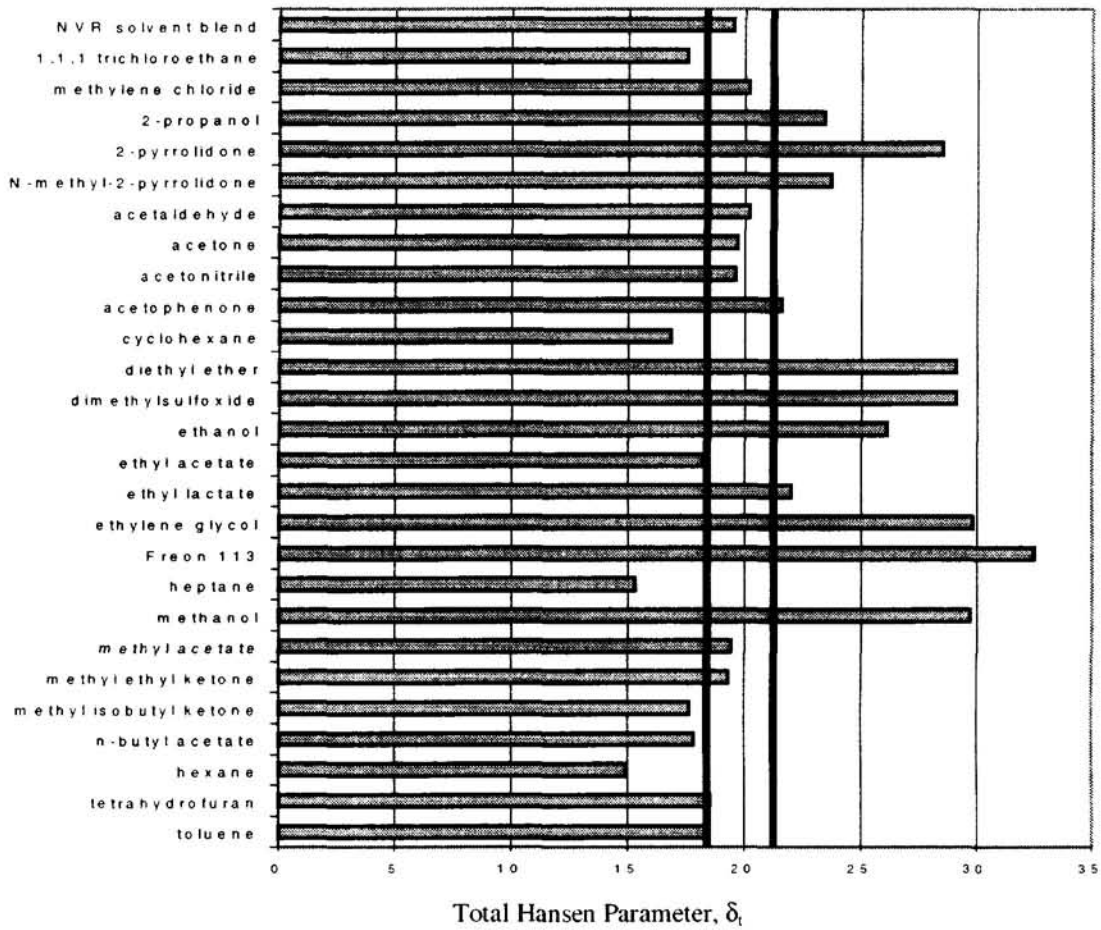

Figure 1. Solvent rankings based on total Hansen solubility parameter, δ_t. The desired replacement solvent for methylene chloride (dichloromethane) lies between 18 amd 20.5 as indicated by heavy black lines.

For a three-component "vector" quantity such as the total Hansen parameter, the vector difference between, say, methylene chloride and any other solvent, designated by *i*, can be defined.

$$d^{MC}_i = [(\delta_{dMC}-\delta_{di})^2+(\delta_{pMC}-\delta_{pi})^2+(\delta_{hMC}-\delta_{hi})^2]^{1/2} \qquad (4)$$

where the vector difference d is made up of the individual differences between the dispersive, polar and hydrogen bonding characteristics of methylene chloride and any other solvent. Though several solvents might have a total Hansen parameter near that of methylene chloride, ethyl acetate has the smallest vector difference. That is, ethyl acetate has the smallest difference between each of the forces: dispersive, polar and hydrogen bonding.

As stated previously, the vapor pressure plays a practical role in the selection of a replacement solvent. A solvent with a high vapor pressure reduces the residence time on the tested surface in a wiping test. A solvent with a low vapor pressure would extend the duration of the evaporation step in either of the NVR tests. Therefore, one seeks a solvent of moderate vapor pressure. Arnold and Uht indicated that diethyl ether would be as high a vapor pressure solvent as one would want to handle and ranks one step above methylene chloride. Isopropyl alcohol (2-propanol) was suggested as the lowest vapor pressure solvent. Ethyl acetate is near the low end of the vapor pressure scale, but higher than that of 2-propanol.

Three figures of merit were examined concerning the flammability and toxicity hazards: the threshold limit value (TLV); the inhalation hazard ratio (IHR); and the "Flash Point." The TLV represents the hazardous exposure level to the material given in ppm. The IHR is the ratio of the saturated vapor concentration at 25°C to the TLV. So-called open cup (OC) and closed cup (CC) flash point measurements give the temperature at which a solvent can be ignited by a hot wire. OC measurements address the possibility of ignition in an open environment as would occur in a spill, while CC tests address the ignition in closed container. Since all potential replacements were both volatile and flammable, the flash point data were not given significant weight in the scoring.

Table 2. Flammability and toxicity assessment for various NVR solvent replacement candidates from Reference 3.

Solvent	Flash Point	TLV, ppm	Inhalation Ratio	Comments
1,1,1 trichloroethane	None	350	451	Class 1 ODC
2-propanol	12	400	140	
2-pyrrolidone	110			No TLV Data
Acetone	-19	750	386	
Aetonitrile	6	40	2888	
Cyclohexane	-18	300	396	
Diethyl ether	-45	400	1806	
Dimethysulfoxide	88			Skin Penetrant, no TLV
Ethanol	12	1000	74	
Ethyl acetate	-4	400	288	
Ethyl lactate	49			No TLV data
Ethylene glycol	111	50	3	
Freon 113	48	1000	434	Class 1 ODC
Heptane	-4	400	141	
Hexane	-22	50	3816	
Methanol	11		796	
Methyl acetate	-16	200	1375	
Methyl ethyl ketone	-6	200	630	EPA 17*
Methylene chloride	None	50	11184	Carcinogen, EPA 17*
n-butyl acetate	22	150	112	
n-methyl-2-pyrrolidone	86			No TLV data
Tetrahydrofuran	-14	200	1086	Explosive hazard in distillation
Toluene	4	50	703	EPA 17*

*"EPA 17" refers to the voluntary reduced emissions of 17 chemicals as part of the EPA's Hazardous Air Pollutant Strategic Implementation Plan.

Most of the candidate solvents are seen to have a higher TLV and lower IHR than methylene chloride, warranting the toxic warnings concerning methylene chloride in the ASTM E1235-95. The exceptions are acetonitrile, with a TLV of 40 ppm versus 50 ppm for methylene chloride.

A series of experimental results was conducted to evaluate the effectiveness of ethyl acetate compared to methylene chloride for use as an NVR solvent. The first test involved stainless steel witness plates exposed for one month in a machine shop environment. They were then bagged together for about three months. The results of subsequent ASTM E1235 testing are shown in Table 3. The agreement is very good.

Table 3. ASTM E1235 test results using methylene chloride and ethyl acetate solvents.

	Methylene Chloride	**Ethyl Acetate**
Sample Mass (g)	0.00093	0.00147
Blank (g)	0.00029	0.00072
NVR Mass (g)	0.00064	0.00075

A series of tests were performed in which known amounts of contaminants were deposited on stainless steel witness plates having one square foot area. The witness plates were then rinsed with solvents to recover the deposited contaminant. The percent contaminant recovered, R_c, is given by:

$$R_c = (m_r - m_b)/m_c \times 100 \qquad (5)$$

Where m_r is the contaminant mass recovered, m_b is mass of the solvent blank and m_c is the known mass of the deposited contaminant. The results for one of the contaminants, tetraphenyl dimethyl disiloxane, a typical represntative of silicones, are shown in Figure 2. Ethyl acetate and methylene chloride are equally effective in removing this contaminant. Methyl acetate is not recommended due to its high vapor pressure and toxicity.

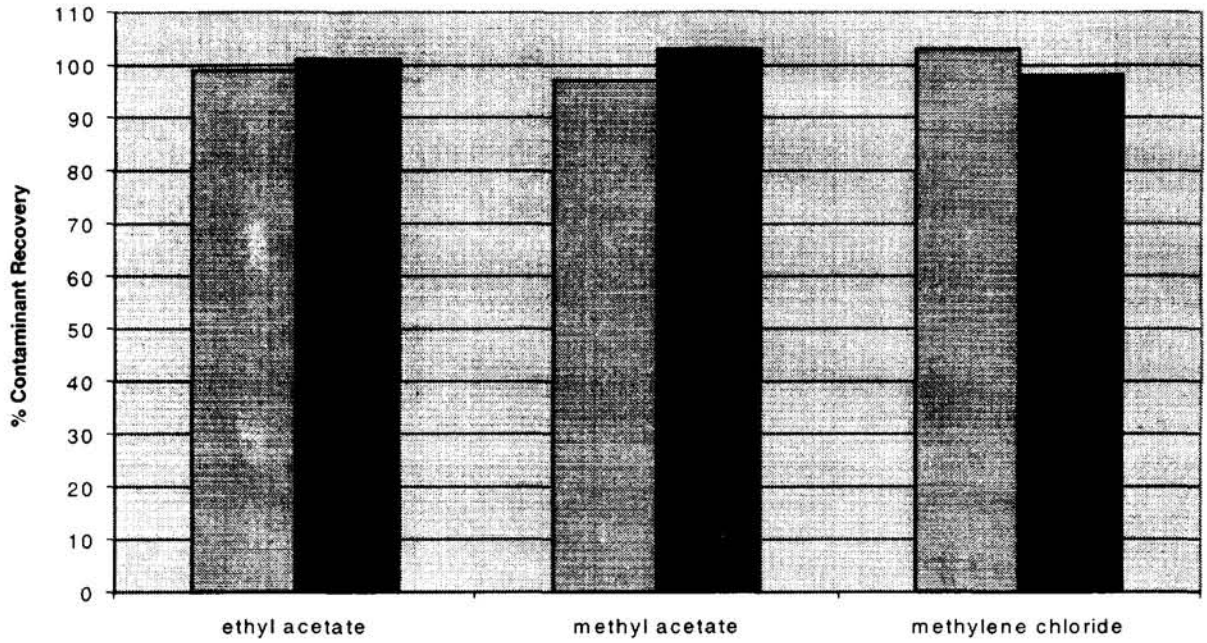

Figure 2. Percent recovery of deposited tetraphenyl dimethyl disiloxane from witness plates using three different solvents.

4.0 Application to Paint Removal

Methylene chloride is used extensively as a paint remover and the search for replacements is vigorous. Paint removal is performed frequently in the aircraft and aerospace industries and a signficant amount of methylene chloride is used for this purpose. As part of the effort to remove hazardous air polluting (HAP) chemicals from DoD processes, an examination was made of solubility parameters as a means of identifying replacements for methylene chloride–based paint removers or strippers.

Paint removal and NVR solvent replacements have similarities and differences. A suitable NVR solvent replacement did not consider specific chemical interactions between solvent and NVR. It was not desired that the solvent replacement remove more NVR than the 1,1,1-trichloroethane/ethanol blend. Rather, the intent was to find a replacement most like the blend. Solubility parameters were therefore an ideal focus, since only the vector differences of the solvents were compared.

The paint removal process can be more complicated than an NVR test. The choice of a paint remover requires the optimization of many steps. It is generally understood that paint stripper solutions must remain on painted surfaces for a long time. In most aircraft paint removal applications the soak time can be 6 – 12 hours. Paint removal solutions containing methylene chloride use a gel or other type of "sealant" to enhance the methlyene chloride residence time on the surface, since methylene chloride has a relatively high vapor pressure. For many

methylene chloride-based paint removers, more than one application is recommended. The methylene chloride must diffuse through multiple layers of paint before reaching the primer and then will cause separation and swelling of the paint from the primer. The solvent must then affect the bond between metal and primer. The solvent must also not damage the underlying metal. References to the actual dissolving of paint by methlyene chloride are difficult to find in the aircraft paint industry but are sometimes referred to in the art restoration area.

Table 4 presents a full listing of the dispersive, polar, hydrogen bonding and total Hansen solubility parameters for the solvents considered as the replacement in the NVR test[4]. The far right column also gives the molecular dipole moment in Debye measured in the gas phase[5]. Dipole moments measured in the liquid phase are also shown and are indicated in parentheses. Dipole moments measured in the liquid phase are described in [5] as less reliable.

Table 4. Hansen parameters and gas phase dipole moments for solvents. Dipole moments in parentheses are measured in the liquid phase.

Solvent	Dispersive	Polar	Hydrogen Bonding	Total	Dipole Moment
Toluene	16.4	8	1.6	18.3	0.36
Tetrahydrofuran	13.3	11	6.7	18.5	1.63
Hexane	14.9	0.0	0.0	14.9	0.00
n-butyl acetate	14.5	7.8	6.8	17.8	(1.9)
Methyl ethyl ketone	14.1	9.3	9.5	19.3	2.50
Methyl acetate	13.3	9.5	10.4	19.4	1.72
Methanol	15.1	12.3	22.3	29.6	1.70
Heptane	15.3	0.0	0.0	15.3	0.00
Ethylene glycol	17	11	26	32.9	2.28
Ethyl acetate	15.8	5.3	7.2	18.1	1.78
Ethanol	12.6	11.2	20	26.1	1.69
Dimethylsulfoxide	18.4	16.4	10.2	26.7	4.49
Diethyl ether	12.4	12.3	23.3	29.1	1.15
Cyclohexane	16.5	3.1	0.0	16.8	0.00
Acetonitrile	10.3	11.1	19.6	24.8	3.92
Acetone	15.5	10.4	7	20	2.88
N-methyl-2-pyrrolidone	16.5	10.4	13.5	23.7	2.66
2-pyrrolidone	19.4	17.4	11.3	28.4	(3.5)
2-propanol	14	9.8	16	23.4	1.66
Methylene Chloride	13.4	11.7	9.6	20.2	1.60
1,1,1-trichloroethane	17	4.3	2.1	17.7	1.78
Average	15.0	9.2	10.6	22.0	1.8
Median	15.1	10.4	9.6	20	1.7

Table 4 shows that methylene chloride does not lie in an extreme range of the parameters. Its values for the three Hansen parameters are very near both the average and median values for the solvents listed. Similarly, its dipole moment is less than the average and median values. It is therefore not strikingly obvious why methylene chloride should be in wide use as a paint remover based on solubility.

By once again using the rule-of-thumb that "like dissolves like," we performed an analysis of solubility parameters and their vector differences for a number of polymeric coatings and solvents. A collection of solubility data for several polymeric coatings was obtained from the literature[6] and is shown in Table 5. This particular collection of polymer coatings was assembled by Burke and includes a radius of interaction, R. R is a measure of how similar a solvent must be in order to dissolve the polymer and is determined empirically.

Table 5. Hansen solubility parameters and interaction radius for several polymer coatings compiled by Burke.

Polymer/Coating	Dispersive	Polar	Hydrogen Bonding	Interaction Radius
Cellulose acetate	18.6	12.7	11	7.6
Chlorinated polypropylene	20.3	6.3	5.4	10.6
Epoxy	20.4	12	11.5	12.7
Isoprene elastomer	16.6	1.4	-0.8	9.6
Cellulose nitrate	15.4	14.7	8.8	11.5
Polyamide, thermoplastic	17.4	-1.9	14.9	9.6
Poly(isobutylene)	14.5	2.5	4.7	12.7
Poly(ethylmethacrylate)	17.6	9.7	4	10.6
Poly(methyl methacrylate)	18.6	10.5	7.5	8.6
Polystyrene	21.3	5.8	4.3	12.7
Poly(vinyl acetate)	20.9	11.3	9.6	13.7
Poly (vinyl butyral)	18.6	4.4	13	10.6
Poly (vinyl chloride)	18.2	7.5	8.3	3.5
Saturated polyester	21.5	14.9	12.3	16.8
Average	18.6	8.0	8.2	
Median	18.6	8.6	8.55	

Like Eq. (4), Burke defines a vector solubility "distance" between solvent and polymer, $D_{S\text{-}P}$ given by:

$$D_{S\text{-}P} = [4(\delta_{dS}-\delta_{dP})^2+(\delta_{pS}-\delta_{pP})^2+(\delta_{hS}-\delta_{hP})^2]^{1/2} \qquad (5)$$

Where δ_{iS} and δ_{iP} are the three Hansen parameters (i=d, dispersive; p, polar; and h, hydrogen) for the solvent and polymer, respectively. $D_{S\text{-}P}$ differs from Eq. (4) by the leading factor of 4 for the dispersive term. It is included to create a spherical "solubility volume." The results of the comparison are shown in Table 6. The designation "Yes" indicates that the vector difference $D_{S\text{-}P}$ is less than R, and the solvent and polymer are therefore closely enough alike that the solvent will dissolve the polymer. These polymer coatings are not necessarily paints, although some paints might contain certain percentages of these polymers in their formulations.

Table 6. Solubility of polymer coatings compiled by Burke[4] in solvents compiled by Arnold and Uht[3].

Solvent / Polymer/Coating	Methhylene Chloride	Toluene	Tetra- -hydrofuran	Hexane	MEK	Cyclo- Hexane	2-pyrro- Lidone	Ethanol
Cellulose acetate	No	No	No	No	No	No	Yes	No
Chlorinated polypropylene	No	Yes	No	No	No	Yes	No	No
Epoxy	No	No	No	No	No	No	Yes	No
Isoprene elastomer	No	Yes	No	Yes	No	Yes	No	No
Cellulose nitrate	Yes	Yes	Yes	No	Yes	No	Yes	No
Polyamide, thermoplastic	No	No	No	No	No	No	No	No
Poly(isobutylene)	Yes	Yes	Yes	Yes	Yes	Yes	No	No
Poly(ethylmethacrylate)	Yes	Yes	Yes	No	Yes	Yes	No	No
Poly(methyl methacrylate)	No	Yes	No	No	No	No	Yes	No
Polystyrene	No	Yes	No	No	No	Yes	No	No
Poly(vinyl acetate)	No	Yes	No	No	Yes	No	Yes	No
Poly (vinyl butyral)	No	No	No	No	Yes	No	No	No
Poly (vinyl chloride)	No	No	No	No	No	No	No	No
Saturated polyester	Yes	Yes	No	No	Yes	No	Yes	No
Number Dissolved	**4**	**9**	**3**	**2**	**6**	**5**	**6**	**0**

Table 6. Continued

Polymer/Coating \ Solvent	Methanol	Ethyl Acetate	Diethyl Ether	DMSO	N-methyl-2-pyrrolidone	Acetone	Ethylene Glycol
Cellulose acetate	No	No	No	No	Yes	No	No
Chlorinated polypropylene	No	Yes	No	No	No	Yes	No
Epoxy	No	Yes	No	Yes	Yes	Yes	No
Isoprene elastomer	No	Yes	No	No	No	No	No
Cellulose nitrate	No	Yes	No	Yes	Yes	Yes	No
Polyamide, thermoplastic	No	No	No	No	No	No	No
Poly(isobutylene)	No	Yes	No	No	Yes	Yes	No
Poly(ethylmethacrylate)	No	Yes	No	Yes	Yes	Yes	No
Poly(methyl methacrylate)	No	Yes	No	Yes	Yes	Yes	No
Polystyrene	No	Yes	No	No	No	Yes	No
Poly(vinyl acetate)	No	Yes	No	Yes	Yes	Yes	No
Poly (vinyl butyral)	No	Yes	No	No	Yes	Yes	No
Poly (vinyl chloride)	No	No	No	No	No	No	No
Saturated polyester	Yes	Yes	No	Yes	Yes	Yes	Yes
Number Dissolved	**1**	**11**	**0**	**6**	**9**	**10**	**1**

Within this group of coatings, we see that methylene chloride does appear to be only a moderate dissolver of polymer coatings. Other solvents that dissolve more than five polymers in the group, including toluene, MEK, N-methyl-2-pyrrolidone, 2-pyrrolidone and acetone, are frequently mentioned as cosolvents with methylene chloride in commercial paint removers. On the other hand, tetrahydrofuran and methanol are also frequently mentioned as cosolvents with methylene chloride but are not indicated by this analysis. The success of ethyl acetate as a dissolver of a wide range of polymers is both surprising and disturbing, as ethyl acetate is now being used to measure NVR on some painted surfaces. So far, there have been no reports of painted surfaces being damaged by the NVR test. Laboratory testing of this and other solvents on painted surfaces would be valuable and is planned.

This study addresses the solubility aspects of paint removal. However, it is generally believed that solubility plays a minor role in the large-scale paint removal from aircraft surfaces. It is thought that the diffusion of molecules through many paint coats and the subsequent interaction with the substrate-polymer bond is more significant. The chemical interaction with this bond is not well quantified and is, so far, a subject that is studied experimentally. More specialized, lower-volume paint removal applications, such as art restoration, are more concerned with the ability of solvents to actually dissolve polymers. There is also no rate information contained in the above analysis. Thus, it could prove that ethyl acetate did indeed dissolve painted surfaces during an NVR test, but at such a slow rate that it would not have been noticed, nor would appreciable amounts of dissolved polymer be found in the non-volatile residue.

5.0 Summary and Conclusions

As part of DoD campaigns to reduce the use of hazardous polluting materials, an effort has been made to identify and reduce the use of methylene chloride, among other materials. In previous work, a literature study of solubility parameters was used to determine a substitute for methylene chloride used as a solvent in ASTM and DoD tests for nonvolatile residue. Ethyl acetate was identified as the best replacement based primarily on the solubility parameter analysis. The results of toxicity and flammability analyses and a modest laboratory test program also contributed to this choice of a replacement solvent.

This year, a formal request was made to the ASTM E21.05 subcommittee to change the specified solvent from methylene chloride to ethyl acetate in ASTM E1235-95 "Standard Test Method for Gravimetric Determination of Non-Volatile Residue in Environmentally Controlled Areas for Spacecraft." A proposed rewriting of ASTM E1235-95 has been submitted and is now being formatted in preparation for a final vote.

The solvent solubility data were used to evaluate the replacement of methylene chloride in the paint removal application. It was found that a much more detailed understanding of the paint removal mechanism is needed than for the NVR test process, and on the basis of solubility, methylene chloride itself is not identified as a good solvent of polymers. Rather, it is thought that methylene chloride has small molar volume and therefore diffuses well through many coats of paint. Several known additives to methylene chloride in commercial paint

removers are identified by their solubility parameters. These include toluene, MEK, tetrahydrofuran, N-methyl-2-pyrrolidone, 2-pyrrolidone and acetone. Methanol, however, which is probably the most common cosolvent with methylene chloride in paint removers, is not identified on the basis of solubility parameters. The results of this analysis show that, in addition to a more mechanistic understanding of paint removal, a supplementary laboratory testing program is essential to finding replacements.

Acknowledgments

The authors gratefully acknowledge valuable technical discussions with Dr. Gidget K. Ternet.

Funding for this work was provided by Air Force Materiel Command (AFMC) through a Pollution Prevention project initiative. The work was done under Air Force contract No. F04701-93-C-0094. The authors would like to acknowledge Mr. Dan Pilson, Project Manager, SMC/AXFV and Dr. Valerie Lang, Office of the Corporate Engineer, The Aerospace Corporation, for their support and administration of this effort.

References

1. *Standard Test Method for Gravimetric Determination of Non-Volatile Residue in Environmentally Controlled Areas for Spacecraft*, ASTM E 1235-95, Vol. 15.03 Space Simulation; Aerospace and Aircraft; High Modulus Fibers and Composites

2. E. N. Borson, E. J. Watts and G. A. To, "Standard Method for Measurement of Nonvolatile Residue on Surfaces", SD-TR-89-63 or TR-0089 (4530-02)-1, The Aerospace Corporation, El Segundo, CA, 10 August 1989. The evaluation of NVR from the cloths is discussed in, *Standard Test Method for Gravimetric Determination of Nonvolatile Residue from Cleanroom Wipers*, ASTM E 1560M.

3. G. S. Arnold and J. C. Uht, "Nonvolatile Residue Solvent Replacement," TR-95(5448)-1, The Aerospace Corporation, 01 March 1995

4. A. F. M. Barton, CRC Handbook of Solubility Parameters and Other Cohesion Parameters, CRC Press, Boca Raton, FL, 1983.

5. CRC Handbook of Chemistry and Physics, 80th Edition, R. C. Weast, ed, CRC Press, Boca Raton, FL, 1999.

6. J. Burke, "Solubility Parameters: Theory and Application," AIC Book and Paper Group, (**3**), 1984, pp. 13-56.

Critical Surface Cleaning and Verification Alternatives

By
Donald M. Melton
Lockheed Martin, Michoud Operations
13800 Old Gentilly Rd
New Orleans, La. 70129
504-257-1782

Abstract

As a result of federal and state requirements, historical critical cleaning and verification solvents such as Freon 113, Freon TMC, and Trichloroethylene (TCE) are either highly regulated or no longer available. Interim replacements such as HCFC 225 have been qualified, however toxicity and future phase-out regulations necessitate long term solutions.

The scope of this project was to qualify a safe and environmentally compliant LOX surface verification alternative to Freon 113, TCE and HCFC 225. The main effort was focused on initiating the evaluation and qualification of HCFC 225G as an alternate LOX verification solvent. The project was scoped in FY 99/00 to perform LOX compatibility, cleaning efficiency and qualification on flight hardware.

Introduction

HCFC 225G, is a cleaning solvent that is an environmentally compatible alternative for HCFC 225 in the areas of metal cleaning, vapor degreasing, and flushing. The major difference between HCFC 225 and HCFC 225G is that HCFC 225G is a single component (3,3-Dichloropentafluoropropane), while HCFC 225 is a two component system (3,3-Dichloropentafluoropropane and 1,3-Dichloropentafluoropropane). By removing the 1,3 isomer HCFC 225G is less toxic than the HCFC 225 product. The respective Threshold Limit Values (TLV) are 250 ppm versus 25 ppm.

Body

A) LOX Compatibility Evaluation of HCFC 225G

The technical approach was to evaluate HCFC 225G for LOX mechanical impact sensitivity testing with liquid oxygen by the procedure outlined in NHB 8060/NASA STD-6001 Test 13 Part #1.

Duplicate lots of Freon 113, HCFC 225G, and HCFC 225 were tested per NHB8060.1B/NASA-STD-6001, test 13A, at Marshall Space Flight Center (MSFC) for LOX compatibility. All solvents submitted passed LOX compatibility tests, as shown in Table 1.

Table 1 LOX Compatibility Test Results

MATERIAL	LOT	TESTS	RESULTS
HCFC 225G	59704211	0/20	PASSED
Freon 113	N/A	0/20	PASSED
HCFC 225	3114	0/20	PASSED

B) HCFC 225G Cleaning Efficiency

The technical approach to evaluate HCFC 225G cleaning efficiency was by applying E.T. contaminants to 2219 Al test panels. Gravimetric analysis was performed in order to determine the percent removal cleaning efficiency for each of the respective contaminants.

The evaluation of the HCFC 225G consisted of preparing Al-2219 test panels for three (3) of the most common E.T. contaminants (J-414 Tape Residue, Safe Tap and CRC 2-26). The respective test panels were weighed before and after the contamination process with each of the respective E. T. contaminants. HCFC 225G was flushed onto the contaminated surface with a controlled stream of 500 mL of solvent from a pressurized vessel that emulated the current process. The test panels were flushed from top to bottom to insure contact with the entire contaminated surface. After flushing, each test panel was placed in a desiccator for 24 hours and then weighed to a constant weight. A percent (%) cleaning efficiency was calculated for each solvent and its respective test panels as shown in Table 2 through 4. Based upon the overall percent removal cleaning efficiency of the three major E.T. contaminants, HCFC 225G cleaning solvent was recommended for additional qualification testing on flight hardware.

Table 2
HCFC 225G Cleaning Efficiency of Safe-Tap Drilling Lubricant

PANEL #:	INITIAL WT.	CONT. Panel Wt.	CONT.	CLEANED WT.	AMT. REMOVED	% CL. EFF
S1	139.107	139.116	0.009	139.108	0.008	88.89
S2	138.542	138.549	0.007	138.541	0.008	114.29
S3	138.164	138.170	0.006	138.164	0.006	100.00
S4	139.914	139.921	0.007	139.913	0.008	114.29
S5	139.085	139.091	0.006	139.085	0.006	100.00
S6	139.537	139.547	0.010	139.537	0.010	100.00
S7	139.889	139.898	0.009	139.889	0.009	100.00
S8	139.593	139.601	0.008	139.592	0.009	112.50
S9	139.531	139.538	0.007	139.530	0.008	114.29
S10	138.939	138.945	0.006	138.938	0.007	116.67
					Average	106.09

Table 3
HCFC 225G Cleaning Efficiency of CRC 2-26 Hydrocarbon Oil

PANEL #:	INITIAL WT.	CONT. Panel Wt.	Cont.	CLEANED WT.	AMT. REMOVED	% CL. EFF
C1	138.974	138.997	0.023	138.975	0.022	95.65
C2	138.753	138.775	0.022	138.753	0.022	100.00
C3	138.818	138.830	0.012	138.817	0.013	108.33
C4	139.110	139.140	0.030	139.11	0.030	100.00
C5	139.520	139.548	0.028	139.52	0.028	100.00
C6	138.587	138.602	0.015	138.586	0.016	106.67
C7	139.653	139.672	0.019	139.653	0.019	100.00
C8	139.285	139.304	0.019	139.286	0.018	94.74
C9	138.406	138.423	0.017	138.406	0.017	100.00
C10	139.773	139.805	0.032	139.771	0.034	106.25
					AVERAGE	101.16

Table 4
HCFC 225G Cleaning Efficiency of J-414 Tape Residue

PANEL #:	INITIAL WT.	CONT. Panel Wt.	Cont.	CLEANED WT.	AMT. REMOVED	% CL. EFF
T1	139.441	139.448	0.007	139.442	0.006	85.71
T2	139.936	139.94	0.004	139.936	0.004	100.00
T3	139.193	139.196	0.003	139.194	0.002	66.67
T4	139.922	139.925	0.003	139.923	0.002	66.67
T5	139.816	139.818	0.002	139.817	0.001	50.00
T6	139.300	139.305	0.005	139.301	0.004	80.00
T7	139.831	139.839	0.008	139.834	0.005	62.50
T8	140.236	140.243	0.007	140.239	0.004	57.14
T9	139.052	139.154	0.102	139.048	0.106	103.92
T10	140.061	140.066	0.005	140.062	0.004	80.00
					Average	75.26

HCFC 225G performed better than Freon 113 (PCA) as a cleaning solvent replacement for HCFC 225. HCFC 225 is the current implemented replacement for Freon 113 (PCA). Percent (%) cleaning efficiency comparative results are listed in Table 5. Therefore a qualification plan was established to compare Freon 113 (PCA) and HCFC 225 to HCFC 225G as baselines for all replacement solvent.

Table 5
Percent (%) Cleaning Efficiency Comparative Results

Contaminant	Solvent	Average % Efficiency
CRC 2-26 Oil	Freon 113	98.4
	HCFC 225	91.8
	HCFC 225G	101.0
Safe Tap	Freon 113	64.7
	HCFC 225	96.6
	HCFC 225G	106.0
J-414	Freon 113	61.3
	HCFC 225	31.5
	HCFC 225G	75.2

C) Perform Qualification of HCFC 225G as an Alternative Cleaning Solvent for HCFC 225

The technical approach to support qualification was to evaluate replacement solvent cleaning ability on the following flight and non-flight items:

20 ft LOX feedline (80971028425-010)
LH Clean Kit (80924061028M900)
Tube Assembly (80923021036-050)
Mask Tool (non-flight), T31K2026

The plan consisted of cleaning flight hardware per Marshall Space Flight Center specification MSFC-SPEC-164B or C and process instruction (PI) 5008. Four (4) representatives of flight hardware were selected to evaluate using HCFC 225G per NASA's operational directive (99/OD/0571).

The flight hardware cleaning evaluation consisted of flushing metallic flight hardware with HCFC 225G by the clean-room operators, upon completion an NVR sample was taken and analyzed. After each cleaning and NVR verification with HCFC 225G, an NVR verification sample (500 mL) of the hardware was immediately taken using HCFC 225 and analyzed to insure that the removal of the organic production contamination had been accomplished with HCFC 225G. Two (2) tube assemblies were evaluated in FY 00. The results are shown in Table 6.

Table 6
Flight Hardware Qualification Results

Flight Hardware	Solvent	MG/FT2
Tube Assembly	HCFC 225G	1.5
	HCFC 225	0.7
Tube Assembly	HCFC 225G	1.6
	HCFC 225	0.7

The results in Table 6 indicate HCFC 225G removed the contamination to an acceptable level of 1 mg/ft2. The outstanding flight hardware qualification items will be evaluated in FY 00. In summary HCFC 225G is an excellent cleaning and verification solvent for common External Tank contaminates.

CP/533/IN/26

F2

FIRST

EFFECTS OF CRYOGENIC TREATMENT ON THE RESIDUAL STRESS AND MECHANICAL PROPERTIES OF AN AEROSPACE ALUMINUM ALLOY

by

Po Chen
IIT Research Institute
Building 4612, Marshall Space Flight Center
George C. Marshall Space Flight Center, AL 35812
(256) 544-4171 (pchen@iitri.org)

Tina Malone
National Aeronautics and Space Administration
Building 4612, Marshall Space Flight Center
George C. Marshall Space Flight Center, AL 35812
(256) 544-2593 (tina.malone@msfc.nasa.gov)

Robert Bond
IIT Research Institute
Building 4612, Marshall Space Flight Center
George C. Marshall Space Flight Center, AL 35812
(256) 544-8277 (rbond@iitri.org)

Pablo Torres
National Aeronautics and Space Administration
Building 4612, Marshall Space Flight Center
George C. Marshall Space Flight Center, AL 35812
(256) 544-2616 (pablo.d.torres@msfc.nasa.gov)

ABSTRACT

Investigators at Marshall Space Flight Center (MSFC) are studying the potential benefits of cryogenic treatment for aerospace Aluminum (Al) alloys. This paper reports the effects of cryogenic treatment on residual stress, tensile strength, hardness, fatigue life, and stress corrosion cracking (SCC) resistance.

INTRODUCTION

Al alloys have long been of interest to the aerospace community, due to their modest specific strength, ease of manufacture, and low cost. Fusion welding is a common method of joining these alloys. However, such techniques can generate defects and high residual stresses. Defects are detected with standard nondestructive evaluation (NDE) techniques. However, residual stresses may generate cracks following proof testing, adding significant costs and schedule delays as repair, inspection, and proof cycles must be repeated.

Methods are continually being sought to improve the weldability of Al alloys for aerospace applications. At MSFC, attempts are being made to determine how cryogenic treatment affects residual stress, tensile strength, hardness, high cycle fatigue (HCF), and SCC resistance. Reports published in the United States and Europe suggest that cryogenic treatment may have the potential to relieve residual stress without sacrificing tensile strength. Treating tool steels at a low temperature near -320 °F (-196 °C) may result in improved mechanical properties, wear resistance, dimensional stability, and tool life.[1,2] Recent claims have also been made that cryogenic treatment can improve the material properties of copper, high-temperature alloys, carbides, plastics, and composite materials.[3-5]

TECHNICAL APPROACH

Cryogenic treatment was applied to an Al alloy that had already been heat treated or welded, as follows:

- Slowly cool without thermal shock to approximately -300 °F (-184 °C).
- Hold at approximately -300 °F (-184 °C) for 24 hours.
- Reheat slowly without thermal shock to ambient temperature.

Test temperatures were reduced from ambient to –300 °F (–184 °C) using liquid nitrogen (LN_2) to significantly slow atomic and molecular activity in the material. Slow temperature changes cause thermal compression and expansion to occur equally from the core to the surface, releasing residual stresses and homogeneously stabilizing the alloy. This process may take 48 hours or longer to keep the entire mass in equilibrium throughout temperature cycling.

EXPERIMENTAL PROCEDURES

This study used rolled plates with a thickness of 1.85 inch (4.7 cm). The material was solutionized and stretched 3% at ambient temperature. Variable Polarity Plasma Arc (VPPA) welding was conducted with the weld bead perpendicular to the rolling direction. As-welded and cryogenically treated weld specimens were then prepared to allow comparison of test results. Residual stress was measured before and after cryogenic treatment. The Bragg law states:

$$n\lambda = 2d\sin\theta$$

where n is an angle denoting the order of diffraction, λ is the x-ray wavelength, d is the lattice spacing of crystal planes, and θ is the diffraction angle. These measurements allow the residual stress state to be evaluated. Here, the X-ray diffraction method was used to calculate the d spacing by measuring the shift of reflected angle θ.

Tensile tests were performed at ambient temperature using round specimens. SCC specimens were tested in the short transverse (ST) orientation at 50% and 75% of yield strength. Three specimens were tested for each condition in a 3.5% NaCl alternate immersion solution per ASTM G44. Unstressed specimens were removed for tensile testing after exposures of various durations.

RESULTS & DISCUSSION

- **Residual Stress Analysis**

As-welded specimens contained significant amounts of residual stress near the fusion line in the heat affected zone (HAZ). Cryogenically treated specimens showed residual stress reductions of up to 12 ksi in the HAZ. Figure 1 shows no significant changes in the weld bead, fusion line, or parent metal.

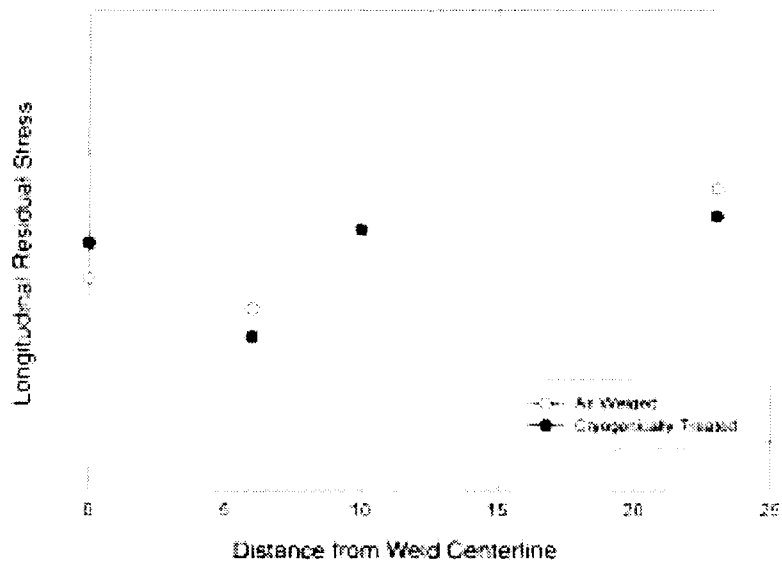

Figure 1. Longitudinal residual stress distribution across a VPPA welded panel

Figure 2 indicates that residual stress was reduced by up to 9 ksi when cryogenic treatment was conducted prior to artificial aging for the rolled plate.

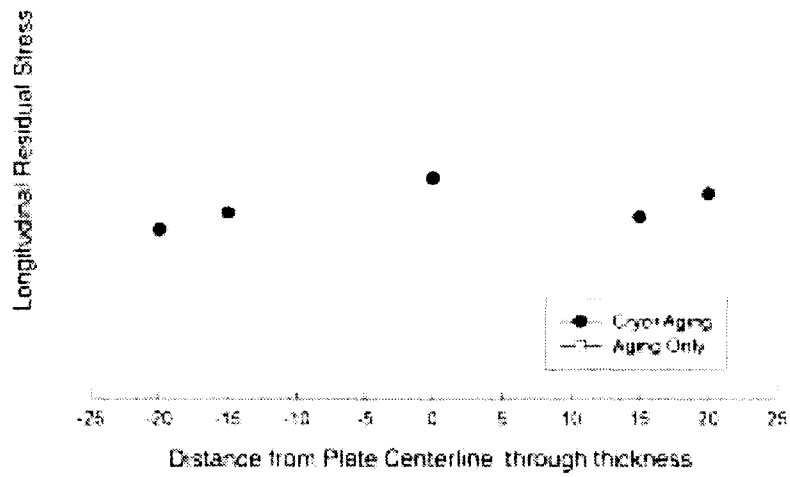

Figure 2. Residual stress profiles for rolled plate with a thickness of 1.85 inch (4.7 cm), with and without cryogenic treatment

- **Tensile and Hardness Tests**

Average hardness increased for parent metal that was artificially aged and then subjected to cryogenic treatment. No significant differences were seen in tensile strength for as-welded and cryogenically treated specimens.

- **High Cycle Fatigue (HCF) Tests**

HCF testing was performed at ambient temperature for as-welded and cryogenically treated specimens. Figure 3 indicates that no noticeable improvements were seen in cryogenically treated specimens.

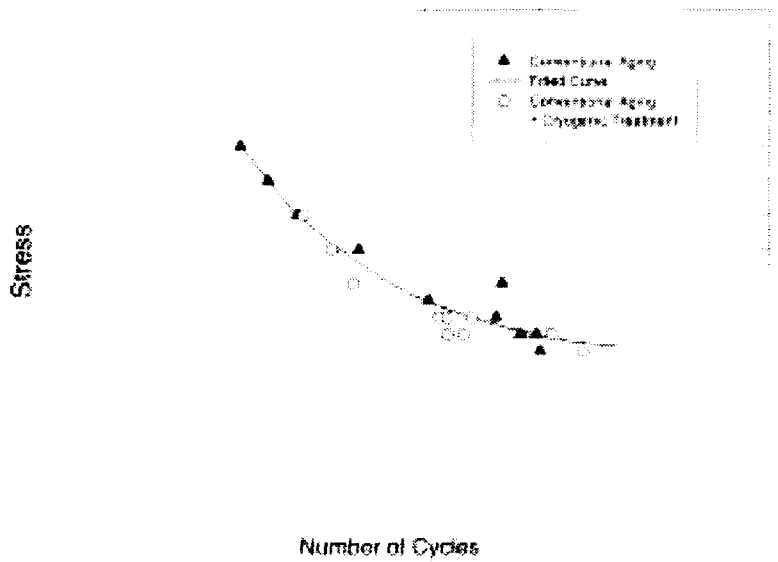

Figure 3. HCF strength

- **Stress Corrosion Cracking (SCC) Tests**

Table 3 shows significant improvements in SCC lives for cryogenically treated specimens.

Table 3 - Stress Corrosion Results for Weld Specimens

Specimen Condition	Stress Level (%YS)	Failure Ratio	Highest Residual Stress in HAZ	Days to Failure
As-welded	50	1/3	23.9 ksi	65
	75	2/3		3, 6
Cryogenically treated	50	0/3	12.2 ksi	--
	75	2/3		22, 84

CONCLUSIONS

The following results were observed for this particular Al alloy after cryogenic treatment:

1. Residual stress was reduced by up to 12 ksi in the HAZ of weld specimens and by up to 9 ksi in parent metal.
2. Significant improvements in SCC performance were seen for weld specimens.
3. Minor increases in tensile strength and hardness were noted for parent metal.
4. No significant changes were found in tensile properties for weld specimens or in fatigue properties for parent metal.

REFERENCES

1. Collins, D.N. "Cryogenic Treatment of Tool Steels," *Advanced Materials & Processes*, 154: 6 (December 1998): 23-27.
2. Kamody, D.J. "Using Deep Cryogenic to Advantage," *Advanced Materials & Processes*, 154:4 (October 1998): 215-218.
3. Gary, J. "A Review of Deep Cryogenic Treatment of Steel." Spring 1999. Department of Mechanical Engineering, University of Texas at Austin. <http://ccwf.cc.utexas.edu/~jwgary/cryo/title.html>. Accessed April 1999.
4. Gillin, J.P. "Cryogenically Treated Electrical Contacts." US Patent No. 5442929, 1995.
5. Brunson, R.W. "300 Below, Inc." Home page. <www.300below.com>. Accessed April 1999.

Toughness of Ultra High Strength AF1410 Type Steels

Luana E. Iorio and Warren M. Garrison Jr.
Department of Materials Science and Engineering
Carnegie Mellon University
Pittsburgh, PA 15213
412-268-3593; wmg@andrew.cmu.edu

1. Introduction:

This paper focuses on low to medium carbon secondary hardening steels in which the secondary hardening response is enhanced by cobalt additions. These steels are associated with both high strength and remarkably high toughnesses at these strength levels. The first steels of this type were the steels HP9-4-20 and HY180. The steel HY180 has been the basis for further development of steels in this class, such as AF1410 and AerMet 100.

Factors which influence the toughnesses of these steels when the fracture mode is ductile or micro-void coalescence are discussed. Ductile fracture is emphasized because high upper shelf toughness can significantly improve toughness at test temperatures in the transition region where the toughness increases with increasing test temperature. When fracture is ductile the toughness is influenced by both the fine-scale microstructure and the inclusion particles distributed through the fine-scale microstructure. While these steels have fracture resistant fine-scale microstructures, inclusions can degrade the inherent toughness of the fine-scale microstructures. One can minimize the detrimental effects of inclusions on toughness by minimizing the inclusion volume fraction, by altering inclusion type to achieve the largest possible inclusion spacing when the inclusions are not resistant to void nucleation or by altering inclusion type to make the inclusions resistant to void nucleation.

To getter sulfur as inclusions which are resistant to void nucleation one can use small titanium additions to form particles of titanium carbosulfide (Ti_2CS). These particles are much more resistant to void nucleation than are particles of other sulfide types such as MnS, CrS or La_2O_2S. This resistance of particles of Ti_2CS to void nucleation leads to large improvements in toughness in HY180, a steel with a carbon content of 0.10 wt.%. In the last section of this paper the results of recent studies of the effects of gettering sulfur as Ti_2CS on toughness as a function of carbon content at a constant inclusion volume fraction are reported.

2. Development of ultra high strength secondary hardening steels of high toughness:

Developed by Speich and coworkers[18], HY180 has a nominal composition of 0.10 wt.% C, 10 wt.% Ni, 8 wt.% Co, 2 wt.% Cr and 1 wt.% Mo. The Charpy impact energy, yield strength and ultimate tensile strength of a heat of HY180 steel are plotted as a function of tempering temperature for a five hour temper in Figure 1. The yield strength increases with increasing tempering temperature to a maximum of about 1250 MPa, reached after tempering at 510°C. Tempering at temperatures greater than 510°C for five hours results in a decrease in the yield strength. The Charpy impact energy decreases with increasing tempering temperature when tempered above 300°C and has a minimum on tempering at about 425°C. As the tempering temperature is increased above 425°C, the Charpy impact energy increases with increasing tempering temperature. After tempering at 425°C the only intra-lath carbides observed were cementite; the cementite particles had a lath shape and a length of about 200 nm. After tempering at 510°C for five hours Speich et al.[18]observed intra-lath precipitation of needles of M_2C, but no intra-lath cementite. The needles of M_2C were about 10 nm in length. Speich et al. concluded that when the steel is tempered at 510°C the fine alloy carbides contribute substantially to the strength of the alloy and that maximum toughness is obtained only when all of the coarse intra-lath cementite particles have been replaced by the fine particles of M_2C.

Speich et al.[18] found that cobalt additions enhanced the secondary hardening response and they attributed this to the following effects of cobalt. First, they noted that cobalt additions delayed recovery to higher tempering temperatures and suggested that the resulting higher dislocation densities would provide a greater number of nucleation sites for M_2C precipitation which should lead to smaller and more closely spaced particles of M_2C and hence to higher strength. Further, they pointed out that cobalt additions can lead to a finer M_2C dispersion by increasing the activity of carbon, leading to a greater M_2C nucleation rate and ultimately a higher strength. Speich et al. [18] also investigated the effects of varying amounts of chromium and molybdenum on toughness and strength as a function of tempering temperature and time and noted that higher chromium results in more rapid coarsening of the alloy carbides and shifts the secondary hardening peak to lower tempering temperatures. Increasing the molybdenum has the opposite effect. They concluded on the basis of strength and toughness that, at a carbon level of about 0.12 wt.%, the optimum amounts of chromium and molybdenum were 2 and 1 wt.%, respectively.

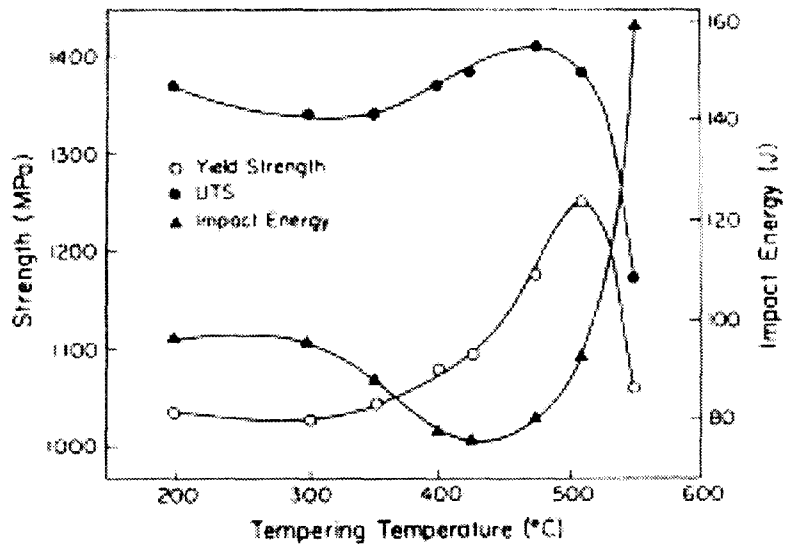

Figure 1. Charpy impact energy, yield strength and ultimate strength as a function of tempering temperature for a heat of HY180 steel.[4]

AF1410 was developed by General Dynamic[13] using the principles outlined by Speich et al.[18] and has the composition 0.16 wt.% C, 14 wt.% Co, 10 wt.% Ni, 2 wt.% Cr and 1 wt.% Mo. This steel, like HY180, is normally tempered for five hours at 510°C and achieves a yield strength of about 1500 MPa after this tempering treatment. The higher strength of AF1410 is attributed to the higher carbon and cobalt levels. The steel AF1410M has a nominal composition identical to that of AF1410 except for the carbon content, which is increased to 0.20 wt.%. When AF1410M is tempered for five hours at 510°C it has a yield strength of 1575 MPa. The Charpy impact energy and yield strength of a heat of AF1410 are plotted as a function of tempering temperature in Figure 2a. In AF1410 the maximum yield strength is obtained after aging at 475°C, not after aging at 510°C as observed for HY180. As observed for HY180 steel the Charpy impact energy of AF1410 has a minimum after aging at 425°C and increases with increasing tempering temperature for aging temperatures above 425°C. This minimum in toughness coincides with the minimum in the retained austenite in the microstructure, as shown in Figure 2b.

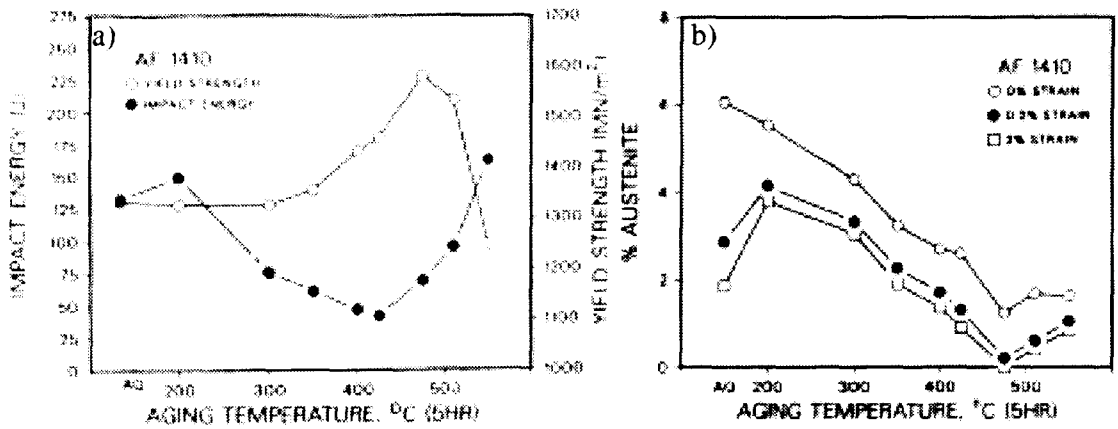

Figure 2. a) Charpy impact energy and yield strength and b) Volume percent retained austenite as a function of aging temperature for AF1410 steel.[8]

Subsequent to the development of AF1410 and AF1410M, Carpenter Technology developed an even higher strength version of this alloy type[15]. The nominal composition of this alloy, called AerMet 100, is 0.24 wt.% C, 13.4 wt.% Co, 11.5 wt.% Ni, 3 wt.% Cr and 1.2 wt.% Mo. The yield strength and Charpy impact energy of oil quenched AerMet 100 are plotted as a function of tempering temperature in Figure 3. As for AF1410, the maximum in the yield strength is obtained after tempering at 475°C. The Charpy impact energy also has a minimum on tempering at about 425°C. However, the decrease in strength associated with increasing the tempering temperature from 475°C to 510°C is much greater for AerMet 100 than for AF1410.

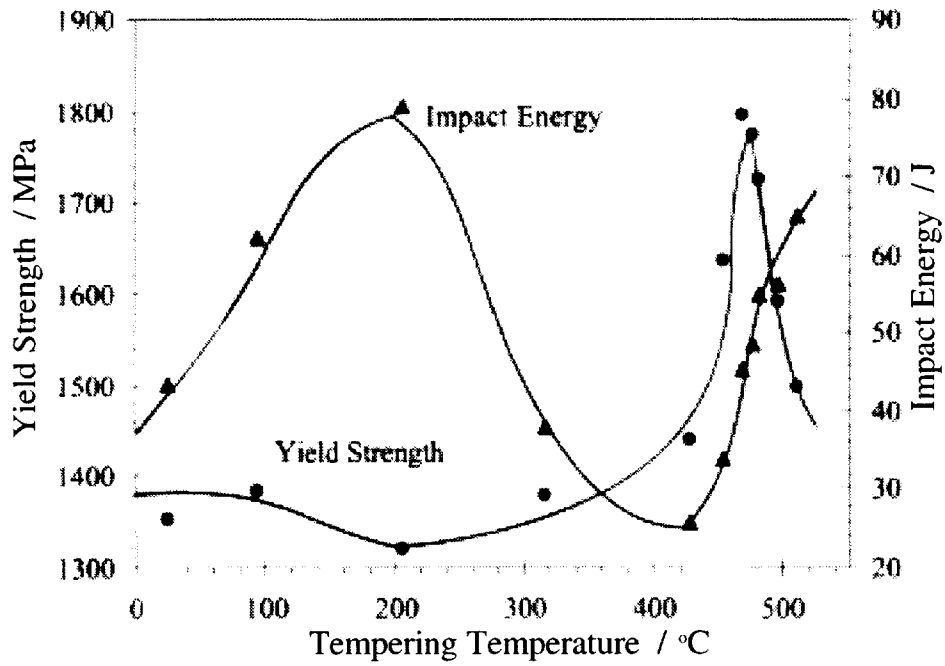

Figure.3. Charpy impact energy and yield strength as a function of tempering temperature for oil quenched AerMet 100 steel.[16]

The primary objective in the development of new alloys of this class has been to increase strength while achieving the highest possible toughness. The primary approach taken to increasing the strength of these steels has been to increase the carbon content which changes the fine-scale microstructure in a number of ways. First, if all of the carbon is precipitated as M_2C then one would expect, if coherency strains remain constant, that the strengthening due to M_2C precipitation would increase as the square root of the carbon content, which is consistent with the results obtained by Speich et al.[18] on the effect of carbon content on yield strength in alloys of the HY180 composition. Second, increasing the carbon content increases the amounts of inter-lath cementite and intra-lath cementite in the microstructure after tempering at 510°C.[10] While no intra-lath cementite is observed after tempering of HY180 at 510°C, there is cementite present in AF1410 steel and the amount of cementite increases as the carbon content is further increased, with a particularly large increase when the carbon content is increased from 0.20 to 0.25 wt. %. In addition, increasing carbon should increase the volume fraction of carbides inherited from the austenitizing temperature, the amount of retained austenite and the extent of twinning of the martensite.

3. Microstructure and toughness:

When a measure of toughness or ductility is plotted as a function of test temperature for a given microstructure the following behavior is normally observed. At low test temperatures the toughness is low and remains relatively constant as the test temperature is increased; this region is often referred to as the lower shelf. For sufficiently high test temperatures the toughness is high but remains constant as the test temperature is varied; this region is often referred to as the upper shelf. Between these two ranges of test temperature there is a region where the toughness increases relatively quickly with increasing test temperature. At test temperatures above this transition region the fracture mode is normally ductile. For test temperatures below this transition region the fracture mode is normally intergranular or a form of cleavage. In the transition region both ductile fracture and brittle fracture modes are observed with the amount of ductile fracture increasing with test temperature.

Ductile fracture is the growth and coalescence of voids typically nucleated at second phase particles. In a given material several particle types can be present. Normally, there are particle types at which voids are nucleated first, either by particle fracture or by separation of the particle-matrix interface. These particles are referred to as primary particles. Voids nucleated at primary particles either grow to impingement or coalesce by a void sheet mechanism. Void sheet coalescence [5] of the voids nucleated at the primary particles requires fracture of the ligaments between these voids, often by the coalescence of voids nucleated at secondary particles, which are particles more resistant to void nucleation than the primary particles and at which voids are nucleated much later in the fracture process.

In steels the primary particles are the inclusions which, in many steels, are sulfide and oxide particles. The inclusions are embedded within a fine-scale microstructure. The secondary particles, considered to be part of the fine-scale microstructure, include the fine carbides, nitrides and carbonitrides inherited from the austenitizing temperature and particles precipitated on tempering. Secondary particles directly influence fracture if they nucleate voids. Secondary particles inherited from the austenitizing temperature can indirectly influence toughness by pinning austenite grain boundaries during austenitizing and thus influence austenite grain size. Secondary particles precipitated on tempering can influence the flow behavior of the material.

When fracture is ductile the toughness of steel is determined by both the fine-scale microstructure and the inclusions. The fracture toughness of ultra high strength steels can be improved by both developing fracture resistant fine-scale microstructures and by minimizing the detrimental effects of inclusion particles on toughness. For a fixed inclusion type the toughness can be increased by decreasing the inclusion volume fraction.[12] However, at a fixed inclusion volume fraction the inclusion type can significantly influence toughness because inclusion type can influence inclusion spacing[3,6] and the void nucleation resistance of the inclusion particles.[9,14] The fine-scale microstructure can influence toughness by influencing matrix strength which can influence the strain at which voids nucleate, the rate of growth of voids nucleated at primary particles and also by influencing coalescence.

For a fixed fine-scale microstructure the inclusion distribution can influence toughness in the transition region because in the transition region the fracture mode is mixed. One would expect the inclusion distributions to influence the toughness in the transition region because of their effect on the energy absorbed during ductile fracture. Thus one would expect increasing the upper shelf toughness to lead to increases in toughness throughout the transition region.

4. Effects of inclusion distributions on the upper shelf toughness:

One objective of prior work has been to determine for a given fine-scale microstructure and constant inclusion volume fraction how to minimize the detrimental effects of inclusions on upper shelf fracture toughness. The plane strain fracture toughness is K_{IC} and is related to δ_{IC}, the crack tip opening displacement at fracture, and J_{IC}, the critical value of the J integral at fracture, through the equations $\delta_{IC} = J_{IC} / 2\sigma_o$ and $J_{IC} = (K_{IC})^2 / E'$ where E' equals Young's modulus, E, for plane stress and E' equals $E/(1-\nu^2)$ for plane strain and σ_o is the flow stress of the material and ν is Poisson's ratio.[2,11]

The Rice and Johnson[17] model predicts that δ_{IC} will scale with the inclusion spacing when the inclusion volume fraction is held constant. Results with HY180 and AF1410 indicate that increasing the inclusion spacing does lead to improved toughness. In this work small inclusion spacings have been achieved by gettering sulfur as small particles of CrS or MnS and large inclusion spacings have been achieved by small additions of lanthanum to getter the sulfur as large particles of La_2O_2S. X_O, the inclusion spacing, is the average nearest-neighbor distance in the volume and has been calculated from $X_O = 0.89R_Of^{-1/3}$ [1], where R_O is the average inclusion radius and f is the inclusion volume fraction.

The effect of inclusion spacing on the toughness of HY180 steel can be seen by comparing heats A792 and G032 in Tables 1 through 3. In A792 the sulfur has been gettered as small, closely spaced particles of MnS and in heat G032 the sulfur has been gettered as large, widely spaced particles of La_2O_2S. The fracture toughness of heat A792 is 233 MPa√m while that of heat G032 is 336 MPa√m. This increase in toughness is ascribed to the increase in inclusion spacing as other microstructural features such as carbides inherited from the austenitizing temperature and grain size have not be altered by the chemistry differences required to vary sulfide type. The effect of inclusion spacing on the toughness of AF1410 steel can be seen by comparing heats G031 and CY2 in Tables 4 through 6. In G031 the sulfur has been gettered as small, closely spaced particles of MnS and in heat CY2 the sulfur has been gettered as large, widely spaced particles of La_2O_2S. The fracture toughness of heat G031 is 158MPa√m while the toughness of heat CY2 is 199 MPa√m. CY2 has considerably higher toughness than heat G031 even though the inclusion volume fraction in heat CY2 is three times greater than that in G031.

The effect of gettering sulfur as particles resistant to void nucleation on the toughness of HY180 can be assessed by comparing the results for heats G027 and G028 which contain no manganese or lanthanum but 0.01 and 0.02 wt. % titanium, respectively, and in which the sulfur is gettered as Ti_2CS to the results for A792 in which the sulfur is gettered as MnS and G032 in which the sulfur is gettered as La_2O_2S. The fracture toughnesses of G027 and G028 were 480 MPa√m and 550 MPa√m, respectively, and those of the A792 and G032 were 233 MPa√m and 336 MPa√m, respectively. As shown in Figure 4 voids are nucleated at much higher strains when the sulfur is gettered as Ti_2CS than when voids are nucleated at particles of MnS or La_2O_2S. It is believed the higher toughnesses of the titanium modified heats are due to the particles of Ti_2CS being more resistant to void nucleation than particles of MnS or La_2O_2S. However, the titanium additions required to alter sulfide type also influence the carbides inherited from the austenitizing temperature and reduce austenite grain size; these changes in fine-scale microstructure could play some role in improving toughness.

Table 1. Chemistries of HY180 Heats*

Heat	C	Ni	Co	Cr	Mo	Si	Mn	S	P	Ti	La	N_2**	O_2**
A792	.10	9.86	7.96	1.98	1.02	.01	.31	.002	.004	.004	<.002	3	6
G032	.12	9.88	8.07	1.99	1.0	.01	.01	.001	.003	.003	.005	3	8
G028	.11	9.88	8.07	1.99	1.00	.01	.01	.001	.003	.021	<.002	1	4
G027	.11	9.90	8.02	1.99	1.01	.01	.01	.001	.003	.012	<.002	1	12

* in wt% ; ** in wt. ppm

Table 2. Inclusion Characteristics of HY180 Heats

Heat	Sulfide Type	f	R_O(μm)	X_O(μm)
A792	MnS	0.00021	0.16	2.4
G032	La_2O_2S	0.00015	0.44	7.5
G028	Ti_2CS	0.00019	0.10	1.5
G027	Ti_2CS	0.00011	0.10	1.9

f = volume fraction; R_O = average radius; X_O = spacing

Table 3. Mechanical Properties of HY180 Heats

Heat	YS (MPa)	UTS (MPa)	Fracture Strain	n	J_{IC} (MPa-m)	K_{IC} (MPa√m)	δ_{IC} (μm)	C_V (J)
A792	1208	1343	1.39	0.043	0.25	233	98	174
G032	1236	1379	1.54	0.048	0.52	336	199	213
G028	1240	1369	1.58	0.044	1.06	480	406	267
G027	1260	1392	1.65	0.046	1.35	550	509	290

Table 4. Compositions of AF1410 Heats *

Heat	C	Ni	Co	Cr	Mo	Si	Mn	S	P	Ti	La	N_2**	O_2**
G031	0.17	9.88	13.90	2.06	1.10	.01	.28	.001	.002	.004	-	3	1
CY2	0.16	10.10	14.04	2.10	1.00	.03	.03	.004	.004	.002	.006	3	9
G618	0.16	9.98	14.10	2.01	1.01	.01	<.01	.001	.003	.013	-	2	7

* wt%, ** wt ppm

Table 5. Inclusion Characteristics of AF1410 Heats

Heat	Sulfide type	f	R_O (μm)	X_O(μm)
G031	MnS	0.00014	0.11	1.90
CY2	La_2O_2S	0.00042	0.64	7.60
G618	Ti_2CS	0.000067	0.069	1.15

f = volume fraction; R_O = average radius; X_O = spacing

Table 6. Mechanical Properties of AF1410 Heats

Heat	YS (MPa)	UTS (MPa)	Fracture Strain	n	J_{IC} (MPa-m)	δ_{IC} (μm)	K_{IC} (MPa√m)	C_V (J)
G031 (MnS)	1505	1661	1.22	0.048	0.123	39	158	70
CY2 (La_2O_2S)	1489	1666	1.24	0.058	0.209	66	199	88
G618 (Ti_2CS)	1472	1672	1.43	-	0.55	175	347	205

Titanium additions would appear to have a similar effect on the toughness of the higher strength steel AF1410. The fracture toughness of heat G618 in which the sulfur is gettered as Ti_2CS is 347MPa√m while the fracture toughness of the heat G031 in which the sulfur is gettered as MnS is 158 MPa√m and the toughness of heat CY2 in which the sulfur is gettered as La_2O_2S is 199 MPa√m. However, the inclusion volume fraction of heat G618 is much lower than the inclusion volume fractions of heats G031 or CY2. Thus, the results obtained using G618 do not conclusively show that gettering sulfur as Ti_2CS can lead to improved fracture toughness in AF1410. For this reason the effects of titanium additions on the inclusion void nucleation behavior and toughness in AF1410 type steels have been explored as a function of carbon content at sulfur levels similar to those obtained in commercial practice and our previous heats of HY180 steel. The results of this study will be covered in section six.

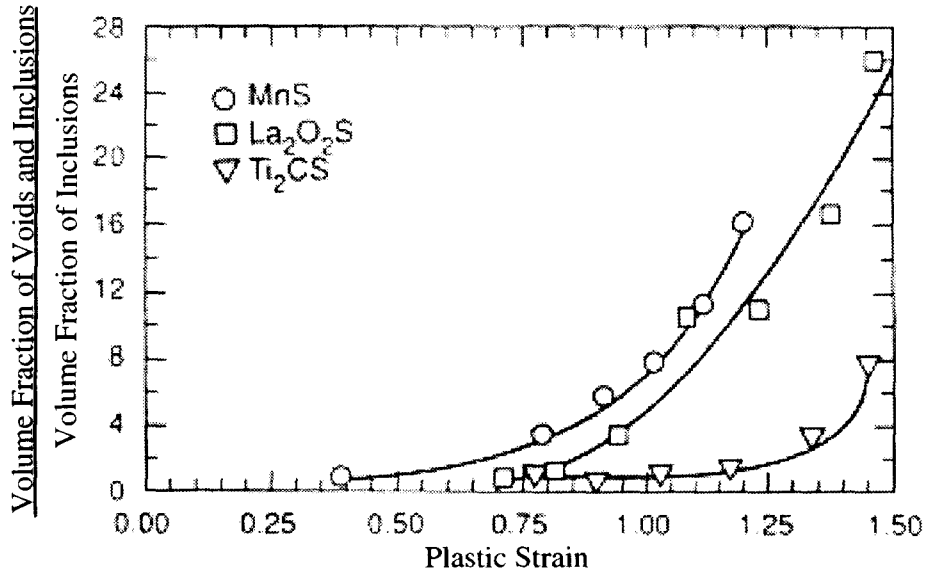

Figure 4. The void + inclusion volume fraction normalized by the inclusion volume fraction plotted as a function of strain for heats of HY180 steel in which the sulfur is gettered as MnS (A792), La_2O_2S (G032) and Ti_2CS (G028). Voids have nucleated when this ratio is greater than one.[7]

5. Effects of inclusion distributions on toughness in the transition region:

Charpy impact energies are given as a function of test temperature in Figure 5 for heats CY2 and 811 of AF1410. In heat CY2 the sulfur is gettered as La_2O_2S particles and the inclusion volume fraction was 0.00042. In heat 811 the sulfur was gettered as Ti_2CS and the inclusion volume fraction was 0.00012. The chemistry, inclusion characteristics and mechanical properties of heat CY2 are summarized in Tables 4, 5 and 6, respectively; those of heat 811 are summarized in Tables 7, 8 and 9, respectively. Heat 811 which has the higher upper shelf toughness has higher toughness throughout the transition region. Since heat 811 has a lower inclusion volume fraction than heat CY2 the higher toughness of heat 811 in the transition and upper shelf ranges cannot be attributed entirely to the differences in sulfide type. However, the data does demonstrate that raising the upper shelf toughness can result in higher toughnesses throughout the transition region.

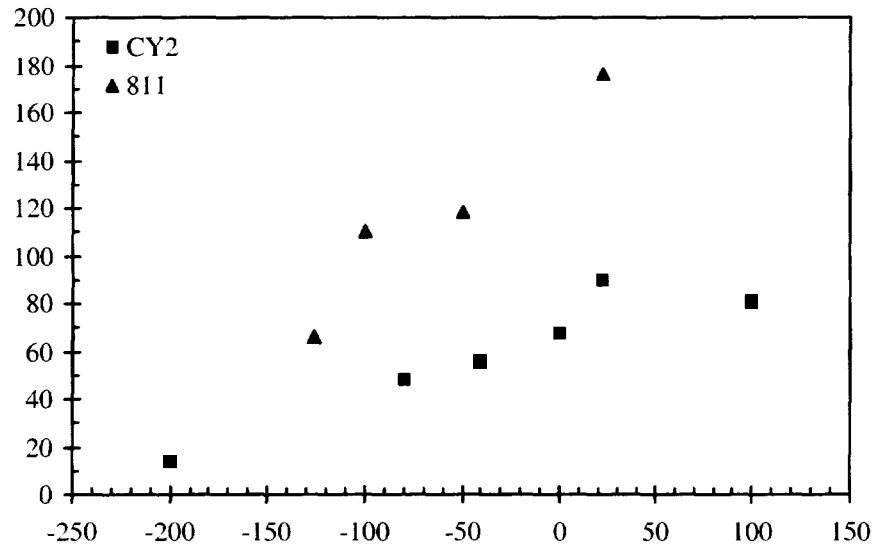

Figure 5. Charpy impact energy versus test temperature for heats CY2 and 811 of AF1410.

6. Effects of carbon content on the toughness of AF1410 type steels:

In section 5 it was noted that gettering sulfur as Ti_2CS might be effective in raising the toughness of AF1410, but the heat of AF1410 initially used, heat G618, had an exceptionally low inclusion volume fraction; thus it was difficult to determine the extent to which gettering sulfur as Ti_2CS improved the toughness of AF1410. Consequently, "control" heats were prepared at three carbon levels (0.16, 0.20 and 0.25 wt. %) in which the sulfur was gettered as Ti_2CS and as CrS but which contain sulfur in amounts similar to those observed in the HY180 heats, 0.0010 wt.%.The sulfur was gettered as Ti_2CS in heats 811, 812 and 813 and, as shown in Table 7, these heats had sulfur, nitrogen and oxygen levels very similar those in the HY180 heats. A second series of alloys was prepared with no titanium, manganese or lanthanum additions and the sulfur in these heats was gettered as CrS. The chemistries of these three heats, 91, 92 and 93, are given in Table 7.

The only sulfur-rich particles found in heats 811, 812 and 813 were Ti_2CS. The Ti_2CS particles were found to have a large size range, with particle diameters varying from 0.05 μm to 3.8 μm. The inclusion characteristics for heats 811, 812 and 813 are given in Table 8. The volume fraction of inclusions in the three heats are very similar. However, differences emerge when the cumulative volume fractions of these heats are plotted as in Figure 6. Particles greater than 0.5 μm in dimension make the largest contribution to the volume fraction of heat 813, while heat 811 has the finest particle distribution. Heats 812 falls between heats 811 and 813. These results suggest that the proportion of large particles of Ti_2CS increases with increasing carbon content.

In heats 91, 92 and 93 all of the sulfur is gettered as CrS. The chromium sulfides are spherical in cross-section and have a much smaller size range than the Ti_2CS particles, with particle diameters varying from 0.05 to approximately 0.30 μm. The inclusion characteristics for the heats 91, 92 and 93 are summarized in Table 8. Inclusion volume fractions for these heats are similar but smaller than those of heats 811, 812 and 813.

Table 7. Compositions of AF1410 Control Heats *

Heat	C	Ni	Co	Cr	Mo	Si	Mn	S	P	Ti	La	N_2**	O_2**
811	0.16	10.20	13.93	2.01	1.00	0.01	0.01	.0010	0.001	0.02	-	1	5
812	0.20	10.15	13.95	2.02	1.01	0.01	0.01	.0008	0.001	0.02	-	2	6
813	0.25	10.14	13.94	2.01	1.01	0.01	0.01	.0010	0.001	0.02	-	1	4
91	0.16	9.98	13.99	1.99	1.03	0.01	0.01	.0012	0.001	<0.01	-	1	6
92	0.20	10.00	13.99	2.00	1.04	0.01	0.01	.0011	0.001	<0.01	-	1	6
93	0.24	9.96	14.00	2.o1	1.02	0.01	0.01	.0013	0.001	<0.01	-	2	5

* wt%, ** wt ppm

Table 8. Inclusion Characteristics of AF1410 Control Heats

Heat	Sulfide type	f	R_o (μm)	X_o(μm)
811	Ti_2CS	0.000120	0.079	1.42
812	Ti_2CS	0.000091	0.075	1.49
813	Ti_2CS	0.000106	0.072	1.36
91	CrS	0.000065	0.070	1.55
92	CrS	0.000078	0.075	1.55
93	CrS	0.000088	0.072	1.44

f = volume fraction; R_o = average radius; X_o = spacing

Table 9. Mechanical Properties of AF1410 Control Heats

Heat	YS (MPa)	UTS (MPa)	Fracture Strain	J_{IC} (MPa-m)	δ_{IC} (μm)	K_{IC} (MPa√m)	C_v (J)
811 (Ti_2CS)	1530	1610	1.4	0.251	80	235	176
812 (Ti_2CS)	1590	1720	1.3	0.156	47	177	103
813 (Ti_2CS)	1690	1830	1.1	0.089	25	135	68
91 (CrS)	1490	1650	1.3	0.137	44	168	107
92 (CrS)	1610	1770	1.2	0.084	25	132	68
93 (CrS)	1730	1880	1.1	0.046	13	95	43

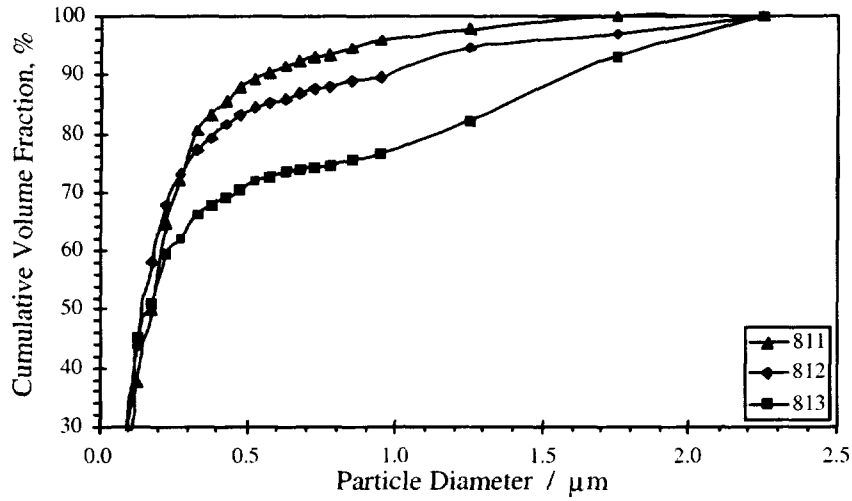

Figure 6. Cumulative volume fraction curves for heats 811, 812 and 813.

The fracture toughnesses of HY180 and of AF1410 at carbon levels of 0.16, 0.20 and 0.25 wt. % are plotted in Figure 7 as a function of yield strength for heats in which the sulfur is gettered as MnS or CrS and when the sulfur is gettered as Ti_2CS for materials in which the sulfur is about 0.001 wt. %. First, for all strength levels higher fracture toughnesses are obtained when the sulfur is gettered as Ti_2CS. Second, the fracture toughness decreases with increasing yield strength when the sulfur is gettered as Ti_2CS and when the sulfur is gettered as MnS or as CrS but this rate of decrease is much more rapid when the sulfur is gettered as Ti_2CS. It would appear that at strength levels of about 1800 MPa the toughness would be independent of sulfide type.

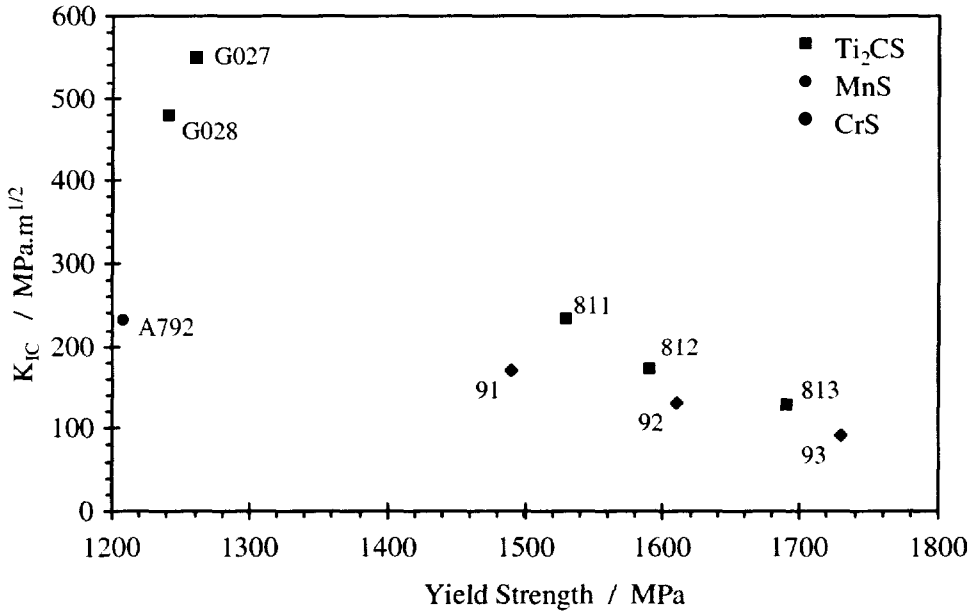

Figure 7. The fracture toughness plotted as a function of yield strength for HY180 and AF1410 at carbon levels of 0.16, 0.20 and 0.25 wt.% when the sulfur is gettered as MnS, CrS and Ti_2CS.

The higher toughnesses of the heats in which the sulfur is gettered as Ti_2CS are associated with the particles of Ti_2CS being more resistant to void nucleation than particles of MnS or CrS. Void generation curves for the 0.16 wt. % carbon heats in which the sulfur is gettered as CrS (heat 91) and in which sulfur is gettered as Ti_2CS (heat 811) are compared in Figure 8. While voids are generated at very low strains at the inclusions in the CrS heat, void generation does not become apparent until a strain of about one for the Ti_2CS heat. There are microstructural differences between these two heats other than sulfide type which could influence toughness. The prior austenite grain size and martensite packet size are larger in heat 91 than in heat 811 and it is possible that the toughness of heat 91 could be improved by a refinement of prior austenite grain size because the inclusions in heat 91 are small and closely spaced. It has been shown in 0.07 wt.% carbon / 9 wt.% nickel steels that increasing austenite grain size is

detrimental to toughness when the inclusion spacing is small, as when the sulfur is gettered as MnS or CrS, but has very little effect on toughness when the inclusion spacing is large, as it is when the sulfur is gettered as La_2O_2S.[7]

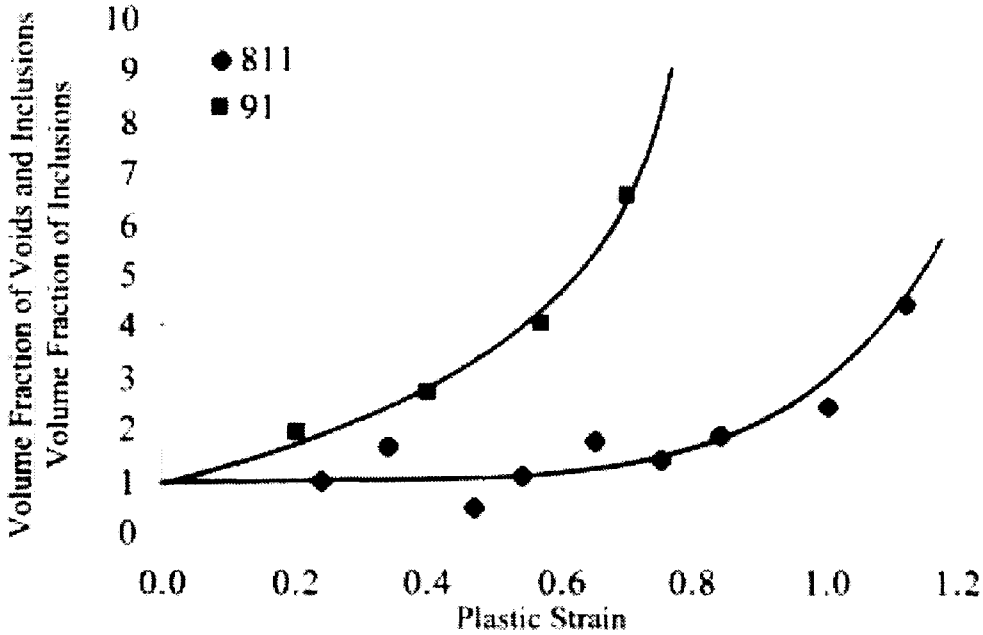

Figure 8. The void + inclusion volume fraction normalized by the inclusion volume fraction plotted as a function of strain for heats of AF1410 in which the sulfur is gettered as CrS (91) and Ti_2CS (811). Voids have nucleated when this ratio is greater than one.

A number of factors could contribute to the toughness decreasing more rapidly with increasing yield strength when the sulfur is gettered as Ti_2CS than when the sulfur is gettered as MnS or CrS. First, inclusion void nucleation resistance does not change as the carbon level is increased from 0.16 to 0.25 wt. % when the sulfur is gettered as CrS; void generation curves for heats 91 and 93 are the same. However, the strains at which voids are generated at inclusions decreases with increasing carbon content when the sulfur is gettered as Ti_2CS. Void generation studies carried out at elevated temperatures for 813 and at low temperatures for heat 811 suggest that the decreasing void generation resistance with increasing carbon level is due, not to an increase in strength, but rather to the effect of carbon on the size distribution of Ti_2CS particles with void generation occurring at lower strains as the number of larger particles of Ti_2CS increases. Thus the effect of carbon content on Ti_2CS size appears to be one reason that the toughness decreases more rapidly with increasing strength when the sulfur is gettered as Ti_2CS than as CrS.

However, that the toughness decreases more rapidly with increasing strength when the sulfur is gettered as Ti_2CS than as CrS cannot be attributed entirely to the effect of carbon on Ti_2CS size. A number of factors suggest that fine-scale microstructural changes play a large role in this decrease in toughness as the carbon level is increased from 0.16 to 0.25 wt.%. To eliminate particles of Ti_2CS specimens were first solution treated at 1390°C, a temperature sufficient to dissolve all of the titanium carbosulfides, then water quenched and then given the standard heat treatment. The effects of this heat treatment on Charpy impact energy are summarized in Table 9.

Table 9. The Effects of High Temperature Solutionizing on Charpy Impact Energies

Heat	Charpy Impact Energy (J)	
	Standard Heat Treatment	1390°C/1hr +Water Quench + Standard Heat Treatment
811	176	240
812	103	143
813	68	80

The increases in Charpy energy for heats 811, 812 and 813 were 64 J, 40 J and 12 J, respectively. The microstructures of the materials which were first solutionized at 1390°C differed from those receiving just the standard heat treatment in that no large titanium carbosulfides were present, no undissolved carbides inherited from the austenitizing temperature could be detected and the austenite grain sizes were quite large, indicating that the standard heat treatment were insufficient to refine the austenite grain size established by first solutionizing at

1390°C. Both removing the large titanium carbosulfides and the carbides inherited from the austenitizing temperature should lead to improved toughness as observed. However, the degree to which removing these particles improves toughness diminishes as the carbon content increases. In fact, at the carbon level of 0.25 wt. % this heat treatment results in an increase in the Charpy impact energy of only 12 J. These results suggest that fine-scale microstructure dominates the fracture behavior at the higher carbon level and that fine-scale microstructural changes due to increasing carbon content play a substantial role in determining the decrease in toughness as the carbon level is increased.

Fine-scale microstructural features which could change with increasing carbon content and which might influence toughness include retained austenite content, the amount and nature of the carbides inherited from the austenitizing temperature, the amount of inter-lath and intra-lath cementite and the amount of twinning. No austenite could be detected in heats 811, 812, 813, 91, 92 and 93. While the number density of carbides inherited from the austenitizing temperature does increase with increasing carbon content, eliminating such carbides through the heat treatment beginning with the solutionizing at 1390°C does not have a significant effect on toughness at the 0.25 wt. % carbon level. Measurements of the amounts of inter-lath and intra-lath cementite in steels of the AF1410 type indicate that the amount of cementite does increase with increasing carbon content. However, no cementite was found on extractions taken from fracture surfaces. This result is certainly contrary to our expectations. While it is possible that the cementite particles in these materials influence fracture indirectly, they to do not appear to nucleate voids. While our results suggest that fine-scale microstructure becomes increasingly dominant in determining fracture behavior as the carbon level is increased the aspects of the fine-scale microstructure which are active have not been identified.

7. Acknowledgments:

The support of the National Science Foundation under DMR-971260 is gratefully acknowledged. The authors also appreciate the preparation of materials by Carpenter Technology and by Teledyne-Allvac.

8. References:

1. Ashby, M F and Ebeling, R, Trans. AIME, 235 (1966), 1396-1404.
2. Begley, J A and Landes, J D, in Fracture Toughness, ASTM STP 514, American Society for Testing and Materials, Philadelphia, PA, (1974), 201.
3. Birkle, A J, Wei, R P and Pellissier, G E, Trans. ASM, 59, (1966), 981-990.
4. Bray, J W Maloney, J L, Raghavan, K S, Garrison, W M, Met. Trans., 22A, (1991), 2277-2285.
5. Cox, T B and Low, J R, Met. Trans., 5A, (1974), 1457-1470.
6. Garrison, W M, Met. Trans., 17A, (1986), 669-678.
7. Garrison, W M, Wojcieszynski, A L and Iorio, L E, in Recent Advances in Fracture (eds. Mahidhara, R K, Geltmacher, A B, Matic, P, Sadananda, K), Orlando, Florida, Feb 10-13, TMS, (1997), 361-372.
8. Handerhan, K J, Garrison W M and Moody, N R, Met. Trans., 20A, (1989), 105-123.
9. Hippsley, C A and Druce S G, Acta Metall., 31, (1983), 1861-1872.
10. Iorio, L E, Maloney, J L and Garrison, W M, in 40th Mechanical Working and Steel Processing Conference, Pittsburgh, Oct. 25-28, Iron & Steel Society, (1998), 901-919.
11. Knott, J F, in Fundamentals of Fracture Mechanics, Butterworths, London, (1973).
12. Knott, J F, Metal Science, 14, (1980), 327-336.
13. Little, C D and Machmeier, P M, Development of a Weldable High Strength Steel, Report AFML-TR-75-148, (1975)
14. Maloney, J L and Garrison, W M, Scripta Met., 23, (1990), 2097-2100.
15. Novotny, P M and Dahl, J M, in 32nd Mechanical Working and Steel Processing Conference, Cincinnati, Ohio, Oct. 21-24, 1990, Iron & Steel Society, (1991), 275-281.
16. Novotny, P M, in Gilbert R. Speich Symposium (eds. Krauss, G and Repas, P E.), Montreal, Canada, Oct. 25-28, Iron & Steel Society, (1992), 215-236.
17. Rice, J R and Johnson, M A, in Inelastic Behavior of Solids, (eds. Kanninen, M F, Adler, W G, Rosenfield, A R and Jaffee, R I) McGraw-Hill, New York, (1970), 641-672.
18. Speich, G R, Dabkowski, D S and Porter, L F, Met. Trans., 4, (1973), 303-315.

SEGREGATION BEHAVIOR OF SULFUR AND OTHER IMPURITIES ONTO THE FREE SURFACES OF ED-NI DEPOSITS

by

Binayak Panda
IIT Research Institute
Building 4628, Marshall Space Flight Center
George C. Marshall Space Flight Center, AL 35812
(256) 544-6349 (bpanda@iitri.org)

and

Gregory Jerman
National Aeronautics and Space Administration
Building 4612, Marshall Space Flight Center
George C. Marshall Space Flight Center, AL 35812
(256) 544-5346 (gregory.a.jerman@msfc.nasa.gov)

ABSTRACT

Most researchers attribute grain boundary embrittlement in electro-deposited Nickel (ED-Ni) to the presence of small quantities of Sulfur as an impurity. It occurs in a highly mobile form that segregates to the grain boundaries. Evaluation of Sulfur segregation requires that a sample be fractured through the grain boundaries. However, this action may not always be possible. ED-Ni is inherently tough at ambient temperature, especially if a low level of Sulfur was intentionally maintained.

A new method was developed to study Sulfur and other migrant species to the grain boundaries, which also migrate to free surfaces. A test specimen is heated by a quartz lamp within the sample preparation chamber, allowing the mobile species to migrate to polished free surfaces. There the mobile species are analyzed using X-ray photoelectron spectroscopy (XPS) also known as Electron Spectroscopy for Chemical Analysis (ESCA).

INTRODUCTION

ED-Ni is one of the structural materials used in the main combustion chamber (MCC) of the Space Shuttle Main Engine (SSME). During manufacture, a Nickel sulfamate bath is used to obtain a deposit of high-purity Nickel. Table 1 shows impurity levels commonly seen in the composition of ED-Ni, given in parts per million (ppm).[1]

Table 1 – Impurity levels in ED-Ni (ppm)[1]

Carbon	Copper	Iron	Manganese	Silicon	Cobalt	Hydrogen	Oxygen	Nitrogen	Sulfur
50	<100	<100	<5	<10	1000	8	20	6	10

Functional characteristics can be seriously impaired by some impurities, even at very low levels, especially in material exposed to elevated temperatures during annealing or welding. High-temperature exposure promotes diffusion of some impurities to grain boundaries, which may result in grain boundary embrittlement characterized by loss of ductility at high temperature. Most researchers[1-3] associate such degraded mechanical properties with Sulfur segregation, while others attribute them to Carbon reacting with Oxygen to form Carbon Monoxide at grain boundaries.[4] Both groups consider Sulfur (in the absence of Oxygen) to be the most important cause of grain boundary embrittlement.

Sulfur has very low solubility in Nickel, with strong segregation tendencies toward grain boundaries. Even at the small ppm level, Sulfur present in a bulk composition can segregate up to several atomic percentages at the grain boundaries.[3] Sulfur is gettered by other elements such as manganese, magnesium, and calcium, which prevent its migration to the grain boundaries.

Measurement of grain boundary Sulfur is an important means of predicting embrittlement. All previous work has made such measurements using Auger electron spectroscopic analysis,[1,3] requiring exposure of the grain boundaries. This action is usually accomplished by introducing large quantities of Sulfur that induce the sample to break easily within the Auger sample preparation chamber.

EXPERIMENTAL PROCEDURE

This paper describes a new method to measure the amount of diffusing species onto a free surface. This phenomenon is considered to be directly related to the amount of diffusing species present on the grain boundaries. XPS was used to identify and quantitatively measure segregating species on a polished surface. This technique allowed the analysts to use a large diameter monochromatic X-ray beam (800 micrometers) for better sensitivity. They were also able to use X-rays as the excitation source in order to prevent heating effects and evaluate polished samples instead of fractured samples.

Both mounted and unmounted samples were analyzed using an SSX-100 ESCA instrument. Mounted and polished ED-Ni samples were introduced into the sample preparation chamber and allowed to outgas. The samples were then introduced into the main analytical chamber. Selected areas of each polished surface were then cleaned using an argon ion sputter gun. After cleaning, the samples were removed from the analytical chamber, reintroduced into the sample preparation chamber, and heated by a quartz lamp for 2 hours. See Figure 1 for heating and cooling curves. After about 4 hours, the cooled samples were reintroduced into the analytical chamber where the cleaned regions were analyzed for possible migration of species.

RESULTS

The limits of elemental sensitivity for XPS are generally in the same range as that of Auger. An element must be present as at least a fraction of a percent in order to be detected. Elements detected on the clean surface are assumed to be species segregating from inside the material. Several runs were made to confirm this phenomenon, as well as to eliminate spurious deposits from the vacuum atmosphere. Therefore two groups of results were obtained. The first was to ascertain the origin of various species found on the sample surface, the second to provide quantitative determination of these species.

To establish this method's effectiveness, analysis was conducted on a sample taken from an MCC (S/N 6014). It was mounted in Bakelite and then polished for microstructural and elemental analysis. Combustion analysis was used to determine that it contained 3 ppm bulk Sulfur. This low amount permitted the XPS method of detection to be effective if Sulfur segregation occurs to the free surface of the sample.

A quartz lamp was used to heat the mounted and polished sample in the XPS sample preparation chamber for 2 hours to remove volatile matter. After cooling, the sample was introduced into the main analytical chamber for analysis. Regional scans were taken between the 150 and 350 eV binding energy range at two locations for an iteration of 10 times each. These scans included positions for Carbon and Sulfur peaks. Table 2 indicates that these locations produced nearly identical scans showing both Carbon and Sulfur on the sample surface. Then the second location was sputtered with argon ions for 2 minutes to remove adsorbed contaminants. After sputtering, the Sulfur peak was eliminated and the Carbon peak reduced. The sample was removed to the sample preparation chamber again, heated with a quartz lamp for 1 hour and then reintroduced into the analytical chamber. Analysts noted a small Sulfur peak and a significant Carbon peak, although not as large as the one seen after heating for 2 hours. Both peaks were removed by 2 minutes of sputter with the argon gun.

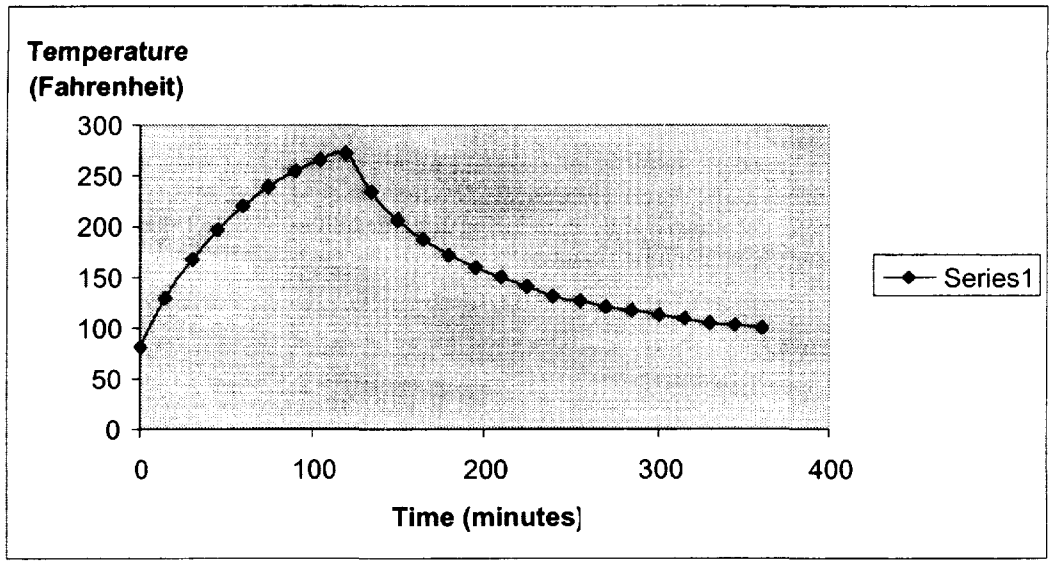

Figure 1 – Sample heating/cooling cycle

Due to sample outgassing, the pressure was elevated to 2 x 10^{-8} torr inside the analytical chamber. An attempt was made to determine whether the appearance of Carbon and Sulfur lines was due to adsorption of gaseous species from the chamber atmosphere. The sample surface was cleaned by sputter with the argon gun, left inside the analytical chamber for 4 hours, and then scanned for Carbon and Sulfur. No evidence of Sulfur was seen, although the Carbon peak had grown somewhat. It was inferred that, for the Bakelite-mounted samples, surface Carbon content could increase either from the atmosphere or through diffusion from inside the sample. In another attempt, the sample was cleaned and then placed in the preparation chamber. It was heated for 2 hours while shielded from direct radiation from the quartz lamp. No Sulfur was observed. Analysts noted the presence of a Carbon peak as large as the one produced by direct heating.

Analysis was conducted on Bakelite-mounted material, as well as on silver paste applied to the mounted samples to improve conductivity during electron microprobe evaluations. Each was analyzed twice. Both showed broader Carbon peaks, but no Sulfur. Upon cleaning, reheating, and analysis, Sulfur was again detected on the same sample.

Table 2 – Peak Areas for Carbon and Sulfur (Preliminary Studies)

Run	Description	Carbon (1s) Counts	Sulfur (2p) Counts	Comments
13	After heating for 2 hr	68,546	10,312	First location
14	After heating for 2 hr	56,787	5,900	Second location
15	After sputter for 2 min.	5,851	-	Second location
16	After sputter, heating for 1 hr	46,200	4,299	Second location
17	Clean surface exposed to analysis chamber vacuum for 4 hr	21,524	-	Second location
18	After heating for 2 hr without direct radiation	67,347	-	Second location (Carbon pickup only)
24	As in Run #13, but at another location	52,061	7,989	Third location

After Sulfur was observed migrating to the clean surface, overall scans were performed between 0 and 1100 eV to determine whether other species were migrating. During Run #24, regional scans were performed between 150 and 350 eV. They showed evidence of Bromine, which was identified from the position of three peaks (182, 189, and 256 eV) and their relative heights. During Run #25, an overall scan was performed from 0 to 550 eV, as shown in part in Figure 2. Bromine and Cadmium species were seen with Carbon, Oxygen, Nitrogen, and Sulfur.

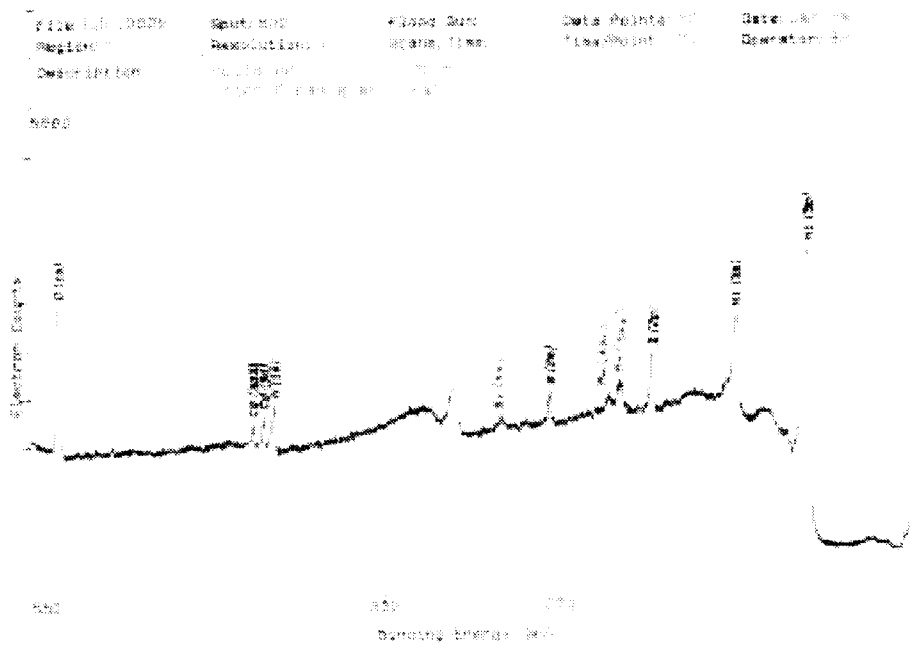

Figure 2 – Scan which shows several elements segregating to surface of Sample 6014

In Table 3, surface analysis is shown in atomic percentages. Carbon and Oxygen covered most of the Nickel surface. A sputtered surface shows about 75% Nickel, 10% Nitrogen, 10% Oxygen, and 5% Carbon. These percentages are approximate. Their accuracy depends upon degree of surface cleanliness, peak-to-background ratio of the peak being evaluated, and the test instrument's inherent machine characteristics. Here, the standard deviation should be around 0.8% for strong lines such as Nickel (10 iterations) and close to 1.8% for Carbon and other light elements (11 iterations).

Table 3 – Quantitative Surface Analysis for Sample 6014
(Atomic Percentages)

Nickel	Oxygen	Cadmium	Nitrogen	Carbon	Sulfur	Bromine
17.93	10.52	0.17	4.24	59.68	4.71	2.75

Systemic analysis was then conducted on several samples from actual MCC liners, using the methodology discussed above. Analysis was conducted on a sample taken from an MCC liner (S/N 6021), which contained more bulk Sulfur than was seen in Sample 6014. Sample 6021 was longitudinally sectioned, polished, and then removed from the mount to eliminate any elemental interference of species emanating from mounting materials. Combustion analysis indicated that it contained 6 to 7 ppm of bulk Sulfur, while the microprobe analysis indicated that it contained 3.5-ppm Sulfur. Combustion analysis gives data for the bulk material, whereas the microprobe gives data for a region of only a few micrometers on the surface.

Table 4 shows that the sample showed Sulfur, Bromine, and Cadmium, as well as small amounts of Chlorine on the surface. Despite higher levels of Sulfur in combustion analysis seen between the two samples, the migrating quantity was less than that seen in the 3 ppm material. Several readings were taken on the same sample, in order to find out whether segregation might be dependent upon location, previous exposure, or polishing. The sample was also repolished and reexamined. Run #36 showed about 11.6% Sulfur on the surface. Afterwards, a depth profiling evaluation indicated that Sulfur was present on the surface to a depth of around 0.7 nm. Thus nearly two monolayers of Sulfur were present on the sample surface.

Table 4 - Surface Analysis Results for Sample 6021
(Atomic Percentages)

Run	Nickel	Oxygen	Cadmium	Nitrogen	Carbon	Sulfur	Bromine	Chlorine	Comments
36	41.00	5.14	0.00	0.00	42.27	11.60	0.00	0.00	First location, first attempt
42	31.08	6.11	1.16	3.54	50.78	3.71	1.28	2.33	Second location, first attempt
48	37.08	7.06	0.72	2.77	43.88	6.32	2.15	0.00	First location, second attempt
49	34.69	7.01	0.42	2.88	46.76	6.41	1.82	Trace	Second location, second attempt
76	34.22	4.21	0.23	3.73	51.04	1.87	2.47	2.23	Third location after grinding

Table 5 shows results for a sample taken from the aft area of an MCC liner (S/N 6005) analyzed at two locations. Both microprobe and combustion analysis showed very small amounts of Sulfur (~1.2 ppm).

Table 5 – Surface Analysis Results for Sample 6005
(Atomic Percentages)

Nickel	Oxygen	Cadmium	Nitrogen	Carbon	Sulfur	Bromine	Chlorine
26.90	10.04	0.23	-	58.03	2.67	2.09	-
28.79	9.80	0.20	1.71	54.28	1.84	3.35	-

Another high-Sulfur sample taken from an MCC liner (S/N 6018) was analyzed at two locations. Sample 6018 contained around 5 to 6 ppm of bulk Sulfur, as confirmed by both combustion and microprobe analyses. Table 6 reports XPS analysis results indicating the presence of traces of Cadmium and Nitrogen on the surface, in addition to Sulfur.

Table 6 – Surface Analysis Results for Sample 6018
(Atomic Percentages)

Nickel	Oxygen	Cadmium	Nitrogen	Carbon	Sulfur	Bromine	Chlorine
26.98	9.33	Trace	Trace	58.36	2.96	2.38	-
25.88	8.93	-	Trace	58.89	3.66	2.65	-

Analysis was also conducted on a sample taken from an MCC liner (S/N 6016). It contained an intermediate amount of Sulfur, with a bulk analysis of approximately 4 ppm. Table 7 shows negligible amounts of Cadmium, with Tin seen as one of the species seen migrating onto the surface.

Table 7 – Surface Analysis for Sample 6016
(Atomic Percentages)

Nickel	Oxygen	Cadmium	Nitrogen	Carbon	Sulfur	Bromine	Chlorine	Tin
23.96	10.44	Trace	3.04	57.80	2.78	1.68	-	0.28
22.28	10.13	Trace	3.89	57.63	3.39	2.23	-	0.43

DISCUSSIONS

Impurities are common in Nickel sulfamate baths. The common impurities in Nickel deposits are Oxygen, Carbon, Sulfur, and Chlorine.[5] These impurities occur in amounts that vary largely depending upon the operating parameters. Metallic impurities generally originate as contamination and additives. Such impurities are generally present in very small concentrations. Their presence and origins are generally not apparent unless the species are specifically sought out. Earlier publications[6] discussed possible sources of these species. Here, the XPS used a residual gas analyzer in the sample preparation chamber to identify species present in the vacuum chamber. During heating, the sample preparation chamber contained Oxygen, Nitrogen, moisture, Carbon dioxide, and Hydrogen gases. No additional species were found after heating for 2 hours using gold samples, unlike results for the ED-Ni material.

Several studies have found Sulfur in Nickel, which is known to segregate to grain boundaries, as well as to free surfaces. That phenomenon occurred here after heating to 275°F. Segregation effects will be faster for high-temperature exposure. The amount migrating to grain boundaries will depend upon how much free Sulfur remains after compounding with other elements (e.g., calcium and/or manganese) that may be present in ED-Ni. Several readings for Sample 6021 showed scatter in surface Sulfur compositions. However, average analyses at different locations for different liners correspond well with the findings of total Sulfur by combustion and microprobe analysis. Table 8 compares average results for surface analysis and combustion analysis.

While the origin of Cadmium and Bromine is unclear, they may be present in very small quantities in ED-Ni. However, additional study is needed as to their segregation propensity, in addition to that of Sulfur. Investigation is also required to determine whether synergistic effects exist among such segregating species.

Table 8 – Comparison of Average Results for Sulfur
During Surface Analysis and Combustion Analysis

MCC Liner Serial Number	Sulfur by Combustion Analysis (ppm)	Average Sulfur on Surface (Atomic Percent)
6021	6.5	5.98
6005	1.2	2.25
6018	5.5	3.31
6016	4.0	3.08

CONCLUSIONS:

1. A viable experimental method using XPS has been shown to conduct a quantitative assessment of migrating species in ED-Ni.

2. This method can be used to evaluate small amounts of segregating species as they accumulate on the free surface.

3. Elements other than Sulfur (such as Cadmium, Tin, and Bromine) were also seen segregating onto the free surface.

ACKNOWLEDGEMENTS

The authors would like to express appreciation to the SSME Program Office for providing funds for this research. Thanks are also due to Mr. Steven J. Gentz for valuable comments, Mr. Steve Hudson for helpful discussions, and Mrs. Susan Hessler for technical editing support.

REFERENCES

1. Dini, J.W.; Johnson, H.R.; and West, L.A., "On High Temperature Ductility Properties of Electro-Deposited Sulfamate Nickel," *Plating and Surface Finish,* February 1978, p. 36-40.

2. Kraai, D.A. and Floreen, S.A., "Hot Ductility of Nickel," *Transactions Metallurgical Society of AIME,* vol. 230, 1964, p. 833.

3. Walsh, J.M. and Anderson, N.P., "Application of Auger Electron Spectroscopy to the Study of Embrittlement in Nickel." *ASTM STP 596*, 1976, p. 58 – 67.

4. Harris, S.J. and Braddick, D.M., "The Elevated Temperature Tensile Properties of Electro-Deposited Nickel," *Transactions IMF,* vol. 51, 1973, p. 165.

5. Safranek, W.H., ed., "The Properties of Electro-Deposited Metals and Alloys," *Handbook*, AESF, 1986, p. 261.

6. Harris, L.A., "Some Observations of Surface Segregation by Auger Electron Emission," *Journal of Applied Physics*, Vol. 39, February 1968, p.1428 – 1431.

86 N 26

F2/4/11

STATISTICAL ANALYSIS OF STRENGTH DATA FOR AN AEROSPACE ALUMINUM ALLOY

by

Lynn Neergaard
IIT Research Institute
215 Wynn Drive NW, Suite 101
Huntsville, AL 35805-1926
(256) 382-4773 (lneergaard@iitri.org)

and

Tina Malone
National Aeronautics and Space Administration
Building 4612, Marshall Space Flight Center
George C. Marshall Space Flight Center, AL 35812
(256) 544-2593 (tina.malone@msfc.nasa.gov)

ABSTRACT

Aerospace vehicles are produced in limited quantities that do not always allow development of MIL-HDBK-5 A-basis design allowables.[1] One method of examining production and composition variations is to perform 100% lot acceptance testing for aerospace Aluminum (Al) alloys. This paper discusses statistical trends seen in strength data for one Al alloy. A four-step approach reduced the data to residuals, visualized residuals as a function of time, grouped data with quantified scatter, and conducted analysis of variance (ANOVA).

BACKGROUND

A test article was fabricated to demonstrate full-scale performance of a production-sized alloy ingot, as well as to qualify rolling, annealing, and weld approaches. Each panel was subjected to 100% lot acceptance testing to verify specification compliance. The test directions were:

- Longitudinal (L) or parallel to the rolling direction
- Long transverse (LT) or perpendicular to the rolling direction in the plane of the plate
- Short transverse (ST) or perpendicular to the rolling direction in the plane of the plate
- 45° from the rolling direction in the plane of the plate

This lot acceptance testing involved multiple tiers of testing and evaluation. Each lot was sampled by machining test coupons in the L, LT, and 45° directions. The coupons were then subjected to tensile tests to determine ultimate tensile strength (UTS), yield strength (YS), and elongation. Thicker plates were also tested in the ST direction. Failed lots were retested twice to confirm the validity of the original test. If possible, failed lots were recovered by solution heat treatment. Failure stresses in this plate material followed a severely truncated distribution. Plates with nominal values were easily found, but plates with marginal values were rare.

The first step in quality control is to verify whether the current distribution is acceptable. If not, the process used to fabricate the parts is improved to produce material with a tighter distribution of critical properties. Here, the distribution appears acceptable and sufficient sampling has been performed to verify the process produces few plates with unacceptable properties. The second step is to introduce continual monitoring to ensure the parts remain defined by the acceptable distribution. This step is more difficult to implement because the distribution has a sharp drop-off after lot acceptance testing.

Process control techniques normally require the presence of some distance between the upper control limit (UCL) and the upper specification limit (USL). The UCL is often the mean plus three sigma, which is a probability <1/740 of having an out-of-bounds signal generated by an in-control process. If the process begins to drift, samples begin to produce values above the UCL. This development is a signal that the process must be brought under control again before an out-of-specification part is produced. However, the UCL is close to the mean in this alloy, due to the sharp drop-off of the distribution. If the USL is placed near the UCL, only a small probability exists that the USL would be exceeded if the current distribution continued. As a result, process malfunctions would probably not be caught before unacceptable parts had been produced.

The alloy specifications included requirements for both strength and toughness. These properties cannot be independently controlled. Process operations intended to increase toughness inadvertently decrease strength, while increases in strength are generally accompanied by decreases in toughness. What might appear to be two single-sided distributions of bulk strength and toughness is actually a single double-sided distribution of the plate's thermomechanical history. The anisotropy of most rolled Al plate results in different properties for different directions. Each plate thickness contains a range of microstructures distributed throughout the plate. Intentional process variations include different amounts of cold work and heat treatment used for various parts of the tank. Gradual process changes may also lead to property or variability changes.

A statistical analysis was performed on lot acceptance data for an Al alloy intended for use in an aerospace vehicle. A-basis design allowables were calculated based on MIL-HDBK-5 procedures. Some property distributions were Normal, others Weibull. A lack of process-stable data limits the usefulness of this analysis.

This paper discusses data taken early in an aerospace project to provide approaches to analyzing lot acceptance data for gradual changes in properties. The data constitute 400 lots and 3,200 specimens.

ANALYSIS

In Figure 1, UTS and YS are plotted for all samples to demonstrate the correlation of strength with processing. OM-temper data fall in the lower left-hand corner, T-3 temper data in the middle, and T-8 temper data in the upper right-hand corner. X-Y plots usually show the dependence of one variable (y) on another (x), with YS or UTS plotted as a function of intentional process variations. However, these processes are difficult to express as a single dimension. Instead of showing cause (x) and effect (y), this plot represents two effects (YS and UTS) of the same cause (processing).

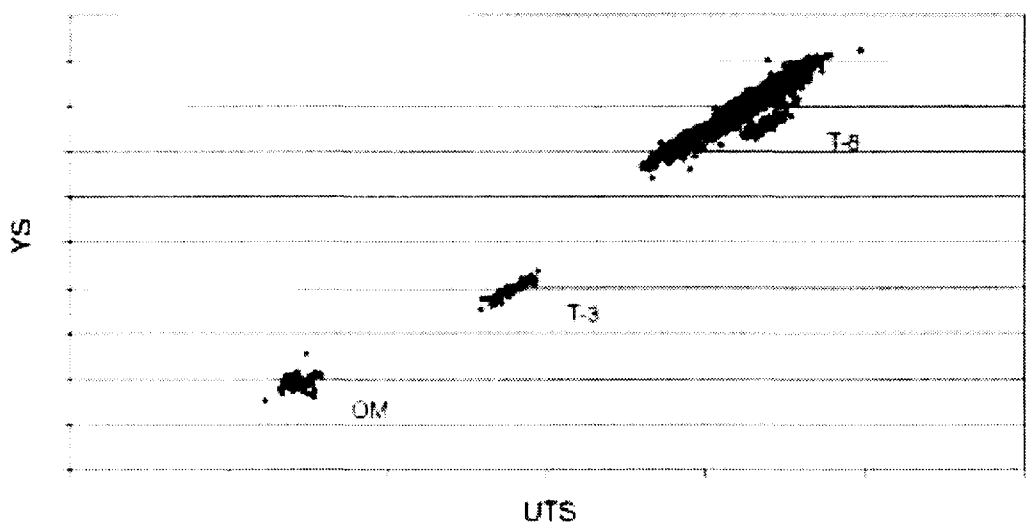

Figure 1. UTS versus YS

Figure 1 demonstrates the effect of intentional differences in processing. As expected, materials with high YS also have high UTS. Deviations from a simple thin line are due to random rather than systematic variation. A direct comparison would normalize values for systematic changes in process and geometry by plotting differences between UTS and YS and averages for each sample type. Such comparisons might be set up for different values of heat treatment, thickness, orientation, etc. The residual is the difference between the expected value based upon all input variables and the actual value for a given point.[2] Intentional variations are extracted to leave the effect of unintentional process variations intact.

Figures 2 through 6 show results of the four-step method used for this study. Figure 2 shows analysis results for the first step (reducing the data to residuals) and compares residuals for UTS and YS. This plot would look different had all the data fallen at either extreme. One extreme distribution might have been plotted as a thin straight line, with all variation due to unintentional process variation. Another might have appeared as a circle around the origin, with all variation due to such random effects as inherent material variability or measurement error. The correlation coefficient is used to quantify the degree of variation and randomness. Here, the correlation coefficient squared of the data group is 80%. This result indicates that 80% of the property variation is due to variations in process and 20% is caused by random effects.

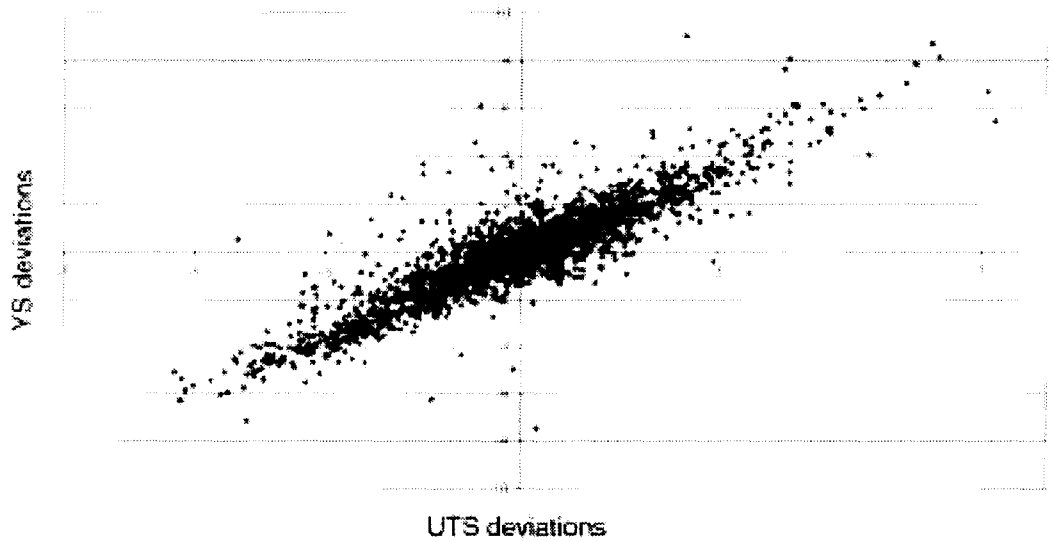

Figure 2. UTS versus YS residuals

Figure 3 shows analysis results for the second step (visualizing residuals as a function of time) with UTS residuals plotted by test date. Time is used as a proxy for process improvements based on the assumption that the processes continuously changed. Such process improvements might include a new heat treat control philosophy, composition retargeting, rolling practices, etc. The data do not show any obvious drift toward progressively higher UTS or a narrowing of the data envelope, which would indicate better process control. Residuals are considered a good metric for process control, with large values indicating significant process variations.

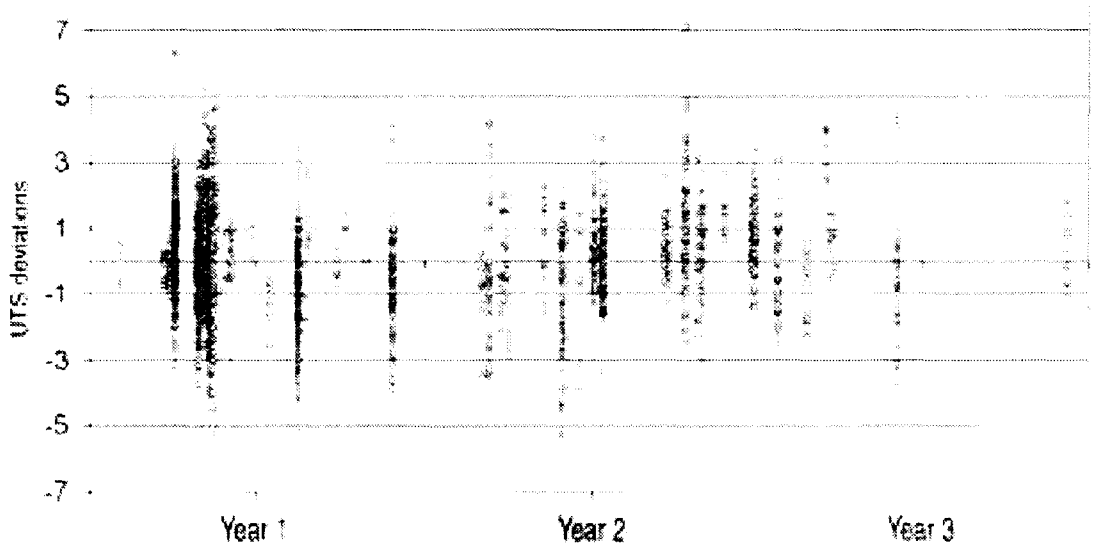

Figure 3. UTS residuals versus time

Figure 4 shows analysis results for the second and third steps (grouping data and quantifying scatter). Twelve data groups may develop when residuals are divided into subgroups to facilitate measurements of data scatter and mean. These boundaries reflect natural divisions between testing efforts and keep the size of each group within one order of magnitude of the other groups. Unlike the UTS data, the elongation data show a gradual narrowing of the data envelope.

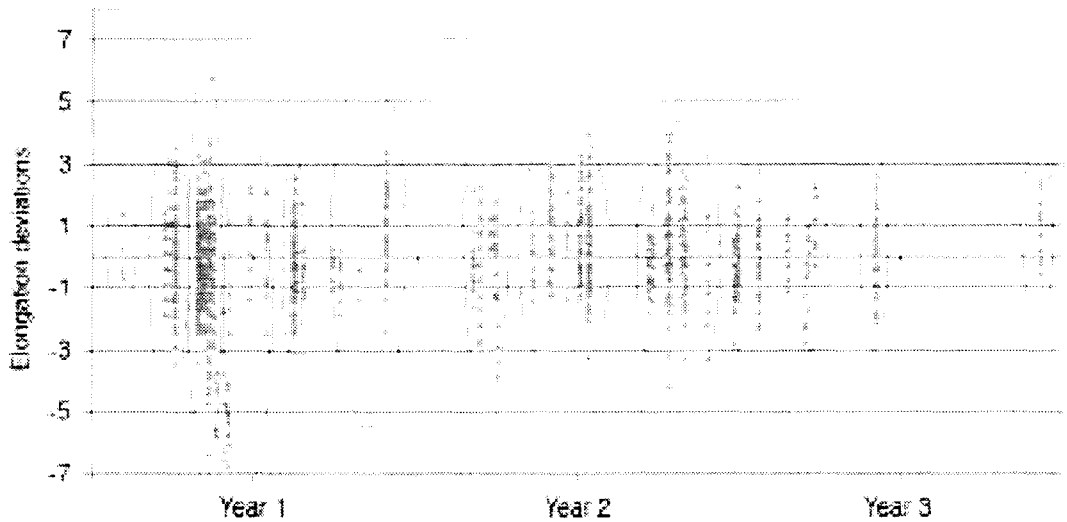

Figure 4. Elongation residuals versus time

Figures 5 through 6 show other analysis results for the third step. Here, Figure 5 shows the size of the groups generated. All data groups fall between 60 and 600 points, except for the two groups at the ends.

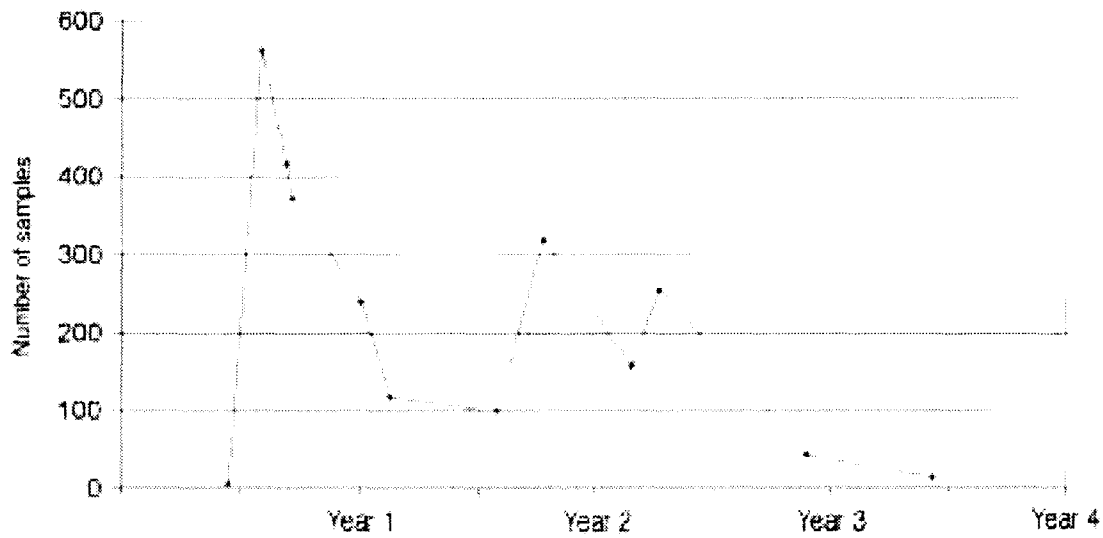

Figure 5. Number of points versus time

Figure 6 includes lines that represent averages for each group. These data do not indicate a trend with time. The error bars indicate plus and minus one variance (i.e., one standard deviation squared) while short horizontal lines show maxima and minima for data groups. Neither variance nor range shows any systematic narrowing with time, although they show significant differences from group to group. High variance occurs together for YS and UTS, primarily due to process variations.

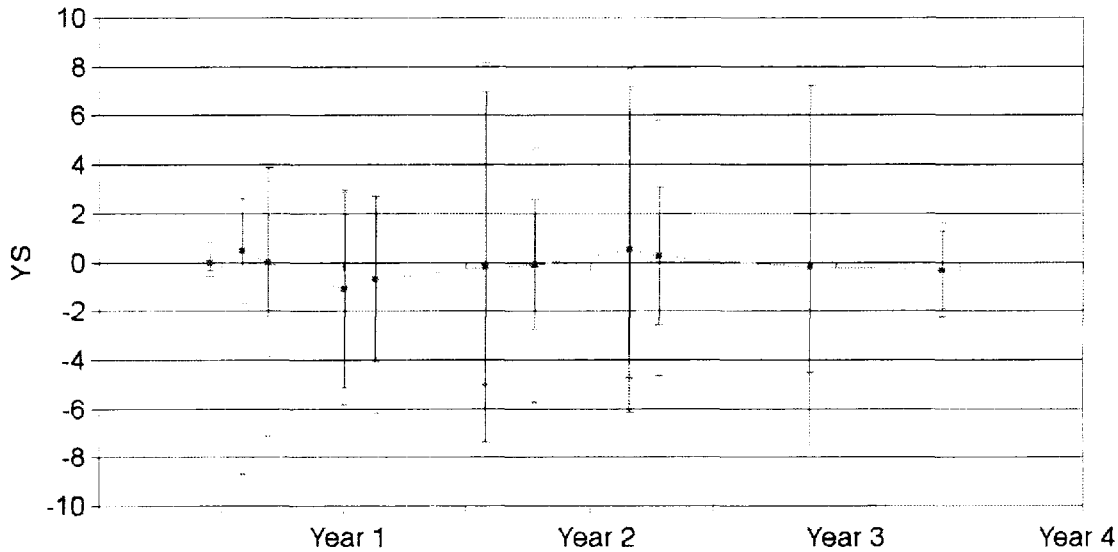

(a) YS

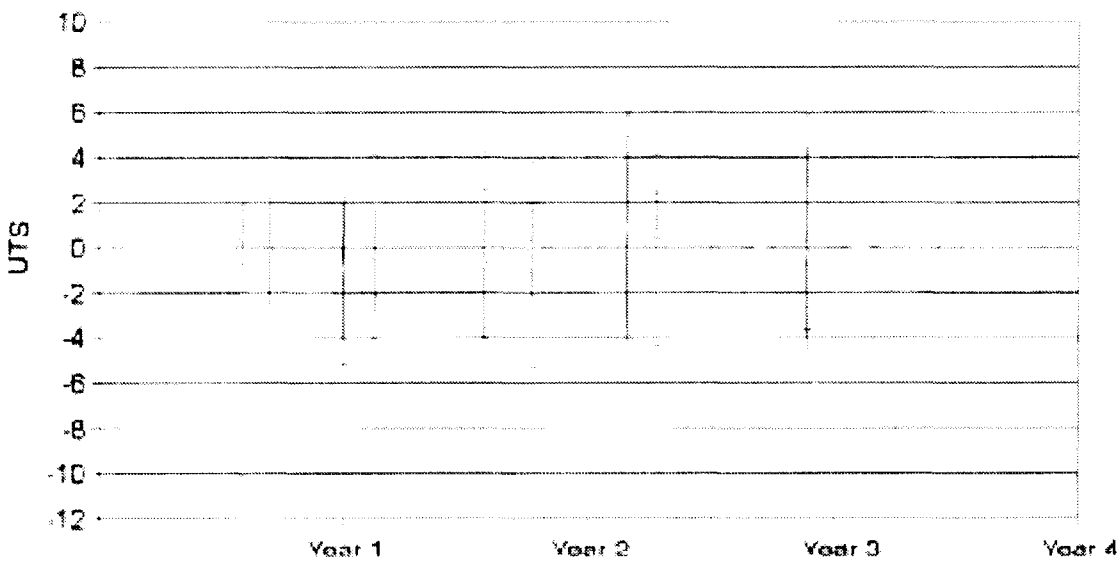

(b) UTS

Figure 6. Summary of Variance for Three Properties

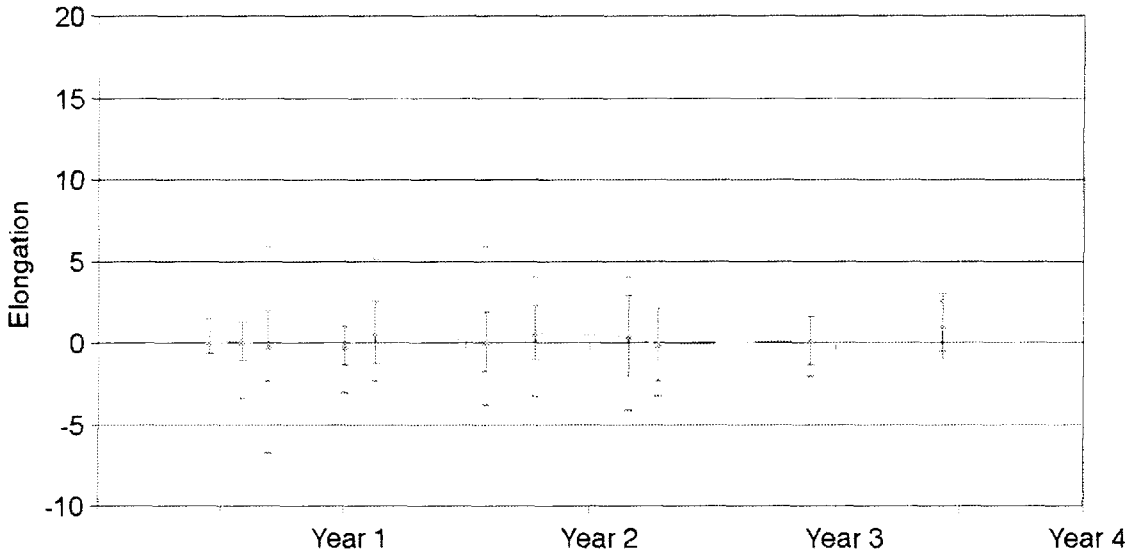

(c) Elongation

Figure 6. Summary of Variance for Three Properties (continued)

Process variations are considered the primary source of property variability. No clear patterns emerge when raw residuals are examined as a function of time or when discrete groups of data are analyzed separately. Data variation is quantified as a function of input variables when ANOVA[3] is used to track process control for sets of acceptance data. However, this technique presents an inherent problem. A well-designed ANOVA experiment should have the same number of data points for each combination of input variables. If the data points are not evenly distributed, the input variables are considered to be convoluted. For example, Table 2 shows convolution when a number of data points are compared as a function of heat treatment and time.

Table 2 – Number of Samples Tested
(Heat Treatment versus Time)

Start Date (1st test run)	Tempers					
	(1) OM	(1) OM	(1) T3M4	(1) T3M4	(1) T3M4	(1) T8M4
	(2) OM	(2) T8L4	(2) T8M4	(2) T3M4	(2) T8L4	(2) T8M4
Year 1	6	-	-	-	-	-
	162	400	-	-	-	-
	37	227	56	15	-	82
	18	88	-	-	-	367
	11	66	-	16	128	18
Year 2	16	72	-	2	18	12
	1	6	-	-	-	92
	13	72	-	21	176	37
Year 3	2	12	-	5	40	98
	11	59	-	5	40	140
	5	24	-	1	8	6
Year 4	-	-	-	-	-	15

Note: Two tempers were applied to the material, the first after it was rolled and the second after it was slightly stretched. "OM" is a temper designation which means that the material was not heat treated during this step.

Several blanks appear in the matrix. However, many spaces can be eliminated by culling the data. Table 3 shows a new matrix that should produce better ANOVA results, although the refined data are still convoluted.

Table 3 - Refined Data
(Heat Treatments versus Time)

Start Date (1st test run)	Tempers				
	(1) OM	(1) OM	(1) T3M4	(1) T3M4	(1) T8M4
	(2) OM	(2) T8L4	(2) T3M4	(2) T8L4	(2) T8M4
Year 1	162	400	-	-	-
	37	227	15	-	82
	18	88	-	-	367
	11	66	16	128	18
Year 2	16	72	2	18	12
	1	6	-	-	92
	13	72	21	176	37
Year 3	2	12	5	40	98
	11	59	5	40	140
	5	24	1	8	6

Note: Two tempers were applied to the material, the first after it was rolled and the second after it was slightly stretched. "OM" is a temper designation which means that the material was not heat treated during this step.

Table 4 shows ANOVA results for the refined data, which involve four different gage thicknesses. Two thin gages were heat treated under one set of conditions while two thick gages were heat treated under another set of conditions. Such differences indicate that the data will be convoluted for plate thickness and heat treat variables. This situation was addressed by combining the thinnest gages into one group for a given set of heat treatments.

Table 4 - Sources of Variance
Indicated by ANOVA Results for Culled Data

Variable	Number of Levels	UTS (%)	YS (%)	Elongation (%)
Time	10	3	3	5
Gage	2	2	2	2
Direction	4	17	19	32
Heat Treatment	5	78	76	61
Error	-	0	0	0

These results are not as precise as they would be for well-conditioned data resulting from a designed experiment. However, the ANOVA suggests that anisotropy and heat treatment control over 90% of the data variability studied. Small but significant contributions also come from gage thickness and time. Together, these four variables account for most of the variability seen in this particular Al alloy.

CONCLUSIONS

1. This study considered a large set of lot acceptance data for an aerospace Al alloy. However, the final ANOVA results are not entirely accurate because the original data inputs were convoluted.
2. Over 90% of the data variability can be attributed to the effects of anisotropy and heat treatment.
3. Process variation did not systematically increase or decrease during this period of time.

REFERENCES

1. U.S. Department of Defense, Information Handling Services. *Military Handbook 5H: Metallic Materials and Elements for Aerospace Vehicle Structures.* Document MIL-HDBK-5H (December 1, 1998): 9-18 – 9-64.

2. Montgomery, Douglas C. *Design and Analysis of Experiments.* (NY: John Wiley & Sons, 1991): 465.

3. Miller, Irwin; Freund, John E.; and Johnson, Richard A. *Probability and Statistics for Engineers.* (Englewood Cliffs, NJ: Prentice Hall, 1990): 376 – 413.

Electrostatic Levitation Processing of Bulk Metallic Glass Forming Liquids

C. C. HAYS, J. Schroers, U. Geyer, W. L. Johnson

Division of Engineering & Applied Science, 138-78
California Institute of Technology
Pasadena, CA 91125 USA
E-mail: chays@hyperfine.caltech.edu

Bulk metallic glass forming alloys are a novel group of multicomponent metallic alloys that exhibit exceptionally high resistance to crystallization in the undercooled liquid state. Compared with the rapidly quenched metallic glasses studied prior to 1990, these alloys can be vitrified at cooling rates <10 K/sec. With critical cooling rates this low, standard processing methods can be employed. This point, together with their high mechanical strengths, shows that bulk metallic glasses are a promising material system for application as an engineering material. Considerable success has recently been achieved in toughening bulk metallic glasses using *in situ* formed ductile phase dendrites in a bulk metallic glass matrix [1]. Processing of these composites involves interfacial reactions and atomic transport in the molten state; thus, knowledge of atomic diffusion constants is critical in this work, as it directly impacts the evolution of the microstructure during processing. Electrostatic levitation (ESL) processing provides an excellent means for examining the thermophysical properties of an undercooled liquid metal system. The advantages of this method are ideal for the study of liquid state properties of bulk metallic glass forming liquids. In this talk, we will discuss results obtained from recent ESL experiments conducted at the Marshall Space Flight Center ESL facility. We will review some of the experimental details required to use the ESL method as a platform for the determination of diffusion coefficients in the high temperature liquid and undercooled liquid regimes of a bulk metallic glass forming liquid, the latter topic being the experimental goal of our proposed NASA flight experiment. The determination of atomic diffusion constants is critical to understanding the processing and control of the dendritic structures in the *in situ* formed composites. Recently, we used the ESL to examine the bulk metallic glass forming ability in the Zr-Nb-Cu-Ni-Al alloy system. We have identified a composition that exhibits a substantially improved glass forming ability in comparison to neighboring compositions: $Zr_{58.5}Nb_{2.8}Cu_{15.6}Ni_{12.8}Al_{10.3}$. This alloy is easily vitrified by standard techniques, *e.g.*, arc melting and melting on a water-cooled silver boat apparatus. When examined in the ESL, the alloy is vitrified by purely radiative cooling. This is the first non-Be containing alloy to be vitrified on free cooling in the ESL. This places the critical cooling rate for this composition <7 K/sec. The TTT diagram for this alloy has been determined and exhibits a single c-shaped branch and a nose time centered at ~20 seconds. Microstructural properties of the ESL processed materials were examined by x-ray diffraction, electron- and optical-microscopy, and thermal analysis methods. These results are used to interpret the complex evolution of glass forming properties observed in this alloy system [2]. As an excellent example of technology transfer, we will discuss use of this new bulk metallic glass as a solar wind collector in the NASA sponsored Genesis Mission, scheduled for launch in February 2001 (Prof. Don Burnett, California Institute of Technology, Principal Investigator).

[1]. C. C. Hays, C. P. Kim, and W. L. Johnson, Phys. Rev. Lett. **84**, 2901 (2000).

[2]. C. C. Hays, J. Schroers, U. Geyer, and W. L. Johnson (to be submitted to Appl. Phys. Lett.).

"Residual Stress Prediction in Machined Workpiece Surfaces"

Marusich, T. D.

Third Wave Systems, Inc

Abstract

The increasing drive for productivity improvements and consistent part dimensionality in aerospace structures has lead to the advent of machined monolithic parts. High speed machining technology employed affords the manufacture of thin-walled parts from single billets of material, resulting in the removal of approximately 85% of the initial workpiece material. With thin-walled monolithic parts come the increased propensity for workpiece distortion and few arresting mechanisms for crack propagation, largely due to potentially unfavorable residual stress states. These imposed states of stress can be a result of the machining conditions used (e.g., feeds, speeds and cutter geometry). A general method is presented to model the residual stress state induced by metal cutting operations which takes into account workpiece thermo-mechanical properties, cutter geometry and process parameters. In this paper the model is specifically applied to Al7050. Results indicate the magnitude and sign of the state of stress is shown to have no intuitive correlation to machining process parameters such as speed and chip load. Similar results are shown for stress-induced bending moments, a potential strong contributor to part distortion. In addition, the machining-affected layer is shown to be on the order of 1mm, easily on the same length scale as the wall thickness of aerospace structures.

Introduction

In order to improve metal cutting processes, i.e. lower part cost, it is necessary to model metal cutting processes at a system level (Ehmann *et. al., 1997*). A necessary requirement of such is the ability to model interactions at the tool chip interface and thus, predict cutter performance. Many approaches such as empirical, mechanistic, analytical and numerical have been proposed. Some level of testing for model development, either material, machining, or bothis required for all. However, the ability to model cutting tool performance with a minimum amount of testing is of great value, reducing costly process and tooling iterations. In this paper, a validated finite element-based machining model is presented and employed to determine the effects of cutting process parameters such as speed and chip load on the induced state of residual stress.

Typical approaches for numerical modeling of metal cutting are Lagrangian and Eulerian techniques. Lagrangian techniques, the tracking of discrete material points, has been applied to metal cutting for over a decade (Strenkowski and Carroll, 1985; Komvopoulos and Erpenbeck, 1991; Sehkon and Chenot, 1993; Obikawa and Usui, 1996; and Obikawa *et. al.*, 1997.). Techniques typically used a predetermined line of separation at the tool tip, propagating a fictitious crack ahead the tool. This method precludes the resolution of the cutting edge radius and accurate resolution of the secondary shear zone due to severe mesh distortion. To alleviate element distortions, others used adaptive remeshing techniques to resolve the cutting edge radius (Sehkon and Chenot, 1993; and Marusich and Ortiz, 1995; Marusich, 2000). Eulerian approaches, tracking volumes rather than materialparticles, did not have the burden of rezoning distorted meshes (Strenkowski and Athavale, 1997). However, steady state free-surface tracking algorithms were necessary and relied on assumptions such as uniform chip thickness, precluding the modeling of milling processes or segmented chipformation .

In this paper, a Lagrangian finite element-based machining model is applied to orthogonal cutting of Al7050. Techniques such as adaptive remeshing, explicit dynamics and tightly couple transient thermal analysis are integrated to model the complex interactions of a cutting tool and workpiece.

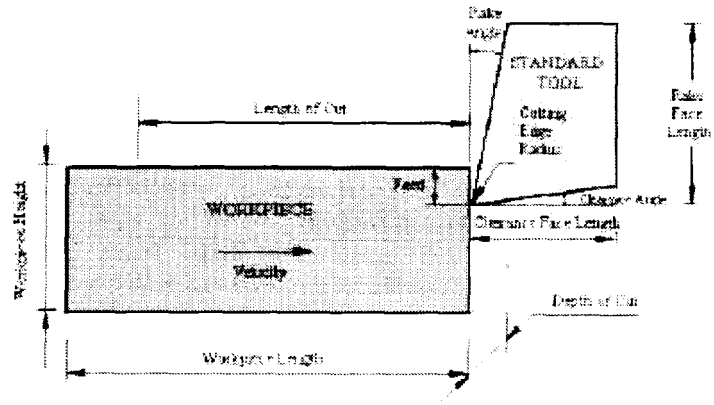

Figure 1 Schematic of orthogonal cutting conditions

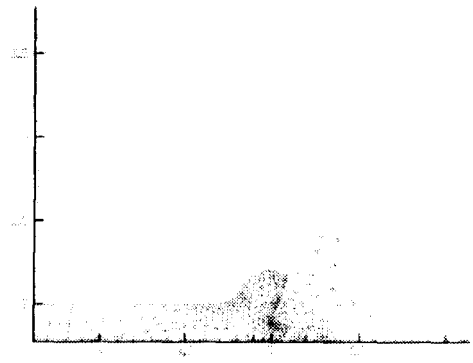

Figure 2 Initial tool indentation

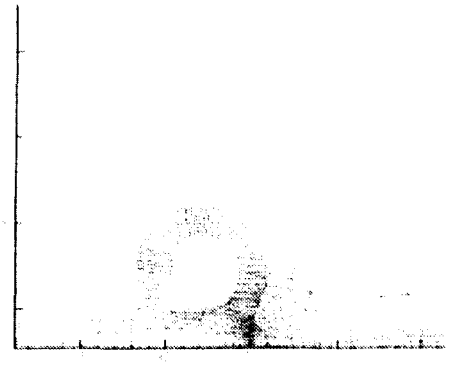

Figure 3 Chip formation

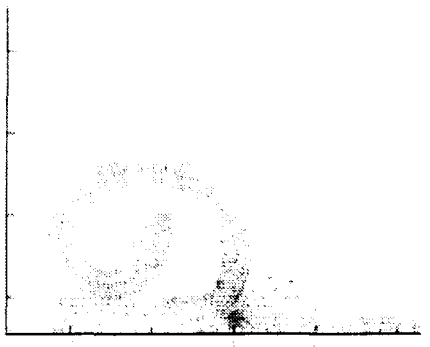

Figure 4 Fully developed continuous chip

Machining Simulation System

Simulations were performed with Third Wave Systems ***AdvantEdge*** machining simulation software, which integrates advanced finite element numerics and material modeling appropriate for machining. The orthogonal cutting system is described in Fig. 1 where the observer is in the frame of reference of the cutting tool with the workpiece moving with velocity v. The cutting tool is parameterized by rake and clearance angles, and a cutting edge radius, but can also accommodate general chip breaker geometries. In the plane strain case the depth of cut into the plane is considered to be large in comparison to the feed. The cutting tool initially indents the workpiece, Fig. 2, the chip begins to form Fig. 3, and finally curls over hitting the workpiece ahead of the cut, Fig. 4.

Modeling Approach

AdvangEdge, Third Wave Systems (2000), is an explicit dynamic, thermo-mechanically coupled finite element model specialized for metal cutting. Features necessary to model metal cutting accurately include adaptive remeshing capabilities for resolution of multiple length scales such as cutting edge radius, secondary shear zone and chip load; multiple body deformable contact for tool-workpiece interaction, and transient thermal analysis. For example, in the vicinity of the cutting edge radius the workpiece material is allowed to flow around the edge radius. The initial mesh, Fig. 5, becomes distorted after a certain length of cut, Fig. 6, and is remeshed in this vicinity to form a regular mesh again, Fig. 7. For a comprehensive discussion on the numerical techniques the reader is referred to Marusich and Ortiz (1995) and to Marusich (2000) for validation examples.

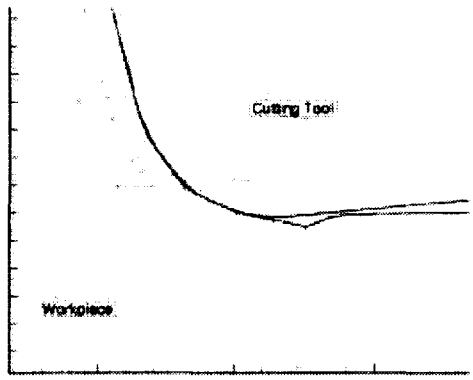

Figure 5. Initial mesh magnified in the cutting tool edge vicinity.

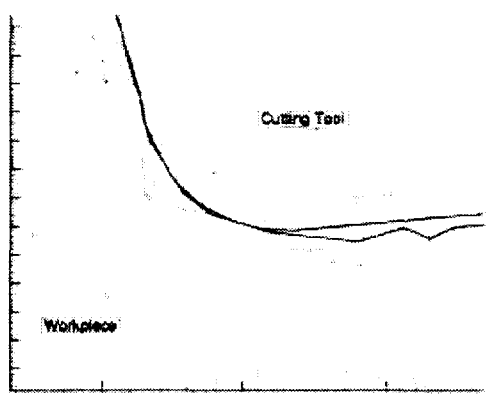

Figure 6 Deformed mesh.

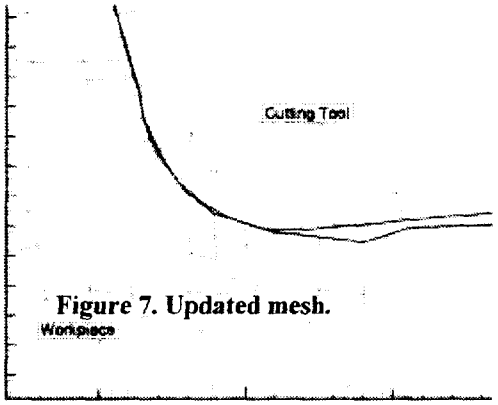

Figure 7. Updated mesh.

Due to the transient thermal and dynamic behavior of the model it is necessary to thermo-mechanically relax the workpiece after the cutting process to accurately model the state of residual stress. The milling operation modeled is idealized by a single cutting tooth in a plane strain, orthogonal cutting, mode with a constant chip load, typically set to be the maximum in the cut.

Material Modeling

In order to model chip formation, constitutive modeling for metal cutting requires determination of material properties at high strain rates, large strains, and short heating times and is quintessential for prediction of segmented chips due to shear-localization (Sandstrom and Hodowany 1998; Childs, 1998). Specific details of the constitutive model used are outlined in Marusich and Ortiz (1995). The model contains deformation hardening, thermal softening and rate sensitivity tightly coupled with a transient heat conduction analysis appropriate for finite deformations.

Results

Residual stress predictions were made for several cutting conditions, varying speed, chip load and radial rake angle, Table 1. The normalized residual stress is plotted as a function of depth from the workpiece surface, Fig. 8. While no clear trend with process parameters is evident, two distinct residual stress signatures appear. Singling out three cutting conditions and comparing with the baseline conditions the two distinct stress signatures are apparent, Fig 9. A resulting bending moment per unit length can be computed from the stresses and plotted as a function of speed and chip load for the four cases, Fig. 10. Finally, the normalized moment is plotted as a function of tangential cutting force for all the cutting conditions, Fig. 11.

Table 1. Cutting conditions

Case	Chip Load per Tooth (mm)	Cutting Speed (m/min)	Tool Geometry
1	0.2	275	12° rake
2	0.4	138	12° rake
3	0.4	275	12° rake
4	0.2	275	25° rake
5	0.2	550	12° rake, 50mm dia.
6	0.4	550	12° rake, 50mm dia.
7	0.2	138	12° rake
8	0.3	275	12° rake
9	0.3	138	12° rake
10	0.1	275	12° rake

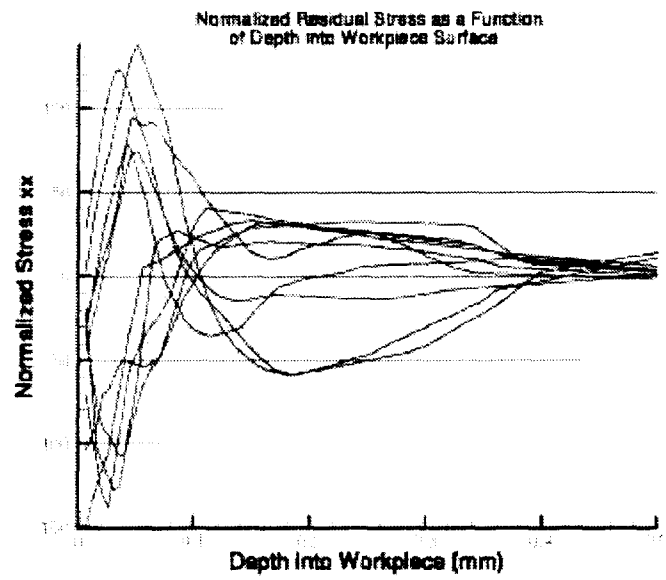

Figure 8 Residual stress profiles into workpiece surface for 10 different cutting conditions

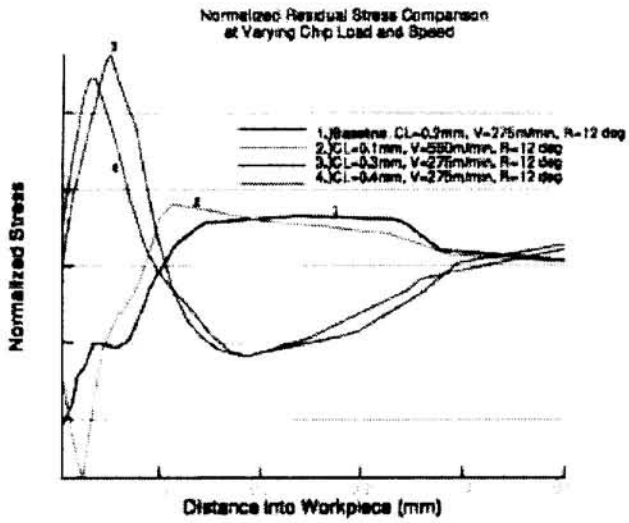

Figure 9. Select cutting conditions tested with substantially different residual stress signatures

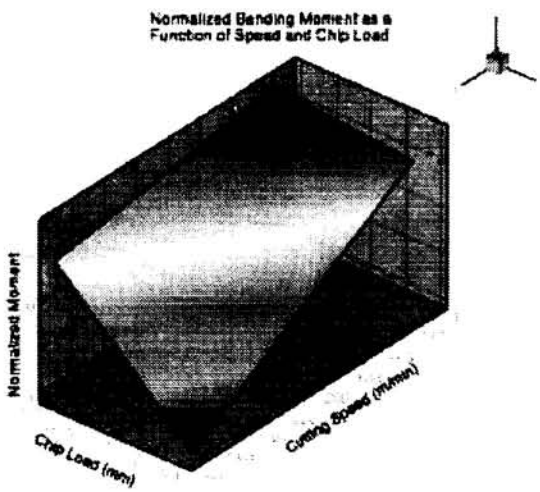

Figure 10. Normalized bending moment as a function of cutting speed and chip load for select cutting conditions.

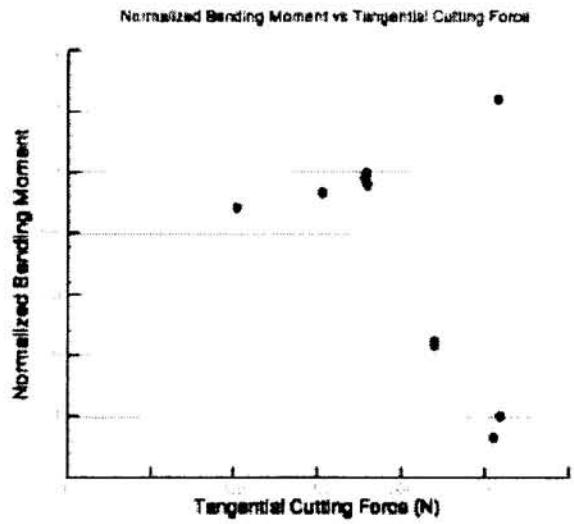

Figure 11. Normalized bending moment as a function of tangential cutting force for 10 different cutting conditions.

Discussion

The residual stress profiles for the entire test matrix are plotted as a function of depth into the workpiece, Fig. 8. The profiles typically decay to zero around 0.5mm beneath the workpiece surface, varying from positive to negative in order to satisfy equilibrium. Since thin walled aerospace parts can be on the order of a couple of millimeters in thickness, the machined-affected zone can be significant. When looking for correlation with process parameters, residual stress profiles were analyzed over a range of chip loads, cutting speeds and a pair of rake angles and exhibited no clear trends. Stress profiles in this parameter space appear to be most influenced by the chip load rather than speed or rake angle. The bending moments computed for these cases show a change in sign, i.e. an opposite tendency for bending, when the chip load is increased from 0.1mm to 0.3mm per tooth, Fig. 10. However, when the entire test matrix is plotted against tangential cutting force there appears to be either no trend or a bifurcation point, Fig 11.

Conclusion

A general method is presented to model the residual stress state induced by metal cutting operations which takes into account workpiece thermo-mechanical properties, cutter geometry and process parameters. In this paper the model is specifically applied to Al7050. Results indicate the magnitude and sign of the state of stress is shown to have no intuitive correlation to machining process parameters such as speed and chip load. Similar results are shown for stress-induced bending moments, a potential strong contributor to part distortion. In addition, the machining-affected layer is shown to be on the order of 1mm, easily on the same length scale as the wall thickness of aerospace structures.

References

Childs, T. H. C., "Material Property Needs inModelling Metal Machining," *CIRP Workshop on Modeling Metal Cutting* , (1998).

Flom, D. G., ``High-Speed Machining," inBruggeman and Weiss (eds.)
Innovations in Materials Processing, Plenum Press, (1983) 417-439.

Kobayashi, S.,Herzog, R. P., Eggleston, D. M. andThomsen, E. G., "A Critical Comparsion of Metal-Cutting Theories with New Experimental Data", Trans. ASME J. Eng. Ind. (1960), 333-347.

Marusich, T. D. and Ortiz, M., "Modeling and Simulation of High-Speed Machining",
Int. J. Num. Meth. Eng **38** (1995), 3675-94.

Marusich, T. D., "Effects of Friction and Cutting Speed on Cutting Force", Submitted to ASME
Journal of Manufacturing Science and Engineering (2000).

Sandstrom, D. R. and Hodowany, J. N., "Modeling the Physics of Metal Cutting in High-Speed Machining," Machining Science and Technology**2** (1998), 343-353.

Stevenson, R. and Stephenson, D. A., "The Mechanical Behavior of Zinc During Machining," Journal of Engineering Materials and Technology,**177** (1995), 172-178.

Strenkowski, J. S. and Athavale, S. M., "A Partially Constrained Eulerian Orthogonal Cutting Model for Chip Control Tools," Journal of Manufacturing Science, **119** (1997), 681-688.

Third Wave Systems, Inc. 2000 "***AdvantEdge v3.3*** Machining Simulation Software", Minneapolis, MN

Obikawa, T. and Usui, E., "Computational Machining of Titanium Alloy-Finite Element Modeling and a Few Results," Journal of Manufacturing Science and Engineering, **118** (1996).

Obikawa, T., Sasahara, H., Shirakashi, T. and Usui, E. "Application of Computational Machining Method to Discontinuous Chip Formation," Journal of Manufacturing Science and Engineering,**119** (1997), 667-674.

Contact

Troy D. Marusich
Troym@thirdwavesys.com
7301 Ohms Lane Suite 580
Minneapolis, MN 55439
www.thirdwavesys.com

EASILY PROCESSABLE HIGH TEMPERATURE AND FLAME RESISTANT PHTHALONITRILE COMPOSITES FOR AEROSPACE APPLICATIONS

Teddy M. Keller
Advanced Materials Section, Code 6127
Chemistry Division
Tel: 202-767-3095
E-Mail: keller1@ccf.nrl.navy.mil

Harry N. Jones
Materials Characterization Section, Code 6325
Materials Science and Technology Division
Tel: 202-767-1278
E-Mail: jones@anvil.nrl.navy.mil

Naval Research Laboratory
Washington, DC 20375-5320

INTRODUCTION

The aerospace industry is utilizing structural composites in airframes and skins to reduce weight and to improve fuel efficiency (1). With an increase in future composite usage, materials with low flammability and high strength will be needed to maintain airframe loads in the next generation, reusable, and expendable aeronautical and space vehicle systems. Polymer-based materials are currently being used in non-structural and semi-structural applications in cabin interiors. The materials are fairly flammable and/or generate copious amounts of smoke in a fire scenario and do not meet the FAA goal of generating survivable aircraft cabin conditions for 15 minutes in post-crash fuel fire. Fiber-reinforced composites utilizing high temperature polymers are more resistant to ignition but can suffer from poor processing characteristics and mechanical properties. Increased usage of polymers and composites by the aerospace industry will demand materials with better fire performance, structural integrity, and ease of processability.

Phthalonitrile-based composites under development at the NRL show excellent flame resistant properties and thermo-oxidative stability (2) approaching 375 ^{0}C. The phthalonitrile cure reaction is not accompanied by evolution of volatile by-products. Therefore, void-free components can be made easily from this resin system. The advantages and versatility of the phthalonitrile polymer may be realized in terms of ease of processing and superior properties. The phthalonitrile monomer can be cured into a thermoset resin using a wide variety of curing additives (2-5). Additionally, a prepolymer (B-staged resin) or prepolymerization composition may be prepared and stored for later usage with an indefinite shelf life under ambient conditions. The polymerization rate is also easily controllable as a function of curing additive and processing temperature for thick section composite fabrication. With regard to the thermal properties, the fully cured resins do not show a glass transition temperature up to 450^{0}C and exhibit good mechanical property retention at elevated temperatures. The current state-of-the-art high temperature resin based on PMR polyimide, designated as PMR-15, shows promise up to 316 ^{0}C but is accompanied by processing problems such as volatiles from residual solvent and a short processing or reaction time (6,7). The short reaction time translates to inadequate resin flow for fabricating thick and complicated composite structures. In light of these drawbacks with existing resin systems, phthalonitrile matrices show promise and may help further the usage of polymeric composites in applications that need high temperature and flame resistant capabilities.

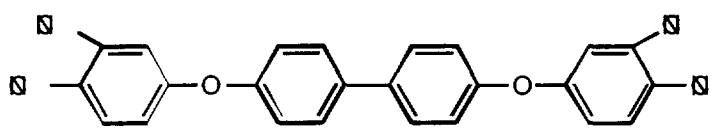

Phthalonitrile Monomer

Phthalonitrile monomer, [4,4'-Bis (3,4-dicyanophenoxy)biphenyl], has been commercialized by Eikos, Inc. and is being used as a matrix resin for composite formulations. Composite panels have been processed by conventional prepreg consolidation and by resin infusion and filament winding methods using carbon tape (8), carbon fabric (9) and glass fabric (10) as reinforcements. Since the initial resin melt viscosity is low (100-200 cp) and can be controlled by

the proper selection of curing additive and curing temperature, the phthalonitrile composites are amenable to processing by more cost effective methods such as resin transfer molding and resin infusion molding. Mechanical properties and thermal and oxidative stability of phthalonitrile-based composites are superior to that of many state-of-the-art high temperature composites. With regard to fire performance, phthalonitrile composites excel over other polymeric composites. The phthalonitrile composites are the only materials that meet the Navy's stringent requirements of MIL-STD-2031 (11) for use of polymeric composites aboard Navy submarines. The specification contains test methods and requirements for flammability characteristics such as flame spread index, specific optical density, heat release, time to ignition, oxygen-temperature index, combustion gas generation, etc. A large fraction of our current efforts at NRL are targeted toward the optimization of curing parameters, property determination, and working with industry and other research organizations to further develop these new composite materials for marine and aerospace applications.

PROCESSABILITY

Most of our composite efforts have involved using aromatic diamines with ether linkages connecting the terminal aromatic amine moieties as curing additives. The amount of aromatic amine that can be used to form a prepolymer is limited due to the reactivity of the amine toward the phthalonitrile monomer. A prepolymer is defined as a low molecular weight B-staged polymeric composition, which is formed from reaction of the amine with the melt of the monomer. Upon cooling, the B-staged prepolymer is a frangible solid, which can be pulverized into a powder. In contrast to prepolymers from other resin systems, the phthalonitrile prepolymer can be stored indefinitely at room temperature. In the fabrication of thick composite components from either a prepreg, by resin infusion molding, or by resin transfer molding (RTM), processing difficulties may arise if the polymerization proceeds too rapidly. This is not a problem in the phthalonitrile systems due to the low cure exotherm.

An improved, more cost effective processing method, which involves a prepolymerization composition formed from mixing various amounts of phthalonitrile monomer and aromatic amine curing additive at room temperature, is under development at the NRL. Upon melting, the polymerization rate depends on the composition of the mixture and melt temperature. These phthalonitrile/curing additive prepolymerization compositions are especially useful for fabrication of composite components by resin transfer molding (RTM), filament winding, injection molding, or prepreg formulation from the melt in the absence of solvent. The composition is completely stable under ambient conditions before melting occurs. Any amine curing additive that is stable and shows non-volatility at the processing or polymerization temperatures can be used to polymerize phthalonitrile monomers. The prepolymerization composition is heated until complete melting occurs, which depends on the melting point of the phthalonitrile monomer. In the melt stage, the curing additive reacts with the phthalonitrile monomer. The viscosity of the resulting B-staged prepolymer at a given temperature and time depends on the amount and reactivity of curing additive in the composition. The composition can be used upon melting (B-stage) in the fabrication of composite components.

$$\text{Phthalonitrile Monomer} + \text{Curing Additive} \xrightarrow{\text{mix}} \text{Prepolymerization Composition}$$

Rheometric studies on phthalonitrile prepolymers with the same molar concentrations of 1,3-bis (3-aminophenoxy)benzene (APB) and bis[4-(4-aminophenoxyphenyl) phenyl] sulfone (BAPS) as curing agents were conducted to monitor the viscosity changes accompanying the cure reaction. Figure 1 shows the melt viscosity as a function of reaction time at 260 °C. The initial melt viscosity is low and range between 50-300 cp. From the plots, it is evident that the melt viscosity of prepolymers containing APB increase at a faster rate than the BAPS-containing compositions. Differential scanning calorimetry (DSC) analyses show that both curing additives react readily with the monomer between 250-260°C. The difference in the reactivity of APB and BAPS toward the phthalonitrile monomer is attributed to the differences in the basicity of the two amines. The basicity of the BAPS is lower due to the presence of the electron withdrawing sulfone group when compared to APB that has an electron donating phenoxy group. Based on this study, cure of the phthalonitrile monomer with BAPS may be advantageous to slow down the polymerization and thus broaden the processing window. Previous cure studies with APB (8) have indicated that the melt viscosity is very sensitive to small changes in the diamine concentration used to make the prepolymer. The preferred amount of APB for composite component fabrication is 1.5-2.3 weight percent. When larger amounts are used, the viscosity of the prepolymer advances too rapidly to consolidate a quality composite panel or component. Given the lower reactivity and a higher molecular mass of BAPS, the amine concentration range for prepolymer formulations can be broadened to 2-4 weight percent.

COMPOSITE FABRICATION

Phthalonitrile composite panels have been fabricated by consolidation of prepreg (undirectional carbon, woven glass and carbon) and by resin infusion molding (woven glass and carbon) techniques for testing in a research size United McGill Corporation autoclave at the National

Figure 1. Viscosity vs.Time Plots for Phthalonitrile Cure with Two Different Amines at 260^{0}C

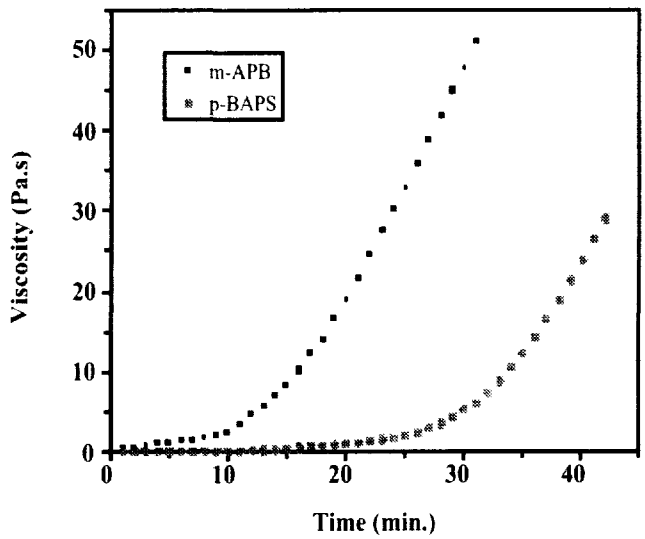

Institute of Standard and Technology (NIST). The resin infusion process is similar to the prepregging process in that the resin flows over the surface of dry fibers. Resin infusion may be viewed as similar to the cure and consolidation process since the viscosity of the resin changes with time and temperature due to the cure process. In this process, the melt viscosity, which controls the resin flow, is of paramount importance. Resin infusion simplifies the composite manufacturing process where impregnationand consolidation are combined in a single step. In this process, unlike with prepregs, each ply is made up of dry fibers and the matrix resin is placed at the top or bottom. A mold is formed from sealant tape and bagging materials and the matrix resin may be in the form of a film, powder, pellet or viscous liquid. This processing technique is particularly attractive for resins that can realize very low viscosity values. Regardless of the technique used to fabricate the phthalonitrile panels, consolidation is accomplished by heating for 1h at 250 °C and 3h at 325 °C under 200 psi pressure (1.3 MPa). The panels were postcured up to 375 °C to improve the physical properties. An alternate cure cycle involves heating for 1 h at 250 °C, for 2h at 325 °C, and for 1-4 h at 375 °C under 200 psi pressure (1.3 MPa). Heating and cooling rates are at 4 °C/min and high vacuum is applied at the start of the cycle. After a dwell at 250 °C for 0-60 min., pressure is applied, which is completed within 1/2h, followed by the cessation of vacuum.

The glass transition temperature (T_g) of the panels is estimated from the modulus vs. temperature plots obtained by dynamic mechanical analysis (DMA). A carbon reinforced panel that had been fabricated from a prepreg and cured for 1h at 250 °C and 3h at 325 °C exhibited a glass transition temperature in excess of 350 °C and maintained 75% of the initial modulus at 400 °C. With an additional postcure for 2h at 350 °C, the T_g is shifted to temperatures above 400 °C. Specimens that are postcured at 375 °C for 2, 4 and 6h do not exhibit a T_g in the measurement range (<450 °C) and appear to retain about 73, 75 and 83%, respectively, of their storage modulus at 450 °C. With an even longer postcure cycle of 8h each at 350 and 375 °C, approximately 90% of the room temperature modulus is maintained at 450 °C.

Table 1. Mechanical Properties of Unidirectional Composite Panels (*Denotes Values Measured for A Panel Made from Different Batch of Prepreg)

Property	Phthalonitrile/IM7	PMR-15/IM7
0_ Tension		
Strength, MPa (±%)	2000 [2400]* (1)	2500 (7)
Modulus, GPa (±%)	183 [162]* (2)	146 (3)
Strain, % (±%)	1.0 [1.36]* (7)	1.6 (4)
90_ Tension		
Strength, MPa (±%)	41 (10)	29 (7)
Modulus, GPa (±%)	10 (8)	9 (3)
Strain, % (±%)	0.4 (12)	0.5 (30)
0_ Flexure		
Strength, MPa (±%)	2350 (2)	1530 (5)
Modulus, GPa (±%)	174 (2)	122 (4)
Strain, % (±%)	1.3 (18)	1.3 (6)
90_ Flexure		
Strength, MPa (±%)	80 (1.3)	
Modulus, GPa (±%)	11 (9)	
Strain, % (±%)	0.6 (4)	
Short Beam Shear		
Strength, MPa (±%)	85 (2)	105 (2)

MECHANICAL PROPERTIES

Composite mechanical properties, in general, are governed by many factors including processing parameters (time, temperature and pressure), type of fibers and fiber orientation, prepreg quality, post-curing environment (e.g., air or nitrogen), specimen size and configuration, and composite composition (fiber, resin and void content). Data on the mechanical properties of carbon-based phthalonitrile (8) and PMR-15 composites (12) are summarized in Table 1. These results reveal that some of the mechanical properties of phthalonitrile-based composites are superior while others are comparable to PMR-15. For instance, the flexural strength of the phthalonitrile composite is substantially higher than that for the PMR-15 analog (2350 MPa vs. 1530 MPa). Similarly, the transverse tensile strength of the phthalonitrile composite is 41 MPa, which is higher than the corresponding PMR-15 composite value by about 40%. Although the measured longitudinal tensile strength for the phthalonitrile system is low (2010 MPa), panels fabricated from a different batch of prepreg and processed by a different method yield a strength value (2400 MPa) comparable to that of the PMR-15 composite (2500 MPa). This improvement suggests that there is additional room for property improvement with optimization of the prepregging and consolidation processes. The measured tensile and flexural modulii of the phthalonitrile composite are also superior to those of the PMR-15 composite. However, the short beam shear strength of the phthalonitrile composite is slightly lower than that of the PMR-15 system. This test is particularly sensitive to relative sample and fixture dimensions and specimen surface preparation.

WATER ABSORPTION AND FLAMMABILITY CHARACTERIZATION

To be considered for advanced aerospace (aircraft and space vehicle) applications, a polymeric composite should have low water absorption and outstanding flame resistant properties. Phthalonitrile based glass and carbon reinforced composites exhibit water uptake level <1% after immersion in water for over 30 months. Tables 2 and 3 present heat release and ignitable data of phthalonitrile/glass and phthalonitrile/carbon composites. Pertinent data for other state-of-the-art polymeric composites and the Navy specification MIL-STD-2031 are also presented in these tables for comparison. Heat release is defined as the heat generated in a fire due to various chemical reactions occurring within a given weight or volume of the material. This characteristic provides a relative fire hazard assessment in that the material with low heat release rate per unit weight or volume will do less damage to the surroundings than the one with a high

heat release rate. It has been suggested that the heat release rate of a material measured in a small scale test under simulated radiant exposure conditions is the single most important parameter in characterizing the hazardous nature of a material in a fire (13). The peak heat release (PHR) and time to ignition (T_{ig}), which serve as a measure of resistance of a material to participate in fire, are very impressive for carbon and glass reinforced phthalonitrile composites.

For usage of organic polymeric composites inside of a submarine, Navy specification MIL-STD-2031 requires a maximum peak heat release (PHR) of 150 kW/m^2 and a minimum time to ignition (T_{ig}) of 60 sec. at a radiant heat flux of 100 kW/m^2. When compared with other high temperature, high performance composites, cone calorimetric studies have shown that a phthalonitrile carbon composite (8) is the only polymeric material that satisfies the Navy's flame retardant specification (PHR and T_{ig}) for using lightweight, polymeric composites for submarine applications (Table 3). At 100 kW/m^2 irradiance heat treatment, phthalonitrile carbon composites meet the requirement and exhibit PHR and T_{ig} values of 118 and 75, respectively. This is an important finding given the fact that high performance composites that meet the Navy's flammability specification have not been available. Preliminary cone calorimetric data has also been obtained on a phthalonitrile glass composite panel (9) containing a fiber volume fraction of 54. The PHR and T_{ig} values are 106 and 59, respectively (Table 2). This study will be repeated on a panel containing a higher volume fraction of fiber.

Table 2: Summary of Heat Release Data for Phthalonitrile and Other Polymeric Composites. *NI Stands for No Ignition

Composite	Time to Ignition (s) at Heat Flux (kW/m^2) of				Peak Heat Release at Heat Flux (kW/m^2) of			
	25	50	75	100	25	50	75	100
MIL-STD-2031	300	150	90	60	50	65	100	150
Gl/Phthalonitrile	NI	NI	84	59	NI	NI	98	106
Gl/Vinyl Ester	278	74	34	20	188	199	300	256
Gl/Epoxy	535	105	60	40	39	178	217	232
Gl/Bismaleimide	503	141	60	38	128	176	245	285
Gl//Phenolic	NI	214	57	25	NI	47	97	133
Gl/Polyimide	NI	175	75	55	NI	40	78	85

The superior flame resistance of the phthalonitrile/carbon composite also meets the FAA requirement (no flammability at 35 kW/m^2 irradiance) for composite usage in an aircraft cabin. The flammability parameters derived from micro-scale calorimetric measurements (14) are the char yield at 650°C, the peak rate of heat release, and the total heat release at 900°C. The peak heat release rate is originally measured in W/g but is subsequently normalized by dividing with the heating rate to obtain the heat release with units of J/g-K. The total heat release in KJ/g is obtained from a numerical integration of the heat release rate curve and the char yield from the residual mass after the test. The char yield and total heat release of the phthalonitrile polymer are 87% and 2.1 kJ/g, respectively. The char yield and the total heat release values for the phthalonitrile polymers are far superior to those of other polymers such as polyimide (kapton), polybenzimidazole (PBI), phenolic triazine (PT-30), etc (15).

Table 3. Flammability Results for Carbon Fiber-Reinforced Composites

Composite	**Time to Ignition (sec.)**	**Peak Heat Release (kW/m^2)**
Carbon/Phthalonitrile	75	118
Carbon/PMR-15	55	85
Carbon/BMI	22	270
Carbon/PEEK	42	85

Carbon/Epoxy	28	232
Carbon/Phenolic	25	96

While the maximum temperature limit at which polymer matrix composites are normally considered for use is around 316-375 °C (600-700 °F), there are many applications such as missile structures, where the temperatures encountered are much higher but exist for only a few minutes. An example of this situation is found in some components of medium range tactical missiles, which may experience maximum surface temperatures from aerodynamic heating of from 399-538 °C (750-1000 °F) for a period of time approaching 70 sec (16). High temperature tensile testing was performed on 8 ply unidirectional IM7 carbon reinforced phthalonitrile composite specimens up to 593 °C (1100°F) at a heating rate of 28 °C/min. The phthalonitrile composite did not start to lose its tensile strength until temperatures of 538 °C (1000 °F) were approached. The sample exhibited a 6-7% weight loss at this temperature, which translated into about 0.004 gm/cm^2 of a real weight loss resulting in a resin loss penetration depth into the composite surface of 0.08 mm. If we assumed the loss of resin on the surface is equivalent to the loss of load carrying of the fibers within the penetration depth, a 13-14% knock down in tensile strength can be calculated. The average loss in tensile strength observed at 538°C (1000°F) was 20% when compared to the room temperature average which is in reasonable agreement. A significant change was observed at 593 °C (1100 °F) where resin loss was rapidly occurring. It would appear based on these observations that the primary strength loss mechanism for carbon reinforced phthalonitrile composites is resin loss at the surface. Accompanying the surface loss of resin there are other changes occurring in the phthalonitrile resin structure at these high temperatures, which may have an additional effect on composite strength. This involves a carbonization of the material but this effect has not been investigated in detail.

Figure 2. Phthalonitrile Composite Variation of Failure Load with Temperature

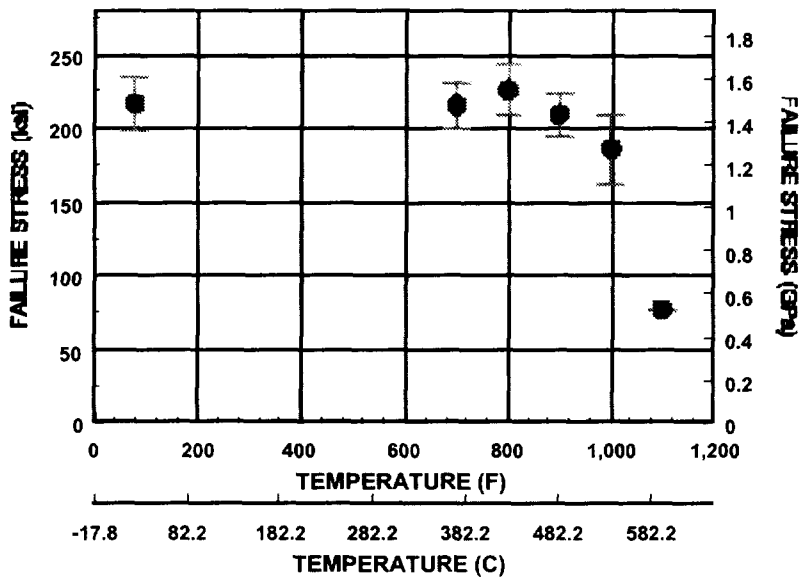

CONCLUSIONS

The use of polymeric composite materials for airframe and spacecraft cabin applications offers benefits in a variety of areas such as improvements in weight, maintenance, corrosion control, and lower thermal conductivity. High performance composites that fit the Navy's flammability requirements of MIL-STD-2031 for application in hull, machinery and structural applications inside naval submarines have not been available. The superior performance of phthalonitrile-based composites on exposure to a flame should enhance their importance for consideration by the aerospace industry in the design of a totally fire resistant cabin for future spacecraft.

The phthalonitrile polymer offers many advantages as flame resistant and high temperature matrix materials for composite applications. The mixed prepolymerization composition and B-staged prepolymer are completely stable under ambient conditions and below the melt temperature. These compositions are especially useful in the fabrication of fiber reinforcedcomposites by RTM, filament winding, resin infusion molding, resin injection molding, and prepreg formulation from the melt in the absence of solvent. A user can readily make changes in the phthalonitrile/curing additive prepolymerization composition to meet the processing needs. No reaction occurs between the monomer and curing additive until melting commences. Conventional resins such as epoxies and polyimides must be stored under freezer conditionsand used in a short time frame upon addition of curing additive. The phthalonitrile resin can be easily processed into void-free composite components. The data reveal that the phthalonitrile composites exhibit mechanical properties that are either superior or comparable to the state-of-the-art high temperature PMR-15 composites. Panels post-cured at 375 °C do not exhibit a glass transition temperature up to 450 °C and retain about 90% of their initial modulus. Based on the excellent physical properties and ease of processability, phthalonitrile composites are finding uses in both marine and aerospace applications.

ACKNOWLEDGEMENT

The authors wish to thank the Office of Naval Research for financial support of this work.

REFERENCES

1. Lyon, R. E., *SAMPE J.*, 32(3), 29 (1996)
2. Keller, T. M. and Price, T. R., *J. Macromol. Sci.-Chem.*, **A18(6)**, 931 (1982).
3. Keller, T. M. and Griffith, J. R., *ACS Symp. Ser.:Resins for Aerospace*, **132**, 25 (1980).
4. Keller, T. M., *ACS Polym. Prep.*, **33(1)**, 422 (1992).
5. Burchill, P. J., *J. Polym. Sci., Part A: Polym. Chem.*, **32**, 1 (1994).
6. Critchley, J. P. and Wright, W. W., *Reviews on High Temperature Materials*, **4**, 107 (1979).
7. Pater, R. H., *NASA Technical Memorandum 53050* (1982).
8. Sastri, S. B., Armistead, J. P., and Keller, T. M., *Polym. Comp.*, **17 (6)**, 816 (1996).
9. Sastri, S. B., Armistead, J. P., and Keller, T. M., *Polym. Comp.*, **18 (1)**, 48 (1997).
10. Sastri, S. B., Armistead, J. P., Keller, T. M. and Sorathia, U., *SAMPE Symp. Ser.*, **42**, 1032 (1996).
11. *Fire and Toxicity Test Methods and Qualification Procedure for Composite Materials Systems Used in Hull, Machinery and Structural Applications Inside Naval Submarines* (1991).
12. Srinivasan, K., Johnston, N. J., and Prater, R. H., *High Temple Workshop XII Document (1992)*.
13. Babrauskas, V. and Peacock, R. D., *Fire Safety Journal*, **18**, 255 (1992).
14. Micro-scale calorimetric experiments were performed by R. E. Lyon and R. N. Walters at the Fire Research Section, Federal Aviation Administration, Atlantic City, New Jersey.
15. Lyon, R. E., *Thrust Area Project Update, 7th Meeting of the Interagency Working Group on Fire and Materials (IWGFM-7)*, (1996).
16. DiGiovanni, P. R., and Paterson, D., "High Temperature, Short Term Tensile Strength of C6000/PMR-15 Composites", *High Temperature Polymer Matrix Composites*, Noyes Data Corporation, New Jersey, 1987, pp. 254-266.

Real Time Video Recording of Extremely High Temperature Processes

Thad Hoffman
Control Vision Incorporated
PO BOX 51505
Idaho Falls, ID 83405
Phone: 208.523.5506
Email: vision@controlvisioninc.com

Introduction

Surface details of materials at extremely high temperatures are quite difficult to monitor with the human eye or with standard video and photographic cameras. Details such as the behaviors of the solid or molten material, surface contaminants or cracks are obscured by the incandescence coming from the surface itself. Additionally, when attempting to view processes with relatively small areas of overwhelming brightness, such as laser welding, the image is additionally degraded by the extreme brightness variation across the image area, making it impossible to achieve proper exposure throughout the scene.

The key to obtaining an image that is properly exposed and shows surface detail lies in using reflected illumination. Reflected illumination provides the basis for almost all of our natural viewing capabilities relying on either natural or artificial lighting to see almost everything in our daily lives. A good example of the principle of reflected illumination can be found in the difference of appearance when viewing the Sun versus the moon. Viewing the sun directly, even with heavy attenuating filters, tells us nothing about the surface since the sun radiates intensely across the visible spectrum. The moon, however, does not radiate in the visible spectrum. Our image of the moon is created by reflected light from the sun. Using the sun's illumination, we are able to see a tremendous amount of surface detail such as craters, valleys and peaks.

Recent electro-optical innovations in charged coupled device (CCD) chip technology and various efficient light sources have provided the basis for implementation of real-time videographic techniques for viewing and recording surface conditions of high temperature processes. This paper describes a basic system design and the implementation of these techniques to a variety of high temperature industrial processes.

High Temperature Video System Description

A video system used for viewing the surface of high-temperature processes, includes a custom designed CCD video camera head, an external light source, a controller unit, a video monitor and a video recorder. Figure 1 shows a block diagram of such a system.

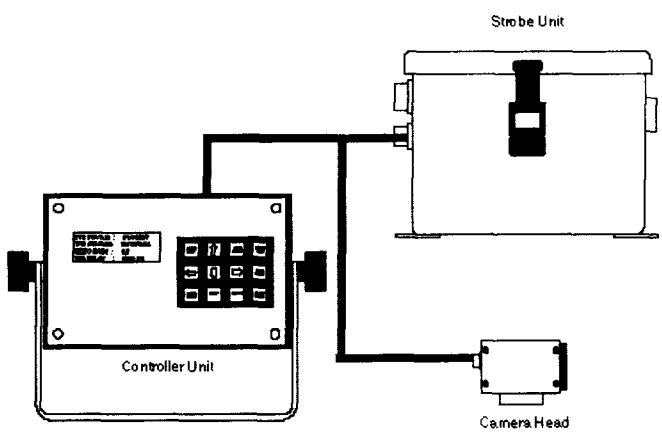

Figure 1

Strobe Unit

The video system is able to overcomes brightness associated with high energy industrial processes with use of an intense pulse of light. A xenon flashlamp strobe unit is typically used, but pulsed laser illumination is also an option for very demanding applications. The broadbanded output energy of the of the typical strobe unit is about 20 millijoules per flash. The strobe output is intense enough to overpower the brightness typically associated with high temperature, high energy processes. Use of a pulsed light source such as a strobe also provides an additional benefit when dealing with motion. The 5 microsecond pulse is sufficient to eliminate any motion-induced blur within the image.

Strobe energy can be delivered to an area of interest in several ways. For close-up applications such as laser welding, the most common delivery method is through the use of a fiberoptic bundle. Typical bundle diameters are under 0.75" and the bundle can be configured in a variety of lengths depending upon installation requirements. The fiber strands are encased within flexible stainless steel sheathing for strength and protection. A transparent protective window is usually secured to the output end of the bundle for protection from welding spatter, etc. For applications that may require larger stand-off distances, projection optics can be mounted onto the strobe unit. These optics produce a well-collimated beam and uniform illumination spot from distances of up to 60 feet away.

Camera Head

The custom-designed video camera head incorporates CCD technology into a small, lightweight package. Pixel resolution is 480 by 640 providing 256 levels of gray scale output. The camera head is approximately the size of a pack of cigarettes and weighs only a few ounces. The head is teathered to the controller unit by means of a 20-foot multiconductor cable and can be situated remotely from the controller unit at even greater distances, if necessary. A variety of optical components specifically designed for typical operating conditions are available for use with the camera head. A standard C-mount lens attachment also allows for integration with standard video camera optics ranging from video microscopes to ordinary wide-angle and zoom lenses.

Controller Unit

The controller unit fires the strobe unit synchronously with the video framing cycle of the camera head. The video image is then created predominately by means of reflected strobe illumination, which overwhelms the brightness of the scene and produces very highly contrasted video imagery of the high temperature surface. Additionally, the controller unit controls various other system functions, such as video framing rate and camera sensitivity. The standard RS-170A video output signal is compatible with all video recording and display systems. The system is typically used with a video recorder and microphone to monitor the audio signature of a particular sequence and to allow the operator to describe specific operating conditions of the process under investigation. In more advanced applications, the camera provides video to a desktop PC configured for digital video image processing.

Example Applications

Pulsed Yag Laser Welding

Pulsed Yag laser welding can typically be characterized by peak power levels in the multi-kilowatt range, usually delivered through a fiberoptic cable for relatively small-scale, precision welding applications. Figure 2 shows a typical pulsed Yag welding operation. Note the bright plume emanating from the weld. Unfortunately this plume causes severe saturation and blooming in the video image when a standard video camera is used for close-up viewing .

Figure 2

Figures 3 and 4, however, show very clear images of the welding process. No evidence of the plume is seen.

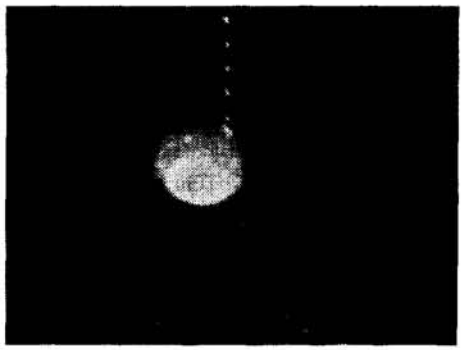

Figure 3

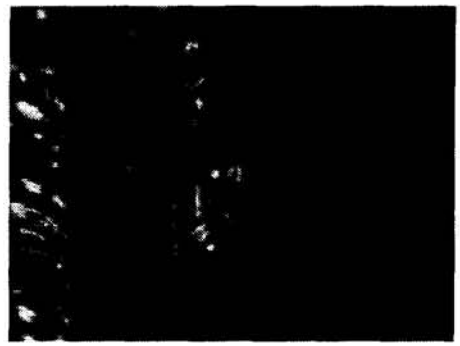

Figure 4

Through the use of an external trigger function, it is possible to view the laser welding pulse at various stages of development. A timing pulse from the laser power supply is used to trigger the video camera system. In these examples, the laser pulse energy is about 10 Joules, with a 2.5 ms pulse duration and 4 Kw peak power. The welding pool diameter is approximately 2 mm across and the transverse field of view is about 9 mm. Figure 3 shows the weld at 1.64 ms of shutter trigger delay, so as to capture a picture during the laser pulse. (Trigger delay is the time between receipt of the leading edge of a pulse from the Yag laser welder power supply and triggering of the camera system.) Note the incandescence of the pool of molten metal. Figure 4, however, was taken at 3.2 ms trigger delay, following the laser pulse. Note the ejection of molten metal and a drop in incandescence of the molten metal that indicates a drop in the temperature the pool.

C02 Laser Heat Treatment

Figure 5 shows heat treatment of a metal surface using a CW C02 laser beam with a rectangular cross-section. The heated material appears as light gray against the darker, un-heated surface. The purge gas nozzle is seen in the upper right hand corner of the video frame. The goal is to heat the surface almost to the point of melting, but the dark splotches on the light gray surface indicate the presence of some molten areas, thus indicating a need to decrease the laser beam power or increase the travel speed of the beam across the surface.

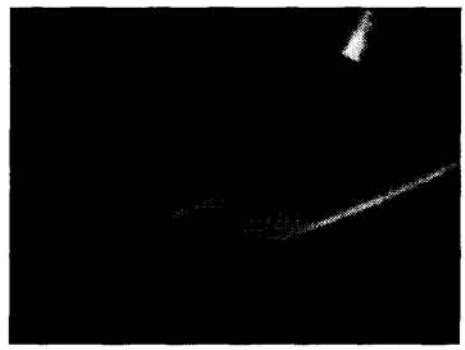

Figure 5

Pulsed Gas Metal Arc Welding (GMAW)

Figure 6 shows an example of typical camcorder video of a pulsed gas metal arc welding process. Figure 7 shows video obtained using the high temperature video camera system. In this case, intense laser illumination is used to illuminate the welding wire and molten pool. The behavior of the wire and droplets is observed during the weld. An external timing reference can be obtained through a small sensor that, when placed around the work lead, senses changes in weld current. Using this timing reference it is possible to selectively view the transfer of droplets from the wire to the molten pool at specific delay times from the weld pulse.

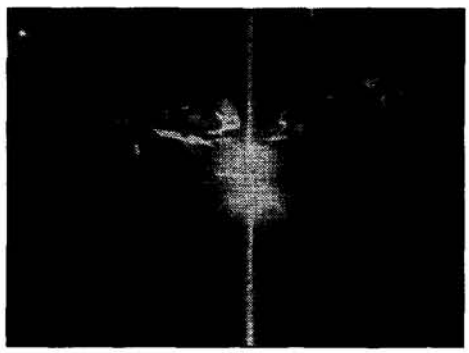

Figure 6

Figure 7

Iron Making

The high temperature video technique has been used in steel making operations. As an example, Figure 8 shows a video frame taken from an ordinary video camcorder. We see a natural gas flame coming from a trough filled with molten iron which has been tapped from a blast furnace. The surface temperature of the iron is over 1,500 degrees centigrade. Figure 9 is taken with the high temperature video system. In this image the flame and incandescence in the scene are overcome by strobe illumination in order to observe the surface of the molten iron. The molten iron appears as pool of mercury at room temperature. Small amounts of slag can be observed on the surface. The reflective nature of the slag is different from molten iron in that the slag is diffuse while the molten iron is specular, tending to reflect strobe energy away from the camera.

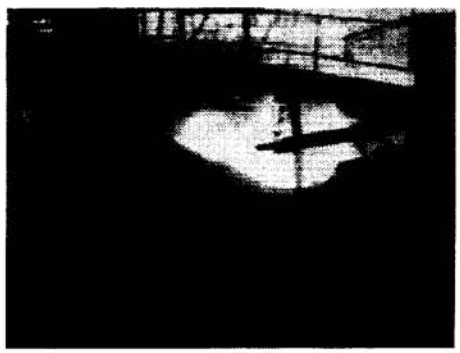

Figure 8

Figure 9

Continuous Casting

Another example of high temperature video camera use can be found with viewing the output of a continuous caster machine. Figure 10 is a camcorder shot of the cast product as it exits the casting mold. The surface temperature is very near molten steel temperatures. Figure 11 shows the high temperature video camera image of the same surface. Use of reflected strobe illumination makes the surface appear as if it was at room temperature. Surface features such as the crack seen on the right third of the video frame are readily apparent. In this case, the strobe illuminator was placed at 90 degrees to the viewing direction and obliquely to the surface of the cast product. This approach to illuminating accentuates surface details, such as the crack, by creating shadows.

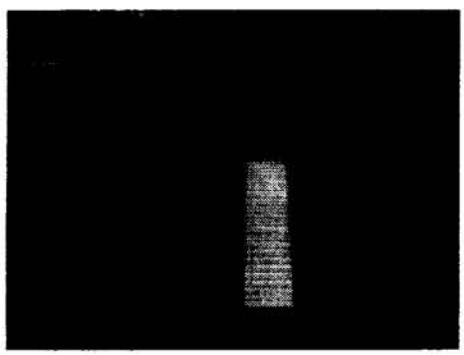

Figure 10

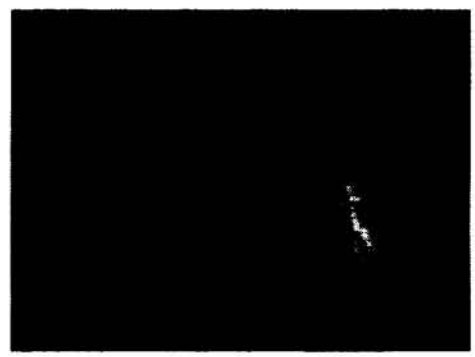

Figure 11

Twin Wire Arc Spray

With twin wire arc spray an electrical arc is generated between the two consumable wire electrodes exiting the orifice of a spray gun. Pressurized air is used to accelerate the molten droplets against a substrate. Figure 12 shows a camcorder shot of a typical twin wire arc spray process. In contrast, figure 13 shows the close-up details of the twin wire arc spray process using the high temperature video camera system. As with pulsed gas metal arc welding, a small, pulsed laser is used to illuminate the process, creating detailed video of wire atomization without arc light overwhelming the image.

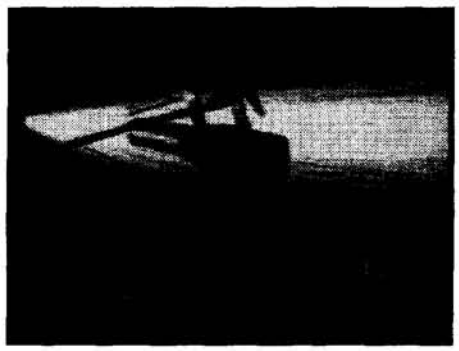

Figure 12

Figure 13

Conclusion

Highly contrasted video observation of details on high temperature, incandescent surfaces requires viewing the surface by means of reflected illumination rather than relying upon the visible radiation coming from the surface itself. Recent innovations in the field of electro-optics make such a video system practical and affordable.

VAPOR GROWN CARBON FIBER/PHENOLIC MATRIX COMPOSITES FOR ROCKET NOZZLES AND HEAT SHIELDS

R.D. Patton[a], C.U. Pittman, Jr.[b], L. Wang[c], J.R. Hill[d], A. Day[e]
[a]Mech. Eng. Dept., PO Box ME, Mississippi State University, Mississippi State, MS 39762
ph: (662) 325-7311 fax: (662) 325-7223 e-mail: patton@me.msstate.edu (corr. author)
[b]Chemistry Dept., PO Box 9573, Mississippi State University, Mississippi State, MS 39762
[c]Chem. Eng. Dept., PO Box C H, Mississippi State University, Mississippi State, MS 39762
[d]3536 Idaho Rd., Charleston AFB, SC 29404
[e]Thiokol Propulsion, PO Box 9033, Huntsville, AL 35812

ABSTRACT

The ablation, mechanical and thermal properties of vapor grown carbon fiber (VGCF) (Pyrograf III™ Applied Sciences, Inc.)/phenolic resin (SC-1008, Borden Chemical, Inc.) composites were evaluated to determine the potential of using this material in solid rocket motor nozzles. Composite specimens with varying VGCF loading (30%-50% wt.) including one sample with ex-rayon carbon fiber plies were prepared and exposed to a plasma torch for 20 sec. with a heat flux of 16.5 MW/m^2 at approximately 1650°C. Low erosion rates and little char formation were observed, confirming that these materials were promising for rocket motor nozzle materials. When fiber loadings increased, mechanical properties and ablative properties improved. The VGCF composites had low thermal conductivities (approximately 0.56 W/m-°C) indicating they were good insulating materials. If a 65% fiber loading in VGCF composite can be achieved, then ablative properties are projected to be comparable to or better than the composite material currently used on the Space Shuttle Reusable Solid Rocket Motor (RSRM).

Keywords: A. Carbon fiber; B. Ablation; Thermal properties; Mechanical properties

INTRODUTION

The ablation, mechanical and thermal properties of some recently prepared vapor grown carbon fiber (VGCF) (Pyrograf III™ Applied Sciences, Inc.)/phenolic resin (SC-1008, Borden Chemical, Inc.) composites are reported herein. The purpose was to begin evaluation of this material for use in solid rocket motor nozzles and related applications.

Applied Science, Inc. (ASI) manufactures the only commercially available supply of vapor grown carbon fibers, (VGCF). The Pyrograf III™ vapor grown carbon fibers from ASI have a diameter range of between 100 - 300 nm and of lengths varying between 10 and 100 μm[1-4] The aspect ratio, l/d (length/diameter), for VGCF ranges between 100 and 1000[1]. Unlike most fibers used for composite reinforcement, VGCFs come in a fluffy mass where the fibers are curved and intertwined[1-4]. Figure 1 shows a Scanning Electron Microscope (SEM) view of a sample of Pyrograf III™ VGCF.

Figure 1 Scanning Electron Microscope View of Pyrograf III™ VGCF

Vapor grown carbon fibers are produced by introducing an aerosol spray of a metal salt (usually Fe^{+3}) into a chamber of hydrocarbon gas (i.e., methane or natural gas) heated to 1000 - 1200 °C [2-4]. Figure 2 depicts the production of VGCF [2].

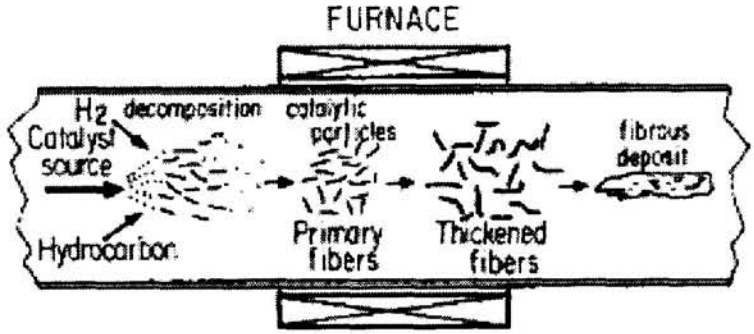

Figure 2 Three-Dimensional Growth of Fibers in a Reaction Chamber [2]

The activation of the iron particle catalyst causes the initial graphitic carbon filaments to form [2-4]. The carbon filaments may lengthen for several minutes until the catalyst deactivates [5,6]. Since the iron particle becomes the nucleation site for the fiber tip, the initial carbon fiber diameter is directly proportional to the iron particle diameter, i.e., 10 nm [2,5,7]. The filaments then lengthen and thicken further by chemical vapor deposition of carbon onto the graphitic substrate [5]. The thickening process forms concentric, cylindrical sheaths around the initial filament [2,5]. These cylindrical sheaths develop a cross-sectional tree-ring morphology [5,6]. The final filament structure has a graphitized core covered with layers of pyrolytic carbon of lower graphitization [6,7]. This tree-ring morphology is illustrated in Figure 3 [5].

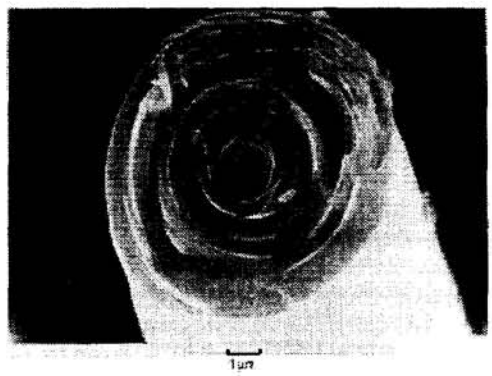

Figure 3 Transverse Section of a Vapor Grown Carbon Fiber Showing Tree Ring Morphology [5].

Vapor grown carbon fibers have two main advantages, cost and availability. VGCF can be very inexpensive due to their size and by the use of natural gas as the source of hydrocarbon gas [3,4]. Fiber diameter is a cost driver for VGCF [4]. The smaller fibers like Pyrograf III™ require less time in the reaction chamber, thus reducing cost [3,4]. Pyrograf I,™which has a fiber diameter between 1 - 100 μm (i.e., 10 to 300 times the size of Pyrograf III™), is much more expensive.

Disadvantages of Pyrograf III™ VGCFs include obtaining a non-standardized product, lack of a detailed knowledge of their material properties, and packing problems. Since Pyrograf III™ fibers are so small, the individual fiber material properties can not be readily measured [3,4,7], although Patton and Pittman have recently reported lower limits for their flexural moduli and flexural strengths [3,8]. Mechanical properties have been measured for much smaller carbon nanotubes by atomic force spectroscopy [9]. However, these techniques can not be used on Pyrograf III™ fiber, because they are too large. Pyrograf III™ material properties are assumed to be similar to Pyrograf I™ material properties, since their preparation differs only in the growth time used. However,

the ratio of pyrolytic carbon outer region to the tubular graphite inner core is different for these two classes of fibers. Table 1 lists the material properties for Pyrograf I™ fibers.

Table 1, Properties of Pyrograf I™ Fibers[a]

Property	Value	Units
Fiber Diameter	1 – 100	μm
Tensile Strength[b]	2.7	Gpa
Tensile Modulus[b]	400	Gpa
Ultimate Strain	1.5	%
Density	1.8	g/cm^3
Coefficient of Thermal Expansion	-1.0	ppm/°C
Electrical Resistance	1000	μΩ-cm
Thermal Conductivity	20	W/m-°K

[a]Source: Applied Sciences, Inc.
[b]Pyrograf III™ ranges: tensile strength 1.7-3.38 GPa, tensile modulus 88-166 GPa [8]

Mechanical properties control many applications of composites, and much VGCF composite research has focused on determining these properties [10]. Chellappa et. al. [11] Shui and Chung, [12] as well as Ciminelli et. al. [1] obtained poor mechanical properties when testing VGCF composites. Chellappa et. al. [11] attributed poor mechanical results in the VGCF composites they prepared to (1) poor fiber/matrix adhesion, (2) poor fiber dispersion, (3) the presence of voids, and (4) using a weak thermoplastic elastomer matrix having a 0.1 MPa ultimate strength. Shui and Chung[12] as well as Ciminelli et. al. [1] attributed the poor mechanical properties to insufficient bonding between the VGCF and the matrix. It is also likely that they achieved poor fiber wetting and poor fiber dispersion.

The first strength improvements in VGCF composites were observed at Mississippi State University by Patton, Pittman, and Wang. [3,4,8]. The main variable contributing to these strength improvements was the use of pre-cure high shear mixing techniques. This aided in resin infusion, which is one of the two most important problems associated with making VGCF composites. Composites with high fiber volume fractions did not have any strength improvements. These composites had poor mechanical properties due to their high porosity resulting from fiber packing problems. Packing is the second significant problem. Random three-dimensional packing of the VGCF, which have a high aspect ratio, leads to a low theoretical packing fraction. Hence, void free composites require high resin volume fractions.

The thermal properties of VGCF composites have not been as widely studied. Shui and Chung [12] showed the thermal conductivity of VGCF/polyether sulfone composites increased with fiber loading. Our group showed the thermal conductivity of VGCF composites with acrylonitrile-butadiene-styrene (ABS) and epoxy matrices increased with an increase in the fiber loading [8]. However, these increases were small. VGCF composites are not thermal conductors.

VGCF composites are being considered as a new material for the rocket nozzle of the space shuttle reusable solid rocket motor (RSRM). Currently NASA uses MX-4926, which is composed of two different reinforcements: woven ex-rayon carbon fiber from Avtex Fibers, Inc., and carbon black filler. The matrix is a phenolic matrix, SC-1008 Borden Chemical, Inc [13]. The high-temperature and high-velocity exhaust produces a pressure of 6.89 MPa and a temperature of 1650 °C in the RSRM's rocket nozzle during firing [14,15]. Not only does the rocket nozzle material have to be a good insulator, but it also must have superb ablative properties [14,15].

MANUFACTURING VAPOR GROWN CARBON FIBER/PHENOLIC COMPOSITES

VGCF/phenolic resin composite specimens were prepared by high shear mixing followed by thermal curing. Table 2 lists the 19 composite specimens made, mixing method used, their composition (wt.), density, void content, and fiber volume fraction, and the tests performed on each specimen. The VGCF/phenolic

composite specimens were tested for ablation, mechanical, and thermal properties. The cure cycles for all samples were held constant. Four types of samples were made for material testing. The compositions, expressed as wt./wt., were 30/70 VGCF/Phenolic, 40/60 VGCF/Phenolic, 40/60 VGCF/Phenolic (where ball milled as-received VGCF was used) and 45/5/50 VGCF/ex-Rayon woven cloth/Phenolic. Two types of fiber were received from ASI: as-received and compacted fiber. The compacted fiber was from a different batch than the as-received fiber, and it had been subjected to post-production compaction processing. VGCF composites made from compacted fiber had significantly higher flexure strengths than comparable samples made from as-received fiber. Compacted fiber was not used in any ablation test specimens. Due to supply problems, the compacted fiber was employed in the 45/5/50 VGCF/ex-rayon/phenolic samples, which were used in mechanical and thermal tests. These properties may differ somewhat from the baseline properties established with as-received fiber. All specimens used in ablation testing were made from as-received VGCF, so they are directly comparable.

Table 2, VGCF/Phenolic Composite Sample Properties

Sample Number	Fiber wt. (%)	Fiber Type	Sample Weight (g)	Sample Density (g/cc)	Void (%)	Fiber Volume (%)	Test Type[a]	Mixing Type[b]
1	30	As-received	16.25	1.416	1.5	20.23	M	CG
2	30	As-received	17.21	1.399	2.73	19.99	M	CG
3	30	As-received	17.87	1.396	2.95	19.94	T	CG
4	30	As-received	n/a	n/a	n/a	n/a	A	HS
5	40	As-received	18.45	1.461	3.02	27.83	M	CG
6	40	As-received	18.58	1.453	3.59	27.68	M	CG
7	40	As-received	18.29	1.462	2.95	27.85	T	CG
8	40	As-received	n/a	n/a	n/a	n/a	A	HS
9	40	Ball milled	14.99	1.484	1.42	28.27	M	HS
10	40	Ball milled	15.21	1.485	1.35	28.29	M	HS
11	40	Ball milled	14.92	1.481	1.63	28.21	T	HS
12	40	Ball milled	n/a	n/a	n/a	n/a	A	HS
13	45/5[c]	Compacted	25.53	1.477	6.04	31.7/4.3[c]	–	CG
14	45/5[c]	Compacted	26.20	1.426	9.81	30.6/4.2[c]	M	CG
15	45/5[c]	Compacted	26.62	1.426	9.81	30.6/4.2[c]	T	CG
16	45/5[c]	As-received	n/a	n/a	n/a	n/a	A	HS
17	40	Compacted	22.15	1.491	0.95	28.40	M	CG
18[d]	0	n/a	20.17	1.312	3.5	0	T	n/a
19	40	As-received	n/a	n/a	n/a	n/a	3DT	HS

[a] M=mechanical testing, T=thermal conductivity, A=ablation, 3DT=3D thermal conductivity
[b] HS=high shear sequence using Brabender and two roll mill after coffee grinder, CG=coffee ground only
[c] Ex-Rayon Carbon Fiber
[d] Pure Phenolic Sample

Ablation test specimens (specimens 4,8,12,16) were prepared as 79.4x54x35.6 mm blocks. They were cut into six specimens, which were 25.4x25.4x35.6 mm in size. Specimens 1-3, 5-7, 17 and 18 were 69.9x41.3x2.5 mm in size. Specimens 9-11 were 69.9x41.3x2.5 mm specimens and had been cut from one larger block. Similarly, specimens 13-15 were also 69.9x41.3x2.5 mm and cut from a larger block. Specimen 19 was the same size as the ablation specimens 4, 8, 12 and 16. Thermal conductivity specimens were cut from three different faces of specimen 19 in order to test for the anisotropy of thermal conductivity in these specimens.

The thermal conductivity specimens 3, 7, 11, 15 and 18 were cut into two identical 31.8x31.8x2.5 mm pieces for use in the guarded hot plate thermal conductivity test. Mechanical test specimens 1, 2, 5, 6, 9, 10, 13, 14 and 17, each of which are 69.9x41.3x2.5 mm in size, were cut into five specimens of 40x10x2.5 mm for the 3-point bending test.

1) Volume reduction

Ball milling was used to reduce the volume (increase the volume fraction) of the as-received VGCF. The ball mill consists of a cylindrical container with internal side brackets fastened to its walls, which continually lifted and dropped the balls onto the fiber. Three different ball diameters are used; 3.18 mm, 6.35 mm, and 12.7 mm; and approximately 300 balls are placed inside the ball mill. The fibers were ground in a high-speed blender before ball milling. A small amount of water was used during the grinding to aid the volume reduction. Significant volume reduction occurs after approximately 30 seconds of grinding. Then the fibers were dried at 121°C for 4 to 6 hours. Dry fibers were necessary for ball milling because excess water in the fiber cushions the impact during ball milling. The VGCF was ball milled for 16 hours. The results of this two step grinding process on VGCF are shown in Table 3. The volume reduction factors ranged between 2.94 - 11.5. The average total reduction factor was 5.34 for these samples.

Table 3, Volume Reduction of VGCF by Grinding and Ball Milling

Sample Number	Weight (g)	Original Volume (mL)	Volume After Grinding (mL)	Volume After Ball Milling (mL)	Total Factor Reduction
1	20.10	687.5	500.0	233.8	2.94
2	40.67	1437.5	887.5	300.0	4.79
3	42.31	1500.0	875.0	312.5	4.80
4	40.67	1500.0	1020.0	250.0	6.00
5	40.81	1480.0	812.5	375.0	3.95
6	40.80	1450.0	687.5	437.5	3.31
7	40.13	1500.0	625.0	250.0	6.00
8	40.24	1500.0	1000.0	312.0	4.80
9	40.24	1437.5	875.0	125.0	11.50
Average	**38.44**	**1388.1**	**809.2**	**288.4**	**5.34**

2) Mixing

VGCF/phenolic resin composites were prepared by a multi-step mixing process followed by a vacuum treatment to remove the isopropyl alcohol solvent from the phenolic resin. First, the fiber and resin were hand mixed for approximately one min. Then, the fiber/resin mixture was placed into a high speed coffee grinder and ground for 2 min. A further two step high shear mixing sequence was used when preparing the ablation test specimens 4, 8, 12 and 16 and mechanical test specimens 9-11. In the first step, the fiber/resin mixture was put into a Brabender high shear mixer at 100 rpm for 30 min. This was followed by 2-roll milling at 50° C at speeds between 50-80 rpm for 30 min. Other composite samples, used for mechanical and thermal conductivity tests, (samples 1-3, 5-7, 13-15 and 17) were not large enough for the high shear mixing in the available sized equipment. Once mixing was complete, the isopropyl alcohol was removed, *in vacuo*, at 70 mm Hg for 48 h.

3) Composite Curing

Samples were cured by heating under pressure in a mold. The mold was placed into the hot press and heated to 80°C at 5.1 MPa for 30 min. Then the temperature and pressure were increased to 104°C with 15.3 MPa for 90 min. Finally the temperature was again increased to 138°C while the pressure is held steady at 15.3 MPa for another 30 min. This allowed the water of curing to diffuse out without distorting the composite or causing voids.

TESTING PROCEDURES AND RESULTS

Density

Density measurements were made so that the percent voids and fiber volume fractions could be calculated. The void percent indirectly indicates the quality of the resin infusion. Composite density and weight measurements were made with the Electronic Densimeter Pyknometer Model # ED-120T, AFD Ltd. Density measurements were performed on the composite samples used for mechanical and thermal conductivity

measurements. The ablation test samples were too large for the densimeter's reservoir. Table 2 lists the VGCF composite samples, their fiber weight fractions, densities, percent voids, mixing regime and which tests were performed.

The void percent was less than 3% for most of the samples (Table 2) indicating relatively good resin infusion; however, the void contents in samples 13, 14, and 15 are much higher than 3%. This is probably due to delamination cracking between the ex-rayon carbon fiber layers, which occurred when specimens 13-15 were cut.

Mechanical Testing

The flexural strengths and flexural moduli were obtained from 3-point bending tests, and conducted in accordance with ASTM standard D 790M-93 using a Zwick Materials Testing Model #1435 (± 1% accuracy). A total of ten 3-point bending tests were performed for each composite type. The span was 30 mm, the width was 10 mm, and the thickness was 2.5 mm. Calculated values of the flexural strength and flexural modulus have an accuracy of ± 5%. The 3-point bending tests were performed on specimens 1, 2, 5, 6, 9, 10, 14 and 17. The results are shown in Table 4.

Table 4, VGCF/Phenolic Composite Flexural Strength and Flexural Modulus

Composite Sample #	$\%W_f$ (%)	Flex. Strength (MPa)	Flex. Modulus (GPa)
1	30	25.6 ± 1.3	1.07 ± 0.05
2	30	25.1± 1.3	0.92± 0.05
5	40	26.1 ± 1.3	1.11± 0.06
6	40	32.4 ± 1.6	1.20 ± 0.06
9	40[a]	33.2± 1.7	2.76 ± 0.14
10	40[a]	35.2± 1.8	2.21 ± 0.11
14	45/5[b]	50.7 ± 2.5	2.26 ± 0.11
17	40[b]	54.0 ± 2.7	2.69 ± 0.14

[a] Ball Milled Fiber and Extra High Shear Mixing
[b] Compacted Fiber

The flexural strengths and moduli were low for these samples. Significant modulus increases occur for the ball milled and high shear mixed samples 9 and 10, which had lower void volumes. The two specimens made with compacted fiber, sample 14 and sample 17, had higher flexural moduli and strengths. Sample 14 suffered some delamination cracking when being cut, which probably reduced its strength and modulus.

Thermal Conductivity Testing

The thermal conductivities were measured according to the ASTM C 177-85 standard test method for steady-state heat flux measurements and thermal transmission properties using a guarded-hot-plate apparatus [15]. Testing temperatures ranged between 22.2 °C and 93.3 °C. This temperature range is much lower than conditions inside the space shuttle solid rocket motor nozzle. A specimen size was 31.8x31.8x2.5 mm was used.

Table 5 displays the measured thermal conductivities. All of the composite samples exhibited similar thermal conductivities (.54 to .62 W/m--°C). These values were only about twice that of the cured phenolic resin without fiber (.28 W/m-°C).

Table 5, VGCF/Phenolic Composite Thermal Conductivities

Composite Sample #	Fiber wt. (%)	Thermal Conductivity (W/m-°C)
18	0	0.28 ± 0.07
3	30	0.57 ± 0.02
7	40	0.54 ± 0.01
11	40[a]	0.62 ± 0.01
15	45/5[b]	0.57 ± 0.03

[a] Ball Milled Fiber and Extra High Shear Mixing
[b] Compacted Fiber

The thermal conductivities in three dimensions were obtained on a 40/60 VGCF/phenolic ablation test composite sample (sample 19, Table 2). Specimens were cut out of the top, side and front of the ablation test specimen. The results are shown in Table 6. They indicate that the material is roughly isotropic, differing by less than ± 9.1% from the average in all 3 directions.

Table 6, Three-Dimensional Thermal Conductivity Testing

40/60 VGCF/Phenolic Specimen Orientation	Thermal Conductivity (W/m-°C)	Percent Difference (%)
Top	0.7788 ± 0.0374	-----
Side 1	0.8275 ± 0.0407	6.25
Side 2	0.7080 ± 0.0276	9.09

Ablation Testing

Thiokol, Inc performed all ablation testing at the NASA Marshall Space Flight Center. A Plasma Torch Test Bed was used for ablation testing. This test simulates the firing conditions of the Reusable Solid Rocket Motor (RSRM), with the exception of the 6.89 MPa pressure produced inside the RSRM rocket nozzle. The plasma torch has a standoff distance of 25.4 mm and uses an argon/nitrogen mixture. A heat flux of 16.47 MW/m^2 is produced at a plasma temperature of 1649 °C. The ablation test has a 20-second burn time. Before each test began, the sample was preloaded with a 444.82 N force, called the starting load. At the end of the burn, the final load was measured. The final load was greater than the starting load due to restrained thermal expansion. Six tests were completed for each composition and the results were averaged (Table 7).

Table 7, NASA/MSFC Plasma Torch Ablation Test Results[a]

Composite Sample	Erosion Rate µm/sec (mils/sec)	% Weight Change (%)	Load Change N (lb)
30/70 VGCF/PH	1.372 ± 0.203 (0.0543 ± 0.0076)	7.7 ± 0.14	668.7 ± 82.3 (150.3 ± 18.5)
40/60 VGCF/PH	1.245 ± 0.203 (0.0487 ± 0.0076)	8.6 ± 0.19	771.0 ± 76.6 (173.3 ± 17.2)
40/60 VGCF/PH[b]	1.689 ± 0.157 (0.0665 ±0.0062)	9.37 ± 0.30	614.6 ± 107.6 (138.2 ± 24.2)
45/5/50 VGCF/Ex-Rayon/PH	1.278 ± 0.229 (0.0503 ± 0.009)	8.76 ± 0.21	635.3 ± 53.3 (142.8 ± 12.0)
MX-4926	0.787 ± 0.080 (0.031 ± 0.0034)	10.4 ± 0.21	1952.8 ± 281.2 (439.0 ± 63.2)

[a] Plasma torch test temperature 1649°C and heat flux 16.5 MW/m^2.
[b] Ball Milled Fiber

Ablation behavior was characterized by three parameters in the plasma torch test: erosion rates, specimen percent weight change, and the increase in load. NASA's standard nozzle material, MX-4926, was tested along with the VGCF composites. The MX-4926 composite is composed of woven ex-rayon carbon fiber, carbon black

filler and a phenolic matrix. The MX-4926 has a larger total carbon loading, with 65% of the composite weight constituting either carbon fiber or filler.

As compared to the MX-4926 baseline, the VGCF composites experienced: 1) higher (58-114%) erosion rates, 2) lower weight losses (10-26%), and 3) lower load changes (60.5-68.5%). Thus, the VGCF specimens had less char and heat penetration than MX-4926. Therefore, more weight was being lost at or near the surface of the specimen versus weight loss from subsurface thermal decomposition. The load did not change much with increasing VGCF content (30%-50% wt.). Furthermore, the load changes for the VGCF composites are significantly lower than that of the MX-4926 composite. Load change is an indirect measure of heat penetration and char depth. Increases in load change indicate an increase in heat penetration and char depth. The VGCF composites appear to be far better insulators than the MX-4926. The higher erosion rates of the VGCF samples probably reflect their lower carbon content. The VGCF samples had a significantly lower carbon loading (30-50%) than the MX-4926 composite (65%).

Qualitative Observations of Ablation

Several interesting observations were made of the ablative action of these specimens.

1) There was no bright spot where the torch impinged on the specimen. The heat appeared to be spread uniformly across the surface, indicating good in-plane thermal conductivity.
2) The ablation proceeded with a flaking action. Very thin, small flakes of heated material would peel off from the specimen. This flaking action was uniform across the specimen for the higher carbon loading specimens (>30% wt.).

Because the load change was low during these ablation tests, the heat penetration, and hence out-of-plane thermal conductivity, was low. Thus, in ablative conditions, the specimens appeared to have higher in-plane than out-of-plane thermal conductivity. This apparently contradicts the results for room temperature thermal conductivity, which were nearly isotropic. A possible mechanism to explain this would be the formation of VGCF/carbon matrix (with high thermal conductivity) flakes on the surface, followed by flaking. This is speculative; much further work needs to be done in this area.

CONCLUSIONS

VGCF/phenolic composites, prepared with extensive high shear mixing, should be made with higher carbon loadings (50%-65% wt.) and subjected to the plasma torch tests. They have exhibited good erosion resistance at low carbon loadings while exhibiting less weight loss and load change than the material currently used on the RSRM.

The plasma torch testing indicates that this class of composites is a good candidate for future development for rocket nozzles and heat shielding materials. This is particularly true since both the VGCF manufacturing and processing technology is in its infancy. The carbon loadings used in VGCF composites so far have been much lower than that used in the MX-4926 composite. Much further work needs to be done at higher carbon loadings.

The mechanical properties of the VGCF composites need improvement. Lower void volumes, better surface treatments for fiber/matrix adhesion and mixed VGCF/carbon fiber weaves/carbon filler combinations should be investigated. VGCF/phenolic composites are virtually unstudied and should be the target of future efforts.

The VGCF/phenolic composites have a low thermal conductivity, and that they have roughly equal conductivity in all directions. This might imply that the fiber alignment is 3-D random, or if a higher order alignment exists in microregions, such microregions are randomly oriented within the macroscopic sample.

ACKNOWLEDGEMENTS

We acknowledge NASA/Marshall Space Flight Center, contract number NAS8-97091, task order number H-30190D, and the Air Force Office of Scientific Research, Grant number F49620-99-1-0191, for support of this research.

REFERENCES CITED

[1] Ciminelli DL. Kearns KM. Ragland WR. Vapor Grown Carbon Fiber (VGCF) Composites *41st International SAMPE Symposium*, March 24-28, 1996: 496-501.

[2] Dresselhaus MS. *Graphite Fibers and Filaments*, New York: Springers-Verlag, 1988.

[3] Patton, RD. Pittman Jr. CU. Wang L. Vapor Grown Carbon Fiber Composites with Epoxy and PPS Matrices. Proceedings of the 29th International SAMPE Technical Conference Series. 29, Oct. 28-Nov. 1, 1997. pp 77-87.

[4] Pittman Jr. CU. Wang L. Patton RD. Vapor Grown Carbon Fiber Composites with Epoxy and PPS Matrices. Extended Abstracts of the 23rd Biennial Conference on Carbon. II, July 18-23, 1997. pp 298-299.

[5] Tibbetts GG. Beetz Jr. CP. Mechanical Properties of Vapour-Grown Carbon Fibers. J Physics D, 1987;20:292.

[6] Madronero, A. Ariza E. Verdu Brandl MW. C. Barda C. Some Microstructual Aspects of Vapor-Grown Carbon-Fibers to Disclose Their Failure Mechanisms. J Material Science 1996;31(23):6189-6193.

[7] Tibbetts GG. Doll GL. Gorkiewicz DW. Moleski JJ. Perry TA. Dasch CJ. Balogh MJ. Physical-Properties of Vapor-Grown Carbon Fibers. Carbon 1993;31(7):1037-1047.

[8] Patton RD. Pittman Jr. CU. Wang L. Hill JR. Vapor Grown Carbon Fiber Composites with Epoxy and PPS Matrices. Composites: A 1999;30:1081-1091.

[9] Chemical Eng News 1997; 75(39):23.

[10] Vanhattum FWJ. Serp PH. Figueriredo JL. Bernardo CA. The Effects of Morphology on the Properties of Vapour-Grown Carbon-Fiber. Carbon 1997;35(6):860-863.

[11] Chellappa V. Chiu ZW. Jang BZ. Electrical Behavior of Carbon Whisker Reinforced Elastomer Matrix Composites. Proceedings of the 26th SAMPE Technical Conference, 26, Oct 17-20, 1994, pp 112-118.

[12] Shui, X. Chung DDL. Conducting Polymer-Matrix Composites Containing Carbon Filaments of Submicron Diameter. 38th International SAMPE Symposium. May 10-13, 1993, pp 1869-1875.

[13] SC 1008, Durite Phenolic Resin, Borden Chemical, Inc., Louisville, KY.

[14] ASTM D 790-92 Standard Test Method for Flexural Properties of Unreinforced and Reinforced Plastics and Electrical Insulating Materials. 1994 Annual Book of ASTM Standards, Vol. 8.01 Plastics, pp 176-184.

[15] ASTM C 177-85 Standard Test Method for Steady-State Heat Flux Measurements and Thermal Transmission Properties by Means of the Guarded-Hot-Plate Apparatus. 1994 Annual Book of ASTM Standards, Vol. 4.06 Thermal Insulation; Environmental Acoustics, pp 20-29.

CR/542/N 45

F4/1ST

Ambient Air Monitoring of Respirable Particulate Matter (PM_{10}) And Total Suspended Particulate (TSP) From the RD180 Rocket Engine Tests at the NASA Marshall Space Flight Center

John Hughes & Kathy Lehr
John.Hughes@ssc.nasa.gov

Lockheed Martin Stennis Operations
Test and Engineering Directorate
GB Tech Sciences Laboratory
SSC, MS 39529-6000

Introduction

The Sciences Laboratory operated by GB Tech was tasked by the Environmental Office at the NASA Marshall Space Flight Center (MSFC) to assess the impact of air particulate matter as a result of RD 180 engine testing. The method used for monitoring ambient air included measuring particles smaller than or equal to 10 micron (PM_{10}), particles with diameters smaller than or equal to 2.5 microns ($PM_{2.5}$) and Total Suspended Particles (TSP) that have a diameter size of 25 to 50 microns. This particulate matter represents small "dust like" particles of soot which are sufficiently small to disperse essentially like a permanent gas. Due to their small particle size, these particulates can be inhaled. The airborne concentrations are regulated and set by the EPA to prevent adverse effects associated with the inhalation of high levels of particulates.

Dedicated samplers were used to collect the correct particle size from the ambient air. The samplers also maintained a controlled flow rate to determine the volume of air sampled. Particles were collected on micro quartz or glass fiber filters that were equilibrated and weighed (tare) and after (gross) sampling to determine the weight (net mass) gain of the sample. The concentration of the particles captured from the air was then computed as the net mass collected by the volume of air sampled. This method provides a measurement of the mass concentration of airborne particulate matter for the determination of compliance with National Ambient Air Quality Standards.

Facility Description

Marshall Space Flight Center (MSFC) is located in Huntsville, Alabama. (Madison County). The facility comprises about 1841 acres and is located within the confines of the 38781 acre Redstone Arsenal. A general location map is provided in Figure 1.

Figure 1 – MSFC Vicinity Map

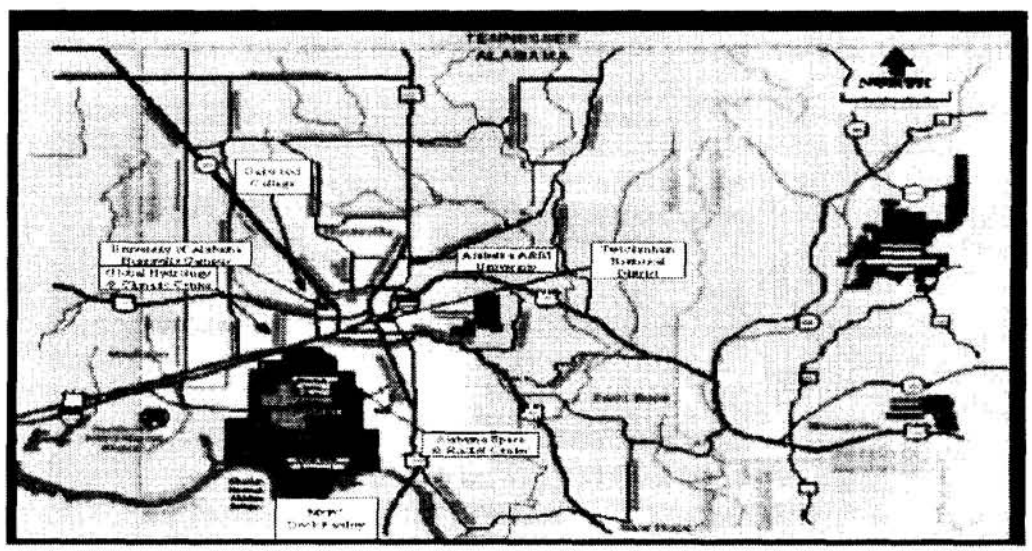

Determination of Sampling Locations

Predicted surface meteorological conditions at the time of testing were the determining factors in the selection of the general sampling locations wind direction and speed being the prime considerations. Other siting criteria included vertical placement, spacing from obstructions and roadways, availability of adequate electricity and security of equipment and monitoring personnel.

Vertical Placement

The optimal placement of the sampler inlet for PM_{10} and TSP monitoring should be at the breathing level. The sampler air intake was located between 2 and 7 meters above ground level. The lower limit is based on a compromise between ease of servicing the sampler and the desire to avoid re-entrainment from dusty surfaces. The upper limit represents the desire to have measurements which are most representative of population exposures. The distance between the PM_{10} inlet and the TSP was at least 2 meters to preclude airflow interference.

Space from Obstructions and Roadways

The samplers were located a minimum of 20 meters from trees and the nearest traffic lanes. An effort was made to locate all samplers away from obstacles such as buildings, so that the distance between obstacles and the samplers was at least twice the height that the obstacle protrudes above the sampler. This could not be accomplished at the on-site station (F-1 Test Stand). The samplers did have an unrestricted airflow of a minimum of 270 degrees around the sampler.

Ground Preparation

Each off-site location was selected using the siting location criteria provided above. It was not possible to locate all stations on a paved area to reduce the impact of fugitive dusts on the sample. The background samplers located at the F-1 Test Stand were placed on a paved area. The samplers at two stations on Redstone Arsenal Test Area #1: Redstone #1 Laser Tracker Trailer and Redstone #6 North Dodd Road were placed on concrete slabs. All other samplers were placed on the ground.

The logistics associated with setting up the air sampling equipment are difficult and time consuming making it necessary to structure a decision as to the placement of the air samplers on the day prior to the test. Weather forecast information (Attachment 1) obtained from the Meteorology Branch of the Redstone Technical Test Center was used in that decision- making process. Using a look- up table referencing "Distance from Test Stand to Maximum Projected Pollutant Concentration for Various Stability Classes and Wind Speeds" (Modeling for RD-180 Test Firings at MSFC - Carolyn Kennedy, September 1998) as a guide, possible sites for sampler placement were determined using a topo map of the area.

October Test (002)- On Site Location

The on-site monitoring station was located in the West Test Area at the F-1 Test Stand, northeast of Test Stand 4670 (S1-C). The on-site station consisted of one (1) PM_{10} Volumetric Flow Controlled (VFC) High Volume

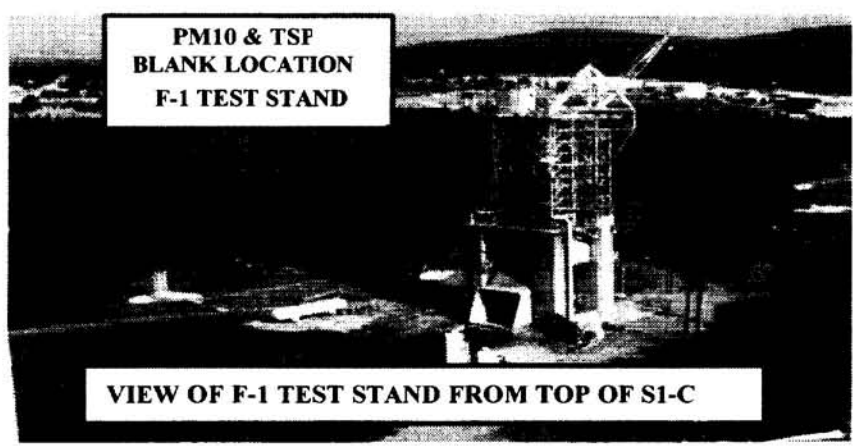

VIEW OF F-1 TEST STAND FROM TOP OF S1-C

sampler and one (1) TSP Volumetric Flow Controlled (VFC) High Volume sampler. This monitoring station was established to obtain background PM_{10} and TSP data.

October Test (002) - Off-site Locations

Based on the information gathered from the aforementioned sources, which forecasted winds from a northeasterly direction, the sites selected fell within the Redstone Technical Test Center, south of the S1-C Test Stand. Permission to locate equipment on the test range was received from the Test Center Director, Wes Widner. The Director provided the team with an escort familiar with the facility who was able to help identify on the map

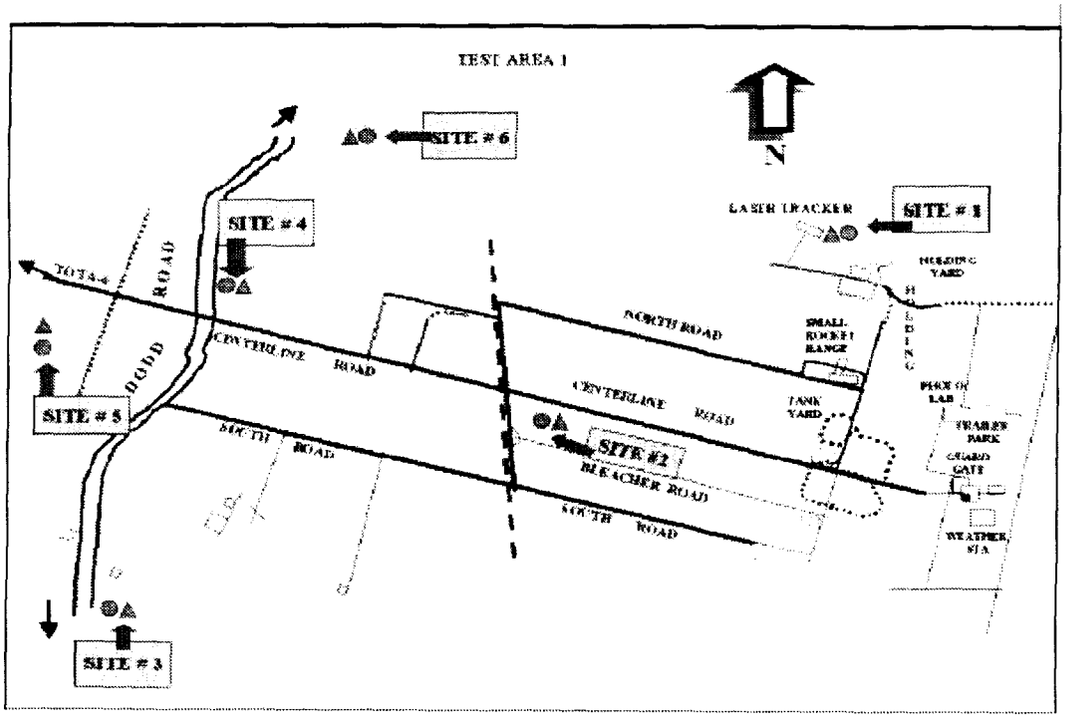

FIGURE 2

the pre-selected sampling locations. Six sets of air samplers were transported into the test area and one set each placed at six different locations. Each off-site station consisted of one (1) PM_{10} (VFC) High Volume sampler and one (1) TSP (VFC) High Volume sampler. The off-site stations are depicted in Figure 2.

Although the firing was scheduled for 4:40 pm, it seemed likely that the firing would not actually take place until later. The stability class for nightfall dramatically changes the distance from the test stand for which sampling equipment should be placed. Sampler sets numbers four, five and six were placed to incorporate this possibility of a later firing into the sampling plan, and in fact, the firing did not actually take place until 7:55 pm. The test duration was 2.7 seconds of a scheduled 56- second test.

As established in Table 1, which shows wind speed and direction for the immediate hours following the firing, winds were predominately from the north- northeast and ranged from 0 to 1 knot.

TABLE 1

Date	Time	Wind Dir Compass °	Wind Dir Cardinal	Wind Spd (kts)	Wind Spd (mph)
10/14/98	1600	311	NNW	4	4.55
	1700	332	NNW	4	4.55
	1800	105	ENE	1	1.14
	1900	30	NNE	1	1.14
* 19:55	2000	31	NNE	0	0.00
	2100	50	ENE	1	1.14
	2200	26	NNE	1	1.14
	2300	36	NNE	1	1.14
	2400	19	NNE	1	1.14

* Engine Ignition

Based on the least and the greatest angle of wind direction, an approximate plume path is demonstrated in the illustration below. This indicates sampler sets numbers three and five were in position to intercept the plume.

DIAGRAM 1

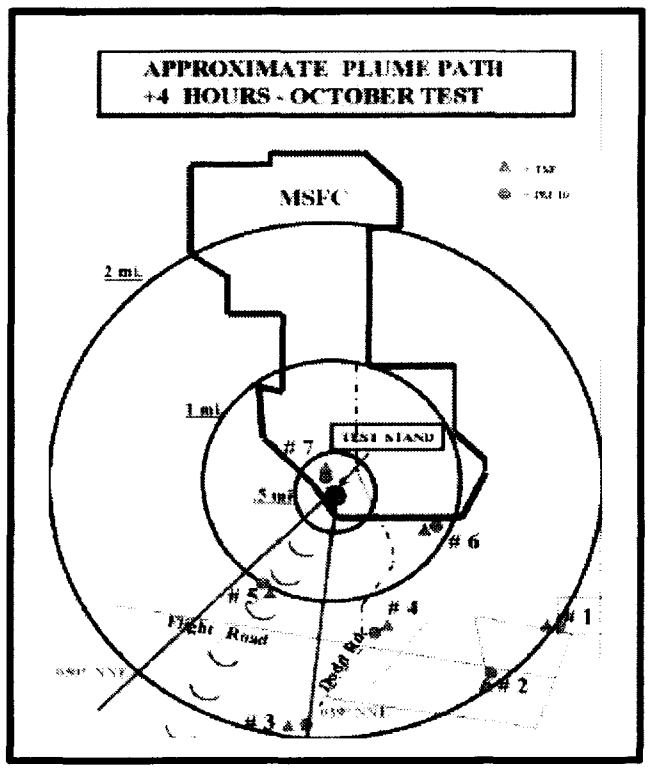

November Test (003)

Forecasted weather information for the November 14th test indicated winds from the northwest. (Attachment 1). The Redstone Test Director had allowed the air sampling team to leave all the equipment in place since the October firing. With the prediction of winds from the northwest, the decision was made to leave all samplers in situ. The test was delayed and firing did not occur until 6:27 pm. The November test duration was 56 seconds.

TABLE 2

		Wind Dir	Wind Dir	Wind Spd	Wind Spd
Date	Time	Compass °	Cardinal	(kts)	(mph)
11/04/98	1600	357	NNW	5	5.68
	1700	356	NNW	5	5.68
* 18:27	1800	1	NNE	5	5.68
	1900	346	NNW	5	5.68
	2000	357	NNW	5	5.68
	2100	1	NNE	4	4.55
	2200	10	NNE	4	4.55
	2300	358	NNW	3	3.40
	2400	350	NNW	4	4.50

* Engine Ignition

As seen in Table 2, winds for a 4- hour period after the test were from the north-northeast or north-northwest at 3 to 4 knots.

The approximate plume path for this test, as seen in the Diagram 2 below, indicates that sampler sets numbers three and four were in position to intercept.

DIAGRAM 2

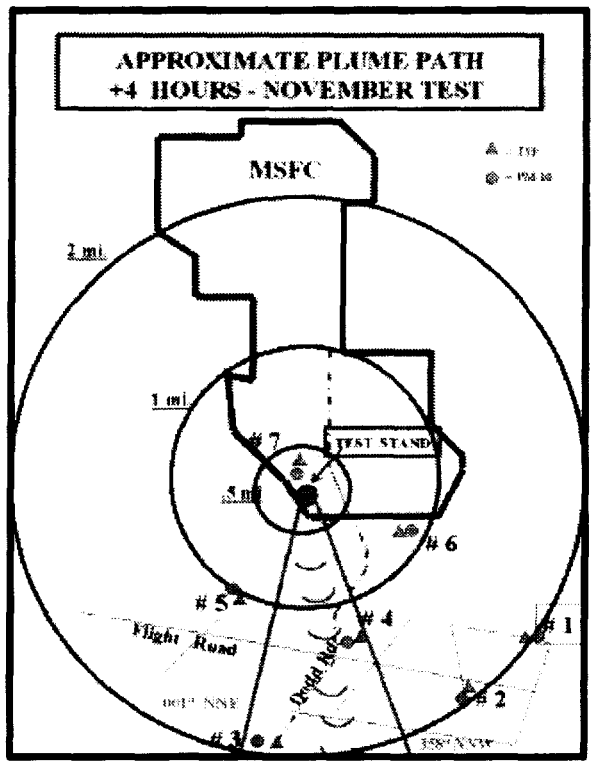

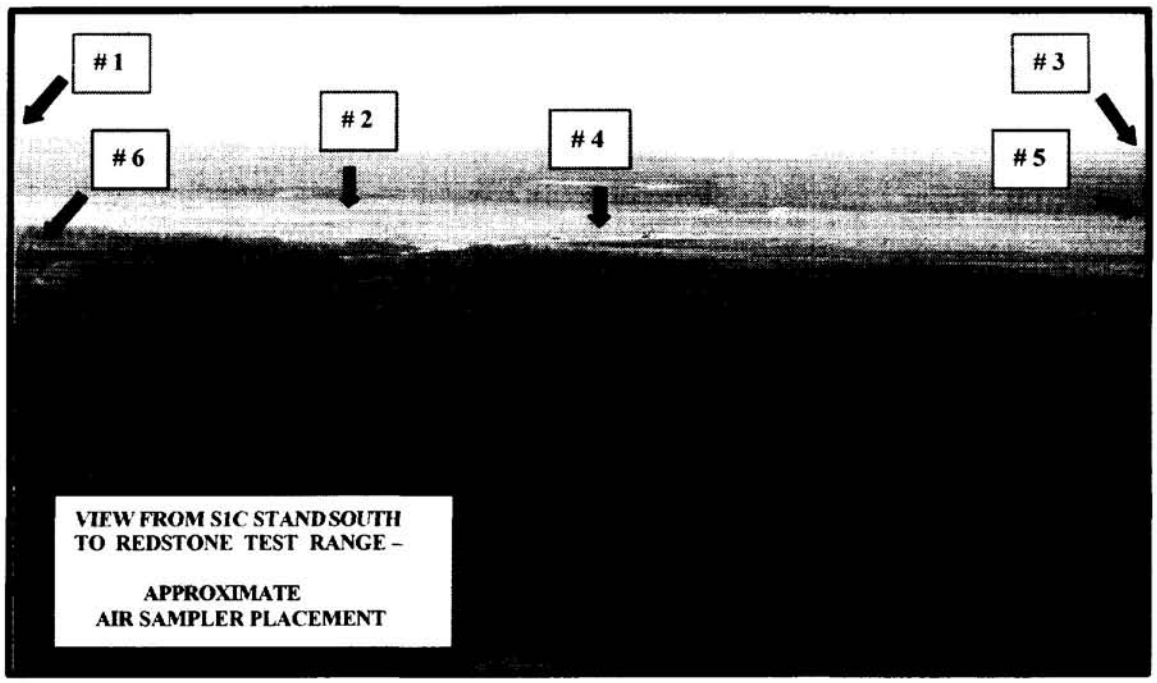

December Test (004)– The afternoon before the December 16th test, the air sampling team met with Redstone meteorologists, Jim Young and Billy Longgrear in an effort to determine sampling strategy for the upcoming test. Another cold front was scheduled to move through the area possibly around the time of testing and northerly winds would prevail. Ahead of the front, wind directions and speeds were variable making it difficult to determine an appropriate placement for the equipment. In the expectation of northerly winds with the passage of the front, the existing sampling positions were maintained. Testing was delayed until 5:49 pm and lasted for 64 seconds. Table 3 indicates that at the time of firing and for considerable time thereafter, the winds were swinging from south- southwest to west- northwest at 4 to 7 knots. The anticipated flow from the north did not in fact occur until around 0900 hrs, December 17th.

TABLE 3

		Wind Dir	Wind Dir	Wind Spd	Wind Spd
Date	Time	Compass °	Cardinal	(kts)	(mph)
12/16/98	1600	211	SSW	4	4.55
	1700	249	WSW	4	4.55
* 17:49	1800	192	SSW	3	3.41
	1900	214	SSW	4	4.55
	2000	243	WSW	4	4.55
	2100	240	WSW	4	4.55
	2200	258	WSW	5	5.68
	2300	264	WSW	7	7.90
	2400	282	WNW	7	7.90

* Engine Ignition

The approximate plume path seen illustrated below in Diagram 3, indicates that none of the samplers were in position to intercept the plume at the time of firing.

Diagram 3

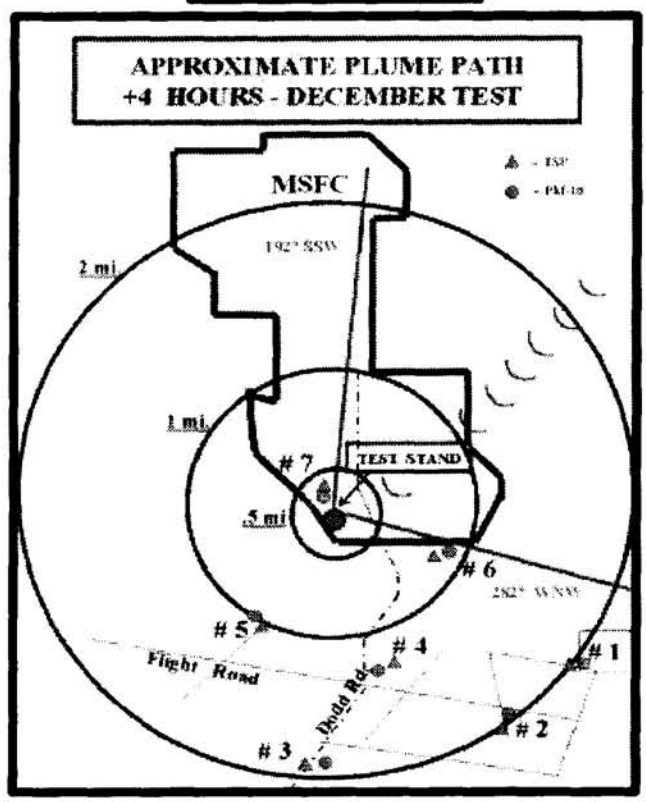

Principle of Operation

Suspended particles in the air were sampled at 1.13 cubic meters per minute (± 10%) through the circumferential inlet of the size selective inlet. The particles were then accelerated through 9 circular impactor nozzles. Because of their larger momentum, particles greater than the 10 micron cut-point impacted onto the greased impaction surface (shim).

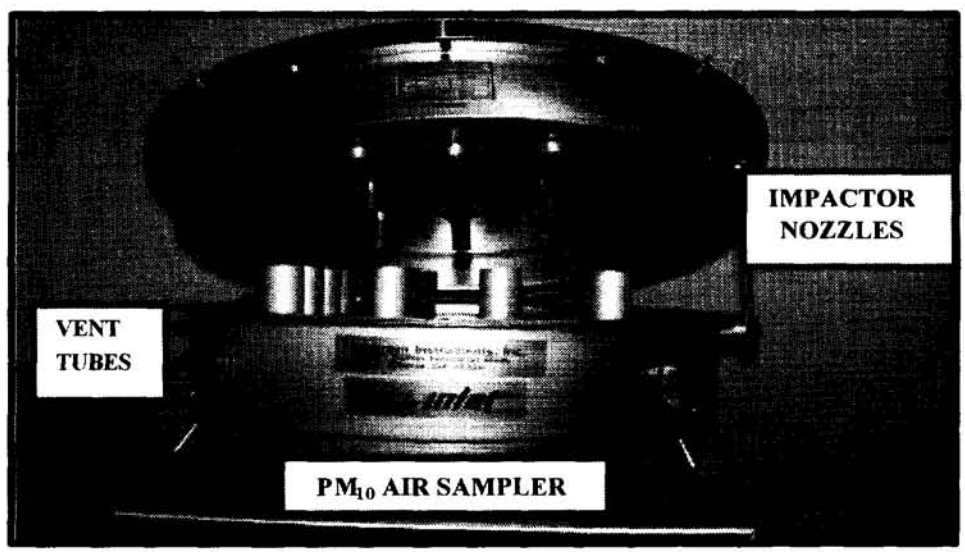

Analytical Procedures

Analytical procedures were based on inertial separation occurring within the sampler unit and gravimetric analysis of the filter medium in the laboratory. The analysis of the filter consisted of determining the mass concentration of the filter by weighing the filter after sampling and moisture equilibration. The analytical balance utilized had a minimum sensitivity of 0.1 mg. The net mass gain was then divided by the total volume of air sampled, corrected to EPA reference conditions of 25^0C (298 K) and 760 mm Hg. The total volume of air sampled was determined from the measured volumetric flow rate and the sampling time.

Data Handling and Retention

All log sheets, recorder charts and logbooks associated with the ambient air stations were maintained. Calibration records on all equipment were also maintained. Analytical results were compiled in a database.

Analytical Results

TABLE 4 – PM-10 Particulate Data Summary

S/N &	PM- 10 CONCENTRATION µg / std m^3	PM-10 CONCENTRATION µg / std m^3	PM-10 CONCENTRATION µg / std m^3
LOCATION	10/14/98	11/04/98	12/16/98
P1209 #1	14.027	10.493	7.39
P1206 #2	11.077	10.549	7.146
P1215 #3	10.530	8.502	5.585
P1216 #4	10.924	10.485	15.989
P1208 #5	12.268	9.978	6.824
P1207 #6	15.241	7.314	NC
P1214 #7	14.831	10.325	8.715

NC = Not Calculated Due to Equipment Malfunction

TABLE 5 – 2.5 Particulate Data Summary

S/N &	PM-2.5 CONCENTRATION µg / std m^3	PM-2.5 CONCENTRATION µg / std m^3	PM-2.5 CONCENTRATION µg / std m^3
LOCATION	10/14/98	11/04/98	12/16/98
P1215 #3	8.785	7.454	3.761
P1207 #6	11.205	6.144	NC

NC = Not Calculated Due to Equipment Malfunction

TABLE 6 – TSP Particulate Data Summary

S/N &	TSP CONCENTRATION µg / std m^3	TSP CONCENTRATION µg / std m^3	TSP CONCENTRATION µg / std m^3
LOCATION	10/14/98	11/04/98	12/16/98
P1185 #1	23.216	22.052	16.785
P1187 #2	22.250	18.732	16.001
P1193 #3	21.579	18.272	16.253
P1197 #4	25.985	20.334	50.759
P1192 #5	22.672	18.963	15.444
P1184 #6	26.636	19.351	NC
P1194 #7	27.797	17.691	15.361

NC = Not Calculated Due to Equipment Malfunction

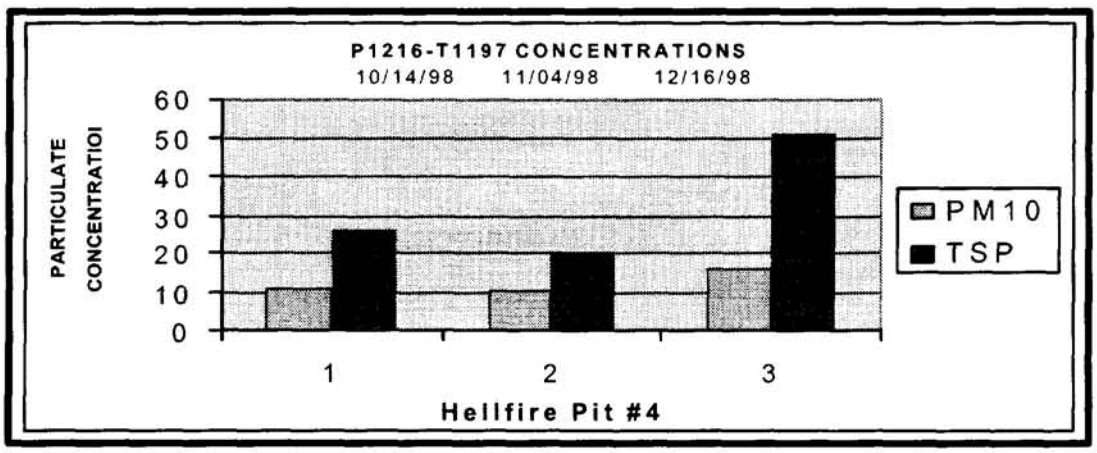

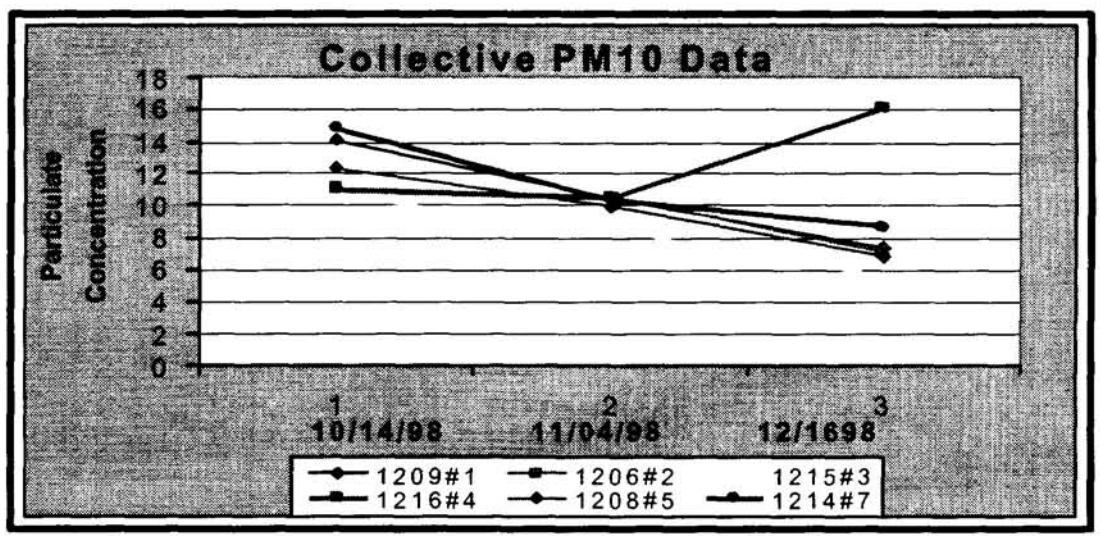

Conclusions

Although the approximate plume path indications were excellent for the October test (002), the firing itself was only 2.4 seconds in duration. The particulate data for this test indicates that heavier concentrations were collected than for the tests 003 and 004. It is probable that the hazy "smog-like" conditions during this period depreciated the general air quality of the area and is responsible for the elevated background levels. Results from a diminished plume are not expected to be as representative as results from a full duration test.

Environmental sampling conditions for the December test were such that it is unlikely that any particulates generated from the test firing were captured. The December data charts show lower concentrations of collected particulates with the exception of the spike seen at the #4 monitoring station. Shortly after the air samplers were prepared and set for the last engine test, Stennis personnel were asked to evacuate the RSA test range due to ordinance testing at the Hellfire Pit. Stennis personnel observed the Army's testing activity near the monitoring station, #4 "Hellfire Pit". Conceivably, detonating explosives near this monitoring station was responsible for the increased particulate loadings.

With respect to cooperative sampling conditions and a full duration firing, the November test was probably the most representative of the sampling events. Taking into consideration the existing general weather conditions for the duration of each test period and the related particulate collection data, it appears that the air sampling events reflect the background particulate levels of the area. Consequently, RD-180 testing had little or no effect on ambient air quality.

Gas Emission Measurements from the RD 180 Rocket Engine Tests at the NASA Marshall Space Flight Center

H. Richard Ross
Rick.Ross@ssc.nasa.gov

Lockheed Martin Stennis Operations
Test and Engineering Directorate
GB Tech Sciences Laboratory
SSC, MS 39529-6000

Introduction

The Science Laboratory operated by GB Tech was tasked by the Environmental Office at the NASA Marshall Space Flight Center (MSFC) to collect rocket plume samples and to measure gaseous components and airborne particulates from the hot test firings of the Atlas III / RD 180 test article at the MSFC. This data will be used to validate plume prediction codes and to assess environmental air quality issues.

This project was funded and administered through the NASA Environmental Office at the John C Stennis Space Center under Stennis Work Request MDS8800100.

Background

NASA's Marshall Space Flight Center in Huntsville, Ala., was under a Space Act agreement with Lockheed Martin Astronautics of Denver to provide a series of test firings of the Atlas III propulsion system configured with a Russian designed RD-180 engine. The RD-180 is being evaluated for use in the evolved Atlas that will replace the current MA-5 engine class.

Plume samples were collected and analyzed for hot test firings 3 and 4 from the S1C test stand area on November 4 and December 16, 1998. Fourier Transform Infrared (FTIR) spectroscopy was used to measure carbon dioxide (CO_2), nitrogen oxides (NO_X), and sulfur dioxide (SO_2). A dual beam non-dispersive infrared (NDIR) process was used to provide concentrations of carbon monoxide (CO). Total hydrocarbon content (THC) was measured using a flame ionization method. All gas components were measured in the ppm range.

The EPA has set National Ambient Air Quality Standards (NAAQS's) for criteria pollutants that identify ambient concentrations necessary to protect human health and welfare from any known or anticipated adverse effects of a pollutant. Four criteria air pollutants relevant to the releases associated with RD 180 engine testing have NAAQS's. The pollutants include CO, NO2, SO2, and suspended particulate matter less than 10 microns in size (PM10) which are airborne particles that are so small in size that they can remain airborne and disperse as a gas. Airborne particles were also collected and analyzed and is discussed in Part II of this report.

The state of Alabama and the city of Huntsville have adopted the National Ambient Air Quality Standards (NAAQS's) for criteria pollutants.

Engine Description

Pratt & Whitney at West Palm Beach has joined with NPO Energomash of Russia to market and to develop the license technology for the RD-180 engine. The engines are powered with liquid oxygen / kerosene propellants that feature a LOX lead start and a staged combustion cycle that provide 860,400 lbs. of thrust at sea level.

The RD 180 is a total propulsion unit that has the following features:

- High-pressure turbopump assembly that exhibits a two stage fuel pump and a single stage oxygen pump

- Oxidizer rich preburner and an oxidizer start and shutdown modes,

- 2 thrust chambers with a chamber pressure of 3,734 psia

- 50 – 100 % continuous throttling

- Total system dry weight 11,675 lbs.

- Self contained hydraulic system powered by kerosene from the fuel pump

Facility Location & Description

MSFC is located on approximately 1,841acres and is surrounded by a large federally owned area consisting of the U.S. Army's, Redstone Arensal (RSA) and the Wheeler Wildlife Refuge. This area is a physical barrier between engine testing and the general public. Huntsville, Alabama borders on the east, north, and west; Madison on the west-northwest; and Decatur on the west-southwest.

Development of space propulsion systems has been the primary mission of the MSFC since its establishment in 1960. The U.S. Army has been developing and testing rocket engines at RSA soon after World War II.

RD 180 engine testing occurred at the Alternate Test Facility (AETF). The AETF is located in the southwest portion of MSFC and orientated to the west-southwest. This location places the AETF within the boundary of the Wheeler National Wildlife Refuge and is approximately 1000ft (305m) from the Wheeler Lake wetlands.

The AETF was constructed in 1964 for the static testing of the Saturn V engines. This facility has also been known as the Propulsion and Structural Test Facility, S-1C Stand, Saturn Test Stand, and Technology Test Bed. The stand was modified in 1974 to perform shuttle external tank structural tests and again in 1986 to accommodate Space Shuttle Main Engine (SSME) testing.

Sample Location and Collection

At some location downstream of the nozzle exit, the exhaust temperature will be quenched or reduced below the temperature necessary for sustained combustion. Discussions with Dr. T Wang at NASA/ MSFC indicated the exhaust emission levels would achieve stability at a distance of approximately of 300 feet from the nozzle exit plane. The temperature at the sampling assembly was monitored during both engine tests and is discussed in the Test & Environmental Conditions section.

A 20-foot sampling assembly was used to elevate the sampling cylinders. The sampling assembly was constructed from a 6 inch I beam steel column with a 5-foot horizitional platform welded to the top end. The platform was used for securing the sampling cylinders and thermocouples.

Samples were collected in stainless steel G1 cylinders with an internal volume of 2100 cu. inches. The Samplers were evacuated to less than 20 microns of Hg and were carried to the site approximately 8 hours before the test firing. The cylinders, thermocouples and electromagnetic valve cables were connected to test equipment and were fastened to the sampling assembly at ground level. After a final check was performed on all sampling hardware, a crane was used to lift and place the sampling assembly next to a 20-ton concrete block.

The concrete block was used to the secure the sampling assembly. Chains were placed around the lower section of the I beam column and were fastened around the anchor block. Thermocouple cables and the electromagnetic valve control wires were fastened down the I beam column. Data loggers were connected to the output of the thermocouple cables to record plume temperatures. Each data logger was placed in a double wall plastic bag and was secured to the back of the I beam column 2 feet below the top of the concrete block.

Sampling Assembly Installation

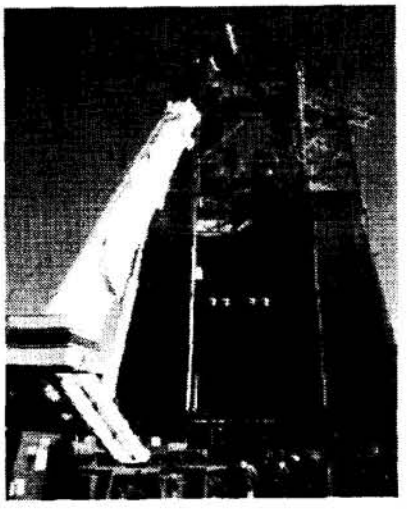

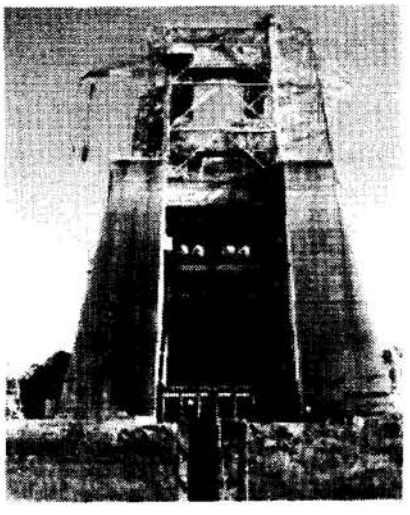

Sampling Assembly Installed and Secured for Engine Exhaust Collection

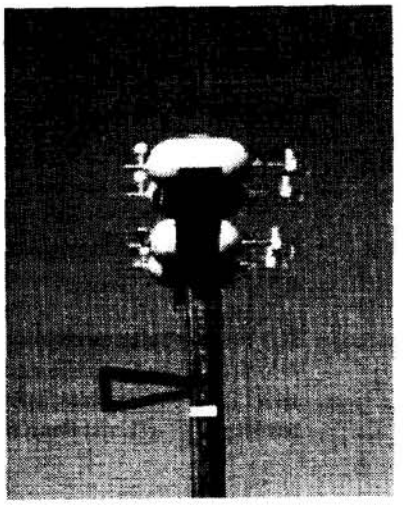

Sample Location Diagram

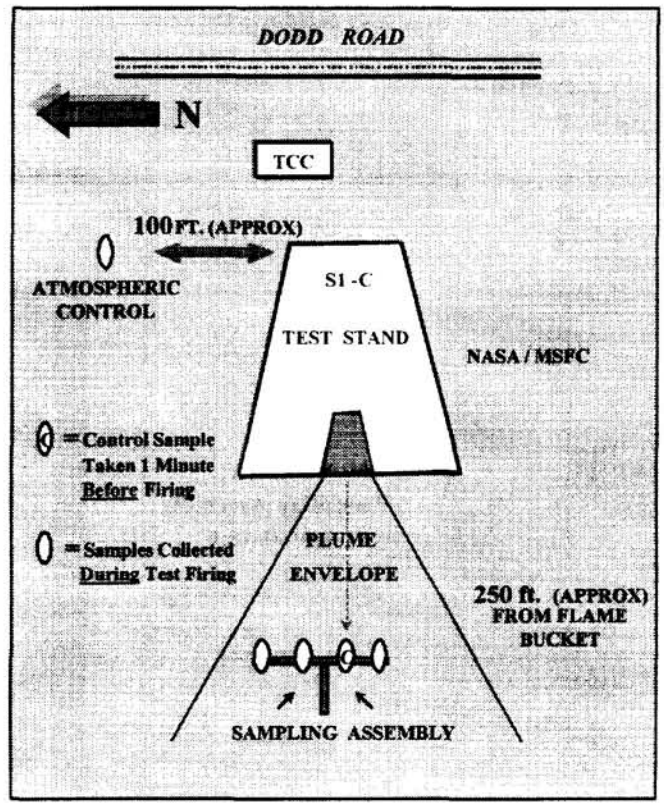

Sampling Features

- The plume control and sampling cylinders were elevated 20 feet at a distance of 250 feet west (downfield) from the flame bucket's exit or 300 feet aft of the nozzle exit plane.

- The plume sampling assembly (sample collection lines and the gas cylinders) was located 4 to 6 feet north from the center horizontal axis of the flame bucket.

- The atmospheric control sample was not placed in the plume envelope and was located approximately 100 feet north from the east boundary plane (front side) of the test stand at an approximate height of 10 feet. This control was used to determine if any background contaminants were present during engine testing (e.g. exhaust from diesel engines that pump water to the AETF deluge system).

- A 90 degree, ¼" x 3" stainless steel sample line was connected to the inlet port on each sampling cylinder through a two position electromagnetic valve. The atmospheric entrance of the sampling lines was pointed toward the flame bucket and was directed downward 90 degrees to minimize water intrusion. All sampling components are constructed from 304 stainless steel, except for the aluminum components of the electromagnetic valve.

- The plume samples and atmospheric control sample were collected over a test period starting at T+3 seconds. Sample collection was terminated at T+56 seconds. The plume control was collected

over a period of T minus 2 minutes through T minus 1 minute. Time events of the sample collection were controlled by actuating the electromagnetic valves on the sampling cylinders via the firing sequence program at the Test Control Center (TCC). When the valve is open the sample flows into the evacuated cylinder under its own atmospheric pressure.

- 3 Way, 2 Position, Electromagnetic Valves, Model - MV543 were used for collecting all samples. Operating Volts, 24VDC @ 1.33 Amps. When no voltage is applied to the sampling valve, the sampling configuration is closed. The closed configuration or "off" condition is the default setting for the sampling valves. Prior to T minus 2 minutes, all valves were in the default or closed configuration.

- The plume deflector on the AETF (S1-C) test stand has a J shaped configuration. The flame bucket boundary exit faces west-southwest and has a 15 degree-inclination.

Test & Environmental Conditions

Air temperature measurements were performed at the sampling assembly to assure that the exhaust gas temperature was quenched or reduced below the temperature necessary for sustaining combustion. At this point no further production of combustion products will occur. A temperature rise was noted for each test, but is within the normal living range. Approximately 50% of temperature increase is attributed to the activation of the water deluge system. This condition has been observed on previous tests when water was flowing at the maximum rate to the flame bucket, but was suddenly shut off or reduced due to unplanned test delays.

Water for the deluge is pumped to the test stands from above ground storage tanks at approximately 6 minutes before testing. NASA reported the water deluge system delivered 200,000 gallons of water per minute. The water exits the sides of the flame bucket through several hundred openings. Each opening has a diameter of 5/32" at a pressure of 160 psig. This configuration generates an enormous spray volume that blankets the flame bucket and surrounding area, including the sampling assembly.

To assure valid temperature measurements, two independent measurement systems were used. Each system consists of an Omega Model OM160 Data Logger, Model MOD-03/31 Signal Conditioner with a thermocouple probe, temperature range –40C to 110 C / -40F to 230 F. The thermocouple probes were fastened at the top of the sampling assembly adjacent to the inlet port of the sampling cylinders. A distance of 3 feet separated each thermocouple. The temperature recording session started 8 hours before the test and ended approximately 18 hours later. The recorded measurements were down loaded to a PC and are reported for each test firing. Temperature measurements for both systems agreed within 10%.

Test Firing 3

Prior to the engine test, the air temperature at the plume sampling cylinders was approximately 8 degrees C^0. The maximum temperature recorded was approximately 27 degrees C^0.

The firing occurred on November 4, 1998 at approximately 6:27PM. There was a heavy cloud ceiling at the time of the firing and it had been cloudy most of the day. Winds were out of the north – northwest at 5 mph.

Test Firing 4

Prior to the engine test, the air temperature at the sampling assembly was approximately 12 degrees C^0. The maximum plume temperature recorded during the firing was approximately 30 degrees C^0.

The firing occurred on December 16, 1998 at 5:47PM. The weather was clear with sunny skies for most of the day. Between 5:00 PM and 6:00 PM wind direction was variable (southwest to west southwest) due to an approaching weather front. Maximum wind speed was 10 mph.

Max. Air Temperature at the Sampling Assembly

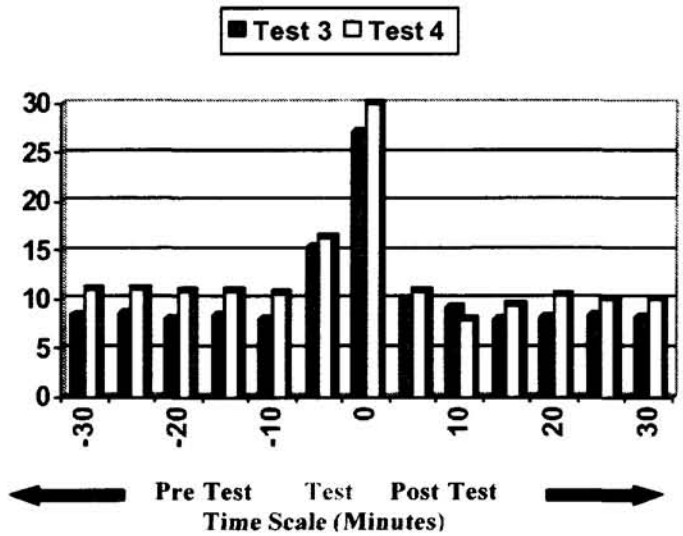

Engine Test Profile

The LOX/fuel mixture for both tests was 2.72. Maximum throttle run of 90% occurred on test 3 and lasted 26.55 seconds. The maximum throttle level for test 4 was 85%; this level was maintained for 12 seconds.

Sample Pressure Measurements

A Ruska Series 6200 Digital pressure gage (NASA ECN 036448) was used to measure the absolute pressure (psia) for all sampling cylinders. The Standards and Calibration laboratory at the NASA Stennis Space Center calibrated the gage. The gage is temperature compensated and has an accuracy of ±0.06 % full scale (50psia).

To collect the field samples, the sampling cylinders were evacuated in the laboratory to less than 20 microns of Hg and were carried to the sampling site. The vacuum level in the samplers was the only process used to draw in the ambient air samples. After all samples were collected, the samplers were removed from the sampling assembly and returned to the laboratory. Initial pressure measurements (P_s) were performed 48 to 72 hours later. This settling period allowed the samples to adjust to the laboratory environment and to achieve thermal equilibrium. Afterwards, research grade nitrogen (99.99995% purity / B6939) was added to the sample cylinders and final pressure readings (P_f) were performed to determine the volumetric expansion (dilution).

The addition of nitrogen provided a positive pressure to the samplers and diluted any elevated moisture levels that could potentially interfere with the analysis results. The final results for each analyzed component are based on the raw data analysis corrected for the volumetric addition of nitrogen

Total Hydrocarbon Analysis

A Rosemount 400A Hydrocarbon analyzer was used to measure the concentration of hydrocarbons expressed as methane. The analyzer is designed for monitoring atmospheric air for low level hydrocarbon contaminants and determining the hydrocarbon concentration of exhaust emissions from internal combustion engines.

Principle of Operation

The analyzer utilizes the flame ionization method of detection. The sensor is housed in a burner where a regulated flow of sample gas passes through a flame sustained by regulated flows of a fuel gas and air. Within

the flame, the hydrocarbon components of the sample stream undergo an ionization that produces electrons and positive ions. Polarized electrodes inside the burner collect these ions, causing current to flow through an electronic measuring circuit. The ionization current is proportional to the amount of carbon atoms that enter the burner, and is therefore a measure of the concentration of total hydrocarbons in the sample.

To ensure stable drift free operation, an internal temperature controller was used to maintain the analyzer interior at a constant 48 degrees C. This feature minimizes temperature dependent variations in electronic current measuring circuitry and adsorption / desorption equilibrium of background hydrocarbons within the internal flow system.

The analyzer is equipped with a mixed fuel mixture (40% hydrogen / 60% helium) to minimize any error introduced by oxygen synergism and for improving the equality of response to the various species of hydrocarbons.

Calibration

Calibration consists of setting two points, a zero point and a span (upscale) point.

A 4.9 ppm hydrocarbon gas standard (B6680 / AP) in nitrogen was used to span the analyzer. The calibration gas accuracy (± 2%) was certified by a specialty gas supplier and is NIST traceable. The total hydrocarbon (THC) value is expressed as methane. Hydrocarbon free air (B7784/ UC, THC <0.1 ppm) was used to adjust the background sensitivity (bias) of the analyzer. Thus with a hydrocarbon free gas flowing, the applied zero suppression compensates for the background current in the detector.

Quality Control

Zero and upscale calibration/verification checks were conducted both before (n=2) and after (n=4) each sample set in order to quantify calibration drift and measurement system bias. During these checks, the calibration gases were analyzed in the same manner as the plume samples. The maximum calibration drift of the span gas measurements was 2.04%. The zero bias remained unchanged.

Long term instrument precision error based on measuring a NIST traceable gas standard over a 3-month period with over 20 sampling points (n=20) is less than 2 sigma or 3 % of the actual reported value of the standard.

Analysis

The analysis results are listed in tables 1, 2 and 3.

Carbon Monoxide

Determination of carbon monoxide in the samples was performed using a Rosemount 880A Dual Beam Nondispersive Infrared Photometer.

Principle of Operation

The photometer uses a selective filter to pass infrared radiation within a narrow range that matches the vibrational energy of the CO molecule. This configuration reduces stray radiation and allows only CO

to be measured. While the absorption frequency depends on the molecular frequency, the absorption intensity is based on the amount of CO present. (See *Principle of Operation* in the "Other Targeted Emissions Section" for further discussion on the interaction of IR radiation with matter).

Calibration

Calibration consists of setting two points, a zero point and a span (upscale) point.

An 84.7 ppm CO gas standard (B6294) in nitrogen was used to span the analyzer. The supplier's reported accuracy for the NIST traceable standard is 2%. CO free nitrogen was used to adjust the background sensitivity (bias) of the analyzer. Thus with a CO free gas flowing, the applied zero suppression compensates for the background bias in the measurement system.

Analysis

The analysis results are listed in tables 1, 2 and 3.

Quality Control

Multipoint calibration error checks were conducted before and after sample testing by introducing 4 different calibration gases directly into the analyzer and recording responses. The maximum error was less than 3%.

Other Targeted Emissions

Other targeted gasses were analyzed using a Bio Rad FTS-40 Fourier Transform Infrared Spectrometer using a multiple reflection gas cell with an optical path of 7.2 meters. Gasses measured were carbon dioxide, (CO_2), nitrogen dioxide (NO_2) and sulfur dioxide (SO_2).

Principle of Operation

IR spectroscopy relies on the fact that all molecules except those with a homogeneous diatomic molecular structure (e.g. O_2, N_2, H_2...etc.) and inert gasses (Ar, He, Ne...etc.) will react and absorb infrared radiation in a characteristic manner. The absorption causes changes in the molecular rotation and vibration. The pattern of absorption is determined by the physical properties of the molecule such as the number and type of atoms, the bond angles and bond strengths. This means that each component spectrum differs from all others and may be considered the molecular signature. By measuring and recording absorption strength as a function of wavelength over the infrared spectral region, the molecules present in the sample can be identified and quantified.

In IR spectroscopy as applied here, two energy spectra have to be recorded, the spectrum of the measurement system without a sample (I_0 or background) and the spectrum of the gas cell containing the sample (I). For the quantitative analyses the absorbance spectrum $A_i(v)$

$$A_i(v) = \log(I_0(v)/(I(v)) = a_i(v) \cdot b \cdot c \qquad \textbf{(1)}$$

is calculated with $a_i(v)$absorptivity of component i at wavenumber v; b sample path length; c_i concentration (partial pressure) of component i ; v wavenumber in cm^{-1}.

Equation 1 is known as Beer's law. Beer's law strictly holds only for isolated molecules, interacting with the radiation. This requirement is best met with gases at low partial pressures diluted in an nonabsorbing (inert) buffer (e.g. ppm concentrations of components in air mixed with nitrogen, as was done in this analysis.

Absorptivity is measured by preparing or using calibration standards of components at known concentrations and measuring the spectra against a reference (background) gas that does not contain the components of interest. These calibration spectra are then used in the sampling analysis: (1) The compounds are detected by matching sample absorbance bands with the bands in the calibration - standard spectra and (2) concentrations are measured by comparing sample band intensities with the calibration intensity levels.

Data Collection

FTIR data collection was set for 4000-650 wavenumbers (cm^{-1}), 16 co-added scans, $1 cm^{-1}$ resolution and a gain of 1.5 for the deuterated triglycine sulfate (DTGS) detector. Data was collected and stored as single beam spectra.

Sampling

Samples and standard gasses were measured in a Model 6 IR absorption cell manufactured by Infrared Analysis Inc. The cell has an internal volume of 530 cc and is equipped with two stainless steel valves with a flow-through tube to allow monitoring of flowing samples. The IR beam is reflected within the gas cell by the three spherical mirrors, which gives multiple passing in increments of 4 passes. The 7.2-meter optical path was obtained by 48 passes with a base path of 0.15meters.The cell was set in the FTIR sample compartment; the compartment was sealed from the atmosphere by using a magnetized rubber gasket.

Samples and calibration gasses were continuously drawn through the inlet of the gas cell and vented to the atmosphere. The sampling flow rate was ~ 500cc/min; the cell was purged with a minimum of 10 cell volumes of the calibration or sample gas before any spectral measurements were acquired. In between each sample and calibration run, the gas cell was purged with at least 5 cell volumes of nitrogen gas.

Carbon Dioxide

Calibration

A comparison between the sample spectrum to research grade nitrogen (B6939) was performed to differentiate the relative spectral contribution from CO_2. Four calibration standards were used to bracket the concentration range of the samples. In addition, a 425 ppm CO_2 calibration gas standard (B6294 / MG) prepared by a specialty gas supplier was also used. The gas standard is a NIST traceable gravimetric standard and has a reported accuracy of 2%.

A multicomponent calibration gas mixture (1920 ppm CO_2, 192 ppm NO_2 and 96.4 ppm SO_2) in air (B7009) was used to prepare three calibration standards. The lower concentrations were obtained by diluting the calibration gas with research grade nitrogen (B6939). Measuring the absolute pressures with a digital pressure gage before and after the dilutions were made, the concentration values for the prepared standards were derived. The primary gas (NIST traceable) standard was certified by the vendor and has a reported accuracy of 2%. Linear regression files were constructed that included reference spectra representing the CO_2 standards. The correlation coefficient (r) for the calibration regression line is 0.99936.

Analysis

The analysis results are listed in tables 1, 2 and 3.

Nitrogen dioxide and sulfur dioxide represent integrated samples that must be seen through water interference bands. Moisture possesses a feature rich and complicated infrared spectrum; the major moisture bands occur in two regions 4000-3400 cm^{-1} and 2000-1300 cm^{-1}. Nitrogen dioxide shows two strong spectral regions near 1600 cm^{-1}. Sulfur dioxide is centered at 1360cm^{-1}.

Because of the strong interference from water vapor, a subtractive technique was employed to reconcile the sample spectrum for NO_2 and SO_2. Screening tests were performed to make reasonable assumptions about the moisture absorption in the samples. Absorbance bands near 3700cm^{-1} were measured to determine the moisture absorption level. Several trial and error steps were attempted to prepare a suitable background by mixing humidified nitrogen in dry nitrogen. The goal was to develop a background (reference) that would subtract 80 to 95% of the moisture bands from all of the samples. This range is optimal for seeing through the water bands without over subtraction. Complete or over subtraction of the spectrum can introduce spectral artifacts (e.g. introduction of noise, spike lines, etc.) and degrade spectral features (i.e., band shapes). The trade off is between sensitivity and risk of measuring a residual feature.

After the moisture background is removed, the sample absorbance spectra are compared with the calibration spectra that were acquired with a dry nitrogen background. This process is similar in nature with the analytical method used to measure CO_2.

Calibration

A NIST traceable multicomponent calibration gas mixture (1920 ppm CO_2, 192 ppm NO_2 and 96.4 ppm SO_2) in air (B7009) was used to prepare four calibration standards. The lower concentrations were obtained by diluting the calibration gas with pure nitrogen. Linear regression files were constructed that included reference spectra representing the NO2 and SO2 standards. The correlation coefficients for NO2 and SO2 are 0.99610 and 0.99299 respectively.

Quality Control

Interference responses were assessed and compensated prior to testing. The position and the slope of the spectral base line were monitored as successive spectra were collected. If the base line within a data set for a particular sample run began to deviate by more than 10%, a new background would be required. No deviations were encountered during the sample runs.

The time domain detector response (interferogram) for the spectrometer remained stable within 2 sigma or 10% over a 4-month period.

Table 1

Exhaust Summary Results					
Test #	**THC**	**CO2**	**CO**	**NO2**	**SO2**
3	1.8 ppm	1581 ppm	40 ppm	< 10 ppm	< 10 ppm
4	1.7 ppm	2097 ppm	48 ppm	< 10 ppm	< 10 ppm

Table 2

Plume Control Data					
Test #	**THC**	**CO2**	**CO**	**NO2**	**SO2**
3	1.1 ppm	409 ppm	< 1 ppm	< 10 ppm	< 10 ppm
4	1.9 ppm	410ppm	< 1 ppm	< 10 ppm	< 10 ppm

Table 3

Atmospheric Control Data					
Test #	**THC**	**CO2**	**CO**	**NO2**	**SO2**
3	1.0 ppm	429 ppm	< 1 ppm	< 10 ppm	< 10 ppm
4	1.9 ppm	401ppm	< 1 ppm	< 10 ppm	< 10 ppm

Overview of the City of Huntsville Air Pollution Control Program

DANIEL SHEA
Division of Natural Resources and Environmental Management, City of Huntsville
P. O. Box 308
Huntsville, AL 35804 USA
Phone: (256) 427-5750
Fax: (256) 427-5751
E-mail: dshea@ci.huntsville.al.us

The City of Huntsville implements one of the two local air pollution control programs in the State of Alabama. Program implementation responsibilities include monitoring of ambient air quality, issuance of pollution control permits, inspection of point sources of emissions, and enforcement of Federal, State, and local air pollution control regulations. This session provides a brief overview of the air pollution control program in Huntsville.

Potential Effects on the Huntsville Area of Revised National Ambient Air Quality Standards for Ozone and Fine Particulate Matter

DANIEL SHEA
Division of Natural Resources and Environmental Management, City of Huntsville
P. O. Box 308
Huntsville, AL 35804 USA
Phone: (256) 427-5750
Fax: (256) 427-5751
E-mail: dshea@ci.huntsville.al.us

In 1997, EPA promulgated a more stringent Federal ozone standard and a new standard for very small particulate matter ($PM_{2.5}$). Ozone concentrations in Huntsville over the past 3 years exceed the tighter ozone standard. Consequently, Huntsville and many other urban areas that are currently classified as "attainment" or "clean air" areas could be redesignated as "non-attainment areas." (The U. S. Supreme Court will hear the case challenging the standards in November 2000). The ramifications of non-attainment designation will be briefly discussed. Preliminary data on fine particulate concentrations in the Huntsville airshed will also be summarized.

Development of Lead Free Energy Absorber for Space Shuttle Blast Container

Donald Balles, Thomas Ingram, Howard Novak, Albert Schricker

United Space Alliance
8550 Astronaut Blvd.
Cape Canaveral, FL 32920

INTRODUCTION

USA SRB Element is responsible for the assembly and refurbishment of the non-motor components of the SRB as part of the Space Shuttle Vehicle (SSV) system shown in Figures 1 and 2, and which is developed and managed by Marshall Space Flight Center (MSFC) in Huntsville, Alabama. Programs are underway to develop and evaluate environmentally acceptable materials for use on aerospace flight hardware in order to eliminate materials such as lead, and also; by effective re-design, provide lighter and more efficient systems. The SRB blast container (BC) is made primarily from Inconel 718 material that interfaces with either Inconel 718 or aluminum alloy materials. Four (4) Inconel 718 studs are used to holddown each of the SRBs to the Mobile Launch Platform (MLP), and each stud is held in place by an upper frangible nut and lower conventional nut. The additional assembly of pyrotechnic initiators and booster cartridges to the frangible nuts allow for detonation on command, which splits the nuts in halves and releases the SRBs and attached SSV. The present BC along with a cast Lead liner / Shock absorber, contain the high energy pyrotechnic fragments as well as frangible nut elements after detonation, and protects the SSV from Foreign Object Damage (FOD). This paper discusses the benefits of replacing the cast lead liner with an open cell aluminum foam.

DISCUSSION

Material Selection and Preliminary Testing

An incident had occurred where the lead liner used in the present BC had corroded, and the hazardous lead oxides resulting from corrosion required special hazardous material handling and disposal. USA, Inc., is actively pursuing lead abatement programs, and the potential replacement of the lead BC liner followed those initiatives. A replacement material for the lead BC liner was sought by the Materials and Process Engineering Department. After an intensive search, the Energy Research and Generation, Inc. (ERG, Inc.) located in Oakland, California; was found to be a company that produces a unique type of open cell aluminum alloy foam designed specifically for energy absorption. The open cell aluminum foam feature allowed for a larger volume of material to be used in the confines of the BC without raising chamber pressure. Conventional materials such as honeycomb, and closed cell foams were found to be unacceptable. Mechanical Engineering contracted ERG, Inc. to provide flat test panels of various thickness and pore size / density configurations, in preparation for static drop testing. Full size frangible nuts were dropped from appropriate heights onto lead and aluminum foam targets below, thereby simulating relative impact energies of high velocity nut segments. It was found from these preliminary tests that the aluminum foam allowed for improved energy absorption over the present lead liner, and would potentially save 200 pounds at liftoff. As a result of these successful tests, USA SRB Element and NASA-MSFC decided to set-up a series of follow-on Proof-of Principle tests to determine the dynamic characteristics of the open cell aluminum foam under actual BC configuration.

Proof-of Principle Tests

A series of follow-on Proof-of-Principle tests were performed at the NASA-Kennedy Space Center (KSC) Launch Equipment Test facility (LETF), which simulated the SRB hold-down post, with actual BC hardware and pyrotechnics assembled. After BC assembly and calibration of instrumentation, the hardware was then test fired. Figures 3, 4, 5, and 6 show the set-up required to perform the dynamic testing. Figures 7, 8, 9, and 10 show the results after test firing. Post-test results revealed that the aluminum foam had excellent energy absorption characteristics, and performed as expected. In addition, operator satisfaction was high, in part caused by the ease of handling and installation of the light weight aluminum foam energy absorber, blast attenuator. A cohesive team composed of USA SRB Element Mechanical Engineering, Production Engineering and Operations, Launch Support

Services, and Materials and Processes Engineering, as well as NASA-MSFC and NASA-KSC personnel and contractors took part in the successful test program.

CONCLUSION

Development and Proof-of Principle testing of an open cell aluminum foam energy absorber / blast attenuator has been completed. Data reduction continues, and the initial results were excellent. It was found that selected aluminum foam densities, and pore sizes worked better than others for the SRB frangible nut application. Excellent instrumentation allowed for accurate measurement of exit stud velocities, chamber pressures, and pyrotechnics firing order. Digital cameras, along with high speed, and conventional video taping recorded key elements of the test program, and helped with the interpretation of data.

ACKNOWLEDGEMENTS

The authors would like to thank the various USA departments both in Huntsville, Alabama and Kennedy Space Center, Florida for supporting and assisting in program management, production operations, logistics and testing. Many thanks to the NASA-MSFC SRB Program Office personnel who were supportive of this program, and NASA-KSC personnel and contractors, who performed the physical testing, and instrumentation at the LETF. Additional thanks are given to ERG, Inc. management and engineering personnel who helped make this test program a success.

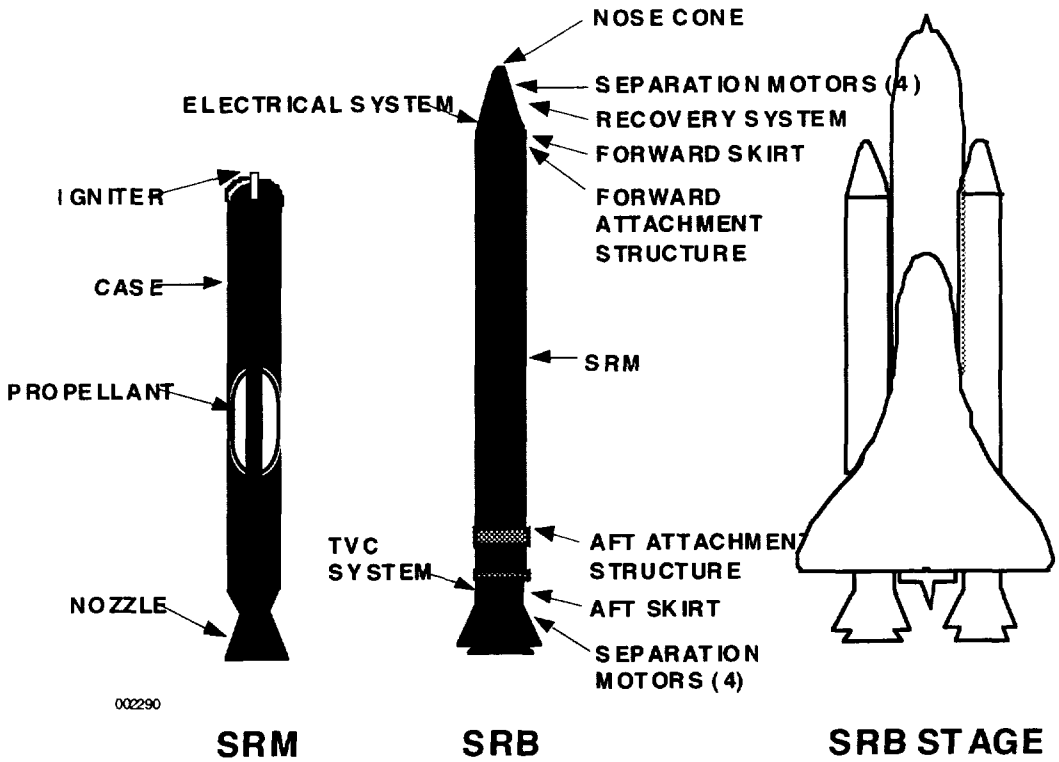

Figure 1. Space Shuttle Vehicle and Solid Rocket Booster

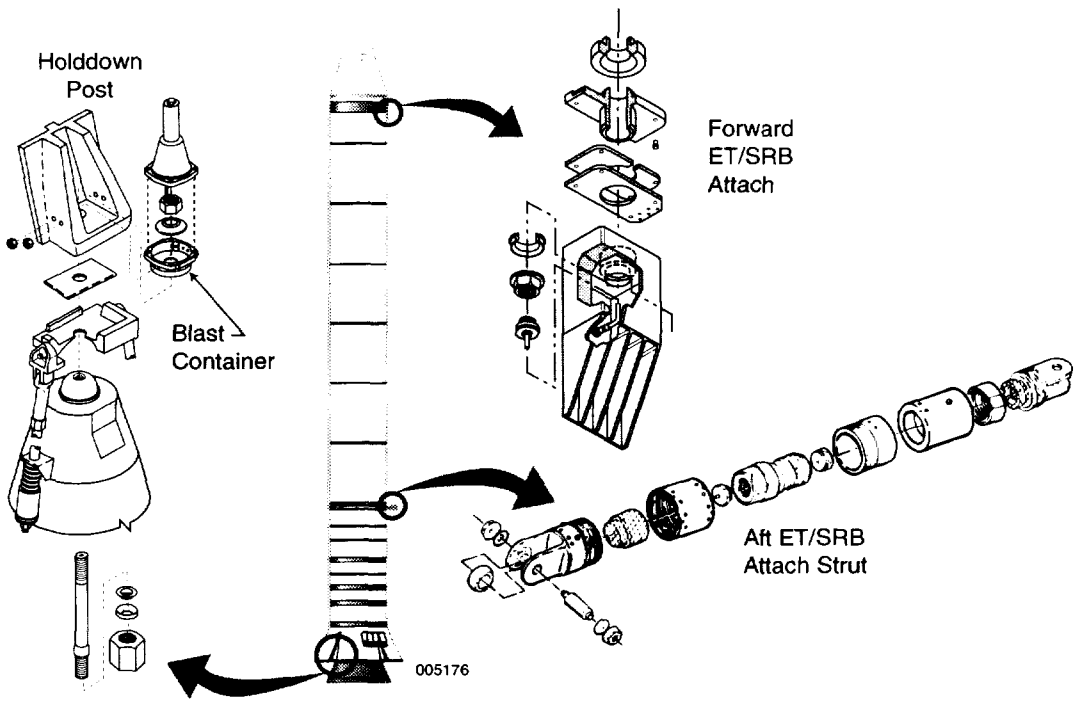

Figure 2. Solid Rocket Booster with Blast Container

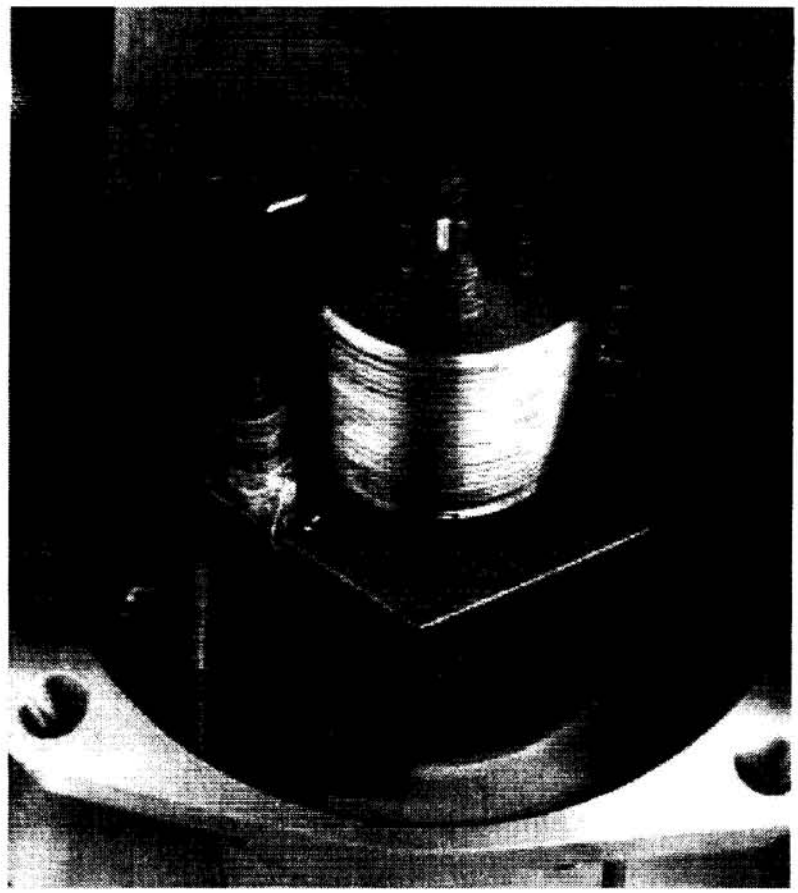

Figure 3. Holddown Stud, Frangible Nut, Booster Cartridges

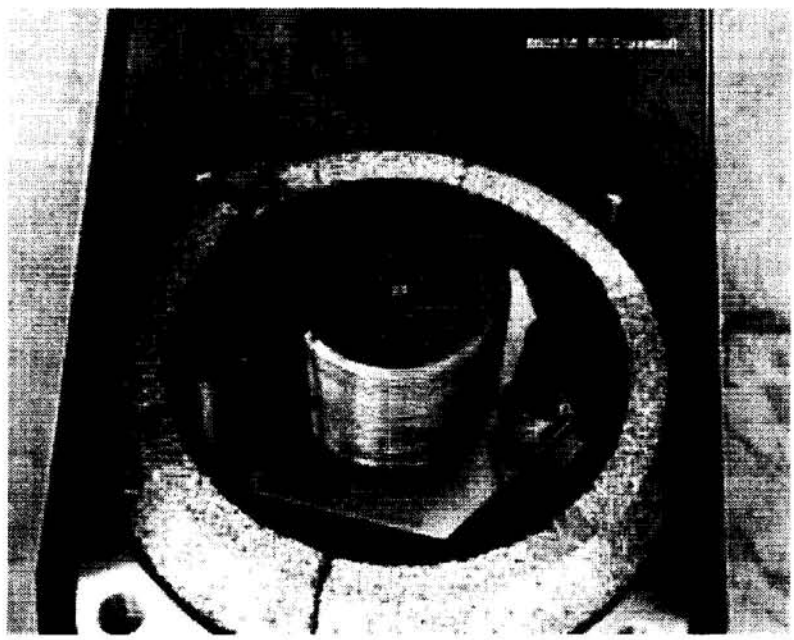

Figure 4. Aluminum Foam in Place

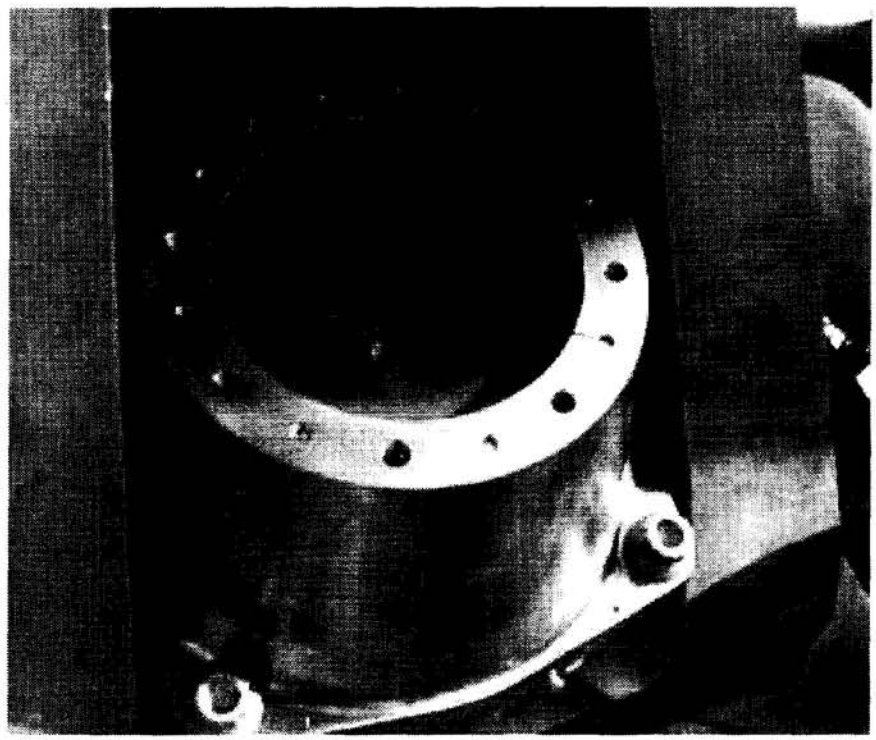

Figure 5. Top Section of Blast Container Assembled

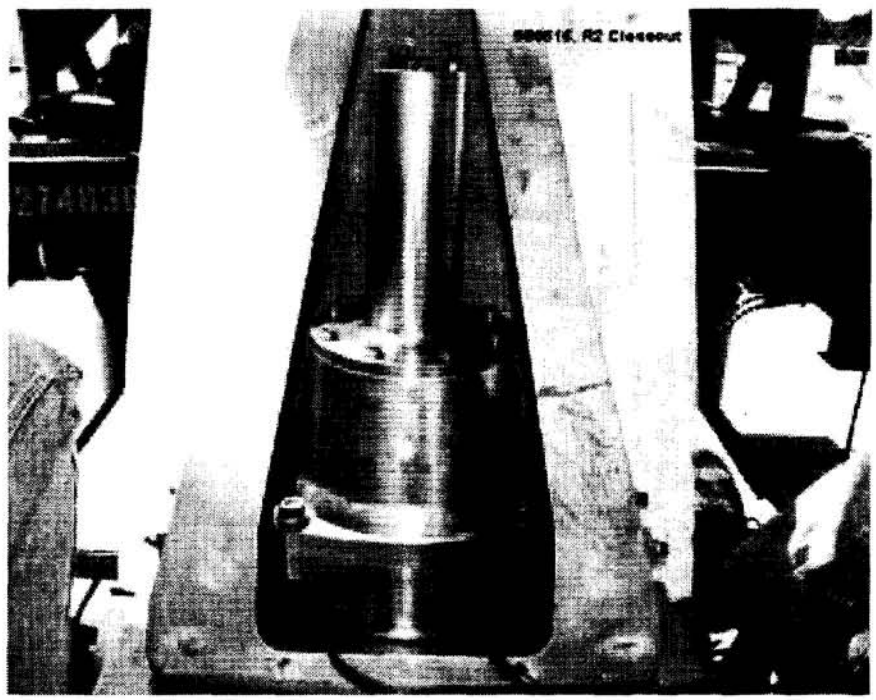

Figure 6. Final Assembly with Spring Housing

Figure 7. Post Test Frangible Nut Segments and Webs

Figure 8. Post-Test Showing Foam Impact, Frangible Nut, etc.

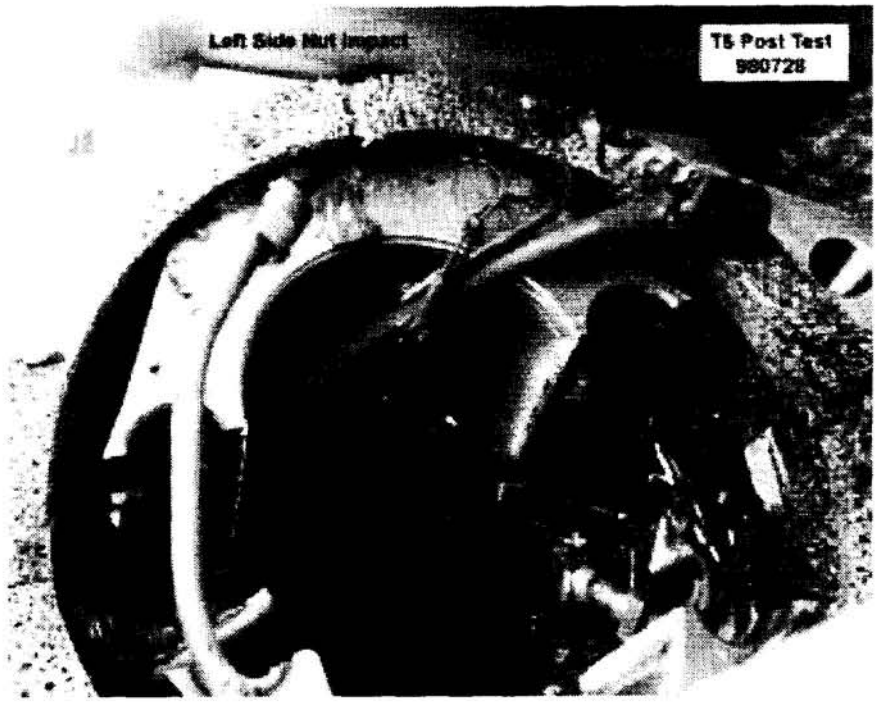

Figure 9. Close-up Showing Foam Impact, Frangible Nut, Pyrotechnics

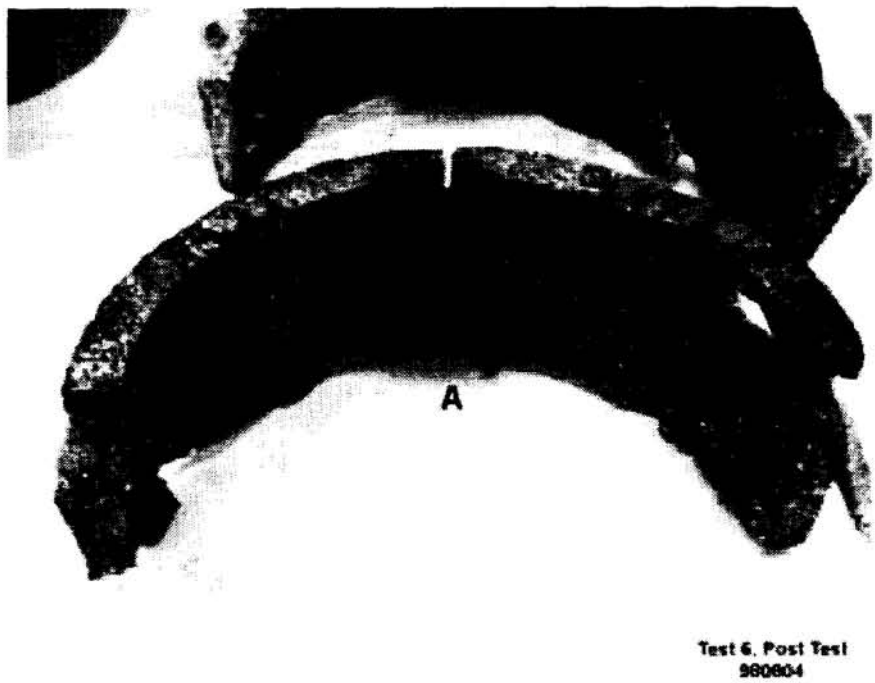

Figure 10. Post-Test Showing Aluminum Foam Energy Absorber

Polymer Matrix Composites (PMCs) Cryopipe for Rocket Engine Lines and Ducts

DAVID BETTINGER

The Technology Partnership
8030 Coventry
Grosse Ile, MI 48138-1119 USA
Phone: 734-675-8295
Fax: 734-675-8296
E-mail: techpart@home.com

Alloy rocket engine ducts and lines have been targeted for conversion to lighter, polymer composites. The concern with polymer composites is assured performance for multiple reuse. The need is for stress control and polymer protection from LOX and LH_2. A suite of seven polymer composite technologies is presented that make the component fabrication, assembly, and performance of polymer cryopipe practical and economical. Flanges are eliminated and expensive expansion alloy bellows are replaced by more efficient and lightweight components.

These technologies use stress design to configure superior performance composites with existing space-qualified materials. The Air Force Research Laboratory and the Ballistic Missile Defense Organization have funded these developments.

CP/58 N. 76
NBS only
Poster Session

Nanotechnology Concepts at Marshall Space Flight Center – Engineering Directorate

BILIYAR BHAT, Raj Kaul, Sandeep Shah, Gweneth Smithers, and Michael D. Watson

Marshall Space Flight Center/ ED33
Huntsville, Alabama 35812 USA
Phone: 256-544-2596
Fax: 256-544-5877
E-mail: Biliyar.Bhat@msfc.nasa.gov

Nanotechnology is the art and science of building materials and devices at the ultimate level of finesse: atom by atom. Our nation's space program has need for miniaturization of components, minimization of weight, and maximization of performance, and nanotechnology will help us get there. MSFC's Engineering Directorate is committed to developing nanotechnology that will enable MSFC missions in space transportation, space science, and space optics manufacturing. MSFC has a dedicated group of technologists who are currently developing high-payoff nanotechnology concepts. This poster presentation will outline some of the concepts being developed including, nanophase structural materials, carbon nanotube reinforced metal and polymer matrix composites, nanotube temperature sensors, and aerogels. The poster will outline these concepts and discuss associated technical challenges in turning these concepts into real components and systems.

Microstructure, Mechanical Properties, Hot-Die Forming, and Joining of 47XD Gamma TiAl Rolled Sheets

G. DAS

Pratt & Whitney
P.O. Box 109600
West Palm Beach, FL 33410-9600 USA
Phone: 561-796-6744
Fax: 561-796-7454
E-mail: dasgopal@pwfl.com

S. Draper, J.D. Whittenberger, and P.A. Bartolotta
Glenn Research Center
2100 Brookpark Road
Cleveland, OH 44135-3191 USA
Phone: 216-433-3257 (Draper); 216-433-3196 (Whittenberger); 216-433-3338 (Bartolotta)
Fax: 216-433-8000
E-mail: Susan.L.Draper@lerc.nasa.gov; John.D.Whittenberger@lerc.nasa.gov; Paul.A.Bartolotta@lerc.nasa.gov

The microstructure and mechanical properties, along with the hot-die forming and joining of Ti-47Al-2Nb-2Mn-0.8 vol% TiB_2 sheets (known as 47XD), produced by a low-cost rolling process, were evaluated. A near-gamma microstructure was obtained in the as-rolled condition. The microstructures of heat-treated sheets ranged from a recrystallized equiaxed near-gamma microstructure at 1,200 to 1,310 °C, to a duplex microstructure at 1,350 °C, to a fully lamellar microstructure at 1,376 °C. Tensile behavior was determined for unidirectionally rolled and cross-rolled sheets for room temperature (RT) to 816 °C. Yield stress decreased gradually with increasing deformation temperature up to 704 °C; above 704 °C, it declined rapidly. Ultimate tensile strength exhibited a gradual decrease up to 537 °C before peaking at 704 °C, followed by a rapid decline at 816 °C. The modulus showed a gradual decrease with temperature, reaching ~72 percent of the RT value at 816 °C. Strain to failure increased slowly from RT to 537 °C; between 537 °C and 704 °C, it exhibited a phenomenal increase, suggesting that the ductile-brittle transition temperature was below 704 °C. Fracture mode changed from transgranular fracture at low temperature, to a mixture of transgranular and intergranular fracture at intermediate temperature, to ductile fracture at 816 °C, coupled with dynamic recrystallization at large strains. Creep rupture response was evaluated between 649 and 816 °C over the stress range of 69 to 276 MPa. Deformation parameters for steady-state creep rate and time-to-rupture were similar: activation energies of ~350 kJ/mol and stress exponents of ~4.5. Hot-die forming of sheets into corrugations was done at elevated temperatures in vacuum. The process parameters to join sheets by diffusion bonding and brazing with TiCuNi 70 filler alloy were optimized for test coupons and successfully used to fabricate large truss-core and honeycomb structures. Nondestructive evaluation methods, *e.g.*, ultrasonic C-scans and thermography along with metallography, were used to characterize bond quality. Microstructural evaluation during heat treatment, identification of phases at the braze/matrix interface, determination of shear strengths of brazed joints, and deformation mechanisms during tensile and creep processes will be discussed.

Poster Session

At Last, Something New!
Cleaning without Chemistry, and Reusing the Waste Water!

JOHN DURKEE

Creative EnterpriZes
105 Anyway, Suite 209
Lake Jackson, TX 77566
Phone: 815-547-5650 x200
Fax: 815-544-2287
E-mail: jdurkee@precisioncleaning.com

The poster describes research performed by Creative EnterpriZes and a client firm to investigate management of industrial soils from their existence on parts to their disposal as a concentrate in water. These soils came from the manufacture of metal parts and include oils used for drawing, forming, cutting, grinding, lubricating, and honing; phosphate-based lubricants used in compression threading; dry lubricants, such as molybdenum disulfide; and other materials whose composition was unknown.

The research produced the following knowledge:

- How these soils could be cleaned from parts using only ultrasonic energy and without use of cleaning chemistry
- How these soils could be made so as to not reinfect the parts in the cleaning bath
- The surprising effects of temperature and cleaning time on surface finish
- How to construct an evaporator for separation of the soils from water
- Specifications about recycle of the distilled and condensed liquid water.

The technology had been used at both high-precision and low-quality levels of cleaning. This knowledge has been implemented in full-scale cleaning machines, which also will be described.

Polymer Matrix Composite (PMC) Analog Processes for Lightweight Aluminum Matrix Composite (AMC) Structures

BRIAN GORDON

Touchstone Research Laboratory
RD1 Box 100B
The Millennium Center
Triadelphia, WV 26059 USA
Phone: 304-547-5800
Fax: 304-547-4069
E-mail: blg@trl.com

Next-generation hypersonic aircraft, reusable launch vehicles, and low-cost spacecraft require new materials to meet decreasing vehicle weights, increasing payload capacity, and dramatically lower operating costs. Materials that have improved specific strength and specific stiffness, especially at cryogenic and elevated temperatures, enable commercial and Government customers to meet these aggressive program goals by supporting development of stronger, lighter, and more thermally stable integrated components. Touchstone's Brazed Aluminum Matrix Composite (AMC) material has nearly twice the specific strength and specific stiffness of structural aluminum alloys and maintains these properties at higher temperatures than current aerospace alloys. When *in situ* brazed from thin tape, the manufacturing of large highly integrated structures is possible with minimal tooling. As such, this material and associated manufacturing process can serve as an enabling technology for many aircraft and spacecraft applications, including engine and thrust structures, feed lines and ducts, propellant tanks, and thermally stable satellite structures. This poster presentation discusses a new material and, more specifically, a new manufacturing system that enables development of high-performance aircraft and spacecraft components.

IP/512/IN/25

Further Studies of Materials Compatibility in High-Test Hydrogen Peroxide

RUDY GOSTOWSKI

Department of Chemistry
Austin Peay State University
Box 4547
Clarksville, TN 37044 USA
Phone: 931-648-7624
Fax: 931-648-5996
E-mail: gostowskir@apsu01.apsu.edu

Tom Owens
Marshall Space Flight Center
Huntsville, AL 35812 USA

Assessment of the compatibility of high-test hydrogen peroxide (HTP) with materials, in particular new materials such as composites, is critical to the development of new propulsion systems meeting requirements of reduced cost and environmental impact. While compatibility with HTP has been addressed previously, newer materials were not considered. The focus of this project was to develop a scheme for evaluation of HTP with all materials. In the previous summer, methods were developed for production of HTP on site, and preliminary steps were taken to evaluate materials. Methods investigated this summer have included accelerated aging by heating, coupled with assay of concentration and stabilization loss, observation of reactivity by means of Isothermal Microcalorimetry, and evaluation of changes to the materials by Short Beam Shear testing and by Photoacoustic-Fourier Transform Infrared Spectroscopy. Various metals, polymers, and composites were examined in this study.

X-traktor: A Rookie Robot, Simple, Yet Complex, Impeccably Designed, A Very Innovative Multidisciplinary Engineering Masterpiece

ARTHUR J. HENDERSON, JR.

Marshall Space Flight Center/ED36
Huntsville, AL 35812 USA
Phone: 256-544-2577
Fax: 256-544-5877
E-mail arthur.henderson@msfc.nasa.gov

FIRST is the acronym of For Inspiration and Recognition of Science and Technology. FIRST is a 501.C.3 non-profit organization whose mission is to generate an interest in science and engineering among today's young adults and youth. This mission is accomplished through a robot competition held annually in the spring of each year. NASA's Marshall Space Flight Center, Education Programs Department, awarded a grant to Lee High School, the sole engineering magnet school in Huntsville, Alabama. MSFC awarded the grant in hopes of fulfilling its goal of giving back invaluable resources to its community and engineers, as well as educating tomorrow's work force in the high-tech area of science and technology.

Marshall engineers, Lee High School students and teachers, and a host of other volunteers and parents officially initiated this robot design process and competitive strategic game plan. The FIRST Robotics Competition is a national engineering contest, which immerses high school students in the exciting world of science and engineering. Teaming with engineers from government agencies, businesses, and universities enables the students to learn about the engineering profession. The students and engineers have 6 weeks to work together to brainstorm, design, procure, construct, and test their robot. The team then competes in a spirited, "no-holds barred" tournament, complete with referees, other FIRST-designed robots, cheerleaders, and time clocks.

The partnerships developed between schools, government agencies, businesses, and universities provide an exchange of resources and talent that build cooperation and expose students to new and rewarding career options. The result is a fun, exciting, and stimulating environment in which all participants discover the important connections between classroom experiences and real-world applications.

This paper will highlight the story, engineering development, and evolutionary design of X-traktor, the rookie robot, a manufacturing marvel and engineering achievement.

Laser Surface Modification of TiAl Intermetallics

SHERMAN McELROY

Department of Metallurgical and Materials Engineering
The University of Alabama
Tuscaloosa, AL 35487-0202 USA
Phone: 205-348-4982
E-mail: smcelroy@hotmail.com

Ramana G. Reddy
ACIPCO Professor
Department of Metallurgical and Materials Engineering,
The University of Alabama
Tuscaloosa, AL 35487-0202 USA
Phone: 205-348-4246
E-mail: rreddy@coe.eng.ua.edu

Using a Nd-YAG laser, laser processing of a series of Ti-Al alloys, including pure Ti, pure Al, and Ti-Al intermetallic compounds, has been studied. SEM, XPS, and optical microscopy were used to determine the surface morphological, chemical, and compositional characteristics of the laser processed samples. Analysis of results showed that cracks along grain boundaries caused by rapid heating and cooling of laser processing were the dominant characteristics of the surface morphologies of the laser processed samples. Al content in the Ti-Al alloys plays a very important role in crack initiation and/or development. The more Al content in the samples, the more severe the cracks that developed after laser processing under the same conditions.

These experiments were conducted at ambient conditions, resulting in surface oxidation layers being observed on the processed samples. XPS results indicate that the oxidation layer consists of adsorbed O_2, Al_2O_3, TiO_2, and TiO. In addition, Al enrichment was found in the oxide film of TiAl as well as in the oxidation layers formed on the surfaces of TiAl and Ti_3Al intermetallics that were processed by the laser; which is different from the reported results for traditional oxidation of TiAl at elevated temperature.

Poster Session

Characterization of Ceramic Matrix Composite Combustor Components: Pre and Post Exposure

G. OJARD

United Technologies Research Center
411 Silver Lane M/S 129-24
East Hartford, CT 06108 USA
Phone: 860-610-7013
E-mail: OjardGC@utrc.utc.com

G. Linsey and J. Brennan
United Technologies Research Center
411 Silver Lane
East Hartford, CT 06108 USA

R. Naik, R. Cairo, R. Stephan, and J. Hornick
Pratt & Whitney
United Technologies Corporation
400 Main Street
East Hartford, CT 06108 USA

D. Brewer
Glenn Research Center/MS 49 - 7
21000 Brookpark Road
Cleveland, OH 44135 USA
Phone: 216-433-3304
Fax: 216-433-8000
E-mail: David.N.Brewer@lerc.nasa.gov

The pursuit of lower emissions and higher performance from gas turbine engines requires the development of innovative concepts and the use of advanced materials for key engine components. One key engine component is the combustor, where innovative design and material improvements have the potential to lower emissions. Efforts to develop a High Speed Civil Transport with low emissions were focused on the evaluation of combustor concepts with liners fabricated from a ceramic matrix composite of silicon carbide fibers in a silicon carbide matrix (SiC/SiC). The evaluation of SiC/SiC composites progressed from simple coupons (to establish a first-order database and identify operant failure mechanisms and damage accumulation processes), to feature-based subelements (to assess fabricability and *in situ* material response), to actual components (to assess structural integrity, dimensional, and compositional fidelity) tested under simulated engine conditions.

As in the case of all evolutionary material and process work, a key element to resolving fabrication issues is the evaluation of witness areas taken from fabricated components before testing the actual component. The witness material from these components allowed microstructural and mechanical testing to be performed and compared to the ideal, flat panel, conditions and data that are typical of basic characterization. This also allowed samples of similar design to be taken from components after 115 hours of combustion exposure. Testing consisted of tensile, double notch shear, ring burst, and thermal conductivity that sampled various regions of the components. The evaluation of the witness material allowed an understanding of the fabrication process, highlighting critical issues, in an early phase of the learning curve development of these configuration and material unique parts. Residual property testing, after exposure, showed if degradation of the material under actual service conditions was occurring. This paper will present the results of this critical testing. Evaluations that consider the degree of complexity of the fabricated part were established to relate *in situ* performance to that of flat panel based coupons. Nondestructive evaluation was used throughout the evaluation process. These results will also be discussed as an aid in understanding the test results.

CP/5106/IN/82

(11)

Automated Acquisition and Analysis of Digital Radiographic Images

Richard Poland, David Immel, Boyd Howard
Randy Singer, and Bob Moore
Westinghouse Savannah River Company
Savannah River Site
Aiken, SC 29808
(803) 725-1998

Keywords
Automated Image Analysis Digital Radiography X-ray

Abstract
Engineers at the Savannah River Technology Center have designed, built, and installed a fully automated small field-of-view, lens-coupled, digital radiography imaging system. The system is installed in one of the Savannah River Site s production facilities to be used for the evaluation of production components. Custom software routines developed for the system automatically acquire, enhance, and diagnostically evaluate critical geometric features of various components that have been captured radiographically. Resolution of the digital radiograms and accuracy of the acquired measurements approaches 0.001 . To date, there has been zero deviation in measurement repeatability. The automated image acquisition methodology will be discussed, unique enhancement algorithms will be explained, and the automated routines for measuring the critical component features will be presented. An additional feature discussed is the independent nature of the modular software components, which allows images to be automatically acquired, processed, and evaluated by the computer in the background, while the operator reviews other images on the monitor.

System components were also a key in gaining the required image resolution. System factors such as scintillator selection, x-ray source energy, optical components and layout, as well as geometric unsharpness issues are considered in the paper. Finally the paper examines the numerous quality improvement factors and cost saving advantages that will be realized at the Savannah River Site due to the implementation of the Digital Imaging & Measurement System (DIMS).

Background
At the Savannah River Site, a U.S. Department of Energy facility, a joining technique called "pinch welding" is used to seal highly pressurized containers, known as reservoirs. Pinch welding seals the tube by applying high force and high current over time to heat a portion of the metal tube to the plastic state, deform the tube, and ultimately seal the tube. *Figure 1.*

Because it is not possible to perform destructive testing of the pinch welds sealing the reservoirs, the qualification process begins with a weld development cycle where welding techniques are developed. Development welds are pressure tested and then destructively analyzed. At the completion of the weld development cycle the acceptable ranges for physical characteristics of the qualified weld are recorded and used as acceptance criteria for production welds.

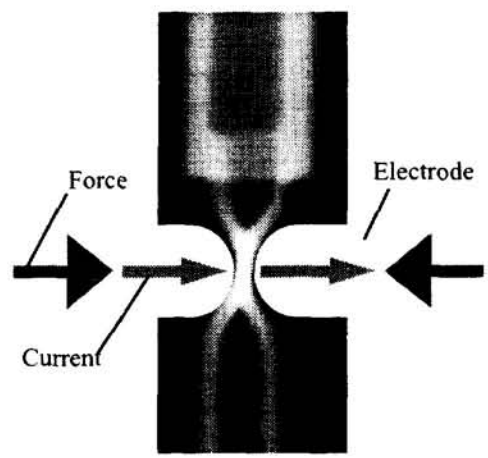

Pinch Weld

Figure 1

The key physical characteristics of these pinch welds are:

- minimum wall thickness,
- closure length,
- electrode alignment,
- tube alignment, and
- open bore length.

Each characteristic is described in detail below.

Since the inception of the program, conventional film radiography has been the method utilized to obtain the physical characteristics of the pinch welds. Film radiography is an expensive and labor intensive method to perform this evaluation; however, quantitative data was a prerequisite prior to component acceptance. Until recently it was not possible to obtain the required radiographic sensitivity and spatial resolution required for these evaluations with digital radiography; however recent developments in large format CCD imaging cameras have made this project possible. The authors presented the customer an opportunity to install a state-of-the-art imaging device that would provide improvements in quality factors as well as yield considerable cost savings. The customer immediately supported a program to evaluate, develop, and install the high resolution imaging system.

System Overview

The most important aspect of any automated digital radiography imaging system is x-ray image quality. Without a sharp, high resolution, high sensitivity radiographic image the accuracy of the automated measurements is very low, and may even be useless. Therefore considerable thought must be given to the selection of the x-ray components, the scintillating detector, and the optical components. Furthermore, the geometric unsharpness of the x-ray image must be considered to ensure that unsharpness is the lowest practicable value. (The lower the geometrical unsharpness, the better the image resolution.)

Each of these factors was considered in the design and development of the system, and each will be discussed in this section. The following section discusses the software that processes the images created by the digital radiographic system.

The system is a classical lens-coupled digital radiography system. The x-ray source is a 150 kVp, 3 mA Varian x-ray tube with a 1.5 mm spot size. The tube is housed in an interlocked x-ray cabinet with an imaging chamber 16 x 18 x 48 . A 2 x 2 x 6mm Industrial Quality, Inc. (IQI)-401 terbium-doped high-density glass scintillator was selected to provide high resolution x-ray to light conversion. A 26 source to scintillator distance, with an object to scintillator distance of one-eighth inch yields a geometric unsharpness of 0.29 mils, which is over three times sharper than the optical resolution of the system.

The scintillator was placed slightly out of the center of the x-ray cone beam to allow room for all of the production components to fit in the cabinet. The plane of the scintillator was therefore tilted at a 5 degree angle toward the x-ray spot ensuring that the scintillator plane is perpendicular to the incident x-rays. This maintains the sharpest possible images for this geometrical arrangement.

The optical imaging components are commercially available. A double turning mirror technique was used protect the CCD camera from high-intensity x-rays. The base optical breadboard table and the scintillator shelf are both lead-backed, and a riser connecting the two tables is also backed with lead. This totally shields the camera from direct exposure, thus nearly eliminating x-ray hits to the camera. The camera is a Photometrics Series 300 camera head with a KAF-4200 CCD. The KAF-4200 is a scientific grade 2,000 pixel by 2,000 pixel imager selected specifically to provide 0.001 resolution with a 2 x 2 field-of-view.

The calibrated optical resolution of the system is 0.927 mils, exceeding the stated customer requirement. The pinch weld essentially is in contact with the scintillator during image acquisition; therefore system geometric enlargement is one.

Figure 2 shows the measured Modulation Transfer Function (MTF). The system MTF is approximately 10 lp/mm at 14% modulation.

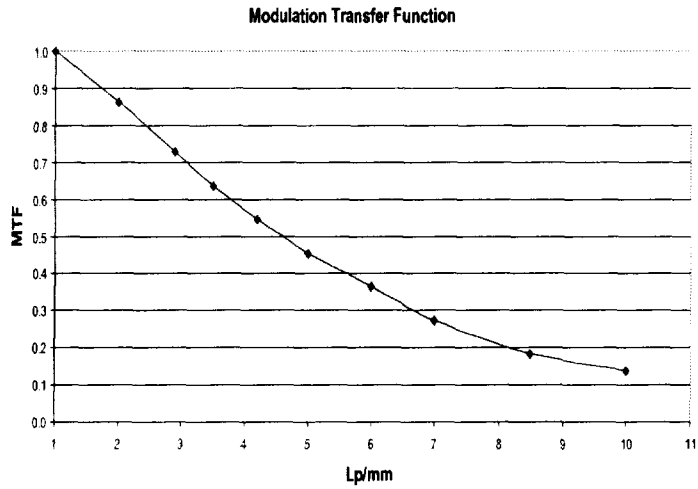

Figure 2

The system, as designed and installed, provides high spatial resolution images with high contrast sensitivity and a dynamic range far greater than that of conventional x-ray film.

Automated Software Modules

Once a high quality radiographic image was assured, the next step was to automate the acquisition and analysis of the image to provide accurate measurements of all pertinent pinch weld features. The software to accomplish these tasks has been designed in modular form, and will be described in detail for each of four modules. The four modules are Acquisition, Processing, Analysis, and Review. It is important to note that each module runs independently and concurrently. After the image is acquired it is passed to the processing module, and from the processing module to the analysis module. Following the automated computer analysis, a qualified operator reviews the image and the measurement results and makes the final accept/reject decision.

Acquisition Module

Prior to the evaluation of each group of reservoirs an ASTM penetrameter is imaged. The #5 penetrameter is placed on a 60 mil thick steel shim, imaged, and automatically evaluated by the software. The evaluation includes verification of the visibility of the 1T hole, where the software evaluates the contrast change from the area surrounding the 1T hole versus the contrast in the hole, and then evaluates the ratio versus a defined threshold. In addition, the dimensional verification of the pixel size is performed by tracing the penetrameter edges and measuring the diagonal dimensions of the penetrameter. These measurements are compared to National Institute of Standards and Technology (NIST) traceable values. If measurements are outside a pre-defined range of values, imaging tests are halted until the discrepancies are resolved.

The operator then places the reservoir in a fixture that precisely places the pinch weld on the surface of the scintillator. The fixture, however, does not align the pinch weld parallel to the x-ray beam, and therefore the vertical pinch weld alignment is dependent on the operator. To ensure that each image is properly rotationally aligned, the software checks the alignment by evaluating the slope of the line profile at the center of the pinch. Essentially, the center of a pinch is similar to a rectangle, and for high resolution imaging of the pinch weld the rectangle must be precisely aligned with the path of the x-ray photons. *Figure 3.* If the rectangle is misaligned, the slope is less, and the operator is prompted to realign the pinch weld.

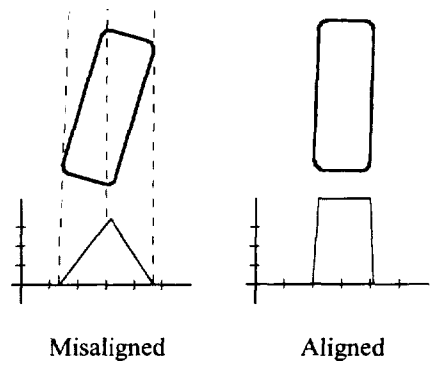

Figure 3

This alignment procedure is performed on a low resolution postage stamp image that requires only 15 seconds to acquire. This postage stamp image is also used to define the region of interest (ROI) that is required for the full resolution image. A very small amount of the 2 x 2 field-of-view (FOV) is required to image the tube, therefore to save data storage space only the required data is acquired and archived. This ROI is automatically detected and set by the software for each image (the ROI changes depending on the reservoir being evaluated). The software also extracts the pinch weld characteristics to determine which measurements will be performed in the analysis module. When the alignment is acceptable and the

operator has verified proper ROI placement, the software begins a four minute exposure to acquire the full resolution image. Following the acquisition the image data is presented to the processing module for data processing.

Processing Module

De-fog

A de-fogging algorithm is applied to the recently acquired pinch weld image, I_0, and to the background image, I_B, that was acquired at the beginning of the run sequence. The de-fogging routine is used to remove effects of x-ray scatter and scintillator cross talk in the background image and the pinch weld image. Incident x-rays transmitted through the pinchweld generate the light in the scintillator that makes up the true image, however light is also generated by scattered x-rays. Further, the light in the transparent scintillator is transmitted in three dimensions, thus there is light cross talk for neighboring pixels within the scintillator. The closer the pixels are together, the greater the cross talk effect. The algorithm effectively removes both the scatter effect as well as a large portion of the cross talk effect. *Figure 4* shows the light generation components of a single scintillating pixel. The x-ray intensity transmitted through the subject, I_{Tx}, the x-ray scatter intensity incident upon the pixel, I_S, and the cross talk light, L_X, all contribute to the total light, L_T, detected by the camera at that pixel.

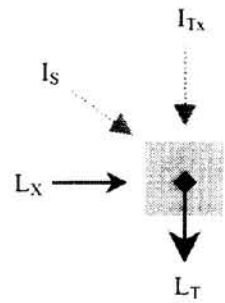

Figure 4

$$L_T = L_{ITx} + L_{IS} + L_X \qquad \text{(Eq. 1)}$$

The desired light to be detected is L_{ITx}, therefore the effects of all extraneous light must be removed from the data. This is accomplished using the equation

$$L_{ITx} = L_T - \sum_i \sum_j F(i,j) * L_T(i,j)\,, \qquad \text{(Eq. 2)}$$

where a function, F(i,j) scales the effect of the total light, L_T, generated in neighboring pixels for a two dimensional surrounding area, i by j. F(i,j) reduces the effect as the distance away from the pixel increases.

The effects of the de-fog routine are tremendous. The edge definitions in the image are greatly enhanced due to the removal of the low frequency cross talk between neighboring pixels. Further, the contrast within the part is greatly increased. *Figure 5* shows a comparison of the de-fogged image (bottom) versus the unprocessed image (top). Comparison of the contrast curves taken through the base, the pinch, and the tube show the increased contrast, the more defined edges, and the removal of the low frequency shadowing apparent near the edges of the tube.

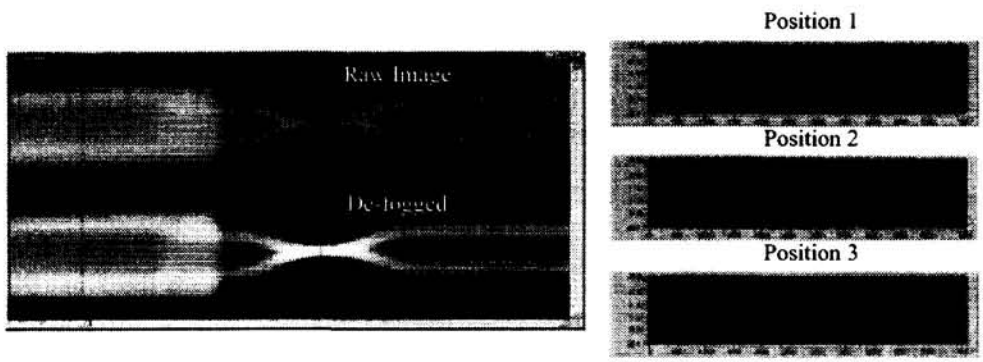

Figure 5

Background and Dark Correction
Beer s Law,

$$I_R = \frac{I_B' - I_D}{I_0' - I_D} \quad , \qquad \text{(Eq. 3)}$$

is applied with the de-fogged background image, I_B , and the dark image, I_D. I_0 is the de-fogged full resolution pinch weld image. Beer s Law processing removes effects such as scintillator imperfections, optical aberrations, differences in pixel responsiveness, as well as other system abnormalities. I_R is the resultant image data.

De-speckle
In the final step of the processing module, the de-speckle routine is applied to I_R. The de-speckle routine is used to remove bad pixels or pixels that have been over-exposed due to a direct strike of an x-ray photon. The center pixel being evaluated, P_C, is compared to the eight surrounding pixels. If P_C is greater than the median surrounding pixel by a specified threshold, then P_C is replaced with that median pixel value.

The processed image is now ready for automated analysis, and is placed in the analysis module s cue.

Analysis Module
Two analyses are performed on the radiographic data. The first is the quantitative measurements of the weld characteristics performed here in the Analysis Module. The second is actually completed by the operator in the Review Module. The operator visual verifies the automated measurements, and then visually examines the tube and the weld area for defects.

The quantitative evaluations are automatically performed by the computer using custom developed software to define the characteristics and then measure the parameters. Four edges form the basis from which all measurements are determined. *Figure 6.* These edges are the left and right outer edges of the tube (red), and the inner edges on the reservoir side of the pinch weld and on the open side of the tube (green).

Figure 6

The outer edges are determined by simple intensity thresholding. The edge is detected at a percentage level above the background contrast level. The inner edges are set by a slope threshold method. The slope threshold method detects an inner edge by first finding the zero-slope point for the tube s contrast curve. The inner edge is then set at a point a percentage below the zero slope on the row s contrast curve. Both threshold levels were set and verified by comparison to a calibrated standard tube. As stated previously, all edge detection levels have been set, calibrated, and verified numerous times.

With the edges defined, all parametric measurements can be determined. There are presently seven parameters that are automatically determined by software. These are:

Minimum Wall Thickness
Minimum wall thickness is a critical process parameter that measures the thinnest portion of the tube wall on the reservoir side of the weld. The minimum wall thickness measurement must be greater than that specified for the reservoir being evaluated. The minimum wall thickness is determined by measuring the distance from every point on the reservoir inner wall edge to every point on each of the outer wall edges. The minimum wall thickness value is extracted from these measurements.

Weld Closure Length
The weld closure length is the minimum distance between the reservoir inner edge and the open-end inner edge. This measurement is obtained by determining the distance from every point on the reservoir inner edge to every point on the open-end inner edge, and then extracting the minimum value. This value therefore measures the minimum closure length of the pinch weld. The designer specifies the minimum length, and the measurement must be greater than the specification for the unit to be accepted.

Electrode Alignment
The electrode alignment parameter measures the vertical alignment of the two electrodes used to make the weld. The alignment is critical because electrodes greater than the acceptable offset could cause a failure of the weld process resulting in considerable expense. The software calculates the offset by first generating a best-fit electrode from the pinch region of each outer edge. A line is then extended from the center of the electrode toward the center of the electrode s deformation in the pinch. The measurement is the offset measured at the vertical centerline of the pinch.

Tube Alignment
The tube alignment measurement is a measurement of the angular difference of the tube extending from the pinch to the reservoir versus the tube extending from the pinch to the open end. This parameter is determined by measuring the angular difference between projected centerlines generated from the outer edges above and below the pinch area. The customized software provides additional information, the tube-centerline offset value. The value is the offset of the centerlines when extended vertically to the center of the weld.

Open Bore Length
Open Bore Length is the location where the inner edge diameter drops below a threshold specified by the designer. This measurement is acquired by defining two value, the location where the tube extends from the reservoir base, and the point at which the reservoir inner edge separation (tube I.D.) drops below the threshold.

Closure Characteristics
Closure Characteristics comprise two different measurements. There are two types of welds which must be evaluated by the system, and each has unique closure characteristics. The software automatically classifies the type of weld, then measures the closure diameter or the extrusion characteristics depending on the classification.

Review Module
The Review Module is somewhat of an extension of the Analysis Module, however the two run independently and therefore are considered separate modules. The Review Module is the most interactive module requiring the operator not only to verify the placement of the inner and outer edges, and the location of the measurements, but also perform a visual inspection of the radiographic image.

Although the software has been thoroughly tested, the designers believed that at least initially the operator should be required to verify the placement of the edges and concur with the locations of the measurement values. Therefore, when the operator reviews an inspection, he is presented with the edge traces and each measurement visually. He either accepts the parameter or rejects the parameter with a comment. The parameter cannot be rejected without a comment explaining the concern. This allows the production engineer to key in on an anomaly during a subsequent examination.

Operators performing the visual examinations must be minimally qualified as an ASNT limited level II x-ray technician. The operator is presented the processed image with mathematically generated 1T holes placed on mathematically generated shims ranging from 30 mils to 150 mils. The virtual #5 penetrameter 1T hole ensures the contrast sensitivity of the system. The extended dynamic range of the digital radiograph contains qualitative data throughout this large range of material thickness, unlike the conventional film method that was qualified for material thickness of only 50 to 78 mils. This alone is a leap forward in the qualitative evaluation of the weld area, which has a material thickness of greater than 120 mils.

The system allows the operator to vary the contrast levels, while viewing the pinch weld image and the 1T penetrameter swatches. The operator has the ability to reduce the display intensity range to produce a higher contrast in a limited range, or expand the range to produce an image similar to film. By ranging through the entire range of contrast levels the operator performs a very thorough evaluation of the tube as

well as the weld area. Again, the operator is permitted to comment on anomalies. These comments are written to the file history and permanently stored with the image data.

Results

The installation of the automated digital radiography system provides many benefits to the customer in this application. The two key benefits are quality improvement and cost savings. Both are obviously critical factors when any organization attempts to justify the installation of a capital piece of equipment.

Quality Improvements

Calibrated Measurements

The Digital Imaging & Measurement System (DIMS) measurements are calibrated and traceable to NIST. On the other hand, there is no way to provide calibration of an operator subjectively determining the edges of the x-ray image, and then performing the measurement of the characteristics.

Greater Measurement Repeatability

The automated measurement algorithms provide zero variation in repeated measurements of the same image, and assure consistent evaluation of pinch welds throughout the life of the system. The conventional method of operator evaluation yielded greater than 25% variation in measurements from operator to operator for evaluations of the same radiographic images.

More Thorough Radiographic Evaluation

The DIMS provides code quality evaluation of the pinch weld radiograph throughout the required thickness range (i.e. 0.030" - 0.130"), and allows the operator to change the contrast levels for a more through evaluation. The conventional method was set up to radiographically image the pinch weld to allow for evaluation of the pinch weld characteristics (0.050" - 0.070"), not for anomalies in the weld area (0.125").

Process Control Feedback

The DIMS allows the operator to evaluate the image within minutes of the exposure, and provides the pinch weld characteristic measurements within minutes as well. If there is an unacceptable parameter, the process can be immediately evaluated and the problem corrected prior to additional reservoirs being sealed. This valuable feedback can typically take two weeks with the conventional film method currently in use.

Cost Savings

Reduced Labor Expenses

Time is money, and labor hours consume budgets. This first installation of the DIMS will have a considerable effect on reducing the labor required for analysis of these welds, however the larger savings will be realized following the conversion of an additional three locations to digital systems. At that point, due to the automated nature of the system, full-time subcontract radiographers will no longer be required at the facility, saving well over a $100,000 per year. Further, due to the contaminated nature of the inspection location, no longer will Radiation Control specialists be required to bag-in/bag-out film because the digital images will be digitally transmitted from the camera to the computer. In all, labor savings alone are estimated to total over $250,000.

Reduced Film Evaluation Time

Since the parameters are automatically measured by the software, no longer do operators have to laboriously determine several measurements for each pinch weld film, moving from two different measurement instruments. Due to the automated and modular nature of the software the operator can be performing other tasks while the computer is imaging, processing, and analyzing images.

Reduced Film and Chemical Requirements

A considerable cost savings will be realized due to the reduced need for x-ray film and development chemicals. Although this cost savings will not scale to the magnitude of the labor savings, this benefit is also important to reduce resource consumption and reduce waste streams.

Reduced Number of Rejected Units
If a parameter is outside of an acceptable range, the reservoir is rejected and the unit must be re-worked. This is a very timely and costly process extending into the hundreds of thousands of dollars. The immediate feedback of the DIMS will reduce the number of re-work units, thus providing considerable cost savings as well as process quality improvement.

Additional Benefits
Digital Nature
There are obvious advantages of the system being digital, such as the data being stored on compact storage disks, replacing film and paper storage. An additional feature of digital storage is that the digital data never degrades, unlike film which will fade over time. Further, the digital images and measurement data may be quickly shared electronically for evaluation and discussion.

Reduced Waste Streams
As mentioned above, the complete installation of the DIMS will eliminate the bag-out scenario and reduce that waste stream, as well as the reduction of waste film and development chemicals.

Summary
Throughout the development of the DIMS several advances in digital radiography techniques have been developed. A key breakthrough is the de-fogging algorithm that removes cross talk effects that have plagued glass scintillators, thus increasing attainable resolution. The display of the virtual penetrameter to ensure equivalency to film is another development in the presentation of digital x-ray images. This virtual penny display allows for code-quality examination of the entire dynamic range of the digital data.

In conclusion, the pinch weld image acquisition and analysis system is a production-ready system with customized, automated software that controls the imaging and analysis process through the complete imaging cycle. The system delivers accurate, repeatable, digital results by eliminating operator bias in the imaging process as well as the analysis processes.

CP/2109/IN/20
ABS ONLY

Poster Session

Fabrication of Low-Cost, High-Temperature Composites for Rocket Propulsion Systems

MARK J. RIGALI, Manish Sutaria, Anthony C. Mulligan, and Ranji Vaidyanathan

(12)

Advanced Ceramics Research, Inc.
3292 E. Hemisphere Loop
Tucson, AZ 85706 USA
Phone: 520-573-6300
Fax: 520-573-2057
E-mail r.vaidyanathan@acrtucson.com

Advanced Ceramics Research, Inc., (ACR) is currently developing two low-cost, flexible manufacturing processes to produce high-temperature composites with zirconium carbide (ZrC) matrices for use in current and future NASA and Department of Defense (DoD) propulsion applications. As a monolithic material, ZrC exhibits corrosion and ablation resistance at high temperatures. ZrC, however, does not possess the toughness and thermal shock resistance necessary to survive in many propulsion system applications. To enhance its toughness and thermal shock resistance, ACR is fabricating ZrC-based composites using two novel and low-cost composite fabrication techniques called Fibrous Monolith (FM) processing and Continuous Composite Co-extrusion (C^3) processing.

Fibrous Monolith processed composites are a new class of low-cost, bi- and multi-component structural ceramics. They exhibit mechanical properties similar to fiber composites or laminate structures, including very high fracture energies, damage tolerance, and graceful failure. Since they are monolithic powder-based composites, however, they can be manufactured by conventional powder processing techniques using inexpensive raw materials. In the FM process, an interpenetrating microstructure of elongated polycrystalline 'cells' of the matrix material (in this case, the high-temperature carbides and diborides) are separated and encapsulated by thin cell boundaries of a low shear strength material (BN, graphite, *etc.*) or a ductile material (W, Re, Mo, *etc.*) This interpenetrating microstructure imparts the necessary toughness and thermal shock resistance to the composite that is lacking in the monolithic carbides. The weak interface composites and many of the ductile interface composites exhibit fracture behavior similar to fiber reinforced ceramic composites, including the ability to fail in a non-catastrophic manner

C^3, based on the Fibrous Monolith processing technology, utilizes an innovative approach to produce continuous fiber reinforced composites. In the C^3 process, carbon fiber tow is passed through the center of a ceramic powder/thermoplastic binder feedstock during melt extrusion to produce a 'green' filament. The resulting filament is flexible, robust, and easily handled using traditional processing methods, *i.e.*, hand lay-up or filament winding; it is then pyrolyzed and hot pressed to produce dense parts. Although it was originally developed for the fabrication of ZrC and HfC carbon fiber composites for propulsion systems, the C^3 process promises to be applicable to the fabrication of a wide variety of other fiber-reinforced composites.

This paper highlights the mechanical and physical properties of the ZrC-based composites currently under development by ACR using the both the FM and C^3 fabrication processes. In addition, ACR is applying solid freeform fabrication (SFF) techniques to the production of these composite components currently being developed for several high-temperature DoD and NASA applications, including hot gas valves components, nozzles, thrust cells, and leading edges.

Electro Spark Alloy Processing for Aerospace Components

MICHAEL RILEY

Surface Treatment Technologies, Inc.
8600 Drumwood Road
Towson, MD 21286 USA
Phone: 410-828-5914
Fax: 410-828-1993
E-mail: mriley@stt-inc.com

Surface Treatment Technologies has employed the Electro Spark Alloying (ESA) process for three NASA hardware needs:

- Repair of pitting corrosion on Solid Rocket Booster (SRB) o-ring grooves
- Repair of 24K gold coatings on Space Shuttle engine components
- Formation of burn-resistant alloy coatings on oxygen delivery hardware.

The ESA process is a low-voltage arc welding technique in which an electrode deposits itself on a conductive metal or ceramic substrate. The resultant coating has the following key features:

- Full metallurgical bond to the substrate
- Nano-grain structure
- No heat-affected zone in the base alloy
- Capability of coating inside diameters and non-line-of-sight geometries.

Nano-grain coatings of metal, intermetallic, and ceramic layers have been formed on test specimens and subjected to relevant customer tests. Process information, metallurgical data, and test results from Phase I Small Business Innovation Research and NASA-related contracts will be presented.

Detection, Identification, and Quantification of Surface Contamination

M. MARTIN SZCZESNIAK, Michael Beecroft, and Phillip Mattison

Surface Optics Corporation
11555 Rancho Bernardo Road
San Diego, CA 92127
Phone: 858-675-7404
Fax: 858-675-2028

Even low levels of surface contamination can affect in a negative way physical properties of metal surfaces: adhesion, bonding, heat radiation. Detection of low contamination levels (below 1 microgram/cm^2) on large surfaces (more than 1 inch in diameter) is a challenge. A portable infrared reflectometer is applied to this application with a high level of success. The reflectometer covers the spectral region required to detect both the hydrocarbons and silicones. It is achieved with a Fourier Transform Infrared spectrometer. The sampling interface depends on the finish of the studied surface. The highly finished mirror-like surfaces can be analyzed with a specular reflectance accessory. The rough surfaces (grit-blasted) can be analyzed with the diffuse reflectance accessory. The reflectometer measures infrared spectra of suspected areas. The measurable infrared spectrum is an indication of surface contamination. The infrared spectra can be searched against standard or custom spectral libraries, which results in contaminant identification. The level of contamination can be predicted by applying calibration curves or chemometrics, PLS, CLS. The surface, which can not be accessed directly, can be swabbed and the residue extracted into the VSphere™. The VSphere™ is a patented accessory for the detection of nonvolatile residues. The minimum detection limits will be presented and discussed.

Quadruple Lap Shear Processing Evaluation

Tony N. Thornton

Thiokol Propulsion
SEHO
P. O. Box, 707, M/S 200
Brigham City, UT 84302

ABSTRACT

The Thiokol, Science and Engineering Huntsville Operations (SEHO) Laboratory has previously experienced significant levels of variation in testing Quadruple Lap Shear (QLS) specimens. The QLS test is used at Thiokol / Utah for the qualification of Reusable Solid Rocket Motor (RSRM) nozzle flex bearing materials. A test was conducted to verify that process changes instituted by SEHO personnel effectively reduced variability, even with normal processing variables introduced. A test matrix was designed to progress in a series of steps; the first establishing a baseline, then introducing additional solvents or other variables. Variables included normal test plan delay times, pre-bond solvent hand-wipes and contaminants. Each condition tested utilized standard QLS hardware bonded with natural rubber, two separate technicians and three replicates. This paper will report the results and conclusions of this investigation.

INTRODUCTION

In 1993, the first QLS specimens were processed at SEHO during the down-selection of aqueous cleaners for the replacement of 1,1,1 trichloroethane (TCA) in vapor-degreasers. Over the course of a year, specimens were processed on five different occasions, each producing unacceptable and unexplainable levels of variation. A team comprised of NASA, SEHO and Utah S&E was established to investigate the problem, but was dissolved when all possible efforts to render a solution were exhausted. The QLS portion of the test was then transferred to Utah.

QLS testing at SEHO was revived again in the latter part of 1999, with changes to processing methodology that provided ample positive results to proceed with a formal Engineering Test Plan. These changes included the use of polyurethane foam brushes for primer, adhesive and tackifier applications instead of nylon bristle brushes, shimming the QLS molds instead of the cure press and changing the cure cycle to include a temperature ramp before initiating the cure cycle.

© 2000 Thiokol Propulsion, a Division of Cordant Technologies Inc.

The primary objective of this test was to demonstrate QLS specimens could be successfully bonded at the SEHO lab after implementing the changes to our processing methodology. The secondary objective was to introduce typical variables and contaminants that may be encountered during hardware processing to demonstrate that the method was robust.

The test was designed to progress in a series of steps, each step introducing another variable. First, using standard QLS hardware and specified processing protocol, three replicates of four QLS specimens were processed at different times by two separate technicians. The second iteration incorporated normal test plan delay times for contamination purposes, with no contaminant. The third iteration incorporated normal test plan delay times that are encountered for contamination purposes, with no contaminant and a pre-bond hand wipe with TCA. The fourth and fifth iterations introduced the contaminants Conoco HD-2® grease and Permacel® tape adhesive respectively, delay times and a pre-bond hand-wipe cleaning with TCA. The test matrix is shown below in Table I.

Table I: Test Matrix

Test	Specimens	Replicates	Technicians	Specimens per Test
Baseline	4	3	2	24
Normal Time-Delay	4	3	2	24
TCA Hand-Wipe	4	3	2	24
TCA Hand-Wipe HD-2	4	3	2	24
TCA Hand-Wipe Permacel Tape	4	3	2	24
Total				**120**

TESTING

The test specimens consisted of steel QLS plates bonded together with natural rubber using a primer (Chemlok® 205); a rubber-to-metal adhesive (Chemlok® 220); and a tackifier (Tycement). A typical QLS specimen is illustrated below in Figure I.

Figure I: QLS Specimen

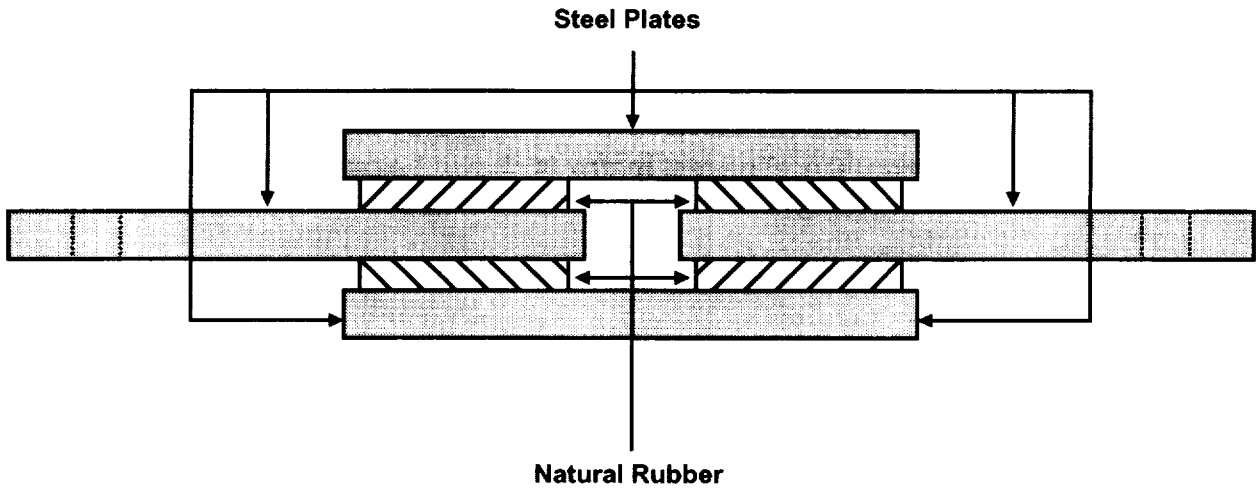

All QLS hardware utilized for this test was measured to the nearest .001" and placed in sets not varying more than .002". All bonding surfaces were grit blasted and spray-in-air cleaned after which they received a final grit blast before processing. Baseline specimens were bonded the same day as the final grit blast. Normal time delay specimens were allowed to sit undisturbed for 36-48 hours after the final grit blast prior to bonding. TCA hand-wipe specimens were allowed to sit undisturbed for 36-48 hours after which they were wiped using the double hand-wipe method prior to bonding. Specimens contaminated with HD-2 grease and yellow tape adhesive were placed in an oven for 24 hours at 100°F, allowed to sit at ambient for an additional 12-24 hours then cleaned with TCA using the double hand-wipe method prior to bonding.

Test specimens were cured for 2 hours at 300°F then allowed to condition for a minimum of 24 hours at ambient. Mechanical testing was conducted at ambient laboratory temperature and humidity using a test rate of 0.5 inches per minute.

RESULTS

Average results for the Baseline specimens exceeded the 500 psi minimum shear strength requirement for this bondline by 35%. Results also yielded a 73% increase over specimens tested previously at SEHO and surpassed our parent lab's historic average by 15%. Shear results are shown in Figure II.

Figure II: Baseline Shear Comparison

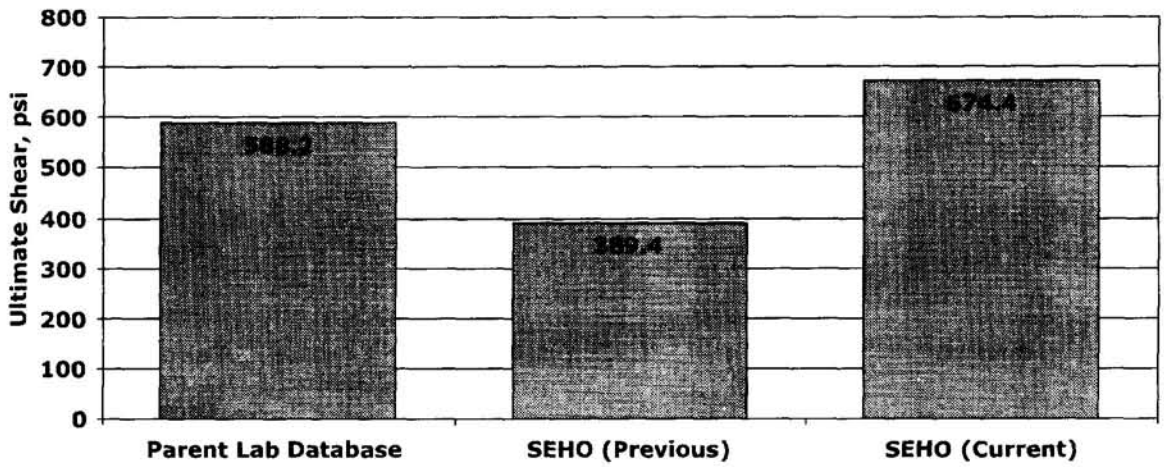

Results also denote a significant decrease in the Coefficient of Variance (CV) compared to previous SEHO testing and our parent lab's historic database as shown in Figure III.

Figure III: Baseline CV Comparison

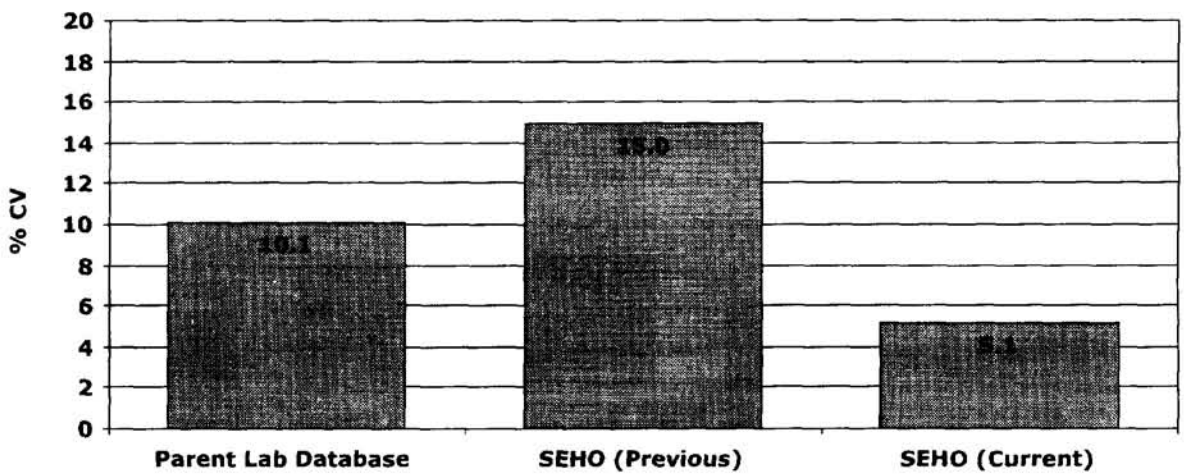

Figure IV summarizes average shear strength results obtained from the test conditions that were shown in Table I. As with the Baseline specimens, all conditions tested significantly exceeded the minimum shear strength requirements for this bondline.

Figure IV: SEHO Current Shear Results

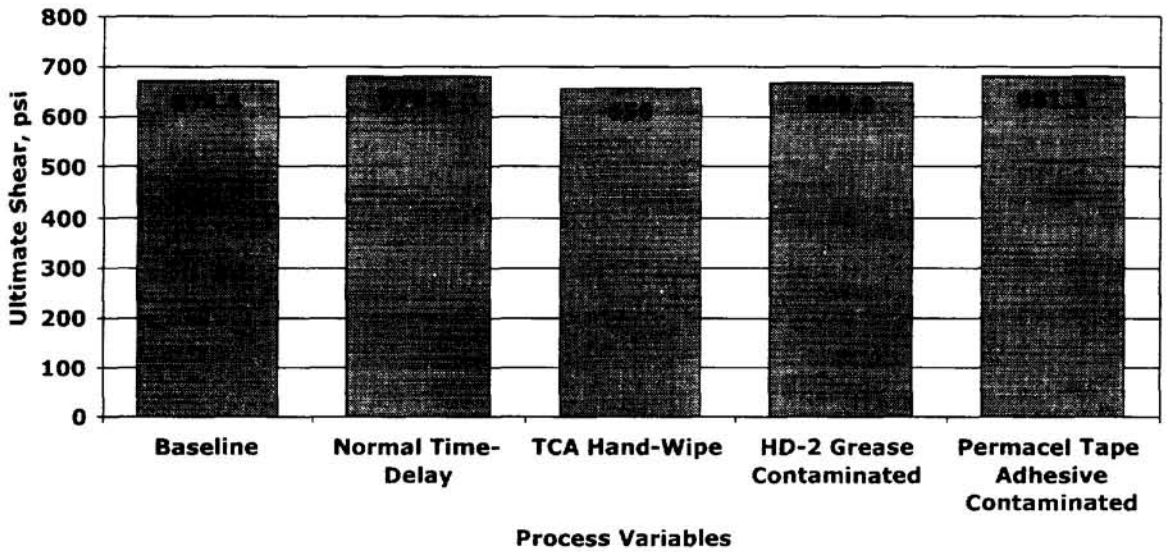

Figure V summarizes average CV results obtained from this testing. As with the Baseline specimens, all conditions tested displayed minimal percentages of variation.

Figure V: SEHO Current CV Results

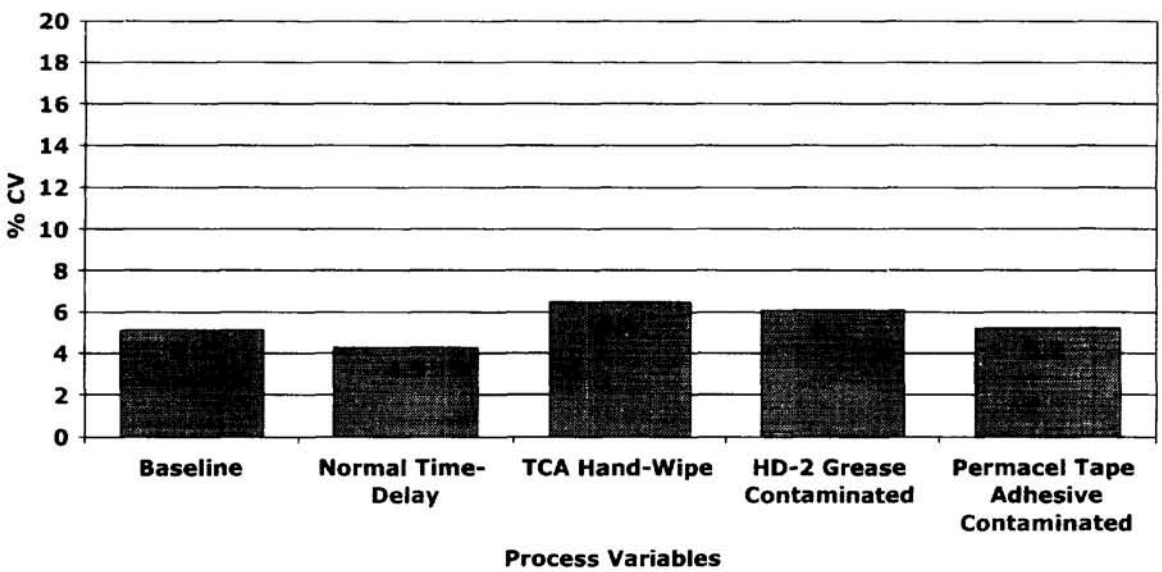

CONCLUSIONS

The program objectives were accomplished demonstrating that SEHO can reliably process QLS specimens without unexplainable variation in test results. Successful QLS processing can be achieved with or without intentional test variables introduced. Current testing demonstrated shear strengths that significantly exceeded minimum requirements.

The success of this program can be attributed to changes made to processing methodology that included:

- Brushes
  - Nylon bristle brushes previously used for application of the primer, adhesive and tackifier were found to be conducive to introducing "streaks" on the surface that seemed to be causing adhesive bond failure
  - Polyurethane foam brushes currently used produce a thin, uniform coating that eliminates streaks and significantly reduces adhesive bond failure
- QLS mold pre-heat
  - The previous method of shimming the cure press did not allow top platen to contact the QLS molds during pre-heat
  - The current method of shimming the molds allows maximum heat transfer from the top platen directly to the molds
- Cure cycle:
  - The cure cycle previously used did not allow time for the press to reach cure temperature before initiating the 2 hour cure
  - Cure cycle currently used incorporates a ramp to cure temperature before the 2 hour cure cycle is initiated

ACKNOWLEDGEMENTS

This effort was accomplished as the result of a collaboration of many individuals. The following people played significant roles in this work: Richard Boothe, Troy Daugette, Charlie Davis, Jill Keen, Ken Peacock and the SEHO Test Lab.

REPORT DOCUMENTATION PAGE

Form Approved
OMB No. 0704-0188

Public reporting burden for this collection of information is estimated to average 1 hour per response, including the time for reviewing instructions, searching existing data sources, gathering and maintaining the data needed, and completing and reviewing the collection of information. Send comments regarding this burden estimate or any other aspect of this collection of information, including suggestions for reducing this burden, to Washington Headquarters Services, Directorate for Information Operation and Reports, 1215 Jefferson Davis Highway, Suite 1204, Arlington, VA 22202-4302, and to the Office of Management and Budget, Paperwork Reduction Project (0704-0188), Washington, DC 20503

1. AGENCY USE ONLY *(Leave Blank)*	2. REPORT DATE	3. REPORT TYPE AND DATES COVERED
	February 2001	Conference Publication

4. TITLE AND SUBTITLE

Proceedings of the 4th Conference on Aerospace Materials, Processes, and Environmental Technology

5. FUNDING NUMBERS

6. AUTHORS

D.E. Griffin, D. Cross Stanley, Editors

7. PERFORMING ORGANIZATION NAMES(S) AND ADDRESS(ES)

George C. Marshall Space Flight Center
Marshall Space Flight Center, AL 35812

8. PERFORMING ORGANIZATION REPORT NUMBER

M–988

9. SPONSORING/MONITORING AGENCY NAME(S) AND ADDRESS(ES)

National Aeronautics and Space Administration
Washington, DC 20546–0001

10. SPONSORING/MONITORING AGENCY REPORT NUMBER

NASA/CP—2001–210427

11. SUPPLEMENTARY NOTES

Prepared for Materials, Processes, and Manufacturing Department, Engineering Directorate.
Proceedings of a conference held in Huntsville, AL, September 18–20, 2000.

12a. DISTRIBUTION/AVAILABILITY STATEMENT

Unclassified-Unlimited
Subject Category 23
Standard Distribution

12b. DISTRIBUTION CODE

13. ABSTRACT *(Maximum 200 words)*

The next millennium challenges us to produce innovative materials, processes, manufacturing, and environmental technologies that meet low-cost aerospace transportation needs while maintaining U.S. leadership. The pursuit of advanced aerospace materials, manufacturing processes, and environmental technologies supports the development of safer, operational, next-generation, reusable, and expendable aeronautical and space vehicle systems. The Aerospace Materials, Processes, and Environmental Technology Conference (AMPET) provided a forum for manufacturing, environmental, materials, and processes engineers, scientists, and managers to describe, review, and critically assess advances in these key technology areas.

14. SUBJECT TERMS

environment, replacement technology, solvents, propulsions, precision cleaning, coating technology, lessons learned, manufacturing, advanced materials, metal processes, nonmetal processes, ceramic matrix composites, rapid prototyping, pollution prevention, cleanliness verification

15. NUMBER OF PAGES

1,084

16. PRICE CODE

A99

17. SECURITY CLASSIFICATION OF REPORT	18. SECURITY CLASSIFICATION OF THIS PAGE	19. SECURITY CLASSIFICATION OF ABSTRACT	20. LIMITATION OF ABSTRACT
Unclassified	Unclassified	Unclassified	Unlimited